Complexity

Modeling, Simulation and Decision-Making of Complex Management Systems

Lead Guest Editor: Gang Kou
Guest Editors: Haobin Li, Hui Xiao, and Yu Zhou

Modeling, Simulation and Decision-Making of Complex Management Systems

Complexity

Modeling, Simulation and Decision-Making of Complex Management Systems

Lead Guest Editor: Gang Kou
Guest Editors: Haobin Li, Hui Xiao, and Yu Zhou

Contents

Contents

Hindawi
Complexity
Volume 2023, Article ID 9481790, 25 pages
https://doi.org/10.1155/2023/9481790

Review Article

Powder Bed Fusion via Machine Learning-Enabled Approaches

Utkarsh Chadha,[1,2] **Senthil Kumaran Selvaraj**,[2] **Abel Saji Abraham**,[2] **Mayank Khanna**,[2] **Anirudh Mishra**,[3] **Isha Sachdeva**,[4] **Swati Kashyap**,[5] **S. Jithin Dev**,[2] **R. Srii Swatish**,[2] **Ayushma Joshi**,[3] **Simar Kaur Anand**,[3] **Addisalem Adefris**,[6] **R. Lokesh Kumar**,[3] **Jayakumar Kaliappan**,[3] **and S. Dhanalakshmi**[7]

[1]*Department of Materials Science and Engineering, aculty of Applied Sciences and Engineering, University of Toronto, St. George Campus, Toronto, Ontario M5S 1A1, Canada*
[2]*Department of Manufacturing Engineering, School of Mechanical Engineering (SMEC), Vellore Institute of Technology, Vellore, Tamilnadu 632014, India*
[3]*School of Computer Science and Engineering (SCOPE), Vellore Institute of Technology, Vellore, Tamilnadu 632014, India*
[4]*School of Information Technology & Engineering (SITE), Vellore Institute of Technology, Vellore, Tamilnadu 632014, India*
[5]*School of Electronics Engineering (SENSE), VIT-AP University, Amaravati, Andhra Pradesh 522237, India*
[6]*School of Mechanical and Automotive Engineering, College of Engineering and Technology, Dilla University, P.O. Box 419, Dilla, Ethiopia*
[7]*Combat Vehicles Research & Development Establishment (CVRDE), Defence Research and Development Organization (DRDO), Ministry of Defence, Government of India, Avadi, Chennai, Tamilnadu 600054, India*

Correspondence should be addressed to Senthil Kumaran Selvaraj; senthilkumaranselvaraj82@gmail.com and Addisalem Adefris; addisalem@du.edu.et

Received 23 April 2022; Revised 14 September 2022; Accepted 6 October 2022; Published 30 April 2023

Academic Editor: Yu Zhou

Powder bed fusion (PBF) applies to various metallic materials used in the metal printing process of building a wide range of complex parts compared to other AM technologies. PBF process has several variants such as DMLS (direct metal laser sintering), EBM (electron beam melting), SHS (selective heat sintering), SLM (selective laser melting), and SLS (selective laser sintering). For PBF to reach its maximum potential, machine learning (ML) algorithms are used with suitable materials to achieve goals cost-effectively. Various applications of neural networks, including ANNs, CNNs, RNNs, and other popular techniques such as KNN, SVM, and GP were reviewed, and future challenges were discussed. Some special-purpose algorithms were listed as follows: GAN, SeDANN, SCNN, K-means, PCA, etc. This review presents the evolution, current status, challenges, and prospects of these technologies in terms of material, features, process parameters, applications, advantages, disadvantages, etc., to explain their significance and provide an in-depth understanding of the same.

1. Introduction

Powder bed fusion is an additive manufacturing (AM) technique widely used to create products with complex geometries and various materials, especially those with good mechanical properties [1]. PBF is considered the best and most used AM process due to its ability to fabricate metallic or nonmetallic parts with a resolution as small as ±0.02 mm and manufacture homogeneous alloy parts with high strength free-form fabrication with other advantages. Therefore, it is applicable in different sectors, including the medical, automotive, and aerospace industries, because it allows lightweight construction and freedom of design, with fewer parts manufactured locally [2]. Also, it has advantages such as fast prototyping, timesaving manufacturing custom quality designs, and economic benefits such as cost-effectiveness.

Laser powder bed fusion (LPBF) is an ever-growing type of additive manufacturing (AM) technology. This paper studies the

different types of LPBF methods, namely, the direct laser sintering method (DLSM), selective laser melting (SLM), selective heat sintering (SHS), electron beam melting (EBM), and selective laser sintering (SLS). Each of these AM techniques differs fundamentally in its working principle. PBF processes are either full melting or successive sintering processes. Powder material coalesces into solid by heating and direct liquefaction and solidifying powder by intense melting in PBF methods such as SLM, while successive sintering of material is performed to achieve net components in PBF processes such as DMLS. The heating source can be laser and electron beam for high precision fabricated parts.

Moreover, the paper discusses the various process parameters common to all types of AM technology such as laser power, laser spot size, layer thickness, scan speed, and hatch spacing. Optimizing process parameters leads to the efficient part density at lesser lead time. Raw materials are powders classified into aluminum alloys, tool steels, titanium, stainless steel, refractory, and superalloys. The material properties of the fabricated 3D part desired by the end user, such as density, tensile strength, yield strength, elongation at break, hardness value, and roughness value, determine the type and characteristics of the powder used. The powder can have many characteristic aspects that can be varied or changed, such as the grain size or coarseness, diameter, packing density, morphology, and microstructure properties that affect the quality of the fabricated part. This paper reviews process parameters and powder characteristics to minimize the various defects in the LPBF methodology. Defects are undesirable errors due to melt-pool instability, preheat built temperature, and improper process conditions at the in situ and ex situ levels. Some common defects discussed in this review are spherical defects such as porosity, residual stresses at melt-pool, delamination, and geometric defects due to tolerance and balling. The causes and solutions to each defect under various LPBF methods are comprehensively reviewed. Table 1 informs us about some of the most common defects that can be seen in components manufactured using AM techniques, their causes, and their solutions. Integration of ML with AM processes can help us prevent these defects in the very initial phases and even stop manufacturing a defective component as soon as the defect appears with the help of real-time data tracking and decision-making techniques, which can benefit economically as well as avert wastage. By implementing ML, we can optimize input and output characteristics or even predict a component's properties for a given set of input parameters. Thus, ML has immense application in improving AM processes' speed, accuracy, and efficiency and can influence quality outcomes [8].

The current scenario of additive manufacturing has wide applications in aerospace, automotive, prototyping, and medical among many other industries in the 4.0 era [9]. However, it also has limitations in various scenarios such as high residual stress, reproducibility, low porosity, etc. Different types of PBF processes such as DMLS (direct metal laser sintering), EBM (electron beam melting), SHS (selective heat sintering), SLM (selective laser melting), and SLS (selective laser sintering) [10] were studied along with their applications to gain in-depth knowledge of these concepts. Due to the PBF process being step-by-step and working layer-by-layer, there are many conditions and parameters to be kept track of for ideal processing. Since numerous attributes determine the outcome, keeping them manually becomes practically impossible, especially if it has to be done in real time during the procedure. That is where machine learning is employed in this field for smooth, fast, effortless processing.

Today, the use of ML can be seen in many different areas of the AM process [11]. It can help optimize input parameters and output characteristics to get optimal results much faster. Combined with multispectral data used for learning and predicting product quality, it can enhance the printers' efficiency and productivity. It can also enhance build-time estimations, speed up design iterations, optimize cost and weight performance, and enhance our capability to influence part performance by examining the powder and its characteristics. With the introduction of machine learning (ML) such as supervised learning, unsupervised learning, and reinforcement learning algorithms, methods, and techniques depicted in Figure 1 were used to implement tasks such as defect detection, in situ monitoring, real-time process monitoring, quality monitoring, porosity analysis, optimizing process and parameters, parameter selection, prediction of inherent strain, fatigue life, part distortions, and anomalies and parameters like laser power [12–14].

ML can also aid with defects speeding up defect identification and deciding the usability of the component produced via AM. However, one main limitation is that there is a serious lack of technology or application of ML for real-time tracking of the AM process that can simultaneously follow both input parameters and output characteristics observed in every printed layer. This kind of real-time tracking can help keep an eye on the component being manufactured and parallelly keep an eye on the defect formation or development of material properties. Furthermore, with such application, the AM process can be immediately stopped when an undesirable defect such as huge porosity, stress accumulation, or excessive coarsening of grain is formed after a layer of molten powder has coalesced, etc. Stopping the AM process from completing in such cases will help us avoid using more material uselessly when we know the end product will get rejected anyway. It can also save time that will, otherwise, be wasted. All these applications can significantly improve AM process efficiency, productivity, and quality. This real-time tracking can also help maintain stricter and more accurate geometry. In PBF processes, the powders' fluidity, spreading, or flow pattern can significantly influence the defect formation, geometric tolerance, and material characteristics. However, current ML technology for AM applications cannot predict, track, or manipulate such parameters in real time. Scientists are building ML algorithms that can handle huge amounts of data about various input and output parameters, observed and recorded in real time, and simultaneously control these parameters dynamically in real time to achieve required results. These algorithms will be able to do this by being able to predict the powders' flow or spreading. This

Table 1: Applications and advantages of different powders.

Problems	Causes	Solutions	Ref.
Residual stress	The rapid heating and cooling rate resulted in a high-temperature gradient	Postprocess techniques include short peening, heat treatment, age hardening, grinding, and polishing; in-process methods such as controlling scan strategy, feedback control, and mechanical control	[3]
Balling phenomenon	Inadequate input energy results in roughened balls and capillary instability due to the Plateau-Raleigh effect	Lowering the scan speed, increasing laser power, and reducing layer thickness	[4]
Porosity	Gas entrapment in the hollow powders that do not precipitate on solidification. The direct relationship between energy density and cooling time	Scan strategy where the output is scanned twice by the laser at different laser powers; powder flowability and packing density must be optimized	[5]
Delamination	High residual stress-to-yield strength ratio	The temperature gradient at the solid laser freedom must be low	[6]
Geometrical deviations	Alterations in data preprocessing, machine errors, stochastic errors, and deviations in material processing	The compensation cycle algorithm studied by Hartmann et al. concluded to reduce the shrinkage effect	[7]

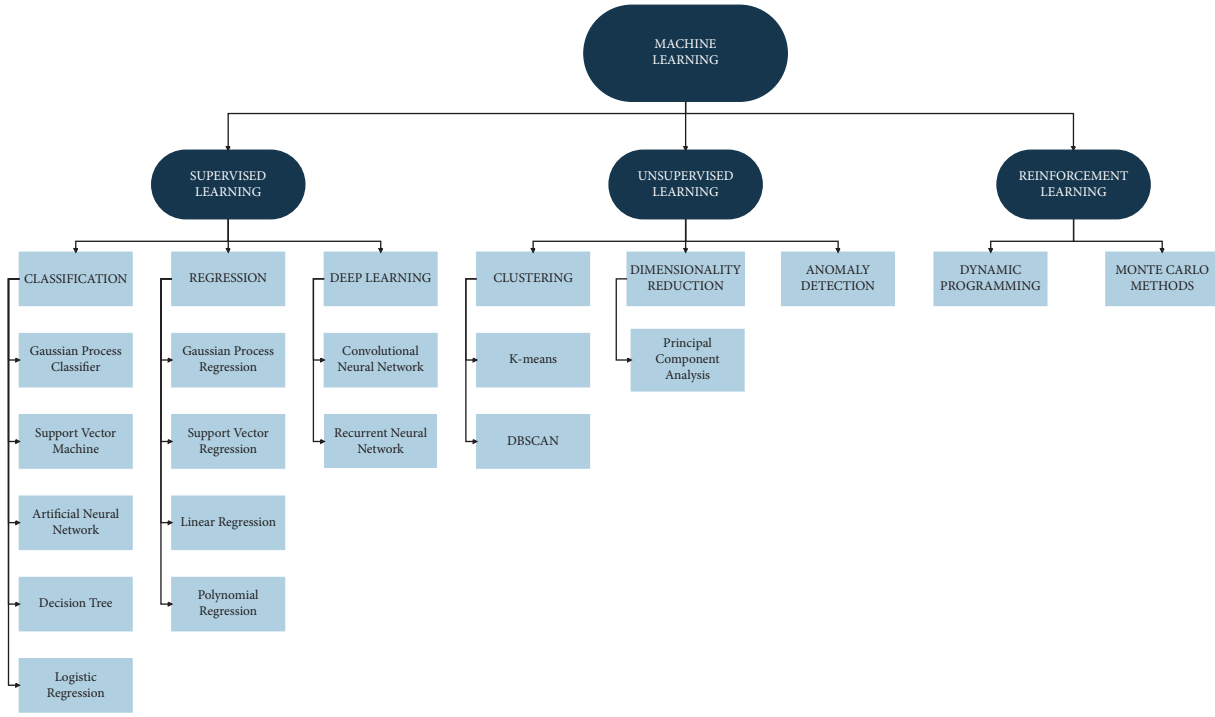

Figure 1: Machine learning algorithms are involved in various additive manufacturing processes, including powder bed fusion.

development could also mean faster qualification times and more flexibility for the AM machine user to buy feedstock materials.

Along with the wide applications, machine learning is a recent and developing field. It paves the way for numerous other applications and enhancements concerning the PBF process that are yet to be discovered. For example, architectures/algorithms could be improved upon with ongoing developments and transfer learning. New parameters could also be looked upon, and the accuracy of parameter readings could be improved with the advent of newer technology, such as sensors.

2. Powder Bed Fusion and 3D Printing Technologies

Powder bed fusion is an additive manufacturing technique that enables it to create complex geometries that could not be made/achieved by any other means. Laser powder bed fusion's metal components/parts can incorporate complex designs and achieve the required mechanical properties. Most of the time, reprinting and discarding these parts is observed to eliminate defects. The methods are optimized so that no time and money are wasted in reprinting and discarding these parts. Prototypes and simulations help in achieving the goal.

The PBF process, from the initial stages of data interpretation to the product capability steps, is diagrammatically shown (Figure 2). Data interpretation includes 3D models of all the various formats and defects. The next PBF process proceeds with its process parameters and material requirement. Each and everything is reviewed and then it moves to the next step where product capability is tested, such as its strength, dimension accuracy, and even roughness [4, 15].

Powder bed fusion is an actively used technique in the current day-to-day industry used in producing original and conventional components' sensing, which is available by machine. Manufacturers imply detection of factors like thermal emissions from melt pool; less-known detection is of the emission system for the excited gases which are present as a result of emission of highly excited evaporations can finally conclude that the sensing systems rely on plume monitoring for powder bed fusion [16–19].

Powder bed fusion techniques give out the best results based on factors such as reproductivity and dimensional accuracy in the aspect of part production, and the PBF process uses to fabricate components is a step-by-step procedure repeated layer-by-layer to fabricate a whole component [20–23]. Using a material, various conclusions were drawn out lack of fusion porosity was due to the overlap of the melt pool, where PBF techniques can be used to improve geometric designs, and more complex models of the melt pools dimensionally can be used to predict accuracy [2, 24–27]. As well increased deposition efficiency, characterization, and quantification may result in a more excellent window to identify defects. Powder bed fusion uses methods such as in the process to increase user confidence and encourage further adoption in high-value manufacturing sectors' systems to assess system accuracy and precision [2, 28–31]. The high-value sectors such as biomedical and automobiles have complex geometrical components and different design capabilities and are much more accurate and preferred as the process is layer-by-layer building to achieve such high design complexities [32–37].

One of the forms of AM is powder bed fusion, which has been in the limelight for a few years now because of its unique capabilities of producing 3-D geometries, complex structures,

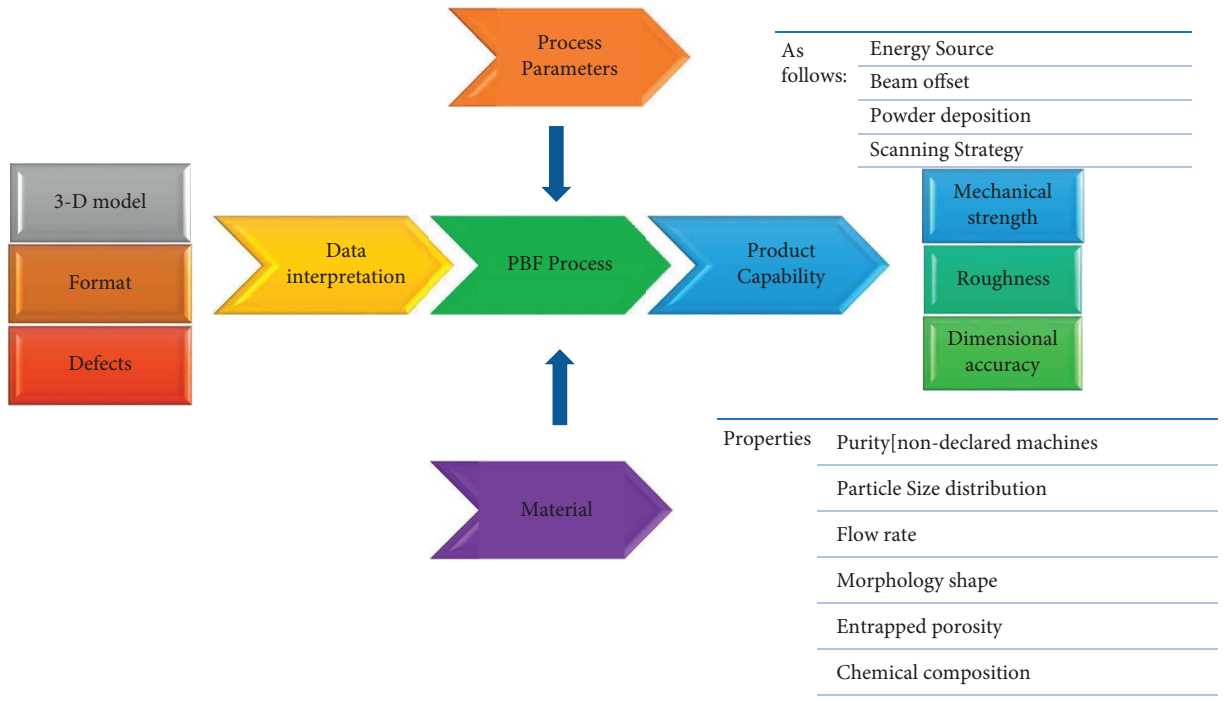

Figure 2: PBF processes.

and quality as required, so high-value industries have a keen interest in this process. The layer-by-layer deposition has many advantages as milling, turning, and postprocessing are less involved [38–43].

Powder bed fusion (PBF) is the earliest additive manufacturing process. It is one of the most popular powder-based sintering used for prototyping and in the end-use application in many industries that compete with injection molding and any other polymer manufacturing process [44–46]. These are generally used for low-medium complex parts manufacturing. The laser and electron methods are one of the fastest-growing methods in the industries of methods in DED. They are mostly used for aerospace and biomedical applications due to their properties to make any complex part and excellent material properties. This is a layer-by-layer method, improved build quality, and comparative reduction in cost. The future of this method is quite bright in various fields such as Aerospace Component Manufacturing For Complicated Components and Medical and Industrial Applications [47–49]. One study highlighted this by investigating the dental implants manufactured by the PBF method compared to other conventional methods. The study particularly examined the geometric and dimensional accuracy of the manufactured parts. An approximate increase of around 20% was seen in the PBF samples [50].

3. Types of PBF Processes

Figure 3 explains the various types of processes based on their energy sources. Selective heat sintering comes under thermally fused, selective laser sintering comes under laser fused, and electron beam melting comes under electron beam fused.

3.1. Direct Metal Laser Sintering. Direct Metal Laser Sintering (DMLS) is an additive manufacturing methodology in which metal powder such as Inconel 625, cobalt chrome, and stainless steel is used to generate a solid three-dimensional model by sintering [1]. The process of joining two entities into one compound by heating and fusing, without melting, is called sintering. The recent advancements in the field of DLMS have found it to be a superior additive manufacturing technology over SLS in reduction of part porosity, manufacturing reliability, postprocessing, and processing time. The DMLS working process consists of the following parts: laser unit, which uses a CO_2 laser, scan head, fiber that connects the laser unit and the scan head, the building platform for layer-by-layer deposition of metal powder, dispenser platform, recoated blade, and collector platform. Metal powder in the dispenser is released one layer at a time from the dispenser platform to the building platform. The relative heights are placed so that the dispenser platform is above the building platform to enable the recoater blade to move without any obstruction. The recoater arm sweeps the powder from left to right motion, and the excess powder is deposited at the collector platform. An inert gas such as argon or neon controls the atmosphere in the chamber construction [2, 9].

In contrast to SLM, the DLMS processes the fabricated parts are generated at 95% density. Thus, it cancels the required successive sintering of the produced parts [2]. In the DMLS process, each layer of powder does not undergo melting and solidification with successive layers, but each layer is heated to a point below the recrystallization temperature, allowing each to fuse with the next one without achieving the melting of the substrate. This is completely different from AM techniques such as SLM as it involves

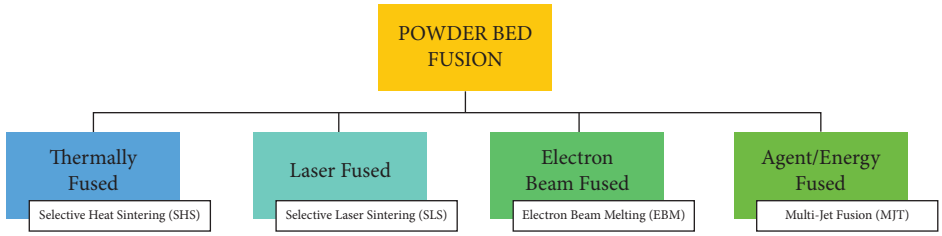

Figure 3: Powder bed fusion types based on energy sources.

melting, welding, and solidifying each successive layer. In such a process, the temperature will cross the recrystallization temperature and reach well up to the melting point. In DMLS, the metal powder deployed does not contain fluxing agent or binder and is sintered using a high-power CO_2 laser at 20 to 40 μm layers. The energy absorbed by the metal powder material is measured as absorbance. It is a ratio between the energy flux absorbed by powder matter to the energy flux irradiated by the laser source.

Absorbance can be increased by multiple laser beam reflections, implying a higher optical penetration depth. Apart from absorbance, another important physical phenomenon is the balling effect. Riza et al. found that using a low-power laser resulted in undercooling of the sintered powder, thus forming coarsened balls. Moreover, the balling effect was observed at higher scan speeds along with large-diameter powder balls (~10 μm) [10]. This unwanted phenomenon could be avoided by increasing the volumetric density of energy at the input. The main parameters in DSLM include laser scan speed, hatch spacing, layer thickness, and laser power. The relationship between energy density with the four parameters is given by

$$\mathbf{E} = \frac{\mathbf{P}}{\mathbf{Vhd}}, \quad (1)$$

where E => energy density (J/mm$\hat{3}$), P => laser power (W), V => laser scan speed (mm/s), h = >hatch distance (mm), d => layer thickness of the powder bed (mm).

The surface roughness depended on the four parameters' laser power and scan speed. Higher laser power and lower scan speed meant more surface roughness. However, it does not depend on the energy density [17].

Upon studying the factors that affect overhanging structures Yap et al., found that higher hatch distance values intensify distortion and accelerate the separation of the part material. Thus, an optimal hatch distance of 0.5 mm was obtained [12]. It was also concluded that laser scan speed does not significantly affect the heat flux in the powder material but reduces the total laser heating time [12]. The scan speed, however, determines the growth of the microstructure. A higher scan speed indicated the presence of small spheroidal balls, giving rise to the balling phenomena [9]. A lower scan speed indicated interagglomerated sintering necks resulting in surface roughness [15]. The layer thickness is a significant process parameter in final surface quality. Decreasing the layer thickness gives a greater surface quality as the spheroidal balls become fully densified. An optimal range for layer thickness is 0.15–0.25 mm, and flat surfaces were obtained in the preheated tracks [4, 9].

The laser sintering process has four stages. In the first stage, powder atoms from two different surfaces make initial contact. Due to the high surface energy of the particles at contact, necking is formed at a slow growth rate. The particles coalesce, and grain boundary size increases while the surface area decreases. Finally, a full merging of the two particles occurs at an infinite time, and the powder is said to be sintered.

The DLMS process is widely used in implants such as joint reconstructions at the medical forefront. The Ti6Al-4V alloy is used as the powder material as it has good biocompatibility, corrosion resistance, and fatigue resistance. Intricate manufacturing applications in scaffolding find DLMS in demand as it can produce materials with fine porous structures and higher density [10, 16].

However, support structures are required during the sintering process to avoid overhangs. The final fabricated metal part requires postprocessing technologies such as short peening, removal of support structures, and heat treatment [2, 9].

3.2. Electron Beam Melting. Electron beam melting (EBM) is an additive manufacturing methodology often considered rapid prototyping (RP) (Figure 4). EBM uses a high-power electron beam source, unlike the other AM processes, which deploy a laser beam as a heat source for melting and fusing the metal powder. Developed by ARCAM AB, EBM machines have biomedical, automotive, and aerospace applications. A typical EBM machine consists of the following components: a filament made of tungsten, a grid cup for directing the electrons to the anode, anode plates connected to the positive end of the DC voltage supply, focus and deflection coils to adjust the position, and determine the diameter of the beam. The sliced data from the CAD file is differentiated into contours and squares. During the part fabrication, contours are boundaries forming the geometry, which behave as an interface between the metallic powder and part. Squares are the regions formed between the set contours [25]. The build table is placed in an inert vacuum chamber with helium or argon (~10^{-2}-10^{-3} Pa) [29]. The reason is to maintain the integrity of the electron beam, yield high tensile strength, remove any impurities, and maximize the density of the fabricated part. The built platform is initially preheated to a temperature ranging from ~500 to 700°C [27]. Powder materials such as titanium, cobalt chrome, 316 L steel, maraging steel, and Inconel 718 are used as they can conduct electric charge having a particle size ranging between 45 and 100 microns. Electron beam melting

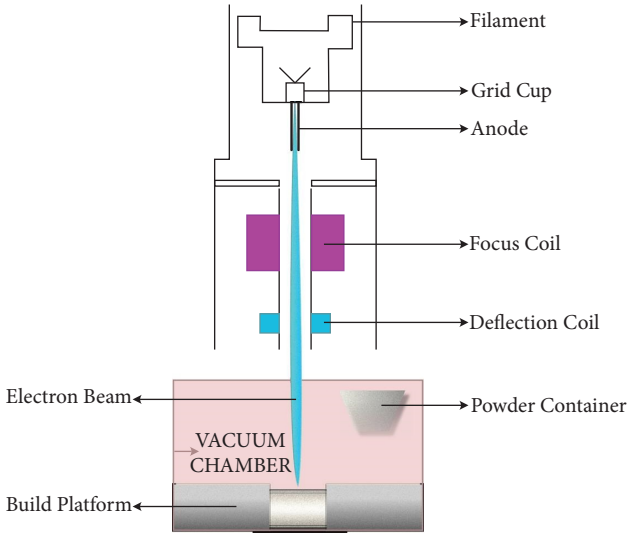

Figure 4: EBM processes.

process parameters are classified into scanning parameters such as scan speed and line offset and beam parameters such as beam current and accelerating voltage. The amount of energy incident by the beam on a powder bed is termed energy density. This occurs due to an elastic or inelastic collision of electrons with the material atoms. The significant interactions between the accelerated electrons with the substrates are scattering, backscattering (energy loss), and transmission (energy penetration) [19]. Silvestri et al. found that the backscattering coefficient was directly dependent on beam intensity.

Moreover, the scattering value depends on the target substrate's depth [19]. Surface roughness increased with the decrease in scan speed and beam current. A linear speed calculated as the ratio between beam intensity and scan speed was found to increase with the temperature rise. Scan speed was a deciding parameter in the thermal diffusion time as melt pool temperature was higher at a shorter duration of scan speed. This implies that surface roughness decreases with an increase in temperature. Line offset, the distance between hatch lines was observed to influence material hardness, i.e., with a decrease in a line offset, energy density was higher, leading to rougher microstructures [20]. While studying the surface roughness of inclined parts, Dolimont et al. found that the underside had a lower value for surface roughness than the upper side [18]. Ding et al. studied the correlation between process parameters and melt pool geometry for a single bead experiment at various preheating temperatures, beam powers, and scan speeds. It was deduced that as the line energy (beam power and scan speed) increased, the width and depth of the melt pool strictly increased in accordance with Rosenthal's model for welding [28].

The advantages of EBM type additive manufacturing are mainly the following: reduction in lead time, residual stress reduced due to high process temperature, and the inert gas providing an oxidation-reduction environment. Large-scale industrial production of light switches was developed by an Italian company, BTicino, where EBM technology was used by injection molding [2]. Conformal cooling channels in cobalt chromium alloys with anti-corrosion and high abrasive resistance were deployed to conduct uniform cooling of the molded part [23, 24]. The fabricated tool displayed 43 HRC Rockwell hardness, yielding 600 MPa, and tensile strength of 900 MPa. The total lead time was effectively one week.

3.3. Selective Laser Melting. Selective laser melting is a type of additive manufacturing process in which a powder bed is melted and layers fused at a high-power laser beam. The setup for the SLM process is similar to DLSM, the difference being the sintering of powder (coalesces without being converted into liquid) instead of melting. The part fabrication begins with slicing CAD file data into layers, and layer thickness ranges from 20 to 100 μm. Each slice is selectively fused using support structures if needed. The final three-dimensional part has up to 99.98% part density as the laser spot size ranges from 20 to 30 μm, creating a melt pool smaller than the EBM process. However, this increases the depth and surface tension of particles around the melt pool, giving rise to more defects in SLM than in EBM. Therefore, a skin-core strategy is used here [30]. The part to be fabricated is classified into an inner core and an outer core forming the skin. The process parameters and focus diameters are distinct in these separate areas. The inner core is manufactured with a beam diameter of 1000 μm and higher laser power (1000 W), subsequently obtaining a higher value of process-relatedbuild-up rate. However, the outer skin is fabricated using a smaller laser beam diameter of 200 μm, focusing on the precision and surface finish of the part.

One of the key undesirable effects of SLM production is residual stress. The direct cause of residual stresses is the varying fluctuations in thermal energy resulting in the crack formation of the fabricated part. Mugwagwa et al., found that upon heat treatment of SLM parts at a range between 600 and 700°C for one hour, the residual stress was reduced by 70% [37]. A recent study by Yasa et al. addresses a newfound scanning strategy termed "sectorial scanning," significantly reducing residual stresses. This method consolidates the various layers into square grids, and adjacent grids are scanned perpendicular to each other [36]. However, ceramic powders show properties of high melting point and low thermal conductivity, resulting in a significantly high thermal gradient during the process. This could be fixed by mixing a eutectic mixture of ammonia and zirconia to reduce the melting temperature to 1860°C [34]. Dross formation is another undesirable formation in low melting metals such as aluminum and tin. In the SLM process, the dross formation was found to reduce in a 30 μm layer thickness compared to 50 μm demonstrating higher strength and lower elongation of the fabricated part [31]. Porosities are spherical defects that occur when gas between powder particles dissolves into the molten pool due to the low packing density of metal powders. Balling effect is an undesirable phenomenon in the SLM process; it occurs when the molten powder does not wet the primary substrate due to surface tension [32]. This increases the surface roughness

and decreases the density of the produced part. Yadroitsev et al. study has concluded that a scan speed of 1 mm/s and laser power of 10 W produced no balling effect as the scan track is widened due to heat conduction, similar to the shrinkage effect [33].

Moreover, in a combination of high scan speed and high laser power, the balling phenomenon does not occur as rapid melt pool solidification occurs behind the laser spot. In a study by Özel et al., increasing the scan velocities tends to decrease the grain sizes in both 67° and 90° rotation strategies. Increasing hatch distance tends to reduce the grain average grain diameters in the case of 90° rotation and is not significant at 67° [35].

SLM materials such as 316 L stainless steel are widely used in the medical industry to develop body implants. Tubular bone, orthodontic products, and mandibular canal segment are a few examples of gradient porosity and stainless steel's strength [32]. Inox 904 L steel produces conformal cooling channels as the wall thickness is about 100 μm. Other applications include microtooling of steel X110CrMoV Al 8-2, and this metal was produced with high hardness and fine structure simultaneously.

3.4. Selective Laser Sintering. Powder bed fusion is an additive manufacturing process. This can spawn products and make them with precision/accurately. This technique of 3d printing enables the manufacture of complex geometrical components with heat sources, like laser/electron beam, which would fuse the particles of the layer above the layer and finally becomes a solid component. This process substantially gives the manufactures the freedom to design through PBF. It uses a laser to sinter the powdered material layer-by-layer to form a solid material. The product is then brushed to remove the extra or loose powder. The material used in this process SLS is polyamides (basically nylons), alumite (a mixture of polyamide blended with gray aluminum), and rubber-like material. Each material has specific properties, like nylons are strong and flexible, making it one of the best materials for manufacturing springs, brackets, and snap. Designers also consider the possibility of cracking and shrinkage. Sometimes CO_2 laser beam is used. In contrast to DMLS, which can only be used to manufacture parts made of metals, the SLS process can also produce parts made of nonmetals such as composites and polymers. This is one of the main differences between DMLS and SLS.

3.5. Selective Heat Sintering. The SHS process uses a heated thermal head for sintering plastic powders, which get fused due to the heated head as it is touched and moves on the STL model slides. Generally, this process is used to manufacture structural parts, mostly prototypes (concept-based). Selective heat sintering (SHS) process plastic powder particles fuse by a heated head. The heated head touches the powder and moves based on the sliced STL model. This method is used to manufacture structural parts and conceptual prototypes, usually made using polymer or plastic materials. Figure 5 shows the schematics of SHS.

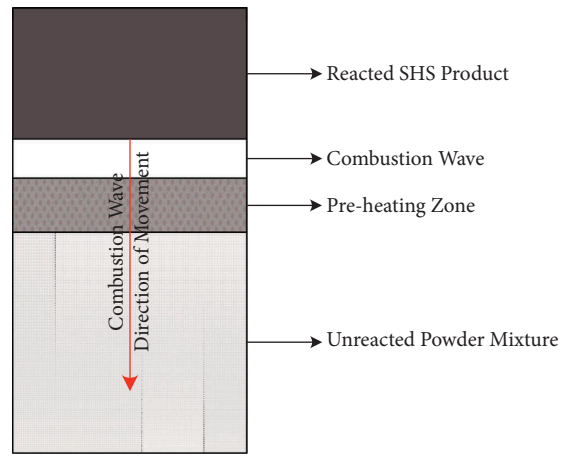

Figure 5: Schematic representation of SHS processes.

4. Application of ML in Powder Bed Fusion

Powder bed fusion is an additive manufacturing methodology used to manufacture three-dimensional metallic objects or parts per requirement, i.e., 3D printing of metallic equipment in short. This procedure is carried out by first dividing the part to be manufactured into layers with the help of computer-aided design (CAD) software that gives a model to be followed while constructing. Then, the manufacturing procedure is carried out layer-by-layer sequentially by the spreading of the metallic constituent powder on top of the previous layer, which is then subjected to a moderate amount of heat, usually with the help of a laser power source resulting in their consolidation to form a solid structured layer. For this layer construction, specific parameters must be considered and monitored throughout to ensure that the procedure is carried out in the desired manner and produces the expected outcome, i.e., a flawless part. The production of a flawless part is an entirely ideal situation and is not practically possible. However, the procedure can be worked upon by continuous monitoring to achieve an almost ideal outcome. The manufacturing procedure consists of several parameters that directly affect the outcome, which must be set and kept at specific value ranges throughout the optimal product. This is where machine learning comes into play.

Machine learning is a developing subsection of Artificial Intelligence currently being used in several application areas. It involves a machine trying to learn, as the name suggests, to perform tasks without any explicit programming relating to that specific task. Initially, the machine is passed some inputs and their known correct outputs with the aim of the machine to come up with a correlation between the two so that when an unknown input is passed onto it, it can come up with the output. This particular feature could be twisted to benefit many scenarios in the industry, one of which is in the PBF process. The process consists of specific parameters that a trained machine learning model can monitor. The model is first passed on some particular example readings that resulted in a successfully manufactured product through which it can establish a cooperative relationship between the

parameters and the outcome for an optimal workflow. After being trained on these examples, the model is employed to monitor these parameters and report or change them if it predicts a failed outcome based on the values of the parameters captured then. This particular feature of in situ observation makes the application of machine learning unique and incredibly helpful, as this can help stop the procedure in between if it leads to the manufacturing of a failed product, thus saving a lot of time and resources [51].

There are numerous application areas of machine learning in the field of PBF. Machine learning consists of various algorithms depending on the desired functionality. Some of the algorithms used in this process are K-nearest-neighbors [52], support vector machines [52–55], K-means clustering [56], principal component analysis [57, 58], polynomial regression [59], and Gaussian process regression [58, 60]. These algorithms cover both the supervised and unsupervised learning domains of machine learning.

Supervised learning involves learning the trend between the input and the output to predict the outcome of custom-supplied input accordingly. Thus, the data given to the model for training consists of the parameter values and the target values, i.e., whether the product was successful or not for that particular set of parameter values. These models then come in handy for in situ observation of the procedure.

Unsupervised learning does not involve anything with the output or target values. It aims to separate or cluster the data according to suitability or similarity. Therefore, the data provided to the model does not consist of target values but only of parameter values. These algorithms come in handy when dealing with high-dimensional data, say if the number of parameters under consideration is huge, as the PBF process consists of numerous parameters that affect the quality of the outcome. In this particular scenario, it is hard for supervised algorithms to operate on this data as the complexity and amount of computation are severely high. Thus, unsupervised algorithms, particularly dimensionality reduction algorithms such as the PCA, convert the high dimensional data supplied into a low dimensional data space by either removal of insignificant parameters or simplifying the correlation between numerous parameters.

The parameters described above are basically process parameters or settings based on which the product quality is decided. Those parameters include laser power, scanning speed, beam diameter, melt pool size, and layer angles. All these various algorithms coupled with these numerous parameters to be considered lead to several possibilities where machine learning may be applied in the process and hence serves useful.

In some cases, the complexity of computations becomes high, resulting in the inability of statistical machine learning algorithms to operate effectively. This paves the way for deep learning. Deep learning is a subsection of machine learning, particularly dealing with neural networks, an artificial mimic of the biological brain consisting of a model of a network of interconnected neurons. These neurons communicate with each other and map complex relations between the input and output space, which simple statistical algorithms might be ineffective.

A wide variety of networks exist in this particular domain as well, some of which are artificial neural networks [53, 54, 61–65], convolutional neural networks [53, 54, 64, 66–69], generative adversarial networks [62], spectral convolutional neural networks [70], and sequential decision analysis neural networks [71]. Again, these specialize in different requirements, as seen in the case of statistical algorithms. Thus, this leads to another area of application of machine learning in this field. Algorithms such as the IT2 fuzzy TOPSIS model, vector evaluation genetic algorithm (VEGA), evolutionary algorithms (EAs), and multiobjective evolutionary algorithms (MOEAs) can help in monitoring pBF input parameters in real-time and dynamically controlling them by varying the input values of the most influential input parameters for the elimination of errors and defects, and development of particular properties without compromising on other properties. This ML algorithm application can help reduce uncertainties, errors, and defects during production [69, 72].

The PBF process has numerous stages, from product design development to manufacturing and postprocessing, where ML implementation can be performed. The various stages include the digital phase, where the geometric and material design of the product is decided, and ML algorithms can be integrated into this process to help us in predicting the design or process parameters we need to consider to get a desirable product; in the stage of file preparation we worry about the LPBF part orientation, position, and arrangement on the build platform, all of which can have significant effects on the processing speed, process stability, and part properties. They can also affect the build cost, time, and quality. To improve machine utilization and decrease cost, it is more efficient to pack as many parts as possible in the building envelope. In addition, support structures may also be needed to fix the part onto the build platform and to support overhanging structures.

Furthermore, they are also needed for heat dissipation to avoid residual stresses. However, it is needed to minimize the volume of necessary support structures as they lead to additional material cost, prolong the build time and require postprocess removal. Alternative build orientations are generated efficiently using a nonsupervised ML method and K-means clustering with Davies-Bouldin criterion cluster measuring. Thus, optimizing parameters involved in file preparation; then comes the manufacturing and monitoring phase, where ML techniques can be used to optimize input parameters for the PBF process, monitor these parameters in real time, and dynamically manipulate their values to avoid the formation of defects or uncertainties; and finally, the postprocessing and quality control phases where ML methods can be implemented to automate and improve the efficiency of quality checking of the products produced and also optimize postprocessing input parameters for getting good quality products [73]. ML algorithms can also be implemented to learn from the monitoring and quality checking phases to train themselves to better optimize input parameters for manufacturing and postprocessing.

Applications of machine learning in powder bed fusion include in situ melt pool monitoring, in situ parameter monitoring, in situ defect detection, dimensionality reduction of data, clustering of data points based on parameter values, optimizing parameter values for an optimal outcome, maintaining uniform print quality in all printers, prediction of product density, and prediction of fatigue life. As can be seen, machine learning has a huge number of applications in each of the mentioned areas, along with great scope for future enhancements.

5. Discussion

Figure 6 shows the summary of all the parameters concerning the LPBF process, both in situ and ex situ, describing all the various parameters in PBF. There are three parameters such as process, signature, and product quality. So, under process parameter space, there are 2 subdivisions, namely, controllable and predefined. Next comes the signature parameter space with three subdivisions such as melt pool, track, and layer. Regarding product quality parameter space, there are three subdivisions such as geometric, physical, and mechanical.

Common process parameters in LPBF methods such as DLSM, EBM, SHS, SLS, and SLM include laser scan speed, hatch spacing, laser power source, layer thickness, bed temperature, and scan strategy. The dimensional tolerances which border secondary stresses in part formation are mainly affected by the scanning angle, overhang ratio, and curvature. The relationship between overhang length (L), build angle (s), and thickness of powder layer (t) is given by: $L = t * \tan(s)$ [42]. As the build angle increases, the overhanging surface smoothness increases. In the working chamber, an inert environment is necessary for powder bed fusion as the fabricated part does not come in contact with reactive gases in the atmosphere such as oxygen, nitrogen, and carbon dioxide to produce contaminants. Renishaw's AM250 is an AM machine that deploys a unique approach to maintaining inert gas. First, present gases and humidity within the chamber are removed by forming a vacuum. Subsequently, the chamber is then charged 600 L of pure argon. The atmosphere levels are set at <1000 ppm (0.1% Oxygen), and it deploys gas feed at rates as low as <30 L/hr [74]. Residual stresses caused by rapid changes in temperature gradient can be decreased by postprocessing techniques such as shot peening, heat treatment, age hardening, grinding, and polishing.

Low laser power causes a low cooling rate and lesser formation of liquid, giving rise to coarsened balls. The high scan speed of the laser beam induced melt splashes, causing an agglomeration of the powdered balls. Therefore, the balling effect can be avoided by lowering the scan speed, increasing laser power and reducing layer thickness. Porosities in part fabrication are of two types such as keyhole and contour. Keyhole porosities happen when gas bubbles are trapped due to improper melting/sintering. Contour porosities occur due to substantial differences between hatch and contour tracks [41]. In LBPF, the temperature gradient is largest in the layer build direction (Z direction) as the cooling occurs more towards the base substrate via conduction and less towards the ambient at the top layer. The production time decreases as the number of lasers increases due to an increase in the build rate per layer.

Increase in the number of lasers increases average powder bed temperature and more area of Heat Affected Zone, which reduces temperature gradient and cooling rate. The peak melt pool temperature value was independent of the scan strategy, and several lasers were used per layer [43]. LPBF in medical field applications seeks material characteristics such as resistance to corrosion, biocompatibility, shear strength, positive elastic modulus, density, and osseointegration. Ti-6AL-4V alloy is, therefore, excellent for surgical and implant applications. Powder morphology, such as particle size distribution, and shape characteristics of individual particles, make for an important parameter in the preprocessing stage. This powder morphology is critical in determining the powder bed's optical penetration depth, thermal conductivity and packing density. Optical penetration leads to the formation of a melt pool. It is defined as the depth at which the radiation intensity inside the material falls to 1/e of the original value. The melt pool's size and cross-section heavily depend on the powder bed's thermal conductivity. A higher densely packed powder bed leads to better ultimate tensile strength [44]. The tensile residual stress developed during the manufacturing process can be minimized by shot peening. It was obtained that anisotropy in the residual stress fields can be controlled by altering the laser pattern of the print, island scan methods, and rotating patterns to reduce anisotropy. Thermal diffusivity and thermal conductivity play a major role in correlation to residual stress. Overall, it was found that such thermal properties played a heavier role than material properties, such as ultimate tensile strength and yield strength in the LPBF process [45].

A 3-D finite element analysis (FEA) is generally deployed to allow the prediction of residual stress and distortion in the multilayer build models. All the common sources of failures in additively manufactured components are the unwanted residual stress and distortion. It is observed that the newly deposited layer generally experiences greater tensile stress while the layers beneath them generally experience compressive stress. The residual stress drives the workpiece's mechanical responses [75].

A Dynamic strategy of adaptive meshing has been developed for the laser powder bed fusion (LPBF) process. This process keeps the fine mesh in the melt pool with the steepest gradient while coarse the rest of its mesh. Updating the mesh at each time frame as the heat source moves, its utility and its accuracy of using dynamic adapting meshing for its simulation (thermal) for the LPBF process is used to predict material properties as well the lack of fusion in it or not [76].

The LPBF process parameters are classified into in situ parameters and significant powder characteristics in Figure 7.

One of the greatest advantages of polymer laser sintering is that it does not require any support structures, which means it has design freedom and fewer post-processing efforts are utilized. The ones where there are overhangs

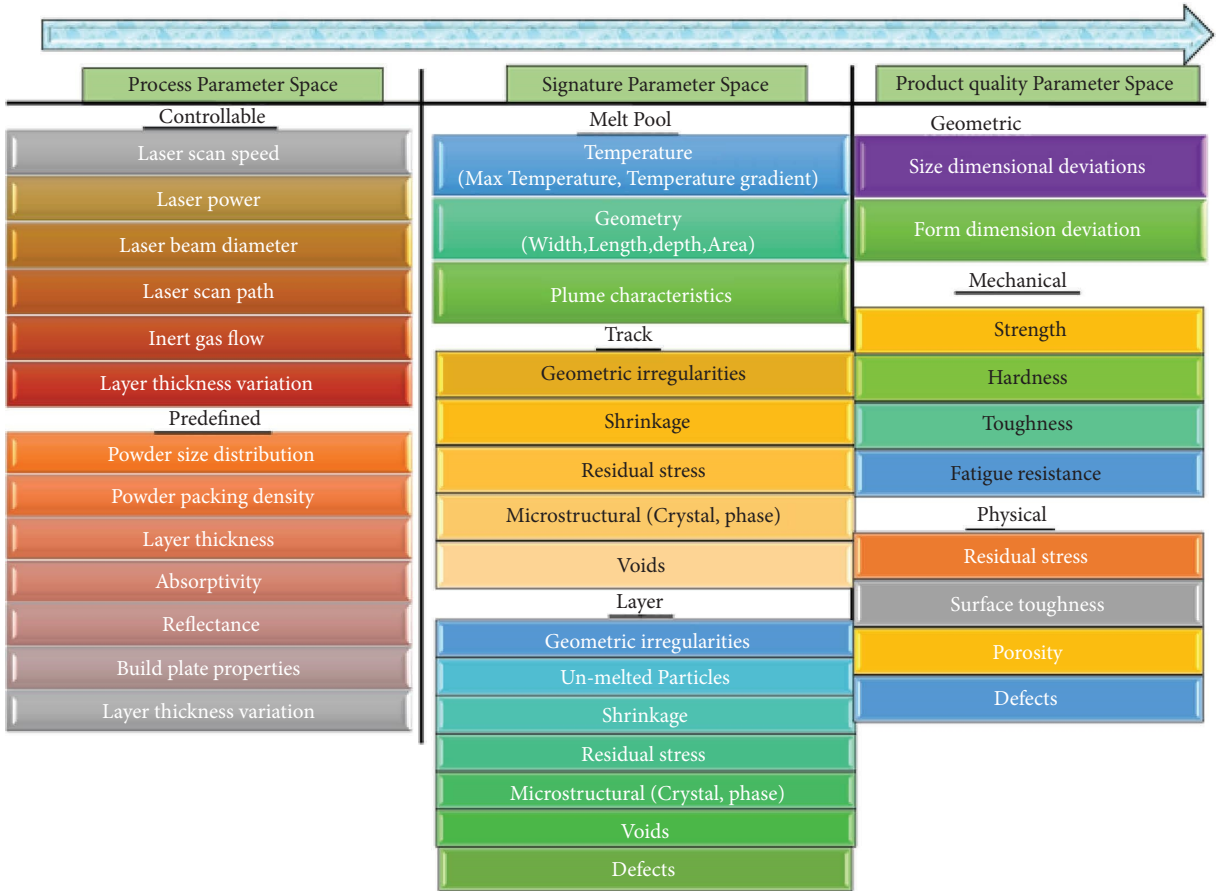

Figure 6: Process parameters of the PBF process.

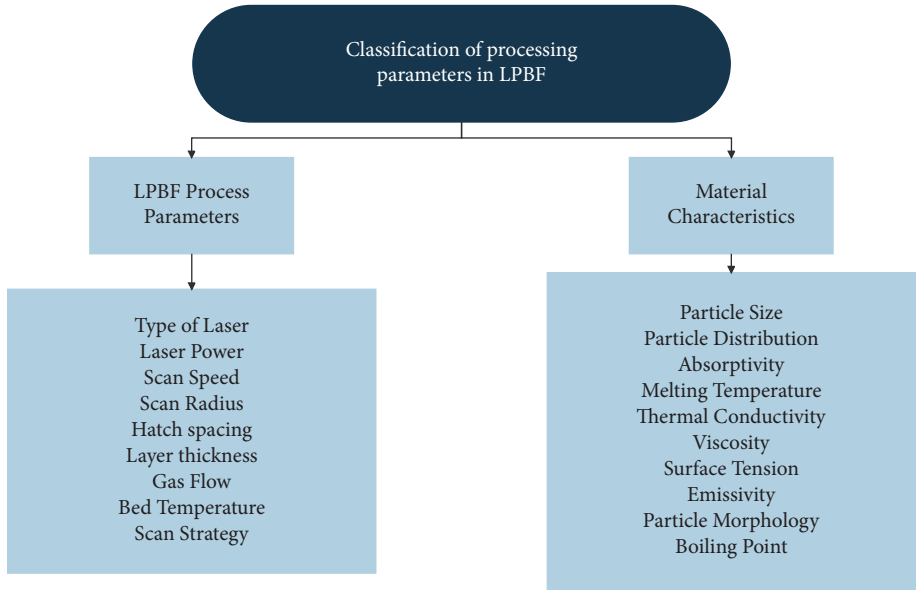

Figure 7: Classification of processing parameters.

used for support must be removed after the completion of the structure or basically when a build is completed/done.

The laser sintering polymer processing can increase the variety of polymers available for usage due to this technique. However, it was suggested that the concentration must not be only on single layer phenomena but also consider building up bigger/whole structures. All the factors, from monitoring to control, all improvised strategies contribute to

the process that can compete with the conventional manufacturing process [77]. Additive manufacturing to produce an improved version of the useful simulations would significantly reduce wasteful behavior so that it could eliminate the failed parts. It ultimately makes AM a useful, economically feasible, and more widely accepted manufacturing technique [48].

5.1. PostProcessing of LPBF. The first step in postprocessing is the removal of support structures [39]. In order to avoid collapsing the fabricated part due to its weight, support structures are needed. To optimize and automate this step, ML algorithms can be applied. Regarding the postprocessing of LPBF processed components, handling defects formed and finishing operations to be performed on the component are the most important factors to worry about. Defects that occur in part fabricated by LPBF can be internal or external. Porosities such as spherical, keyhole, or contour are internal defects that affect the part density, thus varying the mechanical and physical properties when measured in different directions. External defects are caused due to rapid melting and solidification, residual stresses, and balling phenomenon resulting in surface roughness and cracking. Internal pores are treated using a hot isostatic press [41].

Moreover, optimizing input parameters for HIPing such as load, dwell time, and pressure to get the best possible component will the least amounts of defects retained, avoid excessive grain coarsening in the case of using certain materials or retainment or enhancement of mechanical properties, can be achieved by the implementation of ML algorithms designed to predict optimal solutions based on extensive trial and error knowledge already accumulated from literature and industry. Doing so can also eliminate human error associated with the trial and error method and aid in faster and more efficient postprocessing. Although the heat treatment helps improve the mechanical properties of the fabricated part, it does not ensure surface smoothness. Nelaturi et al., worked on a refined grain structure protective coating that can be produced in the tiny regions near the surface using drag finishing, vibratory surface finishing, and finished machining processes. Therefore, the fabricated part's microstructural and mechanical characteristics are improved [40]. ML can again help optimize input parameters such as cutting force, use of cutting fluid, depth of cut, and cutting velocity, to get desired results after finishing. Implementing ML can also reduce the chances of human error and help efficiently automize these finishing operations. ML can also be implemented to study, predict, and validate structural and material properties and even correlate material structures of metallic AM and machining properties [78].

5.2. Applications of LPBF Produced Parts. LPBF finds the most usage of applications in the field of medical, automotive, and aerospace industries. Healthcare systems require parts that are biocompatible along with other characteristics. The production here is low volume. However, it requires rapid prototyping for patients. Parts such as dentures, bone implants, splints, and surgical guides are some examples. Tissue engineering is another good example of the SLS process [46]. LPBF is used in the aerospace industry to produce door clamps for engine front bearing housing. Rolls Royce uses EBM-type AM to produce a titanium front bearing part. Turbine blades, rotor turbines, stators, combustion chambers, fuel nozzles, and air ducts are other components produced using this technique.

Moreover, applications in the field of the automotive industry find use in producing wireless sensors which connect vehicles. Other examples include gear shift knobs, pneumatic and hydraulic systems, prototypes of the headlamp, fuel tanks, gearbox pump impeller, wheel rims, and turbine blades [47]. LPBF is also used as a biomanufacturing technique in the field of tissue engineering, which has enabled the quick fabrication of three-dimensional personalized scaffolds designed to promote tissue regeneration and organs [79]. This is one place where deep learning and ML concepts can help refine and develop better scaffold models that promote enhanced vascularization and better osseointegration. The use of ML can also enable one to predict the appropriate structure and develop various scaffolds with different gradients, mixing different materials in the same scaffold, its properties, and the prediction and correction of their complex architectures [80, 81]. Some commonly used powder materials seen across our review and the properties exhibited by samples made from them with the help of PBF have been listed in Table 2.

5.3. Machine Learning Implementations and Outcomes. Supervised and unsupervised learning algorithms are used in the powder bed fusion process. Supervised algorithms mainly used in this procedure include linear and logistic regression, support vector machines, Gaussian process regression, and k-nearest neighbors. Linear polynomial regression deals with determining the relationship between an independent and a dependent variable, respectively, or parameters in the case of this process. Using polynomial regression with two models having an average relative error magnitude (AREM) of 23% and 17%, respectively, and the latter being implemented, melt pool variation saw a reduction by a massive 78% by updating the laser power as per the observations of the model [91]. Gaussian process regression has a similar intuition apart from the fact that instead of finding a polynomial relation, it defines a Gaussian distribution that suits the data points. It is used in [57] to determine the relationship between the relative density of the produced part and the laser power and scan speed, giving a prediction error of only 0.3%. It is also used in [74] to assist in the design process of powder bed fusion by giving an idea of the remelted depth of single tracks, which signifies whether the energy used for sintering the powder layers is sufficient or not. K-nearest neighbors (KNN) is another supervised algorithm used both in the case of regression and classification. In [52], KNN is used for regression in which the mean of target values of k-nearest neighbors is taken in the feature space of all parameters, i.e., location, morphology, and size of the defect being the

Table 2: Different powders and their properties.

Powder type	Layer thickness (mm)	Density (g/cm^3)	Tensile strength (MPa)	Yield strength (MPa)	E-modulus (GPa)	Elongation at break (%)	Roughness, Ra (μm)	Roughness, Rz (μm)	Hardness (HV)	Ref
AlSi10Mg	0.03–0.1	>2.59	>250	>180	70	>1.0	<20	<80	>80	[82]
Ti-6Al-4V	0.03–0.6	>4.36	>900	>830	110	>10	<20	<80	>310	[83]
IN718	0.03–0.1	>8.07	>940	>750	220	>8	<15	<60	>300	[84]
SS316L	0.03–0.1	—	—	—	—	—	—	—	—	[85]
H13	0.05–0.1	>7.80	>1200	>370	210	>9.0	—	—	—	[86]
IN625		>8.44	>990	>670	170	>35.0	—	—	>30	[87]
ABS-M30	0.18–0.25	1.04	36	—	—	4	—	—	—	[88]
PA 12 (SLS)	0.12	0.95	48	—	—	20	—	—	—	[89]
Polypropylene (PP)	0.12	0.84	32	—	—	529		—	—	[90]

parameters and fatigue life being the target value with a mean squared error value of 1.2736×10^{-3} and R-squared value of 0.96761.

Support vector machine is yet another supervised algorithm that can be used for classification and regression, where it constructs a hyperplane or boundary that contains the maximum average margin value from the associated data points in the feature space [52]. We used an SVM along with a KNN for fatigue life prediction as a function of morphology, location, and defect size with a mean squared error value of 7.0665×10^{-5} and an R-squared value of 0.99418. It is also used in [59] for product density prediction from raw optical signals and can do so with an accuracy of about 93% [55]. We used an SVM to determine whether an abnormality in the produced part is a flaw or a nominal build condition, giving accuracy as high as 85%. As mentioned in [54], SVMs are also used in in situ monitoring of the procedure and reduce defects in the produced part during the process. Unsupervised algorithms include K-means clustering and principal component analysis (PCA), mainly used in the PBF process. K-means clustering involves dividing the data points into "K" clusters, with each point belonging to the cluster with the nearest mean of the cluster to the point itself. In [56], the researchers use K-means clustering for zoning process histories based on thermal data. Principal component analysis is a dimensionality reduction method used to reduce the data's complexity by mapping high feature space data into lower feature space without any significant data loss. The authors of [57, 58] use PCA to reduce the data dimensions for ease of further computation.

Deep learning is another branch of machine learning and artificial intelligence dealing with neural networks that are some of the most advanced algorithms. Neural networks mimic the human nervous system consisting of nodes in place of neurons and the whole network of nodes instead of the nervous system. This interconnection of numerous nodes consisting of innumerable connections in layers helps map complex relations between parameters that statistical machine learning algorithms might fail to perform upon. The neural networks used in the PBF process include artificial neural networks, convolutional neural networks, spectral convolutional neural networks, generative adversarial networks, and sequential decision analysis neural networks (SeDANN).

Artificial neural networks (ANNs) are the simplest neural networks consisting of layers of nodes interconnected to the preceding and the following layer, respectively, along with an input and an output layer and activation functions to remove linearity [61]. We used ANNs to control and manage the quality of produced parts by identifying the mapping between input process parameters and product quality. Inherent strain prediction is carried out as a function of hatch layer, i.e., angles between different layers of the produced part that gives an idea of product distortions in [63] with the help of an ANN consisting of a single hidden layer and a mean prediction error of 2.78% [64]. We used an ANN consisting of an input layer of 3600 nodes, 9 hidden layers, and an output layer consisting of a single node for prediction of laser power value based on an in situ image of the process, giving an accuracy of about 99%. An ANN with two input nodes, two hidden layers, and four output nodes is used in [65] to map the relation between spreader speeds and layer properties, giving an accuracy of around 96%. Also, as mentioned in [54], ANNs are used for process parameter optimization, in situ observation, control of part geometry, tailoring microstructure and properties, and reducing defects.

Convolutional neural networks (CNNs) is a type of neural network specializing in image-based processing, using the convolution operation between layers. The roughness of produced part from the hyperspectral image is carried out in [66] using a CNN consisting of four convolutional layers, including maxpool layers, a flatten layer, and two dense layers, along with the application of a dropout value of 0.4 to reduce overfitting which yields a final mean absolute error of 2.1 μm [53]. We used CNNs for density prediction from raw optical signals with the architectures of VGG-16 and Alex Net using transfer learning, thus obtaining a training accuracy of 94.88%, validation accuracy of 88.54%, and testing accuracy of 81.24%. The research in [64] also uses CNNs for melt pool monitoring to predict laser power values. In the CNN, three filter sizes (3×3, 5×5, 7×7) and three channel sizes are considered, making the comparison span up to 9 CNNs. In all the CNNs, 4 convolutional layers are used with a stride of 1 and no zero

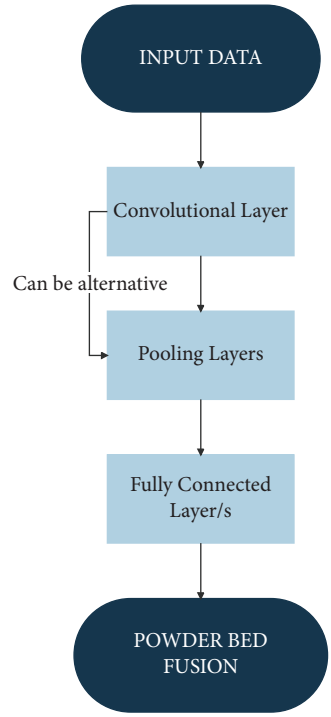

Figure 8: Example of a CNN architecture [68].

padding. Maxpool layers follow the first three layers with a stride of 2 and the application of zero padding. The last layer's output shape is adjusted to 1×1 by changing the filter input size. The 3×3 CNN gave lower RMSE values on increasing the channel size. All $R\hat{2}$ values of the 9 CNNs were closer to 1, but the value of the 3×3 CNNs was comparatively closer than others. The 7×7 CNN obtained the best RMSE value with a channel size of $k = 3$. Similarly, [67] uses CNNs for in situ monitoring by taking in situ images as input and predicting the build quality of the produced part with an architecture having four structures consisting of a convolutional layer, rectified linear unit activation, a layer for batch normalization, and an average pooling layer, along with a fully-connected layer, regression layer, input, and output layer. Again, [68] we used CNN for in situ monitoring and thus default detection yielding a mean accuracy of 97.87%. Figure 8 shows a flowchart that depicts a typical example of a CNN architecture, consisting of convolutional and pooling layers in possibly an alternative manner of order, connected in a network for classification with one or more fully-connected layers at the end.

A generative adversarial network (GAN) is a special type of neural network that, if trained adequately, can generate custom images on the required theme. They are used in [62] for generating artificial images of produced parts to train the CNN.

In [71], a sequential decision analysis neural network (SeDANN) is used for monitoring the process to establish reliable part production and reduce quality assessments after obtaining the produced part. It consists of three echelons/levels traversed sequentially by the data for processing. Each echelon plays a role in the processing by giving some significant detail used by the subsequent echelons as input. A SeDANN approach uses elementary statistical attributes that are obtained based on the physical reasoning of the process mechanism, which also facilitates understanding. The first echelon, an ANN, is tasked with predicting laser velocity and power as a function of four variables of the pyrometer signals such as mean, standard deviation, skewness, and kurtosis of the signature of the pyrometer. The second echelon, an ANN, uses these predicted values of power and velocity alongside melt pool image features obtained from rapid video camera images as input and predicts the single-track width.

Additionally, the single-track width standard deviation is obtained by approximating the mean width over three sections of the single-track. The third echelon predicts the percentage continuity as a function of melt pool characteristics and the statistical features predicted in the second echelon. It performed better than all its counterparts, i.e., CNN, LSTM RNNs, SVMs, and KNN, with an average R-squared value of 0.836.

Work in [70] uses a spectral convolutional neural network which is an extension of the convolutional neural networks (CNNs) but can process data of a more complex configuration achieved using irregular convolutions. A

Table 3: Additive manufacturing techniques and ML algorithms used, their performance accuracy, and datasets (if available).

Accuracy	ML algorithm used	Additive manufacturing process used	Datasets	Ref
High	SVR, KNN	LPBF	Scanning electron microscopy (SEM) was used for generating 2D defect features. 3D defect features were generated via statistical analysis with the help of high-resolutionX-ray microcomputed tomography; fatigue life data was obtained via high-cycle fatigue tests; using both these features, the dataset was constructed	[92]
High	SVM, SVR, KNN	LPBF or SLM	The data set is established by combining the samples of fatigue life and defect geometry; the dataset is later divided into training and testing data sets	[52]
Not mentioned	CNN	LPBF	From [85], values were acquired in order to decide the laser process parameters, and three-parameter combinations of laser power and scan speed were selected which, includes one having excess energy input (50 W; 40 mm/s) and one with good reproducibility and dense parts (50 W; 75 mm/s), and one with very little energy input (20 W; 75 mm/s) as well as 2 samples were built for these parameter sets for which R_z and the number of frames were later determined	[66]
Not mentioned	SVR	LPBF	Computation of the local thermal histories and the analytical model based on the discrete source approach along with the assumptions and validation studies were utilized from [86], and overall energy input efficiency (η) and the depth-to-width ratio of the volumetric energy source (σ_z/σ_x) were the 2 key parameters for the analytical thermal model which were also described in detail in [86]; moreover, to predict the calibration values in the "full" model, the experimental data that was used in concert with the functions $\int_1 = \eta(P, v, w, d)$ and $\int_2 = \sigma_z/\sigma_x(P, v, w, d)$ was selected from [86]; the reported width and depth for the "direct" model were also from [86]	[57]
Defect recognition accuracy of 94.18%, 94.32% and 95% from SVM, MLP, and CNN respectively	SVM, MLP, CNN	LPBF	The dataset is extracted from optical data generated involving raw signals; the steps involved are selecting and extracting statistical features, labeling the data, normalization, and then splitting the data into sets	[91]
High accuracy beyond 99% for laser power prediction with FFNN performing better than CNN	FFNN, CNN	LPBF	The melt-pool images used in the dataset were obtained by a metal additive manufacturing equipment monitoring system	[63]
Defect detection validation accuracy of 97.87%	CNN	LPBF	Thermographic off-axis imaging was used to obtain images to form the dataset	[93]

Table 3: Continued.

Accuracy	ML algorithm used	Additive manufacturing process used	Datasets	Ref
Spreading prediction accuracy above 96%	Backpropagation neural network	LPBF	Polydispersed digital elevation model simulations are used to obtain data attribute values devoid of noise in contrast to data obtained by physical sensors	[94]
96.80% (mean balanced accuracy) 98.80% (top balanced accuracy) (good)	Deep learning-based neural network (CNN)	LPBF	4,314 RGB color images	[68]
Classification accuracy (83–89%)	SCNN (spectral convolutional neural networks)	SLM	The energy was calculated with the help of the work from [87] Experiment mechanism details are from [88] WPT (details are described in [90]) was used to extract the frequency bands. Feature extraction analysis details where daubechies wavelet was resulted to be the best choice are from [89] All details of the methods: details of the experiment determining the number of layers of SCNN used for classification are from [96] and SCNN through FFT are from [97]	[95]

Table 4: Advantages and disadvantages of the above-stated papers in Table 3.

Advantages	Disadvantages	Ref
(i) In addition to model development and optimization, the statistical analysis helped develop up-to-date mathematical descriptions of powder bed fusion processes (ii) A combination of two or more methods helps improve the final product quality, for example, FEM (finite element modeling) and ML (machine learning) or statistical analysis with FEM and ML (iii) Additional costs are reduced as all the methods use the same type of inputs (iv) Experimental and predicted fatigue life are compared and concluded to agree in the case of the SVR model, resulting in a highly accurate regression analysis of SLM processed Ti-6Al-4V alloy (v) Using kernel function led to highly efficient regression analysis and non-linear classification. In contrast, the radial basis function was used due to its efficiency and accuracy as compared to models consisting of linear or polynomial kernels (vi) KNN and SVR models are highly accurate as they fall under the 1.5 times dispersion line (vii) However, compared with KNN, SVM was more accurate in predicting the test set and has good generalization ability (viii) Reliable CV was carried out as the result of coefficient of determination corresponds to 0.99 (approx. 1), which is a perfect fit (ix) Snapshot hyperspectral imaging combines both spatial and spectral resolution. Therefore, it comes with the benefits of both worlds (x) At 1070 nm, the direct reflections of laser light could affect the camera; therefore, a short pass filter of 875 nm was used to protect the camera (xi) After the laser exposure in FOV, the saved images are processed to improve data handling (xii) The camera's orientation was done to collect the maximum number of frames from the scan vectors center (xiii) SAX and PCA techniques were used for dimensionality reduction of thermal histories because of various benefits, including statistical, representational, and dimensional (xiv) DBSCAN algorithm was used to cluster reduced thermal histories compared to K-means because it is a nonparametric algorithm, and a 5 N-component feature vector is obtained (xv) Thermal history is considered an appropriate analytical model to obtain process equivalence by finding input energy-efficient strategies. Also, it provides a representation of AM processing of metal that is precise and concise (xvi) The discrete source analytical method was used to process the scan path's geometric features, such as scan raster properties and vector length in its thermal solution	(i) Modeling the sintering process has been difficult as it requires deep information on parameters and properties, especially physical data (ii) Mathematical modeling in combination with FEA (finite element analysis) needs to be improved regarding accuracy and material phase changes in preheating or fabrication of new parts (iii) Statistical analysis and ML need a large amount of data to achieve accuracy (iv) In terms of structural integrity assessment of metals using additive manufacturing, other parameters such as surface roughness, microstructure, and residual stress should be considered as a collaboration with more testing as well as complex geometrical specimens to generate more practical and definite results for the SVR model (v) Correction/calibration is necessary for snapshot hyperspectral imaging (vi) Data requirements are high to validate the findings statistically; due to limited samples, the results observed are considered preliminary (vii) In comparison with other different sensor technologies, it was found that snapshot hyperspectral imaging has lower temporal as well as spatial resolution when compared to high-speed cameras (viii) Also, snapshot hyperspectral imaging has a lower spectral resolution compared to spectrometers (ix) The configuration formed by the 5×5 patterns called mosaics of Fabry-Pérot filters spread on the CMOS sensor chip is prone to noise induced by nonparallel light beams cross talks, dark currents, chromatic aberration, and vignetting effects of the optical setup (x) The training process ends with slight overfitting, as observed during the training (xi) Thermal history does not capture occurrences on subsequent layers like lack of fusion defects due to denudation of powder either because of occlusion of the laser beam by spattering or the convection in the vapor (xii) The discrete source approach also has limitations, like it does not process the dynamics of melt pool, including sloshing, convection, and waves (xiii) In order to represent processing space completely as thermal history, a few important features are neglected, which could drastically influence the microstructure	[92] [52] [66] [57]

Table 4: Continued.

Advantages	Disadvantages	Ref
(xvii) The approach used showed good density prediction performance with 90% accuracy (xviii) The proposed approach is useful in assisting the ML methods to become more accurate and fast (xix) The statistical features-based approach outperformed the deep learning framework in predicting the various density classes (xx) Leave-one-out (LOO) method evaluation showed high inference success rate provided by the proposed CNN	(xiv) It is important to have a sufficiently dense part manufactured to avoid failure during application since porosity/internal pores affect fatigue and mechanical strength as well as causing rupture due to elongation	[91]
(xxi) The proposed model is expected to predict laser power values from melt-pool images to find the difficult position instead of using the AM product tests, which are considered destructive (xxii) The proposed model will be used to check the AM process's reliability, including the accuracy of powder coating, laser irradiation, and laser power values, and to evaluate the defective parts	(xv) The feed-forward neural network showed higher inference accuracy than the proposed network consisting of the 9 CNN's parametric experiment data due to the sensitive reaction of CNN to the variation of the melt-pool images and leading to predicting erroneous laser power(w) values	[63]
(xxiii) CNN provides highly excellent classification results. It was shown by the confusion matrix that all the delamination defects are classified correctly and are very relevant too (xxiv) The model outperformed with 96.80% of mean balanced accuracy and 98.80% of top balanced accuracy	(xvi) CNN cannot detect defects such as pores, unfused powder, balling, and cracks	
(xxv) The proposed model processes the entire image, which is useful in detecting large defect types such as metal splatters. Therefore, considered better for classification as compared to pool monitoring or pixel-wise classification methods (xxvi) The model proposed in this paper is light on computational costs (xxvi) It is a small model, which makes it more specialized and results in highly accurate values (xxvii) It does not require extensive data pre-processing (xxviii) The BP-NN with 96% accuracy was used to provide a spreading process map which, when installed in a 3D printer, helps with layer-wise control over spreading defects. It is also used to regress between extensively nonlinear spread layer properties. The model proposed is small, meaning it is more centered to solve a given task and results in higher accuracy	(xvii) The current model only used one geometrical shape and material for training and evaluation	[93]
(xxix) It requires very less computational costs and resources (xxx) It does not require powerful hardware for training (xxxi) The compilation is fast (xxxii) Also, the temperature difference between delaminated and nondelaminated parts is considered, which is very important for the results. Therefore, heat maps played an important role in the evaluation of the model (xxxiii) The model is not dependent on X-ray imaging and does not require huge data processing	(xviii) The architecture used by the neural network is far too simple and specialized to model the data produced by simulations devoid of noise, thus making it hard for them to generalize to real-time data	[94]

Table 4: Continued.

Advantages	Disadvantages	Ref
(xxxiv) The model proposed is small, meaning it is more centered to solve a given task and results in higher accuracy (xxxv) It requires very less computational costs and resources (xxxvi) It does not require powerful hardware for training (xxxvii) The compilation is fast (xxxviii) Also, the temperature difference between delaminated and nondelaminated parts is considered, which is very important for the results; therefore, heat maps played an important role in the evaluation of the model (xxxix) The model is not dependent on X-ray imaging and does not require huge data processing (xxxx) AE has many benefits, such as high sensitivity, nondestructive, highly efficient, and cost-effective, over other techniques used in AM processing from past decades for crack initiation and propagation or tracking surface defects	(xix) Incorrect identification of splatter cases, twenty-two images were classified wrong in which no splatter was present (xx) CNN only has the potential to detect delamination and splatter defects cases, whereas defects such as balling, cracks, unfused powder, and pores remain undetected in the current experimental setup (xxi) Various materials are required to be tested due to variations in their temperature fields, and different geometrical shapes should be used in the training and evaluation of the model, also, to determine the generalizability of the setup towards various types of defects	[68]
(xxxxi) FBG sensor has both high time resolution and sensitivity (xxxxii) SCNN can process irregular data, which can later be optimized using an extern tool during training, which is not possible using traditional convolutional NN (xxxxiii) It was concluded that signals recorded with FBG and processed using SCNN could be highly potential in real-time and in situ monitoring of the AM process	(xxii) In conditions like strong or high-pitch noise backgrounds and weak signals, AE is not very efficient; to overcome these conditions, optical fibers-based AE sensors are used, which are highly sensitive; with the help of ML, AE patterns were extracted even in the presence of noises	[98]

sparse signal representation with a wavelet spectrogram is passed to the neural network using which it can classify the data based on the parameter values calculated from the spectrogram. The model seemed to give an accuracy between 83% and 89%, with the highest accuracy being in the poor-quality part images. It has been discovered that the most common parameters considered in most papers are laser power and scanning speed because they represent the fundamental characteristics of the power source for melting the metal, which is a laser in this case. This assertion is backed by several papers showing prediction and detection accuracies of (>90%) when used with appropriate algorithms. Table 3 gives a list of the ML techniques implemented in various types of PBF methods. Table 4 states the corresponding advantages and disadvantages of the papers stated in Table 3.

6. Summary and Conclusion

Laser powder bed fusion is an additive manufacturing methodology for fabricating metal components. LPBF processes use a high power-density laser beam to selectively fuse a region of powder material; successive layers of a powder material are stacked to build a three-dimensional part. The fused portion of powder material forms a liquid pool, called the melt pool, which solidifies and cools down rapidly [64, 67, 93, 99–101]. The process parameters include laser scan velocity, spot size, hatch spacing, and power. The most common powder used is Ti-6Al-4V alloy. The microstructure properties include relative density, grain size, orientation, and growth direction. The correlation between microstructure properties and possible concerns over the preprocessed three-dimensional component is studied depending on a set of constant process parameters [55, 68, 70, 94, 102]. Melt-pool instability, keyhole effect, irregular microstructure, and subsurface integrity are some of the named concerns. Various reasons and solutions to the part defects are discussed. The postprocessing of LPBF has three stages—support structure removal, heat treatment, and surface smoothening. Each stage is explained to optimize the cost of production. The applications of the LPBF process exponentially grew in the industry 4.0 era. Its usage in automotive, aerospace, medical, and other minor fields is discussed. Additive manufacturing is preferred over subtractive manufacturing for the following reasons: flexibility in design, cost of geometric complexity, need for assemblage, and better lead time. AM can produce any complex geometry as it is a layer-wise fabrication process. However, subtractive manufacturing requires various tooling and fixtures making it harder to cut into depths [56, 60, 65, 69]. Thus, AM has only a few constraints and more degrees of freedom to achieve design functionality. The geometric complexity is directly proportional to the mold cost. Intricate designs require support structures that add to postprocessing. However, compared to traditional injection molding AM does not have an additional cost as there is an absence of tooling and fixturing. This decreases the operational intensity and lead time. Moreover, AM provides dimensional accuracies up to a hundredth of a millimeter. dimensional tolerance for SLS is ±0.3% (lower limit: ±0.3 mm). AM provides for "single-part assemblies," avoiding the need for integrating different components as in conventional manufacturing.

Further research needs to be done to optimize the process parameters for assessing the manufacturability of LPBF. The defects, including porosities, need further research on correlating them with the existing scan strategies. Process parameters such as laser power and scan speed affect the residual stresses induced in the melt pool, on which the degree of vaporization depends. Moreover, powder morphology and its characteristics play a vital role in microhardness. The formation of overhangs in part fabrication and their dimensional tolerance plays a significant role in postprocessing. One of the factors that affect dimensional tolerance of overhang features is the overhang ratio which is the ratio between self-supported contours and the total value of admissible and inadmissible contours. A direct relationship between borders effect and overhang ratio is found and needs further study to prevent shape deviations of overhangs [98, 103–105]. Melt pool occurs when a laser strikes the powder causing spheroidization and roughness at the track. In order to produce high-quality fabricated parts, melt-pool behavior at various energy parameters (laser power and scanning speed) needs to be studied to reduce the balling effect. The scan strategy rotation is found to determine the size of the powder particle. Desirable powder characteristics, such as high temperature, high tensile strength, and corrosion resistance, must be analyzed at a minimal cost. Applications in tissue engineering are on the rise for SLS type AM. Various biocompatible materials must be researched to obtain medical scaffolds for tissue restoration. Moreover, composite polymeric materials should be investigated for bioactive response to obtain reinforcements such as bioglass, Ag, Cu, and HAp [106–107].

In this era of artificial intelligence, machine learning and deep learning algorithms are used in this PBF process to enhance its quality and reliability. Various algorithms are used, from supervised statistical algorithms such as linear and logistic regression, SVMs, KNNs, and unsupervised algorithms such as K-means clustering to deep learning approaches making use of ANNs, CNNs, GANs, and SeDANNs to carry out tasks such as in situ monitoring of melt-pool signature, process parameters such as laser power and scanning speed, defect detection, quality prediction, and relative density prediction. This monitoring of various factors is carried out in real time, thus reducing the wastage of time and resources to a great extent [108].

Out of these, the most significant algorithm that stands out comparatively regarding metal melting procedures is the ANN. Since it is an artificial mimic of the biological brain, it can capture and process complex relations between parameters effortlessly due to the numerous interconnections between nodes [78, 109–111]. ANNs see applications in several areas in this procedure as described in [54], including process parameter optimization, in situ observation, control of part geometry, tailoring microstructure and properties, and reduced defects. Thus, ANNs are seen to be versatile, thus being helpful in this procedure [112–116]. Most of the

results obtained using this mechanism are also promising, supported by various papers [64, 65] showing the model's accuracy varying in the range of 90's in percentages [109, 117, 118].

However, a few limitations are encountered while applying machine learning in the LPBF process. Statistical analysis and machine learning models, in general, require a huge amount of data conforming to certain standards for effective training and testing, which is hard to gather. Modeling for producing data to train these models is also a complex and difficult procedure due to the huge number of parameters involved. The numerous parameters make it harder for the model to decide on relevant parameters, which might vary based on the material properties [119–126]. The dimensionality reduction models used for reducing the numerous attributes to a few might not generalize well and scrap useful attributes that might turn out relevant on newly encountered data. Even if the data turns out to be sufficient, there is the problem of underfitting and overfitting. A very simple architecture is used in some papers on a smaller biased dataset, thus resulting in a biased model. The other potential problem might be a highly sophisticated architecture specializing in the training data a little too much, thus failing to generalize well with new unseen data. This paves the way for numerous future enhancements that could address these issues, thus improving the model performance significantly than achieved already [127–129].

Abbreviations

SVM:	Support vector machine
ANN:	Artificial neural network
ML:	Machine learning
SVR:	Support vector regression
KNN:	K-nearest neighbor
LPBF:	Laser powder bed fusion
SLM:	Selective laser melting
GridSearchCV:	Grid search with cross-validation
CV:	Cross-validation
MSE:	Mean square error
*R*2:	Coefficient of determination
K:	Number of folds in *K*-fold CV
AM:	Additive manufacturing
CNN:	Convolutional neural network
MAE:	Mean absolute error
FOV:	Field of view
NN:	Neural networks
AE:	Acoustic emission
SCNN:	Spectral convolutional neural network
SAX:	Symbolic aggregate approximation
PCA:	Principal component analysis
FFNN:	Feed forward neural network
FBG:	Fiber Bragg grating
MLP:	Multilayer perceptron.

Data Availability

All data used to support the findings of the study are included within the article.

Conflicts of Interest

The authors declare that they have no conflicts of interest.

References

[1] T. H. Chio, G. L. Huang, and S. G. Zhou, "Application of direct metal laser sintering to waveguide-based passive microwave components, antennas, and antenna arrays," *Proceedings of the IEEE*, vol. 105, no. 4, pp. 632–644, 2017.

[2] S. Rahmati, "10.12–direct rapid tooling," *Comprehensive materials processing*, vol. 10, pp. 303–344, 2014.

[3] C. Li, Z. Y. Liu, X. Y. Fang, and Y. B. Guo, "Residual stress in metal additive manufacturing," *Procedia CIRP*, vol. 71, pp. 348–353, 2018.

[4] D. Gu and Y. Shen, "Balling phenomena in direct laser sintering of stainless-steel powder: metallurgical mechanisms and control methods," *Materials and Design*, vol. 30, no. 8, pp. 2903–2910, 2009.

[5] A. Du Plessis, I. Yadroitsev, I. Yadroitsava, and S. G. Le Roux, "X-ray microcomputed tomography in additive manufacturing: a review of the current technology and applications," *3D Printing and Additive Manufacturing*, vol. 5, no. 3, pp. 227–247, 2018.

[6] M. Alimardani, E. Toyserkani, J. P. Huissoon, and C. P. Paul, "On the delamination and crack formation in a thin wall fabricated using laser solid freeform fabrication process: an experimental–numerical investigation," *Optics and Lasers in Engineering*, vol. 47, no. 11, pp. 1160–1168, 2009.

[7] C. Hartmann, P. Lechner, B. Himmel, Y. Krieger, T. C. Lueth, and W. Volk, "Compensation for geometrical deviations in additive manufacturing," *Technologies*, vol. 7, no. 4, p. 83, 2019.

[8] P. Gupta, C. Krishna, and R. Rajesh, "Industrial internet of things in intelligent manufacturing a review, approaches, opportunities, open challenges, and future directions," *International Journal of Interactive Design Manufacturing*, 2022.

[9] A. Sharma, A. Chouhan, L. Pavithran, U. Chadha, and S. K. Selvaraj, "Implementation of LSS framework in automotive component manufacturing: a review, current scenario and future directions," *Materials Today Proceedings*, vol. 46, pp. 7815–7824, 2021.

[10] S. H. Riza, S. H. Masood, and C. Wen, "Laser-assisted additive manufacturing for metallic biomedical scaffolds," *Comprehensive Materials Processing*, vol. 10, pp. 285–301, 2014.

[11] U. Chadha, S. K. Selvaraj, A. S. Lamsal et al., "Directed energy deposition via artificial intelligence enabled approaches," *Complexity*, vol. 2022, Article ID 2767371, 32 pages, 2022.

[12] C. Y. Yap, C. K. Chua, Z. L. Dong et al., "Review of selective laser melting: materials and applications," *Applied Physics Reviews*, vol. 2, no. 4, Article ID 041101, 2015.

[13] A. Raj, U. Chadha, and A. Chadha, "Weld quality monitoring via machine learning-enabled approaches," *International Journal Interactive Design Manufacturing*, 2023.

[14] A. Raj, A. Gyaneshwar, and U. Chadha, "Green manufacturing via machine learning enabled approaches," *International Journal of Interactive Design Manufacturing*, 2022.

[15] S. Pal, H. R. Tiyyagura, I. Drstvenšek, and C. S. Kumar, "The effect of post-processing and machining process parameters on properties of stainless steel PH1 product produced by

direct metal laser sintering," *Procedia Engineering*, vol. 149, pp. 359–365, 2016.

[16] A. L. Jardini, M. A. Larosa, C. A. de Carvalho Zavaglia et al., "Customized titanium implant fabricated in additive manufacturing for craniomaxillofacial surgery: this paper discusses the design and fabrication of a metallic implant for the reconstruction of a large cranial defect," *Virtual and Physical Prototyping*, vol. 9, no. 2, pp. 115–125, 2014.

[17] Ö. Poyraz, E. Yasa, G. Akbulut, A. Orhangül, and S. Pilatin, "Investigation of support structures for direct metal laser sintering (DMLS) of IN625 parts," in *Proceedings of the Solid Freeform Fabrication Symposium*, pp. 560–574, Austin, TX, USA, August, 2015.

[18] A. Dolimont, S. Michotte, E. Rivière-Lorphèvre et al., "Influence on surface characteristics of electron beam melting process (EBM) by varying the process parameters," in *Proceedings of the AIP Conference Proceedings*, College Park, MD, USA, October 2017.

[19] A. T. Silvestri, S. Foglia, R. Borrelli, S. Franchitti, C. Pirozzi, and A. Astarita, "Electron beam melting of Ti6Al4V: role of the process parameters under the same energy density," *Journal of Manufacturing Processes*, vol. 60, pp. 162–179, 2020.

[20] A. Mohammad, A. M. Alahmari, M. K. Mohammed, R. K. Renganayagalu, and K. Moiduddin, "Effect of energy input on microstructure and mechanical properties of titanium aluminide alloy fabricated by the additive manufacturing process of electron beam melting," *Materials*, vol. 10, no. 2, p. 211, 2017.

[21] N. Hrabe and T. Quinn, "Effects of processing on microstructure and mechanical properties of a titanium alloy (Ti–6Al–4V) fabricated using electron beam melting (EBM), Part 2: energy input, orientation, and location," *Materials Science and Engineering: A*, vol. 573, pp. 271–277, 2013.

[22] D. Deng, J. Moverare, R. L. Peng, and H. Söderberg, "Microstructure and anisotropic mechanical properties of EBM manufactured Inconel 718 and effects of post heat treatments," *Materials Science and Engineering: A*, vol. 693, pp. 151–163, 2017.

[23] P. Peças, I. Ribeiro, E. Henriques, and A. Raposo, "Additive manufacturing in injection molds—life cycle engineering for technology selection," in *Advanced Applications in Manufacturing Enginering*, pp. 105–139, Woodhead Publishing, Sawston, UK, 2019.

[24] A. Ataee, Y. Li, G. Song, and C. Wen, "Metal scaffolds processed by electron beam melting for biomedical applications," in *Metallic Foam Bone*, pp. 83–110, Woodhead Publishing, Sawston, UK, 2017.

[25] R. Singh, S. Singh, and M. S. J. Hashmi, *Implant Materials And Their Processing Technologies*, Reference Module in Materials Science and Materials Engineering, Elsevie, 2016.

[26] Oshida Y, Bioscience and Bioengineering of Titanium Materials, Elsevier, 2010.

[27] L. C. Zhang, Y. Liu, S. Li, and Y. Hao, "Additive manufacturing of titanium alloys by electron beam melting: a review," *Advanced Engineering Materials*, vol. 20, no. 5, Article ID 1700842, 2018.

[28] X. Ding, Y. Koizumi, D. Wei, and A. Chiba, "Effect of process parameters on melt pool geometry and microstructure development for electron beam melting of IN718: a systematic single bead analysis study," *Additive Manufacturing*, vol. 26, pp. 215–226, 2019.

[29] F. J. Zanner and L. A. Bertram, "Vacuum arc remelting: an overview," *NASA STI/Recon Technical Report N*, vol. 86, Article ID 16417, 1985.

[30] S. Bremen, W. Meiners, and A. Diatlov, "Selective laser melting," *Laser Technik Journal*, vol. 9, no. 2, pp. 33–38, 2012.

[31] A. Charles, A. Elkaseer, L. Thijs, V. Hagenmeyer, and S. Scholz, "Effect of process parameters on the generated surface roughness of down-facing surfaces in selective laser melting," *Applied Sciences*, vol. 9, no. 6, p. 1256, 2019.

[32] B. Zhang, Y. Li, and Q. Bai, "Defect formation mechanisms in selective laser melting: a review," *Chinese Journal of Mechanical Engineering*, vol. 30, no. 3, pp. 515–527, 2017.

[33] I. Yadroitsev, I. Yadroitsava, P. Bertrand, and I. Smurov, "Factor analysis of selective laser melting process parameters and geometrical characteristics of synthesized single tracks," *Rapid Prototyping Journal*, vol. 18, no. 3, pp. 201–208, 2012.

[34] J. P. Kruth, L. Froyen, J. Van Vaerenbergh, P. Mercelis, M. Rombouts, and B. Lauwers, "Selective laser melting of iron-based powder," *Journal of Materials Processing Technology*, vol. 149, no. 1-3, pp. 616–622, 2004.

[35] T. Özel, A. Altay, A. Donmez, and R. Leach, "Surface topography investigations on nickel alloy 625 fabricated via laser powder bed fusion," *International Journal of Advanced Manufacturing Technology*, vol. 94, no. 9-12, pp. 4451–4458, 2018.

[36] E. Yasa, J. Deckers, J. P. Kruth, M. Rombouts, and J. Luyten, "Investigation of sectoral scanning in selective laser melting," in *Proceedings of the Engineering Systems Design and Analysis*, vol. 49187, pp. 695–703, Istanbul, Turkey, January, 2010.

[37] L. Mugwagwa, D. Dimitrov, S. Matope, and I. Yadroitsev, "Influence of process parameters on residual stress related distortions in selective laser melting," *Procedia Manufacturing*, vol. 21, pp. 92–99, 2018.

[38] Y. L. Hu, X. Lin, Y. L. Li et al., "Plastic deformation behavior and dynamic recrystallization of Inconel 625 superalloy fabricated by directed energy deposition," *Materials and Design*, vol. 186, Article ID 108359, 2020.

[39] K. Cooper, P. Steele, B. Cheng, and K. Chou, "Contact-free support structures for part overhangs in powder-bed metal additive manufacturing," *Inventions*, vol. 3, no. 1, 2017.

[40] S. Nelaturi, M. Behandish, A. M. Mirzendehdel, and J. de Kleer, "Automatic support removal for additive manufacturing post processing," *Computer-Aided Design*, vol. 115, pp. 135–146, 2019.

[41] M. Bayat, A. Thanki, S. Mohanty et al., "Keyhole-induced porosities in laser-based powder bed fusion (L-PBF) of Ti6Al4V: high-fidelity modelling and experimental validation," *Additive Manufacturing*, vol. 30, Article ID 100835, 2019.

[42] L. Dowling, J. Kennedy, S. O'Shaughnessy, and D. Trimble, "A review of critical repeatability and reproducibility issues in powder bed fusion," *Materials and Design*, vol. 186, Article ID 108346, 2020.

[43] Renishaw, "Atmosphere-generation," 2020, https://www.renishaw.com/en/inert-atmosphere-generation--31885.

[44] M. Masoomi, S. M. Thompson, and N. Shamsaei, "Laser powder bed fusion of Ti-6Al-4V parts: thermal modeling and mechanical implications," *International Journal of Machine Tools and Manufacture*, vol. 118-119, pp. 73–90, 2017.

[45] A. Mussatto, R. Groarke, A. O'Neill, M. A. Obeidi, Y. Delaure, and D. Brabazon, "Influences of powder morphology and spreading parameters on the powder bed topography uniformity in powder bed fusion metal additive

manufacturing," *Additive Manufacturing*, vol. 38, Article ID 101807, 2021.

[46] A. Kempf and K. Hilgenberg, "Influence of sub-cell structure on the mechanical properties of AlSi10Mg manufactured by laser powder bed fusion," *Materials Science and Engineering: A*, vol. 776, Article ID 138976, 2020.

[47] K. H. Tan, C. K. Chua, K. F. Leong et al., "Selective laser sintering of biocompatible polymers for applications in tissue engineering," *Bio-Medical Materials and Engineering*, vol. 15, no. 1-2, pp. 113–124, 2005.

[48] L. J. Kumar and C. G. Krishnadas Nair, "Current trends of additive manufacturing in the aerospace industry," *Advances in 3D Printing and Additive Manufacturing Technologies*, pp. 39–54, 2016.

[49] M. Gouge and P. Michaleris, "An introduction to additive manufacturing processes and their modelling challenges," in *Thermo-mechanical Modeling of Additive Manufacturing*, pp. 3–18, Butterworth-Heinemann, Oxford, UK, 2018.

[50] Y. Liu, S. L. Sing, R. Xin En Lim, W. Y. Yeong, and B. T. Goh, "Preliminary investigation on the geometric accuracy of 3D printed dental implant using a monkey maxilla incisor model," *International Journal of Bioprinting*, vol. 8, no. 1, pp. 476–573, 2022.

[51] G. K. Sarkon, B. Safaei, M. S. Kenevisi, S. Arman, and Q. Zeeshan, "State-of-the-art review of machine learning applications in additive manufacturing; from design to manufacturing and property control," *Archives of Computational Methods in Engineering*, vol. 29, 2022.

[52] M. Marrey, E. Malekipour, H. El-Mounayri, and E. J. Faierson, "A framework for optimizing process parameters in powder bed fusion (pbf) process using artificial neural network (ann)," *Procedia Manufacturing*, vol. 34, pp. 505–515, 2019.

[53] R. Liu, S. Liu, and X. Zhang, "A physics-informed machine learning model for porosity analysis in laser powder bed fusion additive manufacturing," *International Journal of Advanced Manufacturing Technology*, vol. 113, no. 7-8, pp. 1943–1958, 2021.

[54] A. Gaikwad, F. Imani, H. Yang, E. Reutzel, and P. Rao, "In situ monitoring of thin-wall build quality in laser powder bed fusion using deep learning," *Smart and Sustainable Manufacturing Systems*, vol. 3, no. 1, Article ID 20190027, 2019.

[55] S. P. Donegan, E. J. Schwalbach, and M. A. Groeber, "Zoning additive manufacturing process histories using unsupervised machine learning," *Materials Characterization*, vol. 161, Article ID 110123, 2020.

[56] E. J. Schwalbach, S. P. Donegan, M. G. Chapman, K. J. Chaput, and M. A. Groeber, "A discrete source model of powder bed fusion additive manufacturing thermal history," *Additive Manufacturing*, vol. 25, pp. 485–498, 2019.

[57] A. Gaikwad, B. Giera, G. M. Guss, J. B. Forien, M. J. Matthews, and P. Rao, "Heterogeneous sensing and scientific machine learning for quality assurance in laser powder bed fusion–A single-track study," *Additive Manufacturing*, vol. 36, Article ID 101659, 2020.

[58] L. Li and S. Anand, "Hatch pattern based inherent strain prediction using neural networks for powder bed fusion additive manufacturing," *Journal of Manufacturing Processes*, vol. 56, pp. 1344–1352, 2020.

[59] T. DebRoy, T. Mukherjee, H. L. Wei, J. W. Elmer, and J. O. Milewski, "Metallurgy, mechanistic models and machine learning in metal printing," *Nature Reviews Materials*, vol. 6, pp. 48–68, 2020.

[60] M. Gieseke, C. Noelke, S. Kaierle, V. Wesling, and H. Haferkamp, "Selective laser melting of magnesium and magnesium alloys," in *Magnesium Technology 2013*, pp. 65–68, Springer, Cham, Switzerland, 2013.

[61] S. Srinivasan, B. Swick, and M. A. Groeber, "Laser powder bed fusion parameter selection via machine-learning-augmented process modeling," *Journal of Occupational Medicine*, vol. 72, no. 12, pp. 4393–4403, 2020.

[62] H. Yeung, Z. Yang, and L. Yan, "A meltpool prediction based scan strategy for powder bed fusion additive manufacturing," *Additive Manufacturing*, vol. 35, Article ID 101383, 2020.

[63] O. Kwon, H. G. Kim, W. Kim, G. H. Kim, and K. Kim, "A convolutional neural network for prediction of laser power using melt-pool images in laser powder bed fusion," *IEEE Access*, vol. 8, pp. 23255–23263, 2020.

[64] M. Amini, S. I. Chang, and P. Rao, "A cybermanufacturing and AI framework for laser powder bed fusion (LPBF) additive manufacturing process," *Manufacturing Letters*, vol. 21, pp. 41–44, 2019.

[65] K. Wasmer, C. Kenel, F. Saeidi, C. Leinenbach, and S. A. Shevchik, "In situ and real-time monitoring of powder-bed AM by combining acoustic emission and machine learning," in *Proceedings of the Conference proceedings, Laser in Manufacturing (LiM2017)*, Munich, Germany, June 2017.

[66] X. Zhang, J. Saniie, and A. Heifetz, "Detection of defects in additively manufactured stainless steel 316L with compact infrared camera and machine learning algorithms," *Journal of Occupational Medicine*, vol. 72, no. 12, pp. 4244–4253, 2020.

[67] O. Fergani and K. Eissing, "A machine learning-based digital twin of the manufacturing process: metal powder-bed fusion case," 2020, https://engrxiv.org/preprint/view/878.

[68] L. Meng, "Machine learning and probabilistic design framework for laser powder bed FUSION process," Doctoral dissertation, Purdue University Graduate School, West Lafayette, IN, USA, 2020.

[69] G. Kou, H. Xiao, M. Cao, and L. H. Lee, "Optimal computing budget allocation for the vector evaluated genetic algorithm in multi-objective simulation optimization," *Automatica*, vol. 129, Article ID 109599, 2021.

[70] H. Elwarfalli, D. Papazoglou, D. Erdahl, A. Doll, and J. Speltz, "In Situ process monitoring for laser-powder bed fusion using convolutional neural networks and infrared tomography," in *Proceedings of the 2019 IEEE National Aerospace and Electronics Conference (NAECON)*, pp. 323–327, IEEE, Dayton, OH, USA, July 2019.

[71] Y. Zhu, Z. Wu, W. D. Hartley, J. M. Sietins, C. B. Williams, and H. Z. Yu, "Unraveling pore evolution in post-processing of binder jetting materials: X-ray computed tomography, computer vision, and machine learning," *Additive Manufacturing*, vol. 34, Article ID 101183, 2020.

[72] G. Kou, O. Olgu Akdeniz, H. Dincer, and S. Yuksel, "fintech investments in European banks: a hybrid IT2 fuzzy multi-dimensional decision-making approach," *Financial innovation*, vol. 7, no. 1, p. 39, 2021.

[73] S. L. Sing, C. N. Kuo, C. T. Shih, C. C. Ho, and C. K. Chua, "Perspectives of using machine learning in laser powder bed fusion for metal additive manufacturing," *Virtual and Physical Prototyping*, vol. 16, no. 3, pp. 372–386, 2021.

[74] R. F. Pereira and P. J. Bártolo, "Recent advances in additive biomanufacturing," *Comprehensive Materials Processing*, vol. 10, 2014.

[75] E. R. Denlinger, "Development and numerical verification of a dynamic adaptive mesh coarsening strategy for simulating

laser power bed fusion processes," in *Thermo-Mechanical Modeling of Additive Manufacturing*, pp. 199–213, Butterworth-Heinemann, Oxford, UK, 2018.

[76] C. Vyas, G. Poologasundarampillai, J. Hoyland, and P. Bartolo, "3D printing of bio composites for osteochondral tissue engineering," in *Biomedical Composites*, pp. 261–302, Woodhead Publishing, Sawston, UK, 2017.

[77] S. Sun, M. Brandt, and M. J. L. A. M. Easton, "Powder bed fusion processes: an overview," *Laser Additive Manufacturing*, pp. 55–77, Woodhead Publishing, Sawston, UK, 2017.

[78] X. Gong, D. Zeng, W. Groeneveld-Meijer, and G. Manogharan, "Additive manufacturing: a machine learning model of process-structure-property linkages for machining behavior of Ti-6Al-4V," *Mater Sci Add Manuf*, vol. 1, no. 1, p. 6, 2022.

[79] E. R. Denlinger, M. Gouge, J. Irwin, and P. Michaleris, "Thermomechanical model development and in situ experimental validation of the Laser Powder-Bed Fusion process," *Additive Manufacturing*, vol. 16, pp. 73–80, 2017.

[80] R. Goodridge and S. Ziegelmeier, "Powder bed fusion of polymers," in *Laser Additive Manufacturing*, pp. 181–204, Woodhead Publishing, Sawston, UK, 2017.

[81] S. L. Sing, "Perspectives on additive manufacturing enabled beta-titanium alloys for biomedical applications," *International Journal of Bioprinting*, vol. 8, no. 1, pp. 478–8, 2022.

[82] S. Vock, B. Klöden, A. Kirchner, T. WeiBgarber, and B. Kieback, "Powders for powder bed fusion: a review," *Prog Addit Manuf*, vol. 4, pp. 383–397, 2019.

[83] Stratasys, "Direct Metal Laser Sintering (DMLS)," 2023, https://www.stratasysdirect.com/technologies/direct-metal-laser-sintering.

[84] Matweb, "AISI Type H13 Hot Work Tool Steel," 2022, http://www.matweb.com/search/datasheet_print.aspx?matguid=e30d1d1038164808a85cf7ba6aa87ef7.

[85] Matmatch, "Learn material," 2022, https://matmatch.com/learn/material/inconel-625.

[86] Javelin, "ABS-M30 FDM Plastic," 2023, https://www.javelin-tech.com/3d/stratasys-materials/abs-m30.

[87] H. Christina, "Materials Spotlight: The Properties of Nylon 12," 2022, https://www.cableorganizer.com/learning-center/articles/materials-nylon12.html.

[88] Simplify3d, "Polypropylene," 2020, https://www.simplify3d.com/support/materials-guide/polypropylene/#:%7E:text=Polypropylene%20is%20a%20semi%2Drigid,it%20challenging%20to%203D%20print.

[89] I. Arasu, K. Chockalingam, C. Kailasanathan, and M. Sivabharathy, "Optimization of surface roughness in selective laser sintered stainless steel parts," *International Journal of ChemTech Research*, vol. 6, no. 5, pp. 2993–2999, 2014.

[90] T. D. Ngo, A. Kashani, G. Imbalzano, K. T. Nguyen, and D. Hui, "Additive manufacturing (3D printing): a review of materials, methods, applications and challenges," *Composites Part B: Engineering*, vol. 143, pp. 172–196, 2018.

[91] W. Zouhri, J. Y. Dantan, B. Häfner et al., "Optical process monitoring for laser-powder bed fusion (L-PBF)," *CIRP Journal of Manufacturing Science and Technology*, vol. 31, pp. 607–617, 2020.

[92] I. Baturynska, O. Semeniuta, and K. Martinsen, "Optimization of process parameters for powder bed fusion additive manufacturing by combination of machine learning and finite element method: a conceptual framework," *Procedia CIRP*, vol. 67, pp. 227–232, 2018.

[93] H. Baumgartl, J. Tomas, R. Buettner, and M. Merkel, "A deep learning-based model for defect detection in laser-powder bed fusion using in-situ thermographic monitoring," *Progress in Additive Manufacturing*, vol. 5, no. 3, pp. 277–285, 2020.

[94] P. S. Desai and C. F. Higgs, "Spreading process maps for powder-bed additive manufacturing derived from physics model-based machine learning," *Metals*, vol. 9, no. 11, p. 1176, 2019.

[95] L. Thijs, F. Verhaeghe, T. Craeghs, J. V. Humbeeck, and J. P. Kruth, "A study of the microstructural evolution during selective laser melting of Ti–6Al–4V," *Acta Materialia*, vol. 58, no. 9, pp. 3303–3312, 2010.

[96] P. O'Regan, P. Prickett, R. Setchi, G. Hankins, and N. Jones, "Metal based additive layer manufacturing: variations, correlations and process control," *Procedia Computer Science*, vol. 96, pp. 216–224, 2016.

[97] R. Singh, A. Gupta, O. Tripathi et al., "Powder bed fusion process in additive manufacturing: an overview," *Materials Today Proceedings*, vol. 26, pp. 3058–3070, 2020.

[98] S. Bland and N. T. Aboulkhair, "Reducing porosity in additive manufacturing," *Metal Powder Report*, vol. 70, no. 2, pp. 79–81, 2015.

[99] M. Grasso and B. M. Colosimo, "A statistical learning method for image-based monitoring of the plume signature in laser powder bed fusion," *Robotics and Computer-Integrated Manufacturing*, vol. 57, pp. 103–115, 2019.

[100] B. Yuan, G. M. Guss, A. C. Wilson et al., "Machine-learning-based monitoring of laser powder bed fusion," *Advanced Materials Technologies*, vol. 3, no. 12, Article ID 1800136, 2018.

[101] C. Gobert, E. W. Reutzel, J. Petrich, A. R. Nassar, and S. Phoha, "Application of supervised machine learning for defect detection during metallic powder bed fusion additive manufacturing using high resolution imaging," *Additive Manufacturing*, vol. 21, pp. 517–528, 2018.

[102] K. Wasmer, C. Kenel, C. Leinenbach, and S. A. Shevchik, "In situ and real-time monitoring of powder-bed AM by combining acoustic emission and artificial intelligence," in *Proceedings of the International Conference on Additive Manufacturing in Products and Applications*, pp. 200–209, Springer, Cham, Switzerland, September, 2017.

[103] I. Daubechies, "Ten lectures on wavelets," *Society for industrial and applied mathematics*, 1992.

[104] M. V. Tazebay and A. N. Akansu, "Adaptive subband transforms in time-frequency excisers for DSSS communications systems," *IEEE Transactions on Signal Processing*, vol. 43, no. 11, pp. 2776–2782, 1995.

[105] S. A. Shevchik, C. Kenel, C. Leinenbach, and K. Wasmer, "Acoustic emission for in situ quality monitoring in additive manufacturing using spectral convolutional neural networks," *Additive Manufacturing*, vol. 21, pp. 598–604, 2018.

[106] T. Ghimire, A. Joshi, S. Sen, C. Kapruan, U. Chadha, and S. K. Selvaraj, "Blockchain in additive manufacturing processes: recent trends and its future possibilities," *Materials Today Proceedings*, vol. 50, pp. 2170–2180, 2022.

[107] U. Chadha, A. Abrol, N. P. Vora, A. Tiwari, S. K. Shanker, and S. K. Selvaraj, "Performance evaluation of 3D printing technologies: a review, recent advances, current challenges, and future directions," *Prog Addit Manuf*, vol. 7, no. 5, pp. 853–886, 2022.

[108] R. Sivasubramani, A. Verma, G. Rithvik, U. Chadha, and S. Senthil Kumaran, "Influence on nonhomogeneous microstructure formation and its role on tensile and fatigue performance of duplex stainless steel by a solid-state welding process," *Materials Today Proceedings*, vol. 46, pp. 7284–7296, 2021, 17.

[109] A. Raj, S. Ram Kishore, L. Jose, A. K. Karn, U. Chadha, and S. K. Selvaraj, "A survey of electromagnetic metal casting computation designs, present approaches, future possibilities, and practical issues," *The European Physical Journal Plus*, vol. 136, no. 6, p. 704, 2021.

[110] K. Virmani, C. Deepak, S. Sharma, U. Chadha, and S. K. Selvaraj, "Nanomaterials for automotive outer panel components: a review," *The European Physical Journal Plus*, vol. 136, no. 9, p. 921, 2021.

[111] U. Chadha, S. K. Selvaraj, A. K. Ravinuthala et al., "Bio-inspired techniques in freeze casting: a survey of processes, current advances, and future directions," *International Journal of Polymer Science*, vol. 2022, Article ID 9169046, 22 pages, 2022.

[112] S. K. Selvaraj, A. Raj, R. Rishikesh Mahadevan, U. Chadha, and V. Paramasivam, "A review on machine learning models in injection molding machines," *Advances in Materials Science and Engineering*, vol. 2022, Article ID 1949061, 28 pages, 2022.

[113] S. K. Selvaraj, A. Raj, M. Dharnidharka et al., "A cutting-edge survey of tribological behavior evaluation using artificial and computational intelligence models," *Advances in Materials Science and Engineering*, vol. 2021, Article ID 9529199, 17 pages, 2021.

[114] M. Dharnidharka, U. Chadha, L. M. Dasari, A. Paliwal, Y. Surya, and S. K. Selvaraj, "Optical tomography in additive manufacturing: a review, processes, open problems, and new opportunities," *The European Physical Journal Plus*, vol. 136, no. 11, p. 1133, 2021.

[115] V. Madhavadas, D. Srivastava, U. Chadha et al., "A review on metal additive manufacturing for intricately shaped aerospace components," *CIRP Journal of Manufacturing Science and Technology*, vol. 39, pp. 18–36, 2022.

[116] U. Chadha, S. K. Selvaraj, A. Raj et al., "AI-driven techniques for controlling the metal melting production: a review, processes, enabling technologies, solutions, and research challenges," *Materials Research Express*, vol. 9, no. 7, Article ID 072001, 2022.

[117] S. S. Patel, M. Surjith Shiva, T. Kataray et al., "Trends in tribological behaviour of materials for compressors," *Journal of Physics: Conference Series*, vol. 2272, no. 1, Article ID 012023, 2022.

[118] U. Chadha, S. K. Selvaraj, N. Gunreddy et al., "A survey of machine learning in friction stir welding, including unresolved issues and future research directions," *Material Design and Processing Communications*, vol. 2022, Article ID 2568347, 28 pages, 2022.

[119] V. Carlota, "The Complete Guide to Electron Beam Melting (EBM) in 3D Printing," 2023, https://www.3dnatives.com/en/electron-beam-melting100420174/.

[120] Aniwaa, "Arcam Q20 overview," 2023, https://www.aniwaa.com/product/3d-printers/arcam-q20/.

[121] Slm-solutions, "The makers industrial metal am machines scroll down," 2023, https://www.slm-solutions.com/products-and-solutions/machines/.

[122] L. Meng, B. McWilliams, W. Jarosinski et al., "Machine learning in additive manufacturing: a review," *Journal of Occupational Medicine*, vol. 72, no. 6, pp. 2363–2377, 2020.

[123] H. Bao, S. Wu, Z. Wu, G. Kang, X. Peng, and P. J. Withers, "A machine-learning fatigue life prediction approach of additively manufactured metals," *Engineering Fracture Mechanics*, vol. 242, Article ID 107508, 2021.

[124] N. Gerdes, C. Hoff, J. Hermsdorf, S. Kaierle, and L. Overmeyer, "Snapshot hyperspectral imaging for quality assurance in laser powder bed fusion," *Procedia CIRP*, vol. 94, pp. 25–28, 2020.

[125] L. Scime, D. Siddel, S. Baird, and V. Paquit, "Layer-wise anomaly detection and classification for powder bed additive manufacturing processes: a machine-agnostic algorithm for real-timepixel-wise semantic segmentation," *Additive Manufacturing*, vol. 36, Article ID 101453, 2020.

[126] Q. Liu, H. Wu, M. J. Paul et al., "Machine-learning assisted laser powder bed fusion process optimization for AlSi10Mg: new microstructure description indices and fracture mechanisms," *Acta Materialia*, vol. 201, pp. 316–328, 2020.

[127] M. Mathieu, M. Henaff, and Y. LeCun, "Fast training of convolutional networks through FFTS: international conference on learning representations (ICLR2014), CBLS, april 2014," in *Proceedings of the 2nd International Conference on Learning Representations, ICLR 2014*, Banff, Canada, January, 2014.

[128] I. Sachdeva, S. Ramesh, U. Chadha, H. Punugoti, and S. K. Selvaraj, "Computational AI models in VAT photopolymerization: a review, current trends, open issues, and future opportunities," *Neural Computing and Applications*, vol. 34, no. 20, pp. 17207–17229, 2022.

[129] A. Bhat, R. S. Elsen, D. Abishai et al., "Prediction and experimental verification of distortion due to residual stresses in a Ti-6Al-4V control arm plate," *Advances in Materials Science and Engineering*, vol. 2022, Article ID 5211623, 11 pages, 2022.

Hindawi
Complexity
Volume 2023, Article ID 2701439, 22 pages
https://doi.org/10.1155/2023/2701439

Research Article

Extended Framework for Preventive Maintenance Planning: Risk and Behaviour Analysis of a Proposed Optimization Model

Pablo Viveros, Marco Espinoza, Rodrigo Mena, and Fredy Kristjanpoller

Department of Industrial Engineering, Universidad Técnica Federico Santa María, Valparaíso, Chile

Correspondence should be addressed to Pablo Viveros; pablo.viveros@usm.cl

Received 20 April 2022; Revised 26 September 2022; Accepted 1 October 2022; Published 8 February 2023

Academic Editor: Yu Zhou

The considerable increase in the complexity associated with the formulation of maintenance plans has enabled the development of new techniques to bring maintenance scheduling optimization models to more realistic environments. In this sense, a previous optimization model was proposed considering the use of time windows for the formation of grouping schemes under an opportunistic strategy for maintenance activities considering non-negligible execution times, thus offering the possibility of analysing scenarios with limited resources. This article proposes a risk analysis based on the failure probability of each component involved in the maintenance scheduling optimization model, which has the particularity of enabling a greater number of combinations of grouped PM activities. Moreover, it seeks to identify the general behaviour of the optimization model against different scenarios of periodicities and execution times of each maintenance activity. The proposed optimization model is formulated under a mixed integer linear programming (MILP) paradigm and its objective function seeks to minimize the unavailability of the system associated with the execution times of the activities developed, generating different experimental cases, and varying the start time scheduling under a tolerance factor from 0% up to a maximum of 25% for advance or delay. Results show in contrast with the base optimization model, an 8% less unavailability when the tolerance factor is 10%. Finally, it was possible to quantify the risk present in each maintenance schedule, at the same time a behaviour towards advancing PM activities is evidenced by the optimization model proposed over the delay.

1. Introduction

During the last decades, maintenance management has been a fundamental pillar for certain organizations with production processes in their operation, since it enables the correct use and optimization of resources, generating significant savings in terms of performing and programming maintenance activities, where statistics show that a company can save up to 18% of their total costs destined to this work. So much so that its role in modern production systems has become a much more important task in companies that adopt maintenance as an element of the business that generates profit [1]. Given this, it could be safely stated that the objective of maintenance is to contribute to the benefit of the organization in which it is incorporated, developing a necessity for strategy oriented maintenance operations aligned with the objectives of all incumbent organizational levels. This is, recognizing that current production systems operate more efficiently, effectively, and economically to sustain themselves in the long term [2].

The latter has led a large group of researchers to focus their efforts on finding increasingly precise ways to generate maintenance plans that adapt to the requirements of different industries and their different operational contexts. However, given the large number of factors that can be considered within the spectrum of the problem, it has become a task with immense complexity. To this, it must be added that, not too long ago, many mathematical or computational tools had not been developed, therefore the current potential of the hand with technological advancement is tremendous. Given this, as technology evolves, the complexity of modern engineering systems and maintenance systems also do [3]. Therefore, the continuous developments of technical systems and the growing

dependence on equipment have led the importance of the effectiveness of maintenance plans to grow [4], which has enabled the finding of different and new techniques to face the complexity of each scenario. In addition, the real contribution of forming efficient maintenance plans is in the minimization of the impact of the costs associated with the execution of these activities within industries that have large-scale production processes, which can reach from 15% to 70% of total production costs [5].

The types of systems used within the framework of this document correspond to "multiunit systems." This term can refer to a single asset consisting of multiple components (multicomponent system) or a system with multiple assets (multiasset system). Given this, the fact that multiunit systems operate collectively to produce or deliver a service, creating a maintenance policy for each unit separately might not prove efficient [6]. Therefore, maintenance planning should be performed considering all requirements and constraints of system components at the same time. However, in the presence of multicomponent systems, it is necessary to account for the interactions between them, which can be classified into 3 types: economic, structural, and stochastic. Economic dependence is the most common within these [7] and implies that the combination or grouping of maintenance activities will be cheaper than carrying them out separately (positive dependence), while negative economic dependence occurs when the combination of maintenance activities is more expensive than maintaining the components individually [8]. Structural dependence refers to the fact that to carry out a maintenance activity in a certain component, it is necessary to intervene in others. Finally, stochastic dependence implies that the condition of one component influences the condition of others, or when these are subject to failures for common causes. The latter can often be observed in redundant mechanical systems, where the degradation of one component leads to a distribution of the internal force of the system, and therefore overloads other components [9].

As it was mentioned, maintenance planning aims to reduce the negative impact rising from the execution of maintenance activities. Thus, a method to address these impacts is to minimize failure risk through planning focusing mostly on minimizing the cost associated with failure [10]. The latter is known as risk-based maintenance planning and to be performed it may be supported by different policies such as condition-based maintenance (CBM) or preventive maintenance (PM) policies. Risk-based planning is especially attractive for contexts in which failure brings costly consequences and a cost-effective tool is required to reduce the probability of failure [11] or measure the preventive maintenance effectiveness [12]. Most risk-based maintenance planning does not focus on the effects of economic dependence or the system's unavailability due to scheduled detentions [13]. Moreover, in cases with high uncertainty, it becomes necessary to disregard some costs when availability and reliability are critical [14]. These have pushed the focus away from the context in which high economic dependence is present.

This fosters the development of maintenance plans through the opportunistic maintenance strategy, which is an effective method to reduce interference between maintenance and production operations in a multi-component system [15]. The advantage of this strategy is to be able to carry out several PM activities by stopping the system only once, forming packages or groups of activities. These activity packages and their impact within a certain scheme will be determined by their "time windows." This term refers to a certain time in which the executions of each PM activity may be advanced or delayed with respect to their tentative moment (or equivalently, default moment) of execution previously defined by the periodicity of each of these activities, enabling other PM activities to be partially or totally executed within the same period of time, thus reducing "set up" costs and increasing the availability of a single machine or a multicomponent system [16]. The formation of these groups of PM activities, in which certain activities can be executed together with others minimizing the downtime of the system, will consequently generate, within an established time horizon, and increased generation of groups. Hence, inefficiency and set up costs will be considerably reduced over the time horizon.

The way in which these schemes are formed is through the development and formulation of an optimization model, which aims to obtain the most appropriate maintenance schedule in terms of the tolerance (time window) assigned to each scenario. Each scenario will consider one fixed tolerance for each activity of the studied scenario. It should be also noted that each model will depend exclusively on the variables and assumptions they incorporate, thus giving them certain characteristics that bring them closer or far from what really happens in certain production processes.

On the other hand, one of the challenges posed by the reduction or minimization of the maintenance costs of multicomponent systems is that maintenance plans that have been developed are not based on the maintenance history or condition of each component, which would imply a considerable increase in the risk of failure [17]. Specifically, there is an inherent cost when wasting the useful life of the components when maintenance activities are advanced; on the other hand, an increase in the probability of failure of the components is generated if the activities are delayed [18], increasing the failure risk and shutdown probability. Given this, it is important to consider and quantify the risk associated with maintenance plans, to prefer those that best suit the requirements of each industry or production process.

Therefore, many studies have been developed that cover maintenance planning from different edges, where each of them incorporates different assumptions and characteristics that are typical of the systems studied. In addition, different techniques are revealed to address both the formation of maintenance plans and the implications they have in terms of risk. In the first place, with respect to maintenance planning, each job differs from the other with respect to the assumptions they incorporate, that is, type of system, types of interactions between components, characteristics of maintenance activities, feasibility of grouping through time

windows, and tolerance level thus each of these responds to what is sought in certain problems, situations, or industries. Regarding the interactions between components of a system, commonly, the dependence incorporated into the assessment is the economic one, which refers to the possible decrease in the costs of grouping maintenance activities [5, 16–19]. For its part, stochastic dependence from the point of view of component degradation and its effect on the distribution of the useful life of others has been addressed in conjunction with economic dependence in [2, 8, 20–23]. In fact, several studies have been conducted addressing more accurate and robust modelling, accounting for the interactions, criticality of components [24], and the downstream effect of components that after failure allow normal performance for a limited time [25]. On the other hand, from the point of view of the configuration of the systems, due to the high complexity represented by parallel or hybrid systems such as the one proposed in [26], serial systems are used.

One of these grouping models was early developed in [27] were they sought to maximize the number of groups to, consequently, lower inefficiencies related to availability. They further develop the model in [16] were the objective is to minimize the number of detentions instead of maximizing the groups achieving higher levels of availability and precision in comparison with the original proposed model. More recently, they presented a model available for implementation, also addressing the opportunistic grouping strategy for maintenance scheduling presented in [5] aiming to minimize detentions, but considering the use of resources in the modelling. Now, regarding the characteristics of maintenance activities, it can be considered that their execution times are usually considered negligible, as in [16]; however, in [5], their model is adapted to more realistic contexts, where the incorporation of non-negligible executions stands out, which is an important window of opportunities for the formation of grouping packages.

Furthermore, there are several ways to address the risk associated with scheduling maintenance activities, such as penalty functions, condition-based maintenance, and Bayesian networks. One of the models that raises the penalty functions considering that there is a risk when advancing and delaying maintenance activities corresponds to that carried out in [18], where an optimization model is analysed with a framework similar to the current one, with the particularity of having a dynamic component; that is, maintenance planning can be updated over time considering the existence of events in the short term. Different works emerge that incorporate risk in dynamic contexts [28, 29]; however, from a point of view in which maintenance scheduling is carried out for the entire planning horizon without being subject to possible corrective activities, there is no history of using the probability of failure and corrective cost of each asset using "event space method" for the different groups of activities to be formed within a scheme, as is the method to be developed in the present research.

Considering the above-given theory, this article proposes an extension to the model developed in [5]; that is, maintenance planning is performed by developing a model for optimizing opportunistic maintenance activities in a multicomponent system, incorporating time windows for the formation of grouping packages that allow reducing the downtime of the system by modifying certain key constraints of the original model to facilitate a greater number of groupings. This is achieved by relaxing a certain restriction of the base model that imposes that all maintenance activities that are part of the same working group must begin at the same moment. Although the extension of the original model means adding extra complexity a multiobjective approach such as [30] would improve the solver efficiency, it would at the same time, push to greater changes to the modelling, losing the focus of this article.

The activities can be grouped under two scenarios: their time windows generate an opportunity for grouping when two or more overlap between them; or there is no overlap between the time windows, but since the model contemplates non-negligible execution times, the grouping can be carried out by intercepting the execution times of each activity. In this way, an activity could make use of all the allowed tolerance to delay or advance its execution, without overlapping with the tolerance of another activity, and still be able to generate a grouping package with another activity, as long as its execution times allow it. This will generate two effects: recognizing as joint groupings of activities those that the base model does not consider and provides a new spectrum of possibilities to form groupings, favouring the minimization of the downtime of the system.

Therefore, the main objective of this research is to generate a postoptimal risk analysis on an optimization model that allows a greater number of groupings (and hence a greater minimization in downtime) to recognize the behaviour of the model and deliver valuable information to a decision maker about maintenance scheduling in different scenarios. As mentioned, the quantification of risk is based on the probability of failure of each component; however, it is necessary to emphasize that for each of these components or equipment, parameters are added that define their behaviour by assuming a certain function of the probability distribution of failure, in this case as a Weibull function of scale parameters (α) and shape (β). The quantification of the risk is postoptimal, that is, first a maintenance schedule is obtained disregarding the risk and then each of these schemes proposed by the optimisation model (which differ from the level of tolerance allowed to advance or delay PM activities) are calculated the associated risk (failure probability when delaying and wasted useful life when advancing). We seek to obtain the optimal tolerance levels according to the risk that a decision maker intends to assume in each industry or production line, delivering a series of indicators and numerical results that accompany this decision.

2. Framework Definition

The framework presented in [5] is an extension to the original model developed in [16], which seeks to expand its scope and technical characteristics, incorporating tolerance of time windows, non-negligible duration of preventive maintenance activities, changes in the configuration of the

system and the application of limitations to the technical feasibility in the performance of certain activities, thus generating a better adherence to real maintenance scenarios in the industry. Therefore, some of the most important and considerable assumptions to be incorporated in the current model from the original model, except for (iv) and (vi) are discussed as follows:

(i) The system contemplates a multicomponent series configuration, where each of the equipment has only one failure mode: previously defining that the components involved will have exclusively one failure mode, reduces the degree of analytical and computational complexity.

(ii) The execution of grouped PM activities always involves a simultaneous/parallel execution: this point is important to be able to formulate the optimization model, if there were serial executions, the stopping times of the system would be considerably longer, which would not allow to find the minimum unavailability. The latter is approachable when the activities are performed in parallel and the total time of unavailability for the execution of a package of PM activities corresponds to the longest individual execution time of the activities.

(iii) The execution of PM activities returns the component to its initial operational conditions (perfect maintenance): defining that the components return to their original state of life after the PM activity is executed is an extremely accurate assumption in the context in which computational and analytical complexity is intended to be avoided. If not, the analysis should incorporate degradation models, such as those discussed in [31], which propose the incorporation of the concept of "virtual age," which precisely refers to imperfect maintenance actions.

(iv) It is considered that there are technical feasibility constraints: the incorporation of this assumption promotes and supports the main objective in [5], that is, to adapt the original model to real industrial environments, since it limits the simultaneous execution of certain PM activities due to technical nonfeasibility, which may be attributable to lack of personnel, shortage of tools, etc. Since the scope of this investigation does not contemplate this restriction, the analysis of the technical nonfeasibility of some activities is set aside, considering it as an input parameter that any combination of activities can be executed without problems.

(v) Duration of the executions of the PM activities nonnegligible: in the same way as in the previous case, this assumption is also important to adapt and extend the original model to real production environments, since in these the duration of PM activities translates into a productive cessation, directly impacting on the inefficiency costs.

(vi) Simultaneous start of grouped activities: although this is not considered as an assumption within the article, the constraints associated with the base optimization model support it and it translates into a limitation for the system to form grouping packages that further minimize the unavailability of the system.

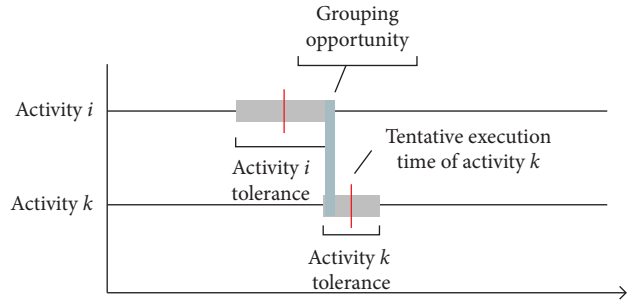

Figure 1: Feasibility of opportunistic grouping between the activities i and k.

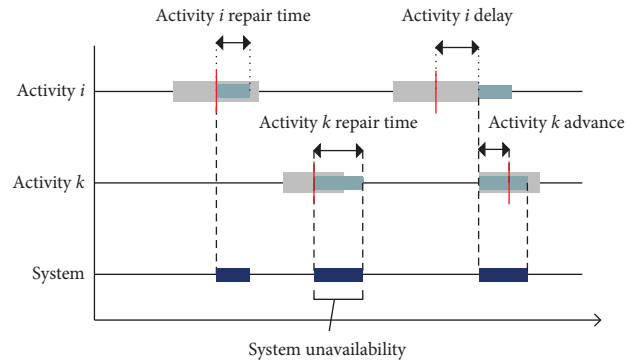

Figure 2: Scheme of grouping two activities of different components configured in series.

On the other hand, from this discussion emerge the differences and key contributions that are implemented in this research for a correct extension of the work carried out in [5], which are divided into two essential points:

2.1. Nonsimultaneous Start of Grouped Activities. For the original model to establish the opportunity to group two or more maintenance activities, it is necessary that the time windows (with their respective tolerances) of these activities are intercepted in some sections (see Figure 1).

That being said, based on what has been mentioned, the following grouping scheme arises, consisting of the same two activities i and k, where the execution of any of the maintenance activities (belonging to different components) always implies a stop of the system. In addition, when there is grouping, both activities may or may not be executed in parallel, hence the total downtime of the system associated with a package of activities is given by the total time in which the maintenance activities are developed. Furthermore, it is assumed that when all PM activities associated with a certain clustering package have ended, the system returns to normal operation immediately (see Figure 2).

As mentioned, restricting the optimization model to grouped activities starting at the same moment limits certain activities, at particular moments, from being able to generate work packages that at first sight seem to be obvious. As an example, Figure 3 shows a grouping scheme subject to tolerances in which the activity i is grouped with the activity k. In this sense, it is necessary to emphasize that although the time windows of each of the grouped activities are not intercepted; in the same way, a grouping package was formed. This grouping is generated by advancing the execution of the activity i and delaying that of the activity k, where it is also appreciated that the time in which the activity i begins is within the execution time of the activity k. That is, the activities make use of all their tolerance (to delay or advance, as the case may be), to allow the minimization of unavailability to be the greatest. Given the above-mentioned theory, in general terms, relaxing this restriction allows the grouping of activities to have different start and end moments; then, the total time out of service of the system in each grouping package will be defined as the period between the earliest start time and the latest completion time of the executions. This enables situations in which could even generate that when there are no time windows available to advance or delay activities, grouping schemes can be formed, which *a priori* could imply times of the unavailability of the system considerably reduced in lower tolerance percentages compared to the extended model.

2.2. Risk Analysis. As mentioned, this research main objective is to incorporate a postoptimal analysis of the risk associated with the use of time windows under an extended framework and optimization model, in order to provide a decision maker with the necessary information to opt for the planning of maintenance activities that best suits the defined requirements and know the behaviour of the model itself. In this context, it is proposed that the risk associated with the change in the tentative moments of execution is represented by the increase or decrease in the probability of failure of the components, that is, both the advance and delay will include a certain level of risk, so that each activity, regardless of whether or not it is grouped with others, will have its own risk component determined by its probability of failure at that moment. However, this is not trivial when there are grouping packages, since for activities to begin their executions, it is necessary to assume that none of the components will present a previous failure state, so the reliability of such a scenario is conditioned on the behaviour of the individual probability of failure of each of the equipment or components and the number of them. In practical terms, the fact of forming an opportunistic preventive maintenance scheme will imply that certain activity executions are performed at their tentative moment, or as part of a grouping package in which the risk is analysed together with other activities that are part of it. On the other hand, it is necessary to establish that the fact of advancing a PM activity will always be beneficial in terms of the probability of failure; hence, there must be some form of associated penalty. That is why the quantification of the risk associated with each grouping scheme is composed of 3 parts.

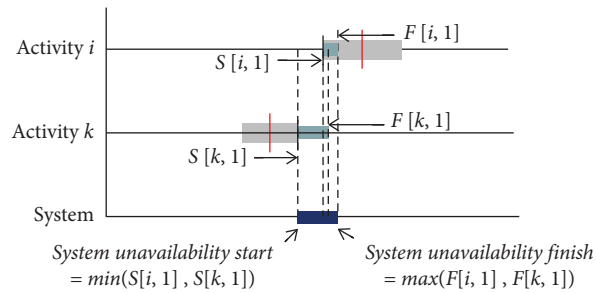

Figure 3: Example of a grouping scheme possible by relaxing the start restriction on grouped activities.

(a) Tentative risk: the first of these refers to the risk that involves executing a certain activity that has not been grouped, and therefore, is executed at its tentative moment. Usually, a random variable is the way in which such a risk is quantified is determined by the cumulative failure probability function of the component or failure state, which is determined by those responsible for having developed the maintenance plans. Given this, the distribution for the random variable will be considered as an input parameter, and considering its widely use to model failure and survival [32–34], it will correspond to a Weibull distribution of scale and shape parameters equally incorporated as exogenous parameters from the previous maintenance planning. The mathematical expression of this quantification is detailed as follows:

$$R_{\text{tentative}} = \left(1 - e^{-\left(rs_{i,j} - rf_{i,j-1}/\alpha\right)^{\beta}}\right) * C_{pf_i}. \quad (1)$$

Here, $rs_{i,j}$ represents the moment of the beginning of the execution pair (i, j). Furthermore, $rf_{i,j-1}$ represents the moment of completion of the previous execution of (i, j). In addition, C_{pfi} refers to the cost associated (in monetary units) to all the management and activities involved in the preventive intervention of the component i, assumed as an arbitrary parameter.

(b) Grouping risk: as mentioned, grouping implies assuming that none of the components involved will fail before the PM activity execution; since otherwise, it would not be possible to execute these activities within the planned interval. Given this, this assumption involves a risk, which corresponds to all scenarios in which at least one of the grouped components fails. That is why the number of scenarios to be analysed will depend exclusively on the number of activities (n) within the grouping package, generating a total of 2^n cases, however, because one of the combinations corresponds to the scenario where none of the equipment fails; that is, the case that is not intended to be studied since it delivers a scenario of good functioning, the number of cases to be analysed corresponds to $2^n - 1$. As an example, a hypothetical case is developed where

Table 1: Analysis of a two-components case, which shows how to calculate each of the three fault scenarios costs.

Sce	Comp 1	Comp 2	Occurrence prob.	Cost
1	Fault	No fault	$P_1 = F(t)_1 * (1 - F(t)_2)$	$C_1 = P_1 * C_{cf_1} + P_1 * p_1 * C_d$
2	No fault	Fault	$P_2 = (1 - F(t)_1) * F(t)_2$	$C_2 = P_2 * C_{cf_2} + P_2 * p_2 * C_d$
3	Fault	Fault	$P_3 = F(t)_1 * F(t)_2$	$C_3 = P_3 * (C_{cf_1} + C_{cf_2}) + P_3 * \max(p_1, p_2) * C_d$

there is a grouping package of two different component activities to be executed at a certain moment t (see Table 1). Given this, the number of scenarios to analyse will be $2^2 - 1 = 3$.

As can be seen in the table, by generating different scenarios for each grouping scheme will deliver different probabilities of occurrences for them, and therefore, different associated costs. In the first of the scenarios, it is observed that the component i is in a state of failure while the second is not, given this, the probability of occurrence of said scenario corresponds to the probability of failure of the first component by the reliability of the second (probability of nonfailure). Moreover, the cost associated with each scenario has two components. The first one is the cost associated with the corrective repair of the component or components that present a state of failure, while the second term corresponds to the cost of inefficiency that would be incurred by having to stop the system to perform such activity. The first term is calculated by multiplying the probability of occurrence of the scenario under study by the costs of repairing the asset or assets that have failed (C_{cf}). On the other hand, the second component is the one resulting from the multiplication between the probability of occurrence of the scenario by the time it takes to carry out the maintenance activity by the cost of stopping the system (C_d). Finally, the total risk associated to this package corresponds to the sum of every scenario cost, i.e., $C_1 + C_2 + C_3$. In addition, it is necessary to emphasize that when there are joint failure scenarios, such as the third scenario in the table, the cost of inefficiency will be calculated based on the maximum execution time of the components that fail at the same time, since it is assumed that they can be executed in parallel without any problem.

(c) Useful life cost: considering the previous risks, it is important to note that when a maintenance activity is advanced, its risk will decrease, since its probability of failure decreases. On the other hand, delaying PM activities translates into an increase of the associated risk. This could imply that advancing is always more convenient than delaying; however, this is not the case, since when advancing a maintenance activity and therefore not taking advantage of the total useful life of the component, it has an associated extra risk component which can be quantified as cost. The way to calculate this cost is done by multiplying the total number of weeks that the activities are advanced by a unit cost associated with the useful life of the components (C_{ul}), assumed in this case as 10 (μm) for each week of useful life used.

$$\left(\text{tent}_{\text{exc}_{i,j}} - \left(\text{tent}_{\text{exc}_{i,j-1}} + T_i\right)\right) \cdot C_{ul}, \quad \forall (i,j) \in IJ^+. \tag{2}$$

3. Problem Formulation

The formulation of the optimization model gives shape to a mixed integer linear programming (MILP) problem; that is, the model is made up of linear constraints and objective function, together with real and binary variables. On this occasion, the solver "Gurobi" will be used, which is a specialized and free use tool to solve problems of this nature. The notation and definition of parameters, sets, and decision variables of the problem presented in the previous section is shown as follows:

Sets:

I set of PM activities to perform on the component, indexed by i or n
J_i set of executions of the PM activity $i \in I$ within the horizon T, indexed by j or o
N set of possible grouping pair combinations (i, j, n, o) in the planning horizon T, where $(i, j), (n, o) \in I \times J_i : i \neq n$
K set of possible grouping pair permutations (i, j, n, o) in the planning horizon T, where $(i, j), (n, o) \in I \times J_i : i \neq n$

Parameters:

T planning horizon, in $[u.t]$.
T_i periodicity of the activity i, $i \in \{1, 2, \ldots |I|\}$
M "Big-M" parameter, where $M \gg T$
e tolerance for the execution of the activity i, $i \in \{1, 2, \ldots |I|\}$
p_i activity execution time i, $i \in \{1, 2, \ldots |I|\}$
ε parameter of negligible value, where $\varepsilon \longrightarrow 0$

Decision variables:

S_{ij} start time of the j-th execution of the activity i, $j \epsilon J_i$, $i \epsilon I$
F_{ij} completion time of the j-th execution of the activity i, $j \epsilon J_i$, $i \epsilon I$
$w_{i,j,n,o}$ clustering activation binary variable, where $w_{i,j,n,o} = 1$ if the j-th execution of the activity i is grouped with the o-th execution of the activity n, $j, o \epsilon J_i$, $i, n \epsilon I$
$z_{i,j,n,o}$ instant of start of the system stop associated with the grouping of the activity (i, j) with (i', j') yes and only if $w_{i,j,n,o} = 1$. Otherwise, $z_{i,j,n,o} = 0$
$y_{i,j,n,o}$ instant of completion of the system stop associated with the grouping of the activity (i, j) with (n, o) yes and only if $w_{i,j,n,o} = 1$. Otherwise, $y_{i,j,n,o} = 0$

$rs_{i,j}$ instant of start of the system stop associated with the j-th execution of the activity i, $j \epsilon J_i$, $i \epsilon I$
$rf_{i,j}$ instant of completion of the system shutdown associated with the j-th execution of the activity i, $j \epsilon J_i$, $i \epsilon I$
$r_{i,j}$ total system downtime associated with the j-th execution of the activity i, $j \epsilon J_i$, $i \epsilon I$
$d_{i,j}$ time out of service associated with the j-th execution of the activity i, $j \epsilon J_i$, $i \epsilon I$

Objective function

$$\min \sum_{i \in I, j \in Ji} d_{ij}, \quad \forall (i, j) \in J. \tag{3}$$

Restrictions

$$F_{i,j} \geq S_{n,o} - M \cdot \left(1 - o_{i,j,n,o}\right), \quad \forall (i, j, n, o) \in K, \tag{4}$$

$$S_{\mathrm{n,o}} \geq F_{i,j} - M \cdot \left(1 - o_{n,o,i,j}\right), \quad \forall (i, j, n, o) \in K, \tag{5}$$

$$o_{i,j,n,o} + o_{n,o,i,j} \leq 1 + w1_{i,j,n,o}, \quad \forall (i, j, n, o) \in N, \tag{6}$$

$$o_{i,j,n,o} + o_{n,o,i,j} \geq 1 + w1_{i,j,n,o}, \quad \forall (i, j, n, o) \in N, \tag{7}$$

$$w1_{i,j,n,o} + w2_{i,j,n,o} \leq w_{i,j,n,o}, \quad \forall (i, j, n, o) \in N, \tag{8}$$

$$w1_{i,j,n,o} + w2_{i,j,n,o} \geq w_{i,j,n,o}, \quad \forall (i, j, n, o) \in N, \tag{9}$$

$$rs_{i,j} \leq rs_{n,o} + M \cdot w1_{i,j,n,o} + M \cdot \left(1 - w2_{i,j,n,o}\right), \quad \forall (i, j, n, o) \in N, \tag{10}$$

$$rs_{i,j} \geq rs_{n,o} - M \cdot w1_{i,j,n,o} - M \cdot \left(1 - w2_{i,j,n,o}\right), \quad \forall (i, j, n, o) \in N, \tag{11}$$

$$rs_{i,j} \leq rs_{n,o} - ep + M \cdot w1_{i,j,n,o} + M \cdot w2_{i,j,n,o} + A1_{i,j,n,o} \cdot M, \quad \forall (i, j, n, o) \in N, \tag{12}$$

$$rs_{i,j} \geq rs_{n,o} + ep - M \cdot w1_{i,j,n,o} - M \cdot w2_{i,j,n,o} - \left(1 - A1_{i,j,n,o}\right) \cdot M, \quad \forall (i, j, n, o) \in N. \tag{13}$$

$$z_{i,j,n,o} \leq S_{i,j} + \left(1 - w_{i,j,n,o}\right) \cdot M, \quad \forall (i, j, n, o) \in N, \tag{14}$$

$$z_{i,j,n,o} \leq S_{n,o} + \left(1 - w_{i,j,n,o}\right) \cdot M, \quad \forall (i, j, n, o) \in N, \tag{15}$$

$$z_{i,j,n,o} \leq w_{i,j,n,o} \cdot M, \quad \forall (i, j, n, o) \in N, \tag{16}$$

$$z_{i,j,n,o} \geq S_{i,j} - \left(1 - w_{i,j,n,o}\right) \cdot M - M \cdot VZ1_{ijno}, \quad \forall (i, j, n, o) \in N, \tag{17}$$

$$z_{i,j,n,o} \geq S_{n,o} - \left(1 - w_{i,j,n,o}\right) \cdot M - M \cdot VZ1_{ijno}, \quad \forall (i, j, n, o) \in N, \tag{18}$$

$$VZ1_{ijno} + VZ2_{ijno} = 1, \quad \forall (i, j, n, o) \in N, \tag{19}$$

$$y_{ijno} \geq F_{ij} - \left(1 - w_{ijno}\right) \cdot M, \quad \forall (i, j, n, o) \in N, \tag{20}$$

$$y_{ijno} \geq F_{no} - \left(1 - w_{ijno}\right) \cdot M, \quad \forall (i, j, n, o) \in N, \tag{21}$$

$$y_{ijno} \geq w_{ijno} \cdot M, \quad \forall (i, j, n, o) \in N, \tag{22}$$

$$y_{ijno} \leq F_{ij} + \left(1 - w_{ijno}\right) \cdot M + M \cdot VY1_{ijno}, \quad \forall (i, j, n, o) \in N, \tag{23}$$

$$y_{ijno} \leq F_{no} + \left(1 - w_{ijno}\right) \cdot M + M \cdot VY2_{ijno}, \quad \forall (i, j, n, o) \in N, \tag{24}$$

$$VY1_{ijno} + VY2_{ijno} = 1, \quad \forall (i, j, n, o) \in N, \tag{25}$$

$$rs_{ij} \leq z_{ijno} + \left(1 - w_{ijno}\right) \cdot M, \quad \forall (i, j, n, o) \in N, \tag{26}$$

$$rs_{no} \leq z_{ijno} + \left(1 - w_{ijno}\right) \cdot M, \quad \forall (i, j, n, o) \in N, \tag{27}$$

$$rs_{ij} \leq S_{ij} + w_{ijno} \cdot M, \quad \forall (i, j, n, o) \in N, \tag{28}$$

$$rs_{no} \leq S_{ij} + w_{ijno} \cdot M, \quad \forall (i, j, n, o) \in N, \tag{29}$$

$$rs_{ij} \geq z_{ijno} - \left(1 - V1_{ijno}\right) \cdot M, \quad \forall (i, j, n, o) \in N, \tag{30}$$

$$rs_{no} \geq z_{ijno} - \left(1 - V1_{ijno}\right) \cdot M, \quad \forall (i, j, n, o) \in N, \tag{31}$$

$$rs_{ij} \geq S_{ij} - \left(1 - Ul_{ij}\right) \cdot M, \quad \forall j \in J_i, \forall i \in I, \tag{32}$$

$$Ul_{ij} + \sum_{(a,b,n,o) \in N} Vl_{ijno} \geq 1, \quad \forall j \in J_i, \forall i \in I, \tag{33}$$

$$rf_{ij} \geq y_{ijno} - \left(1 - w_{ijno}\right) \cdot M, \quad \forall (i, j, n, o) \in N, \tag{34}$$

$$rf_{no} \geq y_{ijno} - \left(1 - w_{ijno}\right) \cdot M, \quad \forall (i, j, n, o) \in N, \tag{35}$$

$$rf_{ij} \geq F_{ij} - w_{ijno} \cdot M, \quad \forall (i, j, n, o) \in N, \tag{36}$$

$$rf_{no} \geq F_{ij} - w_{ijno} \cdot M, \quad \forall (i, j, n, o) \in N, \tag{37}$$

$$rf_{ij} \leq y_{ijno} + \left(1 - V_{ijno}\right) \cdot M, \quad \forall (i, j, n, o) \in N, \tag{38}$$

$$rf_{no} \le y_{ijno} + \left(1 - V_{ijno}\right) \cdot M, \quad \forall (i,j,n,o) \in N, \tag{39}$$

$$rf_{ij} \le F_{ij} + \left(1 - U_{ij}\right) \cdot M, \quad \forall j \in J_i, \forall i \in I, \tag{40}$$

$$U_{ij} + \sum_{(i,j,n,o)\in N} V_{ijno} \ge 1, \quad \forall j \in J_i, \forall i \in I, \tag{41}$$

$$V_{ijno} \le w_{ijno}, \quad \forall (i,j,n,o) \in N, \tag{42}$$

$$r_{ij} = rf_{ij} - rs_{ij}, \quad \forall j \in J_i, \forall i \in I, \tag{43}$$

$$r_{ij} \le M \cdot \left(1 - w_{ijno}\right) + r_{no}, \quad \forall (i,j,n,o) \in N, \tag{44}$$

$$r_{ij} \ge -M \cdot \left(1 - w_{ijno}\right) + r_{no}, \quad \forall (i,j,n,o) \in N, \tag{45}$$

$$d_{ij} \ge r_{ij} - M \cdot \sum_{(i,j,n,o)\in N} w_{ijno}, \quad \forall (i,j,n,o) \in N, \tag{46}$$

$$d_{ij} \le r_{ij} + M \cdot \sum_{(i,j,n,o)\in N} w_{ijno}, \quad \forall j \in J_i, \forall i \in I, \tag{47}$$

$$F_{ij} = S_{ij} + p_i, \quad \forall j \in J_i, \forall i \in I, \tag{48}$$

$$S_{ij} \le rf_{i,j-1} + T_i + T_i \cdot e, \quad \forall j \in J_i, \forall i \in I, \tag{49}$$

$$S_{ij} \ge rf_{i,j-1} + T_i - T_i \cdot e, \quad \forall j \in J_i, \forall i \in I, \tag{50}$$

$$S_{ij} \le rf_{i,j-1} + T_i + M\left(\sum_{(a,b,n,o)\in N} w_{abno} + \sum_{(c,d,n,o)\in N} w_{cdno}\right),$$
$$\forall j \in J_i, \forall i \in I, \ (a,b) = (c,d) = (i,j), \tag{51}$$

$$S_{ij} \ge rf_{i,j-1} + T_i - M\left(\sum_{(a,b,n,o)\in N} w_{abno} + \sum_{(c,d,n,o)\in N} w_{cdno}\right),$$
$$\forall j \in J_i, \forall i \in I, \ (a,b) = (c,d) = (i,j), \tag{52}$$

$$F_{ij} \ge rf_{ij} - M \cdot \sum_{(i,j,n,o)\in N} w_{ijno}, \quad \forall j \in J_i, \forall i \in I, \tag{53}$$

$$F_{ij} \le rf_{ij} + M \cdot \sum_{(i,j,n,o)\in N} w_{ijno}, \quad \forall j \in J_i, \forall i \in I, \tag{54}$$

$$S_{ij} \ge rs_{ij} - M \cdot \sum_{(i,j,n,o)\in N} w_{ijno}, \quad \forall j \in J_i, \forall i \in I, \tag{55}$$

$$S_{ij} \le rs_{ij} + M \cdot \sum_{(i,j,n,o)\in N} w_{ijno}, \quad \forall j \in J_i, \forall i \in I, \tag{56}$$

$$rs_{ij} \le M \cdot \left(1 - w_{ijno}\right) + rs_{\mathrm{no}}, \quad \forall j \in J_i, \forall i \in I, \tag{57}$$

$$rs_{ij} \ge rs_{\mathrm{no}} - M \cdot \left(1 - w_{ijno}\right), \quad \forall j \in J_i, \forall i \in I, \tag{58}$$

$$rf_{ij} \le M \cdot \left(1 - w_{ijno}\right) + rf_{\mathrm{no}}, \quad \forall j \in J_i, \forall i \in I, \tag{59}$$

$$rf_{ij} \ge rf_{\mathrm{no}} - M \cdot \left(1 - w_{ijno}\right), \quad \forall j \in J_i, \forall i \in I. \tag{60}$$

Now, regarding the development of the optimization model: the set of constraints (3)–(12) are responsible for satisfying the condition that the grouped activities can begin or end at different moments. Constraints (13)–(24) pretend to formulate the variables z_{ij} and y_{ij}, which take the start and end values, respectively, of each of the activities that are grouped, leaving with a value = 0 for those that are not part of any grouping package, which would be used in the group of constraints. On the other hand, restrictions (25)–(41) are responsible for establishing the start and end moments of each of the maintenance activities, whether they are grouped or not. Specifically (25)–(32), determine the moments of beginning (see Figure 4), while (33)–(41) are responsible for establishing the moments of completion of each activity (see Figure 5).

Constraint (43) is used to generate the variable r_{ij}, which measures the amount of downtime of the system that generates the execution of such execution (44) and (45) determine that, if a grouping between two activities is generated, they must have the same duration in their interval to execute the activities (45) and (46) are used to determine the variable d_{ij}, which delivers the duration of each of the grouping schemes, designating this value only to one of the executions of the grouped activities. In this way, the time out of service of the system can be counted. The restriction (48) is simply responsible for establishing that the time of completion of an activity corresponds to the time of initiation plus the duration of the activity. Restrictions (49) and (50) determine the window of time that each activity must be able to advance or delay its execution in case of forming a grouping package, which depends on the percentage of tolerance and assigned, establishing that tolerance, in terms of time units, is calculated as $e \cdot T_i$. On the other hand, (51) and (52) imply that if a certain execution is not part of some grouping scheme, it must be executed at its tentative moment, which, in turn, is determined by its periodicity. (52)–(55) are responsible for satisfying that, if there is no grouping in a certain execution (i, j), both the individual start and end variables (S_{ij} and F_{ij}) must coincide with the group end start values. In this way, each execution or grouping of them is treated as a group of activities. On the other hand (56)–(59), adjusts the start and end variables of each of the grouping schemes, determining that, if the activity (i, j) is grouped with (n, o) its values rf and rs must be the same.

3.1. Performance Indicators. It is imperative to incorporate the use of performance indicators for the postoptimal analysis and discussion of the results when carrying out the development of this research hand in hand with the computational implementation of the optimization model since it allows to identify the real contribution to the problem raised. Hence, two types of indicators are presented,

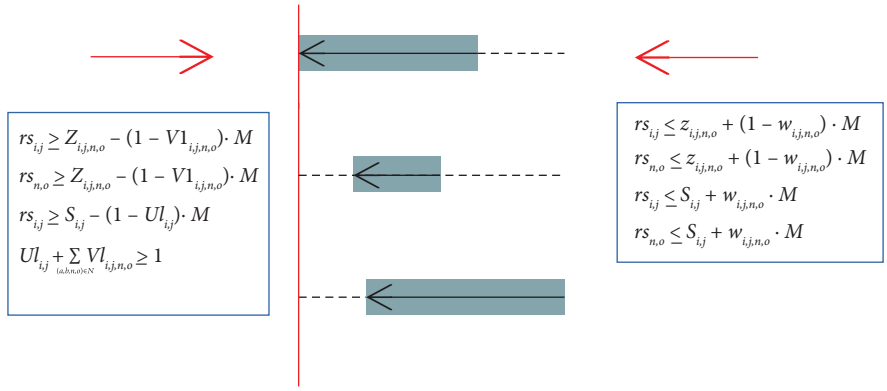

Figure 4: Operation of the constraints associated with the calculation of rs_{ij}.

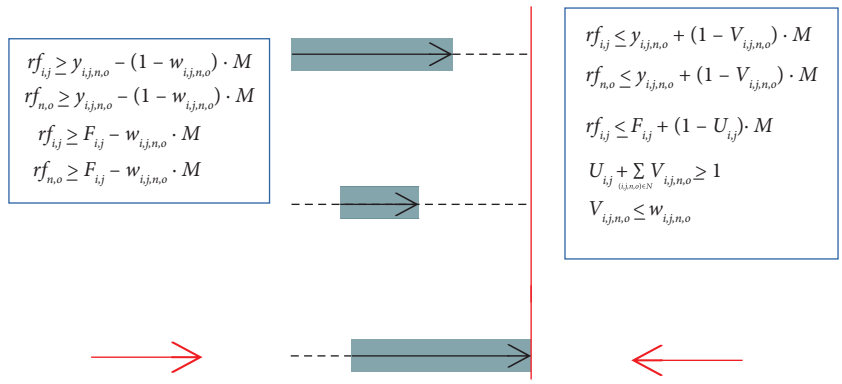

Figure 5: Operation of the constraints associated with the calculation of rf_{ij}.

indicators related to the quality of the grouping scheme (i)–(vi), and the indicators associated with the efficiency of the programming code in terms of the search for feasible solutions (vii), (viii), with a total of 8 indicators. Indicators (ii) to (vi) will allow to know the behaviour of the maintenance activities according to the delay or advance of their moments of execution with respect to the tentative moments. It should be noted that these indicators are extracted from [5].

(i) **Unav**: since this research is an extension to the model proposed by [5], the unavailability of the system in the activity grouping scheme is used as an indicator, which is presented as a direct result of the computational model. This allows to finally make visible the main objective of executing the optimization model, prior to the risk analysis.

(ii) $\mathbf{f_A}$: determines the percentage of activities that are advanced with respect to their tentative moments.

$$f_A = \frac{|IJ^-|}{\sum_{i\in I}|J_i|}. \tag{61}$$

(iii) $\mathbf{f_D}$: determines the percentage of activities that are delayed with respect to their tentative moments.

$$f_D = \frac{|IJ^+|}{\sum_{i\in I}|J_i|}. \tag{62}$$

(iv) $\mathbf{f_J}$: determines the percentage of activities that are executed in their tentative instants.

$$f_J = \frac{|IJ^0|}{\sum_{i\in I}|J_i|}. \tag{63}$$

(v) $\mathbf{A^{AV}}$: indicates the average tolerance usage percentage of those activities that are advanced with respect to their tentative instants.

$$A^{AV} = \frac{\sum_{(i,j)\in IJ^-0}\left(\left(t_{\text{exc}_{i,j-1}} + T_i\right) - t_{\text{exc}_{i,j}}\right)/e \cdot T_i}{\sum_{i\in I}|J_i|}. \tag{64}$$

(vi) $\mathbf{D^{AV}}$: indicates the average tolerance usage percentage of those activities that are delayed with respect to their tentative instants.

$$D^{AV} = \frac{\sum_{(i,j)\in IJ^-0}\left(t_{\text{exc}_{i,j}} - \left(t_{\text{exc}_{i,j-1}} + T_i\right)\right)/e \cdot T_i}{\sum_{i\in I}|J_i|}. \tag{65}$$

(vii) **Optimality gap:** this indicator refers to the percentage difference between the lower limit and the upper limit of the results obtained when executing the developed optimization model. In general, if the GAP takes values other than 0, it means that the model failed to obtain a point solution, that is, the

Table 2: Input parameters of the maintenance activities involved in the comparative case study.

Act$i$	$p_{i\,[\text{hours}]}$	$T_{i[\text{weeks}]}$
1	15	4.2
2	30	6.6
3	40	11.8
4	48	13.2
5	36	5.3

solution will be in a range determined by both limits.

(viii) **Resolution time:** as for the optimality GAP, the resolution times emanate directly from the tool used to solve the optimization model and indicates the time it took to the system to find the solution presented.

Where the sets IJ^-, IJ^+, and IJ^0 are defined as follows:

$$\begin{aligned} IJ^- &= \left\{(i,j):\ \text{tent}_{\text{ext}_{i,j}} - \left(\text{tent}_{\text{exc}_{i,j-1}} + T_i\right) < 0,\right. \\ &\forall i \in I, j \in J_i, IJ^+ = \left\{(i,j):\ \text{tent}_{\text{ext}_{i,j}} - \left(\text{tent}_{\text{exc}_{i,j-1}} + T_i\right) > 0,\right. \\ &\forall i \in I, j \in J_i, IJ^0 = \left\{(i,j)\text{tent}_{\text{ext}_{i,j}} - \left(\text{tent}_{\text{exc}_{i,j-1}} + T_i\right) = 0,\right. \\ &\forall i \in I, j \in J_i. \end{aligned} \tag{66}$$

4. Results and Discussion

The computational results are obtained from a computer with an Intel Core i5-9300H processor at a speed of 2.40 GHz, with 8 GB of RAM and an operating system built under a 64 bit architecture.

The extension of the optimization model was made using a Python interface, for which the Pyomo optimization model language/tool was used, and the results were obtained through the aforementioned "Gurobi" solver.

The results will be divided into two sections. The first of these will deal with a single case of numerical experimentation with a maximum of 10% tolerance allowed for the formation of grouping schemes, which will be evaluated in both the base optimization model presented in [5] and the one developed in this research, with the aim of comparing the results and experimentally obtaining the benefits of the changes applied to the optimization model. To perform a risk analysis, four different study cases will be presented with a maximum tolerance level of 20%. This will make it possible to know the behaviour in the formation of grouping schemes with greater precision.

4.1. Base Case Comparison. Before executing the model, we give way to the presentation of the numerical experimentation case with which the optimization model is intended to be developed and evaluated. Given this, it is necessary to establish the basic parameters for its operation, which correspond to the number of preventive maintenance activities (PM), their periodicities (T_i), and execution times (p_i). It should be noted that the planning horizon (T) corresponds to 52 weeks, as established in the base case (see Table 2).

First, to determine the impact of the programming algorithm when relaxing the restriction of starting the grouped activities at the same moment, a comparison is made between the results of minimizing the unavailability of the base model and the currently developed one. For this, identical input parameters are assumed for each of the comparative instances, that is, the same execution times, periodicities, and number of activities. The latter is quite relevant, since the number of activities will depend exclusively on the tolerance of each scenario, so it does not affect the results in comparative terms. Given this, the way in which the number of activities is calculated is determined by the following formulation:

$$J_i = \left\{ j \in J_i:\ j = 1, 2, \ldots, \left| \frac{T}{\max\left(p_i,\ i \in I\right) + T_i + T_i \cdot e} \right| \right\}, \quad \forall i \in I. \tag{67}$$

Equation (67) defines the set J_i, that is, the number of executions of each of the maintenance activities and is the same as that used in [5]. Its operation is given by the division of the planning horizon into as many sections as maintenance activities can be performed for each component or equipment. In this sense, a pessimistic scenario is used, that is, it is assumed that each maintenance cycle is given by the total use of the time windows to delay the activities. In this way, the minimum number of activities that could be executed in the given planning horizon is obtained.

For each model, 10 instances are executed, which differ in the percentage of tolerance that is allowed so that each execution can be advanced or delayed, starting with a value of 0% escalating to 10%. Table 3 shows the results regarding the total unavailability of the system along with their respective variations:

As it can be observed, the results are sensitized with respect to the percentage of tolerance that is allowed for each scheme, which has a resolution of 1%. For each of these instances, 7 different indicators are obtained.

Regarding the Optimality GAP, this time it always acquires values of 0%, which implies that the execution of the optimization model is always yielding a punctual optimum, that is, both the lower and upper limits have the same values. While there are certain differences in the order of 10^{-12} it is considered negligible.

As for the resolution times, up to 8% tolerance relatively low values are obtained, and not greater than 23 seconds; however, when there are tolerances of 9% or 10%, due to the increase in computational complexity and the wider range of possible solutions, times of up to 140 seconds are reached. However, they are considerably low times. It is necessary to establish that the model with which it is compared has notoriously shorter resolution times, reaching in each of the instances values no greater than 2 seconds. This, although it does not imply a major problem when generating results, is explained due to the greater number of restrictions of the proposed model.

Table 3: Comparative results of total unavailability of the system for different tolerance scenarios between both models.

e (%)	Optimality GAP (%)	Resolution time (s)	Base case unav. (weeks)	Base case opt. (%)	Extended case unav. (sem)	Extended case opt. (%)	Difference (%)
0	0	0.5	5.74	—	5.56	3.1	3.1
1	0	0.6	5.35	6.8	5.26	8.5	1.6
2	0	1.3	5.03	12.5	4.86	15.3	2.8
3	0	1.5	4.86	15.3	4.80	16.4	1.0
4	0	3.8	4.77	16.9	4.60	19.8	3.0
5	0	9.3	4.56	20.6	4.13	28.0	7.4
6	0	8.5	3.83	33.4	3.79	34.0	0.6
7	0	21.6	3.70	35.5	3.70	35.5	0.0
8	0	22.7	3.61	37.1	3.61	37.1	0.0
9	0	140.0	3.61	37.1	3.60	37.3	0.2
10	0	92.4	3.55	38.2	3.06	46.7	8.5
				25		28	2.6

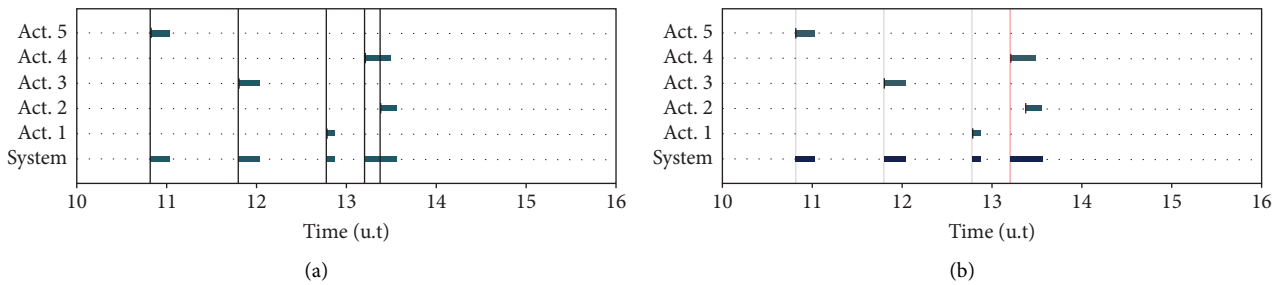

Figure 6: Comparative scheme between both models with $e = 0\%$. (a) Base case. (b) Current case.

Moreover, when analysing the values taken by the objective function in each of the models, that is, the total time (in weeks) of unavailability of the system in a 1year horizon, the optimization model proposed in this research obtains, in the most extreme case, a reduction of 46.7% of the unavailability with respect to the unavailability obtained in the scenario of 0% tolerance with the base model (column 7), in contrast to 38.2% when 10% tolerance is also evaluated in the latter (column 5).

Regarding the graphical results, it is interesting to observe the first scenario for both models, given that there is a variation of 3.1%. In this, since there is no tolerance, the reduction of unavailability of the system is given simply by the fact of having relaxed the restrictions of the optimization model proposed in [5] that limit the start times of every activity that is part of a same group to be equals. This is explained by the fact that the original model cannot count the scenarios where there is overlap in the execution times of the activities as a grouping, thus generating that the periodicities of each of the activities are not respected and a real grouping scenario cannot be chosen. That is, without the need to make use of tolerance, the model can group activities so that the least possible availability is achieved.

In Figure 6, it can be seen that in the executions of activities 2 and 4 there is an overlap; however, the base model does not recognize it. This generates that the next execution of activity 4 has a certain bias when accounting for its periodicity, since, by not recognizing the grouping, the model is assuming that after the activity is executed the associated component immediately returns to operate, which does not turn out to be the case, since activity 2 continues to run. To avoid this bias in the accounting of periodicities, the model currently developed does recognize this as a grouping and both activities schedule the following execution in view of the system resuming at the instant both maintenance activities have been completed.

Furthermore, by correcting the way in which the periodicities of the activities are used would allow for those future ones to be able to form grouping packages with other activities. Moreover, in this same scenario (see Figure 7(b)), the fact of having delayed the subsequent executions of activity 4 generated that the third execution of this activity can generate a grouping package with the sixth execution of activity 2, thus minimizing the times of the unavailability of the system, since now the downtime associated with such executions corresponds to the interval that begins with the execution of activity 4 and ends with the completion of activity 2, in contrast to the base model (see Figure 7(a)) where the time out of service will simply be the sum of both execution times.

This same phenomenon occurs in scenarios where the percentage of tolerance for activities to modify their tentative moments of execution increases, in fact, now not only will the accounting of the periodicities of each activity be corrected (favouring grouping), but the model will be able to advance or delay executions intelligently to obtain the shortest times of unavailability, obtaining even 8.5% less unavailability than in the base model.

On the other hand, analysing only the scenario where the advance or delay of the tentative executions of a

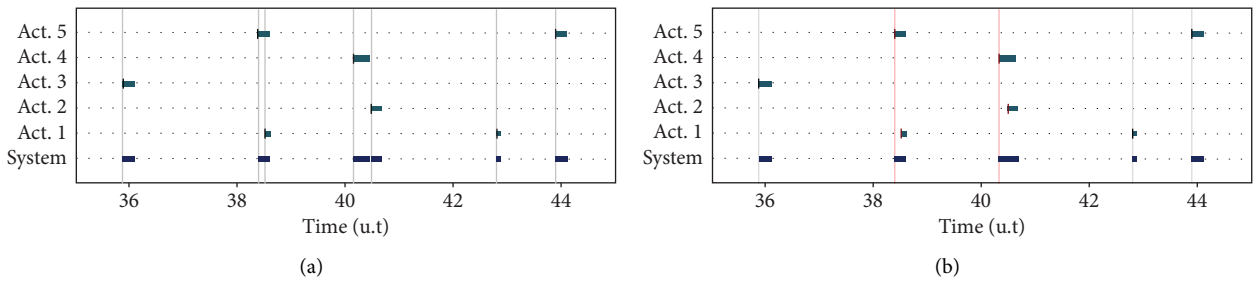

Figure 7: Comparative scheme between both models with $e = 0\%$. (a) Base case. (b) Current case.

maintenance activity is not allowed is not entirely valid, therefore, it is necessary to analyse all the cases reported in Table 2. It can be observed that in all scenarios, from 0% to 6% tolerance there is some degree of difference in the optimization of unavailability. Subsequently, from 7% to 9% there is no difference, to finally, in the case in which the maximum tolerance is defined, generate an 8% optimization above the base case.

These periods in which there is no optimization are related to the periodicity of each activity; since, if the tentative executions of different activities are separated by very large time intervals, it is difficult in all tolerance scenarios to reduce unavailability; hence, the tolerance percentage must be large enough so that their time windows can intersect to form new alternatives to optimize the scheme.

The latter enables the possibility to establish the final results in respect to the comparison between the programming algorithms of both models. For values between 0% and 10% tolerance allowed to modify the tentative moments of execution of maintenance activities, the model developed in the current research generates on average 2.6% extra optimization in each sensitized scenario. However, if only the scenarios where there is indeed a certain degree of improvement were considered, that is, without counting the cases where the tolerance is between the range of 7% to 9%, an optimization of 3.5% is achieved over what is delivered by the base model by tolerance level. Now, in general terms, improvements in the optimization algorithm generate an extra 8.5% in the total unavailability of the system, decreasing it from a value of 5.74 (weeks) to 3.06 (weeks), that is, when activities are allowed to make use of 10% of their tolerances, the unavailability of the system is reduced by 2.68 (weeks), or in percentage terms, 46.7%.

In short, the results presented allow us to recognize the importance of eliminating the bias present in the programming of tasks when there is the possibility of generating grouping due to the overlap of the execution times of the activities. However, it is important to note that in this particular case the results were favourable to be able to generate work packages, such as those shown graphically in Figures 6 and 7, since it is possible, theoretically, to generate a new way of counting the periodicities of the equipment, maintaining or increasing the availability of the system. This is easy to visualize if it were considered that the periodicity of activity number 4 was greater than planned, in this way there would be no possibility of grouping its third execution with the sixth execution of activity 2. Despite this, the fact of determining the precise results will always generate a great added value compared to just delivering an approximation.

Table 4: Parameters associated with the quantification of risk in the case of current experimentation.

Act$i$	C_{cf_i} (μm)	C_{pf_i} (μm)	α	β
1	12	2	7.5	1.8
2	18	3	9.2	1.9
3	30	5	16.4	2.0
4	33	5.5	20.4	1.9
5	15	2.5	8.5	2.2

4.2. Risk Analysis. As mentioned in previous sections, one of the research objectives is to determine which are the optimal tolerance levels based on the risk of all the instances worked by the optimization algorithm. In this sense, the fact of minimizing unavailability and raising awareness regarding the tolerance factor with the developed model is tremendously useful, since it allows to obtain better results and eliminate the existing bias in the base research, however, it is not enough. Given this, it is necessary to obtain the results associated with the risk inherent in the formation of grouping packages, since in this way it would be possible to make coherent decisions based on both variables.

The way in which the risk associated with each individual execution or grouping packages is addressed and quantified is detailed in Section 2, where in general terms it is established that the fact of generating groups of activities implies a risk associated with all scenarios where the system (in series) presents a state of failure. In addition, when a certain execution of some activity is not part of a package of activities to be grouped, it is considered that its cost will be determined exclusively by its probability of failure until its instant of tentative execution.

In order to make visible the risk behaviour associated with each of the grouping schemes, the corresponding analysis will be divided into two parts. The first of these will be an analysis focused on knowing sufficient information to determine the optimal tolerance level in the case of experimentation presented above (see Table 2). Furthermore, with the aim of knowing the behaviour and use of tolerances in general terms, a study will be carried out with 4 different cases of experimentation, which are sensitized from 0% to 25% tolerance, with a resolution of 5%.

Table 5: Number of executions of each of the activities for the different tolerance levels.

e (%)	Act 1	Act 2	Act 3	Act 4	Act 5
0	12	7	4	3	9
1	12	7	4	3	9
2	12	7	4	3	9
3	12	7	4	3	9
4	12	7	4	3	9
5	12	7	4	3	9
6	12	7	4	3	9
7	12	7	4	3	9
8	12	7	4	3	9
9	12	7	4	3	9
10	12	7	4	4	8
11	12	7	4	4	8
12	12	7	4	4	8
13	12	7	4	4	8
14	12	7	4	4	8
15	12	7	4	4	8
16	12	7	4	4	8
17	12	7	4	4	8
18	12	7	4	4	8
19	12	7	4	4	8
20	12	7	4	4	8

Table 6: Number of executions of each of the activities for the different tolerance levels.

e (%)	Cost for attempted executions (μm)	Cost per grouping (μm)	Total cost (μm)	Ind. System (without)
0	230	90	320	5.65
1	214	106	319	5.35
2	177	140	317	4.95
3	173	145	318	4.90
4	91	227	319	4.68
5	83	223	306	4.35
6	83	220	303	4.01
7	78	245	323	3.92
8	69	239	308	3.92
9	82	288	370	3.90
10	54	244	298	3.29
11	54	244	298	2.98
12	39	329	368	2.71
13	39	334	373	2.71
14	39	347	386	2.71
15	39	305	344	2.71
16	39	241	280	2.71
17	39	253	292	2.71
18	39	233	272	2.71
19	39	245	284	2.71
20	39	244	238	2.71

4.2.1. Case Analysis of Base Experimentation. The necessary parameters, as it can be seen in Table 4, are added to the case study to continue with the analysis, incorporating the costs associated with the corrective (C_{cfi}) and preventive intervention (C_{pfi}) and also, since it is considered that the function that best suits the failure behaviour of these is the Weibull distribution, their respective parameters of scale and shape α and β are presented. From the latter, it is possible to obtain the probability of failure associated with each of the programmed executions depending on their actual execution moments (rs_{ij}). In addition, it should be noted that a cost of unavailability of the system (C_d) with a value of 50 (μm), which represents the cost of stopping the system for a unit of time is incorporated.

Now, it is important to note that in the case of the experimentation presented above, a fair comparison is made, where each for tolerance scenario, individually, there is the same amount of activity (J_i) to be executed in the planning horizon. However, in this second part of the analysis, since tolerance cases of different models are not being

incorporated, but the different risk values for certain tolerance levels in the same model, the way in which the number of activities per tolerance level is obtained is by testing, that is, find manually and iteratively the number of activities that are achieved to execute within the given planning horizon (see Table 5).

As it can be observed, for all tolerance levels from 0% to 9% there is the same number of executions per activity; however, for scenarios in which the tolerance exceeds this last value, the number of executions is different: one less activity 5 is executed and an extra activity 4 is executed. Now, with the parameters already incorporated in the model, it is possible to calculate the risk associated with each grouping scheme. Given this, the following are the results, in tabular form, of the risk costs sensitized by tolerance level from 0% to 20%, together with the levels of unavailability obtained (see Table 6).

To know the behaviour of each of the costs presented, a line graph is generated where these 3 variables are unified:

From the graphical representation in Figure 8 it can be observed how the total risk associated with each grouping scheme behaves together with its two components, the cost of tentative risk and cost of grouping risk. If the first case is analysed, where a 0% tolerance is contemplated to advance or delay maintenance activities, there is a total cost of 320 (μm), in which 230 (μm) correspond to the tentative risk and 90 (μm) represent the cost of grouping. The fact that the costs of tentative risk are greater than those of grouping makes total sense, given that, since there are not so many cases of grouping, most of the activities are executed in their tentative moments. In addition, it is noteworthy that the costs per grouping mean 28.2% of the total costs, since at that level of tolerance there is a fairly small number of grouped activities, so it is evident the importance, in terms of cost, of generating grouping packages.

However, when the percentage of tolerance allowed increases, each of the variables presented has some variation and trend. In particular, grouping costs increase more than tentative costs decrease, causing total costs to increase due to the formation of grouping packages. This is entirely consistent with the implication of increasing tolerance levels, since theoretically and practically increasing time windows so that activities can modify their execution moments favours the creation of grouping packages. It is observed that both cost components have similar increases and reductions. If certain points are analyzed, it is interesting to analyse the scenario in which the results are sensitized with a tolerance 14%, where the total cost reaches the highest value of the entire series and with a total unavailability of 2.71 (sem). In addition, in terms of the trend generated in this cost function, preferably the total cost tends to stabilize, even more, to go down along with the increase in the level of tolerance, except for certain intervals where the local maximums are located. On the other hand, when the tolerance increases from 3% to 4%, a greater increase is generated than the trend with which the grouping costs increase to that level. In the same way, the costs for tentative executions suffer the greatest drop of the entire series. In short, there is no considerable increase or decrease in total costs, however, it is interesting to note that the origin of this behaviour is due to the fact that the generation of grouping packages at that tolerance level is such that their quantity is allowed and increased more than at any other tolerance level. Furthermore, it is evident that the minimum value of unavailability is reached in the scenario of 12%, maintaining this value up to 20%, which is equivalent to a reduction of 52% with respect to unavailability in the scenario in which there is no tolerance. Now, regarding the risk, in this set of tolerance levels there is a downward trend, which is attributable to the preference of advancing maintenance activities by the optimization model, that is, the greater the permissibility to form grouping schemes, the model will choose to advance activities.

To complement the basis for making a correct decision, it is necessary to know the behaviour of the indicators proposed in Section 3.1. In view of this, each of the 5 indicators regarding the grouping schemes determined by the tolerance level is presented (see Table 7).

As for the first three indicators, which measure the percentage of activities advanced, delayed, and executed in their tentative moments (f_A, f_D, and f_J, respectively), it can be observed that as the level of tolerance increases, the number of activities executed in their tentative instant decreases rapidly, going from a 89% when there is no tolerance to only 23% at the highest level. On the other hand, the activities advanced or delayed increase consecutively with the increase in tolerance between 0% and 5%, and then, at the end of the series, show certain downward trends for the activities advanced and upwards for the delayed activities. Now, in order to visualize the behaviour graphically, the following line graph of these three indicators is presented (see Figure 9).

Figure 9 makes it possible to observe the behaviour that each of these indicators has, due to the increase in the level of tolerance allowed. From 0% to 4% tolerance, categorically there is a decrease in the activities carried out in their tentative moments together with an increase in advanced or delayed activities. From 5% to 11% there is a balanced behaviour between the three indicators without implications between them, given that the percentage of activities advanced or delayed do not have a defined behaviour, but in some tolerance levels there is greater advance than delay, while between 12% and 20% there is an upward trend for advanced activities and a decrease for delayed activities. To analyse the two remaining performance indicators, which represent the percentage of use of the tolerance of advanced activities (A^{AV}) or delayed activities (D^{AV}), a line graph is presented to define their behaviour (see Figure 10).

As can be seen, the percentage of use of the tolerance of the advanced activities represented by the green line presents a higher value than the delayed activities in all scenarios, except for two points, corresponding to 3% and 9% tolerance. The latter will eventually make it possible to identify why costs behave in such a way.

In this sense, if one analyses particularly the case in which the tolerance has a 9%, it can be noted that in the cost function a local maximum is reached, with 370 (μm). In addition, the percentage of delayed activities is 8% higher

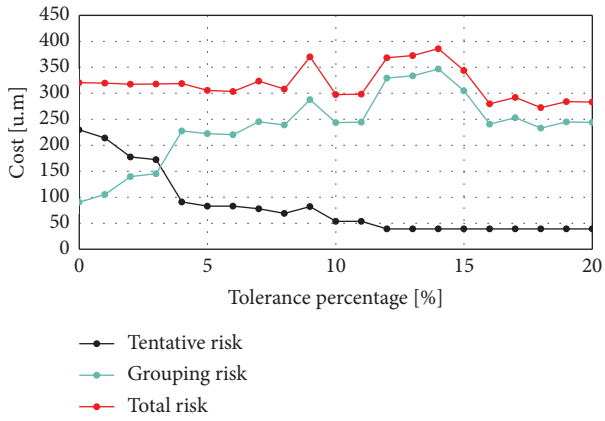

Figure 8: Cost per probability of failure for the different tolerance levels.

Table 7: Variation of the five performance indicators regarding the use of time window tolerances.

e (%)	f_A (%)	f_D (%)	f_J (%)	A^{AV} (%)	D^{AV} (%)
0	11	0	89	—	—
1	20	9	71	42	0
2	17	20	63	18	16
3	14	26	60	12	21
4	23	43	34	47	29
5	40	26	34	46	17
6	37	26	37	32	23
7	37	31	31	30	21
8	31	37	31	32	23
9	29	37	34	18	25
10	34	34	31	36	24
11	31	37	31	31	24
12	43	34	23	41	25
13	43	34	23	39	22
14	43	34	23	38	20
15	43	34	23	36	18
16	51	26	23	39	12
17	51	26	23	41	9
18	51	26	23	42	7
19	57	20	23	42	6
20	71	6	23	43	6

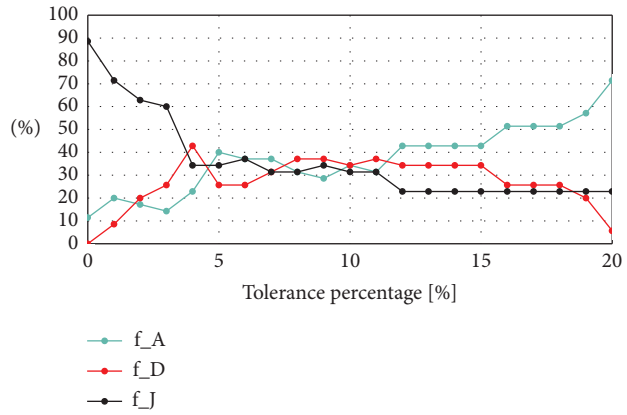

Figure 9: Evolution of the performance indicators of the activities advanced, delayed, or executed in their tentative moments.

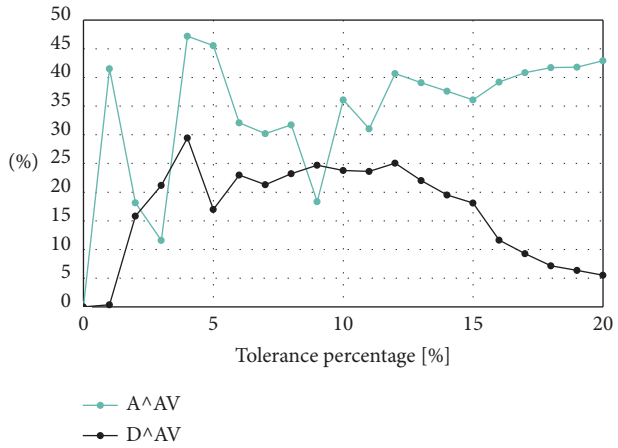

Figure 10: Evolution of the performance indicators of the use of tolerance of delayed or delayed activities.

than those advanced and 3% higher than those executed in their tentative moments. On the other hand, complementing this data with the one exposed in the previous paragraph, it can be explained in greater detail why this increase in costs exists, and it is only due to the fact of decreasing the use of tolerances in advanced activities and, on the other hand, increasing that of delayed activities. This generates that by further delaying the activities, the probability of failure of the components increases, pushing the cost function values to increase.

In short, the risk results are consistent with each of the grouping schemes obtained from the previous optimization of the unavailability of the system. At a higher level of risk, the grouping schemes display a behaviour that favours delaying a greater number of activities, or failing that, using in greater quantity the tolerances of each of these, or, as the cost decreases, a greater number of advanced activities can be observed accompanied by a greater use in the tolerance to advance these activities. However, in order to obtain results with respect to the optimal tolerance level of each grouping scheme, the third risk component is incorporated, which corresponds to the use of the useful life of the components with respect to advance in their execution times. Given this, the results associated with each tolerance level along with their respective graphical representation of this new risk are presented (see Table 8), generated by the sum of costs per grouping, costs for tentative executions, and cost of useful life.

Regarding these results, it can be observed that as the tolerance level increases, the imputed costs per useful life used of each of the components increase, making it clear that the fact of increasing tolerance levels implies an increase in the use of tolerance and therefore, an increase in these useful life costs. Now, with respect to the total costs by risk, that is, if the costs for grouping, tentative executions, and useful life are added, the cost function shown in Figure 11 (green) is obtained, where it is observed that with the increase in tolerance the costs would tend to increase, however, with certain drops, followed by prominent increases.

Table 8: Variation of useful life costs and total costs with respect to tolerance levels.

e (%)	Total cost (μm)	Useful life cost (μm)	Total cost + useful life cost (μm)
0	320	6.6	327
1	319	8.3	328
2	317	7.2	325
3	318	10.1	328
4	319	26.3	345
5	306	56.1	362
6	303	39.5	343
7	323	59.6	383
8	308	65.2	373
9	370	67.0	437
10	298	106.6	404
11	298	104.7	403
12	368	119.2	488
13	373	123.7	496
14	386	127.8	514
15	344	131.2	475
16	280	178.9	459
17	292	196.0	488
18	272	211.7	484
19	284	234.3	518
20	238	222.8	461

Given the above, in order to make a correct decision regarding the optimal tolerance levels, the commented bumps allow to establish which scenario is the most appropriate, however, it will always depend on who makes the decision to choose the tolerance levels. This, given that each decision maker must previously recognize what their objectives and limitations are. For example, if decision makers want to maximize the level of unavailability without sacrificing more than 360 (μm), the most advisable option would be to use a grouping scheme with 6% tolerance. However, if for any reason, it is not technically possible to establish such a tolerance level, it would not be advisable to choose the grouping scheme associated with 5%, since with a level of 4% a relatively similar level of unavailability is obtained without an unjustifiable increase in costs. On the other hand, if the only thing that interests is to minimize the unavailability of the system without cost restrictions, the recommended option would be to use a 16% tolerance. In this way, whenever a decision maker wants to select their appropriate tolerance level, they will have all the necessary information to carry out their choice in the most informed way possible, considering both the costs of failure probability, the costs of useful life, and the unavailability of the system associated with each of the grouping schemes.

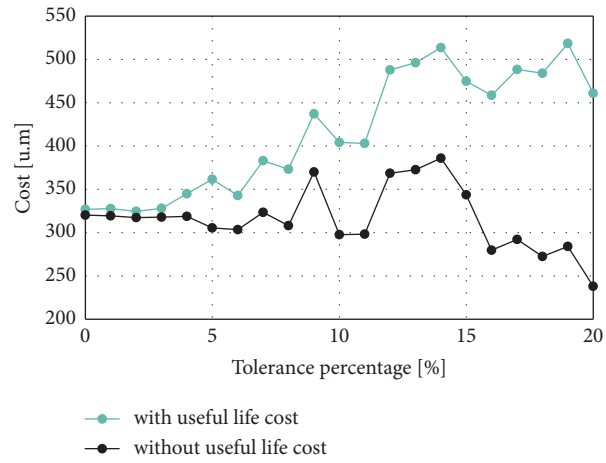

Figure 11: Evolution of total and lifetime costs with respect to each permitted tolerance level.

4.2.2. Analysis for Different Instances. Although the corresponding risk analysis has been performed, the question arises of knowing the behaviour of the results provided by the optimization model in general terms, that is, establishing whether the behaviour of using tolerances and distribution of activities is similar for any case of experimentation or will depend exclusively on the input parameters of the model. Given this, 4 new cases are presented below, which differ from the one presented in the previous section in the periodicities and execution times of each of the activities, in addition to reducing the number of components to 4 with the aim of reducing the computational complexity and resolution times of the optimization model. In this sense, the reason why the number of activities is reduced is due to the fact that in these 4 new cases of experimentation, from 0% to 25% tolerance will be sensitized with a resolution of 5%, in order to know the behaviour of the activities with a higher level of freedom to configure the moments of execution of the PM activities. That is, the number of equipment or components, cost parameters, and failure probability distribution parameters are maintained (see Table 9).

First, the results of unavailability and resolution times for each of the instances analysed are presented (see Table 10). Regarding the resolution times, it can be observed that these increase exponentially as the tolerance level increases, even reaching more than 11 hours in the third case

Table 9: Executions times and periodicities of each PM activity.

Act	Case 1		Case 2		Case 3		Case 4	
	p_i (hrs)	T_i (wks)	p_i (hrs)	T_i (wks)	p_i (hrs)	T_i (wks)	p_i (hrs)	T_i (wks)
1	15	4	20	5	15	3	15	4
2	30	7	15	6	25	8	20	5
3	40	10	35	9	36	9	30	9
4	48	13	50	10	48	13	48	11

Table 10: Resolution times and unavailability results in order to tolerance factor e.

e (%)	Case 1		Case 2		Case 3		Case 4	
	Res. time (secs)	Unav. (weeks)	Res. time (secs)	Unav. (weeks)	Res. time (secs)	Unav. (weeks)	Res. time (secs)	Unav. (weeks)
0	0.8	4.1	1.0	3.7	1.2	4.1	1.8	4.0
5	3.3	3.4	10.9	3.4	14.3	3.1	5.4	3.4
10	16.8	3.0	49.3	2.4	64.6	2.7	328.6	2.7
15	46.3	2.5	133.0	2.1	1499.5	2.6	808.0	2.2
20	445.7	2.4	1677.2	2.1	13837.9	2.5	2304.5	2.1
25	22850	2.3	22323.2	2.1	40808.8	2.3	18917.7	2.1

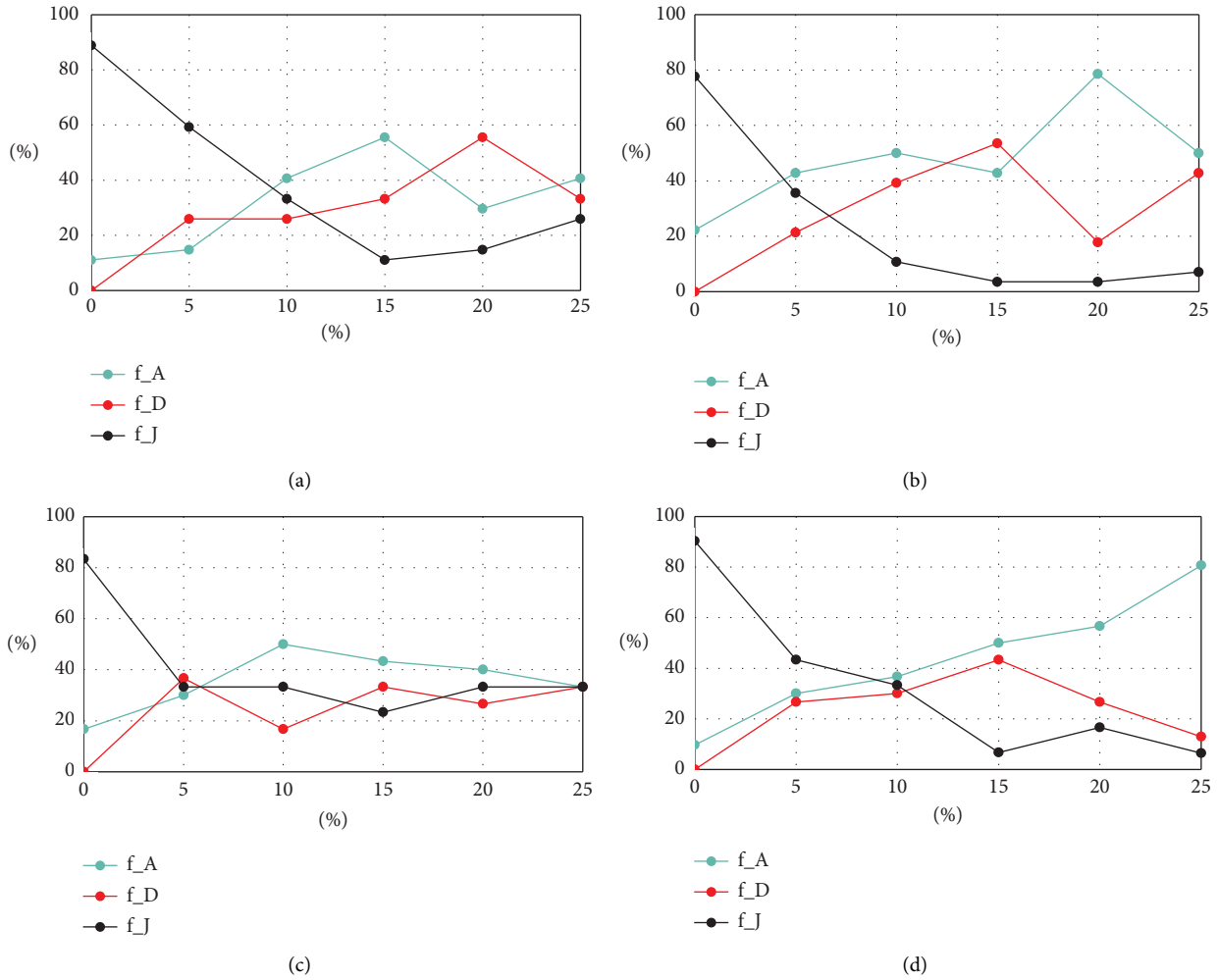

Figure 12: f_A, f_D and f_J evolution, from 0% to 25% of tolerance factor e. (a) Case study 1. (b) Case study 2. (c) Case study 3. (d) Case study 4.

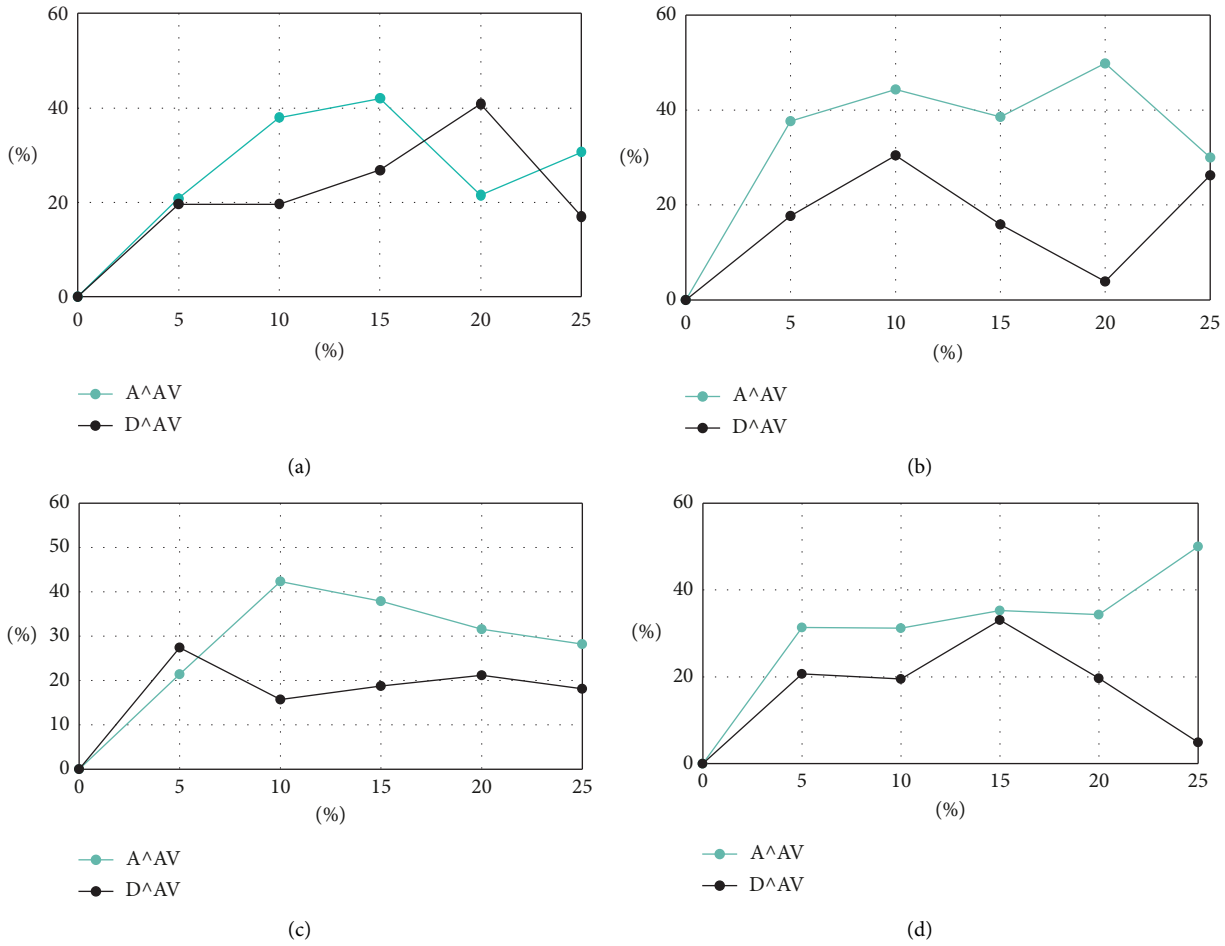

FIGURE 13: A^{AV} and D^{AV} evolution, from 0% to 25% of tolerance factor e. (a) Case study 1. (b) Case study 2. (c) Case study 3. (d) Case study 4.

of experimentation at 25%. Moreover, regarding the total unavailability of the system in the planning horizon of 52 weeks, it is obtained that at 10% tolerance a reduction of between 28% and 35% is achieved with respect to the scenario in which there is no permissibility for the activities to change their moments of tentative execution, while when the tolerance is 20% the reduction of unavailability varies between 39% and 48%, to finally, in the 25% tolerance, vary between 43% and 48%.

Furthermore, in order to know the behaviour of the number of executions that are advanced, delayed, or executed in their tentative moments, the results associated with the indicators are presented f_A, f_D, and f_J through the following line graphs (see Figure 12). In the first place, it can be observed that as in the case of original experimentation, all new cases show a similar behaviour in terms of the decrease in the activities carried out in their tentative moments together with the increase of those that are delayed or delayed. In the first tolerance range, between 0% and 5%, cases 2, 3, and 4 tend to level the number of executions of each type of activity, with percentages within 20% to 40% each, while case 1 is the only scenario where levelling is reached at 10%. On the other hand, from 5% to 15% tolerance, cases 1 and 3 maintain a certain stabilization, while in cases 2 and 4 the number of activities carried out at their tentative moment tends to decrease considerably along with the increase in delayed or advanced activities. Subsequently, between 15% and 25% tolerance, cases 2 and 4 show a behaviour similar to the base case, where the activities carried out in their tentative moments maintain a downward trend, while the advanced ones tend to increase, which obviously implies a decrease in the delayed ones. It should also be noted that, in general, the activities carried out in advance have a higher proportional percentage than those delayed, implying that the optimization model would tend to privilege the advancement of PM activities for the minimization of total unavailability of the system.

Now, with respect to the indicators A^{AV} and D^{AV}, their evolution within the same tolerance range is shown below (see Figure 13). On this occasion, the behaviour of the indicators is not so similar with respect to the base case in terms of the trend generated when graphing the results; however, it can be seen that in only 2 of the 24 resolved instances the percentage of use of the time windows to delay activities is greater than that of advancing them, which if it is consistent with what is stated in the development of the case of base experimentation; that is, independent of the number of activities that are delayed or advanced, the use of tolerance is greater for advanced activities and increases with the tolerance level.

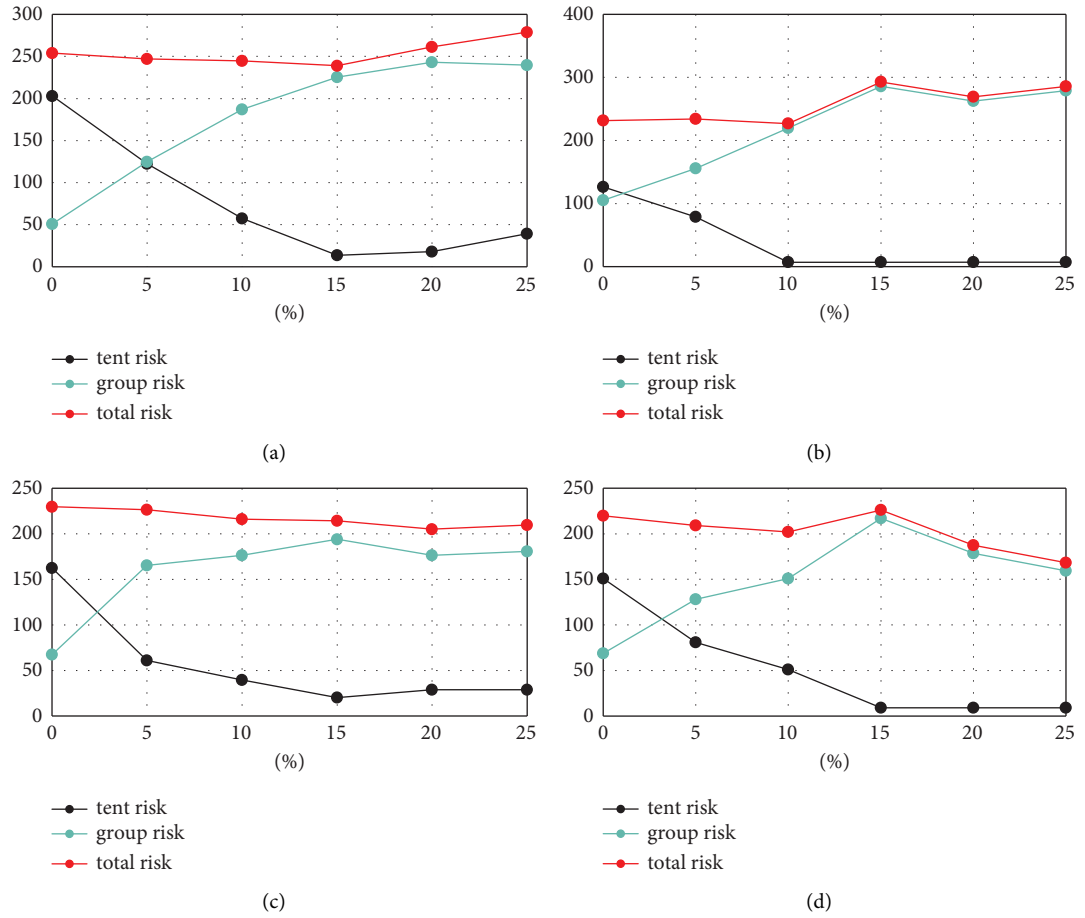

Figure 14: Tentative, grouping and total risk evolution, from 0% to 25% of tolerance factor e. (a) Case study 1. (b) Case study 2. (c) Case study 3. (d) Case study 4.

Finally, in terms of the risk analysis of each of the cases presented, the graphic results of tentative risk, pooling risk, and total risk per instance are shown as follows (see Figure 14). It can be observed that in each of the cases the same behaviour is obtained as in the base case, that is, a prominent increase in the risk by grouping and an abrupt fall in the risk by activities carried out in their tentative moments. On the other hand, in cases 1 and 2, there is an upward trend in risk, while in cases 3 and 4, a decrease, as is obtained in the case of base experimentation. In this sense, the behaviour and trend of total risk, consisting of tentative risk and groping risk, is fully consistent with the results of the performance indicators, however, as in the analysis of the base case, to know the real behaviour of the risk, it is necessary to add the component of risk for useful life, which penalizes the advancement of maintenance activities.

As observed, in each of the cases the trend of the total cost considering useful life is to increase, which establishes and confirms the correct relationship between the fact of penalizing the activities for units of useful life not used of a component. However, it is important to clarify that these results depend exclusively on the cost parameters added to the analysis.

Therefore, it can be observed in Figure 15 that the level of optimal tolerance that emanates from the sensitization of these 4 cases of experimentation does not have a specific value, since it will depend on: the risk that the decision maker intends to assume before the execution of a maintenance plan; the percentage of tolerance in which it is allowed to delay or delay the tentative activities; and what is the value to the that you are satisfied with the optimization of the unavailability of the system. In this sense and given that we are in presence of a risk function that delivers results with local minimums and maximums, the recommendation of the optimal tolerance percentages will vary by sections. On the other hand, since the risk analysis will vary according to the cost parameters of each case of experimentation, the real contribution of this is to generate a practical tool that has the utility of knowing the implications of forming schemes of the grouping of PM activities in terms of the probability of failure of the components, which adapts to different scenarios. However, from the point of view of the optimization model, the results are interesting, since it is found that it tends to advance maintenance activities and to make greater use of tolerance to advance, which is evident in each of the case studies.

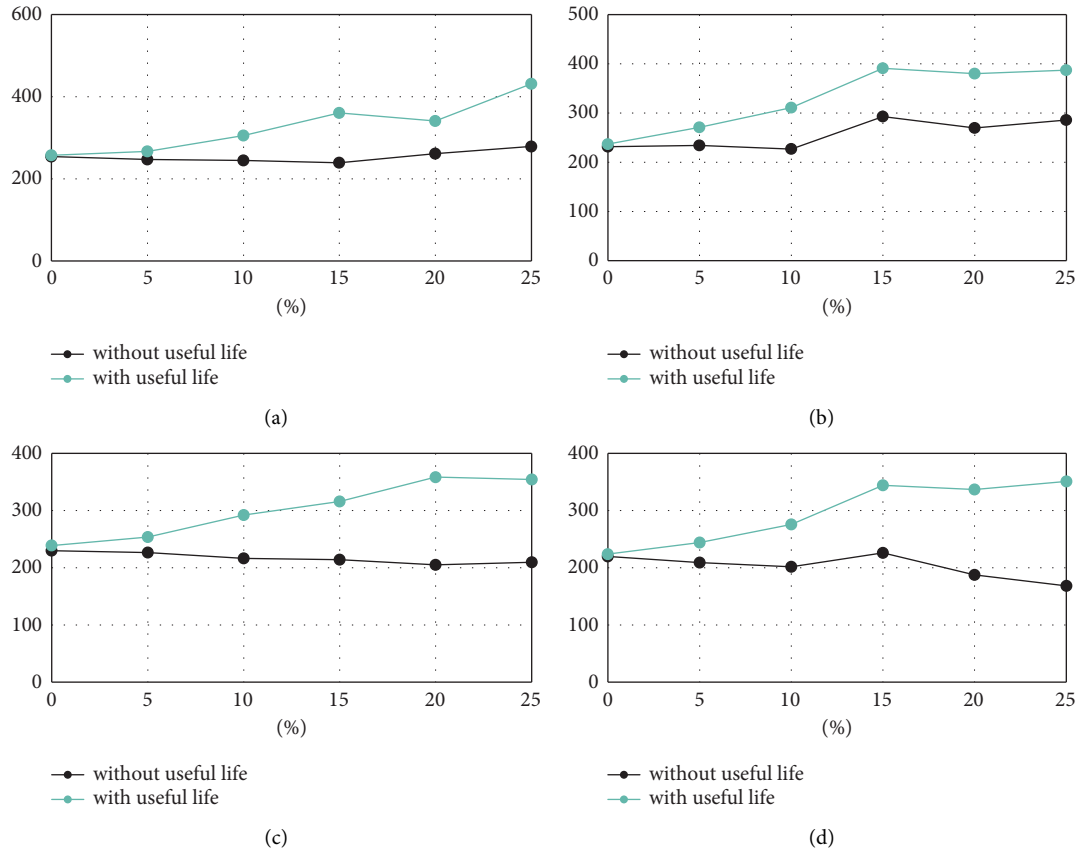

Figure 15: Useful lifetime risk evolution, from 0% to 25% of tolerance factor e. (a) Case study 1. (b) Case study 2. (c) Case study 3. (d) Case study 4.

5. Conclusions

The main objectives of this research are: to be able to provide a decision maker with sufficient tools to choose the best alternative, in terms of risk, within a spectrum of schemes of preventive maintenance activities; and to know the general behaviour of the optimization model for different scenarios. That is why with everything exposed through this article, and in coherence with the objectives set at the beginning, it can be confirmed that these have been fully fulfilled. In specific terms, it has been necessary to meet certain essential milestones, such as the identification of assumptions, criteria, and limitations for the formulation of an optimization model, and the subsequent generation of a tool capable of quantifying risk and behaviour in the formation of grouping schemes.

In terms of results, quite conclusive and interesting behaviours are evidenced with respect to the optimization model developed, particularly in the trend towards the advance in maintenance activities and the formation of new grouping packages that allow to further minimize the times of total unavailability of the system. In contrast with the original framework, the proposed extended framework has achieved:

(1) More flexibility to advance or delay overlapping activities: the original framework forced the start moment of grouped activities and disregarded the importance of overlapping activities.

(2) Risk analysis: the postoptimal analysis along with the proposed performance indicators enables the decision maker to better inform their decisions and have more options available.

Furthermore, although the objectives of the research have been achieved, it is essential to establish that there were certain limitations within the computational formulation of the optimization model. While it is true that the main objective of the research is to establish an optimal tolerance level with respect to the risk represented by a grouping scheme, this analysis is carried out after minimizing the unavailability of the system. Given this, each time the risk level is obtained, it is limited to the fact that the grouping scheme obtained after executing the optimization model disregards the risk associated with the formation of PM activity grouping packages. Therefore, to eventually eliminate the bias present in such a situation, it is advisable to formulate an objective function within the optimization algorithm that incorporates the risk component. For this, one of the best known and most proven methods is that of a multi-objective model, for which it is necessary to establish the weights of each of the variables that are intended to be incorporated, which in this case would correspond to unavailability and the risk of advancing or delaying activities. Another alternative corresponds to that of including within the objective function of the current model, a cost function

that involves the risks and costs due to the unavailability of the system, in this way, within the same function both variables would be incorporated. This last recommendation arises after that, in the first instance, it was the way in which it was intended to address the problem, however, the fact of including the risk function within the objective function transformed the nature of the problem, going from being a MILP model to an MINLP model, which corresponds to a mixed integers nonlinear programming. These types of problems have the characteristic of having a high mathematical and computational complexity, so to solve them it is necessary to solve some "solver" capable of handling them since the "Gurobi" that is the one that was used in the research only manages to solve the MILP problems. Given this, using the "Mindtpy" tool, which is able to incorporate a solver of the NP type and another of the MILP type through a degradation algorithm, the problem was addressed, however, the computational complexity of incorporating the Weibull accumulated probability function turned out to be so high that the model proved infeasible. Under this scenario, other tools were sought and unfortunately, those that potentially seemed useful, such is the case of the "Baron" solver. In this context, it is recommended to reduce the computational complexity of the model to incorporate the probability function.

Data Availability

The data used to support the findings of this study are included within the article.

Conflicts of Interest

The authors declare that they have no conflicts of interest.

References

[1] A. Sharma, G. S. Yadava, and S. G. Deshmukh, "A literature review and future perspectives on maintenance optimization," *Journal of Quality in Maintenance Engineering*, vol. 17, no. 1, pp. 5–25, 2011.

[2] C. Wang and S. Hwang, "A stochastic maintenance management model with recovery factor," *Journal of Quality in Maintenance Engineering*, vol. 10, no. 2, pp. 154–165, 2004.

[3] D. W. Coit and E. Zio, "The evolution of system reliability optimization," *Reliability Engineering & System Safety*, vol. 192, Article ID 106259, 2019.

[4] B. de Jonge and P. A. Scarf, "A review on maintenance optimization," *European Journal of Operational Research*, vol. 285, no. 3, pp. 805–824, 2020.

[5] P. Viveros, R. Mena, E. Zio, L. Miqueles, and F. Kristjanpoller, "Integrated planning framework for preventive maintenance grouping: a case study for a conveyor system in the Chilean mining industry," *Proceedings of the Institution of Mechanical Engineers - Part O: Journal of Risk and Reliability*, p. 1748006X2110537, 2021.

[6] S. Petchrompo, H. Li, A. Erguido, C. Riches, and A. K. Parlikad, "A value-based approach to optimizing long-term maintenance plans for a multi-asset k-out-of-N system," *Reliability Engineering & System Safety*, vol. 200, Article ID 106924, 2020.

[7] C. Zhu, S. Tang, Z. Li, and X. Fang, "Dynamic study of critical factors of explosion accident in laboratory based on FTA," *Safety Science*, vol. 130, p. 104877, 2020.

[8] V. Vijayan and S. K. Chaturvedi, "Multi-component maintenance grouping optimization based on stochastic dependency," *Proceedings of the Institution of Mechanical Engineers - Part O: Journal of Risk and Reliability*, vol. 235, no. 2, pp. 293–305, 2021.

[9] R. Laggoune, A. Chateauneuf, and D. Aissani, "Impact of few failure data on the opportunistic replacement policy for multi-component systems," *Reliability Engineering & System Safety*, vol. 95, no. 2, pp. 108–119, 2010.

[10] J. S. Nielsen and J. D. Sørensen, "Computational framework for risk-based planning of inspections, maintenance and condition monitoring using discrete Bayesian networks," *Structure and Infrastructure Engineering*, vol. 14, no. 8, pp. 1082–1094, 2017.

[11] E. Arzaghi, M. M. Abaei, R. Abbassi, V. Garaniya, C. Chin, and F. Khan, "Risk-based maintenance planning of subsea pipelines through fatigue crack growth monitoring," *Engineering Failure Analysis*, vol. 79, pp. 928–939, 2017.

[12] Y. Zhou, G. Kou, H. Xiao, Y. Peng, and F. E. Alsaadi, "Sequential imperfect preventive maintenance model with failure intensity reduction with an application to urban buses," *Reliability Engineering & System Safety*, vol. 198, Article ID 106871, 2020.

[13] A. Consilvio, A. D. Febbraro, and N. Sacco, "A rolling-horizon approach for predictive maintenance planning to reduce the risk of rail service disruptions," *IEEE Transactions on Reliability*, vol. 70, no. 3, pp. 875–886, 2021.

[14] Z. Liang, H. Chen, S. Chen, Y. Wang, C. Zhang, and C. Kang, "Robust transmission expansion planning based on adaptive uncertainty set optimization under high-penetration wind power generation," *IEEE Transactions on Power Systems*, vol. 36, no. 4, pp. 2798–2814, 2021.

[15] M. Li, M. Wang, J. Kang, L. Sun, and P. Jin, "An opportunistic maintenance strategy for offshore wind turbine system considering optimal maintenance intervals of subsystems," *Ocean Engineering*, vol. 216, Article ID 108067, 2020.

[16] R. Mena, P. Viveros, E. Zio, and S. Campos, "An optimization framework for opportunistic planning of preventive maintenance activities," *Reliability Engineering & System Safety*, vol. 215, Article ID 107801, 2021.

[17] T. Wu, L. Yang, X. Ma, Z. Zhang, and Y. Zhao, "Dynamic maintenance strategy with iteratively updated group information," *Reliability Engineering & System Safety*, vol. 197, Article ID 106820, 2020.

[18] P. Do Van, A. Barros, C. Bérenguer, K. Bouvard, and F. Brissaud, "Dynamic grouping maintenance with time limited opportunities," *Reliability Engineering & System Safety*, vol. 120, pp. 51–59, 2013.

[19] E. Rezaei and D. M. Imani, "Maintenance risk based inspection optimization model in multi-component repaiable system with economic failure interaction," in *Curr. Trends Reliab. Availability, Maintainab. Saf*, U. Kumar, A. Ahmadi, A. K. Verma, and P. Varde, Eds., pp. 611–620, Springer International Publishing, Cham, 2016.

[20] H. Li, W. Zhu, L. Dieulle, and E. Deloux, "Condition-based maintenance strategies for stochastically dependent systems using Nested Lévy copulas," *Reliability Engineering & System Safety*, vol. 217, p. 108038, Article ID 108038, 2022.

[21] J. L. Oakley, K. J. Wilson, and P. Philipson, "A condition-based maintenance policy for continuously monitored multi-component systems with economic and stochastic

dependence," *Reliability Engineering & System Safety*, vol. 222, Article ID 108321, 2022.

[22] H. Moakedi, M. S. Seyedhosseini, and K. Shahanaghi, "A block-based inspection policy for a multi-component system subject to two failure modes with stochastic dependence," *Journal of Quality in Maintenance Engineering*, vol. 25, no. 2, pp. 314–339, 2019.

[23] T. Nguyen, E. Deloux, and L. Dieullez, "Maintenance policies for an heterogeneous two-component system with stochastic and economic dependencies," *IFAC-PapersOnLine*, vol. 49, no. 12, pp. 787–792, 2016.

[24] F. Kristjanpoller, N. Cárdenas-Pantoja, P. Viveros, and R. Mena, "Criticality analysis based on reliability and failure propagation effect for a complex wastewater treatment plant," *Applied Sciences*, vol. 11, no. 22, p. 10836, 2021.

[25] F. Kristjanpoller, P. Viveros, N. Cárdenas, and R. Pascual, "Assessing the impact of virtual standby systems in failure propagation for complex wastewater treatment processes," *Complexity*, vol. 2021, pp. 1–12, 2021.

[26] A. Jiang, Z. Huang, J. Xu, and X. Xu, "Condition-based opportunistic maintenance policy for a series–parallel hybrid system with economic dependence," *Journal of Quality in Maintenance Engineering*, vol. 28, no. 3, pp. 584–605, 2021.

[27] P. Viveros, R. Mena, E. Zio, and S. Campos, "Optimal grouping and scheduling of preventive maintenance activities," in *Proceedings of the 30th Eur. Saf. Reliab. Conf. 15th Probabilistic Saf. Assess. Manag. Conferences*, pp. 2915–2922, Research Publishing Services, Venice, May 2020.

[28] H. C. Vu, P. Do, A. Barros, and C. Bérenguer, "Maintenance grouping strategy for multi-component systems with dynamic contexts," *Reliability Engineering & System Safety*, vol. 132, pp. 233–249, 2014.

[29] P. Do and A. Barros, "Maintenance grouping models for multicomponent systems," in *Math. Appl. To Eng*, pp. 147–170, Elsevier, London, United Kingdom, 2017.

[30] G. Kou, H. Xiao, M. Cao, and L. H. Lee, "Optimal computing budget allocation for the vector evaluated genetic algorithm in multi-objective simulation optimization," *Automatica*, vol. 129, p. 109599, Article ID 109599, 2021.

[31] M. Kijima, "Some results for repairable systems with general repair," *Journal of Applied Probability*, vol. 26, no. 1, pp. 89–102, 1989.

[32] M. Szymkowiak, "Characterizations of distributions through aging intensity," *IEEE Transactions on Reliability*, vol. 67, no. 2, pp. 446–458, 2018.

[33] X. Zhang, "Statistical inference of varying-stress accelerated life test with competing failures based on three-parameter Weibull distribution," *Journal of Mechanical Engineering*, vol. 50, no. 14, p. 42, 2014.

[34] J. Moubray, *Reliability-Centered Maintenance*, Butterworth-Heinemann, China, 1999, https://www.elsevier.com/books/reliability-centered-maintenance/moubray/978-0-7506-3358-1, 2nd edition.

Hindawi
Complexity
Volume 2022, Article ID 4935834, 12 pages
https://doi.org/10.1155/2022/4935834

Research Article

Linking Psychological Ownership to Innovative Behaviour in the Workplace: Empirical Evidence from Complex Management Systems in Pakistan

Minhas Mahsud,[1] Hao Jinxing,[2] Zafar Mahsud,[2] Zhiqiang Chen,[2] and Mumuni Napari Hanifatu[3]

[1]*National University of Sciences and Technology, Islamabad, Pakistan*
[2]*School of Economics and Management, Beihang University, Beijing, China*
[3]*Tamale Technical University, Tamale, Ghana*

Correspondence should be addressed to Mumuni Napari Hanifatu; hanifatu@aims.edu.gh

Received 22 May 2022; Accepted 16 September 2022; Published 5 October 2022

Academic Editor: Yu Zhou

This research work investigates the association between psychological ownership and innovative behaviour with knowledge hiding and knowledge sharing as mediators. The latter variables are presented as focal antecedents of preventive and promotive psychological ownership. To conduct the study, a theoretical framework was proposed, and data was collected from professionals working in complex management systems in Pakistan. The analysis revealed that knowledge hiding and knowledge sharing can exist simultaneously, and psychological ownership can evoke both positive and negative feelings in employees, which poses a challenge for the management. The results illustrate that psychological ownership has significant associations with knowledge hiding, knowledge sharing, and innovative behaviour. Consequent theoretical contributions and important managerial implications are discussed at the end.

1. Introduction

Research extensively illustrates that innovative behaviour is the most besought quality in employees for sustaining competitive advantage in today's dynamic workplace environment. Given increasingly turbulent conditions, intense competition, and rapid technological advancement, organizational leaders are acknowledging that they need to design frameworks that facilitate innovative behaviour in employees. With these notions, a theoretical model linking psychological ownership (PO) with innovative behaviour (IB) via knowledge sharing (KS) and knowledge hiding (KH) within complex management systems in Pakistan was built and tested. One of the most compelling means of producing PO is when one creates something [1], and employees that come up with new ideas and techniques may be thought of as having a greater sense of PO. Ownership was once only talked about with respect to legality and shares, but recently, studies in management have observed the growth of the PO construct as a significant individual-level predictor of workplace behaviours. Theories for PO have been developed to a certain degree, but empirical research is inadequate.

Considering the innate necessity to own and the significance of claiming in organizations, it is interesting to explore the feelings of ownership (promotive and preventive) by examining its linkages with other important constructs such as knowledge sharing, knowledge hiding, and innovative behaviour. Prior studies have mostly researched the factors that lead to KS [2], but those leading to KH have not been investigated enough, creating a gap for research into the lack of knowledge transfer within organizations. Since knowledge transfer has been cited as the most important factor for inducing IB, it is imperative to understand why employees hide knowledge and what could drive them

to share knowledge. PO theory may provide a potential explanation for the way employees behave with respect to knowledge; preventive PO (territoriality) results in KH, and promotive PO (accountability, belongingness, self-efficacy, and self-identity) results in KS. We extend past research on PO, IB, and KS and endeavour to fill the research gaps in KH in the organizational context.

1.1. Theoretical Foundations. Prior research has investigated how people begin to assume themselves as owners of an object and how they assimilate that object within the self-domain. For PO development in employees, three sources have been identified [3]. The first is "control," where one feels like the owner of the objects over which one has control. Next is "intimate knowledge," where the more one knows something well, the more one feels tied to that object/task. The third source is "self-investment," where one feels a sense of ownership because one has invested resources and/or time into an entity. PO has primarily been categorized into two types [4]. One is preventive, which is characterized as territoriality. Territoriality is the sense of being defensive or possessive, including not wanting to share and assuming oneself solely responsible for a certain entity (resource/idea). The second type is promotive, which is comprised of four elements (accountability, self-efficacy, belongingness, and self-identity). Preventive PO is the more defensive form, and promotive PO is the more constructive one [5]. PO theory implies that the form is driven by situational considerations; one's perceived or cognitive ownership is driven to immensely impact expressed mannerism in cooperative settings [6]. A sense of ownership towards knowledge, ideas, and creativity could hence have a critical part in the transfer of knowledge and IB of employees in different work environments. Researchers have deliberated on how people functioning in differing circumstances with distinct possession aims carry unique motives to trigger the sense of ownership [7, 8]. Theorists claim that both positive and negative outcomes could be generated by PO. Positive outcomes comprise most of the organizational citizenship behaviours, including innovation and striving for competitive advantage, whereas the unfavourable outcomes comprise reluctance to accept advice, relational conflict, defiance to change, etc.

Preventive PO signifies that one wants to control the object of PO as their territory. One wants to control who may enter the territory or what kind of activities can happen in that territory. Territoriality or preventive PO leads to marking, signaling, and defending the object of ownership from others. In the organizational context, it can be the feeling of protecting the ideas and/or resources from others, or withholding them for oneself, thinking it is beneficial to limit the target of ownership (here, knowledge) to oneself by hiding it from others. Hence, in situations where one colleague needs certain information and the other conceals it, a KH action transpires [9]. Based on this logic, it may be argued that employees experiencing preventive PO are more likely to engage in KH to restrict the access of others to his/her ownership claim (knowledge in this case).

Therefore, we hypothesize the following:

H1a: "Preventive PO has a positive relationship with KH."

The opportunity to access specialized knowledge is one key resource of negotiating power that employees have against organizations [10]. This means that having control over that specific information (knowledge) gives the employee the power to define what compensation and/or position that employee can have and can also manipulate other terms of employment to his/her benefit. The ability to own and control information/knowledge in the organization guarantees that employee's power and status relationship. This leads to the argument that employees will build a deep preventive PO over knowledge, as it is so valuable for their survival in their employment domain. Sharing the entity one owns would mean letting go of control, leading to an unwillingness to share knowledge with others. This kind of attitude obstructs cooperation between people [11]. This could become the basis of a disagreement over the subject entity, forcing employees to retain control over the entity to prevent themselves from loss and uncomfortable emotions, thereby withholding the target. In this stream of thought, we believe a negative relationship exists between preventive PO and KS.

H1b: "Preventive PO has a negative relationship with KS."

The sense of self-worth in any employee encapsulates the degree to which one sees oneself as offering value to the organization through different practices, one of which is KS. Here, the concept of self-worth could also refer to the scale of fondness for oneself, based on competence and efficacy. Some studies [12, 13] that have presented linkages between PO and KS with a positive relationship have suggested that sharing gives employees the feeling of being appreciated and needed in the organization, which is why they are likely to engage in KS. Respect, reputation, pride, personal identification with colleagues, and even stronger feelings of commitment originate from the same stream. Individuals who believe knowledge belongs to oneself are prone to transfer knowledge as per PO theory, which postulates that PO arises in a framework where one can identify with and where one believes that outcomes that matter to them can be attained [14]. PO is prone to arise if individuals feel they exert control over the entity, know the entity well, and can probe themselves relative to the same entity. Here, we assume the target to be knowledge and the promotive PO (accountability, belongingness, self-efficacy, and self-identity) to drive the individual to have positive feelings regarding the target and strive to achieve positive outcomes for the said target, which in this context would be KS. Drawing from these theories, it is hypothesized.

H2a: "Promotive PO has a positive relationship with KS."

Prior research has recognized KS as a favourable consequence of assumed ownership [15, 16]. Organizational education captures the process from external knowledge attainment to bringing that knowledge inward and the application of the same to shape and integrate it into the social structure of the organization. PO has also been shown to increase KS and is instrumental in the enhanced value of contributions, letting one share values and knowledge [17]. The ability to identify oneself with a particular faction or organization is also considered a key component of knowledge transfer mannerism in cyber societies [6, 18]. Employees with a strong promotional PO consider themselves significant and invaluable to the workplace and thereby develop profound self-esteem [19]. Such employees invest their energies in actions that will add value and help their organizations in an attempt to augment their self-image. Such employees are not prone to commit actions that could possibly hamper the progress of their organizations. Spreading knowledge can benefit organizations in innovation and sustain their competitive advantage. On the other hand, KH is the intentional concealment of knowledge. This workplace behaviour falls into the category of counterproductive work attitudes. Employees with a strong sense of promotional PO will not practice KH in the best interest of their organizations.

These foundations support the following statement:

H2b: "Promotive PO has a negative relationship with KH."

A substantial number of theoretical and empirical inquiries have explored the constructs of creativity (idea generation) and innovation (idea exploitation), but the link between these two domains has been ignored: that is the employees' prerogative to share or restrict their new ideas with colleagues [20]. Innovation entails the continuous pursuit of novelty and rare knowledge. It follows an incessant course where limitations and restrictions originating from inadequate individual cognition are stretched and conquered by attaining a fresh dimension, a different view, or new knowledge [21]. By transferring knowledge to others, one may boost one's scope to understand a situation or problem and employ one's knowledge to provide a way out or a solution [22]. The knowledge management literature reveals that various means and processes of KS in different types of associations have constructive influences on organizational innovation capabilities, whether individual or collective [23], and that KS is necessary for crafting innovation and maiden knowledge [24].

Innovative behaviour involves three distinct tasks: idea generation (developing a new idea), idea promotion (gaining external backing), and idea application (making a model or prototype). Employees engaging in IB at work must manage knowledge continuously, in specific terms, distribute tacit knowledge [25]. Idea generation entails the creation of knowledge which recombines both external and internal knowledge into new structures [26]. Innovative work behaviour is described as "behaviour that aims to achieve the initiation and intentional introduction (within a work role, group, or organization) of new and useful ideas, processes, products, or procedures" [27]. The condition of employees internalizing more knowledge and engaging in KS fosters IB in them. IB at work can be promoted effectively by incorporating knowledge directly into the organization's business plan and encouraging norms coherent with KS. Academic researchers have emphasized the role of KS in improving IB [28]. When knowledge resources are managed in a better way, organizations ensure their improved performance [29]. It propels them towards more knowledge creation, thereby increasing their intellectual assets [30]. Employees supportive of KS internalize more knowledge, which leads to IB. Individual innovation is influenced by character, knowledge, cognitive ability, motives, and social links [31]. It has been observed that KS facilitates the nurturing of creativity [32]. Researchers revealed that knowledge movement in all directions through the organization affect the IB in mid-level managers [33]. Thus, we proposed the third hypothesis:

H3: "KS positively affects IB in employees."

Legal ownership entails legal rights, whether it is a house, a bike, or an idea, and the implications of legal ownership influence one's beliefs and actions. At the workplace, the objects signified for an individual's use are generally not taken home for personal use. If any worker understood that he/she legally owned a certain object given to him/her at work, he/she may feel justified in taking it anywhere. It is unlikely to assert legal ownership of office objects, even though one may feel tied to those objects. However, all or some of the intellectual inventions of an individual's work, even ideas, generate ownership feelings, amounting to the stance of claiming legal ownership. Consequently, if this right of ownership allows them to protect and keep their ideas from others, organizations would be restricted from innovative production. We have theorized earlier that this belief in ownership, called preventive PO will lead to KH in employees. By keeping ideas and creativity to themselves, employees prevent their employers from producing new innovations, which makes it difficult for them to continue to compete effectively. Organizational knowledge is considered the major foundation of innovation [34, 35], even though a limitation of organizational capacity is suggested [36].

Despite steps taken by the management to encourage knowledge transfer in organizations and to ease the process, employees may be hesitant to engage in KS, resulting in hindrance to innovation. The literature suggests that KH has three classifications: playing dumb, evasive hiding, and rationalized hiding [37]. The unavailability of knowledge obstructs creative and

innovative processes, whereas creativity is related to explorative and exploitative actions [38]. Moreover, innovation involves the exploitation of existing knowledge in a useful way. Researchers have suggested that KH can weaken collaboration within a team and hamper idea generation, which could negatively impact team performance [39]. KH impacts the knowledge acquisition mannerisms of both, the one who hides and the one who seeks knowledge, the communication process being a two-way stream [40]. KH exhibits a negative linkage with individual creativity, whereas creativity and IB are considered dependent upon information and knowledge sharing, thereby being affected by KH [41, 42].

This leads to the following argument:

H4: "KH negatively affects IB in employees."

Integration of knowledge resources into substantial capabilities is a key function of the organizational innovation process. This phenomenon has been given some attention by researchers; however, the IB of employees has received less attention [43]. This emphasizes the need to explore its antecedents. In this connection, PO can be regarded as a model that includes the shared notion that all workers are part owners, having the authority and responsibility to act in ways that foster positive consequences for the organization. One of the core beliefs of PO is that employees are party to the long-term interests of the organization and take actions that are motivated by this sense. These employees exhibit behaviours such as good job performance, minimizing costs, and maximizing profit innovatively [44]. Employees having a strong sense of PO consider that they are responsible for behaving in the best interest of the organization and achieving goals through innovative activities. The feelings of pride and concern, which are associated with PO, may be positively related to IB in employees. While legal ownership establishes the right of strategic control, PO focuses on the motivation to engage in it [45, 46]. Integrating the two can give a comprehensive view of how PO can be linked to IB. Since the outcome of innovation springs from a continual search for better solutions, and employee actions in the organization's best interest are triggered by the sense of PO, it can possibly explain the linkage between PO and IB.

Following such reasoning, PO addresses the need to feel effective (self-efficacy) in bringing about improvement and change, a motive which is satisfied by solving problems at work. Furthermore, a workplace is considered an employee's place to dwell (belongingness) satisfying the longing to have a place, fulfilled by the sense of having a physical space and tasks with which one identifies (self-identity). Moreover, the three routes to PO involve a high level of psychological attachment to the ownership target. This results in individuals wanting to protect their organizations, taking care of them, and improving them. In addition, the inherent motivation to safeguard what is psychologically owned forces individuals to align their actions [47]. A range of attitudes and behaviours have been indicated by Dawkins and colleagues [48], such as accomplishments and aspirations relating to the promotive form of PO and duties and obligations being concerned with the preventive form. The promotive characteristics of PO are associated with satisfying aspirations [4], encouraging one to seek new opportunities and further exploit current ones. Employees will bring about improvements and generate innovative outcomes by investing more time and energy at their workplace. Employees with a profound sense of ownership for the organization can align prospective opportunities with these anticipations, resulting in innovative outcomes [49]. In this line of thought, PO is considered an important factor for IB. The desire to engage with the ownership target and the sense of being answerable for the target will nurture IB. Such IB of employees stemming from their feelings of PO could be the antecedent for innovative outcomes in organizations. This leads us to believe that PO has a positive relationship with IB. We conclude the argument with the following hypothesis:

H5: Promotive PO positively affects an employee's IB.

Life at the workplace is territorial in nature. Every office displays nametags on the doors, personal items like photographs or mementos on desks, and arrangement of objects in a definite order, all signifying the employees' reserved regions. This kind of marking of items and spaces generates safety for the employees and makes them feel comfortable at work [11]. PO is linked with several organizational and personal effects which have a negative nature; for example, stress, resistance to change, information hoarding, and the burden of responsibility. The reasoning for the burden of responsibility and related stress here is that employees who have developed profound PO may be motivated to take on responsibility for the ownership target as a way of protecting and defending it. Depending upon the "weight" of the responsibility and/or the amount of time that one is exposed to it, taking on responsibility can cause a feeling of being overburdened. Accompanying the burden, there is likely to be a tiring effect which eventually gives way to feelings of anger and stress. This anger may not only originate in the responsibility burden, but it could be an emotional reaction arising from the invasion of marked territory. As a real-life example, those who assume responsibility for elderly parents or even children are frequently overwhelmed by the burden. Frustration and stress originating from a sense of personal loss could result when one faces the alteration of marked entities. Research suggests that stress and burnout are sure to have an unfavourable effect on creativity and innovativeness in an employee [50]. This feeling of being overwhelmed by responsibility could impede performance, making an employee unwilling and unable to innovate and go the

extra mile. Thus, we can infer that preventive PO by motivating responsibility and related stress will negatively affect IB in employees. In our previous hypotheses, we have reasoned that KS has a positive and KH has a negative relationship with IB. Continuing in this vein, if preventive PO (territoriality) causes employees to withhold knowledge and resist change, it would also have a negative effect on IB as KS is considered central to innovation.

Where employees are expected to be innovative, we anticipate "win-lose" competitive situations to arise, making the psychological owner act in self-interest against the colleagues with whom one is competing. Under such circumstances, strong territorial feelings will lead to an unwillingness to share, thereby inhibiting creativity, cooperation, quality work, and the hoarding of knowledge and information [51]. The territorial employees will possibly try to preserve their ideas and innovations to retain control and avoid risk and uncertainty. To defend ideas and innovations, one indulges in dysfunctional behaviours, such as KH, and resorts to preventive methods to beat a prospective conflict through hiding strategies, as explained in our preventive PO and KH argument. As per the evolutionary theory, innovation is endogenous, with constant and steady changes, and it is a complex process involving various players. Based on this approach, knowledge, know-how, ideas, and suggestions for problem-solving have to be shared within the organization and not "marked" and "defended" in fear of invasion. Foregoing in view, it is hypothesized:

H6: Preventive PO negatively affects an employee's IB.

The nuanced effect of PO on IB can be much more complicated if we consider it being transferred through mediators such as KS and KH. The authors focus on PO resulting in an altruistic spirit with an understanding that KS and KH are not simple constructs.

2. Methodology

To assess and confirm the causal linkages between all our variables (preventive PO with KH, promotive PO with KS, KH and KS with IB, and PO with IB), we adopted an empirical research approach. To test the hypotheses, the data was gathered from organizations having complex management systems in Pakistan. This empirical study's conduct and design followed the tenets of methodological triangulation and adept regulations for qualitative and quantitative methods [52].

2.1. Construct's Operationalization. The questionnaire was formed with the help of established scales from related PO, knowledge management, and IB literature. Table 1shows each construct's measurement details, with scale range and measurable items used in the questionnaire. Questionnaire items were gauged employing the 5-point Likert scales, ranging from 1 (strongly disagree) to 5 (strongly agree) for PO. For the other constructs, KH, KS, and IB, item responses were determined by incorporating the 5-point Likert scales anchored between 1 (never) and 5 (very frequently).

2.2. Measurements. Following Avey and colleagues [4], PO was operationalized as a construct rooted in individuals' internal motives of territoriality (preventive PO), accountability, belongingness, self-efficacy, and self-identity (promotive PO). The scale comprises 16 items that account for employees' feelings of possession. The measurement items for employees' IB were operationalized with a scale of six questions [53], which were modified to a self-reported version. For example, "develops adequate plans and schedules for the implementation of new ideas" was rephrased to "I develop adequate plans and schedules for the implementation of new ideas." For self-reported measures of innovation, empirical evidence endorses the concept that evaluating IB in terms of self-reported figures of new products or processes output is commonplace.

We were aware of the struggle of finely drawing the thin line between "innovativeness, "innovation", and "innovative behaviour." In general terms, a portfolio of indicators could be employed to calculate innovative activity, which typically include the research and development budget, number of trademarks, patents or copyrights obtained, or other subjective measures of innovation. Creativity and innovation are frequently used synonymously in literature, and the difference between these constructs is more of emphasis than of substance [27]. Creativity is, in fact, one of the inputs for innovation. The participants responded on a five-point scale stretching from "never, rarely, occasionally, frequently and very frequently."

The measurement scale for KS was developed with the help of the measurement scale of Bock and colleagues [54] that prepared items for "intention to share knowledge." The six items were modified (intention to action) to suit our study in the following way: "I intend to share any articles from newspapers/magazines/journals that I find useful and related to our work with members of my organization" was rephrased as "I share any articles from newspapers/magazines/journals that I find useful and related to our work with members of my organization." The items (three of each type) reflect whether implicit or explicit knowledge sharing occurs. For KH, the measurement scale developed by Connelly and colleagues was adopted [9]. The dimensions of KH selected for this study are playing dumb, rationalized hiding, and evasive hiding, each having four items and twelve in total. For this construct too, we rephrased the statements as follows: "agreed to help him/her but instead gave him/her information different from what s/he wanted" was modified to "I agree to help my colleagues but instead give them information different from what they want".

2.3. Sample and Data Collection. Non-probability sampling with a purposive technique was used in this study. This is effective where individuals with specific characteristics are selected as the sample. We needed organizations that were

Table 1: Reliability and convergent validity of the measurement model.

Constructs and measures	Loadings
Territoriality (T) (composite reliability = 0.87; AVE = 0.70; Cronbach's alpha = 0.78)	
T1. I feel I need to protect my ideas from being used by others in my organization.	0.86***
T2. I feel that people I work with in my organization should not invade my workspace.	0.79***
T3. I feel I need to protect my property from being used by others in the organization.	0.86***
Accountability (A) (composite reliability = 0.82; AVE = 0.61; Cronbach's alpha = 0.68)	
A1. I would challenge anyone in my organization, if I thought something was done wrong.	0.78***
A2. I would not hesitate to tell my organization, if I saw something that was done wrong.	0.73***
A3. I would challenge the direction of my organization to assure it's correct.	0.83***
Self-efficacy (SE) (composite reliability = 0.83; AVE = 0.62; Cronbach's alpha = 0.69)	
E1. I am confident in my ability to contribute to my organization's success.	0.83***
E2. I am confident that I can make a positive difference in this organization.	0.80***
E3. I am confident setting high performance goals in my organization.	0.73***
Self-identity (SI) (composite reliability = 0.86; AVE = 0.68; Cronbach's alpha = 0.76)	
SI1. I feel this organization's success is my success.	0.88***
SI2. I feel being a member in this organization helps define who I am.	0.80***
SI3. I feel the need to defend my organization when it is criticized.	0.78***
Belongingness (B) (composite reliability = 0.89; AVE = 0.73; Cronbach's Alpha = 0.81)	
B1. I feel I belong in this organization.	0.85***
B2. This place is home for me.	0.84***
B3. I am totally comfortable being in this organization.	0.87***
Evasive hiding (EH) (composite reliability = 0.95; AVE = 0.82; Cronbach's alpha = 0.93)	
EH1. I agree to help my colleagues but do not really intend to.	0.86***
EH2. I agree to help my colleagues but instead give them information different from what they want.	0.93***
EH3. I offer them some other information instead of what they really want.	0.92***
EH4. I tell them that I shall help but I stall/delay as much as possible.	0.92***
Playing dumb (PD) (composite reliability = 0.95; AVE = 0.84; cronbach's alpha = 0.94)	
PD1. I say that I do not know even though I do.	0.90***
PD2. I say that I am not very knowledgeable about the topic.	0.90***
PD3. I pretend that I do not know the information.	0.94***
PD4. I pretend that I do not know what they are talking about.	0.91***
Rationalized hiding (RH) (composite reliability = 0.93; AVE = 0.76; cronbach's alpha = 0.89)	
RH1. I explain that I would like to help them but I am not supposed to.	0.83***
RH2. I explain that the information is confidential and only available to people on a particular project.	0.89***
RH3. I explain that my boss does not let anyone share this knowledge.	0.88***
RH4. I say that I will not answer their questions.	0.89***
Explicit knowledge (EK) (composite reliability = 0.84; AVE = 0.64; cronbach's alpha = 0.70)	
EK1. I share my work reports and official documents with members of my organization.	0.87***
EK2. I provide my manuals, methodologies, and models for members of my organization.	0.89***
EK3. I share articles from newspapers/magazines/journals that I find useful and related to work with my colleagues.	0.61***
Implicit knowledge (IK) (composite reliability = 0.85; AVE = 0.65; cronbach's alpha = 0.73)	
IK1. I share my experiences or know-how from work with my colleagues.	0.79***
IK2. I provide my know-where or know-whom at the request of my colleagues.	0.82***
IK3. I try to share my expertise from my education or training with my colleagues in a more effective way.	0.80***
Innovative behaviour (composite reliability = 0.88; AVE = 0.55; cronbach's alpha = 0.84)	
IB1. I search out new technologies, processes, techniques, and/or product ideas.	0.73***
IB2. I generate creative ideas.	0.73***
IB3. I promote and champion ideas to others.	0.77***
IB4. I investigate and secure funds needed to implement new ideas.	0.74***
IB5. I develop adequate plans and schedules for the implementation of new ideas.	0.73***
IB6. I am innovative.	0.74***

*** $p < 0.01$.

known to have complex management systems requiring employees to exhibit IB (an important variable in this study). To control biases, the questionnaires were distributed to all employees across the selected organizations, and we made sure to follow up on the non-responding ones. Despite Pakistan's native language being Urdu, English is the official language and is commonly understood by the majority of the population. Hence, all the respondents had a good command over English, relieving us of the effort of having to translate the questionnaire. However, we did introduce the main constructs to them. The definitions were written below the constructed title in the questionnaires for ease of

understanding. The respondents were assured of anonymity and confidentiality of the sensitive firm information. Employing the gatekeeper approach to reach our target audience, a senior human resources executive from each organization was requested to circulate the questionnaires for the voluntary participation of employees [55]. Out of the 800 questionnaires distributed, 493 responses were obtained, yielding a response rate of 61.6%. Completed ones were mailed back to the authors with prepaid postage. After eliminating some low-quality samples, we finally retained data from 400 respondents for this study. Table 2 contains a summary of the demographic information.

2.4. Control Variables. Six demographic variables were controlled. These have been found to be significantly related to our study [56]. Organization type, that is, public or private, was measured as a dichotomous variable coded 0 for public and 1 for private. Gender was measured as a dichotomous variable coded as 0 for female and 1 for male, whereas age was measured in years. Tenure in the organization was measured as the number of years that an employee had been working for the specific company. Education was measured as 1, 2, and 3 for the levels corresponding to Bachelors, Masters, and PhD. Job area was assessed as a dichotomous dummy variable with code 0 for technical participants (e.g., engineering and the R&D work areas) and code 1 for non-technical participants (e.g., those from the administration and other functional departments). The information is presented in Table 2.

Table 2: Demographic information.

Demographic variables	Percent	Mean	S.D.
Organization		0.47	0.50
Public (0)	52.7		
Private (1)	47.3		
Gender		0.62	0.49
Male (1)	61.7		
Female (0)	38.3		
Education		1.88	0.76
Undergraduate (1)	35.4		
Postgraduate (2)	40.9		
Doctorate (3)	23.7		
Work area		0.43	0.50
Technical (0)	56.8		
Nontechnical (1)	43.2		
Respondents' mean age (years)	—	30.42	5.67
Tenure (years)	—	5.70	3.75

3. Results and Discussion

Analysis of the data was performed as a whole, employing the Partial Least Squares (PLS) coupled with the bootstrap resampling technique. PLS supports the concurrent application of formative and reflective measurements. It is also capable of modelling latent constructs under non-normality conditions, along with being useful for small and medium-sized samples [57]. Adopting the preferred two-phase analytical technique, structural associations were assessed after evaluating the measurement model [58]. Likewise, suitable safeguards were observed to curtail the likely common method bias as endorsed by researchers [59]. The Harman's single-factor analysis and the partial correlation analyses were also performed, with the findings indicating a low level of common method bias in this research effort.

3.1. Measurement Model Assessment. The measurement model for reflective constructs was evaluated by assessing reliability, convergent validity, and discriminant validity. Cronbach's alpha is the most extensively adopted measure for assessing reliability [60]. The convergent validity was reviewed by analyzing composite reliability and average variance extracted (AVE) from the scales. As Table 1 depicts, Cronbach's alpha was within the range of 0.68– 0.94 for all constructs, suggesting high internal consistency. The reflective constructs' composite reliability surpasses the ceiling of 0.70, signifying that these instruments are good to go with [61]. The range of AVE values is between 0.55 and 0.84, surpassing the advised point of 0.50. The path loadings of all reflective items to constructs are above 0.60, giving support for the convergent validity of measures.

For the formative measures, high loadings are not needed. The weight of each item is to be applied to assess the extent to which it contributes to the overall factor (see Figure 1). Discriminant validity was tested by contrasting the square roots of the AVE value of the concerned construct to the correlation between the respective construct and other constructs. Discriminant validity statistics are shown in Table 3. The square roots of the AVE scores are greater than the correlations among the constructs, proving their discriminant validity.

3.2. Structural Model Assessment. The PLS analysis results of the theoretical model are shown in Figure 1, comprising the following: overall explanatory power ($R2$), weights (for formative measures) and path coefficients (for relationships between latent variables). It describes 28.4% of the variance in IB, with nearly every path coefficient result being substantially significant. This offers sufficient leverage for the research model. The linkages between preventive PO and IB in the full-model testing were not to an extent to be considered significant. In the future, the mediation effects of KH and KS can be further verified through a sequence of tests employing the Sobel-Test, with t-values in the range of 2.40 to 10.46 [62]. Such findings validate the complete mediation effect [63].

The aim of this study was to examine relationships among PO, IB, KS, and KH. As per analysis, the preventive PO (T) and promotive PO (SE, A, B, SI) show significant relationships with both KH and KS, confirming H1a, b, as well as H2a, b. KH and KS have significant links with IB to the magnitude of -0.09 ($p < 0.05$) and 0.41 ($p < 0.01$), respectively, which validates the H3 and H4 hypotheses of this study. Promotive PO has a significant impact on IB ($t = 4.39$, $p < 0.01$), thus verifying H5. H6 found meagre support in the results with a value of only -0.001, which is not significant. Overall, the results support the research model and validate the theoretical foundations.

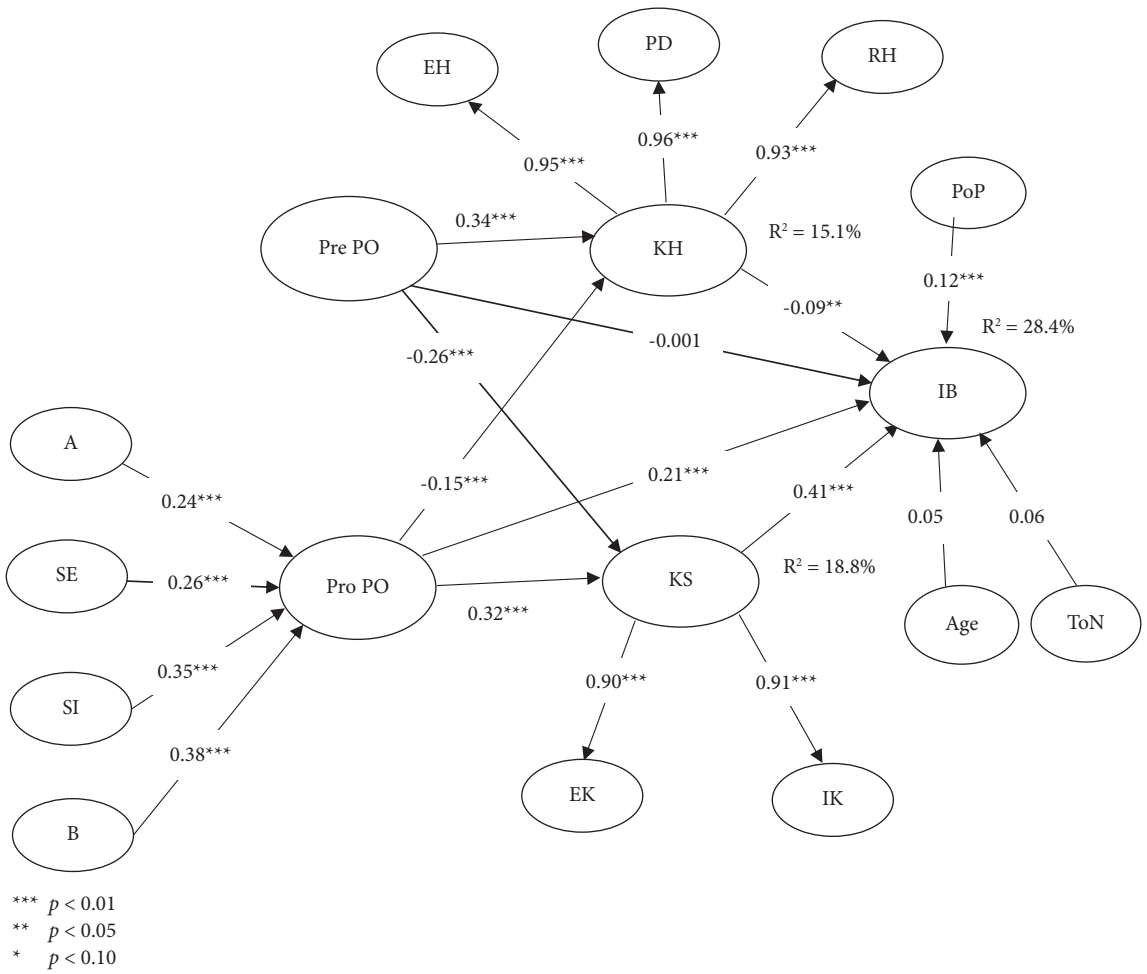

Figure 1: Results of the structural model.

Table 3: Assessment of discriminant validity of variables.

Constructs	1	2	3	4	5	6	7	8	9	10	11	12	13	14
(1) IB	0.74													
(2) T	−0.14	0.84												
(3) A	0.22	−0.01	0.78											
(4) SE	0.31	−0.03	0.45	0.79										
(5) SI	0.28	−0.15	0.52	0.46	0.82									
(6) B	0.29	−0.17	0.53	0.39	0.74	0.85								
(7) EH	−0.19	0.32	−0.07	−0.09	−0.22	−0.25	0.91							
(8) PD	−0.17	0.33	−0.06	−0.06	−0.17	−0.21	0.89	0.92						
(9) RH	−0.13	0.37	0.00	−0.06	−0.19	−0.23	0.81	0.84	0.87					
(10) EK	0.41	−0.25	0.12	0.19	0.29	0.31	−0.28	−0.23	−0.26	0.80				
(11) IK	0.46	−0.29	0.12	0.30	0.32	0.30	−0.18	−0.15	−0.18	0.63	0.81			
(12) PoP	−0.04	0.43	−0.08	0.00	−0.16	−0.21	0.48	0.52	0.44	−0.25	−0.12	—		
(13) ToN	−0.03	0.00	−0.09	−0.01	−0.18	−0.18	0.11	0.09	−0.01	−0.10	−0.07	0.05	—	
(14) Age	0.04	−0.05	0.02	−0.05	−0.01	0.01	−0.04	−0.07	−0.02	0.01	0.00	−0.07	−0.28	—

It is revealed that preventive PO causes employees to engage in KH, and it also negatively affects KS. However, promotive PO causes employees to engage in KS and prevents them from hiding knowledge. With every one unit increase in promotive PO, there is an increase of 0.32^{***} in KS, and with every one unit increase in promotive PO, there is a decrease of -0.15^{***} in KH. This means that the greater the sense of promotive PO, the more employees will practice KS, and the greater the sense of promotive PO, the lesser employees will engage in KH practices. Similarly, for the second type of PO i.e., preventive PO, with a single unit increase in preventive PO, there is a 0.34^{***} increase in KH,

and with a single unit increase in preventive PO, there is a -0.26^{***} effect on KS. This means that a stronger sense of preventive PO leads to more KH by employees and a stronger sense of preventive PO also negatively impacts the KS practices by employees, confirming our theory. Employees who feel like a part of their organization (self-identity) and consider it a second home (belongingness) for themselves are concerned (accountability) about the well-being and prosperity (self-efficacy) of their organization will engage in beneficial practices. They know that their positive attitude towards better managerial practices like KS and IB will benefit their organization and therefore they make efforts to share their knowledge and contribute to their organization's success.

On the other hand, employees are also aware that any form of KH, evasive, rationalized, or playing dumb, would put their organization at the risk of failure, which they do not want as they feel they have a stake in that organization. They avoid hiding knowledge to make sure their home does not suffer. Our results for these relationships can thus be considered a demonstration of employees' stewardship approach [47]. Consistent with the stewardship perspective, PO accentuates the value of KS as a tool to convert employees' cognitive and affective mindsets into organizational-level consequences, the outcome in this case being IB. As knowledge is obtained, controlled, or invented by employees, they typically consider knowledge as their marked territory or personal property. The preventive PO (territoriality) theory can ideally be used to explain KH. Researchers have noted that "territoriality or feelings of ownership have not been explored enough" and recommended employing this tactic in the management of knowledge-related studies [64]. Consistent with PO theory, this research effort found preventive PO and promotive PO play important roles in the links with KS and KH.

We thus enlarge the cluster of variables empirically associated with PO by providing a maiden look at its relationship in the form of prevention and promotion-oriented behaviours [7]. One potentially dysfunctional behaviour is KH (preventive), and productive behaviour is KS (promotive). As knowledge has progressively become a means for organizations' competitive advantage, withholding of knowledge is thus seen as counterproductive [40]. For instance, the need for control is understood to be the reason for clinically noted possessive acts such as, denial in sharing of items (e.g., tools, ideas, office space) and exerting command over the object of possession (e.g., not letting other colleagues share responsibility for a given task). Thus, one might predict that preventive PO (territoriality) promotes counterproductive work behaviours such as KH with respect to the object of ownership, where the feelings of bereavement or damage of the psychologically possessed entity is expected to cause frustration and unease. On the contrary, the promotive PO literature postulates that ownership targets grow into a portion of the extended self [51] and it is believed that development of the same will result in an enrichment of the sense of self and thereby the motivation to safeguard and improve the target of ownership.

Central to PO theory is the notion that there has been a fusion between the target of ownership and the psychological owner. It has been theorized that this relationship satisfies one or more motives that serve as the genesis for PO, and it is this bonding process that sustains the PO object-person relationship [4]. Hence, it is understandable for employees driven by promotional PO to share their knowledge and try for the betterment of their organizations. Research has linked PO with KS and proposed the positive effects [12, 13]. Our findings go one step ahead and reveal that these feelings also lead to counter-productive work behaviours such as KH. Organizations can reduce KH by taking measures (e.g., adopting open workspaces) to decrease individuals' territorial orientation and by promoting teamwork, stressing collective ownership of knowledge. Organizational knowledge-sharing culture may also inhibit the negative effect of preventive PO. In such a climate, territoriality will be thought of as unacceptable and those who transgress organizational norms will feel left out. When employees have a deep sense of positive PO, they believe they own the organization and are more likely to engage in IB because, through their contributions, they feel needed and appreciated. As a means of self-expression, IB could have personal benefits such as pride, increased personal identification with co-workers or the organization, more respect from others, and a better reputation. This reduces alienation and encourages stronger feelings of commitment. Our results show that a single unit increase in promotive PO is produces a 0.21^{***} increase in IB, which is very significant, confirming our belief and theory. Individual extra-role IB is typically exhibited on employees' own initiative. By enhancing the promotional aspects of PO, employees will take the initiative to contribute new ideas and suggest better ways of performing job functions and improving quality assurance.

3.3. Theoretical and Managerial Implications. This paper offers a sound theoretical perspective on PO, KS, KH, and IB, serving as a useful springboard for additional theorizing. To ascertain the generalizability of empirical observations emerging from western studies, we examined the emergence and possible effects of PO on work outcomes in emerging economies with a Pakistani sample. The legal ownership framework of a firm does not explain IB in a comprehensive way. However, through this work we have demonstrated a connection between PO and IB in employees. Our findings support the notion that a greater sense of PO would lead the employees towards IB. Gaining insight from prior research limitations, we have drawn attention to the "dark" side of PO. Most of the research attention to date has been directed toward those outcomes that are positive in nature (for example, job satisfaction, organizational commitment, performance, and citizenship behaviours). We have tried to fill this research gap by identifying negative behaviours like KH and their adverse effects on IB due to strong feelings of possessiveness. Preventive PO can hamper the efforts of managers to inculcate KS practices. Yet, by providing ample recognition to employees for their contributions,

involvement in decision making, and assigning them rights to their psychological property or objects of ownership, they can develop a strong sense of self-identity, efficacy, accountability, and belongingness, which can in turn benefit the organization through their positive workplace behaviours.

Studying KH between dyads in organizations is novel. Given increased calls for research to investigate the failure of KS initiatives in organizations, our exploration of KH is timely and advantageous. Our results demonstrate that KH occurs together with KS. The evidence discovered in our research here implies that interrelationships between PO and knowledge management behaviours serve to provide a sustained advantage to organizations through IB and are therefore important to understand. Innovativeness is a much-sought attribute in employees, given the continued turbulence that characterizes many industries. Under such conditions, organizations are advised to invest in their most valuable resource, human resources. Additionally, the management may plan and implement innovative activities within the framework of these antecedent constructs. The central message from the evidence provided is that the perceptions and feelings of employees are a strong base for positive outcomes to take place. Organizations are less likely to achieve their performance goals if employees' psychological orientation is not channelized in the right direction. If innovativeness is important for organizational performance, the task for the management is to design and implement an organizational environment that recognizes its employees' contributions and makes them feel worthwhile and fosters a sense of belonging.

3.4. Limitations and Future Directions. Limitations in this research effort open future research opportunities. Firstly, we would have preferred a bigger sample size from a wider choice of organizations. Next, the nature of the issues being investigated necessitated the use of self-reported data. Indeed, it is difficult to ask supervisors or co-workers to assess an employee's feelings. For example, for KH behaviours, the actions involved are likely to be concealed. Supervisor or co-worker ratings would reflect the observer's broad impressions and implicit theories about the target employees [65]. There is a possibility in research that deals with potentially awkward interpersonal behaviours that participants respond in socially desirable ways. We attempted to mitigate this issue by ensuring the confidentiality of responses and anonymity. However, future research could include some items to assess if participants are actively altering their responses in a socially desirable manner. Measures of KH could include "lie" statements like those used in personality measures. In the future, it may be explored as to which nature and types of jobs generate a greater sense of PO. It is felt that certain types of jobs could lead to a deeper sense of ownership as compared to others that may be repetitive, boring, or lacking meaning. Another interesting direction could be situational considerations, such as the recent pandemic or other peculiar settings in the environment. The cultural aspects of societies are another future direction. Individualistic societies could be expected to draw different results as compared to Pakistan, which is collectivist. Considering our results concerning the role of preventive PO in predicting KH, it would be exciting to ascertain what other interpersonal dynamics affect this behaviour. Future research may identify specific consequences of knowledge management behaviours at individual, interpersonal, and organizational levels, exploring whether they have consequences on interpersonal relationships in the workplace or not.

4. Conclusion

This research effort examines the status quo of PO and asserts that organizations need to explicitly address feelings of ownership in employees, which were found to be common and consistent with past research. The study observed the existence of PO among employees, no matter whether formal ownership and/or familial association exist or not, and further established the differences between public and private organizations. Identification with mutual goals and values enhances a sense of shared ownership, and can give organizations that invaluable competitive advantage they always seek. When we think of firms pulling through for many generations, the most liable conclusion comes from emotional ties that bind employees to their workplace and push them to contribute to its continuous success. This cognitive linking and emotional bondage are PO, which can serve as a strong base for organizational citizenship behaviours in employees such as KS and IB. PO is not a "cure-all," but it does have considerable power in explaining a rich number of phenomena in the work and organizational context.

We can conclude that promotive PO positively affects KS between employees and the preventive form of PO has a causal relationship with KH. Most practitioners are interested in developing strategies to minimize KH and encourage KS as knowledge is crucial for innovativeness, which is in turn vital for organizational effectiveness and prosperity. Through IB, managers can devise solutions to problems and face challenges, providing the basis for the survival and success of the firm well into the future. To encourage such behaviour in employees, a strong sense of ownership of their workplace needs to be developed. When employees know they count and can make a difference for better or worse, they will assume responsibility and exhibit positive behaviours such as KS and IB. Thus, we can sum up with the suggestion that organizations cannot limit themselves to employee stock ownership plans only. Fostering a sense of PO is equally vital or more so, as we saw in the relationships with KS, KH, and IB. Public sector managers and leaders can rethink their strategies for developing organizational citizenship behaviours and limiting counter-productive work behaviours in their employees based on the PO theory. After all, when a team takes ownership of its problems, the problems get solved. It is true on the battlefield, in business, and in everyday life (Jocko Willink).

Data Availability

The data for this study is available with the submitting author.

Conflicts of Interest

The authors declare that they have no conflicts of interest.

References

[1] M. Baer and G. Brown, "Blind in one eye: how psychological ownership of ideas affects the types of suggestions people adopt[J]," *Organizational Behavior and Human Decision Processes*, vol. 118, no. 1, pp. 60-71, Elsevier, 2012.

[2] S. Wang and R. A. Noe, "Knowledge sharing: a review and directions for future research," *Human Resource Management Review*, vol. 20, no. 2, pp. 115–131, 2010.

[3] J. L. Pierce, I. Jussila, and A. Cummings, "Psychological ownership within the job design context: revision of the job characteristics model," *Journal of Organizational Behavior*, vol. 30, no. 4, pp. 477–496, 2009.

[4] J. B. Avey, B. J. Avolio, C. D. Crossley, and F. Luthans, "Psychological ownership: theoretical extensions, measurement and relation to work outcomes," *Journal of Organizational Behavior*, vol. 30, no. 2, pp. 173–191, 2009.

[5] J. L. Pierce and I. Jussila, "Collective psychological ownership within the work and organizational context: construct introduction and elaboration," *Journal of Organizational Behavior*, vol. 31, no. 6, pp. 810–834, 2010.

[6] J. Li, L. Yuan, L. Ning, and J. Li-Ying, "Knowledge sharing and affective commitment: the mediating role of psychological ownership," *Journal of Knowledge Management*, vol. 19, no. 6, pp. 1146–1166, 2015.

[7] J. L. Pierce, T. Kostova, and K. T. Dirks, "The state of psychological ownership: integrating and extending a century of research," *Review of General Psychology*, vol. 7, no. 1, pp. 84–107, 2003.

[8] E. Karahanna, S. X. Xu, and Z. N. (Andy), "Psychological ownership motivation and use of social media," *Journal of Marketing Theory and Practice*, vol. 23, no. 2, pp. 185–207, 2015.

[9] C. E. Connelly, D. Zweig, J. Webster, and J. P Trougakos, "Knowledge hiding in organizations," *Journal of Organizational Behavior*, vol. 33, no. 1, pp. 64–88, 2012.

[10] B. Bacharach Samuel and J. Lawler Edward, "Power and politics in organizations: the social psychology of conflict, coalitions, and bargaining," *American political science review*, vol. 75, no. 03, pp. 736-737, Cambridge University Press, 1981.

[11] G. Brown, C. Crossley, and S. L. Robinson, "Psychological ownership, territorial behavior, and being perceived as a team contributor: the critical role of trust in the work environment," *Personnel Psychology*, vol. 67, no. 2, pp. 463–485, 2014.

[12] D. Constant, S. Kiesler, and L. Sproull, "What's mine is ours, or is it? A study of attitudes about information sharing[J]," *Information Systems Research*, vol. 5, no. 4, pp. 400–421, 1994.

[13] S. L. Jarvenpaa and D. S. Staples, "Exploring perceptions of organizational ownership of information and expertise," *Journal of Management Information Systems*, vol. 18, no. 1, pp. 151–183, 2001.

[14] J. L. Pierce, T. Kostova, and K. T. Dirks, "Toward a theory of psychological ownership in organizations," *Academy of Management Review*, vol. 26, no. 2, pp. 298–310, 2001.

[15] D. P. Ford and S. Staples, "Are full and partial knowledge sharing the same?" *Journal of Knowledge Management*, vol. 14, no. 3, pp. 394–409, 2010.

[16] M. McLure Wasko and S. Faraj, ""It is what one does": why people participate and help others in electronic communities of practice," *The Journal of Strategic Information Systems*, vol. 9, no. 2–3, pp. 155–173, 2000.

[17] J. Lee and A. Suh, "How do virtual community members develop psychological ownership and what are the effects of psychological ownership in virtual communities?" *Computers in Human Behavior*, vol. 45, pp. 382–391, 2015.

[18] P. J. Bateman, P. H. Gray, and B. S. Butler, "**Research note**—the impact of community commitment on participation in online communities," *Information Systems Research*, vol. 22, no. 4, pp. 841–854, 2011.

[19] J. L. Pierce and L. Rodgers, "The psychology of ownership and worker-owner productivity," *Group & Organization Management*, vol. 29, no. 5, pp. 588–613, 2004.

[20] M. M. Crossan, H. W. Lane, and R. E. White, "An organizational learning framework: from intuition to institution," *Academy of Management Review*, vol. 24, no. 3, pp. 522–537, 1999.

[21] M. Subramaniam and M. A. Youndt, "The influence of intellectual capital on the types of innovative capabilities," *Academy of Management Journal*, vol. 48, no. 3, pp. 450–463, 2005.

[22] I. Nonaka, G. Von Krogh, and S. Voelpel, "Organizational knowledge creation theory: evolutionary paths and future advances," *Organization Studies*, vol. 27, no. 8, pp. 1179–1208, 2006.

[23] L. Hu and A. E. Randel, "Knowledge sharing in teams: social capital extrinsic incentives and team innovation," *Group & Organization Management*, vol. 39, no. 2, pp. 213–243, 2014.

[24] K. Dalkir, *Knowledge Management in Theory and Practice*, p. 4, Elsevier Butterworth Heinemann, Amsterdam, Netherlands, 2005.

[25] I. Nonaka, "A dynamic theory of organizational knowledge creation," *Organization Science*, vol. 5, no. 1, pp. 14–37, 1994.

[26] S. Popadiuk and C. W. Choo, "Innovation and knowledge creation: how are these concepts related," *International Journal of Information Management*, vol. 26, no. 4, pp. 302–312, 2006.

[27] J. L. Farr and C. M. Ford, "Individual innovation," in *Innovation and Creativity at Work: Psychological and Organizational Strategies*, pp. 63-80, M. A. West and J. L. Farr, Eds., 1990.

[28] P. Akhavan, S. M. Hosseini, M. Abbasi, and M. Manteghi, "Knowledge-sharing determinants, behaviors, and innovative work behaviors: an integrated theoretical view and empirical examination[J]," *Aslib Journal of Information Management*, vol. 67, no. 5, pp. 562–591, 2015.

[29] T.-S. Han, H.-H. Chiang, and A. Chang, "Employee participation in decision making, psychological ownership and knowledge sharing: mediating role of organizational commitment in Taiwanese high-tech organizations," *International Journal of Human Resource Management*, vol. 21, no. 12, pp. 2218–2233, 2010.

[30] J. Liebowitz, "Knowledge management and its link to artificial intelligence," *Expert Systems with Applications*, vol. 20, no. 1, pp. 1–6, 2001.

[31] R. W. Woodman, J. E. Sawyer, and R. W. Griffin, "Toward a theory of organizational creativity," *Academy of Management Review*, vol. 18, no. 2, pp. 293–321, 1993.

[32] S. F. Holub, "Knowledge sharing is a change-management exercise," *Tax Practice Management*, vol. 34, pp. 361–363, 2003.

[33] T. J. M. Mom, F. A. J. Van Den Bosch, and H. W. Volberda, "Investigating managers' exploration and exploitation activities: the influence of top-down, bottom-up, and horizontal knowledge inflows," *Journal of Management Studies*, vol. 44, no. 6, pp. 910–931, 2007.

[34] X. Xie, L. Fang, S. Zeng, and J. Huo, "How does knowledge inertia affect firms product innovation?" *Journal of Business Research*, vol. 69, no. 5, pp. 1615–1620, 2016.

[35] A. S. Cui and F. Wu, "Utilizing customer knowledge in innovation: antecedents and impact of customer involvement on new product performance," *Journal of the Academy of Marketing Science*, vol. 44, no. 4, pp. 516–538, 2016.

[36] D. Khajeheian and R. Tadayoni, "User innovation in public service broadcasts: creating public value by media entrepreneurship," *International Journal of Technology Transfer and Commercialisation*, vol. 14, no. 2, pp. 117–131, 2016.

[37] H. Zhao, Q. Xia, P. He, G. Sheard, and P. Wan, "Workplace ostracism and knowledge hiding in service organizations," *International Journal of Hospitality Management*, vol. 59, pp. 84–94, 2016.

[38] K. Rosing, M. Frese, and A. Bausch, "Explaining the heterogeneity of the leadership-innovation relationship: ambidextrous leadership," *The Leadership Quarterly*, vol. 22, no. 5, pp. 956–974, 2011.

[39] H. Peng, "Why and when do people hide knowledge?" *Journal of Knowledge Management*, vol. 17, no. 3, pp. 398–415, 2013.

[40] A. Serenko and N. Bontis, "Understanding counterproductive knowledge behavior: antecedents and consequences of intra-organizational knowledge hiding," *Journal of Knowledge Management*, vol. 20, no. 6, pp. 1199–1224, 2016.

[41] A. Y. Zhang, A. S. Tsui, and D. X. Wang, "Leadership behaviors and group creativity in Chinese organizations: the role of group processes," *The Leadership Quarterly*, vol. 22, no. 5, pp. 851–862, 2011.

[42] M. Černe, C. G. L. Nerstad, A. Dysvik, and M Skerlavaj, "What goes around comes around: knowledge hiding, perceived motivational climate, and creativity," *Academy of Management Journal*, vol. 57, no. 1, pp. 172–192, 2014.

[43] M. Li and C. H. C. Hsu, "A review of employee innovative behavior in services," *International Journal of Contemporary Hospitality Management*, vol. 28, no. 12, pp. 2820–2841, 2016.

[44] S. H. Wagner, C. P. Parker, and N. D. Christiansen, "Employees that think and act like owners: effects of ownership beliefs and behaviors on organizational effectiveness," *Personnel Psychology*, vol. 56, no. 4, pp. 847–871, 2003.

[45] F. Bernhard and M. P. O'Driscoll, "Psychological ownership in small family-owned businesses: leadership style and nonfamily-employees' work attitudes and behaviors," *Group & Organization Management*, vol. 36, no. 3, pp. 345–384, 2011.

[46] N. Rantanen and I. F.-C. P. O. Jussila, "F-CPO: a collective psychological ownership approach to capturing realized family influence on business," *Journal of Family Business Strategy*, vol. 2, no. 3, pp. 139–150, 2011.

[47] M. Hernandez, "Toward an understanding of the psychology of stewardship," *Academy of Management Review*, vol. 37, no. 2, pp. 172–193, 2012.

[48] S. Dawkins, A. W. Tian, A. Newman, and A. Martin, "Psychological ownership: a review and research agenda," *Journal of Organizational Behavior*, vol. 38, no. 2, pp. 163–183, 2017.

[49] K. A. Eddleston and F. W. Kellermanns, "Destructive and productive family relationships: a stewardship theory perspective," *Journal of Business Venturing*, vol. 22, no. 4, pp. 545–565, 2007.

[50] T. M. Amabile, C. N. Hadley, and S. J. Kramer, "Creativity under the gun," *Harvard Business Review*, vol. 80, no. 8, pp. 52–61, 147, 2002.

[51] J. Pierce and I. Jussila, *Psychological Ownership and the Organizational Context*, Edward Elgar Publishing, Cheltenham, United Kingdom, 2011.

[52] A. S. Lee, "Integrating positivist and interpretive approaches to organizational research," *Organization Science*, vol. 2, no. 4, pp. 342–365, 1991.

[53] S. G. Scott and R. A. Bruce, "Determinants of innovative behavior: a path model of individual innovation in the workplace," *Academy of Management Journal*, vol. 37, no. 3, pp. 580–607, 1994.

[54] Z. Bock, Kim, Kim, and Lee, "Behavioral intention formation in knowledge sharing: examining the roles of extrinsic motivators, social-psychological forces and organizational climate," *MIS Quarterly*, vol. 29, no. 1, p. 87, 2005.

[55] F. A. Yamoah and A. U. Haque, "Strategic management through digital platforms for remote working in the higher education industry during & after the COVID-19 pandemic," *Forum Scientiae Oeconomia*, vol. 10, no. 2, pp. 111–128, 2022.

[56] J. Zhou and J. M. George, "When job dissatisfaction leads to creativity: encouraging the expression of voice," *Academy of Management Journal*, vol. 44, no. 4, pp. 682–696, 2001.

[57] W. W. Chin, "The partial least squares approach to structural equation modeling," *Modern methods for business research*, pp. 295–336, 1998.

[58] J. C. Anderson and D. W. Gerbing, "Structural equation modeling in practice: a review and recommended two-step approach," *Psychological Bulletin*, vol. 103, no. 3, pp. 411–423, 1988.

[59] P. M. Podsakoff, S. B. MacKenzie, J.-Y. Lee, and N. P Podsakoff, "Common method biases in behavioral research: a critical review of the literature and recommended remedies," *Journal of Applied Psychology*, vol. 88, no. 5, pp. 879–903, 2003.

[60] L. J. Cronbach, "Coefficient alpha and the internal structure of tests," *Psychometrika*, vol. 16, no. 3, pp. 297–334, 1951.

[61] J. C. Nunnally and I. H. Bernstein, *Psychometric Theory*, Vol. 3, McGraw-Hill, New York, 1994.

[62] M. E. Sobel, "Asymptotic confidence intervals for indirect effects in structural equation models," *Sociological Methodology*, vol. 13, pp. 290–312, 1982.

[63] W. Zheng, B. Yang, and G. N. McLean, "Linking organizational culture, structure, strategy, and organizational effectiveness: mediating role of knowledge management," *Journal of Business Research*, vol. 63, no. 7, pp. 763-771, Elsevier, 2010.

[64] J. Webster, G. Brown, and D. Zweig, "Beyond knowledge sharing: withholding knowledge at work[J]," *Research in Personnel and Human Resources Management*, vol. 27, pp. 1–37, 2008.

[65] S. Tangirala and R. Ramanujam, "Employee silence on critical work issues: the cross level effects of procedural justice climate," *Personnel Psychology*, vol. 61, no. 1, pp. 37–68, 2008.

Hindawi
Complexity
Volume 2022, Article ID 8155929, 36 pages
https://doi.org/10.1155/2022/8155929

WILEY | Hindawi

Research Article

Estimation for Parameters of Life of the Marshall-Olkin Generalized-Exponential Distribution Using Progressive Type-II Censored Data

Ahmed Elshahhat,[1] **Abdisalam Hassan Muse**,[2,3] **Omer Mohamed Egeh**,[3] **and Berihan R. Elemary**[4]

[1]*Faculty of Technology and Development, Zagazig University, Zagazig 44519, Egypt*
[2]*Department of Mathematics (Statistics Option), Pan African University, Institute for Basic Sciences, Technology, and Innovation (PAUSTI), Faculty of Commerce, Damietta University, Nairobi 62000-00200, Kenya*
[3]*Department of Mathematics and Statistics, School of Postgraduate Studies and Research, Amoud University, Borama, Somalia*
[4]*Department of Applied, Mathematical and Actuarial Statistics, Faculty of Commerce, Damietta University, Damietta 22052, Egypt*

Correspondence should be addressed to Omer Mohamed Egeh; 1933@amoud.edu.so

Received 13 April 2022; Revised 9 August 2022; Accepted 18 August 2022; Published 3 October 2022

Academic Editor: Yu Zhou

A new three-parameter extension of the generalized-exponential distribution, which has various hazard rates that can be increasing, decreasing, bathtub, or inverted tub, known as the Marshall-Olkin generalized-exponential (MOGE) distribution has been considered. So, this article addresses the problem of estimating the unknown parameters and survival characteristics of the three-parameter MOGE lifetime distribution when the sample is obtained from progressive type-II censoring via maximum likelihood and Bayesian approaches. Making use of the s-normality of classical estimators, two types of approximate confidence intervals are constructed via the observed Fisher information matrix. Using gamma conjugate priors, the Bayes estimators against the squared-error and linear-exponential loss functions are derived. As expected, the Bayes estimates are not explicitly expressed, thus the Markov chain Monte Carlo techniques are implemented to approximate the Bayes point estimates and to construct the associated highest posterior density credible intervals. The performance of proposed estimators is evaluated via some numerical comparisons and some specific recommendations are also made. We further discuss the issue of determining the optimum progressive censoring plan among different competing censoring plans using three optimality criteria. Finally, two real-life datasets are analyzed to demonstrate how the proposed methods can be used in real-life scenarios.

1. Introduction

Several extensions of the exponential distribution such as Weibull, gamma, generalized-exponential, and Nadarajah-Haghighi distributions among others have been proposed in literature. A general technique that allows to adding a new shape parameter to expand a family of distributions is originally proposed by Marshall and Olkin [1]. Applying the Marshall-Olkin technique to generalized-exponential distribution, Ristić and Kundu [2] introduced the three-parameter Marshall-Olkin generalized-exponential (MOGE) distribution. However, suppose that the lifetime random variable X of an individual testing item follows a three-parameter MOGE(α, β, θ). Hence, its cumulative distribution function (CDF) $F(\cdot)$, probability density function (PDF) $f(\cdot)$, reliability function (RF) $R(\cdot)$, and hazard function (HF) $h(\cdot)$, at distinct time t, are given, respectively, by

$$F(x;\alpha,\beta,\theta)=\frac{\left(1-e^{-\theta x}\right)^{\alpha}}{\beta+\overline{\beta}\left(1-e^{-\theta x}\right)^{\alpha}},\quad x>0, \tag{1}$$

$$f(x;\alpha,\beta,\theta)=\frac{\alpha\beta\theta e^{-\theta x}\left(1-e^{-\theta x}\right)^{\alpha-1}}{\left(\beta+\overline{\beta}\left(1-e^{-\theta x}\right)^{\alpha}\right)^{2}},\quad x>0, \tag{2}$$

$$R(t;\alpha,\beta,\theta)=\frac{\beta\left(1-\left(1-e^{-\theta t}\right)^{\alpha}\right)}{\beta+\overline{\beta}\left(1-e^{-\theta t}\right)^{\alpha}},\quad t>0, \tag{3}$$

$$h(t;\alpha,\beta,\theta)=\frac{\alpha\theta e^{-\theta t}\left(1-e^{-\theta t}\right)^{\alpha-1}}{\left(\beta+\overline{\beta}\left(1-e^{-\theta t}\right)^{\alpha}\right)\left(1-\left(1-e^{-\theta t}\right)^{\alpha}\right)},\quad t>0, \tag{4}$$

where $\overline{\beta}=1-\beta$, $\alpha>0$, and $\beta>0$ are the shape parameters and $\theta>0$ is the scale parameter. Ristić and Kundu [2] derived several properties of the MOGE distribution and estimated its parameters using the likelihood method.

Using some specified values on the range of α, β, and θ, different shapes of the density and failure rate functions of the MOGE distribution are displayed in Figure 1. It shows that the density shapes are decreasing or unimodal while the HF shapes can be increasing, decreasing, bathtub, or inverted tub. Since the bathtub HF shape is quite beneficial in several lifetime data, therefore the MOGE distribution is justly flexible and can be used to provide a good description of different types of censored data, for details, it can be seen in Ristić and Kundu [2]. From (1), three lifetime submodels can be obtained as special cases from the MOGE distribution, namely,

(i) Marshall–Olkin exponential distribution, by Marshall and Olkin [1]; if setting $\alpha=1$.

(ii) Generalized-exponential distribution, by Gupta and Kundu [3]; if setting $\theta=1$.

(iii) Exponential distribution, discussed by Johnson and Kotz [4]; if setting $\alpha=\theta=1$.

Statistical life distributions under censoring plans have received great interest owing to their wide application in numerous fields such as engineering, social sciences, marketing, and medicine. One of the most popular censoring mechanisms, which is of great importance in reliability studies, is known as type-II progressive censoring scheme (PCS-T2). This censoring scheme can be described as follows: suppose that n identical and independent units are put on a life-testing experiment at time zero and the progressive censoring scheme $\mathbf{R}=(R_1,R_2,\ldots,R_m)$ is prefixed, where $m(<n)$ is the number of observed failures that is decided by the experimenter in advance. At the time of the first failure occur (say $x_{1:m:n}$), R_1 of survival items are randomly removed from the remaining live $(n-1)$ units. Again, at the time of the next failure occur (say $x_{2:m:n}$), R_2 of survival items are randomly removed from the remaining live $(n-R_1-2)$ units and continue the test. This procedure continues until all remaining live R_m units are removed from the experiment at the time of the mth failure observed. It is clear that $n-m=\sum_{i=1}^{m}R_i$. For more details, one may refer to an excellent monograph presented by Balakrishnan and Cramer [5].

However, the likelihood function of the PCS-T2 sample $x_{i:m:n}$ for $i=1,2,\ldots,m$, is defined as

$$L(\Theta\mid\mathbf{x})=C\prod_{i=1}^{m}f\left(x_{i:m:n};\Theta\right)\left[1-F\left(x_{i:m:n};\Theta\right)\right]^{R_i}, \tag{5}$$

where $C=n(n-R_1-1)\ldots(n-\sum_{i=1}^{m-1}(R_i+1))$ and Θ is parameter vector.

In literature, several authors including Amin [6], Kim et al. [7], Huang and Wu [8], Dey et al. [9], Panahi [10], Muhammed and Almetwally [11], Elshahhat and Rastogi [12], Maiti and Kayal [13], Dey et al. [14], Maiti et al. [15], and Elshahhat and Abu El Azm [16] studied a wide variety of inferential problems for different lifetime distributions under type-II progressively censored samples.

In the context of censoring mechanisms, to the best of our knowledge, we have not encountered any work related to the estimation of parameters and/or survival characteristics of the MOGE distribution under incomplete (censored) sampling, which is of considerable interest and practical significance in many practical situations. So, in this study, we shall exclusively focus on both classical and Bayesian approaches of estimation to derive the both point and interval estimators of the MOGE parameters α, β, and θ, as well as its time parameters $R(t)$ and $h(t)$ under PCS-T2. Our objectives in this study are as follows: first, deriving the maximum likelihood estimators (MLEs) for the unknown MOGE parameters or any function of them. Correspondingly, using observed Fisher information matrix, two-sided asymptotic confidence intervals are also established. Second, obtain the Bayes estimators of the unknown quantities α, β, θ, $R(t)$, and $h(t)$ using independent gamma priors based on the two popular symmetric and asymmetric loss functions. Markov chain Monte Carlo (MCMC) techniques are also used to carry out the Bayes estimates and associated credible interval estimates from the complex posterior functions. Third, determine the optimum progressive censoring plan from a class of all possible removal patterns that contain a magnificent amount of information regarding the unknown model parameter under consideration. Lastly, the performance of the proposed methods is compared through an extensive simulation study in terms of their simulated root mean squared-error, mean relative absolute bias, average confidence lengths, and coverage percentages. To discuss how the proposed methods can be applied in a real phenomenon, two real-life data sets are analyzed. We also suggest the use of "maxLik" and "coda" statistical packages in R programming software to evaluate the theoretical findings. Finally, some specific recommendations are made.

The rest of the paper is arranged as follows: classical and Bayes estimations of unknown parameters and the reliability characteristics are presented in Sections 2 and 3, respectively. Optimum progressive censoring plans are discussed in Section 4. Monte Carlo simulation is performed in Section

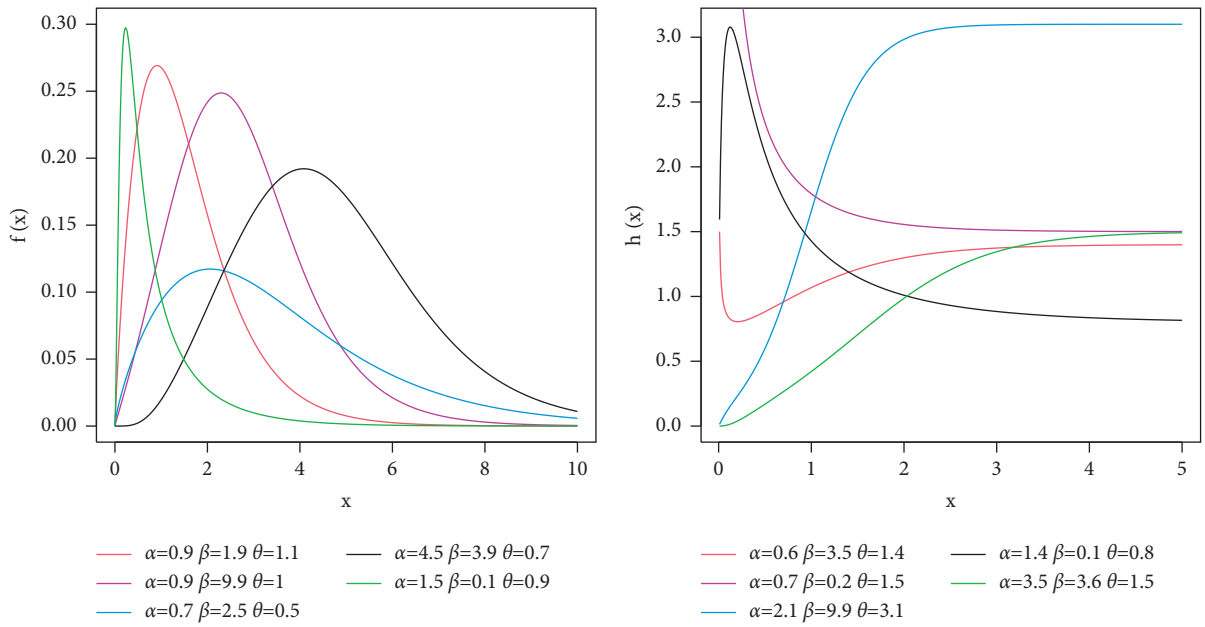

Figure 1: Plots of the density and hazard rate functions of the MOGE distribution.

5. Two applications using real data sets are presented in Section 6. Finally, we conclude the paper in Section 7.

2. Likelihood Inference

In this section, the point and interval estimators of the unknown parameters and the reliability characteristics of the MOGE distribution based on PCS-T2 are derived.

2.1. Point Estimators. Suppose $\mathbf{x} = \{(x_{1:m:n}, R_1), (x_{2:m:n}, R_2), \ldots, (x_{m:m:n}, R_m)\}$ is a PCS-T2 data obtained from MOGE(α, β, θ). From (1) and (2), with ignoring any additive constant, the likelihood function (5) becomes

$$L(\alpha, \beta, \theta|\mathbf{x}) \propto \beta^n (\alpha\theta)^m e^{-\theta \sum_{i-1}^{m} x_i} \cdot \prod_{i=1}^{m} \psi_i^{\alpha-1}(\theta)\left(1-\psi_i^{\alpha}(\theta)\right)^{R_i}\left(\beta+\overline{\beta}\psi_i^{\alpha}(\theta)\right)^{-(R_i+2)}, \tag{6}$$

where x_i is used instead of $x_{i:m:n}$ and. $\psi_i(\theta) = 1 - \exp(-\theta x_i), i = 1, 2, \ldots, m$.

From (6), the log-likelihood function, $\ell(\cdot) = \log L(\cdot)$, can be written as

$$\ell(\alpha, \beta, \theta|\mathbf{x}) \propto n\log(\beta) + m\log(\alpha\theta) - \theta m\overline{x} + (\alpha-1)\sum_{i=1}^{m}\log\left(\psi_i(\theta)\right) + \sum_{i=1}^{m} R_i \log\left(1-\psi_i^{\alpha}(\theta)\right) - \sum_{i=1}^{m}(R_i+2)\log\left(\beta+\overline{\beta}\psi_i^{\alpha}(\theta)\right). \tag{7}$$

Setting the first-partial derivatives of (7) with respect to each unknown parameter to zero, the respective MLEs of α, β, and θ are the solutions to the following normal equations as

$$0 = \frac{m}{\widehat{\alpha}} + \sum_{i=1}^{m}\log\left(\widehat{\psi}_i(\widehat{\theta})\right) - \sum_{i=1}^{m} R_i \log\left(\widehat{\psi}_i(\widehat{\theta})\right)\widehat{\psi}_i^{\widehat{\alpha}}(\widehat{\theta})\left(1-\widehat{\psi}_i^{\widehat{\alpha}}(\widehat{\theta})\right)^{-1} - \overline{\widehat{\beta}}\sum_{i=1}^{m}(R_i+2)\log\left(\widehat{\psi}_i(\widehat{\theta})\right)\widehat{\psi}_i^{\widehat{\alpha}}(\widehat{\theta})\left(\widehat{\beta}+\overline{\widehat{\beta}}\widehat{\psi}_i^{\widehat{\alpha}}(\widehat{\theta})\right)^{-1}, \tag{8}$$

$$0 = \frac{n}{\widehat{\beta}} - \sum_{i=1}^{m}(R_i+2)\left(1-\widehat{\psi}_i^{\widehat{\alpha}}(\widehat{\theta})\right)\left(\widehat{\beta}+\overline{\widehat{\beta}}\widehat{\psi}_i^{\widehat{\alpha}}(\widehat{\theta})\right)^{-1}, \tag{9}$$

$$0 = \frac{m}{\widehat{\theta}} - m\overline{x} + (\widehat{\alpha}-1)\sum_{i=1}^{m}\widehat{\psi}_i'(\widehat{\theta})\widehat{\psi}_i^{-1}(\widehat{\theta}) - \widehat{\alpha}\sum_{i=1}^{m}R_i\widehat{\psi}'_i(\widehat{\theta})\left(\widehat{\psi}_i(\widehat{\theta})\right)^{\widehat{\alpha}-1}\left(1-\widehat{\psi}_i^{\widehat{\alpha}}(\widehat{\theta})\right)^{-1}$$
$$-\widehat{\alpha}\overline{\overline{\beta}}\sum_{i=1}^{m}(R_i+2)\widehat{\psi}_i'(\widehat{\theta})\left(\widehat{\psi}_i(\widehat{\theta})\right)^{\widehat{\alpha}-1}\left(\widehat{\beta}+\overline{\overline{\beta}}\widehat{\psi}_i^{\widehat{\alpha}}(\widehat{\theta})\right)^{-1}, \tag{10}$$

where $\widehat{\psi}_i'(\widehat{\theta}) = x_i(1-\widehat{\psi}_i(\widehat{\theta}))$ for $i = 1,\ldots,m$.

Obviously, from (8) and (10), the MLEs $\widehat{\alpha}$, $\widehat{\beta}$, and $\widehat{\theta}$ of the parameters α, β, and θ, respectively, cannot be obtained analytically but can be evaluated using any iterative approximation technique. Once $\widehat{\alpha}$, $\widehat{\beta}$, and $\widehat{\theta}$ calculated, using the invariance property of MLEs, the corresponding MLEs $\widehat{R}(t)$ and $\widehat{h}(t)$ of $R(t)$ and $h(t)$ at any given time $t>0$ can be easily derived by replacing α, β, and θ with $\widehat{\alpha}$, $\widehat{\beta}$, and $\widehat{\theta}$ in (3) and (4), respectively.

2.2. Asymptotic Intervals. To construct the $100(1-\tau)\%$ two-sided ACIs for the unknown parameters α, β, and θ, or any life function such as $R(t)$ and $h(t)$ (say φ), the asymptotic variances or covariances (by inverting the Fisher information matrix $\mathbf{I}(\cdot)$) of the MLEs $\widehat{\alpha}$, $\widehat{\beta}$, and $\widehat{\theta}$ must be obtained as

$$\mathbf{I}^{-1}(\widehat{\varphi}) = \begin{bmatrix} \mathscr{L}_{11} & & \\ \mathscr{L}_{12} & \mathscr{L}_{22} & \\ \mathscr{L}_{31} & \mathscr{L}_{32} & \mathscr{L}_{33} \end{bmatrix}^{-1}_{\varphi=\widehat{\varphi}} = \begin{bmatrix} \widehat{\sigma}_{11} & & \\ \widehat{\sigma}_{21} & \widehat{\sigma}_{22} & \\ \widehat{\sigma}_{31} & \widehat{\sigma}_{32} & \widehat{\sigma}_{33} \end{bmatrix}. \tag{11}$$

Under some mild regularity conditions of the MLEs, using the concept of large sample theory, we have the asymptotic normality approximation (NA) of $\widehat{\varphi}$ is approximately multivariate normal with mean vector φ and variance-covariance matrix $\mathbf{I}^{-1}(\varphi)$, i.e., $\widehat{\varphi} \sim N_3[\varphi, \mathbf{I}^{-1}(\widehat{\varphi})]$, where $\varphi = (\alpha,\beta,\theta)^\top$ is the parametric vector of α, β, and θ. By differentiating (7) partially with respect to α, β, and θ, locally at their MLEs $\widehat{\alpha}$, $\widehat{\beta}$, and $\widehat{\theta}$, the Fisher's elements $\mathscr{L}_{ij}$ for $i,j = 1,2,3$, are obtained and provided in Appendix A.

Similarly, based on NA of the MLEs $\widehat{R}(t)$ and $\widehat{h}(t)$, it is clear that $\widehat{R} \sim N[R(t), \widehat{\sigma}^2_{R(t)}]$ and $\widehat{h}(t) \sim N[h(t), \widehat{\sigma}^2_{h(t)}]$. Thus, ACIs for $R(t)$ and $h(t)$ can be constructed using the corresponding normality. To obtain ACIs of $R(t)$ and $h(t)$, we need to compute their variances. Following Greene [17], the delta method is used to find $\widehat{\sigma}^2_R$ and $\widehat{\sigma}^2_h$ of $R(t)$ and $h(t)$, respectively, as:

$$\widehat{\sigma}^2_R = \left[\nabla_R, \mathbf{I}^{-1}(\varphi), \nabla_R^\top\right]|_{\varphi=\widehat{\varphi}},$$
$$\widehat{\sigma}^2_h = \left[\nabla_h, \mathbf{I}^{-1}(\varphi), \nabla_h^\top\right]|_{\varphi=\widehat{\varphi}}, \tag{12}$$

where,

$$\nabla_R = \left(\frac{\partial}{\partial\alpha}R(t), \frac{\partial}{\partial\beta}R(t), \frac{\partial}{\partial\theta}R(t)\right),$$
$$\nabla_h = \left(\frac{\partial}{\partial\alpha}h(t), \frac{\partial}{\partial\beta}h(t), \frac{\partial}{\partial\theta}h(t)\right). \tag{13}$$

Then, based on NA, the $100(1-\tau)\%$ two-sided ACIs for the unknown parameter α, β, θ, $R(t)$ or $h(t)$ (say κ) is given by:

$$\widehat{\kappa} \pm z_{\tau/2}\sqrt{\widehat{\sigma}^2_{\widehat{\kappa}}}, \tag{14}$$

where $z_{\tau/2}$ is the upper $(\tau/2)^{\text{th}}$ quantile of the standard normal distribution.

Though, the main problem of asymptotic NA confidence interval is that it may give a negative value in lower bound for a lifetime parameter. To handling this drawback, Meeker and Escobar [18] developed the normal approximation for the log-transformed (NL) of MLE. They also showed that ACI has better CP based on NL compared to NA. However, based on NL, the $100(1-\tau)\%$ two-sided ACI of κ is given by

$$\widehat{\kappa}\exp\left(\mp\frac{z_{\tau/2}\sqrt{\widehat{\sigma}^2_{\widehat{\kappa}}}}{\widehat{\kappa}}\right). \tag{15}$$

3. Bayesian Inference

In this section, we discuss the Bayes inference of the model parameters α, β, and θ, as well as, the reliability parameters $R(t)$ and $h(t)$ using progressively type-II censoring.

3.1. Prior Information and Loss Functions. Since the gamma $G(\cdot)$ density provides various shapes based on parameter values and is flexible in nature, so the utilizing of independent gamma priors are relatively simple which may yield to results with more explicit posterior density expressions Muse et al. [19]; for more details, it can be seen in [14, 20, 21]. Thus, the gamma conjugate priors $G_\alpha(a_1,b_1)$, $G_\beta(a_2,b_2)$, and $G_\theta(a_3,b_3)$ are used to adapt the support of MOGE parameters α, β, and θ, respectively. However, the joint prior PDF of α, β, and θ becomes

$$\pi(\alpha,\beta,\theta) \propto \alpha^{a_1-1}\beta^{a_2-1}\theta^{a_3-1}e^{-\left(b_1\alpha+b_2\beta+b_3\theta\right)}, \quad \alpha,\beta,\theta>0, \tag{16}$$

where the hyperparameters a_i, b_i, $i = 1,2,3$, are chosen to reflect prior knowledge about the unknown parameters α, β, and θ, and they assumed to be known as non-negative.

The choice of (symmetric and/or symmetric) loss function is an important issue in Bayesian analysis. So, to develop the objective estimates, two well-known loss functions namely, squared-error loss (SEL) and linear-exponential loss (LL), are considered. However, any other loss

function can be easily incorporated. The SEL function is defined as

$$\mathfrak{T}_S(\phi, \widetilde{\phi}) = (\widetilde{\phi} - \phi)^2, \tag{17}$$

where $\widetilde{\phi}$ being an estimate of ϕ. Under (13), the Bayes estimate $\widetilde{\phi}$ is the posterior mean of ϕ.

On the other hand, the LL function, $\mathfrak{T}_L(\cdot)$, is defined as

$$\mathfrak{T}_L(\phi, \widetilde{\phi}) = \exp(\upsilon(\widetilde{\phi} - \phi)) - \upsilon(\widetilde{\phi} - \phi) - 1, \quad \upsilon \neq 0. \tag{18}$$

The sign and magnitude of υ represent the direction and degree of symmetry, respectively (if $\upsilon > 0$, overestimation is more serious than underestimation and $\upsilon < 0$ means the opposite). Using (14), the Bayes estimator $\widetilde{\phi}_L$ of ϕ is given by:

$$\widetilde{\phi}_L = -\upsilon^{-1}\ln\left(E_\phi\left[e^{-\upsilon\phi}|\mathbf{x}\right]\right), \quad \upsilon \neq 0, \tag{19}$$

provided the above exception exists, and is finite. When υ close to 0, the LL function is approximately the SEL function and it can become almost symmetric, as can be seen in Pandey and Rai [22].

3.2. Posterior Analysis. Using (6) and (12), the joint posterior PDF of α, β, and θ can be written as

$$\pi(\alpha, \beta, \theta|\mathbf{x}) = K^{-1}\alpha^{a_1+m-1}\beta^{a_2+n-1}\theta^{a_3+m-1}e^{-(\alpha b_1+\beta b_2+\theta(b_3+m\overline{x}))} \times \prod_{i=1}^{m}\psi_i^{\alpha-1}(\theta)(1-\psi_i^{\alpha}(\theta))^{R_i}\left(\beta+\overline{\beta}\psi_i^{\alpha}(\theta)\right)^{-(R_i+2)}, \tag{20}$$

where K is the normalizing constant of (15).

Due to nonlinear expression in (6), the closed-form of the marginal PDF for each unknown parameter is not possible. Thus, we purpose to apply some simulation algorithms such as the MCMC methods to approximate the Bayesian estimates and to find associated credible intervals. So the MCMC methods have been widely used in Bayesian computational analysis. At first, from (15), we derive the conditional posterior distributions of α, β, and θ, respectively, as

$$\pi_\alpha^*(\alpha|\beta, \theta, \mathbf{x}) \propto \alpha^{a_1+m-1}e^{-\alpha b_1^*(\theta)}\prod_{i=1}^{m}(1-\psi_i^{\alpha}(\theta))^{R_i}\left(\beta+\overline{\beta}\psi_i^{\alpha}(\theta)\right)^{-(R_i+2)}, \tag{21}$$

$$\pi_\beta^*(\beta|\alpha, \theta, \mathbf{x}) \propto \beta^{a_2+n-1}e^{-\beta b_2}\prod_{i=1}^{m}\left(\beta+\overline{\beta}\psi_i^{\alpha}(\theta)\right)^{-(R_i+2)}, \tag{22}$$

$$\pi_\theta^*(\theta|\alpha, \beta, \mathbf{x}) \propto \theta^{a_3+m-1}e^{-\theta(b_3+m\overline{x})}\prod_{i=1}^{m}\psi_i^{\alpha-1}(\theta)(1-\psi_i^{\alpha}(\theta))^{R_i}\left(\beta+\overline{\beta}\psi_i^{\alpha}(\theta)\right)^{-(R_i+2)}, \tag{23}$$

where $b_1^*(\theta) = b_1 - \sum_{i=1}^{m}\log(\psi_i(\theta))$.

It can be seen, from (16)–(18), that the conditional distributions of α, β, and θ cannot be reduced to any standard distribution so that the exact inferences from their marginal densities cannot be easily obtained. Thus, to generate samples from posterior distribution whenever the posterior PDF cannot be reduced to any familiar distribution, the Metropolis–Hastings algorithm can be easily used for this purpose (see Gelman et al. [23] for detail).

3.3. M-H Algorithm. The Metropolis-Hastings (M-H) algorithm is a general member of the MCMC family of simulation techniques. In this subsection, the M-H algorithm with normal proposal distributions is conducted to generate samples of α, β, and θ from (16), (17), and (18), respectively. Precisely, Figure 2 indicates that the distribution of MOGE parameters behaves similar to the normal distribution. Next, to obtain the Bayes estimates and the associated credible intervals, do the following generation steps:

Step 1: Put $g = 1$.

Step 2: Set initial values $(\alpha^{(0)}, \beta^{(0)}, \theta^{(0)}) = (\widehat{\alpha}, \widehat{\beta}, \widehat{\theta})$.

Step 3: Generate α^*, β^*, and θ^* from (16)–(18) with normal distributions $N(\widehat{\alpha}, \widehat{\sigma}_\alpha^2)$, $N(\widehat{\beta}, \widehat{\sigma}_\beta^2)$, and $N(\widehat{\theta}, \widehat{\sigma}_\theta^2)$, respectively, as follows:

(a) Calculate $Q_\alpha = \pi_\alpha^*(\alpha^*|\ \beta^{(g-1)}, \theta^{(g-1)}, \mathbf{x})/\pi_\alpha^*(\alpha^{(g-1)}|\beta^{(g-1)}, \theta^{(g-1)}, \mathbf{x})$, $Q_\beta = \pi_\beta^*(\beta^*|\alpha^{(g)}, \theta^{(g-1)}, \mathbf{x})/\pi_\beta^*(\beta^{(g-1)}|\alpha^{(g)}, \theta^{(g-1)}, \mathbf{x})$ and $Q_\theta = \pi_\theta^*(\theta^*|\alpha^{(g)}, \beta^{(g)}, \mathbf{x})/\pi_\theta^*(\theta^{(g-1)}|\alpha^{(g)}, \beta^{(g)}, \mathbf{x})$.

(b) Generate sample variates u_1, u_2, and u_3 from the uniform $U(0, 1)$ distribution.

(c) If $u_1 \leqslant \min\{1, Q_\alpha\}$, set $\alpha^{(g)} = \alpha^*$, else set $\alpha^{(g)} = \alpha^{(g-1)}$.

(d) If $u_2 \leqslant \min\{1, Q_\beta\}$, set $\beta^{(g)} = \beta^*$, else set $\beta^{(g)} = \beta^{(g-1)}$.

(e) If $u_3 \leqslant \min\{1, Q_\theta\}$, set $\theta^{(g)} = \theta^*$, else set $\theta^{(g)} = \theta^{(g-1)}$.

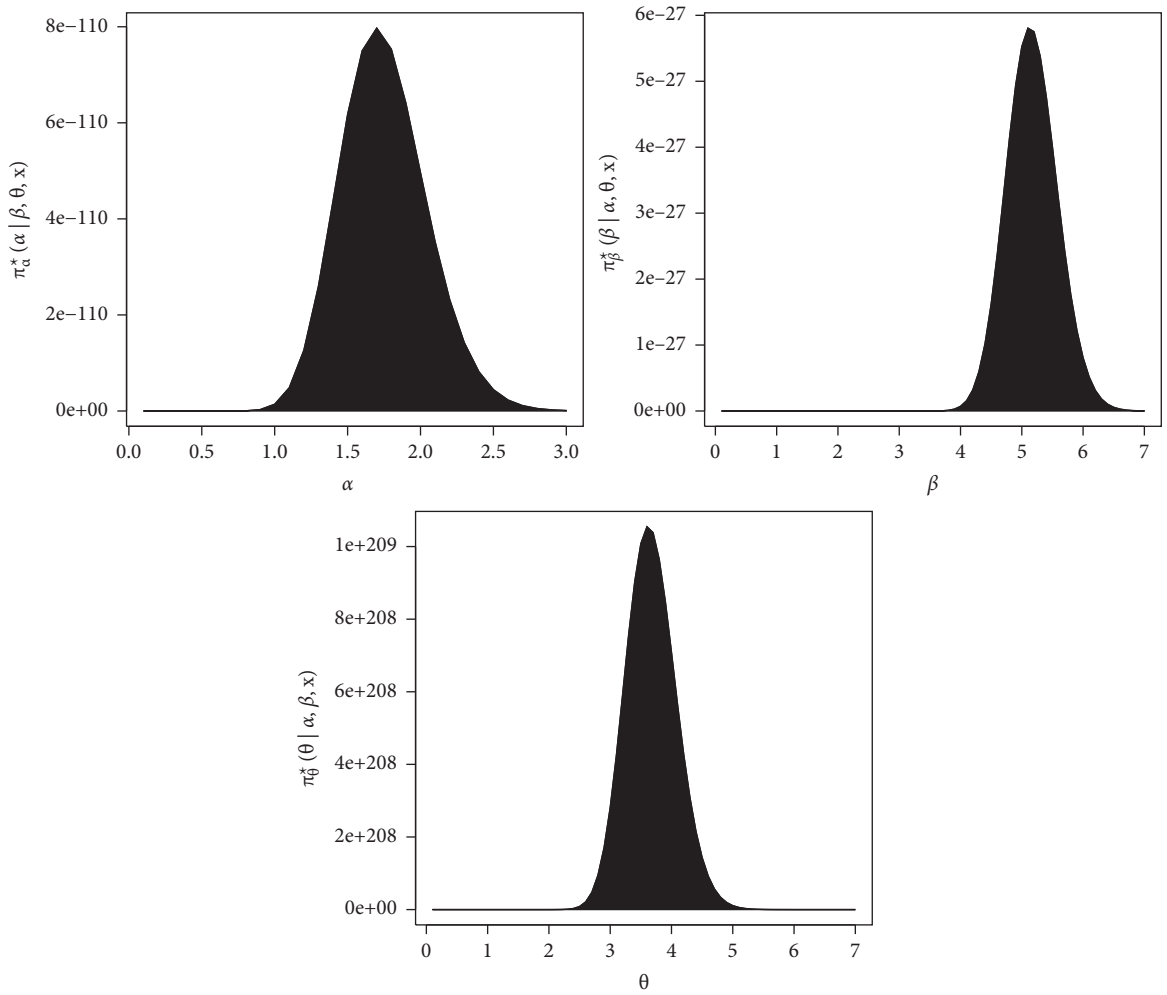

Figure 2: Plots of the conditional distributions of α, β, and θ.

Step 4: Obtain $R^{(g)}(t)$ and $h^{(g)}(t)$, for a specified time $t > 0$ by replacing α, β, and θ with their $\alpha^{(g)}$, $\beta^{(g)}$, and $\theta^{(g)}$, respectively.

Step 5: Put $g = g + 1$.

Step 6: Redo Steps 3–5 G times to obtain the MCMC simulated variates of α, β, θ, $R(t)$, or $h(t)$ (say κ) as $\kappa^{(g)} = (\alpha^{(g)}, \beta^{(g)}, \theta^{(g)}, R^{(g)}(t), h^{(g)}(t))$ for $g = 1, 2, \ldots, G$.

Step 7: Use outputs in Step 6, compute the Bayesian estimates of κ under SEL and LL functions given in (13) and (14), respectively, as:

$$\widetilde{\kappa}_S = \frac{\sum_{g=G_0+1}^{G} \kappa^{(g)}}{(G - G_0)}, \tag{24}$$

$$\widetilde{\kappa}_L = -\frac{1}{v}\log\left[\frac{\sum_{g=G_0+1}^{G} \exp\left(-v\kappa^{(g)}\right)}{(G - G_0)}\right], \quad v \neq 0, \tag{25}$$

where G_0 is the burn-in period.

3.4. Credible Intervals. To construct the Bayes credible interval (BCI) and highest posterior density (HPD) credible interval for the parameter of interest, the MCMC simulated variates of the target parameter are used. Under HPD credible interval, for every point inside the interval, the study distribution must be greater than that for every point outside the interval. Therefore, it has the shortest length among all possible credible intervals. According to the procedure proposed by Chen and Shao [24], the HPD credible interval can be constructed. Now, to establish the BCIs (or HPD credible intervals) of the unknown parameters α, β, and θ or the survival characteristics $R(t)$ and $h(t)$, for short say κ, one can be easily perform the following process:

Step 1: Order the simulated MCMC variates of $\kappa^{(g)}$ for $g = G_0 + 1, \ldots, G$, as $\kappa_{(G_0+1)}, \kappa_{(G_0+2)}, \ldots, \kappa_{(G)}$.

Step 2: Set the level of significance τ.

Step 3: Obtain the $100(1-\tau)$ BCI of κ as $(\kappa_{(G-G_0)(\tau/2)}, \kappa_{(G-G_0)(1-\tau/2)})$.

Step 4: Obtain the $100(1-\tau)$% HPD credible interval κ is given by,

$$\kappa_{(g^*)}, \kappa_{(g^*+(1-\tau)(G-G_0))}, \tag{26}$$

where $g^* = G_0 + 1, \ldots, G$ is chosen, such that,

$$\kappa_{(g^*+[(1-\tau)(G-G_0)])} - \kappa_{(g^*)} = \min_{1\leqslant g\leqslant \tau(G-G_0)} \left(\kappa_{(g+[(1-\tau)(G-G_0)])} - \kappa_{(g)}\right). \tag{27}$$

Here, $[x]$ denotes the largest integer less than or equal to x.

4. Optimum Progressive Censoring Plans

In reliability field, the problem to determine the "optimal" censoring scheme from a set of available censoring schemes is main issue. So, to great the information included in the unknown parameters under consideration, Balakrishnan and Aggarwala [25] first discussed the optimal censoring plan via several setups. Following Ng et al. [26], the values of n (total test units) and m (effective sample) must be fixed in advance, then one can be easily determine the optimal censoring design $(R_1, R_2, \ldots, R_m$ where $\sum_{i=1}^{m} R_i = n - m)$ under type-II progressive censoring by considering the following optimum criteria:

(i) Criterion-A: Minimize $\longrightarrow$ trace$(\mathbf{I}^{-1}(\cdot))$.

(ii) Criterion-B: Minimize $\longrightarrow$ det$(\mathbf{I}^{-1}(\cdot))$.

(iii) Criterion-C: Maximize $\longrightarrow$ trace$(\mathbf{I}(\cdot))$.

Regarding to criteria A and B, our goal is to minimize the trace and determinant of $\mathbf{I}^{-1}(\cdot)$ while regarding to the criterion C our goal is to maximize the main diagonal elements of $\mathbf{I}(\cdot)$, with respect to MLE $\widehat{\varphi}$ of φ. The optimized PCS-T2 plan that provides more information corresponds to the smallest value of criteria (A and B) with the highest value of C-criterion.

5. Monte Carlo Simulation

To show the performance of the proposed estimators of the unknown parameters α, β, and θ as well as the survival characteristics $R(t)$ and $h(t)$, a Monte Carlo simulation study is carried out. Using various combinations of n (total test units), m (effective sample size), and $\mathbf{R}$ (progressive censoring), a large 1,000 PCS-T2 samples are generated from the MOGE distribution when the true value of parameters α, β, θ is taken as $(0.8, 0.5, 0.2)$. Thus, for time $t = 0.1$, the actual value of the reliability and hazard functions is used as 0.91683 and 0.68856, respectively. In this study, some specified values of n, m, and $\mathbf{R}$ are also taken in account such as $n = 30$ (small), 60 (moderate), and 90 (large). As soon as the number of failed subjects achieves (or exceeds) m, where the failure proportion (FP), $(m/n)100\%$, is taken as 30, 60, and 90%, the experiment is terminated.

Moreover, for given n and m, different censoring schemes $\mathbf{R}$ to remove survival items during the test are also considered as:

$$\begin{aligned} &\text{CS}-1\text{: } R_1 = n - m, \\ &\qquad R_i = 0 \text{ for } i \neq 1, \\ &\text{CS}-2\text{: } \begin{cases} R_{m/2} = n - m, R_i = 0 \text{ for } \dfrac{i \neq m}{2}, \text{if } m \text{ is even}, \\ R_{(m+1)/2} = n - m, R_i = 0 \text{ for } \dfrac{i \neq (m+1)}{2}, \text{if } m \text{ is odd}, \end{cases} \\ &\text{CS}-3\text{: } R_m = n - m, R_i = 0 \text{ for } i \neq m. \end{aligned} \tag{28}$$

To examine the effects of the prior parameters a_i and b_i for $i = 1, 2, 3$ on the Bayesian analysis, two informative sets of the hyperparameters are used; called Prior-1 (say P1): $(a_1, a_2, a_3) = (1.6, 1, 0.4)$ and $b_i = 2, i = 1, 2, 3$, and Prior-II (say P2): $(a_1, a_2, a_3) = (4, 2.5, 1)$ and $b_i = 5, i = 1, 2, 3$. These values are specified in such a way that the expected value of prior became the expected value of the corresponding parameter. If one setting $a_i, b_i = 0$, $i = 1, 2, 3$, the posterior distribution (20) is reduced in proportion to the corresponding likelihood function (6). So, if one does not have prior information on the unknown parameter, we recommend to use the frequentist estimates instead of the Bayes estimates because the latter are more computationally expensive.

To develop the Bayesian calculations, following the M–H algorithm proposed in Section 3.3, we generate $G = 12,000$ MCMC samples and then the first $G_0 = 2,000$ iterations have been discarded as burn-in. Hence, using 10,000 MCMC samples, the average Bayes point estimates and associated BCI/HPD credible intervals of the unknown parameters α, β, θ, $R(t)$, and $h(t)$ are computed. Here, the Bayesian estimates relative to SEL and LL $(\upsilon(= -3, -0.03, +3))$ are developed.

For each considered setting, the average point estimates (APEs) using the proposed frequentist and Bayes approaches of α, β, θ, $R(t)$, or $h(t)$ (say η) are computed by

$$\mathrm{APE}\left(\widehat{\eta}_q\right) = \frac{1}{\mathscr{B}}\sum_{j=1}^{\mathscr{B}}\widehat{\eta}_\tau^{(j)}, q = 1,2,3,4,5, \tag{29}$$

where $\widehat{\eta}$ is the desired estimate of the parametric function η, $\widehat{\eta}_q^{(j)}$ denotes the obtained estimate at the $j-th$ sample of the unknown parameter η_q, $\mathscr{B}$ is number of generated sequence data, $\eta_1 = \alpha$, $\eta_2 = \beta$, $\eta_3 = \theta$, $\eta_4 = R(t)$, and $\eta_5 = h(t)$.

Comparison between different point estimates of α, β, θ, $R(t)$, or $h(t)$ (say η) is made based on their root mean squared-error (RMSE) and mean relative absolute bias (MRAB) values using the following formulae, respectively, as

$$\mathrm{RMSE}\left(\widehat{\eta}_q\right) = \sqrt{\frac{1}{\mathscr{B}}\sum_{j=1}^{\mathscr{B}}\left(\widehat{\eta}_q^{(j)} - \eta_q\right)^2}, \quad q = 1,2,3,4,5, \tag{30}$$

$$\mathrm{MRAB}\left(\widehat{\eta}_q\right) = \frac{1}{\mathscr{B}}\sum_{j=1}^{\mathscr{B}}\frac{\left|\widehat{\eta}_q^{(j)} - \eta_q\right|}{\eta_q}, \quad q = 1,2,3,4,5. \tag{31}$$

Further, the performances of different type of the $(1-\tau)$% two-sided asymptotic/credible intervals estimates are compared using their average confidence lengths (ACLs) and the average coverage percentages (CPs) as:

$$\mathrm{ACL}\left(\eta_q\right) = \frac{1}{\mathscr{B}}\sum_{j=1}^{\mathscr{B}}\left(\mathscr{U}\left(\widehat{\eta}_q^{(j)}\right) - \mathscr{L}\left(\widehat{\eta}_q^{(j)}\right)\right), \quad q = 1,2,3,4,5, \tag{32}$$

$$\mathrm{CP}\left(\eta_q\right) = \frac{1}{\mathscr{B}}\sum_{j=1}^{\mathscr{B}}1_{\left(\mathscr{L}\left(\widehat{\eta}_q^{(j)}\right),\mathscr{U}\left(\widehat{\eta}_q^{(j)}\right)\right)}\left(\eta_q\right), \quad q = 1,2,3,4,5, \tag{33}$$

where $\mathscr{L}(\cdot)$ and $\mathscr{U}(\cdot)$ denote the lower and upper bounds, respectively, of $(1-\tau)$% asymptotic (or credible) interval of the unknown parameter η_q.

All numerical computations were performed using *R* 4.0.4 software with three useful packages, namely: (i) "coda" package proposed by Plummer et al. [27]; (ii) "maxLik" package proposed by Henningsen and Toomet [28]; (iii) "GoFKernel" package by Pavia [29]. Recently, the same packages are also recommended by Elshahhat and Nassar [30].

The simulation results of α, β, θ, $R(t)$, and $h(t)$ are presented in Tables 1–10 and are also displayed with heatmaps in Figures 3–7. In each heatmap plot, the "x-lab" display the proposed estimation point (or interval) methods while the "y-lab" represents the different choices of n, FP%, and censoring schemes. For specification, using P1 for example, we have used the notation "SEL-P1" for the Bayes (SEL) estimates; "LL1-P1" for the Bayes (LL) estimates when $\upsilon = -3$; "LL2-P1" for the Bayes (LL) estimates when $\upsilon = -0.03$; "LL3-P1" for the Bayes (LL) estimates when $\upsilon = +3$; "BCI-P1" and "HPD-P1" denote to the BCI and HPD credible intervals, respectively. Also, "ACI-NA" and "ACI-NL" denote to ACI based on NA and NL methods, respectively. All simulation results are presented in Appendix B. Now, we can make the following observations:

(i) In general, all estimates of the unknown parameters α, β, and θ or the time parameters $R(t)$ and $h(t)$ are very good in term of minimum RMSEs and MRABs.

(ii) As n (or m) increases, the proposed estimate become more better. This pattern is also observed when $\sum_{i=1}^{m} R_i$ decreases.

(iii) Due to gamma prior information, the Bayesian estimates perform better than the competing frequentist estimates.

(iv) Bayes estimates using LL function of all unknown parameters are or may be overestimates (or underestimates) when $\upsilon < 0$ (or $\upsilon > 0$).

(v) RMSEs and MRABs of the Bayes (LL) estimates are smaller than the Bayes (SEL) estimates, in most cases, when υ close to a positive value.

(vi) On the basis of smallest ACLs and highest CPs, it is noted that the ACI-NA approach is the best compared to those obtained based on the ACI-NL approach, similarly, the interval estimates based on the HPD method are the best compared to those obtained based on the BCI method.

(vii) Comparing CSs 1 and 3, it is observed that RMSEs, MRABs, and ACLs of α, β, and θ are greater based on CS-3 than CS-1, thus the associated CPs of the same unknown parameters are greater based on CS-1 than CS-3.

(viii) It is also a predictable fact because of the expected duration of the test items using CS-1 (where $n-m$ subjects at the time of 1^{st} failure observed are removed) is greater than the CS-3 (where $n-m$ subjects are withdrawn at the time of m^{th} failure observed).

(ix) Estimates of $R(t)$ and $h(t)$ have the lowest RMSEs, MRABs, and ACLs as well as the highest CPs based on CS-3 than CS-1.

(x) Since the corresponding variance of P2 is less than the variance of P1, one can be seen that the Bayes (point/interval) estimates performed satisfactory based on P2 than P1 as expected.

Table 1: The APEs (first-line), RMSEs (second-line), and MRABs (third-line) of α.

t				SEL		LL					
Prior ⟶	FP	Scheme	MLE	I	II	I			II		
v ⟶						−3	−0.03	+3	−3	−0.03	+3
	30%	1	0.8465	0.7242	0.7955	0.7305	0.7243	0.7100	0.8022	0.7957	0.7759
			0.3001	0.1508	0.0898	0.1081	0.1190	0.1361	0.0306	0.0307	0.0557
			0.2790	0.1484	0.0512	0.1347	0.1482	0.1681	0.0344	0.0357	0.0394
		2	0.9038	0.8281	0.8056	0.8360	0.8282	0.8050	0.8124	0.8057	0.7892
			0.3662	0.1113	0.0949	0.0632	0.0719	0.0906	0.0350	0.0436	0.0659
			0.3144	0.0924	0.0729	0.0785	0.0888	0.1077	0.0427	0.0524	0.0720
		3	0.9373	0.7476	0.8241	0.7547	0.7477	0.7268	0.8312	0.8242	0.8026
			0.5291	0.1148	0.0943	0.0599	0.0695	0.0919	0.0321	0.0306	0.0536
			0.3934	0.0861	0.0579	0.0744	0.0858	0.1085	0.0391	0.0360	0.0563
	60%	1	0.8669	0.7651	0.8201	0.7764	0.7653	0.7396	0.8271	0.8202	0.8023
			0.2799	0.1105	0.0879	0.0698	0.0766	0.0956	0.0078	0.0186	0.0503
			0.2573	0.0948	0.0312	0.0869	0.0947	0.1125	0.0087	0.0157	0.0531
		2	0.8742	0.8039	0.7980	0.8136	0.8040	0.7771	0.8050	0.7981	0.7827
30			0.2755	0.1029	0.0847	0.0371	0.0351	0.0633	0.0162	0.0205	0.0482
			0.2568	0.0640	0.0494	0.0450	0.0411	0.0621	0.0190	0.0231	0.0404
		3	0.8447	0.7963	0.7312	0.8034	0.7964	0.7837	0.7405	0.7314	0.7132
			0.2701	0.1045	0.0819	0.0462	0.0559	0.0907	0.0199	0.0278	0.0452
			0.2573	0.0700	0.0535	0.0567	0.0653	0.0914	0.0199	0.0327	0.0466
	90%	1	0.8641	0.7906	0.6813	0.7961	0.7907	0.7767	0.6922	0.6814	0.6655
			0.2482	0.1094	0.0771	0.0245	0.0377	0.0769	0.0077	0.0176	0.0442
			0.2382	0.0797	0.0271	0.0295	0.0434	0.0755	0.0065	0.0129	0.0301
		2	0.8580	0.7288	0.7580	0.7372	0.7290	0.7138	0.7659	0.7581	0.7424
			0.2566	0.0994	0.0848	0.0165	0.0231	0.0585	0.0153	0.0193	0.0463
			0.2383	0.0602	0.0485	0.0176	0.0224	0.0484	0.0177	0.0208	0.0380
		3	0.8714	0.7785	0.8176	0.7841	0.7786	0.7656	0.8261	0.8177	0.8001
			0.2576	0.0926	0.0796	0.0289	0.0290	0.0521	0.0198	0.0248	0.0426
			0.2412	0.0658	0.0434	0.0332	0.0268	0.0430	0.0207	0.0238	0.0346
	30%	1	0.8904	0.8470	0.8063	0.8543	0.8472	0.8280	0.8141	0.8064	0.7824
			0.2091	0.1016	0.0956	0.0563	0.0532	0.0609	0.0160	0.0203	0.0602
			0.2003	0.0842	0.0436	0.0678	0.0607	0.0718	0.0186	0.0228	0.0494
		2	0.8819	0.7575	0.7643	0.7637	0.7576	0.7406	0.7704	0.7644	0.7491
			0.2231	0.0962	0.0891	0.0493	0.0561	0.0760	0.0302	0.0383	0.0631
			0.2098	0.0693	0.0542	0.0608	0.0671	0.0830	0.0370	0.0445	0.0636
		3	0.8770	0.7792	0.8481	0.7847	0.7793	0.7661	0.8551	0.8482	0.8291
			0.2592	0.1015	0.0843	0.0654	0.0617	0.0622	0.0206	0.0303	0.0602
			0.2262	0.0956	0.0341	0.0805	0.0728	0.0737	0.0235	0.0306	0.0507
	60%	1	0.8690	0.8154	0.7935	0.8219	0.8155	0.7958	0.7994	0.7936	0.7761
			0.1940	0.0890	0.0835	0.0238	0.0255	0.0528	0.0090	0.0200	0.0532
			0.1836	0.0466	0.0248	0.0277	0.0302	0.0519	0.0088	0.0158	0.0374
		2	0.8592	0.7462	0.8143	0.7513	0.7463	0.7336	0.8200	0.8144	0.7997
60			0.1919	0.0933	0.0877	0.0419	0.0455	0.0740	0.0299	0.0298	0.0513
			0.1829	0.0672	0.0475	0.0511	0.0530	0.0743	0.0355	0.0352	0.0543
		3	0.8461	0.7755	0.8581	0.7812	0.7756	0.7594	0.8644	0.8582	0.8422
			0.1838	0.1013	0.0803	0.0569	0.0539	0.0615	0.0191	0.0253	0.0509
			0.1773	0.0864	0.0340	0.0689	0.0618	0.0727	0.0222	0.0259	0.0475
	90%	1	0.8621	0.7934	0.7912	0.7986	0.7935	0.7810	0.7959	0.7912	0.7796
			0.1801	0.0743	0.0715	0.0098	0.0186	0.0418	0.0082	0.0171	0.0395
			0.1721	0.0317	0.0230	0.0090	0.0144	0.0291	0.0059	0.0116	0.0260
		2	0.8568	0.8221	0.8339	0.8284	0.8222	0.8032	0.8408	0.8341	0.8132
			0.1848	0.0914	0.0801	0.0369	0.0397	0.0560	0.0219	0.0228	0.0412
			0.1767	0.0532	0.0443	0.0454	0.0460	0.0633	0.0253	0.0270	0.0421
		3	0.8436	0.8102	0.7770	0.8164	0.8103	0.7920	0.7824	0.7771	0.7632
			0.1808	0.0858	0.0782	0.0201	0.0292	0.0550	0.0166	0.0226	0.0492
			0.1726	0.0394	0.0310	0.0220	0.0286	0.0460	0.0192	0.0265	0.0424

Table 1: Continued.

t				SEL		LL					
Prior ⟶	FP	Scheme	MLE	I	II	I			II		
v ⟶						−3	−0.03	+3	−3	−0.03	+3
	30%	1	0.8978	0.7893	0.7682	0.7945	0.7894	0.7753	0.7737	0.7683	0.7535
			0.1915	0.0840	0.0783	0.0272	0.0353	0.0613	0.0174	0.0259	0.0512
			0.1805	0.0397	0.0259	0.0329	0.0396	0.0581	0.0193	0.0252	0.0416
		2	0.8705	0.7742	0.7940	0.7794	0.7743	0.7607	0.7994	0.7941	0.7791
			0.1889	0.0825	0.0809	0.0233	0.0317	0.0576	0.0136	0.0197	0.0475
			0.1816	0.0357	0.0302	0.0280	0.0348	0.0531	0.0159	0.0216	0.0409
		3	0.8751	0.8020	0.8011	0.8076	0.8021	0.7866	0.8067	0.8012	0.7856
			0.1910	0.0830	0.0748	0.0181	0.0276	0.0551	0.0117	0.0193	0.0470
			0.1772	0.0326	0.0247	0.0199	0.0265	0.0447	0.0138	0.0197	0.0385
	60%	1	0.8762	0.7918	0.7805	0.7978	0.7919	0.7746	0.7857	0.7806	0.7667
			0.1686	0.0835	0.0770	0.0250	0.0332	0.0588	0.0094	0.0203	0.0496
			0.1598	0.0370	0.0253	0.0301	0.0367	0.0548	0.0074	0.0145	0.0410
		2	0.8516	0.7721	0.8036	0.7776	0.7722	0.7575	0.8093	0.8037	0.7876
90			0.1590	0.0797	0.0784	0.0221	0.0305	0.0555	0.0086	0.0186	0.0473
			0.1534	0.0322	0.0201	0.0258	0.0321	0.0492	0.0082	0.0147	0.0332
		3	0.8507	0.7787	0.7884	0.7841	0.7788	0.7642	0.7932	0.7885	0.7764
			0.1505	0.0804	0.0729	0.0135	0.0209	0.0501	0.0102	0.0189	0.0429
			0.1493	0.0271	0.0207	0.0157	0.0217	0.0414	0.0120	0.0173	0.0296
	90%	1	0.8489	0.7797	0.7705	0.7846	0.7798	0.7672	0.7759	0.7706	0.7562
			0.1504	0.0825	0.0757	0.0160	0.0251	0.0536	0.0089	0.0195	0.0469
			0.1460	0.0226	0.0173	0.0179	0.0243	0.0360	0.0068	0.0132	0.0309
		2	0.8454	0.7981	0.7920	0.8035	0.7982	0.7835	0.7970	0.7921	0.7791
			0.1413	0.0780	0.0745	0.0105	0.0189	0.0459	0.0083	0.0179	0.0431
			0.1373	0.0231	0.0193	0.0120	0.0180	0.0359	0.0060	0.0120	0.0281
		3	0.8471	0.8010	0.8007	0.8071	0.8011	0.7845	0.8058	0.8008	0.7875
			0.1474	0.0800	0.0800	0.0127	0.0195	0.0468	0.0101	0.0168	0.0410
			0.1432	0.0291	0.0281	0.0149	0.0207	0.0393	0.0085	0.0144	0.0334

Table 2: The APEs (first-line), RMSEs (second-line), and MRABs (third-line) of β.

n				SEL		LL					
Prior ⟶	FP	Scheme	MLE	I	II	I			II		
v ⟶						−3	−0.03	+3	−3	−0.03	+3
	30%	1	1.9985	0.5629	0.5427	0.5691	0.5630	0.5571	0.5471	0.5428	0.5390
			1.9726	0.0894	0.0749	0.0692	0.0630	0.0571	0.0480	0.0432	0.0402
			2.4722	0.1327	0.1067	0.1383	0.1260	0.1142	0.0941	0.0855	0.0788
		2	1.8432	0.5834	0.5514	0.5870	0.5834	0.5804	0.5586	0.5515	0.5449
			1.5105	0.0957	0.0859	0.0874	0.0836	0.0805	0.0741	0.0680	0.0643
			2.1497	0.1668	0.1355	0.1739	0.1668	0.1608	0.1454	0.1350	0.1282
		3	6.0528	0.5304	0.4064	0.5336	0.5304	0.5279	0.4145	0.4065	0.4009
			1.6522	0.1195	0.1161	0.0899	0.0904	0.0961	0.0835	0.0954	0.1001
			2.9469	0.2079	0.2070	0.1710	0.1777	0.1914	0.1539	0.1870	0.1983
	60%	1	1.0393	0.5479	0.4952	0.5490	0.5480	0.5470	0.5055	0.4953	0.4887
			1.7948	0.0672	0.0546	0.0493	0.0482	0.0472	0.0381	0.0392	0.0393
			1.5525	0.0973	0.0961	0.0980	0.0959	0.0940	0.0729	0.0762	0.0780
		2	0.9105	0.5565	0.5675	0.5583	0.5565	0.5548	0.5727	0.5675	0.5641
30			1.4539	0.0852	0.0660	0.0592	0.0566	0.0549	0.0586	0.0522	0.0458
			1.3115	0.1350	0.1129	0.1171	0.1129	0.1097	0.1167	0.1030	0.0898
		3	1.6928	0.4110	0.5678	0.4243	0.4111	0.4043	0.5715	0.5678	0.5641
			2.1120	0.0841	0.0612	0.0715	0.0679	0.0642	0.0353	0.0316	0.0286
			2.1506	0.1420	0.0803	0.1429	0.1356	0.1282	0.0671	0.0609	0.0557
	90%	1	0.8250	0.5188	0.4619	0.5214	0.5188	0.5169	0.4635	0.4619	0.4606
			1.1076	0.0501	0.0429	0.0238	0.0201	0.0177	0.0282	0.0168	0.0155
			1.1141	0.0873	0.0490	0.0427	0.0376	0.0339	0.0408	0.0305	0.0289
		2	0.8093	0.4851	0.5093	0.4869	0.4851	0.4837	0.5117	0.5093	0.5071
			0.9211	0.0409	0.0363	0.0158	0.0163	0.0171	0.0154	0.0125	0.0100
			1.0725	0.0623	0.0484	0.0295	0.0302	0.0326	0.0233	0.0186	0.0142
		3	0.7959	0.4810	0.5145	0.4866	0.4811	0.4770	0.5180	0.5145	0.5122
			0.8940	0.0536	0.0461	0.0261	0.0254	0.0270	0.0229	0.0170	0.0136
			1.1052	0.0696	0.0413	0.0486	0.0460	0.0478	0.0359	0.0290	0.0245

Table 2: Continued.

n				SEL		LL					
Prior ⟶	FP	Scheme	MLE	I	II	I			II		
v ⟶						−3	−0.03	+3	−3	−0.03	+3
	30%	1	0.8289	0.4609	0.5271	0.4696	0.4609	0.4563	0.5292	0.5271	0.5254
			1.2792	0.0775	0.0648	0.0484	0.0458	0.0457	0.0302	0.0312	0.0347
			1.1895	0.1102	0.0973	0.0955	0.0910	0.0874	0.0584	0.0606	0.0688
		2	0.8221	0.5196	0.5524	0.5226	0.5197	0.5177	0.5534	0.5524	0.5515
			1.0056	0.0674	0.0582	0.0536	0.0525	0.0522	0.0246	0.0206	0.0181
			1.1491	0.1150	0.1069	0.1048	0.1049	0.1031	0.0451	0.0393	0.0353
		3	2.3964	0.4963	0.4363	0.4996	0.4964	0.4943	0.4451	0.4363	0.4319
			1.2605	0.0918	0.0505	0.0275	0.0279	0.0289	0.0632	0.0661	0.0691
			1.7870	0.1550	0.0725	0.0508	0.0512	0.0551	0.1159	0.1273	0.1361
	60%	1	0.6404	0.5408	0.4696	0.5440	0.5408	0.5387	0.4756	0.4697	0.4656
			0.6240	0.0585	0.0582	0.0452	0.0435	0.0440	0.0280	0.0277	0.0258
			0.7339	0.0910	0.0817	0.0880	0.0817	0.0876	0.0519	0.0543	0.0509
		2	0.6507	0.4515	0.5102	0.4552	0.4515	0.4490	0.5145	0.5102	0.5072
60			0.6429	0.0503	0.0485	0.0475	0.0504	0.0516	0.0203	0.0136	0.0093
			0.7673	0.0564	0.0897	0.0477	0.0970	0.1020	0.0290	0.0205	0.0145
		3	0.8705	0.4746	0.5283	0.4780	0.4747	0.4725	0.5325	0.5283	0.5257
			1.2345	0.0552	0.0500	0.0212	0.0207	0.0217	0.0355	0.0294	0.0293
			1.5016	0.0726	0.0595	0.0404	0.0385	0.0421	0.0651	0.0566	0.0562
	90%	1	0.5737	0.5100	0.5455	0.5139	0.5100	0.5078	0.5478	0.5455	0.5438
			0.4576	0.0458	0.0447	0.0438	0.0414	0.0390	0.0197	0.0129	0.0091
			0.6049	0.0639	0.0317	0.0820	0.0794	0.0773	0.0277	0.0201	0.0155
		2	0.5792	0.4880	0.5030	0.4920	0.4881	0.4857	0.5072	0.5030	0.5004
			0.4528	0.0478	0.0448	0.0182	0.0156	0.0157	0.0179	0.0107	0.0068
			0.6110	0.0440	0.0462	0.0342	0.0294	0.0291	0.0208	0.0140	0.0105
		3	0.6153	0.4814	0.4741	0.4855	0.4814	0.4790	0.4780	0.4742	0.4719
			0.5390	0.0523	0.0421	0.0143	0.0100	0.0085	0.0284	0.0284	0.0261
			0.7138	0.0596	0.0348	0.0235	0.0184	0.0159	0.0531	0.0525	0.0514
	30%	1	0.6918	0.4963	0.4965	0.4988	0.4963	0.4947	0.4989	0.4966	0.4950
			1.0070	0.0400	0.0370	0.0184	0.0138	0.0110	0.0143	0.0097	0.0070
			0.8784	0.0299	0.0305	0.0271	0.0221	0.0190	0.0186	0.0150	0.0132
		2	0.6603	0.5138	0.4904	0.5163	0.5138	0.5122	0.4936	0.4904	0.4885
			0.7114	0.0442	0.0435	0.0283	0.0245	0.0223	0.0222	0.0163	0.0131
			0.8485	0.0469	0.0285	0.0518	0.0467	0.0435	0.0343	0.0276	0.0245
		3	1.4694	0.4988	0.5048	0.5026	0.4988	0.4967	0.5082	0.5049	0.5029
			1.2001	0.0448	0.0425	0.0181	0.0154	0.0149	0.0176	0.0112	0.0075
			1.0183	0.0425	0.0250	0.0334	0.0288	0.0272	0.0190	0.0136	0.0106
	60%	1	0.5322	0.5110	0.5059	0.5136	0.5111	0.5095	0.5083	0.5059	0.5044
			0.4071	0.0387	0.0365	0.0159	0.0107	0.0083	0.0120	0.0082	0.0067
			0.5394	0.0277	0.0198	0.0225	0.0181	0.0158	0.0166	0.0125	0.0099
		2	0.5573	0.5193	0.5138	0.5212	0.5194	0.5181	0.5171	0.5138	0.5118
90			0.3903	0.0440	0.0391	0.0234	0.0205	0.0187	0.0171	0.0143	0.0130
			0.5467	0.0399	0.0388	0.0424	0.0387	0.0362	0.0317	0.0270	0.0237
		3	0.6249	0.4900	0.5005	0.4935	0.4901	0.4879	0.5033	0.5005	0.4988
			0.8033	0.0442	0.0403	0.0175	0.0104	0.0076	0.0155	0.0096	0.0061
			1.0769	0.0251	0.0204	0.0247	0.0178	0.0141	0.0187	0.0126	0.0088
	90%	1	0.5475	0.5075	0.5008	0.5103	0.5075	0.5057	0.5029	0.5008	0.4994
			0.3430	0.0377	0.0345	0.0133	0.0098	0.0075	0.0110	0.0080	0.0059
			0.4828	0.0228	0.0171	0.0206	0.0150	0.0114	0.0165	0.0118	0.0087
		2	0.5332	0.4969	0.5234	0.5004	0.4969	0.4948	0.5259	0.5234	0.5217
			0.3258	0.0426	0.0378	0.0198	0.0156	0.0138	0.0165	0.0110	0.0088
			0.4729	0.0296	0.0281	0.0325	0.0276	0.0252	0.0264	0.0199	0.0166
		3	0.5489	0.5036	0.5049	0.5073	0.5036	0.5015	0.5079	0.5049	0.5031
			0.4135	0.0438	0.0390	0.0168	0.0101	0.0064	0.0137	0.0088	0.0060
			0.5669	0.0203	0.0198	0.0198	0.0126	0.0085	0.0162	0.0102	0.0067

Table 3: The APEs (first-line), RMSEs (second-line), and MRABs (third-line) of θ.

n				SEL		LL					
Prior ⟶	FP	Scheme	MLE	I	II	I			II		
v ⟶						−3	−0.03	+3	−3	−0.03	+3
	30%	1	0.3717	0.1597	0.1297	0.1647	0.1597	0.1562	0.1365	0.1297	0.1250
			0.3998	0.0943	0.0671	0.0398	0.0421	0.0445	0.0676	0.0719	0.0758
			1.1666	0.4028	0.2552	0.1830	0.2015	0.2188	0.3174	0.3513	0.3750
		2	0.5022	0.0924	0.2262	0.1026	0.0925	0.0868	0.2341	0.2262	0.2212
			0.6359	0.1299	0.0712	0.1031	0.1093	0.1139	0.0462	0.0384	0.0339
			1.7861	0.6028	0.2124	0.4870	0.5376	0.5658	0.2090	0.1817	0.1645
		3	1.1230	0.1331	0.1982	0.1378	0.1332	0.1298	0.2000	0.1982	0.1968
			1.8096	0.0854	0.0654	0.0655	0.0686	0.0713	0.0354	0.0362	0.0381
			1.6811	0.3790	0.2378	0.3108	0.3342	0.3509	0.1651	0.1677	0.1849
	60%	1	0.2717	0.1672	0.2235	0.1730	0.1673	0.1636	0.2256	0.2235	0.2218
			0.1825	0.0653	0.0430	0.0346	0.0356	0.0377	0.0273	0.0246	0.0225
			0.6336	0.2301	0.1441	0.1605	0.1641	0.1818	0.1281	0.1177	0.1092
		2	0.2958	0.1643	0.2363	0.1719	0.1643	0.1591	0.2418	0.2363	0.2329
30			0.2429	0.0753	0.0656	0.0376	0.0396	0.0430	0.0427	0.0311	0.0245
			0.7644	0.2776	0.2008	0.1738	0.1798	0.2045	0.1705	0.1312	0.1058
		3	0.3477	0.1967	0.1665	0.2017	0.1967	0.1922	0.1724	0.1666	0.1630
			0.4242	0.0683	0.0401	0.0074	0.0074	0.0099	0.0104	0.0089	0.0082
			1.4417	0.3104	0.1088	0.0313	0.0316	0.0440	0.0427	0.0386	0.0363
	90%	1	0.2443	0.2157	0.1969	0.2191	0.2157	0.2133	0.1986	0.1970	0.1957
			0.1392	0.0467	0.0316	0.0234	0.0180	0.0146	0.0090	0.0074	0.0067
			0.4836	0.1247	0.0788	0.0955	0.0785	0.0667	0.0394	0.0344	0.0318
		2	0.2546	0.2167	0.2185	0.2196	0.2168	0.2148	0.2215	0.2185	0.2165
			0.1539	0.0433	0.0450	0.0218	0.0178	0.0152	0.0254	0.0208	0.0179
			0.5352	0.1202	0.1101	0.0978	0.0838	0.0738	0.1073	0.0926	0.0827
		3	0.2506	0.2621	0.1967	0.2633	0.2621	0.2609	0.1995	0.1967	0.1947
			0.1698	0.0564	0.0335	0.0635	0.0622	0.0610	0.0095	0.0067	0.0064
			0.6328	0.2147	0.1031	0.3167	0.3105	0.3047	0.0377	0.0307	0.0297
	30%	1	0.2633	0.1889	0.1408	0.1903	0.1889	0.1878	0.1469	0.1408	0.1372
			0.1908	0.0827	0.0574	0.0586	0.0614	0.0639	0.0243	0.0149	0.0132
			0.6170	0.3539	0.1095	0.2683	0.2960	0.3142	0.0965	0.0685	0.0614
		2	0.3201	0.1452	0.2157	0.1526	0.1452	0.1406	0.2207	0.2158	0.2129
			0.2967	0.0842	0.0538	0.0541	0.0572	0.0606	0.0292	0.0204	0.0157
			0.8839	0.3342	0.1129	0.2474	0.2738	0.2972	0.1037	0.0789	0.0645
		3	0.6700	0.2126	0.1977	0.2147	0.2126	0.2112	0.1994	0.1977	0.1965
			1.1081	0.0626	0.0543	0.0408	0.0431	0.0452	0.0218	0.0133	0.0083
			1.2887	0.2553	0.1497	0.1921	0.2103	0.2237	0.0771	0.0508	0.0336
	60%	1	0.2305	0.1945	0.1990	0.2011	0.1946	0.1912	0.2039	0.1990	0.1958
			0.1106	0.0551	0.0477	0.0398	0.0347	0.0319	0.0193	0.0127	0.0101
			0.4023	0.1675	0.1050	0.1853	0.1676	0.1566	0.0698	0.0538	0.0468
		2	0.2409	0.2121	0.2267	0.2135	0.2121	0.2109	0.2298	0.2267	0.2245
60			0.1442	0.0640	0.0428	0.0467	0.0484	0.0500	0.0182	0.0167	0.0168
			0.4870	0.2808	0.1113	0.2199	0.2366	0.2472	0.0855	0.0776	0.0760
		3	0.2676	0.1579	0.2101	0.1616	0.1579	0.1553	0.2154	0.2102	0.2067
			0.2763	0.0509	0.0333	0.0219	0.0207	0.0213	0.0093	0.0070	0.0060
			1.0459	0.1464	0.0734	0.1029	0.0950	0.0967	0.0390	0.0322	0.0287
	90%	1	0.2121	0.2098	0.2335	0.2140	0.2098	0.2073	0.2371	0.2335	0.2313
			0.0846	0.0526	0.0315	0.0197	0.0128	0.0123	0.0128	0.0127	0.0087
			0.3163	0.1479	0.0971	0.0698	0.0593	0.0579	0.0601	0.0492	0.0366
		2	0.2148	0.1527	0.1875	0.1560	0.1527	0.1506	0.1904	0.1875	0.1856
			0.0909	0.0502	0.0319	0.0324	0.0281	0.0252	0.0148	0.0128	0.0113
			0.3345	0.1478	0.0931	0.1492	0.1336	0.1225	0.0676	0.0604	0.0546
		3	0.2157	0.1836	0.1973	0.1877	0.1837	0.1810	0.1992	0.1973	0.1960
			0.1115	0.0368	0.0314	0.0183	0.0147	0.0124	0.0089	0.0068	0.0058
			0.4229	0.0721	0.0691	0.0737	0.0632	0.0561	0.0375	0.0311	0.0274

Table 3: Continued.

n				SEL		LL					
Prior ⟶	FP	Scheme	MLE	I	II	I			II		
v ⟶						−3	−0.03	+3	−3	−0.03	+3
	30%	1	0.2435	0.2101	0.1928	0.2126	0.2101	0.2085	0.1957	0.1928	0.1911
			0.1384	0.0424	0.0398	0.0175	0.0129	0.0101	0.0165	0.0124	0.0115
			0.4771	0.0896	0.0543	0.0763	0.0640	0.0584	0.0443	0.0588	0.0538
		2	0.2616	0.2103	0.1986	0.2134	0.2104	0.2085	0.2009	0.1986	0.1972
			0.1991	0.0451	0.0413	0.0243	0.0190	0.0160	0.0153	0.0118	0.0108
			0.6324	0.1075	0.0840	0.1025	0.0863	0.0764	0.0685	0.0560	0.0506
		3	0.4731	0.2010	0.2066	0.2035	0.2010	0.1995	0.2090	0.2066	0.2052
			0.7870	0.0494	0.0422	0.0367	0.0333	0.0313	0.0194	0.0140	0.0107
			0.9913	0.1631	0.0824	0.1755	0.1630	0.1549	0.0615	0.0465	0.0371
	60%	1	0.2107	0.1925	0.2057	0.1957	0.1926	0.1906	0.2086	0.2058	0.2040
			0.0837	0.0410	0.0382	0.0169	0.0137	0.0127	0.0162	0.0110	0.0077
			0.3132	0.0853	0.0525	0.0628	0.0504	0.0426	0.0432	0.0291	0.0204
		2	0.2203	0.1892	0.1933	0.1929	0.1892	0.1871	0.1964	0.1933	0.1915
90			0.0973	0.0420	0.0357	0.0198	0.0146	0.0144	0.0125	0.0090	0.0071
			0.3522	0.0948	0.0549	0.0813	0.0690	0.0666	0.0486	0.0388	0.0330
		3	0.2094	0.1940	0.2326	0.1962	0.1940	0.1926	0.2351	0.2326	0.2310
			0.2080	0.0442	0.0366	0.0263	0.0218	0.0193	0.0126	0.0104	0.0096
			0.8395	0.1030	0.0737	0.1167	0.1024	0.0936	0.0577	0.0492	0.0451
	90%	1	0.2093	0.2057	0.2060	0.2088	0.2057	0.2039	0.2086	0.2060	0.2044
			0.0672	0.0406	0.0381	0.0161	0.0112	0.0081	0.0154	0.0102	0.0066
			0.2584	0.0505	0.0493	0.0448	0.0322	0.0244	0.0401	0.0289	0.0196
		2	0.2087	0.2021	0.2172	0.2044	0.2022	0.2007	0.2205	0.2173	0.2153
			0.0718	0.0410	0.0354	0.0174	0.0140	0.0106	0.0116	0.0073	0.0047
			0.2694	0.0607	0.0510	0.0672	0.0518	0.0425	0.0331	0.0226	0.0162
		3	0.2053	0.2093	0.2205	0.2123	0.2093	0.2074	0.2233	0.2205	0.2187
			0.0925	0.0369	0.0355	0.0156	0.0111	0.0082	0.0129	0.0084	0.0058
			0.3563	0.0453	0.0434	0.0454	0.0337	0.0263	0.0429	0.0312	0.0241

Table 4: The APEs (first-line), RMSEs (second-line), and MRABs (third-line) of $R(t)$.

n				SEL		LL					
Prior ⟶	FP	Scheme	MLE	I	II	I			II		
v ⟶						−3	−0.03	+3	−3	−0.03	+3
	30%	1	0.9212	0.9094	0.9365	0.9151	0.9095	0.8942	0.9430	0.9366	0.9177
			0.1454	0.0984	0.0797	0.0564	0.0625	0.0761	0.0095	0.0203	0.0696
			0.1394	0.0673	0.0236	0.0612	0.0672	0.0788	0.0099	0.0166	0.0444
		2	0.9191	0.9565	0.9112	0.9636	0.9566	0.9349	0.9164	0.9112	0.8991
			0.1461	0.1013	0.0742	0.0480	0.0456	0.0717	0.0209	0.0280	0.0473
			0.1377	0.0671	0.0325	0.0510	0.0461	0.0612	0.0218	0.0269	0.0390
		3	0.9240	0.9206	0.9016	0.9285	0.9207	0.8929	0.9070	0.9017	0.8869
			0.1425	0.1006	0.0854	0.0324	0.0367	0.0736	0.0124	0.0224	0.0513
			0.1365	0.0380	0.0340	0.0346	0.0380	0.0524	0.0107	0.0166	0.0326
	60%	1	0.9237	0.9146	0.9096	0.9226	0.9148	0.8882	0.9135	0.9096	0.9007
			0.1385	0.0942	0.0658	0.0280	0.0284	0.0510	0.0090	0.0179	0.0477
			0.1342	0.0450	0.0176	0.0286	0.0293	0.0461	0.0060	0.0108	0.0271
		2	0.9200	0.9284	0.9097	0.9363	0.9285	0.9004	0.9138	0.9097	0.9007
30			0.1364	0.1002	0.0656	0.0362	0.0425	0.0615	0.0113	0.0196	0.0419
			0.1315	0.0478	0.0298	0.0390	0.0446	0.0566	0.0097	0.0143	0.0264
		3	0.9246	0.8979	0.9074	0.9001	0.8979	0.8942	0.9141	0.9075	0.8898
			0.1371	0.0793	0.0651	0.0179	0.0244	0.0466	0.0105	0.0184	0.0502
			0.1328	0.0319	0.0236	0.0183	0.0231	0.0449	0.0108	0.0140	0.0297
	90%	1	0.9242	0.9072	0.8551	0.9113	0.9073	0.8978	0.8607	0.8552	0.8446
			0.1346	0.0889	0.0643	0.0093	0.0168	0.0353	0.0074	0.0166	0.0337
			0.1303	0.0314	0.0171	0.0065	0.0104	0.0207	0.0052	0.0106	0.0202
		2	0.9216	0.8758	0.8921	0.8811	0.8759	0.8649	0.8968	0.8921	0.8810
			0.1348	0.0819	0.0542	0.0220	0.0262	0.0590	0.0106	0.0178	0.0348
			0.1305	0.0401	0.0246	0.0221	0.0268	0.0555	0.0079	0.0117	0.0210
		3	0.9240	0.8820	0.9195	0.8851	0.8820	0.8757	0.9235	0.9196	0.9108
			0.1354	0.0636	0.0484	0.0161	0.0213	0.0275	0.0069	0.0147	0.0294
			0.1316	0.0228	0.0213	0.0163	0.0206	0.0247	0.0045	0.0108	0.0228

Table 4: Continued.

n				SEL		LL					
Prior ⟶	FP	Scheme	MLE	I	II	I			II		
v ⟶						−3	−0.03	+3	−3	−0.03	+3
	30%	1	0.9268	0.9228	0.9327	0.9266	0.9229	0.9143	0.9403	0.9328	0.9073
			0.1321	0.0985	0.0778	0.0255	0.0278	0.0656	0.0129	0.0199	0.0482
			0.1285	0.0436	0.0237	0.0258	0.0288	0.0537	0.0132	0.0160	0.0289
		2	0.9206	0.9200	0.9031	0.9261	0.9201	0.9024	0.9082	0.9031	0.8891
			0.1291	0.0844	0.0777	0.0341	0.0396	0.0545	0.0158	0.0216	0.0486
			0.1248	0.0409	0.0295	0.0365	0.0408	0.0509	0.0160	0.0199	0.0344
		3	0.9256	0.9011	0.9167	0.9047	0.9011	0.8933	0.9205	0.9168	0.9079
			0.1295	0.0765	0.0658	0.0180	0.0210	0.0435	0.0109	0.0183	0.0384
			0.1258	0.0299	0.0206	0.0182	0.0194	0.0306	0.0111	0.0160	0.0268
	60%	1	0.9248	0.9223	0.9042	0.9281	0.9224	0.9056	0.9095	0.9043	0.8903
			0.1285	0.0822	0.0629	0.0147	0.0222	0.0487	0.0123	0.0159	0.0291
			0.1254	0.0285	0.0232	0.0150	0.0196	0.0370	0.0080	0.0137	0.0246
		2	0.9216	0.8793	0.9102	0.8834	0.8794	0.8701	0.9138	0.9103	0.9022
60			0.1268	0.0774	0.0770	0.0209	0.0223	0.0516	0.0118	0.0196	0.0402
			0.1235	0.0356	0.0177	0.0211	0.0231	0.0378	0.0094	0.0149	0.0302
		3	0.9219	0.9144	0.9296	0.9196	0.9145	0.9005	0.9331	0.9297	0.9222
			0.1271	0.0762	0.0622	0.0140	0.0203	0.0430	0.0092	0.0169	0.0309
			0.1238	0.0222	0.0175	0.0133	0.0171	0.0284	0.0093	0.0135	0.0258
	90%	1	0.9240	0.9096	0.9071	0.9129	0.9096	0.9024	0.9104	0.9071	0.9000
			0.1270	0.0586	0.0584	0.0097	0.0161	0.0301	0.0083	0.0148	0.0288
			0.1242	0.0125	0.0114	0.0070	0.0106	0.0184	0.0047	0.0082	0.0160
		2	0.9226	0.9307	0.9244	0.9358	0.9307	0.9170	0.9297	0.9245	0.9101
			0.1261	0.0745	0.0613	0.0137	0.0204	0.0426	0.0084	0.0154	0.0309
			0.1229	0.0272	0.0162	0.0141	0.0193	0.0360	0.0056	0.0093	0.0179
		3	0.9207	0.9165	0.9013	0.9217	0.9166	0.9027	0.9052	0.9014	0.8922
			0.1263	0.0633	0.0606	0.0139	0.0187	0.0353	0.0085	0.0148	0.0267
			0.1230	0.0182	0.0170	0.0127	0.0169	0.0257	0.0085	0.0130	0.0224
	30%	1	0.9295	0.9050	0.9032	0.9091	0.9051	0.8953	0.9079	0.9033	0.8911
			0.1275	0.0769	0.0677	0.0142	0.0224	0.0455	0.0107	0.0185	0.0385
			0.1247	0.0178	0.0133	0.0130	0.0178	0.0302	0.0085	0.0138	0.0238
		2	0.9207	0.9028	0.9090	0.9070	0.9028	0.8926	0.9132	0.9091	0.8991
			0.1228	0.0720	0.0696	0.0127	0.0206	0.0405	0.0088	0.0169	0.0365
			0.1201	0.0194	0.0154	0.0108	0.0153	0.0264	0.0054	0.0099	0.0233
		3	0.9246	0.9120	0.9108	0.9162	0.9121	0.9021	0.9151	0.9109	0.9006
			0.1243	0.0712	0.0676	0.0159	0.0217	0.0406	0.0106	0.0190	0.0351
			0.1217	0.0184	0.0196	0.0158	0.0194	0.0242	0.0078	0.0124	0.0273
	60%	1	0.9257	0.9125	0.9050	0.9178	0.9126	0.8984	0.9092	0.9051	0.8950
			0.1239	0.0732	0.0666	0.0120	0.0210	0.0447	0.0107	0.0184	0.0374
			0.1210	0.0179	0.0130	0.0097	0.0148	0.0292	0.0083	0.0128	0.0235
		2	0.9208	0.9094	0.9168	0.9141	0.9095	0.8974	0.9213	0.9169	0.9058
90			0.1226	0.0684	0.0670	0.0098	0.0171	0.0403	0.0083	0.0162	0.0361
			0.1201	0.0144	0.0131	0.0100	0.0143	0.0261	0.0052	0.0102	0.0208
		3	0.9218	0.9054	0.8990	0.9097	0.9054	0.8949	0.9024	0.8991	0.8918
			0.1214	0.0689	0.0614	0.0098	0.0185	0.0395	0.0093	0.0163	0.0342
			0.1190	0.0144	0.0141	0.0071	0.0119	0.0240	0.0067	0.0110	0.0221
	90%	1	0.9232	0.9055	0.9004	0.9092	0.9055	0.8969	0.9049	0.9005	0.8891
			0.1230	0.0717	0.0635	0.0109	0.0189	0.0440	0.0091	0.0179	0.0347
			0.1203	0.0153	0.0126	0.0083	0.0128	0.0281	0.0084	0.0123	0.0217
		2	0.9212	0.9104	0.9084	0.9143	0.9105	0.9013	0.9121	0.9084	0.9000
			0.1214	0.0645	0.0625	0.0086	0.0159	0.0336	0.0081	0.0157	0.0324
			0.1188	0.0121	0.0117	0.0056	0.0098	0.0198	0.0052	0.0092	0.0184
		3	0.9221	0.9094	0.9074	0.9140	0.9094	0.8980	0.9110	0.9074	0.8994
			0.1213	0.0667	0.0609	0.0085	0.0166	0.0366	0.0083	0.0160	0.0320
			0.1187	0.0140	0.0116	0.0070	0.0113	0.0222	0.0064	0.0103	0.0190

Table 5: The APEs (first-line), RMSEs (second-line), and MRABs (third-line) of $h(t)$.

n				SEL		LL					
Prior ⟶	FP	Scheme	MLE	I	II	I			I		
v ⟶						−3	−0.03	+3	−3	−0.03	+3
	30%	1	0.6786	0.6490	0.4730	1.0081	0.6503	0.6053	0.8772	0.4746	0.4135
			0.4189	0.3983	0.3037	0.3506	0.2297	0.2758	0.2550	0.0978	0.1235
			0.4643	0.4215	0.1969	0.3822	0.3112	0.3995	0.2773	0.1351	0.1792
		2	0.7198	0.3130	0.7049	0.7986	0.3149	0.2535	1.0613	0.7064	0.6347
			0.4300	0.4258	0.3264	0.4134	0.3863	0.3559	0.3609	0.1400	0.0874
			0.4225	0.3955	0.2592	0.4186	0.3267	0.3182	0.3559	0.1918	0.1243
		3	0.7028	0.5604	0.7902	0.9726	0.5619	0.5121	1.0398	0.7911	0.7488
			0.4035	0.3519	0.2761	0.3228	0.2499	0.2226	0.2378	0.1138	0.0916
			0.3973	0.2968	0.2013	0.3362	0.2596	0.2563	0.2216	0.1490	0.1329
	60%	1	0.6373	0.6189	0.7311	1.0722	0.6206	0.5652	0.9240	0.7318	0.7019
			0.2817	0.2489	0.2273	0.2967	0.2206	0.2524	0.2053	0.0696	0.0235
			0.3326	0.2614	0.1357	0.2540	0.2630	0.2644	0.2421	0.0655	0.0281
		2	0.6791	0.5351	0.7158	1.0068	0.5368	0.4875	0.9794	0.7168	0.6678
30			0.2723	0.2760	0.2196	0.2166	0.2310	0.2026	0.2084	0.0909	0.0682
			0.3064	0.2625	0.2374	0.2433	0.2363	0.2921	0.2290	0.0960	0.0863
		3	0.6295	0.8216	0.6625	0.9191	0.8221	0.7905	1.0846	0.6642	0.5971
			0.2569	0.2416	0.2293	0.2519	0.1547	0.1796	0.2307	0.0712	0.0825
			0.3064	0.2601	0.1867	0.2792	0.2070	0.2231	0.2102	0.0982	0.1188
	90%	1	0.6354	0.7311	1.0063	0.9878	0.7320	0.6968	1.2238	1.0074	0.9395
			0.2435	0.2181	0.2073	0.2160	0.0735	0.0835	0.2031	0.0685	0.0108
			0.2830	0.2400	0.1280	0.2346	0.1007	0.1209	0.2316	0.0631	0.0119
		2	0.6478	0.9153	0.8195	1.1731	0.9164	0.8494	1.0931	0.8206	0.7742
			0.2392	0.2236	0.2048	0.2042	0.1767	0.1625	0.1868	0.0784	0.0412
			0.2783	0.2421	0.1951	0.2037	0.2210	0.1594	0.1876	0.0743	0.0504
		3	0.6329	0.9357	0.6420	1.0617	0.9362	0.9110	0.8771	0.6429	0.6068
			0.2520	0.2101	0.1811	0.2309	0.1368	0.1021	0.2238	0.0674	0.0605
			0.2906	0.2589	0.1722	0.2419	0.1940	0.1481	0.2047	0.0899	0.0874
	30%	1	0.6572	0.6334	0.5008	0.8137	0.6341	0.6085	0.9592	0.5025	0.4503
			0.2770	0.2216	0.1936	0.2428	0.2062	0.2392	0.2269	0.0965	0.0813
			0.3112	0.2877	0.1898	0.2408	0.2760	0.2461	0.2334	0.1031	0.1162
		2	0.7069	0.5881	0.7386	0.9764	0.5896	0.5409	1.0929	0.7398	0.7037
			0.2509	0.2335	0.1953	0.2291	0.1600	0.1669	0.2032	0.1093	0.1201
			0.2686	0.2560	0.1108	0.2125	0.1755	0.2144	0.1871	0.1484	0.1724
		3	0.6664	0.7734	0.6881	0.9706	0.7741	0.7482	0.8778	0.6888	0.6640
			0.2240	0.2168	0.2107	0.2125	0.1148	0.1314	0.1838	0.0797	0.0778
			0.2495	0.1789	0.1540	0.2096	0.1546	0.1901	0.2033	0.1071	0.1123
	60%	1	0.6459	0.6104	0.7490	1.0076	0.6118	0.5727	1.0645	0.7502	0.7022
			0.2024	0.1942	0.1316	0.1860	0.1100	0.1175	0.1846	0.0753	0.0318
			0.2390	0.2236	0.1566	0.1953	0.1509	0.1682	0.1622	0.0895	0.0338
		2	0.6694	0.9138	0.7268	1.0909	0.9145	0.8849	0.9477	0.7276	0.6962
60			0.1812	0.1645	0.1403	0.1761	0.1295	0.1656	0.1558	0.0855	0.0192
			0.2099	0.1719	0.1248	0.1844	0.1522	0.2052	0.1763	0.0744	0.0220
		3	0.6636	0.6473	0.5887	0.9432	0.6483	0.6112	0.8412	0.5896	0.5577
			0.1903	0.1728	0.1686	0.1814	0.0976	0.0758	0.1754	0.0712	0.0536
			0.2194	0.1673	0.1129	0.1995	0.1243	0.1041	0.1723	0.0982	0.0770
	90%	1	0.6474	0.7180	0.7401	0.9405	0.7188	0.6931	0.9683	0.7409	0.7137
			0.1790	0.1405	0.1203	0.1800	0.0752	0.0272	0.1548	0.0597	0.0099
			0.2122	0.0968	0.0691	0.1662	0.0760	0.0365	0.1597	0.0445	0.0082
		2	0.6556	0.5421	0.6030	0.8506	0.5432	0.5095	0.9075	0.6041	0.5698
			0.1668	0.1608	0.1393	0.1537	0.1288	0.1496	0.1505	0.0675	0.0146
			0.1916	0.1562	0.1220	0.1589	0.1328	0.1600	0.1442	0.0567	0.0136
		3	0.6640	0.6565	0.7657	0.9680	0.6576	0.6169	0.9671	0.7664	0.7416
			0.1719	0.1650	0.1341	0.1667	0.0918	0.0600	0.1616	0.0520	0.0279
			0.1975	0.1260	0.0966	0.1957	0.1130	0.0866	0.1522	0.0610	0.0367

Table 5: Continued.

n				SEL			LL				
Prior ⟶	FP	Scheme	MLE	I	II	I			I		
v ⟶						−3	−0.03	+3	−3	−0.03	+3
	30%	1	0.6373	0.7468	0.7389	0.9890	0.7476	0.7205	1.0140	0.7398	0.7106
			0.2188	0.1862	0.1647	0.2079	0.0963	0.0513	0.1662	0.0791	0.0461
			0.2541	0.1226	0.0864	0.1992	0.1135	0.0733	0.1727	0.0876	0.0618
		2	0.6982	0.7529	0.7146	1.0105	0.7538	0.7262	0.9498	0.7154	0.6888
			0.1849	0.1549	0.1386	0.1543	0.0876	0.0640	0.1480	0.0622	0.0268
			0.2073	0.1416	0.1010	0.1675	0.0975	0.0902	0.1481	0.0641	0.0373
		3	0.6728	0.6961	0.7050	0.9358	0.6969	0.6698	0.9488	0.7059	0.6785
			0.1762	0.1599	0.1423	0.1481	0.1236	0.0880	0.1320	0.0724	0.0236
			0.2017	0.1664	0.0849	0.1652	0.1668	0.1274	0.1401	0.0650	0.0304
	60%	1	0.6504	0.6771	0.7389	0.9836	0.6782	0.6460	0.9926	0.7398	0.7121
			0.1648	0.1605	0.1503	0.1567	0.0791	0.0329	0.1555	0.0735	0.0257
			0.1910	0.1122	0.0848	0.1524	0.0857	0.0464	0.1492	0.0774	0.0342
		2	0.6759	0.6928	0.6549	0.9933	0.6938	0.6629	0.9278	0.6559	0.6264
90			0.1509	0.1448	0.1258	0.1360	0.0715	0.0395	0.1291	0.0585	0.0118
			0.1721	0.0948	0.0710	0.1494	0.0947	0.0547	0.1402	0.0499	0.0205
		3	0.6722	0.7314	0.8027	0.9686	0.7322	0.7050	1.0055	0.8034	0.7763
			0.1462	0.1419	0.1124	0.1359	0.0734	0.0281	0.1249	0.0696	0.0228
			0.1706	0.1277	0.0841	0.1440	0.0768	0.0393	0.1268	0.0634	0.0296
	90%	1	0.6526	0.7377	0.7658	0.9747	0.7386	0.7119	1.0271	0.7667	0.7390
			0.1459	0.1422	0.1259	0.1526	0.0764	0.0251	0.1394	0.0696	0.0249
			0.1686	0.0889	0.0783	0.1441	0.0744	0.0339	0.1416	0.0726	0.0320
		2	0.6702	0.7082	0.7249	0.9323	0.7089	0.6833	0.9652	0.7258	0.6980
			0.1391	0.1232	0.1142	0.1305	0.0639	0.0121	0.1202	0.0562	0.0105
			0.1616	0.0880	0.0665	0.1471	0.0540	0.0144	0.1388	0.0487	0.0137
		3	0.6626	0.7148	0.7406	0.9811	0.7157	0.6822	0.9649	0.7414	0.7156
			0.1380	0.1259	0.1109	0.1211	0.0611	0.0190	0.1201	0.0583	0.0169
			0.1637	0.0882	0.0833	0.1407	0.0626	0.0239	0.1091	0.0587	0.0226

Table 6: The ACLs/CPs of asymptotic/credible interval estimates of α.

n			ACI-NA		BCI			
	FP	Scheme	ACI-NL		HPD			
Prior ⟶					I	II	I	II
			ACL	CP	ACL	CP	ACL	CP
	30%	1	1.5136	0.963	0.3198	0.988	0.2507	0.999
			2.0153	0.935	0.2705	0.959	0.1942	0.972
		2	1.6241	0.963	0.3085	0.988	0.2710	0.999
			2.0466	0.933	0.2496	0.957	0.2316	0.970
		3	1.8642	0.930	0.2966	0.954	0.2804	0.967
			2.0752	0.931	0.2569	0.955	0.2393	0.968
	60%	1	1.2520	0.966	0.2967	0.991	0.2257	0.999
			1.4132	0.942	0.2644	0.966	0.1706	0.979
		2	1.2288	0.970	0.2835	0.995	0.2668	0.999
30			1.3672	0.947	0.2401	0.972	0.2202	0.984
		3	1.1503	0.948	0.2776	0.973	0.2344	0.985
			1.6574	0.935	0.2320	0.959	0.1790	0.972
	90%	1	1.1156	0.982	0.2389	0.997	0.2069	0.999
			1.2204	0.958	0.1992	0.983	0.1595	0.996
		2	1.1042	0.978	0.2630	0.994	0.2420	0.999
			1.2040	0.949	0.2074	0.974	0.1959	0.986
		3	1.1252	0.966	0.2347	0.991	0.2147	0.999
			1.2621	0.941	0.1799	0.965	0.1697	0.978

Table 6: Continued.

n	FP	Scheme	ACI-NA		BCI			
			ACI-NL		HPD			
Prior ⟶					I	II	I	II
			ACL	CP	ACL	CP	ACL	CP
60	30%	1	1.0578	0.971	0.2607	0.997	0.2495	0.999
			1.1375	0.939	0.2003	0.964	0.1968	0.977
		2	1.0423	0.965	0.2327	0.991	0.2083	0.999
			1.1156	0.943	0.1841	0.968	0.1577	0.982
		3	1.3312	0.953	0.2442	0.979	0.2028	0.992
			1.6050	0.930	0.1917	0.955	0.1597	0.968
	60%	1	0.8704	0.979	0.2009	0.995	0.1897	0.999
			0.9127	0.947	0.1452	0.973	0.1349	0.986
		2	0.8333	0.971	0.2249	0.997	0.1962	0.999
			0.8713	0.949	0.1687	0.973	0.1460	0.985
		3	0.9457	0.956	0.2241	0.982	0.1908	0.995
			1.0345	0.938	0.1770	0.963	0.1386	0.976
	90%	1	0.7658	0.990	0.1903	0.997	0.1730	0.999
			0.7945	0.961	0.1457	0.987	0.1294	0.999
		2	0.7514	0.987	0.2059	0.996	0.1925	0.999
			0.7789	0.949	0.1600	0.974	0.1404	0.988
		3	0.7766	0.969	0.1927	0.995	0.1848	0.999
			0.8087	0.942	0.1419	0.967	0.1334	0.980
90	30%	1	0.8749	0.977	0.1865	0.997	0.1730	0.999
			0.9156	0.945	0.1338	0.973	0.1243	0.988
		2	0.8202	0.968	0.1867	0.997	0.1801	0.999
			0.8548	0.945	0.1376	0.973	0.1283	0.988
		3	1.0393	0.958	0.2030	0.987	0.1799	0.999
			1.1490	0.938	0.1517	0.966	0.1292	0.981
	60%	1	0.7025	0.981	0.1818	0.999	0.1674	0.999
			0.7232	0.949	0.1322	0.977	0.1177	0.992
		2	0.6679	0.985	0.1783	0.999	0.1702	0.999
			0.6866	0.950	0.1281	0.979	0.1193	0.993
		3	0.7937	0.974	0.1869	0.999	0.1658	0.999
			0.8015	0.940	0.1358	0.968	0.1183	0.983
	90%	1	0.6217	0.996	0.1817	0.999	0.1575	0.999
			0.6369	0.969	0.1318	0.998	0.1104	0.999
		2	0.6081	0.998	0.1731	0.998	0.1664	0.999
			0.6224	0.961	0.1247	0.990	0.1188	0.999
		3	0.6364	0.981	0.1730	0.999	0.1645	0.999
			0.6531	0.947	0.1230	0.975	0.1179	0.990

(xi) In summary, the Bayesian inference via M-H algorithm of the unknown life parameters α, β, θ, $R(t)$, and $h(t)$ of the Marshall-Olkin generalized-exponential lifetime model is recommended.

6. Real-Life Applications

To show the potentiality and flexibility of the proposed methodologies to real phenomenon, in this section we shall provide two real data sets obtained from different fields. First data set (denoted by Data-I) represents the failure times of $n = 18$ electronic devices, as can be seen in Wang [31]. Recently, this data set has also been discussed by Elshahhat and Abu El Azm [16]. Other data set (denoted by data-II), reported by Hinkley [32], consists of the amount of precipitation (inches) having $n = 30$ successive values in March at Minneapolis/St Paul. The lifetime points (in order) of both data sets I and II are presented in Table 11.

Using Table 11, plots of the empirical/estimated scaled TTT-transform of the MOGE distribution are provided in Figure 8. It shows that the scaled TTT-transform is (a) convex and then concave for data-I while is concave for data-II. It also suggests that increasing and bathtub shaped failure rates are suitable for the fitting MOGE lifetime model.

Before discussing our proposed estimators, the MOGE distribution is compared with seven popular Marshall-Olkin

Table 7: The ACLs/CPs of asymptotic/credible interval estimates of β.

n	FP	Scheme	ACI-NA		BCI			
			ACI-NL		HPD			
Prior ⟶					I	II	I	II
			ACL	CP	ACL	CP	ACL	CP
30	30%	1	2.1029	0.935	0.2470	0.959	0.1885	0.970
			2.8978	0.946	0.2156	0.965	0.1737	0.976
		2	2.5156	0.933	0.2201	0.968	0.1847	0.979
			2.9665	0.947	0.2080	0.970	0.1693	0.981
		3	2.6728	0.930	0.2628	0.941	0.1667	0.951
			3.2831	0.931	0.2238	0.945	0.1612	0.955
	60%	1	2.0646	0.947	0.1941	0.968	0.1159	0.975
			2.8450	0.959	0.1883	0.968	0.0998	0.979
		2	2.1457	0.949	0.1811	0.969	0.1210	0.980
			2.9067	0.953	0.1541	0.975	0.1088	0.986
		3	2.2594	0.935	0.2288	0.949	0.1598	0.959
			3.1135	0.935	0.2030	0.967	0.1436	0.978
	90%	1	2.0477	0.961	0.1289	0.968	0.1022	0.979
			2.4218	0.967	0.1099	0.970	0.0925	0.981
		2	2.0345	0.959	0.1401	0.975	0.1055	0.986
			2.7836	0.968	0.1266	0.982	0.0899	0.993
		3	2.0779	0.942	0.1986	0.956	0.1369	0.967
			2.8034	0.952	0.1746	0.977	0.1134	0.988
60	30%	1	1.2260	0.942	0.2037	0.966	0.1402	0.975
			1.3398	0.960	0.1696	0.966	0.1155	0.981
		2	1.5492	0.943	0.1570	0.968	0.1501	0.984
			1.4873	0.976	0.1351	0.973	0.1247	0.986
		3	1.6245	0.936	0.1887	0.946	0.1353	0.957
			1.8239	0.946	0.1531	0.965	0.1128	0.961
	60%	1	1.1900	0.949	0.1913	0.969	0.1296	0.984
			1.1409	0.968	0.1652	0.975	0.1129	0.984
		2	1.2970	0.959	0.1435	0.971	0.1233	0.985
			1.2537	0.981	0.1177	0.983	0.0968	0.992
		3	1.1520	0.941	0.1408	0.955	0.1259	0.965
			1.3875	0.965	0.1152	0.971	0.1005	0.983
	90%	1	0.8932	0.964	0.1273	0.978	0.1136	0.984
			1.0309	0.973	0.1007	0.979	0.0948	0.986
		2	0.9701	0.970	0.1225	0.976	0.0947	0.992
			1.1368	0.988	0.1010	0.985	0.0809	0.999
		3	1.0142	0.947	0.1339	0.966	0.1202	0.972
			1.2175	0.978	0.1074	0.980	0.0927	0.994
90	30%	1	0.6642	0.945	0.1061	0.979	0.0905	0.985
			0.7152	0.979	0.0833	0.977	0.0676	0.985
		2	0.7568	0.945	0.1033	0.975	0.0900	0.987
			0.9429	0.979	0.0799	0.978	0.0671	0.992
		3	0.8374	0.940	0.1188	0.977	0.1022	0.965
			1.1004	0.948	0.0938	0.980	0.0753	0.984
	60%	1	0.5277	0.958	0.1021	0.980	0.0874	0.988
			0.6272	0.981	0.0811	0.979	0.0643	0.995
		2	0.5950	0.967	0.1031	0.975	0.0817	0.990
			0.6820	0.982	0.0775	0.985	0.0612	0.998
		3	0.8045	0.947	0.1046	0.985	0.0979	0.974
			0.8527	0.979	0.0771	0.984	0.0737	0.990
	90%	1	0.3216	0.969	0.0882	0.983	0.0800	0.998
			0.4431	0.986	0.0658	0.980	0.0589	0.999
		2	0.4885	0.981	0.1019	0.988	0.0996	0.996
			0.6032	0.989	0.0770	0.987	0.0716	0.998
		3	0.5997	0.958	0.1037	0.986	0.0973	0.985
			0.6263	0.980	0.0760	0.986	0.0724	0.998

Table 8: The ACLs/CPs of asymptotic/credible interval estimates of θ.

n	FP	Scheme	ACI-NA		BCI			
			ACI-NL		HPD			
Prior ⟶					I	II	I	II
			ACL	CP	ACL	CP	ACL	CP
30	30%	1	1.0555	0.956	0.2068	0.967	0.1862	0.973
			1.6742	0.947	0.1822	0.960	0.1589	0.970
		2	1.5785	0.951	0.2301	0.964	0.2296	0.972
			1.9251	0.943	0.2042	0.956	0.2004	0.969
		3	1.8426	0.950	0.2061	0.962	0.1821	0.973
			2.1218	0.947	0.1950	0.960	0.1556	0.972
	60%	1	0.6223	0.959	0.1748	0.972	0.1369	0.978
			0.9152	0.952	0.1504	0.969	0.1103	0.978
		2	0.7489	0.959	0.2242	0.966	0.1769	0.975
			1.2099	0.950	0.1894	0.963	0.1497	0.973
		3	1.4160	0.955	0.1805	0.969	0.1349	0.978
			1.8741	0.951	0.1577	0.964	0.1156	0.973
	90%	1	0.4788	0.965	0.1491	0.978	0.1036	0.985
			0.6136	0.956	0.1224	0.971	0.0871	0.974
		2	0.5126	0.967	0.1378	0.972	0.1291	0.978
			0.6598	0.951	0.1168	0.964	0.1065	0.976
		3	1.2041	0.957	0.1161	0.972	0.1029	0.984
			1.5174	0.962	0.0979	0.974	0.0951	0.975
60	30%	1	0.6254	0.960	0.1750	0.969	0.1545	0.974
			1.5286	0.948	0.1455	0.965	0.1210	0.977
		2	0.8538	0.958	0.1975	0.971	0.1460	0.978
			1.4900	0.962	0.1668	0.974	0.1171	0.978
		3	1.6051	0.959	0.1680	0.963	0.1561	0.975
			1.6117	0.958	0.1409	0.965	0.1338	0.976
	60%	1	0.4083	0.973	0.1679	0.976	0.1254	0.984
			0.4828	0.960	0.1421	0.973	0.1088	0.981
		2	0.4731	0.960	0.1305	0.974	0.1234	0.980
			0.5953	0.965	0.1100	0.978	0.0998	0.983
		3	1.1866	0.958	0.1392	0.972	0.0940	0.980
			1.4610	0.960	0.1143	0.969	0.0759	0.977
	90%	1	0.3181	0.979	0.1205	0.985	0.0916	0.986
			0.3563	0.962	0.0956	0.975	0.0771	0.981
		2	0.3324	0.968	0.1193	0.980	0.0992	0.982
			0.3783	0.968	0.0965	0.982	0.0855	0.984
		3	0.4527	0.962	0.0971	0.975	0.0902	0.987
			1.0251	0.964	0.0773	0.975	0.0726	0.982
90	30%	1	0.4902	0.971	0.1126	0.984	0.1041	0.986
			0.9675	0.961	0.0877	0.974	0.0799	0.983
		2	0.6296	0.962	0.1087	0.975	0.1066	0.979
			0.9274	0.967	0.0839	0.980	0.0784	0.989
		3	1.2145	0.965	0.1153	0.978	0.1017	0.982
			1.4497	0.967	0.0912	0.980	0.0793	0.984
	60%	1	0.3222	0.976	0.0979	0.986	0.0959	0.987
			0.3627	0.967	0.0722	0.980	0.0707	0.984
		2	0.3707	0.976	0.0954	0.989	0.0945	0.991
			0.4293	0.972	0.0713	0.985	0.0709	0.986
		3	0.9149	0.968	0.1003	0.981	0.0863	0.990
			0.9867	0.969	0.0756	0.982	0.0643	0.992
	90%	1	0.2581	0.980	0.0936	0.989	0.0885	0.990
			0.2776	0.968	0.0704	0.983	0.0656	0.986
		2	0.2686	0.979	0.0927	0.990	0.0920	0.992
			0.2911	0.975	0.0694	0.988	0.0695	0.995
		3	0.3640	0.978	0.0880	0.988	0.0825	0.991
			0.5262	0.970	0.0650	0.983	0.0596	0.990

Table 9: The ACLs/CPs of asymptotic/credible interval estimates of $R(t)$.

n	FP	Scheme	ACI-NA		BCI			
			ACI-NL				HPD	
Prior ⟶					I	II	I	II
			ACL	CP	ACL	CP	ACL	CP
30	30%	1	0.2452	0.947	0.2138	0.961	0.1930	0.970
			0.1823	0.948	0.1936	0.962	0.1731	0.971
		2	0.2263	0.952	0.1981	0.966	0.1601	0.975
			0.1658	0.950	0.1605	0.964	0.1536	0.973
		3	0.2355	0.941	0.2297	0.955	0.2101	0.964
			0.2134	0.946	0.1770	0.960	0.1699	0.969
	60%	1	0.1968	0.954	0.1637	0.968	0.1555	0.977
			0.1639	0.950	0.1593	0.964	0.1449	0.973
		2	0.2215	0.944	0.1865	0.958	0.1522	0.967
			0.1621	0.947	0.1524	0.961	0.1427	0.970
		3	0.1848	0.949	0.1804	0.963	0.1386	0.972
			0.1857	0.948	0.1349	0.962	0.1033	0.971
	90%	1	0.1571	0.955	0.1504	0.969	0.1112	0.979
			0.1506	0.952	0.1150	0.966	0.1107	0.975
		2	0.2060	0.942	0.1761	0.956	0.1494	0.965
			0.1608	0.945	0.1496	0.959	0.1365	0.968
		3	0.1571	0.956	0.1609	0.970	0.1291	0.980
			0.1467	0.953	0.1163	0.967	0.1012	0.976
60	30%	1	0.2225	0.968	0.1797	0.981	0.1412	0.989
			0.1599	0.961	0.1413	0.973	0.1267	0.982
		2	0.1952	0.962	0.1693	0.975	0.1144	0.983
			0.1419	0.968	0.1200	0.981	0.1145	0.989
		3	0.1764	0.965	0.1425	0.978	0.1417	0.986
			0.1272	0.968	0.1028	0.981	0.1009	0.989
	60%	1	0.1868	0.969	0.1423	0.982	0.1210	0.990
			0.1356	0.965	0.1211	0.978	0.1023	0.986
		2	0.1694	0.965	0.1603	0.978	0.1092	0.986
			0.1203	0.970	0.1156	0.983	0.1078	0.991
		3	0.1738	0.967	0.1450	0.980	0.1316	0.988
			0.1246	0.971	0.1104	0.984	0.0996	0.992
	90%	1	0.1271	0.972	0.1304	0.985	0.1096	0.993
			0.1097	0.974	0.0911	0.987	0.0896	0.995
		2	0.1664	0.969	0.1441	0.982	0.1077	0.990
			0.1182	0.973	0.1092	0.986	0.1048	0.994
		3	0.1408	0.968	0.1465	0.981	0.1283	0.989
			0.1130	0.976	0.1151	0.989	0.0961	0.997
90	30%	1	0.1641	0.964	0.1391	0.977	0.1165	0.988
			0.1166	0.960	0.1032	0.972	0.0964	0.984
		2	0.1542	0.970	0.1476	0.983	0.0933	0.994
			0.1068	0.968	0.1018	0.981	0.0934	0.992
		3	0.0969	0.968	0.1398	0.981	0.1129	0.992
			0.1153	0.974	0.0992	0.987	0.0979	0.998
	60%	1	0.1502	0.972	0.1389	0.985	0.1002	0.996
			0.1144	0.976	0.1003	0.989	0.0956	0.998
		2	0.1411	0.974	0.1398	0.987	0.0904	0.998
			0.0980	0.973	0.0961	0.986	0.0904	0.997
		3	0.0932	0.977	0.1397	0.990	0.1103	0.998
			0.0933	0.975	0.1007	0.988	0.0940	0.999
	90%	1	0.1459	0.965	0.1256	0.978	0.0911	0.989
			0.0986	0.961	0.0896	0.973	0.0883	0.985
		2	0.1344	0.975	0.1244	0.988	0.0899	0.999
			0.0940	0.976	0.0922	0.989	0.0899	0.998
		3	0.0895	0.978	0.1376	0.991	0.1091	0.998
			0.0895	0.976	0.1091	0.989	0.0888	0.999

Table 10: The ACLs/CPs of asymptotic/credible interval estimates of $h(t)$.

n	FP	Scheme	ACI-NA		BCI			
			ACI-NL		HPD			
Prior ⟶					I	II	I	II
			ACL	CP	ACL	CP	ACL	CP
30	30%	1	1.5013	0.949	0.9965	0.962	0.9859	0.973
			1.8475	0.958	0.8069	0.966	0.8042	0.974
		2	1.3225	0.946	1.0254	0.961	1.0064	0.970
			1.5260	0.951	0.8197	0.962	0.8468	0.972
		3	1.1862	0.960	1.0191	0.965	0.9190	0.972
			1.3247	0.948	0.8363	0.960	0.7316	0.971
	60%	1	1.0750	0.960	0.8859	0.964	0.8399	0.974
			1.2229	0.962	0.7755	0.968	0.6627	0.975
		2	0.9821	0.966	0.9481	0.967	0.8518	0.973
			1.0785	0.961	0.8087	0.964	0.7109	0.975
		3	0.9753	0.950	0.7517	0.962	0.6660	0.973
			0.9963	0.958	0.6133	0.965	0.5898	0.972
	90%	1	0.9178	0.955	0.7219	0.966	0.6399	0.977
			1.0102	0.965	0.5738	0.974	0.4976	0.982
		2	0.8950	0.968	0.9327	0.970	0.8243	0.982
			0.9778	0.962	0.7221	0.975	0.6718	0.984
		3	0.8953	0.954	0.7328	0.968	0.5662	0.980
			0.9828	0.962	0.5670	0.971	0.4578	0.983
60	30%	1	1.0510	0.959	0.9113	0.974	0.7610	0.986
			1.1716	0.961	0.7126	0.972	0.5693	0.983
		2	0.8889	0.959	0.8581	0.972	0.7133	0.983
			0.9495	0.959	0.6782	0.974	0.5331	0.985
		3	0.8095	0.964	0.7332	0.975	0.6713	0.982
			0.8654	0.957	0.5011	0.969	0.5254	0.980
	60%	1	0.7787	0.966	0.8358	0.975	0.5622	0.985
			0.8301	0.964	0.6715	0.973	0.4359	0.984
		2	0.6770	0.960	0.6730	0.974	0.6690	0.985
			0.7076	0.960	0.5248	0.975	0.5102	0.986
		3	0.7082	0.966	0.6931	0.976	0.5625	0.986
			0.7527	0.960	0.5689	0.970	0.4243	0.981
	90%	1	0.6606	0.969	0.5723	0.976	0.5362	0.986
			0.6917	0.965	0.4253	0.974	0.3939	0.985
		2	0.6405	0.967	0.6526	0.978	0.6484	0.989
			0.6680	0.961	0.5093	0.973	0.4960	0.985
		3	0.6488	0.968	0.6590	0.975	0.5191	0.987
			0.6765	0.967	0.5528	0.978	0.3816	0.984
90	30%	1	0.8486	0.966	0.6336	0.977	0.5739	0.986
			0.9153	0.964	0.4651	0.973	0.4120	0.984
		2	0.6994	0.966	0.6088	0.977	0.5780	0.988
			0.7293	0.971	0.4337	0.982	0.4182	0.990
		3	0.6569	0.969	0.5669	0.979	0.5424	0.988
			0.6857	0.968	0.4324	0.976	0.4062	0.990
	60%	1	0.6434	0.967	0.5452	0.978	0.5434	0.989
			0.6713	0.971	0.3947	0.978	0.3889	0.990
		2	0.5641	0.969	0.5525	0.982	0.5402	0.990
			0.5685	0.970	0.4125	0.981	0.3821	0.991
		3	0.6081	0.972	0.5508	0.983	0.5379	0.992
			0.6571	0.969	0.4015	0.979	0.3904	0.990
	90%	1	0.5399	0.968	0.5339	0.982	0.5300	0.993
			0.5562	0.973	0.3789	0.984	0.3728	0.995
		2	0.5448	0.970	0.5272	0.982	0.5153	0.992
			0.5414	0.972	0.3959	0.983	0.3681	0.993
		3	0.5299	0.977	0.5475	0.984	0.5206	0.994
			0.5447	0.971	0.3964	0.980	0.3738	0.989

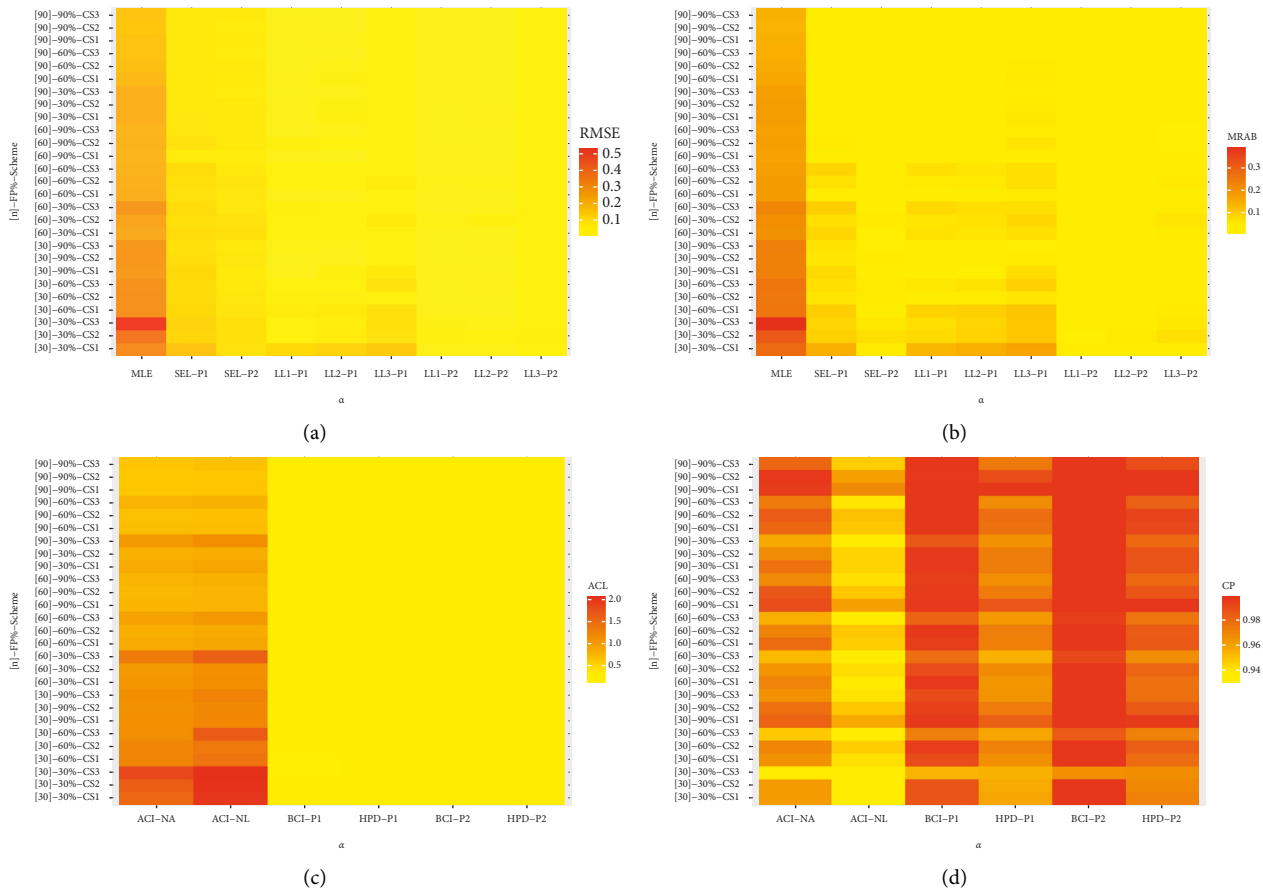

Figure 3: Heatmaps for the simulated results. (a) RMSE, (b) RMAB, (c) ACL, and (d) CP of α.

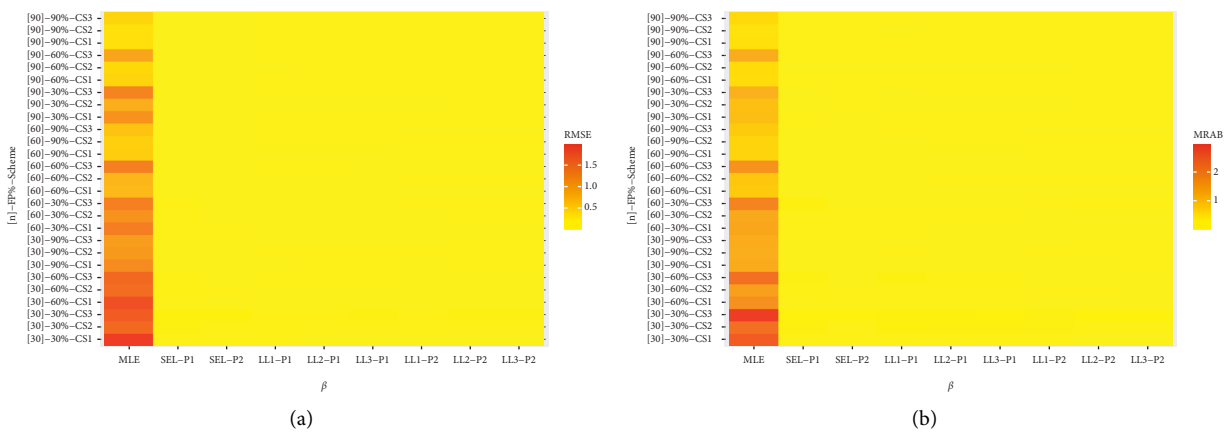

Figure 4: Continued.

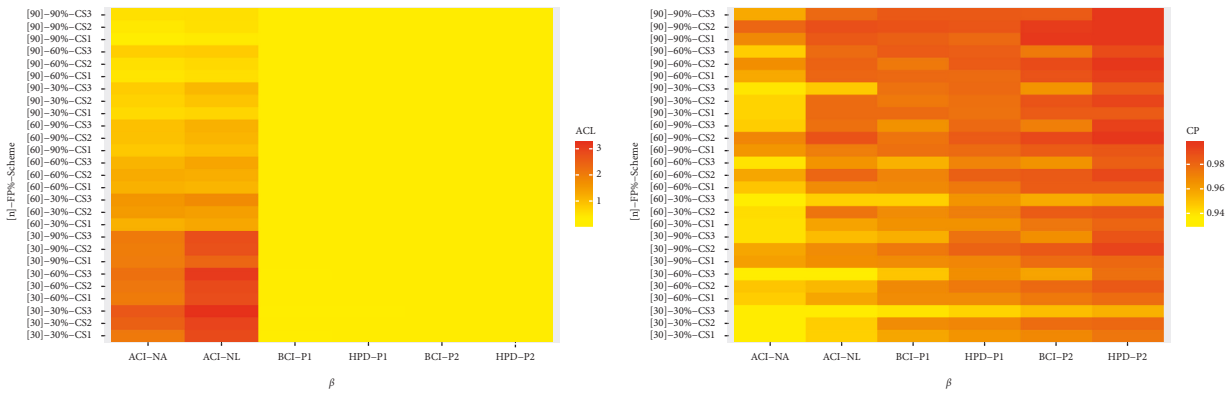

Figure 4: Heatmaps for the simulated results. (a) RMSE, (b) RMAB, (c) ACL, and (d) CP of β.

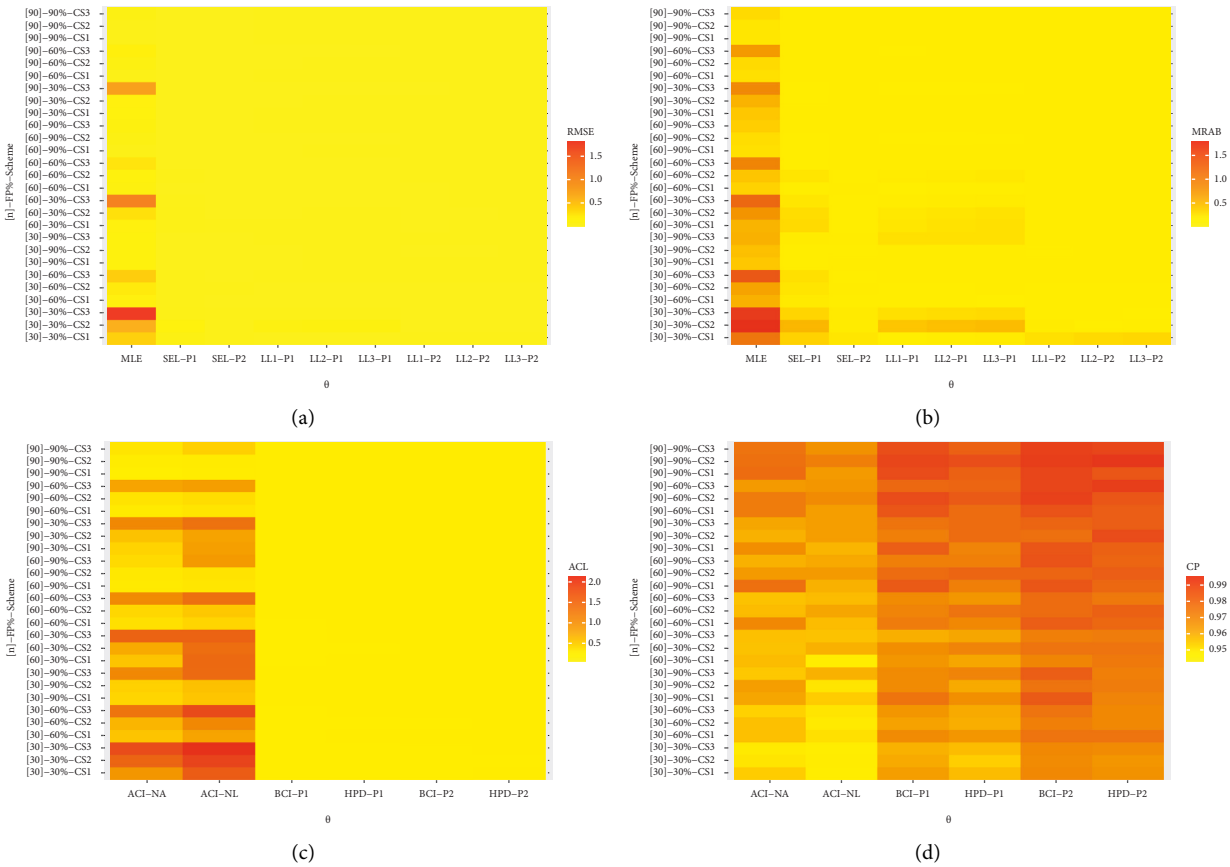

Figure 5: Heatmaps for the simulated results. (a) RMSE, (b) RMAB, (c) ACL, and (d) CP of θ.

extended distributions as competitors, namely: Marshall-Olkin extended Weibull (MOEW), Marshall-Olkin logistic exponential (MOLE), Marshall-Olkin alpha power exponential (MOAPE), Marshall-Olkin Nadarajah-Haghighi (MONH), Marshall-Olkin Gompertz (MOG), Marshall-Olkin Lomax (MOL), and Marshall-Olkin exponential (MOE) distributions. The corresponding probability densities of the competing models (for $x > 0$ and $\alpha, \beta, \theta > 0$) are tabulated in Table 12.

To judge the performance of the considered models, several goodness-of-fit criteria, namely, estimated negative log-likelihood (ENL), Akaike information (AI), consistent

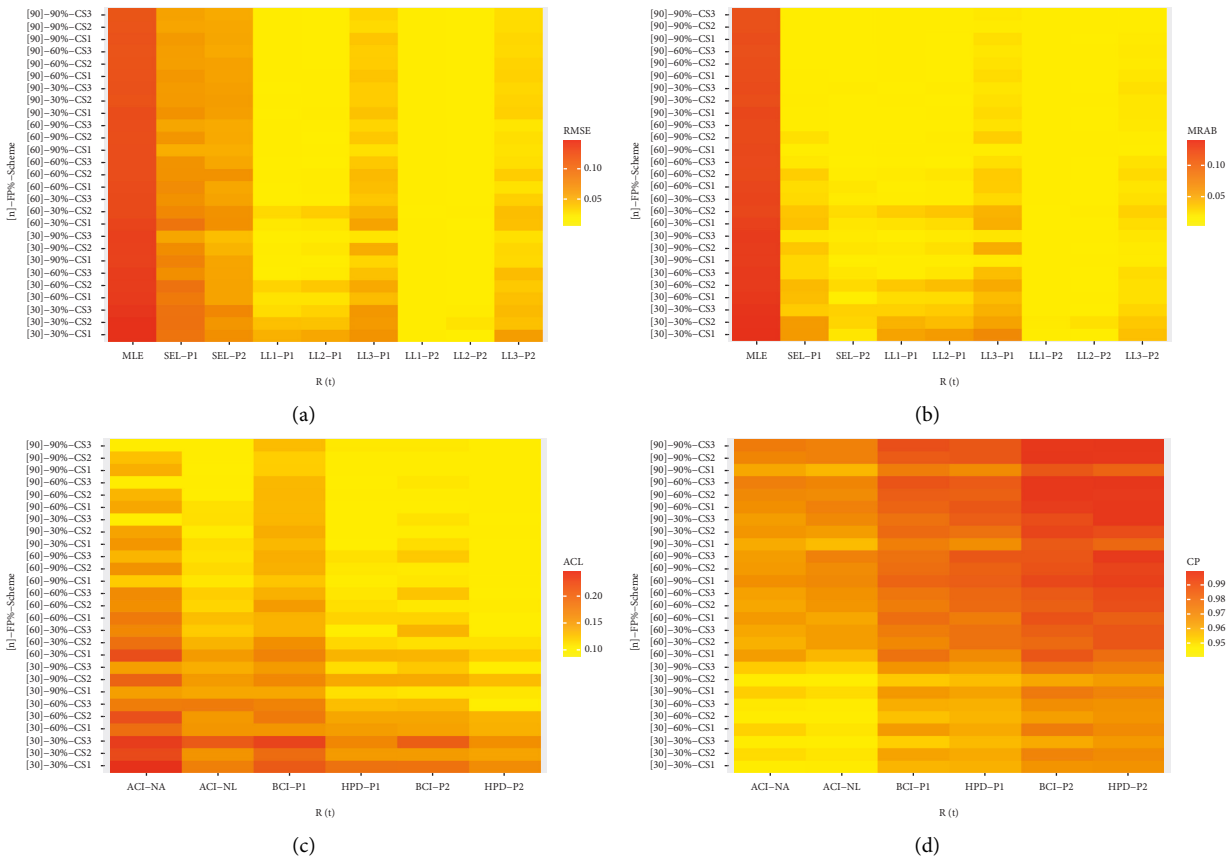

Figure 6: Heatmaps for the simulated results. (a) RMSE, (b) RMAB, (c) ACL, and (d) CP of $R(t)$.

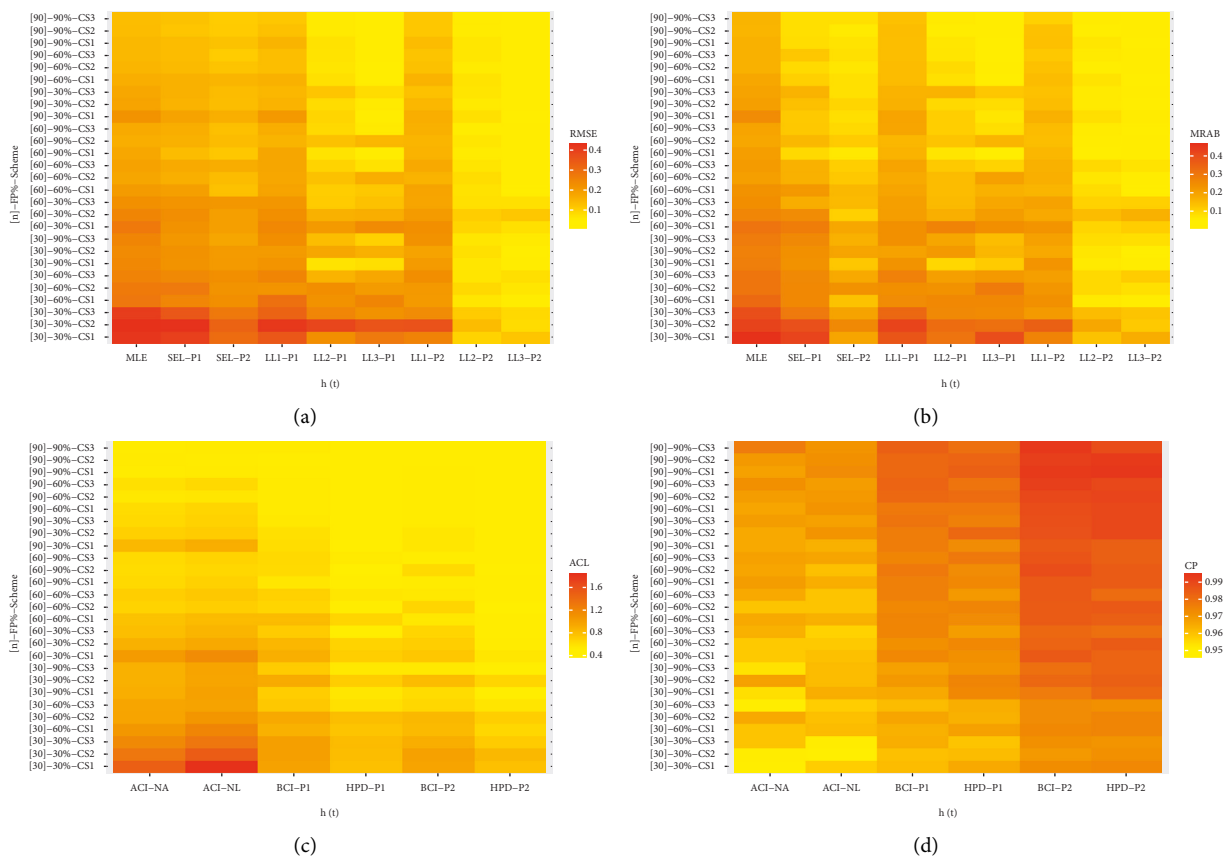

Figure 7: Heatmaps for the simulated results. (a) RMSE, (b) RMAB, (c) ACL, and (d) CP of $h(t)$.

Table 11: Failure times of data sets I and II.

Data	Times									
I	5	11	21	31	46	75	98	122	145	165
	196	224	245	293	321	330	350	420		
II	0.32	0.47	0.52	0.59	0.77	0.81	0.81	0.90	0.96	1.18
	1.20	1.20	1.31	1.35	1.43	1.51	1.62	1.74	1.87	1.89
	1.95	2.05	2.10	2.20	2.48	2.81	3.00	3.09	3.37	4.75

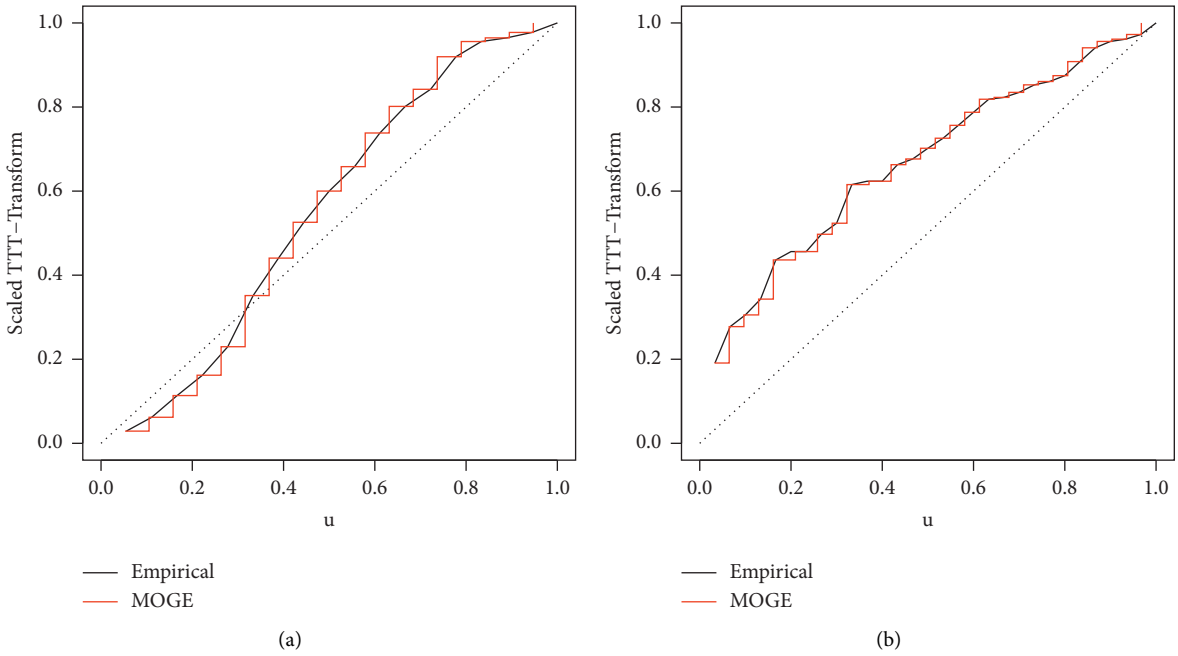

Figure 8: Empirical and estimated scaled TTT-transform plot of the MOGE distribution. (a) Data-I. (b) Data-II.

Table 12: Some useful Marshall-Olkin life models.

Model	$f(x)$	Author(s)
MOEW	$\alpha\beta\theta x^{\alpha-1}\exp(-\theta x^{\alpha})/(1-\overline{\beta}\exp(-\theta x^{\alpha}))^2$	Cordeiro and Lemonte [33]
MOLE	$\alpha\beta\theta\exp(\theta x)(\exp(\theta x)-1)^{-\alpha-1}/(1+\beta(\exp(\theta x)-1)^{-\alpha})^2$	Mansoor et al. [34]
MOAPE	$\theta\beta\log(\alpha)\exp(-\theta x)\alpha^{1-\exp(-\theta x)}/(\alpha-1)(\beta+\overline{\beta}(1/(\alpha-1))(\alpha(^{1-\exp}(-\theta x))-1))^2$	Nassar et al. [35]
MONH	$\theta\beta\alpha(1+\theta x)^{\alpha-1}\exp(1-(1+\theta x)^{\alpha})/(1-\overline{\beta}\exp(1-(1+\theta x)^{\alpha}))^2$	Lemonte et al. [36]
MOG	$\alpha\beta\exp(\theta x)\exp(-(\alpha/\theta)(\exp(\theta x)-1))/(1-\overline{\beta}\exp(-(\alpha/\theta)(\exp(\theta x)-1)))^2$	Eghwerido et al. [37]
MOL	$\alpha\beta\theta(1+\theta x)^{\alpha-1}/((1+\theta x)^{\alpha}-\overline{\beta})^2$	Ghitany et al. [38]
MOE	$\theta\beta\exp(-\theta x)/(\beta+\overline{\beta}(1-\exp(-\theta x)))^2$	Marshall and Olkin [1]

Akaike information (CAI), Bayesian information (BI), Hannan-Quinn information (HQI), Anderson-Darling (AD), Cramer von Mises (CvM) and Kolmogorov-Smirnov (KS) distance with its P-value are used. For each model, we estimate the parameters with their standard errors (SEs) by utilizing the method of maximum likelihood, see Table 13. Generally, the lowest values of these statistics (except the highest P-value) represent the best fit to the given data. The calculated statistics based on data sets I and II are reported in Table 14. It indicates that the MOGE model provides the best fit than other competing models for the given data sets. Plots of the estimated densities and reliability functions of all fitted models are displayed in Figure 9. It shows that the MOGE distribution for both data sets I and II captures the general pattern of the histograms and also supports the numerical findings established here. Also, quantile-quantile plots of the

Table 13: MLEs with their (SEs) of the competing distributions.

Model	MLE (SE)		
	α	β	θ
Data-I			
MOGE	0.6490 (0.5526)	4.5237 (6.4116)	0.0090 (0.0030)
MOEW	0.6927 (0.1490)	0.2761 (0.2874)	0.0114 (0.0157)
MOLE	0.8497 (0.2631)	1.9676 (1.5960)	0.0086 (0.0048)
MOAPE	1.0462 (2.6066)	2.3850 (3.5866)	0.0086 (0.0029)
MONH	1.0053 (0.5547)	2.6755 (2.7688)	0.0088 (0.0106)
MOG	0.0139 (0.0148)	4.8900 (7.7044)	0.0014 (0.0045)
MOL	2.4924 (1.0329)	2.6491 (2.4099)	0.0055 (0.0035)
MOE	—	9.8556 (3.5453)	0.0132 (0.0051)
Data-II			
MOGE	3.3527 (1.2959)	1.2211 (1.5027)	1.2271 (0.4267)
MOEW	2.4651 (0.5673)	0.1748 (0.2675)	0.0624 (0.0951)
MOLE	1.9930 (1.0694)	0.9614 (4.5808)	0.4598 (0.7649)
MOAPE	17.022 (34.498)	2.4018 (2.9264)	1.4241 (0.3697)
MONH	0.7013 (0.4966)	24.895 (59.086)	4.5347 (11.584)
MOG	1.9963 (0.9514)	13.623 (12.192)	0.1311 (0.2301)
MOL	12.687 (10.343)	12.129 (8.4767)	0.1508 (0.1575)
MOE	—	9.8857 (6.2279)	1.5511 (0.3205)

Table 14: Summary fit for the competing models.

Model	ENL	AI	CAI	BI	HQI	AD	CvM	KS (P-value)
Data-I								
MOGE	109.9511	225.9023	227.6165	228.5734	226.2706	0.2602	0.0349	0.0994 (0.9863)
MOEW	115.9579	237.9373	239.6516	240.6084	238.3056	0.6553	0.1059	0.2019 (0.4019)
MOLE	110.0574	226.1147	227.8290	228.7858	226.4830	0.2956	0.0419	0.0857 (0.9977)
MOAPE	110.1670	226.3339	228.0482	229.0051	226.7022	0.2966	0.0417	0.1122 (0.9580)
MONH	110.1754	226.3507	228.0650	229.0218	226.7190	0.2880	0.0401	0.1199 (0.9309)
MOG	110.9341	227.8682	229.5825	230.5393	228.2365	0.3399	0.0481	0.1288 (0.8898)
MOL	111.6748	229.3495	231.0638	232.0206	229.7178	0.4579	0.0673	0.1349 (0.8565)
MOE	111.7332	227.4664	228.2664	229.2471	227.7119	0.2395	0.0310	0.1993 (0.4172)
Data-II								
MOGE	38.0814	82.1628	83.0858	86.3664	83.5075	0.1030	0.0141	0.0601 (0.9999)
MOEW	38.1435	82.2871	83.2102	86.4907	83.6318	0.1107	0.0149	0.0602 (0.9999)
MOLE	38.3690	82.7381	83.6611	86.9417	84.0828	0.1163	0.0157	0.0585 (0.9999)
MOAPE	38.9348	83.8696	84.7927	88.0732	85.2144	0.1744	0.0228	0.0538 (0.9999)
MONH	39.0908	84.1817	85.1047	88.3852	85.5264	0.1860	0.0246	0.0549 (0.999)
MOG	39.1869	84.3738	85.2968	88.5773	85.7185	0.1740	0.0230	0.0661 (0.9994)
MOL	39.2394	84.4788	85.4019	88.6824	85.8236	0.1039	0.0140	0.0603 (0.9999)
MOE	39.3771	82.7542	83.1986	85.5566	83.6507	0.2401	0.0328	0.0646 (0.9996)

fitted models are also investigated in Figure 10. It yields that the MOGE model fits the given data sets more closely and supports the numerical findings.

Now, using some specified choices of m and R, different PCS-T2 samples are generated from data sets I and II, see Table 15. For brevity, the PCS $(2, 0, 0, 0, 2)$ is abbreviated by $(2, 0^3, 2)$. Using the M-H algorithm described

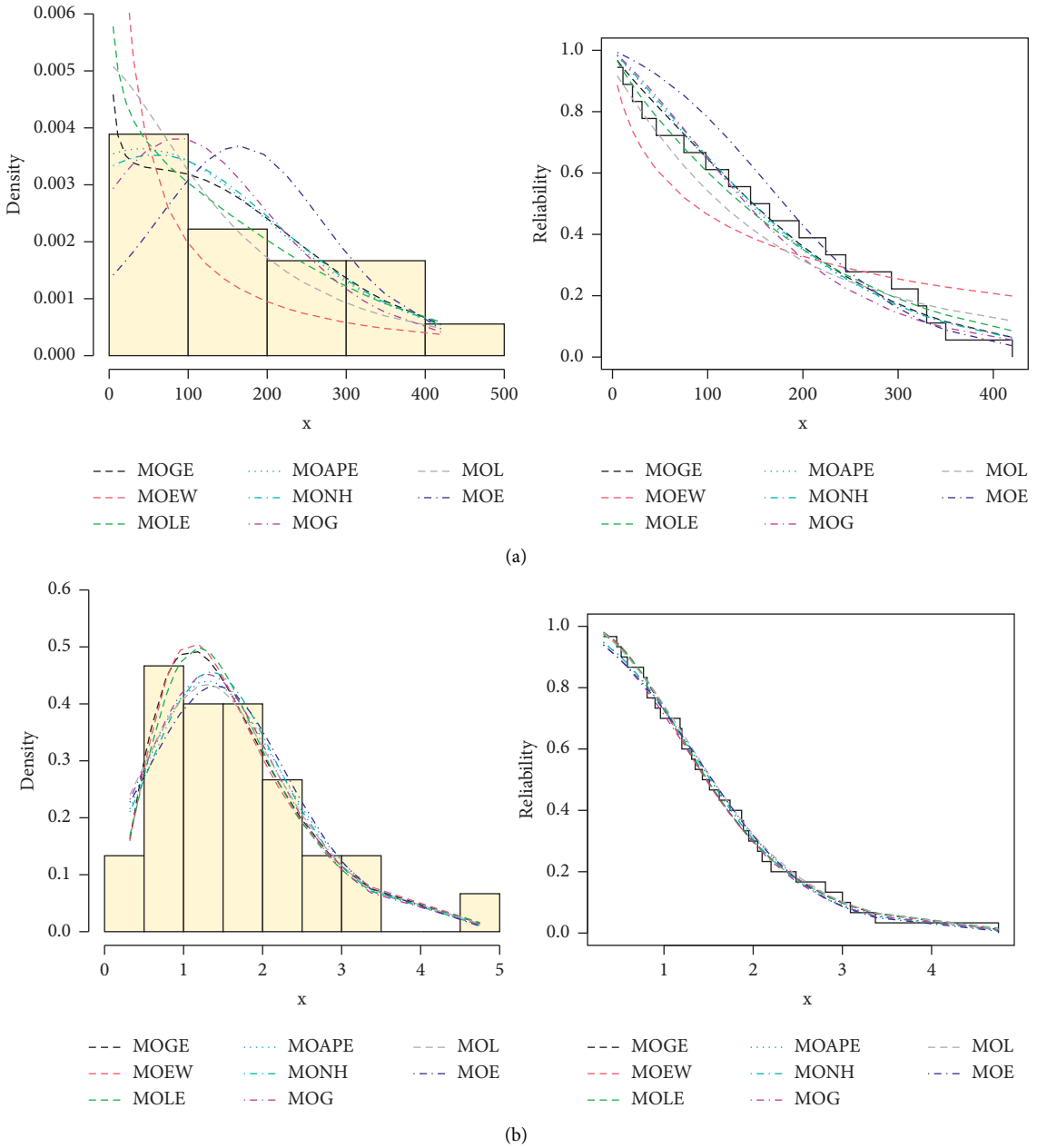

FIGURE 9: Plots of histogram and fitted PDFs (left-panel) fitted/empirical RFs (right-panel) of MOGE and competing models under data sets I and II. (a) Data-I. (b) Data-II.

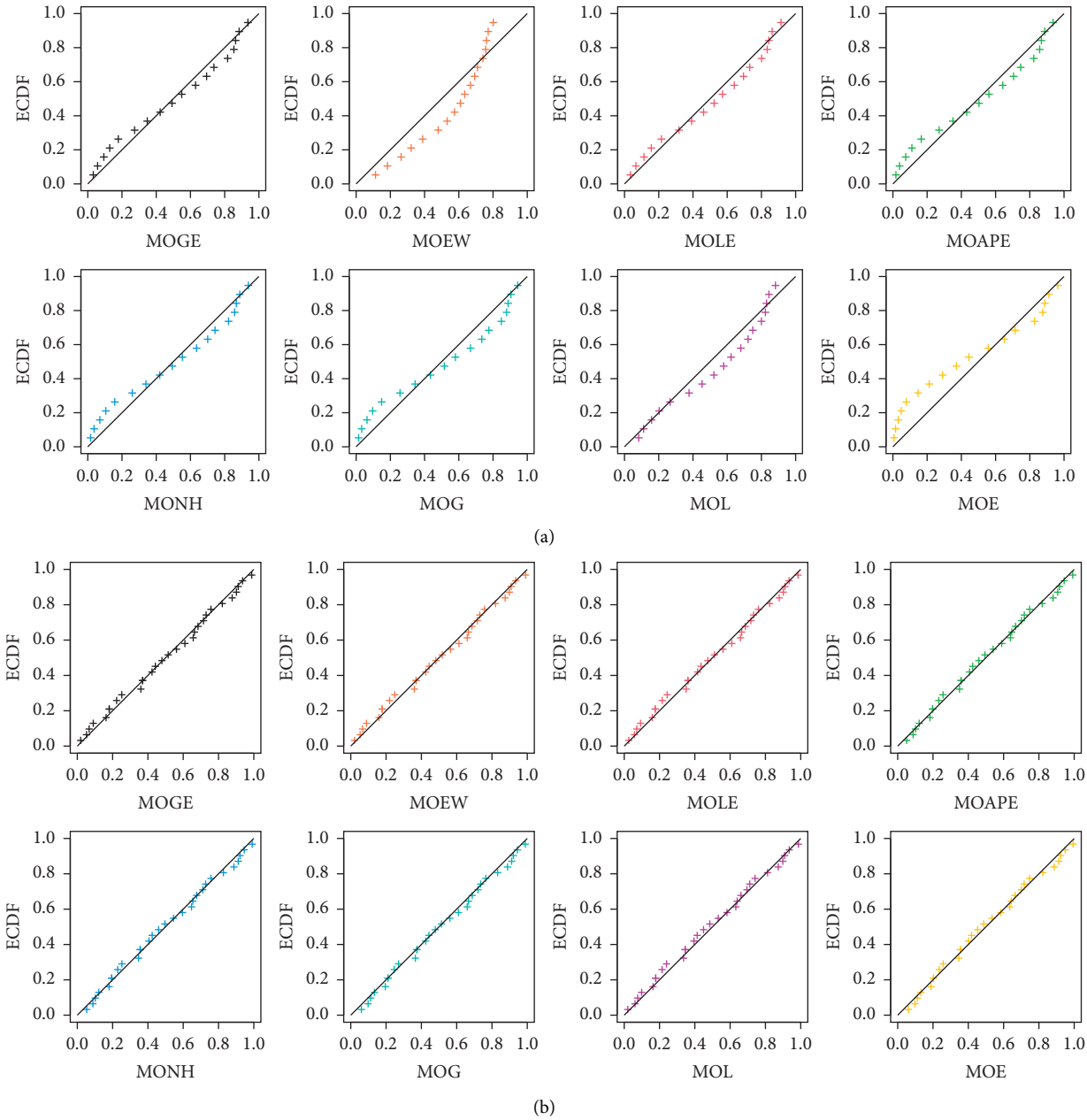

Figure 10: The Q-Q plots of MOGE and competing models under data sets I and II. (a) Data-I. (b) Data-II.

Table 15: Three generated PCS-T2 samples from data sets I and II.

Data	$n(m)$	Scheme	Censored data
I	18 (9)	$\mathbf{R}_1 = (9, 0^8)$	5, 196, 224, 245, 293, 321, 330, 350, 420
		$\mathbf{R}_2 = (0^4, 9, 0^4)$	5, 11, 21, 31, 46, 321, 330, 350, 420
		$\mathbf{R}_3 = (0^8, 9)$	5, 11, 21, 31, 46, 75, 98, 122, 145
II	30 (15)	$\mathbf{R}_1 = (15, 0^{14})$	0.77, 1.31, 0.32, 0.59, 0.81, 2.81, 1.87, 1.18, 1.35, 4.75, 2.48, 0.96, 1.89, 0.90, 2.05
		$\mathbf{R}_2 = (0^7, 15, 0^7)$	0.77, 1.74, 0.81, 1.20, 1.95, 1.20, 0.47, 1.43, 1.35, 4.75, 2.48, 0.96, 1.89, 0.90, 2.05
		$\mathbf{R}_3 = (0^{14}, 15)$	0.77, 1.74, 0.81, 1.20, 1.95, 1.20, 0.47, 1.43, 3.37, 2.20, 3.00, 3.09, 1.51, 2.10, 0.52

Table 16: The frequentist and bayes estimates (with their SEs) under data sets I and II.

Scheme	Parameter	MLE	SEL	LL		
$v \longrightarrow$				-2	-0.02	2
Data-I						
	α	0.2442 (0.3133)	0.2441 (1.10×10^{-5})	0.2442 (2.38×10^{-8})	0.2442 (3.33×10^{-8})	0.2442 (9.16×10^{-8})
	β	302.82 (2.9810)	302.82 (1.09×10^{-5})	302.82 (1.14×10^{-7})	302.82 (5.71×10^{-8})	302.82 (1.19×10^{-9})
$\mathbf{R}_1$	θ	0.0156 (0.0042)	0.0157 (9.77×10^{-6})	0.0157 (5.05×10^{-7})	0.0157 (4.90×10^{-7})	0.0157 (4.75×10^{-7})
	$R(100)$	0.9471 (0.0451)	0.9462 (5.84×10^{-5})	0.9463 (6.21×10^{-6})	0.9462 (6.75×10^{-6})	0.9461 (7.29×10^{-6})
	$h(100)$	0.0010 (0.0006)	0.0009 (1.54×10^{-5})	0.0010 (2.24×10^{-7})	0.0010 (2.23×10^{-7})	0.0010 (2.23×10^{-7})
	α	0.6520 (0.4854)	0.6520 (1.90×10^{-5})	0.6520 (3.68×10^{-8})	0.6519 (1.94×10^{-8})	0.6520 (7.68×10^{-8})
	β	2.7522 (4.3540)	2.7521 (1.89×10^{-5})	2.7521 (4.54×10^{-8})	2.7522 (1.02×10^{-7})	2.7521 (1.59×10^{-7})
$\mathbf{R}_2$	θ	0.0057 (0.0031)	0.0057 (5.44×10^{-6})	0.0057 (2.06×10^{-7})	0.0057 (2.02×10^{-7})	0.0057 (1.97×10^{-7})
	$R(100)$	0.6659 (0.1229)	0.6646 (2.45×10^{-4})	0.6661 (5.21×10^{-6})	0.6646 (4.17×10^{-6})	0.6661 (1.37×10^{-5})
	$h(100)$	0.0039 (0.0016)	0.0039 (4.16×10^{-6})	0.0039 (2.52×10^{-7})	0.0039 (2.49×10^{-7})	0.0039 (2.47×10^{-7})
	α	0.9315(0.5133)	0.9315 (6.31×10^{-6})	0.9315 (1.10×10^{-7})	0.9315 (1.16×10^{-7})	0.9315 (1.23×10^{-7})
	β	0.5257 (2.5912)	0.5257 (6.29×10^{-6})	0.5257 (1.36×10^{-7})	0.5257 (1.42×10^{-7})	0.5257 (1.48×10^{-7})
$\mathbf{R}_3$	θ	0.0026 (0.0098)	0.0027 (2.81×10^{-6})	0.0027 (8.15×10^{-7})	0.0027 (8.13×10^{-7})	0.0027 (8.12×10^{-7})
	$R(100)$	0.6057 (0.1072)	0.5974 (2.75×10^{-4})	0.5993 (5.39×10^{-5})	0.5974 (6.59×10^{-5})	0.5955 (7.79×10^{-5})
	$h(100)$	0.0043(0.0020)	0.0044 (3.69×10^{-6})	0.0044 (9.90×10^{-7})	0.0044 (9.88×10^{-7})	0.0044 (9.86×10^{-7})
Data-II						
	α	4.2551 (1.4664)	4.2535 (5.09×10^{-4})	4.2600 (3.12×10^{-5})	4.2536 (9.42×10^{-6})	4.2471 (5.09×10^{-5})
	β	0.3270 (0.8587)	0.3455(4.39×10^{-4})	0.3504 (1.48×10^{-4})	0.3456 (1.17×10^{-4})	0.3407 (8.69×10^{-5})
$\mathbf{R}_1$	θ	0.8510 (0.8031)	0.8586 (4.28×10^{-4})	0.8632 (7.69×10^{-5})	0.8586 (4.82×10^{-5})	0.8540 (1.90×10^{-5})
	$R(1)$	0.7602 (0.0747)	0.7600 (3.06×10^{-4})	0.7623 (1.39×10^{-5})	0.7600 (6.12×10^{-7})	0.7576 (1.58×10^{-5})
	$h(1)$	0.7139 (0.2696)	0.7119 (8.57×10^{-4})	0.7310 (1.07×10^{-4})	0.7121 (1.18×10^{-5})	0.6942 (1.25×10^{-4})
	α	4.9887 (2.1453)	4.9941 (1.25×10^{-3})	5.0334 (2.83×10^{-4})	4.9945 (3.63×10^{-5})	4.9548 (2.14×10^{-4})
	β	0.9138 (2.3699)	0.9500 (1.15×10^{-3})	0.9835 (4.41×10^{-4})	0.9503 (2.31×10^{-4})	0.9173 (2.20×10^{-5})
$\mathbf{R}_2$	θ	1.0688 (0.9528)	1.0867 (7.30×10^{-4})	1.1002 (1.98×10^{-4})	1.0868 (1.14×10^{-4})	1.0735 (2.98×10^{-5})
	$R(1)$	0.8674 (0.0514)	0.8619 (2.42×10^{-4})	0.8633 (2.57×10^{-5})	0.8619 (3.47×10^{-5})	0.8604 (4.42×10^{-5})
	$h(1)$	0.4216 (0.1402)	0.4359 (6.97×10^{-4})	0.4485 (1.70×10^{-4})	0.4360 (9.14×10^{-5})	0.4242 (1.64×10^{-5})
	α	4.3478 (1.9903)	4.3514 (1.92×10^{-3})	4.4437 (6.07×10^{-4})	4.3523 (2.83×10^{-5})	4.2601 (5.55×10^{-4})
	β	1.6147 (2.4821)	1.6355 (1.82×10^{-3})	1.7195 (6.63×10^{-4})	1.6363 (1.37×10^{-4})	1.5536 (3.86×10^{-4})
$\mathbf{R}_3$	θ	1.4146 (0.5795)	1.4307 (1.04×10^{-3})	1.4583 (2.77×10^{-4})	1.4310 (1.04×10^{-4})	1.4042 (6.55×10^{-5})
	$R(1)$	0.7918 (0.0788)	0.7835 (3.61×10^{-4})	0.7867 (3.23×10^{-5})	0.7835 (5.24×10^{-5})	0.7802 (7.35×10^{-5})
	$h(1)$	0.5857 (0.2394)	0.6097 (9.78×10^{-4})	0.6348 (3.11×10^{-4})	0.6099 (1.53×10^{-4})	0.5869 (7.61×10^{-6})

Table 17: The 95% asymptotic/credible interval estimates [with their CLs] under data sets I and II.

Scheme	Parameter	ACI-NA	ACI-NL	BCI	HPD
Data-I					
	α	(0.0000, 0.8595) [0.8582]	(0.0198, 3.0176) [2.9978]	(0.2382, 0.2501) [0.0118]	(0.2382, 0.2501) [0.0118]
	β	(296.14, 307.82) [11.680]	(296.19, 307.88) [11.691]	(302.81, 302.83) [0.0117]	(302.81, 302.83) [0.0117]
$\mathbf{R}_1$	θ	(0.0073, 0.0239) [0.0166]	(0.0092, 0.0265) [0.0173]	(0.0127, 0.0188) [0.0061]	(0.0126, 0.0187) [0.0060]
	$R(100)$	(0.8588, 0.9999) [0.1411]	(0.8628, 0.9999) [0.1371]	(0.9260, 0.9620) [0.0360]	(0.9280, 0.9636) [0.0356]
	$h(100)$	(0.0000, 0.0022) [0.0022]	(0.0003, 0.0036) [0.0033]	(0.0006, 0.0015) [0.0009]	(0.0006, 0.0015) [0.0009]
	α	(0.0000, 1.6033) [1.6033]	(0.1515, 2.8051) [2.6536]	(0.6460, 0.6578) [0.0118]	(0.6461, 0.6579) [0.0118]
	β	(0.0000, 11.286) [11.286]	(0.1239, 61.137) [61.137]	(2.7463, 2.7581) [0.0118]	(2.7465, 2.7583) [0.0118]
$\mathbf{R}_2$	θ	(0.0000, 0.0118) [0.0118]	(0.0019, 0.0166) [0.0147]	(0.0041, 0.0075) [0.0034]	(0.0041, 0.0075) [0.0034]
	$R(100)$	(0.4251, 0.9067) [0.4816]	(0.4638, 0.9560) [0.4922]	(0.5889, 0.7407) [0.1518]	(0.5900, 0.7417) [0.1516]
	$h(100)$	(0.0007, 0.0070) [0.0063]	(0.0017, 0.0088) [0.0071]	(0.0027, 0.0053) [0.0026]	(0.0026, 0.0052) [0.0026]
	α	(0.0000, 1.9375) [1.9375]	(0.3163, 2.7428) [2.4264]	(0.9296, 0.9335) [0.0039]	(0.9295, 0.9334) [0.0039]
	β	(0.0000, 5.6043) [5.6043]	(0.0001, 8244.3) [8244.3]	(0.5237, 0.5276) [0.0039]	(0.5237, 0.5276) [0.0039]
$\mathbf{R}_3$	θ	(0.0000, 0.0219) [0.0219]	(0.0001, 4.0602) [4.0601]	(0.0019, 0.0036) [0.0017]	(0.0019, 0.0036) [0.0017]
	$R(100)$	(0.3956, 0.8159) [0.4203]	(0.4282, 0.8569) [0.4287]	(0.5170, 0.6866) [0.1696]	(0.5164, 0.6854) [0.1690]
	$h(100)$	(0.0004, 0.0082) [0.0078]	(0.0017, 0.0107) [0.0090]	(0.0033, 0.0056) [0.0023]	(0.0033, 0.0056) [0.0023]
Data-II					
	α	(1.3811, 7.1292) [5.7481]	(2.1656, 8.3608) [6.1952]	(4.0952, 4.4105) [0.3153]	(4.0955, 4.4107) [0.3152]
	β	(0.0000, 2.0101) [2.0101]	(0.0019, 56.228) [56.226]	(0.2136, 0.4867) [0.2731]	(0.2147, 0.4873) [0.2726]
$\mathbf{R}_1$	θ	(0.0000, 2.4250) [2.4250]	(0.1338, 5.4104) [5.2765]	(0.7269, 0.9931) [0.2662]	(0.7294, 0.9952) [0.2659]
	$R(1)$	(0.6137, 0.9066) [0.2929]	(0.6270, 0.9216) [0.1371]	(0.6563, 0.8470) [0.1906]	(0.6664, 0.8539) [0.1875]
	$h(1)$	(0.1854, 1.2424) [1.0570]	(0.3405, 1.4967) [1.1562]	(0.4684, 1.0015) [0.5331]	(0.4530, 0.9793) [0.5263]

Table 17: Continued.

Scheme	Parameter	ACI-NA	ACI-NL	BCI	HPD
	α	(0.7840, 9.1933) [8.4093]	(2.1475, 11.588) [9.4409]	(4.6080, 5.3856) [0.7776]	(4.6064, 5.3816) [0.7752]
	β	(0.0000, 5.5587) [5.5587]	(0.0057, 147.40) [147.39]	(0.6005, 1.3118) [0.7113]	(0.5975, 1.3079) [0.7103]
$\mathbf{R}_2$	θ	(0.0000, 2.9362) [2.9362]	(0.1862, 6.1331) [5.9469]	(0.8663, 1.3248) [0.4585]	(0.8644, 1.3219) [0.4574]
	$R(1)$	(0.7667, 0.9680) [0.2013]	(0.7723, 0.9741) [0.2018]	(0.7776, 0.9269) [0.1494]	(0.7851, 0.9325) [0.1474]
	$h(1)$	(0.1468, 0.6964) [0.5496]	(0.2197, 0.8090) [0.5894]	(0.2458, 0.6759) [0.4301]	(0.2370, 0.6642) [0.4272]
	α	(0.4469, 8.2488) [7.8018]	(1.7726, 10.664) [8.8915]	(3.7588, 4.9459) [1.1871]	(3.7527, 4.9383) [1.1856]
	β	(0.0000, 6.4795) [6.4795]	(0.0794, 32.851) [32.772]	(1.0759, 2.2085) [1.1326]	(1.0858, 2.2128) [1.1270]
$\mathbf{R}_3$	θ	(0.2788, 2.5505) [2.2717]	(0.6338, 3.1576) [2.5238]	(1.1212, 1.7705) [0.6493]	(1.1070, 1.7542) [0.6472]
	$R(1)$	(0.6373, 0.9463) [0.3090]	(0.6515, 0.9624) [0.3109]	(0.6612, 0.8832) [0.2220]	(0.6740, 0.8934) [0.2194]
	$h(1)$	(0.1165, 1.0548) [0.9383]	(0.2629, 1.3048) [1.0419]	(0.3420, 0.9462) [0.6042]	(0.3258, 0.9194) [0.5936]

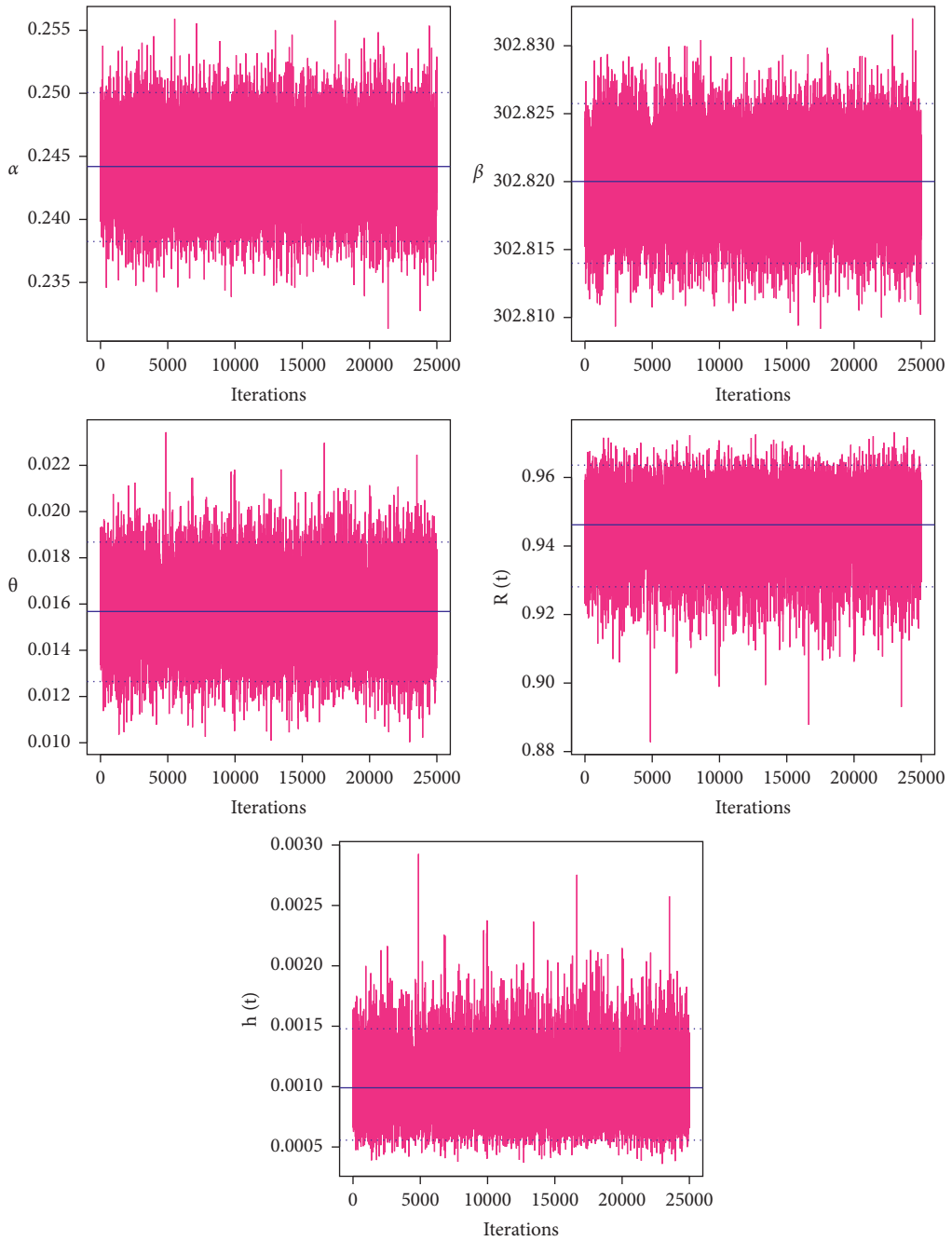

(a)

Figure 11: Continued.

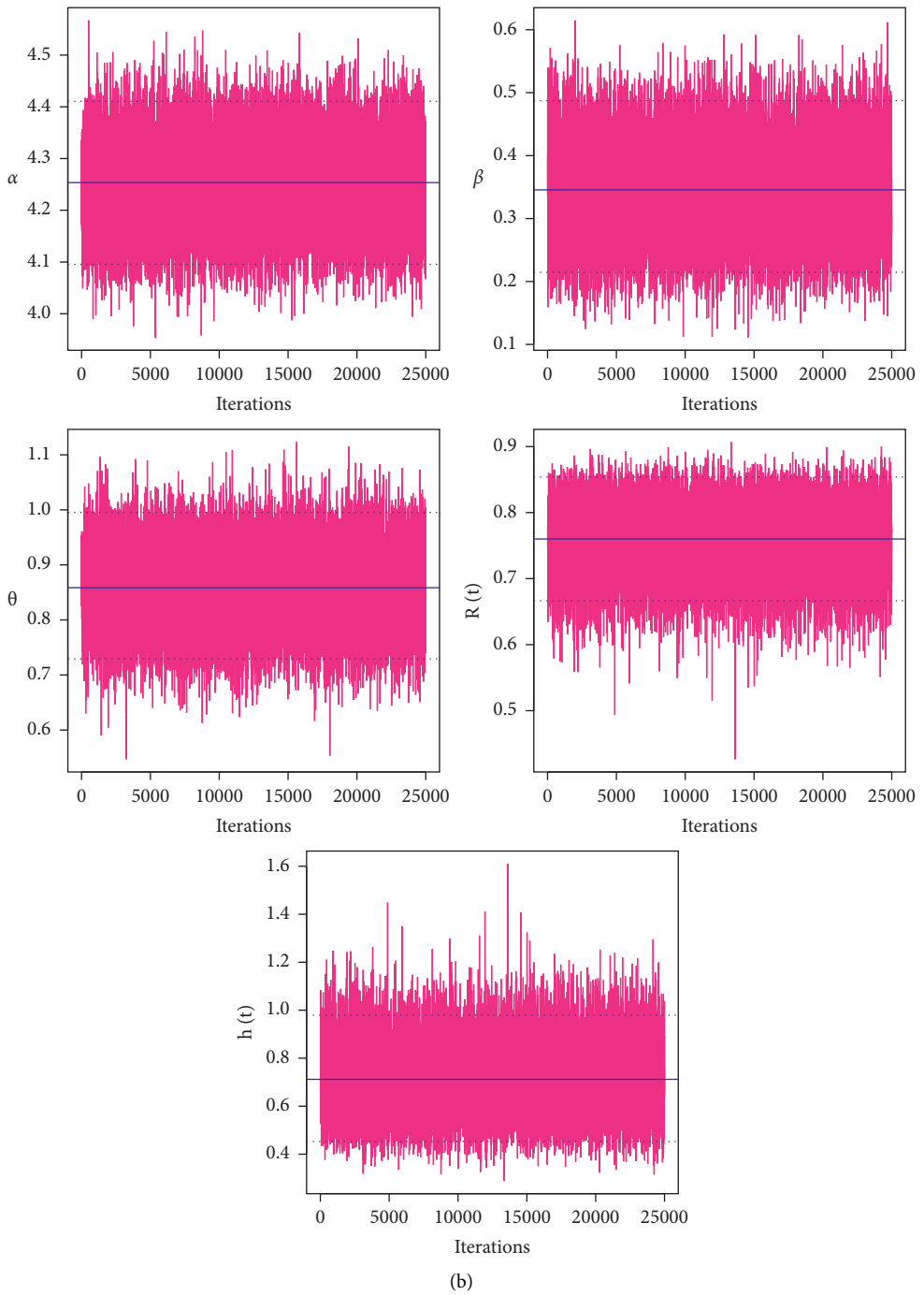

Figure 11: Trace plots for MCMC draws of the unknown parameters under data sets I and II. (a) $\mathbf{R}_1$ of data-I. (b) $\mathbf{R}_1$ of data-II.

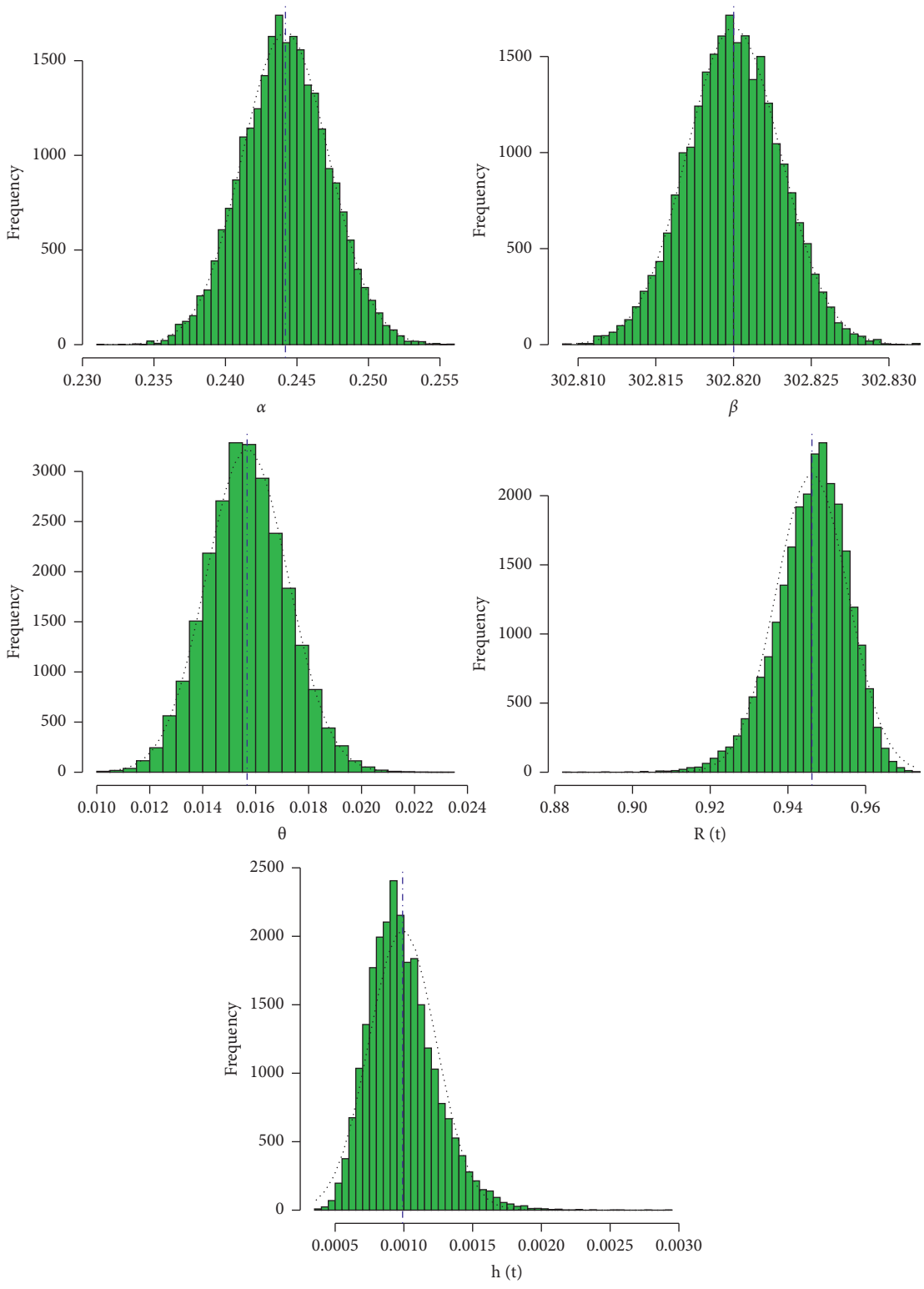

(a)

Figure 12: Continued.

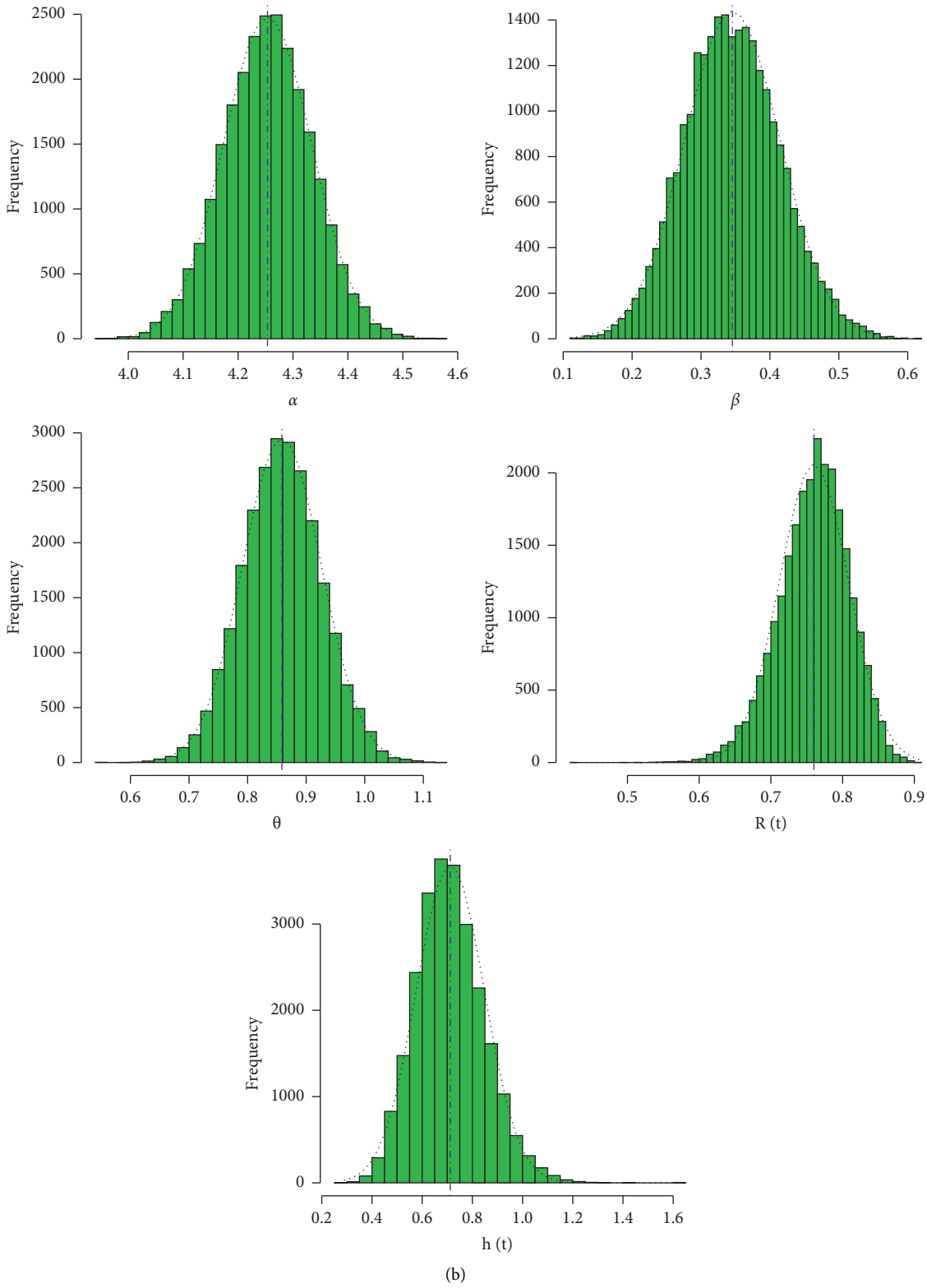

Figure 12: Histogram plots of the unknown parameters under data sets I and II. (a) $\mathbf{R}_1$ from data-I. (b) $\mathbf{R}_1$ from data-II.

Table 18: Optimum censoring scheme under data sets I and II.

Data	Scheme	Criterion		
		A	B	C
I	$\mathbf{R}_1$	8.9824	2.822×10^{-6}	306091.5
	$\mathbf{R}_2$	19.193	4.203×10^{-6}	330194.6
	$\mathbf{R}_3$	6.9776	7.775×10^{-7}	943744.4
II	$\mathbf{R}_1$	3.5326	1.988×10^{-2}	138.9751
	$\mathbf{R}_2$	11.127	3.890×10^{-1}	76.48990
	$\mathbf{R}_3$	10.458	6.801×10^{-1}	31.96376

in Section 3.3, we generate 30,000 MCMC samples and discard the first 5,000 samples as burn-in. Under SEL and LL (with $v(= -2, -0.02, +2)$), the Bayesian MCMC estimates and associated credible intervals of α, β, $\theta R(t)$, and $h(t)$ using noninformative priors are developed. Also, MLEs and two-sided 95% asymptotic (NA and NL) interval estimates of the unknown parameters are computed. The estimates of RF and HF are calculated when the mission time t is taken as 100 and 1 for data sets I and II, respectively. The point estimates (with their SEs) and interval estimates with their confidence lengths (CLs) and reported in Tables 16 and 17, respectively. It is noted that the proposed point and interval estimates, obtained based on data sets I and II, of α, β, $\theta R(t)$, and $h(t)$ are very similar to each other, as expected.

To examine the convergence of M-H algorithm, trace plot based on 25,000 MCMC simulated variates of each unknown parameter (for $\mathbf{R}_1$ as an example) using data sets I and II, is plotted in Figure 11. For each trace plot, the sample mean and two bounds of 95% HPD credible intervals are mentioned by solid (—) and dashed (- - -) lines, respectively. It indicates that the M-H algorithm converges very well. Using the Gaussian kernel density, the corresponding histogram plot of each unknown parameter (for $\mathbf{R}_1$ as an example) is also plotted and represented in Figure 12. In each histogram, the sample mean is depicted as vertical dash-dotted line (:). It represents that the simulated posteriors of α, β, and θ are fairly symmetric while the simulated posteriors of $R(t)$ and $h(t)$ are close to negative and positive skewed, respectively.

Using the optimum criteria given in Section 4, using the observed Fisher information (11) obtained from both data sets I and II, the concept of optimal censoring is illustrated, see Table 18. It shows that the scheme $\mathbf{R}_3$ is the optimal censoring (for data set I) while $\mathbf{R}_1$ is the optimal censoring (for data set II) than other competing scheme plans. However, the parameter and optimal estimates examined here support the same findings reported in the simulation study.

7. Conclusion Remarks

This article investigates the problem of estimating the unknown parameters and reliability characteristics of the MOGE distribution when the data are collected under type-II progressive censoring. Besides the likelihood inference, the Bayes MCMC estimates of the unknown parameters, reliability, and hazard functions are derived. As expected the joint posterior density cannot be obtained explicitly. Therefore, using gamma informative priors under different loss functions, the Bayes point and interval estimates of the unknown parametric functions are approximated utilizing the Metropolis–Hasting algorithm. From the simulation outputs, the Bayes MCMC estimation method for any unknown function of the MOGE parameters is recommended. To show the practical utility of the proposed methods in real-life phenomenon and to determine the optimum censoring plan, two data sets from engineering and physics are analyzed for this purpose. Additionally, based on the given data sets, we showed that the proposed model provides an adequate fit with respect to its competing Marshall–Olkin extended models. We hope that the results and methodologies discussed in this paper will be beneficial to data analyst and reliability practitioners. [39, 40].

Appendix

A. Fisher's Elements

Differentiating (7) partially with respect to α, β, and θ, the Fisher elements $\mathscr{L}_{ij}, i, j = 1, 2, 3$, are expressed as

$$
\begin{aligned}
\mathscr{L}_{11} &= -\frac{m}{\alpha^2} - \sum_{i=1}^{m} R_i \log^2 \psi_i(\theta) \psi_i^{\alpha}(\theta) \left(1 - \psi_i^{\alpha}(\theta)\right)^{-1} \left[1 + \psi_i^{\alpha}(\theta) \left(1 - \psi_i^{\alpha}(\theta)\right)^{-1}\right] \\
&\quad - \overline{\beta} \sum_{i=1}^{m} (R_i + 2) \log^2 \psi_i(\theta) \psi_i^{\alpha}(\theta) \left(\beta + \overline{\beta} \psi_i^{\alpha}(\theta)\right)^{-1} \left[1 - \overline{\beta} \psi_i^{\alpha}(\theta) \left(\beta + \overline{\beta} \psi_i^{\alpha}(\theta)\right)^{-1}\right], \\
\mathscr{L}_{22} &= -\frac{n}{\beta^2} + \sum_{i=1}^{m} (R_i + 2) \left(1 - \psi_i^{\alpha}(\theta)\right)^2 \left(\beta + \overline{\beta} \psi_i^{\alpha}(\theta)\right)^{-2}, \\
\mathscr{L}_{33} &= -\frac{m}{\theta^2} + (\alpha - 1) \sum_{i=1}^{m} \psi_i^{-1}(\theta) \left[\psi_i''(\theta) - \psi_i'^2(\theta) \psi_i^{-1}(\theta)\right] \\
&\quad - \alpha \sum_{i=1}^{m} R_i \psi_i^{\alpha-1}(\theta) \left(1 - \psi_i^{\alpha}(\theta)\right)^{-1} \left[\psi_i''(\theta) - \psi_i'^2(\theta) \psi_i^{-1}(\theta) \left\{1 - \alpha - \alpha \psi_i^{\alpha}(\theta) \left(1 - \psi_i^{\alpha}(\theta)\right)^{-1}\right\}\right] \\
&\quad - \alpha \overline{\beta} \sum_{i=1}^{m} (R_i + 2) \psi_i^{\alpha-1}(\theta) \left(\beta + \overline{\beta} \psi_i^{\alpha}(\theta)\right)^{-1} \left[\psi_i''(\theta) - \psi_i'^2(\theta) \psi_i^{-1}(\theta) \left\{1 - \alpha + \alpha \overline{\beta} \psi_i^{\alpha}(\theta) \left(\beta + \overline{\beta} \psi_i^{\alpha}(\theta)\right)^{-1}\right\}\right], \\
\mathscr{L}_{12} &= \sum_{i=1}^{m} (R_i + 2) \log\left(\psi_i(\theta)\right) \psi_i^{\alpha}(\theta) \left(\beta + \overline{\beta} \left(\psi_i(\theta)\right)^{\alpha}\right)^{-1} \left[1 + \overline{\beta} \left(1 - \psi_i^{\alpha}(\theta)\right) \left(\beta + \overline{\beta} \psi_i^{\alpha}(\theta)\right)^{-1}\right], \\
\mathscr{L}_{23} &= \alpha \sum_{i=1}^{m} (R_i + 2) \psi_i'(\theta) \psi_i^{\alpha-1}(\theta) \left(\beta + \overline{\beta} \psi_i^{\alpha}(\theta)\right)^{-1} \left[1 + \overline{\beta} \left(1 - \psi_i^{\alpha}(\theta)\right) \left(\beta + \overline{\beta} \psi_i^{\alpha}(\theta)\right)^{-1}\right],
\end{aligned}
\tag{A.1}
$$

$$
\begin{aligned}
\mathscr{L}_{13} &= \sum_{i=1}^{m} \psi_i'(\theta) \psi_i^{-1}(\theta) - \sum_{i=1}^{m} R_i \psi_i'(\theta) \left(\psi_i(\theta)\right)^{\alpha-1} \left(1 - \left(\psi_i(\theta)\right)^{\alpha}\right)^{-1} \left[1 + \alpha \log\left(\psi_i(\theta)\right) \left\{1 + \psi_i^{\alpha}(\theta) \left(1 - \psi_i^{\alpha}(\theta)\right)^{-1}\right\}\right] \\
&\quad - \overline{\beta} \sum_{i=1}^{m} (R_i + 2) \psi_i'(\theta) \psi_i^{\alpha-1}(\theta) \left(\beta + \overline{\beta} \psi_i^{\alpha}(\theta)\right)^{-1} \left[1 + \alpha \log\left(\psi_i(\theta)\right) \left\{1 - \overline{\beta} \psi_i^{\alpha}(\theta) \left(\beta + \overline{\beta} \psi_i^{\alpha}(\theta)\right)^{-1}\right\}\right],
\end{aligned}
\tag{A.2}
$$

where $\psi_i''(\theta) = -x_i^2 (1 - \psi_i(\theta)), i = 1, 2, \ldots, m$.

Appendix B. Simulation Outputs

All simulation outputs including APEs, RMSEs, MRABs, ACLs, and CPs of α, β, θ, $R(t)$, and $h(t)$ based on different choices of progressive censoring schemes (also different complete and effective sample sizes) are reported here.

Data Availability

The data that support the findings of this study are available from the corresponding author upon reasonable request.

Conflicts of Interest

The authors declare that they have no conflicts of interest.

References

[1] A. W. Marshall and I. Olkin, "A new method for adding a parameter to a family of distributions with application to the exponential and Weibull families," *Biometrika*, vol. 84, no. 3, pp. 641–652, 1997.

[2] M. M. Ristić and D. Kundu, "Marshall-Olkin generalized exponential distribution," *Metron*, vol. 73, no. 3, pp. 317–333, 2015.

[3] R. D. Gupta and D. Kundu, "Generalized exponential distribution: different method of estimations," *Journal of Statistical Computation and Simulation*, vol. 69, no. 4, pp. 315–337, 2001.

[4] N. L. Johnson and S. Kotz, *Continuous Univariate Distribution*, Wiley, New York, NY, USA, 1970.

[5] N. Balakrishnan and E. Cramer, *The Art of Progressive Censoring*, Springer, Birkhäuser, New York, NY, USA, 2014.

[6] Z. H. Amin, "Bayesian inference for the Pareto lifetime model under progressive censoring with binomial removals," *Journal of Applied Statistics*, vol. 35, no. 11, pp. 1203–1217, 2008.

[7] C. Kim, J. Jung, and Y. Chung, "Bayesian estimation for the exponentiated Weibull model under Type II progressive censoring," *Statistical Papers*, vol. 52, no. 1, pp. 53–70, 2011.

[8] S. R. Huang and S. J. Wu, "Bayesian estimation and prediction for Weibull model with progressive censoring," *Journal of Statistical Computation and Simulation*, vol. 82, no. 11, pp. 1607–1620, 2012.

[9] S. Dey, M. Nassar, R. K. Maurya, and Y. M. Tripathi, "Estimation and prediction of Marshall–Olkin extended exponential distribution under progressively type-II censored data," *Journal of Statistical Computation and Simulation*, vol. 88, no. 12, pp. 2287–2308, 2018.

[10] H. Panahi, "Interval estimation of Kumaraswamy parameters based on progressively Type-II censored sample and record values," *Miskolc Mathematical Notes*, vol. 21, no. 1, pp. 319–334, 2020.

[11] H. Z. Muhammed and E. M. Almetwally, "Bayesian and non-Bayesian estimation for the bivariate inverse Weibull distribution under progressive Type-II censoring," *Annals of Data Science*, pp. 1–32, 2020.

[12] A. Elshahhat and M. K. Rastogi, "Estimation of parameters of life for an inverted Nadarajah–Haghighi distribution from Type-II progressively censored samples," *Journal of the Indian Society for Probability and Statistics*, vol. 22, no. 1, pp. 113–154, 2021.

[13] K. Maiti and S. Kayal, "Estimation of parameters and reliability characteristics for a generalized Rayleigh distribution under progressive type-II censored sample," *Communications in Statistics - Simulation and Computation*, vol. 50, no. 11, pp. 3669–3698, 2021.

[14] S. Dey, A. Elshahhat, and M. Nassar, "Analysis of progressive Type-II censored gamma distribution," *Computational Statistics*, 2022.

[15] K. Maiti, S. Kayal, and D. Kundu, "Statistical inference on the Shannon and Rényi entropy measures of generalized exponential distribution under the progressive censoring," *SN Computer Science*, vol. 3, no. 4, pp. 317–321, 2022.

[16] A. Elshahhat and W. S. Abu El Azm, "Statistical reliability analysis of electronic devices using generalized progressively hybrid censoring plan," *Quality and Reliability Engineering International*, vol. 38, no. 2, pp. 1112–1130, 2022.

[17] W. H. Greene, *Econometric Analysis*, Prentice-Hall, New York, NY, USA, 2000.

[18] W. Q. Meeker and L. A. Escobar, *Statistical Methods for Reliability Data*, John Wiley & Sons, New York, NY, USA, 1998.

[19] A. H. Muse, S. Mwalili, O. Ngesa, H. M. Alshanbari, S. K. Khosa, and E. Hussam, "Bayesian and frequentist approach for the generalized log-logistic accelerated failure time model with applications to larynx-cancer patients," *Alexandria Engineering Journal*, vol. 61, no. 10, pp. 7953–7978, 2022.

[20] A. H. Muse, S. Mwalili, O. Ngesa, S. J. Almalki, and G. Abd-Elmougod, "Bayesian and classical inference for the generalized log-logistic distribution with applications to survival data," *Computational Intelligence and Neuroscience*, vol. 2021, Article ID 5820435, 24 pages, 2021.

[21] A. H. Muse, O. Ngesa, S. Mwalili, H. M. Alshanbari, and A. A. H. El-Bagoury, "A flexible Bayesian parametric proportional hazard model: simulation and applications to right-censored healthcare data," *Journal of Healthcare Engineering*, pp. 1–28, 2022.

[22] B. N. Pandey and O. Rai, "Bayesian estimation of mean and square of mean of normal distribution using LINEX loss function," *Communications in Statistics - Theory and Methods*, vol. 21, no. 12, pp. 3369–3391, 1992.

[23] A. Gelman, J. B. Carlin, H. S. Stern, and D. B. Rubin, *Bayesian Data Analysis*, Chapman and Hall/CRC, New York, NY, USA, 2004.

[24] M. H. Chen and Q. M. Shao, "Monte Carlo estimation of Bayesian credible and HPD intervals," *Journal of Computational & Graphical Statistics*, vol. 8, no. 1, pp. 69–92, 1999.

[25] N. Balakrishnan and R. Aggarwala, *Progressive Censoring Theory, Methods and Applications*, Birkhäuser, Boston, MA, USA, 2000.

[26] H. K. T. Ng, P. S. Chan, and N. Balakrishnan, "Optimal progressive censoring plans for the Weibull distribution," *Technometrics*, vol. 46, no. 4, pp. 470–481, 2004.

[27] M. Plummer, N. Best, K. Cowles, and K. Vines, "coda: convergence diagnosis and output analysis for MCMC," *R News*, vol. 6, pp. 7–11, 2006.

[28] A. Henningsen and O. Toomet, "maxLik: a package for maximum likelihood estimation in R," *Computational Statistics*, vol. 26, no. 3, pp. 443–458, 2011.

[29] J. M. Pavia, "Testing goodness-of-fit with the kernel density estimator: GoFKernel," *Journal of Statistical Software*, vol. 66, pp. 1–27, 2015.

[30] A. Elshahhat and M. Nassar, "Bayesian survival analysis for adaptive Type-II progressive hybrid censored Hjorth data," *Computational Statistics*, vol. 36, no. 3, pp. 1965–1990, 2021.

[31] F. K. Wang, "A new model with bathtub-shaped failure rate using an additive Burr XII distribution," *Reliability Engineering & System Safety*, vol. 70, no. 3, pp. 305–312, 2000.

[32] D. Hinkley, "On quick choice of power transformation," *Applied Statistics*, vol. 26, no. 1, pp. 67–69, 1977.

[33] G. M. Cordeiro and A. J. Lemonte, "On the Marshall–Olkin extended Weibull distribution," *Statistical Papers*, vol. 54, no. 2, pp. 333–353, 2013.

[34] M. Mansoor, M. H. Tahir, G. M. Cordeiro, S. B. Provost, and A. Alzaatreh, "The Marshall-Olkin logistic-exponential distribution," *Communications in Statistics - Theory and Methods*, vol. 48, no. 2, pp. 220–234, 2019.

[35] M. Nassar, D. Kumar, S. Dey, G. M. Cordeiro, and A. Z. Afify, "The Marshall–Olkin alpha power family of distributions with applications," *Journal of Computational and Applied Mathematics*, vol. 351, pp. 41–53, 2019.

[36] A. J. Lemonte, G. M. Cordeiro, and G. Moreno–Arenas, "A new useful three-parameter extension of the exponential distribution," *Statistics*, vol. 50, no. 2, pp. 1–26, 2015.

[37] J. T. Eghwerido, J. O. Ogbo, and A. E. Omotoye, "The Marshall-Olkin Gompertz distribution: properties and applications," *Statistica*, vol. 81, no. 2, pp. 183–215, 2021.

[38] M. E. Ghitany, F. A. Al-Awadhi, and L. A. Alkhalfan, "Marshall–Olkin extended Lomax distribution and its application to censored data," *Communications in Statistics - Theory and Methods*, vol. 36, no. 10, pp. 1855–1866, 2007.

[39] N. Balakrishnan and R. A. Sandhu, "A simple simulational algorithm for generating progressive Type-II censored samples," *The American Statistician*, vol. 49, no. 2, pp. 229-230, 1995.

[40] S. Dey and A. Elshahhat, "Analysis of Wilson-Hilferty distribution under progressive Type-II censoring," *Quality and Reliability Engineering International*, 2022.

Hindawi
Complexity
Volume 2022, Article ID 2767371, 32 pages
https://doi.org/10.1155/2022/2767371

Review Article

Directed Energy Deposition via Artificial Intelligence-Enabled Approaches

Utkarsh Chadha,[1] **Senthil Kumaran Selvaraj**,[1] **Aakrit Sharma Lamsal**,[2] **Yashwanth Maddini**,[1] **Abhishek Krishna Ravinuthala**,[1] **Bhawana Choudhary**,[2] **Anirudh Mishra**,[2] **Deepesh Padala**,[3] **Shashank M**,[3] **Vedang Lahoti**,[1] **Addisalem Adefris**,[4] **and Dhanalakshmi S**[5]

[1]*Department of Manufacturing Engineering, School of Mechanical Engineering (SMEC), Vellore Institute of Technology (VIT), Vellore 632014, Tamil Nadu, India*
[2]*School of Computer Science and Engineering (SCOPE), Vellore Institute of Technology (VIT), Vellore 632014, Tamil Nadu, India*
[3]*School of Electronics Engineering (SENSE), Vellore Institute of Technology, Vellore 632014, Tamil Nadu, India*
[4]*School of Mechanical and Automotive Engineering, College of Engineering and Technology, Dilla University, P.O. Box 419, Dilla, Ethiopia*
[5]*Combat Vehicles Research & Development Establishment (CVRDE), Defence Research & Development Organization (DRDO), Ministry of Defence, Government of India, Avadi, Chennai 600054, Tamil Nadu, India*

Correspondence should be addressed to Senthil Kumaran Selvaraj; senthilkumaranselvaraj82@gmail.com and Addisalem Adefris; addisalem@du.edu.et

Received 16 April 2022; Revised 2 August 2022; Accepted 23 August 2022; Published 29 September 2022

Academic Editor: Yu Zhou

Additive manufacturing (AM) has been gaining pace, replacing traditional manufacturing methods. Moreover, artificial intelligence and machine learning implementation has increased for further applications and advancements. This review extensively follows all the research work and the contemporary signs of progress in the directed energy deposition (DED) process. All types of DED systems, feed materials, energy sources, and shielding gases used in this process are also analyzed in detail. Implementing artificial intelligence (AI) in the DED process to make the process less human-dependent and control the complicated aspects has been rigorously reviewed. Various AI techniques like neural networks, gradient boosted decision trees, support vector machines, and Gaussian process techniques can achieve the desired aim. These models implemented in the DED process have been trained for high-precision products and superior quality monitoring.

1. Introduction

Artificial intelligence (AI) is a branch of computer science that deals with self-learning mathematical models. For example, weather prediction systems predict weather using AI based on various parameters. Similarly, artificial intelligence has been beneficial in the field of mechanical engineering. This review will rigorously explain that artificial intelligence has made the process of development in the DED process more effortless. It has successfully achieved various goals, including modeling the correlation between the microstructure of alloys and their properties, i.e., with the help of microstructural characteristics like volume fraction and thickness of phase to predict its tensile properties like tensile strength, yield strength, and so on. Experiments can be carried on these alloys more effectively with the properties of the alloys predicted using AI. We have studied a few techniques used in various stages of the DED process, including prediction of single clad geometry, modeling correlation between properties and microstructure of elements, and predicting tensile properties of alloys formed using DED. Using some neural networks and a proper dataset, a

good model can be built to predict temperatures with higher accuracy and precision, leading to an even more efficient deposition technology, which will help build complex and unique parts, especially in biomedical and aerospace industries. We studied how various AI techniques like NN, SVM, GP, GBT, and so on have helped achieve various goals, and we have tried to present an overview of all the techniques [1, 2].

Directed energy deposition (DED) is defined as an additive manufacturing process in which a focused energy source, such as laser arc, electron, or laser beam, melts a material as a nozzle is depositing them [3, 4].

A typical setup of all the components is shown in Figure 1. As seen, the feedstock delivers material (wire or powder) to the deposition point where it is melted by concentrating a laser or an electron beam.

Like many similar additive manufacturing processes, the DED method involves a feeder which directs the feedstock through a heat source to form a weld pool in the presence of a controlled environment such as a vacuum or an inert gas. The feedstock is either a metal wire or powder that deposits on the target object's surface when melted. As shown in Figure 2, there are three widely used heat sources in the DED process [5]. They are electron beam, electric arc or plasma, and laser. In the directed energy deposition process, the heat source is generally focused on the feedstock at the point where metal deposition occurs. G-Code controls the nozzle of the gun or tool in such a way that it follows a specific tool path around the object [6, 7]. The melt pool formed is directed along the tool path by carefully controlling the feed material and the heat source.

2. Understanding Directed Energy Deposition

Figure 3 shows a brief description of how the DED process is generally carried out. The process starts at the point where the material is injected in the form of a wire or powder and completes at the point where all the layers of the material are deposited on the substrate [8]. One must be careful about the residual stresses formed by the enormous magnitude of the thermal gradients created in the heat-affected zone. This results in final products with lesser strength due to the distortion of the grain structure. To reduce these thermal-induced stresses, complex heat treatment processes might be necessary [9, 10]. Due to this reason, the printing process might sometimes be interrupted. Thus, to avoid such circumstances, the printing process must be closely monitored at all times.

The print speed is one of the essential aspects of the DED process. The wire-based DED processes have lower resolution compared to powder-based DED processes. Powder DED processes maintain lower speeds and tend to produce products with higher resolution. Wire-based systems are generally used to create large parts with low printing costs. This is achieved by using low-cost feed materials and higher print speeds. To get higher resolutions and lesser material waste, powder processes can get a near net shape [10]. However, powder processes are relatively expensive compared to the wired processes. We get a near net shape with a much lesser resolution, limited geometric variety, and higher costs for post-processing using wired processes.

As already mentioned in Figure 4, the DED process is conducted in the presence of a vacuum or an inert gas (shielding gas) in order to prevent the weld pool from oxidizing [10, 11]. Reactive metals such as titanium (and its alloys), tungsten, and niobium are some of the most used feed materials used in the DED process. These metals tend to oxidize if there is no shielding gas or vacuum around them. Table 1 shows the pros and cons of these shielding mediums.

Oxidation reactions that might occur during the process:

$$\mathrm{Ti}_{(s)} + \mathrm{O}_{2(g)} \longrightarrow \mathrm{TiO}_2 \tag{1}$$

$$2\mathrm{W}_{(S)} + 3\mathrm{O}_{2(g)} \longrightarrow 2\mathrm{WO}_3 \tag{2}$$

Table 2 provides a deep insight and comparison of the additive manufacturing processes on various parameters.

There are many pros as well as some cons of using the directed energy deposition process. One of the main advantages of using this process is that it can be used for various metals, polymers, and ceramics. All the other additive manufacturing processes are usually confined to using metals as the feed material. Many industrial sectors often use this process to repair their existing parts by which they can reduce repairing or replacing costs. The laser or electron beam takes very minimal time to melt the material. Hence, this process has a relatively higher deposition rate when compared to other additive manufacturing techniques. Therefore, the build rate is also high. The nature of the materials used as the feed is selected to cool faster to form round bead-like structures. This makes sure that the parts created are more robust and denser. Also, the precision rate is high, so that there is rarely any need for post-processing or texture enhancements [13]. The DED process makes it convenient for us to change the material whenever needed to make different parts. This is one of the desirable and essential qualities that other additive manufacturing processes do not possess. This process produces near net shape products, and hence the material wastage is low.

Moreover, finally, the DED process can produce very complex objects and through traditional manufacturing processes. This process is also better at making more oversized products when compared to similar processes. This method also has some disadvantages that are to be noted to avoid any manufacturing issues. One such major disadvantage is that the products made by this process have a relatively poorer surface finish than those from other additive manufacturing methods [3]. This is because wire-based DED systems tend to have higher speeds which reduce the resolution of the product. Also, premium features such as overhangs and interior customizing are not possible as support structures are not possible in the DED process. Moreover, finally, the equipment used in this process, such as the shielding systems, energy sources like laser and electron beams, and material feeding systems, is costly, and great care and effort should be taken to manage them.

2.1. Applications of DED. DED is used to fabricate parts but is specially used to add material to existing products or repair. In general, the DED applications come under three

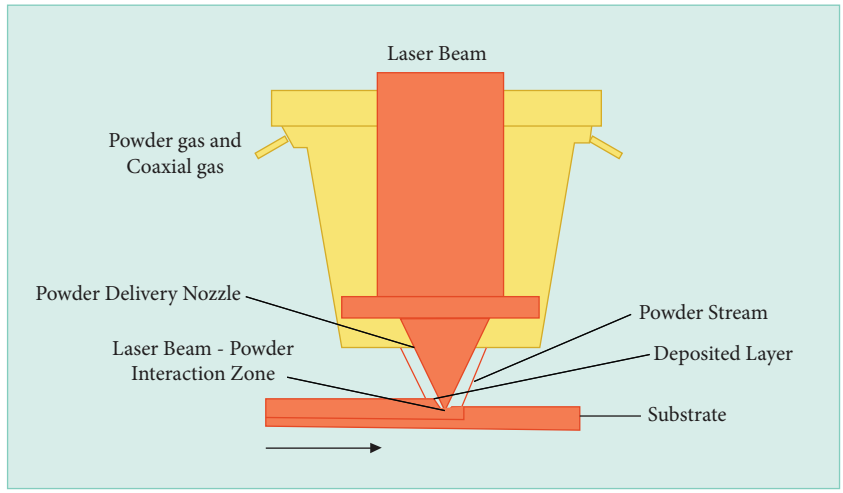

Figure 1: DED process setup.

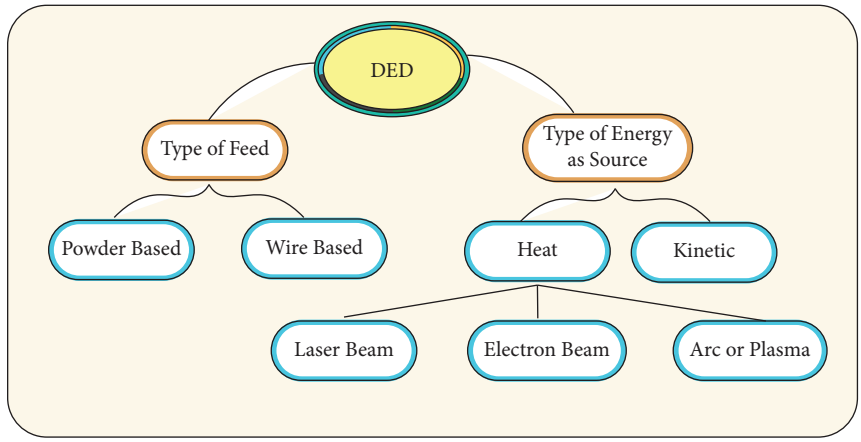

Figure 2: DED classification.

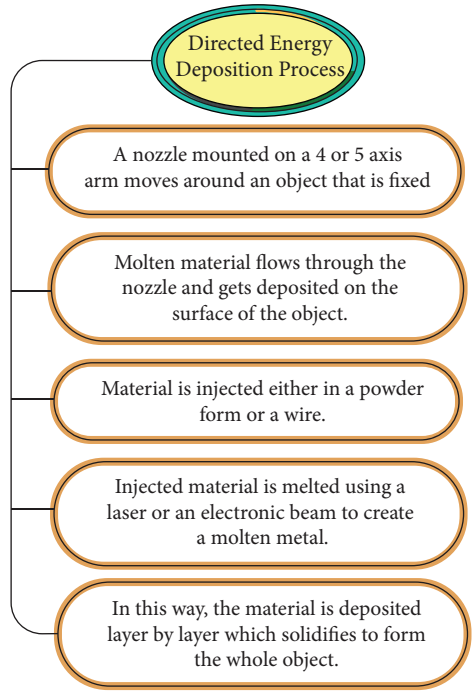

Figure 3: DED process flowchart.

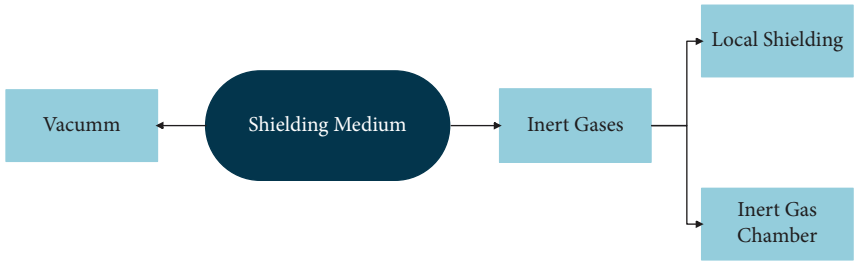

Figure 4: Shielding medium.

Table 1: Pros and cons involving the use of these shielding mediums.

Pros/ cons	Vacuum chamber	Inert chamber	Local shielding	Ref.
Pros	(i) It provides the highest quality environment.	(i) It provides the highest quality environment.	(i) There are some quality compromises which is acceptable.	[10]
Cons	(i) It requires a heavy and expensive reinforced chamber to withstand vacuum forces. (ii) Elements in the melt pool evaporate because of the low-pressure environment.	(i) It is costly and time consuming to fill the whole chamber with inert gas.	(i) It is pretty expensive because of its enclosed environment. (ii) It provides less consistency and atmosphere purity.	[10]

categories (Figure 5). They are near net shape parts, feature additions, and repair. DED is primarily used in manufacturing near net shape parts such as airplane and marine-related parts, saving a lot of time and money. DED can thus produce complex shapes while reducing material wastage. DED can also be used to add some additional features to pre-existing objects. DED uses industrial robots and software tools for the same. It is introduced to add layers to surfaces by using a cladding process with the help of robots. Adding features to objects increases the value of the product. DED makes sure that the machining time is reduced while the only disadvantage being an expensive process. Also, bonding of dissimilar metals is possible by changing the feedstock during printing. A lot more research needs to be done to increase this feature addition process [3, 14]. Finally, DED is used in many industrial sectors to repair existing equipment. A repairing process that was previously done manually got much easier with the help of DED. DED does component repairs often extending the life of the part. It also simplifies the process by reducing the lead time.

2.2. Types of DED Processes concerning Energy Sources

2.2.1. Electron Beam Directed Energy Deposition. Most of the customers choose DED processes to manufacture more significant parts because the DED process has a high deposition rate compared to other additive manufacturing processes. In the DED process, there is a feature addition method that helps to bond two dissimilar metals.

The DED process is subdivided into three categories: electronic beam, laser, and plasma or electric arc. The electron beam additive manufacturing (EBAM) process uses a wire feeder to feed metal wire which directs into an electronic beam to perform on substrate pool. Electron beam gun controls the material and substrate when power is transferred to material [13, 14]. The power values in DED vary with deposition rate, material, and geometry. Most of the time, the power values range from 4 to 20 kw. The EBAM process can be controlled using CAD software to change machine path and axis of tools. This total operation is performed in the vacuum chamber to prevent oxidation. EBAM produces near net shape parts because of its layer-by-layer deposition and is faster than traditional manufacturing methods. This process is used to create parts or components for the aerospace industry as it creates final geometry to components [15, 16]. EBAM works for hours to produce large parts and reduce material wastage. DED works in such a way to get flexible designs. Figure 6 summarizes the characteristics of an EBAM process.

2.2.2. Laser Directed Energy Deposition. The laser directed energy deposition (LDED) process is used to achieve small parts with high resolution, and it does not require any vacuum environment as EBAM. This process comes under powder bed fusion which gives high-resolution parts and maintains low speed [13, 17]. In the powder bed fusion process, parts are built by powdered metal particles that are melted and combined using a laser energy source. Laser DED uses inert gas for shielding and creates finer microstructures.

The main drawback of the laser DED process is that this process requires inert gas for shielding, and manipulation of energy sources also occurs. During building large-scale components, there is a possibility of getting spot sizes [14, 15]. Significant characteristics of the LDED process are summarized in Figure 7.

2.2.3. Arc Directed Energy Deposition. Arc directed energy deposition (ADED) produces or builds more significant parts than the other two DED processes. This is by far the

Table 2: Additive manufacturing processes (comparisons).

Process type	Powder bed fusion	Directed energy deposition	Material extrusion	VAT photopolymerization	Material jetting	Ref
Brief description	Thermal energy selectively fuses regions of a powder bed.	Focused thermal energy is used to fuse materials by melting as the material is being deposited.	Material is selectively dispensed through a nozzle.	Liquid photopolymer in a VAT is selectively cured by light activation.	Droplets of build material are selectively deposited.	[12]
Related technologies	Electron beam melting (EBM), selective laser sintering (SLS), selective heat sintering (SHS), direct metal laser sintering (DMLS)	Laser metal deposition (LMD)	Fused deposition melting (FDM)	Stereolithography (SLA), digital light processing (DLP)	Multi-jet modeling (MJM)	[12]
Materials	Metals, polymers	Metals, polymers, and ceramics	Typically polymer-based	Photopolymer	Polymers, waxes	[12]

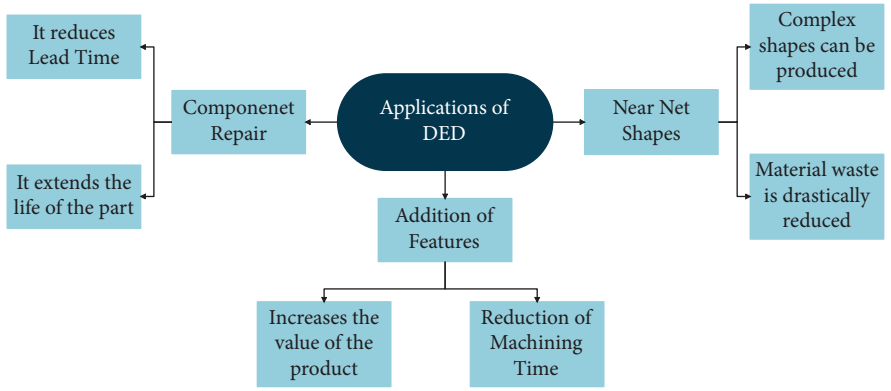

Figure 5: Applications of DED.

most commonly available DED method in the market. The arc DED process is used in many industries because it is less expensive than other DED processes [16, 17]. Mainly steel alloys are used to create near net shape parts with high power.

However, there are few drawbacks to the arc DED process. One of the major drawbacks is that the deposition rate is considerably low compared to other DED processes. High deposition rates can be reached with higher traveling speeds under a large volume of shielding gases. Shielding gases used in this process are pure inert gases such as argon which are highly expensive and potentially hazardous [13, 15–17]. All the significant characteristics of an ADED process are listed out as a flowchart in Figure 8.

3. Types of Feed Materials Used in DED

Feed materials are the primary sources for any additive manufacturing process. Feed materials are of two types in the DED (directed energy deposition) process: wire and powder. The selection of suitable feed material is essential to determine various process parameters like viscosity, thermal conductivity, or the coefficient of expansion, and it depends upon the desired features, complexity, and geometry of the final component.

Technology is advancing daily with research searching for new and efficient feed materials that can be used in additive manufacturing processes. While metals and some alloys were the only feed materials used in the primitive stages of DED, a broad spectrum of materials are currently being used in the additive manufacturing industry [13]. Unconventional materials such as superalloys, polymers, nanomaterials, biomaterials, or even bio-waste materials have proven to be suitable replacements for conventional metals and alloys [18–25]. Even though not ready to be used at an industrial scale, recent research on these new materials has shown promising results about using them for mass production in the future.

3.1. Pure Metals. Most of the metals in their pure form have limited applications and very few desirable properties. This is one of the main reasons why pure metals are rarely used for mainstream manufacturing. When combined with other metals, these metals bring out unique properties used in many industrial applications. Even after all these, some of the metals are being used in 3D printing for the sake of research. Some of those metals are listed and briefly discussed below. Table 3 provides a comparison of the pure metal feed materials in the DED process.

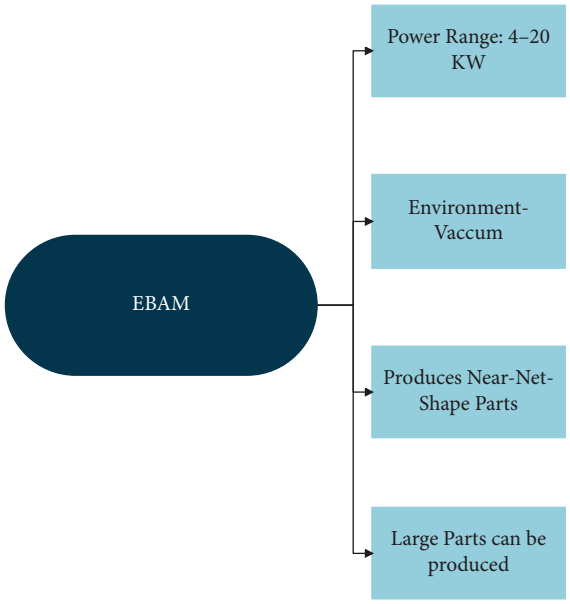

Figure 6: Characteristics of EBAM process.

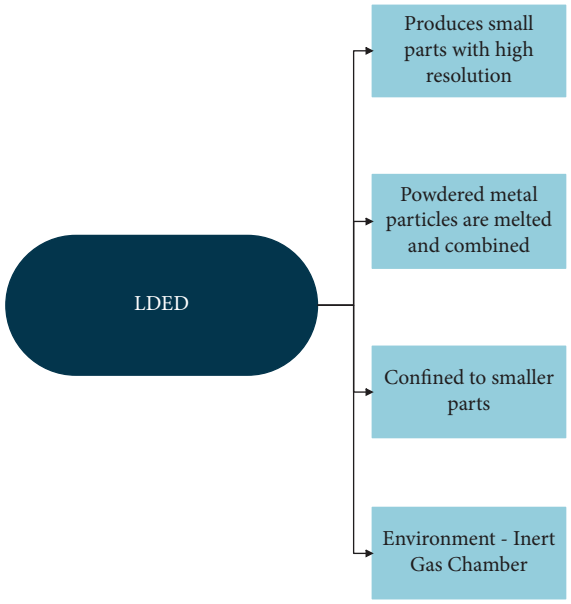

Figure 7: Characteristics of LDED process.

3.1.1. Copper. Many aviation and marine industries manufacture heat exchangers, induction coils, or heat sinks for different mechanisms. The DED process allows printing of these products with 99.99% pure copper as the feed material. Copper is considered one of the best metals used for manufacturing such components because it has an exceptional thermal and electrical conducting capacity. Also, it has an excellent heat-retaining capacity and is also said to have anti-bacterial properties. Recent research has shown that the average micro-hardness values obtained by the LDED process are more significant than ordinary Cu samples. One such research is the experiment done by Yadav et al., where they created a block of pure copper by using a 2 kW LDED system [26]. The average micro-hardness value they obtained was 77 ± 3.5 HV0.98 N, which is greater than the average micro-hardness value of copper, which is 57 HV [27]. The results have shown that pure Cu components made using the LDED process have more refined grain structures and better hardness values.

3.1.2. Tungsten. Another metal that is widely used in many industries is tungsten. While tungsten is not directly used in its pure form, it is made into tungsten carbide, a hard material for cutting wood or metals, refining metals, and drilling [28]. Tungsten has many desirable qualities, such as excellent corrosion resistance, low vapor pressure, high thermal conductivity, high melting point, and higher density. This makes it suitable to be used in aerospace and space technologies and nuclear systems. Although fabrication of tungsten is done by using powder bed fusion or spark plasma sintering, recent research studies have shown that DED can also be a suitable process to fabricate pure tungsten. The methods mentioned above are usually time consuming and cannot produce complex geometries [30]. According to Jeong et al., fabricating tungsten through the DED process can solve both problems simultaneously. By the end of their experiment, they could print a pure tungsten structure over 100 mm size, density up to 19.0 g/cm^2, and up to 3.9 GPa hardness. Also, it is concluded that the oxygen level should be less than 300 ppm in the tungsten powder to avoid any oxidation due to the repeated melting and solidification process [29].

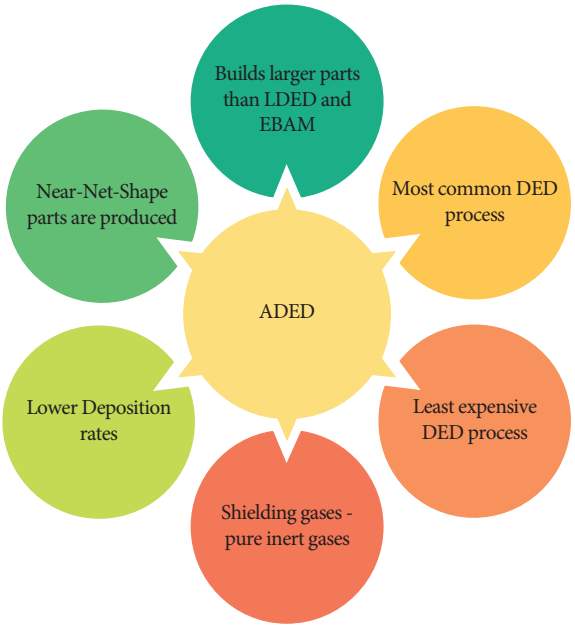

Figure 8: Characteristics of an ADED process.

3.2. Metal Alloys. Table 4 shows the various metallic alloys as feed materials which are used in the DED process.

3.2.1. Hastelloy-X. Jinoop et al. studied that laser addition manufacturing using directed energy deposition (LAM-DED) is an excellent process to create complex Hastelloy-X

Table 3: Types of feed materials (pure metals).

S.no	Materials	Properties	Exploitation on DED	Applications	References
1	Copper	High thermal and electrical conducting capacity, high heat-retaining capacity, and anti-bacterial properties.	LDED	Heat exchangers, induction coils, or heat sinks	[26, 27]
2	Tungsten	Excellent corrosion resistance, low vapor pressure, high thermal conductivity, high melting point, and higher density.	Powder bed fusion, plasma laser sintering, LDED	Wood and metal cutting, drilling, machining, aerospace and space industries, nuclear systems	[28, 29]

Table 4: Types of feed materials (metal alloys).

S.no	Materials	Properties	Exploitation on DED	Applications	References
1	Hastelloy-X (nickel-chromium iron-molybdenum)	High mechanical strength, high yield strength, high ductility, high resistance.	LAM-DED	Gas turbine engines, heat exchangers and heat shielding, etc.	[31]
2	Nickel-based superalloy Inconel 718	High tensile and impact strength, good resistance to corrosion and oxidation.	LAM-DED	Jet engines and gas turbines, etc.	[32]
3	Titanium-molybdenum (Ti-15Mo)	Excellent corrosion resistance, hardness, and fatigue.	EBAM-DED	Bioimplants and aerospace industries.	[33]
4	Other titanium alloys	High tensile and toughness.	EBAM-DED	Military, aircraft, spacecraft, etc.	[34]
5	Stainless steel (300 series)	Resistance to corrosion, high strength at high temperature.	EBAM-DED	Plates, sheets, pipes, tube, and fits	[35]
6	Zirconium alloys (Zircaloy)	High hardness, ductility, corrosion resistance.	EBAM-DED	Nuclear technology, water reactor, etc.	[36]
7	4043 aluminum alloy	Good corrosion resistance.	EBAM-DED	Welding and brazing, etc.	[37]

(Hast-X) components on weld pool. Hastelloy-X is used in many engineering applications, especially in gas turbines, heat exchangers, and shields. All these applications are made of Hastelloy-X because of their high resistance and stress corrosion with high strength. An inert gas such as argon has been used for powder feeding. Similarly, laser addition manufacturing uses powder bed fusion (LAM-PBF) to melt Hastelloy-X on the powder bed. Samples built using the LAM-DED process have higher ultimate strength and yield strength than compared to conventional processes. However, it is lower compared to LAM-PBF. Components built using LAM-DED have higher ductility than components built using LAM-PBF. Most complex Hast-X components are being built using LAM-DED because these samples are used for high-temperature applications [31].

3.2.2. Nickel-Based Superalloy Inconel 718. Careri et al. showed that additive manufacturing is the best method to produce complex parts in various automotive, aerospace, and medical industries. Manufacturing parts produced by additive manufacturing processes are more flexible to create near net shape parts. Nickel-based superalloy Inconel 718 is taken in powder with sizes varying from 45 to 106 μm. Inconel 718 is used in nuclear reactors and gas turbine engines because of its high tensile and impact strength. It has good resistance to corrosion and oxidation. The manufacturing process followed by the machining process shows excellent machinability due to the high ductility of Inconel 718 [32].

3.2.3. Titanium-Molybdenum (Ti-15Mo). Titanium-molybdenum (Ti-15Mo) is also called a biomedical alloy since it is used to build biomedical implants, especially orthopedic and dental implants. Laser deposition is used to deposit metal powder on the substrate. Because of its fabulous process parameters, Ti-15Mo is used to build biocompatible implants. The chemical composition of Ti in the deposition part is $85.02 \pm 2.44\%$, and Mo is $14.98 \pm 2.58\%$. Ti alloys are the best alloys for biomedical applications. Two types of Ti alloys are used for biomedical implants: α-type Ti and $\alpha + \beta$ type. Ti-15Mo is used for biocompatible implants because of its excellent corrosion resistance, hardness, and fatigue. Ti-15Mo is quite feasible for bioimplants because of its properties. Similarly, there are some applications used in the aerospace industry. Some advanced research works focus on Ti-15M to learn its applications in biomedical industries [33].

3.2.4. Other Titanium alloys. Compared to the conventional process, manufacturing near net shape (NNS) parts using metal additive manufacturing is more suitable. Near net shape components are built using the conventional process which has various disadvantages such as removing a large amount of material and high cost. Ti alloys in the form of wire and powder have been used to produce NNS components. Ti alloys have high corrosion resistance and can withstand high temperatures. Alloys such as Ti-6Al-4V and Ti-6Al-6V-2Sn are used in the military, aircraft, and spacecraft because of their high tensile strength and

toughness. Metal additive manufacturing is the best method to build NNS because it is more cost-efficient and less costly than conventional manufacturing. For Ti alloys, powder bed fusion is the best way to manufacture components [34].

3.3. Polymers

3.3.1. Polymethyl Methacrylate (PMMA). PMMA is a transparent polymer used as a substitute for standard glass. It is shatterproof and a very rigid thermoplastic material [38]. PMMA is highly resistant to UV light or harsh weather conditions. It has higher chemical resistance when compared to other transparent polymers. It is also highly resistant to scratches. PMMA is mainly used in the biomedical industry to make bone implants, bone types of cement, and drug delivery systems. It is also used to make dental implants where it is substituted for dental roots [39]. Mitsouras et al. described that 3D printed endoprostheses used for the palliative care of patients were created using selective laser sintering and directed energy deposition of PMMA and were sterilized using γ radiations [40]. When these materials are observed for 486 days (about one and a half years), the functional outcome was good in 70% of the patients and was fair in the remaining patients.

3.3.2. Polyether Ether Ketone (PEEK). PEEK is a semicrystalline thermoplastic with high performance. PEEK is used in the medical industry as supporting parts of endoscopes, dialyzers, and dental instruments. This is mainly because of its high heat and electrical resistance. It is used in the aircraft industry to replace parts made of aluminum [41]. PEEK has a high melting point, and thus it can withstand high temperatures. Therefore, it is used in critical engine parts in aircraft. It also has similar applications in the automobile industry [42]. Rinaldi et al. fabricated nanosat structures using PEEK as the feed material and FDM process. They described that the part was made, but there were many thermal-related issues in part. Despite these hurdles, they achieved an acceptable value of thermal conductivity (5 w/mK). Thermal conductivity needs to be within the acceptable values to ensure a minimal number of hotspots forming on the surface. Also, it was understood that the temperature should not exceed the polymer glass transition temperature to ensure no drop in the mechanical properties [43].

3.3.3. Acrylonitrile Butadiene Styrene (ABS). ABS is majorly used in automotive applications to reduce weight by replacing conventional metallic parts. Dashboard parts and bumper parts are some examples. ABS has high impact strength and heat resistance. This makes it very apt to be used in pipe materials, and fittings can withstand earth loads and high temperatures. ABS is used in many structural applications due to its stain resistance and stability over time [44]. ABS fused with MOF (metal-organic framework) materials can also be extensively used for gas storing, filtering, sensing, and catalysis, as described by Bible et al. in their research. They were able to fabricate an ABS-MOF composite without any visible defects successfully. Bible et al. created two ABS-MOF materials ABS-ZIF-8 and ABS-HKUST-1 and tried adsorbing N2 and found that the printed ABS-HKUST-1 adsorbs more N2 (70) than ABS-ZIF-8 (55) [45].

3.3.4. Polypropylene (PP). Polypropylene is one of the cheapest crystalline thermoplastics available in the market. PP is produced when a propene monomer is polymerized. PP is extensively used in the packaging industry due to its excellent barrier properties and low cost. This is used in food packaging because of its low moisture-vapor transmission and exceptional optical clarity. It is also used as battery cases and instrumental panels in the automotive industry. In the medical industry, polypropylene is used in making disposable syringes, Petri dishes, diagnostic devices, etc. due to its high bacterial and thermal resistance [46]. Polypropylene is also used as water filter nets and feed spacers to treat sewage and wastewater in wastewater treatment plants. Tan et al. successfully created polypropylene net-like structures through SLS (selective laser sintering) to measure the effectiveness of polypropylene as a suitable material for feed spacers. It was found from the results that Young's modulus and the ultimate strength are directly proportional to the amount of energy density used [47]. They have also concluded that raw PP powder is not suitable to be 3D printed with the process parameters they have taken, and much research about the ideal process parameters needs to be conducted.

Table 5 shows all the polymer-based feed materials for DED process.

3.4. Ceramics. The additive manufacturing (AM) process is appropriate to shape different ceramic parts. There are two types of AM processes: direct and indirect. The indirect AM process is used to produce appropriate components, and direct AM produces large parts. The AM process can produce pore and crack-free ceramic parts. In the traditional DED process, ceramic powder has been used to melt and solidifies on the substrate. In the hybrid fused DED process, the wire has been used to build parts [49]. Ceramics are widely used for dental applications. Ceramics with high chemical stability, biocompatibility, aesthetic, and mechanical properties replace or restore damaged teeth.AM is used for mass production, and it is the least expensive [50].

3.4.1. Alumina. Alumina is one of the widely used ceramic materials. It is well known for excellent electric insulation and is highly resistant to corrosion. It has a wide range of applications such as automotive sensors, dental implants, and electronics [51].

3.4.2. Zirconia. Zirconia ceramic is the most studied and more robust material in ceramics. It provides unique properties which provide high demand to its applications. It offers high toughness, high strength, and corrosion

Table 5: Types of feed materials (polymers).

S.no	Materials	Properties	Exploitation on DED	Applications	References
1	Polymethyl methacrylate (PMMA)	Shatterproof, rigid, UV and harsh weather-resistant, highly resistant to scratches	Selective laser sintering (SLS), DED	Biomedical industry, automotive and transportation industries, furniture industry	[38–40]
2	Polyether ether ketone (PEEK)	High heat and electrical resistance and can withstand high temperatures	FDM (fused deposition method)	Medical industry, aircraft, and automotive industries	[42, 43]
3	Acrylonitrile butadiene styrene (ABS)	High impact strength and heat resistance, high strain resistance, and stability over time.	DED	The automotive industry, pipes and fittings, structural applications	[44, 45]
4	Polypropylene (PP)	Excellent barrier properties, low cost, low moisture-vapor transmission, exceptional optical clarity, high bacterial and thermal resistance	SLS	The packaging industry, automotive industry, medical industry	[46, 47]
5	Polylactic acid (PLA)	Biobased, biodegradable, biocompatible, compostable, non-toxic polymer	DED	The packaging industry, health and medical industry, structural applications	[48]

Table 6: Types of feed materials (ceramics).

S.no	Materials	Properties	Exploitation on DED	Applications	References
1	Alumina	Electric insulation and resistant to corrosion	LAM-DED	Automotive sensors, dental implants, electronics, etc.	[51]
2	Zirconia	Toughness, high strength, and corrosion resistance	LAM-DED	Dental crowns, insulators, rollers, pistons, etc.	[52]
3	Magnesium aluminate spinel	High strength	LAM-DED	Bulletproof glass, aerospace, and defence.	[53]

resistance. Widely used applications include pistons, rollers, insulators, bushings, dental crowns, and more. It has been used for dental crowns because of its high strength and longevity [52].

3.4.3. Magnesium Aluminate Spinel. Laser directed energy deposition is feasible to fabricate magnesium aluminate spinel (MAS) ceramic parts. Because it is costly to manufacture using the traditional method [51], MAS is a high-strength ceramic used for bulletproof glass applications. These applications are used in industries such as aerospace and defense [53].

Table 6 compares the feed materials based on ceramics, which are used in the DED process.

4. Implementation of Computational/AI Models in DED

Additive manufacturing was founded with the Internet. Hence, it has always had the networking and communication capabilities that its traditional counterparts did not. Because AM is a digital process, it may produce large datasets throughout a build. The value of additive manufacturing resides in creating components that are performance-optimized and can only be created using AM technologies. AM aids in reducing assembly and, all with it, touch labor by allowing components that would normally be formed of various pieces to be created in a single piece. This information or digital input may then be utilized to maximize the physical output using machine learning and artificial intelligence. We expect that this translates into greater productivity, higher production, and the capacity to seal the quality control loop rather than depending on expensive inspection techniques.

Artificial intelligence can make additive manufacturing processes less tedious than they presently are as well as increase the precision of the process. Computer vision may be used to analyze current physical items to reverse engineer them and create a new, enhanced product design based on the current model. This can help to speed product development and improve processes while also reducing the time taken to produce new items.

Machine learning and artificial intelligence are indeed assisting in generative design, in which a software program generates design models automatically depending on the needs and restrictions stated by the technical department. This allows design engineers to investigate novel design solutions to address the most challenging problems. These designs may be swiftly turned into tangible prototypes or operational models by utilizing additive manufacturing processes.

Product development is typically a time-consuming operation that necessitates the investigation of multiple viable design possibilities before arriving at a final solution. With AI-driven generative design, this approach of

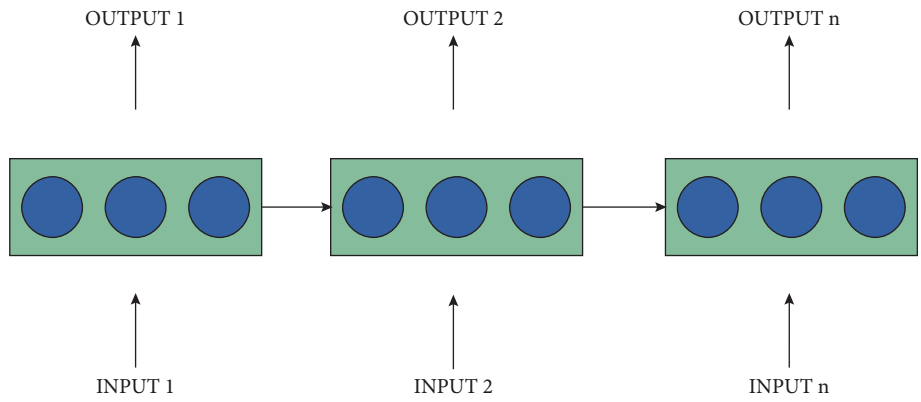

Figure 9: RNN chain.

iteratively evaluating multiple concepts may be significantly amplified. Design teams may use additive manufacturing techniques to undertake fast prototyping to transform designs into 3D models for evaluation and approval for large-scale production in an unparalleled short time frame, increasing design productivity.

The application of AI in DED also helps to improve the quality of the product by designing products with good quality standards paired with consumer-friendly functionality. This assures greater client satisfaction, which may result in increased profits and revenue. Following the implementation of IoT in production, the advent of AI applications in DED will most likely be the industry's upcoming revolutionary surge. AI-driven additive manufacturing can be the major technique of making new models in the future if advances in disciplines such as precision automation and machine learning continue.

Although machine learning is already used in creating AM products, the interconnections have not yet been completely realized. We are witnessing data, which could be from multi-dimensional data or existing sources, advising algorithms that can alert consumers of chances for improvement. Machine learning is now strongly a part of the progress of AM, from designing materials to powder feedstocks, through the AM equipment in the form of variables, and eventually with parts.

4.1. Machine Learning (ML) to Predict the Temperature of the Melt Pool. ML can be used to predict the temperature of the melt pool by looking at other parameters surrounding it. Two such ML algorithms are tested, namely, XGBoost and an LSTM. Both are good at predicting melt pool temperature.

Recurrent neural network (RNN) is a special type of artificial neural network. RNNs in general are capable of remembering and using previous results to predict the next result by sensing patterns in the sequential data given to it. But as the length of these dependencies grow, the traditional RNN starts to have less accurate results. This is because of the vanishing gradient problem [54]. The problem is accentuated in prolonged sequences of data. The gradient decays with each update as it propagates backwards in the data stream. This causes the backpropagation algorithm to gain more insights from the last data point when compared to the first one; for example, in Figure 9, the RNN will learn more from input n than it will from input 1. This could prove detrimental to the accuracy of the algorithm as it may miss important signs from the earlier stages in the stream of data given to it.

This issue can be remedied using LSTM [55]. LSTMs are special as they are capable of handling long-term dependencies. LSTM neural networks consist of a chain of repeating modules of neural networks too, unlike RNNs. The major difference is that it has a different structure in each module as you can see in Figure 10. The core idea behind LSTM is the cell state, which runs through the entire chain of modules, with only minor linear interaction. It basically helps in the ease of the flow of information. Another huge advantage of the LSTM is the ability to selectively read, write, and forget information [55] which are taken care of by the various operations shown in Figure 10. These help it derive information from the entire dataset without giving any data point preference just because of its position in the sequence. This makes it a very robust algorithm, which can easily recognize sequences, irrespective of the length of the data chain.

Extreme gradient boosting (XGBoost) is a highly scalable algorithm, capable of handling wide range of problems with high accuracy. Benefiting from the automatic parallel computation and customized tree structures, the algorithm is reported to be ten times faster than normal boosting tree algorithms. XGBoost algorithm involves creation of sequential decision trees where each tree is capable of fitting the residual of previous tree. Each tree can be understood as a weak base learner having relatively low predictive accuracy, and combined (as shown in Figure 11), these trees give a boosted performance. Also for the best results, few hyperparameters like the number of trees, maximum depth, learning rate, and minimum child weight of leaves are tuned based on previous research.

The prediction was similar, with a significant variation in the melt pool temperature. LSTM performs slightly better with low variations, but the efficiency is lower when compared to XGBoost. XGBoost is 400 times faster than LSTM in one of the situations in the testing. Their performance is

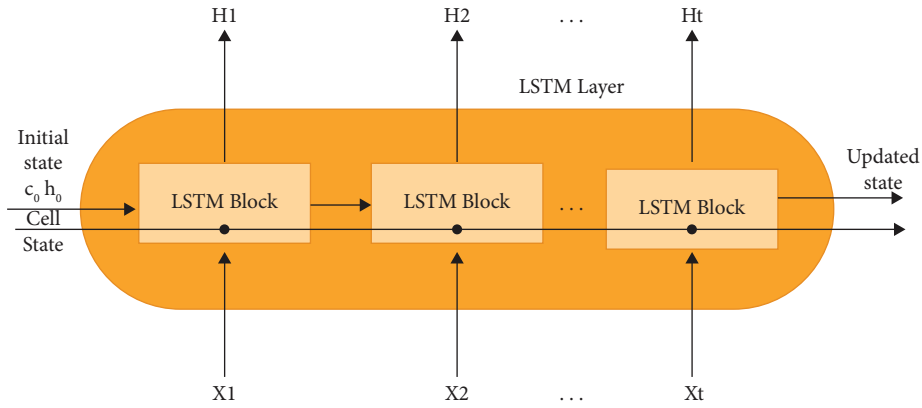

Figure 10: Working of LSTM.

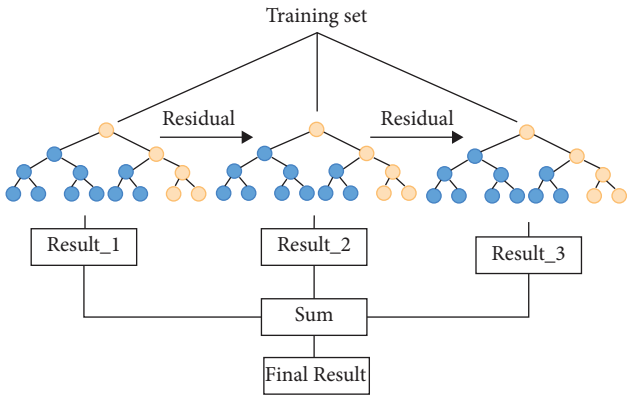

Figure 11: XGBoost algorithm.

compared with ridge regression, which turned out to be inferior [56].

Some hyperparameters were adjusted for XGBoost, such as learning rate, number of trees, maximum depth, subsample rate, and the minimum child weight. This was done according to the findings from previous experiments [56]. Similarly, for LSTM, some hyperparameters were adjusted, such as mini-batch size, the number of epochs, the learning rate, the sequence length, the number of hidden layers, and the hidden layer size. This was done according to the findings from previous experiments [56].

Data from 24 experiments were used for training the model for the predictive model, and the rest were used for validations and testing. The data consisted of input variables and an output which is the melt pool temperature [56].

4.2. Using a Convolutional Neural Network (CNN) to Predict Scanning Speed and Laser Power. Identification of additive manufacturing processes is carried out via the application of deep learning. The algorithm employed map supplied input images to corresponding output labels based on the features extracted from the training data passed onto the model. In this case, the input supplied is in the form of thermal images of the time series collected by a camera consisting of various settings of the DED process. These thermal images were used for feature extraction and pattern recognition by the CNN model. Authentic images of the DED process were used for testing the validity of the model. Such a strategy produced convincing results at recognizing patterns in parameters such as scanning speed and laser power in [57].

Convolutional neural networks (CNNs) come under the category of deep learning algorithms specialized for working on images (applications such as segmentation, classification, and object detection). They consist of convolutional layers, maxpool layers, and dense layers. Convolutional layers make use of the convolution operation (i.e., element-wise multiplication) of the image with other tensors known as filters in convolutional layers, whose weights are assigned relevant to the processing to achieve the desired mapping between input and output using the backpropagation algorithm [54]. Since images are heavy on capacity and computation, maxpool layers (Figure 12) work on compressing the image size with minimal loss in important features.

Image tensors being of the form of multi-dimensional tensors have to be flattened out in order to correspond to a single output label after which further linear and non-linear processing is carried out in dense layers on the converted tensor leading to the output label. The thermal images were passed to a deep CNN architecture (Figure 13) for image extraction and classification.

4.3. Using a Recurrent Neural Network (RNN) to Predict the Thermal History of the DED Process. An RNN structure (shown in Figure 14) alongside a gated recurrent unit design predicts thermal history in the directed energy deposition process with distinct geometry, laser power, build dimensions, toolpath strategy, scan speed, and toolpath strategy. RNN was the best choice simply because RNNs permit the learning of the data's temporal dependencies without further specifying things. Also, the traditional time series need precise adjustment every simulation. This makes RNN suitable for this kind of particular setup [58].

A stacked recurrent neural network structure with GRU formulation is used in the research. Each GRU cell receives an input feature (xt) for a particular time step and a hidden state from the time step before this step (ht1). The output is a new hidden state (ht). The dimension is the number of units

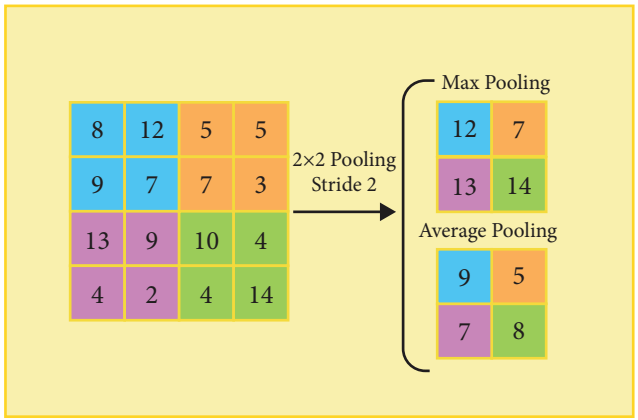

Figure 12: Pooling layer functionality.

per GRU cell. With the help of weights and biases, the state connects to other cells [58].

Developed using the Keras deep learning library, the model was built. The Adam optimizer was used, and the MSE function was used to evaluate the costs and results. The data were prepared using GAMMA. GAMMA is an in-house finite element code for thermal analysis [58].

4.4. Finding Surface Cracks Using LSTMs. The laser spot scanning system is designed to produce a multi-mode heat source with various modes with a controlled spatial position and excitation time. Depending on the detection system, combining the LST method with the neural network's short-term neural network (LSTM) (represented in Figure 15), a new process of finding surface cracks was introduced. A post-processing algorithm was developed to extract the feature signal after the LST scan method indicated the split distribution: temperature and temperature gradient. The signal that is to be inserted into the neural network for training went on to predict the crack width. When verification of the reliability of the LSTM neural network was performed, cracks in the actual surface of the LENS variety were predicted. The estimated total error of the LSTM neural network for predicting crack width was observed to be 2.0 μm (and the total error detected was 6.1 μm) of crack with a range ranging from 3–68 μm [59].

The numerical mesh was created for modeling a cracked sample using the ABAQUS software. A periodic thermal source with a square wave pattern was touched on the model's surface using a FORTRAN code [59].

LSTM neural network is used in this project for its ability to analyze sound and text. It has the following layers: an input layer, a recurrent hidden layer containing memory blocks, and an output layer. The memory blocks contain special memory cells that aid in self-connections for storing temporal states and gate units. The flow is controlled with the input gate (it) and the output gate (ot) [59].

The amplitude and heat source radius were finely adjusted. Then, the task was executed to see the thermal response for the cracks having different depths and widths. Lastly, the thermal response with no noise, which was

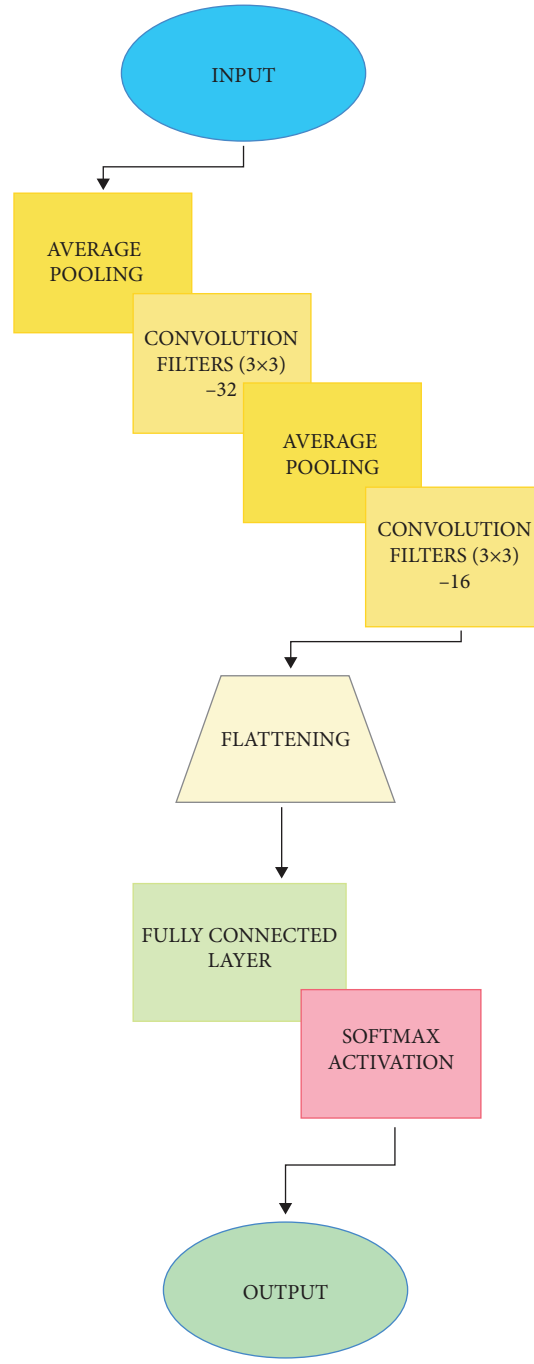

Figure 13: CNN architecture [57].

obtained via the experiment, was used to determine the structure of the neural network. The next step was to modify network elements and apply the model to detect artificial cracks [59].

LSTM NN was trained with data gathered from the FEM simulations and artificial crack tests. To obtain (surface) temperature field, numerical replications were used. The surface temp was observed to rise due to our sample's thermal excitation having cracks of varying widths and depths. The temp features required were gathered from the thermal image of the location of the cracks. The data were

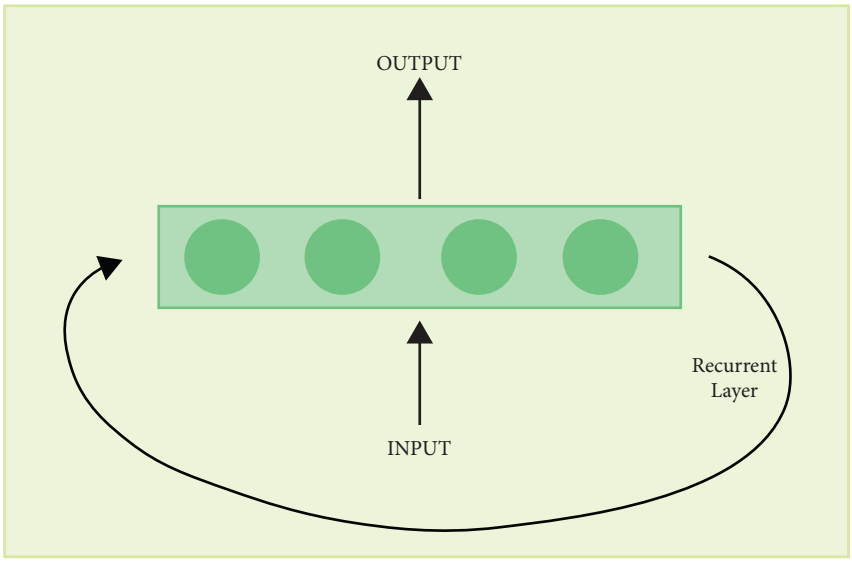

Figure 14: Recurrent neural network.

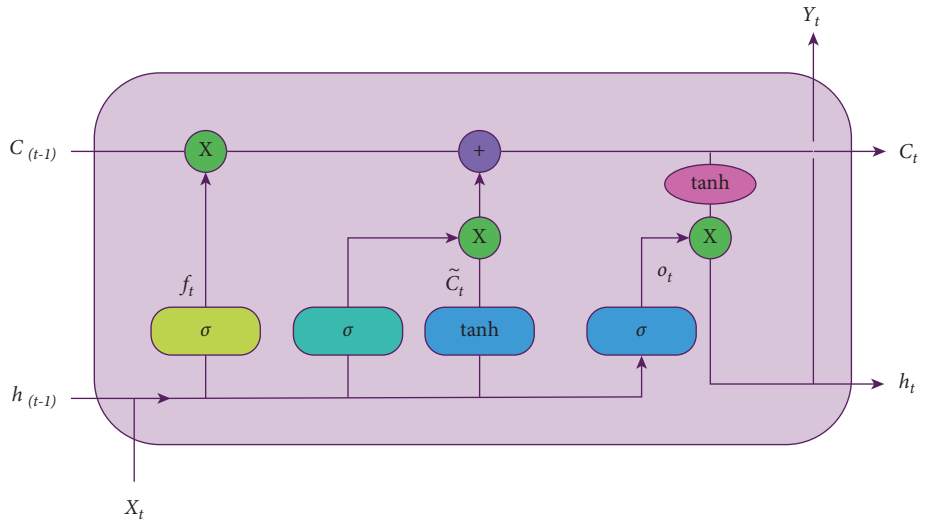

Figure 15: An LSTM block.

gathered from three crack widths and depths. The structure has the following layers:

(i) Input layer
(ii) LSTM layer
(iii) Fully connected layer
(iv) Dropout layer
(v) Fully connected layer
(vi) Regression layer [59]

4.5. Prediction of Tear Rates Using ANNs. In another paper, an artificial neural network (ANN) was used to validate and optimize the process and results. Data used were selected and pre-processed. The input parameters were L0 orthogonal array and three input variables, namely, layer thickness (LT), orientation, and temperature. The output consisted of a single variable: wear rate. The neural network had 10 neurons in its hidden layer and was trained using an accelerated gradient descent algorithm with an adaptive learning rate [60]. Gradients were generated using the mean squared loss metric.

4.6. Using ML to Predict the Depositing Height (DH). This implementation was made with laser engineered net shaping (LENS) in mind, as one of its main drawbacks is controlling the DH. This is mainly because of the large number of parameters that affect the process. This is where ML algorithms come in. They can easily predict the DH by parsing all the parameters that affect the DH.

The algorithms tested are the backpropagation and adaptive learning rate and momentum coefficient (BP-AM)

and the LS-SVM (least squares support vector machine). Input specimen comprised of main parameters that affected the DH. Also, the DH (output of the algorithms) of a single track was accumulated with the help of LENS experiments [61].

The BP-AM consists of only one input layer. Since there are three inputs, three nerve cells were also required. The input consists of PFR, laser power, and scanning speed. When the hidden layers were increased to 3 in size, the training time also increased, with the equivalent error for the same training sets. Due to this, the hidden layer was set to consist of only one layer.

The output consisted of one neuron, producing the DH of a single track. The thresholds and weights were initialized using random values in the range of 1 and -1 for BP-AM, while the increment was initialized to 0. The maximum loop time, goal error, momentum factor, and learning rate were optimized as 100,000, 0.01, 0.95, and 0.03, respectively.

The training data were provided, which included the parameters and the results from the experiments. This was acquired before the training of the BP-AM model. The data were normalized [62] before the training was done. After the successful training, this model was tested in the LENS process for predictions [61].

Like the BP-AM model, the LS-SVM model was also facilitated with the normalized training datasets and trained. For the optimization of the model, the MSE value was calculated and used. As for the performance index, MSE and relative error from the predictions were calculated and used [61].

4.7. CNNs to Classify DED Patterns. DED patterns caused by different types of particles might look similar to the human eye, albeit with subtle differences. It is these differences that a CNN will easily be able to pick up on and categorize which can aid the manufacturing process.

The input layer of the CNN had a size of 28×28 (2D image), and the architecture had two convolution layers. Layer 1 consisted of ten filters of kernel size (6×6), and layer 2 had 20 filters of kernel size (4×4), both with a stride of (1×1) to ensure that the filters were passed over every pixel. These layers helped in feature extraction (edges and shapes). The ReLU activation function was applied to the outputs to introduce non-linearity to the neural network. The output of the convolution layers was reduced by a max-pooling layer of pool size 2×2, which reduced the dimension of the images by 50% on each max-pool operation. After flattening the $20 \times 20 \times 7$ output, 980 values were obtained, which were then passed to a fully connected layer connected to another fully connected layer containing 2000 neurons. To prevent the model from overfitting, a 50% dropout rate was applied; this means that while training, the gradients were applied to only 50% of the neurons at each update. This prevented one set of neurons from dominating the decision-making process [63].

As for the dataset, the authors used 100,000 images, 50,000 of each class. The images were categorized as follows:

(i) 60,000: training

(ii) 20,000: validation

(iii) 20,000: testing

4.8. Using RNNs to Predict Thermal History. A stacked RNN structure can be used with a GRU design to predict the high dimensional thermal history at a given point. The model was showing an MSE of $2.97e-5$ after 100 epochs of training. The predictions were further examined for a more extended period and non-trained geometry. In additive manufacturing processes, RNN can make predictions of complicated behavior. The model could be further enhanced by incrementing the number of epochs the model goes through while training and increasing the different types of geometries present in the datasets [58].

The inputs consist of the time step (ht) and a previous time step's hidden state (ht-1). This gave out a new hidden state (ht) as the output. The dimension (hidden state) is equal to the number of units per GRU cell. The hidden state makes a connection to other states using weights and biases. To comprehend the deep-lying correlation in the data, the model uses multiple layers of the GRU structure. To combine the different outputs into one time-series temp output, the fully connected layers were used. Keras library was used to build the model. Adam optimization was used for optimization, and for the evaluation of the model, MSE cost function was considered [58].

The RNN model was trained with various configurations. It involved GRU units (100–500), 1–5 RNN layers, and 1–3 fully connected layers. Reaching the MSE value of $1e-4$, the model displayed promising results in just 100 epochs and a few layers and units. When increased to 3 stacked GRU layers, the model had only $3.210e-5$ MSE on training and $3.84e-5$ on testing with 100 epochs. The training time was observed to be approximately 40 h on Nvidia Quadro P5000 [58].

4.9. Predicting the Correlation between Microstructures Using ANNs. To explore the effect of microstructure on mechanical properties of Ti-6Al-4V, an alloy, few experiments like forging, heat treatment, and tensile tests at room temperature were done on the alloy. A relational model between microstructure and mechanical properties was documented using an artificial neural network (ANN) where the proposed model took quantitative microstructural characteristics, volume fraction and thickness of phase, and the Feret ratio as input and gave tensile properties like ultimate tensile strength, yield strength, increment, and decrement in the area as the output as shown in Figure 16. ANN techniques are believed to be one of the most effective ways and are enormously used in material science for various tasks like developing intrinsic relationships, predicting mechanical properties, and optimizing processing attributes. In this case, the architecture with a single hidden layer was chosen because these kinds of three-layer neural networks can approximate most of the simple functions given that the hidden layer has the right number of neurons. Had the number of neurons taken in the hidden layer been

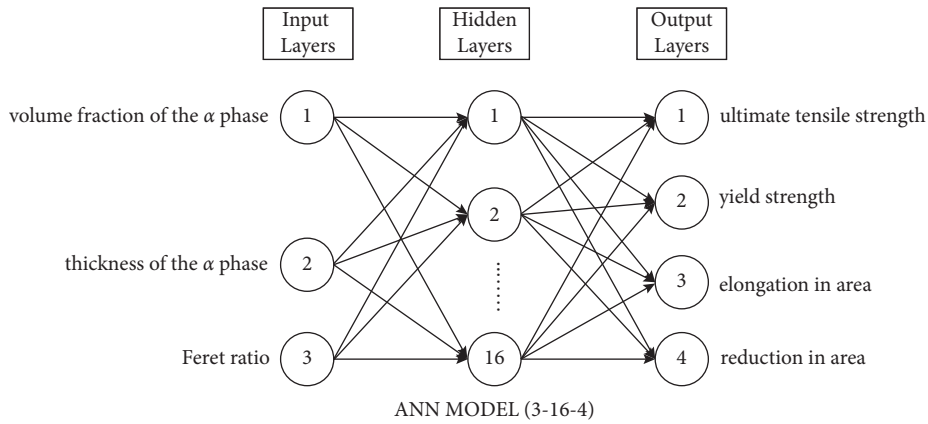

Figure 16: Overview of an ANN model.

less than what was required, then ANN would not have the desired approximating capability, and if they were more than what was required, then the model will get overfit, which is the phenomenon in which the neural network picks up on unwanted variations in the training data, making it seem highly accurate, while performing badly when presented with previously unseen data. Hence, several permutations were processed by a computer program compiled by the authors. Considering the number of neurons in the hidden layer and its effect on the network's performance, the number of neurons was altered from 1 to 20. To avoid overfitting, architectures containing more than 20 neurons in the hidden layer were not tested. Based on these experiments, it was found that the network with 16 hidden layer neurons gave the best output with desired error tolerance. The structure was deduced to be 3–16–4 in the model. The input layer had three nodes: volume fraction of the α phase, the thickness of the α phase, and Feret ratio. Moreover, the output layer had four nodes: ultimate tensile strength, yield strength, elongation, and reduction in area. To train the model more efficiently, input and output data had been scaled to a range of 0.1 to 0.9. There was less than 5% error between the expected and tested values, which showed that the model could predict the necessary relations. The collective impact of characteristic microstructural constraints on the mechanical properties of the alloy had been examined using this model to check the completeness ability of the model. When calculated, all the values of R were more significant than 0.90 and MAPE was 1.22%, which showed that the prediction results were fit for at least 90% of experimental results and that the model could successfully predict the internal relationship between microstructure and mechanical properties of the alloy with operational reliability [64].

Similarly, a model was developed to predict the same alloy's tensile properties using the hybrid ANN and genetic algorithm approach. At first, the ANN was trained and then tested, with the assumption that fitting did not occur. As a result, the authors got an n-variable response surface where variables were microstructural parameters and their composition. The ANN was also explored using virtual experiments to estimate the importance of each input by keeping other input values average. These experiments are then used in conjunction with theory to estimate "loadings" (a set of possible ranges) that unknown pre-factors and exponents for a physically-based equations might take. Then, the GA finds an ideal solution. As the GA is about to meet the solution, the response surfaces produced by both the models, GA and ANN, are compared using the virtual experiment. Then, based on how identical both models are, models closer to theoretical values of the terms and models with minimum scatter between predicted and experimental values are given higher weights. In this way, a physically-based model with predictive capability as an adequately trained ANN model can be produced but with a basis of physically understood strengthening mechanisms. The authors, for achieving the aim, used convolutional neural network (for feature extraction in thermal image data) and ANN approaches (to identify parameter effects) to investigate thermal history images of the build process and process parameter influences in distortion to develop the approach [65].

4.10. Using ML to Predict Single Clad Geometry in DED. There can be a sequential description of physical events occurring at directed energy decomposition with powder injection. When the laser energy hits the substrate, a significant fraction of its energy is imparted there. The residual energy is distributed among reflection and energizing powder particles, making their path to the substrate. This process can be said alternately as the laser creating a melt pool into which metal powder is injected to build the clad. To better understand this process of directed energy decomposition and cladding, models have been established to predict the outcomes and dynamics of the process. When classified broadly, there are two types of these models: physics-based model and empirical-statistical-based model. The basic physical phenomenon gives analytic results of heat transfer, mass transfer, and continuity under certain sets of assumptions and boundary conditions. However, these models lose predictive power in the face of process variability. The author had devised a method that falls under the empirical-statistical model of data science. Empirical-statistical models address process variability by taking direct

measurements and constructing process maps to predict directly tested behavior. Moreover, even in empirical-statistical models, regression models are the best and most studied form. They are easy to use and have significant value in the practical sense [66].

The dataset used to train this algorithm is a collection of process parameter study data points. The input set comprises powder material (one hot encoded [67]), substrate material (one hot encoded), spot size (mm), power (W), mass flow rate (g/min), travel velocity (mm/min) and the deposition resultants (height (mm), width (mm), and contact angle (deg)). For classification to be performed, the output of interest and aspect ratio (H/W) had to be split into classes before applying the ML techniques. Since the original data were continuous, a target value of 0.5 was chosen, and intervals of increasing distance were formed around that target value, discretizing the data, making it easier for the algorithm to parse. The author developed dataset-wide models based on ML techniques to assess the predictive power of those models. The ML techniques used were neural networks, gradient boosted decision trees, support vector machines, and Gaussian process techniques. Results of all these models were compared to check which one performed the best. With the dataset pre-processed, the application of the previously mentioned machine learning techniques was performed. The neural network architecture used in this study borrows from McGhee and uses what is termed a linear "skip connection" [68] to evade the vanishing gradient problem. The generalized notion is that this set of neurons with only a linear activation function will capture linear artifacts in the data while the non-linear neurons will then capture the non-linear artifacts. McGhee suggests this architecture as a means to increase the effectiveness of NNs on tabular data [66].

Neural network regression exhibited a response plot similar to logarithmic curves inherent in the empirical-statistical models. There was a fair amount of variance still present in the results of the regression model. This indicates a shortcoming in the model when provided with a high variance dataset. However, the success of the model is that it produces a generalization between material and processing conditions. This non-reduction of variance is seen when examining the classification results of the neural network model. The network is only a binary classifier, even though it was subject to multi-class input. The response surface of the GP model indicates a departure from the logarithmic curves of the NN and empirical-statistical models. This departure results in minor variance than those models. This is further supported by the classification results where the GP model is more than simply a binary classifier. The inclusion of more classes yields a better predictive model. The deduction is that the Gaussian inductive prior of the GP model is more informative at a high dimension than the radial basis kernel in this dataset. SVMs, when compared to the NNs, have lower variance and better classification accuracy, even though the SVMs and NNs both entirely overestimate non-optimal clads as classifiers. The gradient boosted decision tree (GBT) model lends credence to its effectiveness on tabular data. The resulting classification distribution closely follows that of the dataset. However, the coefficient of determination, r^2 value, is the lowest of all models examined. This suggests that outliers might be over-penalized by the model, lowering the R^2 value [66].

4.11. Predicting Surface Characteristics in CO2 Laser Micro-Milling. For predicting the surface characteristics, i.e., depth and surface roughness of plastic composite augmented by glass fiber, an approach using ANN to be applied after CO2 laser milling consisting of layers and neurons has to be developed and optimized. In ANN, there are three types of layers, i.e., input layer, hidden layer, and output layer. Hidden layers are responsible for establishing a connection between the rest of the layers based on learning by the data. Neurons include inputs, weights, a summation function, an activation function, and outputs. The summation equation as given in the below equation finds the total input of the neuron:

$$\mathrm{NET}_i = \sum n_j = 1 w_{ij} x_j + w b_i, \tag{3}$$

where NET_i is a weighted sum of inputs to the ith processing element, wb_i represents the weights of biases between layers, x_j is the output of the jth processing element, w_{ij} represents the weights of the connections between the ith and jth processing elements, i and j are the processing elements, and the number of processing elements in the last layer. It used various network structures like 3-1-3, 3-3-3, 3-6-3, 3-7-3, 3-1-1-3, 3-3-3-3, 3-6-6-3, 3-7-7-3 based on trial-and-error process. The previously mentioned sequences of numbers are the orders of the number of neurons in the layers of the ANN. For the training dataset, many parameters such as the availability of material, cost, and time required for conducting the experiments were considered. The dataset of 60 experiments was considered and assumed to provide the most accurate results in predicting surface roughness using ANN for testing the model. The algorithm chosen to implement was the feed-forward backpropagation algorithm. The approach used log sig transfer function, and evaluation of the model was done based on mean square error (MSE) performance function. The mean prediction error for each network structure was calculated, and based on results, two hidden layers with six nodes in each were found to be the most accurate one, i.e., 3-6-6-3. Hence, it was concluded that the ANN approach using a 3-6-6-3 network structure is the most suitable one [69].

4.12. ANN to Predict the Grain Boundary Tilt Angle While Performing DED with Titanium Alloys. An ANN model was developed to investigate the connection between grain-boundary tilt angle and three causative factors, i.e., thermal gradient, crystal orientation, and Marangoni effect in DED. Experiments like EBSD, melt pool cross section observation, and grain-boundary tilt angle measurement were performed to extract and train the model. Using these experiments, 50 groups of data were collected to evaluate the ANN model. This model followed a feed-forward neural network with network structure 1-5-10-1, i.e., input and output layer with

one neuron each and two hidden layers with 5 and 10 neurons, respectively. The input consisted of three different angles: thermal gradient, crystal orientation, and Marangoni effect. Moreover, prediction results for the grain-boundary tilt angle were given as output by the output layer. It was implemented on PyTorch, an open-source machine learning platform. The model's accuracy, i.e., training and testing performance, was calculated using mean squared error metric (MSE). The model was tested 20 times by randomly changing training and test sets to calculate the mean MSE and the corresponding variance [70].

4.13. AI in 3D Printing Metals. Few studies in past years showed how 3D metal printing is not consistent, repeatable, or traceable because of many independent variables. To solve those problems, AI can be adopted. In addition to solving the problems mentioned above, it will also help improve the technology. Due to AI, the printers learn with the help of fed data to make assumptions and take decisions like assembling correct parameters independently. To observe the internal process and control it, sensors and cameras are accommodated at the nozzle in the printer. The observed data are fed into specific software for measuring and analyzing the multiple real-time builds. This method helps the printer learn and understand the problem and therefore find the best solution using AI. When the machine can understand the relation of one parameter to another, it can decide which parameter will be best to get which output [71].

4.14. Decision Support Systems in Laser-Based Additive Manufacturing. The modern technology of laser-based metal products AM using powder compositions comprises theoretical models and a lot of experimental data. A decision support system (DSS) can be used for the laser-based AM process [72].

The input comprises the type of process, the equipment for the process, and terms of reference while operating, such as the shapes, structures, characteristics of the product, the characteristics of the processed part, its geometric form, and the chemical composition properties. The output information includes settings of the controlled process parameters, the laser power, the laser emission mode, beam diameter, linear velocity of the laser beam on the metal surface, offsets between the layers, powder flow rate, carrier, shielding, compression gas flow rate, and characteristics of the substrate. The corresponding ontologies inspire the database and the knowledge base. The database contains information about the components of the AM system and the materials required for AM. The software components include editors for the creation and maintenance of the DSS, the tools for structuring the cases, the control parameters of the process, and the interaction between the DSS and the external tools of the mathematical modeling of physio-chemical [72].

5. Results and Discussion

5.1. DED Process and Advancements. While directed energy deposition is gaining popularity, many researchers are quite enthusiastic about conducting various types of research on this topic. The most desirable intention is to improve the process in whichever way possible by analyzing different outcomes of different research studies until we reach certain favorable process parameters. One such research was conducted by Heigel et al. to develop a thermo-mechanical model of the DED process with Ti-6Al-4V as the feed material. Many researchers consider free convection on all surfaces while creating a thermo-mechanical model. That may not result in accurate simulation results. Here, the measurement-based convection model is done with three depositions with different geometries and dwell times. An additional model is developed using the assumption of free convection on all surfaces. The difference in the results shows why a measurement-based convection model is required to produce accurate simulation results. An Optomec LENS MR-7 system is used with 500 W IPG Photonics fiber laser for the three depositions [73]. An argon atmosphere is created with an argon jet of 30 L/min capacity with an oxygen percentage less than 15 parts per million. The Ti-6Al-4V powder (44–149 μm diameter) is supplied by four jets with a combined flow rate of 4 L/min. After all the three depositions, the forced convection model produced more accurate results with an error rate of 10.4%, whereas the free convection model had an error rate of 43.8%. This shows that the measurement-based forced convection model generates more reliable results than the free convection model. Even though the measurement based on forced convection is efficient, it can be improved in some ways the authors prescribe. The mechanical model can be improved by performing more detailed measurements to explore the effects of specific part geometries on convection. Also, we can use approved CFD analysis to validate the CFD of the gas flow. This work also indicates that a more detailed mechanical model is required as this model produces accurate deflection in only one of the cases, despite having superior thermal results. Similarly, Yang et al. developed a three-dimensional Ti-6A-4V elastic model to check the thermo-mechanical behavior in the laser energy net shape (LENS) process. The quasi-static and dynamic analysis has been predicted using the FMEA process. The comparison of experimental and simulation of quasi-static and dynamic analysis is performed. They both compared mechanically to reduce computational costs. Mesh analysis is performed, and it consists of 6094 elements and 10378 nodes. The laser used in this process is 400 w IPG fiber laser, and its intensity is around 300 W [74]. Determining the thermal characteristics of the melt pool and solidification parameters is also important to get a consistent and fine microstructure. However, determining them using the current methods is a lengthy process and takes up much time. Huang et al. researched rapid prediction of real-time thermal characteristics, solidification parameters, and microstructures in laser DED. This research correlates localized transient thermal characteristics such as cooling rate, temperature, and so on and solidification parameters like thermal gradient and solidification rate to the process parameters for rapid prediction of the microstructural evolution. This correlation is validated by depositing stainless steel 316 L and Inconel

625 and conducting experiments on them. This research is conducted by using LPF_AM apparatus with Inconel particle size of 45–125 μm. 1.1 kW IPG Photonics fiber laser is used for creating the melt pool. The measured temperatures of the melt pool were well in coordination with results obtained from various previous research studies at various speeds and different energy densities. It was found that the DAS (dendritic arm spacing) is more delicate to scanning speed than the laser power. Also, this research found that high scanning speed and lower laser power result in a finer microstructure. Better microstructures were found in the top zones for SS 316 L and Inconel 625 due to cooling rates from the bottom to the top. The count time for the cooling rate ($G \times R$) and G/R proportion is found to be around 40 ms with a tolerance of 10-3 in this experiment, affirming the capability of this work to be utilized for the in situ forecast of warm and hardening qualities [75]. Xu et al. studied that AM process slicing method is used to improve quality and eliminate support structures. There are three types of slicing methods: powder, multi-directional, and non-layer-wise slicing methods. Few traditional processes are efficient to prefer in the powder bed fusion (PBF) system because they require costly support in the DED process. The multi-directional and non-layer-wise methods are used to achieve quality and require costly support. In the traditional slicing method, the contour extrapolation method is used to slice solid models, and the step-wise uniform method is used to slice CAD models to achieve high surface accuracy. To build desirable shapes with shorter build time, the accurate exterior and fist interior method is used. Local adaptive slicing is used to reduce fabrication time and maintain high surface quality. To build normal complex parts, decomposition-regrouping slicing time has been used, but their method is inefficient for making inner holes. The multi-directional slicing method is used to build parts without support structures and increase the quality of the surface. A non-layer-wise method is used to build components without support structures (Table 7). So, it saves material costs [76].

In situ monitoring is used to understand the physical phenomena. It influences process parameters such as porosity formation and powder flow. High-velocity X-beam that uncovers the laser-matter collaborations in different methods of DED preparing can help in the approval of warm, thermo-liquid dynamic, and thermo-mechanical models. A piezo-driven powder delivery system that controls power delivery in the AM process influences the geometry of the melt pool and mechanical behavior. High-voltage amplifier controls piezo element and vibration which induces gravitational flow. A surface strain of the softened pool entrains particles on the surface to enter the pool or discharges hot particles. Particles that stream into the dissolved pool impact the strength of the laser-instigated hole and the encompassing melt pool. Changes in mass entering the softened pool impact the cooling speed of the softened pool, reaching up to 106 k/s [77]. Hsu et al. worked on a publication that proposed a trinocular vision-based review framework to assess the cladding stature in the DED interaction utilizing a reference point estimation technique. The exactness of the proposed technique has been improved by using an alignment bar procedure to redress for the FOV impact and viewpoint marvel. Strikingly, the proposed technique is vigorous toward test arrangement mistakes and is computationally direct and exact.

Notwithstanding, the technique depends on the utilization of picture finders with the worthy goal since, something else, the unit distance addressed by every pixel in the caught picture is extraordinary in various districts of the picture. Consequently, the straight suspicions fundamental to the proposed estimation calculation presently do not hold. In executing the proposed estimation strategy, a separating strategy is utilized to eliminate commotion and the undesirable foundation locales of the caught pictures. Using infrared cameras to catch the soften pool picture may give more exact estimations of the cladding stature than those acquired utilizing the computerized cameras utilized in the current examination since the noticeable range comprises many noises. Be that as it may, an infrared camera is significantly more costly than an advanced camera.

Moreover, the outcomes acquired utilizing the present computerized cameras go amiss by close to 4.2% from the specific outcomes acquired utilizing an optical 3D scanner and caliper [78]. Hence, this outcomes the technique proposed in this examination gives a minimal effort which is helpful and the exact methodology for estimating the "cladding tallness" in the DED process. Laser beam additive manufacturing (LBAM) processes can be employed to generate practical parts via layer-wise-cladding to provide a chance to generate complex shaped parts and functionally graded parts that are utilized to build a variety of engineering components. Thompson et al. focused on thermal phenomena during the fed direct laser deposition (DLD) process. In AM metallic parts, PBF and DED processes are the most feasible methods. In PBF laser, selective laser melting (SLM) is used to create metallic parts. PBF is used to finish parts with more refined quality. The DLD process is used to produce parts, but it requires post-processing to get high surface quality parts. Not only surface quality, but this process is advantageous to get overhanging parts. In the PBF process, the powder acts as support, which does not require any other supporting structures. Both single and multi-nozzle can be used to feed powder [79].

Types of lasers used are neodymium-doped yttrium aluminum garnet (Nd: YG) laser and C02-type end pulsed-wave lasers, as shown in Figure 17. Nd: YG laser power ranges from 1 to 5 kW, and CO2 laser has capacities near 18 kw. There are two types of feed materials: powder and wire. Mainly DLD process has been commonly used to get finer deposition. Both DLD and PBF-L processes are operating in the inert gas chamber. This process utilizes an electron beam in a vacuum chamber. Challenges in the DED process are DLD efficiency, DLD control, numerical modeling, process parameters, industrial adoption, process monitoring limitations, DLD graded materials, and near net shapes. NNS is perfectly manufactured in the DLD process, and no further machining process is required. Both PBF-L and DLD are appealing added substance-producing strategies for metals since their working chambers should be cleansed with inert gas. Powder-bed and DED methods that

Table 7: Types of slicing methods (advantages and disadvantages).

Category	Feature	Advantage	Disadvantage	Ref.
Adaptive slicing	Constant layer height.	(i) Easy application. (ii) Highly versatile.	(i) It can handle only simple geometric parts. (ii) Rough accuracy.	[76]
Basic slicing	(i) Accuracy or complexity requirement. (ii) Different layer heights concerning surface.	(i) High surface quality. (ii) Easily applicable.	(i) It cannot handle overhangs. (ii) Complex structures are still restricted.	[76]
Non-layer-wise slicing	(i) It requires fewer support structures. (ii) Multiple depositions.	(i) Reduces support structures. (ii) Complexity in several directions.	(i) It may need a manual inspection.	[76]
Multi-direction slicing	It does not require any support structures.	(i) No need for support structures. (ii) Implement Complexity in infinite direction.	(i) Lack of universality.	[76]

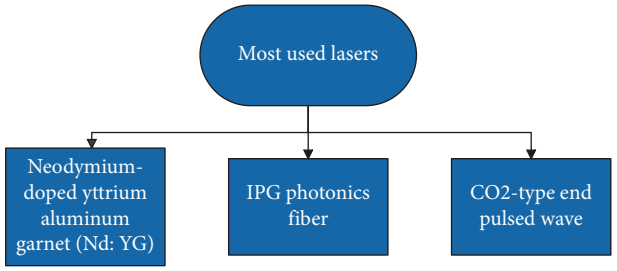

Figure 17: Frequently used lasers.

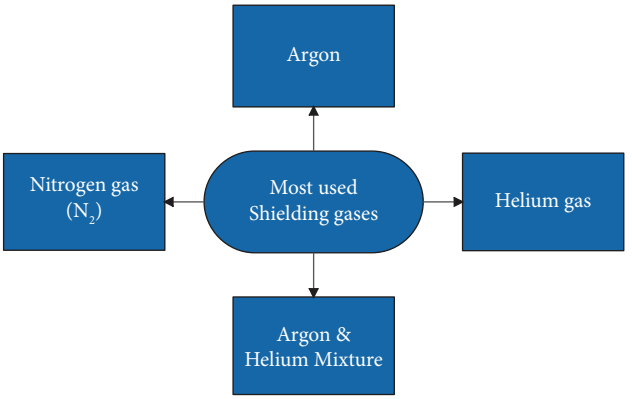

Figure 18: Frequently used shielding gases.

use electron radiates require chambers with full vacuum conditions, which are regularly more exorbitant [79].

A lot of research was done on materials like Ti-6Al-4V, stainless steels, and Inconel, and aluminum and its alloys are the most used materials. One such research was done on Al-Si alloys by Javidani et al. Al-Si alloys are most suitable for welding purposes and hence are one of the most used materials in many applications. In this research, AlSi10Mg powder particles were deposited layer by layer on the substrate using 500 W IREPA IPG Photonics fiber laser along with a powder hopper as the material feeder. 45–90 μm was set to be the acceptable range of particle size for the deposition. According to the authors, the final deposition was nearly defect-free. It was found that cellular dendrites were found in the region near to the substrate, followed by columnar dendrites in the middle layers and then equiaxed dendritic morphology in the topmost layers of the deposit. The hardness test results showed that the region nearer to the substrate (cellular dendrites) showed the highest hardness value (nearly 65 HV) and the topmost layers (equiaxed dendrites) had the lowest hardness value (nearly 53 HV) due to its coarser microstructure [80]. It was also found that the microstructure was coarser near the boundary layers than the layers closer to the core. This work has proved that the DED process can efficiently print Al-Si alloys for many applications. The DED process finds many applications in fabricating thin-walled honeycomb structures and complex heat exchangers having thin walls. These applications are accomplished only when the walls created are fragile. One such work conducted by Jinoop et al. focuses on DED's ability to fabricate thin walls using the LAM-DED process and Inconel 718 as the feed material. A 2 kW in-house developed fiber laser is used in the LAM-DED system. The substrate is sandblasted SS304L (10 mm thick, 75 mm diameter), which is fixed on a 5-axis CNC laser workstation. Argon of 99.99% purity is used as the shielding gas with oxygen less than 2 ppm, nitrogen less than 3 ppm, and hydrocarbons less than 0.2 ppm. The flow rate of the shielding gas was set to be 6–8 L per min for all the experiments (Figure 18).

Widely available IN718 powder with particle sizes ranging from 45–106 μm is used. After the final part is created, it is soaked for 1 hour at 950°C and then water quenched. A similar post-treatment is done to another final component where it is soaked for an hour at 1050°C and water quenched. It was found that the maximum laser energy per unit length (E_{max}) is 210 kJ/m, and the minimum of the same (E_{min}) is around 105 kJ/m. Also, the maximum powder feed rate per unit length (F_{max}) is 12.5 g/m, and the minimum value for the same (F_{min}) is around 4 g/m to fabricate defect-free thin walls. The walls had a dendritic microstructure free from any defects. The ideal process parameters for uniform deposition and high deposition rates were 1400 W laser power, a scan speed of 0.01 m/s, and a 0.117 g/s powder feed rate. Post-heat treatment processes resulted in reduced residual stress on the surface of the

component. While the as-built component had residual stress of 512 ± 15.46 MPa, it was reduced to 422 ± 12.99 MPa when heat-treated at 950°C (HT950) and was further reduced to 254 ± 11.80 MPa when treated at 1050°C (HT1050). This means that the residual stresses are reduced by 50% after the heat treatment process. Due to post-heat treatment, the surface microstructure was found to be recrystallized. The ductility increased by 62.5%, while the hardness is reduced by 12% [81]. Also, the energy storage capacity is increased by 2.4 times. This proves that the LAM-DED process is suitable for the desired applications and can be effectively used for thin-wall fabrication.

Saboori et al. studied microstructures and mechanical performance of DED AISI316L stainless steel. DED has an advantage in fabricating near net shape and high functional components. DED provides high valued parts for different engineering applications. However, there is a lack of knowledge regarding the mechanical characteristics and microstructure of built parts. There are different deposition patterns due to motion between deposition head and substrate. Because of its high deposition rate, this process is widely used to build large components. Demerits of the DED process show low powder efficiency, and roughness of surface should be done by machining process. The thermal history of DED, such as temperature gradient, high cooling rate, and high heating rate, defines the size of grains in DED components. Since all these parameters are important to build parts, effective parameters such as temperature gradient and local solidification rate at solid/liquid interface define the microstructure's solidification. The cooling rate at 103 to 104 k/s can get desired microstructures and mechanical properties in DED components. During heat transfer in the DED process, it is found that columnar structures grow in the direction of a thermal gradient, which dominates the middle height of the sample. Higher microhardness and finer microstructure are formed at the bottom top of DED components. There is a possibility of affecting thermal history due to the cooling rate, and it is one critical process. The cooling rate in DED of AISI316L ranges from 103–104 ks, which has a typical cooling rate. When the laser power increases, the average primary cellular arm spacing (PACS) of AISI316 produced in DED ranges from 3 to 9 μm. In order to reduce oxidation content, these should be done in a reliable atmosphere. From an industrial point of view, mechanical properties such as hardness and tensile properties are the main quality indicators. The main factors in achieving high mechanical properties are to reduce grain size and dendrite size. The building parameters such as feeding rate, scan feed, and laser power are key factors to improve quality. The factors that affect tensile properties are texture, elongated dendrites, and grain morphology. The powder quality influences porosity and consolidation and plays an important role quality of the component. The high mechanical properties can be gained when this process is held in N2 filled chamber. However, inert gas can affect the microstructure of the alloy. The different heat treatment process is carried out to reduce internal stress. AISI316L, with high corrosion resistance and good mechanical properties, is used in different sectors, such as the petrochemical and automotive industries [82]. The DED process can fabricate customized and complex parts and prototype metallic parts and repair valuable components that traditional techniques cannot repair. Titanium is a commonly used alloy in aircraft, aerospace, biomedical, and automotive industries because of its corrosion resistance, significant strength, and fracture toughness. However, it is challenging for some applications due to its low thermal conductivity, which results in poor machinability. The ratio of thermal gradient (G) and temperature gradient (R) affects the shape of solidification, whereas thermal gradient and temperature gradient affect microstructure dimensions. The low ratio of G/R shows the equiaxed morphology of grains, and the high ratio of G/R shows the predominant morphology of grains. The G and R values are affected by several factors such as material features, machine condition, and other process parameters [83]. Ti-6Al-4V structures produced by the DED process are porosity-free components using high laser power and low powder-free rate. Thermal gradient and cooling rate influence the microstructures of Ti-6Al-4V components. It is important to know the thermal history of components because it affects the anisotropy of microstructures. Stainless steel is one of the major feed materials used in DED processes. DED fabricates many stainless-steel parts that are widely used in many real-world applications. Therefore, there is a high risk of the material being corroded in the long run. Hence, the corrosion properties of the stainless steel made through DED processes need to be studied to come up with solutions to reduce it in the future. One such research was conducted by Melia et al. on the corrosion properties of SS304L and compared with wrought SS304L to assess its effectiveness against corrosion. Commercially available SS304L powder with a diameter range of 45–90 μm is used as the feed material. Two types of DED systems are used in this research. One is a low-power (LP) DED using an Optomec LENS MR-7, and the other is a high power (HP) DED using a home-built high power and deposition DED system. Heat input given to the LP system is 0.03 kJ/mm, whereas the heat input for the HP system is decided to be 0.45 kJ/mm. The resulting parts were tested for corrosion using techniques like potentio-static holds, cyclic potentiodynamic polarization, and double loop electrochemical potentio-kinetic reactivation (DLEPR). The SS304L that is finally deposited showed microstructures having scattered nanoscale oxide particles, lack of fusion (LOF), and gas porosity. It was found that the LOF pores created can act as crevice sites and affect the part's corrosion resistance. The intradendritic parts control the breakdown resistance. In the absence of LOF pores, the Eb of the HP process was 100 mV lower than that of the LP process. The SS304L part produced by DED showed lower corrosion resistance than wrought SS304L due to LOF pore formation in the microstructure. The authors suggest that corrosion resistance can be enhanced considerably by minimizing LOF defects and achieving higher

cooling rates. The authors also suggest long-term research in this area for those materials to be useful in corrosive environments [84].

5.2. Process Parameters: A Guide to Efficient DED Process. Using the currently available literature, the process parameters are designed to lead to an efficient DED process. These parameters guide the researchers to understand the process and execute it efficiently concerning the core mechanical process.

(1) Many researchers have used a home-based DED system that uses different parts from various companies connected as a single system. This is a much better way to reduce costs than to use 3D printers from certified companies like Optomec. While this method effectively reduces costs, it has many notable drawbacks that can affect the research results. This is because of the following reasons. The first and foremost reason is that home-based DED systems are not reliable. Using cheap parts can result in fluctuating laser power and scan speeds. High laser power and scan speeds mean coarser microstructure and larger DAS (dendritic arm spacing) [75]. Using home-based DED systems can also lead to varying powder feed rates, resulting in irregular depositions and overlapping layers. Even though costly, using reliable DED systems such as Optomec LENS MR-7 is much better due to their stability in the long run. These 3D printers use a CNC control system (3 axes or five-axis) to better position the deposit on the substrate. It uses inbuilt 500 W IPG Photonics fiber laser which constantly delivers laser with a power of 410 W. This laser is also upgradeable to 1 kW if needed. These premium printers are also equipped with thermal imaging cameras with analysis software. This feature is beneficial to determine the number of thermal stresses on the surface of the part. These systems come with a better atmosphere control to monitor shielding gas and oxygen in the gas chamber. Home-based DED systems cannot monitor the amount of oxygen in the inert gas chamber with such accuracy, and the melt pool may oxidize if the amount of oxygen is high. Systems like Optomec LENS MR-7 also come with more powder feeders to create parts with different materials. Every layer can be different from the previous layer. Therefore, the use of a proper DED system is essential to ensure correct results and successful research.

(2) Heat treatment shows different characteristics of tool steel in the DED process. However, the heat treatment process is used to improve the mechanical properties of components. Tool steel such as H13 and D2 was deposited on the substrate using the DED process as the hardness of deposited H13 steel is higher than a wrought H13 steel substrate. At the same time, the hardness of deposited D2 is lower compared to wrought D2. Microstructures and heat treatment vary with different materials used in DED. For Ni-based alloys, post-weld heat treatment is carried out to relieve stress from materials and increase strength. For steel, heat treatment is carried out to get relief from residual stress and grain refining. The mechanical properties such as hardness, tensile strength, and impact strength can be improved using heat treatment. As research studies suggest, heat treatment can eliminate boundaries between newly deposited layer and pre-existing layer. It seems that after the heat treatment process, microstructures of H13 steel were changed and similar to wrought H13 steel. Both microstructures seem to be tempered. Martensite and XRD results show that the phase of H13 steel was ferrite. After heat treatment, the equilibrium of H13 steel was austenite and maintains the temperature at 1293 K. After heat treatment, the chemical composition of deposited H13 and wrought H13 seems to be similar. However, the microstructure of D2 steel is dendritic and eutectic. The microstructure of deposited D2 and wrought D2 is different. The deposited D2 consists of fine carbide, which is dissimilar to wrought D2. However, wrought D2 has martensitic structures. The microstructures without heat treatment process consist of columnar crystals [85]. During the printing process, materials can gather tension and internal stress, which affects mechanical properties. Such effects can be reduced by heat treatment. So, it can provide external features such as tensile strength and heat resistance. The value-based heat treatment process can benefit alloys such as titanium alloys, stainless steel, nickel superalloys, and so on [86].

(3) Selection of the type of feed material is also very essential in DED processes. The feed material can be a wire or powder according to the type of outcome desired by the researcher. In some cases, using a wire or powder does not matter to the researcher as long as the material is being deposited on the substrate. In such cases, powder feeding can be used because powders of most metals and ceramics are widely available in the market. However, one major drawback of using powder-based feed materials is that the powder capture efficiency is always less than 100% [87]. That is, all the powder that is fed into the feeder is not captured in the melt pool. Therefore, the excess powder is utilized. Also, the thickness of the deposit made by powder feed is more than the thickness deposited by wire feed. This thickness helps overcome some wrinkled surface physiography associated with directed energy deposition. If the amount of feed material is one of the essential characteristics considered in detailed research, it is always advisable to use wire-based feed material because the wire capture efficiency is nearly 100%. When particular research involves fabricating basic geometries, either thick or thin, and some block-like structures, it is better to use wire feed. Wire-based

feeds produce pore-free parts so that the densities of the parts produced are high compared to parts made by powder feed. Wire-based feeds indeed produce parts with lower dimensional accuracy when compared with powder-based wire feeds. This can be significantly improved by controlling the process parameters such as wire feed rate and wire thickness. The optimal process parameters for doing this varies for different materials and can be found through further research. Therefore, if the surface texture and quality are not an issue, wire-based feeds are the best way to reduce material wastage and create parts with greater densities.

(4) Layer thickness is one of the most critical process parameters which build components layer by layer in the AM-DED process. Layer thickness can be determined based on the single-layer height given during deposition. Layer thickness plays a significant role in maintaining the strength and good surface quality of the component. The DED technology involves two kinds of energy sources: laser energy and electron beam, to build metallic components layer by layer. It can be used for part repair or to build new parts. As many researchers said, the geometry and structure of components depend on the thickness of the layer. An increase in melt pool volume and reduction in layer thickness can have benefits over roughness. The slicing strategy can help in the decrease in manufacturing time and depositing layer thickness depends on process parameters.

(5) Layer thickness improves not only the accuracy of geometry but also the mechanical properties of components. The main disadvantage of slicing in the DED process is that it requires additional machining processes to improve accuracy [88]. There are three slicing methods: feedback control, conventional, and adaptive slicing methods. The conventional method can reach target height till 1.5 mm and adaptive slicing can reach target height till 1.82 mm. In steel, micro-hardness increases from the first layer to the top deposition layer. The top layer shows the highest hardness. The layer height can increase either due to energy source or powder feed. Feedback control relents the performance concerning geometry. The conventional and adaptive method is also called an open-loop process. The open-loop process sets defined values, and there is no feedback from process output. Adaptive slicing is a beneficial method to build quality parts and decrease production time.

(6) One of the significant process parameters in the directed energy deposition process is laser power. The amount of laser power used in the system determines many essential attributes, such as the size of the melt pool, the density of the deposit, and its thickness. Firstly, increased laser power leads to increased melt pool size. This is because as the temperature of the melt pool increases, the material expands to a specific limit, increasing the melt pool's size. An increase in the size of the melt pool means a reduction in density [89]. Therefore, when this melt pool is deposited, it covers more area on the substrate, and hence the height track width will increase. The laser power shows its effect not only on the melt pool but also on the substrate. Generally, the laser slightly melts the substrate to create a better bond with the deposit. This is known as dilution. If the laser power is high, the substrate dilution increases, and therefore the depth of penetration increases for the deposit. This results in lower deposit heights than planned by the researcher. Also, lower laser powers (100 W–400 W in general) lead to the melt pool's rapid solidification. Even partial solidification of the melt pool increases the density on the whole. Many researchers found that scale formation can be created on the deposit's surface due to the melt pool's rapid solidification [90]. Sometimes, deposits with smooth surfaces or low surface roughness are the required attributes for researches. In that case, it was found that high gas flow rate combined with high laser power can deposit materials with low surface roughness. Finally, it was found that crucial output parameters such as clad thickness, dilution, temperature, and thermal stresses will increase with the increase of the laser power. Of these parameters, dilution and temperature become constant because they reach a point called the saturation level [91].

(7) Powder flow rate is essential to improve reproductivity and reliability in industrial applications. Due to the lack of sensors, it became difficult to measure powder flow rate. However, these days, many different methods have been introduced to measure powder flow rate. Industries use the equipment called weight-loss metering system to regulate the powder flow rate. The online powder flow rate is not recommended because of the low powder flow rate. The optoelectronic sensor is used to sense powder flow rate, and it consists of a photodiode, glass window, and laser diode. The laser energy is used to regulate power flow, and it sends process feedback signals. Another sensor, such as a compact pressure sensor, can be used to sense powder flow rate, and this high flow rate requires high pressure. Suppose there is a constant powder flow rate deposited at a point that causes dilution and porosity. The variable powder flow rate (VPFR) is the best strategy to adopt because the idea of VPFR is the constant distribution of powder along the path. It even helps to measure uniform morphology if the system decelerates or accelerates. The powder flow rate system consists of a PC that controls the powder flow rate. The circle-shaped or fish-shaped parts were fabricated using three different powder flow rate references: variable-based, constant, and modified [92].

(8) Scan speed is yet another vital process parameter that can primarily affect the melt pool dimensions. There

is no ideal scan speed defined for a process. Optimum scan speed values change from one material to another material and one process to another process. However, lower scan speeds generally result in large melt pools with considerable build heights and meager dilution rates. When the scan speeds are low, the flexural strength improves remarkably due to reducing grain sizes and suppressing macroscopic cracks. High scan speeds have a decreasing effect on melt pool dimensions. An increase in scan speeds results in low melting or lack of fusion. So, a melt pool is not produced [93]. As scanning speed increases, clad height, temperature, stresses, and clad height decreases [91]. This is because there is low energy density or heat input due to less interaction time. At high scanning speeds, the thermal stresses decrease, and directional grain growth weakens, which causes significant suppression of the cracks on the part's surface. At higher scanning speeds, porosity increases due to an increase in molten pool viscosity. This increase in porosity notably decreases the strength of the final component. Also, with increasing scanning speeds, the fracture toughness of the final components increases. This is caused due to the microstructure refinement, and the flexural strength shows a parabolic course. However, using high or low scanning speeds can be neutralized using medium scanning speeds (400–500 mm/sec). By using medium scan speeds, the sample shows excellent comprehensive properties along with balanced toughness and strength.

5.3. Artificial Intelligence in DED. The results from the use of AI seem promising in the DED technology. AI has brought on a significant impact on the quality and efficiency of the technology while also reducing wastage. The results discussed from the experiments performed will help justify the impact of AI in this section.

The accuracies of the models were evaluated based on RMSE, RE, and the coefficient of determination (R^2). The LSTM prediction demonstrates the model's strength against noises. However, the XGBoost shows its relative weakness when there is variation or unsteadiness in the temperature. This resulted in line with spikes. The observed values for RMSE, RE, and R^2 of the model having XGBoost are 95.9, 3.7%, and 54.4%, respectively. Likewise, the three measurements of the prediction using LSTM are 88.2, 3.4%, and 60.1%. Compared to XGBoost, the RMSE, RE, and R^2 are improved by 8.0%, 8.1%, and 10.5%, respectively, on the model based on LSTM [56].

It was also observed that for temperatures below approximately 2000°C, the LSTM model generates more accurate predictions. However, for values above approximately 2000°C, both models (XGBoost and LSTM) fail to give highly accurate results [56].

From the seventh experiment, the laser power was 350 W with 11 mm/s of the scanning speed. The RMSE, RE, and R^2 prediction using XGBoost are 24.0, 1.0%, and 51.8%, respectively. Likewise, the RMSE, RE, and R^2 of LSTM are 20.1, 0.8%, and 67.1%. The prediction accuracy of LSTM over XGBoost according to the observed values of RMSE, RE, and R^2 is improved by a whopping 16.3%, 20.0%, and 29.5%, respectively. Given overall smaller variations, the model based on LSTM delivers much better performance than XGBoost [56].

Table 8: The difference in performance of LSTM and XGBoost.

Network/algorithm	RMSE	RE	R^2	Ref.
LSTM	88.2	3.4	60.1	[56]
XGBoost	95.9	3.7	54.4	[56]

Finally, it was observed that the model built with LSTM has higher accuracy than the model built using XGBoost. XGBoost is faster than LSTM, and so LSTM is suitable for smaller datasets. For the particular case in the experiment, LSTM was suitable, but this cannot be said for all cases [56]. From [3], we can have the following comparison as shown in Table 8.

The Levenberg–Marquardt algorithm, constructed using the TRAINLM function in MATLAB, was allocated 70% of the data for training, 15% for testing, and 15% for validation. It was found that the minimum MSE reached $10.6 \times 10{-}5$ (after four epochs), and the correlation coefficients for the areas; For training: 14 data is 0.983; validation: 3 data is 0.999; testing: 3 data is 0.999; overall data 20 runs are 0.987. As for mean absolute percentage error, the calculated value of MAPE for RSM and ANN is 0.587 and 0.188, respectively. Finally, it is determined that ANN performed significantly better than RSM, yielding better predictions. A decrease of 67.97% was observed in MAPE with ANN over RSM [94].

Two stacked RNN models were trained. The models were trained for 20 s and 50 s, and they were tested for 100 seconds of thermal history. The model trained for 20 seconds continues to make good predictions for about 60 seconds of thermal history, showing an MSE of $7.05e-5$ for the 100 seconds. The model trained for 50 seconds had only $3.17e-5$ MSE for 100 seconds of thermal history prediction. This decrease in MSE comes at the cost of more training time and resources [58].

The four tests show that an accuracy of 80% can easily be achieved in various tasks. This result shows that the model is effective in process monitoring. This also outperforms the DNN model in some situations. It is concluded that the DCNN structure is more suitable for problems related to thermal image processing in additive manufacturing [57].

The RNN model proposed by the authors is trained in different arrangements. This included the number of layers, GRU units, and fully connected layers. RNN layers: 1–5, GRU units: 100–500, and fully connected layers: 1–5. The model had an MSE of $1e-4$ after 100 epochs of training with a smaller number of layers. It reached an MSE of $3.210e-5$ on training and $3.84e-5$ on testing with many layers and units on 100 epochs of training. The time consumption for training was approximately 40 h on Nvidia Quadro P5000. Finally, the results showed that the

Table 9: A comparison of two training networks.

Network	MSE	Training time	Regression R-value	Maximum relative error (%)	Minimum relative error (%)	Mean relative error (%)	Ref.
BP-AM	$8.792E-05$	6 min	0.979	24.98	0.0018	7.745	[56]
LS-SVM	$2.89E-08$	0.016 s	1	0.7	0	0.18	[56]

model could reach $2.97e-5$ MSE on testing after 100 epochs of training [58].

In the width prediction, for sample 10, a maximum absolute error of 13.9 μm was found with a relative error of 8.2%. From FEM data, the average error of 6.88 μm was achieved for cracks of 50–170 μm. For sample 3, a max error of 18 μm was found. The prediction through artificial crack data was 7.41 μm for cracks of 56–160 μm. From FEM simulation and artificial crack data, it is observed that LSTM NN is pretty reliable. For this application, though, the combined technique of LSR-NN was tested to detect crack width of LENS with wear-resistant coating. The mean error of the prediction was 2.0 μm, and the max error was 6.1 μm for cracks of 3–68 μm [59].

LS-SVM, compared to BP-AM (Table 9), shows better ability in generalization and its strength in function approximation. Hence, LS-SVM is more useable in the LENS process for more accurate predictions [60].

With the help of the plots that compare the performances of CNN and BDT, BDT had a 68.73% background rejection, whereas CNN had 93.02% for 60% signal efficiency. This was for the 1st case. For the 2nd scenario, BDT had 86.84% background rejection against 96.39% CNN for 60% signal efficiency. CNN outperformed BDT for more considerable signal efficiencies [63].

Ever since the processing power proliferated, so did the field of deep learning. Numerous advanced techniques have taken a form and can outperform CNN as well. Caps Net is one of the examples which aims to make optimizations and enhancements to the CNN to handle the spatial relationship with more efficiency. Likewise, PointNet++ is another pioneering project that seeks to apply ML on point clouds (collection of high dimensional objects). Another such advancement is GNN which stands for graph neural network. This operates directly on graph functions and has found wide use in many physics-related applications, including high energy [63].

Using an ANN to model the correlation between microstructure and the Ti-6Al-4V alloy properties proved to be very efficient with absolute percentage errors between the predicted and experimental values less than or equal to 5.0%, which is an acceptable range. Moreover, the developed ANN model can predict the mechanical properties of Ti-6Al-4V alloy in the future [64].

Similarly, when compared the efficiency of GP, NN, SVM, and GBT models to predict single clad geometry, the Gaussian process (GP) model by the metrics was more successful, though only marginally, at regression and classification than neural network (NN) models. Support vector machines (SVMs) underperformed when compared against the GP model. SVMs, when compared to the NNs, had lower variance and better classification accuracy. As a classifier, the GBT model outperformed the other models. As a regressor, GBT showed the lowest variance [66].

In another research, a CNN and an ANN successfully predicted tensile properties of Ti-6Al-4V, where CNN was used for feature extraction in thermal image data, and ANN approached to identify parameter effects. 84% of the data lay within the ±5% deviation from a perfect prediction of yield strength, 90% of the data lay within ±5.85% deviation, and 70% of the data lay within ±3.48% deviation. The median deviation was 2.4%, and the average deviation was 3.0%. The maximum error was calculated to be 8.2%. Most importantly, these data represented three distinctly different heat treatments which was never done before. The average knockdown effects due to texture for the alloy were calculated to be 3% using the wrought structure equation as a baseline [65].

For predicting surface characteristics in CO2 laser micro-milling of glass fiber reinforced plastic composite, ANN model with 3-6-6-3 network structure was the most efficient with the mean, maximum, and minimum prediction errors of 0.82%, 2.26%, and 0.0004%, respectively. The difference between experimental and model values of milling depth was within ±2%, and the coefficient of determination R^2 was found to be 0.999. For surface roughness, the difference between experimental and model values was again ±2%, whereas the value of R^2 was found to be 0.997 and 0.993 for parallel and perpendicular to the fiber during milling, respectively [69].

In another paper where an ANN model was developed to study grain-growth behavior, the MSE for the model was 3.45 and 6.42 for training and testing data, respectively. The average distance between the prediction of the grain-boundary angle and their experimental results was 1.83 and 2.43, and the standard deviation was 0.32 and 0.73, respectively, for training and testing. The tolerance range of this model was found to be about ±4. An average prediction error of 2.43 showed that a feed-forward neural network is an appropriate tool for this task [70].

When incorporated with 3D printers, AI's resultant system helps aerospace manufacturers make more accurate and precise products like aero-parts, which are more flexible, less costly, and produce less waste [71].

In this ontology, the authors proposed a hybrid approach to solve the current problem of DSS in laser-based AM. The researchers combined the knowledge engineering methods and case-based search by analogy. This includes continuous updating of the knowledge base by experts for improvement in the process. This work was later implemented, and the

Table 10: Comparison between various network models used.

Algorithm used	Depth, layer sizes, training time, and testing time	Dataset	Accuracy	Variation from experimental value	Ref.
ANN	1 hidden layer, 7 neurons 3-7-1, feed-forward, backpropagation neural network model	Not mentioned.	98.7%	67.9% MAPE	[94]
CNN	(i) Avg pooling layer (ii) Convolution layer (3×3; 32 filters) (iii) Avg pooling layer (iv) Convolution layer (3×3; 16 filters) (v) Flattening layer (vi) Fully connected layer (vii) Softwax function (confidence values into probabilities)	The time-series thermal images were collected with the help of the cameras and other multiple DED process settings.	80%	Not mentioned	[57]
RNN	(i) 1–5 layers (ii) 100–500 GRU units (iii) 1–3 fully connected layers	Self-made using GAMMA.	MSE: $2.97e-5$ after 100 epochs	Not mentioned	[58]
LSTM	(i) Input layer (ii) LSTM layer (iii) Fully connected layer (iv) Dropout layer (v) Fully connected layer (vi) Regression layer	FEM sim data and data from artificial crack experiments.	The average absolute error of prediction: 2.0 μm	(i) Abs error for FEM data: 6.88 μm (ii) Avg error for artificial crack data: 7.41 μm.	[59]
ANN: feed-forward backpropagation	Input parameters: L0 orthogonal array Input variables: 3	Self-prepared, pre-processed, and labeled data	97.08% R-squared	Not mentioned	[60]
CNN	2 convolution layers: (i) Layer 1: 10 filters of kernel size 6×6; (ii) Layer 2: 20 filters of kernel size 4×4 max-pooled with pool size of 2×2 convolution $(20 \times 7 \times 7)$ images $\longrightarrow$ max-pooling $\longrightarrow$ fully connected layer (with 200 nodes) $\longrightarrow$ activation function RELU $\longrightarrow$ 50% dropout	100,000 images of both classes. Training images: 60,000	96.02%: case one 93.69%: case two	24%: case one 9.6%: case two	[63]
Stacked RNN	(i) 1–5 hidden layers (ii) 100–500 GRU units (iii) 1–3 fully connected layers Training time: 40 h on Nvidia Quadro P5000	Built using GAMMA.	MSE: $3.17e-5$	N/A	[58]
ANN	Single hidden layer (3-16-4)	Trained dataset using ANN backpropagation.	90%	5%	[64]
Neural network (I), gradient boosted decision tree (II), SVM (III), and Gaussian process (IV)	(I) For regression: linear neurons = 283, non-linear = 210, learning rate: 0.000871 For classification: linear neurons = 358, non-linear = 744, LR = 0.000465; 1 hidden layer. (IV) LR = 0.01; max depth = 20	Previously unpublished experimental results of this author. Input set (powder material, substrate material, spot size, power, Mass flow rate, travel velocity)	II > IV > III > I ensemble regression accuracy of 70.5% and an ensemble classification accuracy of 72.3%	Not mentioned	[66]

Table 10: Continued.

Algorithm used	Depth, layer sizes, training time, and testing time	Dataset	Accuracy	Variation from experimental value	Ref.
Hybrid of ANN and genetic algorithm approach	Not mentioned	Experimentally measured process variables.	84%	5%	[65]
ANN	Neural networks with hidden layer containing nodes in the following orders were tested: 3-1-3, 3-3-3, 3-6-3, 3-7-3, 3-1-1-3, 3-3-3-3, 3-6-6-3, 3-7-7-3	Prepared after conducting 60 experiments. Constraints like availability of material, cost, and time required for experiment were considered	82%	2%	[69]
ANN	1-5-10-1	50 groups of data were gathered from the experiment.	Not mentioned	4%	[70]

process of AM of metal products using laser-based tech was created on the IACPaaS cloud platform. This work has been used to date in various works, with the components of the knowledge portal improved further, helping to create new components and bringing improvement on the current ones [72].

Table 10 provides an exhaustive comparison between various network models used in the DED processes to date, and their accuracy, datasets, and various other parameters for industrial significance have been addressed and accumulated.

6. Summary and Conclusions

Based on the above results, we can conclude that AI has been beneficial in making various processes of DED easier. The products made using DED technology and monitored by the AI-trained system have become of superior quality. The products are superior, and also there are fewer failure rates as well as fewer wastes. With the suitable model and proper amount of training dataset, a system with accurate and reliable prediction can be prepared, which helps to make a good DED manufacturing technology. Throughout this literature review, we have seen high use of CNNs, ANNs, and RNNs based on the type of use. These network models have shown significant improvement in results compared to the results from the DED technology without AI. RNN architecture excels at predicting thermal history in the DED process. The CNN architecture excels at applications such as speech recognition, image processing, fault diagnosis, and feature extraction from high-dimensional signals. In DED, CNN can be used as a tool for pattern recognition and ultimately in process monitoring. The ANN architecture on the other hand is also a non-linear machine learning model that can effectively predict track dilution values in the DED process with different setting parameters. In our reviews, CNN showed accuracy in prediction as high as 96% and as low as 80%, while ANN also showed great fit with the R_2 value of 97%. The RNN is highly effective in predicting values in which the previous output affects the current output and has shown MSE as low as $2.97e-5$. Few algorithms like ANN are more useful when developing a predicting model, but few others, like GBT, are more efficient when we need geometry prediction. GBT (gradient boost decision tree) is a technique in ML that effectively solves regression and classification problems which have data in tabular form. A prediction model is produced from a group of weaker prediction models where each model is optimized using a loss function, called gradient descent. NN and GBT have this optimization thing in common. Similarly, SVM and Gaussian process have a commonality too, as they both can be called kernel methods. In these processes, a kernel is produced among all the data, which can best describe all other data. SVM and GP can be disadvantageous as they do not provide probability estimates directly. Various parameters, like MSE, accuracy, variation, and standard deviation, make a basis for comparing the efficiency of all these algorithms. We have tried to present most of the efficiency determining parameters of the AI techniques used in the DED process. If studied further, we can explore many more techniques that are more efficient than those explained previously. These AI techniques can be used to achieve similar goals in areas other than DED. We can study more about AI and its contributions to mechanical engineering and improve already known techniques, as there is always room for improvement.

The directed energy deposition (DED) process and its key parameters are thoroughly discussed by reviewing various research or journal papers published in recent times. Firstly, the basic structure of any DED system is depicted as a well-labeled diagram showing all its components. As already discussed, there are two types of feed material in the DED process, namely, powder-based and wire-based, which are thoroughly discussed in the later sections. Also, there are three types of heat sources, namely, electron beam, laser beam, and plasma or arc. A brief description of the overall process is given as a flowchart which helps the reader better understand the overview of the process. The types of environments in which the DED system is conducted are also discussed as a flowchart showing all types of shielding gases or vacuum that create the environment. According to the flowchart, there are two shielding mediums—local shielding and inert gas chamber. Pros and cons of these shielding mediums are listed in a table. A vacuum chamber, even

though heavy and expensive, creates the best environment for the process. In mediums created by inert gases, an inert gas chamber gives the best results as it provides a better environment when compared to local shielding. Next, the DED process is compared with similar additive manufacturing processes based on their basic description, related technologies, and materials. Then, the major pros and cons of using the DED process are elaborately discussed. One of the main advantages of using this process is that it can be used for varied materials such as metals, polymers, and ceramics, and one major disadvantage is that the products made by this process have a relatively poorer surface finish than other additive manufacturing methods. There are three types of applications of the DED process in any industry. DED is used for the addition of features in pre-existing parts. It increases the value of the product and reduces machining times. This process is used in the repair of pre-existing components in many industries. In component repair, it reduces lead time and extends the life of the part. Also, the DED process is used to fabricate near net shapes where the material wastage is reduced while fabricating complex shapes.

Next, the types of energy sources—an electron beam (EBAM), a laser beam (LDED), and arc (ADED)—are thoroughly discussed. The EBAM process is done at a power range of 4–20 kW in a vacuum chamber. This process is mainly used to produce near net shape parts and large parts. While EBAM is used to produce large parts, the LDED process produces smaller parts with higher resolution. The powder is the primary feed material used in the LDED process. Many types of feed materials that can be used in the DED process were discussed one by one. The types discussed are pure metals, metal alloys, polymers, and ceramics. In pure metals, copper and tungsten are the two most used metals due to the following properties. Copper is majorly used as feed material in the LDED process. While copper is used in aviation and marine industries, tungsten is used in aerospace, space, and nuclear industries, such as wood and metal cutting, drilling, and machining, due to its excellent corrosion resistance, low vapor pressure, high thermal conductivity, high melting point, and higher density. Tungsten finds its uses as feed material in AM processes like powder bed fusion, plasma laser sintering, and LDED. The most used materials as the feed in any DED process are metal alloys. Some of the key metal alloys on which much research has been done are discussed in detail in this paper. Hastelloy-X is a nickel-chromium iron-molybdenum alloy that shows high mechanical strength, high yield strength, high ductility, and high corrosion resistance. Therefore, it is used to fabricate gas turbine engines, heat exchangers, etc. Moreover, it is used as feed material in the LAM-DED process. Inconel 718 is a nickel-based superalloy used to create jet engines, gas turbines, etc., as it has high tensile and impact strength and good resistance to corrosion and oxidation. It is mostly used as feed material in the LAM-DED process. Titanium-molybdenum (Ti-15Mo) shows excellent corrosion resistance, high hardness, and fatigue. Hence, this material is used as bioimplants and in aerospace industries. The EBAM-DED process uses this material as feed. Similarly, other titanium alloys are also used in similar military, aircraft, and aerospace industries due to their high tensile strength and toughness.

Stainless steel is one of the highest standard alloys that is used almost everywhere. It has high resistance toward corrosion and displays high strength even at high temperatures. It is mainly used as feed material in the EBAM-DED process. Zirconium alloys such as Zircaloy are used to create parts in the nuclear industry, water reactors, etc., due to their high ductility, hardness, and corrosion resistance. Also, some aluminum alloys, such as 4043 aluminum alloy, display good corrosion resistance and are used in welding and brazing metals. The DED process is not only applicable to metals and metal alloys but also polymers and ceramics. Some of the most used polymers in the DED processes are discussed in detail. One such material is polymethyl methacrylate (PMMA). It is shatterproof, rigid, UV and harsh weather-resistant, and highly resistant to scratches. These properties are used in the biomedical industry, automotive and transportation industries, and the furniture industry.

Selective laser sintering (SLS) and DED processes use this material as a feed material. Polyether ether ketone (PEEK) is a polymer with high heat and electrical resistance to withstand high temperatures. Therefore, it is used in the medical industry, aircraft, and automotive industries. Even though it can be used as feed material in the DED process, it is mainly utilized in the fused deposition method (FDM) process. Another important polymer is acrylonitrile butadiene styrene (ABS). It is used in the automotive industry, pipes and fittings, and structural applications due to its high impact strength and heat resistance, high strain resistance, and stability over time. Polypropylene (PP) has excellent barrier properties, low cost, low moisture-vapor transmission, exceptional optical clarity, and high bacterial and thermal resistance and is used in the packaging industry, automotive industry, and medical industry. SLS process uses this material as feed to fabricate components in these industries.

Moreover, finally, polylactic acid (PLA) is a biobased, biodegradable, biocompatible, compostable, and non-toxic polymer used in the packaging industry, health and medical industry, and many structural applications. Some of the ceramics are also used as feed materials in the DED process. One such ceramic is alumina which has high electrical insulation and resistance to corrosion. Hence, it is used in automotive sensors, dental implants, and electronics. It is mainly used as feed material in the LAM-DED process. Another ceramic that is widely used in the DED process is zirconia. It has high toughness, high strength, and corrosion resistance and is used in producing dental crowns, insulators, rollers, pistons, etc. Another ceramic widely used in the DED process is magnesium aluminate spinel which is used in bulletproof glass, aerospace, and defense industries. It is mainly used as feed material in the LAM-DED process.

Then, a wide variety of works done by many researchers are thoroughly studied, and their research outcomes are drafted in this paper. While many researchers discussed the thermal effects of laser power and scanning speeds on the

weld pool, some focused on a trinocular vision-based system that can measure the clad height in the DED process. One of the main results presented in these papers is that a measurement-based forced convection model can produce meager error rates. This model can be used for any research work that focuses on thermal characteristics. A CFD analysis can also be added, and high scanning speed and lower laser power are always preferable to achieve finer microstructures while working with stainless steel and Inconel. It is established that a trinocular vision system is always better than a binocular vision system which gives a minimal effort and helpful and exact methodology for estimating the cladding tallness in the DED interaction. Also, many papers tried to find out the types of materials that can be used as feed in the DED process. Many researchers tried and are still trying to fabricate defect-free components of various metals and metal alloys through the DED process. Metal alloys such as AlSi10Mg are proved to be very suitable as feed materials in the LAM-DED process as they showed higher hardness values than the AlSi10Mg parts created by other manufacturing methods. Many studies were inclined toward finding the properties of final parts created by the DED process. This includes finding out the final hardness values and corrosive properties in which it was found that stainless steel that are fabricated from DED processes. They have less corrosion resistance than parts manufactured through traditional methods and their thermo-mechanical properties and other various other properties may vary. It is also seen that slicing is a critical but less used process in additive manufacturing processes such as DED.

Slicing can be very useful to increase the quality and eliminate support structures. The types of slicing processes, namely, additive slicing, essential slicing, non-layer-wise slicing, and multi-direction slicing, are exhaustively discussed with the help of a table and concerning their features, advantages, and disadvantages. Also, three types of laser beams are extensively used in DED processes. IPG Photonics lasers, neodymium-doped yttrium aluminum garnet (Nd: YG) laser, and C02-type end pulsed-wave laser were used. These are depicted as a flowchart in the part of the discussion. There are four mainly used shielding gases in the DED processes. They are argon, helium, argon-helium mixtures, and nitrogen. These, too, are depicted as a flowchart in the part of the discussion. Finally, to improve the quality of the components, the building parameters such as feeding rate, scan feed, and laser power are vital factors [41, 95–98].

After studying and analyzing many research works, a set of process parameters that can be useful for a particular process is drafted and discussed in detail in the process parameters section. The first and foremost process parameter discussed is that using certified or reliable DED systems is always better than cheap or home-based DED systems. This is because cheap DED systems can have a fluctuating laser power or powder delivery rate, whereas reliable DED systems can provide constant rates at all times. Also, relevant examples are given from research papers to justify the same. The second process parameter tells that post-heat treatment processes are essential to enhance the mechanical properties of materials such as hardness, tensile strength, and impact strength. Adverse effects such as tension and internal stresses can also be removed using post-heat treatment processes. This is proven for two types of tool steels – H13 and D2 in the recent research works conducted, which is also mentioned in the process parameters section [99–104].

The third parameter is about the selection of feed material in DED processes. There are two types of feed material—wire and powder. The advantages and disadvantages of both wire and powder feed are discussed in detail, and it is seen that powder-based feed is best suitable for the LDED process, and wire-based feed is used when the material wastage is not to be encouraged. The difference between them is also discussed in length. The following process parameter is about the layer thickness of the deposited layer in the DED process. It is said that the geometry and structure of components depend on the thickness of layers. Lower thickness and increased melt pool volume produce components with better roughness. The fifth process parameter is about the laser power and how it affects the geometry of the component. Higher laser powers (800 W+) mean increased dilution and penetration depth, which reduces the total component's height. At the same time, lower power (100–400 W) leads to rapid solidification of the melt pool, increasing the deposit density. Scale formations can be seen in such deposits. Finally, it was found that crucial output parameters such as clad thickness, dilution, temperature, and thermal stresses will increase with the increase of the laser power. Of these parameters, dilution and temperature become constant because they reach a point called the saturation level. The following process parameter is about the powder flow rate of DED processes. Monitoring the powder flow rate is essential to improve the reliability of components in industries. Many different types of methods are mentioned which can efficiently measure the powder flow rate. Maintaining constant flow rates at all times is very important to regulate dilution and porosity. Even distribution of powder feed is also essential [19–23, 105–107].

The final parameter discussed in this review talks about the scan speeds of lasers in the DED process. Lower scan speeds result in significantly large melt pools with considerable build heights and meager dilution rates, whereas increase in scan speeds results in low melting or lack of fusion [108–113]. So, a melt pool is not produced. As scanning speed increases, clad height, temperature, stress, and clad height decrease. However, using high or low scanning speeds can be neutralized using medium scanning speeds (400–500 mm/sec). By using medium scan speeds, the sample shows excellent comprehensive properties along with balanced toughness and strength. Also, the role of artificial intelligence (AI) is an added flavor to the directed energy deposition process and has a scope that is very promising shortly. Recent signs of progress in artificial intelligence have made it a technology that can be used in any

application with the DED process as no exception to reduce the human effort [114–116].

Data Availability

The data used to support the findings of this study are included within the article.

Conflicts of Interest

The authors declare that they have no conflicts of interest.

References

[1] G. Kou, H. Xiao, M. Cao, and L. H. Lee, "Optimal computing budget allocation for the vector evaluated genetic algorithm in multi-objective simulation optimization," *Automatica*, vol. 129, Article ID 109599, 2021.

[2] G. Kou, Ö. Olgu Akdeniz, H. Dinçer, and S. Yüksel, "Fintech investments in European banks: a hybrid IT2 fuzzy multidimensional decision-making approach," *Financial Innovation*, vol. 7, no. 1, pp. 39–28, 2021.

[3] Twi Global (n.d.), https://www.twi-global.com/technical-knowledge/faqs/directed- energy-deposition, 2021.

[4] Autonomous Manufacturing, "Metal 3D printing: what is directed energy deposition?," 2018, https://amfg.ai/2018/09/27/metal-3d-printing-what-is-directed-energy- deposition/.

[5] A. Dass and A. Moridi, "State of the art in directed energy deposition: from additive manufacturing to materials design," *Coatings*, vol. 9, no. 7, p. 418, 2019.

[6] M. Ramesh and K. Niranjana, "Effect of process parameters on fused filament fabrication printed composite materials," in *High-Performance Composite Structures*, pp. 155–178, Springer, Singapore, 2022.

[7] M. Ramesh, L. Rajeshkumar, and D. Balaji, "Influence of process parameters on the properties of additively manufactured fiber-reinforced polymer composite materials: a review," *Journal of Materials Engineering and Performance*, vol. 30, no. 7, pp. 4792–4807, 2021.

[8] Additive Manufacturing Research Group, "Loughborough university," https://www.lboro.ac.uk/research/amrg/about/the7categoriesofadditivemanufacturing/directedenergydeposition/.

[9] X. Lu, X. Lin, M. Chiumenti et al., "Residual stress and distortion of rectangular and S-shaped Ti-6Al-4V parts by Directed Energy Deposition: modelling and experimental calibration," *Additive Manufacturing*, vol. 26, pp. 166–179, 2019.

[10] Y. Bandai, "Directed energy deposition (DED), digital alloys' guide to metal additive manufacturing – Part 9," 2019, https://www.digitalalloys.com/blog/directed-energy-deposition/.

[11] J. Ruiz, M. Cortina, J. Arrizubieta, and A. Lamikiz, "Study of the influence of shielding gases on laser metal deposition of Inconel 718 superalloy," *Materials*, vol. 11, no. 8, p. 1388, 2018.

[12] Total Materia, "Introduction to additive manufacturing: Part Two," 2018, https://www.totalmateria.com/page.aspx?ID=CheckArticle&site=ktn&LN=FR&NM= 432.

[13] Engineering product design, "Directed energy deposition (DED)," 2019, https://engineeringproductdesign.com/knowledge-base/directed-energy-deposition/.

[14] Beam Machines, "Ded - directed energy deposition," https://www.beam-machines.com/applications-process-3d-printing.

[15] Sciaky Inc, "What is directed energy deposition (DED) 3D printing? https://www.sciaky.com/additive-manufacturing/what-is-ded-3d-printing.

[16] EWI, "What is directed energy deposition? https://ewi.org/capabilities/additive- manufacturing/what-is-directed-energy-deposition/.

[17] 3D Experience, "3D printing – ADDITIVE, Directed energy deposition - DED, LENS,"https://make.3dexperience.3ds.com/processes/directed-energy- deposition.

[18] S. K. Selvaraj, R. Ramesh, T. M. V. Narendhra et al., "New deveLopments in carbon-based nanomaterials for automotive brake pad applications and future challenges," *Journal of Nanomaterials*, vol. 2021, Article ID 6787435, 24 pages, 2021.

[19] U. Chadha, P. Bhardwaj, R. Agarwal et al., "Recent progress and growth in biosensors technology: a critical review," *Journal of Industrial and Engineering Chemistry*, vol. 109, pp. 21–51, 2022.

[20] A. Tiwari, A. Tiwari, A. Bhatia et al., "Nanomaterials for electromagnetic interference shielding applications: a review," *Nano*, vol. 17, no. 2, Article ID 2230001, 2022.

[21] U. Chadha, P. Bhardwaj, S. K. Selvaraj et al., "Advances in chitosan biopolymer composite materials: from bioengineering, wastewater treatment to agricultural applications," *Materials Research Express*, vol. 9, no. 5, Article ID 052002, 2022.

[22] U. Chadha, S. Sinha, J. Jonna et al., "Review—chemical structures and stability of carbon-doped graphene nanomaterials and the growth temperature of carbon nanomaterials grown by chemical vapor deposition for electrochemical catalysis reactions," *ECS Journal of Solid State Science and Technology*, vol. 11, no. 4, Article ID 041003, 2022.

[23] U. Chadha, S. K. Selvaraj, H. Ashokan et al., "Complex nanomaterials in catalysis for chemically significant applications: from synthesis and hydrocarbon processing to renewable energy applications," *Advances in Materials Science and Engineering*, vol. 2022, Article ID 1552334, 72 pages, 2022.

[24] U. Chadha, S. K. Selvaraj, S. Vishak Thanu et al., "A review of the function of using carbon nanomaterials in membrane filtration for contaminant removal from wastewater," *Materials Research Express*, vol. 9, no. 1, Article ID 012003, 2022.

[25] K. Kulkarni, U. Chadha, S. Yadav et al., "Latest trends and advancement in porous carbon for biowaste organization and utilization," *ECS Journal of Solid State Science and Technology*, vol. 11, no. 1, Article ID 011003, 2022.

[26] S. Yadav, C. P. Paul, A. N. Jinoop, A. K. Rai, and K. S. Bindra, "Laser directed energy deposition based additive manufacturing of copper: process development and material characterizations," *Journal of Manufacturing Processes*, vol. 58, pp. 984–997, 2020.

[27] J. Yu, G. Wang, and Y. Rong, "Experimental study on the surface integrity and chip formation in the micro cutting process," *Procedia Manufacturing*, vol. 1, pp. 655–662, 2015.

[28] Stanford Advanced Materials, "Application of Tungsten in modern industry," https://www.samaterials.com/content/application-of-tungsten-in-modern-industry.html.

[29] W. Jeong, Y. S. Kwon, and D. Kim, "Three-dimensional printing of tungsten structures by directed energy deposition," *Materials and Manufacturing Processes*, vol. 34, no. 9, pp. 986–992, 2019.

[30] V. Madhavadas, D. Srivastava, U. Chadha et al., "A review on metal additive manufacturing for intricately shaped aerospace components," *CIRP Journal of Manufacturing Science and Technology*, vol. 39, no. 2022, pp. 18–36.

[31] A. N. Jinoop, C. P. Paul, and K. S. Bindra, "Laser assisted directed energy deposition of Hastelloy-X," *Optics & Laser Technology*, vol. 109, pp. 14–19, 2019.

[32] F. Careri, S. Imbrogno, D. Umbrello, M. M. Attallah, J. Outeiro, and A. C. Batista, "Machining and heat treatment as post-processing strategies for Ni-superalloys structures fabricated using directed energy deposition," *Journal of Manufacturing Processes*, vol. 61, pp. 236–244, 2021.

[33] T. Bhardwaj, M. Shukla, C. P. Paul, and K. S. Bindra, "Directed energy deposition-laser additive manufacturing of titanium-molybdenum alloy: parametric studies, microstructure and mechanical properties," *Journal of Alloys and Compounds*, vol. 787, pp. 1238–1248, 2019.

[34] A. N. Jinoop, C. P. Paul, and K. S. Bindra, "Laser-assisted directed energy deposition of nickel super alloys: a review," *Proceedings of the Institution of Mechanical Engineers - Part L: Journal of Materials: Design and Applications*, vol. 233, no. 11, pp. 2376–2400, 2019.

[35] Atlantic Steels, "300 series stainless steel," https://www.atlanticstainless.com/steel-grades/300-series-stainless-steel/.

[36] Wikipedia, "Zirconium alloy,".

[37] AlcoTechnics, "Alloy 4043 weld data sheet," http://www.alcotec.com/us/en/support/upload/a4043tds.pdf.

[38] Omnexus, "PMMA or acrylic: guide to support your future "transparent" developments," https://omnexus.specialchem.com/selection-guide/polymethyl- methacrylate-pmma-acrylic-plastic.

[39] O. S. Manoukian, N. Sardashti, T. Stedman et al., "Biomaterials for tissue engineering and regenerative medicine," *Encyclopedia of Biomedical Engineering*, pp. 462–482, 2019.

[40] D. Mitsouras, P. Liacouras, A. Imanzadeh et al., "Medical 3D printing for the radiologist," *RadioGraphics*, vol. 35, no. 7, pp. 1965–1988, 2015.

[41] S. K. Selvaraj, K. Srinivasan, U. Chadha et al., "Contemporary progresses in ultrasonic welding of aluminum metal matrix composites," *Frontiers in Materials*, vol. 8, p. 126, 2021.

[42] Omnexus, "Popular application of polyetheretherketone (PEEK)," https://omnexus.specialchem.com/selection-guide/polyetheretherketone-peek- thermoplastic/key-applications.

[43] M. Rinaldi, F. Cecchini, L. Pigliaru, T. Ghidini, F. Lumaca, and F. Nanni, "Additive manufacturing of polyether ether Ketone (PEEK) for space applications: a nanosat polymeric structure," *Polymers*, vol. 13, no. 1, p. 11, 2020.

[44] Omnexus, "A detailed guide on acrylonitrile Butadiene Styrene," https://omnexus.specialchem.com/selection-guide/acrylonitrile-butadiene-styrene-abs- plastic.

[45] M. Bible, M. Sefa, J. A. Fedchak et al., "3D-Printed acrylonitrile Butadiene styrene-metal organic framework composite materials and their gas storage properties," *3D Printing and Additive Manufacturing*, vol. 5, no. 1, pp. 63–72, 2018.

[46] Omnexus, "The definitive guide to polypropylene (PP)," https://omnexus.specialchem.com/selection-guide/polypropylene-pp-plastic.

[47] W. S. Tan, C. K. Chua, T. H. Chong, A. G. Fane, and A. Jia, "3D printing by selective laser sintering of polypropylene feed channel spacers for spiral wound membrane modules for the water industry," *Virtual and Physical Prototyping*, vol. 11, no. 3, pp. 151–158, 2016.

[48] M. Nofar, D. Sacligil, P. J. Carreau, M. R. Kamal, and M.-C. Heuzey, "Poly (lactic acid) blends: processing, properties and applications," *International Journal of Biological Macromolecules*, vol. 125, pp. 307–360, 2019.

[49] J. Deckers, J. Vleugels, and J.-P. Kruth, "Additive manufacturing of ceramics: a review," *Journal of Ceramic Science and Technology*, vol. 5, 2014.

[50] R. Galante, C. G. Figueiredo-Pina, and A. P. Serro, "Additive manufacturing of ceramics for dental applications: a review," *Dental Materials*, vol. 35, no. 6, pp. 825–846, 2019.

[51] Elan Technology, "96% alumina ceramic," https://www.elantechnology.com/ceramics/ceramic-materials/alumina-ceramics/96- alumina/#:~:text=Alumina%20ceramic%20(Aluminum%20Oxide%20or,resistant%20 to%20wear%20and%20corrosion.&text=Elan%20Technology%20offers%20a%20ran ge,meet%20your%20most%20demanding%20applications.

[52] Superior Technical Ceramics, "Zirconia ceramics," https://www.ceramics.net/ceramic- materials-solutions/zirconia-ceramics.

[53] J. M. Pappas, E. C. Kinzel, and X. Dong, "Laser direct deposited transparent magnesium aluminate spinel ceramics," *Manufacturing Letters*, vol. 24, pp. 92–95, 2020.

[54] D. E. Rumelhart, R. Durbin, R. Golden, and Y. Chauvin, "Backpropagation: the basic theory," *Backpropagation: Theory, architectures and applications*, pp. 1–34, 1995.

[55] F. A. Gers, N. N. Schraudolph, and J. Schmidhuber, "Learning precise timing with LSTM recurrent networks," *Journal of Machine Learning Research*, vol. 3, pp. 115–143, 2002.

[56] Z. Zhang, Z. Liu, and D. Wu, "Prediction of melt pool temperature in directed energy deposition using machine learning," *Additive Manufacturing*, vol. 37, Article ID 101692, 2021.

[57] X. Li, S. Siahpour, J. Lee, Y. Wang, and J. Shi, "Deep learning-based intelligent process monitoring of directed energy deposition in additive manufacturing with thermal images," *Procedia Manufacturing*, vol. 48, pp. 643–649, 2020.

[58] M. Mozaffar, A. Paul, R. Al-Bahrani et al., "Data-driven prediction of the high-dimensional thermal history in directed energy deposition processes via recurrent neural networks," *Manufacturing letters*, vol. 18, pp. 35–39, 2018.

[59] W. Shi, Z. Ren, W. He, J. Hou, H. Xie, and S. Liu, "A technique combining laser spot thermography and neural network for surface crack detection in laser engineered net shaping," *Optics and Lasers in Engineering*, vol. 138, Article ID 106431, 2021.

[60] M. Pant, R. M. Singari, P. K. Arora, G. Moona, and H. Kumar, "Wear assessment of 3–D printed parts of PLA (polylactic acid) using Taguchi design and Artificial Neural Network (ANN) technique," *Materials Research Express*, vol. 7, no. 11, Article ID 115307, 2020.

[61] Z. L. Lu, D. C. Li, B. H. Lu, A. F. Zhang, G. X. Zhu, and G. Pi, "The prediction of the building precision in the Laser Engineered Net Shaping process using advanced networks," *Optics and Lasers in Engineering*, vol. 48, no. 5, pp. 519–525, 2010.

[62] B. Li, F. Wu, S. N. Lim, S. Belongie, and K. Q. Weinberger, "On feature normalization and data augmentation," in *Proceedings of the IEEE/CVF Conference on Computer Vision and Pattern Recognition*, pp. 12383–12392, Nashville, TN, USA, June 2021.

[63] B. Bhattacherjee, S. Mukherjee, and R. Sengupta, "Study of energy deposition patterns in hadron calorimeter for prompt

and displaced jets using convolutional neural network," *Journal of High Energy Physics*, vol. 2019, no. 11, pp. 156–232, 2019.

[64] Y. Sun, W. Zeng, Y. Han et al., "Modeling the correlation between microstructure and the properties of the Ti–6Al–4V alloy based on an artificial neural network," *Materials Science and Engineering: A*, vol. 528, no. 29-30, pp. 8757–8764, 2011.

[65] B. J. Hayes, B. W. Martin, B. Welk et al., "Predicting tensile properties of Ti-6Al-4V produced via directed energy deposition," *Acta Materialia*, vol. 133, pp. 120–133, 2017.

[66] M. Juhasz, "Machine learning predictions of single clad geometry in directed energy deposition," *OSF Preprints - Open Science Framewor*, 2020.

[67] L. Yu, R. Zhou, R. Chen, and K. K. Lai, "Missing data preprocessing in credit classification: one-hot encoding or imputation?" *Emerging Markets Finance and Trade*, vol. 58, no. 2, pp. 472–482, 2022.

[68] J. Yamanaka, S. Kuwashima, and T. Kurita, "Fast and accurate image super resolution by deep CNN with skip connection and network in network," in *Proceedings of the International Conference on Neural Information Processing*, pp. 217–225, Springer, Bangkok, Thailand, November 2017.

[69] S. Prakash and S. Suman, "Neural network-based prediction for surface characteristics in CO 2 laser micro-milling of glass fiber reinforced plastic composite," *Neural Computing & Applications*, vol. 33, no. 18, pp. 11517–11529, 2021.

[70] J. Li, M. Sage, X. Guan, M. Brochu, and Y. F. Zhao, "Machine learning- enabled competitive grain growth behavior study in directed energy deposition fabricated Ti6Al4V," *Journal of Occupational Medicine*, vol. 72, no. 1, pp. 458–464, 2020.

[71] A. Syuhada, M. S. Shamsudin, M. F. Omar, S. K. Ghoshal, S. W. Harun, and M. S. Aziz, "Incorporating 3D metal printing with artificial intelligence in meeting aerospace demands," in *Journal of Physics: Conference Series*vol. 1892, no. 1, IOP Publishing, Article ID 012015, 2021.

[72] V. Gribova, Y. Kulchin, A. Nikitin, and V. Timchenko, "The concept of support for laser-based additive manufacturing on the basis of artificial intelligence methods," in *Russian Conference on Artificial Intelligence*, pp. 403–415, Springer, Berlin, Germany, 2020.

[73] J. C. Heigel, P. Michaleris, and E. W. Reutzel, "Thermo-mechanical model development and validation of directed energy deposition additive manufacturing of Ti–6Al–4V," *Additive Manufacturing*, vol. 5, pp. 9–19, 2015.

[74] Q. Yang, P. Zhang, L. Cheng, Z. Min, M. Chyu, and A. C. To, "Finite element modeling and validation of thermo-mechanical behavior of Ti-6Al-4V in directed energy deposition additive manufacturing," *Additive Manufacturing*, vol. 12, pp. 169–177, 2016.

[75] Y. Huang, M. Ansari, H. Asgari et al., "Rapid prediction of real-time thermal characteristics, solidification parameters and microstructure in laser directed energy deposition (powder-fed additive manufacturing)," *Journal of Materials Processing Technology*, vol. 274, Article ID 116286, 2019.

[76] J. Xu, X. Gu, D. Ding, Z. Pan, and K. Chen, "A review of slicing methods for directed energy deposition based additive manufacturing," *Rapid Prototyping Journal*, vol. 24, no. 6, pp. 1012–1025, 2018.

[77] S. J. Wolff, H. Wu, N. Parab et al., "In-situ high-speed X-ray imaging of piezo-driven directed energy deposition additive manufacturing," *Scientific Reports*, vol. 9, no. 1, p. 962, 2019.

[78] H.-W. Hsu, Y.-L. Lo, and M.-H. Lee, "Vision-based inspection system for cladding height measurement in directed energy deposition (DED)," *Additive Manufacturing*, vol. 27, pp. 372–378, 2019.

[79] S. M. Thompson, L. Bian, N. Shamsaei, and A. Yadollahi, "An overview of Direct Laser Deposition for additive manufacturing; Part I: transport phenomena, modeling, and diagnostics," *Additive Manufacturing*, vol. 8, pp. 36–62, 2015.

[80] M. Javidani, J. Arreguin-Zavala, J. Danovitch, Y. Tian, and M. Brochu, "Additive manufacturing of AlSi10Mg alloy using directed energy deposition: microstructure and hardness characterization," *Journal of Thermal Spray Technology*, vol. 26, no. 4, pp. 587–597, 2016.

[81] A. N. Jinoop, C. P. Paul, S. K. Mishra, and K. S. Bindra, "Laser Additive Manufacturing using directed energy deposition of Inconel-718 wall structures with tailored characteristics," *Vacuum*, vol. 166, pp. 270–278, 2019.

[82] A. Saboori, A. Aversa, G. Marchese, S. Biamino, M. Lombardi, and P. Fino, "Microstructure and mechanical properties of AISI 316L produced by directed energy deposition-based additive manufacturing: a review," *Applied Sciences*, vol. 10, no. 9, p. 3310, 2020.

[83] A. Saboori, D. Gallo, S. Biamino, P. Fino, and M. Lombardi, "An overview of additive manufacturing of titanium components by directed energy deposition: microstructure and mechanical properties," *Applied Sciences*, vol. 7, no. 9, p. 883, 2017.

[84] M. A. Melia, H.-D. A. Nguyen, J. M. Rodelas, and E. J. Schindelholz, "Corrosion properties of 304L stainless steel made by directed energy deposition additive manufacturing," *Corrosion Science*, vol. 152.

[85] J. S. Park, M.-G. Lee, Y.-J. Cho et al., "Effect of heat treatment on the characteristics of tool steel deposited by the directed energy deposition process," *Metals and Materials International*, vol. 22, no. 1, pp. 143–147, 2016.

[86] A. Fiorese, "The advantages of heat treating metals following additive manufacturing," 2020, https://www.industrialheating.com/articles/95878-the-advantages-of-heat-treating-metals-following-additive-manufacturing.

[87] I. Gibson, D. Rosen, and B. Stucker, "Directed energy deposition processes," *Additive Manufacturing Technologies*, Springer, Berlin, Germany, pp. 245–268, 2015.

[88] D.-S. Shim, G.-Y. Baek, J.-S. Seo, G.-Y. Shin, K.-P. Kim, and K.-Y. Lee, "Effect of layer thickness setting on deposition characteristics in directed energy deposition (DED) process," *Optics & Laser Technology*, vol. 86, pp. 69–78, 2016.

[89] D. R. Feenstra, A. Molotnikov, and N. Birbilis, "Utilisation of artificial neural networks to rationalise processing windows in directed energy deposition applications," *Materials & Design*, vol. 198, 2021.

[90] R. M. Mahamood, "Effect of laser power and gas flow rate on properties of directed energy deposition of titanium alloy," *Lasers in Manufacturing and Materials Processing*, vol. 5, no. 1, pp. 42–52, 2018.

[91] R. Parekh, R. K. Buddu, and R. I. Patel, "Multiphysics simulation of laser cladding process to study the effect of process parameters on clad geometry," *Procedia Technology*, vol. 23, pp. 529–536, 2016.

[92] L. Tang, J. Ruan, R. G. Landers, and F. Liou, "Variable powder flow rate control in laser metal deposition processes," *Journal of Manufacturing Science and Engineering*, vol. 130, no. 4, Article ID 041016, 2008.

[93] Y. Huang, D. Wu, D. Zhao et al., "Process optimization of melt growth alumina/aluminum titanate composites directed energy deposition: effects of scanning speed," *Additive Manufacturing*, vol. 35, Article ID 101210, 2020.

[94] T. Bhardwaj and M. Shukla, "Laser additive manufacturing-directed energy deposition of Ti-15Mo biomedical alloy: artificial neural network based modeling of track dilution," *Lasers in Manufacturing and Materials Processing*, vol. 7, no. 3, pp. 245–258, 2020.

[95] R. Sivasubramani, A. Verma, G. Rithvik, U. Chadha, and S. Senthil Kumaran, "Influence on nonhomogeneous microstructure formation and its role on tensile and fatigue performance of duplex stainless steel by a solid-state welding process," *Materials Today Proceedings*, vol. 46, pp. 7284–7296, 2021.

[96] A. Sharma, A. Chouhan, L. Pavithran, U. Chadha, and S. K. Selvaraj, "Implementation of LSS framework in automotive component manufacturing: a review, current scenario, and future directions," *Materials Today Proceedings*, vol. 46, pp. 7815–7824, 2021.

[97] A. Raj, S. Ram Kishore, L. Jose, A. K. Karn, U. Chadha, and S. K. Selvaraj, "A survey of electromagnetic metal casting computation designs, present approaches, future possibilities, and practical issues," *The European Physical Journal Plus*, vol. 136, no. 6, pp. 704–733, 2021.

[98] K. Virmani, C. Deepak, S. Sharma, U. Chadha, and S. K. Selvaraj, "Nanomaterials for automotive outer panel components: a review," *The European Physical Journal Plus*, vol. 136, no. 9, pp. 921–929, 2021.

[99] T. Ghimire, A. Joshi, S. Sen, C. Kapruan, U. Chadha, and S. K. Selvaraj, "Blockchain in additive manufacturing processes: recent trends & its future possibilities," *Materials Today Proceedings*, vol. 50, pp. 2170–2180, 2022.

[100] T. Pati, S. Kabra, and U. Chadha, "Statistical quality study of the parts produced in an automobile industry: a daimler India case study," *IOP Conference Series: Materials Science and Engineering*, IOP Publishing, vol. 1206, no. 1, , Article ID 012022, 2021.

[101] M. Dharnidharka, U. Chadha, L. M. Dasari, A. Paliwal, Y. Surya, and S. K. Selvaraj, "Optical tomography in additive manufacturing: a review, processes, open problems, and new opportunities," *The European Physical Journal Plus*, vol. 136, no. 11, pp. 1133–1228, 2021.

[102] S. K. Selvaraj, A. Raj, M. Dharnidharka et al., "A cutting-edge survey of tribological behavior evaluation using artificial and computational intelligence models," *Advances in Materials Science and Engineering*, vol. 2021, Article ID 9529199, 17 pages, 2021.

[103] S. K. Selvaraj, A. Raj, R. Rishikesh Mahadevan, U. Chadha, and V. Paramasivam, "A review on machine learning models in injection molding machines," *Advances in Materials Science and Engineering*, vol. 2022, Article ID 1949061, 28 pages, 2022.

[104] U. Chadha, A. Abrol, N. P. Vora, A. Tiwari, S. K. Shanker, and S. K. Selvaraj, "Performance evaluation of 3D printing technologies: a review, recent advances, current challenges, and future directions," *Progress in Additive Manufacturing*, 2022, In press.

[105] U. Chadha, S. K. Selvaraj, H. Pant et al., "Phase change materials in metal casting processes: a critical review, and future possibilities," *Advances in Materials Science and Engineering*, vol. 2022, Article ID 7520308, 14 pages, 2022.

[106] U. Chadha, S. K. Selvaraj, A. K. Ravinuthala et al., "Bio-inspired techniques in freeze casting: a survey of processes, current advances, and future directions," *International Journal of Polymer Science*, vol. 2022, Article ID 9169046, 22 pages, 2022.

[107] A. Adefris, D. Desalegn, S. K. Selvaraj, V. Paramasivam, and U. Chadha, "Experimental investigation of sorghum stalk and sugarcane bagasse hybrid composite for particleboard," *Advances in Materials Science and Engineering*, vol. 2022, Article ID 1844004, 17 pages, 2022.

[108] T. Pereira, J. V. Kennedy, and J. Potgieter, "A comparison of traditional manufacturing vs additive manufacturing, the best method for the job," *Procedia Manufacturing*, vol. 30, pp. 11–18, 2019.

[109] M. Attaran, "The rise of 3-D printing: the advantages of additive manufacturing over traditional manufacturing," *Business Horizons*, vol. 60, no. 5, pp. 677–688, 2017.

[110] A. Ge, "What is additive manufacturing? https://www.ge.com/additive/additive-manufacturing.

[111] K. Stevenson, "How could additive manufacturing replace traditional manufacturing?," 2020, https://www.fabbaloo.com/news/how-could-additive-manufacturing- replace-traditional-manufacturing.

[112] American Manufacturing, "3D printing vs traditional manufacturing," 2015, https://www.marlinwire.com/blog/3d-printing-vs-traditional-manufacturing.

[113] S. Hochreiter, "The vanishing gradient problem during learning recurrent neural nets and problem solutions," *International Journal of Uncertainty, Fuzziness and Knowledge-Based Systems*, vol. 6, no. 2, pp. 107–116, 1998.

[114] U. Chadha, S. K. Selvaraj, N. Gunreddy et al., "A survey of machine learning in friction stir welding, including unresolved issues and future research directions," *Material Design & Processing Communications*, vol. 2022, Article ID 2568347, 28 pages, 2022.

[115] U. Chadha, S. K. Selvaraj, A. Raj et al., "AI-driven techniques for controlling the metal melting production: a review, processes, enabling technologies, solutions, and research challenges," *Materials Research Express*, vol. 9, no. 7, Article ID 072001, 2022.

[116] I. Sachdeva, S. Ramesh, U. Chadha, H. Punugoti, and S. Kumaran Selvaraj, "Computational AI models in VAT photopolymerization: a review, current trends, open issues, and future opportunities," in *Neural Computing and Applications*, Springer, Berlin, Germany, 2022.

Hindawi
Complexity
Volume 2022, Article ID 8298451, 13 pages
https://doi.org/10.1155/2022/8298451

Research Article

Optimal Decision-Making in Chinese Cross-Border Mergers and Acquisitions: A Perspective of Overbidding

Yanping Bao,[1,2] **Chan Lyu**,[1] **Xia Wu**,[3] **and Jun Lian**[3]

[1]*School of Business, Macau University of Science and Technology, Macau, China*
[2]*Chongqing Finance and Economics College, Chongqing 401320, China*
[3]*School of International Business and Management, Sichuan International Studies University, Chongqing 400031, China*

Correspondence should be addressed to Chan Lyu; chlyu@must.edu.mo

Received 9 May 2022; Accepted 12 September 2022; Published 27 September 2022

Academic Editor: Yu Zhou

Chinese domestic firms engage actively in the cross-border merger and acquisition (CBMA) markets, which are crucial in China's foreign investment economics. Acquisition premium has attracted stakeholders' attention to determine whether the CBMA decision is optimal. This study employs a novel model to assess decision-making efficiency by overbidding based on a profit maximization assumption. Based on the Chinese CBMA transaction data from 2009 to 2019 of Chinese acquiring firms, the descriptive analysis indicates the widespread overbidding phenomenon in Chinese CBMAs. Moreover, empirical findings reveal that SOEs (vs. non-SOEs) experience less overbidding among acquiring firms. This study also shows that firms from the high-tech industry tend to be less overbidding (more efficient) in the CBMAs' setting. The findings may have policy implications for China's outward investment efficiency.

1. Introduction

Chinese cross-border mergers and acquisitions (CBMAs) are important foreign investments, accounting for 58.6% of China's total outward foreign direct investment in 2019 [1]. Government policies such as "Going Out policy," "Five-Year Plans," and other supporting policies help to ensure the safeguard of Chinese investors and contribute to Chinese firms' dynamic engagement in CBMAs [2, 3]. Despite the increasing number and deal value of CBMAs announced in recent years, acquisition overpayment in merger and acquisition (M&A) transactions is another fascinating economic phenomenon, which attracts the attention of scholars and practitioners. Acquisition overpayment, also called acquisition premium or takeover premium, refers to the price offered to the target firm over its preacquisition price [4]. To account for the market anticipation of the pending offer, prior studies have commonly used the base price 42 trading days before the deal announcement. For example, based on US stock market data, shreds of empirical evidence have shown that the average initial offer premium is 45% across the total sample with premium data [5]. The higher premium is more likely to be recognized in cross-border M&As (CBMAs) due to the higher transaction and negotiation costs and institutional differences [6]. Hope et al. documented the overpayment provided by firms from emerging markets from the perspective of national pride embedded in the management team [7]. The Chinese firms' active role in CBMAs activities is said to "never beat on willingness to pay for a target" (The Economist, 2010), and they tend to pay a higher premium than other acquirers from developed countries [8].

Some scholars try to explain the premium phenomenon of Chinese CBMAs from the perspective of state-owned equity nature [8, 9], arguing that state-owned enterprises (SOEs) pay higher acquisition premiums due to financial and policy support from the government and inefficiency in financial management. However, overpayment does not necessarily mean value-destroying or inefficiency in the decision-making process of CBMAs, as long as the shareholder's profits are maximized.

The innovation-driven CBMAs taken by Chinese firms are encouraged by the Chinese government to improve the domestic firms' innovative capability [10]. Bidding costs rise due to the sensitivity of advanced technology in the high-tech industry. Furthermore, due to the increased complexity of the deals, the information asymmetry between acquirers and targets in high-tech industries may be more severe in cross-border settings, resulting in overpayment by target firms. Chinese firms are regarded as late entrants in science development and innovative technologies [11], and Chinese acquiring firms are motivated by innovative capability at the expense of higher bidding prices. However, whether the bidding decision-making is optimal when acquiring firms from high-tech industries remains unclear.

This study examines whether the decision-making of Chinese CBMAs is relatively optimal from the perspective of overbidding, based on the first-order condition (FOC) of the acquirer's expected profit maximization [12]. In the complex economic environment, decision-makers often encounter problems of optimization. Existing studies developed an algorithm to help to derive Pareto set by minimizing the uncertainty in the complex process [13, 14], while this paper focuses on the single objective optimization considering profit maximization. In our paper, the measure of overbidding takes into account both the probability of the M&A's success and the acquirer's abnormal return. To measure overbidding, we first estimated the probability of acquisition success using CBMA transactions of completed and uncompleted ones. The bidder's profit is then the abnormal returns over the transaction's acquisition cost (proxied by the premium). In the empirical test, the bidder's profit is calculated as the cumulative abnormal returns (CARs) scaled by the probability of acquisition success [15]. If the FOC equals 0, a maximized profit is realized by taking a partial derivative of the bidder's profit for the bid premium. Overbidding is then measured as the FOC of the bidder's profit, with a negative value indicating that the pricing decision is overbidding. To make it easier to interpret overbidding, we transform the process of overbidding by multiplying −100 [16].

Based on the Chinese CBMA data from 2009 to 2019 of Chinese listed acquiring firms, the empirical results show that the overbidding phenomenon is pervasive among Chinese acquiring firms engaged in CBMAs. When the acquiring firms are grouped into SOEs and non-SOEs, the overbidding is notably more severe in non-SOEs. A different-in-different (DID) method is further applied to examine whether the institutional environment change plays a role in overbidding. The evidence shows that the efficiency of a bidding strategy in SOEs is more optimal than in nonSOEs. An interesting finding is that the bidding decisions in CBMA deals by high-tech firms tend to be more optimal, regardless of whether the bidder or the target firm belongs to the high-tech industry.

This study contributes to the Chinese CBMA literature from the perspective of overbidding based on the theory of optimal decision-making. Previous studies have examined the premium phenomenon of Chinese acquiring firms, whereas this study extends this line of literature more comprehensively to obtain a better understanding of Chinese outward investment efficiency. The findings on the state-ownership nature's effect on overbidding, which is inconsistent with previous findings [8], suggest that the efficiency of SOEs in overseas investment deserves further research as the institutional environment is changing.

The remainder of this paper is organized into the following sections: Section 2 provides a review of the related literature on overbidding, and Section 3 develops the hypothesis. Section 4 summarizes the sampling procedure, statistics, and overbidding measurement. Section 5 delves into the empirical findings. Section 6 provides further analysis. Finally, Section 7 concludes the paper.

2. Literature Review

An extensive body of research has explored the economic phenomenon of acquisition premiums in M&A activities. One stream of the literature focuses on the determinants of overpayment in CBMAs. The process of M&As, which involves various stakeholders such as acquirers, targets, intermediary parties, investors, and the government, is complex. Hence, prior studies have proposed different explanations to address why acquirers offer acquisition premiums, which is either irrational or inefficient decision-making.

2.1. Hubris or Overconfidence Hypothesis and Irrational Decision-Making. There is a significant body of literature on the acquisition premium from the standpoint of the top management team. The top management team is crucial in decision-making, especially for strategic decisions such as mergers and acquisitions (M&As). According to Hambrick and Mason upper echelons theory [17], the demographic traits of managers (e.g., gender, age, education background, and experience) influence a firm's strategic decisions. This research focuses on the ex-ante determinants of acquisition premium based on managers' personal characteristics. For example, Roll explained why bidding firms pay too much for their targets from the perspective of irrational behavior due to hubris, assuming that negative stockholder reaction indicates management hubris [18]. The irrational overbidding theoretical framework suggests that management's hubris and overconfidence cause the valuation error and result in acquirers overpaying for the target. This behavioral bias-driven overbidding is based on the assumption that people do not always make rational decisions, especially when faced with uncertainty. In the context of CBMAs, the acquirer management must exercise professional judgment and evaluate potential targets based on their experience and cognition. Other factors being equal, those managers with hubris and overconfidence in the bidding process for a potential target are more likely to make biased valuations and ignore the "winner's curse" [5, 12, 19].

Hayward and Hambrick further examined the hubris hypothesis by directly investigating the dynamics of managerial confidence [20], which reflects the individual bidder's decision process. Scholars have advanced this stream of

literature and extended our understanding of the role of management in the premium paid in M&A transactions. Overconfident CEOs overestimate their ability to gain synergies in M&A transactions and overpay for potential targets [21]. Another source of irrational behavior in strategic decision-making is CEO narcissism [17].

Scholars' attention has been drawn to firms from emerging markets that are actively engaged in CBMA transactions. A higher premium phenomenon has been observed in CBMAs of acquirers from developing countries targeting developed countries. In particular, Hope et al. [7] explained the phenomenon from a phycology standpoint, stating that national pride plays a role when acquirer managers consider the bidding premium decision. They contend that national pride can amplify the effects of individual pride, leading to a desire for pride in CBMA investment decisions.

2.2. Agency Theory and Inefficiency in M&A Strategic Decisions. Another well-accepted neoclassical theory that considers corporate governance is the agency theory [22]. The agency theory argues that managers may take advantage of the information asymmetry for their personal benefits or even make value-destroying strategic decisions. Intuitively, managers from acquiring firms and target firms may have an unequal information advantage, and the asymmetric bargaining power may result in different influences on the pricing negotiation process. Due to the conflicts between the principal and the agent, management (the agent) would be incentivized to make decisions that maximize their own interests at the expense of the shareholders (the principal). Moreover, managers may have an incentive to entrench when acquiring firms with rich internal resources, leading to rent-extracting behavior [18, 19, 23], especially when governance quality is poor. Meanwhile, managers from target firms may trade the premium in the M&A negotiation process for their post-M&A control rights in the newly merged firm, which could harm the target's shareholders [24]. In support of this claim, Qiu et al. presented evidence of a significant negative relationship between target CEO retention and takeover premium [25]. Jenter and Lewellen found that firms with retirement-age CEOs are more likely to be chosen as negotiation targets, arguing that these CEOs are more willing to accept takeover bids at their retirement age [26].

Either the hubris hypothesis or the agency conflict theory predicts that the shareholders' value will not be maximized. However, irrational behavior due to managers' hubris or overconfidence may differ from agency conflict theory in that managers may be acting in the best interests of their principals [21], even if their hubris reduces shareholder value. Meanwhile, the agency theory posits that agents may entrench for personal gain at the expense of their principals.

Several studies have been conducted based on the Chinese CBMAs setting to investigate the role of governance on acquisition from the perspectives of the principal-principal issue of governance [9], the efficiency of SOEs [8], and government involvement [27]. Chen and Young [9] specified that the Chinese government is the largest owner and has the controlling power to influence the firm's decisions based on the critical role of government ownership in Chinese public listed companies. In SOEs, this principal-principal governance conflict reduces the value of minority shareholders because the dominant owner is more likely to be motivated by political considerations rather than the firm's profit maximization.

In a similar vein, Guo et al. argued that the Chinese government, as the biggest shareholder in Chinese SOEs, plays an important role in CBMA transactions [8]. The Chinese government provides SOEs with preferential outward investment policy support, such as access to finance, interest subsidies, special fund projects, and tax privileges. The government's involvement indeed affects the CBMA activities of SOEs. Compared with non-SOEs, SOEs have the advantage of accessing CBMA transactions and the ability to pay a higher premium to beat rivals. The findings of the poor efficiency of Chinese SOEs' financial management in the CBMA call for further exploration. The authors argue that SOEs are the agents of the government and have the dual objectives of both social welfare and economic development. Moreover, management in SOEs is motivated to make decisions in favor of political benefits at the expense of the firm's profitability when the two objectives are in conflict. However, the two objectives might also be complementary because a well-developed economy can generate better social benefits, especially when managerial incentives change as the institutional environment changes.

The aforementioned studies have provided consistent evidence of the Chinese SOEs' inefficiency in CBMAs, assuming that the managers have self-incentives to conduct opportunistic behavior based on the traditional agency theory or that the dominant power from the controlling owner is more propolitically motivated. What other noneconomic motives may impact the decision-making process and the efficiency of Chinese SOEs in CBMAs remains unclear.

2.3. Stewardship Theory and Management Behavior in Decision-Making. Governance theories, such as the agency theory, assume that managers maximize their own self-interest; however, managers may be motivated by incentives other than monetary ones. Davis et al. proposed the stewardship theory [28], which challenges neoclassical economic theory and calls on researchers to pay attention to managers' personal needs, from social and psychological viewpoints. This theory questions agency theory's individualistic and financially self-interested assumptions [29]. It provides a dynamic perspective for understanding the role of managers' needs in the governance context, releasing the assumption of individualistic utility motivations in agency theory. Stewards prefer pro-organizational, collectivistic behaviors; hence, the nuanced view of treating managers as firm stewards may broaden our understanding of corporate governance. Traditional Chinese culture emphasizes collectivism and maintaining positive social relationships. For example, Confucian culture emphasizes the importance of stewardship and sustainable decision-making.

In the CBMA setting, the strategic decision-making of acquiring a potential target firm generally indicates the acquiring firm's goal of expanding or strengthening its competitive advantage. The acquiring firm's top management is in charge of strategic decision-making and implementation. The degree to which management's interests align with those of the firm has a significant impact on decision-making efficiency. In China, contemporary corporate managers have been educated with the socialist values of public service as the first and most valuable doctrine. Individuals in traditional Chinese culture are encouraged to engage in pro-organizational collectivist behavior rather than self-fulfilling individualistic behavior. Moreover, managers tend to take on the role of steward when their personal interests align with those of the company. Empirical evidence also suggests that the stewardship theory, rather than the agency theory, can better explain the situation of corporate governance in Chinese firms [30].

3. Hypothesis Development

3.1. Decision-Making Efficiency and Institutional Background. The ownership structure of Chinese public firms has improved as a result of the corporatization and privatization processes. However, the government still controls the majority of the shares in specific industries (e.g., natural resources, banking, and transportation) [31], indicating that the government continues to play a crucial role. Because of the highly concentrated ownership of Chinese listed firms, the agency conflict between management and shareholders may differ depending on the type of shareholder. Chen et al. proposed that the major agency conflict is between minority and controlling shareholders and their appointed managers [32]. The controlling shareholders' and managers' agency conflict is minimal. The controlling shareholders motivate managers to make corporate decisions that are aligned with the interests of the controlling shareholder. According to the institutional theory [33], formal social structures and informal cultural factors influence managers' behavior. From a cultural standpoint, China is known for embracing collectivist culture [34], which encourages people to prioritize group harmony and achievement over individual interests [35]. Based on the context of Chinese social development, managers in Chinese SOEs may act as stewards of controlling shareholders rather than merely as agents. The agency theory focuses on economic rewards, whereas the stewardship theory explains human behavior in a broader sense, in that stewards are motivated by nonfinancial goals in addition to basic financial needs from a firm [29]. The manager's behavior as a steward is more likely to be pro-organizational and responsible for the firm's best development. The rationale behind this is also intuitive; only a well-organized firm with promising growth development can secure individual needs. If the stewardship theory can explain the managers' behavior, Chinese SOE managers are expected to perform their duties. In the complicated CBMA transaction, which is more aligned with the strategic development at the country level, managers of SOEs may feel pride in fulfilling their goals. Furthermore, based on the favorable financial and other resource support from the government, SOEs enjoy the advantages of competing rivals in the CBMA transaction. Hence, if the stewardship theory holds, the decision-making efficiency of SOEs is better than that of non-SOEs in CBMAs. To obtain a better understanding of the decision-making efficiency, we must measure it by overbidding based on an optimal model [12].

The preceding argument leads to the following hypothesis:

> H1: the decision-making efficiency is relatively more optimal in SOEs than in non-SOEs in Chinese CBMA transactions.

3.2. Decision-Making Efficiency of CBMAs in the High-Tech Industry. Encouraged by the government's "Go Global" policy, Chinese firms have been actively engaged in CBMAs to seek advanced technology, knowledge, and managerial experience [36–38], which benefit the firm's sustainable development. For the acquirer, acquiring high-tech firms rather than developing the technology internally by themselves is more efficient [39], either because of the limited technical barriers or the high uncertainty of R&D, which is commonly time-consuming and costly.

However, due to the security sensitivity of high-tech industries, CBMA deals are more likely to be intervened by the native country's protectionists, increasing the costs for foreign firms to acquire targets with extensive knowledge and technological resources. The host country may be more active in intervening against foreign acquirers targeting firms in the high-tech industry, either by directly opposing the entry of foreign acquirers or by supporting domestic firms with competitive advantages to succeed in the bid. This is consistent with the viewpoint of economic nationalism [40], which refers to "the preference for natives over foreigners in economic activities."

Furthermore, the information asymmetry between acquirers and targets in high-tech industries may be more severe in cross-border settings due to the increased complexity of transactions. Seeking and assessing knowledge-based targets are expensive and frequently error-prone [41], resulting in an overpayment in most deals. Acquirers have less perfect information because of the tacitness of the knowledge resident in the targets; thus, the biased valuation may differ from the intrinsic value of the target firms. In the emerging markets, for example, China, acquirers do not have much bargaining power over the targets (especially high-tech firms) because Chinese firms are considered the latecomers in science development and innovative technologies [42, 43]. Therefore, targeting high-tech firms may require higher bidding prices.

Acquiring high-tech firms with advanced technology is expensive, and the potential synergies are expected to be value-enhancing; thus, managers have incentives to make efficient decisions. Meanwhile, managers are also under pressure if the acquisition price paid for the target is too high and the decision-making is damaging to shareholders' value. In this case, they would probably encounter the risk of losing their jobs. According to the stewardship theory, managers

can act as the shareholders' trusted agents and share the same interests as the shareholders. Moreover, managers have an incentive to actively participate in the due diligence process and negotiate a fair price, especially for CBMAs dealing with higher uncertainty. If the determined bidding price is higher than what the shareholders expected, they will make the best use of the acquisition to generate potential synergies and demonstrate that the investment is worthwhile by focusing on the optimal consideration. Therefore, although the bidding price for targets in high-tech industries may be higher, the decision-making process is more optimal.

SOEs receive more government support than non-SOEs in terms of outward investment, such as lower capital costs or state-funding guarantees [8]. The favorable policies, combined with ample financial support for SOEs, increase the chances of winning the CBMA deal. As the importance of the high-tech industry in economic and social development grows, SOEs in the high-tech industry are becoming one of the primary areas of government concern. In addition, the CBMA process is attracting the attention of all parties. In line with the stewardship hypothesis, the managers in SOEs are more likely to act with due diligence in the best interest of the controlling shareholder. Even if the agency conflict between the managers and the minority shareholders is inevitable, the decision-making process is less likely to be influenced by minority shareholders.

Based on these arguments, we propose the following hypotheses:

H2a: the overbidding of Chinese CBMAs is less pronounced in targets for high-tech industries

H2b: the overbidding of Chinese CBMAs is less pronounced when the acquiring firm is from the high-tech industry

H2c: the overbidding of Chinese CBMAs is less pronounced when the high-tech acquiring firms are state-owned

4. Research Methodology

4.1. Measurement of Overbidding. Following De Bodt et al. [12] and Bartov et al. [16], this study measures the overbidding of the acquirer in CBMAs based on the assumption of value maximization. In a competitive market without transaction costs or agency conflicts, rational managers make optimal decisions to realize the shareholders' expectations of value maximization. The maximization of a CBMA transaction is stated as follows:

$$\max_{bid} E(\text{Bidder's Profit}) = \Pr(\text{Success}) \times E(\text{Synergy} - \text{Bid Premium}|\text{Success}), \tag{1}$$

where Pr (.|.) is the probability function and E (.|.) is the expectation on condition. Specifically, Pr (Success) is the probability of a completed acquisition, and E (Synergy-Bid_Premium | Success) is the expected net profit from a successful acquisition. The bid premium is the value overpaid to the target firm.

According to the mathematical condition for optimization, for obtaining maximization of the bidder's profit, the FOC should be satisfied. In other words, the first derivative of (1) is zero. Given that Pr (Success) and E (Synergy-Bid_Premium | Success) are functions of bid premium, the corresponding FOC of (1) is derived by taking the partial derivative with respect to bid premium.

$$\begin{aligned} FOC = \frac{\partial E(\text{Bidder's Profit})}{\partial \text{Bid}} &= \frac{\partial \Pr(\text{Success})}{\partial \text{Bid}} \\ &\times E(\text{Snergy} - \text{Bid Premium}|\text{Success}) \\ &+ \Pr(\text{Success}) \\ &\times \frac{\partial E(\text{Synergy} - \text{Bid Premium}|\text{Success})}{\partial \text{Bid}} \\ &= \alpha \times E(\text{Snergy} - \text{Bid Premium}|\text{Success}) \\ &+ \beta \times \Pr(\text{Success}), \end{aligned} \tag{2}$$

where α denotes $\partial \Pr(\text{Success})/\partial \text{Bid}$, indicating the effect of one unit change in the bid premium on the changes in the success probability. α is predicted to have a positive sign because the probability increases as the bid premium increases. β denotes $\partial E(\text{Synergy} - \text{Bid Premium}|\text{Success})/\partial \text{Bid}$, and it is expected to have a negative sign because the net profit will decrease as the bid premium increases. A zero value of FOC denotes an optimal bidding decision to maximize the bidder's profit. Accordingly, a positive value of FOC indicates underbidding, whereas a negative value of FOC shows overbidding. To estimate FOC, this study follows De Bodt et al.'s way of estimating α and β by using the following two equations (17):

$$\Pr(\text{Success}) = \alpha_0 + \alpha_1 \times \text{Bid Premium} + \sum \text{Control} + \varepsilon_1, \tag{3}$$

$$\text{Bidder's Profit} = \beta_0 + \beta_1 \times \text{Bid Premium} + \sum \text{Control} + \varepsilon_2. \tag{4}$$

The error terms of ε_1 and ε_2 are potentially correlated. As the independent variables on the right-hand side of (3) and (4) are the same, the estimation should apply seemingly unrelated regression (SUR), (in a multivariate regression model, the errors in different equations might be correlated. Here, the efficiency of the estimation can be improved by considering these cross-equation correlations. Like OLS, the seemingly unrelated regression (SUR) method assumes that all regressors are independent variables, but SUR uses the correlations among the errors in different equations to

Table 1: Variables and definitions.

Variables	Definition
Premium	Takeover premium = (Transaction deal value − Target's market value of equity)/Target's market value of equity
Cash_payment	Dummy variable equals 1 if the CBMA deal is paid in cash
Target_size	Target's total assets before the CBMA announcement (logarithm is used in regression)
Target_turnover	Target's total revenue before the CBMA announcement (logarithm is used in regression)
Target_ROA	Target's net profit divided by its total assets before the CBMA announcement
Target_lev	Target's total liability is divided by its total equity
Target_hightech	Dummy variable equals 1 if the target firm is from the high-tech industry
Acquirer_size	Acquirer's total assets before the CBMA announcement (logarithm is used in regression)
Relative_size	Target size divided by the acquirer size
Acquirer_listed	Dummy variable equals 1 if the acquirer is a public listed company and 0 otherwise
Acquirer_hightech	Dummy variable equals 1 if the acquiring firm is from high-tech industry
Toehold	Dummy variable equals 1 if the acquirer holds a nonzero percentage of the target's shares before the announcement and 0 otherwise
Final_control	Dummy variable equals 1 if the acquirer holds a percentage of the target's share greater than 51% after the M&A deal and 0 otherwise
Horizontal	Dummy variable equals 1 if the target and acquirer are from the same industry and 0 otherwise
GDP	Nominal GDP in US$ translated using purchasing power parity exchange rates, divided by population (logarithm is used in regression)
TFP_FAPG	Total factor productivity is part of economic output, calculated by dividing GDP growth by employment growth and estimated growth in the capital stock
Export	Exports of goods and services at constant market prices of a country, rebased to 2010 constant prices and translated into US$ using the local currency unit:$ exchange rate in 2010 (logarithm is used in regression)
LogDistance	Geographical distance between the capital cities of the acquiring and target countries (logarithm is used in regression)

improve the regression estimates) which is the simplification of the general linear model. $\widehat{\alpha_1}$ is the estimate of $\partial \Pr(\text{Success})/\partial \text{Bid}$ and $\widehat{\beta_1}$ of $\partial E(\text{Synergy}-\text{Bid Premium}|\text{Success})/\partial \text{Bid}$.

The bidder's profit is calculated using CARs scaled by the probability of success, as described by Bhagat et al. [15]. CARs are based on a three-day event window that captures market reactions to CBMA announcements [44]. The abnormal return (AR) is the difference between the actual stock return and the estimated expected stock return based on Brown and Warner's standard market model [45]. Specifically, in equations (5) and (6), R_{it} is the actual daily stock return of firm i on day t, and R_{mt} is the market daily return from the Shanghai stock exchange composite index and Shenzhen stock exchange composite index. AR_{it} is the AR of firm i on day t, calculated by the estimated γ_i and φ_i. The coefficients γ_i and φ_i are estimated from the OLS regression of R_{it} on R_{mt}. CAR_t is then calculated as the sum of the cumulated AR for the period of day −1 to day +1.

$$R_{it} = \gamma_i + \varphi_i \times R_{mt} + \varepsilon, \tag{5}$$

$$AR_{it} = R_{it} - \left(\widehat{\gamma} + \widehat{\varphi} \times R_{mt}\right), \tag{6}$$

$$\text{CAR}_t = \sum_{t=1}^{n} AR_t. \tag{7}$$

4.2. Regression Model. Model (8) is designed to examine whether the state-ownership nature matters in the decision-making efficiency in Chinese CBMAs, with overbidding as the dependent variable, SOE as the main explaining variable (independent variable), and a set of control variables.

$$\begin{aligned}\text{Overbidding}_{it} = {} & \mu_0 + \mu_1 SOE_{it} + \gamma \sum \text{Deal level Control} \\ & + \delta \sum \text{Firm level Control} \\ & + \omega \sum \text{Coutry level Control} \\ & + \text{Year} + \text{Industry} + \varepsilon_i.\end{aligned} \tag{8}$$

Overbidding is the FOC described in the previous section. The dummy variable SOE_{it} takes the value of 1 if the acquiring firm is owned by the state and 0 otherwise. Table 1 defines the other variables in the model.

Model (9) is designed to test whether high-tech target firms with innovative capacity require higher overbidding.

$$\begin{aligned}\text{Overbidding}_{it} = {} & \delta_0 + \delta_1 \text{High Tech}_{it} + \delta_2 SOE_{it} \\ & + \delta_3 SOE \times \text{High Tech}_{it} \\ & + \omega \sum \text{Control} + \text{Year} + \text{Industry} + \varepsilon_i.\end{aligned} \tag{9}$$

Overbidding is the FOC described in the previous section. The dummy variable High Tech_{it} takes the value of 1 if a firm is from high-tech industries and 0 otherwise. The other variables in the model are defined in Table 1.

4.3. Sampling Procedure and the Overbidding Measurement

4.3.1. Sampling Procedure for Estimating the Success Probability of a CBMA. To estimate the probability of success in CBMAs, we collected a sample of 3,586 Chinese CBMA deals targeting member countries of the Organization for Economic Co-operation and Development (OECD) from 2009

Table 2: Sampling procedure for estimating the probability of success.

Cross-border mergers and acquisitions deals on and after January 1, 2009, and up to December 31, 2019, with the acquirer originating from China and the targets' countries from members of the Organization for Economic Co-operation and Development (OECD)	3,586
Less acquirer from banking, insurance, and other financial industry sectors	(1,602)
	1,984
Less missing financial or other deal information observations	(896)
	1,088

Data source: the cross-border merger and acquisition data are from the Zephyr database.

to 2019. Table 2 reports a summary of the sampling procedure.

4.3.2. Estimating the Probability of Acquisition Success. Using the 1,088 observations of Chinese CBMA transactions (with both completed and uncompleted deals), logistic regression is applied to estimate the probability of acquisition success. Table 3 reports the logistic regression results. Based on the regression coefficients, the predicted probability of the success of each CBMA is then calculated.

4.3.3. Sampling Procedure for Estimating the Bidder's Profits and the Measurement of Overbidding. In this section, observations of completed CBMAs are selected in regression because only completed CBMAs yield the bidder's profit.

The data used in this section are sampled as follows, with a detailed sampling procedure reported in Table 4.

From 2009 to 2019, 291 of the 1,088 samples of total Chinese CBMAs targeting OECD members were uncompleted. We obtained a sample of 346 observations for the empirical test after removing 290 observations with unlisted acquiring firms and 161 observations with missing data.

The bidder's profit is calculated by multiplying CAR by the estimated profitability of acquisition success from the previous section. The CARs are based on a three-day event window that captures market reactions to the CBMA announcement. Due to data availability, we estimated the CARs of the acquiring firms using the listed acquiring firms' stock returns and other financial data from the China Stock Market and Accounting Research Database (CSMAR).

4.3.4. Descriptive Statistics of Main Variables Used in SUR Regression for Estimating Overbidding. Table 5 presents the descriptive statistics of the main variables in the regression models (3) and (4).

4.3.5. SUR Regression Results. The regression estimation of (3) and (4) is obtained using the SUR procedure. The dependent variable in column (1) is the predicted probability of success and that in column (2) is the bidder's profits. The two key coefficients of interest are the coefficients on premium: $\widehat{\alpha}_1$ is the estimate of $\partial \Pr(\text{Success})/\partial \text{Bid}$ and $\widehat{\beta}_1$ of $\partial E(\text{Synergy} - \text{Bid Premium}|\text{Success})/\partial \text{Bid}$

Table 3: Logistic regression results in the probability of acquisition success.

Variables	Coefficients
Intercept	28.8620** (16.3420)
Premium	0.1365 (0.1439)
Cash_payment	−0.1381 (0.4966)
Toehold	−0.7451 (0.6350)
Horizontal	−0.3473 (0.4295)
Final_control	−1.9143*** (0.5816)
Target_Hightech	−0.3259 (0.5297)
Target_patent	0.0322 (0.1073)
Target_size	−0.6203** (0.3426)
Target_ROA	−0.3684 (0.5611)
Target _LEV	0.8450 (0.8860)
Acquirer_size	−0.8300*** (0.3134)
Acquirer_list	−0.3542 (0.4721)
GDP	−6.5926 (3.7833)
TFP_FAPG	0.3207 (0.2849)
Export	0.8058*** (0.2990)
LogDistance	2.3290** (1.3716)
No. of observations	1,088
Hosmer and Lemeshow test chi-square (pr > ChiSq)	8.4478 (0.3910)

Note. The dependent variable (success) is a dummy variable, with the value of 1 if the CBMA deal is finally completed and 0 otherwise. Standard errors are in parentheses; ***, **, and *indicate significance at 1%, 5%, and 10% levels, respectively.

$$\Pr(\text{Success}) = \alpha_0 + \alpha_1 \times \text{Bid Premium} + \sum \text{Control} + \varepsilon_1, \tag{10}$$

$$\text{Bidder's Profit} = \beta_0 + \beta_1 \times \text{Bid Premium} + \sum \text{Control} + \varepsilon_2. \tag{11}$$

The estimated $\widehat{\alpha}_1$ is significantly negative at the 1% level; however, it is inconsistent with the previous literature [12, 16]. Previous research suggests that the premium should be positively related to the probability of success. It turns out to be the opposite in this study. One possible explanation is that sample sources and size in Chinese CBMAs differ from those in other developed economies. The other factor could be the particular institutional

Table 4: Sample for estimating the bidder's profit.

Items	Number of deals
Cross-border merger and acquisition deals on and after January 1, 2009, and up to December 31, 2019, with the acquirer originating from China and the targets' countries from members of the Organization for Economic Co-operation and Development (OECD)	1,088
Less: uncompleted deals	(291)
Less: unlisted acquiring firms	(290)
Less: observation with missing data	(161)
	346

Data source: the cross-border merger and acquisition data are from the Zephyr database. The financial data and stock return data are from the China Stock Market and Accounting Research Database (CSMAR).

Table 5: Summary statistics.

Variables	Min	P25	Mean	Median	P75	Max	St. dev
Bidder's CAR	−0.2308	−0.0156	0.0092	0	0.0267	0.4247	0.0662
Probability of acquisition success	0.1646	0.6169	0.7156	0.7492	0.8531	0.9713	0.1783
Bidder's profit	−0.0857	−0.0102	0.00847	0	0.0146	0.2744	0.0492
Premium	−0.00001	−0.000012	0.4272	9.35E-7	0.3816	5.8334	0.9132

Table 5 reports the summary statistics of three main variables in SUR regression models (3) and (4). The sample size comprised 346 Chinese completed CBMAs. Bidder's CAR measures the bidder's abnormal returns in the [−1, +1] window around the CBMA announcement. The probability of acquisition success is the predicted probability of transaction completion. The bidder's profit is measured as the bidder's CAR is scaled by the estimated probability of success. Premium denotes the percentage of excess transaction deal value over the target's market value of equity relative to the target's market value of equity.

Table 6: SUR regression results of estimating the probability of acquisition success and the bidder's profit.

Variables	(1) Dependent variable: probability of success	(2) Dependent variable: bidder's profit
Intercept	−0.5844 (−1.23)	1.03691 (1.57)
Premium	**−0.02387 *** (−4.37)**	**−0.00385 (−0.51)**
Cash_payment	0.1174*** (9.22)	−0.02285 (−1.29)
Toehold	−0.0579*** (−4.33)	−0.0238 (−1.29)
Horizontal	0.0031 (0.27)	0.0059 (0.38)
Final_control	−0.1645*** (−11.84)	−0.0464** (2.40)
Target_size	−0.1996*** (−3.25)	0.14462* (1.69)
Target_Hightech	−0.08948*** (−7.20)	−0.01365 (−0.79)
Target_patent	−0.00399 (−1.16)	−0.0109** (−2.30)
Target_ROA	−0.03535** (−2.22)	−0.04454* (2.01)
Target _LEV	0.0661** (2.29)	0.0219 (0.55)
Acquirer_size	0.0105 (0.20)	−0.14108* (1.97)
RelativeSize	0.7517** (2.01)	−0.9646* (−1.85)
GDP	0.3039*** (3.54)	−0.00715 (−0.06)
TFP_FAPG	0.02467*** (3.63)	−0.00184 (−0.19)
Export	0.03534*** (5.17)	0.0033 (0.35)
LogDistance	0.0444 (1.33)	−0.02916 (−0.63)
No. of observations	346	346
Adj R^2	0.9513	0.023

Table 6 summarizes the estimation results of (3) and (4) for calculating overbidding. T-statistics are in parentheses. ***, **, and *indicate significance at 1%, 5%, and 10% levels, respectively. The regression estimation is obtained using the SUR procedure. The dependent variable in column (1) is the probability of success and that of column (2) is the bidder's profits. The two key coefficients of interest are the coefficients on premium: $\hat{\alpha}_1$ is the estimate of $\partial \Pr(\text{Success})/\partial \text{Bid}$ and $\hat{\beta}_1$ of $\partial E(\text{Synergy} - \text{Bid Premium}|\text{Success})/\partial \text{Bid}$.According to the research data we collected, we did not find significance for the regression coefficient of Premium in Column (2). The T-statistics (−0.51) are reported in parentheses.

context of China's transitional economy. In general, the higher the premium paid by the acquirer, the greater the likelihood of success. However, when a firm from an emerging market acquires targets from well-developed economies, the higher premium paid by the acquirer indicates that the target firm is crucial for the acquiring firm's development. Whether it is technology-oriented or resource-driven, the CBMA deals may probably be intervened by the target regulators, and the probability of success may be negatively influenced. The estimated $\hat{\beta}_1$ is negatively related to the bidder's profits, as expected; however, it is not significant.

Table 7: Summary of the statistics of the first-order condition test.

Variable	Min	P25	Mean	Median	P75	Max	Std
FOC	−0.0230	−0.0203	−0.0171	−0.0178	−0.0146	−0.0039	0.0042

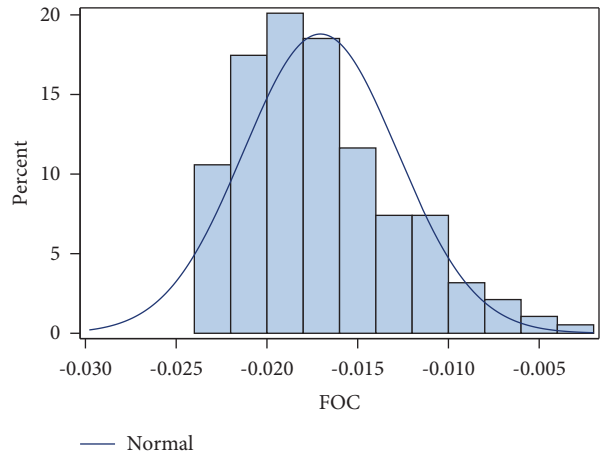

Figure 1: Histogram of the first-order condition test.

Table 8: Difference in premiums and overbidding between SOEs and non-SOEs.

	N	Mean of premium	Difference	*T*-test (Pr > |*t*|)
SOEs	92	0.5469	0.163	1.47 (0.1428)
Non-SOEs	254	0.3839		
	N	Mean of overbidding	Difference	*T*-test (Pr > |*t*|)
SOEs	92	1.5297	−0.2338***	3.36 (0.0009)
Non-SOEs	254	1.7635		

Note. The premium is the percentage of the transaction deal value over the target's market value of equity, and overbidding is calculated by −100 multiplied by FOC, assuming the maximization of the bidder's profits. ***, **, and *indicate significance at 1%, 5%, and 10% levels, respectively.

$$\Pr(\text{Success}) = \alpha_0 + \alpha_1 \times \text{Bid Premium} + \sum \text{Control} + \varepsilon_1, \tag{12}$$

$$\text{Bidder's Profit} = \beta_0 + \beta_1 \times \text{Bid Premium} + \sum \text{Control} + \varepsilon_2. \tag{13}$$

4.3.6. Overbidding Measurements. To obtain the FOC, we estimated the coefficients of α and β in (3) and (4) using the SUR method. The overbidding is then calculated as follows:

$$\text{FOC} = \widehat{\alpha_1} \times \text{Probability of Success} + \widehat{\beta_1} \times \text{Bidder's Profit}. \tag{14}$$

As a negative value of FOC indicates overbidding, in the empirical testing, the FOC is multiplied by −100. That is, the higher the value, the more overbidding and inefficiency it represents. Thus, overbidding = $(-100)_{\times \text{FOC}}$.

Table 7 presents the summary of the FOC test, and Figure 1 displays the histogram for 346 transactions included in the sample. The descriptive statistics indicate that all transactions tend to be overbidding as the values of FOC are negative, and they are centered in the range of [−0.025, −0.01]. In terms of profit maximization, the bidding strategies of these transactions in the sample period are not optimal (overbidding) because the FOC is negative.

Based on the assumption of the bidder's expected profit maximization, FOC denotes the marginal change in the bidder's profit given one unit change in bid premium [12]. Negative FOC values indicate overbidding, whereas positive values indicate underbidding.

5. Results

5.1. Difference in Premium and Overbidding Based on the T-Test. Table 8 provides the difference in premium and the overbidding of both SOEs and non-SOEs. Interestingly, the premium paid in the CBMA transaction is higher in SOEs on average, but the difference between SOEs and non-SOEs is not significant. However, the mean of overbidding is lower in SOEs, and it is significantly different from that of non-SOEs, which provides some evidence that the efficiency of SOEs in CBMAs is better than that of non-SOEs.

Table 9: Regression results.

Variables	(1)	(2)	(3)	(4)	(5)	(6)
Intercept	−0.53 (1.20)	−0.378 (−0.28)	−0.372 (−0.27)	−0.567 (−0.61)	−0.704 (−0.76)	−0.635 (−0.67)
SOE	−0.12*** (−2.79)	−0.13*** (−3.07)	−0.124** (−2.58)		−0.046* (−1.65)	−0.0429 (−1.47)
Target_hightech		−0.105** (−2.47)	−0.09** (−2.08)			
SOE ∗ Target_hightech			−0.058 (−0.55)			
Acquirer-hightech				−0.07*** (−2.65)	−0.08*** (−2.92)	−0.07*** (−2.63)
SOE ∗ Acquirer_hightech						−0.042 (−0.38)
Cash_payment	0.31*** (8.22)	0.32*** (8.53)	0.32*** (8.53)	0.29*** (13.17)	0.29*** (13.07)	0.29*** (12.89)
Horizontal	0.015 (0.39)	0.018 (0.47)	0.018 (0.45)	−0.04 (−1.65)	−0.038 (−1.56)	−0.036 (−1.48)
Toehold	−0.18*** (−3.97)	−0.19*** (−4.16)	−0.19*** (−4.19)	−0.13*** (−4.65)	−0.12*** (−4.42)	−0.12*** (−4.43)
Final_control	−0.27*** (−5.55)	−0.28*** (−5.97)	−0.28*** (−5.94)	−0.30*** (−10.7)	−0.29*** (−10.5)	−0.29*** (−10.44)
Target_turnover	−0.29*** (−11.75)	−0.29*** (11.96)	−0.29*** (−11.95)	−0.10*** (−5.72)	−0.10*** (−4.12)	−0.10*** (−5.58)
Target_ROA	−0.012 (−0.33)	0.006 (0.18)	0.007 (0.19)	−0.07*** (−3.47)	−0.07*** (−3.42)	−0.07*** (−3.43)
Target _LEV	−0.09 (−1.54)	−0.087 (−1.42)	−0.088 (−1.42)	0.12*** (3.11)	0.118*** (3.42)	0.121*** (3.10)
Relative_size	0.222 (1.50)	0.191 (1.31)	0.193 (1.32)	0.77** (1.81)	0.907** (2.09)	0.87** (1.98)
GDP	0.53 (1.63)	0.521 (1.63)	0.517 (1.61)	0.65*** (3.37)	0.66*** (3.46))	0.65*** (3.37)
TFP_FAPG	0.04 (1.36)	0.05 (1.55)	0.05 (1.58)	0.03** (1.88)	0.03** (1.79)	0.033** (1.78)
Export	0.07*** (2.91)	0.08*** (3.31)	0.08*** (3.29)	0.07*** (4.79)	0.068*** (4.79)	0.069*** (4.79)
LogDistance	0.168 (1.51)	0.145 (1.32)	0.149 (1.35)	0.189*** (2.91)	0.17*** (2.62))	0.169** (2.57)
Year fixed	Yes	Yes	Yes	Yes	Yes	Yes
Industry fixed	Yes	Yes	Yes	Yes	Yes	Yes
R-square	0.766	0.775	0.775	0.921	0.922	0.922
No. of observations	346	346	346	346	346	346

Note. The dependent variable is overbidding. *T*-values are in parentheses. ***, **, and *indicate significance at 1%, 5%, and 10% levels, respectively.

Table 10: Difference-in-difference regression results.

Variables	Coefficients
Intercept	−0.7443 (1.2789)
SOE	−0.1752** (0.0847)
POST	−0.0003 (0.059)
SOE ∗ POST	0.0522 (0.0976)
Cash_payment	0.3047*** (0.0371)
Toehold	−0.1979*** (0.0450)
Horizontal	0.0205 (0.0348)
Final_control	−0.2815*** (0.0460)
Target_turnover	−0.2939*** (0.0234)
Target_ROA	0.0042 (0.0331)
Target_LEV	−0.1012* (0.0612)
Relative_size	0.2059 (0.1377)
GDP	0.5512* (0.3002)
TFP_FAPG	0.0707*** (0.0211)
Export	0.0870*** (0.0225)
LogDistance	0.1498 (0.1080)
No. of observations	346

Note. The dependent variable is overbidding. Standard errors are in parentheses. ***, **, and *indicate significance at 1%, 5%, and 10% levels.

5.2. Regression Results. Table 9 summarizes the regression results in testing H1 and H2.

Column (1) summarizes the findings regarding the relationship between overbidding and the nature of state-ownership. After controlling for deal-level, firm-level, and country-level variables, we determined that the coefficient is negatively related to overbidding and significant at the 1% level. The findings show that the overbidding in CBMA deals of acquiring firms that are SOEs is lower than non-SOEs. In other words, SOEs are more efficient than non-SOEs, thus providing empirical evidence to support H1.

We then test whether the overbidding phenomenon is clearer when the Chinese acquiring firms target firms in the high-tech industry. Due to the increased complexity in the high-tech firm's valuation, the target firm likely requires a higher payment. However, a higher premium paid does not necessarily lead to inefficiency in the pricing decision-making.

Except in column (6), the coefficient of SOE is significantly negative to overbidding, indicating that bidding efficiency in SOEs is higher than in non-SOEs, which is consistent with the results in the previous section. The negative coefficient of Target_hightech is significant at the 5% level in columns (2) and (3), indicating that when Chinese firms target high-tech firms overseas, the bidding strategy is more optimal. The findings support the argument that acquirer management is sensitive to high-tech targets, and it strives to maximize the target's technology and knowledge to achieve potential synergy. Hence, H2a is supported.

Examining whether the acquired firms from the high-tech industry have the same effect is interesting. In columns (4)–(6), the results show analogical negative coefficients on Acquirer_hightech at the 1% significance level. When the acquiring firms belong to the high-tech industry, the bidding strategy tends to be optimal, probably due to the realized potential merging synergy. Again, this evidence supports the hypothesis that the overbidding of Chinese CBMAs is lower when the acquiring firm is from the high-tech industry.

When state-owned equity is considered, as proposed in the previous section, the effects of the high-tech industry may be exacerbated because state-owned high-tech firms are one of the critical focus areas. The government attaches great importance to the development of high-tech firms to improve the country's competitiveness in the international market and the stability of its economic growth. The results of the interaction of SOE and high-tech are negative, as expected, but they are not statistically significant in empirical testing.

6. Further Analysis: Difference-In-Difference (DID) Analysis of the Corporate Governance Reform on SOEs

To obtain a better understanding of the institutional environment in China, we further analyze whether the corporate governance reform in SOEs impacts the efficiency of the CBMA transaction decision-making. In the theoretical framework of the stewardship theory, managers of the firm act as stewards who make decisions that maximize the firm value. In the previous section, we find supporting evidence of the stewardship theory in explaining the efficiency of Chinese CBMAs' decision-making. We used an exogenous shock of the anticorruption campaign in 2013 to apply a DID analysis and examine whether governance reform matters in efficient decision-making.

The Communist Party of China issued "Rule 18" in October 2013, with the goal of reducing corruption between businesses and officials by requiring party and government officials to resign from enterprises. Prior to this rule, many Chinese SOE managers were appointed by the government and were more sensitive to their political careers. Managers of SOEs are more likely to build their empires through firm expansion or overinvestment. The Chinese government's anticorruption campaign demonstrates its desire to improve governance quality, which may result in a better institutional environment and benefits for long-term economic development. Research based on China's anticorruption campaign has shown that it does improve internal corporate governance in SOEs at the firm level [46]. However, whether the anticorruption campaign's improved corporate governance has an impact on decision-making in the context of Chinese CBMAs has not yet been fully understood. According to the stewardship theory, management in Chinese SOEs is more likely to be pro-organizational and responsible for the firm's best development.

The DID regression results are shown in Table 10. The SOE coefficient is negatively related to overbidding and significant at the 5% level, indicating that overbidding is lower in SOEs than in non-SOEs. In other words, SOEs have higher bidding efficiency. However, the coefficients of POST and the interaction term of SOE ∗ POST are not significant, indicating that the efficiency of a CBMA transaction bidding strategy has not changed significantly in SOEs since the 2013 anticorruption campaign. This finding contrasts with

previous studies [8, 9] that found the inefficient performance of SOEs based on the agency theory. As society and corporate ownership change, the role of managers in SOEs should be reconsidered. The stewardship theory offers a novel perspective on whether managers in SOEs serve as stewards of shareholders rather than as agents focused on economic rewards. If stewardship plays an important role, the efficiency of corporate performance is unlikely to be impacted by the anticorruption campaign, which improves transparency and governance quality. The insignificant coefficients of the interaction term of SOE ∗ POST in DID regression results confirm this argument, providing further evidence of the explaining power of stewardship theory in Chinese CBMA decision-making efficiency.

7. Conclusion

The phenomenon of acquisition premium has piqued the interest of academics and practitioners, with a focus on why it occurs and how it may affect firm value. This study adds to the literature on the phenomenon by employing a novel model to assess overbidding in Chinese CBMAs, focusing on optimal decision-making. In response to the overbidding phenomenon, descriptive statistics results indicate that overbidding is prevalent in Chinese CBMA transactions during the sample period from 2009 to 2019. Interestingly, compared with non-SOEs, SOEs experience less overbidding, and the decision-making is relatively more optimal. This finding is inconsistent with previous empirical results of Chinese SOEs' inefficient performance due to agency conflicts and poor corporate governance. The phenomenon is explained by the stewardship theory, which posits that managers in SOEs are stewards rather than agents who focus solely on economic rewards. Empirical evidence also suggests that firms in the high-tech industry are less likely to overbid.

In a subsequent analysis, this study examines whether the role of state-ownership has an impact on the overbidding of the CBMAs transaction within the changing institutional environment, using the exogenous shock of the Chinese government's anticorruption campaign in 2013. The DID analysis shows that governance reform in SOEs has no significant effect on CBMA decision-making efficiency, confirming the explanatory power of stewardship theory.

This study contributes to the Chinese CBMAs' literature on the overbidding phenomenon by providing evidence of the various overbidding of Chinese SOEs and non-SOEs' CBMAs transactions, focusing on optimal decision-making. Furthermore, from a theoretical perspective, the stewardship theory used to explain the efficiency of SOEs broadens our understanding of corporate governance. The findings may have policy implications for China's outward investment policy, particularly in terms of improving the efficiency of foreign investment.

Data Availability

The data for the cross-border merger and acquisition is released from Zephyr database, and the acquiring firms' stock returns and other financial data are supplied by the China Stock Market and Accounting Research Database (CSMAR). Both databases are under license and cannot be made freely available without permission. The data used to support the findings of this study are available from the corresponding author upon request.

Conflicts of Interest

The authors declare that they have no conflicts of interest.

Acknowledgments

This work was supported by the Chongqing Federation of Social Science Planning Project (Grant number: 2021NDYB079).

References

[1] Unctad, *World Investment Report 2020*, UNCTAD, Geneva, Switzerland, 2020.

[2] J. Chaisse and K. F. Olaoye, "The tired dragon: casting doubts on China's investment treaty practice," vol. 17, no. 1, pp. 134–193, 2020.

[3] Q. Xu, "Scoping the impact of the Comprehensive Agreement on investment: liberalization, protection, and dispute resolution in the next era of EU–China relations," *Asia Pacific Law Review*, vol. 30, no. 1, pp. 93–122, 2022.

[4] T. Laamanen, "On the role of acquisition premium in acquisition research," *Strategic Management Journal*, vol. 28, no. 13, pp. 1359–1369, 2007.

[5] B. E. Eckbo, "Bidding strategies and takeover premiums: a review," *Journal of Corporate Finance*, vol. 15, no. 1, pp. 149–178, 2009.

[6] M. Maung, M. Shedden, Y. Wang, and C. Wilson, "The investment environment and cross-border merger and acquisition premiums," *Journal of International Financial Markets, Institutions and Money*, vol. 59, pp. 19–35, 2019.

[7] O. K. Hope, W. Thomas, and D. Vyas, "The cost of pride: why do firms from developing countries bid higher," *Journal of International Business Studies*, vol. 42, no. 1, pp. 128–151, 2011.

[8] W. Guo, J. A. Clougherty, and T. Duso, "Why are Chinese MNES not financially competitive in cross-border acquisitions? The role of state ownership," *Long Range Planning*, vol. 49, no. 5, pp. 614–631, 2016.

[9] Y. Y. Chen and M. N. Young, "Cross-border mergers and acquisitions by Chinese listed companies: a principal-principal perspective," *Asia Pacific Journal of Management*, vol. 27, no. 3, pp. 523–539, 2010.

[10] A. Howell, J. Lin, and S. Worack, "Going out to innovate more at home: impacts of outward direct investments on Chinese firms' domestic innovation performance," *China Economic Review*, vol. 60, Article ID 101404, 2020.

[11] P. J. Buckley, L. J. Clegg, A. R. Cross, X. Liu, H. Voss, and P. Zheng, "The determinants of Chinese outward foreign direct investment," *Journal of International Business Studies*, vol. 38, no. 4, pp. 499–518, 2007.

[12] E. De Bodt, J. G. Cousin, and R. Roll, "Empirical evidence of overbidding in M&A contests," *Journal of Financial and Quantitative Analysis*, vol. 53, no. 4, pp. 1547–1579, 2018.

[13] G. Kou, H. Xiao, M. Cao, and L. H. Lee, "Optimal computing budget allocation for the vector evaluated genetic algorithm in multi-objective simulation optimization," *Automatica*, vol. 129, Article ID 109599, 2021.

[14] G. Kou, O. Akdeniz, H. Dinçer, and S. Yüksel, "Fintech investments in European banks: a hybrid IT2 fuzzy multidimensional decision-making approach," *Financ. Innov.*, vol. 7, no. 1, pp. 39–67, 2021.

[15] S. Bhagat, M. Dong, D. Hirshleifer, and R. Noah, "Do tender offers create value? New methods and evidence," *Journal of Financial Economics*, vol. 76, no. 1, pp. 3–60, 2005.

[16] E. Bartov, C. S. A. Cheng, and H. Wu, "Overbidding in mergers and acquisitions: an accounting perspective," *The Accounting Review*, vol. 96, no. 2, pp. 55–79, 2021.

[17] D. C. Hambrick and P. A. Mason, "Upper echelons: the organization as a reflection of its top managers," *Academy of Management Review*, vol. 9, no. 2, pp. 193–206, 1984.

[18] R. Roll, "The hubris hypothesis of corporate takeovers," *Journal of Business*, vol. 59, no. 2, pp. 197–216, 1986.

[19] N. Aktas, E. de Bodt, and R. Roll, "MicroHoo: deal failure, industry rivalry, and sources of overbidding," *Journal of Corporate Finance*, vol. 19, no. 1, pp. 20–35, 2013.

[20] M. L. A. Hayward and D. C. Hambrick, "Explaining the premiums paid for large acquisitions: evidence of CEO hubris," *Administrative Science Quarterly*, vol. 42, no. 1, pp. 103–127, 1997.

[21] U. Malmendier and G. Tate, "Who makes acquisitions? CEO overconfidence and the market's reaction," *Journal of Financial Economics*, vol. 89, no. 1, pp. 20–43, 2008.

[22] M. C. Jensen, "Agency problems of free cash flow," *Mark. Corp. Control*, vol. 76, no. 2, pp. 323–329, 1986.

[23] A. Pan, W. Liu, and X. Wang, "Managerial overconfidence, debt capacity and merger & acquisition premium," *Nankai Business Review International*, vol. 10, no. 4, pp. 570–590, 2019.

[24] J. Wulf, "Do CEOs in mergers trade power for premium? Evidence from 'mergers of equals," *Journal of Law, Economics, and Organization*, vol. 20, no. 1, pp. 60–101, 2004.

[25] B. Qiu, S. Trapkov, and F. Yakoub, "Do target CEOs trade premiums for personal benefits?" *Journal of Banking & Finance*, vol. 42, no. 1, pp. 23–41, 2014.

[26] D. Jenter and K. Lewellen, "CEO preferences and acquisitions," *The Journal of Finance*, vol. 70, no. 6, pp. 2813–2852, 2015.

[27] Q. Gu, C. Ju, and F. Bao, "The cross-border mergers and acquisitions of local state-owned enterprises: the role of home country government involvement," *Sustainability*, vol. 12, no. 7, p. 3020, 2020.

[28] J. H. Davis, F. D. Schoorman, and L. Donaldson, "Toward a stewardship theory of management," *Academy of Management Review*, vol. 22, no. 1, pp. 20–47, 1997.

[29] R. E. Till and M. B. Yount, "Governance and incentives: is it really all about the money?" *Journal of Business Ethics*, vol. 159, no. 3, pp. 605–618, 2019.

[30] M. W. Peng, S. Zhang, and X. Li, "CEO duality and firm performance during China's institutional transitions," *Management and Organization Review*, vol. 3, no. 2, pp. 205–225, 2007.

[31] Y. Luo, Q. Xue, and B. Han, "How emerging market governments promote outward FDI: experience from China," *Journal of World Business*, vol. 45, no. 1, pp. 68–79, 2010.

[32] Z. Chen, B. Ke, Z. Yang, Z. Chen, and B. Ke, "Minority shareholders ' control rights and the quality of corporate decisions in weak investor protection countries: a natural experiment from China," *The Accounting Review*, vol. 88, no. 4, pp. 1211–1238, 2013.

[33] W. R. Scott, K. G. Smith, and M. A. Hitt, "Institutional theory: contributing to a theoretical research program chapter prepared for great minds in management: the process of theory," *Gt. minds Manag. Process theory Dev*, pp. 460–485, 2004.

[34] G. Hofstede, *Geert Hofstede, Culture's Consequences: Comparing Values, Behaviours, Institutions, and Organizations across Nations*, pp. 1–621, Sage Publications, Thousand Oaks, California, USA, 2001.

[35] C. Lyu, D. C. Y. Yuen, and X. Zhang, "Individualist-collectivist culture, ownership concentration and earnings quality," *Asia-Pacific Journal of Accounting & Economics*, vol. 24, no. 1–2, pp. 23–42, 2017.

[36] P. Deng, "Why do Chinese firms tend to acquire strategic assets in international expansion?" *Journal of World Business*, vol. 44, no. 1, pp. 74–84, 2009.

[37] L. Cui, K. E. Meyer, and H. W. Hu, "What drives firms' intent to seek strategic assets by foreign direct investment? A study of emerging economy firms," *Journal of World Business*, vol. 49, no. 4, pp. 488–501, 2014.

[38] N. Zheng, Y. Wei, Y. Zhang, and J. Yang, "In search of strategic assets through cross-border merger and acquisitions: evidence from Chinese multinational enterprises in developed economies," *International Business Review*, vol. 25, no. 1, pp. 177–186, 2016.

[39] N. Kohers and T. Kohers, "Takeovers of technology firms: expectations vs. Reality," *Financial Management*, vol. 30, no. 3, p. 35, 2001.

[40] I. Serdar Dinc and I. Erel, "Economic nationalism in mergers and acquisitions," *The Journal of Finance*, vol. 68, no. 6, pp. 2471–2514, 2013.

[41] A. Mukherji, J. Mukherji, C. Dibrell, and J. D. Francis, "Overbidding in cross-border acquisitions: misperceptions in assessing and valuing knowledge," *Journal of World Business*, vol. 48, no. 1, pp. 39–46, 2013.

[42] W. Guo, *Cross-border mergers and acquisitions from emerging market nations: evidence from Chinese acquirers*, Ph.D. Dissertation, University of Illinois Urbana-Champaign, Urbana, IL, USA, 2014.

[43] X. Wu, X. Yang, H. Yang, and H. Lei, "Cross-border mergers and acquisitions by Chinese firms: value creation or value destruction?" *Journal of Contemporary China*, vol. 25, no. 97, pp. 130–145, 2016.

[44] S. Betton, B. E. Eckbo, R. Thompson, and K. S. Thorburn, "Merger negotiations with stock market feedback," *The Journal of Finance*, vol. 69, no. 4, pp. 1705–1745, 2014.

[45] S. J. Brown and J. B. Warner, "Using daily stock returns," *Journal of Financial Economics*, vol. 14, no. 1, pp. 3–31, 1985.

[46] Q. Jin, Y. Jin, G. G. Tian, and Y. Xuan, "Does internal corporate governance complement or substitute for external auditing? Evidence from China's anti-corruption campaign," *Abacus*, vol. 57, no. 1, pp. 153–182, 2021.

Hindawi
Complexity
Volume 2022, Article ID 5288187, 12 pages
https://doi.org/10.1155/2022/5288187

Research Article

Codes over Lattice-Valued Intuitionistic Fuzzy Set Type-3 with Application to the Complex DNA Analysis

Asra Riaz,[1] **Sajida Kousar**,[1] **Nasreen Kausar**,[2] **Dragan Pamucar**,[3] **and Gezahagne Mulat Addis**[4]

[1]*Department of Mathematics and Statistics, International Islamic University Islamabad, Islamabad, Pakistan*
[2]*Department of Mathematics, Faculty of Arts and Sciences, Yildiz Technical University, Esenler 34210, Istanbul, Turkey*
[3]*Faculty of Organizational Sciences, University of Belgrade, Belgrade 11000, Serbia*
[4]*Department of Mathematics, University of Gondar, P.O. Box 196, Gondar, Ethiopia*

Correspondence should be addressed to Gezahagne Mulat Addis; gezahagne412@gmail.com

Received 1 June 2022; Accepted 4 August 2022; Published 21 September 2022

Academic Editor: Yu Zhou

In this article codes over lattice valued intuitionistic fuzzy set type-3 (LIFS-3) are defined. Binary block codes and linear codes are constructed over LIFS-3. Hamming distance and related properties of these newly established codes are examined. The research findings are applied to genetic codes. The set L of sixty-four codons is converted into a lattice and then codes are created over the set S of twenty amino acids by defining membership and nonmembership functions from the set of twenty amino acids to the sixty-four codon set. Comparison of codes over L-fuzzy set and LIFS-3 conducted in terms of hamming distance for codon system that ensures the efficiency of newly established codes.

1. Introduction

Probability theory was once believed to be an ideal tool to deal with any uncertain situation. However, there are many problems where the uncertainty appears as an imprecision and ambiguity rather than a statistical variation. The classical probability theory is not efficient and suitable for handling the uncertainties and imprecision that appear in pattern recognition. Zadeh [1] presented the notion of fuzzy set as an extension of the ordinary set. This notion is used for describing vagueness and ambiguity mathematically. The formulation of fuzzy sets over a nonempty set S is based on an allocation of a grade of membership to each element of S. The allocated grades are precisely the real numbers ranging between 0 and 1. Mathematically, a fuzzy set μ over S is characterized by a map $\mu\colon S \longrightarrow [0,1]$ termed as membership function and the value $\mu(x)$ as grade of membership of x in S. For instance, let X be the set of seven days of a week and $p(x)$ be the number of codes transmitted from a source center S and $q(x)$ be the number of codes received accurately at the receiver end R in the day $x \in X$. Then the function $\mu\colon X \longrightarrow [0,1]$ defined as $\mu(x) = q(x)/p(x)$, for all $x \in X$, provides a fuzzy set over X (that is, the collection of ordered pairs $(x, \mu(x))$). For example, if on x = Monday, 100 codes were transmitted from S and the supervisor at R reported that 75 codes were received properly at R, then $\mu(x) = 75/100 = 0.75$ would be the grade of membership of x in X, or we can say that the supervisor's statement's truth value was 0.75. According to classical probability, 25 codes were not received at R, but in real practice, mostly the interpreter at R can decode the partially transmitted codes for further processing. In this example, if ten partially received codes are processed, then the supervisor's statement's truth value increases from 0.75 to 0.85; the falsity value (nonmembership) decreases from 0.25 to 0.15. Let $\nu(x) = 0.15$ represent the falsity value of the supervisor's statement; then $1 - \{\mu(x) + \nu(x)\} = 0.10$ is the degree of uncertainty caused by the performance of interpreter at R. So, the membership grades are not enough to communicate the correct information in this case and need to introduce the idea of nonmembership grades; these grades should not be confused with the probability of non-occurrence $P(\overline{A}) = 1 - P(A)$ of an event A.

Atanassov [2], first introduced the notion of nonmenbership grages. The generalization of fuzzy sets that involves both the membership and nonmembership grades is known as the intuitionistic fuzzy set (IFS). Atanassov proposed fundamental properties, various arithmetic operations for his development in fuzzy sets. In continuation, Atanassov [3] presented the geometric interpretation of intuitionistic fuzzy objects. There are several other generalizations of fuzzy sets that mostly depend upon membership, nonmembership, hesitancy and indeterminacy grades. As in a fuzzy set, the grades $\mu(x)$ belong to the close interval $[0, 1]$, which is naturally endowed with a partial order. The assumption of order structures outside the unit interval laid the foundations of ordered fuzzy sets. Partial orderings and fuzzy uncertainties are features of many real-world problems. These kinds of problems are ill-posed most of the time, because either they have infinite solutions or no solutions at all. For instance, the selection of a grocery bundle from various packages is subjected to various contradictory and conflicting criteria. Nutritional value, quality, variety and above all cost, are some of the factors that a person can think about a bundle. Thus, the partial ordering of the bundles is an essential feature of this problem. Goguen [4] introduced the concept of L-fuzzy subsets of S where the interval $[0, 1]$ is replaced by a partially ordered set L. He discovered remarkable features of this generalized concept and concluded that L-fuzzy set theory works more efficiently in real-world problems. After IFS Atanassov and Stoeva [5] enrich the area and replaced the lattice [0, 1] by arbitrary complete lattice L, to relate membership and nonmembership functions $\mu, \nu\colon S \longrightarrow L$ he involved an involutive order reversing unary operation $N\colon L \longrightarrow L$. The new structure is known as lattice valued intuitionistic fuzzy set (LIFS-1). But it has certain limmitation mostly occurred due to the incorporation of the operator N. Gerstenkorn and Tepavcevic [6] made an attempt to upgrade Atanassov idea and proposed a new variant, that is, the lattice valued intuitionistic fuzzy set type 2 (LIFS-2) simply by exchanging the operator N with a linearization function $\ell\colon L \longrightarrow [0, 1]$. This modification is quite helpful in the establishment of decomposition theorem and synthesis but fails to deal with basic set operations. Choice of the linearization function is the main reseaon behind this failure. Finally, lattice homomorphism $\alpha\colon L \longrightarrow [0, 1]$ is used to relate membership and nonmembership functions and the new LIFS is called a lattice valued intuitionistic fuzzy set type-3 (LIFS-3). This new sturcture has certain advantages over the previously defined fuzzy sets and L-fuzzy sets mostly occurs due to the inclusion of lattices and lattice homomorphism. The lattice homomorphim is applicable to any collection of lattices unlike the unary operator N of LIFS-1 and satisfy all the basic set operations unlike the linearization function ℓ of LIFS-2.

A code is a system of rules used for data communication and information process. These rules are designed in the form of letters, symbols, images, sounds or numbers. Coding theory was established to study these rules mathematically and make them workable in daily communication. In communication, algebraic codes are used for data compression and error correction. Coding theory is concerned with the reliability of communication over a noisy channel. Algebraic codes are studied in a variety of domains and they have a wide range of applications across a large range of disciplines. Murugan and Ananthanarayana [7] presented the WordTrie, a specialised trie for storing words in order to facilitate fast coding. The code combination is generated in such a manner that the size of the WordCode for a word must be less than the entire size of the character coding. To improve the detection rate of NLOS nodes in any safety application of VANET, the WDHPBDS protocol was designed by Arjunan and Kaviarasan [8] in order to permit reliable delivery of emergency information to the targeted node in a timely manner. Nagaraju et al. [9] explored that by using a hybrid area exploration technique, mobility assisted localization for mission critical wireless sensor network applications can be achieved.

When data are transmitted through a noisy channel, some errors may arise. The vagueness in data transmission can be handled by involving theoretical fuzzy set concepts in the coding and decoding process. There are two ways to incorporate theoretical fuzzy set concepts in coding. One method was proposed by von Kaenel and Pierre [10], termed fuzzy code, and is defined as a fuzzy subset of n-dimensional vector space $\mathbb{F}^n$ over the field $\mathbb{F}$. He investigated the Hamming distance for newly established fuzzy codes. Kaenel's theory is based on the symmetric nature of the error—that is, the probability of $1 \longrightarrow 0$ crossover failure and $0 \longrightarrow 1$ is equally likely. However, in computer memories and VLSI circuits, the error may not be symmetric. Hall and Dial [11] discussed the asymmetric nature of fuzzy codes and generalized the results of Kaenel. They worked on the distance between fuzzy code words and proved that the distance is independent of the dimension of the vector space $\mathbb{F}^n$. Tsafack et al. [12] established a fuzzy linear code, fuzzy cyclic code over Gralois ring $\mathbb{Z}_{p^k}$. Amudhambigai and Neeraja [13] discussed arithmetic operations on fuzzy codes and introduced their super increasing sequences. Shijina [14] introduced multi-fuzzy code in terms of a multi-fuzzy subset of n-tuples over a set S, and produced some essential results for Hamming distance. Du [15] analyzed arithmetic operations of subtraction and division on intuitionistic fuzzy subsets that were induced by the Hamming distance. Ali et al. [16] developed soft algebraic codes over soft sets. They also defined soft canonical generator matrix and soft canonical parity check to decode these algebraic codes. Seselja and Tepavcevic [17] introduced another method of involving fuzzy theory in coding, which is based on defining a map $\overline{A}$ from a nonempty set $S = \{1, 2, \ldots, n\}$ for partially ordered set P. Seselja et al. [18] carried the concept and defined binary block codes over lattice valued fuzzy sets (L-fuzzy sets). Mališa and Lazarević [19] discussed the length and cardinality of block codes over L-fuzzy sets. The concepts of fuzzy codes and codes of ordered fuzzy sets are relatively new, but crucial for modifying the data communication and pattern recognition in deep learning [20] and fault detection for distributed components [21, 22]. However, these codes are unable to identify and handle any expected error in the information process while codes are transmitted in a noisy channel, for example, a spell

checker and machine reader. Moreover, the already existing fuzzy codes or codes over fuzzy sets are based solely on the degree of membership; the degree of nonmembership was not incorporated in any previous method. Lattice valued intuitionistic fuzzy set type-3 is a generalization of basic fuzzy set that incorporates both the degree of membership and the degree of nonmembership, so it is a more workable framework for modeling uncertain data. The effectiveness of LIFS-3 motivated us to construct codes over these fuzzy sets.

2. Preliminaries

2.1. Bounded Lattice. A relation ϱ on a nonempty set L is precisely a subset of $L \times L$. The elements of ϱ are more commonly denoted by $a\varrho b$; a is ρ related to b. Based on the nature of elements in the relation ϱ, it can have different names. For instance, if $x\varrho x$ for all $x \in L$, then ϱ is called reflexive; if $x \rangle y \Longrightarrow y \rangle x$, then ϱ is called symmetric; if $x\varrho y$ and $y \succ x \Longrightarrow x = y$, then ϱ is called anti-symmetric; if $x\varrho y$ and $y \rangle z \Longrightarrow x \rangle z$, then ϱ is called transitive. A reflexive, anti-symmetric and transitive relation is called a partial order of L. In this case, the set L is called a partially ordered set. For example, " $\leq$ " (less than or equal) is a partial order on the set of real numbers. The symbol " $\leq$ " is used for partial order in general and is also used in this article for better understanding by a wider audience. A subset Y of a partially ordered set L is said to be bounded above (below) if there exists $\ell \in L$ such that $\ell' \leq \ell$ ($\ell \leq \ell'$) for all $\ell' \in Y$. The element ℓ is called an upper (lower) bound of Y. The set Y may possess more than one upper (lower) bound. The least (greatest) member in the set of upper (lower) bounds of Y is called the supremum (infimum) of Y denoted by $\sup(Y)$ ($\inf(Y)$). More precisely, if $\ell = \sup(Y)$ then. $\ell \leq \xi$ ($\xi \leq \ell$).

The partially ordered set L is called a *lattice* if $\inf\{l_1, l_2\}$ and $\sup\{l_1, l_2\}$ exist for any pair of elements $l_1, l_2 \in L$. The symbols $\wedge$ and $\vee$ are used to indicate the infimum and supremum of l_1 and l_2. Thus, we can write $l_1 \wedge l_2 = inf\{l_1, l_2\}$ and $l_1 \vee l_2 = \sup\{l_1, l_2\}$. The lattice L is said to be *complete* if and only if $\inf(Y)$ and $\sup(Y)$ exist for all $Y \subset L$. The lattice L is said to be *bounded* if it has a greatest a element T and a least element B. These elements are also called the *top* and *bottom* elements of L, respectively. Thus, in a bounded lattice $B \leq l \leq T$ for all $l \in L$. If $\vee$ and $\wedge$ are distributive over each other, then such a lattice is called a distributive lattice. A complemented distributive lattice is called a Boolean lattice.

A lattice L can be represented geometrically by means of a Hasse diagram whose vertices are labeled by elements of L, and any two vertices a and b are joined by a line segment or a curve that goes upward from a to b whenever $a < b$ and there is no member $c \in L$ between a and b. These edges may cross each other but must not touch any vertex other than their endpoints. Such a diagram uniquely determines the partial order defined on L. In a partial order, the existence of $l_1 \wedge l_2$ and $l_1 \vee l_2$ is essential for the formulation of lattices. Being nonempty sets, we can define several maps between any two lattices. Any map that preserves the three essential components that constitute a lattice is called a *lattice homomorphism*. Mathematically, a map α from a lattice L_1 into a lattice L_2 is called a lattice homomorphism if for all $l_1, l_1' \in L_1$, $\alpha(l_1 \wedge l_1') = \alpha(l_1) \wedge \alpha(l_1')$ and $\alpha(l_1 \vee l_1') = \alpha(l_1) \vee \alpha(l_1')$.

If L_1 is a bounded lattice with top element T_{L_1} and bottom element is a bounded lattice with $\alpha(T_{L_1})$ and $\alpha(B_{L_1})$ as top and bottom elements. If L_1 and L_2 both are bounded lattices, then α maps top and bottom elements of L_1 onto the top and bottom elements of L_2 respectively.

Example 1. Let $L = \{B, T, a, c, d, e, f, g, h, i, j, k\}$ be a lattice [6] with partial order presented by the Hasse diagram in Figure 1.

The map α: $L \longrightarrow [0, 1]$ de is a lattice homomorphism.

A filter F of a lattice L is a subset $F \subseteq L$ satisfying two conditions stated as

(i) If $\ell \in F$ and $\ell' \ell'$, then $\ell' \in F$;

(ii) If $\ell, \ell' \in F$, then $\ell \wedge \ell' \in F$.

Let L be a lattice. The principal filter denoted by $\uparrow p$ is de Clearly, the principal filter is the smallest filter that contains the given element p. Let L be a bounded lattice. If M is a subset of L, then M_p: $= \uparrow p \cap M$.

2.2. Lattice Valued Intuitionistic Fuzzy Set Type-3. Zadeh [1] formulated the fundamental definition of fuzzy sets. A fuzzy subset A of a nonempty set S is perhaps the collection of ordered pairs with first components from S, and second components are images of the map μ: $S \longrightarrow [0, 1]$ (called membership function). Mathematically, A can be written as $A = \{(x, \mu(x))\colon x \in S\}$. The grades of membership for elements of S under μ can be used to define crisp subsets of S termed level or cut sets. For any $\alpha \in [0, 1]$, the α-level set of μ is de. The idea of a fuzzy set is a major breakthrough in mathematical logic giving a better approximation than the classical probability theory. However, in real-life problems, membership is not the only option in all cases; there is the chance of nonmembership to handle as well. For such cases, Atanassov introduced the concept of the intuitionistic fuzzy set (IFS). An intuitionistic fuzzy set (IFS) A over S is a triplet (A, μ, ν), where μ, ν: $S \longrightarrow [0, 1]$ (called membership and nonmembership functions). Thus, the IFS A can be written as $A = \{\langle x, \mu(x), \nu(x)\rangle\colon x \in S\}$ with $0 \leq \mu(x) + \nu(x) \leq 1$. "Less than or equal to" ($\leq$) constitutes a natural partial order on the closed interval $[0, 1]$ and turns it into a lattice. The replacement of $[0, 1]$ by any other lattice L gives us the concept of L-fuzzy and L-intuitionistic fuzzy sets. A lattice valued intuitionistic fuzzy set type-1 (LIFS-1) [6] is the set (S, L, μ, ν, N), where S is a non empty set; L is a lattice; μ: $S \longrightarrow L$ and ν: $S \longrightarrow L$ are membership and nonmembership functions; and N: $L \longrightarrow L$ is an involutive order reversing unary operator on L such that $\mu(x) \leq N(\nu(x))$ for all $x \in S$. The replacement of unary operator N by the linearization map ℓ: $L \longrightarrow [0, 1]$ satisfying $\ell(\mu(x)) + \ell(\nu(x)) \leq 1$ for all $x \in S$ constitutes a lattice valued intuitionistic fuzzy set type-2 (LIFS-2). A lattice valued intuitionistic fuzzy set type-3 (LIFS-3) is the quintuplet (S, L, μ, ν, α), where S is a nonempty set; L is a bounded lattice with top element T and bottom element B; μ: $S \longrightarrow L$

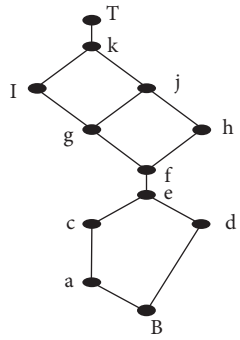

Figure 1: Lattice $L = \{B, T, a, c, d, e, f, g, h, i, j, k\}$.

and $\nu: S \longrightarrow L$ are membership and nonmembership functions; and $\alpha: L \longrightarrow [0,1]$ is a lattice homomorphism with $\alpha(\mu(x)) + \alpha(\nu(x)) \leq 1$ for all $x \in S$. For $p \in L$, two level sets in LIFS-3 are defined as:

$$\mu_p = \{X \in S \mid \mu(x) \geq p\}; \nu_p = \{X \in S \mid \nu(x) \geq p\}. \quad (1)$$

Two level functions generally called characteristics functions $\overline{\mu}_p$ and $\overline{\nu}_p$ are defined as:

$$\overline{\mu}_p(x) = 1 \Longleftrightarrow \mu(x) \geq p, \overline{\nu}_p(x) = 1 \Longleftrightarrow \nu(x) \geq p. \quad (2)$$

Proposition 1. *[6] Let S be a nonempty set and (S, L, μ, ν, α) be an LIFS-3. Then the following statements are true:*

(i) Let L be a lattice with bottom element B. Then $\mu_B = \nu_B = S$.

(ii) If $p \leq q$, then $\mu_q \subseteq \mu_p$ and $\nu_q \subseteq \nu_p$.

(iii) If $Z \subseteq L$, then $\wedge\{\mu_P | p \in Z\} = \mu_{\vee\{p|p\in Z\}}$ and $\wedge\{\nu_P | p \in Z\} = \nu_{\vee\{p|p\in Z\}}$.

Remark 1. The functions μ: S $\longrightarrow$ L and ν: S $\longrightarrow$ L define a partitioning of L under the equivalence relation $\sim$ defined as $g \sim h$ if and only if $\mu_g = \mu_h$ and $\nu_g = \nu_h$.

For every $g \in L$, the equivalence class of g is $[g]_\sim = \{h \in L | g \sim h\}$. As we know, the join (supremum) of a set may or may not be an element of that set, but for these classes $\vee [g] \sim \in [g] \sim$.

3. Codes over LIFS-3

Let $S = \{1, 2, \ldots, r\}$ and $S^{\alpha}_{L\mu\nu} = (S, L, \mu, \nu, \alpha)$ be an LIFS-3. For $p \in L$, define $\overline{\mathscr{C}}_p: S \longrightarrow \{0,1\}$ as:

$$\begin{aligned} \overline{\mathscr{C}}_p &= \overline{\mu}_p \wedge \overline{\nu}_p \\ &= u_p \wedge v_p \\ &= (a_1, \ldots, a_n) \wedge (b_1, \ldots, b_n) \\ &= (a_1 \wedge b_1)(a_2 \wedge b_2) \ldots (a_n \wedge b_n), \end{aligned} \quad (3)$$

where u_p and v_p are the codewords—also called vectors—for the element $p \in L$. The map $\overline{\mathscr{C}}_p$ is called a binary block codeword over $S^{\alpha}_{L\mu\nu}$. The LIFS-3 codewords inherit a partial order from the lattice L in such a way that $a_1 \ldots a_n \leq b_1 \ldots b_n$ if and only if $a_1 \geq b_1, a_2 \geq b_2, \ldots, a_n \geq b_n$ in L. The number of elements in S that are mapped onto $p \in L$ under μ and ν are called the degrees of u_p and v_p denoted by $s(u_p)$ and $s(v_p)$. Moreover, the degree of c_p is exactly equal to the sum of the maxima of $s(u_p)$ and $s(v_p)$. For a binary block code $\mathscr{C} \subseteq \{0,1\}^n$, a nonempty set S, a lattice L and lattice homomorphism $\alpha: L \longrightarrow [0,1]$, the set $S^{\alpha}_{L\mu\nu\mathscr{C}}$ is an LIFS-3 if the binary block code constructed on it is equal to $\mathscr{C}$.

Example 2. Let us consider a nonempty set $S = \{x, y, z\}$ and lattice L described in example 1. Define membership and nonmembership functions as

$$\mu = \begin{pmatrix} x & y & z \\ a & g & e \end{pmatrix} \nu = \begin{pmatrix} x & y & z \\ f & \mathrm{d} & j \end{pmatrix}. \quad (4)$$

Clearly, for all $s \in S$, the lattice homomorphism α satisfies $0 \leq \alpha(\mu(s)) + \alpha(\nu(s)) \leq 1$. Now for $a \in L$, $\overline{\mu}_a = 111$ and $\overline{\nu}_a = 101$ because $a \leq \mu(x), a \leq \mu(y), a \leq \mu(z)$ and $a \leq \nu(x)$, $a \geq \nu(y), a \leq \nu(z)$. Thus, $\mathscr{C}_a = (1 \wedge 1)(1 \wedge 0)(1 \wedge 1) = 101$.

Codewords corresponding to other elements of L can be computed in a similar fashion and are presented in Table 1.

As $s(u_a) = 1$ and $s(v_a) = 0$, the degree of a code word $c_a \subseteq \mathscr{C}$ is. $s(c_a) = \max\{s(u_a), s(v_a)\} = \max\{1, 0\} = 1$.

Theorem 1. *The binary block code $\mathscr{C} \subseteq \{0,1\}^n$ constitutes a lattice valued intuitionistic fuzzy set type-3 if and only if code $\mathscr{C}$ is closed under an intersection and the identity vector $11 \ldots 1$ belongs to $\mathscr{C}$.*

Proof. Let $\mathscr{C} \subseteq \{0,1\}^{\mathrm{n}}$ be a code and $S^{\alpha}_{L\mu\nu\mathscr{C}}$ be the corresponding LIFS-3. As L is a lattice, the families $\{\mu_p: p \in L\}$ and $\{\nu_p: p \in L\}$ are closed under a set theoretical intersection, which implies that the code $\mathscr{C}$ is closed. Hence, binary block code is closed under intersection. Moreover, $\mu_B = S$ and $\nu_B = S$ imply that $11 \ldots 1 \in \overline{\mu}_B$ and $11 \ldots 1 \in \overline{\nu}_B$ for the bottom element $B \in L$. Thus $\overline{\mathscr{C}}_B = \overline{\mu}_B \wedge \overline{\nu}_B = 11 \ldots 1$ belongs to $\mathscr{C}$. Conversely, suppose that $\mathscr{C}$ is closed under a set theoretical intersection and non-zero codeword $11 \ldots 1 \in \mathscr{C}$. Now we show that there is an LIFS-3 corresponding to the code $\mathscr{C}$. Consider $S = \{1, 2, \ldots, n\}$. The complements of the subsets of S obtained by the codewords of $\mathscr{C}$ in terms of characteristic functions constitute a lattice L with inclusion as a partial order. Now for $p \in L$, $\overline{\mathscr{C}}_p$ is a codeword such that $\overline{\mu}_p(i) = \overline{\nu}_p(i) = 0$ if and only if $i \in p$. The collection $\overline{\mathscr{C}}_p: p \in L$ gives an LIFS-3 having cod for all $x \in S$. □

3.1. Hamming Distance. The Hamming distance $d(s,t)$ defined in [23] is the number of places in which the two vectors (codewords) s and t differ. In other words, $d(s,t)$ represents the component-wise difference of the two codewords s and t. That is,

$$d(s,t) = \left|\{i: s_i = t_i\}\right|. \quad (5)$$

Consider a code $\mathscr{C}$. Then the distance $d(\mathscr{C})$ of a code $\mathscr{C}$ is defined in [23] as the minimum distance between two

Table 1: Codewords over LIFS-3.

$\overline{\mu}_p$	$\overline{\nu}_p$	$\overline{\mathscr{C}}_p = \overline{\mu}_p \wedge \overline{\nu}_p$	$\overline{\mu}_p$	$\overline{\nu}_p$	$\overline{\mathscr{C}}_p = \overline{\mu}_p \wedge \overline{\nu}_p$	$\overline{\mu}_p$	$\overline{\nu}_p$	$\overline{\mathscr{C}}_p = \overline{\mu}_p \wedge \overline{\nu}_p$
111	101	101	010	101	000	000	001	000
011	101	001	010	001	000	000	000	000
011	111	011	000	001	000	111	111	111
011	101	001	000	000	000	000	000	000

distinct codewords in $\mathscr{C}$. The number of non-zero components of a codeword is known as its Hamming weight denoted by $\|c_p\|$.

Proposition 2. *For any code $\mathscr{C}$, $d(\mathscr{C}) \geq min_{p\in\overline{\mu}(s),\overline{\nu}(s)}\, s(c_p)$.*

Proof. Let L be a lattice and $\mathscr{C}$ be a binary block code over $S^{\alpha}_{L\mu\nu}$. Then for any $p \in L$ and codeword c_p, the degree of c_p is equal to the maximum of $s(\mu_p)$ and $s(\nu_p)$. Ultimately if c_p differs at the i^{th} coordinate, then it will differ at each j^{th} coordinate, which is an outcome of some $x \in S$ mapped onto p under μ and ν. Thus, the distance of code $\mathscr{C}$ is at least equal to $s(c_p)$. □

Proposition 3. *For any $c_p \in \mathscr{C}$, the Hamming weight*

$$\left\|c_p\right\| \geq \max\left\{s\left(c_q\right) :\ q \in \mu(S), \nu(S) \text{ and } c_p \leq c_q\right\}. \tag{6}$$

Proof. Let $S^{\alpha}_{L\mu\nu}$ be an LIFS-3. Then $\overline{u}_q(x) = \overline{v}_q(x) = 1$ if $\mu(x), \nu(x) \geq q \Rightarrow c_q(x) = 1$ if $p = \mathscr{C}(x) \geq q$. Hence, $c_q(x)$ is non-zero if both $u_q(x)$ and $v_q(x)$ are non-zero, implying that the number of non-zero coordinate is equal to or greater than the degree of $s(c_q)$. □

Proposition 4. *Let $c_p, c_q \in \mathscr{C}$, such that $?_p \leq ?_q$. Then, $d(c_p, c_q) = \sum_{c_t \in T} s(c_t)$ where*

$$T = \left\{c_t \in \mathscr{C} :\ c_t \geq c_p \text{ and } c_t \leq c_q\right\}. \tag{7}$$

Proof. Let $S^{\alpha}_{L\mu\nu}$ be an LIFS-3. Let $\overline{u}_p$ and $\overline{u}_q$ be two vectors corresponding to the membership function. For $c_p \leq c_q$ we have $\overline{u}_p \leq \overline{u}_q$; this implies that the number of non-zero elements in $\overline{u}_q$ is not more than the number of non-zero elements in $\overline{u}_p$. Let $t \in \mu(S)$ such that $\overline{u}_t \geq \overline{v}_p$ and $\overline{u}_t \leq \overline{v}_q$. Then for each element $x \in S$ which is mapped onto t, we have $u_p(x) = 1$ and $u_q(x) = 0$.

A similar argument for the nonmembership function implies. $v_p(x) = 1$ and $v_q(x) = 0$.

Hence $c_p(x) = u_p(x) \wedge v_p(x) = 1$ and. $c_q(x) = u_q(x) \wedge v_q(x) = 0$.

As $c_p \leq c_q$, for each $x \in S$ there exist non-zero coordinates in c_q that belong to c_p and are mapped onto t. □

Theorem 2. *If c_p and c_q are two different codewords, then $d(c_p, c_q) = d(c_p, c_{p\vee q}) + d(c_q, c_{p\vee q})$.*

Proof. Suppose we have two vectors $\overline{u}_p$ and $\overline{v}_p$ corresponding to the membership and nonmembership functi in this case $p \vee q = q$, and $d(c_p, c_q) = d(c_p, c_{p\vee q}) + d(c_q, c_{p\vee q})$. Now let us consider the case when two vectors $\overline{u}_p$ and $\overline{u}_q$ are non-comparable. Then any coordinate which is non-zero in $\overline{u}_{p\vee q}$ will be non-zero in $\overline{u}_p$ and $\overline{u}_q$. A similar case exists for two vectors $\overline{v}_p$ and $\overline{v}_q$ corresponding to the nonmembership function. Let m be the coordinates at which two code words $\overline{u}_p$ and $\overline{u}_q$ and $\overline{v}_p$ and $\overline{v}_q$ differ, that is, $u_q(m) = 1$ and $u_p(m) = 0$.

In addition, $v_q(m) = 1$ and $v_p(m) = 0$, imply $c_q(m) = 1, c_p(m) = 0$.

Hence, c_p and c_q differ at m. If $\mu(m) = t$, then. $\overline{u}_t \geq \overline{u}_q$ and $\overline{u}_t \leq \overline{u}_p$.

If $\nu(m) = t$, then $\overline{v}_t \geq \overline{v}_q$ *an d* $\overline{v}_t \leq \overline{v}_p$. Hence $\overline{u}_t \leq \overline{u}_{p\vee q}, u_{p\vee q}(m) = 0$ and. $\overline{v}_t \leq \overline{v}_{p\vee q}, v_{p\vee q}(m) = 0$

Imply

$$c_{p\vee q}(m) = 0. \tag{8}$$

Hence c_q and $c_{p\vee q}$ differ at the coordinate m. □

3.2. Linear Codes over LIFS-3. A linear (n, k) code is defined in [23] is a k-dimensional subspace of a vector space $\{0, 1\}^n$ under the binary operation $\oplus$ of componentwise addition modulo 2.

Theorem 3. *Let $\mathscr{C}$ be a linear (r, k) code satisfying the conditions of Theorem 1. Then the lattice L of $S^{\alpha}_{L\mu\nu}$ corresponding to $\mathscr{C}$ is Boolean.*

Proof. Let $\mathscr{C}$ be a linear (r, k) code satisfying the conditions of Theorem 1. Then, corresponding to code $\mathscr{C}$, we have an LIFS-3, where L consists of all the elements which are the complement of subsets of the set S. The lattice is distributive and the elements 0 and 1 are in L. As in distributive lattice, every element has a unique complement and $\overline{r} = r \oplus 11 \ldots 1$, so this lattice is complemented, and hence it is a Boolean lattice.

The relation in Remark 2.4. is modified in the following result. □

Theorem 4. *If for μ: $S \longrightarrow L$ and ν: $S \longrightarrow L$ in $S^{\alpha}_{L\mu\nu}$ we have $M = \mu(S)$ and $N = \nu(S)$, then for any pair of elements p,q in $Lp \sim q$ if and only if $M_p = M_q$ and $N_p = N_q$.*

Proof. For $S^{\alpha}_{L\mu\nu}$, the relation $\sim$ defined by $p \sim q$ if and only if $\mu_p = \mu_q$ and $\nu_p = \nu_q$ is an equivalence relation on L. As $\mu_p = \{x \in S | \mu_P = 1\} = \{x \in S | \mu_P \in \uparrow p\}$ and $\nu_p = \{x \in S | \nu_P = 1\} = \{x \in S | \nu_P \in \uparrow p\}$. We get that

$$\begin{aligned} p \sim q &\Leftrightarrow \mu_p = \mu_q, \\ \nu_p &= \nu_q \\ \Leftrightarrow \{x \in S | \mu(x) \in \uparrow p\} &= \{x \in S | \mu(x) \in \uparrow q\}, \\ \{x \in S | \nu(x) \in \uparrow p\} &= \{x \in S | \nu(x) \in \uparrow q\}, \\ \Leftrightarrow \uparrow p \cap M &= \uparrow q \cap M \\ \uparrow p \cap N &= \uparrow q \cap N, \\ \Leftrightarrow M_p &= M_q, \\ N_p &= N_q. \end{aligned} \tag{9}$$

Thus for $g, h \in L$, $g \neq h$ implies $\uparrow g \cap M \neq \uparrow h \cap M$ turns out to be the necessary and sufficient condition for an equivalence class to be a singleton. □

Theorem 5. *The sets $\mu(S)$ and $\nu(S)$ consists of all coatoms of the Boolean lattice L of lattice valued intuitionistic fuzzy set type-3 $S^{\alpha}_{L\mu\nu}$ constituted by a linear (r, k) code.*

Proof. Let $S^{\alpha}_{L\mu\nu}$ be an LIFS-3 corresponding to the linear code $\mathscr{C}$. From Theorem 4. if $x \neq y \in L$, then.

$$\begin{aligned} [x) \cap \mu(S) &\neq [y) \cap \mu(S), \\ [x) \cap \nu(S) &\neq [y) \cap \nu(S). \end{aligned} \tag{10}$$

Hence, the top element 1_L of the lattice L does not belong to $\mu(S)$ and $\nu(S)$ otherwise, the code $\mathscr{C}$ does not contain the codeword $00\ldots0$, which contradicts the linearity of the code. Now on the contrary, suppose that one co-atom, say, y, is not present in $\mu(S)$ and $\nu(S)$; then

$$\begin{aligned} [y) \cap \mu(S) &= [1) \cap \mu(S), \\ [y) \cap \nu(S) &= [1) \cap \nu(S). \end{aligned} \tag{11}$$

Thus $|\mathscr{C}| < |L|$, which leads to a contradiction. In fact, each codeword that corresponds to a co-atom has only non-zero coordinates, and forms a basis for the code $\mathscr{C}$. Let t be an element in $\mu(S)$ and $\nu(S)$ but not a co-atom. Then each codeword corresponding to t has a zero coordinate. If $\overline{c}_t$ is a codeword corresponding to t, then it is linearly independent of all those elements which are in the base that are not true. Hence $\mu(S)$ and $\nu(S)$ will consist of all co-atoms of a Boolean lattice. □

Theorem 6. *The linear (r, k)-code $\mathscr{C}$ corresponds to an LIFS-3 if and only if $\mathscr{C}$ is closed under intersection and for each $j \in \{1, \ldots, r\}$ there is a codeword in $\mathscr{C}$ having a non-zero j th coordinate.*

Proof. Let $S^{\alpha}_{L\mu\nu}$ be the LIFS-3 corresponding to $\mathscr{C}$. Then by Theorem 3, $\mathscr{C}$ is closed under an intersection, and non-zero vector $11\ldots1$ belongs to the families $\overline{\mu}_p$ and $\overline{\nu}_p$ for an element $p \in L$. As codeword $\overline{c}_p \in \mathscr{C}$ is a meeting of these two families, it is a non-zero vector contained in $\mathscr{C}$. Hence, satisfies the required condition. Conversely, suppose $\mathscr{C}$ is a linear (r, k) code satisfying the given conditions. The closeness of $\mathscr{C}$ under intersection ensures the existence of $11\ldots1$ in $\mathscr{C}$, which implies the constitution of LIFS-3. □

Theorem 7. *Let $S^{\alpha}_{L\mu\nu}$ be an LIFS-3 over a Boolean lattice L. If $\mu(S)$ and $\nu(S)$ include the maximum element of the set of all co-atoms of L, then the code constructed on $S^{\alpha}_{L\mu\nu}$ is linear.*

Proof. Consider $S^{\alpha}_{L\mu\nu}$ over a Boolean lattice L. The codewords corresponding to the maximum elements of co-atoms of a boolean lattice are linearly independent and thus can be extended to a basis that will be used to generate other codewords from the former codewords. If, corresponding to a maximum number of co-atoms, we have n codewords, then the code $\mathscr{C}$ consists of exactly 2^n codewords. Thus $\mathscr{C}$ is closed under the binary operation $\oplus$, and hence it is linear. □

Example 3. Consider the lattice $L = \{0, 1, a, b, c, d, e, f\}$ with partial order presented in Figure 2.

Construct an LIFS-3 on $S = \{1, 2\}$ by defining μ and ν as $\mu = \begin{pmatrix} 1 & 2 \\ e & f \end{pmatrix}$ and $\nu = \begin{pmatrix} 1 & 2 \\ f & d \end{pmatrix}$. Then a linear code is obtained as shown in Table 2.

Theorem 8. *Let $\mathscr{C}$ be a linear code over where a set T consists of maximum elements of the classes of co-atoms of Boolean lattice.*

Proof. For the linear code $\mathscr{C}$ over $S^{\alpha}_{L\mu\nu}$, the sets $\mu(S)$ and $\nu(S)$ consist of all the maximum elements of co-atoms. Hence $\mu(S) = \nu(S) = T$ and by Proposition 2.

$$d(\mathscr{C}) \geq \min_{p \in \overline{\mu}(s), \overline{\nu}(s)} s\left(c_p\right). \tag{12}$$

As for $s(u_p)$ and $s(v_p)$, this distance is equal to the minimum value on the codeword corresponding to the class of the co-atoms with minimal degree, and thus $s(c_p)$ is also attained its minimum. □

4. Application

Proteins are the most diverse class of biomolecules, both structurally and functionally, and they carry out many tasks. They are polymers of amino acids which are attached via peptide bonds and arranged in the form of long polypeptide chains [24]. Proteins have an extremely wide range of different functions, and they do not act by themselves. They usually interact with other proteins or macromolecules to form fully functional complexes, and these protein complexes are responsible for carrying out many different functions [25]. Nucleic acids are giant biomolecules made of monomers called nucleotides. Nucleic acids refer to the genetic material present in cells that transfer all the hereditary and transmissible information from parents to offspring. Deoxyribonucleic acid (DNA) and ribonucleic acid (RNA) are the two types of nucleic acids. The key task of nucleic acids is to use their stored genetic information for the synthesis of proteins via processes commonly known as translation and transcription. DNA is transcribed to RNA and then translated into a protein. The translation

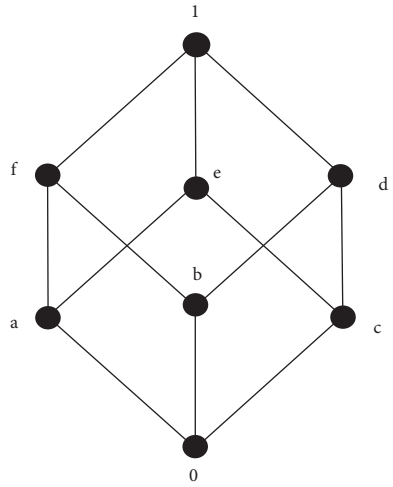

Figure 2: Lattice $L = \{0, 1, a, b, c, d, e, f\}$.

Table 2: Linear code over LIFS-3.

$\overline{\mu}_p$	$\overline{\nu}_p$	$\mathscr{C}$	$\overline{\mu}_p$	$\overline{\nu}_p$	$\mathscr{C}$	$\overline{\mu}_p$	$\overline{\nu}_p$	$\mathscr{C}$	$\overline{\mu}_p$	$\overline{\nu}_p$	$\mathscr{C}$
00	00	00	10	10	10	01	00	00	01	01	01
10	10	10	00	11	00	11	01	01	11	11	11

machinery includes tRNA, mRNA and ribosomes. A ribosomal subunit attaches to an mRNA molecule; then, tRNA molecules that have three complementary bases in their anticodon regions recognize and bind to specific codon sequences on the mRNA molecule. The ribosome moves along the mRNA, matching three base pairs at a time and adding the amino acids to the polypeptide chain [24, 25].

All living cells use a genetic code to translate the information encoded within the genetic material (DNA and RNA) into proteins. The genetic code describes the set of trios of nucleotides which specify particular amino acids (three nucleotides to one amino acid). There are twenty amino acids typically used to build proteins. As there are four bases, there are 64 possible base triplets [26]. A genetic code is a list of codons, and a codon is a consecutive series of three nucleotides. A codon set is an extension of the four letter-alphabet of DNA. There are four DNA bases, adenine (A), guanine (G), cytosine (C) and thymine (T), and thymine is replaced by uracil in RNA. The base guanine is the complementary base of cytosine, and adenine is that of thymine. Each codon corresponds to a specific type of amino acid; for example, the sequence of nucleotides "GUU" corresponds to a specific amino acid known as valine [27]. Two or more different codons can correspond to the same amino acid, making the genetic code degenerate, and such codons are known as synonymous codons. In a coding sequence, the synonymous codons are not used with equal frequencies in many organisms. This phenomenon is called synonymous codon usage bias (SCUB), and this shows that during the translation of genes to proteins, there is nonuniform usage of synonymous codons encoding the same amino acid; e.g., UGC and UGU are two different sequences corresponding to the same amino acid, cysteine [28].

The algebraic structures of the genetic code are essential to understanding the information and applications which are stored within the code. There are various conventional mathematical models of the genetic code, which include binary representations of the DNA bases. The representations of the four DNA bases by Jimenez-Montano et al. [29] are: ?=00, $G = 01$, $U = 10$ and $C = 11$. Stambuk [30] presented the universal metric properties of the human genetic code and described it by using the nucleotide base representation on the square having U or $T = 00$, $C = 01$, $G = 10$ and $A = 11$. A model for topological coding of proteins was proposed by Karasev and Stefanov [31], using: $C = 00$, $U = 01$, $G = 10$ and $A = 11$. Sánchez et al. [32] described the Boolean lattice of the genetic code and showed that the Boolean lattice of the genetic code can be obtained as the third power of the initial lattice. He used two types of lattices, the primal $(B(X), \sup, \inf)$ and the dual $(B(X), \inf, \sup)$, with $X = \{U, C, G, A\}$. The representations of the four bases given to primal lattice are: $G = 00$, $A = 01$, $U = 10$ and $C = 11$. Similarly, for the dual lattice: $C = 00, U = 01, A = 10$ and $G = 11$. A Hasse diagram of the genetic Boolean lattice is presented in the following Figure. It shows that the codons with uracil as a second base encode hydrophobic amino acids, and the codons with adenine as the second base encode hydrophilic amino acids. Additionally, the Hamming distances between pairs of codons reveal distinct hydrophobicities among their encoded amino acids. If XYZ and $X_1Y_1Z_1$ are two codons, then $XYZ \leq X_1Y_1Z_1$ only if $X \leq X_1, Y \leq Y_1$, $Z \leq Z_1$, and we can say that the codons are comparable.

In recent years, a paradigm shift for "new biology" has taken place as a direct result of an expanded awareness of the fuzziness of the processes that occur in biological systems. There is a lot of evidence to suggest that many biological processes are not deterministic but rather include an inherent element of uncertainty. Many studies and observations have shown that fuzzy effects are a very important part of how living things develop and work in their physiology and evolution. Both fuzzy set theory and fuzzy logic, along with many other approaches to computational intelligence, have the potential to solve a numerous challenges that arise in the field of bioinformatics. An analysis of protein sequences can be performed using fuzzy set theory and fuzzy logic. A method was devised to predict the solvent accessibility of each amino acid in a protein sequence by using a k-nearest neighbour approach [33]. In addition, the FKNN algorithm has been used to predict a protein's subcellular location [34], which refers to the region of the cell in which the protein is found (including extracellular, cytoplasm, nucleus). In this study, a class membership function was used in accordance with the dipeptide composition of a protein sequence. Fuzzy logic was used in conjunction with neural networks to describe how protein motifs can change [35].

An information-theoretic-based fuzzy inference engine was created to predict coding areas, or the sequence segments that correspond to proteins, for genomic sequences (DNA) [36]. Polynucleotides (words made up of the letters A, T, C, and G) were also employed by researchers as fuzzy

Table 3: Amino acids and RNA codons.

Amino acid	RNA codons	Abb	Amino acid	RNA codons	Abb
Isoleucine	AUU, AUC, AUA	I	Phenylalanine	UUU, UUC	F
Valine	GUA, GUC, GUG, GUU	V	Lysine	AAA, AAG	K
Tryptophan	UGG	W	Methionine	AUG	M
Alanine	GCA, GCC, GCG, GCU	A	Glycine	GGA, GGC, GGG, GGU	G
Cysteine	UGC, UGU	C	Tyrosine	UAC, UAU	Y
Proline	CCA, CCC, CCG, CCU	P	Threonine	ACA, ACC, ACG, ACU	T
Serine	UCA, UCC, UCG, UCU, AGC, AGU	S	Histidine	CAC, CAU	H
Glutamic acid	GAA, GAG	E	Asparagine	AAC, AAU	N
Glutamine	CAA, CAG	Q	Aspartic acid	GAC, GAU	D
Leucine	CUA, CUC, CUG, CUU, UUA, UUG	L	Arginine	CGA, CGC, CGG, CGU, AGA, AGG	R

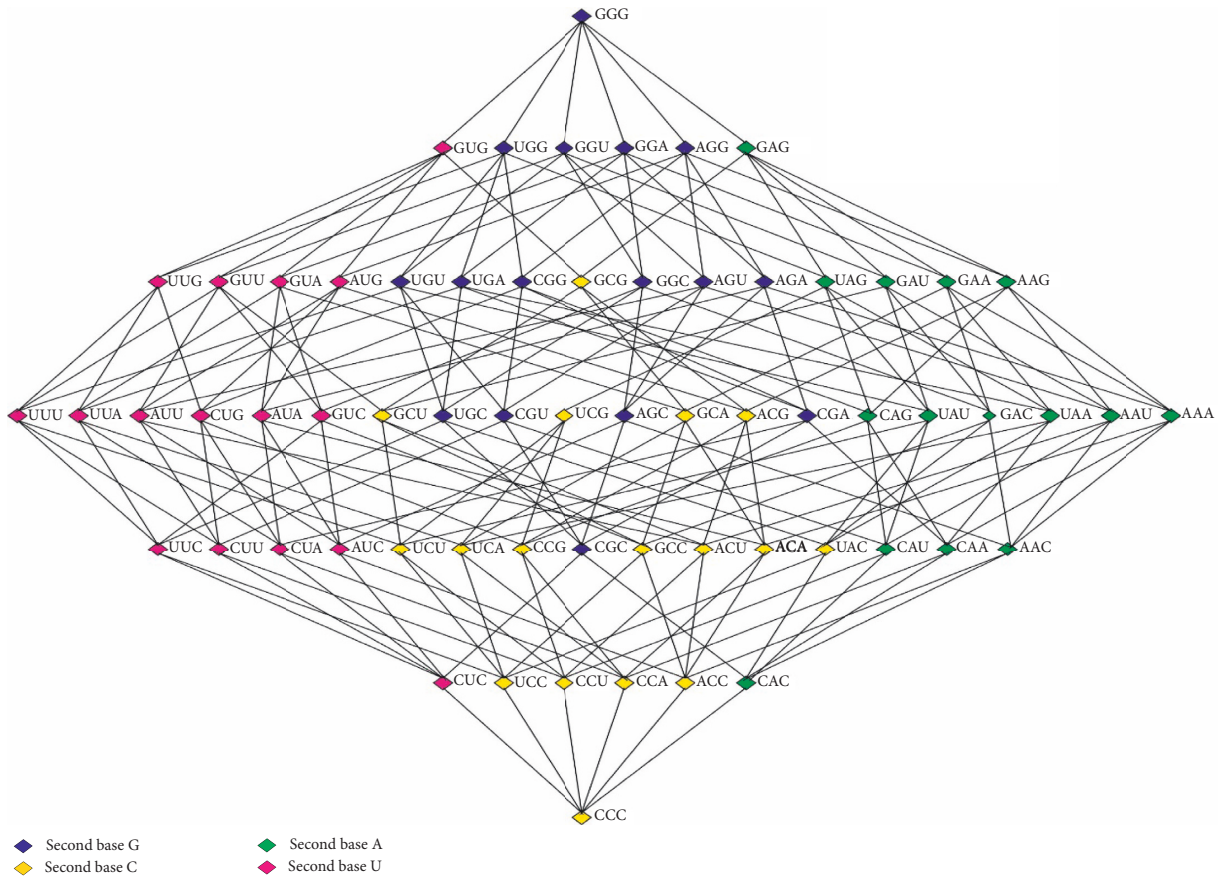

Figure 3: The Boolean lattice of 64 codons.

sets, and they developed a method for calculating the distances between them as points in a hypercube [37, 38]. The procedure served as a tool for comparing various genetic sequences. Additionally, operons, an important structure in bacterial genomes, were predicted using fuzzy scoring functions based on various biological information (e.g., genome sequences, functional annotations, and conservation across multiple genomes) [39]. An operon is a closely related group of neighbouring genes on a DNA sequence.

Ordinary fuzzy sets are used in the literature to model numerous bioinformatics-related problems. In a conventional fuzzy set, the degree of belongingness to the set under discussion is indicated by the membership function, which assigns a number from the unit interval to each element of the discourse universe. A LIFS-3, on the other hand, is distinguished by two functions that, express the degree of belongingness and the degree of non-belongingness. This concept, which is a natural generalization of an ordinary fuzzy set, appears to be helpful in simulating a variety of real-world scenarios. Thus, the idea of LIFS-3 can be used to study biological problems in a more significant way.

In this paper we investigate the genetic code further by considering a lattice valued intuitionistic fuzzy set. We consider S to be the set of 20 amino acids: x_1 = Phenylalanine, x_2 = Leucine, x_3 = Isoleucine, x_4 = Methionine, x_5 = Valine, x_6 = Serine, x_7 = Proline,

Table 4: Genetic codes over LIFS-3.

p	$\overline{\mu}_p$	$\overline{\nu}_p$	$\overline{\mathscr{C}}_p = \overline{\mu}_p \wedge \overline{\nu}_p$
CCC	1111111111111111111	1111111111111111111	1111111111111111111
CUC	11111000000000001111	11111100000000001111	11111000000000001111
UCC	11001100110000111111	11001100110000111101	11001100110000111101
CCU	10111111111010101111	01010000000101010100	00010000000000000101
CCA	01010000000101010110	01010000000101010110	01010000000101010110
ACC	00111001100011110011	00111001100011110011	00111001100011110011
CAC	00000000011111111111	00000000011111111111	00000000011111111111
UUC	11001000000000001101	10010000000000001101	11001000000000001101
CUU	10111000000000001101	01010000000000000111	00010000000000000111
CUA	01010000000000000110	01010000000000000110	01010000000000000110
AUC	00111000000000000011	00111000000000000011	00111000000000000011
UCU	10001100110000101101	01000000000000010101	00000000000000000101
UCA	01000000000000010100	00100000000000010100	01000000000000000100
CCG	00010000000000000100	01010100000100010110	00010000000000010110
CGC	00000000000000000111	00000000000000001111	00000000000000000111
GCC	00001000100000110001	00001000100000110001	00001000100000110001
ACU	00111001100010100001	00010000000001010011	00010000000000000001
ACA	00010000000001010010	00100000000011101010	00010000000001010010
UAC	00000000010000111101	00000000010000111111	00000000110000111101
CAU	00000000000101010111	00000000001000101011	00000000000000000101
CAA	00000000001010110110	00000000000101010110	00000000000101010110
AAC	00000000000011110011	00000000000011110011	00000000000011110011
UUU	10000110000000001101	01000000000000000100	00000000000000000100
UUA	01000000000000000100	01000000000000000100	01100000000000000100
AUU	00111000000000100001	00010000000000000010	00010000000000000001
CUG	00010000000000000100	01010000000000000110	00010000000000000100
AUA	00010000000000000010	00010000000000000010	00010000000000000010
GUC	00000000000000110001	00000000000000110001	00000000000000110001
GCU	00001000100000010001	00000000000000010000	00000000000000000000
UGC	00000000000000001111	00000000000000001111	00000000000000001111
CGU	00000000000000000100	00000000000000000100	00000000000000000100
UCG	00000000000000000100	00000000000000000100	00000000000000000100
AGC	00000000000000000011	00000000000000000011	00000000000000000011
GCA	00000000000000010000	00000000000000010000	00000000000000010000
ACG	00010000000000000000	00010000000001010010	00010000000000000000
CGA	00000000000000000110	00000000000000000110	00000000000000000110
CAG	00000000000000000100	00000000000100010110	00000000000000000100
UAU	00000000010000101101	00000000000000000101	00000000000000000101
GAC	00000000000000110001	00000000000000110001	00000000000000110001
UAA	00000000000000010100	00000000000000010100	00000000000000010100
AAU	00000000000010100001	00000000000000010010	00000000000000000000
AAA	00000000000001010010	00000000000001010010	00000000000001010010
UUG	00000000000000000100	01000000000000001100	00000000000000000100
GUU	00001000000000000001	00000000000000000000	00000000000000000000
GUA	00000000000000000000	00000000000000000000	00000000000000000000
AUG	00010000000000000000	00010000000000000000	00010000000000000000
UGU	00000000000000001101	00000000000000000101	00000000000000000100
UGA	00000000000000000100	00000000000000000100	00000000000000000100
CGG	00000000000000000100	00000000000000000110	00000000000000000100
GCG	00000000000000000000	00000000000000010000	00000000000000000000
GGC	00000000000000000001	00000000000000000001	00000000000000000001
AGU	00000000000000000001	00000000000000000010	00000000000000000000
AGA	00000000000000000010	00000000000000000010	00000000000000000010
UAG	00000000000000000100	00000000000000010100	00000000000000000100
GAU	00000000000000100001	00000000000000010000	00000000000000000000
GAA	00000000000000110000	00000000000000010000	00000000000000010000
AAG	00000000000000000000	00000000000000010010	00000000000000000000
GUG	00000000000000000000	00000000000000000000	00000000000000000000
UGG	00000000000000000100	00000000000000000100	00000000000000000100
GGU	00000000000000000001	00000000000000000000	00000000000000000000

Table 4: Continued.

p	$\overline{\mu}_p$	$\overline{\nu}_p$	$\overline{\mathscr{C}}_p = \overline{\mu}_p \wedge \overline{\nu}_p$
GGA	00000000000000000000	00000000000000000000	00000000000000000000
AGG	00000000000000000100	00000000000000000100	00000000000000000100
GAG	00000000000000000000	00000000000000010000	00000000000000000000
GGG	00000000000000000000	00000000000000000000	00000000000000000000

Table 5: Hamming distance between pairs of Amino acids.

Amino acid	G	W	C	R	S	V	L	F	M	I	E	D	Y	K	N	Q	H	A	T	p
G	0	1.5	2.8	1.8	3.2	1.4	3.8	5.2	1.7	2.5	1	2.9	2.5	2	3	3.5	6	2.4	4.5	8.6
W	1.5	0	1	0.6	2.7	3	2.8	5	2	4	2	2.5	2	2.5	4	2	5.5	2.5	5.5	8.2
C	2.8	1	0	1.2	2.8	2.3	2.8	5.8	3	3.7	3	3	2	3.6	4	2.5	5	3.1	5.4	8
R	1.8	0.6	1.2	0	3.1	2.5	2.8	4.8	2.5	3.5	2	2.8	3	2.5	4.3	2.3	5.5	2.9	5.3	7.9
S	3.2	2.7	2.8	3.1	0	3.8	3.0	5.3	4.0	4.2	3.3	2.9	3.3	4	4.6	3.6	6.5	3.8	5.7	8.5
V	1.4	3	2.3	2.5	3.8	0	4.3	6.2	2	3.7	1.2	1.8	2.8	2.2	3	3.6	6.2	1.6	4.6	8
L	3.8	2.8	2.8	2.8	3.0	6.2	0	6.5	3.2	3.9	4	4.8	3.5	4.8	5.9	4.3	7	4.3	6.3	7.8
F	5.2	5	5.8	4.8	5.3	6.2	6.5	0	7	6.8	6	6	5	5.3	5	5	8	5.8	8.3	8.5
M	1.7	4	3	2.5	4	2	3.2	7	0	2	1.5	2.5	4	2.5	4	4	7.5	2	3.5	8.7
I	2.5	4	3.7	3.5	4.2	3.7	3.9	6.8	2	0	3	4	4.5	3.8	6.3	5.3	7.3	3.6	3.8	4.5
E	1	2	3	2	3.3	1.2	4	6	1.5	3	0	2	3	2	3.5	3.5	7.3	2.2	5.1	8.3
D	2.9	2.5	3	2.8	2.9	1.8	4.8	6	2.5	4	2	0	2.5	2.8	3.3	3.5	6	2	4.6	8.1
Y	2.5	2	2	3	3.3	2.8	3.5	5	4	4.5	3	2.5	0	4	4.2	3.5	4.5	3.6	5.4	8.2
K	2	2.5	3.6	2.5	4	2.2	4.8	5.3	2.5	3.8	2	2.8	4	0	3	4.5	5.3	2.6	5.1	8.4
N	3	4	4	4.3	4.6	3	5.9	5	4	6.3	3.5	3.3	4.2	3	0	4.3	5.5	4.3	4.8	8.6
Q	3.5	2	2.5	2.3	3.6	3.6	4.3	5	4	5.3	3.5	3.5	3.5	4.5	4.3	0	5.5	5	5.8	7.2
H	6	5.5	5	5.5	6.5	6.2	7	8	7.5	7.3	7.3	6	4.5	5.3	5.5	5.5	0	6	8.1	7.2
A	2.4	2.5	3.1	2.9	3.8	1.6	4.3	5.8	2	7.3	2.2	2	3.6	2.6	4.3	5	6	0	4.7	4.5
T	4.5	5.5	5.4	5.3	5.7	4.6	6.3	8.3	3.5	3.8	5.1	4.6	5.4	5.1	4.8	5.8	8.1	4.7	0	4.5
P	8.6	8.2	8	7.9	8.5	9	7.8	8.5	8.7	4.5	8.3	8.1	8.2	8.4	8.6	7.2	4.5	7.2	8.9	0

x_{81} = Threonine, x_9 = Alanine, x_{10} = Tyrosine, x_{11} = Histidine, x_{12} = Glutamine, x_{13} = Aspartic, x_{14} = Lysine, x_{15} = Asparagine, x_{16} = Glutamic, x_{17} = Cysteine, x_{18} = Tryptophan, x_{19} = Arginine, x_{20} = Glycine. The codons related to amino acids are listed in Table 3.

Let L be the lattice (see Figure 3.) consisting of 64 codons. As two or more codons can encode the same amino acid e.g., UUU and UUC encode the same amino acid, phenylalanine we put $\overline{\mu}(x_1) = \text{UUU}$ and $\overline{\nu}(x_1) = \text{UUC}$, where x_1 =phenylalanine. Similarly, we can assign a codon for every other amino acid, and we ha where

$$\begin{aligned}
&a_1 = \text{UUU} \quad a_2 = \text{UUA} \quad a_3 = \text{AUU} \quad a_4 = \text{AUG} \quad a_5 = \text{GUU}\\
&a_6 = \text{UCU} \quad a_7 = \text{CCU} \quad a_8 = \text{ACU} \quad a_9 = \text{GCU} \quad a_{10} = \text{UAC}\\
&a_{11} = \text{CAU} \quad a_{12} = \text{CAA} \quad a_{13} = \text{AAU} \quad a_{14} = \text{AAA} \quad a_{15} = \text{GAU}\\
&a_{16} = \text{GAA} \quad a_{17} = \text{UGU} \quad a_{18} = \text{UGG} \quad a_{19} = \text{AGA} \quad a_{20} = \text{GGU}\\
&b_1 = \text{UUC} \quad b_2 = \text{UUG} \quad b_3 = \text{AUC} \quad b_4 = \text{AUG} \quad b_5 = \text{GUC}\\
&b_6 = \text{UCC} \quad b_7 = \text{CCC} \quad b_8 = \text{ACC} \quad b_9 = \text{GCU} \quad b_{10} = \text{UAC}\\
&b_{11} = \text{CAU} \quad b_{12} = \text{CAG} \quad b_{13} = \text{AAC} \quad b_{14} = \text{AAG} \quad b_{15} = \text{GAC}\\
&b_{16} = \text{GAG} \quad b_{17} = \text{UGC} \quad b_{18} = \text{UGG} \quad b_{19} = \text{AGG} \quad b_{20} = \text{GGC}
\end{aligned} \tag{13}$$

Consider a representation of four bases as $C = 00$, $U = 01$, $A = 10$ and $G = 11$. Let $p = CCC$ be an element of a lattice L. Then, $\overline{\mu}_{CCC}(x_1) = \mu(x_1) \geq CCC$. Now, by using definition of a level function, $\overline{\mu}_{CCC}(x_1) = 1$. Similarly, $\overline{\mu}_{CCC}(x_2), \ldots, \overline{\mu}_{CCC}(x_{20}) = 1$. Thus $\mu_{CCC} = 1111111111111111111$ is a codeword relative to the codon CCC. In similar fashion, the remaining codewords corresponding to the other codewords can be found, which are shown in Table 4.

Hence, we have a binary code corresponding to 64 codons having length 20. Furthermore, the difference

Table 6: Hamming distance between hydrophobic and hydrophilic Amino acids.

Codewords	$\mathscr{C}_{XAZ}$	$\mathscr{C}_{XUZ}$	Codewords	$\mathscr{C}'_{XAZ}$	$\mathscr{C}'_{XUZ}$
$\mathscr{C}_{XAZ}$	8.2	11	$\mathscr{C}'_{XAZ}$	7.6	9.3
$\mathscr{C}_{XUZ}$	9.5	6.5	$\mathscr{C}'_{XUZ}$	9.3	6.1

between two codewords can be calculated by using well known Hamming distance. That is,

$$d_H(\mathscr{C}_{CUC}, \mathscr{C}_{UCC}) = d_H(1111100000000000111, 1100110011000011110) = 8. \quad (14)$$

If we consider only membership values μ_p from the above table, then it is an L-fuzzy code [28]. The distances between different amino acids pairs can be computed in terms of mean distances between their respective codons. For instance, the amino acids glycine (G) and methionine (M) are encoded by the bases GGA, GGC, GGG, GGU and AUG. Thus, the distance between G and M means the distances between the codewords ($\mathscr{C}_{GGA}$, $\mathscr{C}_{GGC}$, $\mathscr{C}_{GGU}$, $\mathscr{C}_{CUG}$ and $\mathscr{C}_{AUG}$) relative to their codons. The distances between all the 20 pairs of amino acids are shown in Table 5.

The Hamming distance between two codons reflects the variations among the physico-chemical properties of the relative amino acids. Amino acids can be categorized by two types, hydrophobic amino acids (codons having U in second base) and hydrophilic amino acids (codons having A in the second base). Consider the collections of codewords $\mathscr{C}_{XAZ}$, $\mathscr{C}_{XUZ}$, $\mathscr{C}'_{XAZ}$ and $\mathscr{C}'_{XUZ}$, where $X, Y, Z \in \{A, C, G, U\}$ over LIFS-3 and L-fuzzy set, respectively. Table 6 shows the Hamming distances between these sets.

It can be seen that the distances between amino acids with larger differences in physico-chemical properties are larger in an LIFS-3 environment than a L-fuzzy set.

5. Conclusion

The authors' main focus was to construct codes over lattice valued intuitionistic fuzzy set type-3. Binary and binary Linear codes are commonly defined in terms of subspaces of $\mathbb{Z}_2^n$. Different attempts were made to incorporate the imprecisions in data into the coding process by involving theoretical fuzzy set concepts. Using membership and nonmembership functions, codes were designed over LIFS-3. Distances of code were examined in relation with the degrees of the codewords. It was concluded that binary block and binary linear codes can be constructed over LIFS-3, and conversely, from any given binary block code, we can formulate an LIFS-3. Code over a lattice valued intuitionistic fuzzy set type-3 was constructed by considering the lattice of a 64-codon system, and we found that the physico-chemical differences can be interpreted by computing the Hamming distances between codewords. In the case of LIFS-3, the Hamming distances between codewords were greater than the Hamming distances between codewords in L-fuzzy sets, which indicates the efficiency of the LIFS-3 compared to the L-fuzzy set. In the future, a variety of extensions will be possible. One of the major directions of this work will be to study the already existing codes, such as Hamming code and Hadamard code, by introducing the concept of LIFS-3. This may be done by encoding the messages by using the decomposition of LIFS-3, which gives the family of characteristic functions. Furthermore, the developed application could be used for the further study of the structure of genetic code. As found in the literature, the variations among different physio-chemical properties of amino acids are described by the Hamming distances between the codons. In LIFS-3 codes, this Hamming distance is related to the degrees of code words (or classes), so we can extend it by incorporating these degrees along with the Hamming distances. Moreover, there are several practically useful generalizations of fuzzy sets including the picture fuzzy sets [40], Pythagorean fuzzy sets [41], hesitant fuzzy sets [42] and neutrosophic sets [43] where the replacement of the interval [0, 1] by lattices L can play a vital role in the development and application of fuzzy coding theory.

Data Availability

No data is used to support this study.

Conflicts of Interest

The authors declare that there were no conflicts of interest regarding the publication of this article.

Authors' Contributions

All authors contributed equally to the preparation of this manuscript.

References

[1] L. A. Zadeh, "Fuzzy sets," *Information and Control*, vol. 8, no. 3, pp. 338–353, 1965.

[2] K. T. Atanassov, "Intuitionistic fuzzy sets," *Fuzzy Sets and Systems*, vol. 20, no. 1, pp. 87–96, 1986.

[3] K. T. Atanassov, "Geometrical interpretation of the elements of the intuitionistic fuzzy objects," *IM-MFAIS*, vol. 20, no. S1, pp. 1–89, 1989.

[4] J. A. Goguen, "L-fuzzy sets," *Journal of Mathematical Analysis and Applications*, vol. 18, no. 1, pp. 145–174, 1967.

[5] K. T. Atanassov and S. Stoeva, "Intuitionistic L-fuzzy sets," in *Cybernetics and System Research*, pp. 539-540, Elsevier, Amsterdam, Netherlands, 1984.

[6] T. Gerstenkorn and A. Tepavcevic, "Lattice valued intuitionistic fuzzy sets," *Central European Journal of Mathematics*, vol. 2, no. 3, pp. 388–398, 2004.

[7] R. S. Murugan and V. S. Ananthanarayana, "WordCode using WordTrie," *Journal of King Saud University-Computer and Information Sciences*, vol. 34, no. 3, pp. 923–933, 2022.

[8] A. R. and R. Kaviarasan, "Weighted distance hyperbolic prediction-based detection scheme for non line of sight nodes in VANETs," *Journal of King Saud University - Computer and Information Sciences*, vol. 33, no. 4, pp. 489–496, 2021.

[9] S. Nagaraju, L. J. Gudino, N. Tripathi, V. C.K., and R. CK, "Mobility assisted localization for mission critical Wireless Sensor Network applications using hybrid area exploration approach," *Journal of King Saud University - Computer and Information Sciences*, vol. 33, no. 5, pp. 608–618, 2021.

[10] P. A. von Kaenel and A. Pierre, "Fuzzy codes and distance properties," *Fuzzy Sets and Systems*, vol. 8, no. 2, pp. 199–204, 1982.

[11] L. O. Hall, G. Dial, On fuzzy codes for asymmetric and unidirectional errors," *Fuzzy Sets and Systems*, vol. 36, no. 3, pp. 365–373, 1990.

[12] S. A. Tsafack, S. Ndjeya, L. Strüngmann, and C. Lele, "Fuzzy linear codes," *Fuzzy Information and Engineering*, vol. 10, no. 4, pp. 418–434, 2018.

[13] B. Amudhambigai and A. A. Neeraja, "New view of fuzzy codes and its application," *Jordan Journal of Mathematics and Statistics*, vol. 12, no. 4, pp. 455–471, 2019.

[14] V. Shijina, "Multi-fuzzy codes," in *Proceedings of the AIP Conference Proceedings*, vol. 2336, no. 1, Article ID 040026, Australia, 2021.

[15] W. S. Du, "Subtraction and division operations on intuitionistic fuzzy sets derived from the Hamming distance," *Information Sciences*, vol. 571, pp. 206–224, 2021.

[16] M. Ali, H. Khan, L. H. Son, F. Kandasamy, and W. B. V. Kandasamy, "New soft set based class of linear algebraic codes," *Symmetry*, vol. 10, no. 10, p. 510, 2018.

[17] B. Seselja and A. Tepavcevic, "On a construction of codes by P-fuzzy sets," *Univ.uNovomSaduZb. Rad. Prirod.-Mat.Fak. Ser. Mat.*vol. 20, no. 2, pp. 71–80, 1990.

[18] B. Seselja, A. Tepavcevic, and G. Vojvodic, "L-fuzzy sets and codes"," *Fuzzy Sets and Systems*, vol. 53, no. 2, pp. 217–222, 1993.

[19] Z. Mališa and V. Lazarević, "Construction of codes by lattice valued fuzzy sets," *Novi Sad Journal of Mathematics*, vol. 35, no. 2, pp. 155–160, 2005.

[20] X. Li, S. Hua, and X. Hua, "Pattern recognition of grating perimeter intrusion behavior in deep learning method," *Symmetry*, vol. 13, no. 1, p. 87, 2021.

[21] Y. Hafeez, S. Ali, N. Jhanjhi, M. Humayun, A. Nayyar, and M. Masud, "Role of fuzzy approach towards fault detection for distributed components," *Computers, Materials & Continua*, vol. 67, no. 2, pp. 1979–1996, 2021.

[22] M. Ali Lilo and M. Jasem Mahammad, "Design and implementation of wireless system for vibration fault detection using fuzzy logic," *IAES International Journal of Artificial Intelligence*, vol. 9, no. 3, pp. 545–552, 2020.

[23] R. M. Roth, *Introduction to Coding Theory, IET Communications*, Cambridge University Press, Cambridge, UK, 2006.

[24] B. Alberts, A. Johnson, J. Lewis, M. Raff, and K. Roberts, "The shape and structure of proteins," in *Molecular Biology of the Cell*, Garland Science, New York, USA, 2002.

[25] D. Voet, J. G. Voet, and C. W. Pratt, *Fundamentals of Biochemistry*, John Wiley & Sons, New Jersey, USA, 2006.

[26] M. V. Zamudio and G. S. Zamudio, "On the importance of asymmetry in the phenotypic expression of the genetic code upon the molecular evolution of Proteins," *Symmetry*, vol. 12, no. 6, p. 997, 2020.

[27] M. W. Nirenberg, "The genetic code: II," *Scientific American*, vol. 208, no. 3, pp. 80–95, 1963.

[28] A. A. Komar, "Synonymous codon usage-a guide for Co-translational protein folding in the cell," *Molecular Biology*, vol. 53, no. 6, pp. 777–790, 2019.

[29] M. A. Jiménez-Montaño, C. R. de la Mora-Basáñez, and T. Pöschel, "The hypercube structure of the genetic code explains conservative and non-conservative aminoacid substitutions in vivo and in vitro," *Biosystems*, vol. 39, no. 2, pp. 117–125, 1996.

[30] N. Stambuk, "Universal metric properties of the genetic code," *Croatica Chemica Acta*, vol. 73, pp. 1123–1139, 2000.

[31] V. A. Karasev and V. Stefanov, "Topological nature of the genetic code," *Journal of Theoretical Biology*, vol. 209, no. 3, pp. 303–317, 2001.

[32] R. Sanchez, E. Morgado, and R. Grau, "The genetic code Boolean lattice," *Match - Communications in Mathematical and in Computer Chemistry*, vol. 52, pp. 29–46, 2004.

[33] J. Sim, S. Y. Lee, and J. Lee, "Prediction of protein solvent accessibility using fuzzy k-nearest neighbor method," *Bioinformatics*, vol. 21, no. 12, pp. 2844–2849, 2005.

[34] Y. Li and Y. Li, "Prediction of protein subcellular locations using fuzzy k-NN method," *Bioinformatics*, vol. 20, no. 1, pp. 21–28, 2004.

[35] B. C. Halgamuge and S. K. Halgamuge, "Protein motif extraction with neuro-fuzzy optimization," *Bioinformatics*, vol. 18, no. 8, pp. 1084–1090, 2002.

[36] T. V. Arredondo, P. S. De Groff, and D. De Groff, "Fuzzy attributes of a DNA complex: development of a fuzzy inference engine for codon-"junk" codon delineation," *Artificial Intelligence in Medicine*, vol. 35, no. 1-2, pp. 87–105, 2005.

[37] A. Nieto and J. J. Nieto, "The fuzzy polynucleotide space: basic properties," *Bioinformatics*, vol. 19, no. 5, pp. 587–592, 2003.

[38] K. Sadegh-Zadeh, "Fuzzy genomes," *Artificial Intelligence in Medicine*, vol. 18, no. 1, pp. 1–28, 2000.

[39] E. Jacob, R. Sasikumar, and K. N. R. Nair, "A fuzzy guided genetic algorithm for operon prediction," *Bioinformatics*, vol. 21, no. 8, pp. 1403–1407, 2005.

[40] R. Sahu, S. R. Dash, and S. Dash, "Career selection of students using hybridized distance measure based on picture fuzzy set and rough set theory," *Decision Making: Applications in Management and Engineering*, vol. 4, no. 1, pp. 104–126, 2021.

[41] F. Xiao and W. Ding, "Divergence measure of Pythagorean fuzzy sets and its application in medical diagnosis," *Applied Soft Computing*, vol. 79, pp. 254–267, 2019.

[42] A. K. Das and C. Granados, "FP-intuitionistic multi fuzzy N-soft set and its induced FP-Hesitant N soft set in decision making," *Decision Making: Applications in Management and Engineering*, vol. 5, no. 1, pp. 67–89, 2022.

[43] F. Smarandache, "Neutrosophic seta generalization of the intuitionistic fuzzy set," *Journal of Defense Resources Management*, vol. 1, no. 1, pp. 107–116, 2010.

Hindawi
Complexity
Volume 2022, Article ID 5043058, 16 pages
https://doi.org/10.1155/2022/5043058

Research Article

Multiobjective Parallel Algorithms for Solving Biobjective Open Shop Scheduling Problem

Seyed Hassan Shams Lahroudi,[1] **Farzaneh Mahalleh**,[2] **and Seyedsaeid Mirkamali**[3]

[1]*Department of Industrial Management, Science and Research Branch, Islamic Azad University, Tehran, Iran*
[2]*Department of Computer, Faculty of Khoy, West Azarbijan Branch, Technical and Vocational University (TVU), Khoy, Iran*
[3]*Department of Computer Engineering and IT, Payame Noor University (PNU), Tehran, Iran*

Correspondence should be addressed to Seyedsaeid Mirkamali; s.mirkamali@pnu.ac.ir

Received 18 February 2022; Revised 15 May 2022; Accepted 5 July 2022; Published 31 August 2022

Academic Editor: Hui Xiao

Open Shop Scheduling Problem (OSSP) is one of the most important scheduling problems in the field of engineering and industry. This kind of problem includes m machines and n jobs, each job contains a certain number of operations, and each operation has a predetermined processing time on its corresponding machine. The order of processing of these operations affects the completion times of all jobs. Therefore, the purpose of OSSP is to achieve a proper order of processing of jobs using specified machines, so that the completion time of all jobs is minimized. In this paper, the strengths and limitations of three methods are evaluated by comparing the results of solving the OSSP in large-scale and small-scale benchmarks. In this case, the minimized completion time and total tardiness are considered the objective functions of the adapted methods. To solve small-scale problems, we adapt a mathematical model called Multiobjective Mixed Linear Programming (MOMILP). To solve large-scale problems, two metaheuristic algorithms including Multiobjective Parallel Genetic Algorithm (MOPGA) and Multiobjective Parallel Simulated Annealing (MOPSA) are adapted. In experimental results, we randomly generated small-scale problems to compare MOMILP with the Genetic Algorithm (GA) and Simulate Annealing (SA). To compare MOPSA and MOPGA with the state of the art and show their strengths and limitations, we use a standard large-scale benchmark. The simulation results of the proposed algorithms show that although the MOPSA algorithm is faster, the MOPGA algorithm is more efficient in achieving optimal solutions for large-scale problems compared with other methods.

1. Introduction

Optimal job scheduling problems are classified into single machine scheduling, job shop scheduling, open shop scheduling, flow shop scheduling, and hybrid scheduling problems; where the single machine scheduling is the simplest problem of scheduling. The problem is to schedule the processing of n jobs with varying processing times on a single machine [1]. In the Job Shop Scheduling Problem (JSSP), the problem is more complex. Here, each job consists of a set of operations ($O1$, $O2$, ..., O_n) that need to be processed in a specific order. Each operation has a unique machine on which it must be performed, and only one operation per task may be performed at the moment [2]. A more complex problem than JSSP is the Open Shop Scheduling Problem (OSSP). OSSP involves m machines $(M_1, M_2, \ldots, M_m)$ to perform n jobs $(J_1, J_2, \ldots, J_n)$, each job involving m operations. Jth operation of J_j is indicated by O_{ij} which should be processed on machine M_i for $p_{ij} \geq 0$ units of time. Therefore, we will have a total of $n \times m$ operations $(O_{11}, O_{12}, \ldots, O_{nm})$ [3]. Like OSSP, each job in the Flow Shop Scheduling Problem (FSSP) consists of precisely m operations. However, the ith operation of the job must be executed on the ith machine. No machine is capable of doing many operations simultaneously. The execution time for each action of each task is provided earlier [4]. The most complex problem in the class of job scheduling problems is the hybrid scheduling problem (HSFP). In this problem, n jobs $(J_1, J_2, \ldots, J_n)$, must be processed in a multistage manufacturing facility in

which each step has several concurrent and identical machines [5].

This paper addresses the problem of Biobjective Open Shop Scheduling. In case of complexity of the problem, the OSSP is in between the job shop scheduling and the flow shop scheduling problems. However, all the problems in this class are considered as NP-Hard problems. The OSSP has a broad range of applications across different sectors that include timetabling, Satellite communication, health care management, transportation, tourism, computer vision, and many other applications. In the following subsection, we introduce some related works that tried to solve the problem of open shop scheduling.

1.1. Related Works. Production scheduling problems have been widely studied in the past years. A detailed review of this type of research work can be found in [6, 7]. Breit et al. [8] solved the OSSP of two machines with a predetermined stop time for one of the machines and proposed a heuristic algorithm. Next, they set some predetermined stop times for both machines and again used heuristic algorithms to approximate the problem. Hsu et al. [9] examined two different periodic maintenance approaches simultaneously in the single-machine scheduling problem. Periodic maintenance approaches considered for their problem are such that the machine stops after a certain period of time (T) or after processing a certain number of jobs (K) in order to perform the maintenance process. Obviously, if either of these conditions occurs earlier, the machine will stop.

To quantitatively characterize the production and distribution optimization issue, Fu et al. [10] formulate a mixed-integer programming model to minimize the maximum completion time. To best handle the presented issue, an improved black widow optimization method is created to address the researched problem. In their suggested method, the solution representation, population initiation, procreation, cannibalism, and mutation, as well as a simulated annealing method, are uniquely constructed.

Another condition that arises in the presence of machines' unavailability constraint is the impermissibility of cutting work due to which in the absence of sufficient time to perform an operation and face the machine stop, the desired operation is not loaded on the machine and its processing is postponed until machine stop is finished. Transportation and movement times between machines are other criteria that have been considered in scheduling problems. Strusevich [11] considered a time interval between the completion of the processing of one activity of a job on one machine and the beginning of the next activity of the same job on another machine for two-machine OSSP and due to occurring transportation in real conditions named it transportation time. He also points out that in chemical and metallurgical applications, these transportation times are equivalent to the times of the heating or cooling processes.

Recently, Fu et al. [12] offer a stochastic biobjective two-stage open shop scheduling problem that mimics a car repair process where duties are delegated to different third-party organizations with specialized equipment. The optimization issue was formulated by reducing the overall lateness and processing costs, subject to different resource restrictions. In order to tackle the open shop issue, a hybrid multiobjective optimization of migratory birds, along with a genetic operation and discrete event system, is developed by considering problem features.

The OSSP is known as an NP-hard problem [13–15] and it is not possible to solve these problems in polynomial time except in small dimensions. Therefore, approximate solution achievements including heuristic and metaheuristic methods can be more efficient than exact methods. Panahi et al. [16] used multiobjective simulated annealing and Ant Colony Optimization (ACO) algorithm to solve Multiobjective Open Shop Scheduling (MOOSS) with the objectives of total delay and the longest completion time. Panahi and Tavakkoli-Moghaddam [17] combined general and multiobjective simulated annealing algorithms with ACO and used it to simultaneous optimization of two objective functions including the longest completion time and total delay in OSSP. Drezner [18] used the Genetic Algorithm (GA) and Simulated Annealing (SA) algorithm for batch scheduling in the case of multifunction parallel machines.

Task scheduling has been studied in much different research works with an array of different applications from task scheduling in cloud computing [19] to the flow shops in factories [20, 21]. Most studies on scheduling problems have been conducted under the basic assumption that machines are available on all planning horizons, while this is not the case in the real world. Machines may not be available for reasons such as preventive maintenance, failure, rest periods, and residual work from the previous planning period that should be processed at the beginning of the new period, [22]. In many cases, unavailability times are known in advance, so the decision-maker can make a more efficient decision by considering them. Karimi et al. [23] considered a predetermined time for machine unavailability in the single machine problem and proposed two heuristic methods to solve it.

In this paper, an OSSP is addressed in which stops occur at different times on machines and its duration is different but specific for different machines.

The intended objective functions include minimizing the longest completion time ($C_{\max}$) and the sum of delays, which are presented as a weight combination in a single function. Also, due to the possibility of using different devices to transport different items in a shop, the movement time in a fixed route is different for each job. Also, the working path from one machine to another is considered different from its return path due to the minimization of material flow interference. Therefore, the work transferring matrix is asymmetric between different workstations. In order to solve problems with small dimensions and when the weight of each target is known, the exact approach of the mixed biobjective linear mathematical model is adapted to use as a problem-solving method, and later the results are compared with the results of GA and SA in solving small-scale OSSP. On the contrary, when the weight of each target is unknown, the achievement of Pareto optimal solutions using

metaheuristic algorithms including Multiobjective Parallel Genetic Algorithm (MOPGA) and Multiobjective Parallel Simulated Annealing (MOPSA) algorithm are adapted to solve large-scale problems. The parameters of the metaheuristic algorithms are adjusted using the Taguchi experimental design method, as a result of which, algorithms show a state of stability in the face of various problems.

1.2. The Contributions of the Study to the Literature. This study has various contributions to the literature from various aspects. These are as follows:

(i) The exact approach of the mixed multiobjective linear mathematical model is adapted to use as a problem-solving method, and later the results are compared with the results of GA and SA in solving small-scale OSSP.

(ii) Multiobjective Parallel Genetic Algorithm (MOPGA) and Multiobjective Parallel Simulated Annealing (MOPSA) methods are adapted to solve large-scale OSSP.

(iii) To improve the exploitation and exploration capabilities of MOPGA, the new candidate generation stage of MOPGA was developed by changing crossover and mutation operators.

(iv) Variations in MOPGA and MOPSA were compared in detail with various heuristic algorithms selected from the literature according to the average RPD, execution time, and best solution criteria.

In the following, Section 2 presents a mixed linear mathematical programming model. The adapted metaheuristic algorithms and their details are described in Section 3. Section 4 describes the design of experiments and computational evaluation. Section 5 provides a conclusion and future studies.

2. Mathematical Model

In this section, the problem is introduced using simplifying assumptions as well as mathematical symbols and then a multiobjective mixed linear programming model is presented and analyzed to accurately solve small-scale problems.

To achieve the mathematical model, the available time of each machine is considered as a packet of a certain length T_i and jobs should be placed in such a way that their total processing time does not exceed the length of the packet. To clarify the issues, see Figure 1, in which $J_{[j]}$ indicates j^{th} job in sequence and B_{il} indicates l^{th} packet of machine i.

2.1. Problem Assumptions. Simplifying assumptions are considered as follows:

(i) Each machine may process up to one task at a time.

(ii) Each machine may process up to one task at a time.

(iii) Jobs can be processed in any order by all or some machines.

(iv) All jobs are available in the shop from the beginning of the planning horizon.

(v) Job cutting is not allowed during processing.

(vi) There is only one machine of each type in the shop (operations of each job are performed by only one specific machine).

(vii) Unavailable times occur at specific times on each machine.

The length of available (and unavailable) times of machines is specific and depends on the machine and is fixed during the planning period.

2.2. Indexes and Parameters

j, k: indexes of job ($j, k = 1,2, \ldots, n$)

i, h: indexes of machines ($i, h = 1,2, \ldots, m$)

l, l': indexes of packets ($l, l' = 1,2, \ldots, b$)

p_{ij}: processing time of job j on machine i

Tr_{ihj}: job transferring time from machine i to machine h

Ti: the length of the available time of machine i

ti: the length of unavailable time of machine i

dj: delivery date of job j

2.3. Decision Variables

st_{ij}: start time of preparing job j on machine i

C_{ij}: completion time of job j on machine i

C_j: completion time of job j on the last machine according to the sequence.

Tard_j: tardiness of completion time of job j from the delivery date

$$Y_{ihj} = \begin{cases} 1 & \text{if job } j \text{ on machine } i \text{ is processed before machine } h \\ 0 & \text{otherwise} \end{cases}$$

$$X_{ijk} = \begin{cases} 1, & \text{if job } j \text{ is processed on machine } i \text{ before job } k \\ 0, & \text{otherwise} \end{cases}$$

$$A_{ijl} = \begin{cases} 1, & \text{if job } j \text{ is located in packet } l \text{ of machine } i\,(Bil) \\ 0, & \text{otherwise} \end{cases}$$

2.4. Multiobjective Mixed Linear Programming Model. In this section, using the above assumptions and symbols, a Multiobjective Mixed Linear Programming Model (MOMILP) is adapted to solve the open shop scheduling problem, taking into account the unavailability of machines, preparation and separation times of jobs and machines, and transmission times between machines to simultaneously minimize the criteria of the longest completion time and the sum of delays as a single function. The MOMILP model is as follows:

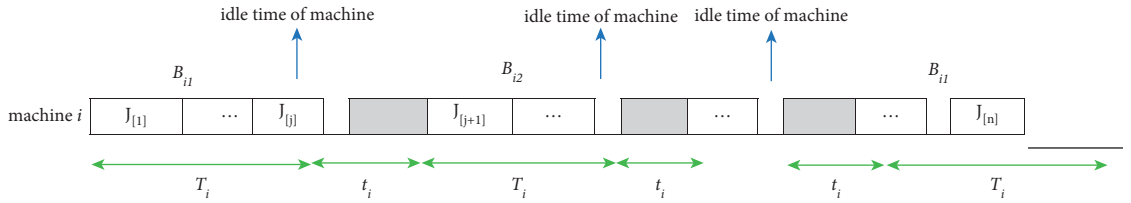

Figure 1: A sequence of jobs on the machine.

$$\min z = \theta_1 C_{\max} + \theta_2 \sum_{j=1}^{n} Tard_j, \tag{1}$$

$$st_{ij} + pi_j = c_{ij} \forall j, jst_{ij} + pi_j = Tr_{ihj} \forall j, h, j; \tag{2}$$

$$M\left(1 - Y_{ihj}\right) \leq st_{hj} i \neq h, \tag{3}$$

$$\begin{aligned} &\leq st_{ik} - M\left(1 - A_{ikl}\right) - M\left(1 - X_{ijk}\right) j \neq k\left(st_{ij} + p_{ij}\right) \\ &- M\left(1 - A_{ijl}\right) \forall i, j, k, l; \end{aligned} \tag{4}$$

$$st_{ij} \geq (l-1)\left(T_i + t_i\right) A_{ijl} \forall_{i,j,l}, \tag{5}$$

$$C_{ij} - M\left(1 - A_{ijl}\right) \leq (l-1) t_i + l.T_i \forall_{i,j,l}, \tag{6}$$

$$C_{ij} + M\left(1 - A_{ijl}\right) \geq (l-1)\left(t_i + T_i\right) \forall i, j, l, \tag{7}$$

$$M\left(1 - A_{ijl}\right) + M\left(1 - A_{ikl'}\right) + X_{ijk} \geq 1 \quad \begin{matrix} \forall i, j, k, l, l' \\ j \neq k, \\ l < b, l' \end{matrix} \tag{8}$$

$$X_{ijk} + X_{ikj} = 1 \begin{matrix} \forall i, k, j; \\ j < n, k < j \end{matrix}, \tag{9}$$

$$Y_{ihj} + Y_{hij} = 1 \begin{matrix} \forall i, j, h; \\ i \langle m, h \rangle i \end{matrix}, \tag{10}$$

$$\sum_{l=1}^{b} A_{ijl} = 1 \forall i, j, \tag{11}$$

$$\sum_{j=1}^{n} p_{ij}.A_{ijl} \leq T_i \forall i, l, \tag{12}$$

$$C_i \geq C_{ij} \forall i, j, \tag{13}$$

$$C_{\max} \geq C_{ij} \forall i, \tag{14}$$

$$Tard_j \geq C_j - d_j \forall j, \tag{15}$$

$$st_{ij}, C_{ij}, C_j, C_{\max}, Tard_j \geq 0_{\forall i,j}, \tag{16}$$

$$X_{ijk}, Y_{ihj}, A_{ijl} \in \{0,1\} \begin{matrix} \forall i, h, j, k, l \\ \neq h, j \\ \neq k \end{matrix} \tag{17}$$

Equation (1) is the objective function of the problem, which includes the convex linear combination of the two criteria: (1) the longest completion time and (2) the sum of the delays.

θ_1 and θ_2 are positive coefficients that represent the weight of each target and $\theta_1 + \theta_2 = 1$. The completion time of each operation (C_{ij}) is obtained by equation (2). If job j on machine i is processed before machine h, we have $Y_{ihj} = 1$, then the start time of preparing job j on machine h ($st_{hj} = 1$) will be larger than the completion time of that job on machine i, this is shown using equation (3). If job j is processed on machine i before job k ($X_{ijk} = 1$) and both jobs are located in the same packet l ($A_{ijl} = A_{ikl} = 1$), then the start time of preparing job k on machine i ($st_{ik} = 1$) will be larger than the completion time of job j on that machine, this criterion is shown in equation (4). Consequently, equation (5) ensures that no preparation takes place when machines are unavailable. Equations (6) and (7) together prevent the completion of operations during machines are unavailable. Equations (8) and (9) simultaneously specify the sequence of jobs on each machine and packets. Equation (10) determines the order of the machines for the operations of each job. Equation (11) ensures that each operation takes place in exactly one packet of each machine. Equation (12) controls the sum of the total processing times of the operations contained in a packet according to the maximum time of that packet, which is the access time of the relevant machine (T_i). The completion time of each job is calculated through equation (13) and according to the objective function. Equations (14) and (15) calculate the longest completion time and the delay time of each operation, respectively. Finally, equations (16) and (17) represent the negative variables and binary variables (0 or 1).

2.5. An Example. Here, to clarify the concept of the problem, we provide an example and solve it using the above MOMILP model. This example includes five jobs ($n = 5$), two machines ($m = 2$), and five packets for each machine ($b = 5$). The rest of the parameters are as follows:

$$
\begin{aligned}
p_{ij} &= \begin{bmatrix} 6 & 11 \\ 12 & 16 \\ 15 & 14 \\ 11 & 15 \\ 9 & 15 \end{bmatrix}, \\
Tr_{ih1} &= \begin{bmatrix} 0 & 0 \\ 2 & 0 \end{bmatrix}, \\
Tr_{ih2} &= \begin{bmatrix} 0 & 0 \\ 0 & 0 \end{bmatrix}, \\
T_i &= (26 \quad 16), t_i = (2 \quad 4), d_j, \\
Tr_{ih3} &= \begin{bmatrix} 0 & 2 \\ 2 & 0 \end{bmatrix}, Tr_{ih4} = \begin{bmatrix} 0 & 0 \\ 2 & 0 \end{bmatrix}, Tr_{ih5} = \begin{bmatrix} 0 & 0 \\ 2 & 0 \end{bmatrix} \\
T_i &= (26 \quad 16), t_i = (2 \quad 4), d_j \\
T_i &= (26 \quad 16), t_i = (2 \quad 4), d_j \\
&= (19 \quad 48 \quad 60 \quad 37 \quad 28)
\end{aligned} \tag{18}
$$

Considering the weight of the targets $\theta_1 = \theta_2 = 0.5$, the global optimal solution $Z = 90.5$ is obtained by solving the MOMILP model in Lingo 8 software; the Gantt chart of which is depicted in Figure 2. As can be seen, no operation is performed during the unavailable times of machines, which are shown in gray. Thus, our main goal of modeling this design has been met. In addition, the sum of the total processing times associated with the operations contained in each packet does not exceed the time of that packet. Also, the obtained sequence indicates that the delivery date has been observed so that the jobs with an earlier delivery time are at the beginning of the sequence and the jobs with a later delivery time are at the end of the sequence. Another noteworthy point is the observance of transfer times; as an example, we can point to the distance between the completion of job J_1 on machine M_2 and starting this job on the next machine ($Tr_{211} = 2$).

2.6. Model Analysis. In this section, the sensitivity of the MOMILP model to the number of jobs (n), machines (m), and packets (b) is investigated. To do so, all indexes related to variables and constraints are shown in Tables 1 and 2, respectively. The effect of increasing the number of jobs, machines, and packets on the number of variables and constraints can also be seen in Table 3.

3. The Genetic Algorithm-Based Method

As mentioned in the introduction, the OSSP is known as an NP-hard problem and only small-scale problems can be solved accurately in a reasonable amount of time [24]. Although the proposed mathematical model achieves an accurate solution, its efficiency decreases as the dimensions of the problem increase. Hence, heuristic methods or approximate algorithms are more effective for solving medium- and large-scale problems that commonly occur in the real world.

Genetic algorithms (GAs) are a class of general-purpose search strategies based on natural selection and genetics. GAs have been used effectively to a wide array of optimization challenges [19, 25, 26]. In contrast to local search algorithms such as SA, which are often focused on manipulating a single viable solution and are extremely quick, GAs retain and modify a population of possible solutions. Despite the fact that GAs have shown to be a diverse and successful search tool for addressing optimization issues, there are still several scenarios in which the basic GA performs poorly. Therefore, several hybridization methods have been reported in the literature. In this section, we also propose to use the Multiobjective Parallel Genetic Algorithm to solve the OSSP.

3.1. Chromosome Display. Chromosomes are in fact encoded solutions and points in solution space. In this paper, each operation is considered as a gene and each chromosome (solution) is represented as a permutation of genes (operations). For example, consider a problem with five jobs and 2 machines, and so 10 operations. A chromosome (or an encoded solution) can be looked at in Table 4 for reference.where O_{ij} is the operation of job j on machine i. According to this chromosome, operation O_{21} will be processed before operation O_{11} (note that these two operations are related to the same job) and operation O_{14} will be processed before operation O_{11} (note that these two operations are related to the same machine).

3.2. Initial Population. Scattering in generations prevents rapid convergence and local optimums. Therefore, we randomly generate the initial population (initial generation) to maintain the scattering of solutions in the solution space as much as possible. That is, a random permutation from the set {1, 2, . . ., $m.n$} is considered as an individual where $m.n$ indicates the number of operations.

3.3. Objective Function. In order to calculate the objective function for each chromosome (solution space points), these so-called coded solutions should be decoded. For this purpose, we place the operations on the machines in ascending order from the first operation to the last one; taking into account their unavailable times as well, we calculate their completion time. Then, taking into account the completion time of all operations, the longest completion time is obtained $C_{\max} = \max_{i,j}\{C_{ij}\}$.

Also, in order to calculate the second expression of the objective function, i.e., the sum of the delays, first the completion time of each job is calculated as $C_{\max} = C_j = \max_i\{C_{ij}\}$ and then the delay of that job is obtained by $\text{Tard}_j = \max[0, C_j - d_j]$. Finally, the sum of delays is calculated as $\sum_{j=1}^{n} \text{Tard}_j$. How to determine the values of the coefficients θ_1 and θ_2 is explained in the next sections. Therefore, the objective function of each chromosome is calculated as $Z = \theta_1 C_{\max} + \theta_2 \sum_{j=1}^{n} \text{Tard}_j$.

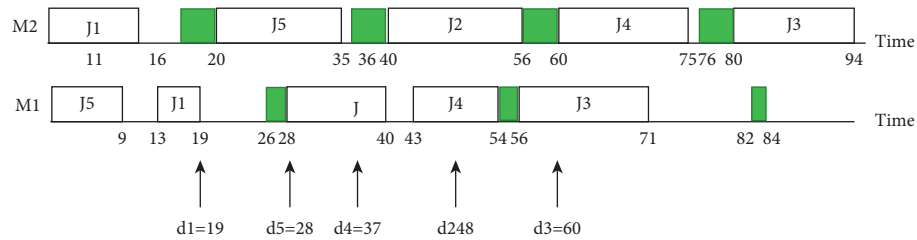

Figure 2: Gantt chart of optimal solving of the example.

Table 1: Number of variables.

Variable	Number
Z, $C_{\max}$	1
Cj, Tard_j	n
St_{ij}, C_{ij}	mn
X_{ijk}	$mn\ (n-1)$
Y_{ijk}	$mn\ (m-1)$
A_{ijl}	mnb

Table 2: Number of constraints.

Constraint	Number
(1)	1
(2), (11), (13)	mn
(3)	$mn\ (m-1)$
(4)	$mbn\ (n-1)$
(5), (6), (7)	mnb
(8)	$mn\ (n-1)\ b\ (b\text{-}1)/2$
(9)	$mn\ (n-1)/2$
(10)	$mn\ (m\text{-}1)/2$
(12)	mb
(14), (15)	n

Table 3: Number of variables and constraints according to the model MOMILP.

Problem size ($m.n.b$)	Number of variables	Number of constraints
2, 4, 4	61	393
3, 4, 4	95	607
2, 5, 5	91	826
3, 5, 5	141	1261
5, 30, 30	7156	2039926
10, 30, 30	15031	4082101
5, 40, 40	12541	6425901
10, 40, 40	26041	12854801

Table 4: An example of a chromosome for a problem with 5 jobs and 2 machines, and 10 operations.

O_{11}	O_{12}	O_{13}	O_{14}	O_{15}	O_{21}	O_{22}	O_{23}	O_{24}	O_{25}
3	6	8	2	5	1	9	10	4	7

3.4. Selection. Selection is the process by which individuals present in a generation are selected in pairs for mating. There are various approaches for selection in the literature [27]. In this paper, we use the roulette wheel selection approach, according to which individuals with higher fitness have a better chance of mating and this is in fact the basis of Darwin's theory. In order to apply the roulette wheel selection, two parameters are required: individual selection probability and individual cumulative probability, which are obtained from equations (18) and (19), respectively:

$$PS_i = \frac{f_i}{\sum_{j=1}^{\text{popsize}} f_j}, \tag{19}$$

$$CP_i = \sum_{j=1}^{i} PS_j. \tag{20}$$

According to the roulette wheel selection approach, a number is randomly generated in the range [0, 1], then individual i that meets the condition $CP_{i-1} < r < CP_i$ is selected as one of the pairs. This process is repeated for the second one.

3.5. Crossover Operation. After selecting a pair of parents using one of the selection methods, a genetic crossover operator with the probability p_c is used to combine the two parents and generate two children. There are several crossover techniques and combining parents: single-point crossover, two-point crossover, multipoint crossover, uniform crossover, and so on [28]. However, the main problem with the crossover operation is that the feasibility of new solutions (newborns) may not be guaranteed. In cases where new chromosomes or newborns produce infeasible solutions, corrective action is usually taken to turn them into feasible solutions, which will lengthen the solving time, by maintaining the feasibility of new chromosomes in each generation and without any modification process [29]. In the following, the crossover operation is described in four steps:

Step 1: Select two operations randomly from chromosome 1 (parent).

Step 2: Transfer the genes from the two selected operations along with all the genes between them from parent 1 to child 1 while maintaining their location.

Step 3: Select the rest of the genes needed by child 1 from left to right until creating a complete chromosome and place them the same way from left to right in the empty spaces of child 1.

Step 4: To create the second child, replace the two parents 1 and 2 and repeat steps 2 and 3 with the genes of the same operations selected in step 1.

Table 5: Chromosomes of parents 1 and 2.

Parent 1	3	6	8	2	5	1	9	10	4	7
Parent 2	4	9	5	6	2	1	7	10	8	3

Table 6: Transfer the genes from the two selected operations along with all the genes between them from parent 1 to child 1 while maintaining their location.

Parent 1	3	6	8	2	5	1	9	10	4	7
Parent 2	4	9	5	6	2	1	7	10	8	3
Child 1				2	5	1	9			

Table 7: Select the rest of the genes needed by child 1 from parent 2 and place them in the empty spaces of child 1.

Child 1	4	6	7	2	5	1	9	10	8	3

Table 8: Exchange the two parents 1 and 2 and repeat steps 2 and 3 until creating child 2.

Child 1	3	8	5	6	2	1	7	9	10	4

For example, consider the two parents in Tables 5–8.

Step 1. Suppose the two operations selected by the parent 1 are O_{14} and O_{22}, in other words, genes 2 and 9, respectively.

Step 2. Transfer genes 2, 5, 1, and 9 from parent 1 to child 1 while maintaining their locations.

Step 3. Select the rest of the genes needed by child 1 (from left to right) from parent 2 and place them (from left to right) in the empty spaces of child 1.

Step 4. Exchange the two parents 1 and 2 and repeat steps 2 and 3 until creating child 2 as follows:

3.6. Mutation. In order to prevent the generated generations from being directed toward the local optimums, a mutation operator with a probability p_m is applied to each of the produced children. This operator exchanges the two randomly selected operations and their genes [29]. For example, suppose that operations O_{12} and O_{24} are selected from child 1. Then, genes 6 and 8 are exchanged and mutated child will be simillar to the result given in Table 9)

3.7. Termination Condition. The GA continues until a termination criterion is met, which is $m.n.\varepsilon s$ from the beginning and produces new generations [30]. Where ε is a coefficient whose value is adjusted through experiments. In the following sections, we explain how to set it up. Also, the reason for choosing this termination condition is that it gives the algorithm more time to solve larger problems.

Table 9: The genes 6 and 8 are exchanged and mutated is generated.

Child 1	4	6	7	2	5	1	9	10	8	3
Mutated Child 1	4	8	7	2	5	1	9	10	6	3

3.8. Primary Genetic Algorithm. Before presenting the GA for solving multiobjective problems, here we describe the structure and performance of the original GA using the above explanations. The following is how the basic genetic algorithm works in 12 steps:

Step 1. Generate popsize individuals (chromosome) randomly as the initial population.

Step 2. Calculate the fitness of each individual

Step 3. Select a pair of parents from individuals based on the selection strategy.

Step 4. Apply crossover operator with the probability p_c on the parents and generate two new children.

Step 5. Apply mutation operator with the probability p_m on each child.

Step 6. Calculate the fitness of children

Step 7. Repeat steps 3–6 until generating popsize new children.

Step 8. Arrange all existing individuals, both old (i.e., the initial population) and new (i.e., generated children), that reach $2 \times$ popsize according to their fitness.

Step 9. Transfer popsize number of individuals with the best fitness to the new generation.

Step 10. Check the termination condition, if it is not met, go to step 3; otherwise, step 11.

Step 11. Select the best solution (the most fitted one) of the last generation as the answer to the algorithm.

Step 12. End.

Values related to the parameters of the GA including p_c, p_m, popsize, and ε will be determined by designing statistical tests in future sections.

3.9. Multiobjective Parallel Genetic Algorithm. There is a lot of research in the literature in which GA has been used to solve multiobjective problems due to its high ability to deal with multiobjective optimization. Since the GAs deal with a population of points (solutions), Pareto optimal multiple solutions can be found in a population of GAs [27]. In the following, we explain how to deal with a multiobjective problem.

In the mathematical model MOMILP, θ_1 and θ_2 are introduced according to the weight of each objective $C_{\max}$ and $\sum_{j=1}^{n} \mathrm{Tard}_j$, and the objective function is written as a single function (1). Now, our biobjective problem has become a single-objective problem. However, determining weights is a delicate and sensitive task. To tackle this problem, we can divide the population into several groups, with individuals in each group searching for one of the possible combinations of goal coefficients, while all groups search in parallel for Pareto optimal solutions. In this way, we can turn a multiobjective problem into a single-objective

problem with different weights. Therefore, we consider a set of λ different weights with a little difference between the two consecutive weights. Equation (20) shows the set of possible combinations.

$$\theta = \left\{\left(\theta_1^1, \theta_2^1\right), \left(\theta_1^2, \theta_2^2\right), \ldots, \left(\theta_1^\lambda, \theta_2^\lambda\right)\right\}. \quad (21)$$

Similarly, we divide the population into λ subpopulations and assign weights of the above set to them. Thus, each subpopulation searches for Pareto optimal solutions in a separate path. Subpopulations act independently and unrelatedly as parallel GAs, but their other parameters and operators, including crossover and mutation, the size of the subpopulation, and termination conditions, are all the same.

In this way, the scattering of solutions is effectively strengthened. Also, Pareto solutions are stored to keep dominant solutions. This prevents losing dominant solutions during the optimization process. This set is updated frequently to get closer to Pareto's optimal solution. The process of MOPGA is as follows:

Step 1. Generate the initial population randomly, including $\lambda \times$ popsize members

Step 2. Divide the initial population into λ subpopulations

Step 3. Create the weights related to the single objective function and assign to the subpopulations

$$\theta = \{(\sup \times \rho, 1 - \text{sub} \times \rho) : \text{sub} = 0, 1, \ldots, \lambda - 1\}. \quad (22)$$

For instance, if we set $\lambda = 21$ and $\rho = 0.05$, we will have:

$$\theta = \{(0.0, 1.0), (0.05, 0.95), \ldots, (1.0, 0.0)\}. \quad (23)$$

Step 4. Perform the initial genetic algorithm process from step 2 for all subpopulations and save the dominant solutions

Step 5. Find the best solution among the dominant ones

Step 6. Finish

3.10. The Simulated Annealing (SA)-Based Method. Another common metaheuristic algorithm for solving NP-hard problems is Simulated Annealing. This algorithm is inspired by physical systems in which the energy of atoms is reduced through the cooling process to a minimum level [30–32]. SA analyzes the complete surface of the goal function and attempts to optimize it while going both uphill and downhill. Consequently, it is essentially independent of the initial values, which are often a crucial input in traditional algorithms. In addition, it can escape from local optimums and locate the global optimum via uphill and downhill maneuvers. In addition, SA makes fewer rigorous assumptions about the objective function than traditional algorithms. Because of these lenient assumptions, it can cope with objective functions with ridges and plateaus more readily. Finally, it is capable of optimizing objective functions that are not even specified for certain parameter values [33].

In this section, we first provide an overview of the SA and then describe the MOPSA.

3.10.1. The Primary Simulated Annealing (SA) Algorithm. SA starts from a solution (energy level) as the basis of an initial temperature (temp 0) and searches in the solution space in the neighborhood of that solution. The search continues until reaching a termination condition, which we set as $m.n.\varphi$ iterations. Parameter φ is a fixed coefficient in range (0, 1). In this algorithm, we also use the method of GA to encode the problem solutions and introduce chromosomes. We also considered a random permutation of operations as the base solution for the beginning. In order to move from one solution to another, the neighborhood search method described in Algorithm 1 is used. After completing the neighborhood search process, the current temperature is reduced by multiplying it by the parameter $\mu\epsilon(0, 1)$ and the neighborhood search process is repeated.

The algorithm continues until reaching the final temperature (temp_f). During iterations and searches, the new solution is accepted if it improves the value of the objective function, otherwise, the new solution is accepted with the probability $\exp(-\Delta/\text{temp}_i)$, in which $temp_i$ is the current temperature and $\Delta = 100 \times (Z_{\text{new}} - Z_{\text{old}})/Z_{\text{new}}$. SA is summarized in Algorithm 2. We consider the final temperature as *1* and the value of other parameters of the algorithm including temp, μ and φ set by the statistical experiment design method is discussed in Section 4.

3.10.2. Multiobjective Parallel Simulated Annealing (SA). MOPSA process is very similar to the process of MOPGA and both use the same approach to deal with multiobjective optimization. Here, the objective function is considered as a single function (1) and several SA examines the different weights of each target in parallel and independently. The difference between starting MOPSA and MOPGA is that, in MOPGA, the initial population is divided into several subpopulations, but since SA starts with only one chromosome, such a division is not possible. The process of MOPSA is as follows:

Step 1. Produce λ chromosomes randomly

Step 2. Produce the weights of the single objective function as equation (22) and assign them to the chromosomes

Step 3. Perform the primary SA as shown in Algorithm 2 for all chromosomes from step 2 and store the dominant solutions

Step 4. Find the best solution among the dominant ones

Step 5. End

4. Experimental Design and Computation Evaluation

In this section, we seek to establish the adapted algorithms through experiments and statistical analysis. For this purpose, different levels of the relevant factors are considered

(1) Choose a gene at random.
(2) If the selected gene is located in the first location of the chromosome, then replace it with the next gene. Otherwise,
(3) If the selected gene is located at the last location of the chromosome replace it with the previous gene. Otherwise,
(6) Evaluate exchanging with the two lateral genes (previous and next).
(7) Replace the selected gene with the lateral gene that gets the most improvement.
(8) End of condition.

Algorithm 1: Neighborhood search simulated annealing algorithm.

(1) Generate a random permutation of operations.
(2) Calculate the value of the objective function.
(3) Set the parameters temp, $\text{temp}_f, \mu, \varphi$.
(4) Check the termination condition, then go to step 5 if not met and go to step 15 if met.
(5) Set repeat = 0.
(6) repeat < Int $(m.n.\varphi)$ go to step 7, otherwise, go to step 14.
(7) Call the neighborhood search process.
(8) If the value of the objective function is improved, go to step 9; otherwise go to step 10.
(9) Accept the new solution, update the value of the objective function, and go to step 13.
(10) Select a random number in (0, 1) and put it in rand.
(11) If $\exp(-\Delta/\text{temp}_i) < ran\ d$ go to step 12; otherwise, go to step 13.
(12) Accept the new solution, and update the value of the objective function.
(13) Set repeat = repeat + 1.
(14) Modify the new temperature as $\text{temp}_{\text{new}} = \mu.\text{temp}_{\text{old}}$ and go to step 4.
(15) End.

Algorithm 2: Steps of the primary simulated annealing algorithm.

and their different combinations are investigated. Therefore, the Taguchi approach is used as an experimental design method in this paper.

In addition, after adjusting the parameters of the proposed algorithms using the Taguchi method and by generating random data, two problem groups, one with small dimensions and the other with large dimensions, are randomly generated and the results of the solution methods are compared.

We also compare the results of our experiments on a large-scale benchmark with other methods that solved the OSSP.

4.1. Taguchi Experiment Design. Taguchi method is one of the statistical analysis methods in which using orthogonal arrays the number of experiments is significantly reduced compared to complete factorial designs [30]. For example, to design an experiment with four factors, each including three levels, a complete factorial design performs $3^4 = 81$ experiments, but Taguchi reduces them to nine experiments.

Taguchi believed that the key to improving quality was to reduce deviations, not just controlling placement within the specified range. Therefore, he tried to reduce the deviations to zero and paid less attention to being on a fixed slope. This is the main reason why the Taguchi method is mentioned as a reliable method [34]. According to the Taguchi method, factors are divided into two categories: controllable factors or signals and uncontrollable factors or noise. In order to reduce the deviations, a fraction called signal to noise (S/N) is defined which indicates the sensitivity of the response variable to uncontrollable factors and shows the deviation around a certain amount of signal. High values of S/N indicate low deviation, which means that controllable factors are more effective than uncontrollable ones. Using the optimal levels of factors obtained by this method, close to the mean value with the least deviation is expected [30].

To convert the objective function to the fraction S/N, three types of criteria can be imagined in the Taguchi method: "the less the better," "the more the better," and "the closer to the nominal value the better" [30]. According to the measurement criterion of the problem discussed in this, which is expressed as a minimization expression, the "less is better" mode is appropriate. The relevant S/N formula is as follows:

$$\frac{S}{N} = -10\ \log_{10}\left(Z^2\right). \tag{24}$$

Also, a well-known performance criterion named RPD is used:

$$\text{RPD} = \frac{\text{Alg}_{\text{sol}} - \text{Min}_{\text{sol}}}{\text{Min}_{\text{sol}}}.100, \tag{25}$$

Where Alg_{sol} is the value of an objective function of an example which is obtained from an algorithm of experiment

design and Min_{sol} is the minimum value of the objective function of that example which is obtained from all the algorithms of experiments. So, it is obvious that low RPD values are more valuable.

4.1.1. Data Generation. To perform Taguchi experiments, a problem with dimensions $(m, n, b) = (10, 5, 20)$ is considered, and five iterations of the same are generated randomly. Also, other literature-inspired [9, 35–37] parameters of the problem are as follows:

(i) Processing times have a continuous uniform distribution in (1, 99).

(ii) Transfer times between machines have a continuous uniform distribution in (1) and (20).

(iii) Consecutive unavailable durations of each machine have a uniform distribution in (1, 50).

(iv) Consecutive machine access times (packet size of each machine) are calculated as follows:

$$T_i = \max\left\{ a \sum_{j=1}^{n} p_{ij}, \max_i p_{ij} \right\}, \tag{26}$$

where a is selected from $\{1/5, 1/4, 1/3\}$ randomly.

Delivery time is calculated as follows:

$$d_j = \sum_{i=1}^{m} p_{ij} + \frac{\left(\sum_{i=1}^{m}\sum_{h=1}^{m} Tr_{ihj}\right)}{m} + U(0\ \ 1).(n-1).\frac{\sum_{i=1}^{m} t_i}{m}. \tag{27}$$

In which d_j is the total time that a job is on all machines. $\sum_{i=1}^{m} p_{ij}$ is the average movement between all machines. $\sum_{i=1}^{m}\sum_{h=1}^{m} Tr_{ihj}/m$ is the average unavailable times of all machines.

4.1.2. Adjusting the Parameters of the MOPGA. Factors to be set in the MOPGA algorithm are as follows: crossover probability (p_c), mutation probability (p_m), population size (popsize), and termination criterion coefficient (ε). According to Table 10, three levels are considered for each factor [29, 30]. So, Orthogonal Array Design L_9 is the most appropriate case because it has exactly the same number of factors and levels as the experiment and meets all objectives. Combinations of different levels of factors in each experiment of the design L_9 for the MOPGA algorithm are shown in Table 11. MOPGA and all experiment designs are programmed in C#.Net visual language and run on a computer with GHz Intel® Core™ and 4 GB ram. According to the results, optimal levels of factors are as follows: $p_c = 0.8$, $p_m = 0.2$, popsize = 30 and $\varepsilon = 0.4$.

In order to find the effect of each factor on the response variable, we perform an analysis of variance (ANOVA). It is important to note that in the designed experiment, the degree of error freedom is 0. To deal with this problem, the factors that have the lowest mean squares are considered errors. In the above experiment, factors p_c and popsize with mean squares of 0.92 and 0.70, respectively, are of the least mean squares and so have the least effect on the response variable. Therefore, these two factors are considered errors. Analysis of the variance of the S/N fraction is given in Table 12. Therefore, the most effective factors are p_m and ε with the percentage of effect of 86.92% and 7.81%, respectively.

Table 10: Factors of MOPGA algorithm and their levels.

Factor	Level		
	(1)	(2)	(3)
Pc	0.4	0.6	0.8
Pm	0.0	0.1	0.2
popsize	20	30	40
ϵ	0.2	0.3	0.4

Table 11: Experiments related to the array L_9 in the MOPGA algorithm.

Experiment	Factor			
	Pc	Pm	popsize	ϵ
1	0.4	0.0	20	0.2
2	0.4	0.1	40	0.3
3	0.4	0.2	30	0.4
4	0.6	0.0	40	0.4
5	0.6	0.1	30	0.2
6	0.6	0.2	20	0.3
7	0.8	0.0	30	0.3
8	0.8	0.1	20	0.4
9	0.8	0.2	40	0.2

4.1.3. Adjusting the Parameters of the MOPSA. According to the description of the SA, three factors should be adjusted: initial temperature (temp_0), temperature reduction coefficient (μ), and the coefficient of the number of iterations per temperature (φ). Considering two levels for each factor, orthogonal array L_4 is suitable and its factors and levels are depicted in Table 13. Also, the combinations of different levels of factors in each experiment of design L_4 of the MOPSA are shown in Table 14. MOPSA and all experiment designs are programmed in C#.Net and run on a computer with GHz Intel® Core™ and 4 GB ram. Optimal levels of factors are as follows: $\text{temp}_0 = 100$, $\mu = 0.7$, and $\varphi = 0.3$.

An analysis of variance is performed to find the effect of each factor. Also, to prevent the error degree of freedom from zeroing, we consider the factor with the lowest mean squares as the error. The results indicate that the factor μ with the mean square 0.03 has the lowest effect on the response variable. Analysis of variance of S/N for the factors of the MOPSA algorithm is shown in Table 15 in which factor φ with the percentage of effect of 66.62% has the highest effect on the response variable. As well, temp_0 is the second effective factor with a percentage of effect of 21.89.

4.2. Computational Evaluation. In order to evaluate the performance of the MOMILP model and the proposed algorithms, two sets of problems including small-scale

Table 12: Analysis of variance of the S/N fraction for the factors of the MOPGA algorithm.

Factor	df	SS	MS	F	Percentage of effect (%)	Cumulative percentage (%)	p-value
popsize	2	108.56	54.28	67.07	86.93	86.93	0.00
ε	2	11.23	5.61	6.94	7.81	94.74	0.05
Error (p_c + popsize	4	3.24	0.81		5.26	100	
Total	8	123.02					

Table 13: Factors of MOPSA algorithm and their levels.

Factor	Level	
	(1)	(2)
temp_0	50	100
μ	0.7	0.8
φ	0.3	0.6

Table 14: Array experiments L_4 in MOPSA algorithm.

Experiment	Factor		
	temp_0	μ	ϕ
1	50	0.7	0.3
2	50	0.8	0.6
3	100	0.7	0.6
4	100	0.8	0.3

Table 15: Analysis of variance of the S/N fraction for the factors of the MOPSA algorithm.

Factor	df	SS	MS	F	Percentage of effect (%)	Cumulative percentage (%)	p-value
temp_0	1	0.17	0.17	6.72	21.89	21.89	0.23
ϕ	1	0.47	0.47	18.40	66.62	88.51	0.15
Error (μ)	1	0.03	0.03		11.49	100	
Total	3	0.66					

Table 16: Performance of MOMILP model and primary GA and SA algorithms in dealing with small-scale problems ($\theta_1 = \theta_2 = 0.5$.).

Problem		Z			Deviation from optimum (%)			Solving time (s)		
	m, n, b	MOMILP	GA	SA	MOMILP	GA (%)	SA (%)	MOMILP	GA	SA
1	2, 4, 8	449.74	449.74	510.53	0	0.00	13.52	11	84	1
2	3, 4, 8	347.31	350.83	668.90	0	1.02	92.60	60	105	1
3	2, 5, 10	492.95	492.95	726.71	0	0.00	47.42	145	106	1
4	3, 5, 10	382.65	466.38	737.00	0	21.88	92.61	1951	147	2
5	2, 6, 12	848.09	859.43	1415.23	0	1.34	66.87	1386	105	3
6	3, 6, 12	—	1026.97	2375.36	—	—	—	38744	168	4
Average					0	4.85	62.60			

Table 17: Average RPD for algorithms MOPGA and MOPSA in solving large-scale problems.

Problem	$m.n.b$	MOPGA	MOPSA	Problem	$m.n.b$	MOPGA	MOPSA
7	5, 10, 20	0.03	0.69	17	5, 20, 40	0.05	0.39
8	5, 10, 20	0.03	0.62	18	5, 20, 40	0.01	0.47
9	5, 10, 20	0.07	1.10	19	5, 20, 40	0.05	0.48
10	5, 10, 20	0.02	0.76	20	5, 20, 40	0.04	0.65
11	5, 10, 20	0.04	0.80	21	5, 20, 40	0.04	0.54
12	10, 10, 20	0.08	0.73	22	10, 20, 40	0.01	0.20
13	10, 10, 20	0.11	0.80	23	10, 20, 40	0.03	0.24
14	10, 10, 20	0.07	0.73	24	10, 20, 40	0.04	0.28
15	10, 10, 20	0.06	0.80	25	10, 20, 40	0.07	0.45
16	10, 10, 20	0.08	0.61	26	10, 20, 40	0.06	0.41
Average RPD of MOPGA: 0.05							
Average RPD of MOPSA: 0.59							

Table 18: Simulation results of the proposed algorithm and comparable algorithms for the Taillard [38] benchmarks.

Benchmarks	Optimal solution	SA	GA	Hybrid GA	Hybrid GA	GA	EGA_OS	ACS	CS	CSO	BA_OS	MOPSA	MOPGA
4 × 4 – 1	193	193	193	213	193	193	193	193	193	193	193	193	193
4 × 4 – 2	236	236	236	240	236	239	239	236	236	236	236	236	236
4 × 4 – 3	271	271	271	293	271	271	271	271	271	271	271	271	271
4 × 4–4	250	250	250	253	250	250	250	250	252	250	250	250	250
4 × 4 – 5	295	295	295	303	295	295	295	295	295	295	295	295	295
4 × 4 – 6	189	189	189	209	189	189	189	189	189	189	189	189	189
4 × 4 – 7	201	201	201	203	201	201	201	201	201	201	201	201	201
4 × 4 – 8	217	217	217	224	217	217	217	217	217	217	217	217	217
4 × 4 – 9	261	261	261	281	261	261	261	261	261	261	261	261	261
4 × 4 – 10	217	217	217	230	217	217	217	217	217	217	217	217	217
5 × 5 – 1	300	300	301	323	300	301	300	301	301	300	300	300	300
5 × 5 – 2	262	262	262	269	262	263	262	262	262	262	262	262	262
5 × 5 – 3	323	323	331	353	323	335	323	331	335	323	323	323	323
5 × 5 – 4	310	310	N/A	N/A	310	316	310	315	314	310	310	310	310
5 × 5 – 5	326	326	N/A	N/A	326	330	326	331	329	326	326	326	326
5 × 5 – 6	312	312	312	327	312	312	312	317	318	312	312	312	312
5 × 5 – 7	303	303	N/A	N/A	303	308	303	308	305	303	303	303	303
5 × 5 – 8	300	300	N/A	N/A	300	304	300	304	303	300	300	300	300
5 × 5 – 9	353	353	353	373	353	358	353	358	358	353	353	353	353
5 × 5 – 10	326	326	326	341	326	328	326	329	329	326	326	326	326
7 × 7 – 1	435	435	438	447	435	436	435	435	436	435	435	435	435
7 × 7 – 2	443	443	455	454	443	447	443	445	447	443	443	443	443
7 × 7 – 3	468	468	N/A	N/A	468	472	468	479	472	468	468	468	468
7 × 7 – 4	463	463	N/A	N/A	463	463	463	467	466	463	463	463	463
7 × 7 – 5	416	416	N/A	N/A	416	417	416	419	416	416	416	416	416
7 × 7 – 6	451	451	N/A	N/A	451	455	451	460	454	452	451	452	451
7 × 7 – 7	422	422	443	450	422	426	422	435	425	422	422	422	422
7 × 7 – 8	424	424	N/A	N/A	424	424	424	424	424	426	424	424	424
7 × 7 – 9	458	458	465	467	458	458	458	458	458	458	458	459	458
7 × 7 – 10	398	398	405	406	398	398	398	398	399	398	398	399	398
10 × 10 – 1	637	637	667	655	637	637	637	638	639	645	637	641	637
10 × 10 – 2	588	588	N/A	N/A	588	588	588	588	688	588	588	588	588
10 × 10 – 3	598	598	N/A	N/A	598	598	598	599	600	599	598	598	598
10 × 10 – 4	577	577	586	581	577	577	577	577	577	577	577	577	577
10 × 10 – 5	640	640	N/A	N/A	640	640	640	640	640	640	640	640	640
10 × 10 – 6	538	538	555	541	538	538	538	538	538	538	538	538	538
10 × 10 – 7	616	616	N/A	N/A	616	616	616	616	616	616	616	616	616
10 × 10 – 8	595	595	N/A	N/A	595	595	595	595	595	595	595	595	595
10 × 10 – 9	595	595	627	598	595	595	595	595	595	595	595	595	595
10 × 10 – 10	596	596	623	605	596	596	596	596	596	596	596	596	596
15 × 15 – 1	937	937	967	937	937	937	937	937	937	937	937	937	937
15 × 15 – 2	918	918	N/A	N/A	918	918	918	918	918	918	918	919	918
15 × 15 – 3	871	871	904	871	871	871	871	871	871	871	871	871	871
15 × 15 – 4	934	934	969	934	934	934	934	934	934	934	934	934	934
15 × 15 – 5	946	946	N/A	N/A	946	946	946	946	946	946	946	948	946
15 × 15 – 6	933	933	N/A	N/A	933	933	933	933	933	933	933	933	933
15 × 15 – 7	891	891	N/A	N/A	891	891	891	891	891	891	891	891	891
15 × 15 – 8	893	893	928	893	893	893	893	893	893	893	893	893	893
15 × 15 – 9	899	899	N/A	N/A	899	899	899	899	902	902	899	913	899
15 × 15 – 10	902	902	N/A	N/A	902	902	902	902	902	902	902	902	902
20 × 20 – 1	1155	1155	1230	1165	1155	1155	1155	1155	1155	1155	1155	1166	1155
20 × 20 – 2	1241	1241	N/A	N/A	1241	1241	1242	1241	1242	1243	1241	1260	1241
20 × 20 – 3	1257	1282	1292	1257	1257	1257	1257	1257	1257	1257	1257	1257	1259
20 × 20 – 4	1248	1274	N/A	N/A	1248	1248	1248	1248	1248	1248	1248	1253	1248
20 × 20 – 5	1256	1289	1315	1256	1256	1256	1256	1256	1256	1256	1256	1256	1256
20 × 20 – 6	1204	1204	1266	1207	1204	1204	1204	1204	1204	1204	1204	1204	1204
20 × 20 – 7	1294	1294	N/A	N/A	1294	1294	1294	1294	1295	1294	1294	1310	1294
20 × 20 – 8	1169	1169	N/A	N/A	1173	1171	1173	1170	1176	1175	1170	1173	1176
20 × 20 – 9	1289	1307	1339	1289	1289	1289	1289	1289	1289	1289	1289	1289	1289
20 × 20 – 10	1241	N/A	1307	1241	1241	1241	1241	N/A	1241	1241	1241	1241	1241

Table 19: Execution time of the proposed algorithm and compared algorithms in terms of seconds.

Benchmarks	CSO	MOPSA	MOPGA	Benchmarks	CSO	MOPSA	MOPGA
4 × 4 – 1	0.001	0.001	0.003	10 × 10 – 1	160.762	158.514	160.216
4 × 4 – 2	0.001	0.001	0.007	10 × 10 – 2	474.782	472.948	474.309
4 × 4 – 3	0.001	0.001	0.018	10 × 10 – 3	68.567	65.781	66.118
4 × 4 – 4	0.156	0.101	0.148	10 × 10 – 4	41.04	40.014	40.783
4 × 4 – 5	0.125	0.097	0.129	10 × 10 – 5	679.018	678.091	678.615
4 × 4 – 6	0.003	0.001	0.009	10 × 10 – 6	126.936	122.726	123.552
4 × 4 – 7	0.109	0.074	0.101	10 × 10 – 7	22.877	20.281	21.227
4 × 4 – 8	0.359	0.231	0.287	10 × 10 – 8	375.292	371.557	374.591
4 × 4 – 9	0.219	0.142	0.186	10 × 10 – 9	263.801	257.890	262.175
4 × 4 – 10	0.156	0.099	0.121	10 × 10 – 10	112.65	110.032	11.758
5 × 5 – 1	0.610	0.451	0.573	15 × 15 – 1	250.323	247.080	248.903
5 × 5 – 2	0.735	0.618	0.691	15 × 15 – 2	501.669	494.118	486.337
5 × 5 – 3	2.235	1.876	2.116	15 × 15 – 3	498.766	492.016	493.768
5 × 5 – 4	8.906	6.569	8.592	15 × 15 – 4	112.994	109.854	11.243
5 × 5 – 5	1.344	1.123	1.338	15 × 15 – 5	834.63	827.603	831.728
5 × 5 – 6	13.813	11.097	12.589	15 × 15 – 6	149.578	147.932	148.005
5 × 5 – 7	14.688	13.458	13.976	15 × 15 – 7	867.539	863.590	564.329
5 × 5 – 8	35.236	31.231	34.811	15 × 15 – 8	176.073	175.327	175.824
5 × 5 – 9	4.032	2.642	3.628	15 × 15 – 9	658.615	652.187	655.442
5 × 5 – 10	2.453	2.321	2.404	15 × 15 – 10	891.272	887.849	890.119
7 × 7 – 1	24.375	21.968	23.211	20 × 20 – 1	457.839	453.202	455.601
7 × 7 – 2	26.065	24.376	24.897	20 × 20 – 2	618.409	607.114	610.105
7 × 7 – 3	51.658	47.612	50.626	20 × 20 – 3	340.266	337.621	338.290
7 × 7 –	227.313	221.874	224.529	20 × 20 – 4	816.467	811.479	814.471
7 × 7 – 5	169.751	167.496	168.004	20 × 20 – 5	432.391	426.719	431.772
7 × 7 – 6	640.466	633.012	137.831	20 × 20 – 6	806.064	805.431	805.712
7 × 7 – 7	349.208	347.890	348.210	20 × 20 – 7	859.499	857.386	859.116
7 × 7 – 8	21.567	20.001	20.901	20 × 20 – 8	695.772	694.329	694.707
7 × 7 – 9	83.953	78.016	81.378	20 × 20 – 9	207.641	203.989	206.752
7 × 7 – 10	112.39	110.731	112.004	20 × 20 – 10	489.458	484.307	488.262

problems ($n = 4, 5, 6$; $m = 2, 3$) and large-scale problems ($n = 10, 20$; $m = 5, 10$) have been generated [26]. Considering one iteration for each of the small-scale problems and five iterations for each of the large-scale problems, we will have a total of 26 problems. The rest of the parameters are considered exactly as in the Data Generation Section. Considering the weights as $\theta_1 = \theta_2 = 0.5$, small-scale problems are solved using the primary GA and SA and the results will be compared to the optimal solutions obtained by the MOMILP model with the mentioned weights. MOMILP model is coded in Lingo 8 and C#.Net is used to code the primary algorithms GA and SA.

The performance of the MOMILP model and primary SA and GA are shown in Table 16. As seen in the table, although the MOMILP model is a suitable method to solve small-scale problems, by increasing the computational time of the MOMILP model while magnifying the problem, the GA method becomes more efficient with a deviation of 4.85% from the optimum. As well, although the SA algorithm shows a relatively large deviation from the optimal solution, its time saving compared to GA is clear.

To solve large-scale problems, MOPGA and MOPSA algorithms are used and each problem is solved five times using each of the algorithms. In addition, in order to compare algorithms, obtained results are converted to relative percentage difference (RPD) criteria and are shown in Table 17. Therefore, MOPGA with an average RPD of 0.05% is more efficient and stable than MOPSA in solving large-scale problems.

In addition, MOPGA and MOPSA are programmed in C#.Net programming language, and all algorithms including models MOMILP, GA, SA, MOPGA, and MOPSA are performed on a computer with CPU 3 GHz Intel® Core™ I and 4 GB RAM.

In order to show the efficiency of the proposed algorithm (MOPGA), we tested the above algorithm on benchmarks by Taillard [38] and compared it with other metaheuristic algorithms including SA [39], GA [40], Hybrid GA [40], GA [41], Hybrid GA [42], Ant Colony System (ACS) [43], Cuckoo Search (CS) [43], Cat Swarm Optimization (CSO) algorithm [44], Extended Genetic Algorithm Open Shop (EGA_OS) [14], and Bat Algorithm Open Shop (BA_OS) [22]. Table 18 shows the simulation results of the proposed algorithm and the comparable algorithms for different benchmarks. As mentioned in this table, the proposed algorithms were able to achieve the optimal solution in most benchmarks and solve the problem well.

As you can see in Table 19, the MOPSA algorithm has less execution time than the other two algorithms and was able to respond in less time. The MOPGA algorithm was able to achieve the optimal answer in less time than the CSO algorithm.

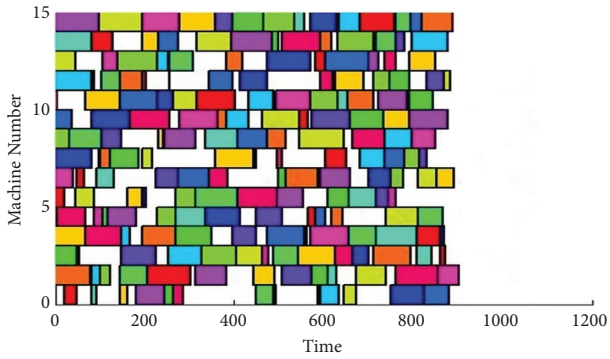

Figure 3: Gantt chart of the MOPGA for the $15 \times 15 - 1$ benchmark.

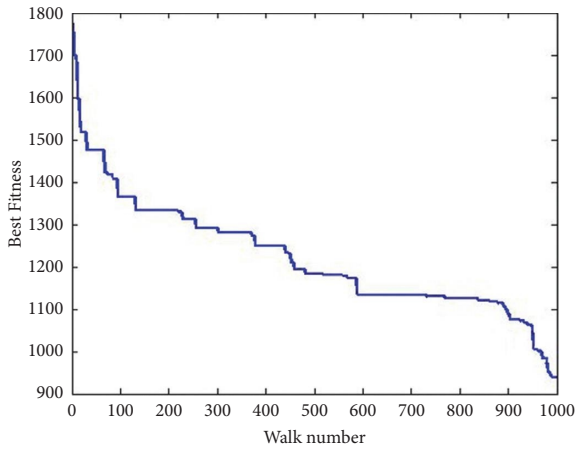

Figure 4: Fitness diagram of the MOPGA for the $15 \times 15 - 1$ benchmark.

The accuracy of the proposed algorithm in programming things well on machines is shown in Figure 3. This figure shows the Gantt chart for the $15 \times 15 - 1$ benchmark. In this case, a few free times left for the machine shows the accuracy of the proposed algorithm.

Figure 4 shows the fitness diagram of the MOPGA for the $15 \times 15 - 1$ benchmark. In this diagram, the best fitness is getting close to 900 while the walk number crosses 900 walks.

Figure 5 shows the dispersion diagram for the $15 \times 15 - 1$ benchmark. Population dispersion is always maintained in the MOPGA. As you can see in the above algorithm, premature convergence of chromosomes is prevented.

5. Conclusion

In this paper, a multiobjective mixed-integer linear programming model is adapted to solve biobjective OSSP considering unavailable times for machines. Also, "maximum completion time" and "total delays" are considered in optimization criteria simultaneously. The efficiency of the MOMILP model is investigated through a number of small-scale problems and compared with the efficiency and execution time of GA and SA. Although the results indicate the high ability of the MOMILP model to solve small-scale

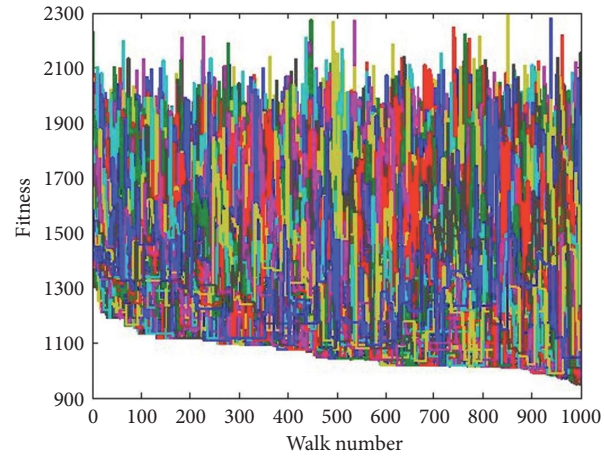

Figure 5: Dispersion diagram of the MOPGA for the $15 \times 15 - 1$ benchmark.

problems, the analyzes performed on the model highlight the need to develop other methods such as heuristic and metaheuristic methods to solve large-scale problems. Therefore, MOPGA and MOPSA algorithms were introduced for multiobjective problems with unknown weights for objectives. Also, the reliability of multiobjective algorithms is evaluated by designing Taguchi experiments. Results show that the MOPGA algorithm is more efficient than the MOPSA algorithm in dealing with large-scale problems. Finally, variations in MOPGA and MOPSA were compared in detail with various heuristic algorithms selected from the literature according to the Average RPD, execution time, and best solution criteria. Our experiments proved the success of the proposed solutions by running MOPGA and MOPSA not only on low- and medium-scaled open shop scheduling samples but also on large-scale open shop scheduling samples.

In the following, some areas of development and expanding the present study are mentioned:

(i) Developing other solution methods, including new heuristic and metaheuristic methods to solve large-scale problems and comparison with the algorithms proposed in this paper can be a good idea for making the model more practical.

(ii) Considering more diverse optimization criteria according to the needs of today's industry can also provide the basis for future studies.

(iii) In this paper, optimizing factors of the algorithms in discrete space are explored. Therefore, another area of development of the present paper can be the optimization of factors in the continuous space.

(iv) A sequence-dependent preparation and separation times can be considered and then a mathematical model can be developed.

(v) The number of vehicles can be used as a constraint on the problem.

(vi) Considering variable speeds for machines seems practical. That is, the processing speed of the

machines decreases after performing a certain number of jobs or a certain period of time and then increases again after performing the maintenance process.

Data Availability

We used data from ref [26] and discussed the same in Section 4.2 of the manuscript.

Conflicts of Interest

The authors declare that they have no conflicts of interest.

References

[1] D. Biskup, "Single-machine scheduling with learning considerations," *European Journal of Operational Research*, vol. 115, no. 1, pp. 173–178, 1999.

[2] A. S. Manne, "On the job-shop scheduling problem," *Operations Research*, vol. 8, no. 2, pp. 219–223, 1960.

[3] M. Sheikhalishahi, N. Eskandari, A. Mashayekhi, and A. Azadeh, "Multi-objective open shop scheduling by considering human error and preventive maintenance," *Applied Mathematical Modelling*, vol. 67, pp. 573–587, 2019.

[4] F. Zhao, R. Ma, and L. Wang, "A self-learning discrete jaya algorithm for multiobjective energy-efficient distributed no-idle flow-shop scheduling problem in heterogeneous factory system," *IEEE Transactions on Cybernetics*, pp. 1–12, 2021.

[5] B. Zhang, Qk. Pan, Ll. Meng, C. Lu, Jh Mou, and Jq Li, "Pan Q-k, Meng L-l, Lu C, Mou J-h, Li J-q: an automatic multi-objective evolutionary algorithm for the hybrid flowshop scheduling problem with consistent sublots," *Knowledge-Based Systems*, vol. 238, p. 107819, 2022.

[6] K. Gao, Z. Cao, L. Zhang, Z. Chen, Y. Han, and Q. Pan, "A review on swarm intelligence and evolutionary algorithms for solving flexible job shop scheduling problems," *IEEE/CAA Journal of Automatica Sinica*, vol. 6, no. 4, pp. 904–916, 2019.

[7] Y. Fu, Y. Hou, Z. Wang, X. Wu, K. Gao, and L. Wang, "Distributed scheduling problems in intelligent manufacturing systems," *Tsinghua Science and Technology*, vol. 26, no. 5, pp. 625–645, 2021.

[8] J. Breit, G. Schmidt, and V. A. Strusevich, "Two-machine open shop scheduling with an availability constraint," *Operations Research Letters*, vol. 29, no. 2, pp. 65–77, 2001.

[9] C.-J. Hsu, C. Low, and C.-T. Su, "A single-machine scheduling problem with maintenance activities to minimize makespan," *Applied Mathematics and Computation*, vol. 215, no. 11, pp. 3929–3935, 2010.

[10] Y. Fu, Y. Hou, Z. Chen, X. Pu, K. Gao, and A. Sadollah, "Modelling and scheduling integration of distributed production and distribution problems via black widow optimization," *Swarm and Evolutionary Computation*, vol. 68, p. 101015, 2022.

[11] V. A. Strusevich, "A heuristic for the two-machine open-shop scheduling problem with transportation times," *Discrete Applied Mathematics*, vol. 93, no. 2-3, pp. 287–304, 1999.

[12] Y. Fu, H. Li, M. Huang, and H. Xiao, "Bi-objective modeling and optimization for stochastic two-stage open shop scheduling problems in the sharing economy," *IEEE Transactions on Engineering Management*, pp. 1–15, 2022.

[13] A. A. R. Hosseinabadi, H. Siar, S. Shamshirband, M. Shojafar, and M. H. N. M. Nasir, "Using the gravitational emulation local search algorithm to solve the multi-objective flexible dynamic job shop scheduling problem in Small and Medium Enterprises," *Annals of Operations Research*, vol. 229, no. 1, pp. 451–474, 2015.

[14] C.-F. Liaw, "Scheduling preemptive open shops to minimize total tardiness," *European Journal of Operational Research*, vol. 162, no. 1, pp. 173–183, 2005.

[15] A. Sedeño-Noda, D. Alcaide, and C. González-Martín, "Network flow approaches to pre-emptive open-shop scheduling problems with time-windows," *European Journal of Operational Research*, vol. 174, no. 3, pp. 1501–1518, 2006.

[16] H. Panahi, M. Rabbani, and R. Tavakkoli-Moghaddam, "Solving an open shop scheduling problem by a novel hybrid multi-objective ant colony optimization," in *2008 Eighth International Conference on Hybrid Intelligent Systems: 2008*, pp. 320–325, IEEE, 2008.

[17] H. Panahi and R. Tavakkoli-Moghaddam, "Solving a multi-objective open shop scheduling problem by a novel hybrid ant colony optimization," *Expert Systems with Applications*, vol. 38, no. 3, pp. 2817–2822, 2011.

[18] Z. Drezner, "A distance based rule for removing population members in genetic algorithms," *4OR*, vol. 3, no. 2, pp. 109–116, 2005.

[19] P. Pirozmand, A. A. R. Hosseinabadi, M. Farrokhzad, M. Sadeghilalimi, S. Mirkamali, and A. Slowik, "Multi-objective hybrid genetic algorithm for task scheduling problem in cloud computing," *Neural Computing & Applications*, vol. 33, no. 19, pp. 13075–13088, 2021.

[20] F. Zhao, X. He, and L. Wang, "A two-stage cooperative evolutionary algorithm with problem-specific knowledge for energy-efficient scheduling of no-wait flow-shop problem," *IEEE Transactions on Cybernetics*, vol. 51, no. 11, pp. 5291–5303, 2021.

[21] F. Zhao, L. Zhao, L. Wang, and H. Song, "An ensemble discrete differential evolution for the distributed blocking flowshop scheduling with minimizing makespan criterion," *Expert Systems with Applications*, vol. 160, p. 113678, 2020.

[22] M. B. Shareh, S. H. Bargh, A. A. R. Hosseinabadi, and A. Slowik, "An improved bat optimization algorithm to solve the tasks scheduling problem in open shop," *Neural Computing & Applications*, vol. 33, no. 5, pp. 1559–1573, 2021.

[23] S. Karimi, Z. Ardalan, B. Naderi, and M. Mohammadi, "Scheduling flexible job-shops with transportation times: mathematical models and a hybrid imperialist competitive algorithm," *Applied Mathematical Modelling*, vol. 41, pp. 667–682, 2017.

[24] D. Bai and L. Tang, "Open shop scheduling problem to minimize makespan with release dates," *Applied Mathematical Modelling*, vol. 37, no. 4, pp. 2008–2015, 2013.

[25] M. Ahmady, S. S. Mirkamali, B. Pahlevanzadeh, E. Pashaei, A. A. R. Hosseinabadi, and A. Slowik, "Facial expression recognition using fuzzified Pseudo Zernike Moments and structural features," *Fuzzy Sets and Systems*, vol. 443, pp. 155–172, 2022.

[26] J. Khodadoust, A. M. Khodadoust, S. S. Mirkamali, and S. Ayat, "Fingerprint indexing for wrinkled fingertips immersed in liquids," *Expert Systems with Applications*, vol. 146, p. 113153, 2020.

[27] C.-F. Liaw, "A hybrid genetic algorithm for the open shop scheduling problem," *European Journal of Operational Research*, vol. 124, no. 1, pp. 28–42, 2000.

[28] M. E. Matta, "A genetic algorithm for the proportionate multiprocessor open shop," *Computers & Operations Research*, vol. 36, no. 9, pp. 2601–2618, 2009.

[29] B. Naderi, S. Fatemi Ghomi, M. Aminnayeri, and M. Zandieh, "Scheduling open shops with parallel machines to minimize total completion time," *Journal of Computational and Applied Mathematics*, vol. 235, no. 5, pp. 1275–1287, 2011.

[30] R. Tavakkoli-Moghaddam, N. Safaei, and F. Sassani, "A memetic algorithm for the flexible flow line scheduling problem with processor blocking," *Computers & Operations Research*, vol. 36, no. 2, pp. 402–414, 2009.

[31] B.-W. Cheng and C.-L. Chang, "A study on flowshop scheduling problem combining Taguchi experimental design and genetic algorithm," *Expert Systems with Applications*, vol. 32, no. 2, pp. 415–421, 2007.

[32] R. Tavakkoli-Moghaddam, A. Rahimi-Vahed, A. Ghodratnama, and A. Siadat, "A simulated annealing method for solving a new mathematical model of a multi-criteria cell formation problem with capital constraints," *Advances in Engineering Software*, vol. 40, no. 4, pp. 268–273, 2009.

[33] A. Corana, M. Marchesi, C. Martini, and S. Ridella, "Minimizing multimodal functions of continuous variables with the "simulated annealing" algorithm—corrigenda for this article is available here," *ACM Transactions on Mathematical Software*, vol. 13, no. 3, pp. 262–280, 1987.

[34] B. Naderi, M. Zandieh, and S. M. T. Fatemi Ghomi, "Fatemi Ghomi S: scheduling sequence-dependent setup time job shops with preventive maintenance," *International Journal of Advanced Manufacturing Technology*, vol. 43, no. 1-2, pp. 170–181, 2009.

[35] G. J. Kyparisis and C. Koulamas, "Open shop scheduling with makespan and total completion time criteria," *Computers & Operations Research*, vol. 27, no. 1, pp. 15–27, 2000.

[36] R. Ruiz, J. Carlos García-Díaz, and C. Maroto, "Considering scheduling and preventive maintenance in the flowshop sequencing problem," *Computers & Operations Research*, vol. 34, no. 11, pp. 3314–3330, 2007.

[37] J. Jungwattanakit, M. Reodecha, P. Chaovalitwongse, and F. Werner, "Algorithms for flexible flow shop problems with unrelated parallel machines, setup times, and dual criteria," *International Journal of Advanced Manufacturing Technology*, vol. 37, no. 3-4, pp. 354–370, 2008.

[38] E. Taillard, "Benchmarks for basic scheduling problems," *European Journal of Operational Research*, vol. 64, no. 2, pp. 278–285, 1993.

[39] H. M. Harmanani and S. B. Ghosn, "An efficient method for the open-shop scheduling problem using simulated annealing. In: *Information technology: New generations.* edn.: Springer," pp. 1183–1193, 2016.

[40] S. Khuri and S. R. Miryala, "Genetic algorithms for solving open shop scheduling problems. In: Portuguese Conference on Artificial Intelligence: 1999: Springer," pp. 357–368, 1999.

[41] R. H-LFaP, "Corne D: a promising hybrid GA/heuristic approach for open-shop scheduling problems," *In: Proceedings of the 11th European conference on artificial intelligence: 1994: Citeseer*, pp. 590–594, 1994.

[42] C. Prins, "Competitive genetic algorithms for the open-shop scheduling problem," *Mathematical Methods of Operations Research*, vol. 52, no. 3, pp. 389–411, 2000.

[43] W. Marrouche and H. M. Harmanani, "Heuristic approaches for the open-shop scheduling problem. In: *information Technology-New Generations.* edn.: Springer," pp. 691–699, 2018.

[44] A. Bouzidi, M. E. Riffi, and M. Barkatou, "Cat swarm optimization for solving the open shop scheduling problem," *Journal of Industrial Engineering International*, vol. 15, no. 2, pp. 367–378, 2019.

Hindawi
Complexity
Volume 2022, Article ID 2400751, 15 pages
https://doi.org/10.1155/2022/2400751

Research Article

Research on the Vulnerability of Government Procurement of Elderly Care Services: A Complex Network Perspective

Yuting Zhang,[1] **Lan Xu**,[2] **and Zhengnan Lu**[1]

[1]*School of Management, Jiangsu University, Zhenjiang 212003, China*
[2]*School of Economics and Management, Jiangsu University of Science and Technology, Zhenjiang 212003, China*

Correspondence should be addressed to Lan Xu; xulan1111@just.edu.cn

Received 31 March 2022; Revised 15 June 2022; Accepted 28 June 2022; Published 29 August 2022

Academic Editor: Hui Xiao

The policy of government procurement of elderly care services has the vulnerability characteristics that all complex systems have. To maintain the policy's robustness, this paper studies the vulnerability of government procurement of elderly care services from the perspective of complex network. Case analysis and sample statistics are used to obtain the vulnerability influencing factors of the policy. Then, complex network diagram of vulnerability influencing factors is constructed through *Pajek* software. The compatibility coefficient is used to investigate the network's overall vulnerability from a macro perspective. From a micro perspective, a vulnerability index of the complex network is applied to measure each node's vulnerability value, and the vulnerability priority of the nodes is established. Results show that government purchasing power and supervisory bodies' diversity are at the first priority. The remaining vulnerability influencing factors are at the second and the third priority.

1. Introduction

With the acceleration of population aging in China, the contradiction between supply and demand of elderly care services has become increasingly prominent. How to innovate the supply mode of elderly care services and effectively allocate the resources of elderly care services is particularly important. China began to implement Government Procurement of Public Services in 1990s. Government procurement of elderly care service means that government purchases elderly care services from qualified service institutions and social organizations through public bidding or direct funding with the financial funds [1]. It is a new and efficient governance mode, making up for the deficiency of the market and governments in supplying the elderly care services. The policy of government procurement of elderly care services aims to meet the diversified needs of the elderly, promote the transformation of government functions, and improve the quality of elderly care services.

With the horizontal and vertical development of government procurement of elderly care services, the "point-to-point" cooperation mode between governments and social organizations for the aged has gradually developed into a network mode of multiagent cooperation. Policy of government procurement of elderly care services has the characteristics of integrity, relevance, purpose, and environmental adaptability that all complex systems should have. These properties and characteristics determine that government procurement of elderly care services is a complex network, with a certain vulnerability. Vulnerability is the objective attribute of complex systems. The higher the vulnerability, the more significant the negative impact of the complex network's weak link on the system and the greater the consequences. To improve the quality of government procurement of elderly care services and maintain the complex system's stability, it is necessary to analyze the network structure. Only by understanding its network structure and mastering the characteristics of its core vulnerability nodes correctly can we maintain the system's robustness. It is a complex system, promoting the implementation and improvement of the policy.

In the literature that utilizes complex network theory to study complex systems, network nodes are mostly physical entities. Although such practice can abstract connections

between entities, it cannot profoundly reflect the vulnerability factors' interaction. Given the purpose of the vulnerability study in this paper, factors influencing the vulnerability are identified as network nodes. In the context of this study, vulnerability influencing factors refer to the weak factors that affect the effectiveness or overall quality of government procurement of elderly care services. Regarding the definition of vulnerability influencing factors, considering that case studies can thoroughly describe the cases and display a comprehensive grasp of the dynamic changes and situations, this study begins with 68 actual government procurement cases of elderly care services. It breaks through traditional practice by combining a qualitative description of case studies with large sample statistics to obtain scientific and effective vulnerability influencing factors.

In summary, this paper studies the vulnerability of government procurement of elderly care services from a complex network perspective. A method of combining case analysis and sample statistics is used to obtain the vulnerability influencing government procurement factors of elderly care services. On this basis, *Pajek* is applied to construct a network topology diagram of vulnerability influencing factors. The topology measurement index of the compatibility coefficient is then applied to analyze the network topology diagram's vulnerability at the macro level. The vulnerability measurement index of the complex network is used to rank the vulnerability influencing factors from the micro level, establishing the vulnerability priority of factors influencing the effectiveness or overall quality of government purchasing elderly care services.

The main contributions of this paper are as follows:

(1) It studies the vulnerability of government procurement of elderly care services from the perspective of a complex system, identifying key vulnerability influencing factors, and establishes the vulnerability priority of influencing factors to provide a decision-making basis for managers.

(2) From the macro level, the network compatibility coefficient is used to examine the network's overall vulnerability. Furthermore, the impact of each node on the network vulnerability is considered from the micro level.

(3) The traditional qualitative method of case studies is improved by combining the case study with large sample statistics, obtaining vulnerability factors scientifically and effectively. *Pajek* is used to construct the network diagram of vulnerability influencing factors of government purchasing pension service.

The remainder of this paper is structured as follows. A literature review is presented in Section 2. Section 3 determines the vulnerability influencing factors by combining the case study and sample analysis. In Section 4, a vulnerability analysis is conducted. Finally, conclusions are presented in Section 5.

2. Literature Review

2.1. Government Procurement of Elderly Care Services. Scholars have begun to focus on government procurement of elderly care services in recent years, and the research mainly focused on empirical studies about existing problems or countermeasures and performance evaluation. In terms of empirical research, Knapp and Bauer [2] studied the procurement of elderly care services and summarized various problems. These include substandard qualifications of institutions for the elderly, poor cooperative relations between parties, and unclear roles and functions of participants. Ma and Hu [3] took Xi'an, China, as the research object and investigated the existing problems of local government purchasing home-based elderly care services. From the perspective of welfare pluralism, Chen [4] analyzed the situation of local government purchasing elderly care services in Wuhan, Hubei Province, and found the existing problems, such as policy fragmentation, imbalance between supply and demand of elderly care services, and insufficient professionals of elderly care services. In addition to the empirical research on the problems existing in government procurement of elderly care services, there are also empirical exploration on purchase mode [5], public satisfaction [6], and fiscal expenditure efficiency [7] of the policy. In terms of performance evaluation research in government procurement of elderly care services, Yang et al. [8] constructed a performance evaluation framework of elderly care services purchased by governments based on the logic of input-process-output-result. To promote the performance of government procurement of elderly care services, Xu [9] explored the influencing factors of policy performance with the help of SEM model. Drawing on existing research results, Milliken and Devlin [10] constructed an evaluation index system of the influencing factors, which are the ability of social organizations to undertake services, the degree of market competition, the ability of government management, and the external procurement environment. In addition to empirical studies and performance evaluation research, risk research is also the focus of government procurement of elderly care services. From the macro perspective, government procurement of elderly care services contains the monopoly risk [11], rent-seeking risk [12], moral hazard, and adverse selection risk [2]. Specifically, Li and Zhang [13] studied the risks of government procurement of elderly care services from the perspective of elderly care service chain and summarized the specific risks in the demand chain, supply chain, and evaluation chain.

Reviewing the relevant literature, it is found that most of the existing studies focus on the institutions which provide elderly care services without considering government procurement of elderly care services as a whole network from a macroperspective. A complex system with multiagent and multitask government procurement of elderly care services possesses the objective attribute of vulnerability. Therefore, to promote the implementation and improvement of the policy and maintain the complex system's stability, it is essential to study the vulnerability of government procurement of elderly care services from the perspective of a complex network.

2.2. Complex Network. A proposal of the "Seven Bridges problem of Ginsberg" in 1736 indicates the birth of complex networks theory. Regarding the specific application of complex network, two research directions and results are summarized as follows.

(1) Research on the importance of the node based on complex network theory: Evaluation of node importance is the focus in the field of network science. The commonly used network node importance ranking indicators include degree value [1], betweenness [14], near centrality [15], K-shell value [16], and eigenvector [17]. Scholars have considered various algorithms to improve these commonly used indicators. For example, Lu and Shang [18] proposed the Local Rank algorithm based on the degree value's centrality, which considered the information contained in the fourth-order neighbors of a node. Lu et al. [19] simultaneously regarded the number of adjacent nodes and the node aggregation coefficient, proposing the Cluster Rank algorithm. An index of H was used to measure individuals' influence on social networks [20]. Gao et al. [21] proposed a network node importance recognition algorithm based on the adjacent information entropy by studying the relationship between a node and its direct and indirect adjacent nodes. In addition to algorithmic research about the importance evaluation indicators of a complex network, scholars have also explored the application of node importance. Xu et al. [22] proposed an importance evaluation method based on mutual information, which had low computational complexity and was suitable for the node importance assessment of large complex networks. Wang et al. [23] used the mutual information method to evaluate node importance of a weighted directed network. Su and Song [24] applied structural hole theory to evaluate node importance to overcome the defects of the local node evaluation algorithm and the computational complexity of the global measurement algorithm. Based on the water network's global network topology, Yu and Yang [25] defined the node importance evaluation index from four aspects: local attribute, global attribute, propagation attribute, and network location. They comprehensively evaluated node importance based on the TOPSIS multiattribute decision-making method.

(2) Research on propagation mechanism based on complex network theory: to aid the decision-making process, Mukul and Rajhans [26] aimed to determine the key influencers in information propagation with the application of network complex. Wang and Chen [27] constructed a risk propagation model of complex products based on the complex network theory to investigate the dynamic propagation process. Using the complex network analysis method, Katerelos and Tsekeris [28] constructed a complex network topology model of microblog public opinion propagation in mobile Internet and analyzed its structural characteristics and evolution mechanism. In addition, propagation behavior in complex network has similar laws with the disease transmission, applying the infectious disease model such as SI model, SIR model, and SIS model [29] to study the propagation mechanism in networks which has become a classic practice in academic circles.

2.3. Vulnerability Study. Vulnerability research originated from the ecosystem and natural disasters and has been applied to many research fields. The research content mainly involves the definition of vulnerability, a qualitative assessment of vulnerability, an analysis of vulnerability causes, and countermeasures research. Based on the framework of "risk-adaptation-sensitivity," He and Zhou [30] constructed a vulnerability evaluation index system of farmers' livelihood. In urban development research, Pei and Guo [31] incorporated the innovation system into the urban vulnerability assessment framework and constructed the urban vulnerability evaluation index system from five dimensions of resources, measuring the urban vulnerability of 11 prefecture-level cities in Shanxi province from 2013 to 2017. In terms of the project system, Zhang and Chen [32] established a System Dynamics model based on sensitivity, adaptability, and exposure to analyze system vulnerability's driving factors. To understand the degree of PPP project system exposure to the external environment's adverse impacts, the ability to resist interference and self-regulation recovery, Yuan et al. [33] proposed a vulnerability assessment method for PPP projects. In addition, due to the complex relationship in the network, research on network vulnerability has become necessary. Complex network theory provides a theoretical basis and a powerful tool for network vulnerability assessment. When measuring the nodes' vulnerability in the nearest neighbor network of smart government, Ma et al. [34] took the node degree value as the vulnerability measurement index. Duan and Zheng [35] designed a vulnerability analysis method for complex networks based on node importance by combining degree value and node betweenness.

In summary, to maintain the objects' robustness and reliability, vulnerability research in various fields has its practical significance. However, when retrieving "government procurement of elderly care services" and "vulnerability" as keywords, no relevant literature is found. Government procurement of elderly care services has developed into a multiagent and multitask complex system, and it is urgent to study its vulnerability.

2.4. Summary of Literature Review. Through a literature review, it is found that scholars at home and abroad have carried out beneficial explorations on government procurement of elderly care services, complex network theory, and vulnerability research, which provides a theoretical basis for this study. However, there are few studies on the vulnerability of government procurement of elderly care services in existing literature, and it is biased to put the research

focus only on the elderly care service institutions, ignoring the vulnerability research on the complex system which contains governments, the public, and institutions for the aged from the perspective of the complex system. In addition, the current literature on government procurement of elderly care services is mostly qualitative research, concentrating on the performance evaluation of the policy, existing problems, and other empirical research. Moreover, the relevant vulnerability literature also focuses on constructing vulnerability evaluation indicators and the definition of vulnerability driving factors, ignoring the importance of the quantitative measurement of each node's vulnerability. This paper combines qualitative case analysis and quantitative sample statistics to scientifically define the vulnerability influencing government procurement factors of elderly care services. Furthermore, the network compatibility coefficient and the loss of network efficiency are selected to examine the vulnerability of government procurement of elderly care services from the macro and micro levels, respectively.

3. Data Analysis of Vulnerability Influencing Factors

3.1. Case Selection. The first step in analyzing the vulnerability of government procurement of elderly care services with the complex network theory is to construct a network topology diagram, which consists of vulnerability influencing factors. Case analysis and sample statistics are used to obtain the scientific vulnerability influencing factors.

As far as the source of cases is concerned, researchers start with the news and media and consult relevant government websites. Network material of cases is collected through snowballing to compile standardized cases that can be used for further academic research. The results of the case summary are shown in Table 1 by collecting and filing the materials. For example, during the collection of the case "Home-Based Care Services in Jing'an District, Shanghai," the basic information was first extracted from a news report on sohu.com entitled "Elaborating on Several Problems Faced by the Government in Purchasing Home-Based Care Services," and it was kept as the preliminary data of "Home-Based Care Services in Jing'an District, Shanghai." Then researchers searched the website of Jing'an District Government of Shanghai and found reports entitled "Notice on Printing and Distributing the implementation measures of Jing'an District on Supporting the Development of Home-Based Care Services" and "Audit and Investigation Results on the Special Funds for Home-Based Elderly Care by Shanghai Jing'an District Civil Affairs Bureau in 2016-2017." On this basis, the scope was expanded, and the "Notices on Adjusting the Relevant Policies of the City's Community Home-Based Elderly Care Services by the Civil Affairs Bureau" and "Notice of the Civil Affairs Bureau on the Allocation of Subsidy Funds for the Home-Based Elderly Care Service Projects in the First Half of 2017 with Municipal Welfare Lottery Public Welfare Fund-Funded Community" were retrieved from the website of the Shanghai Municipal Government. With these reports' help, a complete case of "Home-Based Care Services in Jing'an District, Shanghai" has been compiled.

3.2. Variable Identification and Hypothesis Formulation. To break through the traditional practice of case studies, the case materials are coded into statistical data and combined with sample statistics to complete the statistical inference research aim.

3.2.1. Determination of Dependent Variables. The paper aims to define the key vulnerability influencing nodes and the priority of the vulnerability influencing nodes in government procurement of elderly care services. Vulnerability influencing nodes refer to weak links in the complex network, that is, the factors that negatively impact the overall quality or effectiveness of government procurement of elderly care services. Therefore, the effectiveness or quality of government purchasing elderly care services evaluated by governments or the third-party institutions is the dependent variable. Evaluation results provide a "material" basis for the data collection of the dependent variables.

The central government has issued a series of policies requiring the evaluation of procured services, such as "a strict supervision and evaluation mechanism should be established in government procurement" and "the evaluation mechanism composed of buyers, service objects and the third party shall be established." With the promotion of central policies, many local governments began to evaluate various procurement services' effectiveness or quality. Therefore, data on dependent variables are easy to obtain. For example, the case of "Home-Based Elderly Care Services in Shangcheng District, Hangzhou City, Zhejiang Province" was evaluated as 92 points by the third-party evaluation agency, Hangzhou endowment Promotion Association. Another example is the case "Elderly Care Services in Haishu District, Ningbo City, Zhejiang Province," in which the evaluation result is described as "good." It should be noted that some cases' evaluation results are descriptive interval data rather than specific values. With descriptive interval data, the value of 95 is assigned to "excellent," 85 to "good," 75 to "medium," and 65 to "qualified."

3.2.2. Determination of the Independent Variable. The independent variable is the vulnerability influencing factors of government procurement of elderly care services. Through case analysis, quality problems, and weak links in each specific case are identified to decide whether the effectiveness or quality of government procurement of elderly care services is affected by the ratio of the elderly to nursing workers, number of personalized service items, the proportion of professional nursing workers, construction of elderly care service facilities, government purchasing power, the type of procurement target, procurement methods, number of bidding companies, diversity of supervisory bodies, number of volunteers, support of policies and

Table 1: Case summary of government procurement of elderly care services.

Number	Case	Financial input	Type of procurement target	Procurement method	Operation cycle
1	Home-based care services in Jing'an district, Shanghai	Government invested 2 million yuan in 2019	Social organizations	Directional entrustment	1 year
2	Government of Zhongmu county, Henan province procured elderly care services	1.83 million yuan	Commercial company (Hanjing Project Management Co., Ltd.)	Open and fair competition	2 years
3	Elderly care service in Guangzhou City, Guangdong province	The provincial government raised 30 million yuan in the welfare lottery fund each year from 2010 to 2012	Social organizations; commercial company	Open and fair competition	3 years
4	Elderly care services in Pukou District, Nanjing City, Jiangsu Province	Since 2013, the government has subsidized 1.2 million yuan in fiscal funds every year	Social organizations	Directional entrustment	1 year
5	Elderly care services in Haishu District, Ningbo City, Zhejiang Province	Since 2004, the government has allocated 1.5 million yuan annually	Nonprofit social organization	Internal designation (established by the government)	1 year
6	Home-based elderly care services in Shangcheng District, Hangzhou City, Zhejiang Province	In 2015, the government invested 25 million yuan in financial funds	Social organizations	Directional entrustment	1 year
7	Procurement of home-based care services by Huaian municipal government in Jiangsu Province	In 2016, the government allocated 3 million yuan	Government-affiliated institutions	Internal designation	1 year
8	Procurement of elderly care services in Xiamen City, Fujian Province	In 2012, the government invested 5 million yuan in early-stage start-up funds and 2 million yuan each year after that	Social organizations	Open and fair competition	3 years
9	Procurement of home-based elderly care services in Hefei City, Anhui Province	The government procured home-based care services worth 600 yuan per month for the elderly	Government-affiliated institutions	Directional entrustment	2 years
10	"Home-based elderly care service card" launched by Taiyuan City, Shanxi Province	Government invested 6 million yuan in 2016	Government-affiliated institutions	Directional entrustment	1 year
⋮	⋮	⋮	⋮	⋮	⋮
66	Elderly care services in Zhenjiang, Jiangsu University	Zhenjiang municipal government invested 60 million yuan in 2017	Commercial company	Directional entrustment	1 year
67	Government purchase of home-based elderly-care services in Urumqi	The city has invested 1.86 million yuan in total	Social organizations	Directional entrustment	1 year
68	Smart elderly care services in Shanghai	Government invested 3.6 million yuan	Commercial company	Directional entrustment	2 years

regulations, the coverage rate of service, starting time of procurement, operation cycle of projects, and the economic conditions of the region.

(1) Ratio of the elderly to nursing workers (f1): the ratio between the elderly and nursing workers should be balanced. In actual cases of government procurement of elderly care services, a small number of nursing workers are taking care of a raft of elderly people in the elderly care service center. The ratio of the elderly to nursing workers has reached 15 : 1. Obviously, the higher the ratio of the elderly to nursing workers, the less time and lower the quality of service the elderly get. The shortage of nursing workers is closely related to high prejudice and the poor treatment of the industry. Therefore, the first hypothesis of this study is put forward.

Hypothesis 1. The lower the ratio of the elderly to nursing workers, the higher the effectiveness or quality of government procurement of elderly care services.

(2) Number of personalized service items (f2): elderly people of different age groups and different physical conditions have different service needs. With modernization and urbanization, the needs of the elderly have gradually deviated from basic physiology and safety to emotion, respect, and self-realization. Essential service items of elderly care include meal aid, cleaning aid, and medical aid. As for obtaining the variable data, the specific number of service items can be obtained from the procurement documents. For example, Huai'an, Jiangsu Province, actively explored home-based care services procurement and promulgated

"the 13th five-year plan for the development of the elderly, and the construction of the pension system." Elderly care services include seven items stipulated as daily cooking, meal assistance, cleaning, medical assistance, purchasing assistance, agency, and daily communication.

Hypothesis 2. The more personalized the service items, the higher the effectiveness or quality level of government procurement of elderly care services.

(3) Proportion of professional nursing workers (f3): at present, there are no relevant political restrictions on the qualification of nursing workers in China, and their training is not a priority, which leads to the problem of a "low quality" of nursing workers in elderly care institutions. There are few nursing workers with professional skills in the whole service team. Recently, more attention has been paid to the professional level of nursing workers in government procurement of elderly care services. Some specific requirements for the proportion of professional nursing workers have been released in relevant documents. For example, in the "notice of printing and distributing the implementation opinions on further accelerating the construction of social pension service system in Pukou district" issued by the People's Government of Pukou District, Nanjing, it is recorded that "the proportion of nursing workers with medium and high professional titles must account for more than 10%."

Hypothesis 3. The higher the proportion of professional nursing workers, the higher the government's effectiveness or quality procured pension services.

(4) Construction of elderly care service facilities (f4): the construction of elderly care service facilities is measured by three aspects: the accommodation (area), safety (handrails, nonslip ground, etc.), and the provision of functional facilities (reading room, table tennis room, and opera room). Ostensibly, it is difficult to obtain the measurement data. However, there is a clear record of the institution's facility construction in the government procurement and bidding enterprise documents. The value of f4 is measured by considering all three aspects of accommodation, safety, and functional equipment, and 3 is assigned to f4.

Hypothesis 4. The more complete the construction of elderly care service facilities, the higher the effectiveness or quality of government procurement of elderly care services.

(5) Government purchasing power (f5): governments' financial contribution to the procurement project is used to reflect the government's procurement power. The greater the government's procurement power, the greater the motivation of elderly care service institutions to improve their services, and the more the elderly will benefit.

Hypothesis 5. The greater the purchasing power, the higher the effectiveness or quality of government procurement of elderly care pension services.

(6) Type of procurement target (f6): in China, there are mainly two forms of government procurement in the elderly care service domain: first, governments procurement from social forces (enterprises and social organizations) and second, governments procure from government-affiliated institutions. According to classical theory, once an institution connects with governments closely, it will turn inefficient. Therefore, there is a risk of low efficiency and low quality when government-affiliated institutions provide pension services.

The measurement of the variable "type of procurement target" is processed according to the following model. Social force (enterprises and social organizations) is assigned to 1, and government-affiliated institutions are assigned to 2.

Hypothesis 6. From the perspective of the type of procurement target, the effectiveness and quality of elderly care services provided by social forces are higher than the effectiveness and quality of elderly care services provided by public institutions.

(7) Procurement methods (f7): according to the definition of Government Procurement of Public Services, service procurement refers to open and fair competition with a clear service objective. Market competition is introduced into government procurement to encourage potential targets to improve service level. However, in actual cases, there are three procurement methods: open and fair competition, directional entrustment, and internal designation. Among the three procurement methods, the independence between governments and social organizations is gradually reduced, and the risk of quality problems in government procurement of elderly care services is also gradually increasing.

In the empirical test, the variables of "procurement methods" are assigned as follows: open and fair competition = 3, directional entrustment = 2, and internal designation = 1.

Hypothesis 7. In terms of procurement methods, the effectiveness of elderly care services procured in an open and fair competition is higher than directional entrustment. The effectiveness of elderly care services procured with the above two methods is higher than that of internal designation.

(8) Number of bidding companies (f8): in a fair, just, and open environment, multiple bidding companies are conducive to stimulating market vitality. Candidates providing elderly care services will strive to improve their service capabilities to obtain the opportunity to become procurement targets.

Hypothesis 8. The greater the number of bidding companies, the higher the effectiveness or quality of government procurement of elderly care pension services.

(9) Diversity of supervisory bodies (f9): in the government procurement of elderly care services, governments have changed from its original role as a direct service provider to an indirect provider. As a result, governments tend to ignore their responsibilities as "buyers" and "regulators" in many practical cases. In addition, third-party institutions are considered to be the natural supervisory bodies of government procurement of elderly care services

due to their high objectivity, professionalism, and neutrality. Multisubject supervision will improve supervision efficiency and ensure the effectiveness of procurement. The diversity of supervisory bodies is measured by the following method. If the supervisory body only includes the government, 1 is assigned to the independent variable of f9. If the supervisory bodies include both government and third-party agencies, 2 is assigned to the independent variable of f9.

Hypothesis 9. The higher the diversity of supervisory bodies, the higher the effectiveness or quality of government procurement of elderly care pension services.

(10) Number of volunteers (f10): voluntary service is an important part of the elderly care service system in the new era. In the procurement of elderly care services, professional medical staff, nursing workers, and many volunteers are needed to create a social atmosphere of filial piety and respect for the elderly. The number of volunteers can be obtained from the procurement documents of elderly care services. For example, in the "notice of printing and distributing the implementation opinions on further accelerating the construction of social pension service system in Pukou district" issued by the People's Government of Pukou District, Nanjing, it is mentioned that "voluntary service for the aged should be extensively carried out, and the number of volunteers serving the elderly needs to reach 2000."

Hypothesis 10. The more the volunteers, the higher the effectiveness or quality of government procurement of elderly care pension services.

(11) Support for policies and regulations (f11): it is generally believed that policies and regulations are important factors to induce elderly care services' government procurement effectiveness. The imperfect policies and regulations of procurement standards, procedures, and regulatory systems lead to frequent government corruption, market disorder, and low pension services quality. Data on the support for policies and regulations can be obtained by consulting local government documents related to elderly care services procurement. For example, in the case of "Home-Based Care Services in Jing'an District, Shanghai," consulting the Shanghai municipal government website, the website of Shanghai municipal government procurement, and some news reports, three documents are obtained. These include, "Implementation plan of deepening the elderly care service in Shanghai (2019–2022)," "Some opinions on improving the basic public services for the elderly in Shanghai," and "Suggestions on encouraging social forces to participate in the construction of elderly care service system."

Hypothesis 11. The more the support for policies and regulations, the higher the effectiveness or quality of government procurement of elderly care pension services.

(12) The coverage rate of service (f12). The coverage rate of service is the ratio of the number of elderly people enjoying the policy to the number of elderly people in the area. The purpose of government procurement of elderly- are is to expand pension service resources and popularize pension services. Therefore, a high coverage rate of service should be the intention of the policy. The acquisition of the variable is not complicated. For example, in the case of "Procurement of home-based care services by the Huaian municipal government in Jiangsu province," the city issued a document stipulating that the scope of procurement of home-based care services will be expanded to the age of 60 years, based on the original coverage, benefiting 59000 elderly people. According to the Huaian Municipal Bureau of Statistics data, there are 330000 elderly people over 60. Therefore, the coverage rate of the service is 17.8%.

Hypothesis 12. The higher the coverage rate of service, the higher the effectiveness or quality of government procurement of elderly care pension services.

(13) Starting time of procurement (f13): as a policy to improve elderly care service resources' efficiency, government procurement of elderly care services presents a significant feature of "gradualism." According to the historical experience, the earlier the starting time of procurement, the longer the exploration time will be. Thus the practice of government procurement of elderly care services will be more mature, and the effect will be better, which can be explained by the "first cause-effect." Data on the time of procurement is easy to obtain.

3.2.3. Determination of the Control Variable

Hypothesis 13. The earlier the procurement's starting time, the higher the effectiveness or quality of government procurement of elderly care pension services.

(14) The operation cycle of projects (f14): the operation cycle of projects is not related to the starting time of the procurement. The operation cycle of projects refers to the time from the effective starting date of the procurement to its end. The longer the operation cycle of projects, the greater the risks, and the more difficult the supervision. Therefore, the following hypothesis is formulated.

Hypothesis 14. The longer the operation cycle of projects, the lower the effectiveness or quality of elderly- care pension services' government procurement.

(15) Economic conditions of the region (f15): it refers to the economic conditions of the area where the elderly care services are procured. Generally speaking, the better the regional economic situation, the stronger the vitality of local social organizations, and the stronger its ability to provide elderly care services. The regions' economic conditions can be measured by total GDP, obtained from the "China Statistical Yearbook." According to the ranking of the total GDP of major regions in 2019, the economic conditions of seven regions from Northwest to East China are shown below: northwest: 4,659.2 billion yuan; northeast: 5,543 billion yuan; southwest: 876.3 billion yuan; North China: 1,13672 billion yuan; Central China: 1161100.1 billion yuan; South China: 14.7036 billion yuan; and, East China: 288818 billion yuan.

Table 2: Summary of variables and the measurement method.

Variable	Factors	Measurement
Dependent variables	Effectiveness or quality of government purchasing elderly care services (EFFE)	Evaluated by governments or third-party institutions, the score is 0~100
	Vulnerability influencing factors	Measurement
Independent variables	Ratio of the elderly to nursing workers (f1)	Ratio of the number of the elderly served to the number of nursing workers
	Number of personalized service items (f2)	Number of services provided
	Proportion of professional nursing workers (f3)	Proportion of nursing workers with middle and senior titles
	Construction of elderly care service facilities (f4)	Considering all three aspects, accommodation, safety, and functional equipment, 3 is assigned to f4
	Government purchasing power (f5)	Governments' financial input
	Type of procurement target (f6)	Social forces (enterprises and social organizations) = 1 and government-affiliated institutions = 2.
	Procurement methods (f7)	Open and fair competition = 3, directional entrustment = 2, internal designation = 1
	Number of bidding companies (f8)	Number of companies participating in bidding
	Diversity of supervisory bodies (f9)	If the supervisory body only includes the government, 1 is assigned to f9. If the supervisory bodies include both government and third-party agencies, 2 is assigned to f9.
	Number of volunteers (f10)	Number of volunteers participating in the project
	Support for policies and regulations (f11)	Number of documents related to the policy
	Coverage rate of service (f12)	Proportion of the number of elderly people enjoying the policy to the total number of elderly people in the region
Control variable	Starting time of procurement (f13)	Start time of procurement project
	Operation cycle of projects (f14)	Time period from the effective start date of the procurement to the end of the procurement
	Economic conditions of the region (f15)	The total GDP of the region obtained from the "China Statistical Yearbook"

Table 3: Descriptive statistics of variables.

Variable	Sample size	Mean	Mode	Minimum	Maximum	Standard deviation
f1	68	16.4	15	6	30	5.84
f2	68	4.5	3	3	8	1.57
f3	68	0.12	0.1	0.05	0.2	0.04
f4	68	2.12	3	1	3	0.83
f5	68	185.1	20	0.8	2000	400.4
f6	68	1.3	1	1	2	0.48
f7	68	2.3	3	1	3	0.8
f8	68	2.2	0	0	7	2.3
f9	68	1.5	2	1	2	0.5
f10	68	222.8	100	0	2000	405.4
f11	68	4.2	5	2	10	1.6
f12	68	0.29	0.32	0.1	0.52	0.11
f13	68	2015	2016	2012	2019	1.93
f14	68	1.56	1	1	4	0.82
f15	68	241855.5	288818	46592	1161101	285015.5
E	68	78.4	85	55	95	12.1

Hypothesis 15. The better the region's economic conditions (GDP) where the government procures elderly care services, the higher the effectiveness or quality of government procurement of elderly care pension services.

The specific meaning of each variable and the measurement method is shown in Table 2.

3.3. Results of the Statistical Analysis. After obtaining the data for each variable, researchers clarify the variables' descriptive statistics and test their correlation. Finally, regression testing on the hypothesis is performed step by step.

3.3.1. Descriptive Statistics of Variables. The statistical results of 68 sample data are summarized in Table 3.

3.3.2. Correlation Test of Variables. The correlation test results between variables are shown in Table 4.

Table 4: Correlation test of variables.

Variable	f1	f2	f3	f4	f5	f6	f7	f8	f9	f10	f11	f12	f13	f14	f15	E
f1	1	−0.10	0.15	0.31*	−0.06	−0.14	−0.02	0.03	−0.06	−0.22	−0.06	−0.02	−0.29	0.02	−0.17	0.12
f2	−0.10	1	0.07	−0.31*	0.13	0.03	−0.22	−0.21	0.01	0.23	0.33	0.17	0.04	0.09	0.42	0.03
f3	0.15	0.07	1	0.11	0.18*	0.22	0.03	035	0.25	0.12	0.17	0.42	0.20	0.27	0.09	0.17
f4	0.31*	−0.31*	0.11	1	0.34	0.06	0.16	0.25	0.09	0.19	0.22	0.26	0.61	0.33	0.19	0.23
f5	−0.06	0.13	0.18*	0.34	1	0.14	0.18	0.24	0.37	0.12	0.35	0.41	0.19	0.56	0.72	0.37
f6	−0.14	0.03	0.22	0.06	0.14	1	0.33	0.28	0.47	0.65	0.61	0.73	0.48	0.52	0.64	0.58
f7	−0.02	−2.22	0.03	0.16	0.18	0.33	1	0.37	0.58*	0.18	0.29	0.26	0.48	0.69	0.54	0.64
f8	0.03	−0.21	0.35	0.25	0.24	0.28	0.37	1	0.55	0.64	0.62	0.74	0.67	0.38	0.49	0.71
f9	−0.06	0.01	0.25	0.09	0.37	0.47	0.58*	0.55	1	0.38	0.57	0.53	0.26	0.36	0.38	0.74
f10	−0.22	0.23	0.12	0.19	0.12	0.65	0.18	0.64	0.38	1	0.85	0.61	0.69	0.77	0.63	0.84
f11	−0.06	0.33	0.17	0.22	0.35	0.61	0.29	0.62	0.57	0.85	1	0.85	0.17	0.88	0.79	0.83
f12	−0.02	0.17	0.42	0.26	0.41	0.73	0.26	0.74	0.53	0.61	0.85	1	0.69	0.48	0.52	0.54
f13	−0.29	0.04	0.20	0.61	0.19	0.48	0.48	0.67	0.26	0.69	0.17	0.69	1	0.59	0.33	0.41
f14	0.02	0.09	0.27	0.33	0.56	0.52	0.69	0.38	0.36	0.77	0.88	0.48	0.59	1	0.53	0.64
f15	−0.17	0.42	0.09	0.19	0.72	0.64	0.54	0.49	0.38	0.63	0.79	0.52	0.33	0.53	1	0.49
E	0.12	0.03	0.17	0.23	0.37	0.58	0.64	0.71	0.74	0.84	0.83	0.54	0.41	0.64	0.49	1

Note. $^{*}P < 0.05$ and $^{**}P < 0.01$. The test was double tailed and the correlation coefficient was a Pearson correlation coefficient.

A correlation between variables can be concluded from the results of the testing. The value of the correlation is less than 0.5. It means the possibility of multicollinearity is insignificant, indicating that the variables can be used for a regression test.

3.3.3. Regression Test. The result of the stepwise regression test is shown in Table 5.

It can be seen from Table 4 that, after adding the independent variables one by one, the model is significant at the level of 0.05 and the explanatory ability continues to improve. Model 13 shows that it is statistically significant and can explain 34% of the variance of the dependent variable (R-square = 0.345, $F = 38.723$). The white heteroscedasticity test of Model 13 shows that the p value is 0.79. The original assumption H0: the model is homovariance. The original assumption is accepted, and it is considered that Model 13 does not have heteroscedasticity. Then, Model 13 is tested for sequential correlation. The test results show that there is no sequential autocorrelation in Model 13. According to regression results in Model 13, the following analysis is carried out. The regression coefficient of f1, which is the ratio of the elderly to nursing workers, is −0.122. It is significant at the level of 0.001, indicating that the ratio of the elderly to nursing workers and the effectiveness of government procurement of elderly care services are negatively correlated. Therefore, Hypothesis 1 is supported. The elderly's ratio to nursing workers is indeed the vulnerability influencing factor in government procurement of elderly care services. There is no statistical correlation between the operation cycle of projects and the effectiveness of government procurement of pension services. Therefore, Hypothesis 14 is not supported, and the projects' operation cycle will not be identified as a vulnerability influencing factor. In the same way, other hypotheses can be proved. Therefore, the vulnerability influencing factors of government procurement of elderly care services to include the ratio of the elderly to nursing workers (f1), number of personalized service items (f2), the proportion of professional nursing workers (f3), construction of elderly care service facilities (f4), government purchasing power (f5), type of procurement target (f6), procurement methods (f7), number of bidding companies (f8), diversity of supervisory bodies (f9), number of volunteers (f10), support of policies and regulations (f11), the coverage rate of service (f12), starting time of procurement (f13), and economic conditions of the region (f15).

4. Vulnerability Analysis on Government Procurement of Elderly Care Services

4.1. Construction of Network Topology Diagram. To construct the network topology diagram of the vulnerability influencing factors, it is necessary to clarify the correlation between the factors after defining the vulnerability influencing factors of government procurement of elderly care services. Six experts were investigated, including two directors of the home-based pension service center, two in-service teachers studying government purchasing pension services, and two master's and doctoral students of **university engaged in government procurement research. Firstly, each expert's opinions about the correlation between different vulnerability influencing factors are solicited by face-to-face inquiry, and results are sorted and summarized. The correlation between factors will be fed back to experts, soliciting opinions and summarizing again. In this way, collection and feedback are taken as a cycle, repeating this cycle three times. Finally, an agreement on the relationship between the vulnerability influencing factors is reached.

To realize the analysis and visual operation of the complex network of vulnerability influencing factors of government procurement of elderly care services, the vulnerability influencing factors and their relationships are recorded in Notepad and transformed into NET format with txt2pajek software. Finally, the network topology diagram of vulnerability influencing factors is constructed using *Pajek* and is shown in Figure 1.

Table 5: Result of stepwise regression analysis.

	Variable	M1	M2	M3	M4	M5	M6	M7	M8	M9	M10	M11	M12	M13
Independent variable	f1		−0.135**	−0.172**	−0.164**	−0.174**	−0.158**	−0.139**	−0.126**	−0.178**	−0.166**	−0.134**	−0.147**	−0.122**
	f2			0.124***	0.136***	0.137***	0.129***	0.135***	0.127***	0.179***	0.158***	0.139***	0.166***	0.142***
	f3				0.129*	0.145*	0.128*	0.133*	0.146*	0.065*	0.124*	0.151*	0.123*	0.132*
	f4					0.162**	0.183**	0.142**	0.119**	0.138**	0.127**	0.133**	0.154**	0.162**
	f5						0.151***	0.142***	0.191***	0.114***	0.152***	0.133***	0.127***	0.142***
	f6							−0.163**	−0.116**	−0.127**	−0.136**	−0.162**	−0.119**	−0.121**
	f7								0.104**	0.089**	0.052**	0.126**	0.124**	0.167**
	f8									0.065***	0.043***	0.024***	0.015***	0.062***
	f9										0.062*	0.053*	0.071*	0.043*
	f10											0.137***	0.142***	0.163***
	f11												0.145*	0.127*
	f12													0.123*
Control variable	f13	−0.038*	−0.028*	−0.016*	−0.046*	−0.031*	−0.042*	−0.022*	−0.018*	−0.027*	−0.016*	−0.075*	−0.062*	−0.042*
	f14	0.127*	0.167	0.128	0.121	0.152	0.106	0.103	0.116	0.139	0.126	0.183	0.172	0.152
	f15	0.216**	0.133**	0.145**	0.137**	0.126**	0.107**	0.114**	0.126**	0.173**	0.165**	0.153**	0.142**	0.126**
N		68	68	68	68	68	68	68	68	68	68	68	68	68
F		1.106	3.342	7.431	10.011	13.165	15.342	19.230	23.141	27.103	31.122	33.062	35.621	38.723
R^2		0.023	0.054	0.076	0.098	0.128	0.163	0.194	0.211	0.246	0.268	0.293	0.314	0.345

Note. $^{*}P < 0.05$, $^{**}P < 0.01$, and $^{***}P < 0.001$.

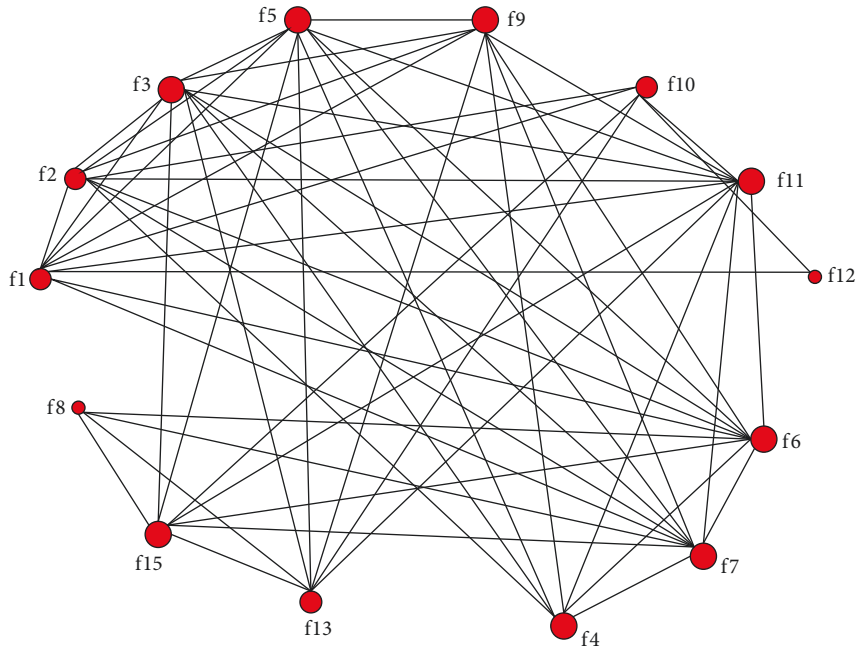

Figure 1: Network topology diagram of the vulnerability influencing factors in government procurement of elderly care services.

Table 6: Statistical characteristics of Figure 1.

Structural parameters	Number of nodes	Density of network	Average degree	Average shortest path	Diameter
	14	0.615	8	1.406	3

Table 7: Degree value of nodes in network topology network of vulnerability influencing factors.

Node	f1	f2	f3	f4	f5	f6	f7	f8	f9	f10	f11	f12	f13	f15
Degree value	9	9	9	7	10	9	10	4	9	6	11	2	7	9

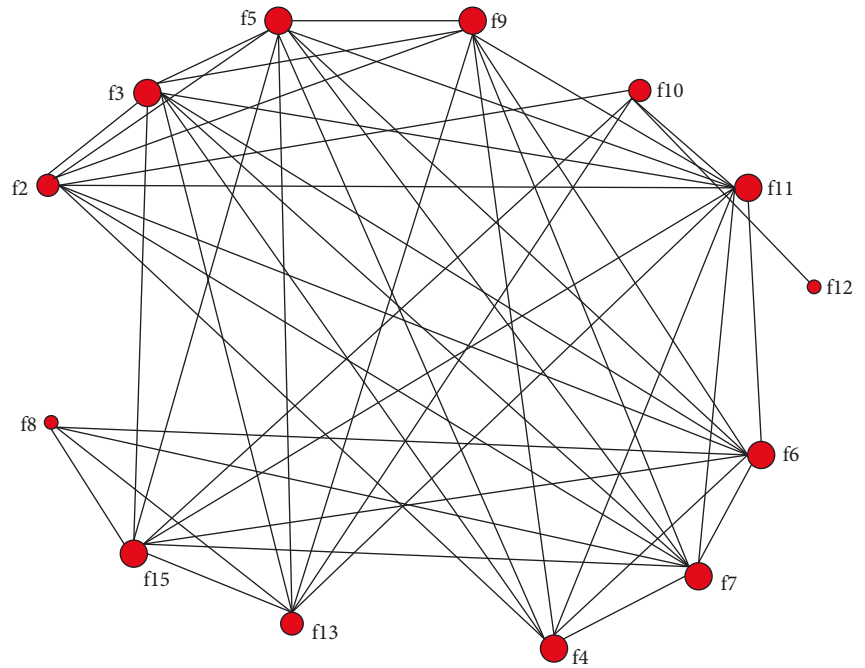

Figure 2: Network topology diagram where $f1$ fails.

The statistical characteristics of Figure 1 are shown in Table 6.

4.2. Calculation of the Compatibility Coefficient. After obtaining the network topology diagram of vulnerability influencing factors and its basic statistical characteristics, the paper examines the network's vulnerability from the macro level by using the compatibility coefficient to judge the overall vulnerability of government procurement of elderly care services. If the node with a high degree tends to connect with the node with a high degree, it is defined as a homomorphic network; otherwise, it is a heteromorphic network. Newman found that, compared with the heterogeneous network, information in the homomorphic network flows easier, and the network is more stable when the nodes are removed. The definition of the compatibility coefficient is as follows:

$$r = \frac{M^{-1}\sum_i j_i k_i - \left[M^{-1}\sum_i 1/2\left(j_i + k_i\right)\right]^2}{M^{-1}\sum_i 1/2\left(j_i^2 + k_i^2\right) - \left[M^{-1}\sum_i 1/2\left(j_i + k_i\right)\right]^2}, \quad (1)$$

where j_i and k_i are the degree value of two endpoints of the i-th edge. M is the total number of edges in the network. If $r > 0$, then the network is homomorphic. If $r < 0s$, then the network is homomorphic.

The degree values of 14 nodes in the network topology diagram are shown in Table 7. After calculation, $\sum_i j_i k_i = 4130$, $\sum_i 1/2\,(j_i + k_i) = 485$, $\sum_i 1/2\,(j_i{}^2 + k_i{}^2) = 4337$, so the compatibility coefficient of the network topology diagram is −0.512. Therefore, as mentioned above, the network of the vulnerability influencing factors of government procurement of elderly care services is heterogeneous. It means that the network topology diagram of Figure 1 is vulnerable, and when some nodes with a high degree value are deleted, the network presents a greater vulnerability. Nodes with a high degree value are not necessarily connected with high degree value nodes. Therefore, the value of the degree cannot directly reflect the vulnerability of the nodes. It is imperative and necessary to study the vulnerability of nodes further and grasp the key vulnerability factors.

4.3. Calculation of Nodes Vulnerability. Concerning the vulnerability measurement of the complex network, a series of measurement indexes have been proposed in the literature, such as degree value, betweenness, and the largest connected subgraph scale. However, according to system vulnerability's general definition and characteristics, vulnerability refers to the network system's sensitivity when the function is damaged during disasters and emergencies [36]. Therefore, the vulnerability of government procurement of elderly care services is defined as the declining ratio of system efficiency under the threat of the vulnerability influencing factors [37]. The vulnerability of nodes can be evaluated by the loss of network efficiency. Vulnerability of node f_i is

$$V\left(f_i\right) = \frac{E(G) - E\left(G, f_i\right)}{E(G)}, \quad (2)$$

where $E(G)$ is the average efficiency of the network under the normal conditions, and $E(G, f_i)$ is the average efficiency of the network in which node f_i fails. Usually, the failure of a node is represented by deleting the node and the edges connected to the node. Network efficiency is the most commonly used and effective index to measure network performance, which is defined as

$$E(G) = \frac{1}{n(n-1)}\sum_{i\neq j}\frac{1}{d(i, j)}, \quad (3)$$

where $d(i, j)$ is the shortest path between node i and node j; n is the number of network nodes. The vulnerability assessment process of government procurement of elderly care services is as follows:

Step 1: calculating the network efficiency $E(G)$ under the normal conditions and the network efficiency $E(G, f_i)$ with node f_i fails by using formula (3).

Step 2: calculating the vulnerability of each node by using formula (2).

Combined with *Pajek*, the new network topology diagram is obtained by deleting each node and its connected edge. The vulnerability of each vulnerable node is calculated according to the above steps.

Vulnerability of node $f1$, which is recorded as $V(f_1)$ is calculated as follows. Firstly, the network efficiency of the initial network, in Figure 1, is 0.418. Secondly, the node $f1$ and its connected edges are deleted to obtain a new network topology shown in Figure 2. With the help of formula (3), the network efficiency of the network is calculated where node $f1$ is deleted, and the value is 0.406. Thus, $V(f_1) = 0.029$. The vulnerability of the ratio of the elderly to nursing workers ($f1$) is 0.029. Following this step, the vulnerability results of the remaining nodes are shown in Figure 3.

4.4. Establishment of Node Vulnerability Priority. After calculating the node vulnerability of government procurement of elderly care services, establishing the vulnerability priority can provide an important reference for promoting government governance. The purpose of establishing node vulnerability priority is to strengthen node vulnerability and complete classification and refinement based on node vulnerability. Nodes with a higher vulnerability priority should be focused on to improve the quality of government procurement of elderly care services and maintain their robustness. Node vulnerability priority is shown in Table 8.

According to the value of node vulnerability of government procurement of elderly care services, the nodes are divided into the three priorities shown in Table 8.

① The first priority includes government purchasing power (f5) and diversity of supervisory bodies (f9), and their vulnerability is 0.067. Compared with other nodes, the vulnerability of these two nodes is very high. Managers should pay more attention to government purchasing power and supervisory bodies' diversity, which are the first priority. Managers are supposed to increase government procurement power, expand the

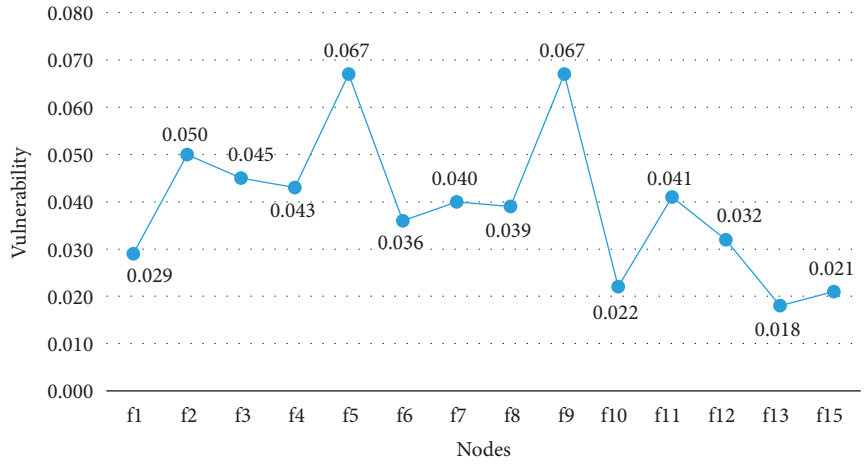

Figure 3: Results of node vulnerability.

Table 8: Vulnerability value of factors.

Priority	Vulnerability influencing factors	Vulnerability
1	Government purchasing power	0.067
	Diversity of supervisory bodies	0.067
2	Number of personalized service items	0.05
	Proportion of professional nursing workers	0.045
	Construction of elderly care service facilities	0.043
	Procurement methods	0.04
	Support of policies and regulations	0.041
3	Ratio of the elderly to nursing workers	0.029
	Type of procurement target	0.036
	Number of bidding companies	0.068
	Number of volunteers	0.022
	Coverage rate of service	0.032
	Starting time of procurement	0.018
	Economic conditions of the region	0.021

policy coverage, and popularize government procurement of elderly care services to enable the efficient and optimized allocation of elderly care service resources. To ensure the effectiveness and quality of government procurement of elderly care services, a diversified regulatory system with government regulation as the main body, third-party professional institutions as the guarantee, and consumer supervision as the auxiliary should be established.

② The second priority includes the number of personalized service items (f2), the proportion of professional nursing workers (f3), the construction of elderly care service facilities (f4), procurement methods (f7), and support of policies and regulations (f11). These nodes' vulnerability value is between 0.04 and 0.05. The vulnerability influencing factors are the "mainstay" in government procurement of elderly care services. Managers should increase the number of personalized service items according to the needs of the elderly. The proportion of professional nursing workers needs to be optimized, and the professional quality of nursing workers should be improved. In addition, enhancing the facility construction of elderly care service institutions is favorable to the effectiveness and quality of government procurement of elderly care services. Finally, open and fair competition should be adopted in the procurement process as much as possible.

③ The third priority includes the ratio of the elderly to nursing workers (f1), type of procurement target (f6), number of bidding companies (f8), number of volunteers (f10), the coverage rate of service (f12), starting time of procurement (f13), and economic conditions of the region (f15). These nodes have an insignificant negative impact on the overall quality or effectiveness of government procurement of elderly care services, but they should not be ignored.

5. Conclusion

Government procurement of elderly care services is necessary to alleviate the contradiction between supply and demand of elderly care service resources and it is important

to study this complex system. With the help of case analysis and sample statistics, the factors affecting the vulnerability of the government procurement of elderly care services are determined after verifying a series of hypotheses. Then, based on the interrelationship of the vulnerability influencing factors, *Pajek* is used to construct the network topology diagram of the vulnerability influencing factors, and the basic statistical characteristics of the diagram are obtained. Mining the key vulnerability nodes in the government procurement of elderly care services is an important way to maintain the complex network's robustness and ensure the procurement project's effectiveness. After calculating and analyzing the compatibility coefficient of the network topology and the vulnerability of each node, the nodes' priority is established, which provides effective countermeasures and suggestions for the policy construction of government procurement of pension services. Simultaneously, the paper's research methods apply to vulnerability research of other complex systems with good adaptability. During the research, several shortcomings were discovered. The relationship between the vulnerability influencing factors is determined subjectively. Even through multiple rounds of feedback from experts, there are still problems and risks, which should be improved in future research.

Data Availability

The data that support the findings of this study can be obtained from the corresponding author upon reasonable request.

Conflicts of Interest

The authors have no relevant financial or nonfinancial interests to disclose.

Authors' Contributions

All authors contributed to the study conception and design. Material preparation, data collection, and analysis were performed by Yuting Zhang and Zhengnan Lu. The first draft of the manuscript was written by Yuting Zhang and all authors commented on previous versions of the manuscript. All authors read and approved the final manuscript.

Acknowledgments

This study was funded by the National Nature Science Foundation of China, under Grant no. 72074100.

References

[1] C. Li and Q. Wang, "On third-party evaluation system in the process of outsourcing government-financed social service for the elderly," *Chinese Public Administration*, vol. 12, pp. 40–44, 2014.

[2] G. Hu, X. Xu, H. Gao, Z. Xianqiang, and Z. Yun, "Node importance recognition algorithm based on adjacency information entropy in networks," *Systems Engineering --Theory & Practice*, vol. 40, no. 3, pp. 172–183, 2020.

[3] D. Chen, L. L¨u, M. S. Shang, Y. C. Zhang, and T. Zhou, "Identifying influential nodes in complex networks," *Physica A: Statistical Mechanics and Its Applications*, vol. 391, no. 4, pp. 1777–1787, 2012.

[4] X. Chen, "Problems and Improvement Countermeasures of government purchase of elderly care services--a case study of Wuhan City, Hubei Province," *Reform and Opening up*, vol. 12, no. 24, pp. 53–56, 2020.

[5] Y. He and C. Zhou, "Evaluation on the livelihood vulnerability of farmers in poor areas," *Statistics & Decisions*, vol. 9, pp. 72–76, 2020.

[6] H. Qian and F. Shen, "Evaluation of financial expenditure efficiency of local government purchasing services--taking hefei municipal government purchasing home-based elderly care services as an example," *Financial Research*, vol. 1, no. 3, pp. 64–67, 2014.

[7] G. Mukul and M. Rajhans, "Spreading the information in complex networks: identifying A set of top-N influential nodes using network structure," *Decision Support Systems*, vol. 149, pp. 21–29, 2021.

[8] Y. Wang and Y. Liu, "Analysis of flight operation risk propagation based on complex network," *Journal of Transportation Systems Engineering and Information Technology*, vol. 01, pp. 198–205, 2020.

[9] S. Shao, "Performance Evaluation of Government Purchasing Community Home Care Services," *CO-Operative Economy Science*, vol. 8, pp. 112–115, 2020.

[10] D. P. Wall, A. E. Hirsh, H. B. Fraser et al., "Functional genomic analysis of the rates of protein evolution," *in Proceedings of the National Academy of Sciences*, vol. 102, no. 15, pp. 5483–5488, 2005.

[11] A. Koulouris, I. Katerelos, and T. Tsekeris, "Multi-equilibria regulation agent-based model of opinion dynamics in social networks," *Interdisciplinary Description of Complex Systems*, vol. 11, no. 1, pp. 51–70, 2013.

[12] X. Su and Y. Song, "Leveraging neighborhood "structural holes" to identifying key spreaders in social networks," *Acta Physica Sinica*, vol. 64, pp. 020101–020111, 2015.

[13] M. E. J. Newman, "Finding community structure in networks using the eigenvectors of matrices," *Physical Review A*, vol. 74, no. 3, Article ID 036104, 2006.

[14] M. Gorsky and S. Sheard, *Financing Medicine: The British Experience 1750*, Routledge, New York, 2016.

[15] J. Wang and H. Chen, "Risk propagation model of complex product supply chain based on complex network," *Statistics & Decisions*, vol. 37, no. 4, pp. 176–180, 2021.

[16] R. Mulgan, "Contracting-out and accountability," *Australian Journal of Public Administration*, vol. 56, no. 4, pp. 106–116, 1997.

[17] B. Wang, R. Ma, and G. Wang, "Improved evaluation method for node importance based on mutual information in weighted networks," *Journal of Computer Applications*, vol. 35, no. 7, pp. 1820–1823, 2015.

[18] M. Knapp, T. Snell, A. Bauer, and M. Perkins, "Building community capital in social care: is there an economic case?" *Community Development Journal*, vol. 48, pp. 313–331, 2013.

[19] H. Ma and J. Hu, "Exploration on the government procurement of home-based elderly care services from social forces-taking L District of Xi'an as an example," *Journal of Hubei Institute of Technology*, vol. 38, no. 6, pp. 34–40, 2021.

[20] W. Kermack and A. McKendrick, "A contribution to the mathematical theory of epidemics," *in Proceedings of the Royal Society of London - Series A: Containing Papers of a*

Mathematical and Physical Character, vol. 115, no. 772, pp. 1095–1934, 1927.

[21] J. Xu, "An empirical study on the influencing factors of the operation performance of community elderly care services purchased by governments--A case study of changsha," *Hunan Social Sciences*, no. 2, pp. 157–165, 2020.

[22] T. Zhou, B. Wang, and Y. Han, "Social network analysis and its application in the prevention and control of propagation for public opinion and the epidemic," *Journal of Systems Engineering*, vol. 25, pp. 742–754, 2010.

[23] J. Ma, Y. Xie, H. Pu, and Y. Zhang, "The node vulnerability of smart government local nearest neighbor network: a research based on shenzhen government online," *Library and Information Service*, vol. 63, no. 15, pp. 13–17, 2018.

[24] B. Xing, J. Zhang, and Y. Chen, "Research on system vulnerability of green buildings based on SD model," *Journal of Engineering Management*, vol. 34, no. 4, pp. 112–117, 2020.

[25] M. Kitsak, L. K. Gallos, S. Havlin et al., "Identification of influential spreaders in complex networks," *Nature Physics*, vol. 6, no. 11, pp. 888–893, 2010.

[26] Y. Zhang, Y. Liu, K. Xu, and R. Zhen, "Evaluation method for node importance based on mutual information in complex networks," *Computer Science*, vol. 6, pp. 88-89, 2011.

[27] C. Ji, W. Huang, and J. Yuan, "Vulnerability evaluation method of infrastructure PPP project," *Systems Engineering--Theory & Practice*, vol. 36, no. 3, pp. 613–622, 2016.

[28] R. Albert, H. Jeong, and A. L. Barabási, "Internet: diameter of the world-wide web," *Nature*, vol. 401, no. 6749, pp. 130-131, 1999.

[29] A. Y. Ni and A. Schneider, "The decision to contract out: a study of contracting for E-government services in state government," *Public Administration Review*, vol. 11, no. 67, pp. 231–242, 2007.

[30] Q. Yang, S. Yang, and J. Wang, "Empirical application of performance evaluation index system of government procurement of elderly-care services," *Social Security Research*, no. 05, pp. 60–71, 2021.

[31] Z. Liu, F. Yang, and H. Yu, "Evaluate the node importance for water network based on complex network theory," *SCIENTIA SINICA Technologica*, vol. 44, pp. 1280–1294, 2014.

[32] V. Latora and M. Marchiori, "How the science of complex networks can help developing strategies against terrorism," *Chaos, Solitons & Fractals*, vol. 20, no. 1, pp. 69–75, 2004.

[33] R. Schick, "Government contracting: from the perspectives of management, ethics and governance," *Public Administration Review*, vol. 71, no. 4, pp. 46–57, 2011.

[34] D. B. Chen, H. Gao, L. L¨u, and T. Zhou, "Identifying influential nodes in large-scale directed networks: the role of clustering," *PLoS One*, vol. 8, no. 10, Article ID e77455, 2013.

[35] H. Schimd, *Organizational and Structural Dilemmas in Nonprofit Human Service Organizations*, Haworth Press Inc, Philadelphia, Pennsylvania, 2014.

[36] O. Milliken, V. Barham, G Russell, S. Dahrouge, and G. Russell, "Comparative efficiency assessment of primary care service delivery models using data envelopment analysis," *Canadian public policy. Analyse de politiques*, vol. 37, no. 1, pp. 85–109, 2011.

[37] L. C. Freeman, "A set of measures of centrality based on betweenness," *Sociometry*, vol. 40, no. 1, pp. 35–41, 1977.

Hindawi
Complexity
Volume 2022, Article ID 3688381, 12 pages
https://doi.org/10.1155/2022/3688381

Research Article

Estimating Performance Efficiency of Mining and Extracting Sectors Using DEA Models: The Case of Jordan

Jamil J. Jaber,[1] **Fatiha Beldjilali**,[2] **Ali A. Shehadeh**,[1] **Nawaf N. Hamadneh**,[3] **Mohammad Saleh**,[1] **Muhammad Tahir**,[4] **and S. Al Wadi**[1]

[1]*Department of Finance, Faculty of Business, The University of Jordan, Aqaba, Jordan*
[2]*Department of Commercial Sciences, Faculty of Economic, Commercial and Management Sciences, University of Ibn Khaldoun Tiaret, BP P 78, Zaâroura 14000, Tiaret, Algeria*
[3]*Department of Basic Sciences, College of Science and Theoretical Studies, Saudi Electronic University, Riyadh 11673, Saudi Arabia*
[4]*College of Computing and Informatics, Saudi Electronic University, Riyadh, Saudi Arabia*

Correspondence should be addressed to Nawaf N. Hamadneh; nhamadneh@seu.edu.sa

Received 26 May 2022; Accepted 9 July 2022; Published 19 August 2022

Academic Editor: Yu Zhou

In this study, we estimated the performance efficiency of the Jordanian mining and extracting sector based on Data Envelopment Analysis (DEA). The utilized dataset includes 6 out of 15 corporations that reflect around 90% of the total market capitalization under the mining and extracting sector in the Amman Stock Exchange (ASE). The sample consists of 126 observations from 2000 to 2020. It should be noted that estimating the efficiency of the sector based on time series for each company is not mentioned in the literature review. Therefore, we applied BCC (Banker–Charnes–Cooper) models to estimate performance efficiency and compared between input and output models under DEA. We also estimated the average performance efficiency of the sector to detect weaknesses/strengths among companies. The market capitalization and the operating revenue are used to evaluate the companies' performance. In addition to the performance variables as output to the DEA models, the current assets, non-current assets, operating expenses, and general administrative expenses are also used as input variables under the DEA models. This study also examined the effect of Gross Domestic Product (GDP) growth and Return on Assets (ROA) on performance efficiency scores for BCC models. In the results, we found that there are differences in performance efficiency across time series in each company based on dynamic BCC models. It is observed that the performance efficiency of NAST Company is better than the other companies based on BCC (Input/output). The GDP growth and ROA reveal the effect on efficiency performance under BCC models. The proposed model can be used to improve the performance efficiency of companies in stock exchange markets.

1. Introduction

The mining sector is a central pillar of Jordan's economy. It is considered most significant to the national economy because of its effective contribution in employing local labor, investment, export, and revenue. In 2020, this sector contributed 24.5% of Jordan's GDP and employed 24% of the workforce [1]. Mining and extracting (mostly phosphate and potash) are among the primary industries. The industrial sector contributes to Jordan's financial stability by providing the government with more than JOD 1 billion in direct and indirect taxes each year [2].

The important role of the industrial sector can identify Jordan's position within the Middle East and North Africa (MENA) region, which is supported by a variety of free trade agreements (FTAs) allowing access to 1.5 billion customers across more than 160 countries. The high volume of industrial investment contributes significantly to the strength of the Jordanian Dinar and to the exchange rate's stability by providing the Kingdom's official reserves with foreign currency (more than US$ 8.0 billion in 2017) [3].

DEA is one of the major and popular techniques employed for analyzing efficiency. Since its introduction through the seminal work of [4], it has seen numerous

developments. Those developments encompass both methodological developments and application developments. Methodological-wise and apart from the basic DEA, several DEA model variations emerge in literature that are dedicated to addressing various technical and modeling issues such as generic DEA models, bootstrap DEA models, network models, multiplier bounds, considerations on the status variables, and data variations. Application-wise, DEA is applied in a wide range of fields for examining and analyzing various aspects of efficiency and productivity. To name but a few, those fields include banking, health care, agriculture and farm, education, transportation, finance, tourism, retailing, fishery, manufacturing, communication, and the list goes on.

From applications perspective [5], survey on DEA application covers the period from 1978 to 2010 that identified banking, health care, agriculture and farm, transportation and education as the top-five industries addressed by DEA. Most recently; [1] a comprehensive survey of DEA-related published articles was conducted that covers the last four decades (1978–2016). This survey includes and analyses all types of articles whether they address theoretical, methodological or real applications. They reported that from 2004 to 2016 the number of DEA-related articles has grown exponentially, with an average of 680 articles per year. In addition, they argued that agriculture, banking, supply chain, transportation, and public policy are the top-five application fields of DEA [1]. References [2, 6] examined the elasticities and casualties of financial performance of the mining and extractive companies listed in the Amman Stock Exchange (ASE) during 2005–2018 period. They applied several models; including Dynamic Ordinary Least Squares (DOLS), Fully Modified Ordinary Least Square (FMOLS), and Pooled Mean Group (PMG). The results showed that company characteristics and GDP growth are most important determinants causing financial performance.

The vast majority of articles, published in the first 20 years of DEA since its development, were purely methodological [5]. However, the accumulated number of application papers exceeds methodological papers starting from 1999 onward. Several authors review and follow the technical and methodological developments as well as application developments of DEA have devoted a considerable endeavor, for example, [7] survey on the developments of DEA from the angle of mathematical programming. Reference [8] tracks the methodological evolutions of DEA over a period of 17 years; from 1978 to 1995. Reference [9] survey analytical models, developed for examining the sensitivity of DEA results to data variations. Over a time period of 30 years, [10] map out the major methodological developments and directions of DEA.

The mining sector is one of the numerous industries where DEA models and techniques can be employed for studying and assessing efficiency. References [3, 11] used bootstrap DEA for assessing the balance of efficiency gains and losses for 33 mining firms in Australia. They tried to identify the behavior of efficiency performance for the 33 firms over the period 2008–2014. Reference [12] employed the DEA models of BCC (Banker, Charnes, and Cooper) and CCR (Charnes, Cooper, and Rhodes) for measuring, analyzing, and comparing the performance of technical efficiency of 24 major global corporations involved in Phosphate rock mining for the year 2012. They examined whether the efficiency of publicly quoted companies differs significantly from that of state-owned companies. References [4, 13] used the DEA model version of the Malmquist index for studying the growth of efficiency and productivity of the coal mining sector in India over the period 1985–1997. The results show that opencast mining does not have more productivity growth than underground mining. Reference [14] conducted a comparative study on the relative technical efficiency performance of the public coal mining companies in China and the USA. Using CCR and BCC models, they found that the USA companies are relatively much more efficient than the Chinese ones. Using DEA techniques, [15] evaluated and analyzed the safety output efficiency in relation to safety input factors for coal mines. Reference [16] employed DEA bootstrapping for assessing the performance of fifteen strip coal mines in Illinois (USA). The results of this approach indicate significant inefficiencies in the analyzed sample. With the application of DEA and stochastic frontier estimation, [17] found that private international oil companies are more efficient than national oil companies in terms of revenue efficiency. With an emphasis on the potential environmental effects, [18] analyzed the efficiency of the cement industry in 21 countries using DEA and directional distance function. Reference [16] applied DEA along with stochastic frontier analysis (SFA) for assessing the efficiency performance of the Greek Bauxite mining sector over the period 1970–1996. This paper is innovative regarding the utilization of a bootstrapping approach in DEA for aggregated sector data.

Several researchers have examined the efficient performance of the mining and extracting sector at the industrial level [19, 20]. Based on the studies, there is a concentration on the efficiency of the mining and extracting sector in developing countries. Reference [19] investigated bootstrap data envelopment analysis to analyze the efficiency performance of 33 mining companies in Australia. They found that most mining companies became more efficient over time in Australia. In addition, there are many researchers have examined the efficiency performance of financial institutions based on traditional DEA [21, 22]. The two-stage network was able to explain more about the variables that affect the efficiency of companies [23–25].

DEA proves to be a common and acceptable tool for studying and analysing various aspects of efficiency and productivity in many sectors and industries, including the mining sector. Different efficiency-related issues in mining industries have been addressed by DEA techniques. Some authors track the efficiency performance of mining sector as a whole over some period of time either on a country-specific level or worldwide, others focus on comparing the efficiency of firms specialized in a specific kind of mining work either in a specific country or globally. Furthermore, some articles try to relate the efficiency of the mining sector to some potential environmental effects [11]. Yet, other papers attempt to relate the efficiency of mining firms to the

type of firms' ownership [19]. In this study, we employ DEA for measuring and analyzing the efficiency of mining sector in Jordan, which is one of the most important industries for the Jordanian economy. In our study, the following are some of the specific contributions:

(i) We identify the efficiency gaps in Jordanian mining and extracting corporations using BCC models under DEA.

(ii) We discover how the efficiency performance of mining and extracting corporations has changed from 2000 to 2020 in each corporation.

(iii) We detect the average performance efficiency level between companies based on BCC models under DEA.

(iv) We determine the role of internal and external factors on efficiency performance in the mining and extracting sector in Jordan.

The remainder of the study proceeds as follows. Section 2 discusses the mathematical models. Section 3 presents a description of the data. Section 4 highlights the empirical results and discusses the efficiency performance of mining and extracting corporations. Section 4draws the conclusion.

2. Methodological Issues

This section gives a background of the main concepts of DEA models; BCC (input/output).

2.1. The Efficiency Models. The efficiency performance at the corporate level has a number of advantages. First, with corporate-level data, we concentrate on a smaller size of data that is more homogenous. Second, with corporate-level analysis, we can explore efficiency performance over years more accurately and discover benchmark years. Third, we can determine both input and output variables more accurately using corporate-level analysis. Fourth, we can identify best practices and benchmarks across comparable firms. Finally, we can decompose the sources of inefficiency into pure technical inefficiency and scale inefficiency based on corporate level. The performance gap between the corporation and the corresponding frontier can be easily assessed using variable returns to scale (BCC) models if the corporation has pure technical inefficiency. The degree to which a corporation operates inefficiently is called scale inefficiency. Constant returns to scale (CRS) efficiency discovers the impact of both scale and pure technical (in) efficiencies. A comparison of efficiency findings from CRS and BCC models can be determined if the cause of inefficiency in the mining and extracting sector is due to pure technical inefficiency.

The measurement of efficiency in the production unit and the identification of sources of their inefficiency are preconditions to improve the performance of any production unit in a competitive environment. The term productive unit refers to a unit producing certain output by spending certain inputs.

In DEA, the organization under study is called a DMU (decision-making unit). Generically, a DMU is regarded as the entity responsible for converting inputs into outputs and whose performances are to be evaluated. In managerial applications, DMUs may include banks, department stores, and supermarkets extending to carmakers, hospitals, schools, public libraries, and so on. Mining and extracting corporations can be treated as production units too. To secure relative comparisons, a group of DMUs is used to evaluate each other with each DMU having a certain degree of managerial freedom in decision making. In general, the group is homogenous units performing the same or similar activities. All inputs and outputs have an impact on the efficient operation of such units, even though some are considered more or less important.

We have a population of n productive units (companies) $\mathrm{DMU}_1, \mathrm{DMU}_2, \ldots, \mathrm{DMU}_n$. We write an input matrix $x_i = (x_{i1}, x_{i2}, \ldots, x_{ip})$ and an output matrix $y_i = (y_{i1}, y_{i2}, \ldots, y_{iq})$ of DMU_i, where $i = 1, 2, \ldots, n$. DMU_0 is the target of DMU. Also, $x_0 = (x_{01}, x_{02}, \ldots, x_{0p})$ and $y_0 = (y_{01}, y_{02}, \ldots, y_{0q})$ are the input and the output vectors of the target DMU_0. The efficiency rate of such a unit can be generally expressed as:

$$\begin{aligned}\text{Efficiency rate} &= \frac{\sum_r \text{weighted sum of outputs}}{\sum_i \text{weighted sum of inputs}} \\ &= \frac{\sum_{r=1}^{q} u_r y_{rj}}{\sum_{i=1}^{p} v_i x_{ij}},\end{aligned} \tag{1}$$

where v_i, $i = 1, 2, \ldots, q$, are weights assigned to i th input u_r, $r = 1, 2, \ldots, p$, are weights assigned to r-th output.

There are several ways to estimate the efficiency rate as defined above, namely multicriteria decision methods and data envelopment analyses (DEA). These approaches differ in how they obtain input and output weights. Multicriterial decision methods usually expect the user to define the weights v_i, and u_r upfront, i.e. the user determines the significance of individual inputs and outputs in the analysis. Such an analysis yields the rate of the utility of given units. It reflects the relative importance of inputs and outputs represented by their respective weights. Based on the analysis, units can be ranked from the worst to the best performer. On the other hand, DEA models derive input and output weights by means of an optimizing calculation. Based on that, units can be classified into efficient and inefficient categories. In inefficient units, they tell us the target values of inputs and outputs, which would lead to efficiency.

2.2. DEA Model. In DEA model, we evaluate n productive units, DMUs, where each DMU takes p different inputs to produce q different outputs. The essence of the DEA model in measuring the efficiency of a productive unit DMUq lies in maximizing its efficiency rate. However, subject to the condition that the efficiency rate of "virtual output" versus "virtual input" should not exceed 1 for every DMU. The objective is to obtain the ratio of the weighted output to the

weighted input weights. By virtue of the constraints, the optimal objective value θ^* is at most 1. Mathematically, the non-negativity constraint is not sufficient for the fractional terms to have a positive value. We do not treat this assumption in the explicit mathematical form at this time. Instead, we put this in managerial terms by assuming that all outputs and inputs have some nonzero worth and this is to be reflected in the weights v and u being assigned some positive value. DMU_0 is CCR-efficient if $\theta^* = 1$ and there exists at least one optimal $u^* > 0$ and $v^* > 0$. The fractional model is initially proposed by [8].

$$\begin{aligned} &\text{Maximize :} \\ &\theta = \frac{v^T y_0}{u^T x_0}, \\ &\text{Subject to :} \\ &v^T y_j \le u^T x_j,\ j = 1, 2, \ldots, n \\ &u_r \ge \varepsilon > 0\, r = 1, 2, \ldots, p \\ &v_i \ge \varepsilon > 0\, i = 1, 2, \ldots, q, \end{aligned} \tag{2}$$

where θ is the efficiency ratio, ε is a constant greater than zero that is called a non-Archimedean element defined to be smaller than any positive real number. It is normally pitched at 10^{-6} or 10^{-8}.

2.3. CCR Model. In 1978, this model was developed to measure the technical efficiency of a given observed decision-making unit (DMU) assuming constant returns to scale (CRS). In other words, the change in inputs has a constant effect on the outputs if moved from one point to another point on the frontier curve. CCR model is considered as a global pure technical efficiency. The linear programming formulation allowed multiple inputs and multiple outputs. However, the CCR model is divided into input-oriented (CCR-I) and output-oriented (CCR-O).

2.3.1. Input–Oriented (CCR-I) Model. This model assumes that the inefficient units can become efficient if they reduce their input while maintaining the same level of production. In other words, they try to find out how to improve the input characteristics of the unit concerned for it to become efficient. In addition, the above fractional program (1) is replaced by the *equivalent* linear program (2). The CCR-I model maximizes the numerator and considers the constant denominator as shown in Table 1.

The dual model (b) in Table 1 has a feasible the solution $\theta^* = 1$, $\lambda_0^* = 1$, $\lambda_j^* = 1$ $(j \ne 0)$. Hence, the optimal value θ^* is not greater than 1 [4, 26]. The optimal solution, θ^*, yields an efficiency score for a particular *DM U*. The process is repeated for each DMU_j, $j = 1, 2, \ldots, n$.DMUs for which $\theta^* < 1$ are inefficient, while DMUs for which $\theta^* = 1$ are boundary points. Some boundary points may be "weakly efficient" because we have nonzero slacks. This may appear to be worrisome because alternate optima may have nonzero slacks in some solutions, but not in others. However, we can avoid being worried even in such cases by invoking the following linear program in which the slacks are taken to their maximal values. In Table 1, we also note that choices of s_i^- and s_r^+ do not affect the optimal θ^*, which is determined from model (b). Where s_i^- and s_r^+ are slack variables used to convert the inequalities in (b) in Table 1 to equivalent equations. This is equivalent to solving (b) in Table 1 in two stages by first minimizing θ and then fixing $\theta = \theta^*$ as in (c) in Table 1, where the slacks are to be maximized without altering the previously determined value of $\theta = \theta^*$.

These developments based on the "relative efficiency" lead to the following. First, the performance of DMU_0 is fully (100%) efficient if we do not have ability to decrease inputs $(s_i^- = 0)$, increase outputs $(s_r^+ = 0)$, and set efficiency ratio $\theta^* = 1$. Second, the performance of DMU_0 is weakly efficient if we have ability to decrease inputs $(s_i^- \ne 0)$, increase outputs $(s_r^+ \ne 0)$, and set efficiency ratio $\theta^* = 1$. Finally, the inefficiency ratio is. $\theta < 1$.

2.3.2. Output–Oriented (CCR-O) Model. CCR-O model assumes that the inefficient units can become efficient if they increase their output while maintaining the same level of input. In other words, they try to find out how to improve the output characteristics of the unit concerned for it to become efficient. In addition, CCR-O model minimizes the denominator and considers the constant numerator (a) in Table 2:

The models in Table 2 assume output-oriented CCR. In equation (b) in Table 2, we use the dual equation to solve equation (a) in Table 2. In equations (c) and (d) in Table 2, we use slacks.

The aim of DEA analysis is not only to determine the efficiency rate of the units reviewed, but in particular to find target values for inputs *X'q* and outputs *Y'q* for an inefficient unit. After reaching these values, the unit would arrive at the threshold of efficiency. Target values are calculated with the following [4]:

(i) The productive unit vectors: $(X_q' = X\lambda^* \text{ and } Y_q' = Y\lambda^*)$, where λ^* is the vector of optimal variable values.

(ii) The efficiency rate and values of additional variables s^- and s^+: input-oriented CCR model $(X_q' = \theta X - s^-$ and $Y_q' = Y_q + s^+)$ and Output-oriented CCR model $(X_q' = X_q - s^-$ and $Y_q' = \phi Y_q + s^+)$, where θ is the efficiency rate in the input-oriented model and ϕ is the efficiency rate in the output-oriented model.

2.4. BCC Models. BCC models extend the CCR model to allow variable returns to scale [16]. They are developed to measure the technical efficiency of a given observed decision-making unit (DMU) assuming variable returns to scale (VRS). This model considers a local pure technical efficiency. The BCC model is divided into input-oriented (BCC–I) and output-oriented (BCC–O)[27].

Table 1: Input-oriented CCR model.

(a)	(b)	(c)	(d)
Maximize:	**Minimize:**	**Maximize:**	**Minimize:**
$\theta = v^T y_0$	$\theta = v^T y_0$	$\sum_{i=1}^{m} s_i - + \sum_{r=1}^{s} s_r^+$	$\theta - \varepsilon(\sum_{i=1}^{m} s_i^- + \sum_{r=1}^{s} s_r^+)$
Subject to:	**Subject to:**	**Subject to:**	**Subject to:**
$u^T x_0 = 1$	$\sum_{j=1}^{n} \lambda_i x_{ij} \le \theta x_{i0}$	$\sum_{j=1}^{n} x_{ij}\lambda_j + s_i^- = \theta^* x_0$	$\sum_{j=1}^{n} x_{ij}\lambda_j + s_i^- = \theta x_0$
$v^T y_j - u^T x_j \le 0,$	$\sum_{j=1}^{n} \lambda_r y_{rj} \ge y_{r0}$	$\sum_{j=1}^{n} y_{rj}\lambda_j - s_r^+ = y_{r0},$	$\sum_{j=1}^{n} y_{rj}\lambda_j - s_r^+ = y_{r0},$
$j = 1, 2, \ldots, n$	$\lambda_j \ge 0$	$\lambda_j, s_i -, s_r^+ \ge 0$	$\lambda_j, s_i -, s_r^+ \ge 0$
$u, v \ge \varepsilon > 0$	$j = 1, 2, \ldots, n$	$j = 1, 2, \ldots, n$	$j = 1, 2, \ldots, n$
	$i = 1, 2, \ldots, p$	$i = 1, 2, \ldots, p$	$i = 1, 2, \ldots, p$
	$r = 1, 2, \ldots, q$	$r = 1, 2, \ldots, q$	$r = 1, 2, \ldots, q$

Table 2: Output-oriented CCR model.

(a)	(b)	(c)	(d)
Maximize:	**Minimize:**	**Maximize:**	**Minimize:**
$\theta = u^T x_0$	$\theta = u^T x_0$	$\sum_{i=1}^{p} s_i^- + \sum_{r=1}^{q} s_r^+$	$\theta - \varepsilon(\sum_{i=1}^{m} s_i^- + \sum_{r=1}^{s} s_r^+)$
Subject to:	**Subject to:**	**Subject to:**	**Subject to:**
	$\sum_{j=1}^{n} \lambda_i x_{ij} \le x_{i0}$	$\sum_{j=1}^{n} x_{ij}\lambda_j + s_i^- = x_{i0}$	$\sum_{j=1}^{n} x_{ij}\lambda_j + s_i^- = x_{i0}$
$v^T y_0 = 1$	$\sum_{j=1}^{n} \lambda_r y_{rj} \ge \theta y_{r0}$	$\sum_{j=1}^{n} y_{rj}\lambda_j - s_r^+ = \phi^* y_{r0},$	$\sum_{j=1}^{n} y_{rj}\lambda_j - s_r^+ = \phi y_{r0},$
$u^T x_j - v^T y_j \ge 0,$	$\lambda_j \ge 0$	$\lambda_j, s_i^-, s_r^+ \ge 0$	$\lambda_j, s_i^-, s_r^+ \ge 0$
$j = 1, 2, \ldots, n$	$j = 1, 2, \ldots, n$	$j = 1, 2, \ldots, n$	$j = 1, 2, \ldots, n$
$u, v \ge \varepsilon > 0$	$i = 1, 2, \ldots, p$	$i = 1, 2, \ldots, p$	$i = 1, 2, \ldots, p$
	$r = 1, 2, \ldots, q$	$r = 1, 2, \ldots, q$	$r = 1, 2, \ldots, q$

Table 3: Input-oriented BCC model.

(a)	(b)	(c)	(d)
Maximize:	**Minimize:**	**Maximize:**	**Minimize:**
$\theta = v^T y_0 - v_0$	$\theta = v^T y_0 - v_0$	$\sum_{i=1}^{m} s_i^- + \sum_{r=1}^{s} s_r^+$	$\theta - \varepsilon(\sum_{i=1}^{m} s_i^- + \sum_{r=1}^{s} s_r^+)$
Subject to:	**Subject to:**	**Subject to:**	**Subject to:**
	$\sum_{j=1}^{n} \lambda_i x_{ij} \le \theta x_{i0}$	$\sum_{j=1}^{n} x_{ij}\lambda_j + s_i^- = \theta^* x_0$	$\sum_{j=1}^{n} x_{ij}\lambda_j + s_i^- = \theta x_0$
	$\sum_{j=1}^{n} \lambda_r y_{rj} \ge y_{r0}$	$\sum_{j=1}^{n} y_{rj}\lambda_j - s_r^+ = y_{r0},$	$\sum_{j=1}^{n} y_{rj}\lambda_j - s_r^+ = y_{r0},$
$u^T x_0 = 1$	$\sum_{j=1}^{n} \lambda_j = 1$	$\sum_{j=1}^{n} \lambda_j = 1$	$\sum_{j=1}^{n} \lambda_j = 1$
$v^T y_j - u^T x_j \le 0,$	$\lambda_j \ge 0$	$\lambda_j, s_i^-, s_r^+ \ge 0$	$\lambda_j, s_i^-, s_r^+ \ge 0$
$j = 1, 2, \ldots, n$	$j = 1, 2, \ldots, n$	$j = 1, 2, \ldots, n$	$j = 1, 2, \ldots, n$
$u, v \ge \varepsilon > 0$	$i = 1, 2, \ldots, p$	$i = 1, 2, \ldots, p$	$i = 1, 2, \ldots, p$
	$r = 1, 2, \ldots, q$	$r = 1, 2, \ldots, q$	$r = 1, 2, \ldots, q$

2.4.1. Input-Oriented (BCC–I) Model. The difference between BCC-I model and CCR-I model is presented in free variable v_0 in equation (a) in Table 3, which is the dual variable (b) in Table 3 associated with the constraint $\sum_{j=1}^{n} \lambda_j = 1$ that also does not appear in the CRR model. The performance of $DM\ U_0$ is fully (100%) efficient in BCC if we cannot decrease inputs ($s_i^- = 0$), increase outputs ($s_r^+ = 0$), and set efficiency ratio $\theta^* = 1$. The BCC-I model is explained in Table 3.

2.4.2. Output-Oriented (BCC–O) Model. The difference between the BCC-O model and the CCR-O model is presented in free variable u_0 in equation (a) in Table 4, which is the dual variable (b) in Table 4 associated with the constraint $\sum_{j=1}^{n} \lambda_j = 1$ that also does not appear in the CRR model. The BCC-O model is explained in Table 4.

2.5. Tobit Model. The Tobit model is a statistical model proposed by Tobin to describe the relationship between a non-negative dependent variable y_i and an independent variable x_i [28]. The benefit of the Tobit model is to draw the relationship between the relative efficiency scores of companies and some of the factors that may affect companies' efficiency. The model supposes that there is a latent (i.e. unobservable) variable y_i. This variable linearly depends on x_i via a parameter (vector) β which determines the

Table 4: Output-oriented BCC model.

(a)	(b)	(c)	(d)
Maximize:	**Minimize:**	**Maximize:**	**Minimize:**
$\theta = u^T x_0 - u_0$	$\theta = u^T x_0 - u_0$	$\sum_{i=1}^{p} s_i^- + \sum_{r=1}^{q} s_r^+$	$\theta - \varepsilon(\sum_{i=1}^{m} s_i^- + \sum_{r=1}^{s} s_r^+)$
Subject to:	**Subject to:**	**Subject to:**	**Subject to:**
$v^T y_0 = 1$	$\sum_{j=1}^{n} \lambda_i x_{ij} \le x_{i0}$	$\sum_{j=1}^{n} x_{ij}\lambda_j + s_i^- = x_{i0}$	$\sum_{j=1}^{n} x_{ij}\lambda_j + s_i^- = x_{i0}$
$u^T x_j - v^T y_j \ge 0,$	$\sum_{j=1}^{n} \lambda_r y_{rj} \ge \theta y_{r0}$	$\sum_{y=1}^{n} y_{rj}\lambda_j - s_r^+ = \phi^* y_{r0},$	$\sum_{j=1}^{n} y_{rj}\lambda_j - s_r^+ = \phi y_{r0},$
$u, v \ge \varepsilon > 0$	$\sum_{j=1}^{n} \lambda_j = 1$	$\sum_{j=1}^{n} \lambda_j = 1$	$\sum_{j=1}^{n} \lambda_j = 1$
$j = 1, 2, \ldots, n$	$\lambda_j \ge 0$	$\lambda_j, s_i^-, s_r^+ \ge 0$	$\lambda_j, s_i^-, s_r^+ \ge 0$
	$j = 1, 2, \ldots, n$	$j = 1, 2, \ldots, n$	$j = 1, 2, \ldots, n$
	$i = 1, 2, \ldots, p$	$i = 1, 2, \ldots, p$	$i = 1, 2, \ldots, p$
	$r = 1, 2, \ldots, q$	$r = 1, 2, \ldots, q$	$r = 1, 2, \ldots, q$

relationship between the independent variable (or vector) x_i and the latent variable y_i (just as in a linear model). In addition, there is a normally distributed error term u_i to capture random influences on this relationship. When the dependent variable y_i is limited to the interval [0, 1], it may be described by the following general model [29, 30]: $Y_i^* = \beta x_i + \varepsilon_i^*$, where the $\varepsilon_i^* \sim N(0, \sigma^2)$ and $i = 1, \ldots, n$. However, we measure $Y_i = Y_i^*$ only if $Y_i^* > \mathrm{L}$ and $Y_i^* < \mathrm{U}$ for some cutpoints L and U. Otherwise we let $Y_i = \mathrm{L}$ or $Y_i = \mathrm{U}$, whatever is closer. The Tobit model is thus a multiple linear regression but with censored responses, if it is below or above certain cut points.

3. Results and Discussion

The source of research data for this study is from financial statements of corporations, listed on the Amman Stock Exchange (ASE) in Jordan. This article studies 6 out of 15 corporations that reflect around 90% of the total market capitalization under the mining and extracting sector from 2000 to 2020. The selected corporations are namely; Arab Aluminum Industry (AALU), National Steel Industry (NAST), Jordan Phosphate Mines (JOPH), The Arab Potash (APOT), Jordan Steel (JOST), and National Aluminum Industrial (NATA). The market capitalization and the operating revenue are used to evaluate companies' performance. The performance variables are used as output in Data Envelopment Analysis models [12, 19]. In addition, the current assets, non-current assets, operating expenses, and general administrative expenses are used as input in DEA models. In order to examine the factors that affect the efficiency performance of the mining and extracting sector in Jordan, the Tobit model has been used. This section will discuss the results of the DEA models and Tobit model. Package "deaR" in R-program is used in the analysis of BCC models [13, 20, 31].

Table 5 shows the descriptive statistics of input/output variables. The mean and standard deviation of current assets are 116096738 and 170279405, respectively. The skewness and kurtosis are 1.413 and 0.681, respectively. In addition, the mean and standard deviation of non-current assets are 154095030 and 238863286, respectively. The skewness and kurtosis are 1.535 and 1.025, respectively. Furthermore, the mean and standard deviation of operating expenses are 124276270 and 174729427, respectively. The skewness and kurtosis are 1.478 and 0.967, respectively. Moreover, the mean and standard deviation of general administration expenses are 14477754 and 24463219, respectively. The skewness and kurtosis are 2.193 and 5.150, respectively. However, the mean and standard deviation of operating revenue are 171383507 and 245544797, respectively. The skewness and kurtosis are 1.376 and 0.481, respectively. In addition, the mean and standard deviation of market capitalization are 396254882 and 820977697, respectively. The skewness and kurtosis are 2.646 and 6.787, respectively.

3.1. Comparative Analysis of CCR and BCC Models. The DEA models' assumptions have been applied before running CCR and BCC models. First, the input/output variable selected is greater than or equal to zero. Second, there are significant positive correlation between inputs and outputs greater than 50%. Third, homogeneity DMUs refer to identical used input/output variables for DMUs. Four, the sample size selected (sample = 126) is greater than or equal to the multiply of input (4 variables) with output (2 variables). Five, also the sample size selected (sample = 126) is greater than or equal to the multiplied by $(3 * \text{input} * \text{output})$. Finally, the full efficiency rate (100%) for DMUs is not greater than or equal to third sample size $((1/3) * 126 = 42)$. The CCR and BCC models is applied after the above conditions.

The comparison between CCR and BCC models is explained in Table 6. We can observe that the performance of DMU is better in BCC models compared to CCR models for several reasons: (i) we find that mining and extracting corporations could improve their performance from a minimum of 0.47 in CCR-I to a minimum of 0.53 in BCC-I. Furthermore, the corporations could improve their performance from a maximum of 2.12 in CCR-O to a maximum of 1.97 in BCC-O. The output-oriented DEA models give the DMUs score values from 1 to infinity. In other words, the DMUs lay on the efficiency frontier if scores go to 1, otherwise it is inefficient. (ii) The number of efficient DMUs in BCC models is more than in CCR models. (iii) We find that the BCC models are better than CCR models because they

Table 5: Descriptive statistic for input and output variables.

Variables	N	Mean	Std. deviation	Skewness		Kurtosis	
				Statistic	Std. error	Statistic	Std. error
Current assets	126	116096738	170279405	1.413	0.216	0.681	0.428
Non-current assets	126	154095030	238863286	1.535	0.216	1.025	0.428
Operating expenses	126	124276270	174729427	1.478	0.216	0.967	0.428
General administration expenses	126	14477754	24463219	2.193	0.216	5.150	0.428
Operating revenue	126	171383507	245544797	1.376	0.216	0.481	0.428
Market capitalization	126	396254882	820977697	2.646	0.216	6.787	0.428

Table 6: Comparison between CCR and BCC models.

Models	No. of DMU	Efficient	Non-efficient	Average score	Max	Min	S.D
CCR-I	126	13	113	0.7865	1	0.4710	0.1279
CCR-O	126	13	113	1.3071	2.1231	1	0.2270
BCC-I	126	23	103	0.8428	1	0.5297	0.1229
BCC-O	126	23	103	1.2274	1.9784	1	0.2040

Table 7: The average efficiency rate and slacks for BCC-I during 2000–2020.

Models	Corporations	Efficiency rate	Rank	Current assets (s^-)	Non-current assets (s^-)	Operating expenses (s^-)	General adm. expenses (s^-)
BCC-I	AALU	0.7185	6	0.0000	4305.9293	0.0000	13382621.4783
	NAST	0.9590	1	68809.9091	2282.5163	0.0000	1190421.0986
	JOPH	0.8055	5	7353350.0924	12033450.8901	0.0000	430138786.3599
	APOT	0.8218	4	0.0000	12877691.8722	215931.5630	119493303.9384
	JOST	0.8808	2	0.0000	0.0000	0.0000	20666331.5067
	NATA	0.8674	3	0.0000	0.0000	0.0000	4981090.9670

use the VRS rather than CRS. This result is consistent with [3, 11]. For this reason, we will select BCC-I and BCC-O in our study.

3.2. The Input-Oriented DEA Model. The average efficiency and slacks for input-oriented in BCC-I models from 2000 to 2020 are shown in Table 7. The corporations should decrease the input variables to approximate the performance efficiency to 100%. For instance, NAST should reduce, on average, current assets to 68809.91 JD, Non-current assets to 2282.52 JD, Operating expenses to 0.00 JD, and general administrative expenses to 1190421.10 JD if we assume BCC. In addition, NAST is the best efficiency performance on average from 2000 to 2020 and AALU is the lowest efficiency performance on average during the same period based on rank in BCC-I. Indeed, the input-oriented DEA model considered a good efficiency performance if the efficiency rate is close to one.

Figure 1 shows the dynamic BCC-I efficiency performance of each corporation over the years from 2000 to 2020. The AALU has a full efficiency performance of 100% in all years except the following cases; the increase in general administration expenses is reduced efficiency performance in 2004, and the increase in current assets reduced efficiency performance in 2007. The increase in non-current assets and operating expenses reduced efficiency performance in 2008, the increase in non-current assets reduced efficiency performance in 2010, and the increase in current assets and operating expenses reduced efficiency performance in 2012. Moreover, the effect of economic crises from 2007 to 2010 reduced the efficiency performance. The NAST also has full efficiency performance of 100% in all years except the following cases; the increase in non-current assets and general administration expenses reduced efficiency performance in (2002, 2003, 2006–2007), the increase in non-current assets is reduced efficiency performance in 2009, the increase in current assets and operating expenses are reduced efficiency performance in 2010 and 2012. The increase in current assets and non-current assets reduced efficiency performance in 2017. The JOPH also has full efficiency performance of 100% in all years except the following cases; the increase in operating expenses is reduced efficiency performance in (2000, 2010, 2012 : 2014, and 2016 : 2020), and the increase in general administration expenses is reduced efficiency performance in (2012 : 2014, 2015, and 2016). The APOT also has full efficiency performance of 100% in all years except the following cases; the increase in current assets is reduced efficiency performance in 2002, the increase in current assets and general administration expenses is reduced efficiency performance in 2009, the increase in non-current assets, operating expenses, and general administrative expenses are reduced efficiency performance in 2013 to 2020. The JOST has also a full efficiency performance of 100% in all years except the

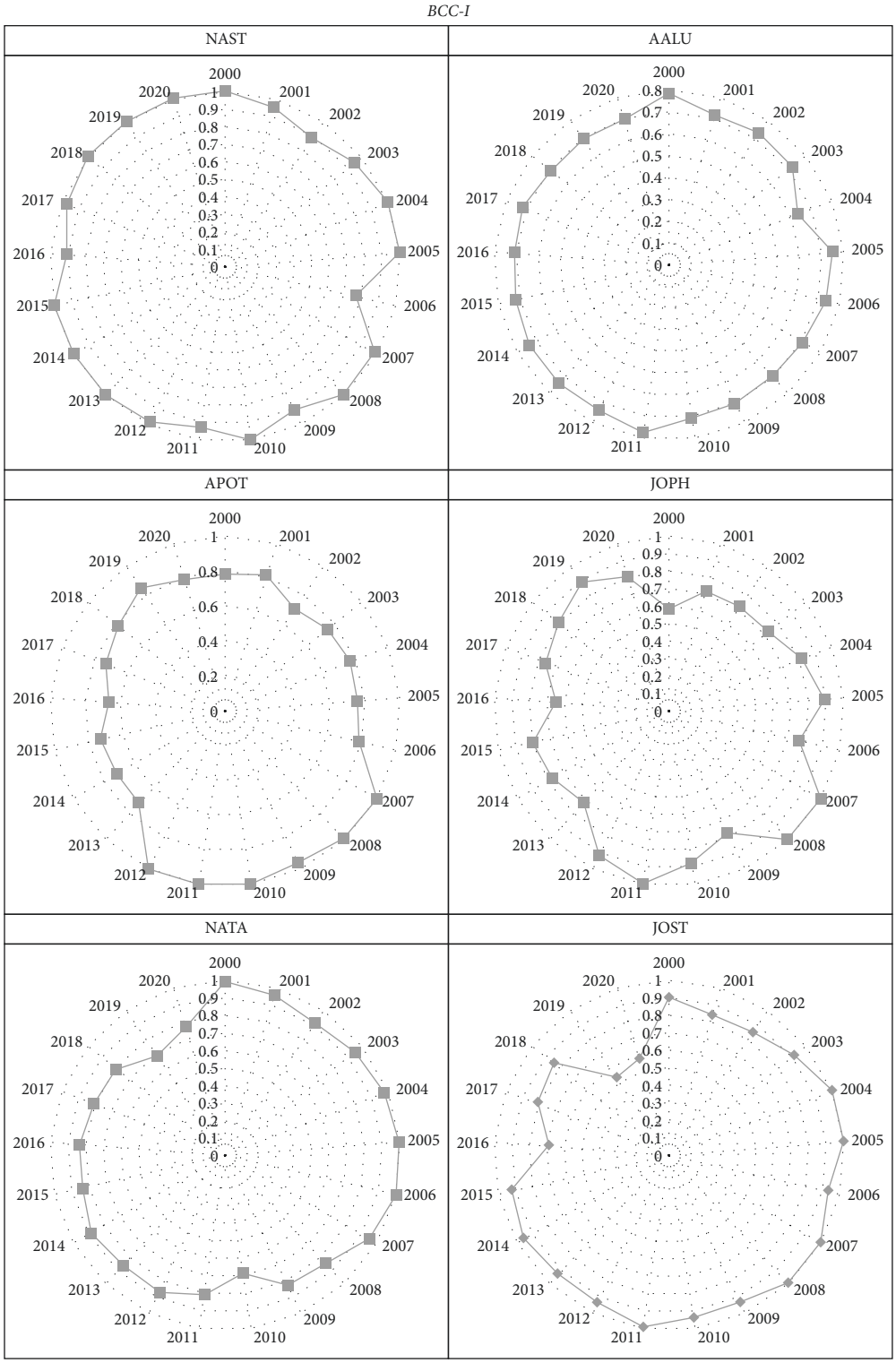

Figure 1: The efficiency rate for each company of BCC-I model during 2000–2020.

following cases; the increase in current assets reduced efficiency performance in (2002, 2010, 2016, 2017, and 2019), the increase in non-current assets is reduced efficiency performance in (2001, 2002, 2010, 2012 : 2013, and 2015 : 2019), the increase in general administration expenses is reduced efficiency performance in (2001, 2002, 2006, 2016, and 2019). The NATA also has full efficiency performance of 100% in all years except the following cases; the increase in current assets is reduced efficiency performance in (2008, 2013, 2014, and 2017). The increase in non-current assets is reduced efficiency performance in 2002, the increase in operating expenses is reduced

Table 8: The average slacks for output-oriented in BCC models during 2000–2020.

Models	Corporations	Efficiency rate	Rank	Operating revenue (s^+)	Market capitalization (s^+)
BCC-O	AALU	1.44024	6	0.00000	21885185.75731
	NAST	1.07258	1	0.00000	1765157.58978
	JOPH	1.24070	5	0.00000	541679987.51728
	APOT	1.22811	4	433577.65242	165482653.94463
	JOST	1.18573	2	0.00000	27123503.81740
	NATA	1.20444	3	0.00000	8506632.47749

efficiency performance in 2008, the increase in general administration expenses is reduced efficiency performance in (2015, 2017, and 2018).

3.3. The Output-Oriented DEA Model. The average efficiency and slacks for output-oriented in BCC models from 2000 to 2020 are shown in Table 8. The corporations should increase the following outputs to get to the efficiency performance of 100%. For instance, NAST should increase, on average, operating revenue to 0.00 JD, and market capitalization to 1765157.59 JD in BCC. In addition, the table shows that NAST is the best efficiency performance on average from 2000 to 2020 and AALU is the lowest efficiency performance on average during the same period based on rank in BCC-O. Indeed, the output-oriented in DEA models is considered a good efficiency performance if the efficiency rate is close to one.

Figure 2 shows the dynamic BCC-O efficiency performance of each corporation over the years from 2000 to 2020. The AALU has full efficiency performance at one in all years except the following cases; the over increase in market capitalization makes efficiency performance become more 100% in (2004, 2007 : 2010, and 2012). The NAST has full efficiency performance also 100% in all years except the following cases; the over increase in operating revenue and market capitalization together make efficiency performance become more 100% in (2002 : 2003, 2007, 2010, and 2012), the over increase in only market capitalization makes efficiency performance become more 100% in (2006, 2009, and 2017). The JOPH has full efficiency performance also 100% in all years except the following cases; the over increase in operating revenue and market capitalization together make efficiency performance become more 100% in (2000, 2010, and 2012 : 2017). The APOT has full efficiency performance also 100% in all years except the following cases; the over increase in operating revenue and market capitalization together make efficiency performance become more 100% in (2000 : 2006 and 2013 : 2020). The JOST has full efficiency performance also 100% in all years except the following cases; the over increase in operating revenue and market capitalization together make efficiency performance become more 100% in (2001 : 2002, 2006, 2010, and 2019). The over increase in market capitalization only make efficiency performance become more 100% in (2015 and 2016 : 2018).The NATA has full efficiency performance also 100% in all years except the following cases; the over increase in operating revenue and market capitalization together make efficiency performance become more 100% in (2008, 2014, and 2018). The over increase in market capitalization only make efficiency performance become more 100% in 2013, 2015, and 2017.

3.4. Tobit Model. The Tobit model proposed by James Tobin in 1958 reference to describe the relationship between a nonnegative dependent variable (efficient ratios) and an independent variable (financial ratios). In this section, we will run the Tobit model, using the VGLM function of the VGAM library in the R-package to find the financial ratios that affect the efficient performance in DEA models. The upper cutpoints in input-oriented equals ($L = 1$) and the upper cutpoints in output-oriented equals ($U = 2.5$) in our analysis.

Table 9 shows the efficient performance of CCR-I as a dependent variable. The return on assets (ROA) and Growth gross domestic product (GDP) are independent variables. The table shows that there is a significant positive relationship between ROA and efficient rate at p value less than 1%. In other words, The ROA value of 0.7269 affects the efficiency rate for corporations. In addition, there is significant positive relationship between GDP growth and the efficient ratio at p value less than 1%. Moreover, the GDP growth value of 1.2916 affects the efficient rate for corporations under CCR-I. Furthermore, the GDP growth and ROA explain about 26.99% (R-square is 0.2699) of efficiency performance under the CCR-I model. The intercept 1 is constant for the model. Moreover, intercept 2 is an ancillary statistic if we exponentiate this value as $e^{-2.13411} = 0.1183$, we get a statistic that is analogous to the square root of the residual variance in OLS regression. The intercept 2 is described as $\ln(\sigma)$. However, the result in Table 9 shows the efficient performance of BCC-I as dependent variable. The return on assets (ROA) and Growth gross domestic product (GDP) are independent variables. The table shows that there is a significant positive relationship between ROA and efficiency performance at p value less than 1%. In other words, the ROA value 0.6003 affects the efficiency performance rate for corporations. In addition, there is a significant positive relationship between GDP growth and efficient performance at p value less than 5%. Moreover, the GDP growth value of 1.0851 affects the efficient rate for corporations under BCC-I. Furthermore, the GDP growth and ROA explain about 14.93% (R-square is 0.1493) of efficiency performance under the BCC-I model. The intercept 1 is constant for the model. Moreover, the intercept 2 is an ancillary statistic if we exponentiate this value as $e^{-2.02410} = 0.1321$, we get a statistic that is analogous to the square root of the residual

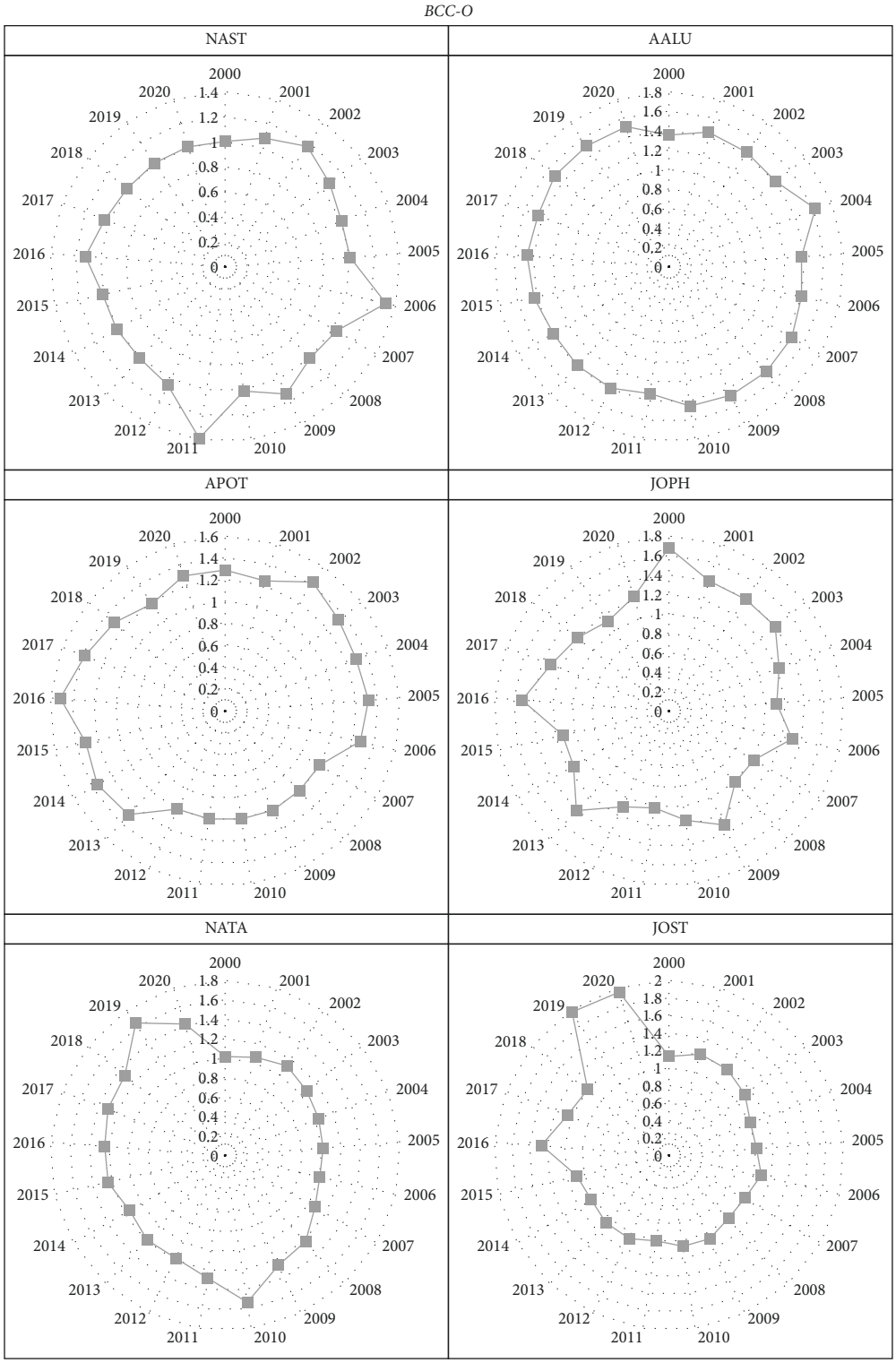

Figure 2: The efficiency rate for each company of BCC-O model during 2000–2020.

variance in OLS regression. The intercept 2 is described as $\ln(\sigma)$. Indeed, the GDP growth and ROA explain affect on efficiency performance under BCC-I less than CCR-I.

Table 9 also highlights the efficient performance of CCR-O as a dependent variable. The return on assets (ROA) and Growth gross domestic product (GDP) are independent variables. The table shows a significant negative relationship between ROA and efficient ratio at p value of less than 1%. In other words, the ROA value of −1.049 affects the efficient performance rate for corporations. In addition, there is significant negative relationship between GDP growth and efficient performance at p value of less than 1%. Moreover,

Table 9: Tobit model.

		Estimate	Std. error	Z-value	Pr (>|z|)	Criteria	Statistic
BCC-I	(Intercept): 1	0.78331	0.02253	34.763	$<2e-16^{***}$	R-squared	0.149387
	(Intercept): 2	−2.02410	0.07129	−28.392	$<2e-16^{***}$	Log-likelihood	40.171
	GDP growth	1.08513	0.45445	2.388	0.0169^{**}	Number of iterations	7
	ROA	0.60033	0.14238	4.216	$2.48e-05^{***}$	Degree of freedom	248
BCC-O	(Intercept): 1	1.32919	0.03069	43.310	$<2e-16^{***}$	R-squared	0.1822066
	(Intercept): 2	−1.69405	0.06299	−26.892	$<2e-16^{***}$	Log-likelihood	34.6641
	GDP growth	−1.51748	0.61798	−2.456	0.0141^{**}	Number of iterations	5
	ROA	−0.78873	0.18354	−4.297	$1.73e-05^{***}$	Degree of freedom	248

Signif. codes: 0.01 "***" 0.05 "**" 0.1 "*".

the GDP growth value of −2.2718 affects the efficient rate for corporations under CCR-O. Furthermore, the GDP growth and ROA explain about 27.90% (R-square is 0.2790) of efficiency performance under the CCR-O model. The intercept 1 is constant for the model. Moreover, intercept 2 is an ancillary statistic if we exponentiate this value as $e^{-1.65042} = 0.1920$, we get a statistic that is analogous to the square root of the residual variance in OLS regression. The intercept 2 is described as $\ln(\sigma)$. However, the result in the table below shows the efficient performance of BCC-O as dependent variable. The return on assets (ROA) and Growth gross domestic product (GDP) are independent variables. The table shows that there is a significant negative relationship between ROA and efficiency performance at p value less than 1%. In other words, the ROA value −0.7887 affects the efficiency performance rate for corporations. In addition, there is a significant negative relationship between GDP growth and efficient performance at p value of less than 1%. Moreover, the GDP growth value −1.5175 affects the efficient rate for corporations under BCC-O. Furthermore, the GDP growth and ROA explain about 18.22% (R-square is 0.1822) from efficiency performance under the BCC-O model. The intercept 1 is constant for the model. Moreover, the intercept 2 is an ancillary statistic that if we exponentiate this value as $e^{-1.69405} = 0.1838$, we get a statistic that is analogous to the square root of the residual variance in OLS regression. The intercept 2 is described as $\ln(\sigma)$. Indeed, the GDP growth and ROA explain the affect on efficiency performance under BCC-O less than CCR-O.

4. Conclusion

In this study, we have proposed successfully an estimation of performance efficiency for mining and extracting corporations in Jordan. This paper selected those mining and extracting corporations that reflect 90% of the total market capitalization in the Amman Stock Exchange (ASE) from 2000 to 2020. The DEA models (CCR (input/output) and BCC (input/output)) are used to analyse the performance efficiency based on the average efficiency ratio of the sector. In addition, the role of internal and external factors on performance efficiency in mining and extracting sector is determined based on the Tobit model. The results show that the performance of DMU is better in BCC models compared to CCR models for several reasons; the sector could improve its performance from a minimum of 0.47 in CCR-I to a minimum of 0.53 in BCC-I, the sector could improve its performance from a maximum of 2.12 in CCR-O to a maximum of 1.97. In BCC-O, the number of efficient *DM Us* in BCC models is more than in CCR models and the BCC models are better than CCR models because they use VRS rather than CRS. This result is consistent with References [3, 4]. However, the average of NAST's performance efficiency is higher than that of other companies based on BCC (Input/Output). Moreover, the performance efficiency ratio variety is based on company level from 2000 to 2020. Finally, GDP growth and ROA have affected BCC's efficiency performance rate based on the Tobit model. In future work, we will use another dynamic DEA models and compare with our study. Managerial implications for enhancing decision-making are expected to contribute to management policies. This study asks mining and extracting companies to take the indicator results to improve their efficiency performance.

Data Availability

The datasets analyzed during the current study are available in the Amman Stock Exchange (ASE) repository, https://www.ase.com.jo/.

Conflicts of Interest

The authors declare that they have no conflicts of interest.

References

[1] A. Yang and G.-l. Yang, "A survey and analysis of the first 40 years of scholarly literature in DEA: 1978-2016," *Socio-Economic Planning Sciences*, vol. 61, pp. 4–8, 2018.

[2] W. Bank, "World bank," *Ministry of Investment-Jordan, Amman, Jordan*, https://www.worldbank.org/en/home, 2021. 3, https://www.moin.gov.jo/en/home-new/, 2022, 2021.

[3] J. J. I. C. Jic, "Jordan investment commission (JIC)," 2021.

[4] A. Charnes, W. W. Cooper, and E. Rhodes, "Measuring the efficiency of decision making units," *European Journal of Operational Research*, vol. 2, no. 6, pp. 429–444, 1978.

[5] J. S. Liu, L. Y. Lu, W.-M. Lu, and B. J. Lin, "A survey of DEA applications," *Omega*, vol. 41, no. 5, pp. 893–902, 2013.

[6] N. Y. Yusop, J. A. Alhyari, and H. A. Bekhet, "Dynamic elasticities between financial performance and determinants of mining and extractive companies in Jordan," *The Journal of Asian Finance, Economics and Business*, vol. 8, no. 7, pp. 433–446, 2021.

[7] L. M. Seiford and R. M. Thrall, "Recent developments in DEA: the mathematical programming approach to Frontier analysis," *Journal of Econometrics*, vol. 46, no. 1-2, pp. 7–38, 1990.
[8] L. M. Seiford, "Data envelopment analysis: the evolution of the state of the art (1978?1995)," *Journal of Productivity Analysis*, vol. 7, no. 2-3, pp. 99–137, 1996.
[9] W. W. Cooper, S. Li, L. M. Seiford et al., "Sensitivity and stability analysis in DEA: some recent developments," *Journal of Productivity Analysis*, vol. 15, no. 3, pp. 217–246, 2001.
[10] W. D. Seiford and L. M. Seiford, "Data envelopment analysis (DEA) - thirty years on," *European Journal of Operational Research*, vol. 192, no. 1, pp. 1–17, 2009.
[11] A. Hosseinzadeh, R. Smyth, A. Valadkhani, and V. Le, "Analyzing the efficiency performance of major Australian mining companies using bootstrap data envelopment analysis," *Economic Modelling*, vol. 57, pp. 26–35, 2016.
[12] B. Geissler, M. C. Mew, O. Weber, and G. Steiner, "Efficiency performance of the world's leading corporations in phosphate rock mining," *Resources, Conservation and Recycling*, vol. 105, pp. 246–258, 2015.
[13] M. Parikh and J. K. Parikh, "Study of efficiency and productivity growth in opencast and underground coal mining in India: a DEA analysis," *Energy Economics*, vol. 24, no. 5, pp. 439–453, 2002.
[14] H. Fang, J. Wu, and C. Zeng, "Comparative study on efficiency performance of listed coal mining companies in China and the US," *Energy Policy*, vol. 37, no. 12, pp. 5140–5148, 2009.
[15] W. Shu-Ming, "Evaluation of safety input-output efficiency of coal mine based on DEA model," *Procedia Engineering*, vol. 26, pp. 2270–2277, 2011.
[16] I. E. Tsolas, "Performance assessment of mining operations using nonparametric production analysis: a bootstrapping approach in DEA," *Resources Policy*, vol. 36, no. 2, pp. 159–167, 2011.
[17] S. L. Eller, P. R. Hartley, and K. B. Medlock, "Empirical evidence on the operational efficiency of national oil companies," *Empirical Economics*, vol. 40, no. 3, pp. 623–643, 2011.
[18] R. Riccardi, G. Oggioni, and R. Toninelli, "Efficiency analysis of world cement industry in presence of undesirable output: application of data envelopment analysis and directional distance function," *Energy Policy*, vol. 44, pp. 140–152, 2012.
[19] A. Hosseinzadeh, R. Smyth, A. Valadkhani, and A. Moradi, "What determines the efficiency of Australian mining companies?" *The Australian Journal of Agricultural and Resource Economics*, vol. 62, no. 1, pp. 121–138, 2018.
[20] C. Maheswari, E. B. Priyanka, S. Thangavel, S. V. R. Vignesh, and C. Poongodi, "Multiple regression analysis for the prediction of extraction efficiency in mining industry with industrial IoT," *Production Engineering*, vol. 14, no. 4, pp. 457–471, 2020.
[21] D. Akbarian, "Network DEA based on DEA-ratio," *Financial Innovation*, vol. 7, no. 1, pp. 73–26, 2021.
[22] G. Kou, H. Xiao, M. Cao, and L. H. Lee, "Optimal computing budget allocation for the vector evaluated genetic algorithm in multi-objective simulation optimization," *Automatica*, vol. 129, Article ID 109599, 2021.
[23] F. Kamarudin, F. Sufian, and A. M. Nassir, "Global financial crisis, ownership and bank profit efficiency in the Bangladesh's state owned and private commercial banks," *Contaduría Y Administración*, vol. 61, no. 4, pp. 705–745, 2016.
[24] P. A. Aghimien, F. Kamarudin, M. Hamid, and B. Noordin, "Efficiency of gulf cooperation council banks: empirical evidence using data envelopment analysis," *Review of International Business and Strategy*, 2016.
[25] K. Hafsal, A. Suvvari, and S. R. S. Durai, "Efficiency of Indian banks with non-performing assets: evidence from two-stage network DEA," *Future Business Journal*, vol. 6, no. 1, pp. 26–29, 2020.
[26] M. Zimková and E. Zimková, "A DEA model for measuring financial intermediation," *Economic Change and Restructuring*, vol. 54, no. 2, pp. 339–370, 2021.
[27] R. D. Morey and R. C. Morey, "Efficiency analysis for exogenously fixed inputs and outputs," *Operations Research*, vol. 34, no. 4, pp. 513–521, 1986.
[28] J. Tobin, "Estimation of relationships for limited dependent variables," *Econometrica*, vol. 26, no. 1, pp. 24–36, 1958.
[29] A. Hoff, "Second stage DEA: comparison of approaches for modelling the DEA score," *European Journal of Operational Research*, vol. 181, no. 1, pp. 425–435, 2007.
[30] B. B. Lin and W. T. Lin, "Technical efficiency analysis of information technology investments: a two-stage empirical investigation," *Information & Management*, vol. 39, no. 5, pp. 391–401, 2002.
[31] G. N. Gregoriou, "Quantitative models for performance evaluation and benchmarking: data envelopment analysis with spreadsheets," *The Journal of Wealth Management*, vol. 17, no. 4, pp. 114-115, 2015.

Hindawi
Complexity
Volume 2022, Article ID 2801930, 12 pages
https://doi.org/10.1155/2022/2801930

Research Article

A Consensus Decision-Making Model considering Empathetic Preferences and Power Structure of the Poverty Alleviation E-Commerce Supply Chain

Ruili Shi,[1,2] **Lianming Zhao**,[2] **Chunxiang Guo**,[3] **and Xin Gu**[3]

[1]*College of Business Administration, Chongqing University of Science and Technology, Chongqing 401331, China*
[2]*Chongqing Business Vocational College, Chongqing 401331, China*
[3]*Business School, Sichuan University, Chengdu 610065, China*

Correspondence should be addressed to Chunxiang Guo; guochunxiang@scu.edu.cn

Received 30 May 2022; Revised 27 June 2022; Accepted 12 July 2022; Published 13 August 2022

Academic Editor: Yu Zhou

This article focuses on the conflict consultation process and empathetic decision-making behavior of a poverty alleviation supply chain composed of farmers, retailers, and third-party e-commerce platforms (e-platforms), and proposes an empathetic preference-based consensus decision-making model. The impact of empathetic preferences and power structure on the consensus reaching process are analyzed. The results indicate that consumers' empathy increases the consensus wholesale price and sales price of products, while retailers' and e-platforms' empathy increase the wholesale price and reduce the sales price of products. The empathetic preferences of consumers, retailers, and e-platforms are helpful for increasing the profits of farmers. The retailer's empathetic preference is not beneficial to its own profits and the supply chain, while the e-platform's empathetic preference can help to improve its own income and increase the overall profit of the supply chain at first, before decreasing. Moreover, the power of retailer is positively correlated with the profits of farmers and the retailer, and negatively correlated with the profits of the e-platform and supply chain. The sales price and commission price are negatively correlated with the power of retailer, but the wholesale price is not related to the change in power structure.

1. Introduction

How to improve the sales and circulation of agricultural products is a key problem to promoting the development of rural industry and improve farmers' income [1–3]. With the development of e-commerce technologies, enterprises cooperate with third-party e-commerce platforms (e-platforms), such as Alibaba, JD, and Amazon, forming the e-commerce supply chain (eSC), which has become an important channel to promote the circulation of agricultural products and plays a vital role in poverty alleviation, especially since the outbreak of COVID-19 [4–8]. With the prominent effectiveness of e-platforms on poverty alleviation, the decision-making process of the agricultural supply chain with the participation of e-platforms has attracted scholarly attention, such as the operational and pricing strategies [9], profit distribution mechanism, and conflict coordination strategies [10–12] of eSC and dual-channel SC. However, the existing research on poverty alleviation eSC (PA-eSC) decision-making is mainly based on game theory for balanced analysis, and rarely analyzes the consensus-reaching process (CRP) of profit conflict within the supply chain.

The CRP is essentially the communication and evolution of preferences or opinions between supply chain subjects, which is very normal in daily life [13, 14]. It was previously assumed that the evolution of preferences is based on individual rationality and self-interest, that is, the hypothesis of "economic man." With the deepening of behavioral research, the hypothesis of "economic man" falls into theoretical confusion when explaining many phenomena in the real-world [15, 16], that is, when making choices or decisions, people pay attention not only to their own profits or feelings but also to the welfare or emotion of others, and will

incorporate them into their decision goals and therefore adjust their decision [15–17]. In the economics area, individuals' understanding of others' emotions and attention to the welfare of others is called empathetic preference [18].

Significantly, when it comes to the poverty alleviation supply chain (PASC), unlike the standard hypothesis that supply chain entities only seek to maximize their own profits, they may care about the profits of farmers and generate empathetic decision-making behavior, which has been proven to be an important basis for social interaction, an important factor in promoting social equity, reducing unfair behavior and altruistic behavior [19–21]. In PASC, consumers may increase their willingness to buy because of their empathy for farmers, and e-platforms may also increase their willingness to participate in the PASC for the same reason. Therefore, taking into account the empathetic preference to explore the CRP of PA-eSC will be more in line with the actual decision-making behavior.

Furthermore, in the real-world situation, it is known that when faced with some strong retail giants (such as Walmart, Jingdong, Suning, and Yonghui), product manufacturers are powerless in the pricing and profit coordination of supply chain, and vice versa, that is, the power of supply chain entities is usually unequal [10–12]. Previous studies have shown that a change in power structure will affect the decision-making and coordination of a supply chain, based on game theory [11, 12, 22, 23]. In practice, when focusing on the PA-eSC, retailers or e-platforms generally occupy a dominant position, have a greater power in supply chain, and usually obtain a larger proportion of supply chain profits. Farmers, on the other hand, have limited sales channels, often passively waiting for retailers' procurement, with lower pricing power and low profits [24].

In summary, existing research on the PA-eSC is mainly based on the game theory to conduct equilibrium analysis of the supply chain decision-making and coordination strategy, rarely analyzing the decision-making process of supply chain entities from the perspective of consensus negotiation. However, supply chain decision-making is often accompanied by negotiation consensus. Meanwhile, consumers and the main entities of the PA-eSC usually have empathetic preference, which will inevitably affect the CRP of the supply chain, but existing research has not yet considered the existence of empathetic preference. Moreover, some scholars have studied the impact of different power structures on traditional supply chain decision-making and dual-channel supply chain decision-making, but have not yet considered the impact of power structure, especially the "non-dominator-follower" structure on the PA-eSC.

Therefore, this article examines the empathetic preference of consumers and supply chain entities; regards the pricing decision of the PA-eSC as a consensus problem with empathetic preference; and analyzes the influence of empathetic preference and power structure on pricing decisions concerning agricultural products, the income of supply chain entities, and the CRP of supply chain.

The main contributions and innovations of this study are as follows.

Firstly, this article focuses on the empathetic preferences of consumers and supply chain members, and explores the impact of empathetic preferences on decisions and member profits of the PA-eSC. The current literature has not yet considered the empathetic preference in the PA-eSC, nor has it researched the impact of empathetic preferences on the pricing decision and profit of the PA-eSC.

Secondly, the "non-dominator-follower" power structure is considered an important factor of supply chain decision-making, improving the reliability of supply chain decision-making. The current research on power structure is mostly limited to the simple "dominator-follower" structure in traditional offline supply chains and dual-channel supply chains.

Moreover, unlike the game equilibrium analysis of supply chain decision-making in existing research studies, this article researches the decision-making process of supply chain from the perspective of consensus negotiation, and a novel CRP model is proposed.

The rest of this article is organized as follows. Section 2 offers a brief introduction to the research on supply chain decision-making. The description and hypothesis of this study is introduced in Section 3. Section 4 constructs the consensus model of pricing decisions via discussing the empathetic preferences and power distribution of the PA-eSC. In Section 5, we use a case study to analyze the influence of empathetic preferences and the power structure on the CRP of PA-eSC. Finally, our conclusions are set out in Section 6.

2. Literature Review

This section features a brief review of the relevant studies on supply chain decision-making. The existing research related to this study mainly focuses on three aspects: supply chain decision-making under social preference, supply chain decision-making under different power structures, and the decision-making of the PA-eSC.

2.1. Supply Chain Decisions under Social Preference. Many behavioral experiments, such as the ultimatum game experiment and the dictator experiment, have proved that many human behaviors are contrary to the expected behavior based on rational hypothesis [15–17]. Thus, scholars began to try to give up the hypothesis of individual rationality, and the theory of social preference was produced and developed rapidly [16–18]. The basic assumption of social preference is that people care not only about their own benefits but also about the interests of others, and this is also known as "other-regarding preferences," "pro-social preferences," or "inter-dependent preferences" [17, 18].

There has been a lot of recent research on the supply chain under social preference, including inequality aversion preference, reciprocity preference, altruism preference, and so on. Ho and Zhang [25] verified the existence of an inequality aversion behavior tendency in the supply chain through empirical methods. Katok et al. [26] found that the weak inequality aversion behavior of members would cause a

loss in efficiency of the supply chain system. Wang et al. [11] studied the decision-making and coordination of a green eSC with manufacturer fairness concerns. Zhang [27] discussed the pricing strategy of supply chain under reciprocity preference, and found that reciprocity preference is beneficial to the income and efficiency of closed-loop supply chain, and an increased reciprocity preference will lead to a decrease in their own income but an increase in others' income. Shi et al. [9] studied the effect of altruism on pricing strategy in two classic dual-channel supply chains using Stackelberg game models, and showed that the altruism preference strongly affects the pricing strategies. Wang et al. [28, 29] studied the impacts of altruistic preference on decisions of retailer-led low-carbon supply chain and e-commerce closed-loop supply chain. Moreover, Sana [30, 31] analyzed the price decision of green products by considering the green preferences of consumers and corporate social responsibility. Nevertheless, when using the theory of social preference to explain individual behavior, one of the major problems encountered is whether the cause of social preference is fairness concerns, reciprocity, or altruism. This problem is often difficult to decompose and test strictly. In fact, the core idea of social preference theory is that people care not only about their own interests but also about the interests of others [15–18]. Psychological research shows that an important factor that leads individuals to pay attention to the interests of others is empathy [19–21].

Empathy is an important inherent ability of human beings to maintain social relations, and it is also an important driving force for people to produce mutual benefit, inequality aversion, and altruistic and other prosocial behavior [18–21]. In the PA-eSC, consumers, e-commerce platforms, and retailers are more likely to empathize with farmers, and may eventually affect supply chain decision-making. Therefore, considering the impact of empathetic preference on supply chain decision-making will be more in line with a realistic decision-making scenario.

2.2. Supply Chain Decision-Making under Different Power Structures. The study of power structure within the supply chain mainly focuses on the discussion of supply chain decision-making under different game power structures, such as retailer dominates, manufacturers dominate, and no one dominates, from a game perspective. Some of the literature discusses the impact of power structure on the traditional supply chain, for example, Gaski and Nevin [32] analyzed the power sources of supply chain members, and discussed the impact of power on supply chain channel decisions. Chen and Wang [33] discovered that power leaders can gain more revenue. Gao et al. [22] found that retailers' profits continued to rise with the increase of their power. Some studies revealed the impact of power on a dual-channel supply chain. Chen et al. [34] studied the influence of power structures on the retailers' dual-channel supply chain. Sun et al. [35] analyzed the influence of power structures on manufacturers' dual-channel supply chain. Cao and Liu [36] compared the optimal strategy and performance of the presale and current sale dual-channel supply chain under three power structures as described above. Furthermore, some scholars have introduced the power structure of supply chain into research of green supply chain, and studied the impact of power structures on product green degree, wholesale price, retail price, and profit of supply chain [37, 38].

The current research mainly focuses on pricing strategy and profit distribution of supply chain decision-making under the game power structure, that is, "dominator and follower" and "no dominator" structure. However, in the actual decision-making, the power structure between supply chain entities is often not a simple "dominator-follower" or "no dominator" relationship, and the difference in power structure will also play a different role in the decision-making of the supply chain.

2.3. Research on the Decisions of PA-eSC. In recent years, the problem of poverty alleviation has received great attention from scholars, and research hotspots focus on the operation mode of social responsibility, the design of cooperation and coordination mechanism between enterprises and the poor, the creation and distribution of shared value, and so on [1–3]. Previous scholars have studied the way in which government funding promotes agricultural development in the PASC. Besley and Kanbur [39] studied the optimal model of grain subsidy. Yuanchang and Jiyu [40] analyzed the optimal boundary of financial subsidy based on the agricultural insurance welfare loss model. Kang et al. [41] examined the impacts of government subsidies and corporate social responsibility on a PASC, and suggested that the most effective poverty alleviation mechanism in most cases is a combination of government subsidies and market efforts. A few scholars have discussed the decision-making and coordination issues related to the PASC. For example, Kang et al. [24] studied the decision-making and coordination strategy with fairness concerns involved in a PASC, and found that the fairness concerns of the farmer enterprise aggravated the double marginalization within the PASC and reduced the profit of both farmer and core enterprises. Zhou et al. [42] studied the influence of enterprise's poverty alleviation preference on the profits of the supply chain and its members considering consumers' altruistic preferences.

With the popularity of e-commerce, e-platforms give full play to big data advantages and actively invest in poverty alleviation. The decision-making of agricultural product eSC has attracted the attention of scholars. Li et al. [43] analyzed the role of governments in developing rural e-commerce ecosystems and the impact of such ecosystems on poverty alleviation, and elucidated a model of poverty alleviation through e-commerce. Peng et al. [44] confirmed that e-commerce has a significantly positive effect on rural poverty alleviation using empirical evidence. Wan et al. [45, 46] explored the impact of the government financial platform incentive mechanism and consumers' poverty alleviation preference on the decision and coordination strategy of the smart supply chain.

In brief, the research on PA-eSC decision-making has achieved certain research results, but few scholars consider

the impact of consumers' and supply chain entities' empathetic preferences, and the non- "dominator-follower" -type power structure of supply chain on the decision-making of the PA-eSC. Thus, this article studies the pricing decision of the PA-eSC under the empathetic preferences and non- "dominator-follower" power structure, and analyzes the impact of empathetic preferences and power structure on the CRP of PA-eSC, which is closer to the actual decision-making scene, and better to provide scientific suggestions for the supply chain decision-making.

3. Model Description

In this section, the assumptions for this study are presented, and the consensus model of the PA-eSC decision is introduced.

3.1. Description and Assumptions. This article focuses on the CRP of a PS-eSC composed of farmers, retailers, and e-commerce platforms, a three-level supply chain model. In the PA-eSC, similar to the traditional agricultural product supply chain, farmers are often in the position of passively waiting for the retailer to purchase, and have limited alternative sales channels, while the retailer and e-platform have more choice and play a leading role. Simultaneously, the difference of the PA-eSC is that the retailers, e-platforms, and consumers care not only about their own interests but also about the interests of farmers, having empathetic preference, which may affect the CRP of the supply chain. The supply chain network can be described as in Figure 1, and the notations involved in this study are presented in Table 1.

The assumptions of this article are as follows.

Assumption 1. Consumers, retailers, and e-platforms have empathetic preferences for farmers. The higher the consumers' empathy, the more willing consumers are to buy the products. The demand function of agricultural products is $q = d_0(1+\rho_a) - ap^s$, where $a\,(a>0)$ is the price elasticity coefficient of agricultural products, and $\rho_a\,(0 \le \rho_a \le 1)$ is the empathy degree of consumers to farmers

Assumption 2. The empathy degree of consumers for farmers is positively related to the poverty degree of farmers they perceived, which is mainly determined by the service level of the e-platform. As stated in the literature [7], the service level has a linear function of the unit product commission. Therefore, the empathy degree of consumers is set as $\rho_a = 1 - 1/\lambda r$, where λ indicates the sensitivity of consumers to agricultural assistance service level.

Assumption 3. The unit service cost of the e-platform is directly proportional to the service level determined by the service fee. Thus, the unit service cost c_3 is a quadratic function of the unit service fee. With reference to the literature [7], we suppose $c_3 = kr^2/2$, where $k\,(k>0)$ is the elasticity coefficient of unit cost, which mainly refers to the funds needed to provide the unit service (marketing promotion service, big data forecast, sales service, logistics service, payment service, and customer service).

Assumption 4. In the PA-eSC, the power of each supply chain entities is different. The power distribution in the supply chain composed of farmers, retailers, and e-platforms is set as (R_1, R_2, R_3), in which R_1, R_2, R_3 are the power indices of farmers, retailers, and e-platforms, respectively. Farmers are powerless, whereas the retailer and e-platform are powerful, that is, $R_1 \ll R_2, R_3$.

Assumption 5. In the PA-eSC, the government only guides and calls on consumers, retailers, and e-platforms to actively participate in supporting agriculture, without any policy subsidy.

3.2. Consensus Model. In this section, we construct a consensus model of the pricing decisions via discussing the empathetic preferences and power distribution of the PA-eSC.

3.2.1. Basic Models. In the PA-eSC composed of farmers, retailers, and e-platforms, the profit functions of farmers, retailers, and e-platforms are as follows:

$$\begin{aligned} v_1 &= (p^c - c_1)q = (p^c - c_1)(d_0(1+\rho_a) - ap^s), \\ v_2 &= (p^s - p^c - r - c_2)q \\ &= (p^s - p^c - r - c_2)(d_0(1+\rho_a) - ap^s), \\ v_3 &= rq - c_3 = r(d_0(1+\rho_a) - ap^s) - \frac{k}{2}r^2. \end{aligned} \tag{1}$$

The total profit function of the supply chain is

$$\begin{aligned} v &= (p^s - c_1 - c_2)q - c_3 \\ &= (p^s - c_1 - c_2)(d_0(1+\rho_a) - ap^s) - \frac{k}{2}r^2. \end{aligned} \tag{2}$$

In the PA-eSC, the difference in the power of supply chain entities leads to a different discourse power in the profit distribution of each member. Hence, the profit utility function of each member is also different. Generally, in the supply chain of agricultural products, farmers have the least power, while the retailers and e-platforms have more power. Therefore, the utility function of farmers, retailers, and e-platforms are as follows:

$$\begin{aligned} u_1 &= v_1^{\alpha} = ((p^c - c_1)(d_0(1+\rho_a) - ap^s))^{\alpha}, \\ u_2 &= v_2^{\beta} = ((p^s - p^c - r - c_2)(d_0(1+\rho_a) - ap^s))^{\beta}, \\ u_3 &= v_3^{\xi} = \left(r(d_0(1+\rho_a) - ap^s) - \frac{k}{2}r^2\right)^{\xi}, \end{aligned} \tag{3}$$

where α, β, ξ determine the concavity and convexity of the utility function of farmers, retailers, and e-platforms, respectively, and they satisfy $1 \ge \alpha, \beta, \xi > 0$ according to the law of diminishing marginal utility. In reality, farmers within the PA-eSC have lower income compared with retailers and e-platforms, and the utility of the same income is necessarily different for farmers, retailers, and e-platforms. Specifically, for the same profits, farmers' utility is the highest, while the

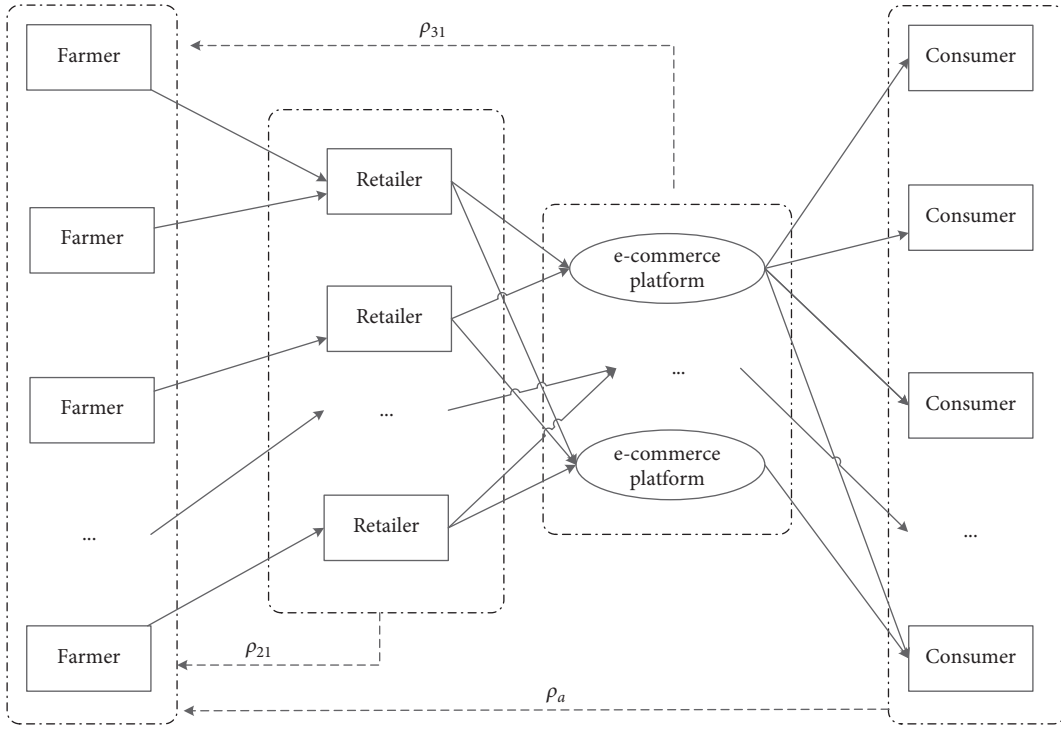

Figure 1: The supply chain network of "Farmers + Retailers + e-platforms."

Table 1: Notations.

Symbols	Notations
d_0	Market demand for products
p^c	The wholesale price
p_1^c	The wholesale quotation of farmers
p_2^c	The wholesale quotation of retailers
p_3^c	The wholesale quotation expected by e-platforms
p^s	The sales price
p_2^s	The sales quotation of retailers
p_3^s	The sales quotation expected by e-platforms
c_1	The unit production cost of farmers
c_2	The unit production cost of retailers
c_3	The unit service cost of e-platforms
r	The unit service fee paid by retailers to the e-platform (the commission price)
r_2	The commission quotation of retailers
r_3	The commission quotation of e-platforms
ρ_a	The consumers' empathetic preference coefficient, $0 \le \rho_a \le 1$
ρ_{21}	The empathetic preference coefficient of retailer to farmers, $0 \le \rho_{21} \le 1$
ρ_{31}	The empathetic preference coefficient of platform to farmers, $0 \le \rho_{31} \le 1$

retailers and e-platforms have relatively low utility. Therefore, α, β, ξ satisfy $1 \ge \alpha > \beta, \xi > 0$ in the proposed model.

In the PA-eSC, not only do consumers have an empathetic preference for farmers but the retailers and e-platforms also care about the interests of farmers and have empathetic preferences, that is, the utility of each member in the supply chain is not only related to their own profit. Thus, the utility function of farmers, retailers, and e-platforms under empathetic preference conditions can be expressed as follows:

$$\begin{aligned}
U_1 &= u_1 = (p^c - c_1)(d_0(1+\rho_a) - ap^s),\\
U_2 &= u_2 + \rho_{21}u_1\\
&= ((p^s - p^c - r - c_2)(d_0(1+\rho_a) - ap^s))^\beta\\
&\quad + \rho_{21}((p^c - c_1)(d_0(1+\rho_a) - ap^s))^\alpha,\\
U_3 &= u_3 + \rho_{31}u_1\\
&= \left(r(d_0(1+\rho_a) - ap^s) - \frac{k}{2}r^2\right)^\xi\\
&\quad + \rho_{31}((p^c - c_1)(d_0(1+\rho_a) - ap^s))^\alpha.
\end{aligned} \tag{4}$$

The total utility function of the supply chain is

$$U = U_1 + U_2 + U_3 = (1 + \rho_{21} + \rho_{31})u_1 + u_2 + u_3, \tag{5}$$

where ρ_{21} and ρ_{31} are the retailers' and e-platforms' empathy degree to farmers, respectively.

3.2.2. Consensus Reaching Process. In the following, we consider pricing consensus model with the empathetic preferences, and the consensus reaching process is proposed.

(1) Initial Pricing Stage. In the pricing decision of agricultural products supply chain, farmers have the least power to decide the price of agricultural products and are in a follower position. Therefore, the initial pricing process of the PA-eSC can be summarized as follows: First, the wholesale price of agricultural products is determined by the retailer, and farmers can only choose to accept or refuse; next, the retailer

determines the product sales price according to the wholesale price and market demand of agricultural products; then, the e-platform determines the unit service fee according to the product sales price, with some consideration of the profit for farmers.

The retailer and e-platform are two independent economic entities maximizing their own profits. The ideal quotation of the retailer is obtained by the model.

$$\begin{aligned}\max U_2 = {} & \left(\left(p^s - p^c - r - c_2\right)\left(d_0\left(1+\rho_a\right) - ap^s\right)\right)^{\beta} \\ & + \rho_{21}\left(\left(p^c - c_1\right)\left(d_0\left(1+\rho_a\right) - ap^s\right)\right)^{\alpha},\end{aligned} \tag{6}$$

$$\text{s.t.}\begin{cases} p^c - c_1 > 0, \\ p^s - p^c - r - c_2 > 0, \\ d_0\left(1+\rho_a\right) - ap^s - \dfrac{k}{2}r > 0. \end{cases} \tag{7}$$

The optimal quotation of the retailer can be obtained by solving the model equation (6) and model equation (7): wholesale price $p_2^c = p_2^{c*}$, sales price $p_2^s = p_2^{s*}$, and platform commission $r_2 = r_2^*$.

The optimal quotation of the e-platform can be obtained by the model equation (8) and model equation (9).

$$\begin{aligned}\max U_3 = {} & \left(r\left(d_0\left(1+\rho_a\right) - ap^s\right) - \frac{k}{2}r^2\right)^{\xi} \\ & + \rho_{31}\left(\left(p^c - c_1\right)\left(d_0\left(1+\rho_a\right) - ap^s\right)\right)^{\alpha},\end{aligned} \tag{8}$$

$$\text{s.t.}\begin{cases} p^c - c_1 > 0, \\ p^s - p^c - r - c_2 > 0, \\ d_0\left(1+\rho_a\right) - ap^s - \dfrac{k}{2}r > 0. \end{cases} \tag{9}$$

The optimal quotation of the e-platform can be obtained by the model equation (8) and model equation (9), that is, wholesale price $p_3^c = p_3^{c*}$, sales price $p_3^s = p_3^{s*}$, and platform commission $r_3 = r_3^*$.

According to the model equation (6) and (7) and model equations (8) and (9), if the optimal quotations of the retailer and e-platform are consistent and in line with the expectation of farmers, then a consensus can be reached and the consultation will be concluded; otherwise, the members will negotiate on the basis of the initial prices, that is, the optimal quotations gained and model equations (6) and (7), and model equations (8) and (9), to reach a consensus.

(2) Consensus Reaching Stage. The negotiation of the supply chain is conducted through a smart decision-making system (SDMS) which encourages all members to reach a consensus based on the supply chain utility maximization rules and their price expectations.

Suppose that the lowest wholesale price acceptable to farmers is $p_1^{c^\circ}$, that is, p_1^c satisfies $p_1^c \geq p_1^{c^\circ}$, the highest wholesale price acceptable to the retailer is $p_2^{c^\circ}$, that is, p_2^c satisfies $p_2^c \leq p_2^{c^\circ}$, and the lowest wholesale price that the e-platform wants the retailer to give to farmers is $p_3^{c^\circ}$, that is, p_3^c satisfies $p_3^c \geq p_3^{c^\circ}$; the lowest commission price acceptable for the e-platform is r_3^0, that is, r_3 satisfies $r_3 \geq r_3^0$.

The above information is the private information provided by each member to the SDMS. Accordingly, the consensus process based on the SDMS is as follows:

(1) Consensus Information Feedback. If the optimal wholesale price of farmers, retailer, and e-platform satisfies $p_1^{c*} = p_2^{c*} = p_3^{c*}$, the optimal sales price of retailer and e-platform satisfies $p_2^{s*} = p_3^{s*}$, and the optimal commission price of retailer and e-platform satisfies $r_2^* = r_3^*$, simultaneously, the supply chain reaches a consensus, and we can get consensus prices and consensus profits directly.

tIf there is no consensus reached among the supply chain members, the SDMS provides feedback consensus information to retailers and offers a suggested quotation to the retailer according to supply chain utility maximization rules, and the provide recommended price to supply chain members based on the following model equations (10) and (11).

$$\max U = U_1^{R_1} + U_2^{R_2} + U_3^{R_3}, \tag{10}$$

$$\text{s.t.}\begin{cases} p_3^{c^\circ} \leq p^c \leq p_2^{c^\circ}, \\ p^s - p^c - r - c_2 > 0, \\ d_0\left(1+\rho_a\right) - ap^s - \dfrac{k}{2}r > 0, \\ r \geq r_3^0. \end{cases} \tag{11}$$

where R_1, R_2, R_3 express the power of farmers, retailer, and e-platform in the supply chain, respectively.

Based on the model equations (10) and (11), the recommended quotation from the SDMS to the retailer can be gained: $p_1^c = \widetilde{p}_2^{c*}, p_3^s = \widetilde{p}_2^{s*}, r = \widetilde{r}_3^*$.

(2) Price Adjustment. According to the recommendations of the SDMS, the retailer adjusts its quotation according to the following rules as model equations (12) and (13):

$$\begin{aligned}\max U_2 = {} & \left(\left(p_2^s - p_2^c - r_2 - c_2\right)\left(d_0\left(1+\rho_a\right) - ap_2^s\right)\right)^{\beta} \\ & + \rho_{21}\left(\left(p_2^c - c_1\right)\left(d_0\left(1+\rho_a\right) - ap_2^s\right)\right)^{\alpha},\end{aligned} \tag{12}$$

$$\text{s.t.}\begin{cases} \dfrac{p_2^{c*} + \widetilde{p}^{c*}}{2} \leq p_2^c \leq \widetilde{p}^{c*}, \text{if } \widetilde{p}^{c*} > {p_2}^{c*}, \\ p_2^c = \widetilde{p}^{c*}, \text{if } \widetilde{p}^{c*} \leq {p_2}^{c*}, \\ \dfrac{r_2^* + \widetilde{r}^*}{2} \leq r_2 \leq \widetilde{r}^*, \text{if } \widetilde{r}^* > r_2^*, \\ r_2 = \widetilde{r}^*, \text{if } \widetilde{r}^* \leq r_2^*, \\ p_2^s - p_2^c - r_2 - c_2 > 0, \\ d_0\left(1+\rho_a\right) - ap_2^s - \dfrac{k}{2}r_2 > 0. \end{cases} \tag{13}$$

The revised quotation given by the retailer according to the model equations (12) and (13) is $\widehat{p}_2^c, \widehat{p}_2^s, \widehat{r}_2$.

Then, the SDMS puts the latest quotation of the retailer $\widehat{p}_2^c, \widehat{p}_2^s, \widehat{r}_2$ feedback to farmers and the e-platform, and they adjust their quotation according to the following model equation (14) and model equations (15) and (16), respectively.

$$\begin{cases} \widehat{p}_1^c = \dfrac{\widehat{p}_2^c + p_1^{c*}}{2}, & \text{if } \widehat{p}_2^c < p_1^{c*}, \\ \widehat{p}_1^c = \widehat{p}_2^c, & \text{if } \widehat{p}_2^c \geq p_1^{c*}, \end{cases} \tag{14}$$

$$\begin{aligned} \max U_3 = &\left(r_3 \left(d_0 \left(1 + \rho_a \right) - a p_3^s \right) - \frac{k}{2} r_3^2 \right)^{\xi} \\ &+ \rho_{31} \left(\left(p_3^c - c_1 \right) \left(d_0 \left(1 + \rho_a \right) - a p_3^s \right) \right)^{\alpha}, \end{aligned} \tag{15}$$

$$\text{s.t.} \begin{cases} p_1^{c*} \leq p_3^c \leq \max\left(\dfrac{\widehat{p}_2^c + p_3^{c*}}{2}, \widehat{p}_2{}^c \right), \\ \min\left(\widehat{p}_2^s, p_3^{s*} \right) \leq p_3^s \leq \max\left(\widehat{p}_2^s, p_3^{s*} \right), \\ r_3^* \leq r_3 \leq \dfrac{\widehat{r}_2 + r_3{}^*}{2}, \text{if } \widehat{r}_2 < r_3^*, \\ r_3 = \widehat{r}_2, \text{if } \widehat{r}_2 \geq r_3{}^*, \\ p_3^s - p_3^c - r_3 - c_2 > 0, \\ d_0 \left(1 + \rho_a \right) - a p_3^s - \dfrac{k}{2} r_3 > 0. \end{cases} \tag{16}$$

According to the model equations (14)–(16), the revised quotation of the e-platform, that is, $\widehat{p}_3^c, \widehat{p}_3^s, \widehat{r}_3$, can be obtained.

(3) Reach a Consensus. The consensus process (1) and (2) above are repeated until a consensus is reached among the members of the supply chain, that is, $p_1^{c*} = p_2^{c*} = p_3^{c*}$, $p_2^{s*} = p_3^{s*}$, and $r_2^* = r_3^*$. Then, we can get the consensus wholesale price, sales price, and commission price of the supply chain, and the optional profits of the farmers, retailer, and e-platform, that is, v_1^*, v_2^*, v_3^*.

4. Analysis and Results

In this section, we describe the empirical application of the proposed consensus model, and discuss the influence of the empathetic preferences and the network power index power distribution on the CRP of PA-eSC.

4.1. Setup. It is supposed that the market demand of a certain agricultural product is $d_0 = 500$, and the price elasticity coefficient of agricultural products is $a = 8$. The elasticity coefficient of the service cost of the e-platform is $k = 20$, the cost of processing and selling unit agricultural products (processing, packaging, transportation, storage, and wear and tear,) is $c_2 = 2$, the unit cost of agricultural products for farmers is $c_1 = 5$, the consumer sensitivity to the e-platform services is $\lambda = 2$, and the government does not give any subsidies to the supply chain. The acceptable wholesale price of farmers satisfies $p_1^c \geq p_1^{c^\circ} = 10$, and farmers' ideal price is $p_1^{c*} = 15$. The acceptable wholesale price of the retailer satisfies $p_2^c \leq p_2^{c^\circ} = 20$. The acceptable commission price for the e-platform satisfies $r_3 \geq r_3^0 = 2$, and the wholesale price that the e-platform wants the retailer to give to the farmer satisfies $p_3^c \geq p_3^{c^\circ} = 15$.

As mentioned in the model equation (3) above, parameters α, β, ξ in the utility functions of farmers, retailers, and e-platforms satisfy $1 \geq \alpha > \beta, \xi > 0$. Although this article pays no more attention to the concave and convexity variation of utility functions, in order to reflect the utility differences of supply chain members and simultaneously not affect the analysis of proposed model, it is assumed that α, β, ξ are known constants and $\alpha = 1, \beta = 0.8, \xi = 0.9$.

In addition, we assume that the empathy degree of the retailer to farmers is $\rho_{21} = 0.1$, and the empathy degree of the e-platform to farmers is $\rho_{31} = 0.2$. We also assume that the power indices of the farmers, retailers, and e-platforms are $R_1 = 0.167, R_2 = 0.5, R_3 = 0.333$, respectively.

4.2. Results and Discussion. We analyze the pricing consensus reaching process using the proposed consensus model equations (1)-(16). The initial quotations and consensus results are shown in Table 2, and the CRP of the PA-eSC is shown in Figure 2.

As shown in Table 2, the optimal quotation agreed upon by the supply chain is $p^{c*} = 19.63, p^{s*} = 68.6, r^* = 7.49$. We can see from Figure 2 that firstly, when the wholesale price given by the retailer is greater than the minimum acceptable price of farmers, they can reach a consensus quickly, while the wholesale price still rises to a certain extent after the consensus has been reached. The main reason for this phenomenon is that the e-platform is concerned about the profits of farmers and tends to urge the retailer to give farmers higher prices. Secondly, the sales price is determined by the retailer based on its own utility maximization, and the sales price rises with the increase of the wholesale price. Moreover, in terms of the platform commission price, it is related to the service level of the platform, which is also an important factor that affects the empathy degree of consumers, and the higher the empathy degree of consumers, the stronger the willingness to buy products. Therefore, the retailer pays more attention to the service level and commission price that maximize their utility, and the consensus process of commission price in Figure 2 verifies this point: the retailer is less able to compromise on commission price.

In order to reach consensus, supply chain members may need to make a compromise, which may harm their own profits. Figure 3 shows the changes in the expected profits of the members during the CRP of supply chain. It can be seen that the expected profits of farmers gradually increased, while the profits of the retailer and the e-platform gradually decreased. This result is consistent with the empathetic preference of the retailer and the e-platform: they are concerned about the interests of farmers, and will make a compromise for farmers to obtain higher profits.

Table 2: Price quotes of farmers, retailers, and e-commerce platforms.

Members	Wholesale price p^{c*}	Sales price p^{s*}	Commission fee r^*
Farmers' initial quotation	15		
Retailer's initial quotation	6	66.04	5.59
E-commerce platform's initial quotation	42.09	58.41	14.32
SDMS' suggested quotation	20	63.1	7.47
Consensus quotation	19.63	68.6	7.49

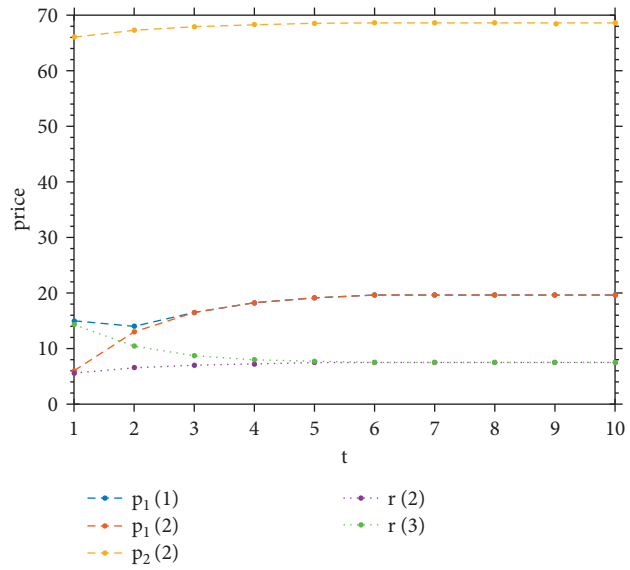

Figure 2: The consensus process of supply chain on sales price, wholesale price, and platform commission. $p_1(1)$ is the optimal wholesale price expected by farmers, $p_1(2)$ represents the wholesale price given by the retailer, $p_2(2)$ is the optimal sales price of the retailer, $r(2)$ is the commission price given by the retailer, $r(3)$ represents the optimal commission price of the platform, and t refers to the number of consultations.

It can be known from the proposed consensus model that empathetic preference and power structure have an important impact on the pricing decisions of the consumers, retailers, and e-platforms. On the one hand, the empathy degree of consumers stimulated by e-platform services level will affect the market demand of products, and thus may affect the pricing strategy of the retailer in relation to wholesale price and sales prices. The empathetic preference of the retailer and e-platform will also affect their pricing decisions based on the utility of farmers. On the other hand, in the CRP, the power structure of supply chain is an important factor affecting profit distribution. In order to make the supply chain reach a consensus as quickly as possible, the SDMS will feedback the optimal quotation according to the power of each member, and thus may affect the pricing strategy of the supply chain. To further understand the

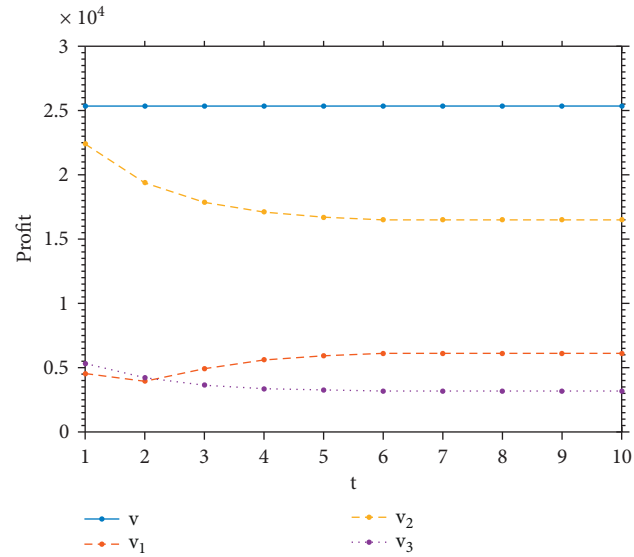

Figure 3: Changes in expected profits in the CRP of PA-eSC. v represents the maximum profit of the supply chain, v_1 is the maximum profit of farmers, v_2 is the maximum profit of the retailer, and v_3 is the maximum profit of the e-commerce platform.

influence of empathetic preferences and power structure on the consensus process, the simulation analysis is conducted as follows.

4.2.1. The Influence of Consumers' Empathy on the CRP of the PA-eSC. The impact of consumers' empathy on the CRP of supply chain is shown in Figure 4.

As shown in Figure 4, with the increase of consumers' sensitivity to the level of the e-platform service, consumers' empathy degree is also increasing. The higher the sensitivity of consumers to the service level, the more the empathy degree of consumers can be stimulated, the higher the wholesale price and the sales price, and the greater the profits that the farmers and retailers receive. On the contrary, the more sensitive consumers are to the service level, the lower the commission price, and the lower the profit earned by the e-platform. At the same time, an improvement in consumers' empathy degree will promote an increase in the overall profit of the supply chain. This shows that the more the e-platform can stimulate the consumers' empathetic preference, the more it will benefit the farmers and retailers.

4.2.2. The Influence of Empathetic Preferences of the Retailer and E-Platform. Figures 5 and 6 show the impact of empathetic preferences of the retailer and e-platform on supply chain consensus.

Firstly, it can be seen from Figure 5 that with the increase of empathy degree of the retailer and the e-platform, the wholesale price obtained by farmers gradually rises until the highest acceptable value of the retailer, and the sales price set by retailer gradually decreases. The commission price of the e-platform increases with the improvement

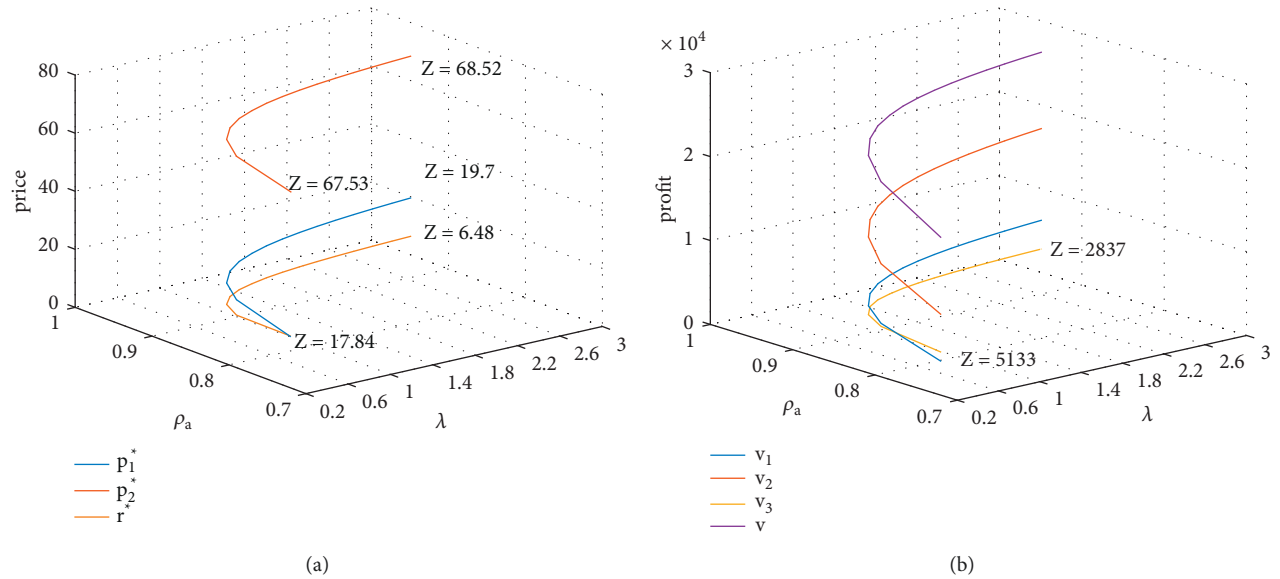

FIGURE 4: The influence of consumers' empathy on supply chain consensus. (a) The effect of empathetic preferences on the consensus prices; (b) the effect of empathetic preferences on the profits of supply chain. λ is the consumers' sensitivity coefficient of services. ρ_a is the consumers' empathy degree to farmers. p_1^*, p_2^*, r^* are the consensus wholesale prices, consensus sales price, and consensus commission price of the supply chain, respectively. v, v_1, v_2, v_3 are the total profits, farmers' profits, retailer's profits, and e-platform's profits when the supply chain reaches a consensus, respectively.

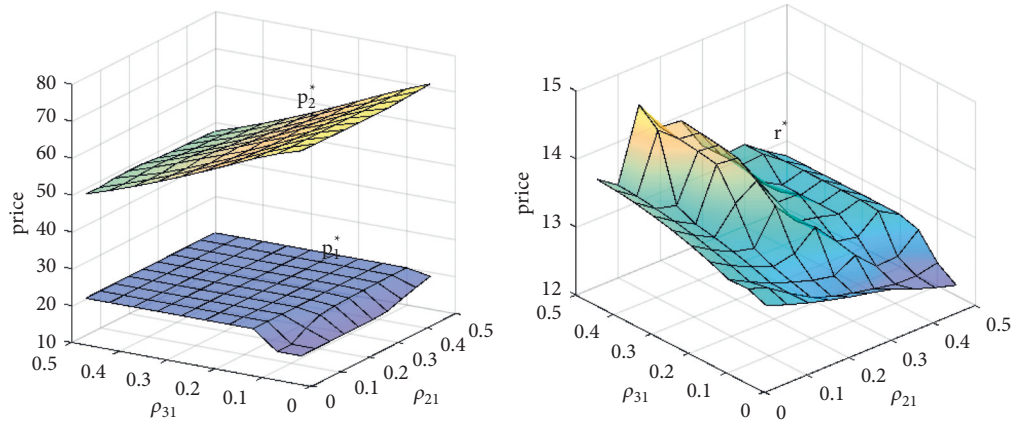

FIGURE 5: The influence of empathetic preference of retailer and e-platform on the prices. (a) The influence on wholesale price and sales price; (b) the influence on commission price. ρ_{21}, ρ_{31} are the empathy degrees of retailers and e-platforms to the farmers, respectively.

of its empathy degree, and it shows a fluctuating decrease trend with the improvement of retailer's empathy degree.

Secondly, in terms of profits, as shown in Figure 6, with the improvement of the empathy of retailer and e-platform toward farmers, the farmers' profits gradually rise and the retailer's profit gradually decrease. The profit of the e-platform increases with the improvement of its empathy degree, and decrease with the improvement of the retailer's empathy degree. This shows that the empathetic preferences of the retailer and the e-platform are helpful to the promotion of the farmers' interests. Meanwhile, the retailer's empathetic preference will reduce its own benefits, and the empathetic preference of the e-platform will help to improve its own benefits. However, in the supply chain where the retailer has a higher power, with the improvement of retailer's empathy degree, the retailer not only cares about the farmers' profits, but also tries maximizing their own benefits, causing them to control the commission price to reduce costs, which may reduce the profit of the e-platform.

Furthermore, it can be seen in Figure 7 that the improvement of retailer's empathy degree will reduce the overall profit of the supply chain, and the overall profit of the supply chain will initially increase and then decrease with the increase of the e-platform's empathy degree toward farmers. This is because when the e-platform's empathy degree toward farmers is high, the supervision intensity of the e-platforms for the

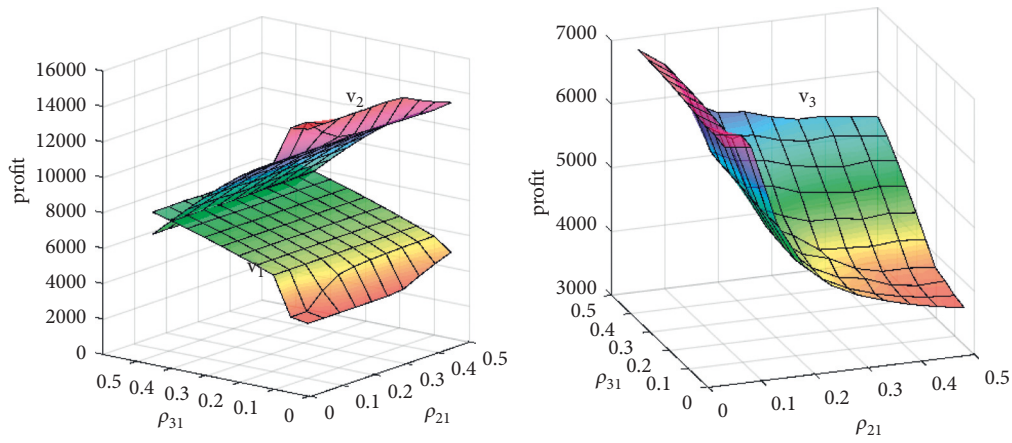

Figure 6: The influence of empathetic preferences of retailer and e-platform on the profits. (a) The impact on the profits of the farmers and the retailer; (b) the impact on the profits of e-commerce platform.

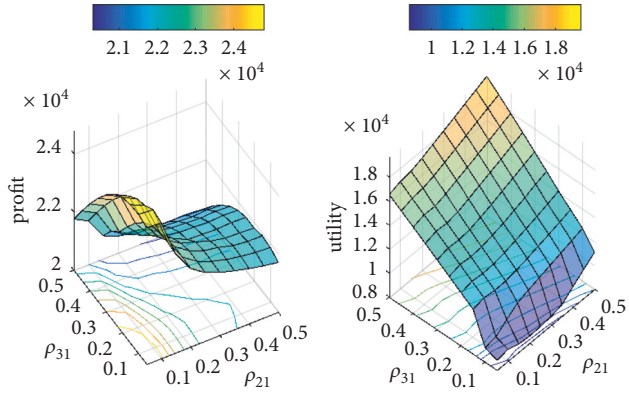

Figure 7: The influence of empathetic preferences of the retailer and the e-platform on the total profits and utility of supply chain. (a) The influence on the total profits; (b) the influence on the utility of supply chain.

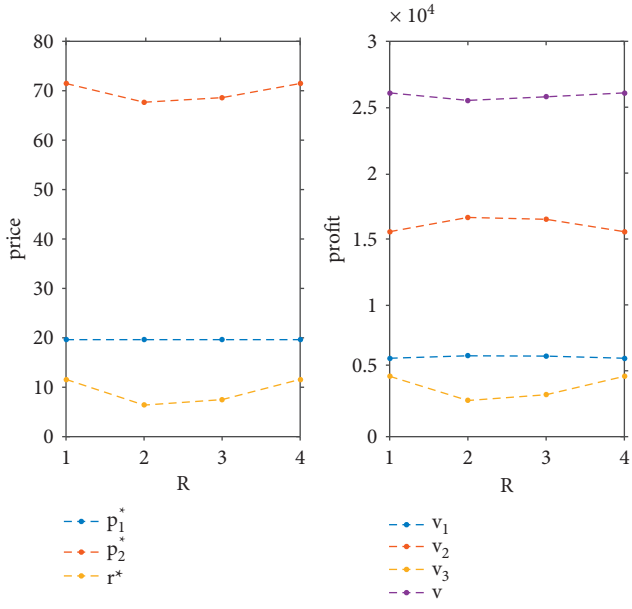

Figure 8: The influence of power structure on the supply chain pricing and profit disposition. (a) The influence on the prices; (b) the influence on the profits.

retailer is at a high level. With the increase in supervision intensity of the e-platform, the interests of farmers and e-platform is lower than the reduced interests of the retailer, resulting in a decreasing trend of the total profit of the supply chain.

4.2.3. The Influence of the Power Structure within Supply Chain on the CRP. Figure 8 shows the impact of power structure within the supply chain on pricing strategy and profit disposition, where horizontal coordinate R represents the power distribution in the supply chain, the four points represent $R = (0.05, 0.35, 0.6)$, $R = (0.05, 0.6, 0.35)$, $R = (0.167, 0.5, 0.333)$, and $R = (0.5, 0.3, 0.2)$, respectively.

The analysis results in Figure 8 show that the change in power distribution will not affect the wholesale price, but has a great impact on the sales price and the commission price of the e-platforms. The sales price and commission price are negatively correlated with the power of the retailer. The greater the power of the retailer, the lower the sales price and commission price of the product. The power of the retailer is positively correlated with the profits of farmers and retailers, and negatively correlated with the profit of e-platform. At the same time, the total profit of the supply chain is negatively correlated with the power of the retailer, and decreases with the growth in power of the retailer.

5. Conclusions

This article proposed a consensus model of the PA-eSC considering the empathetic preference and power structure, and analyzed the influence of empathetic preference and power structure on pricing decisions concerning agricultural products, the income of supply chain entities, and the CRP. The major findings are as follows.

Firstly, consumers' empathy increases the wholesale price and sales price of products. Consumers' empathy has a positive impact on the demand for products, and increases the profits of farmers, retailers, and the supply chain.

Secondly, the wholesale price increases with the improvement of retailers' and e-platforms' empathy to

farmers, but the sales price is the opposite, and commission prices rise with an increase in the e-platforms' empathy. The empathetic preference of retailers will reduce their own profit and the overall profit of the supply chain, while the empathetic preference of e-platforms will help to improve their own profit, and will increase the overall profit of the supply chain at first, before decreasing.

Moreover, the sales price and commission price are negatively correlated with the power of retailer, but the wholesale price is not related to the change in power distribution. The power of retailers is positively correlated with the profits of farmers and retailers, and negatively correlated with the profits of e-platforms and the supply chain.

The conclusions bring various managerial insights to the PA-eSC stakeholders. Firstly, a straightforward managerial insight is that empathetic preferences of consumers have positive impacts on improving the supply chain profits and system efficiency. Therefore, farmers, retailers, and e-platforms should pay attention to the marketing planning and service levels, and improve consumers' empathy for all aspects. In doing this, consumers' purchasing desires can be enhanced, and the profits of supply chain can be increased. Secondly, e-platforms that sell agricultural products should improve the quality of online sales services, strengthen cooperation with retailers and pay appropriate attention to the profits of farmers, but not apply too much interest concessions pressure to retailers because of the empathy to farmers. In this way, it is possible to stabilise and expand the market, and realize the promotion of the overall profit of the supply chain. Moreover, retailers should properly respect the voice of e-platforms and farmers in order to achieve the overall profit growth of the supply chain in the actual supply chain management.

This study has several limitations. First, this research model only considers retailers' and e-platforms' empathy toward farmers, but there is also empathy between retailers and e-platforms in practice, so the empathetic preferences for the supply chain needs further exploration. Moreover, this study only considers the e-commerce supply chain. Further exploration of empathetic preferences in dual-channel supply chains will make the research conclusions on the empathetic preferences more realistic and meaningful.

Data Availability

No data were used to support this study.

Conflicts of Interest

The authors declare that there are no conflicts of interest regarding the publication of this paper.

Acknowledgments

This research was funded by the National Natural Science Foundation of China (grant number 71871150) and the Education Science Planning Project of Chongqing (grant number 2021-GX-056, 2021-GX-058). This work was also funded by Research Foundation of Chongqing University of Science and Technology.

References

[1] M. S. Sodhi and C. S. Tang, "Supply chain research opportunities with the poor as suppliers or distributors in developing countries," *Production and Operations Management*, vol. 23, no. 9, pp. 1483–1494, 2014.

[2] C. N. Liao and Y. J. Chen, "Farmers' information management in developing countries —a highly asymmetric information structure," *Production and Operations Management*, vol. 26, no. 6, pp. 1207–1220, 2017.

[3] X. Li and L. Li, "Evaluation of China's targeted poverty alleviation policies: a decomposition analysis based on the poverty reduction effects," *Sustainability*, vol. 13, no. 21, pp. 1–17, 2021.

[4] A. Abid and S. Jie, "Impact of COVID-19 on agricultural food: a strengths, weaknesses, opportunities, and threats (SWOT) analysis," *Food Frontiers*, vol. 2, no. 4, pp. 396–406, 2021.

[5] S. L. Golicic, D. F. Davis, T. M. Mccarthy, and J. T. Mentzer, "The impact of e-commerce on supply chain relationships," *International Journal of Physical Distribution & Logistics Management*, vol. 32, no. 10, pp. 851–871, 2002.

[6] A. W. Siddiqui and S. A. Raza, "Electronic supply chains: status & perspective," *Computers & Industrial Engineering*, vol. 88, pp. 536–556, 2015.

[7] Y. Wang and Z. Yu, "Decisions of hybrid supply chain considering internet platform service and differences in customer demand," *Systems Engineering-Theory & Practice*, vol. 38, no. 6, pp. 1465–1478, 2018.

[8] K. H. Leung, K. L. Choy, P. K. Siu, G. Ho, H. Y. Lam, and C. K. Lee, "A B2C e-commerce intelligent system for re-engineering the e-order fulfilment process," *Expert Systems with Applications*, vol. 91, pp. 386–401, 2018.

[9] K. Shi, F. Jiang, and Q. Ouyang, "Altruism and pricing strategy in dual-channel supply *chains*"," *American Journal of Operations Research*, vol. 03, no. 4, pp. 402–412, 2013.

[10] P. He, J. Wen, S. Ye, and Z. Li, "Logistics service sharing and competition in a dual-channel e-commerce supply chain," *Computers & Industrial Engineering*, vol. 149, no. 2, Article ID 106849, 2020.

[11] Y. Wang, R. Fan, L. Shen, and M. Jin, "Decisions and coordination of green e-commerce supply chain considering green manufacturer's fairness concerns," *International Journal of Production Research*, vol. 58, no. 24, pp. 7471–7489, 2020.

[12] Q. Han, Y. Wang, L. Shen, and W. Dong, "Decision and coordination of low-carbon e-commerce supply chain with government carbon subsidies and fairness concerns," *Complexity*, vol. 2020, no. 8, pp. 1–19, Article ID 1974942, 2020.

[13] Y. Dong, M. Zhan, G. Kou, Z. Ding, and H. Liang, "A survey on the fusion process in opinion dynamics," *Information Fusion*, vol. 43, pp. 57–65, 2018.

[14] Y. W. Du, Q. Chen, Y. L. Sun, and C. H. Li, "Knowledge structure-based consensus-reaching method for large-scale multiattribute group decision-making," *Knowledge-Based Systems*, vol. 219, no. 1, Article ID 106885, 2021.

[15] W. Güth and R. Tietz, "Ultimatum bargaining behavior: a survey and comparison of experimental results," *Journal of Economic Psychology*, vol. 11, no. 3, pp. 417–449, 1990.

[16] M. A. Nowak, K. M. Page, and K. Sigmund, "Fairness versus reason in the ultimatum game," *Science*, vol. 289, no. 5485, pp. 1773–1775, 2000.

[17] H. Richard, *Thaler, "Misbehaving: The Making of Behavioral Economics*, W. W. Norton & Company, New York, NY, USA, 2016.
[18] A. Salehi-Abari and C. Boutilier, *Empathetic Social Choice on Social Networks*, pp. 693–700, International Foundation for Autonomous Agents and Multiagent Systems, Richland, 2014.
[19] K. M. Page and M. A. Nowak, "Empathy leads to fairness," *Bulletin of Mathematical Biology*, vol. 64, no. 6, pp. 1101–1116, 2002.
[20] A. Edele, I. Dziobek, and M. Keller, "Explaining altruistic sharing in the dictator game: the role of affective empathy, cognitive empathy, and justice sensitivity," *Learning and Individual Differences*, vol. 24, pp. 96–102, 2013.
[21] M. R. Andreychik and N. Migliaccio, "Empathizing with others' pain versus empathizing with others' joy: examining the separability of positive and negative empathy and their relation to different types of social behaviors and social emotions," *Basic and Applied Social Psychology*, vol. 37, no. 5, pp. 274–291, 2015.
[22] J. Gao, H. Han, L. Hou, and H. Wang, "Pricing and effort decisions in a closed-loop supply chain under different channel power structures," *Journal of Cleaner Production*, vol. 112, no. 3, pp. 2043–2057, 2016.
[23] R. Shi, J. Zhang, and J. Ru, "Impacts of power structure on supply chains with uncertain demand," *Production and Operations Management*, vol. 22, no. 5, pp. 1232–1249, 2013.
[24] K. Kang, M. Wang, and X. Luan, "Decision-making and coordination with government subsidies and fairness concerns in the poverty alleviation supply chain," *Computers & Industrial Engineering*, vol. 152, no. 9, Article ID 107058, 2021.
[25] T. H. Ho and J. Zhang, "Designing pricing contracts for boundedly rational customers: does the framing of the fixed fee matter?" *Management Science*, vol. 54, no. 4, pp. 686–700, 2008.
[26] E. Katok, T. Olsen, and V. Pavlov, "Wholesale pricing under mild and privately known concerns for fairness," *Production and Operations Management*, vol. 23, no. 2, pp. 285–302, 2014.
[27] K. Zhang, "Analysis on closed-loop supply chain decision under the reciprocal preference," *Journal of Control and Decision*, vol. 09, pp. 184–189, 2015.
[28] Y. Wang, Z. Yu, M. Jin, and J. Mao, "Decisions and coordination of retailer-led low-carbon supply chain under altruistic preference," *European Journal of Operational Research*, vol. 293, no. 3, pp. 910–925, 2021.
[29] Y. Wang, Z. Yu, L. Shen, and W. Dong, "Impacts of altruistic preference and reward-penalty mechanism on decisions of E-commerce closed-loop supply chain," *Journal of Cleaner Production*, vol. 315, Article ID 128132, 2021.
[30] S. S. Sana, "Price competition between green and non green products under corporate social responsible firm," *Journal of Retailing and Consumer Services*, vol. 55, Article ID 102118, 2020.
[31] S. S. Sana, "A structural mathematical model on two echelon supply chain system," *Annals of Operations Research*, no. 1, pp. 1–29, 2021.
[32] J. F. Gaski and J. R. Nevin, "The differential effects of exercised and unexercised power sources in a marketing channel," *Journal of Marketing Research*, vol. 22, no. 2, p. 130, 1985.
[33] X. Chen and X. Wang, "Free or bundled: channel selection decisions under different power structures," *Omega*, vol. 53, pp. 11–20, 2015.
[34] X. Chen, X. Wang, and X. Jiang, "The impact of power structure on the retail service supply chain with an O2O mixed channel," *Journal of the Operational Research Society*, vol. 67, no. 2, pp. 294–301, 2016.
[35] Z. Sun, X. Wang, J. Ruan, and W. Fan, "Impact of different game power structures on the manufacturer dual-channel supply chain," *Operations Research and Management Science*, vol. 29, no. 9, pp. 106–114, 2020.
[36] X. Cao and X. Liu, "Research on the decision-making of dual-channel supply chain considering advance selling under different power Structures," *Operations Research and Management Science*, vol. 30, no. 09, pp. 93–99, 2021.
[37] M. Xue and J. Zhang, "Impacts of heterogeneous environment awareness and power structure on green supply chain," *RAIRO - Operations Research*, vol. 52, no. 1, pp. 143–157, 2018.
[38] I. E. Nielsen, S. Majumder, S. S. Sana, and S. Saha, "Comparative analysis of government incentives and game structures on single and two-period green supply chain," *Journal of Cleaner Production*, vol. 235, pp. 1371–1398, 2019.
[39] T. Besley and R. Kanbur, "Food subsidies and poverty alleviation," *The Economic Journal*, vol. 98, no. 392, pp. 701–719, 1988.
[40] X. Yuanchang and J. Jiyu, "The optimal boundary of political subsidies for agricultural insurance in welfare economic prospect," *Agriculture and Agricultural Science Procedia*, vol. 1, pp. 163–169, 2010.
[41] K. Kang, X. Luan, W. Shen, Y. Ma, and X. Wei, "The strategies of the poverty-alleviation supply chain with government subsidies and cost sharing: government-led or market-oriented?" *Sustainability*, vol. 12, no. 10, pp. 1–24, 2020.
[42] Y. Zhou, D. Zheng, and X. Ye, "Decision making and contract coordination of three-level agricultural products supply chain with consumer poverty alleviation preference," *Control and Decision*, vol. 35, no. 11, pp. 2589–2598, 2020.
[43] L. Li, K. Du, W. Zhang, and J. Y. Mao, "Poverty alleviation through government-led e-commerce development in rural China: an activity theory perspective," *Information Systems Journal*, vol. 29, no. 4, pp. 914–952, 2019.
[44] C. Peng, B. Ma, and C. Zhang, "Poverty alleviation through e-commerce: village involvement and demonstration policies in rural China," *Journal of Integrative Agriculture*, vol. 20, no. 4, pp. 998–1011, 2021.
[45] X. Wan, Q. Wang, Q. Meng, and D. Y Wei, "Smart supply chain decision and coordination strategy considering poverty alleviation concern based on manufacture diseconomies of scale," *Chinese Journal of Management Science*, vol. 28, no. 2, pp. 153–165, 2020.
[46] X. Wan and X. Qie, "Poverty alleviation ecosystem evolutionary game on smart supply chain platform under the government financial platform incentive mechanism," *Journal of Computational and Applied Mathematics*, vol. 372, Article ID 112595, 2020.

Hindawi
Complexity
Volume 2022, Article ID 7257449, 16 pages
https://doi.org/10.1155/2022/7257449

Research Article

Analysis of Cryptocurrency Market by Using q-Rung Orthopair Fuzzy Hypersoft Set Algorithm Based on Aggregation Operators

Salma Khan,[1] **Muhammad Gulistan**,[1] **Nasreen Kausar**,[2] **Sajida Kousar**,[3] **Dragan Pamucar**,[4] **and Gezahagne Mulat Addis**[5]

[1]*Department of Mathematics and Statistics, Hazara University Mansehra, Mansehra, Pakistan*
[2]*Department of Mathematics, Faculty of Arts and Sciences, Yildiz Technical University, Esenler 34210, Istanbul, Turkey*
[3]*Department of Mathematics and Statistics, International Islamic University Islamabad, Islamabad, Pakistan*
[4]*Faculty of Organizational Sciences, University of Belgrade, Belgrade, Serbia*
[5]*Department of Mathematics, University of Gondar, P.O. Box: 196, Gondar, Ethiopia*

Correspondence should be addressed to Gezahagne Mulat Addis; gezahagne412@gmail.com

Received 2 May 2022; Accepted 25 May 2022; Published 13 July 2022

Academic Editor: Yu Zhou

One of the most important innovations brought by digitization is the cryptocurrency, also called virtual or digital currency, which has been discussed in recent years and in particular is a new platform for investors. Different types of cryptocurrencies such as Bitcoin, Ethereum, Binance Coin, and Tether do not depend on a central authority. Decision making is complicated by categorization and transmission of uncertainty, as well as verification of digital currency. The weighted average and weighted geometric aggregation operators are used in this article to define a multi-attribute decision-making approach. This work investigates the uniqueness of q-rung orthopair fuzzy hypersoft sets (q-ROFHSS), which respond to instabilities, uncertainty, ambiguity, and imprecise information. This research also covers some fundamental topics of q-ROFHSS. The model offered here is the best option for learning about electronic currency. This study validates the complexity of decision-making problems with different attributes and subattributes to obtain an optimal choice. We conclude that Bitcoin has a diverse set of applications and that crypto assets are well positioned to become an important asset class in decision making.

1. Introduction

The concept of cryptocurrency has been widely used in the past. Cryptocurrencies are also known as digital currencies that use encryption for transaction verification. In 2009, Satoshi Nakamoto [1] generated a cryptocurrency to be a peer-to-peer electronic cash transaction. As a result, the first cryptocurrency, Bitcoin, was founded in 2009. Cryptocurrencies are digital currencies that use the cryptographic approach and are based on blockchain technology [2]. With exponential changes in the cryptocurrency market, buying or selling a cryptocurrency is a difficult task in the online market. To cope with this, we need to analyze the cryptocurrency market by decision-making problem. The process of selecting the best options from a dataset is known as decision making. To make the right decision, several researchers have given a number of concepts. Decisions were developed at the beginning of the era on the basis of accurate numerical datasets, but this resulted in insufficient conclusions that were less applicable to real circumstances. Many researchers used different decision-making models in some branches of mathematics, statistics, and artificial intelligence. According to Urquhart [3], trading activity and significant volatility draw people's attention to Bitcoin. However, it noted that no meaningful results for anticipating volatility could be found via online searches. However, David et al. [4]. worked on the feedback cycles between the socio-eooi signals in the bitcoin economy. And the used vector autoregression to identify two positive feedback loops. In 2020, Ramadani and Devianto [5] developed the forecasting model of Bitcoin price with fuzzy time series Markov chain and Chen logical method. Fuzzy time series can model various types of time series data pattern

because this method is free from classical assumption. In the field of fuzzy set theory, Jana et al. [6] developed a dynamic decision-making method based on aggregation operators in complex q-rung orthopair fuzzy environment. In 2022, Palanikumar et al. [7] also developed multi-attribute decision-making problems based on aggregation operators by using Pythagorean neutrosophic normal interval-valued fuzzy sets. After the classical notion of set, Zadeh [8] proposed fuzzy set theory. Bhattacharya and Mukherjee [9] worked on fuzzy set and developed fuzzy relations and fuzzy groups. Yager and Filev [10, 11] in 1994 using fuzzy set developed aggregation operators, fuzzy models, and formal structures. In 1999, Demirci [12] introduced fuzzy functions and their fundamental properties. Atanassov [13] proposed intuitionist fuzzy sets with the condition that the total of these two grades should not exceed unity. In some cases, the sum of membership grade and non-membership grade is greater to one, then intuitionistic fuzzy sets did not completely fulfill this condition. (e.g. $.9 + .6 > 1$), hence intuitionistic fuzzy sets fail. Yager [14] proposed Pythagorean fuzzy sets, an extended version of intuitionist fuzzy sets in which the square sum of the MM and non-membership grades is less than or equal to one. As in the previous study, linear inequalities between membership and non-membership grades are explored. If the decision maker increases the power to 2, however, $.9^2 + .8^2 \not\leq 1$ is obtained, suggesting that the Pythagorean fuzzy set theory is also erroneous. Ali et al. [15] used complex interval-valued Pythagorean fuzzy set in green supplier chain management. Ashraf et al. [16] introduced interval-valued picture fuzzy Maclaurin symmetric mean operator as application in decision-making problem. In the instance of q-rung orthopair fuzzy set (q-ROFS) [17–19], the conditions on membership function and non-membership functions are changed to $0 \leq u^q + v^q \leq 1\,(q \geq 1)$. Even for very large values of "q," we can treat the membership and non-membership grades independently to some extent. As a result, q-ROF set has more ability in terms of processing ambiguous data than intuitionistic and Pythagorean fuzzy set. These theories, on the other hand, are unable to account for the parametric values of the alternatives. Molodtsov [20] presented the concept of soft set theory for dealing with unpredictability in a parametric way in order to overcome these restrictions. He identified some mathematical representations and proposed a soft set theory for solving problems. By using the concepts of soft set, Cagman et al. [21] introduced fuzzy soft sets and also created fuzzy aggregation operators and applied them to real-world applications. Using the soft set scheme, Maji [22, 23] created a fuzzy soft set theory and a neutrosophic soft set theory. The previous study focused only on data gaps caused by membership and non-membership values. These assumptions, on the other hand, are unable to cope with the overall inconsistency and inaccuracy of the data. Previous theories fail to handle such situations when characteristics of a group of parameters contain additional subattributes. In order to overcome the restriction indicated above, Smarandache [24] introduced the hypersoft set theme by using the soft set concept. The basics of the hypersoft set, such as complement, non-set, hypersoft subset, and aggregation operators, were then presented by Saeed et al. [25]. Several scholars have looked into different operators and features under the hypersoft set and its expansions [26–30]. The theme of the fuzzy intuitionistic soft set was then extended and a new theme of the intuitionistic fuzzy hypersoft set was established, as well as aggregation operators for solving MADM problems by Zulqarnain [31].

Motivation. The modeling of the decision-making problems requires deep importance on the attributes, and we cannot directly consider or neglect any attribute without considering its importance. In order to deal with more attributes, it is a dire need to get the benefit of the theory hypersoft set (HSS). Since hypersoft sets deals with attributes and subattributes, while soft theory deals only with attributes, and fuzzy hypersoft sets deal with attributes and sub attributes in an uncertain way. So, that is why we choose the field of hypersoft set theory by considering the nature of subattributes. The main goal of our research is to develop a novel aggregation operator for a q-rung orthopair fuzzy hypersoft environment. We have also created an algorithm to explain multi-criteria decision-making situations, as well as a numerical example to show how the suggested technique works in the q-ROFHS context. In the digital market, the selection and evaluation of cryptocurrency is a vital procedure. As a result, more studies using MCDM approaches in the selection of cryptocurrencies are needed to accurately capture the uncertainty of the cryptocurrency market data as well as that of the manufacturer of decision preferences. We propose some operational principles based on the decision formula in terms of q-ROFH set. We then create two aggregation operators, the q-ROFHWA and q-ROFHWG operators, using operational principles. Score and accuracy functions are also provided to compare the q-ROFH set. To handle decision-making concerns, the algorithm's rule is proposed with the help of the proposed operators. Finally, a numerical example is provided to show the method's efficiency.

2. Materials and Methods

This section collects some fundamental elements that will contribute to the compilation of the remaining part of the article: soft set, hypersoft set, and q-rung orthopair fuzzy hypersoft set and their example.

Definition 1 (see [20]). Let $\mathbb{S}$ be a set of discourse with attributive set E, and $\overline{\overline{\alpha}} \subseteq E$. A pair $(\hookleftarrow_\rho, \overline{\overline{\alpha}})$ is called soft set over $\mathbb{S}$, where $\hookleftarrow_\rho$ is a function such that $\hookleftarrow_\rho : \overline{\alpha} \longrightarrow P^{\mathbb{S}}$ and $P^{\mathbb{S}}$ represents the family of all possible subsets of $\mathbb{S}$. A pair $(\hookleftarrow_\rho, \overline{\overline{\alpha}})$ can be defined as $(\hookleftarrow_\rho, \overline{\overline{\alpha}}) = \{\langle e, \hookleftarrow_\rho(e)\rangle | e \in \overline{\overline{\alpha}}, \hookleftarrow_\rho(e) \in F^{\mathbb{S}}\}$.

Definition 2 (see [24]). Let $\mathbb{S}$ be a universal set with n distinct attributive sets $a_1, a_2, a_3, \ldots, a_{\ddot{n}}$, whose attributive value belong to the sets $\overline{\alpha}_1, \overline{\alpha}_2, \ldots, \overline{\alpha}_{\ddot{n}}$, respectively, such that $\overline{\alpha}_i \cap \overline{\alpha}_j = \phi$, for all $i, j \in \{1, 2, \ldots, n\}$. A pair $(\hookleftarrow_\rho, \overline{\overline{\alpha}})$ is called hypersoft set over $\mathbb{S}$, where $\hookleftarrow_\rho$ is a function such that $\hookleftarrow_\rho : \overline{\overline{\alpha}} \longrightarrow P(U)$ and $\overline{\overline{\alpha}} = \overline{\alpha}_1 \times \overline{\alpha}_2 \times \ldots, \times \overline{\alpha}_{\ddot{n}}$. A pair $(\hookleftarrow_\rho, \overline{\overline{\alpha}})$ can be defined as $(\hookleftarrow_\rho, \overline{\overline{\alpha}}) = \{\langle \overline{\overline{\alpha}}, \hookleftarrow_\rho(\overline{\aleph})\rangle | \overline{\overline{\alpha}} \in \overline{\overline{\alpha}}, \hookleftarrow_\rho(\overline{\aleph}) \in P(U)\}$.

Definition 3 (see [32]). Let Ⓢ be universal set and a_1, a_2, a_3, ..., a_n be n distinct attributes concerning Ⓢ whose corresponding attributive values are members of the sets $\overline{\wedge}_1, \overline{\wedge}_2, \ldots, \overline{\wedge}_{\ddot{n}}$, respectively, such that $\overline{\wedge}_i \cap \overline{\wedge}_j = \phi$, where $i = j$ for each $n > 1$ and $i, j \in \{1, 2, ..., n\}$. A pair $(\leftrightarrow\!\!\!\!\rho, \overline{\overline{\wedge}})$ is called q-ROFHS set, where $\leftrightarrow\!\!\!\!\rho$ is a mapping $\leftrightarrow\!\!\!\!\rho: \overline{\overline{\wedge}} \longrightarrow q - ROFS^{(Ⓢ)}$ and $\overline{\wedge}_1 \times \overline{\wedge}_2 \times \cdots \times \overline{\wedge}_{\ddot{n}} = \overline{\overline{\wedge}} = \{k_1, k_2, \ldots, k_{\ddot{n}}\}$ is a family of subparameters. A pair $(\leftrightarrow\!\!\!\!\rho, \overline{\overline{\wedge}})$ can be expressed as $(\leftrightarrow\!\!\!\!\rho, \overline{\overline{\wedge}}) = \{(\overline{\propto}, \leftrightarrow\!\!\!\!\rho_{\overline{\overline{\wedge}}}(\overline{\aleph})): \overline{\propto} \in \overline{\overline{\wedge}}, \leftrightarrow\!\!\!\!\rho_{\overline{\overline{\wedge}}}(\overline{\aleph}) \in q - ROFS^{Ⓢ} \in 0, 1\}$, where $\leftrightarrow\!\!\!\!\rho_{\overline{\overline{\wedge}}}(\overline{\aleph}) = \{\langle \ddot{y}, \curvearrowright_{\overline{\overline{\wedge}}(\overline{\aleph})}(\ddot{y}), \ddot{\curvearrowright}_{\overline{\overline{\wedge}}(\overline{\aleph})}(\ddot{y})\rangle | \ddot{y} \in Ⓢ \text{ and } q \geq 1\}$. Here $\curvearrowright$ and $\ddot{\curvearrowright}$ represent membership and non-membership functions with the restriction $0 \leq (\curvearrowright_{\overline{\overline{\wedge}}(\overline{\aleph})}(\ddot{y}))^q + (\ddot{\curvearrowright}_{\overline{\overline{\wedge}}(\overline{\aleph})}(\ddot{y}))^q \leq 1$ and $q \geq 1$, where $q - ROFHSN$ can be expressed as $(\leftrightarrow\!\!\!\!\rho, \overline{\overline{\wedge}}) = (\curvearrowright_{\overline{\overline{\wedge}}(\overline{\aleph}_{ij})}, \ddot{\curvearrowright}_{\overline{\overline{\wedge}}(\overline{\aleph}_{ij})})$.

Example 1. Let $Ⓢ = \{y_1, y_2, y_3, y_4\}$ be the set of four houses under consideration say Ⓢ and also consider the set of attributes as

(i) $\top_1$ represents location of the house.

(ii) $\top_2$ represents the price of the house.

(iii) $\top_3$ represents number of bedrooms in the house.

Also, $\top_1 = \{\natural_{11} = \text{the proximity of important services}, \natural_{12} = \text{resale value in future}, \natural_{13} = \text{lifestyle}\}$, $\top_2 = \{\natural_{21} = 5,000,000, \natural_{22} = 8,000,000\}$, $\top_3 = \{\natural_{31} = 5, \natural_{32} = 4\}$ are sets of corresponding parameters. Suppose $\overline{\wedge}_1 = \{\natural_{11}, \natural_{12}\}, \overline{\wedge}_2 = \{\natural_{21}\}, \overline{\wedge}_3 = \{\natural_{31}, \natural_{32}\}$, and $B_1 = \{\natural_{11}\}, B_2 = \{\natural_{21}, \natural_{22}\}, B_3 = \{\natural_{31}, \natural_{32}\}$ are subsets of $\top_i$ for $i = 1, 2, 3$. Then, $\overline{\overline{\wedge}} = \top_1 \times \top_2 \times \top_3$ will contain elements with three tuples, and we will assume $q = 5$:

$$\begin{aligned}
&\overline{\overline{\wedge}} = \{\overline{\aleph}_1, \overline{\aleph}_2, \overline{\aleph}_3, \overline{\aleph}_4, \overline{\aleph}_5, \overline{\aleph}_6, \overline{\aleph}_7, \overline{\aleph}_8, \overline{\aleph}_9, \overline{\aleph}_{10}, \overline{\aleph}_{11}, \overline{\aleph}_{12}\},\\
&\overline{\aleph}_1 = (\natural_{11}, \natural_{21}, \natural_{31}), \overline{\aleph}_2 = (\natural_{11}, \natural_{21}, \natural_{32}), \overline{\aleph}_3 = (\natural_{11}, \natural_{22}, \natural_{31}), \overline{\aleph}_4 = (\natural_{11}, \natural_{22}, \natural_{32}),\\
&\overline{\aleph}_5 = (\natural_{12}, \natural_{21}, \natural_{31}), \overline{\aleph}_6 = (\natural_{12}, \natural_{21}, \natural_{32}), \overline{\aleph}_7 = (\natural_{12}, \natural_{22}, \natural_{31}), \overline{\aleph}_8 = (\natural_{12}, \natural_{22}, \natural_{32}),\\
&\overline{\aleph}_9 = (\natural_{13}, \natural_{21}, \natural_{31}), \overline{\aleph}_{10} = (\natural_{13}, \natural_{21}, \natural_{32}), \overline{\aleph}_{11} = (\natural_{13}, \natural_{22}, \natural_{31}), \overline{\aleph}_{12} = (\natural_{13}, \natural_{22}, \natural_{32}).
\end{aligned} \tag{1}$$

Suppose

$$\begin{aligned}
&\overline{\aleph}_1 = (\natural_{11}, \natural_{21}, \natural_{31}),\\
&\overline{\aleph}_2 = (\natural_{11}, \natural_{21}, \natural_{32}),\\
&\overline{\aleph}_3 = (\natural_{12}, \natural_{21}, \natural_{31}),\\
&\overline{\aleph}_4 = (\natural_{12}, \natural_{21}, \natural_{32}),\\
&\overline{b}_1 = (\natural_{11}, \natural_{21}, \natural_{31}),\\
&\overline{b}_2 = (\natural_{11}, \natural_{21}, \natural_{32}),\\
&\overline{b}_3 = (\natural_{11}, \natural_{22}, \natural_{31}),\\
&\overline{b}_4 = (\natural_{11}, \natural_{22}, \natural_{32}).
\end{aligned} \tag{2}$$

Then, $(\leftrightarrow\!\!\!\!\rho, \overline{\overline{\wedge}})$ and $(\nrightarrow, \overline{\beta} * * *)$, two q-ROFHS sets, may be expressed as

$$\begin{aligned}
(\leftrightarrow\!\!\!\!\rho, \overline{\overline{\wedge}}) &= \left\{\begin{array}{l} c\langle \overline{\aleph}_1, \{(y_1, (.6, .8)), (y_2, (.7, .9)), (y_3, (.8, .6)), (y_4, (.5, .9))\}\rangle \\ \langle \overline{\aleph}_2, \{(y_1, (.5, .8)), (y_2, (.7, .6)), (y_3, (.9, .5)), (y_4, (.9, .8))\}\rangle \\ \langle \overline{\aleph}_3, \{(y_1, (.6, .8)), (y_2, (.7, .6)), (y_3, (.7, .9)), (y_4, (.6, .9))\}\rangle \\ \langle \overline{\aleph}_4, \{(y_1, (.9, .7)), (y_2, (.9, .7)), (y_3, (.7, .8)), (y_4, (.8, .9))\}\rangle \end{array}\right\},\\
(\nrightarrow, \overline{\beta}) &= \left\{\begin{array}{l} c\langle \overline{b}_1, \{(y_1, (.9, .7)), (y_2, (.8, .9)), (y_3, (.7, .9)), (y_4, (.8, .7))\}\rangle \\ \langle \overline{b}_2, \{(y_1, (.7, .8)), (y_2, (.7, .8)), (y_3, (.9, .8)), (y_4, (.9, .7))\}\rangle \\ \langle \overline{b}_3, \{(y_1, (.9, .8)), (y_2, (.8, .9)), (y_3, (.7, .8)), (y_4, (.8, .9))\}\rangle \\ \langle \overline{b}_4, \{(y_1, (.7, .9)), (y_2, (.8, .9)), (y_3, (.9, .8)), (y_4, (.9, .7))\}\rangle \end{array}\right\}.
\end{aligned} \tag{3}$$

Tables 1 and 2 show the tabular forms of q-ROFHS values.

Definition 4. For two q-ROFHS sets $(\leftarrow\!\!\rho, \overline{\overline{\kappa}})$ and $(\leftarrow\!\!\rho, \overline{\overline{\beta}})$ by a universe of discourse $\textcircled{s}$, we define $(\leftarrow\!\!\rho, \overline{\overline{\kappa}})$ as a q-ROFHS subset of $(\leftarrow\!\!\rho, \overline{\overline{\beta}})$, defined as $(\leftarrow\!\!\rho, \overline{\overline{\kappa}})\widetilde{\subseteq}(\leftarrow\!\!\rho, \overline{\overline{\beta}})$, if the following hold.

(1) $\overline{\overline{\kappa}} \subseteq \overline{\overline{\beta}}$.

(2) For any $\overline{\overline{\alpha}} \in \overline{\overline{\kappa}}$, $\leftarrow\!\!\rho(\overline{\overline{\kappa}}) \subseteq \leftarrow\!\!\rho(\overline{\overline{b}})$.

Example 2. In Example 1, we consider these parameters and assume that $(\leftarrow\!\!\rho, \overline{\overline{\kappa}})$ and $(\leftarrow\!\!\rho, \overline{\overline{\beta}})$ are two q-ROFHS sets on $Y = \{y_1, y_2, y_3, y_4\}$. Tabular forms of $(\leftarrow\!\!\rho, \overline{\overline{\kappa}})$ and $(\leftarrow\!\!\rho, \overline{\overline{\beta}})$ are provided in Tables 3 and 4.

It is clear that $(\leftarrow\!\!\rho, \overline{\overline{\kappa}}) \subseteq (\leftarrow\!\!\rho, \overline{\overline{\beta}})$.

Table 1: q-ROFHS values.

$(\leftarrow\!\!\rho, \overline{\overline{\kappa}})$	y_1	y_2	y_3	y_4
$(\natural_{11}, \natural_{21}, \natural_{31})$	(.6, .8)	(.7, .9)	(.8, .6)	(.5, .9)
$(\natural_{11}, \natural_{21}, \natural_{32})$	(.5, .8)	(.7, .6)	(.9, .5)	(.9, .8)
$(\natural_{12}, \natural_{21}, \natural_{31})$	(.6, .8)	(.7, .6)	(.7, .9)	(.6, .9)
$(\natural_{12}, \natural_{21}, \natural_{32})$	(.9, .7)	(.9, .7)	(.7, .8)	(.8, .9)

Table 2: q-ROFHS values.

$(\leftarrow\!\!\rho, \overline{\overline{\beta}})$	y_1	y_2	y_3	y_4
$(\natural_{11}, \natural_{21}, \natural_{31})$	(.9, .7)	(.8, .9)	(.7, .9)	(.8, .7)
$(\natural_{11}, \natural_{21}, \natural_{32})$	(.7, .8)	(.7, .8)	(.9, .8)	(.9, .7)
$(\natural_{12}, \natural_{21}, \natural_{31})$	(.9, .8)	(.8, .9)	(.7, .8)	(.8, .9)
$(\natural_{12}, \natural_{21}, \natural_{32})$	(.7, .9)	(.8, .9)	(.9, .8)	(.9, .7)

3. Aggregation Operators

The score and accuracy function for q-ROFHSNs are discussed in this part, as well as q-ROFHS weighted average and q-ROFHS weighted geometric operators. Furthermore, we discuss the fundamental properties of q-ROFHS weighted averaging and q-ROFHS weighted geometric aggregation operators by utilizing developed q-ROFHSNs.

Definition 5. The score function of q-ROFHSN is defined as

$$\left(\$_{\overline{\kappa}_{ij}}\right) = \curvearrowright_{\overline{\overline{\kappa}}}\left(\overline{\kappa}_{ij}\right) - \ddot{\curvearrowright}_{\overline{\overline{\kappa}}}\left(\overline{\kappa}_{ij}\right). \tag{4}$$

Definition 6. The accuracy function of q-ROFHSN is defined as

$$\beta\left(\$_{\overline{\kappa}_{ij}}\right) = \curvearrowright_{\overline{\overline{\kappa}}}\left(\overline{\kappa}_{ij}\right) + \ddot{\curvearrowright}_{\overline{\overline{\kappa}}}\left(\overline{\kappa}_{ij}\right). \tag{5}$$

For the comparison purpose of q-ROFHSNs, the following laws are classified:

(1) $S(\$_{\overline{\kappa}_{ij}}) > S(\widehat{\$}_{\overline{\kappa}_{ij}})$; then, $\$_{\overline{\kappa}_{ij}} > \widehat{\$}_{\overline{\kappa}_{ij}}$.

(2) $S(\$_{\overline{\kappa}_{ij}}) = S(\widehat{\$}_{\overline{\kappa}_{ij}})$; then,

(i) If $\beta(\$_{\overline{\kappa}_{ij}}) > \beta(\widehat{\$}_{\overline{\kappa}_{ij}})$, then $\$_{\overline{\kappa}_{ij}} > \widehat{\$}_{\overline{\kappa}_{ij}}$.

(ii) If $\beta(\$_{\overline{\kappa}_{ij}}) = \beta(\widehat{\$}_{\overline{\kappa}_{ij}})$, then $\$_{\overline{\kappa}_{ij}} = \widehat{\$}_{\overline{\kappa}_{ij}}$.

Definition 7. Let $\$_{\overline{\kappa}_k} = (\curvearrowright_{\overline{\overline{\kappa}}(\overline{\kappa}_k)}, \ddot{\curvearrowright}_{\overline{\overline{\kappa}}(\overline{\kappa}_k)})$ be a q-ROFHNs and $w_i = \{w_1, w_2, \ldots, w_{\ddot{n}}\}$ and $\nu_i = \{\nu_1, \nu_2, \ldots, \nu_{\ddot{m}}\}$ be the expert weight vectors and selected subattributes, respectively, with the condition that $w_i > 0, \sum_{i=1}^{\ddot{n}} w_i = 1, \nu_i > 0, \sum_{i=1}^{\ddot{m}} \nu_i = 1$. The mapping for the q-ROFHWA operator is thus defined as $q-\text{ROFHWA}: \Delta^{\ddot{n}} \longrightarrow \Delta$, where Δ is the collection of all q-ROFHNs, provided as

$$q-\text{ROFHWA}\left(\$_{\overline{\kappa}_{11}}, \$_{\overline{\kappa}_{12}}, \ldots, \$_{\overline{\kappa}_{mn}}\right) = \oplus_{j=1}^{\ddot{m}} \nu_i \left(\oplus_{i=1}^{\ddot{n}} w_i \$_{\overline{\kappa}_{ij}}\right). \tag{6}$$

Example 3. Let $\textcircled{s}$ be the set of decision makers to decide best laptop given as $\textcircled{s} = \{y_1, y_2, y_3\}$ and also consider the set of attributes as $\urcorner_1$ and $\urcorner_2$, where $\urcorner_1$ represents laptop type and $\urcorner_2$ represents laptop RAM. Then, their corresponding attributive sets can be $\urcorner_1 = \{a_{11} = \text{HP}, a_{12} = \text{Dell}\}$, $\urcorner_2 = \{a_{21} = 8\,\text{GB}, a_{22} = 16\,\text{GB}, a_{23} = 16\,\text{GB}\}$

Suppose $\overline{\kappa}_1 = \{\natural_{11}, \natural_{12}\}, \overline{\kappa}_2 = \{\natural_{21}, \natural_{22}\}$. Then, $\overline{\overline{\kappa}} = \urcorner_1 \times \urcorner_2$ will have 2 tuple elements and we suppose $q = 8$.

Then, q-ROFHS set $(\leftarrow\!\!\rho, \overline{\overline{\kappa}})$ can be written as

$$\begin{aligned} \langle \$_{\overline{\kappa}_{11}} \rangle &= \langle 0.81, 0.88 \rangle, \\ \langle \$_{\overline{\kappa}_{12}} \rangle &= \langle 0.95, 0.97 \rangle, \\ \langle \$_{\overline{\kappa}_{21}} \rangle &= \langle 0.87, 0.84 \rangle, \\ \langle \$_{\overline{\kappa}_{22}} \rangle &= \langle 0.95, 0.91 \rangle. \end{aligned} \tag{7}$$

Let $w_i = (0.2, 0.1, 0.4, 0.3), \nu_j = (0.6, 0.1, 0.3)$, and $q = 8$.

$$\begin{aligned} &q-ROFHWA\left(\$_{\overline{\kappa}_{11}}, \$_{\overline{\kappa}_{12}}, \$_{\overline{\kappa}_{21}}, \$_{\overline{\kappa}_{22}}\right) \\ &= \left(\sqrt[q]{1 - \prod_{j=1}^{3} \left(\prod_{i=1}^{4} \left(1 - \curvearrowright_{\overline{\kappa}_k}^{q}\right)^{w_i} \right)^{\nu_i}}, \prod_{j=1}^{3} \left(\prod_{i=1}^{4} \left(\ddot{\curvearrowright}_{\overline{\kappa}_k} \right)^{w_i} \right)^{\nu_i} \right) \\ &= (0.732, 0.488). \end{aligned} \tag{8}$$

Table 3: q-ROFHS values.

$(\leftarrow_{\rho}, \overline{\overline{\alpha}})$	y_1	y_2	y_3	y_4
$(\natural_{11}, \natural_{21}, \natural_{31})$	(.8, .9)	(.7, .9)	(.7, .8)	(.8, .9)
$(\natural_{11}, \natural_{21}, \natural_{32})$	(.7, .8)	(.6, .9)	(.7, .9)	(.7, .8)
$(\natural_{12}, \natural_{21}, \natural_{31})$	(.7, .9)	(.8, .9)	(.7, .8)	(.7, .9)
$(\natural_{12}, \natural_{21}, \natural_{32})$	(.8, .9)	(.7, .9)	(.7, .9)	(.8, .9)

Table 4: q-ROFHS values.

$(\nrightarrow, \overline{\beta})$	y_1	y_2	y_3	y_4
$(\natural_{11}, \natural_{21}, \natural_{31})$	(.9, .8)	(.9, .8)	(.8, .7)	(.9, .7)
$(\natural_{11}, \natural_{21}, \natural_{32})$	(.8, .7)	(.8, .7)	(.8, .7)	(.8, .7)
$(\natural_{12}, \natural_{21}, \natural_{31})$	(.8, .8)	(.9, .7)	(.9, .7)	(.8, .7)
$(\natural_{12}, \natural_{21}, \natural_{32})$	(.9, .8)	(.9, .8)	(.9, .8)	(.9, .8)

Theorem 1. *Let $\$_{\overline{\kappa}_k} = (\curvearrowright_{\overline{\kappa}_k}, \ddot{\curvearrowright}_{\overline{\kappa}_k})$ be a q-ROFHN. Then, the aggregated result for q − ROFHWA operator is given as*

$$q-\mathrm{ROFHWA}\left(\$_{\overline{\kappa}_{11}}, \$_{\overline{\kappa}_{12}}, \ldots, \$_{\overline{\kappa}_{nm}}\right) = \oplus_{j=1}^{\ddot{m}} \nu_i \left(\oplus_{i=1}^{\ddot{n}} w_i \$_{\overline{\kappa}_{i_j}}\right) = \left(\sqrt[q]{1-\prod_{j=1}^{\ddot{m}}\left(\prod_{i=1}^{\ddot{n}}\left(1-\curvearrowright_{\overline{\kappa}_k}^{q}\right)^{w_i}\right)^{\nu_i}}, \prod_{j=1}^{\ddot{m}}\left(\prod_{i=1}^{\ddot{n}}\left(\ddot{\curvearrowright}_{\overline{\kappa}_k}\right)^{w_i}\right)^{\nu_i}\right), \tag{9}$$

where $w_i = \{w_1, w_2, \ldots, w_{\ddot{n}}\}$ and $\nu_i = \{\nu_1, \nu_2, \ldots, \nu_{\ddot{m}}\}$ are the expert weight vectors and selected subattributes, respectively, with given circumstances $w_i > 0, \sum_{i=1}^{\ddot{n}} w_i = 1, \nu_i > 0, \sum_{i=1}^{\ddot{m}} \nu_i = 1$.

Proof. Consider the principle of mathematical induction to verify the given results: for $\ddot{n} = 1$, we get $w_1 = 1$. Then, we have

$$q-\mathrm{ROFHWA}\left(I_{\overline{\kappa}_{11}}, \$_{\overline{\kappa}_{12}}, \ldots, \$_{\overline{\kappa}_{nm}}\right) = \oplus_{j=1}^{\ddot{m}} \nu_j \$_{\kappa} = \left(\sqrt[q]{1-\prod_{j=1}^{\ddot{m}}\left(1-\curvearrowright_{\overline{\kappa}_k}^{q}\right)^{\nu_i}}, \prod_{j=1}^{\ddot{m}}\left(\ddot{\curvearrowright}_{\overline{\kappa}_k}\right)^{\nu_i}\right) = \left(\sqrt[q]{1-\prod_{j=1}^{\ddot{m}}\left(\prod_{i=1}^{1}\left(1-\curvearrowright_{\overline{\kappa}_k}^{q}\right)^{w_i}\right)^{\nu_i}}, \prod_{j=1}^{\ddot{m}}\left(\prod_{i=1}^{1}\left(\ddot{\curvearrowright}_{\overline{\kappa}_k}\right)^{w_i}\right)^{\nu_i}\right). \tag{10}$$

For $\ddot{m} = 1$, we get $\nu_1 = 1$. Then, we have

$$q-\mathrm{ROFHWA}\left(\$_{\overline{\kappa}_{11}}, \$_{\overline{\kappa}_{12}}, \ldots, \$_{\overline{\kappa}_{nm}}\right) = \oplus_{i=1}^{\ddot{n}} w_i \$_{\overline{\kappa}_{i_j}} = \left(\sqrt[q]{1-\prod_{i=1}^{\ddot{n}}\left(1-\curvearrowright_{\overline{\kappa}_k}^{q}\right)^{w_i}}, \prod_{i=1}^{\ddot{n}}\left(\ddot{\curvearrowright}_{\overline{\kappa}_k}\right)^{w_i}\right) = \left(\sqrt[q]{1-\prod_{j=1}^{1}\left(\prod_{i=1}^{\ddot{n}}\left(1-\curvearrowright_{\overline{\kappa}_k}^{q}\right)^{w_i}\right)^{\nu_j}}, \prod_{j=1}^{1}\left(\prod_{i=1}^{\ddot{n}}\left(\ddot{\curvearrowright}_{\overline{\kappa}_k}\right)^{w_i}\right)^{\nu_j}\right). \tag{11}$$

This verifies that equation (4) is correct for $n = 1$ and $m = 1$. We will now show that equation (5) also holds for $\ddot{m} = 1$ and$\ddot{m} = 2$, thus completing our proof.

$$\begin{aligned}
q-\mathrm{ROFHWA}\left(\$_{\overline{\kappa}_{11}}, \$_{\overline{\kappa}_{12}}, \ldots, \$_{\overline{\kappa}_{nm}}\right) &= \oplus_{j=1}^{2} \nu_j \left(\oplus_{i=1}^{2} w_i \$_{\overline{\kappa}_{i_j}}\right) \\
&= \nu_1\left(\oplus_{i=1}^{2} w_i \$_{\overline{\alpha}_{i_1}}\right) \oplus \nu_2\left(\oplus_{i=1}^{2} w_i \$_{\overline{\alpha}_{i_2}}\right) \\
&= \nu_1\left(w_1 \$_{\overline{\kappa}_{11}} \oplus w_2 \$_{\overline{\kappa}_{21}}\right) \oplus \nu_2\left(w_1 \$_{\overline{\kappa}_{12}} \oplus w_2 \$_{\overline{\kappa}_{22}}\right) \\
&= \nu_1\left\{\left(\sqrt[q]{1-\left(1-\curvearrowright_{11}^{q}\right)^{w_1}}, \tilde{\curvearrowright}_{11}^{w_1}\right) \oplus \left(\sqrt[q]{1-\left(1-\curvearrowright_{21}^{q}\right)^{w_2}}, \ddot{\curvearrowright}_{21}^{w_2}\right)\right\} \\
&\quad \oplus \nu_2\left\{\left(\sqrt[q]{1-\left(1-\curvearrowright_{12}^{q}\right)^{w_1}}, \ddot{\curvearrowright}_{12}^{w_1}\right) \oplus \left(\sqrt[q]{1-\left(1-\curvearrowright_{22}^{q}\right)^{w_2}}, \ddot{\curvearrowright}_{22}^{w_2}\right)\right\} \\
&= \nu_1\left(\sqrt[q]{1-\prod_{i=1}^{2}\left(1-\curvearrowright_{i1}^{q}\right)^{w_i}}, \prod_{i=1}^{\ddot{n}} \ddot{\curvearrowright}_{i1}^{w_i}\right) \oplus \nu_2\left(\sqrt[q]{1-\prod_{i=1}^{2}\left(1-\curvearrowright_{i2}^{q}\right)^{w_i}}, \prod_{i=1}^{\ddot{n}} \ddot{\curvearrowright}_{i2}^{w_i}\right) \\
&= \left(\sqrt[q]{1-\left(\prod_{i=1}^{2}\left(1-\curvearrowright_{i1}^{q}\right)^{w_i}\right)^{\nu_1}}, \left(\prod_{i=1}^{2} \ddot{\curvearrowright}_{i1}^{w_i}\right)^{\nu_1}\right) \oplus \left(\begin{array}{c}\sqrt[q]{1-\left(\prod_{i=1}^{2}\left(1-\curvearrowright_{i2}^{q}\right)^{w_i}\right)^{\nu_2}}, \\ \left(\prod_{i=1}^{2} \ddot{\curvearrowright}_{i2}^{w_i}\right)^{\nu_2}\end{array}\right) \\
&= \left(\sqrt[q]{1-\prod_{j=1}^{2}\left(\prod_{i=1}^{2}\left(1-\curvearrowright_{ij}^{q}\right)^{w_i}\right)^{\nu_j}}, \prod_{j=1}^{2}\left(\prod_{i=1}^{2} \ddot{\curvearrowright}_{ij}^{w_i}\right)^{\nu_1}\right).
\end{aligned} \tag{12}$$

Hence, it is true for $\ddot{m} = k_1 + 1$ and $\ddot{n} = k_2 + 1$. Therefore, equation (28) is true for all $\ddot{m}, \ddot{n} \geq 1$, by mathematical induction. □

Theorem 2. *Let $\$_{\overline{\kappa}_k} = (\curvearrowright_{\overline{\overline{\alpha}}(\overline{\kappa}_k)}, \ddot{\curvearrowright}_{\overline{\overline{\alpha}}(\overline{\kappa}_k)})$ be a q-ROFHN and $w_i = \{w_1, w_2, \ldots, w_{\ddot{n}}\}$ and $\nu_i = \{\nu_1, \nu_2, \ldots, \nu_{\ddot{m}}\}$ be the expert weight vectors and selected subattributes, having the*

condition that $w_i > 0, \sum_{i=1}^{\ddot{n}} w_i = 1, v_i > 0, \sum_{i=1}^{\ddot{m}} v_i = 1$. *Then, the q-ROFHWA operator holds for the following properties:*

(i) Idempotency: if $\S_{\overline{\kappa}_k} = \zeta_{\overline{\kappa}}$ *for all* $(i = 1,2, \ldots, \ddot{n})$ *and* $(j = 1,2, \ldots, \ddot{m})$, *then q-ROFHWA* $(\S_{\overline{\kappa}_{11}}, \S_{\overline{\kappa}_{12}}, \ldots, \S_{\overline{\kappa}_{nm}}) = \zeta_{\overline{\kappa}}$.

Proof. Since we know $\S_{\overline{\kappa}_k} = (\curvearrowright_{\overline{\overline{\wedge}}(\propto\overline{\kappa}_k)}, \ddot{\curvearrowright}_{\overline{\overline{\wedge}}(\overline{\kappa}_k)}) = \zeta_{\overline{\kappa}}$ is a collection of q-ROFHNs, then from Theorem 1, we have

$$\begin{aligned} & q - ROFHWA\left(\S_{\overline{\kappa}_{11}}, \S_{\overline{\kappa}_{12}}, \ldots, \S_{\overline{\kappa}_{nm}}\right) \\ &= \left(\sqrt[q]{1 - \prod_{j=1}^{\ddot{m}} \left(\prod_{i=1}^{\ddot{n}} \left(1 - \curvearrowright_{\overline{\kappa}_k}^{q}\right)^{w_i} \right)^{v_j}}, \prod_{j=1}^{\ddot{m}} \left(\prod_{i=1}^{\ddot{n}} \left(\ddot{\curvearrowright}_{\overline{\kappa}_k}\right)^{w_i} \right)^{v_j} \right) \\ &= \left(\sqrt[q]{1 - \left(\left(1 - \curvearrowright_{\overline{\kappa}_k}^{q}\right)^{\sum_{i=1}^{\ddot{n}} w_i} \right)^{\sum_{j=1}^{\ddot{m}} v_j}}, \left(\left(\ddot{\curvearrowright}_{\overline{\kappa}_k}\right)^{\sum_{i=1}^{\ddot{n}} w_i} \right)^{\sum_{j=1}^{\ddot{m}} v_j} \right) \\ &= \left(\sqrt[q]{1 - \left(1 - \curvearrowright_{\overline{\kappa}_k}^{q}\right)}, \tilde{\curvearrowright}_{\overline{\kappa}_k} \right) \\ &= \zeta_{\overline{\kappa}}. \end{aligned} \tag{13}$$

Therefore,

$$q - \mathrm{ROFHWA}\left(\S_{\overline{\kappa}_{11}}, \S_{\overline{\kappa}_{12}}, \ldots, \S_{\overline{\kappa}_{nm}}\right) = \zeta_{\overline{\kappa}}. \tag{14}$$

(ii) Boundedness: if

$$\S_{\overline{\kappa}_{ij}}^{-} = \left(\min_j \min_i \left\{ \curvearrowright_{\overline{\overline{\wedge}}}\left(\overline{\kappa}_{ij}\right) \right\}, \max_j \max_i \left\{ \ddot{\curvearrowright}_{\overline{\overline{\wedge}}}\left(\overline{\kappa}_{ij}\right) \right\} \right), \tag{15}$$

$$\S_{\overline{\propto}_{ij}}^{+} = \left(\max_j \max_i \left\{ \curvearrowright_{\overline{\overline{\wedge}}}\left(\overline{\kappa}_{ij}\right) \right\}, \min_j \min_i \left\{ \ddot{\curvearrowright}_{\overline{\overline{\wedge}}}\left(\overline{\kappa}_{ij}\right) \right\} \right), \tag{16}$$

then

$$\S_{\overline{\kappa}_{ij}}^{-} \le q - \mathrm{ROFHWA}\left(\S_{\overline{\kappa}_{11}}, \S_{\overline{\kappa}_{12}}, \ldots, \S_{\overline{\kappa}_{nm}}\right) \le \S_{\overline{\kappa}_{ij}}^{+}. \tag{17}$$

□

Proof. $\S_{\overline{\kappa}_{ij}}^{-} = \left(\min_j \min_i \left\{ \curvearrowright_{\overline{\overline{\wedge}}(\overline{\kappa}_{ij})} \right\}, \max_j \max_i \left\{ \tilde{\curvearrowright}_{\overline{\overline{\wedge}}(\overline{\kappa}_{ij})} \right\}\right)$ and $\S_{\overline{\kappa}_{ij}}^{+} = \left(\max_j \max_i \left\{ \curvearrowright_{\overline{\overline{\wedge}}(\overline{\kappa}_{ij})} \right\}, \min_j \min_i \left\{ \ddot{\curvearrowright}_{\overline{\overline{\wedge}}(\overline{\kappa}_{ij})} \right\}\right)$. To prove that $\S_{\overline{\propto}_{ij}}^{-} \le q\text{–ROFHWA}\left(\S_{\overline{\propto}_{11}}, \S_{\overline{\propto}_{12}}, \ldots, \S_{\overline{\propto}_{nm}}\right) \le \S_{\overline{\propto}_{ij}}^{+}$, for each $i = 1, 2, \ldots, n$ and $j = 1, 2, \ldots, m$, we have

$$\begin{aligned} & \min_j \min_i \left\{ \curvearrowright_{\overline{\overline{\wedge}}}\left(\overline{\kappa}_{ij}\right) \right\} \le \curvearrowright_{\overline{\overline{\wedge}}}\left(\overline{\kappa}_{ij}\right) \le \max_j \max_i \left\{ \curvearrowright_{\overline{\overline{\wedge}}}\left(\overline{\kappa}_{ij}\right) \right\} \\ & \Rightarrow 1 - \max_j \max_i \left\{ \curvearrowright_{\overline{\overline{\wedge}}}^{q}\left(\overline{\kappa}_{ij}\right) \right\} \le 1 - \curvearrowright_{\overline{\overline{\wedge}}}^{q}\left(\overline{\kappa}_{ij}\right) \\ & \le 1 - \min_j \min_i \left\{ \curvearrowright_{\overline{\overline{\wedge}}}^{q}\left(\overline{\kappa}_{ij}\right) \right\} \\ & \Leftrightarrow \left(1 - \max_j \max_i \left\{ \curvearrowright_{\overline{\overline{\wedge}}}^{q}\left(\overline{\kappa}_{ij}\right) \right\}\right)^{w_i} \le \left(1 - \curvearrowright_{\overline{\overline{\wedge}}}^{q}\left(\overline{\kappa}_{ij}\right)\right)^{w_i} \\ & \le \left(1 - \min_j \min_i \left\{ \curvearrowright_{\overline{\overline{\wedge}}}^{q}\left(\overline{\kappa}_{ij}\right) \right\}\right)^{w_i} \\ & \Leftrightarrow \left(1 - \max_j \max_i \left\{ \curvearrowright_{\overline{\overline{\wedge}}}^{q}\left(\overline{\kappa}_{ij}\right) \right\}\right)^{\sum_{i=1}^{\ddot{n}} w_i} \le \prod_{i=1}^{\ddot{n}} \left(1 - \curvearrowright_{\overline{\overline{\wedge}}}^{q}\left(\overline{\kappa}_{ij}\right)\right)^{w_i} \end{aligned}$$

$$
\begin{aligned}
&\le \left(1-\min_j\min_i\left\{\sim^{q}_{\overline{\overline{\wedge}}}\left(\overline{\kappa}_{ij}\right)\right\}\right)^{\sum_{i=1}^{\ddot{n}} w_i}\\
&\Leftrightarrow \left(1-\max_j\max_i\left\{\sim^{q}_{\overline{\overline{\wedge}}}\left(\overline{\kappa}_{ij}\right)\right\}\right)^{\sum_{j=1}^{\ddot{m}} v_j} \le \prod_{j=1}^{\ddot{m}}\left(\prod_{i=1}^{\ddot{n}}\left(1-\sim^{q}_{\overline{\overline{\wedge}}}\left(\overline{\kappa}_{ij}\right)\right)^{w_i}\right)^{v_j}\\
&\le \left(1-\min_j\min_i\left\{\sim^{q}_{\overline{\overline{\wedge}}}\left(\overline{\kappa}_{ij}\right)\right\}\right)^{\sum_{j=1}^{\ddot{m}} v_j}\\
&\Leftrightarrow 1-\max_j\max_i\left\{\sim^{q}_{\overline{\overline{\wedge}}}\left(\overline{\kappa}_{ij}\right)\right\} \le \prod_{j=1}^{\ddot{m}}\left(\prod_{i=1}^{\ddot{n}}\left(1-\sim^{q}_{\overline{\overline{\wedge}}}\left(\overline{\kappa}_{ij}\right)\right)^{w_i}\right)^{v_j}\\
&\le 1-\min_j\min_i\left\{\sim^{q}_{\overline{\overline{\wedge}}}\left(\overline{\kappa}_{ij}\right)\right\}\\
&\Leftrightarrow \min_j\min_i\left\{\sim_{\overline{\overline{\wedge}}}\left(\overline{\kappa}_{ij}\right)\right\} \le 1-\prod_{j=1}^{\ddot{m}}\left(\prod_{i=1}^{\ddot{n}}\left(1-\sim^{q}_{\overline{\overline{\wedge}}}\left(\overline{\kappa}_{ij}\right)\right)^{w_i}\right)^{v_j}\\
&\le \max_j\max_i\left\{\sim_{\overline{\overline{\wedge}}}\left(\overline{\kappa}_{ij}\right)\right\}.
\end{aligned}
\tag{18}
$$

Hence,

$$
\min_j\min_i\left\{\sim_{\overline{\overline{\wedge}}}\left(\overline{\kappa}_{ij}\right)\right\} \le \sqrt[q]{1-\prod_{j=1}^{\ddot{m}}\left(\prod_{i=1}^{\ddot{n}}\left(1-\sim^{q}_{\overline{\overline{\wedge}}}\left(\overline{\kappa}_{ij}\right)\right)^{w_i}\right)^{v_j}} \le \max_j\max_i\left\{\sim_{\overline{\overline{\wedge}}}\left(\overline{\kappa}_{ij}\right)\right\}. \tag{19}
$$

Next, for each $i = 1, 2, \ldots, \ddot{n}$ and $j = 1, 2, \ldots, \ddot{m}$, we have

$$
\begin{aligned}
&\min_j\min_i\left\{\ddot{\sim}_{\overline{\overline{\wedge}}}\left(\overline{\kappa}_{ij}\right)\right\} \le \ddot{\sim}_{\overline{\overline{\wedge}}}\left(\overline{\kappa}_{ij}\right) \le \max_j\max_i\left\{\ddot{\sim}_{\overline{\overline{\wedge}}}\left(\overline{\kappa}_{ij}\right)\right\}\\
&\Leftrightarrow \prod_{j=1}^{\ddot{m}}\left(\prod_{i=1}^{\ddot{n}}\left(\min_j\min_i\left\{\ddot{\sim}_{\overline{\overline{\wedge}}}\left(\overline{\kappa}_{ij}\right)\right\}\right)^{w_i}\right)^{v_j} \le \prod_{j=1}^{\ddot{m}}\left(\prod_{i=1}^{\ddot{n}}\left(\ddot{\sim}_{\overline{\overline{\wedge}}}\left(\overline{\kappa}_{ij}\right)\right)^{w_i}\right)^{v_j}\\
&\le \prod_{j=1}^{\ddot{m}}\left(\prod_{i=1}^{\ddot{n}}\left(\max_j\max_i\left\{\ddot{\sim}_{\overline{\overline{\wedge}}}\left(\overline{\kappa}_{ij}\right)\right\}\right)^{w_i}\right)^{v_j}\\
&\Leftrightarrow \prod_{j=1}^{\ddot{m}}\left(\prod_{i=1}^{\ddot{n}}\left(\min_j\min_i\left\{\ddot{\sim}_{\overline{\overline{\wedge}}}\left(\overline{\kappa}_{ij}\right)\right\}\right)^{\sum_{i=1}^{\ddot{n}} w_i}\right)^{\sum_{j=1}^{\ddot{m}} v_j} \le \prod_{j=1}^{\ddot{m}}\left(\prod_{i=1}^{\ddot{n}}\left(\ddot{\sim}_{\overline{\overline{\wedge}}}\left(\overline{\kappa}_{ij}\right)\right)^{w_i}\right)^{v_j}\\
&\le \prod_{j=1}^{\ddot{m}}\left(\prod_{i=1}^{\ddot{n}}\left(\max_j\max_i\left\{\ddot{\sim}_{\overline{\overline{\wedge}}}\left(\overline{\kappa}_{ij}\right)\right\}\right)^{\sum_{i=1}^{\ddot{n}} w_i}\right)^{\sum_{j=1}^{\ddot{m}} v_j},
\end{aligned}
\tag{20}
$$

which implies that

$$
\min_j\min_i\left\{\ddot{\sim}_{\overline{\overline{\wedge}}}\left(\overline{\alpha}_{ij}\right)\right\} \le \prod_{j=1}^{\ddot{m}}\left(\prod_{i=1}^{\ddot{n}}\left(\ddot{\sim}_{\overline{\overline{\wedge}}}\left(\overline{\kappa}_{ij}\right)\right)^{w_i}\right)^{v_j} \le \max_j\max_i\left\{\ddot{\sim}_{\overline{\overline{\wedge}}}\left(\overline{\kappa}_{ij}\right)\right\}. \tag{21}
$$

Therefore, $q-\mathrm{ROFHWA}(\$_{\overline{\kappa}_{11}}, \$_{\overline{\kappa}_{12}}, \ldots, \$_{\overline{\kappa}_{\ddot{n}\ddot{m}}}) = (\curvearrowright_{\overline{\overline{\wedge}}(\overline{\kappa}_{ij})}, \ddot{\curvearrowright}_{\overline{\overline{\wedge}}(\overline{\kappa}_{ij})}) = \$_{\overline{\kappa}_{ij}}$, and thus

$$\min_j \min_i \left\{ \curvearrowright_{\overline{\overline{\wedge}}}(\overline{\kappa}_{ij}) \right\} \leq \sqrt[q]{\curvearrowright^{q}_{\overline{\overline{\wedge}}}(\overline{\kappa}_{ij})} \leq \max_j \max_i \left\{ \curvearrowright_{\overline{\overline{\wedge}}}(\overline{\kappa}_{ij}) \right\}. \tag{22}$$

$$\min_j \min_i \left\{ \ddot{\curvearrowright}_{\overline{\overline{\wedge}}}(\overline{\kappa}_{ij}) \right\} \leq \ddot{\curvearrowright}_{\overline{\overline{\wedge}}}(\overline{\kappa}_{ij}) \leq \max_j \max_i \left\{ \ddot{\curvearrowright}_{\overline{\overline{\wedge}}}(\overline{\kappa}_{ij}) \right\}. \tag{23}$$

So, we have $^{q}S(\$_{\overline{\kappa}_{ij}}) = {}^{q}\min_j \min_i \left\{ \curvearrowright_{\overline{\overline{\wedge}}}(\overline{\kappa}_{ij}) \right\}^{q} - (\ddot{\curvearrowright}_{\overline{\overline{\wedge}}}(\overline{\kappa}_{ij}))^{q} \leq {}^{q}\max_j \max_i \left\{ \curvearrowright_{\overline{\overline{\wedge}}}(\overline{\kappa}_{ij}) \right\}^{q} - \min_j \min_i \left\{ \ddot{\curvearrowright}_{\overline{\overline{\wedge}}}(\overline{\kappa}_{ij}) \right\}^{q} = S(\$^{+}_{\overline{\kappa}_{ij}})$, $S(\$_{\overline{\kappa}_{ij}}) = (\curvearrowright_{\overline{\overline{\wedge}}}(\overline{\overline{\propto}}_{ij}))^{q} - (\ddot{\curvearrowright}_{\overline{\overline{\wedge}}}(\overline{\kappa}_{ij}))^{q} \geq \min_j \min_i \left\{ \curvearrowright_{\overline{\overline{\wedge}}}(\overline{\kappa}_{ij}) \right\}^{q} - \max_j \max_i \left\{ \ddot{\curvearrowright}_{\overline{\kappa}}(\overline{\kappa}_{ij}) \right\}^{q} = S(\$^{-}_{\overline{\kappa}_{ij}})$.

Then,

$$S\left(\$^{-}_{\overline{\kappa}_{ij}}\right) \leq q-\mathrm{ROFHWA}\left(\$_{\overline{\kappa}_{11}}, \$_{\overline{\kappa}_{12}}, \ldots, \$_{\overline{\overline{\propto}}_{\ddot{n}\ddot{m}}}\right) \leq S\left(\$^{+}_{\overline{\kappa}_{ij}}\right). \tag{24}$$

□

Definition 8. Let $\$_{\overline{\kappa}_k} = (\curvearrowright_{\overline{\overline{\wedge}}(\overline{\kappa}_k)}, \ddot{\curvearrowright}_{\overline{\overline{\wedge}}(\overline{\kappa}_k)})$ be a q-ROFHN, $w_i = \{w_1, w_2, \ldots, w_{\ddot{n}}\}$ and $v_i = \{v_1, v_2, \ldots, v_{\ddot{m}}\}$ be the weight vectors of the experts and selected parameters of sub-attributes, respectively, having the condition that $w_i > 0, \sum_{i=1}^{\ddot{n}} w_i = 1, v_i > 0, \sum_{i=1}^{\ddot{m}} v_i = 1$. Then, the mapping for q-ROFHWG operator is defined as $q-\mathrm{ROFHWG}: \Delta^{\ddot{n}} \longrightarrow \Delta$, where Δ is the collection of all q-ROFHNs.

$$q-\mathrm{ROFHWG}\left(\$_{\overline{\kappa}_{11}}, \$_{\overline{\kappa}_{12}}, \ldots, \$_{\overline{\kappa}_{\ddot{n}\ddot{m}}}\right) = \otimes^{\ddot{m}}_{j=1} v_i \left(\otimes^{\ddot{n}}_{i=1} w_i \$_{\overline{\kappa}_{ij}} \right). \tag{25}$$

Example 4. Let ⓢ be the set of decision makers to decide the best car given as $ⓢ = \{y_1, y_2, y_3\}$ and also consider the set of attributes as $\top_1$ and $\top_2$, where $\top_1$ represents colour of the car and $\top_2$ represents price of the car. Then, their corresponding attributive sets can be
$\top_1 = \{a_{11} = \text{black}, a_{12} = \text{white}\}$,
$\top_2 = \{a_{21} = 25\text{lac}, a_{22} = 30\text{lac}, a_{23} = 20\text{laclac}\}$.

Suppose $\overline{\wedge}_1 = \{\natural_{11}, \natural_{12}\}, \overline{\wedge}_2 = \{\natural_{21}, \natural_{22}\}$. Then, $\overline{\overline{\wedge}} = \top_1 \times \top_2$ will have 2 tuple elements and we suppose $q = 8$.

Then, q-ROFHS set $(\hookleftarrow, \overline{\overline{\wedge}})$ can be written as

$$\begin{aligned} \langle \$_{\overline{\kappa}_{11}} \rangle &= \langle 0.91, 0.84 \rangle, \\ \langle \$_{\overline{\kappa}_{12}} \rangle &= \langle 0.85, 0.92 \rangle, \\ \langle \$_{\overline{\kappa}_{21}} \rangle &= \langle 0.80, 0.93 \rangle, \\ \langle \$_{\overline{\kappa}_{22}} \rangle &= \langle 0.95, 0.88 \rangle. \end{aligned} \tag{26}$$

Let $w_i = (0.2, 0.1, 0.4, 0.3), v_j = (0.6, 0.1, 0.3)$, and $q = 8$.

$$\begin{aligned} &q-\mathit{ROFHWG}\left(\$_{\overline{\kappa}_{11}}, \$_{\overline{\kappa}_{12}}, \$_{\overline{\kappa}_{21}}, \$_{\overline{\kappa}_{11}}\right) \\ &= \left(\prod_{j=1}^{3} \left(\prod_{i=1}^{4} \left(\curvearrowright_{\overline{\kappa}_k} \right)^{w_i} \right)^{v_i}, \sqrt[q]{1 - \prod_{j=1}^{3} \left(\prod_{i=1}^{4} \left(1 - \ddot{\curvearrowright}^{q}_{\overline{\kappa}_k} \right)^{w_i} \right)^{v_i}} \right) \\ &= (0.895, 0.569). \end{aligned} \tag{27}$$

Theorem 3. *Let $\$_{\overline{\kappa}_k} = (\curvearrowright_{\overline{\kappa}_k}, \ddot{\curvearrowright}_{\overline{\kappa}_k})$ be a q-ROFHN. Then, the aggregated result for $q-$ROFHWG operator is given as*

$$\begin{aligned} &q-\mathrm{ROFHWG}\left(\$_{\overline{\kappa}_{11}}, \$_{\overline{\kappa}_{12}}, \ldots, \$_{\overline{\kappa}_{nm}}\right) = \otimes^{\ddot{m}}_{j=1} v_i \left(\otimes^{\ddot{n}}_{i=1} w_i \$_{\overline{\kappa}_{ij}} \right) \\ &= \left(\prod_{j=1}^{\ddot{m}} \left(\prod_{i=1}^{\ddot{n}} \left(\curvearrowright_{\overline{\kappa}_k} \right)^{w_i} \right)^{v_i}, \sqrt[q]{1 - \prod_{j=1}^{\ddot{m}} \left(\prod_{i=1}^{\ddot{n}} \left(1 - \ddot{\curvearrowright}^{q}_{\overline{\kappa}_k} \right)^{w_i} \right)^{v_i}} \right), \end{aligned} \tag{28}$$

where $w_i = \{w_1, w_2, \ldots, w_{\ddot{n}}\}$ and $v_i = \{v_1, v_2, \ldots, v_{\ddot{m}}\}$ are the weight vectors of the experts and selected parameters of subattributes, respectively, with given circumstances $w_i > 0, \sum_{i=1}^{\ddot{n}} w_i = 1, v_i > 0, \sum_{i=1}^{\ddot{m}} v_i = 1$.

Proof of Theorem 3. Consider the principle of mathematical induction to verify the given result as follows: for $\ddot{n} = 1$, we get $w_1 = 1$. Then, we have

$$\begin{aligned} &q-\mathrm{ROFHWG}\left(\$_{\overline{\kappa}_{11}}, \$_{\overline{\kappa}_{12}}, \ldots, \$_{\overline{\kappa}_{nm}}\right) = \otimes^{\ddot{m}}_{j=1} \$^{v_j}_{\overline{\kappa}_{ij}} \\ &= \left(\prod_{j=1}^{\ddot{m}} \left(\curvearrowright_{\overline{\kappa}_k} \right)^{v_i}, \sqrt[q]{1 - \prod_{j=1}^{\ddot{m}} \left(1 - \ddot{\curvearrowright}^{q}_{\overline{\kappa}_k} \right)^{v_i}} \right) \\ &= \left(\prod_{j=1}^{\ddot{m}} \left(\prod_{i=1}^{1} \left(\curvearrowright_{\overline{\kappa}_k} \right)^{w_i} \right)^{v_i}, \sqrt[q]{1 - \prod_{j=1}^{\ddot{m}} \left(\prod_{i=1}^{1} \left(1 - \ddot{\curvearrowright}^{q}_{\overline{\kappa}_k} \right)^{w_i} \right)^{v_i}} \right). \end{aligned} \tag{29}$$

For $\ddot{m} = 1$, we get $v_1 = 1$. Then, we have

$$\begin{aligned} &q-\mathrm{ROFHWA}\left(\$_{\overline{\kappa}_{11}}, \$_{\overline{\kappa}_{12}}, \ldots, \$_{\overline{\kappa}_{nm}}\right) = \otimes^{\ddot{n}}_{i=1} \left(\$_{\overline{\kappa}_{i_1}} \right)^{w_i} \\ &= \left(\prod_{i=1}^{\ddot{n}} \left(\curvearrowright_{\overline{\kappa}_k} \right)^{w_i}, \sqrt[q]{1 - \prod_{i=1}^{\ddot{n}} \left(1 - \ddot{\curvearrowright}^{q}_{\overline{\kappa}_k} \right)^{w_i}} \right) \\ &= \left(\prod_{j=1}^{1} \left(\prod_{i=1}^{\ddot{n}} \left(\curvearrowright_{\overline{\kappa}_k} \right)^{w_i} \right)^{v_j}, \sqrt[q]{1 - \prod_{j=1}^{1} \left(\prod_{i=1}^{\ddot{n}} \left(1 - \ddot{\curvearrowright}^{q}_{\overline{\kappa}_k} \right)^{w_i} \right)^{v_j}} \right). \end{aligned} \tag{30}$$

For $\ddot{n} = 1$ and $\ddot{m} = 2$, this proves that equation (28) is true. Now we will prove that equation (28) also holds for $\ddot{n} = 2$ and $\ddot{m} = 1$, so we have

$$
\begin{aligned}
q-\mathrm{ROFHWA}\left(\S_{\overline{\kappa}_{11}},\S_{\overline{\kappa}_{12}},\ldots,\S_{\overline{\kappa}_{nm}}\right)&=\oplus_{j=1}^{2}v_j\left(\otimes_{i=1}^{2}w_i\S_{\overline{\kappa}_{ij}}\right)\\
&=v_1\left(\oplus_{i=1}^{2}w_i\S_{\overline{\kappa}_{i_1}}\right)\otimes v_2\left(\oplus_{i=1}^{2}w_i\S_{\overline{\kappa}_{i_2}}\right)=v_1\left(w_1\S_{\overline{\kappa}_{11}}\otimes w_2\S_{\overline{\kappa}_{21}}\right)\otimes v_2\left(w_1\S_{\overline{\kappa}_{12}}\otimes w_2\S_{\overline{\kappa}_{22}}\right)\\
&=v_1\left\{\left(\sim_{11}^{w_1},\sqrt[q]{1-\left(1-\ddot{\sim}_{11}^{q}\right)^{w_1}}\right)\otimes\left(\sim_{21}^{w_2},\sqrt[q]{1-\left(1-\ddot{\sim}_{21}^{q}\right)^{w_2}}\right)\right\}\otimes v_2\left\{\left(\sim_{12}^{w_1},\sqrt[q]{1-\left(1-\ddot{\sim}_{12}^{q}\right)^{w_1}}\right)\otimes\left(\sim_{22}^{w_2},\sqrt[q]{1-\left(1-\ddot{\sim}_{22}^{q}\right)^{w_2}}\right)\right\}\\
&=v_1\left(\prod_{i=1}^{\ddot{n}}\sim_{i1}^{w_i},\sqrt[q]{1-\prod_{i=1}^{2}\left(1-\ddot{\sim}_{i1}^{q}\right)^{w_i}}\right)\otimes v_2\left(\prod_{i=1}^{\ddot{n}}\sim_{i1}^{w_i},\sqrt[q]{1-\prod_{i=1}^{2}\left(1-\ddot{\sim}_{i2}^{q}\right)^{w_i}}\right)\\
&=\left(\left(\prod_{i=1}^{2}\sim_{i1}^{w_i}\right)^{v_1},\sqrt[q]{1-\left(\prod_{i=1}^{2}\left(1-\ddot{\sim}_{i1}^{q}\right)^{w_i}\right)^{v_1}}\right)\otimes\left(\frac{\left(\prod_{i=1}^{2}\sim_{i2}^{w_i}\right)^{v_2}}{\sqrt[q]{1-\left(\prod_{i=1}^{2}\left(1-\ddot{\sim}_{i2}^{q}\right)^{w_i}\right)^{v_2}}}\right)\\
&=\left(\prod_{j=1}^{2}\left(\prod_{i=1}^{2}\sim_{ij}^{w_i}\right)^{v_1},\sqrt[q]{1-\prod_{j=1}^{2}\left(\prod_{i=1}^{2}\left(1-\ddot{\sim}_{ij}^{q}\right)^{w_i}\right)^{v_j}}\right).
\end{aligned}
\tag{31}
$$

Hence, the result is true for $\ddot{n}=2$ and $\ddot{m}=2$. Further suppose that equation (28) is true for $\ddot{m}=k_1+1,\ddot{n}=k_2$ and $\ddot{m}=k_1,\ddot{n}=k_2+1$, such as

$$
\begin{aligned}
\otimes_{j=1}^{k_1+1}v_j\left(\otimes_{i=1}^{k_2}w_i\S_{\overline{\kappa}_{ij}}\right)&=\left(\prod_{j=1}^{k_1+1}\left(\prod_{i=1}^{k_2}\sim_{ij}^{w_i}\right)^{v_j},\sqrt[q]{1-\prod_{j=1}^{k_1+1}\left(\prod_{i=1}^{k_2}\left(1-\ddot{\sim}_{i1}^{q}\right)^{w_i}\right)^{v_j}}\right),\\
\otimes_{j=1}^{k_1}v_j\left(\otimes_{i=1}^{k_2+1}w_i\S_{\overline{\kappa}_{ij}}\right)&=\left(\prod_{j=1}^{k_1}\left(\prod_{i=1ij}^{k_2+1}\sim^{w_i}\right)^{v_j},\sqrt[q]{1-\prod_{j=1}^{k_1}\left(\prod_{i=1}^{k_2+1}\left(1-\ddot{\sim}_{i1}^{q}\right)^{w_i}\right)^{v_j}}\right).
\end{aligned}
\tag{32}
$$

For $\ddot{m}=k_1+1,\ddot{n}=k_2+1$, we have

$$
\begin{aligned}
\otimes_{j=1}^{k_1+1}v_j\left(\otimes_{i=1}^{k_2+1}w_i\S_{\overline{\kappa}_{ij}}\right)&=\otimes_{j=1}^{k_1+1}v_j\left(\otimes_{i=1}^{k_2}w_i\S_{\overline{\kappa}_{ij}}\otimes w_{k_2+1}\S_{\overline{\kappa}_{(k_2+1)j}}\right)\\
&=\otimes_{j=1}^{k_1+1}\otimes_{i=1}^{k_2}v_jw_i\S_{\overline{\kappa}_{ij}}\otimes\otimes_{j=1}^{k_1+1}v_jw_{k_2+1}\S_{\overline{\kappa}_{(k_2+1)j}}\\
&=\left(\begin{array}{c}\prod_{j=1}^{k_1+1}\left(\prod_{i=1}^{k_2}\sim_{ij}^{w_i}\right)^{v_j}\otimes\prod_{j=1}^{k_1+1}\left(\left(\sim_{\overline{\kappa}(k_2+1)j}\right)^{w_{k_2+1}}\right)^{v_j}\\ \sqrt[q]{1-\prod_{j=1}^{k_1+1}\left(\prod_{i=1}^{k_2}\left(1-\ddot{\sim}_{i1}^{q}\right)^{w_i}\right)^{v_j}}\otimes\sqrt[q]{1-\prod_{j=1}^{k_1+1}\left(\left(1-\ddot{\sim}_{\overline{\kappa}(k_2+1)j}^{q}\right)^{w_{k_2+1}}\right)^{v_j}}\end{array}\right)\\
&=\left(\prod_{j=1}^{k_1+1}\left(\prod_{i=1}^{k_2+1}\sim_{ij}^{w_i}\right)^{v_j},\sqrt[q]{1-\prod_{j=1}^{k_1+1}\left(\prod_{i=1}^{k_2+1}\left(1-\ddot{\sim}_{\overline{\kappa}(k_2+1)j}^{q}\right)^{w_i}\right)^{v_j}}\right).
\end{aligned}
\tag{33}
$$

Hence, it is true for $\ddot{m} = k_1 + 1$ and $\ddot{n} = k_2 + 1$. Therefore, equation (26) is true for all $\ddot{m}, \ddot{n} \geq 1$, by mathematical induction. □

Theorem 4. *Let* $\$_{\overline{\kappa}_k} = (\curvearrowright_{\overline{\overline{\wedge}}(\overline{\kappa}_k)}, \ddot{\curvearrowright}_{\overline{\overline{\wedge}}(\overline{\kappa}_k)})$ *be a q-ROFHN and* $w_i = \{w_1, w_2, \ldots, w_{\ddot{n}}\}$ *and* $v_i = \{v_1, v_2, \ldots, v_{\ddot{m}}\}$ *be the weight vectors of the experts and selected parameters of subattributes, respectively, having the condition that* $w_i > 0, \sum_{i=1}^{\ddot{n}} w_i = 1, v_i > 0, \sum_{i=1}^{\ddot{m}} v_i = 1$. *Then, the q-ROFHWA operator holds for the following properties:*

Idempotency: if $\$_{\overline{\kappa}_k} = \zeta_{\overline{\kappa}}$ *for all (i = 1, 2, . . ., n) and (j = 1, 2, . . ., m), then q-ROFHWA* $(\$_{\overline{\kappa}_{11}}, \$_{\overline{\kappa}_{12}}, \ldots, \$_{\overline{\kappa}_{nm}}) = \zeta_{\overline{\kappa}}$.

Proof. As we know $\$_{\overline{\kappa}_k} = (\curvearrowright_{\overline{\overline{\wedge}}(\overline{\kappa}_k)}, \ddot{\curvearrowright}_{\overline{\overline{\wedge}}(\overline{\kappa}_k)}) = \zeta_{\overline{\kappa}}$ is a collection of q-ROFHNs, then from Theorem 1, we have

$$
\begin{aligned}
q - ROFHWA\left(\$_{\overline{\kappa}_{11}}, \$_{\overline{\kappa}_{12}}, \ldots, \$_{\overline{\kappa}_{nm}}\right) &= \left(\prod_{j=1}^{\ddot{m}}\left(\prod_{i=1}^{\ddot{n}}\left(\curvearrowright_{\overline{\kappa}_k}\right)^{w_i}\right)^{v_j}, \sqrt[q]{1 - \prod_{j=1}^{\ddot{m}}\left(\prod_{i=1}^{\ddot{n}}\left(1 - \ddot{\curvearrowright}_{\overline{\kappa}_k}^{q}\right)^{w_i}\right)^{v_j}}\right) \\
&= \left(\left(\curvearrowright_{\overline{\kappa}_k}\right)^{\sum_{i=1}^{\ddot{n}} w_i}\right)^{\sum_{j=1}^{\ddot{m}} v_j}, \sqrt[q]{1 - \left(\left(1 - \ddot{\curvearrowright}_{\overline{\kappa}_k}^{q}\right)^{\sum_{i=1}^{\ddot{n}} w_i}\right)^{\sum_{j=1}^{\ddot{m}} v_j}} \\
&= \left(\curvearrowright_{\overline{\kappa}_k}, \sqrt[q]{1 - \left(1 - \ddot{\curvearrowright}_{\overline{\kappa}_k}^{q}\right)}\right) \\
&= \zeta_{\overline{\kappa}}.
\end{aligned} \tag{34}
$$

Therefore,

$$
q - \mathrm{ROFHWG}\left(\$_{\overline{\kappa}_{11}}, \$_{\overline{\kappa}_{12}}, \ldots, \$_{\overline{\kappa}_{nm}}\right) = \zeta_{\overline{\kappa}}. \tag{35}
$$

(ii) Boundedness: if

$$
\$_{\overline{\kappa}_{ij}}^{-} = \left(\min_j \min_i \left\{\curvearrowright_{\overline{\overline{\wedge}}}\left(\overline{\kappa}_{ij}\right)\right\}, \max_j \max_i \left\{\ddot{\curvearrowright}_{\overline{\overline{\wedge}}}\left(\overline{\kappa}_{ij}\right)\right\}\right), \tag{36}
$$

$$
\$_{\overline{\kappa}_{ij}}^{+} = \left(\max_j \max_i \left\{\curvearrowright_{\overline{\overline{\wedge}}}\left(\overline{\kappa}_{ij}\right)\right\}, \min_j \min_i \left\{\ddot{\curvearrowright}_{\overline{\overline{\wedge}}}\left(\overline{\kappa}_{ij}\right)\right\}\right), \tag{37}
$$

then

$$
\$_{\overline{\kappa}_{ij}}^{-} \leq q - \mathrm{ROFHWG}\left(\$_{\overline{\kappa}_{11}}, \$_{\overline{\kappa}_{12}}, \ldots, \$_{\overline{\kappa}_{nm}}\right) \leq \$_{\overline{\kappa}_{ij}}^{+}. \tag{38}
$$

□

Proof of Theorem 4. Part ii. $\$_{\overline{\kappa}_{ij}}^{-} = (\min_j \min_i \left\{\curvearrowright_{\overline{\overline{\wedge}}(\overline{\kappa}_{ij})}\right\}, \max_j \max_i \left\{\tilde{\curvearrowright}_{\overline{\overline{\wedge}}(\overline{\kappa}_{ij})}\right\})$ and $\$_{\overline{\kappa}_{ij}}^{+} = (\max_j \max_i \left\{\curvearrowright_{\overline{\overline{\wedge}}(\overline{\kappa}_{ij})}\right\}, \min_j \min_i \left\{\ddot{\curvearrowright}_{\overline{\overline{\wedge}}(\overline{\kappa}_{ij})}\right\})$. To prove that $\$_{\overline{\alpha}_{ij}}^{-} \leq q\text{-ROFHWG}(\$_{\overline{\alpha}_{11}}, \$_{\overline{\alpha}_{12}}, \ldots, \$_{\overline{\alpha}_{\ddot{m}\ddot{m}}}) \leq \$_{\overline{\alpha}_{ij}}^{+}$, for each $i = 1, 2, \ldots, \ddot{n}$ and $j = 1, 2, \ldots, \ddot{m}$, we have

$$
\begin{aligned}
&\min_j \min_i \left\{\curvearrowright_{\overline{\overline{\wedge}}}\left(\overline{\kappa}_{ij}\right)\right\} \leq \curvearrowright_{\overline{\overline{\wedge}}}\left(\overline{\kappa}_{ij}\right) \\
&\leq \max_j \max_i \left\{\curvearrowright_{\overline{\overline{\wedge}}}\left(\overline{\kappa}_{ij}\right)\right\} \\
&\Rightarrow \min_j \min_i \left\{\curvearrowright_{\overline{\overline{\wedge}}}^{q}\left(\overline{\kappa}_{ij}\right)\right\} \leq \curvearrowright_{\overline{\overline{\wedge}}}^{q}\left(\overline{\kappa}_{ij}\right) \leq \max_j \max_i \left\{\curvearrowright_{\overline{\overline{\wedge}}}^{q}\left(\overline{\kappa}_{ij}\right)\right\} \\
&\Leftrightarrow \left(\min_j \min_i \left\{\curvearrowright_{\overline{\overline{\wedge}}}^{q}\left(\overline{\kappa}_{ij}\right)\right\}\right)^{w_i} \leq \left(\curvearrowright_{\overline{\overline{\wedge}}}^{q}\left(\overline{\kappa}_{ij}\right)\right)^{w_i} \\
&\leq \left(\max_j \max_i \left\{\curvearrowright_{\overline{\overline{\wedge}}}^{q}\left(\overline{\kappa}_{ij}\right)\right\}\right)^{w_i} \\
&\Leftrightarrow \left(\min_j \min_i \left\{\curvearrowright_{\overline{\overline{\wedge}}}^{q}\left(\overline{\kappa}_{ij}\right)\right\}\right)^{\sum_{i=1}^{\ddot{n}} w_i} \leq \prod_{i=1}^{\ddot{n}}\left(\curvearrowright_{\overline{\overline{\wedge}}}^{q}\left(\overline{\kappa}_{ij}\right)\right)^{w_i} \\
&\leq \left(\max_j \max_i \left\{\curvearrowright_{\overline{\overline{\wedge}}}^{q}\left(\overline{\kappa}_{ij}\right)\right\}\right)^{\sum_{i=1}^{\ddot{n}} w_i}
\end{aligned}
$$

$$\begin{aligned}
&\Leftrightarrow\left(\min_j\min_i\left\{\sim^{q}_{\overline{\overline{\kappa}}}\left(\overline{\kappa}_{ij}\right)\right\}\right)^{\sum_{j=1}^{\ddot{m}}v_j}\leq\prod_{j=1}^{\ddot{m}}\left(\prod_{i=1}^{\ddot{n}}\left(\sim^{q}_{\overline{\overline{\kappa}}}\left(\overline{\kappa}_{ij}\right)\right)^{w_i}\right)^{v_j}\\
&\leq\left(\max_j\max_i\left\{\sim^{q}_{\overline{\overline{\kappa}}}\left(\overline{\kappa}_{ij}\right)\right\}\right)^{\sum_{j=1}^{\ddot{m}}v_j}\\
&\Leftrightarrow\min_j\min_i\left\{\sim^{q}_{\overline{\overline{\kappa}}}\left(\overline{\kappa}_{ij}\right)\right\}\leq\prod_{j=1}^{\ddot{m}}\left(\prod_{i=1}^{\ddot{n}}\left(\sim^{q}_{\overline{\overline{\kappa}}}\left(\overline{\kappa}_{ij}\right)\right)^{w_i}\right)^{v_j}\\
&\leq\max_j\max_i\left\{\sim^{q}_{\overline{\overline{\kappa}}}\left(\overline{\kappa}_{ij}\right)\right\}\\
&\Leftrightarrow\min_j\min_i\left\{\sim_{\overline{\overline{\kappa}}}\left(\overline{\kappa}_{ij}\right)\right\}\leq\prod_{j=1}^{\ddot{m}}\left(\prod_{i=1}^{\ddot{n}}\left(1-\sim^{q}_{\overline{\overline{\kappa}}}\left(\overline{\kappa}_{ij}\right)\right)^{w_i}\right)^{v_j}\\
&\leq\max_j\max_i\left\{\sim_{\overline{\overline{\kappa}}}\left(\overline{\kappa}_{ij}\right)\right\}.
\end{aligned}\tag{39}$$

Hence,

$$\min_j\min_i\left\{\sim_{\overline{\overline{\kappa}}}\left(\overline{\overline{\alpha}}_{ij}\right)\right\}\leq\prod_{j=1}^{\ddot{m}}\left(\prod_{i=1}^{\ddot{n}}\left(\sim^{q}_{\overline{\overline{\kappa}}}\left(\overline{\kappa}_{ij}\right)\right)^{w_i}\right)^{v_j}\leq\max_j\max_i\left\{\sim_{\overline{\overline{\kappa}}}\left(\overline{\kappa}_{ij}\right)\right\}.\tag{40}$$

Next, for each $i=1,2,\ldots,\ddot{n}$ and $j=1,2,\ldots,\ddot{m}$, we have

$$\begin{aligned}
&\min_j\min_i\left\{\ddot{\sim}_{\overline{\overline{\kappa}}}\left(\overline{\kappa}_{ij}\right)\right\}\leq\ddot{\sim}_{\overline{\overline{\kappa}}}\left(\overline{\kappa}_{ij}\right)\\
&\leq\max_j\max_i\left\{\ddot{\sim}_{\overline{\overline{\kappa}}}\left(\overline{\kappa}_{ij}\right)\right\}\\
&\Leftrightarrow\sqrt[q]{1-\prod_{j=1}^{\ddot{m}}\left(\prod_{i=1}^{\ddot{n}}\left(\min_j\min_i\left\{1-\ddot{\sim}_{\overline{\overline{\kappa}}}\left(\overline{\kappa}_{ij}\right)\right\}\right)^{w_i}\right)^{v_j}}\leq\sqrt[q]{1-\prod_{j=1}^{\ddot{m}}\left(\prod_{i=1}^{\ddot{n}}\left(1-\ddot{\sim}_{\overline{\overline{\kappa}}}\left(\overline{\kappa}_{ij}\right)\right)^{w_i}\right)^{v_j}}\\
&\leq\sqrt[q]{1-\prod_{j=1}^{\ddot{m}}\left(\prod_{i=1}^{\ddot{n}}\left(\max_j\max_i\left\{1-\ddot{\sim}_{\overline{\overline{\kappa}}}\left(\overline{\kappa}_{ij}\right)\right\}\right)^{w_i}\right)^{v_j}}\\
&\Leftrightarrow\sqrt[q]{1-\prod_{j=1}^{\ddot{m}}\left(\prod_{i=1}^{\ddot{n}}\left(\min_j\min_i\left\{1-\ddot{\sim}_{\overline{\overline{\kappa}}}\left(\overline{\kappa}_{ij}\right)\right\}\right)^{\sum_{i=1}^{\ddot{n}}w_i}\right)^{\sum_{j=1}^{\ddot{m}}v_j}}\leq\sqrt[q]{1-\prod_{j=1}^{\ddot{m}}\left(\prod_{i=1}^{\ddot{n}}\left(1-\ddot{\sim}_{\overline{\overline{\kappa}}}\left(\overline{\kappa}_{ij}\right)\right)^{w_i}\right)^{v_j}}
\end{aligned}$$

$$\leq \sqrt[q]{1-\prod_{j=1}^{\ddot{m}}\left(\prod_{i=1}^{\ddot{n}}\left(\max_j\max_i\left\{1-\ddot{\sim}_{\overline{\overline{\wedge}}}\left(\overline{\kappa}_{ij}\right)\right\}\right)^{\sum_{i=1}^{\ddot{n}}w_i}\right)^{\sum_{j=1}^{\ddot{m}}v_j}}, \tag{41}$$

which implies that

$$\min_j\min_i\left\{\ddot{\sim}_{\overline{\overline{\wedge}}}\left(\overline{\kappa}_{ij}\right)\right\} \leq \sqrt[q]{1-\prod_{j=1}^{\ddot{m}}\left(\prod_{i=1}^{\ddot{n}}\left(1-\ddot{\sim}_{\overline{\overline{\wedge}}}\left(\overline{\kappa}_{ij}\right)\right)^{w_i}\right)^{v_j}} \leq \max_j\max_i\left\{\ddot{\sim}_{\overline{\overline{\wedge}}}\left(\overline{\kappa}_{ij}\right)\right\}. \tag{42}$$

Therefore, $q-\mathrm{ROFHWG}\left(\S_{\overline{\kappa}_{11}},\S_{\overline{\kappa}_{12}},\ldots,\S_{\overline{\kappa}_{\ddot{n}\ddot{m}}}\right) = \left(\sim_{\overline{\overline{\wedge}}}\left(\overline{\kappa}_{ij}\right),\ddot{\sim}_{\overline{\overline{\wedge}}}\left(\overline{\kappa}_{ij}\right)\right) = \S_{\overline{\kappa}_{ij}}$, so

$$\min_j\min_i\left\{\sim_{\overline{\overline{\wedge}}}\left(\overline{\kappa}_{ij}\right)\right\} \leq \sqrt[q]{\sim^q_{\overline{\overline{\wedge}}}\left(\overline{\kappa}_{ij}\right)} \leq \max_j\max_i\left\{\sim_{\overline{\overline{\wedge}}}\left(\overline{\kappa}_{ij}\right)\right\}, \tag{43}$$

$$\min_j\min_i\left\{\ddot{\sim}_{\overline{\overline{\wedge}}}\left(\overline{\kappa}_{ij}\right)\right\} \leq \ddot{\sim}_{\overline{\overline{\wedge}}}\left(\overline{\kappa}_{ij}\right) \leq \max_j\max_i\left\{\ddot{\sim}_{\overline{\overline{\wedge}}}\left(\overline{\kappa}_{ij}\right)\right\}. \tag{44}$$

So, we have

$$\begin{aligned} S\left(\S_{\overline{\kappa}_{ij}}\right) &= \left(\sim_{\overline{\overline{\wedge}}}\left(\overline{\kappa}_{ij}\right)\right)^q - \left(\ddot{\sim}_{\overline{\overline{\wedge}}}\left(\overline{\kappa}_{ij}\right)\right)^q \\ &\leq \max_j\max_i\left\{\sim_{\overline{\overline{\wedge}}}\left(\overline{\kappa}_{ij}\right)\right\}^q - \min_j\min_i\left\{\ddot{\sim}_{\overline{\overline{\wedge}}}\left(\overline{\kappa}_{ij}\right)\right\}^q \\ &= S\left(\S^+_{\overline{\kappa}_{ij}}\right), \\ S\left(\S_{\overline{\kappa}_{ij}}\right) &= \left(\sim_{\overline{\overline{\wedge}}}\left(\overline{\kappa}_{ij}\right)\right)^q - \left(\ddot{\sim}_{\overline{\overline{\wedge}}}\left(\overline{\kappa}_{ij}\right)\right)^q \\ &\geq \min_j\min_i\left\{\sim_{\overline{\overline{\wedge}}\overline{\overline{\wedge}}}\left(\overline{\kappa}_{ij}\right)\right\}^q - \max_j\max_i\left\{\widetilde{\sim}_{\overline{\overline{\wedge}}}\left(\overline{\kappa}_{ij}\right)\right\}^q \\ &= S\left(\S^-_{\overline{\kappa}_{ij}}\right). \end{aligned} \tag{45}$$

Then,

$$S\left(\S^-_{\overline{\kappa}_{ij}}\right) \leq q-\mathrm{ROFHWG}\left(\S_{\overline{\kappa}_{11}},\S_{\overline{\kappa}_{12}},\ldots,\S_{\overline{\kappa}_{\ddot{n}\ddot{m}}}\right) \leq S\left(\S^+_{\overline{\kappa}_{ij}}\right). \tag{46}$$

□

4. Proposed Methodology

Decision making is a technique used to choose logical alternatives in different cases/environment. Here, we will use our proposed technique under q rung orthopair fuzzy hypersoft sets environment for multi criteria decision making process. Let $\{Q^1,Q^2,\ldots,Q^s\}$ be a set of s attributes and $\{x_1,x_2,\ldots,x_{\ddot{n}}\}$ be a set of n experts. The weight of experts are given as $w=\{w_1,w_2,\ldots,w_{\ddot{n}}\}^T$. Let $\bar{\omega}=\{\bar{\omega}_1,\bar{\omega}_2,\ldots,\bar{\omega}_{\ddot{m}}\}$ be the set of attributes with their corresponding subattributes as $\bar{\omega}=\{\bar{\omega}_{1a}\times\bar{\omega}_{2a}\times,\ldots\times\bar{\omega}_{mp}\}$ for all $a\in\{1,2,\ldots,t\}$ with weights $v=\{v_{1a}\times v_{2a}\times,\ldots\times v_{\ddot{m}p}\}$ such as $v_a>0,\sum_{p=1}^t a_a=1$. The following algorithm can be used to make a decision:

Step 1. Construct a decision matrix containing subattributes of parameters.

Step 2. Construct a decision matrix based on the experts' evaluations of each alternative in the form of q-ROFNs.

$$(Q,\acute{\bar{\omega}}) = \left[\S^q_{\overline{\kappa}_{ij}}\right]_{\ddot{n}\times\ddot{m}} = \begin{pmatrix} \S^q_{\overline{\kappa}_{11}} & \S^q_{\overline{\kappa}_{12}} & \cdots & \S^{\mathrm{q}}_{\overline{\kappa}_{1m}} \\ \S^q_{\overline{\kappa}_{21}} & \S^q_{\overline{\kappa}_{22}} & \cdots & \S^{\mathrm{q}}_{\overline{\kappa}_{2\ddot{m}}} \\ . & . & \cdots & . \\ . & . & \cdots & . \\ . & . & \cdots & . \\ \S^q_{\overline{\kappa}_{\ddot{n}1}} & \S^q_{\overline{\kappa}_{\ddot{n}2}} & \cdots & \S^{\mathrm{q}}_{\overline{\kappa}_{\ddot{n}\ddot{m}}} \end{pmatrix}. \tag{47}$$

Figure 1: 1BTC = 46004.15 USD (source: price index data from CoinDesk (https://coinmarketcap.com/currencies/bitcoin/?period=7d)).

Table 5: Decision matrix for cryptocurrency market.

A_1	$\overline{\kappa}_1$	$\overline{\kappa}_2$	$\overline{\kappa}_3$	$\overline{\kappa}_4$	$\overline{\kappa}_5$	$\overline{\kappa}_6$	$\overline{\kappa}_7$	$\overline{\kappa}_8$
X_1	(.91, .97)	(.81, .97)	(.96, .98)	(.79, .68)	(.81, .98)	(.79, .98)	(.79, .96)	(.97, .98)
X_2	(.87, .98)	(.98, .88)	(.88, .98)	(.85, .99)	(.87, .99)	(.86, .87)	(.86, .97)	(.90, .98)
X_3	(.87, .89)	(.98, .79)	(.77, .99)	(.88, .97)	(.88, .89)	(.97, .99)	(.79, .98)	(.89, .79)
X_4	(.67, .98)	(.89, .98)	(.87, .99)	(.95, .86)	(.87, .96)	(.78, .89)	(.97, .87)	(.79, .98)

Table 6: Decision matrix for alternative (A_1 = Tether).

A_1	$\overline{\kappa}_1$	$\overline{\kappa}_2$	$\overline{\kappa}_3$	$\overline{\kappa}_4$	$\overline{\kappa}_5$	$\overline{\kappa}_6$	$\overline{\kappa}_7$	$\overline{\kappa}_8$
X_1	(.71, .98)	(.81, .91)	(.91, 0.98)	(.79, .68)	(.81, .98)	(.77, .98)	(.73, .94)	(.79, .98)
X_2	(.81, .88)	(.78, .88)	(.88, .98)	(.85, .99)	(.85, .89)	(.83, .88)	(.83, .87)	(.99, .78)
X_3	(.78, .89)	(.98, .69)	(.77, .69)	(.88, .77)	(.88, .89)	(.98, .89)	(.79, .98)	(.88, .79)
X_4	(.67, .87)	(.69, .88)	(.87, .99)	(.97, .86)	(.87, .96)	(.68, .89)	(.97, .87)	(.69, .88)

Table 7: Decision matrix for alternative (A_2 = Binance Coin (BNB)).

A_1	$\overline{\kappa}_1$	$\overline{\kappa}_2$	$\overline{\kappa}_3$	$\overline{\kappa}_4$	$\overline{\kappa}_5$	$\overline{\kappa}_6$	$\overline{\kappa}_7$	$\overline{\kappa}_8$
X_1	(.74, .98)	(.76, .98)	(.95, .98)	(.81, .91)	(.89, .98)	(.76, .98)	(.83, .94)	(.95, .93)
X_2	(.83, .87)	(.98, .88)	(.98, .88)	(.78, .88)	(.84, .99)	(.93, .88)	(.87, .85)	(.97, .76)
X_3	(.78, .79)	(.85, .89)	(.74, .79)	(.98, .69)	(.85, .89)	(.95, .89)	(.83, .89)	(.89, .74)
X_4	(.97, .87)	(.89, .76)	(.87, .93)	(.69, .88)	(.98, .79)	(.98, .84)	(.94, .86)	(.79, .84)

Step 3. Aggregate all the alternatives according to the proposed aggregation operators, i.e., weighted average and weighted geometric operator.

Step 4. Calculate each alternative's score.

Step 5. Choose the best option by ranking the alternatives according to the descending values of the score value.

4.1. Numerical Example. To demonstrate how each stage of the typical decision-making approach works, we present a practical stepwise procedure based on the following scenario. We want to examine the price stability of specific cryptocurrencies (alternative), denoted as A_1 = Tether, A_2 = Binance Coin, A_3 = Ethereum, and A_4 = Bitcoin. A committee of decision makers having weight vector (.16, .25, .33, .26) decides the best cryptocurrency. The attribute-valued sets ϖ = {security, decentralization, demand} with their corresponding subattributes are given as ϖ_1 = security = {a_{11} = strong level of security, a_{12} = low level of security}, ϖ_2 = decentralization = {a_{21} decentralized application (dApp), a_{22} = decentralized autonomous organization (DAO)}, and ϖ_3 = demand = {more demands, less demand}. Then, $\varpi = \varpi_1 \times \varpi_2 \times \varpi_3$ is a set of subattributes which have 3-tuple elements.

$$\begin{aligned}\varpi' &= \{\mathfrak{y}_{11}, \mathfrak{y}_{12}\} \times \{\mathfrak{y}_{21}, \mathfrak{y}_{22}\} \times \{\mathfrak{y}_{31}, \mathfrak{y}_{32}\} \\ &= \left\{ \begin{matrix} c(\mathfrak{y}_{11}, \mathfrak{y}_{21}, \mathfrak{y}_{31}), (\mathfrak{y}_{11}, \mathfrak{y}_{21}, \mathfrak{y}_{32}), (\mathfrak{y}_{11}, \mathfrak{y}_{22}, \mathfrak{y}_{31}), (\mathfrak{y}_{11}, \mathfrak{y}_{22}, \mathfrak{y}_{32}) \\ (\mathfrak{y}_{12}, \mathfrak{y}_{21}, \mathfrak{y}_{31}), (\mathfrak{y}_{12}, \mathfrak{y}_{21}, \mathfrak{y}_{32}), (\mathfrak{y}_{12}, \mathfrak{y}_{22}, \mathfrak{y}_{31}), (\mathfrak{y}_{12}, \mathfrak{y}_{22}, \mathfrak{y}_{32}) \end{matrix} \right\}. \end{aligned} \tag{48}$$

Table 8: Decision matrix for alternative (A_3 = Ethereum).

A_1	$\overline{\kappa}_1$	$\overline{\kappa}_2$	$\overline{\kappa}_3$	$\overline{\kappa}_4$	$\overline{\kappa}_5$	$\overline{\kappa}_6$	$\overline{\kappa}_7$	$\overline{\kappa}_8$
X_1	(.78, .94)	(.76, .98)	(.95, .98)	(.84, .95)	(.93, .84)	(.76, .94)	(.86, .97)	(.89, .98)
X_2	(.86, .87)	(.85, .89)	(.98, .99)	(.87, .87)	(.77, .65)	(.93, .98)	(.88, .85)	(.84, .99)
X_3	(.78, .77)	(.85, .89)	(.77, .78)	(.95, .79)	(.87, .88)	(.92, .89)	(.86, .89)	(.84, .99)
X_4	(.97, .88)	(.83, .79)	(.83, .97)	(.69, .88)	(.74, .89)	(.91, .88)	(.91, .86)	(.85, .89)

Table 9: Decision matrix for alternative (A_4 = Bitcoin).

A_1	$\overline{\kappa}_1$	$\overline{\kappa}_2$	$\overline{\kappa}_3$	$\overline{\kappa}_4$	$\overline{\kappa}_5$	$\overline{\kappa}_6$	$\overline{\kappa}_7$	$\overline{\kappa}_8$
X_1	(.79, .98)	(.79, .68)	(.95, .92)	(.83, .91)	(.89, .98)	(.76, .98)	(.83, .94)	(.95, .94)
X_2	(.83, .84)	(.88, .69)	(.98, .76)	(.78, .81)	(.84, .99)	(.93, .88)	(.86, .81)	(.97, .86)
X_3	(.88, .72)	(.95, .78)	(.84, .78)	(.98, .91)	(.85, .89)	(.95, .89)	(.88, .81)	(.81, .84)
X_4	(.99, .88)	(.69, .97)	(.89, .73)	(.71, .88)	(.98, .79)	(.98, .84)	(.91, .88)	(.71, .88)

Figure 2: 1ETH = 3760.10 USD (source: price index data from CoinDesk (https://coinmarketcap.com/currencies/ethereum/?period=7d)).

Figure 3: 1BNB = 508.32 USD (https://coinmarketcap.com/currencies/bnb/?period=7d).

Let $\acute{\omega} = \{\overline{\kappa}_1, \overline{\kappa}_2, \overline{\kappa}_3, \overline{\kappa}_4, \overline{\kappa}_5, \overline{\kappa}_6, \overline{\kappa}_7, \overline{\kappa}_8\}$ be a set of all subattributes with (.22,.1,.04,.07,.13,.14.11,.17) weights. Under the examined subattributes, each expert will assess each alternative's ratings in the form of q-ROFHNs. The following are the decision processes to determine the optimal alternative using the q-ROFHWA or q-ROFHWG operators:

Step 1. Develop a matrix containing subattributes of parameters (see Table 5).

Figure 4: 1Tether = 1.00 USD (https://coinmarketcap.com/currencies/tether/?period=7d).

Step 2. Develop the decision matrices (see Tables 6–9) of the experts as follows.

Step 3. Aggregated values of experts from given tables are calculated using the given weighted average aggregation operator as follows:

$$\begin{aligned} &A_1, (.881576, .869115),\\ &A_2, (.879565, .860845),\\ &A_3, (.907279, .881586),\\ &A_4, (.916721, 841755). \end{aligned} \tag{49}$$

Step 4. Score value of alternatives.

$$\begin{aligned} A_1 &= 0.012461,\\ A_2 &= 0.01872,\\ A_3 &= 0.025693,\\ A_4 &= 0.074966. \end{aligned} \tag{50}$$

Step 5. The rank of alternatives shows us that $A_4 > A_3 > A_2 > A_1$, and Bitcoin (alternative A_4) is the best among all these cryptocurrencies (alternatives). According to the team of experts, a Bitcoin has a strong security level and decentralized application. Also, Bitcoin has more market demand as compared to other

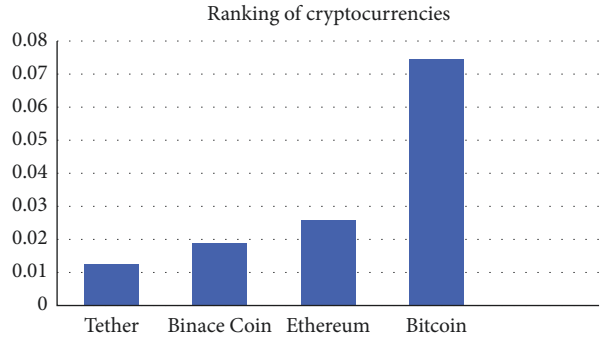

Figure 5: Overall ranking of cryptocurrency.

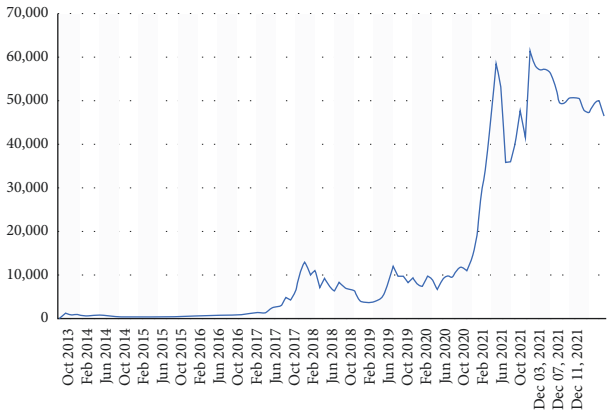

Figure 6: Bitcoin (BTC) price from 2013 to 2021 (source: price index data from CoinDesk (http://www.coindesk.com/price/)).

cryptocurrencies because Bitcoin is a good indicator of the crypto market. Bitcoin's price has rapidly grown in recent months. The latest price rise in the world's most popular cryptocurrency has generated speculation about its future. Therefore, the team of experts announced its decision on Bitcoin. Graphical representation of cryptocurrency (alternatives) is shown in Figure 1.

As we have seen from the result, Bitcoin has a high range compared to other cryptocurrencies. These all have a different price validity in relation to time. First of all, we will discuss the volatility of Bitcoin prices as in April 2011, from 1 USD to a peak of 29.60 USD by June. 2012 was a rather quiet year for Bitcoin, while 2013 saw significant price increases. Bitcoin trading started in January 2013 at 13.28 and peaked at 230 in April. In 2014, its price reached 315.21 USD. Also, its prices still have a big increase from 900 USD in 2016 to 40,000 USD in 2021. The graphical representation of Bitcoin, Ethereum, Binance Coin, and Tether is presented in Figures 2–5.

The combined graphical representation of the price of Bitcoin, Ethereum, Binance Coin, and Tether is shown in Figure 6.

5. Comparison Analysis

We will compare our suggested structure to the present one in this section. Our proposed structure has multiple choices of attributes in which we deal with uncertainty more generally with respect to the fuzzy soft set theory [21], intuitionistic fuzzy soft set [33], the Pythagorean fuzzy soft set [34], and the q-rung orthopair fuzzy soft set [35]. All these existing structures are widely applicable in many fields and areas. However, these theories have restrictions due to their parametrization tool on some specific parameters. On the other hand, when we compare our suggested structure to the hypersoft form of fuzzy sets, such as fuzzy hypersoft set, intuitionistic fuzzy hypersoft set [24], and Pythagorean fuzzy hypersoft set [28], we find that our proposed structure is superior.

The fuzzy hypersoft set, the intuitionistic fuzzy hypersoft set, and the Pythagorean fuzzy hypersoft set are all special cases of the q-rung orthopair fuzzy hypersoft set, as can be shown from these structures. Because our proposed structure provide more information by comparing with existing research. This proposed structure can deal with uncertain data in the decision making process in a very simple way. Therefore, the structure of q rung orthopair fuzzy hypersoft sets is more practical from the existing fuzzy structures. In our proposed structure, we use multiple choices of attributes in order to solve the problems of everyday life. Our proposed structure addressed the uncertainties in a more specific way as compared to the existing structures.

6. Conclusion

To control different types of cryptocurrencies, avoid losses, and continue trading in the online market, an effective and proper analysis of the cryptocurrency market is necessary. The analysis of the cryptocurrency market revealed that security, decentralization, and demand are the most essential elements for Bitcoin investment intentions, followed by financial incentives with a minor difference. Finally, the ranking of subfactors is the high level of security, decentralized application, and increased demand in the cryptocurrency market. As a result, a number of academics and researchers began working on cryptocurrency. Many scholars are turning to fuzzy set theory and its hybrid structures to solve the difficulty of studying the Bitcoin market since ambiguity exists in almost all real-world systems. In this work, a novel scientific instrument is designed that uses a parametric method to expose factual information. The q-rung orthopair fuzzy set and the hypersoft set define the multi-argument functions that provide the set of the q-rung orthopair fuzzy hypersoft. Two aggregation techniques for the q-rung orthopair fuzzy hypersoft sets are weighted mean and weighted geometric. The validity and implementation of the suggested operations and definitions are tested using appropriate examples. This research is also important for decision-making approaches. The main motive of experts in this work is to invest in the cryptocurrency market using a decision-making technique for various attributes and subattributes. In the future, we intend to create new techniques for analyzing the Bitcoin market using decision-making problems.

Data Availability

No data were used to support this study.

Conflicts of Interest

The authors declare that they have no conflicts of interest.

References

[1] S. Nakamoto, ""Bitcoin", A peer-to-peer electronic cash system," 2009, https://bitcoin.org/bitcoin.pdf.

[2] W. Bank Group, *Distributed Ledger Technology (DLT) and Blockchain*, World Bank Group, Washington, DC, USA, 2017.

[3] A. Urquhart, "What causes the attention of Bitcoin?" *Economics Letters*, vol. 166, pp. 40–44, 2018.

[4] D. Garcia, C. J. Tessone, P. Mavrodiev, and N. Perony, "The digital traces of bubbles: feedback cycles between socio-economic signals in the Bitcoin economy," *Journal of The Royal Society Interface*, vol. 11, no. 99, Article ID 20140623, 2014.

[5] K. Ramadani and D. Devianto, "The forecasting model of Bitcoin price with fuzzy time series Markov chain and Chen logical method," in *Proceedings of the AIP Conference Proceedings*, November 2020, Article ID 020095.

[6] C. Jana, M. Pal, and P. Liu, "Multiple attribute dynamic decision making method based on some complex aggregation functions in CQROF setting," *Computational and Applied Mathematics*, vol. 41, no. 3, p. 103, 2022.

[7] M. Palanikumar, K. Arulmozhi, and C. Jana, "Multiple attribute decision-making approach for Pythagorean neutrosophic normal interval-valued fuzzy aggregation operators," *Computational and Applied Mathematics*, vol. 41, no. 3, p. 90, 2022.

[8] L. A. Zadeh, "Fuzzy sets," *Information and Control*, vol. 8, no. 3, 1965.

[9] P. Bhattacharya and N. P. Mukherjee, "Fuzzy relations and fuzzy groups," *Information Sciences*, vol. 36, no. 3, pp. 267–282, 1985.

[10] R. R. Yager, "Aggregation operators and fuzzy systems modeling," *Fuzzy Sets and Systems*, vol. 67, no. 2, pp. 129–145, 1994.

[11] D. Filev and R. R. Yager, "Essentials of fuzzy modeling and control," *Sigart Bulletin*, vol. 6, no. 4, p. 22, 1994.

[12] M. Demirci, "Fuzzy functions and their fundamental properties," *Fuzzy Sets and Systems*, vol. 106, no. 2, pp. 239–246, 1999.

[13] K. T. Atanassov, *Intuitionistic fuzzy sets*, Springer, Berlin, Germany, 1999.

[14] R. R. Yager, "Pythagorean membership grades in multicriteria decision making," *IEEE Transactions on Fuzzy Systems*, vol. 22, no. 4, pp. 958–965, 2014.

[15] Z. Ali, T. Mahmood, T. Mahmood, K. Ullah, and Q. Khan, "Einstein geometric aggregation operators using a novel complex interval-valued pythagorean fuzzy setting with application in green supplier chain management," *Reports in Mechanical Engineering*, vol. 2, no. 1, pp. 105–134, 2021.

[16] A. Ashraf, K. Ullah, K. Ullah, A. Hussain, and M. Bari, "Interval-valued picture fuzzy maclaurin symmetric mean operator with application in multiple attribute decision-making," *Reports in Mechanical Engineering*, vol. 3, no. 1, pp. 301–317, 2022.

[17] R. R. Yager, "Generalized orthopair fuzzy sets," *IEEE Transactions on Fuzzy Systems*, vol. 25, no. 5, pp. 1222–1230, 2017.

[18] M. I. Ali, "Another view on q-rung orthopair fuzzy sets," *International Journal of Intelligent Systems*, vol. 33, no. 11, pp. 2139–2153, 2018.

[19] P. Liu and P. Wang, "Some q-rung orthopair fuzzy aggregation operators and their applications to multiple-attribute decision making," *International Journal of Intelligent Systems*, vol. 33, no. 2, pp. 259–280, 2018.

[20] D. Molodtsov, "Soft set theory-first results," *Computers & Mathematics with Applications*, vol. 37, no. 4-5, pp. 19–31, 1999.

[21] N. Cagman, S. Enginoglu, and F. Citak, "Fuzzy soft set theory and its applications," *Iranian journal of fuzzy systems*, vol. 8, no. 3, pp. 137–147, 2011.

[22] A. R. Roy and P. K. Maji, "A fuzzy soft set theoretic approach to decision making problems," *Journal of Computational and Applied Mathematics*, vol. 203, no. 2, pp. 412–418, 2007.

[23] P. K. Maji, "Neutrosophic soft set," *Annals of Fuzzy Mathematics and Informatics*, vol. 5, no. 1, pp. 157–168, 2013.

[24] F. Smarandache, "Extension of soft set to hypersoft set, and then to plithogenic hypersoft set," *Neutrosophic Sets and Systems*, vol. 22, pp. 168–170, 2018.

[25] M. Saeed, M. Ahsan, M. K. Siddique, and M. R. Ahmad, "A Study of the Fundamentals of Hypersoft Set Theory," *International Journal of Scientific and Engineering Research*, vol. 11, 2020.

[26] S. Rana, M. Qayyum, M. Saeed, F. Smarandache, and B. A. Khan, "Plithogenic Fuzzy Whole Hypersoft Set, Construction of Operators and Their Application in Frequency Matrix Multi Attribute Decision Making Technique," *Neutrosophic Sets and Systems*, vol. 28, 2019.

[27] R. M. Zulqarnain, X. L. Xin, M. Saqlain, and F. Smarandache, "Generalized aggregate operators on neutrosophic hypersoft set," *Neutrosophic Sets and Systems*, vol. 36, pp. 271–281, 2020.

[28] R. M. Zulqarnain, X. L. Xin, and M. Saeed, "A Development of Pythagorean fuzzy hypersoft set with basic operations and decision-making approach based on the correlation coefficient," *Theory and Application of Hypersoft Set*, vol. 6, 2021.

[29] R. M. Zulqarnain, I. Siddique, F. Jarad, R. Ali, and T. Abdeljawad, "Development of topsis technique under pythagorean fuzzy hypersoft environment based on correlation coefficient and its application towards the selection of antivirus mask in covid-19 pandemic," *Complexity*, vol. 2021, Article ID 6634991, 27 pages, 2021.

[30] A. Samad, R. M. Zulqarnain, E. Sermutlu et al., "Selection of an effective hand sanitizer to reduce covid-19 effects and extension of topsis technique based on correlation coefficient under neutrosophic hypersoft set," *Complexity*, vol. 2021, Article ID 5531830, 22 pages, 2021.

[31] R. M. Zulqarnain, X. L. Xin, X. L. Xin, and M. Saeed, "Extension of TOPSIS method under intuitionistic fuzzy hypersoft environment based on correlation coefficient and aggregation operators to solve decision making problem," *AIMS Mathematics*, vol. 6, no. 3, pp. 2732–2755, 2021.

[32] S. K. Khan, M. Gulistan, and H. A. Wahab, "Development of the structure of q-rung orthopair fuzzy hypersoft set with basic operations," *Punjab University Journal of Mathematics*, vol. 53, no. 12, pp. 881–892, 2021.

[33] P. K. Maji, R. Biswas, and A. Roy, "Intuitionistic fuzzy soft sets," *Journal of Fuzzy Mathematics*, vol. 9, pp. 677–692, 2001.

[34] X. Peng, Y. Yang, and J. Song, "Pythagoren fuzzy soft set and its application," *Computer Engineering*, vol. 41, pp. 224–229, 2015.

[35] A. Hussain, M. I. Ali, T. Mahmood, and M. Munir, "q-Rung orthopair fuzzy soft average aggregation operators and their application in multicriteria decision-making," *International Journal of Intelligent Systems*, vol. 35, no. 4, pp. 571–599, 2020.

Hindawi
Complexity
Volume 2022, Article ID 5317738, 18 pages
https://doi.org/10.1155/2022/5317738

Research Article

Reputation Detection for Information Diffusion in Social Network Systems

Yifeng Zhou [1,2] **and Fang Yu** [3]

[1]*School of Information Engineering, Nanjing Audit University, Nanjing 211815, China*
[2]*School of Computer Science and Engineering, Southeast University, Nanjing 211189, China*
[3]*China Electric Power Research Institute, Nanjing 210003, China*

Correspondence should be addressed to Yifeng Zhou; yfzhouseu@gmail.com

Received 15 December 2021; Revised 30 March 2022; Accepted 14 May 2022; Published 7 July 2022

Academic Editor: Yu Zhou

Reputation detection in traditional distributed systems (e.g., electronic commerce systems and peer-to-peer systems) relies heavily on the factor of interaction reputation, which can be derived from direct interactions between agents through bidirectional relationships. However, in the current information diffusion in social network systems (SNS) (e.g., Twitter), the characteristic of the unidirectional relationship between agents and the decay property of diffusion will result in lacking direct interactions; therefore, interaction reputations will be difficult to be obtained by agents in a distributed manner. To solve this problem, a novel distributed reputation detection model following the pattern "*from path to individual*" (*FPTI*) is proposed, which can provide a new reputation factor as an alternative to interaction reputation in such environments. The main idea is that the positive (or negative) observation of an information diffusion process increases (or decreases) the belief of the corresponding diffusion path, which further increases (or decreases) the reputation of each involved agent. Thus, the reputation of a target agent can be assessed by the superimposition of reputations of multiple paths on which this agent has participated in past information diffusion processes. Furthermore, being aware of agent's limited capacity for reputation detection in SNS, we then propose the *enhanced FPTI model* (*eFPTI*), which simplifies the detection source to reduce detection costs and achieve the approximate performance as FPTI. Theoretical analyses and experimental evaluations validate the efficiency and effectiveness of our models and also show several properties of the models, for example, the robustness for dynamic environments.

1. Introduction

Social network systems (SNS) (e.g., Twitter [1, 2] and LinkedIn [3]) provide platforms for online information sharing. Due to the open nature of SNS, some malicious agents may be involved and engage in malicious behavior that will influence the performance of these systems [4–8]. An efficient way to address this problem makes use of the reputation mechanism, which can provide agents with credits for reference that help them make decisions about whom to trust and encourage agents to engage in trustworthy behavior [5, 7, 9–23].

Generally, the reputation of an agent (an agent in a social network system is an autonomous entity that can have interactions with other entities following some interaction rules; for example, an agent in Twitter can interaction with other agents following the rules defined by the Twitter client. It is worth noting that the agent in social network systems can be either a real user or a software bot) is often regarded as the assessment of the behaviors of this agent [15]. Some representative reputation models, for example, Regret (Regret is named by Sabater and Sierra representing "a reputation model for gregarious societies") [16] and FIRE (FIRE, which is from "fides" and "reputation," is named by Huynh et al.) [17], evaluate agents' reputations by integrating reputation factors from various sources, for example, direct interaction experiences, exchange of reputation information, and intrinsic features of agents. Among these

reputation factors, the *interaction reputation* of agents, which is based on direct interactions, is the most crucial because it not only reflects the trustworthiness of agents based on direct interaction experiences, but also can be treated as the basis for reputation information exchange (e.g., neighborhood reputation [16], witness reputation [17]). These reputation models can perform well in traditional distributed systems, for example, electronic commerce systems [13, 15] and P2P systems [24], in which agents have *direct interactions* through bidirectional relationships (the relationship between agents in SNS is the network connection, which is one necessary condition for the behavior transfer; a bidirectional relationship between a pair of agents allows bidirectional behavior transfer, which is often considered as the direct interactions).

However, due to the unidirectional relationship between agents [1, 25], for example, the follower-following topology of Twitter [1], and the decay property of diffusion [26] in the information diffusion scenarios in SNS, direct interactions between agents may be rare. This scarcity of direct interactions makes it difficult to determine the interaction reputations of agents. Traditional reputation models that rely heavily on interaction reputation, for example, Regret [16], FIRE [17], and P2PRep [24], may be of limited use in such environments. This situation will lead to inappropriate formation of trust between agents and may naturally result in the increase of malicious behaviors due to the absence of the effective supervision of agents' behaviors.

To address this problem, we propose a novel reputation detection idea to generate a new reputation factor as an alternative for interaction reputation: a positive observation of an information diffusion process increases the belief of the corresponding diffusion path (a path in this paper represents a queue of agents comprising the information diffusion pathway), which increases the reputation of each involved agent, and conversely, a negative observation decreases the belief of the corresponding diffusion path, which decreases the reputation of each involved agent. This method determines the reputations of agents by following the pattern "*from path to individual*" [27]: the reputation of an agent is evaluated by superimposing the reputations of multiple paths on which this agent participated in previous information diffusion processes. The key contributions of this paper are summarized as follows:

(i) This paper introduces the reputation detection problem considering the unidirectional relationship between agents in information diffusion scenarios in SNS and proposes the detection pattern "*from path to individual*" that employs the path reputation as the intermediate for reputation assessment of agents.

(ii) To detect path reputations in information diffusion processes, *feedback* and *feed-forward* approaches are proposed, which utilize *crossing situations* in information diffusion to check whether malicious behavior has occurred or not and then generate the path reputations.

(iii) To assess the reputations of individual agents from the obtained path reputations, an aggregation approach is proposed on the basis of evidence–belief transformation [28–32], and it especially considers the *suspicion probability* for agents in negative evidences of path reputations.

(iv) With the consideration of agents' limited capacity in SNS, a filtering method is presented, which can simplify the detection source to reduce the detection costs with reputation detection performance guarantee.

The remainder of this paper is organized as follows. In Section 2, we introduce some related research on reputation detection. In Section 3, we present the problem description and the novel reputation detection pattern. In Sections 4 and 5, we introduce the FPTI and eFPTI reputation detection models and conduct theoretical analyses, respectively. Then, in Section 6, we present experimental results that validate our models. Finally, we conclude our paper and discuss the future work in Section 7.

2. Related Work

The eBay model [18] and the Sporas model [19] are two typical reputation models in SNS. The reputation model on eBay [18] estimates the reputations of agents (buyer or seller) by the ratings provided by their partners after transactions. The rating can be −1 (negative rating), 0 (neural rating), or +1 (positive rating). The reputation of an agent (buyer or seller), which is the value of the sum of all the ratings on this agent, is provided on the transaction page attached to the users' screen names. It can indicate the reliability of a buyer or a seller in transactions and can be used as the reference for whether to trade or not. Similar with the eBay model, Sporas [19] also evaluates the reputation of an agent by aggregating the ratings about the agent from others. But by considering that agents may change their behavior patterns over time, which is ignored by the eBay model, Sporas assigned more weight to more recent ratings in the aggregation of reputation evaluation.

Using the eBay [18] and Sporas [19] models, the ratings for reputation evaluation provided by agents (which can be also considered as one kind of interaction reputation) can be generated based on the past experiences of direct interactions between the agents; thus bidirectional relationships between agents are required. Hence, if direct interaction is lacking because of unidirectional relationships between agents [1, 25] and the decay property of diffusion [26], it may be infeasible for reputation evaluation by using these models.

The eBay model [18] and the Sporas [19] model can be classified as single reputation models that assess agents' reputations by a single source. The single reputation model is designed for a specific application scenario and cannot make full use of various information sources in the system. Thus, with the proposal of the integrated reputation model, the single reputation models are often used as key components

to support the reputation aggregation. There are many representative reputation models, such as Regret [16], FIRE [17], FIRE+ (FIRE+ is an extension of FIRE model proposed by Qureshi et al., which can avoid collusion attacks) [20], DISARM (DISARM is a social, distributed, hybrid, rule-based reputation model named by Kravari and Bassiliades, which uses defeasible logic) [21], and AFRAS (AFRAS is from "a fuzzy reputation agent system" named by Carbo et al.) [22], can be classified as integrated reputation models that generate agents' reputations by integrating many reputation factors.

In the Regret model [16], which is implemented in transaction scenarios, the reputations of agents are computed from three dimensions: the individual dimension, the social dimension, and the ontological dimension. The individual dimension component of Regret presents the solution for obtaining the interaction reputation of agents, the social dimension component presents the solutions for producing the indirect reputation factors, and the ontological dimension component can combine different types of reputation factors into a new factor. The FIRE model [17] integrates four types of reputation factors that are derived from direct interaction experiences, witness information, role-based relationships, and certified information. It has been tested in provider and consumer games. The FIRE-+model [20] is devised to avoid collusion attacks that cannot be avoided by the Fire model; it also mainly focuses on the sources of direct and witness-based interaction experiences, but through a graph construction of witness ratings and various interaction policies (direct interaction policy, witness interaction policy, and connection decision policy), collusion among agents can be effectively detected. DISARM [21] introduces a distributed reputation system considering the relationships among agents as a network; DISARM proposes the use of defeasible logic combining the direct and witness information to support accurate reputation assessment. Wu et al. [23] introduce an artificial neural network-based reputation bootstrapping approach, which establishes the reputation of an agent by explicit evidences (direct interaction experiences) and implicit evidences (information that may be relevant with performance) in order to solve the reputation detection problem of newly deployed agents. The AFRAS model [22] introduces the fuzzy logic to represent the agent's reputation; the evaluation of the reputation value of an agent depends on not only the direct interactions, but also the recommendations from other agents of the society.

In these integrated reputation models, the interaction reputation derived from direct interactions can be the most important factor in reputation evaluation. It could be possible to produce some of the indirect reputation factors in these models (e.g., the social dimension reputation in Regret [16] and the witness and certified reputation in FIRE [17], FIRE+ [20], etc.) on the basis of the interaction reputation. However, the studies on these models did not consider the situation that direct interactions were lacking. This situation will not only cause a problem of infeasible interaction reputation generation, but may also make it impossible to determine some indirect reputation factors. In contrast, our models proposed in this paper provide solutions for solving this crucial problem.

3. Problem Description and Our Solutions

Diffusion is a common phenomenon in agents' collective behavior in SNS [33–40]. In previous studies, interaction reputations have often been generated from agents' observations and evaluations of other agents' behaviors [16, 18, 24]. In information diffusion processes (the spread of messages through agents in the network), the diffused *messages* can serve as the measure of the behaviors of agents. Moreover, in current SNS, for example, Twitter [1], messages spreading through agents (users) contain not only the message texts, but also the information of the spreading paths (e.g., the @ behavior in Twitter [1, 25]). This characteristic coincides with the characteristic of the diffusion process of chain letter messages [41]. In information diffusion process, there are two types of agent behaviors when diffusing messages: (a) *malicious behavior*: the agent tampers with the idea or content of some messages it received and diffuses them intentionally or unintentionally [42]; (b) *proper behavior*: the agent diffuses some messages it received with no tampering. To benefit the readers with a quick reference, the major notations of this paper are listed in Table 1.

3.1. Problem Description. Given a SNS, $N = <A, E>$, where A is the set of agents, $\forall <a_i, a_j> \in E$ indicates the existence of an edge directed from agent a_i to a_j. The distributed reputation detection problem in information diffusion scenarios can be described as follows:

$$M_i \longrightarrow \{r_i(j)\}, \tag{1}$$

where M_i represents the local message storage of agent a_i in the information diffusion process, and $r_i(j)$ represents the reputation of a_j produced by a_i. M_i consists of the messages sent by a_i and the messages a_i received from others. (Note that the messages sent by a_i include not only the messages wrote by a_i but also the messages a_i received from others and diffused by itself.)

Based on (1), the process of generating interaction reputations can be simply represented by the following (for brevity, messages with the same ID are labelled by their diffusion paths in the remainder of this paper.):

$$\left[m_{ij}, m_{iji}\right] \in M_i \longrightarrow r_i(j), \tag{2}$$

where m_{ij} indicates one message diffused from a_i to a_j and m_{iji} is the response of m_{ij} from a_j. By observing the response from a_j, a_i can evaluate or update the reputation of a_j.

However, $[m_{ij}, m_{iji}]$, which actually represents the direct interaction in information diffusion, must rely on a bidirectional relationship between a_i and a_j, i.e., $\exists <a_i, a_j>$, $<a_j, a_i> \in E$. Thus, due to the unidirectional relationship between agents in information diffusion, $[m_{ij}, m_{iji}]$ cannot be obtained. Moreover, even if a bidirectional relationship exists, because of the decay property of information diffusion, $[m_{ij}, m_{iji}]$ may also be missing due to the absence of m_{iji}.

Table 1: Major notations.

Notation	Description
A	The set of agents in the system
E	The set of edges in the system; $<a_i, a_j> \in E$ indicates the existence of an edge directed from agent a_i to a_j
$r_i(j)$	The reputation of a_j assessed by a_i
M_i	The local message storage of agent a_i
$m_{o\#i}$	The message with diffusion path $o\#i$, where o indicates the origin agent of this message, i indicates the agent a_i, and "#" represents the upstream path of a_i
$m_{o\#i^*i}$	The message with diffusion path $o\#i^*i$, where o indicates the origin agent of this message, i indicates the agent a_i at the crossing position, and "#" and "*" represent the upstream and downstream paths of a_i, respectively
PR	The path reputation PR = <path, (p, n)>, (p, n) is the corresponding evidence space
$\mathrm{PRF}_j^{\mathrm{PR}_k}$	The path reputation factor of PR_k for agent a_j
$\varepsilon_j^{PR_k}$	The suspicion probability of agent a_j for the negative evidence of PR_k

To solve this problem, a natural approach is to introduce some intermediates for producing the reputations of agents from the message storage. This approach is described as follows:

$$M_i \longrightarrow \{\text{Intermediates}\}_i \longrightarrow \{r_i(j)\}. \quad (3)$$

The intermediates introduced should meet the following requirements: (1) the intermediate can effectively reflect the agents' behaviors in information diffusion processes; and (2) the intermediate can be simply achieved by agents from their local message storage.

Then, the reputation detection problem in information diffusion scenarios in SNS can be divided into three subproblems:

(i) An appropriate intermediate should first be introduced.

(ii) Approaches for obtaining the intermediates should be proposed.

(iii) A mechanism for transforming the intermediates into the reputations of agents should be devised.

3.2. Our Solutions. To solve the above problems, we propose the reputation detection pattern "*from path to individual*." The main idea is that the reputations of agents can be detected according to the observations of their behaviors through the information diffusion paths; hence, the positive (or negative) observation of an information diffusion process increases (or decreases) the belief of the corresponding diffusion path, which further increases (or decreases) the reputation of each involved agent.

(i) To solve the first subproblem, we introduce the concept of *path reputation* (PR) as an intermediate for reputation detection that can meet the requirements for a detection intermediate. (1) Path reputations represent the evidence space for the information diffusion paths, which are past observations of the concatenations of agents' behaviors along the paths. For this reason, each path reputation can partially represent the behavior feature of each agent along the path. (2) Path reputations can be simply detected by agents from their local message storages using path reputation detection approaches described below.

(ii) To solve the second subproblem, *feedback* and *feed-forward* approaches (see Section 4.1) are proposed for path reputation detection. The central idea of these approaches is to find $\{[m]\}_i \subseteq M_i$ that can be used to produce path reputations. Here, $\{[m]\}_i$ represents the message subsets of M_i. The feedback and feed-forward approaches utilize the *crossing situations* in message spreading processes to find appropriate $\{[m]\}_i$, which can provide opportunities for checking whether malicious behaviors exist in the diffusion processes.

(iii) To solve the third subproblem, the *aggregation* approach (see Section 4.2) that can transform the path reputations into reputations of agents is devised. Negative evidence in path reputation can only partially reflect the disbelief of each involved agent because the evidence is the observation of the concatenation of agents' behaviors along the path; that is, the negative evidence may only be caused by the malicious behaviors of partially involved agents. Thus, in the transformation, the *suspicion probability* that can revise the weight of negative evidence for each agent involved is considered.

Figure 1 shows the reputation detection pattern of "*from path to individual*." The reputation detection can be operated synchronously with the operations of information diffusion. When some information diffusion actions result in an update of the local message storage of an agent, the agent can use the path reputation detection component (feedback and feed-forward) to update local path reputations and then update reputations of agents using the aggregation component. In Figure 1, the two dashed boxes represent the reputation detection process and the information diffusion process, respectively, and the arrow between them indicates their synchronous relationship.

4. Reputation Detection Model: *From Path to Individual* (FPTI)

4.1. Path Reputation Detection. Path reputation is composed of two essential parts: (1) the path information, which indicates the track of message spreading from one agent to another (which is actually created based on the information diffusion pathway), and (2) the evidence space, which

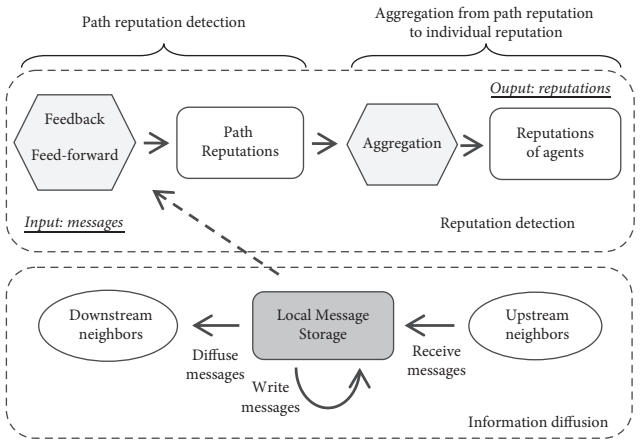

Figure 1: Reputation detection pattern "from path to individual."

contains both positive and negative evidences for the observations of information diffusion along the path. (Positive evidence is derived from the positive observation, which indicates that it is observed that no malicious behavior has been involved during the information diffusion process, and vice versa.) The path reputation is defined as follows:

$$\mathrm{PR} = \langle \mathrm{path}, (p, n) \rangle, \tag{4}$$

where path indicates the path information, and (p, n) is the corresponding evidence space, defined by the number of pieces of positive evidence (p) and negative evidence (n).

For the malicious behavior of tampering in information diffusion, we find that the key factor in detecting the path reputation is to find an appropriate subset of messages to check the correctness of messages that can further generate evidences for their information diffusion paths. In this paper, we utilize the subset of messages whose diffusion paths form a crossing situation, because some messages in such a subset can be treated as a standard for checking the correctness of the other messages. Based on the checking results, the path reputations of their diffusion paths can be generated. For this reason, the messages to be compared in a given subset should have the same ID.

In summary, two types of crossing situations in information diffusion can be utilized:

(1) The *feedback* cross, which is created by a single diffusion path that forms a loop (Figure 2). The corresponding message subset is represented by $[m_{o\#i}, m_{o\#i^*i}]$, where o indicates the origin agent of this message, i indicates the agent a_i at the crossing position, and # and * represent the upstream and downstream paths of a_i, respectively.

(2) The *feed-forward* cross, which is created by multiple diffusion paths joining up (Figure 3). The corresponding message subset is represented by $[m_{o\#i}, m_{o\#'i}, \ldots, m_{o\#''i}]$, in which the messages all have the same ID but have different diffusion paths.

The feedback and feed-forward detection approaches are described in the following sections, with an emphasis on how to provide the checking standard for the feedback and feed-forward crosses.

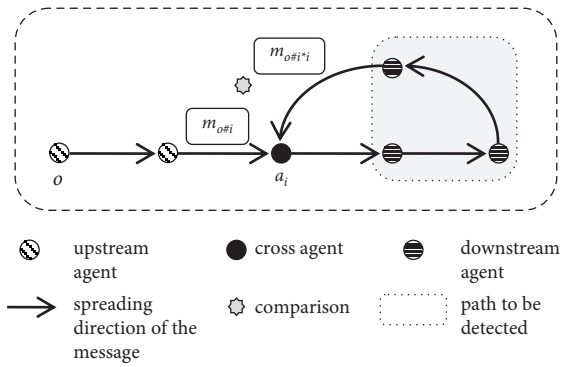

Figure 2: Example for feedback path reputation detection.

4.1.1. Feedback Detection. The feedback detection approach utilizes the feedback crossing situation to generate path reputations. Figure 2 gives an example of a feedback cross. A feedback cross is formed by a single diffusion path of a message having being diffused to cross agent a_i at some time in the past ($m_{o\#i}$) and diffused to a_i again after several diffusion steps ($m_{o\#i^*i}$). The message $m_{o\#i}$ is a previous copy of $m_{o\#i^*i}$; thus, it is used as the standard to check the relative correctness of $m_{o\#i^*i}$, that is, to check whether this message has been tampered with or not along the downstream path after $m_{o\#i}$.

In feedback detection, agents first seek feedback message subsets in their local message storages; then, they check the correctness of the message texts in each message subset; and finally, they generate path reputations of the *downstream paths* based on the checking results.

Figure 2 is an example for feedback detection. To find the feedback message subset, the agents need to find the message whose diffusion path already contains itself twice in its local message storage, i.e., $\exists m_{o\#i^*i} \in M_i$. If $m_{o\#i^*i}$ can be found, the previous version of message $m_{o\#i^*i}$ must also be contained in M_i, i.e., $\exists m_{o\#i} \in M_i$ (See Figure 2). Thus, the feedback message subset $[m_{o\#i}, m_{o\#i^*i}]$ is built. By comparing the texts of the two messages $m_{o\#i}$ and $m_{o\#i^*i}$, evidence for the downstream path "*" can be generated. If there is no difference, a piece of positive evidence is added to the downstream path, i.e., $p = p + 1$, and the number of pieces of negative evidence, n, remains unchanged; otherwise, a piece of negative evidence should be added, i.e., $n = n + 1$, and the number of pieces of positive evidence, p, remains unchanged.

4.1.2. Feed-Forward Detection. The feed-forward detection approach can generate path reputations by utilizing feed-forward crossing situations. A feed-forward crossing situation is formed by multiple diffusion paths joining up. The corresponding messages have the same ID but different diffusion paths.

Thus, the feed-forward message subset is represented by $[m_{o\#i}, m_{o\#'i}, \ldots, m_{o\#''i}]$. To simplify the analysis, the feed-forward message subset is divided into paired messages. For instance, the feed-forward message subset $[m_{o\#i}, m_{o\#'i}, m_{o\#''i}]$ can be divided into $[m_{o\#i}, m_{o\#'i}]$, $[m_{o\#'i}, m_{o\#''i}]$, and $[m_{o\#i},$

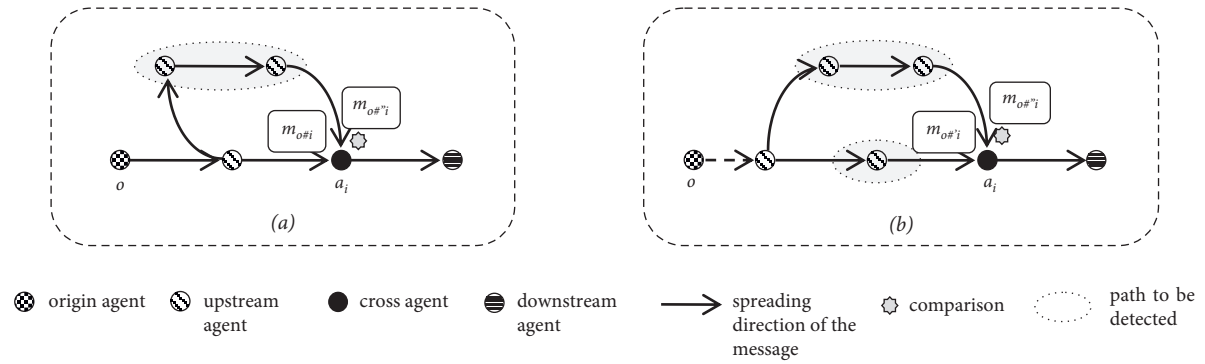

Figure 3: Example for feed-forward path reputation detection.

$m_{o\#''i}$]. Based on the different path relationships, the feed-forward detection approach is studied for two types of paired messages:

(i) The entire diffusion path of one message overlaps with part of the path of another message, as shown in Figure 3(a);

(ii) The diffusion paths of the two messages both have a nonoverlapped part with each other, as shown in Figure 3(b);

Crossing situation (a) can be used to produce the path reputation of the nonoverlapped part of the longer diffusion path. This use is reliable within feed-forward detection because the message with the shorter diffusion path can be treated as the local standard for comparison to check the relative correctness of the other message. Figure 3(a) is an example for crossing situation (a). If there is no difference between the texts of the two messages $m_{o\#i}$ and $m_{o\#''i}$, a piece of positive evidence is added to the path to be detected, i.e., $p = p + 1$, and the number of pieces of negative evidence, n, remains unchanged; otherwise, a piece of negative evidence should be added, i.e., $n = n + 1$, and the number of pieces of positive evidence, p, remains unchanged.

Crossing situation (b) can produce the path reputations of the nonoverlapped part of the message diffusion paths under the condition that the two messages have the same texts. Here, we assume that if a message has been tampered with by different agents, the texts will not be the same; that is, collusion between agents is not considered in this paper. Thus, if the two messages have the same texts, it is presumed that neither message has been tampered with through the nonoverlapping part of the diffusion paths. However, if the texts are different, the crossing situation (b) cannot take effect. Figure 3(b) is an example for crossing situation (b). If there is no difference between the texts of the two messages $m_{o\#'i}$ and $m_{o\#''i}$, a piece of positive evidence is added to each path to be detected, i.e., $p = p + 1$, and the number of pieces of negative evidence, n, remains unchanged; otherwise, the numbers of pieces of positive evidence and negative evidence, p and n, both remain unchanged.

The procedures for executing feed-forward detection are similar to those for feedback detection. For brevity, the procedures are not presented here. Unlike feedback detection, feed-forward detection can detect the *upstream paths* of cross agents.

4.2. Aggregation from Path Reputation to Individual Reputation. After path reputation detections are executed, agents need to transform the path reputations obtained into individual reputations of agents. First, the belief of the path reputation for each agent involved should be calculated. Then, the reputation of a target agent can be evaluated by superimposing the belief values of the multiple paths on which this agent has participated in past information diffusion processes.

4.2.1. Path Reputation Factor Calculation. The path reputation factor (PRF) can be used to reflect the belief of path reputation for each agent involved. Below, agent a_j is considered as the target agent for demonstration purposes.

The main idea in calculating the path reputation factor is to transform the evidence space of the path reputation into a belief value. In each PR, if the positive and negative evidences are treated equally in the transformation, the belief of this PR for each agent will be underestimated, because the negative evidence may be not caused by the action of a_j but rather by other agents within the path. For this reason, the *suspicion probability* of negative evidence for a_j needs to be taken into account. Therefore, the path reputation factor is defined as follows, based on the framework of evidence–belief transformation [28–32].

Let PR_k^p and PR_k^n denote the number of pieces of positive and negative evidence of PR_k, respectively. The path reputation factor of PR_k can be defined as follows:

$$\mathrm{PRF}_j^{\mathrm{PR}_k} = \frac{\mathrm{PR}_k^p + \left(1 - \varepsilon_j^{\mathrm{PR}_k}\right)\mathrm{PR}_k^n}{\mathrm{PR}_k^p + \mathrm{PR}_k^n + 1}, \tag{5}$$

where $\varepsilon_j^{\mathrm{PR}_k}$ denotes the suspicion probability of agent a_i for the negative evidence of PR_k. Thus, $(1 - \varepsilon_j^{\mathrm{PR}_k})\mathrm{PR}_k^n$ denotes the partial belief based on the negative evidences.

In our model, the detection process is executed independently by each agent, none of whom can know the behavior of others (i.e., whether other agents behave properly or maliciously). Thus, the probabilities of other agents behaving maliciously are considered to be 0.5 to reflect neutral opinions. Thus, we have the following:

Theorem 1. *The suspicion probability of each agent for negative evidence is*

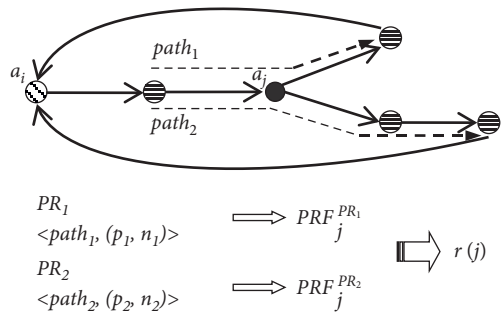

Figure 4: Example for aggregation from path reputations to individual reputations of agents. (The aggregation is taken by agent a_i; and a_j is the target agent).

$$\varepsilon_j^{PR_k} = \frac{\sum_{x=0}^{l-1} C_{l-1}^x}{\sum_{x=1}^{l} C_l^x}, \tag{6}$$

where l is the length (number of agents) along the path of PR_k ($l \geq 1$) and C_l^x indicates the combination in discrete mathematics, which means the number of subsets including x elements from a set of l distinct items.

Proof of Theorem 1. From the perspective of discrete mathematics, the suspicion probability for a_j for each instance of negative evidence should be equal to the ratio of the quantity of combination q that a_j may behave maliciously, no matter how others behave, to the quantity of all possible combinations q'.

$$\begin{aligned} q &= C_{l-1}^0 + C_{l-1}^1 + \cdots + C_{l-1}^{l-1} = \sum_{x=0}^{l-1} C_{l-1}^x, \\ q' &= C_l^1 + C_l^2 + \cdots + C_l^l = \sum_{x=1}^{l} C_l^x. \end{aligned} \tag{7}$$

Therefore, the suspicion probability is represented by the ratio q/q', i.e., $\sum_{x=0}^{l-1} C_{l-1}^x / \sum_{x=1}^{l} C_l^x$ □

From (6), it is observed that the suspicion probability is negatively correlated to the length of the path. If the length is shorter, the suspicion probability of negative evidence for each agent will be higher. According to (6), the suspicion probability for an agent ranges from 0.5 to 1.0. If the length of the path of PR_k is 1, the suspicion probability should have the maximum value of 1.0, and if the length of the path is infinite, the suspicion probability should have the minimum value of 0.5. □

4.2.2. Reputation Aggregation. The idea for the aggregation to evaluate the reputation of the target agent is to consider the superposition of its related path reputation factors (Figure 4). However, the extent of each path reputation factor to be referred to should be different because of their different amounts of evidence.

For this reason, we also investigate the weight of the PRF by considering that the more evidence the PRF is based on, the more dependable it should be. Thus, more evidence will lead to a higher weight value of a PRF. Based on Jøsang's uncertainty proposition in [28, 29], we can define the weight of the PRF of PR_k as follows:

$$w\_PRF_j^{PR_k} = 1 - \frac{1}{PR_k^p + PR_k^n + 1} = \frac{PR_k^p + PR_k^n}{PR_k^p + PR_k^n + 1}. \tag{8}$$

By considering the weight of each PRF, the reputation of a_j is equal to the weighted mean value of all its related path reputation factors. The larger the weight of a PRF is, the more reliable it is for aggregation purposes. Thus, the reputation of a_j as calculated by a_i is as follows:

$$r_i(j) = \frac{\sum_{\forall PR_k \in PR[j]} PRF_j^{PR_k} \times w\_PRF_j^{PR_k}}{\sum_{\forall PR_k \in PR[j]} w\_PRF_j^{PR_k}}, \tag{9}$$

where PR $[j]$ is the set of all relevant path reputations of a_j. PR $[j]$ belongs to PR_i, which is the set of path reputations produced by a_i.

4.3. Analyses of the FPTI Model

4.3.1. Detection Accuracy. The expected reputation of agent, $r_i(j)$, is computed by aggregating all the related path reputation factors. According to (9), we have the following:

$$\Delta_j \leq \max_{1 \leq x \leq |PR[j]|} e_{pa}^x, \tag{10}$$

where Δ_j is the reputation detection error of a_j and e_{pa}^x is the detection error (difference) between the path reputation factors PRF_j and the actual reputation factor AR_j. (Here, the actual reputation factor means the belief of the agent calculated by its real behavior history for each path reputation.) For this reason, we analyze the detection error e_{pa} between each PRF_j and AR_j below.

We set $AR_j = bp_j/(bp_j + bn_j + 1)$ to be the actual reputation factor of a_j here (which is proposed by Jøsang [28] to represent the belief value of an agent), where bp_j and bn_j represent the real number of past proper and malicious behaviors, respectively, of a_j in PRF_j. The total number of pieces of evidence in the path reputation factor PRF_j equals $(bp_j + bn_j)$, i.e., $PR^p + PR^n = bp_j + bn_j$. Note that $PR^p \geq 0$, $PR^n \geq 0$, $bp_j \geq 0$, and $bn_j \geq 0$.

Theorem 2. *The detection error between the path reputation factor and the actual reputation factor of a_j is as follows:*

$$e_{pa} = \left| \left(1 - \varepsilon_j\right) - \frac{\left(1 - \varepsilon_j \left(\prod_{a_k \in A_{pa} - a_j} \omega_k \right)\right) bp_j - \left(1 - \varepsilon_j\right)}{bp_j + bn_j + 1} \right|, \tag{11}$$

where A_{pa} represents the set of agents comprising the path of PRF_j, ω_k is the probability of other involved agent a_k behaving properly within PRF_j, $0 \leq \omega_k \leq 1$, and bp_j and bn_j represent the real number of past proper and malicious behaviors, respectively, of a_j in PRF_j.

Proof of Theorem 2.

$$e_{pa} = \left|\mathrm{PRF}_j - \mathrm{AR}_j\right| = \left|\frac{\mathrm{PR}^p + \left(1-\varepsilon_j\right)\mathrm{PR}^n}{\mathrm{PR}^p + \mathrm{PR}^n + 1} - \frac{bp_j}{bp_j + bn_j + 1}\right|. \tag{12}$$

All the proper behaviors of agents within the path can generate one instance of positive evidence, while one or more agents behaving maliciously will generate one instance of negative evidence. Suppose that the probability of other involved agents a_k behaving properly is ω_k $(0 \le \omega_k \le 1)$. We then have the following:

$$\begin{aligned} &\mathrm{PR}^p + \mathrm{PR}^n = bp_j + bn_j = \Omega, \\ &\mathrm{PR}^p = bp_j\left(\prod_{a_k \in A_{pa} - a_j} \omega_k\right), \\ &\mathrm{PR}^n = bp_j + bn_j - bp_j\left(\prod_{a_k \in A_{pa} - a_j} \omega_k\right). \end{aligned} \tag{13}$$

Hence, $e_{pa} = |(bp_j(\prod_{a_k \in A_{pa}-a_j} \omega_k) + (1-\varepsilon_j)(\Omega - bp_j(\prod_{a_k \in A_{pa}-a_j} \omega_k)))/(\Omega+1) - bp_j/(\Omega+1)|, = |(1-\varepsilon_j) - ((1-\varepsilon_j(\prod_{a_k \in A_{pa}-a_j} \omega_k))bp_j - (1-\varepsilon_j))/(bp_j + bn_j + 1)|$ □

From (11), we find that the detection error e_{pa} should have the minimum value ($e_{pa} = 0$) when bp_j and bn_j satisfy $(1 - \prod_{a_k \in A_{pa}-a_j} \omega_k)\varepsilon_j bp_j = (1-\varepsilon_j)(bn_j + 2)$.

Significantly, we observe one property of the detection accuracy of the FPTI model from (11). In addition to the parameters bp_j and bn_j, which reflect the behavior pattern of a_j, the detection accuracy is also influenced by the parameters ε_j and ω_k, where ε_j is mainly determined by the length of the corresponding diffusion path from equation (6); that is, the number of other involved agents and ω_k indicates the probability of other involved agents behaving properly in diffusion processes along this path. Thus, we have the following: □

Property 1. The detection accuracy of the FPTI model is contextually influenced; that is, the detection accuracy of the FPTI model is determined not only by the behavior pattern of the target agent, but also by the number of other involved agents in the diffusion paths and their behavior patterns.

Based on Property 1, we arrive at the following conclusions, according to (11).

(i) If $bn_j > bp_j$, the larger the difference between them, the greater the degree to which the error e_{pa} is influenced by the suspicion probability ε_j. Assuming that $bn_j >> bp_j$ *and* bn_j is infinite, e_{pa} should equal $1 - \varepsilon_j$.

(ii) If $bp_j > bn_j$, the larger the difference between them, the greater the degree to which the error e_{pa} is influenced by both the suspicion probability ε_j and the probability of other agents behaving properly, ω_j. Assuming that $bp_j >> bn_j$ and bp_j is infinite, e_{pa} should equal $(1 - \prod_{a_k \in A_{pa}-a_j} \omega_k)\varepsilon_j$.

Thus, the more maliciously an agent behaves, the detection accuracy is more likely to be influenced by the number of other involved agents in the diffusion paths; and the more properly an agent behaves, the detection accuracy is more likely to be influenced by both the number and the behavior patterns of other involved agents in the diffusion paths.

4.3.2. Feasibility of FPTI Model. In this section, we analyze the conditions for the implementation of FPTI in the following. Given a SNS, $N = <A, E>$, where A is the set of agents, $\forall <a_i, a_j> \in E$ indicates the edge directed from agent a_i to a_j. Let P_{ij} be a directed path from a_i to a_j. Then, we have the following theorems.

Theorem 3. *Let $C = <A^C, E^C>$ be a subnetwork of N, where $A^C \subseteq A$, $E^C \subseteq E$. If C is a simple cycle (a cycle with no repetitions of agents or edges), then $a_i \in A^C$ can perform feedback detection of FPTI.*

Proof of Theorem 3. $C = <A^C, E^C>$ is a simple cycle and a subnetwork of N. Thus, $a_i \in A^C$ must be a tail of an edge $<a_i, a_x> \in E^C$, and a head of an edge $<a_y, a_i> \in E^C$ where $a_x, a_y \in A^C$; and there exists a directed path P_{xy} from a_x to a_y. Hence, a message can be diffused initially from a_i, then through P_{xy}, and finally back to a_i, where C is the basis on which the feedback cross can form, and a_i is the cross agent of such feedback cross. Therefore, $a_i \in A^C$ can perform feedback detection of FPTI. □ □

Theorem 4. *Let $D = <A^D, E^D>$ be a subnetwork of N, where $A^D \subseteq A$, $E^D \subseteq E$. If D is acyclic (with no cycle), $a_i, a_x \in A^D$, and $\exists P_{xi}, P_{xi}' \subseteq D$, then a_i can perform feed-forward detection of FPTI.*

Proof of Theorem 4. $D = <A^D, E^D>$ is acyclic and a subnetwork of N, and $a_i, a_x \in A^D$. Hence, if $\exists P_{xi}, P_{xi}' \subseteq D$, then $P_{xi} \neq P_{xi}'$. P_{xi} and P_{xi}' provide two different paths for information diffusion from a_x to a_i, and there exist nonoverlapped parts between them. Thus, a message can be diffused respectively through P_{xi} and P_{xi}' and finally reach a_i, so that a feed-forward crossing situation can be formed and a_i is the cross agent. Therefore, $a_i \in A^D$ can perform feed-forward detection of FPTI. □ □

5. Enhanced FPTI Reputation Detection Model

In Section 4, we have presented the FPTI model for reputation detection in information diffusion scenarios in SNS. However, in SNS, the capacity of agents is often limited, for example, the limited capacity of communication [43], and the limited capacity of executing tasks [5, 7]. Hence, the limited capacity of agents in reputation detection should also

be taken into account. As the load of the agent's local message storage increases during the information diffusion process, the detection costs of FPTI sustained by the agents should be larger. Therefore, in this section, we investigate how to achieve satisfactory detection performance but with lower detection costs.

In FPTI, the number of messages used for detection is the key parameter that determines the detection costs. Thus, we design a message filtering method to filter a limited number of messages that are of highest *usability* for reputation detection from the agent's local message storage. The message filtering method promotes the FPTI model to the *enhanced FPTI* (*eFPTI*) model (see Figure 5).

5.1. Message Usability Evaluation. In eFPTI, the effect of the filtered messages on reputation detection can directly determine the reputation detection performance. Thus, to improve the performance of eFPTI, the different effect of the messages on reputation detection should be measured. Hence, we define the *detection value* of the message to reflect its effect on reputation detection. The factors that can reflect the effect of a message on detection performance in FPTI have been shown in Table 2. These factors jointly determine the detection value of a message.

Let S_1^m, S_2^m, S_3^m and S_4^m be the outputs of the four factors in Table 2 for the message m, respectively. The detection value of message m can be defined as

$$V_m = S_1^m \left(\alpha \cdot S_2^m + \beta \cdot S_3^m + \gamma \cdot S_4^m\right), \tag{14}$$

where α, β, and γ are parameters, which reflect the importance of the factors, respectively, shown in Table 2, and $\alpha + \beta + \gamma = 1$, $\alpha > \beta > \gamma$.

Besides the detection value for reputation detection, the *elapsed time* of a message, since it has been received, also needs to be taken into account, because of the timeliness of information diffusion (limited lifetime of the diffusion of the message [44]). If a message has been stored for longer time than other messages, it is considered to have lower probability to be used for reputation detection.

Therefore, jointly considering the detection value and the elapsed time, we give the definition of *usability* of a message. Let T_m denote the elapsed time of the message m; ψ is an attenuation function ($0 \le \psi \le 1$), and the value of $\psi(x)$ decreases monotonically as x increases. The *usability* of m is defined as

$$U_m = \psi(T_m) \cdot V_m. \tag{15}$$

5.2. Usability-Based Filtering. When agents intend to filter messages for reputation detection, they can refer to the usability of each message in their local message storages M_i and then filter the messages with the highest usability for eFPTI.

The filtering method is called *usability-based filtering* and can be described as follows.

[Step 1] Before a_i makes reputation detection, the usability of each message in M_i should be calculated according to (15).

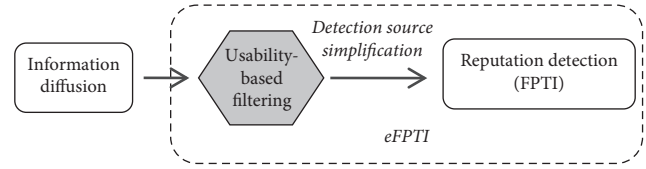

Figure 5: The enhanced FPTI model (eFPTI).

[Step 2] Then, the messages can be sorted according to their usability values.

[Step 3] Finally, the set of messages M_i' with the highest usability will be filtered for eFPTI, where $\forall m' \in M_i'$, $\forall m'' \in M_i - M_i'$, $U_{m'} > U_{m''}$ and $|M_i'| < |M_i|$.

After *usability-based filtering*, the messages, which are most useful for reputation detection in eFPTI, can be available, while the other worthless messages can be excluded from the reputation detection.

5.3. Analyses of the Enhanced FPTI Model

5.3.1. Detection Cost. The detection costs of reputation detection following the pattern "from path to individual" are composed of the following two parts: (1) the detection costs from the detection source (the messages used in detection) to the path reputations, and (2) the detection costs of aggregation from path reputations to individual reputations of agents.

The path reputation detection can be conducted by firstly executing the feedback detection and then executing the feed-forward detection in turn. For the feedback detection, it only needs to check the diffusion path of each recently received message after last detection and update the corresponding path reputation if it meets the conditions (details can be seen in Section 4.1.1); thus, the time complexity is $O(\mu \cdot k)$, where μ is the number of messages received after the last detection, and $k = |E|/|A|$ is the average degree of the system (considering that the length of the information diffusion path can be effectively estimated as proportional to the average degree of the system). For the feedforward detection, it needs to check the diffusion path of each recently received message by comparing with the messages in the local storage and update the related path reputations if it meets the conditions (details can be seen in Section 4.1.2); let $|M|$ be the number of messages in the local storage, and the time complexity is $O(\mu|M|k^2)$, since the time complexity of generating the detection region (paths) and updating the evidence space is $O(k^2)$. Hence, the time complexity of path reputation detection is $O(\mu|M||k|^2)$.

The reputation aggregation transforms the path reputations into individual reputations of agents by firstly calculating the path reputation factors for each agent involved and then evaluating each agent's reputation by superimposing the belief values of multiple paths on which this agent has participated in past information diffusion processes. After path reputation detection, there will be as most $|M|(|M|+1)$ pieces of path reputations ($|M|$ for feedback detection and $|M|^2$ for feed-forward detection); hence, the

Table 2: Factors for evaluating the detection value of a message.

Factors	Measures	Importance* (reason)
Has the message been used for producing path reputation? (F_1)	*Yes,* decreases the value of the message ($S_1^m = 0$) *No,* increases the value of the message ($S_1^m = 1$)	Most important (A message can have little chance to make further advantage for reputation detection if it has been used yet)
Whether the message can be utilized by the feedback detection? (F_2)	*Yes,* increases the value of the message($S_2^m = 1$) *No,* decreases the value of the message($S_2^m = 0$)	Very important (feedback cross can be reliable for path reputation detection)
Whether the message can be utilized by the feed-forward detection? (F_3)	*Yes,* increases the value of the message($S_3^m = 1$) *No,* decreases the value of the message ($S_3^m = 0$)	Important (feed-forward cross cannot be as reliable as feedback cross for path reputation detection)
The diffusion path length of the message. (F_4)	*Longer* length indicates the message has a higher value; *Shorter* length indicates the message has a lower value ($S_4^m = 1 - 1/l$)	Fair (The length of the diffusion path mainly influences the reusability of the corresponding path reputation for reputation aggregation)

time complexity for the calculation of path reputation factors for each agent involved is $O(|M|^2|k|)$. Then, for each agent, the reputation aggregation is conducted by superimposing the belief values of the multiple paths it involved; and the time complexity is $O(|A||M|^2)$. Hence, considering that $k << |A|$ in real social networks, the time complexity of reputation aggregation is $O(|M|^2|A|)$.

The detection costs of reputation detection following the pattern "from path to individual" are composed of (a) the detection costs of path reputation detection, and (b) the detection costs for reputation aggregation. Therefore, the time complexity of the presented FPTI model is $O(\mu|M|k^2 + |M|^2|A|)$. Moreover, the time complexity of eFPTI is $O(\mu|M'|k^2 + |M'|^2|A|)$, where $|M'|$ is the number of messages filtered, while the usability-based filtering is $O(|M'|\log|M'|)$; thus, the detection costs can be reduced effectively because $|M'|$ can be much smaller than $|M|$.

5.3.2. Detection Performance. Let $|M_i'|$ be the limited number of messages in usability-based filtering, let $\mathfrak{t}$ denote the time interval between each implementation of eFPTI to detect agents' reputations (here, we assume the time interval is uniform), and let τ represent the probability that a message can be engaged in the formation of crossing situation. Then, the following theorem can be derived:

Theorem 5. *The optimal limited number of messages of usability-based filtering is $|M_i'|_{OPT} = (Em \cdot \mathfrak{t}) \cdot \tau$, where Em is the expected number of messages stored into the local message storage in a time unit.*

Proof of Theorem 5. The usability-based filtering aims to achieve the best reputation detection performance with the lowest detection costs. Thus, (1) the messages that are valuable for reputation detection should be available after filtering; (2) the limited number of messages in usability-based filtering should be the minimum. Assume that such minimum number is $|M_i'|_{\min}$. In a time interval, $Em \cdot \mathfrak{t}$ is the number of messages received by an agent; thus, $(Em \cdot \mathfrak{t}) \cdot \tau$ can just be the number of messages, which can form the crossing situations that are valuable for reputation detection in eFPTI, so that we can have $|M_i'|_{\min} = (Em \cdot \mathfrak{t}) \cdot \tau$. Therefore, if the eFPTI model is implemented uniformly in such interval, the aim mentioned can be satisfied if $|M_i'|_{\text{OPT}} = |M_i'|_{\min} = (Em \cdot \mathfrak{t}) \cdot \tau$. □

6. Experimental Validation and Analyses

The proposed reputation detection models (FPTI and eFPTI) are validated by experimental evaluations from the following perspectives:

(i) *Feasibility & Effectiveness*: we evaluate the reputation detection performance of our models (FPTI and eFPTI) by using Twitter datasets [45], and we also compare the performance of our two models.

(ii) *Properties*: we first confirm the robustness of the models in different types of dynamic environments. Then, we test the effect of the key parameter, suspicion probability, in the models.

(iii) *Applicability*: we test the applicability of our models by implementing the models into a typical application scenario in information diffusion—misinformation suppression.

6.1. Experimental Settings. The information diffusion scenarios were constructed according to the model presented by Gruhl et al. in their research on information diffusion through blogspace [33]. The details of the information diffusion process in our experiments are described below, and one sketch of the diffusion process is shown in Figure 6. In the information diffusion scenarios considered in this paper, the upstream neighbors of an agent a_i represent the agents that can diffuse messages to a_i, and the downstream neighbors of a_i represent the agents that can receive messages diffused by a_i.

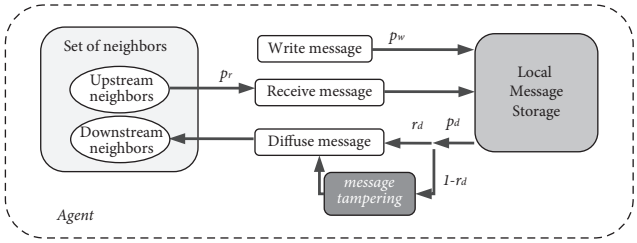

Figure 6: The experimental environment settings.

At the initial state, agents write messages, with probability p_w. At the successive states, agents have the opportunity to receive those messages, with probability p_r. Agents who receive a message can choose whether to diffuse it with diffusion probability p_d. Then, by considering the decay property of information diffusion [26], p_r decreases according to a decreasing function of the time elapsed, which is $p_r = \mathrm{X}(t' - t) \times p_r'$, where t is the time at which the message was initially diffused by the upstream agent, t' is the current time, $\mathrm{X}(t' - t)$ is a function that decreases from 1.0 to 0.0 as $(t' - t)$ increases, and p_r' is the inherent probability of agents receiving messages. Therefore, in the experiments, for each time step, each agent has an opportunity to write messages, receive messages, and diffuse messages, with probabilities of p_w, p_r', and p_d, respectively. The decreasing function $\mathrm{X}(t' - t)$ for receiving probability modification is set to $1/(t' - t)^2$.

The default reputation r_d for each agent is set randomly ranging from 0.0 to 1.0. $1 - r_d$ is the probability that the agent will behave maliciously; for instance, if the r_d of an agent is 0.7, there is a 30% probability that it will engage in malicious behavior at each time step. Moreover, in the eFPTI model, the limited number of message filtering methods, $|M_i'|$, is set to 20.

6.2. Feasibility and Effectiveness of the Models. In this section, we validate the feasibility and effectiveness of our models by using Twitter datasets extracted by Greene and Cunningham [45]: Football (FB), which is the network dataset, consists of 248 football players and clubs active on Twitter and 3819 edges among them, Olympics (OLY), which is the network dataset consists of 464 Twitter accounts of athletes and organizations in London 2012 Summer Olympics and 10642 edges among the accounts, Politics-ie (POL), which is the network dataset of Twitter users including 348 Irish politicians and political organizations and 16856 edges among these users, and Rugby (RUG), which is the dataset of 854 international Rugby Union players, clubs, and organizations active on Twitter and 35757 edges among them. The details of the datasets are shown in Table 3. The datasets include not only the data of network structure, but also the retweeting data among Twitter users, that is, the users and edges actually observed in the retweeting processes, which can be also used to investigate the feasibility of our models.

6.2.1. Feasibility Tests for Path Reputation Detection. To validate the feasibility of FPTI and eFPTI models, we first use the retweeting data (including retweeting relations between paired users and corresponding retweeting weights) to construct real retweeting paths through Twitter users, which are represented by retweeting networks among users. Then, feasible feedback and feed-forward crosses in the retweeting networks, which can support the implementation of reputation detection of the presented FPTI and eFPTI models, have been investigated in depth-first order [46] and breadth-first order [47], respectively.

Table 3: Summary of datasets [45].

Dataset	Users	Edges	Retweeting users	Retweeting edges
Football (FB)	248	3819	234	1350
Olympics (OLY)	464	10642	440	3740
Politics-ie (POL)	348	16856	307	3019
Rugby (RUG)	854	35757	827	12472

Figures 7(a) and 7(b) show the number of feedback and feed-forward crosses discovered from the retweeting networks of the four Twitter datasets. The results show that there are a great number of feasible feedback and feed-forward crosses (even in FB retweeting network with the least nodes and relations) that can be sufficient to support the path reputation detection of FPTI and eFPTI models; namely, the discovered crosses can satisfy the conditions for reputation detection demonstrated by Theorems 2 and 3. Moreover, by comparing the results in Figures 7(a) and 7(b), we find that the numbers of feasible feed-forward crosses in retweeting networks can be much larger than that of feedback crosses; it indicates the higher feasibility of feed-forward detection of our models in path reputation detection. In conclusion, verified by the retweeting data from the Twitter datasets, there are feasible information diffusion structures that can support the implementation of the presented FPTI and eFPTI models for reputation detection in information diffusion scenarios.

6.2.2. Coverage and Accuracy Tests. To test the effectiveness of our models, we first introduce the following baseline model. *The ideal interaction model* (*Ideal model*): in this model, each activity of an agent can be ideally observed by the agent's neighbors immediately as if they have direct interactions during the whole process. In fact, this model cannot be applied in real information diffusion scenarios, but it can be set as the standard (upper bound) for performance evaluation.

The effectiveness tests have been conducted in information diffusion scenarios (see Section 6.1) on Twitter user networks shown in Table 3. The parameters for information diffusion are set as follows: $p_w = 0.05$, $p_r' = 0.1$, and $p_d = 0.1$. The results are obtained at the 500^{th} step of the information diffusion processes.

(1) Coverage Tests. Coverage tests focus on what percentage of the agents in the network can be detected by the reputation model. The detection coverage is defined as $\mathrm{Cov} = |A'|/|A|$, where $|A'|$ is the number of agents whose reputations have been detected, and $|A|$ is the total number of agents in the network.

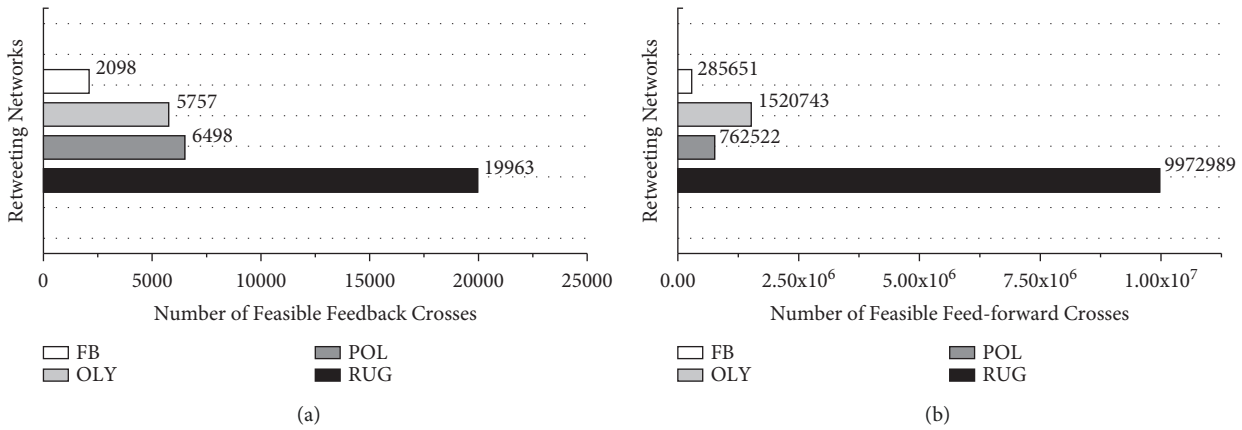

Figure 7: Feasibility validation of path reputation detection of the presented models. (a) Feedback detection. (b) Feed-forward detection.

If employing the ideal model, all the activities of the agents can be ideally observed by their neighbors (which is actually impossible in reality), so that the coverage of the ideal model can keep 1.0 during all the periods. Hence, the results of detection coverage by using the ideal model are omitted here. Table 4 shows the results of the detection coverage of our models (FPTI and eFPTI) in Twitter networks. From Table 4, we find that, using FPTI model, the detection coverage can be equal or greater than 0.74; and in the networks of POL and RUG with relatively higher average degree, the detection coverage can be larger than 0.95, which is close to the optimal results. Then, using eFPTI model, the detection coverage can be closer to that using FPTI model if the average degree of the users is higher; in the POL and RUG networks, the performance loss of eFPTI model can be very low, and the coverage can achieve 0.9. The performance loss using eFPTI is caused by the message filtering introduced in Section 5.

(2) Accuracy Tests. Let er_x be the difference between the detected reputation of an agent and its default reputation set initially. The detection accuracy is defined as $\mathrm{Acc} = \sum_{\forall er_x \in \{er\}} (1 - er_x)/|\{er\}|$, where $\{er\}$ is the set of er_x. The initial er_x in the simulation is set to 0.5.

Figure 8 reports the accuracy test results. The ideal model can obviously have the best performance on detection accuracy. There are two reasons: (1) each activity of an agent can be ideally observed by the agent's neighbors immediately; and (2) the transformation of ideal model from the observed evidences (neighbors' activities) into agents' reputations is set to uniform, which coincides with our experimental settings of agents' behavior pattern. Hence, the ideal model can have a very high accuracy in reputation detection (close to 0.9 in FB and OLY networks, and close to 0.95 in POL and RUG networks).

In Figure 8, we can find that the detection accuracy employing our models can achieve 0.7 on the Twitter user networks. The performance gap between our models and the ideal model is mainly caused by (1) the incomplete information that agents can only obtain in the information diffusion processes, (2) and the transformation error from path reputation into reputations of agents. For the former aspect, the ideal model can have complete information of agents' behaviors in the reputation detection that is actually impossible in reality; then, for the latter aspect, as introduced before, it is very difficult to estimate the reputations of agents from the obtained path reputation because of the concatenation of agents' behaviors through paths in information diffusion scenarios. Therefore, compared with the ideal model, the detection employing FPTI and eFPTI models can be considered to be of high accuracy and satisfying.

Table 4: Detection coverage in twitter networks.

Dataset	FPTI	eFPTI
Football (FB)	0.747 (±0.023)	0.586 (±0.036)
Olympics (OLY)	0.798 (±0.014)	0.718 (±0.015)
Politics-ie (POL)	0.960 (±0.006)	0.939 (±0.006)
Rugby (RUG)	0.980 (±0.002)	0.975 (±0.003)

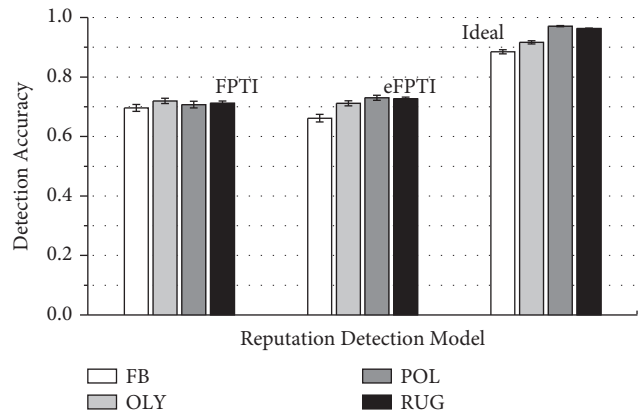

Figure 8: Detection accuracy in twitter networks.

6.2.3. Comparison between Our Two Models. In this section, we compare our presented eFPTI model with the FPTI model. Besides the detection coverage and accuracy, we also compare the detection costs of the two models. Figure 8

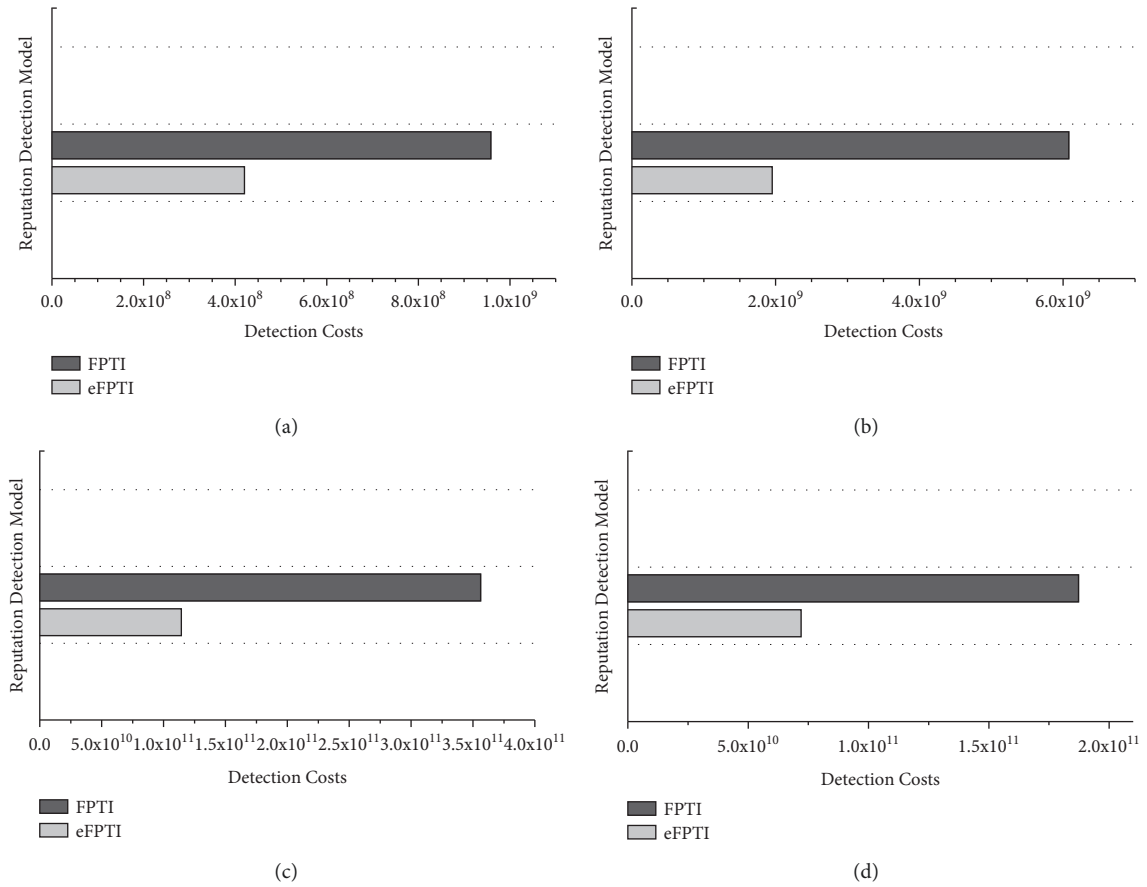

Figure 9: Comparison of the proposed reputation detection models (FPTI vs. eFPTI) on the detection costs. (a) Detection costs in FB network. (b) Detection costs in OLY network. (c) Detection costs in POL network. (d) Detection costs in RUG network.

shows that the eFPTI model can perform as well as the FPTI model on the reputation detection accuracy in all the tested Twitter networks; then, Table 4 indicates that the eFPTI performs a little worse on the detection coverage than the FPTI model, and the performance of eFPTI can be closer to that of FPTI if the network average degree is larger. Finally, in Figure 9, we observe that the reputation detection costs of eFPTI are much lower than those of FPTI in the tested networks. These results validate the advantage of eFPTI. Therefore, the eFPTI model reaches the expected objective to achieve satisfactory performance of reputation detection with lower detection costs.

In conclusion, the presented FPTI and eFPTI models both achieve the corresponding objectives for reputation detection in information diffusion scenarios in SNS, which are verified by several Twitter datasets. The FPTI model performs well on the detection coverage and accuracy; the detection coverage ranges from 0.74 to 0.98, and the detection accuracy can be up to 0.7. The eFPTI model also achieves satisfying performance on detection coverage and accuracy that are close to those of FPTI model in most of the cases, and it can have much lower costs in reputation detection.

6.2.4. Comparison with the Representative. We compare the presented FPTI and eFPTI models with the representative reputation model, *the direct interaction model* (DI) [17, 18] in this section. This benchmark model uses the direct interaction experiences among agents to assess their reputations. It is often considered as the most important component in most of the integrated reputation models, such as Regret [16], FIRE [17], and FIRE+ [20], and can also be used as the source to generate the indirect reputation factors in these models.

The experiments are conducted in a specially set environment where forming bidirectional relationships are facilitated by setting the same probability to construct the relations in both directions between paired users. In the traditional direct interaction model, the agents evaluate the reputations of their neighbors by their direct interaction experiences during the whole information diffusion process.

Figures 10(a) and 10(b) show the results of the detection coverage and accuracy of the presented models and the DI model, respectively. From Figures 9(a) and 9(b), we observe that the presented FPTI and eFPTI models can have much better performance than the DI model on the detection coverage and accuracy. The performance advantage of our models on the detection coverage compared with the DI model is large, which is nearly 0.75; and then, for the detection accuracy, our models can be 0.13 higher than the DI model (only the agents that can be detected are considered).

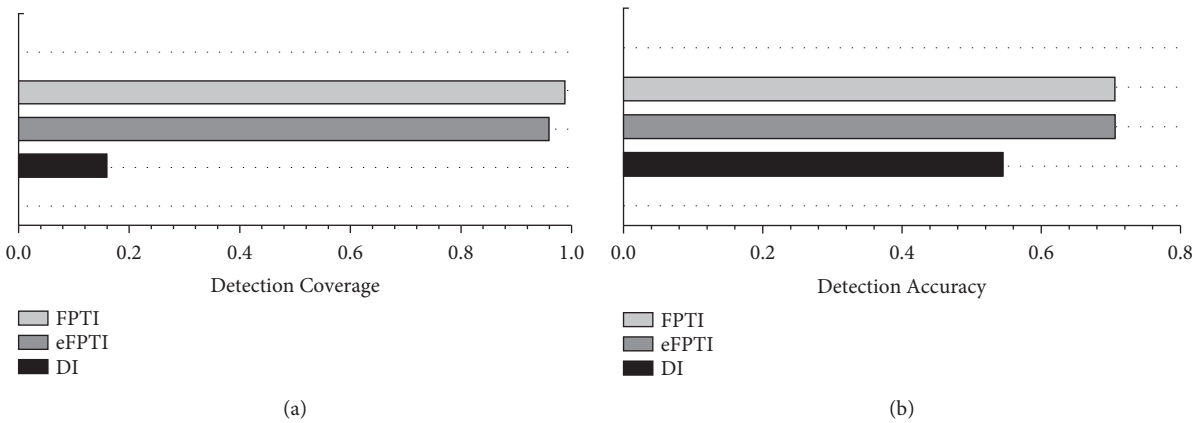

Figure 10: Reputation detection performance of the presented models (FPTI and eFPTI) vs. the direct interaction model (DI). (a) Results of detection coverage. (b) Results of detection accuracy.

The potential reasons for the observed results are as follows: (1) compared with the DI model, our models can detect much more evidences of the agents' behaviors by using path reputation detection through a large amount of diffusion crosses during the information diffusion process, while the DI model can only obtain evidences from the direct interaction experiences, which largely restrict the detection scope and the evidence quantity; (2) then, because more evidences can lead to more accurate assessment of the agents' reputations, the less evidence quantity of the DI model will lead to a lower detection accuracy. In fact, there is another explanation that can be easier to understand: the DI model can be just considered as a special case in the feedback detection of the FPTI and eFPTI models when the path length of the feedback cross is 2. In conclusion, the direct interaction reputation model cannot be well adapted to the information diffusion scenarios considered in this paper. This also gives an insight into the problem that traditional models may have in the information diffusion environment.

6.3. Key Properties of the Models. We investigate the key properties of the presented models: (1) the robustness in dynamic environments, and (2) the effect of suspicion probability in the presented models. For the convenience of property investigation, the initial network for information diffusion is constructed according to the random social network model [48], which initially contains 500 nodes, and the average degree of the initial networks is 10. The parameters for information diffusion are set as follows: $p_w = 0.1$, $p_r' = 0.2$, and $p_d = 0.2$.

6.3.1. Robustness for Dynamic Environments. The dynamic environments in the experiments are set as follows:

(i) Agent behavior pattern reset (*dynamic type i*): the probabilities of agents to behave maliciously can be dynamically reset; namely, the values of their default reputations are reassigned; in this robustness test, the probabilities of all the agents in the system to behave maliciously are reassigned randomly.

(ii) Network relationship rewiring (*dynamic type ii*): the network relationships of the system can be dynamically rewired; namely, old relationships between agents can be destroyed, and, at the same time, new relationships will be created; in this robustness test, there is a 50% probability of rewiring for each edge in the system by selecting paired agents randomly.

(iii) New agent entrance (*dynamic type iii*): considering the open environment, agents can dynamically enter the system and construct relationships with other agents; in this robustness test, new agents, the number of whom is 10% of the initial number of agents, will join the system (i.e., 50 new agents will join the system for each dynamic change).

We also set the mixed dynamic environments (*dynamic type i + ii + iii*) to test the robustness of our models (FPTI and eFPTI). The dynamic changes of the system are conducted at the 100^{th}, 200^{th}, 300^{th}, and 400^{th} steps of the experiments, respectively.

Figure 11 shows the performance of the reputation detection of our models (FPTI and eFPTI) in these dynamic environments. In Figure 11(a), when the probabilities of agents to behave maliciously are dynamically reset, the reputation detection accuracy decreases dramatically. The reason is that the past observations for the agents' reputation estimation can not reflect their behavior pattern after reset. Such situation makes a challenge of fast convergence of reputation detection. But from the plot, we can see that the detection accuracy of our models can recover soon after a short period of time and converge to the former state. In Figure 11(b), we observe that the network relationship rewiring of the system does not have an obvious impact on the performance of our models. The potential reason is that, after relationship rewiring, the past observations that can be used for reputation detection can also reflect the behavior pattern of engaged agents. Thus, our models are robust in this type of dynamic environments where network relationships may be rewired. Figure 11(c) indicates the robustness of our models in the environments where new

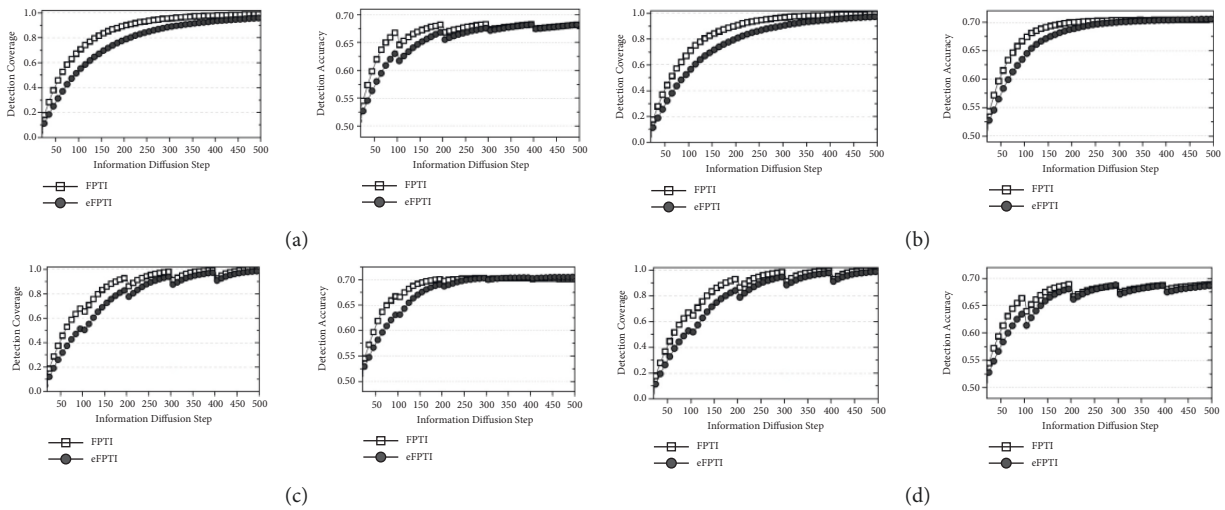

Figure 11: The robustness tests of the FPTI and eFPTI models in different types of dynamic environments. (a) Agent behavior pattern reset. (b) Network relationship rewiring. (c) New agent entrance. (d) Mixed dynamic environment.

agents can enter. We find that when new agents enter the systems, the detection coverage and accuracy have been both influenced. Unlike the dynamic of agent behavior pattern reset, the detection coverage of our models in this type of dynamic environment has obvious fluctuations. But from this plot, we can observe that our models can recover soon and also achieve the expected results. Figure 11(d) shows the test results of our models in the mixed dynamic environments. With several dynamic situations combined in the environment, the detection coverage and accuracy of our models both have obvious fluctuations. But similar to the results in previous dynamic environments, our models can also be robust in this mixed dynamic environment and can achieve good performance. In conclusion, the presented models (FPTI and eFPTI) are robust for the reputation detection in several dynamic environments where agents may dynamically change their behavior patterns, network relationships may be rewired, and new agents may enter the system.

6.3.2. Effect of Suspicion Probability in Reputation Aggregation. In this section, we aim to confirm the effect of suspicion probability introduced in our models. We first ignore the suspicion probability in our models (FPTI and eFPTI) and then employ such modified models to perform the same tests as those in previous section. By comparing the corresponding results, the effect of the suspicion probability can be proved. Here, we only compare their detection accuracy performance, because the modification (ignoring the suspicion probability) cannot influence the detection coverage.

Figure 12(a) shows that there is a large performance difference between the original models and the modified models without considering the suspicion probability. The detection accuracy of modified models is nearly 0.11–0.13 lower than that of the original models. Such results obviously indicate the benefit of considering suspicion probability in reputation aggregation.

Then, in Figure 12(b), we can see how the suspicion probability takes effect in the reputation detection. We first give the definition of the error distribution ratio (*EDR*) as follows: $\mathrm{EDR} = N_{\text{err-}n}/N_{\text{err-}p}$, where $N_{\text{err-}n}$ and $N_{\text{err-}p}$ represent the number of negative detection and positive detection, respectively. The positive (negative) detection indicates that the detected reputation of an agent is higher (lower) than its default reputation set initially. In Figure 12(b), the EDRs of the modified models are much larger than those of the origin FPTI and eFPTI models; namely, there are much more negative detections when not considering the suspicion probability. This validates the aim of introducing suspicion probability into reputation detection, which is to revise the effect of obtained negative evidences on reputation aggregation. If no such revision has been carried out, agents' reputations could be significantly underestimated.

6.4. Applicability of the Models on Misinformation Suppression. In this section, we apply our models (FPTI and eFPTI) in information diffusion scenarios and test the effects of agents' reputations detected by our models on misinformation suppression. A threshold method utilizing the detected reputations is used to suppress the influence of malicious behaviors. Let I_m be the ratio of the number of messages that have been tampered with, thus taking misinformation to the total number of messages in the system, and I_m' be the ratio of the number of messages that take misinformation to number of messages after the suppression approach is implemented. The details of the threshold method are described below. Let A_u and A_d be the set of upstream and downstream neighbors of an agent a_i, and let $r_i(j)$ be the reputation of a_j evaluated by a_i. The agent a_i can first set the threshold values α and β for upstream and downstream neighbors, respectively, and then, it can only receive messages from A_u' and diffuses messages to A_d', where $A_u' \subseteq A_u$, $A_d' \subseteq A_d$, $\forall\ r_i(a_u') > \alpha\ (a_u' \in A_u')$, and $\forall\ r_i(a_d') > \beta\ (a_d' \in A_d')$. In the experiments, we set α and β to be equal to 0.7.

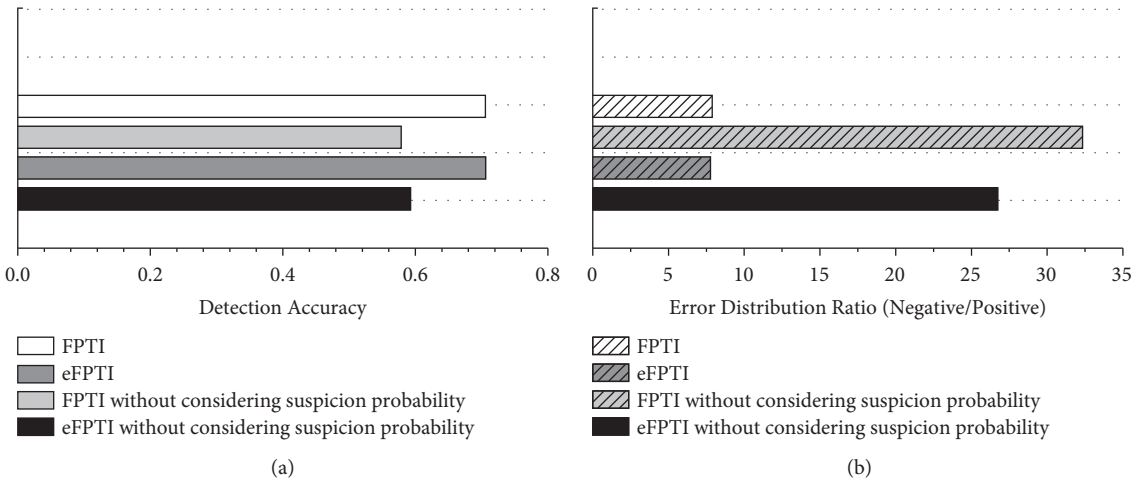

Figure 12: The effects of suspicion probability in the proposed models on (a) the detection accuracy, and (b) the error distribution. (a) Results of detection accuracy. (b) Results of error distribution ratio.

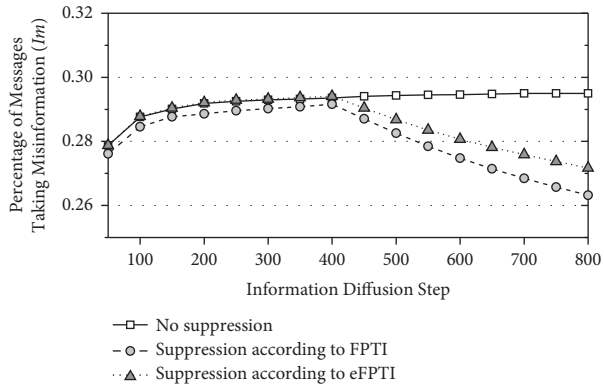

Figure 13: The effect of reputations of agents (generated by the proposed models) for suppressing the influence of malicious behaviors (the suppression approach is implemented at the 400th execution step).

For example, let $A_u = \{a_1, a_2, a_3\}$ be the set of upstream neighbors of agent a_i; that is, there are edges directed from the agent a_1, a_2 and a_3 to a_i, respectively, and $r_i(a_1) = 0.35$, $r_i(a_2) = 0.76$ and $r_i(a_3) = 0.91$; let $A_d = \{a_4, a_5, a_6, a_7\}$ be the set of upstream neighbors of agent a_i; that is, there are edges directed from the agent a_i to a_4, a_5, a_6 and a_7, respectively, and $r_i(a_4) = 0.21$, $r_i(a_5) = 0.83$, $r_i(a_6) = 0.96$ and $r_i(a_7) = 0.62$. If the threshold value for upstream neighbors α is set to 0.7, then the agent a_i can only receive messages from a_2 and a_3 for misinformation suppression; and if the threshold value for downstream neighbors β is set to 0.7, then the agent a_i can only diffuse messages to a_5 and a_6 for misinformation suppression.

Figure 13 provides insight into the effect of the reputations detected by our models in weakening the influence of malicious behaviors in information diffusion. This plot first shows that, with no suppression on malicious behaviors, I_m increases rapidly in the early stages and then gradually tends towards stability; that is, the number of messages tampered with increases as the total number of messages increases. Then, from the results implementing the suppression approach, we can see that a gradual decrease in I_m occurs after the suppression approach is implemented at the 400^{th} execution step. Finally, at the 800^{th} step, the results obtained using the suppression approach can be much better. (The percentage of misinformation after misinformation suppression based on the reputation detection results by FPTI and eFPTI declined by 30.4% and 20.6%, respectively).

7. Conclusion and Future Works

We present a novel distributed reputation detection pattern "*from path to individual*," which can overcome the problem that it may be difficult or impossible to determine interaction reputations in the absence of direct interactions in scenarios of information diffusion in SNS. The main idea is that the positive (negative) observation of an information diffusion process increases (decreases) the belief of the corresponding diffusion path, which further increases (decreases) the reputation of each involved agent.

Based on the detection pattern "*from path to individual*," we then propose the FPTI and eFPTI models. The FPTI model effectively addresses the following issues for the diffusion in SNS: (a) how to detect path reputations from information diffusion process, and (b) how to aggregate obtained path reputations into reputations of agents. Furthermore, the eFPTI (enhanced FPTI) model is proposed in order to address an additional important issue: how to effectively reduce the detection costs on the premise that satisfactory detection performance can be achieved.

Through theoretical analyses and experimental evaluations, we have shown that, in information diffusion scenarios in SNS, (1) the presented models (FPTI and eFPTI) can be effective and efficient in reputation detection, (2) the reputations of agents determined using the presented models can be considered as appropriate alternatives to interaction reputations, and (3) the obtained agents' reputations are valuable for suppressing the influence of malicious behaviors.

In future work, we plan to extend our model in the following ways:

(i) Collusion between agents is not currently considered in the model. However, agents in social network systems may collude to achieve their selfish goals [49]. For this reason, we plan to extend our model for reputation detection in the future to consider collusion between agents in information diffusion scenarios in SNS.

(ii) Recently, the multiplex nature of social networks has received considerable attention [50, 51]. This feature of social networks suggests that it may be useful to study reputation models that suit the characteristics of multiplex social network systems. Thus, we also plan to extend our model to multiplex social network systems by considering their particular network characteristics, for example, diverse relative bias for diffusion in different network layers [51] and the relevance of connectivity between multiple network layers [52].

Data Availability

The data that support the findings of this study are available upon request from the corresponding author.

Conflicts of Interest

The authors declare no conflicts of interest.

Acknowledgments

This research was supported by the National Natural Science Foundation of China (Nos. 61807008, 61806053, and 62076060) and the Natural Science Foundation of Jiangsu Province of China (BK20180369 and BK20180356). Some preliminary results of this paper were presented at the Proceedings of the 12th IEEE/WIC/ACM International Conference on Intelligent Agent Technology.

References

[1] H. Kwak, C. Lee, H. Park, and S. Moon, "What is twitter, a social network or a news media?" in *Proceedings of the 19th International Conference on World Wide Web (WWW'10)*, pp. 591–600, Raleigh, NC, USA, April 26-30, 2010.

[2] H. U. Khan, S. Nasir, K. Nasim, D. Shabbir, and A. Mahmood, "Twitter trends: a ranking algorithm analysis on real time data," *Expert Systems with Applications*, vol. 164, Article ID 113990, 2021.

[3] M. M. Skeels and J. Grudin, "When social networks cross boundaries: a case study of workplace use of facebook and LinkedIn," in *Proceedings of the ACM 2009 International Conference on Supporting Group Work (GROUP'09)*, pp. 95–104, Sanibel Island, Florida, USA, May 10–13, 2009.

[4] H. Yu, C. Miao, B. An, C. Leung, and V. R. Lesser, "A reputation management approach for resource constrained trustee agents," in *Proceedings of the Twenty-Third International Joint Conference on Artificial Intelligence (IJCAI'13)*, pp. 418–424, Beijing, China, August 3-9, 2013.

[5] Y. Jiang and J. C. Jiang, "Understanding social networks from a multiagent perspective," *IEEE Transactions on Parallel and Distributed Systems*, vol. 25, no. 10, pp. 2743–2759, 2014.

[6] H. Ohtsuki, C. Hauert, E. Lieberman, and M. A. Nowak, "A simple rule for the evolution of cooperation on graphs and social networks," *Nature*, vol. 441, no. 7092, pp. 502–505, 2006.

[7] Y. Jiang, Y. Zhou, and W. Wang, "Task allocation for undependable multiagent systems in social networks," *IEEE Transactions on Parallel and Distributed Systems*, vol. 24, no. 8, pp. 1671–1681, 2013.

[8] M. M. de Weerdt, Y. Zhang, and T. Klos, "Multiagent task allocation in social networks," *Autonomous Agents and Multi-Agent Systems*, vol. 25, no. 1, pp. 46–86, 2012.

[9] V. Krishnamurthy and H. V. Poor, "A tutorial on interactive sensing in social networks," *IEEE Transactions on Computational Social Systems*, vol. 1, no. 1, pp. 3–21, 2014.

[10] J. Sabater and C. Sierra, "Review on computational trust and reputation models," *Artificial Intelligence Review*, vol. 24, no. 1, pp. 33–60, 2005.

[11] S. D. Ramchurn, D. Huynh, and N. R. Jennings, "Trust in multi-agent systems," *The Knowledge Engineering Review*, vol. 19, no. 1, pp. 1–25, 2004.

[12] E. Franchi and A. Poggi, "Multi-agent systems and social networks," *Handbook of Research on Business Social Networking*, IGI Global, Pennsylvania, pp. 84–97, 2012.

[13] F. Bergenti, E. Franchi, and A. Poggi, "Enhancing social networks with agent and semantic web technologies," *Collaboration and the Semantic Web: Social Networks, Knowledge Networks, and Knowledge Resources*, pp. 83–100, 2012.

[14] J. Yao, W. Tan, S. Nepal et al., "ReputationNet: reputation-based service recommendation for e-science," *IEEE Transactions on Services Computing*, vol. 8, no. 3, pp. 439–452, 2015.

[15] D. Artz and Y. Gil, "A survey of trust in computer science and the semantic web," *Journal of Web Semantics*, vol. 5, no. 2, pp. 58–71, 2007.

[16] J. Sabater and C. Sierra, "Reputation and social network analysis in multi-agent systems," in *Proceedings of the First International Conference on Autonomous Agents and Multi-agent Systems (AAMAS'02)*, pp. 475–482, Bologna, Italy, July15-19, 2002.

[17] T. D. Huynh, N. R. Jennings, and N. R. Shadbolt, "FIRE: an integrated trust and reputation model for open multi-agent systems," in *Proceedings of the 16th European Conference on Artificial Intelligence (ECAI'04)*, pp. 18–22, Valencia, Spain, August 22-27, 2004.

[18] eBay, "eBay," http://www.ebay.com, 2004.

[19] G. Zacharia and P. Maes, "Trust management through reputation mechanisms," *Applied Artificial Intelligence*, vol. 14, no. 9, pp. 881–907, 2000.

[20] B. Qureshi, G. Min, and D. Kouvatsos, "Countering the collusion attack with a multidimensional decentralized trust and reputation model in disconnected MANETs," *Multimedia Tools and Applications*, vol. 66, no. 2, pp. 303–323, 2013.

[21] K. Kravari and N. Bassiliades, "DISARM: a social distributed agent reputation model based on defeasible logic," *Journal of Systems and Software*, vol. 117, pp. 130–152, 2016.

[22] J. Carbo, J. M. Molina, and J. Davila, "Trust management through fuzzy reputation," *International Journal of Cooperative Information Systems*, vol. 12, no. 01, pp. 135–155, 2003.

[23] Q. Wu, Q. Zhu, and P. Li, "A neural network based reputation bootstrapping approach for service selection," *Enterprise Information Systems*, vol. 9, no. 7, pp. 768–784, 2015.

[24] F. Cornelli, E. Damiani, S. Vimercati, S. Paraboschi, and P. Samarati, "Choosing reputable servents in a P2P network," in *Proceedings of the 11th International Conference on World Wide Web (WWW'02)*, pp. 376–386, Honolulu, Hawaii, USA, May 7-11, 2002.

[25] C. Lee, H. Kwak, H. Park, and S. Moon, "Finding influentials based on the temporal order of information adoption in twitter," in *Proceedings of the 19th International Conference on World Wide Web (WWW'10)*, pp. 1137-1138, Raleigh, NC, USA, April 26-30, 2010.

[26] J. Yang and J. Leskovec, "Modeling information diffusion in implicit networks," in *Proceedings of the 2010 IEEE International Conference on Data Mining (ICDM'10)*, pp. 599–608, Sydney, Australia, December 14-17, 2010.

[27] Y. Zhou and Y. Jiang, "From path to individual: a distributed reputation detection model for information diffusion," in *Proceedings of the 12th IEEE/WIC/ACM International Conference on Intelligent Agent Technology (IAT'12*, pp. 188–195*)*, Macau, China, December 4-7, 2012.

[28] A. JØsang, "A subjective metric of authentication," in *Proceedings of the Computer Security — ESORICS 98*, vol. 1485, pp. 329–344, Louvain-la-Neuve, Belgium, September 16-18, 1998.

[29] A. Jøsang, "A logic for uncertain probabilities," *International Journal of Uncertainty, Fuzziness and Knowledge-Based Systems*, vol. 09, no. 03, pp. 279–311, 2001.

[30] Y. Wang and M. P. Singh, "Formal trust model for multiagent systems," in *Proceedings of the 20th International Joint Conference on Artificial Intelligence (IJCAI'07)*, pp. 1551–1556, Hyderabad, In-dia, January 6-12, 2007.

[31] Y. Wang and M. P. Singh, "Trust representation and aggregation in a distributed agent system," in *Proceedings of the Twenty-first National Conference on Artificial Intelligence (AAAI'06)*, pp. 1425–1430, Boston, Massachusetts, USA, July 16-20, 2006.

[32] C. Hang, Y. Wang, and M. P. Singh, "Operators for propagating trust and their evaluation in social networks," in *Proceedings of the Eighth International Conference on Autonomous Agents and Multiagent Systems (AAMAS'09)*, pp. 1025–1032, Budapest, Hungary, May 10-15, 2009.

[33] D. Gruhl, D. Liben-Nowell, R. Guha, and A. Tomkins, "Information diffusion through blogspace," in *Proceedings of the 13th International World Wide Web Conference (WWW'04)*, pp. 491–501, New York, NY, USA, May 17-20, 2004.

[34] J. L. Iribarren and E. Moro, "Impact of human activity patterns on the dynamics of information diffusion," *Physical Review Letters*, vol. 103, no. 3, Article ID 038702, 2009.

[35] A. Mohaisen, T. AbuHmed, T. Zhu, and M. Mohaisen, "Collaboration in social network-based information dissemination," in *Proceedings of the IEEE International Conference on Communications (ICC'12)*, Ottawa, ON, Canada, June 10-15, 2012.

[36] Y. Jiang, "Concurrent collective strategy diffusion of multiagents: the spatial model and case study," *IEEE Transactions on Systems, Man, and Cybernetics, Part C (Applications and Reviews)*, vol. 39, no. 4, pp. 448–458, 2009.

[37] Y. Jiang and T. Ishida, "A model for collective strategy diffusion in agent social law evolution," in *Proceedings of the 20th International Joint Conference on Artificial Intelligence (IJCAI'07)*, pp. 1353–1358, Hyderabad, India, January 6-12, 2007.

[38] D. Lin and T. Ishida, "Coordination of local process views in interorganizational business process," *IEICE - Transactions on Info and Systems*, vol. E97-D, no. 5, 2014.

[39] Y. Jiang and J. C. Jiang, "Diffusion in social networks: a multiagent perspective," *IEEE Transactions on Systems, Man, and Cybernetics: Systems*, vol. 45, no. 2, pp. 198–213, 2015.

[40] C. Gao, J. Liu, and N. Zhong, "Network immunization with distributed autonomy-oriented entities," *IEEE Transactions on Parallel and Distributed Systems*, vol. 22, no. 7, pp. 1222–1229, 2011.

[41] D. Liben-Nowell and J. Kleinberg, "Tracing information flow on a global scale using internet chain-letter data," *Proceedings of the National Academy of Sciences*, vol. 105, no. 12, pp. 4633–4638, 2008.

[42] J. Caverlee, L. Liu, and S. Webb, "Socialtrust: tamper-resilient trust establishment in online communities," in *Proceedings of the 8th ACM/IEEE-CS Joint Conference on Digital Libraries (JCDL'08)*, pp. 104–114, Pittsburgh, Pennsylvania, USA, June 16-20, 2008.

[43] G. Miritello, R. Lara, M. Cebrian, and E. Moro, "Limited communication capacity unveils strategies for human interaction," *Scientific Reports*, vol. 3, no. 1, p. 1950, 2013.

[44] I. Taxidou and P. Fischer, "Realtime analysis of information diffusion in social media," *Proceedings of the VLDB Endowment*, vol. 6, no. 12, pp. 1416–1421, 2013.

[45] D. Greene and P. Cunningham, "Producing a unified graph representation from multiple social network views," in *Proceedings of the 5th Annual ACM Web Science Conference (WebSci'13)*, pp. 118–121, Paris, France, May 1–5, 2013.

[46] R. Tarjan, "Depth-first search and linear graph algorithms," *SIAM Journal on Computing*, vol. 1, no. 2, pp. 146–160, 1972.

[47] D. E. Knuth, *The Art of Computer Programming*, Vol. Vol 1, Addison-Wesley, Boston, 3rd ed edition, 1997.

[48] M. E. J. Newman, D. J. Watts, and S. H. Strogatz, "Random graph models of social networks," *Proceedings of the National Academy of Sciences*, vol. 99, no. suppl_1, pp. 2566–2572, 2002.

[49] Z. Rui, T. Fu, D. Lai, and Y. Jiang, "Cooperation among malicious agents: a general quantitative congestion game framework," in *Proceedings of the 11th International Conference on Autonomous Agents and Multiagent Systems (AAMAS'12)*, pp. 1331-1332, Valencia, Spain, June 4-8, 2012.

[50] J. Gómez-Gardeñes, I. Reinares, A. Arenas, and L. M. Floría, "Evolution of cooperation in multiplex networks," *Scientific Reports*, vol. 2, no. 1, 620 pages, 2012.

[51] O. Yağan and V. Gligor, "Analysis of complex contagions in random multiplex networks," *Physical Review A*, vol. 86, no. 3, Article ID 036103, 2012.

[52] M. Berlingerio, M. Coscia, F. Giannotti, A. Monreale, and D. Pedreschi, "Multidimensional networks: foundations of structural analysis," *World Wide Web*, vol. 16, no. 5-6, pp. 567–593, 2013.

Hindawi
Complexity
Volume 2022, Article ID 4523287, 27 pages
https://doi.org/10.1155/2022/4523287

Research Article

Evaluation of Network Security Service Provider Using 2-Tuple Linguistic Complex q-Rung Orthopair Fuzzy COPRAS Method

Sumera Naz,[1] Muhammad Akram ,[2] Mohammed M. Ali Al-Shamiri ,[3,4] and Muhammad Ramzan Saeed[1]

[1]*Department of Mathematics, Division of Science and Technology, University of Education, Lahore, Pakistan*
[2]*Department of Mathematics, University of the Punjab, New Campus, Lahore 54590, Pakistan*
[3]*Department of Mathematics, Faculty of Science and Arts, Mahayl Assir, King Khalid University, Abha, Saudi Arabia*
[4]*Department of Mathematics and Computer, Faculty of Science, Ibb University, Ibb, Yemen*

Correspondence should be addressed to Muhammad Akram; m.akram@pucit.edu.pk

Received 23 March 2022; Revised 5 May 2022; Accepted 14 May 2022; Published 26 June 2022

Academic Editor: Yu Zhou

In recent years, network security has become a major concern. Using the Internet to store and analyze data has become an integral aspect of the production and operation of many new and traditional enterprises. However, many enterprises lack the necessary resources to secure information security, and selecting the best network security service provider has become a real issue for many enterprises. This research introduces a novel decision-making method utilizing the 2-tuple linguistic complex q-rung orthopair fuzzy numbers (2TLCq-ROFNs) to tackle this issue. We propose the 2TLCq-ROF concept by combining the complex q-rung orthopair fuzzy set with 2-tuple linguistic terms, including the fundamental definition, operational rules, scoring, and accuracy functions. Aggregation operators are the fundamental mathematical approach used to combine various inputs into a single output. Taking into account the interaction between the attributes, we develop the 2TLCq-ROF Hamacher (2TLCq-ROFH) operators by using the innovative operational rules. These operators include the 2TLCq-ROFH weighted average (2TLCq-ROFHWA), 2TLCq-ROFH ordered weighted average (2TLCq-ROFHOWA), 2TLCq-ROFH hybrid average (2TLCq-ROFHHA), 2TLCq-ROFH weighted geometric (2TLCq-ROFHWG), 2TLCq-ROFH ordered weighted geometric (2TLCq-ROFHOWG), and 2TLCq-ROFH hybrid geometric (2TLCq-ROFHHG) operators. In addition, we talk about the properties of 2TLCq-ROFH operators such as idempotency, commutativity, monotonicity, and boundedness and also examine their spatial cases. To tackle the problems of the 2TLCq-ROF multiattribute group decision-making (MAGDM) environment, we develop a novel approach according to the COPRAS (complex proportional assessment) model. Finally, to validate the feasibility of the given strategy, we employ a quantitative example related to select the best network security service provider. In comparison with existing approaches, the developed decision-making algorithm is most extensively used and reduces the loss of information.

1. Introduction

The use of the computer network has spread to every industry as a result of its popularization and advancement. People in the information society are becoming increasingly reliant on the network, and as the network has grown in size and complexity, network security has become a major concern. Although the Internet and other information technologies empower businesses, financial institutions, and even government agencies with the ease of data storing and processing to efficiently serve society, network security risks also present a threat to enterprises and the entire society. In the information era, data losses are certainly fatal. Many noncyber security organizations find it impractical to maintain a long-term professional network security technology staff due to the extremely professional aspects of network security technology. As a result, many enterprises want to entrust network security defense to professional network security service providers for technical help. This means that choosing the proper network security service

providers has much impact on ordinary enterprises. As a result, selecting the best network security company is a MADM issue. MAGDM is an integrative research field that combines MADM with the group of decision-makers, particularly analyzing different alternatives through different decision-making (DM) approaches. MAGDM usually provides structures to fuse individual preference information into group preference information. Due to the increasing complexity in economics and management, it is almost impossible for decision-makers (DMs) to collect all information about optimal alternatives associated with MAGDM problems. Hence, uncertainty and fuzziness occur in real-life issues, and how to effectively deal with such kind of fuzziness is crucial to select the best alternative. Many scholars and researchers have worked hard to develop different methods to represent fuzzy DM information in the MAGDM process. Recently, for expressing vagueness and uncertainty, various tools have been developed. For some MAGDM problems, DMs experience problems in describing attribute values of alternatives by using crisp numbers. To describe the uncertainties, Zadeh [1] introduced the fuzzy set (FS) as a generalization of the crisp set, and the value of FS lies between $[0, 1]$. However, FS has only a membership degree (MD) and ignores the nonmembership degree (NMD) in DM problems. Furthermore, intuitionistic FS (IFS) [2], Pythagorean FS (PFS) [3], and Fermatean FS (FFS) [4], whose elements are pairs of fuzzy numbers, have been introduced. All of the above described FSs demonstrate the MD and NMD. The limitation of MD and NMD is that the sum, square sum, and cube sum of both would belong to $[0, 1]$. Yager [5] realized that the current IFS, PFS, and FFS frameworks are unable to represent human opinion more realistically and developed the q-rung orthopair FS (q-ROFS), which effectively enhances the scope of information by establishing novel subjective constraints where the qth sum of MD and NMD lies between $[0, 1]$. If $q = 1$, $q = 2$, and $q = 3$, and then, the q-ROFS is reduced into the IFS, PFS, and FFS, respectively.

The q-ROFS theory deals only with one dimension at a time, which sometimes destroys information. However, in real life, we encounter complex natural phenomena in which it becomes significant to integrate the second dimension for the representation of MD and NMD. The development of the second dimension allows complete information to be projected into a set, avoiding any information loss. With the unit disc, Ramot et al. [6] extended the MD range from real number to complex number and proposed the concept of a complex FS (CFS). Furthermore, representing the complex-valued NMD, Alkouri and Salleh [7, 8] extended an idea of CFS to complex IFS (CIFS) and also put forward the concept of CIF relations and a distance measure in CIF circumstances. Ullah et al. [9] developed various distance measures of the complex PFS (CPFS) and an algorithm for addressing pattern recognition problems. Liu et al. [10] put forward an innovative, effective, and powerful tool to describe uncertain phenomena named Cq-ROFSs and introduced the Cq-ROF weighted average operator and Cq-ROF weighted geometric operator. To aggregate complex q-rung orthopair fuzzy numbers, Liu et al. [11] extended the Einstein operations to Cq-ROFSs and proposed a family of Cq-ROF Einstein averaging operators, such as the Cq-ROF Einstein weighted averaging, the Cq-ROF Einstein ordered weighted averaging, the generalized Cq-ROF Einstein weighted averaging, and the generalized Cq-ROF Einstein ordered weighted averaging operators. The newly proposed Cq-ROFSs are incredibly flexible and efficient, as opposed to many existing FS theories, which can clearly describe the DM perspectives of experts in a complex environment. The amplitude term implies the extent to which an object belongs in a Cq-ROFS, while the phase terms are frequently associated with periodicity. The Cq-ROFS differs from typical q-ROFS theories because of these phase terms. Akram et al. developed novel decision-making methods based on complex Pythagorean fuzzy [12] and complex Fermatean fuzzy N-soft circumstances [13].

The above FSs can only represent information from a quantitative perspective. And it is difficult for DMs to provide precise numerical values to describe their point of view. As a result, Zadeh [14] developed the linguistic variable (LV) as a tool to express qualitative information in DM problems. Following that, various innovative concepts based on the LV and FS were proposed, including intuitionistic linguistic numbers [15], single-valued neutrosophic linguistic set [16], and linguistic q-ROF numbers [17]. Furthermore, Herrera and Martnez [18] introduced the concept of a 2-tuple linguistic FS (2TLFS) established by LV and numerical value to reduce information loss in the DM procedure. Zhao et al. [19] presented an advanced TODIM strategy based on 2-tuple linguistic neutrosophic sets and cumulative prospect theory as a novel approach to MAGDM problems. Based on previous research, Zhang et al. [20] improved dramatically the TODIM technique as well as the cumulative prospect theory under the 2TL Pythagorean fuzzy sets. Naz and Akram [21, 22] developed a new DM approach to deal with the MADM problems based on the graph theory. Recently, many research studies [23–27] have developed several DM methods under generalized fuzzy scenario.

Later, many researchers integrated the 2TL model with several FSs and proposed 2TLIFS [28], 2TLPFS [29], and so forth. These extensions can effectively describe uncertain fuzzy information in addressing DM problems. The Cq-ROFS and the 2TL terms, as previously noted, are two strategies for describing the quantitative and qualitative assessment information. Motivated by the concept of a 2TLPFS, Rong et al. [30] introduced the novel concept of 2TLCq-ROFS. The 2TLCq-ROFS is the more universal than existing FSs because we can obtain multiple specific examples by considering some particular circumstances. In the context of 2TLCq-ROFS, the parameters $q = 1$ and $q = 2$ degenerate into the 2TLCIFS and the 2TLCPFS, respectively. Furthermore, if the imaginary part of 2TLCq-ROFS is set to zero, it is reduced to a 2TLq-ROFS. From the previous linguistic set research, the 2TLCq-ROFS is stronger because: (1) it can prevent information distortion throughout the linguistic information procedure; (2) it can avoid information loss by expressing assessment information through complex-valued MD and complex-valued NMD;

and (3) in real-life applications, it can tackle problems with two dimensions of information.

An aggregation operator (AO) is a well-known approach in the field of information fusion, and it has provided lots of new research results on a variety of topics. To design the MAGDM method, Liu and Wang [31] developed a weighted average and geometric operator for q-ROFS. However, in DM problems, these operators fail to evaluate the interrelationship of attributes. Hamacher product and Hamacher sum were first presented by Hamacher [32] as part of the Hamacher operations. Furthermore, as a generalization of the algebraic and Einstein t-norm and t-conorm, the Hamacher t-norm and t-conorm are more general and flexible. According to a review of the 2TL$C$$q$-ROF-AOs, there is limited research by using Hamacher operations to propose new operators. Therefore, it is necessary to research AOs utilizing Hamacher operations with 2TL$C$$q$-ROF information. Moreover, in decision analysis, selecting the appropriate alternative(s) is critical. As a result, it is crucial to use Hamacher operations to develop 2TL$C$$q$-ROF-AOs for solving MAGDM problems. Akram et al. [33] introduced the complex intuitionistic fuzzy Hamacher-weighted averaging operator, complex intuitionistic fuzzy Hamacher ordered weighted averaging operator, complex intuitionistic fuzzy Hamacher weighted geometric operator, and complex intuitionistic fuzzy Hamacher ordered weighted geometric operator. With the use of Hamacher operations and I2TL elements, Faizi et al. [34] developed the intuitionistic 2-tuple linguistic Hamacher weighted average (I2TLHWA) and intuitionistic 2-tuple linguistic Hamacher weighted geometric (I2TLHWG) operators. Rawat [35] introduced q-rung orthopair fuzzy Hamacher Muirhead mean aggregation operators and developed a decision-making approach utilizing proposed operators. Pamucar et al. [36] introduced a novel weighted aggregated sum product assessment approach for advantage prioritization of the electric ferry's sustainable supply chain based on the fuzzy Hamacher weighted averaging function and weighted geometric averaging function.

In recent years, a wide range of methods such as AHP, VIKOR, TOPSIS, and COPRAS that can effectively deal with the ranking procedure has been introduced. The basic purpose of these methods is to select the best alternative by aggregating the information and ranking the objectives according to their significance. Zavadskas et al. [37] proposed the COPRAS method, which compares each alternative and computes their priorities based on attribute weights. COPRAS method is one of the most appropriate methods for ranking the alternatives among all of these methods, and it is widely used for both quantitative and qualitative analyses. The COPRAS method considers direct and proportional reliance of the weights and the utility degree of examined adaptations on a framework of the attributes. To explain logistic regression, boosted regression trees, and random forest, Arabameri et al. [38] built three new ensemble models and assessed them using the COPRAS method. A comparative analysis of COPRAS and the other existing methods such as AHP, TOPSIS, and VIKOR is conducted by Chatterjee et al. [39] and concluded that the COPRAS method indicates good transparency, less calculation time, and a high possibility of graphical understanding of their counterpart strategies. Alipour et al. [40] provided an integrated approach for fuel cell combined with hydrogen supplier selection based on entropy, step-wise weight assessment ratio analysis, and COPRAS methods in a Pythagorean fuzzy environment. Balali et al. [41] utilized the COPRAS approach for risk assessment and the analytic network process technique for determining the weights of each risk assessment criteria. Narang et al. [42] introduced a new hybrid multicriteria decision-making method comprised of group fuzzy COPRAS and fuzzy BCM, followed by a strategy based on the combination of the fuzzy set theory and the COPRAS to rank alternatives in uncertain and ambiguous contexts. This paper extends the COPRAS method to the 2TL$C$$q$-ROF environment, considering the flexibility of 2TL$C$$q$-ROFS and the quality of the COPRAS method. The crucial properties of the COPRAS method are (1) during the execution of the process, it evaluates the proportions of the ideal and worst solutions at the same time; (2) this method evaluates the direct and relative dependencies of the significance and the utility degree of the alternatives under the contrary attribute values; and (3) this method is designed to obtain the decision much more effective and sensible. Thus, considering the advantages of the AOs and the COPRAS method, this article intends to establish an innovative MAGDM approach for managing the information associated with the 2TL$C$$q$-ROFS and some new information measures.

The motivation and objectives of this study are to find the best network security service provider. After conducting several experiments, the MAGDM method is applied to make the final decision. A significant component of MAGDM is the selection of attributes. Attributes are divided into two types: benefit attribute and cost attribute, to select the best alternative in the application based on whether they are beneficial or not. Existing CFS theories fail to depict uncertain information through the 2TL representation model, which has a higher capability to express linguistic information and can avoid information distortion loss while dealing with linguistic decision problems. The 2TL$C$$q$-ROFS and related fundamental theories are developed to enhance CFS theories and provide a reliable tool for experts to express assessment information. Using the 2TL$C$$q$-ROFS in this type of MAGDM method gives rise to the clear thinking of DMs who assigns value to complex membership and complex nonmembership functions. Information fusion is essential for aggregating the opinions of DMs. In addition, in a range of practical problems, the correlation of selected attributes is essentially addressed. Several 2TL$C$$q$-ROFH operators are presented to address two-dimensional fuzzy information in the light of the excellent superiority of the Hamacher operator. The COPRAS method establishes to rank the given 2TL$C$$q$-ROFNs, to develop two algorithms based on COPRAS and AOs to understand DM problems. The approach is described with a numerical illustration to examine the research study.

The main contributions of this research work are as follows:

(i) We introduce the 2TL terms into the complex q-rung orthopair fuzzy environment and propose the construction process of 2TLCq-ROFNs.

(ii) The 2TLCq-ROFHWA and 2TLCq-ROFHWG operators are proposed combining 2TL terms with complex q-rung orthopair fuzzy set, Hamacher weighted average, and Hamacher weighted geometric operators.

(iii) We propose some operational properties and special cases of 2TLCq-ROF Hamacher AOs.

(iv) Based on 2TLCq-ROFNs, we improve the COPRAS method and develop a 2TLCq-ROF-COPRAS method to solve the MAGDM problem for ranking of alternatives.

(v) We apply the 2TLCq-ROF-COPRAS method to the assessment of the network security service provider. This method is verified to provide a new idea for the assessment of the network security service provider.

To achieve the cognitive approach, the overall framework of this article is as follows: In Section 2, we give several fundamental concepts and definitions including 2TL term, Cq-ROFS, and Hamacher operator. Section 4 presents some new 2TLCq-ROFH aggregation operators, that is, 2TLCq-ROFHWA operator, 2TLCq-ROFHOWA operator, 2TLCq-ROFHHA operator, 2TLCq-ROFHWG operator, 2TLCq-ROFHOWG operator, and 2TLCq-ROFHHG operator, and also discussed some desirable properties and particular cases of them. In Section 5, we design an extended COPRAS method for the MAGDM problem based on the 2TLCq-ROFHWA and 2TLCq-ROFHWG operators. Section 6 employs an example of the best network security service provider to show the application of the proposed method. Some sensitive and comparative analysis is also provided. Finally, Section 7 presents the conclusions, remarks, and also future directions.

2. Preliminaries

In this section, some correlative basic concepts of LTS, 2TL, and Cq-ROFS, are recapped to facilitate the next sections.

2.1. 2TL Representation Model and Cq-ROFS

Definition 1 (see [43]). Let there exist a linguistic term set (LTS) $S = \{s_\epsilon | \epsilon = 0, 1, \ldots, \tau\}$ with odd cardinality, where s_ϵ indicates a possible linguistic term for a linguistic variable. For instance, an LTS S having seven terms can be described as follows:

$S = \{s_0 = \text{no influence}, s_1 = \text{very low influence}, s_2 = \text{low influence}, s_3 = \text{same influence}, s_4 = \text{high influence}, s_5 = \text{very high influence}, s_6 = \text{very high influence}\}$.

If $s_\epsilon, s_\kappa \in S$, then the LTS meets the following characteristics:

(i) The set is ordered: $s_\epsilon > s_\kappa$, iff $\epsilon > \kappa$

(ii) Max operator: $\max(s_\epsilon, s_\kappa) = s_\epsilon$, iff $\epsilon \geq \kappa$

(iii) Min operator: $\min(s_\epsilon, s_\kappa) = s_\epsilon$, iff $\epsilon \leq \kappa$

(iv) Negative operator: $\text{Neg}(s_\epsilon) = s_\kappa$ such that $\kappa = \tau - \epsilon$

The 2TL representation model based on the idea of symbolic translation, introduced by Herrera and Martinez [18, 44], is useful for representing the linguistic assessment information by means of a 2-tuple $(s_\epsilon, \upsilon_\epsilon)$, where s_ϵ is a linguistic label from predefined LTS S and υ_ϵ is the value of symbolic translation, and $\upsilon_\epsilon \in [-0.5, 0.5)$.

Definition 2 (see [18, 44]). Let ϑ be the result of an aggregation of the indices of a set of labels assessed in an LTS S, that is, the result of a symbolic aggregation operation, $\vartheta \in [1, \tau]$, where τ is the cardinality of S. Let $\epsilon = \text{round}(\vartheta)$ and $\upsilon = \vartheta - \epsilon$ be two values, such that $\epsilon \in [1, \tau]$ and $\upsilon \in [-0.5, 0.5)$, and then, υ is called a symbolic translation.

Definition 3 (see [18, 44]). Let $S = \{s_\epsilon | \epsilon = 1, \ldots, \tau\}$ be an LTS and $\vartheta \in [1, \tau]$ is a number value representing the aggregation result of linguistic symbolic. Then, the function Δ used to obtain the 2TL information equivalent to ϑ is defined as

$$\Delta: [1, \tau] \longrightarrow S \times [-0.5, 0.5),$$
$$\Delta(\vartheta) = \begin{cases} s_\epsilon, & \epsilon = \text{round}(\vartheta) \\ \upsilon = \vartheta - \epsilon, & \upsilon \in [-0.5, 0.5). \end{cases} \tag{1}$$

Definition 4 (see [18, 44]). Let $S = \{s_\epsilon | \epsilon = 1, \ldots, \tau\}$ be an LTS and $(s_\epsilon, \upsilon_\epsilon)$ be a 2-tuple; there exists a function Δ^{-1} that restore the 2-tuple to its equivalent numerical value $\vartheta \in [1, \tau] \subset R$, where

$$\Delta^{-1}: S \times [-0.5, 0.5) \longrightarrow [1, \tau],$$
$$\Delta^{-1}(s_\epsilon, \upsilon) = \varepsilon + \upsilon = \vartheta. \tag{2}$$

Definition 5 (see [10]). A Cq-ROFS $\mathcal{T}$ is defined as

$$\mathcal{T} = \{(l, \mu_\mathcal{T}(l), \nu_\mathcal{T}(l)): l \in L\}, \tag{3}$$

where $\mu_\mathcal{T}, \nu_\mathcal{T}$ are the complex-valued membership and nonmembership functions, respectively, and are defined as

$$\mu_\mathcal{T}(l) = \eta_\mathcal{T}(l) e^{i2\pi\omega_{\eta_\mathcal{T}}(l)}; \nu_\mathcal{T}(l) = \gamma_\mathcal{T}(l) e^{i2\pi\omega_{\gamma_\mathcal{T}}(l)} \tag{4}$$

where $0 \leq \eta_\mathcal{T}(l), \gamma_\mathcal{T}(l), \eta^q_\mathcal{T}(l) + \gamma^q_\mathcal{T}(l) \leq 1$ and $0 \leq \omega^q_{\eta_\mathcal{T}}(l), \omega^q_{\gamma_\mathcal{T}}(l), \omega^q_{\eta_\mathcal{T}}(l) + \omega^q_{\gamma_\mathcal{T}}(l) \leq 1$. Furthermore, $\pi_\mathcal{T}(l) = (1 - (\eta^q_\mathcal{T}(l) + \gamma^q_\mathcal{T}(l)))^{1/q}$ and $\omega_{\pi_\mathcal{T}}(l) = (1 - (\omega^q_{\eta_\mathcal{T}}(l) + \omega^q_{\gamma_\mathcal{T}}(l)))^{1/q}$ are complex hesitancy degree of l. For simplicity, the pair $\tau = ((\eta, \omega_\eta), (\gamma, \omega_\gamma))$ is called the Cq-ROF number (Cq-ROFN), where $0 \leq \eta, \gamma, \eta^q + \gamma^q \leq 1$, and $0 \leq \omega_\eta, \omega_\gamma, \omega^q_\eta + \omega^q_\gamma \leq 1$.

2.2. Hamacher t-Norm and Hamacher t-Conorm.

To extend the existing operations of t-norm and t-conorm, Hamacher [32] introduced the Hamacher product t-norm and Hamacher sum t-conorm as generalizations of t-norms and t-conorms, respectively, as follows:

$$T_{\varrho}^{H}(\mathfrak{r},\mathfrak{s}) = \begin{cases} \dfrac{\mathfrak{r}\mathfrak{s}}{\varrho + (1-\varrho)(\mathfrak{r}+\mathfrak{s}-\mathfrak{r}\mathfrak{s})} & \text{if } \varrho > 0, \\ \dfrac{\mathfrak{r}\mathfrak{s}}{\mathfrak{r}+\mathfrak{s}-\mathfrak{r}\mathfrak{s}} & \text{if } \varrho = 0. \end{cases}$$
$$\left(T^{*}\right)_{\varrho}^{H}(\mathfrak{r},\mathfrak{s}) = \begin{cases} \dfrac{\mathfrak{r}+\mathfrak{s}-\mathfrak{r}\mathfrak{s}-(1-\varrho)\mathfrak{r}\mathfrak{s}}{1-(1-\varrho)\mathfrak{r}\mathfrak{s}} & \text{if } \varrho > 0, \\ \dfrac{\mathfrak{r}+\mathfrak{s}-2\mathfrak{r}\mathfrak{s}}{1-\mathfrak{r}\mathfrak{s}} & \text{if } \varrho = 0. \end{cases} \tag{5}$$

Clearly, when $\varrho = 1$, the Hamacher t-norm and t-conorm change into the algebraic t-norm and t-conorm as follows:

$$\begin{aligned} P(\mathfrak{r},\mathfrak{s}) &= \mathfrak{r}\mathfrak{s}, \\ P^{*}(\mathfrak{r},\mathfrak{s}) &= \mathfrak{r}+\mathfrak{s}-\mathfrak{r}\mathfrak{s}. \end{aligned} \tag{6}$$

Again, when $\varrho = 2$, the Hamacher t-norm and t-conorm reduce to the Einstein t-norm and t-conorm [45] as follows:

$$\begin{aligned} I(\mathfrak{r},\mathfrak{s}) &= \frac{\mathfrak{r}\mathfrak{s}}{1+(1-\mathfrak{r})(1-\mathfrak{s})}, \\ I^{*}(\mathfrak{r},\mathfrak{s}) &= \frac{\mathfrak{r}+\mathfrak{s}}{1+\mathfrak{r}\mathfrak{s}}. \end{aligned} \tag{7}$$

3. 2-Tuple Linguistic Complex q-Rung Orthopair Fuzzy Set

Definition 6. Let $S = \{s_1, s_2, \ldots, s_\tau\}$ be a LTS with odd cardinality $\tau + 1$. The 2TLCq-ROFS is defined as

$$T = \{(r, \upsilon_T(r), \vartheta_T(r)) : r \in R\}, \tag{8}$$

where υ_T, ϑ_T are termed as 2TL complex-valued membership and nonmembership functions, respectively, and are defined as

$$\begin{aligned} \upsilon_T(r) &= \left(s_{p_\epsilon}, \wp_\epsilon\right)_T(r) e^{i2\pi\omega\left(s_{p_\epsilon},\wp_\epsilon\right)_T(r)}; \\ \vartheta_T(r) &= \left(s_{r_\epsilon}, \mathfrak{R}_\epsilon\right)_T(r) e^{i2\pi\omega\left(s_{r_\epsilon},\mathfrak{R}_\epsilon\right)_T(r)}, \end{aligned} \tag{9}$$

where

$$\begin{aligned} &0 \le \left(\Delta^{-1}\left(s_{p_\epsilon}, \wp_\epsilon\right)\right)_T(r) \le \tau, \\ &0 \le \left(\Delta^{-1}\left(s_{r_\epsilon}, \mathfrak{R}_\epsilon\right)\right)_T(r) \le \tau, \\ &0 \le \left(\Delta^{-1}\left(s_{p_\epsilon}, \wp_\epsilon\right)\right)_T^q(r) + \left(\Delta^{-1}\left(s_{r_\epsilon}, \mathfrak{R}_\epsilon\right)\right)_T^q(r) \\ &\quad \le \tau^q 0 \le \omega^q_{\left(\Delta^{-1}\left(s_{p_\epsilon},\wp_\epsilon\right)\right)_T} \le \tau, \\ &0 \le \omega^q_{\left(\Delta^{-1}\left(s_{r_\epsilon},\mathfrak{R}_\epsilon\right)\right)_T} \le \tau, \\ &0 \le \omega^q_{\left(\Delta^{-1}\left(s_{p_\epsilon},\wp_\epsilon\right)\right)_T}(r) + \omega^q_{\left(\Delta^{-1}\left(s_{r_\epsilon},\mathfrak{R}_\epsilon\right)\right)_T}(r) \le \tau^q. \end{aligned} \tag{10}$$

For simplicity, the pair $(((s_p, \wp), \omega_{(s_p,\wp)}), ((s_r, \mathfrak{R}), \omega_{(s_r,\mathfrak{R})}))$ is called the 2TLCq-ROF number and is defined for $s_p, s_r \in S$ and $\wp, \mathfrak{R} \in [-0.5, 0.5)$, where

$$\begin{aligned} &0 \le \left(\Delta^{-1}\left(s_{p_\epsilon}, \wp_\epsilon\right)\right) \le \tau, \\ &0 \le \left(\Delta^{-1}\left(s_{r_\epsilon}, \mathfrak{R}_\epsilon\right)\right) \le \tau, \\ &0 \le \left(\Delta^{-1}\left(s_{p_\epsilon}, \wp_\epsilon\right)\right)^q + \left(\Delta^{-1}\left(s_{r_\epsilon}, \mathfrak{R}_\epsilon\right)\right)^q \\ &\quad \le \tau^q 0 \le \omega^q_{\left(\Delta^{-1}\left(s_{p_\epsilon},\wp_\epsilon\right)\right)_T} \le \tau, \\ &0 \le \omega^q_{\left(\Delta^{-1}\left(s_{r_\epsilon},\mathfrak{R}_\epsilon\right)\right)_T} \le \tau, \\ &0 \le \omega^q_{\left(\Delta^{-1}\left(s_{p_\epsilon},\wp_\epsilon\right)\right)_T} + \omega^q_{\left(\Delta^{-1}\left(s_{r_\epsilon},\mathfrak{R}_\epsilon\right)\right)_T} \le \tau^q. \end{aligned} \tag{11}$$

In order to compare any two 2TLCq-ROFNs, their score value and accuracy value are defined as follows:

Definition 7. Let $\widetilde{\varsigma} = (((s_p, \wp), \omega_{(s_p,\wp)}), ((s_r, \mathfrak{R}), \omega_{(s_r,\mathfrak{R})}))$ be a 2TLCq-ROFN. Then, the score value F of a 2TLCq-ROFN $\widetilde{\varsigma}$, can be represented as

$$\mathsf{F}(\widetilde{\varsigma}) = \Delta\left(\frac{\tau}{2}\left(\left(1 + \left(\frac{\Delta^{-1}\left(s_p,\wp\right)}{\tau}\right)^q - \left(\frac{\Delta^{-1}\left(s_r,\mathfrak{R}\right)}{\tau}\right)^q\right) + \left(1 + \omega\left(\frac{\Delta^{-1}\left(s_p,\wp\right)}{\tau}\right)^q - \omega\left(\frac{\Delta^{-1}\left(s_r,\mathfrak{R}\right)}{\tau}\right)^q\right)\right)\right). \tag{12}$$

$\mathsf{F}(\widetilde{\varsigma}) \in [0, \tau]$, and its accuracy function $\beth$ is defined as

$$\beth(\widetilde{\varsigma}) = \Delta\left(\tau\left(\left(\frac{\Delta^{-1}\left(s_p,\wp\right)}{\tau}\right)^q + \left(\frac{\Delta^{-1}\left(s_r,\mathfrak{R}\right)}{\tau}\right)^q + \omega_{\left(\Delta^{-1}\left(s_p,\wp\right)/\tau\right)^q} + \omega_{\left(\Delta^{-1}\left(s_r,\mathfrak{R}\right)/\tau\right)^q}\right)\right), \tag{13}$$

$\beth(\widetilde{\varsigma}) \in [0, \tau]$.

Definition 8. Let $\widetilde{\varsigma}_1 = (((s_{p_1}, \wp_1), \omega_{(s_{p_1},\wp_1)}), ((s_{r_1}, \mathfrak{R}_1), \omega_{(s_{r_1},\mathfrak{R}_1)}))$, and $\widetilde{\varsigma}_2 = (((s_{p_2}, \wp_2), \omega_{(s_2,\wp_2)}), ((s_{r_2}, \mathfrak{R}_2), \omega_{(s_{r_2},\mathfrak{R}_2)}))$ be two 2TLCq-ROFNs; then, these two 2TLCq-ROFNs can be compared according to the following rules:

(1) If $\mathsf{F}(\widetilde{\varsigma}_1) > \mathsf{F}(\widetilde{\varsigma}_2)$, then $\widetilde{\varsigma}_1 \succ \widetilde{\varsigma}_2$

(2) If $\mathsf{F}(\widetilde{\varsigma}_1) = \mathsf{F}(\widetilde{\varsigma}_2)$, then

(i) If $\sqsupset(\widetilde{\varsigma}_1) > \sqsupset(\widetilde{\varsigma}_2)$, then $\widetilde{\varsigma}_1 \succ \widetilde{\varsigma}_2$

(ii) If $\sqsupset(\widetilde{\varsigma}_1) = \sqsupset(\widetilde{\varsigma}_2)$, then $\widetilde{\varsigma}_1 \sim \widetilde{\varsigma}_2$

3.1. Operational Laws for 2TLCq-ROFNs. Some operational laws are put forward to compute the 2TLCq-ROFNs like complex numbers:

Definition 9. Let $\widetilde{\varsigma} = (((s_p, \wp), \omega_{(s_p,\wp)}), ((s_r, \mathfrak{R}), \omega_{(s_r,\mathfrak{R})}))$, $\widetilde{\varsigma}_1 = (((s_{p_1}, \wp_1), \omega_{(s_{p_1},\wp_1)}), ((s_{r_1}, \mathfrak{R}_1), \omega_{(s_{r_1},\mathfrak{R}_1)}))$, and $\widetilde{\varsigma}_2 = (((s_{p_2}, \wp_2), \omega_{(s_{p_2},\wp_2)}), ((s_{r_2}, \mathfrak{R}_2), \omega_{(s_{r_2},\mathfrak{R}_2)}))$ be three 2TLCq-ROFNs, then

(1)

$$\widetilde{\varsigma}_1 \oplus \widetilde{\varsigma}_2 = \begin{pmatrix} \Delta\left(\tau\sqrt{[q]1} - \left(1 - \left(\Delta^{-1}\left(s_{p_1}, \wp_1\right)/\tau\right)^q\right)\left(1 - \left(\Delta^{-1}\left(s_{p_2}, \wp_2\right)/\tau\right)^q\right)\right), \\ \Delta\left(\tau\sqrt{[q]1} - \left(1 - \left(\omega_{\Delta^{-1}\left(s_{p_1},\wp_1\right)}/\tau\right)^q\right)\left(1 - \left(\omega_{\Delta^{-1}\left(s_{p_2},\wp_2\right)}/\tau\right)^q\right)\right) \\ \left(\Delta\left(\tau\left(\Delta^{-1}\left(s_{r_1}, \mathfrak{R}_1\right)/\tau\right)\left(\Delta^{-1}\left(s_{r_2}, \mathfrak{R}_2\right)/\tau\right)\right), \Delta\left(\tau\left(\omega_{\Delta^{-1}\left(s_{r_1},\mathfrak{R}_1\right)}/\tau\right)\left(\omega_{\Delta^{-1}\left(s_{r_2},\mathfrak{R}_2\right)}/\tau\right)\right)\right) \end{pmatrix}. \tag{14}$$

(2)

$$\widetilde{\varsigma}_1 \oplus \widetilde{\varsigma}_2 = \begin{pmatrix} \left(\Delta\left(\tau\left(\Delta^{-1}\left(s_{p1}, \wp_1\right)/\tau\right)\left(\Delta^{-1}\left(s_{p2}, \wp_2\right)/\tau\right)\right), \Delta\left(\tau\left(\omega_{\Delta^{-1}\left(s_{p1},\wp_1\right)}/\tau\right)\left(\omega_{\Delta^{-1}\left(s_{p1},\wp_2\right)}/\tau\right)\right)\right), \\ \left(\Delta\left(\tau\sqrt{[q]1} - \left(1 - \left(\Delta^{-1}\left(s_{r_1}, \mathfrak{R}_1\right)/\tau\right)^q\right)\left(1 - \left(\Delta^{-1}\left(s_{r_2}, \mathfrak{R}_2\right)/\tau\right)^q\right)\right), \\ \Delta\left(\tau\sqrt{[q]1} - \left(1 - \left(\omega_{\Delta^{-1}\left(s_{r_1},\mathfrak{R}_1\right)}/\tau\right)^q\right)\left(1 - \left(\omega_{\Delta^{-1}\left(s_{r_2},\mathfrak{R}_2\right)}/\tau\right)^q\right)\right) \end{pmatrix} \tag{15}$$

(3)

$$\lambda\widetilde{\varsigma} = \begin{pmatrix} \left(\Delta\left(\tau\sqrt{[q]1} - \left(1 - \left(\Delta^{-1}\left(s_p, \wp\right)/\tau\right)^q\right)^\lambda\right), \Delta\left(\tau\sqrt{[q]1} - \left(1 - \left(\omega_{\Delta^{-1}\left(s_p,\wp\right)}/\tau\right)^q\right)^\lambda\right)\right), \\ \left(\Delta\left(\tau\left(\Delta^{-1}\left(s_r, \mathfrak{R}\right)/\tau\right)^\lambda\right), \Delta\left(\tau\left(\omega_{\Delta^{-1}\left(s_r,\mathfrak{R}\right)}/\tau\right)^\tau\right)\right) \end{pmatrix}, \lambda 0 \tag{16}$$

(4)

$$\widetilde{\varsigma}^\lambda = \begin{pmatrix} \left(\Delta\left(\tau\left(\Delta^{-1}\left(s_p, \wp\right)/\tau\right)^\lambda\right), \Delta\left(\tau\left(\omega_{\left(\Delta^{-1}\left(s_p,\wp\right)/\tau\right)}\right)^\lambda\right)\right), \\ \left(\Delta\left(\tau\sqrt{[q]1} - \left(1 - \left(\Delta^{-1}\left(s_r, \mathfrak{R}\right)/\tau\right)^q\right)^\lambda\right), \Delta\left(\tau\sqrt{[q]1} - \left(1 - \left(\omega_{\Delta^{-1}\left(s_r,\mathfrak{R}\right)}/\tau\right)^q\right)^\lambda\right)\right), \end{pmatrix}, \lambda > 0 \tag{17}$$

4. Some 2TLCq-ROFH Aggregation Operators

In this section, we present Hamacher operational laws of 2TLCq-ROFS, and based on these Hamacher operational laws, we propose some 2TLCq-ROFH AOs by using weighted average and weighted geometric operators.

Definition 10. Let $\widetilde{\varsigma}_1 = (((s_{p_1}, \wp_1), (\omega_{(s_{p_1},\wp_1)})), ((s_{r_1}, \mathfrak{R}_1), (\omega_{(s_{r_1},\mathfrak{R}_1)})))$, and $\widetilde{\varsigma}_2 = (((s_{p_2}, \wp_2), (\omega_{(s_{p_2},\wp_2)})), ((s_{r_2}, \mathfrak{R}_2), (\omega_{(s_{r_2},\mathfrak{R}_2)})))$ be two 2TLCq-ROFNs, with $\varrho > 0$; then, the basic Hamacher operations between $\widetilde{\varsigma}_1$ and $\widetilde{\varsigma}_2$ are given as follows:

$$1.\tilde{\zeta}_1 \oplus \tilde{\zeta}_2 = \left(\begin{array}{c} \left(\begin{array}{c} \Delta\left(\tau\left(\sqrt[q]{\frac{\left(\Delta^{-1}\left(s_{p_1},\wp_1\right)/\tau\right)^q + \left(\Delta^{-1}\left(s_{p_2},\wp_2\right)/\tau\right)^q - \left(\Delta^{-1}\left(s_{p_1},\wp_1\right)/\tau\right)^q\left(\Delta^{-1}\left(s_{p_2},\wp_2\right)/\tau\right)^q - (1-\varrho)\left(\Delta^{-1}\left(s_{p_1},\wp_1\right)/\tau\right)^q\left(\Delta^{-1}\left(s_{p_2},\wp_2\right)/\tau\right)^q}{1-(1-\varrho)\left(\Delta^{-1}\left(s_{p_1},\wp_1\right)/\tau\right)^q\left(\Delta^{-1}\left(s_{p_2},\wp_2\right)/\tau\right)^q}} \right) \right) \\ \Delta\left(\tau\left(\sqrt[q]{\frac{\left(\omega_{\left(\Delta^{-1}\left(s_{p_1},\wp_1\right)/\tau\right)}\right)^q + \left(\omega_{\left(\Delta^{-1}\left(s_{p_2},\wp_2\right)/\tau\right)}\right)^q - \left(\omega_{\left(\Delta^{-1}\left(s_{p_1},\wp_1\right)/\tau\right)}\right)^q\left(\omega_{\left(\Delta^{-1}\left(s_{p_2},\wp_2\right)/\tau\right)}\right)^q - (1-\varrho)\left(\omega_{\left(\Delta^{-1}\left(s_{p_1},\wp_1\right)/\tau\right)}\right)^q\left(\omega_{\left(\Delta^{-1}\left(s_{p_2},\wp_2\right)/\tau\right)}\right)^q}{1-(1-\varrho)\left(\omega_{\left(\Delta^{-1}\left(s_{p_1},\wp_1\right)/\tau\right)}\right)^q\left(\omega_{\left(\Delta^{-1}\left(s_{p_2},\wp_2\right)/\tau\right)}\right)^q}} \right) \right) \end{array} \right) \\ \left(\begin{array}{c} \Delta\left(\tau\left(\frac{\left(\Delta^{-1}\left(s_{r_1},\mathfrak{R}_1\right)/\tau\right)\left(\Delta^{-1}\left(s_{r_2},\mathfrak{R}_2\right)/\tau\right)}{\sqrt[q]{\varrho + (1-\varrho)\left(\left(\Delta^{-1}\left(s_{r_1},\mathfrak{R}_1\right)/\tau\right)^q + \left(\Delta^{-1}\left(s_{r_2},\mathfrak{R}_2\right)/\tau\right)^q - \left(\Delta^{-1}\left(s_{r_1},\mathfrak{R}_1\right)/\tau\right)^q\left(\Delta^{-1}\left(s_{r_2},\mathfrak{R}_2\right)/\tau\right)^q\right)}} \right) \right) \\ \Delta\left(\tau\left(\frac{\omega_{\left(\Delta^{-1}\left(s_{r_1},\mathfrak{R}_1\right)/\tau\right)}\omega_{\left(\Delta^{-1}\left(s_{r_2},\mathfrak{R}_2\right)/\tau\right)}}{\sqrt[q]{\varrho + (1-\varrho)\left(\left(\omega_{\left(\Delta^{-1}\left(s_{r_1},\mathfrak{R}_1\right)/\tau\right)}\right)^q + \left(\omega_{\left(\Delta^{-1}\left(s_{r_2},\mathfrak{R}_2\right)/\tau\right)}\right)^q - \left(\omega_{\left(\left(\Delta^{-1}\left(s_{r_1},\mathfrak{R}_1\right)/\tau\right)\right)}\right)^q\left(\omega_{\left(\Delta^{-1}\left(s_{r_2},\mathfrak{R}_2\right)/\tau\right)}\right)^q\right)}} \right) \right) \end{array} \right) \end{array} \right),$$

$$2\,\tilde{\zeta}_1 \otimes \tilde{\zeta}_2 = \left(\begin{array}{c} \left(\begin{array}{c} \left(\begin{array}{c} \Delta\left(\tau\left(\frac{\left(\Delta^{-1}\left(s_{p_1},\wp_1\right)/\tau\right)\left(\Delta^{-1}\left(s_{p_2},\wp_2\right)/\tau\right)}{\sqrt[q]{\varrho + (1-\varrho)\left(\left(\Delta^{-1}\left(s_{p_1},\wp_1\right)/\tau\right)^q + \left(\Delta^{-1}\left(s_{p_2},\wp_2\right)/\tau\right)^q - \left(\Delta^{-1}\left(s_{p_1},\wp_1\right)/\tau\right)^q\left(\Delta^{-1}\left(s_{p_2},\wp_2\right)/\tau\right)^q\right)}} \right) \right), \\ \Delta\left(\tau\left(\frac{\omega_{\left(\Delta^{-1}\left(s_{p_1},\wp_1\right)/\tau\right)}\omega_{\left(\Delta^{-1}\left(s_{p_2},\wp_2\right)/\tau\right)}}{\sqrt[q]{\varrho + (1-\varrho)\left(\left(\omega_{\left(\Delta^{-1}\left(s_{p_1},\wp_1\right)/\tau\right)}\right)^q + \left(\omega_{\left(\Delta^{-1}\left(s_{p_2},\wp_2\right)/\tau\right)}\right)^q - \left(\omega_{\left(\Delta^{-1}\left(s_{p_1},\wp_1\right)/\tau\right)}\right)^q\left(\omega_{\left(\Delta^{-1}\left(s_{p_2},\wp_2\right)/\tau\right)}\right)^q\right)}} \right) \right) \end{array} \right) \\ \left(\begin{array}{c} \Delta\left(\tau\left(\sqrt[q]{\frac{\left(\Delta^{-1}\left(s_{r_1},\mathfrak{R}_1\right)/\tau\right)^q + \left(\Delta^{-1}\left(s_{r_2},\mathfrak{R}_2\right)/\tau\right)^q - \left(\Delta^{-1}\left(s_{r_1},\mathfrak{R}_1\right)/\tau\right)^q\left(\Delta^{-1}\left(s_{r_2},\mathfrak{R}_2\right)/\tau\right)^q - (1-\varrho)\left(\Delta^{-1}\left(s_{r_1},\mathfrak{R}_1\right)/\tau\right)^q\left(\Delta^{-1}\left(s_{r_2},\mathfrak{R}_2\right)/\tau\right)^q}{1-(1-\varrho)\left(\Delta^{-1}\left(s_{r_1},\mathfrak{R}_1\right)/\tau\right)^q\left(\Delta^{-1}\left(s_{r_2},\mathfrak{R}_2\right)/\tau\right)^q}} \right) \right) \\ \Delta\left(\tau\left(\sqrt[q]{\frac{\left(\Delta^{-1}\left(s_{r_1},\mathfrak{R}_1\right)/\tau\right)^q + \left(\omega_{\left(\Delta^{-1}\left(s_{r_2},\mathfrak{R}_2\right)/\tau\right)}\right)^q - \left(\Delta^{-1}\left(s_{r_1},\mathfrak{R}_1\right)/\tau\right)^q\left(\omega_{\left(\Delta^{-1}\left(s_{r_2},\mathfrak{R}_2\right)/\tau\right)}\right)^q - (1-\varrho)\left(\omega_{\left(\Delta^{-1}\left(s_{r_1},\mathfrak{R}_1\right)/\tau\right)}\right)^q\left(\omega_{\left(\Delta^{-1}\left(s_{r_2},\mathfrak{R}_2\right)/\tau\right)}\right)^q}{1-(1-\varrho)\left(\omega_{\left(\Delta^{-1}\left(s_{r_1},\mathfrak{R}_1\right)/\tau\right)}\right)^q\left(\omega_{\left(\Delta^{-1}\left(s_{r_2},\mathfrak{R}_2\right)/\tau\right)}\right)^q}} \right) \right) \end{array} \right) \end{array} \right),$$

$$3.\lambda\tilde{\zeta}_1 = \left(\begin{array}{c} \left(\begin{array}{c} \Delta\left(\tau\left(\sqrt[q]{\frac{\left(1+(\varrho-1)\left(\Delta^{-1}\left(s_{p_1},\wp_1\right)/\tau\right)^q\right)^\lambda - \left(1-\left(\Delta^{-1}\left(s_{p_1},\wp_1\right)/\tau\right)^q\right)^\lambda}{\left(1+(\varrho-1)\left(\Delta^{-1}\left(s_{p_1},\wp_1\right)/\tau\right)^q\right)^\lambda + (\varrho-1)\left(1-\left(\Delta^{-1}\left(s_{p_1},\wp_1\right)/\tau\right)^q\right)^\lambda}} \right) \right) \\ \Delta\left(\tau\left(\sqrt[q]{\frac{\left(1+(\varrho-1)\left(\omega_{\left(\Delta^{-1}\left(s_{p_1},\wp_1\right)/\tau\right)}\right)^q\right)^\lambda - \left(1-\left(\omega_{\left(\Delta^{-1}\left(s_{p_1},\wp_1\right)/\tau\right)}\right)^q\right)^\lambda}{\left(1+(\varrho-1)\left(\omega_{\left(\Delta^{-1}\left(s_{p_1},\wp_1\right)/\tau\right)}\right)^q\right)^\lambda + (\varrho-1)\left(1-\left(\omega_{\left(\Delta^{-1}\left(s_{p_1},\wp_1\right)/\tau\right)}\right)^q\right)^\lambda}} \right) \right) \end{array} \right) \\ \left(\begin{array}{c} \Delta\left(\tau\left(\frac{\sqrt[q]{\varrho\left(\Delta^{-1}\left(s_{r_1},\mathfrak{R}_1\right)/\tau\right)^\lambda}}{\sqrt[q]{\left(1+(\varrho-1)\left(1-\left(\Delta^{-1}\left(s_{r_1},\mathfrak{R}_1\right)/\tau\right)^q\right)\right)^\lambda + (\varrho-1)\left(\Delta^{-1}\left(s_{r_1},\mathfrak{R}_1\right)/\tau\right)^{q\lambda}}} \right) \right) \\ \Delta\left(\tau\left(\frac{\sqrt[q]{\varrho\left(\omega_{\left(\Delta^{-1}\left(s_{r_1},\mathfrak{R}_1\right)/\tau\right)}\right)^\lambda}}{\sqrt[q]{\left(1+(\varrho-1)\left(1-\left(\omega_{\left(\Delta^{-1}\left(s_{r_1},\mathfrak{R}_1\right)/\tau\right)}\right)^q\right)\right)^\lambda + (\varrho-1)\left(\omega_{\left(\Delta^{-1}\left(s_{r_1},\mathfrak{R}_1\right)/\tau\right)}\right)^{q\lambda}}} \right) \right) \end{array} \right) \end{array} \right);$$

$$4.\tilde{\varsigma}_1^{\lambda}=\left(\begin{array}{c}\left(\Delta\left(\tau\left(\frac{\sqrt[q]{\varrho\left(\Delta^{-1}\left(s_{p_1},\wp_1\right)/\tau\right)^{\lambda}}}{\sqrt[q]{\left(1+(\varrho-1)\left(1-\left(\Delta^{-1}\left(s_{p_1},\wp_1\right)/\tau\right)^{q}\right)\right)^{\lambda}+(\varrho-1)\left(\Delta^{-1}\left(s_{p_1},\wp_1\right)/\tau\right)^{q\lambda}}}\right)\right)\\ \left(\Delta\left(\tau\left(\frac{\sqrt[q]{\varrho\left(\omega_{\left(\Delta^{-1}\left(s_{p_1},\wp_1\right)/\tau\right)}\right)^{\lambda}}}{\sqrt[q]{\left(1+(\varrho-1)\left(1-\left(\omega_{\left(\Delta^{-1}\left(s_{p_1},\wp_1\right)/\tau\right)}\right)^{q}\right)\right)^{\lambda}+(\varrho-1)\left(\omega\left(\Delta^{-1}\left(s_{p_1},\wp_1\right)/\tau\right)\right)^{q\lambda}}}\right)\right)\end{array}\right)\\ \left(\begin{array}{c}\left(\Delta\left(\tau\left(\sqrt[q]{\frac{\left(1+(\varrho-1)\left(\Delta^{-1}\left(s_{r_1},\mathfrak{R}_1\right)/\tau\right)^{q}\right)^{\lambda}-\left(1-\left(\Delta^{-1}\left(s_{r_1},\mathfrak{R}_1\right)/\tau\right)^{q}\right)^{\lambda}}{\left(1+(\varrho-1)\left(\Delta^{-1}\left(s_{r_1},\mathfrak{R}_1\right)/\tau\right)^{q}\right)^{\lambda}+(\varrho-1)\left(1-\left(\Delta^{-1}\left(s_{r_1},\mathfrak{R}_1\right)/\tau\right)^{q}\right)^{\lambda}}}\right)\right)\\ \left(\Delta\left(\tau\left(\sqrt[q]{\frac{\left(1+(\varrho-1)\left(\omega_{\left(\Delta^{-1}\left(s_{r_1},\mathfrak{R}_1\right)/\tau\right)}\right)^{q}\right)^{\lambda}-\left(1-\left(\omega_{\left(\Delta^{-1}\left(s_{r_1},\mathfrak{R}_1\right)/\tau\right)}\right)^{q}\right)^{\lambda}}{\left(1+(\varrho-1)\left(\omega_{\left(\Delta^{-1}\left(s_{r_1},\mathfrak{R}_1\right)/\tau\right)}\right)^{q}\right)^{\lambda}+(\varrho-1)\left(1-\left(\omega_{\left(\Delta^{-1}\left(s_{r_1},\mathfrak{R}_1\right)/\tau\right)}\right)^{q}\right)^{\lambda}}}\right)\right)\end{array}\right).\tag{18}$$

Definition 11. Let $\tilde{\varsigma}_\varepsilon=(((s_{p_\varepsilon},\wp_\varepsilon),(\omega_{(s_{p_\varepsilon},\wp_\varepsilon)})),((s_{r_\varepsilon},\mathfrak{R}_\varepsilon),(\omega_{(s_{r_\varepsilon},\mathfrak{R}_\varepsilon)})))(\varepsilon=1,2,\ldots,n)$ be a collection of 2TLCq-ROFNs; then, the 2TLCq-ROFHWA operator is defined as

$$2TLCq-ROFHWA_{\varphi}\left(\tilde{\varsigma}_1,\tilde{\varsigma}_2,\ldots,\tilde{\varsigma}_n\right)=\oplus_{\epsilon=1}^{n}\left(\varphi_\epsilon\tilde{\varsigma}_\epsilon\right),\tag{19}$$

where $\varphi=(\varphi_1,\varphi_2,\ldots,\varphi_n)^T$ be the weight vector of $\tilde{\varsigma}_\epsilon(\epsilon=1,2,\ldots,n)$, and $\varphi_\epsilon>0$, $\sum_{\epsilon=1}^{n}\varphi_\epsilon=1$.

We derive the following theorem from Def. 11 using the 2TLCq-ROFH operations.

Theorem 1. *Let* $\tilde{\varsigma}_\epsilon=(((s_{p_\epsilon},\wp_\epsilon),(\omega_{(s_{p_\epsilon},\wp_\epsilon)})),((s_{r_\epsilon},\mathfrak{R}_\epsilon),(\omega_{(s_{r_\epsilon},\mathfrak{R}_\epsilon)})))(\epsilon=1,2,\ldots,n)$ *be a collection of 2TLCq-ROFNs, where* $\varrho>0$. *Then, for any* $q\geq 0$, *the aggregated value by utilizing 2TLCq-ROFHWA operator is also a 2TLCq-ROFN, and*

$$2TLCq-ROFHWA_{\varphi}\left(\tilde{\varsigma}_1,\tilde{\varsigma}_2,\ldots,\tilde{\varsigma}_n\right)=\oplus_{\epsilon=1}^{n}\left(\varphi_\epsilon\tilde{\varsigma}_\epsilon\right)$$

$$=\left(\begin{array}{c}\left(\Delta\left(\tau\left(\sqrt[q]{\frac{\prod_{\epsilon=1}^{n}\left(1+(\varrho-1)\left(\Delta^{-1}\left(s_{p_\epsilon},\wp_\epsilon\right)/\tau\right)^{q}\right)^{\varphi_\epsilon}-\prod_{\epsilon=1}^{n}\left(1-\left(\Delta^{-1}\left(s_{p_\epsilon},\wp_\epsilon\right)/\tau\right)^{q}\right)^{\varphi_\epsilon}}{\prod_{\epsilon=1}^{n}\left(1+(\varrho-1)\left(\Delta^{-1}\left(s_{p_\epsilon},\wp_\epsilon\right)/\tau\right)^{q}\right)^{\varphi_\epsilon}+(\varrho-1)\prod_{\epsilon=1}^{n}\left(1-\left(\Delta^{-1}\left(s_{p_\epsilon},\wp_\epsilon\right)/\tau\right)^{q}\right)^{\varphi_\epsilon}}}\right)\right)\\ \left(\Delta\left(\tau\left(\sqrt[q]{\frac{\prod_{\epsilon=1}^{n}\left(1+(\varrho-1)\left(\omega_{\left(\Delta^{-1}\left(s_{p_\epsilon},\wp_\epsilon\right)/\tau\right)}\right)^{q}\right)^{\varphi_\epsilon}-\prod_{\epsilon=1}^{n}\left(1-\left(\omega_{\left(\Delta^{-1}\left(s_{p_\epsilon},\wp_\epsilon\right)/\tau\right)}\right)^{q}\right)^{\varphi_\epsilon}}{\prod_{\epsilon=1}^{n}\left(1+(\varrho-1)\left(\omega_{\left(\Delta^{-1}\left(s_{p_\epsilon},\wp_\epsilon\right)/\tau\right)}\right)^{q}\right)^{\varphi_\epsilon}+(\varrho-1)\prod_{\epsilon=1}^{n}\left(1-\left(\Delta^{-1}\left(s_{p_\epsilon},\wp_\epsilon\right)/\tau\right)^{q}\right)^{\varphi_\epsilon}}}\right)\right)\end{array}\right),$$

$$\left(\begin{array}{c}\left(\Delta\left(\tau\left(\frac{\sqrt[q]{\varrho}\prod_{\epsilon=1}^{n}\left(\Delta^{-1}\left(s_{r_\epsilon},\mathfrak{R}_\epsilon\right)/\tau\right)^{\varphi_\epsilon}}{\sqrt[q]{\prod_{\epsilon=1}^{n}\left(1+(\varrho-1)\left(\Delta^{-1}\left(s_{r_\epsilon},\mathfrak{R}_\epsilon\right)/\tau\right)^{q}\right)^{\varphi_\epsilon}+(\varrho-1)\prod_{\epsilon=1}^{n}\left(1-\left(\Delta^{-1}\left(s_{r_\epsilon},\mathfrak{R}_\epsilon\right)/\tau\right)\right)^{q\varphi_\epsilon}}}\right)\right)\\ \left(\Delta\left(\tau\left(\frac{\sqrt[q]{\varrho}\prod_{\epsilon=1}^{n}\left(\omega_{\left(\Delta^{-1}\left(s_{r_\epsilon},\mathfrak{R}_\epsilon\right)/\tau\right)}\right)^{\varphi_\epsilon}}{\sqrt[q]{\prod_{\epsilon=1}^{n}\left(1+(\varrho-1)\left(\Delta^{-1}\left(s_{r_\epsilon},\mathfrak{R}_\epsilon\right)/\tau\right)^{q}\right)^{\varphi_\epsilon}+(\varrho-1)\prod_{\epsilon=1}^{n}\left(1-\left(\Delta^{-1}\left(s_{r_\epsilon},\mathfrak{R}_\epsilon\right)/\tau\right)\right)^{q\varphi_\epsilon}}}\right)\right)\end{array}\right),\tag{20}$$

where $\varphi = (\varphi_1, \varphi_2, \ldots, \varphi_n)^T$ *be the weight vector of* $\widetilde{\varsigma}_\epsilon$ $(\epsilon = 1, 2, \ldots, n)$, *and* $\varphi_\epsilon > 0$, $\sum_{\epsilon=1}^{n} \varphi_\epsilon = 1, \varrho > 0$.

Proof. We use the mathematical induction principle, to prove (20). For $n = 2$, utilizing the operational laws (1) and (3) of Def. 10, we obtain the following result:

$$
\begin{aligned}
(\varphi_1\widetilde{\varsigma}_1)\oplus(\varphi_2\widetilde{\varsigma}_2) = &\left(\begin{array}{c}
\left(\Delta\left(\tau\left(\sqrt[q]{\frac{\left(1+(\varrho-1)\left(\Delta^{-1}\left(s_{p_1},\wp_1\right)/\tau\right)^q\right)^{\varphi_1}-\left(1-\left(\Delta^{-1}\left(s_{p_1},\wp_1\right)/\tau\right)^q\right)^{\varphi_1}}{\left(1+(\varrho-1)\left(\Delta^{-1}\left(s_{p_1},\wp_1\right)/\tau\right)^q\right)^{\varphi_1}+(\varrho-1)\left(1-\left(\Delta^{-1}\left(s_{p_1},\wp_1\right)/\tau\right)^q\right)^{\varphi_1}}}\right)\right)\right) \\
\left(\Delta\left(\tau\left(\sqrt[q]{\frac{\left(1+(\varrho-1)\left(\omega_{\left(\Delta^{-1}\left(s_{p_1},\wp_1\right)/\tau\right)}\right)^q\right)^{\varphi_1}-\left(1-\left(\omega_{\left(\Delta^{-1}\left(s_{p_1},\wp_1\right)/\tau\right)}\right)^q\right)^{\varphi_1}}{\left(1+(\varrho-1)\left(\omega_{\left(\Delta^{-1}\left(s_{p_1},\wp_1\right)/\tau\right)}\right)^q\right)^{\varphi_1}+(\varrho-1)\left(1-\left(\omega_{\left(\Delta^{-1}\left(s_{p_1},\wp_1\right)/\tau\right)}\right)^q\right)^{\varphi_1}}}\right)\right)\right) \\
\left(\Delta\left(\tau\left(\frac{\sqrt[q]{\varrho}\left(\Delta^{-1}\left(s_{r_1},\mathfrak{R}_1\right)/\tau\right)^{\varphi_1}}{\sqrt[q]{\left(1+(\varrho-1)\left(1-\left(\Delta^{-1}\left(s_{r_1},\mathfrak{R}_1\right)/\tau\right)^q\right)\right)^{\varphi_1}+(\varrho-1)\left(\Delta^{-1}\left(s_{r_1},\mathfrak{R}_1\right)/\tau\right)^{q\varphi_1}}}\right)\right) \\
\left(\Delta\left(\tau\left(\frac{\sqrt[q]{\varrho}\prod_{1=1}^{n}\left(\omega_{\left(\Delta^{-1}\left(s_{r_1},\mathfrak{R}_1\right)/\tau\right)}\right)^{\varphi_1}}{\sqrt[q]{\left(1+(\varrho-1)\left(1-\left(\omega_{\left(\Delta^{-1}\left(s_{r_1},\mathfrak{R}_1\right)/\tau\right)}\right)^q\right)\right)^{\varphi_1}+(\varrho-1)\left(\omega_{\left(\Delta^{-1}\left(s_{r_1},\mathfrak{R}_1\right)/\tau\right)}\right)^{q\varphi_1}}}\right)\right)
\end{array}\right) \\
\oplus &\left(\begin{array}{c}
\left(\Delta\left(\tau\left(\sqrt[q]{\frac{\left(1+(\varrho-1)\left(\Delta^{-1}\left(s_{p_2},\wp_2\right)/\tau\right)^q\right)^{\varphi_2}-\left(1-\left(\Delta^{-1}\left(s_{p_2},\wp_2\right)/\tau\right)^q\right)^{\varphi_2}}{\left(1+(\varrho-1)\left(\Delta^{-1}\left(s_{p_2},\wp_2\right)/\tau\right)^q\right)^{\varphi_2}+(\varrho-1)\left(1-\left(\Delta^{-1}\left(s_{p_2},\wp_2\right)/\tau\right)^q\right)^{\varphi_2}}}\right)\right)\right) \\
\left(\Delta\left(\tau\left(\sqrt[q]{\frac{\left(1+(\varrho-1)\left(\omega_{\left(\Delta^{-1}\left(s_{p_2},\wp_2\right)/\tau\right)}\right)^q\right)^{\varphi_2}-\left(1-\left(\omega_{\left(\Delta^{-1}\left(s_{p_2},\wp_2\right)/\tau\right)}\right)^q\right)^{\varphi_2}}{\left(1+(\varrho-1)\left(\omega_{\left(\Delta^{-1}\left(s_{p_2},\wp_2\right)/\tau\right)}\right)^q\right)^{\varphi_2}+(\varrho-1)\left(1-\left(\omega_{\left(\Delta^{-1}\left(s_{p_2},\wp_2\right)/\tau\right)}\right)^q\right)^{\varphi_2}}}\right)\right)\right) \\
\left(\Delta\left(\tau\left(\frac{\sqrt[q]{\varrho}\left(\Delta^{-1}\left(s_{r_2},\mathfrak{R}_2\right)/\tau\right)^{\varphi_2}}{\sqrt[q]{\left(1+(\varrho-1)\left(1-\left(\Delta^{-1}\left(s_{r_2},\mathfrak{R}_2\right)/\tau\right)^q\right)\right)^{\varphi_2}+(\varrho-1)\left(\Delta^{-1}\left(s_{r_2},\mathfrak{R}_2\right)/\tau\right)^{q\varphi_2}}}\right)\right) \\
\left(\Delta\left(\tau\left(\frac{\sqrt[q]{\varrho}\prod_{2=1}^{n}\left(\omega_{\left(\Delta^{-1}\left(s_{r_2},\mathfrak{R}_2\right)/\tau\right)}\right)^{\varphi_2}}{\sqrt[q]{\left(1+(\varrho-1)\left(1-\left(\omega_{\left(\Delta^{-1}\left(s_{r_2},\mathfrak{R}_2\right)/\tau\right)}\right)^q\right)\right)^{\varphi_2}+(\varrho-1)\left(\omega_{\left(\Delta^{-1}\left(s_{r_2},\mathfrak{R}_2\right)/\tau\right)}\right)^{q\varphi_2}}}\right)\right)
\end{array}\right) \\
= &\left(\begin{array}{c}
\left(\Delta\left(\tau\left(\sqrt[q]{\frac{\prod_{\epsilon=1}^{2}\left(1+(\varrho-1)\left(\Delta^{-1}\left(s_{p_\epsilon},\wp_\epsilon\right)/\tau\right)^q\right)^{\varphi_\epsilon}-\prod_{\epsilon=1}^{2}\left(1-\left(\Delta^{-1}\left(s_{p_\epsilon},\wp_\epsilon\right)/\tau\right)^q\right)^{\varphi_\epsilon}}{\prod_{\epsilon=1}^{2}\left(1+(\varrho-1)\left(\Delta^{-1}\left(s_{p_\epsilon},\wp_\epsilon\right)/\tau\right)^q\right)^{\varphi_\epsilon}+(\varrho-1)\prod_{\epsilon=1}^{2}\left(1-\left(\Delta^{-1}\left(s_{p_\epsilon},\wp_\epsilon\right)/\tau\right)^q\right)^{\varphi_\epsilon}}}\right)\right)\right) \\
\left(\Delta\left(\tau\left(\sqrt[q]{\frac{\prod_{\epsilon=1}^{2}\left(1+(\varrho-1)\left(\omega_{\left(\Delta^{-1}\left(s_{p_\epsilon},\wp_\epsilon\right)/\tau\right)}\right)^q\right)^{\varphi_\epsilon}-\prod_{\epsilon=1}^{2}\left(1-\left(\omega_{\left(\Delta^{-1}\left(s_{p_\epsilon},\wp_\epsilon\right)/\tau\right)}\right)^q\right)^{\varphi_\epsilon}}{\prod_{\epsilon=1}^{2}\left(1+(\varrho-1)\left(\omega_{\left(\Delta^{-1}\left(s_{p_\epsilon},\wp_\epsilon\right)/\tau\right)}\right)^q\right)^{\varphi_\epsilon}+(\varrho-1)\prod_{\epsilon=1}^{2}\left(1-\left(\omega_{\left(\Delta^{-1}\left(s_{p_\epsilon},\wp_\epsilon\right)/\tau\right)}\right)^q\right)^{\varphi_\epsilon}}}\right)\right)\right) \\
\left(\Delta\left(\tau\left(\frac{\sqrt[q]{\varrho}\prod_{\epsilon=1}^{2}\left(\Delta^{-1}\left(s_{r_\epsilon},\mathfrak{R}_\epsilon\right)/\tau\right)^{\varphi_\epsilon}}{\sqrt[q]{\prod_{\epsilon=1}^{2}\left(1+(\varrho-1)\left(1-\left(\Delta^{-1}\left(s_{r_\epsilon},\mathfrak{R}_\epsilon\right)/\tau\right)^q\right)\right)^{\varphi_\epsilon}+(\varrho-1)\prod_{\epsilon=1}^{2}\left(\Delta^{-1}\left(s_{r_\epsilon},\mathfrak{R}_\epsilon\right)/\tau\right)^{q\varphi_\epsilon}}}\right)\right) \\
\left(\Delta\left(\tau\left(\frac{\sqrt[q]{\varrho}\prod_{\epsilon=1}^{2}\left(\omega_{\left(\Delta^{-1}\left(s_{r_\epsilon},\mathfrak{R}_\epsilon\right)/\tau\right)}\right)^{\varphi_\epsilon}}{\sqrt[q]{\prod_{\epsilon=1}^{2}\left(1+(\varrho-1)\left(1-\left(\omega_{\left(\Delta^{-1}\left(s_{r_\epsilon},\mathfrak{R}_\epsilon\right)/\tau\right)}\right)^q\right)\right)^{\varphi_\epsilon}+(\varrho-1)\prod_{\epsilon=1}^{2}\left(\omega_{\left(\Delta^{-1}\left(s_{r_\epsilon},\mathfrak{R}_\epsilon\right)/\tau\right)}\right)^{q\varphi_\epsilon}}}\right)\right)
\end{array}\right).
\end{aligned}
\tag{21}
$$

The result in (20) holds true for $n = 2$. Suppose the result is true for $n = k$, and we can get the result:

$$\oplus_{\epsilon=1}^{k}\left(\varphi_\epsilon\widetilde{\varsigma}_\epsilon\right)=\left(\begin{array}{c}\left(\begin{array}{c}\Delta\left(\tau\left(\sqrt[q]{\dfrac{\prod_{\epsilon=1}^{k}\left(1+(\varrho-1)\left(\Delta^{-1}\left(s_{p_\epsilon},\wp_\epsilon\right)/\tau\right)^q\right)^{\varphi_\epsilon}-\prod_{\epsilon=1}^{k}\left(1-\left(\Delta^{-1}\left(s_{p_\epsilon},\wp_\epsilon\right)/\tau\right)^q\right)^{\varphi_\epsilon}}{\prod_{\epsilon=1}^{k}\left(1+(\varrho-1)\left(\Delta^{-1}\left(s_{p_\epsilon},\wp_\epsilon\right)/\tau\right)^q\right)^{\varphi_\epsilon}+(\varrho-1)\prod_{\epsilon=1}^{k}\left(1-\left(\Delta^{-1}\left(s_{p_\epsilon},\wp_\epsilon\right)/\tau\right)^q\right)^{\varphi_\epsilon}}}\right)\right),\\ \Delta\left(\tau\left(\sqrt[q]{\dfrac{\prod_{\epsilon=1}^{k}\left(1+(\varrho-1)\left(\omega_{\left(\Delta^{-1}\left(s_{p_\epsilon},\wp_\epsilon\right)/\tau\right)}\right)^q\right)^{\varphi_\epsilon}-\prod_{\epsilon=1}^{k}\left(1-\left(\omega_{\left(\Delta^{-1}\left(s_{p_\epsilon},\wp_\epsilon\right)/\tau\right)}\right)^q\right)^{\varphi_\epsilon}}{\prod_{\epsilon=1}^{k}\prod_{\epsilon=1}^{k}\left(1+(\varrho-1)\left(\omega_{\left(\Delta^{-1}\left(s_{p_\epsilon},\wp_\epsilon\right)/\tau\right)}\right)^q\right)^{\varphi_\epsilon}+(\varrho-1)\prod_{\epsilon=1}^{k}\left(1-\left(\omega_{\left(\Delta^{-1}\left(s_{p_\epsilon},\wp_\epsilon\right)/\tau\right)}\right)^q\right)^{\varphi_\epsilon}}\right)\right)\end{array}\right)\\ \left(\begin{array}{c}\Delta\left(\tau\left(\dfrac{\sqrt[q]{\varrho}\prod_{\epsilon=1}^{k}\left(\Delta^{-1}\left(s_{r_\epsilon},\mathfrak{R}_\epsilon\right)/\tau\right)^{\varphi_\epsilon}}{\sqrt[q]{\prod_{\epsilon=1}^{k}\left(1+(\varrho-1)\left(1-\left(\Delta^{-1}\left(s_{r_\epsilon},\mathfrak{R}_\epsilon\right)/\tau\right)^q\right)\right)^{\varphi_\epsilon}+(\varrho-1)\prod_{\epsilon=1}^{k}\left(\omega_{\left(\Delta^{-1}\left(s_{r_\epsilon},\mathfrak{R}_\epsilon\right)/\tau\right)}\right)^{q\varphi_\epsilon}}}\right)\right)\\ \Delta\left(\tau\left(\dfrac{\sqrt[q]{\varrho}\prod_{\epsilon=1}^{k}\left(\omega_{\left(\Delta^{-1}\left(s_{r_\epsilon},\mathfrak{R}_\epsilon\right)/\tau\right)}\right)^{\varphi_\epsilon}}{\sqrt[q]{\prod_{\epsilon=1}^{k}\left(1+(\varrho-1)\left(1-\left(\omega_{\left(\Delta^{-1}\left(s_{r_\epsilon},\mathfrak{R}_\epsilon\right)/\tau\right)}\right)^q\right)\right)^{\varphi_\epsilon}+(\varrho-1)\prod_{\epsilon=1}^{k}\left(\omega_{\left(\Delta^{-1}\left(s_{r_\epsilon},\mathfrak{R}_\epsilon\right)/\tau\right)}\right)^{q\varphi_\epsilon}}}\right)\right)\end{array}\right)\end{array}\right).\tag{22}$$

When $n = k + 1$, by using the operational laws of Def. 10, we have

$$\oplus_{\epsilon=1}^{k+1}\left(\varphi_\epsilon\widetilde{\varsigma}_\epsilon\right)=\left(\oplus_{\epsilon=1}^{k}\left(\varphi_\epsilon\widetilde{\varsigma}_\epsilon\right)\right)\oplus\left(\varphi_{k+1}\widetilde{\varsigma}_{k+1}\right)$$

$$=\left(\begin{array}{c}\left(\begin{array}{c}\Delta\left(\tau\left(\sqrt[q]{\dfrac{\prod_{\epsilon=1}^{k}\left(1+(\varrho-1)\left(\Delta^{-1}\left(s_{p_\epsilon},\wp_\epsilon\right)/\tau\right)^q\right)^{\varphi_\epsilon}-\prod_{\epsilon=1}^{k}\left(1-\left(\Delta^{-1}\left(s_{p_\epsilon},\wp_\epsilon\right)/\tau\right)^q\right)^{\varphi_\epsilon}}{\prod_{\epsilon=1}^{k}\left(1+(\varrho-1)\left(\Delta^{-1}\left(s_{p_\epsilon},\wp_\epsilon\right)/\tau\right)^q\right)^{\varphi_\epsilon}\prod_{\epsilon=1}^{k}+(\varrho-1)\prod_{\epsilon=1}^{k}\left(1-\left(\Delta^{-1}\left(s_{p_\epsilon},\wp_\epsilon\right)/\tau\right)^q\right)^{\varphi_\epsilon}}}\right)\right)\\ \Delta\left(\tau\left(\sqrt[q]{\dfrac{\prod_{\epsilon=1}^{k}\left(1+(\varrho-1)\left(\omega_{\left(\Delta^{-1}\left(s_{p_\epsilon},\wp_\epsilon\right)/\tau\right)}\right)^q\right)^{\varphi_\epsilon}-\prod_{\epsilon=1}^{k}\left(1-\left(\omega_{\left(\Delta^{-1}\left(s_{p_\epsilon},\wp_\epsilon\right)/\tau\right)}\right)^q\right)^{\varphi_\epsilon}}{\prod_{\epsilon=1}^{k}\left(1+(\varrho-1)\left(\omega_{\left(\Delta^{-1}\left(s_{p_\epsilon},\wp_\epsilon\right)/\tau\right)}\right)^q\right)^{\varphi_\epsilon}+(\varrho-1)\prod_{\epsilon=1}^{k}\left(1-\left(\omega_{\left(\Delta^{-1}\left(s_{p_\epsilon},\wp_\epsilon\right)/\tau\right)}\right)^q\right)^{\varphi_\epsilon}}\right)\right)\end{array}\right)\\ \left(\begin{array}{c}\Delta\left(\tau\left(\dfrac{\sqrt[q]{\varrho}\prod_{\epsilon=1}^{k}\left(\Delta^{-1}\left(s_{r_\epsilon},\mathfrak{R}_\epsilon\right)/\tau\right)^{\varphi_\epsilon}}{\sqrt[q]{\prod_{\epsilon=1}^{k}\left(1+(\varrho-1)\left(1-\left(\Delta^{-1}\left(s_{r_\epsilon},\mathfrak{R}_\epsilon\right)/\tau\right)^q\right)\right)^{\varphi_\epsilon}+(\varrho-1)\prod_{\epsilon=1}^{k}\left(\Delta^{-1}\left(s_{r_\epsilon},\mathfrak{R}_\epsilon\right)/\tau\right)^{q\varphi_\epsilon}}}\right)\right)\\ \Delta\left(\tau\left(\dfrac{\sqrt[q]{\varrho}\prod_{\epsilon=1}^{k}\left(\omega_{\left(\Delta^{-1}\left(s_{r_\epsilon},\mathfrak{R}_\epsilon\right)/\tau\right)}\right)^{\varphi_\epsilon}}{\sqrt[q]{\prod_{\epsilon=1}^{k}\left(1+(\varrho-1)\left(1-\left(\omega_{\left(\Delta^{-1}\left(s_{r_\epsilon},\mathfrak{R}_\epsilon\right)/\tau\right)}\right)^q\right)\right)^{\varphi_\epsilon}+(\varrho-1)\prod_{\epsilon=1}^{k}\left(\omega_{\left(\Delta^{-1}\left(s_{r_\epsilon},\mathfrak{R}_\epsilon\right)/\tau\right)}\right)^{q\varphi_\epsilon}}}\right)\right)\end{array}\right)\end{array}\right)$$

$$\oplus\left(\begin{array}{l}\left(\begin{array}{l}\left(\begin{array}{l}\Delta\left(\tau\left(\sqrt[q]{\dfrac{\left(1+(\varrho-1)\left(\Delta^{-1}\left(s_{p_{k+1}},\wp_{k+1}\right)/\tau\right)^{q}\right)^{\varphi_{k+1}}-\left(1-\left(\Delta^{-1}\left(s_{p_{k+1}},\wp_{k+1}\right)/\tau\right)^{q}\right)^{\varphi_{k+1}}}{\left(1+(\varrho-1)\left(\Delta^{-1}\left(s_{p_{k+1}},\wp_{k+1}\right)/\tau\right)^{q}\right)^{\varphi_{k+1}}+(\varrho-1)\prod_{k+1=1}^{n}\left(1-\left(\Delta^{-1}\left(s_{p_{k+1}},\wp_{k+1}\right)/\tau\right)^{q}\right)^{\varphi_{k+1}}}}\right)\right)\\ \Delta\left(\tau\left(\sqrt[q]{\dfrac{\left(1+(\varrho-1)\left(\omega_{\left(\Delta^{-1}\left(s_{p_{k+1}},\wp_{k+1}\right)/\tau\right)}\right)^{q}\right)^{\varphi_{k+1}}-\left(1-\left(\omega_{\left(\Delta^{-1}\left(s_{p_{k+1}},\wp_{k+1}\right)/\tau\right)}\right)^{q}\right)^{\varphi_{k+1}}}{\left(1+(\varrho-1)\left(\omega_{\left(\Delta^{-1}\left(s_{p_{k+1}},\wp_{k+1}\right)/\tau\right)}\right)^{q}\right)^{\varphi_{k+1}}+(\varrho-1)\left(1-\left(\omega_{\left(\Delta^{-1}\left(s_{p_{k+1}},\wp_{k+1}\right)/\tau\right)}\right)^{q}\right)^{\varphi_{k+1}}}}\right)\right)\end{array}\right)\\ \left(\begin{array}{l}\Delta\left(\tau\left(\dfrac{\sqrt[q]{\varrho}\left(\Delta^{-1}\left(s_{r_{k+1}},\mathfrak{R}_{k+1}\right)/\tau\right)^{\varphi_{k+1}}}{\sqrt[q]{\left(1+(\varrho-1)\left(1-\left(\Delta^{-1}\left(s_{r_{k+1}},\mathfrak{R}_{k+1}\right)/\tau\right)^{q}\right)\right)^{\varphi_{k+1}}+(\varrho-1)\left(\Delta^{-1}\left(s_{r_{k+1}},\mathfrak{R}_{k+1}\right)/\tau\right)^{q\varphi_{k+1}}}}\right)\right)\\ \Delta\left(\tau\left(\dfrac{\sqrt[q]{\varrho}\left(\omega_{\left(\Delta^{-1}\left(s_{r_{k+1}},\mathfrak{R}_{k+1}\right)/\tau\right)}\right)^{\varphi_{k+1}}}{\sqrt[q]{\left(1+(\varrho-1)\left(1-\left(\omega_{\left(\Delta^{-1}\left(s_{r_{k+1}},\mathfrak{R}_{k+1}\right)/\tau\right)}\right)^{q}\right)\right)^{\varphi_{k+1}}+(\varrho-1)\left(\omega_{\left(\Delta^{-1}\left(s_{r_{k+1}},\mathfrak{R}_{k+1}\right)/\tau\right)}\right)^{q\varphi_{k+1}}}}\right)\right)\end{array}\right)\end{array}\right)$$

$$\cdot\left(\begin{array}{l}\left(\begin{array}{l}\Delta\left(\tau\left(\sqrt[q]{\dfrac{\prod_{\epsilon=1}^{k+1}\left(1+(\varrho-1)\left(\Delta^{-1}\left(s_{p_\epsilon},\wp_\epsilon\right)/\tau\right)^{q}\right)^{\varphi_\epsilon}-\prod_{\epsilon=1}^{k+1}\left(1-\left(\Delta^{-1}\left(s_{p_\epsilon},\wp_\epsilon\right)/\tau\right)^{q}\right)^{\varphi_\epsilon}}{\prod_{\epsilon=1}^{k+1}\left(1+(\varrho-1)\left(\Delta^{-1}\left(s_{p_\epsilon},\wp_\epsilon\right)/\tau\right)^{q}\right)^{\varphi_\epsilon}+(\varrho-1)\prod_{\epsilon=1}^{k+1}\left(1-\left(\Delta^{-1}\left(s_{p_\epsilon},\wp_\epsilon\right)/\tau\right)^{q}\right)^{\varphi_\epsilon}}}\right)\right)\\ \Delta\left(\tau\left(\sqrt[q]{\dfrac{\prod_{\epsilon=1}^{k+1}\left(1+(\varrho-1)\left(\omega_{\left(\Delta^{-1}\left(s_{p_\epsilon},\wp_\epsilon\right)/\tau\right)}\right)^{q}\right)^{\varphi_\epsilon}-\prod_{\epsilon=1}^{k+1}\left(1-\left(\omega_{\left(\Delta^{-1}\left(s_{p_\epsilon},\wp_\epsilon\right)/\tau\right)}\right)^{q}\right)^{\varphi_\epsilon}}{\prod_{\epsilon=1}^{k+1}\left(1+(\varrho-1)\left(\omega_{\left(\Delta^{-1}\left(s_{p_\epsilon},\wp_\epsilon\right)/\tau\right)}\right)^{q}\right)^{\varphi_\epsilon}+(\varrho-1)\prod_{\epsilon=1}^{k+1}\left(1-\left(\omega_{\left(\Delta^{-1}\left(s_{p_\epsilon},\wp_\epsilon\right)/\tau\right)}\right)^{q}\right)^{\varphi_\epsilon}}}\right)\right)\end{array}\right)\\ \left(\begin{array}{l}\Delta\left(\tau\left(\dfrac{\sqrt[q]{\varrho}\prod_{\epsilon=1}^{k+1}\left(\Delta^{-1}\left(s_{r_\epsilon},\mathfrak{R}_\epsilon\right)/\tau\right)^{\varphi_\epsilon}}{\sqrt[q]{\prod_{\epsilon=1}^{k+1}\left(1+(\varrho-1)\left(1-\left(\Delta^{-1}\left(s_{r_\epsilon},\mathfrak{R}_\epsilon\right)/\tau\right)^{q}\right)\right)^{\varphi_\epsilon}+(\varrho-1)\prod_{\epsilon=1}^{k+1}\left(\Delta^{-1}\left(s_{r_\epsilon},\mathfrak{R}_\epsilon\right)/\tau\right)^{q\varphi_\epsilon}}}\right)\right)\\ \Delta\left(\tau\left(\dfrac{\sqrt[q]{\varrho}\prod_{\epsilon=1}^{k+1}\left(\omega_{\left(\Delta^{-1}\left(s_{r_\epsilon},\mathfrak{R}_\epsilon\right)/\tau\right)}\right)^{\varphi_\epsilon}}{\sqrt[q]{\prod_{\epsilon=1}^{k+1}\left(1+(\varrho-1)\left(1-\left(\omega_{\left(\Delta^{-1}\left(s_{r_\epsilon},\mathfrak{R}_\epsilon\right)/\tau\right)}\right)^{q}\right)\right)^{\varphi_\epsilon}+(\varrho-1)\prod_{\epsilon=1}^{k+1}\left(\omega_{\left(\Delta^{-1}\left(s_{r_\epsilon},\mathfrak{R}_\epsilon\right)/\tau\right)}\right)^{q\varphi_\epsilon}}}\right)\right)\end{array}\right)\end{array}\right). \tag{23}$$

Hence, (20) is also true for $n = k + 1$, and therefore, (20) holds for all n.

Based on the parameter ϱ, we can derive the following special cases of Theorem 1. □

Remark 1. When $\varrho = 1$, the 2TLCq-ROFHWA operator transforms to the 2TLCq-ROF weighted average (2TLCq-ROFWA) operator as follows:

$$2TLCq-ROFWA_{\varphi}\left(\widetilde{\varsigma}_1,\widetilde{\varsigma}_2,\ldots,\widetilde{\varsigma}_n\right)$$

$$=\left(\begin{array}{c}\left(\Delta\left(\tau\left(\sqrt[q]{1-\prod_{\epsilon=1}^{n}\left(1-\left(\frac{\Delta^{-1}\left(s_{p_\epsilon},\wp_\epsilon\right)}{\tau}\right)^{q}\right)^{\varphi_\epsilon}}\right)\right),\Delta\left(\tau\left(\sqrt[q]{1-\prod_{\epsilon=1}^{n}\left(1-\left(\omega_{\left(\Delta^{-1}\left(s_{p_\epsilon},\wp_\epsilon\right)/\tau\right)}\right)^{q}\right)^{\varphi_\epsilon}}\right)\right)\right)\\ \left(\Delta\left(\tau\left(\prod_{\epsilon=1}^{n}\left(\frac{\Delta^{-1}\left(s_{r_\epsilon},\mathfrak{R}_\epsilon\right)}{\tau}\right)^{\varphi_\epsilon}\right)\right),\Delta\left(\tau\left(\prod_{\epsilon=1}^{n}\left(\omega_{\left(\Delta^{-1}\left(s_{r_\epsilon},\mathfrak{R}_\epsilon\right)/\tau\right)}\right)^{\varphi_\epsilon}\right)\right)\right)\end{array}\right). \tag{24}$$

Remark 2. When $\varrho = 2$, the 2TLCq-ROFHWA operator reduces to the 2TLCq-ROF Einstein weighted average (2TLCq-ROFEWA) operator as follows:

$$2TLCq-ROFEWA_{\varphi}\left(\widetilde{\varsigma}_1,\widetilde{\varsigma}_2,\ldots,\widetilde{\varsigma}_n\right)$$

$$=\left(\begin{array}{c}\Delta\left(\tau\left(\sqrt[q]{\frac{\prod_{\epsilon=1}^{n}\left(1+\left(\Delta^{-1}\left(s_{p_\epsilon},\wp_\epsilon\right)/\tau\right)^{q}\right)^{\varphi_\epsilon}-\prod_{\epsilon=1}^{n}\left(1-\left(\Delta^{-1}\left(s_{p_\epsilon},\wp_\epsilon\right)/\tau\right)^{q}\right)^{\varphi_\epsilon}}{\prod_{\epsilon=1}^{n}\left(1+\left(\Delta^{-1}\left(s_{p_\epsilon},\wp_\epsilon\right)/\tau\right)^{q}\right)^{\varphi_\epsilon}+\prod_{\epsilon=1}^{n}\left(1-\left(\Delta^{-1}\left(s_{p_\epsilon},\wp_\epsilon\right)/\tau\right)^{q}\right)^{\varphi_\epsilon}}}\right)\right)\\ \Delta\left(\tau\left(\sqrt[q]{\frac{\prod_{\epsilon=1}^{n}\left(1+\left(\omega_{\left(\Delta^{-1}\left(s_{p_\epsilon},\wp_\epsilon\right)/\tau\right)}\right)^{q}\right)^{\varphi_\epsilon}-\prod_{\epsilon=1}^{n}\left(1-\left(\omega_{\left(\Delta^{-1}\left(s_{p_\epsilon},\wp_\epsilon\right)/\tau\right)}\right)^{q}\right)^{\varphi_\epsilon}}{\prod_{\epsilon=1}^{n}\left(1+\left(\omega_{\left(\Delta^{-1}\left(s_{p_\epsilon},\wp_\epsilon\right)/\tau\right)}\right)^{q}\right)^{\varphi_\epsilon}+\prod_{\epsilon=1}^{n}\left(1-\left(\omega_{\left(\Delta^{-1}\left(s_{p_\epsilon},\wp_\epsilon\right)/\tau\right)}\right)^{q}\right)^{\varphi_\epsilon}}}\right)\right)\\ \Delta\left(\tau\left(\frac{\sqrt[q]{2}\prod_{\epsilon=1}^{n}\left(\Delta^{-1}\left(s_{r_\epsilon},\mathfrak{R}_\epsilon\right)/\tau\right)^{\varphi_\epsilon}}{\sqrt[q]{\prod_{\epsilon=1}^{n}\left(2-\left(\Delta^{-1}\left(s_{r_\epsilon},\mathfrak{R}_\epsilon\right)/\tau\right)^{q}\right)^{\varphi_\epsilon}+\prod_{\epsilon=1}^{n}\left(\Delta^{-1}\left(s_{r_\epsilon},\mathfrak{R}_\epsilon\right)/\tau\right)^{q\varphi_\epsilon}}}\right)\right)\\ \Delta\left(\tau\left(\frac{\sqrt[q]{2}\prod_{\epsilon=1}^{n}\left(\omega_{\left(\Delta^{-1}\left(s_{r_\epsilon},\mathfrak{R}_\epsilon\right)/\tau\right)}\right)^{\varphi_\epsilon}}{\sqrt[q]{\prod_{\epsilon=1}^{n}\left(2-\left(\omega_{\left(\Delta^{-1}\left(s_{r_\epsilon},\mathfrak{R}_\epsilon\right)/\tau\right)}\right)^{q}\right)^{\varphi_\epsilon}+\prod_{\epsilon=1}^{n}\left(\omega_{\left(\left(\Delta^{-1}\left(s_{r_\epsilon},\mathfrak{R}_\epsilon\right)/\tau\right)\right)}\right)^{q\varphi_\epsilon}}}\right)\right)\end{array}\right). \tag{25}$$

Theorem 2. *Let* $\widetilde{\varsigma}_\epsilon = (((s_{p_\epsilon},\wp_\epsilon),(\omega_{(s_{p_\epsilon},\wp_\epsilon)})),((s_{r_\epsilon},\mathfrak{R}_\epsilon),(\omega_{(s_{r_\epsilon},\mathfrak{R}_\epsilon)})))$ *and* $\widetilde{\varsigma}'_\epsilon = (((s_{p_\epsilon}{}',\wp'_\epsilon),(\omega_{(s_{p_\epsilon}',\wp'_\epsilon)})),((s_{r_\epsilon}',\mathfrak{R}'_\epsilon),(\omega_{(s_{r_\epsilon}',\mathfrak{R}'_\epsilon)})))$ $(\epsilon = 1,2,\ldots,n)$*be two sets of 2TLCq-ROFNs; then, the 2TLCq-ROFHWA operator has the following properties:*

(1) Idempotency. If all 2TLCq-ROFNs $\widetilde{\varsigma}_\epsilon = (((s_{p_\epsilon},\wp_\epsilon),(\omega_{(s_{p_\epsilon},\wp_\epsilon)})),((s_{r_\epsilon},\mathfrak{R}_\epsilon),(\omega_{(s_{r_\epsilon},\mathfrak{R}_\epsilon)})))(\epsilon = 1,2,\ldots,n)$ *are equal, that is,* $\widetilde{\varsigma}_\epsilon = \widetilde{\varsigma} = (((s_p,\wp),(\omega_{(s_p,\wp)})),((s_r,\mathfrak{R}),(\omega_{(s_r,\mathfrak{R})})))$*, then*

$$2TLCq-ROFHWA_{\varphi}\left(\widetilde{\varsigma}_1,\widetilde{\varsigma}_2,\ldots,\widetilde{\varsigma}_n\right)=\widetilde{\varsigma}. \tag{26}$$

(2) Boundedness. Let $\widetilde{\varsigma}_\epsilon\,(\epsilon = 1,2,\ldots,n)$ *be a collection of 2TLCq-ROFNs, and let* $\widetilde{\varsigma}^{-} = \min\widetilde{\varsigma}_{(\epsilon)}$ *and* $\widetilde{\varsigma}^{+} = \max\widetilde{\varsigma}_{(\epsilon)}$*; then,*

$$\widetilde{\varsigma}^{-}\le 2TLCq-ROFHWA_{\varphi}\left(\widetilde{\varsigma}_1,\widetilde{\varsigma}_2,\ldots,\widetilde{\varsigma}_n\right)\le\widetilde{\varsigma}^{+}. \tag{27}$$

(3) Monotonicity. Let $\widetilde{\varsigma}_\epsilon$ *and* $\widetilde{\varsigma}'_\epsilon(\epsilon = 1,2,\ldots,n)$ *be two collections of 2TLCq-ROFNs, if* $\widetilde{\varsigma}_\epsilon\le\widetilde{\varsigma}'_\epsilon$*, for all* ϵ*; then,*

$$\begin{aligned}&2TLCq-ROFHWA_{\varphi}\left(\widetilde{\varsigma}_1,\widetilde{\varsigma}_2,\ldots,\widetilde{\varsigma}_n\right)\\ &\le 2TLCq-ROFHWA_{\varphi}\left(\widetilde{\varsigma}'_1,\widetilde{\varsigma}'_2,\ldots,\widetilde{\varsigma}'_n\right).\end{aligned} \tag{28}$$

Definition 12. Let $\widetilde{\varsigma}_\epsilon = (((s_{p_\epsilon}, \wp_\epsilon), (\omega_{(s_{p_\epsilon}, \wp_\epsilon)})), ((s_{r_\epsilon}, \mathfrak{R}_\epsilon), (\omega_{(s_{r_\epsilon}, \mathfrak{R}_\epsilon)}))(\epsilon = 1, 2, \ldots, n)$ be a collection of 2TLCq-ROFNs, then the 2TLCq-ROFHOWA operator is defined as

$$2TLCq - ROFHOWA_\psi(\widetilde{\varsigma}_1, \widetilde{\varsigma}_2, \ldots, \widetilde{\varsigma}_n) = \oplus_{\epsilon=1}^{n}\left(\psi_\epsilon \widetilde{\varsigma}_{\flat(\epsilon)}\right), \tag{29}$$

where $(\flat(1), \flat(2), \ldots, \flat(n))$ is a permutation of $(1, 2, \ldots, n)$, such that $\widetilde{\varsigma}_{\flat(\epsilon-1)} \geq \widetilde{\varsigma}_{\flat(\epsilon)}$ for all $\epsilon = 2, \ldots, n$, and $\psi = (\psi_1, \psi_2, \ldots, \psi_n)^T$ is the aggregation-associated weight vector such that $\psi_\epsilon \in [0, 1]$ and $\sum_{\epsilon=1}^{n} \psi_\epsilon = 1$, $\varrho > 0$.

Based on Hamacher operations of the 2TLCq-ROF values described, we can derive Theorem 3.

Theorem 3. *Let* $\widetilde{\varsigma}_\epsilon = (((s_{p_\epsilon}, \wp_\epsilon), (\omega_{(s_{p_\epsilon}, \wp_\epsilon)})), ((s_{r_\epsilon}, \mathfrak{R}_\epsilon), (\omega_{(s_{r_\epsilon}, \mathfrak{R}_\epsilon)}))(\epsilon = 1, 2, \ldots, n)$ *be a collection of 2TLCq-ROFNs, where* $\varrho > 0$. *Then, for any* $q \geq 0$, *the aggregated value by utilizing 2TLCq-ROFHOWA operator is also a 2TLCq-ROFN, and*

$$2TLCq - ROFHOWA_\psi(\widetilde{\varsigma}_1, \widetilde{\varsigma}_2, \ldots, \widetilde{\varsigma}_n) = \oplus_{\epsilon=1}^{n}\left(\psi_\epsilon \widetilde{\varsigma}_{\flat(\epsilon)}\right)$$

$$= \left(\begin{array}{c} \left(\Delta\left(\tau\left(\sqrt[q]{\frac{\prod_{\epsilon=1}^{n}\left(1+(\varrho-1)\left(\Delta^{-1}\left(s_{p_{\flat(\epsilon)}}, \wp_{\flat(\epsilon)}\right)/\tau\right)^q\right)^{\psi_\epsilon} - \prod_{\epsilon=1}^{n}\left(1-\left(\Delta^{-1}\left(s_{p_{\flat(\epsilon)}}, \wp_{\flat(\epsilon)}\right)/\tau\right)^q\right)^{\psi_\epsilon}}{\prod_{\epsilon=1}^{n}\left(1+(\varrho-1)\left(\Delta^{-1}\left(s_{p_{\flat(\epsilon)}}, \wp_{\flat(\epsilon)}\right)/\tau\right)^q\right)^{\psi_\epsilon} + (\varrho-1)\prod_{\epsilon=1}^{n}\left(1-\left(\Delta^{-1}\left(s_{p_{\flat(\epsilon)}}, \wp_{\flat(\epsilon)}\right)/\tau\right)^q\right)^{\psi_\epsilon}}}\right)\right) \\ \left(\Delta\left(\tau\left(\sqrt[q]{\frac{\prod_{\epsilon=1}^{n}\left(1+(\varrho-1)\left(\omega_{\left(\Delta^{-1}\left(s_{p_{\flat(\epsilon)}}, \wp_{\flat(\epsilon)}\right)/\tau\right)}\right)^q\right)^{\psi_\epsilon} - \prod_{\epsilon=1}^{n}\left(1-\left(\omega_{\left(\Delta^{-1}\left(s_{p_{\flat(\epsilon)}}, \wp_{\flat(\epsilon)}\right)/\tau\right)}\right)^q\right)^{\psi_\epsilon}}{\prod_{\epsilon=1}^{n}\left(1+(\varrho-1)\left(\omega_{\left(\Delta^{-1}\left(s_{p_{\flat(\epsilon)}}, \wp_{\flat(\epsilon)}\right)/\tau\right)}\right)^q\right)^{\psi_\epsilon} + (\varrho-1)\prod_{\epsilon=1}^{n}\left(1-\left(\omega_{\left(\Delta^{-1}\left(s_{p_{\flat(\epsilon)}}, \wp_{\flat(\epsilon)}\right)/\tau\right)}\right)^q\right)^{\psi_\epsilon}}}\right)\right) \end{array}\right), \tag{30}$$

$$= \left(\begin{array}{c} \left(\Delta\left(\tau\left(\frac{\sqrt[q]{\varrho}\prod_{\epsilon=1}^{n}\left(\Delta^{-1}\left(s_{r_{\flat(\epsilon)}}, \mathfrak{R}_{\flat(\epsilon)}\right)/\tau\right)^{\psi_\epsilon}}{\sqrt[q]{\prod_{\epsilon=1}^{n}\left(1+(\varrho-1)\left(1-\left(\Delta^{-1}\left(s_{r_{\flat(\epsilon)}}, \mathfrak{R}_{\flat(\epsilon)}\right)/\tau\right)^q\right)\right)^{\psi_\epsilon} + (\varrho-1)\prod_{\epsilon=1}^{n}\left(\Delta^{-1}\left(s_{r_{\flat(\epsilon)}}, \mathfrak{R}_{\flat(\epsilon)}\right)/\tau\right)^{q\psi_\epsilon}}}\right)\right) \\ \left(\Delta\left(\tau\left(\frac{\sqrt[q]{\varrho}\prod_{\epsilon=1}^{n}\left(\omega_{\left(\Delta^{-1}\left(s_{r_{\flat(\epsilon)}}, \mathfrak{R}_{\flat(\epsilon)}\right)/\tau\right)}\right)^{\psi_\epsilon}}{\sqrt[q]{\prod_{\epsilon=1}^{n}\left(1+(\varrho-1)\left(1-\left(\omega_{\left(\Delta^{-1}\left(s_{r_{\flat(\epsilon)}}, \mathfrak{R}_{\flat(\epsilon)}\right)/\tau\right)}\right)^q\right)\right)^{\psi_\epsilon} + (\varrho-1)\prod_{\epsilon=1}^{n}\left(\omega_{\left(\Delta^{-1}\left(s_{r_{\flat(\epsilon)}}, \mathfrak{R}_{\flat(\epsilon)}\right)/\tau\right)}\right)^{q\psi_\epsilon}}}\right)\right) \end{array}\right),$$

where $(\flat(1), \flat(2), \ldots, \flat(n))$ *is a permutation of* $(1, 2, \ldots, n)$, *such that* $\widetilde{\varsigma}_{\flat(\epsilon-1)} \geq \widetilde{\varsigma}_{\flat(\epsilon)}$ *for all* $\epsilon = 2, \ldots, n$, *and* $\psi = (\psi_1, \psi_2, \ldots, \psi_n)^T$ *is the aggregation-associated weighted vector such that* $\psi_\epsilon \in [0, 1]$ *and* $\sum_{\epsilon=1}^{n} \psi_\epsilon = 1, \varrho > 0$.

The 2TLCq-ROFHOWA operator has the same properties as Theorem 2.

Definition 13. Let $\widetilde{\varsigma}_\epsilon = (((s_{p_\epsilon}, \wp_\epsilon), (\omega_{(s_{p_\epsilon}, \wp_\epsilon)})), ((s_{r_\epsilon}, \mathfrak{R}_\epsilon), (\omega_{(s_{r_\epsilon}, \mathfrak{R}_\epsilon)}))(\epsilon = 1, 2, \ldots, n)$ be a collection of 2TLCq-ROFNs, then the 2TLCq-ROFHHA operator is defined as

$$2TLCq - ROFHHA_{\psi,\varphi}(\widetilde{\varsigma}_1, \widetilde{\varsigma}_2, \ldots, \widetilde{\varsigma}_n) = \oplus_{\epsilon=1}^{n}\left(\psi_\epsilon \dot{\widetilde{\varsigma}}_{\flat(\epsilon)}\right), \tag{31}$$

where $\psi = (\psi_1, \psi_2, \ldots, \psi_n)$ is the associated weighting vector such that $\psi_\epsilon \in [0, 1]$ and $\sum_{\epsilon=1}^{n} \psi_\epsilon = 1$, and $\dot{\widetilde{\varsigma}}_{\flat(\epsilon)}$ is the ϵ-th largest element of 2TLCq-ROF arguments $\dot{\widetilde{\varsigma}}_\epsilon (\dot{\widetilde{\varsigma}}_\epsilon = (n\varphi_\epsilon)\widetilde{\varsigma}_\epsilon, \epsilon = 1, 2, \ldots, n)$, $\varphi = (\varphi_1, \varphi_2, \ldots, \varphi_n)$ is the weighted vector of 2TLCq-ROF arguments $\widetilde{\varsigma}_\epsilon$, with $\varphi_\epsilon \in [0, 1]$ and $\sum_{\epsilon=1}^{n} \varphi_\epsilon = 1$, and n is the balancing coefficient. Especially, if $\psi = ((1/n), (1/n), \ldots, (1/n))^T$, then 2TLC$q$-ROFHHA is reduced to the 2TLCq-ROFHWA operator; if $\varphi = ((1/n), (1/n), \ldots, (1/n))$, then 2TLC$q$-ROFHHA is reduced to the 2TLCq-ROFHOWA operator.

Based on Hamacher sum operations of the 2TLCq-ROF values described, we can derive Theorem 4.

Theorem 4. *Let* $\widetilde{\varsigma}_\epsilon = (((s_{p_\epsilon}, \wp_\epsilon), (\omega_{(s_{p_\epsilon}, \wp_\epsilon)})), ((s_{r_\epsilon}, \mathfrak{R}_\epsilon), (\omega_{(s_{r_\epsilon}, \mathfrak{R}_\epsilon)}))(\epsilon = 1, 2, \ldots, n)$ *be a collection of 2TLCq-ROFNs, where* $\varrho > 0$. *Then, its aggregated value by utilizing the 2TLCq-ROFHHA operator is also a 2TLCq-ROFN, and*

$$2TLCq-ROFHHA_{\psi,\varphi}(\tilde{\varsigma}_1,\tilde{\varsigma}_2,\ldots,\tilde{\varsigma}_n)$$

$$=\oplus_{\epsilon=1}^{n}\left(\psi_\epsilon\dot{\tilde{\varsigma}}_{\flat(\epsilon)}\right)=\left(\begin{array}{c}\Delta\left(\tau\left(\sqrt[q]{\frac{\prod_{\epsilon=1}^{n}\left(1+(\varrho-1)\left(\Delta^{-1}\left(\dot{s}_{p_{\flat(\epsilon)}},\dot{\wp}_{\flat(\epsilon)}\right)/\tau\right)\right)^{q}\right)^{\psi_\epsilon}-\prod_{\epsilon=1}^{n}\left(1-\left(\Delta^{-1}\left(\dot{s}_{p_{\flat(\epsilon)}},\dot{\wp}_{\flat(\epsilon)}\right)/\tau\right)\right)^{q}\right)^{\psi_\epsilon}}{\prod_{\epsilon=1}^{n}\left(1+(\varrho-1)\left(\Delta^{-1}\left(\dot{s}_{p_{\flat(\epsilon)}},\dot{\wp}_{\flat(\epsilon)}\right)/\tau\right)\right)^{q}\right)^{\psi_\epsilon}+(\varrho-1)\prod_{\epsilon=1}^{n}\left(1-\left(\Delta^{-1}\left(\dot{s}_{p_{\flat(\epsilon)}},\dot{\wp}_{\flat(\epsilon)}\right)/\tau\right)\right)^{q}\right)^{\psi_\epsilon}}}\right)\right)\\ \Delta\left(\tau\left(\sqrt[q]{\frac{\prod_{\epsilon=1}^{n}\left(1+(\varrho-1)\left(\omega_{\left(\Delta^{-1}\left(\dot{s}_{p_{\flat(\epsilon)}},\dot{\wp}_{\flat(\epsilon)}\right)/\tau\right)}\right)^{q}\right)^{\psi_\epsilon}-\prod_{\epsilon=1}^{n}\left(1-\left(\omega_{\left(\Delta^{-1}\left(\dot{s}_{p_{\flat(\epsilon)}},\dot{\wp}_{\flat(\epsilon)}\right)/\tau\right)}\right)^{q}\right)^{\psi_\epsilon}}{\prod_{\epsilon=1}^{n}\left(1+(\varrho-1)\left(\omega_{\left(\Delta^{-1}\left(\dot{s}_{p_{\flat(\epsilon)}},\dot{\wp}_{\flat(\epsilon)}\right)/\tau\right)}\right)^{q}\right)^{\psi_\epsilon}+(\varrho-1)\prod_{\epsilon=1}^{n}\left(1-\left(\omega_{\left(\Delta^{-1}\left(\dot{s}_{p_{\flat(\epsilon)}},\dot{\wp}_{\flat(\epsilon)}\right)/\tau\right)}\right)^{q}\right)^{\psi_\epsilon}}}\right)\right)\\ \Delta\left(\tau\left(\frac{\sqrt[q]{\varrho}\prod_{\epsilon=1}^{n}\left(\Delta^{-1}\left(\dot{s}_{r_{\flat(\epsilon)}},\dot{\mathfrak{R}}_{\flat(\epsilon)}\right)/\tau\right)^{\psi_\epsilon}}{\sqrt[q]{\prod_{\epsilon=1}^{n}\left(1+(\varrho-1)\left(1-\left(\Delta^{-1}\left(\dot{s}_{r_{\flat(\epsilon)}},\dot{\mathfrak{R}}_{\flat(\epsilon)}\right)/\tau\right)^{q}\right)\right)^{\psi_\epsilon}+(\varrho-1)\prod_{\epsilon=1}^{n}\left(\Delta^{-1}\left(\dot{s}_{r_{\flat(\epsilon)}},\dot{\mathfrak{R}}_{\flat(\epsilon)}\right)/\tau\right)^{q\psi_\epsilon}}}\right)\right)\\ \Delta\left(\tau\left(\frac{\sqrt[q]{\varrho}\prod_{\epsilon=1}^{n}\left(\omega_{\left(\Delta^{-1}\left(\dot{s}_{r_{\flat(\epsilon)}},\dot{\mathfrak{R}}_{\flat(\epsilon)}\right)/\tau\right)}\right)^{\psi_\epsilon}}{\sqrt[q]{\prod_{\epsilon=1}^{n}\left(1+(\varrho-1)\left(1-\left(\omega_{\left(\Delta^{-1}\left(\dot{s}_{r_{\flat(\epsilon)}},\dot{\mathfrak{R}}_{\flat(\epsilon)}\right)/\tau\right)}\right)^{q}\right)\right)^{\psi_\epsilon}+(\varrho-1)\prod_{\epsilon=1}^{n}\left(\omega_{\left(\Delta^{-1}\left(\dot{s}_{r_{\flat(\epsilon)}},\dot{\mathfrak{R}}_{\flat(\epsilon)}\right)/\tau\right)}\right)^{q\psi_\epsilon}}}\right)\right)\end{array}\right),\tag{32}$$

where $\psi=(\psi_1,\psi_2,\ldots,\psi_n)$*is the aggregation-associated weighting vector such that* $\psi_\epsilon\in[0,1]$ *and* $\sum_{\epsilon=1}^{n}\psi_\epsilon=1$*, and* $\dot{\tilde{\varsigma}}_{\flat(\epsilon)}$ *is the* ϵ*-th largest element of 2TLCq-ROF arguments* $\dot{\tilde{\varsigma}}_\epsilon(\dot{\tilde{\varsigma}}_\epsilon=(n\varphi_\epsilon)\tilde{\varsigma}_\epsilon,\epsilon=1,2,\ldots,n)$*,* $\varphi=(\varphi_1,\varphi_2,\ldots,\varphi_n)$ *is the weighting vector of 2TLCq-ROF arguments* $\tilde{\varsigma}_\epsilon$*, with* $\varphi_\epsilon\in[0,1]$ *and* $\sum_{\epsilon=1}^{n}\varphi_\epsilon=1$*, and n is the balancing coefficient.*

The 2TLCq-ROFHHA operator has the same properties as Theorem 2.

Definition 14. Let $\tilde{\varsigma}_\epsilon=(((s_{p_\epsilon},\wp_\epsilon),(\omega_{(s_{p_\epsilon},\wp_\epsilon)})),((s_{r_\epsilon},\mathfrak{R}_\epsilon),(\omega_{(s_{r_\epsilon},\mathfrak{R}_\epsilon)}))(\epsilon=1,2,\ldots,n)$ be a collection of 2TLCq-ROFNs; then, the 2TLCq-ROFHWG operator is defined as

$$2TLCq-ROFHWG_\varphi(\tilde{\varsigma}_1,\tilde{\varsigma}_2,\ldots,\tilde{\varsigma}_n)=\otimes_{\epsilon=1}^{n}(\tilde{\varsigma}_\epsilon)^{\varphi_\epsilon},\tag{33}$$

where $\varphi=(\varphi_1,\varphi_2,\ldots,\varphi_n)^T$ be the weight vector of $\tilde{\varsigma}_\epsilon(\epsilon=1,2,\ldots,n)$, and $\varphi_\epsilon>0$, $\sum_{\epsilon=1}^{n}\varphi_\epsilon=1$.

Using the 2TLCq-ROFH operations, we deduce the following theorem from Def. 14.

Theorem 5. *Let* $\tilde{\varsigma}_\epsilon=(((s_{p_\epsilon},\wp_\epsilon),(\omega_{(s_{p_\epsilon},\wp_\epsilon)})),((s_{r_\epsilon},\mathfrak{R}_\epsilon),(\omega_{(s_{r_\epsilon},\mathfrak{R}_\epsilon)})))(\epsilon=1,2,\ldots,n)$ *be a collection of 2TLCq-ROFNs, where* $\varrho>0$*. Then, its aggregated value by utilizing 2TLCq-ROFHWG operator is also a 2TLCq-ROFN, and*

$$2TLCq-ROFHWG_\varphi(\tilde{\varsigma}_1,\tilde{\varsigma}_2,\ldots,\tilde{\varsigma}_n)=\otimes_{\epsilon=1}^{n}(\tilde{\varsigma}_\epsilon)^{\varphi_\epsilon}$$

$$=\left(\begin{array}{c}\Delta\left(\tau\left(\frac{\sqrt[q]{\varrho}\prod_{\epsilon=1}^{n}\left(\Delta^{-1}\left(s_{p_\epsilon},\wp_\epsilon\right)/\tau\right)^{\varphi_\epsilon}}{\sqrt[q]{\prod_{\epsilon=1}^{n}\left(1+(\varrho-1)\left(1-\left(\Delta^{-1}\left(s_{p_\epsilon},\wp_\epsilon\right)/\tau\right)^{q}\right)\right)^{\varphi_\epsilon}+(\varrho-1)\prod_{\epsilon=1}^{n}\left(\Delta^{-1}\left(s_{p_\epsilon},\wp_\epsilon\right)/\tau\right)^{q\varphi_\epsilon}}}\right)\right)\\ \Delta\left(\tau\left(\frac{\sqrt[q]{\varrho}\prod_{\epsilon=1}^{n}\left(\omega_{\left(\Delta^{-1}\left(s_{p_\epsilon},\wp_\epsilon\right)/\tau\right)}\right)^{\varphi_\epsilon}}{\sqrt[q]{\prod_{\epsilon=1}^{n}\left(1+(\varrho-1)\left(1-\left(\omega_{\left(\Delta^{-1}\left(s_{p_\epsilon},\wp_\epsilon\right)/\tau\right)}\right)^{q}\right)\right)^{\varphi_\epsilon}+(\varrho-1)\prod_{\epsilon=1}^{n}\left(\omega_{\left(\Delta^{-1}\left(s_{p_\epsilon},\wp_\epsilon\right)/\tau\right)}\right)^{q\varphi_\epsilon}}}\right)\right)\\ \Delta\left(\tau\left(\sqrt[q]{\frac{\prod_{\epsilon=1}^{n}\left(1+(\varrho-1)\left(\Delta^{-1}\left(s_{r_\epsilon},\mathfrak{R}_\epsilon\right)/\tau\right)^{q}\right)^{\varphi_\epsilon}-\prod_{\epsilon=1}^{n}\left(1-\left(\Delta^{-1}\left(s_{r_\epsilon},\mathfrak{R}_\epsilon\right)/\tau\right)^{q}\right)^{\varphi_\epsilon}}{\prod_{\epsilon=1}^{n}\left(1+(\varrho-1)\left(\Delta^{-1}\left(s_{r_\epsilon},\mathfrak{R}_\epsilon\right)/\tau\right)^{q}\right)^{\varphi_\epsilon}\prod_{\epsilon=1}^{n}+(\varrho-1)\prod_{\epsilon=1}^{n}\left(1-\left(\Delta^{-1}\left(s_{r_\epsilon},\mathfrak{R}_\epsilon\right)/\tau\right)^{q}\right)^{\varphi_\epsilon}}}\right)\right)\\ \Delta\left(\tau\left(\sqrt[q]{\frac{\prod_{\epsilon=1}^{n}\left(1+(\varrho-1)\left(\omega_{\left(\Delta^{-1}\left(s_{r_\epsilon},\mathfrak{R}_\epsilon\right)/\tau\right)}\right)^{q}\right)^{\varphi_\epsilon}-\prod_{\epsilon=1}^{n}\left(1-\left(\omega_{\left(\Delta^{-1}\left(s_{r_\epsilon},\mathfrak{R}_\epsilon\right)/\tau\right)}\right)^{q}\right)^{\varphi_\epsilon}}{\prod_{\epsilon=1}^{n}\left(1+(\varrho-1)\left(\omega_{\left(\Delta^{-1}\left(s_{r_\epsilon},\mathfrak{R}_\epsilon\right)/\tau\right)}\right)^{q}\right)^{\varphi_\epsilon}+(\varrho-1)\prod_{\epsilon=1}^{n}\left(1-\left(\omega_{\left(\Delta^{-1}\left(s_{r_\epsilon},\mathfrak{R}_\epsilon\right)/\tau\right)}\right)^{q}\right)^{\varphi_\epsilon}}}\right)\right)\end{array}\right),\tag{34}$$

where $\varphi=(\varphi_1,\varphi_2,\ldots,\varphi_n)^T$ *be the weight vector of* $\tilde{\varsigma}_\epsilon(\epsilon=1,2,\ldots,n)$*, and* $\varphi_\epsilon>0$*,* $\sum_{\epsilon=1}^{n}\varphi_\epsilon=1,\varrho>0$.

Based on the parameter ϱ, we can derive the following special cases of Theorem 5.

Remark 3. When $\varrho = 1$, the 2TLCq-ROFHWG operator transforms to the 2TLCq-ROF weighted geometric (2TLCq-ROFWG) operator as follows:

$$2TLCq-ROFWG_{\varphi}(\widetilde{\varsigma}_1,\widetilde{\varsigma}_2,\ldots,\widetilde{\varsigma}_n)=\left(\begin{array}{c}\Delta\left(\tau\left(\left(\prod_{\epsilon=1}^{n}\left(\Delta^{-1}\left(s_{p_\epsilon},\wp_\epsilon\right)/\tau\right)^{\varphi_\epsilon}\right)\right),\Delta\left(\tau\left(\prod_{\epsilon=1}^{n}\left(\omega_{\left(\Delta^{-1}\left(s_{p_\epsilon},\wp_\epsilon\right)/\tau\right)}\right)^{\varphi_\epsilon}\right)\right)\right),\\ \Delta\left(\tau\left(\sqrt{[q]}\,1-\prod_{\epsilon=1}^{n}\left(1-\left(\Delta^{-1}\left(s_{r_\epsilon},\mathfrak{R}_\epsilon\right)/\tau\right)^{q}\right)^{\varphi_\epsilon}\right),\Delta\left(\tau\left(\sqrt{[q]}\,1-\prod_{\epsilon=1}^{n}\left(1-\left(\omega_{\left(\Delta^{-1}\left(s_{r_\epsilon},\mathfrak{R}_\epsilon\right)/\tau\right)}\right)^{q}\right)^{\varphi_\epsilon}\right)\right)\right)\end{array}\right). \tag{35}$$

Remark 4. When $\varrho = 2$, the 2TLCq-ROFHWG operator reduces to the 2TLCq-ROF Einstein weighted geometric (2TLCq-ROFEWG) operator as follows:

$$2TLCq-ROFEWG_{\varphi}(\widetilde{\varsigma}_1,\widetilde{\varsigma}_2,\ldots,\widetilde{\varsigma}_n)$$

$$=\left(\begin{array}{c}\left(\begin{array}{c}\Delta\left(\tau\left(\frac{\sqrt[q]{2}\prod_{\epsilon=1}^{n}\left(\Delta^{-1}\left(s_{p_\epsilon},\wp_\epsilon\right)/\tau\right)^{\varphi_\epsilon}}{\sqrt[q]{\prod_{\epsilon=1}^{n}\left(2-\left(\Delta^{-1}\left(s_{p_\epsilon},\wp_\epsilon\right)/\tau\right)^{q}\right)^{\varphi_\epsilon}+\prod_{\epsilon=1}^{n}\left(\Delta^{-1}\left(s_{p_\epsilon},\wp_\epsilon\right)/\tau\right)^{q\varphi_\epsilon}}}\right)\right)\\ \Delta\left(\tau\left(\frac{\sqrt[q]{2}\prod_{\epsilon=1}^{n}\left(\omega_{\left(\Delta^{-1}\left(s_{p_\epsilon},\wp_\epsilon\right)/\tau\right)}\right)^{\varphi_\epsilon}}{\sqrt[q]{\prod_{\epsilon=1}^{n}\left(2-\left(\omega_{\left(\Delta^{-1}\left(s_{p_\epsilon},\wp_\epsilon\right)/\tau\right)}\right)^{q}\right)^{\varphi_\epsilon}+\prod_{\epsilon=1}^{n}\left(\omega_{\left(\Delta^{-1}\left(s_{p_\epsilon},\wp_\epsilon\right)/\tau\right)}\right)^{q\varphi_\epsilon}}}\right)\right)\end{array}\right)\\ \left(\begin{array}{c}\Delta\left(\tau\left(\sqrt[q]{\frac{\prod_{\epsilon=1}^{n}\left(1+\left(\Delta^{-1}\left(s_{r_\epsilon},\mathfrak{R}_\epsilon\right)/\tau\right)^{q}\right)^{\varphi_\epsilon}-\prod_{\epsilon=1}^{n}\left(1-\left(\Delta^{-1}\left(s_{r_\epsilon},\mathfrak{R}_\epsilon\right)/\tau\right)^{q}\right)^{\varphi_\epsilon}}{\prod_{\epsilon=1}^{n}\left(1+\left(\Delta^{-1}\left(s_{r_\epsilon},\mathfrak{R}_\epsilon\right)/\tau\right)^{q}\right)^{\varphi_\epsilon}+\prod_{\epsilon=1}^{n}\left(1-\left(\Delta^{-1}\left(s_{r_\epsilon},\mathfrak{R}_\epsilon\right)/\tau\right)^{q}\right)^{\varphi_\epsilon}}}\right)\right)\\ \Delta\left(\tau\left(\sqrt[q]{\frac{\prod_{\epsilon=1}^{n}\left(1+\left(\omega_{\left(\Delta^{-1}\left(s_{r_\epsilon},\mathfrak{R}_\epsilon\right)/\tau\right)}\right)^{q}\right)^{\varphi_\epsilon}-\prod_{\epsilon=1}^{n}\left(1-\left(\omega_{\left(\Delta^{-1}\left(s_{r_\epsilon},\mathfrak{R}_\epsilon\right)/\tau\right)}\right)^{q}\right)^{\varphi_\epsilon}}{\prod_{\epsilon=1}^{n}\left(1+\left(\omega_{\left(\Delta^{-1}\left(s_{r_\epsilon},\mathfrak{R}_\epsilon\right)/\tau\right)}\right)^{q}\right)^{\varphi_\epsilon}+\prod_{\epsilon=1}^{n}\left(1-\left(\omega_{\left(\Delta^{-1}\left(s_{r_\epsilon},\mathfrak{R}_\epsilon\right)/\tau\right)}\right)^{q}\right)^{\varphi_\epsilon}}}\right)\right)\end{array}\right)\end{array}\right). \tag{36}$$

Theorem 6. *Let* $\widetilde{\varsigma}_\epsilon = (((s_{p_\epsilon},\wp_\epsilon),(\omega_{(s_{p_\epsilon},\wp_\epsilon)})),((s_{r_\epsilon},\mathfrak{R}_\epsilon),(\omega_{(s_{r_\epsilon},\mathfrak{R}_\epsilon)})))$ *and* $\widetilde{\varsigma}'_\epsilon = (((s_{p_\epsilon},\wp'_\epsilon),(\omega_{(s_{p_\epsilon},\wp'_\epsilon)})),((s_{r_\epsilon},\mathfrak{R}'_\epsilon),(\omega_{(s_{r_\epsilon},\mathfrak{R}'_\epsilon)})))$ $(\epsilon = 1,2,\ldots,n)$*be two sets of 2TLCq-ROFNs; then, the 2TLCq-ROFHWG operator has the following properties:*

(1) Idempotency. If all 2TLCq-ROFNs $\widetilde{\varsigma}_\epsilon = (((s_{p_\epsilon},\wp_\epsilon),(\omega_{(s_{p_\epsilon},\wp_\epsilon)})),((s_{r_\epsilon},\mathfrak{R}_\epsilon),(\omega_{(s_{r_\epsilon},\mathfrak{R}_\epsilon)}))(\epsilon = 1,2,\ldots,n)$ *are equal, that is,,*$\widetilde{\varsigma}_\epsilon = \widetilde{\varsigma} = (((s_p,\wp),(\omega_{(s_p,\wp)})),((s_r,\mathfrak{R}),(\omega_{(s_r,\mathfrak{R})})))$*, then*

$$2TLCq-ROFHWG_{\varphi}(\widetilde{\varsigma}_1,\widetilde{\varsigma}_2,\ldots,\widetilde{\varsigma}_n)=\widetilde{\varsigma}. \tag{37}$$

(2) Boundedness. Let $\widetilde{\varsigma}_\epsilon\,(\epsilon = 1,2,\ldots,n)$ *be a collection of 2TLCq-ROFNs, and let* $\widetilde{\varsigma}^- = \min\widetilde{\varsigma}_{(\epsilon)}$ *and* $\widetilde{\varsigma}^+ = \max\widetilde{\varsigma}_{(\epsilon)}$*; then,*

$$\widetilde{\varsigma}^- \le 2TLCq-ROFHWG_{\varphi}(\widetilde{\varsigma}_1,\widetilde{\varsigma}_2,\ldots,\widetilde{\varsigma}_n)\le\widetilde{\varsigma}^+. \tag{38}$$

(3) Monotonicity. Let $\widetilde{\varsigma}_\epsilon$ *and* $\widetilde{\varsigma}'_\epsilon\,(\epsilon = 1,2,\ldots,n)$ *be the two collections of 2TLCq-ROFNs, if* $\widetilde{\varsigma}_\epsilon \le \widetilde{\varsigma}'_\epsilon$*, for all* ϵ*; then,*

$$\begin{aligned}&2TLCq-ROFHWG_{\varphi}(\widetilde{\varsigma}_1,\widetilde{\varsigma}_2,\ldots,\widetilde{\varsigma}_n)\\ &\le 2TLCq-ROFHWG_{\varphi}(\widetilde{\varsigma}'_1,\widetilde{\varsigma}'_2,\ldots,\widetilde{\varsigma}'_n).\end{aligned} \tag{39}$$

Definition 15. Let $\widetilde{\varsigma}_\epsilon = (((s_{p_\epsilon}, \wp_\epsilon), (\omega_{(s_{p_\epsilon}, \wp_\epsilon)})), ((s_{r_\epsilon}, \mathfrak{R}_\epsilon), (\omega_{(s_{r_\epsilon}, \mathfrak{R}_\epsilon)}))(\epsilon = 1, 2, \ldots, n)$ be a collection of 2TLCq-ROFNs, then the 2TLCq-ROFHOWG operator is defined as

$$2TLCq - ROFHOWG_\psi(\widetilde{\varsigma}_1, \widetilde{\varsigma}_2, \ldots, \widetilde{\varsigma}_n) = \otimes_{\epsilon=1}^{n}\left(\widetilde{\varsigma}_{\flat(\epsilon)}\right)^{\psi_\epsilon}, \tag{40}$$

where $(\flat(1), \flat(2), \ldots, \flat(n))$ is a permutation of $(1, 2, \ldots, n)$, such that $\widetilde{\varsigma}_{\flat(\epsilon-1)} \geq \widetilde{\varsigma}_{\flat(\epsilon)}$ for all $\epsilon = 2, \ldots, n$, and $\psi = (\psi_1, \psi_2, \ldots, \psi_n)^T$ is the aggregation-associated weighted vector such that $\psi_\epsilon \in [0, 1]$ and $\sum_{\epsilon=1}^{n} \psi_\epsilon = 1$.

Theorem 7. *Let* $\widetilde{\varsigma}_\epsilon = (((s_{p_\epsilon}, \wp_\epsilon), (\omega_{(s_{p_\epsilon}, \wp_\epsilon)})), ((s_{r_\epsilon}, \mathfrak{R}_\epsilon), (\omega_{(s_{r_\epsilon}, \mathfrak{R}_\epsilon)}))(\epsilon = 1, 2, \ldots, n)$*be a collection of 2TLCq-ROFNs, where* $\varrho > 0$*. Then, its aggregated value by utilizing the 2TLCq-ROFHOWG operator is also a 2TLCq-ROFN, and*

$$2TLCq - ROFHOWG_\psi(\widetilde{\varsigma}_1, \widetilde{\varsigma}_2, \ldots, \widetilde{\varsigma}_n) = \otimes_{\epsilon=1}^{n}\left(\widetilde{\varsigma}_{\flat(\epsilon)}\right)^{\psi_\epsilon}$$

$$= \left(\begin{array}{c} \left(\Delta\left(\tau\left(\dfrac{\sqrt[q]{\varrho}\prod_{\epsilon=1}^{n}\left(\Delta^{-1}\left(s_{p_{\flat(\epsilon)}}, \wp_{\flat(\epsilon)}\right)/\tau\right)^{\psi_\epsilon}}{\sqrt[q]{\prod_{\epsilon=1}^{n}\left(1 + (\varrho - 1)\left(1 - \left(\Delta^{-1}\left(s_{p_{\flat(\epsilon)}}, \wp_{\flat(\epsilon)}\right)/\tau\right)^q\right)\right)^{\psi_\epsilon} + (\varrho - 1)\prod_{\epsilon=1}^{n}\left(\Delta^{-1}\left(s_{p_{\flat(\epsilon)}}, \wp_{\flat(\epsilon)}\right)/\tau\right)^{q\psi_\epsilon}}}\right)\right) \\ \left(\Delta\left(\tau\left(\dfrac{\sqrt[q]{\varrho}\prod_{\epsilon=1}^{n}\left(\omega_{\left(\Delta^{-1}\left(s_{p_{\flat(\epsilon)}}, \wp_{\flat(\epsilon)}\right)/\tau\right)}\right)^{\psi_\epsilon}}{\sqrt[q]{\prod_{\epsilon=1}^{n}\left(1 + (\varrho - 1)\left(1 - \left(\omega_{\left(\Delta^{-1}\left(s_{p_{\flat(\epsilon)}}, \wp_{\flat(\epsilon)}\right)/\tau\right)}\right)^q\right)\right)^{\psi_\epsilon} + (\varrho - 1)\prod_{\epsilon=1}^{n}\left(\omega_{\left(\Delta^{-1}\left(s_{p_{\flat(\epsilon)}}, \wp_{\flat(\epsilon)}\right)/\tau\right)}\right)^{q\psi_\epsilon}}}\right)\right) \\ \left(\Delta\left(\tau\left(\sqrt[q]{\dfrac{\prod_{\epsilon=1}^{n}\left(1 + (\varrho - 1)\left(\Delta^{-1}\left(s_{r_{\flat(\epsilon)}}, \mathfrak{R}_{\flat(\epsilon)}\right)/\tau\right)^q\right)^{\psi_\epsilon} - \prod_{\epsilon=1}^{n}\left(1 - \left(\Delta^{-1}\left(s_{r_{\flat(\epsilon)}}, \mathfrak{R}_{\flat(\epsilon)}\right)/\tau\right)^q\right)^{\psi_\epsilon}}{\prod_{\epsilon=1}^{n}\left(1 + (\varrho - 1)\left(\Delta^{-1}\left(s_{r_{\flat(\epsilon)}}, \mathfrak{R}_{\flat(\epsilon)}\right)/\tau\right)^q\right)^{\psi_\epsilon} + (\varrho - 1)\prod_{\epsilon=1}^{n}\left(1 - \left(\Delta^{-1}\left(s_{r_{\flat(\epsilon)}}, \mathfrak{R}_{\flat(\epsilon)}\right)/\tau\right)^q\right)^{\psi_\epsilon}}}\right)\right) \\ \left(\Delta\left(\tau\left(\sqrt[q]{\dfrac{\prod_{\epsilon=1}^{n}\left(1 + (\varrho - 1)\left(\omega_{\left(\Delta^{-1}\left(s_{r_{\flat(\epsilon)}}, \mathfrak{R}_{\flat(\epsilon)}\right)/\tau\right)}\right)^q\right)^{\psi_\epsilon} - \prod_{\epsilon=1}^{n}\left(1 - \left(\omega_{\left(\Delta^{-1}\left(s_{r_{\flat(\epsilon)}}, \mathfrak{R}_{\flat(\epsilon)}\right)/\tau\right)}\right)^q\right)^{\psi_\epsilon}}{\prod_{\epsilon=1}^{n}\left(1 + (\varrho - 1)\left(\omega_{\left(\Delta^{-1}\left(s_{r_{\flat(\epsilon)}}, \mathfrak{R}_{\flat(\epsilon)}\right)/\tau\right)}\right)^q\right)^{\psi_\epsilon} + (\varrho - 1)\prod_{\epsilon=1}^{n}\left(1 - \left(\omega_{\left(\Delta^{-1}\left(s_{r_{\flat(\epsilon)}}, \mathfrak{R}_{\flat(\epsilon)}\right)/\tau\right)}\right)^q\right)^{\psi_\epsilon}}}\right)\right) \end{array}\right), \tag{41}$$

where $(\flat(1), \flat(2), \ldots, \flat(n))$*is a permutation of* $(1, 2, \ldots, n)$*, such that* $\widetilde{\varsigma}_{\flat(\epsilon-1)} \geq \widetilde{\varsigma}_{\flat(\epsilon)}$ *for all* $\epsilon = 2, \ldots, n$*, and* $\psi = (\psi_1, \psi_2, \ldots, \psi_n)^T$ *is the aggregation-associated weighted vector such that* $\psi_\epsilon \in [0, 1]$ *and* $\sum_{\epsilon=1}^{n} \psi_\epsilon = 1, \varrho > 0$.

The 2TLCq-ROFHOWG operator has the same properties as Theorem 2.

Definition 16. Let $\widetilde{\varsigma}_\epsilon = (((s_{p_\epsilon}, \wp_\epsilon), (\omega_{(s_{p_\epsilon}, \wp_\epsilon)})), ((s_{r_\epsilon}, \mathfrak{R}_\epsilon), (\omega_{(s_{r_\epsilon}, \mathfrak{R}_\epsilon)}))(\epsilon = 1, 2, \ldots, n)$ be a collection of 2TLCq-ROFNs; then, the 2TLCq-ROFHHG operator is defined as

$$2TLCq - ROFHHG_{\psi,\varphi}(\widetilde{\varsigma}_1, \widetilde{\varsigma}_2, \ldots, \widetilde{\varsigma}_n) = \otimes_{\epsilon=1}^{n}\left(\dot{\widetilde{\varsigma}}_{\flat(\epsilon)}\right)^{\psi_\epsilon}, \tag{42}$$

where $\psi = (\psi_1, \psi_2, \ldots, \psi_n)$ be the associated weighting vector with $\psi_\epsilon \in [0, 1]$, $\sum_{\epsilon=1}^{n} \psi_\epsilon = 1$, and $\dot{\widetilde{\varsigma}}_{\flat(\epsilon)}$ is the ϵ-th largest element of 2TLCq-ROF arguments $\dot{\widetilde{\varsigma}}_\epsilon(\widetilde{\varsigma}_\epsilon = (n\varphi_\epsilon)\widetilde{\varsigma}_\epsilon, \epsilon = 1, 2, \ldots, n)$, $\varphi = (\varphi_1, \varphi_2, \ldots, \varphi_n)$ is the weighting vector of 2TLCq-ROF arguments $\widetilde{\varsigma}_\epsilon$, with $\varphi_\epsilon \in [0, 1]$ and $\sum_{\epsilon=1}^{n} \varphi_\epsilon = 1$, and n is the balancing coefficient, $\varrho > 0$. Especially, if $\psi = ((1/n), (1/n), \ldots, (1/n))^T$, then 2TLC$q$-ROFHHG is reduced to the 2TLCq-ROFHWG operator; if $\varphi = ((1/n), (1/n), \ldots, (1/n))$, then 2TLC$q$-ROFHHG is reduced to the 2TLCq-ROFHOWG operator.

Based on Hamacher sum operations of the 2TLCq-ROF values described, we can derive Theorem 8.

Theorem 8. *Let* $\widetilde{\varsigma}_\epsilon = (((s_{p_\epsilon}, \wp_\epsilon), (\omega_{(s_{p_\epsilon}, \wp_\epsilon)})), ((s_{r_\epsilon}, \mathfrak{R}_\epsilon), (\omega_{(s_{r_\epsilon}, \mathfrak{R}_\epsilon)}))(\epsilon = 1, 2, \ldots, n)$ *be a collection of 2TLCq-ROFNs, where* $\varrho > 0$*. Then, its aggregated value by utilizing the 2TLCq-ROFHHG operator is also a 2TLCq-ROFN, and*

$$2TLCq-ROFHHG_{\psi,\varphi}\left(\tilde{\varsigma}_1,\tilde{\varsigma}_2,\ldots,\tilde{\varsigma}_n\right)=\otimes_{\epsilon=1}^{n}\left(\tilde{\varsigma}_{\flat(\epsilon)}\right)^{\psi_\epsilon}$$

$$=\left(\begin{array}{c}\left(\Delta\left(\tau\left(\frac{\sqrt[q]{\varrho}\prod_{\epsilon=1}^{n}\left(\Delta^{-1}\left(\dot{s}_{p_{\flat(\epsilon)}},\dot{\wp}_{\flat(\epsilon)}\right)/\tau\right)^{\psi_\epsilon}}{\sqrt[q]{\prod_{\epsilon=1}^{n}\left(1+(\varrho-1)\left(1-\left(\Delta^{-1}\left(\dot{s}_{p_{\flat(\epsilon)}},\dot{\wp}_{\flat(\epsilon)}\right)/\tau\right)^{q}\right)\right)^{\psi_\epsilon}+(\varrho-1)\prod_{\epsilon=1}^{n}\left(\Delta^{-1}\left(\dot{s}_{p_{\flat(\epsilon)}},\dot{\wp}_{\flat(\epsilon)}\right)/\tau\right)^{q\psi_\epsilon}}}\right)\right)\right)\\ \left(\Delta\left(\tau\left(\frac{\sqrt[q]{\varrho}\prod_{\epsilon=1}^{n}\left(\omega_{\left(\Delta^{-1}\left(\dot{s}_{p_{\flat(\epsilon)}},\dot{\wp}_{\flat(\epsilon)}\right)/\tau\right)}\right)^{\psi_\epsilon}}{\sqrt[q]{\prod_{\epsilon=1}^{n}\left(1+(\varrho-1)\left(1-\left(\omega_{\left(\Delta^{-1}\left(\dot{s}_{p_{\flat(\epsilon)}},\dot{\wp}_{\flat(\epsilon)}\right)/\tau\right)}\right)^{q}\right)\right)^{\psi_\epsilon}+(\varrho-1)\prod_{\epsilon=1}^{n}\left(\omega_{\left(\Delta^{-1}\left(\dot{s}_{p_{\flat(\epsilon)}},\dot{\wp}_{\flat(\epsilon)}\right)/\tau\right)}\right)^{q\psi_\epsilon}}}\right)\right)\right)\\ \left(\Delta\left(\tau\left(\sqrt[q]{\frac{\prod_{\epsilon=1}^{n}\left(1+(\varrho-1)\left(\Delta^{-1}\left(\dot{s}_{r_{\flat(\epsilon)}},\dot{\mathfrak{R}}_{\flat(\epsilon)}\right)/\tau\right)^{q}\right)^{\psi_\epsilon}-\prod_{\epsilon=1}^{n}\left(1-\left(\Delta^{-1}\left(\dot{s}_{r_{\flat(\epsilon)}},\dot{\mathfrak{R}}_{\flat(\epsilon)}\right)/\tau\right)^{q}\right)^{\psi_\epsilon}}{\prod_{\epsilon=1}^{n}\left(1+(\varrho-1)\left(\Delta^{-1}\left(\dot{s}_{r_{\flat(\epsilon)}},\dot{\mathfrak{R}}_{\flat(\epsilon)}\right)/\tau\right)^{q}\right)^{\psi_\epsilon}+(\varrho-1)\prod_{\epsilon=1}^{n}\left(1-\left(\Delta^{-1}\left(\dot{s}_{r_{\flat(\epsilon)}},\dot{\mathfrak{R}}_{\flat(\epsilon)}\right)/\tau\right)^{q}\right)^{\psi_\epsilon}}}\right)\right)\right)\\ \left(\Delta\left(\tau\left(\sqrt[q]{\frac{\prod_{\epsilon=1}^{n}\left(1+(\varrho-1)\left(\omega_{\left(\Delta^{-1}\left(\dot{s}_{r_{\flat(\epsilon)}},\dot{\mathfrak{R}}_{\flat(\epsilon)}\right)/\tau\right)}\right)^{q}\right)^{\psi_\epsilon}-\prod_{\epsilon=1}^{n}\left(1-\left(\omega_{\left(\Delta^{-1}\left(\dot{s}_{r_{\flat(\epsilon)}},\dot{\mathfrak{R}}_{\flat(\epsilon)}\right)/\tau\right)}\right)^{q}\right)^{\psi_\epsilon}}{\prod_{\epsilon=1}^{n}\left(1+(\varrho-1)\left(\omega_{\left(\Delta^{-1}\left(\dot{s}_{r_{\flat(\epsilon)}},\dot{\mathfrak{R}}_{\flat(\epsilon)}\right)/\tau\right)}\right)^{q}\right)^{\psi_\epsilon}+(\varrho-1)\prod_{\epsilon=1}^{n}\left(1-\left(\omega_{\left(\Delta^{-1}\left(\dot{s}_{r_{\flat(\epsilon)}},\dot{\mathfrak{R}}_{\flat(\epsilon)}\right)/\tau\right)}\right)^{q}\right)^{\psi_\epsilon}}}\right)\right)\end{array}\right),\tag{43}$$

where $\psi=(\psi_1,\psi_2,\ldots,\psi_n)$ *be the associated weighting vector with* $\psi_\epsilon\in[0,1]$, $\sum_{\epsilon=1}^{n}\psi_\epsilon=1$, *and* $\dot{\tilde{\varsigma}}_{\flat(\epsilon)}$ *is the* ϵ*-th largest element of 2TLC*q*-ROF arguments* $\tilde{\varsigma}_\epsilon$ $(\dot{\tilde{\varsigma}}_\epsilon=(\tilde{\varsigma}_\epsilon)^{n\varphi_\epsilon})$, $(\epsilon=1,2,\ldots,n)$, $\varphi=(\varphi_1,\varphi_2,\ldots,\varphi_n)$ *is the weighting vector of 2TLC*q*-ROF arguments* $\tilde{\varsigma}_\epsilon$, *with* $\varphi_\epsilon\in[0,1]$ *and* $\sum_{\epsilon=1}^{n}\varphi_\epsilon=1$, *and* n *is the balancing coefficient,* $\varrho>0$.

The 2TLCq-ROFHHG operator has the same properties as Theorem 2.

5. An Extended COPRAS Method for MAGDM Approach

In this section, the 2TLCq-ROFHWA and 2TLCq-ROFHWG operators are used to integrate the evaluation values of the 2TLCq-ROF-MAGDM problem and develop a ranking procedure based on the COPRAS method for the 2TLCq-ROF-MAGDM problem. Firstly, we demonstrate the MAGDM problem with the 2TLCq-ROFS. For the 2TLCq-ROF-MAGDM problem, we build an extended COPRAS method, and then, with the assistance of the 2TLCq-ROFHWA and 2TLCq-ROFHWG operators, we fuse the individual input arguments into a combined viewpoint and also describe the DM algorithm.

5.1. An Extended COPRAS Method with 2TLCq-ROFH Aggregation Operators. In this section, we will extend COPRAS method to solve a MAGDM problem within the 2TLCq-ROF environment. According to the work of Zhang [46], group decision-making problems can be solved from two angles: (1) aggregation stage and (2) exploitation stage.

In the aggregation stage, collective evaluation values are obtained from the individual evaluation values of the alternatives. Therefore, we employ the 2TLCq-ROFHWA and 2TLCq-ROFHWG operators to combine the individual decision matrices into a group decision matrix. In the exploitation stage, the best alternative(s) is selected according to the priorities of the cumulative evaluation values. We will develop an extended COPRAS method based on the 2TLCq-ROFH aggregation operator, named the 2TLCq-ROFH-COPRAS method, to tackle the information in the group decision matrix.

By utilizing the 2TLCq-ROFHWA operator, the overall value of alternative $\daleth_\kappa$ based on attributes $\hbar_\epsilon$ is calculated, the result is computed as follows.

Phase 1. Establish the attributes as well as the alternatives.

The goal of the MADM process is to choose the best alternative from a set of m alternatives $\daleth=\{\daleth_1,\daleth_2,\ldots,\daleth_m\}$ under the attributes set $\hbar=\{\hbar_1,\hbar_2,\ldots,\hbar_n\}$. Assume a group of DEs appointed to serve on a panel $E=\{e_1,e_2,\ldots,e_\Lambda\}$, which was formulated in order to find the optimal alternative(s). Let $\daleth=(\daleth_{\kappa\epsilon}^{\lambda})$, $\kappa=1(1)m,\epsilon=1(1)n$ be the linguistic decision matrix provided by the DEs, where $\daleth_{\kappa\epsilon}^{\lambda}$ shows the assessed values of an alternative $\daleth_\kappa$ over attributes $\hbar_\epsilon$ in the form of linguistic values for λ^{th} the expert.

Phase 2. Construct the aggregated 2TLCq-ROF decision matrix.

We stimulate the 2TLCq-ROFHWA and 2TLCq-ROFHWG operators to obtain the decision matrix subsequently and achieve $R = (\eta_{\lambda\epsilon})_{\Lambda\times n}$ from (20) and (34).

Phase 3. Calculate the assessment values of the favorable-type and nonfavorable-type attributes.

Each alternative is defined throughout the designed model in terms of its total of maxima $\breve{\alpha}_\kappa$ (favorable-type) and minima $\breve{\beta}_\kappa$ (nonfavorable-type); that is, maxima and minima, respectively, produce the optimal outcomes. In such circumstances, $\breve{\alpha}_\kappa$ and $\breve{\beta}_\kappa$ can be obtained as described below.

Let $\Delta = \{1, 2, \ldots, \mathfrak{l}\}$ be a favorable-type attribute. Afterward, for every alternative, we compute the greatest possible index value in contexts of 2TLCq-ROFNs, as follows:

$$\breve{\alpha}_\kappa = \oplus_{\epsilon=1}^{\mathfrak{l}} \varphi_\epsilon \eta_{\kappa\epsilon}, \quad \kappa = 1\,(1)m. \tag{44}$$

Let $\nabla = \{\mathfrak{l}+1, \mathfrak{l}+2, \ldots, n\}$ be a nonfavorable-type attribute. Afterward, for every alternative, we assess the index value in contexts of 2TLCq-ROFNs as follows:

$$\breve{\beta}_\kappa = \oplus_{\epsilon=\mathfrak{l}+1}^{n} \varphi_\epsilon \eta_{\kappa\epsilon}, \quad \kappa = 1\,(1)m, \tag{45}$$

where $\mathfrak{l}$ represents favorable types and n represents the attributes.

Phase 4. Furthermore, we calculate the relative degree Γ_κ of each alternative $\beth_\kappa (\kappa = 1\,(1)m)$. Obviously, the bigger the value of Γ_κ, the higher the importance of the alternative. Γ_κ can be obtained as follows:

$$\Gamma_\kappa = \mathsf{F}\left(\breve{\alpha}_\kappa\right) + \frac{\min_\kappa \mathsf{F}\left(\breve{\beta}_\kappa\right) \sum_{\kappa=1}^{p} \mathsf{F}\left(\breve{\beta}_\kappa\right)}{\mathsf{F}\left(\breve{\beta}_\kappa\right) \sum_{\kappa=1}^{p} \min_\kappa \mathsf{F}\left(\breve{\beta}_\kappa\right) / \mathsf{F}\left(\breve{\beta}_\kappa\right)}, \quad \kappa = 1\,(1)m, \tag{46}$$

where $\mathsf{F}(\breve{\alpha}_\kappa)$ is the score value of $\breve{\alpha}_\kappa$ and $\mathsf{F}(\breve{\beta}_\kappa)$ is the score value of $\breve{\beta}_\kappa$.

Equation (46) can be simplified as

$$\Gamma_\kappa = \mathsf{F}\left(\breve{\alpha}_\kappa\right) + \frac{\sum_{\kappa=1}^{p} \mathsf{F}\left(\breve{\beta}_\kappa\right)}{\mathsf{F}\left(\breve{\beta}_\kappa\right) \sum_{\kappa=1}^{p} 1/\mathsf{F}\left(\breve{\beta}_\kappa\right)}, \quad \kappa = 1\,(1)m. \tag{47}$$

Γ_κ from (47) reflects the satisfaction measure of each alternative. Based on the Γ_κ, maximal value F can be determined.

Phase 5. Calculate the summary of priority.

$$\mathsf{F} = \max_\kappa \Gamma_\kappa, \kappa = 1\,(1)m. \tag{48}$$

Thus, the alternative(s) with the associated maximal relative degree is selected among the possible alternatives. Moreover, we can ascertain the utility degree $\mathscr{U}_\kappa$ of each alternative with the aid of the Γ_κ. $\mathscr{U}_\kappa$ can be determined by using the following formula:

$$\mathscr{U}_\kappa = \left(\frac{\Gamma_\kappa}{\Gamma_{\max}}\right) \times 100\%, \kappa = 1\,(1)m. \tag{49}$$

Hence, the bigger the value $\mathscr{U}_\kappa$, the higher the rank of the alternative $\beth_\kappa$.

Table 1: Network security service providers (alternatives).

$\beth_1$	Delta tech
$\beth_2$	Catalytic security
$\beth_3$	PakCERT
$\beth_4$	Tranchulas
$\beth_5$	Tier 3 cyber security services
$\beth_6$	Cyber security consultancy company
$\beth_7$	Institute of cyber security

6. Numerical Example

In this part, we present a numerical example to evaluate how well our strategy works. With the increased reliance on technology, it is becoming increasingly important to protect all aspects of Internet information and data. Data integrity has become one of the most critical issues for enterprises to address, as the Internet and computer networks increase over time. No matter how little or large your enterprises is, network security is one of the most crucial factors to consider while working over the Internet, LAN, or other technology. While no network is immune to cyber threats, a solid and effective network security solution is critical for securing client data. An effective network security solution minimizes the danger of data theft and tampering in the workplace. Workstations will be protected from malicious software, thanks to network security service provider. It also assures the safety of shared information. In this section, we illustrate the application of 2TLCq-ROF COPRAS method on the choice of network security service provider.

By the above analysis, let $L = \{\beth_1, \beth_2, \beth_3, \beth_4, \beth_5, \beth_6, \beth_7\}$ be a set of seven network security service providers (see Table 1) and let $A = \{\hbar_1, \hbar_2, \hbar_3, \hbar_4\}$ be a set of four attributes with weighting vector $\xi = (0.17, 0.31, 0.27, 0.25)^T$. Suppose, seven network security service providers are evaluated by three experts $E = \{e_1, e_2, e_3\}$, with weighting vector $\varphi' = (0.2, 0.5, 0.3)^T$ for choosing the best network security service provider. To quantify each LTS, three experts provide their opinions. Based on their experience, each decision expert has an opinion for the selection of the best network security service provider according to four attributes, including

(1) $\hbar_1$: web security

(2) $\hbar_2$: data loss prevention

(3) $\hbar_3$: antivirus and anti-malware software

(4) $\hbar_4$: mobile device security

Experts should evaluate the effectiveness of network security service provider concerning all attributes in

Table 2: 2TLCq-ROF decision matrix by e_1.

	$\hbar_1$	$\hbar_2$	$\hbar_3$	$\hbar_4$
λ_1	$\langle((s_1,0),(s_4,0)),((s_7,0),(s_3,0))\rangle$	$\langle((s_2,0),(s_3,0)),((s_3,0),(s_5,0))\rangle$	$\langle((s_5,0),(s_2,0)),((s_6,0),(s_{63},0))\rangle$	$\langle((s_4,0),(s_3,0)),((s_2,0),(s_3,0))\rangle$
λ_2	$\langle((s_1,0),(s_4,0)),((s_5,0),(s_3,0))\rangle$	$\langle((s_3,0),(s_4,0)),((s_2,0),(s_3,0))\rangle$	$\langle((s_2,0),(s_4,0)),((s_2,0),(s_4,0))\rangle$	$\langle((s_2,0),(s_4,0)),((s_5,0),(s_3,0))\rangle$
λ_3	$\langle((s_3,0),(s_2,0)),((s_2,0),(s_3,0))\rangle$	$\langle((s_3,0),(s_3,0)),((s_4,0),(s_2,0))\rangle$	$\langle((s_2,0),(s_4,0)),((s_3,0),(s_1,0))\rangle$	$\langle((s_3,0),(s_3,0)),((s_2,0),(s_5,0))\rangle$
λ_4	$\langle((s_2,0),(s_2,0)),((s_1,0),(s_3,0))\rangle$	$\langle((s_2,0),(s_5,0)),((s_5,0),(s_4,0))\rangle$	$\langle((s_4,0),(s_1,0)),((s_4,0),(s_5,0))\rangle$	$\langle((s_4,0),(s_3,0)),((s_2,0),(s_3,0))\rangle$
λ_5	$\langle((s_2,0),(s_3,0)),((s_2,0),(s_4,0))\rangle$	$\langle((s_3,0),(s_2,0)),((s_4,0),(s_2,0))\rangle$	$\langle((s_3,0),(s_2,0)),((s_1,0),(s_5,0))\rangle$	$\langle((s_2,0),(s_3,0)),((s_5,0),(s_1,0))\rangle$
λ_6	$\langle((s_1,0),(s_5,0)),((s_6,0),(s_3,0))\rangle$	$\langle((s_5,0),(s_1,0)),((s_3,0),(s_6,0))\rangle$	$\langle((s_5,0),(s_6,0)),((s_3,0),(s_2,0))\rangle$	$\langle((s_6,0),(s_5,0)),((s_2,0),(s_3,0))\rangle$
λ_7	$\langle((s_3,0),(s_4,0)),((s_5,0),(s_2,0))\rangle$	$\langle((s_5,0),(s_4,0)),((s_2,0),(s_3,0))\rangle$	$\langle((s_3,0),(s_4,0)),((s_5,0),(s_2,0))\rangle$	$\langle((s_6,0),(s_3,0)),((s_1,0),(s_3,0))\rangle$

Table 3: 2TLCq-ROF decision matrix by e_2.

	$\hbar_1$	$\hbar_2$	$\hbar_3$	$\hbar_4$
λ_1	$\langle((s_4,0),(s_2,0)),((s_2,0),(s_4,0))\rangle$	$\langle((s_1,0),(s_5,0)),((s_6,0),(s_5,0))\rangle$	$\langle((s_2,0),(s_3,0)),((s_2,0),(s_3,0))\rangle$	$\langle((s_3,0),(s_5,0)),((s_3,0),(s_2,0))\rangle$
λ_2	$\langle((s_1,0),(s_3,0)),((s_4,0),(s_3,0))\rangle$	$\langle((s_7,0),(s_2,0)),((s_2,0),(s_5,0))\rangle$	$\langle((s_3,0),(s_4,0)),((s_2,0),(s_4,0))\rangle$	$\langle((s_2,0),(s_4,0)),((s_3,0),(s_2,0))\rangle$
λ_3.	$\langle((s_4,0),(s_2,0)),((s_4,0),(s_3,0))\rangle$	$\langle((s_2,0),(s_2,0)),((s_5,0),(s_3,0))\rangle$	$\langle((s_3,0),(s_4,0)),((s_3,0),(s_3,0))\rangle$	$\langle((s_2,0),(s_3,0)),((s_5,0),(s_2,0))\rangle$
λ_4	$\langle((s_3,0),(s_4,0)),((s_2,0),(s_3,0))\rangle$	$\langle((s_3,0),(s_4,0)),((s_3,0),(s_5,0))\rangle$	$\langle((s_5,0),(s_3,0)),((s_2,0),(s_6,0))\rangle$	$\langle((s_4,0),(s_2,0)),((s_4,0),(s_2,0))\rangle$
λ_5	$\langle((s_1,0),(s_5,0)),((s_4,0),(s_2,0))\rangle$	$\langle((s_5,0),(s_1,0)),((s_2,0),(s_4,0))\rangle$	$\langle((s_5,0),(s_2,0)),((s_4,0),(s_6,0))\rangle$	$\langle((s_2,0),(s_5,0)),((s_6,0),(s_4,0))\rangle$
λ_6	$\langle((s_6,0),(s_5,0)),((s_3,0),(s_4,0))\rangle$	$\langle((s_5,0),(s_6,0)),((s_4,0),(s_3,0))\rangle$	$\langle((s_1,0),(s_2,0)),((s_5,0),(s_4,0))\rangle$	$\langle((s_2,0),(s_1,0)),((s_4,0),(s_5,0))\rangle$
λ_7	$\langle((s_3,0),(s_2,0)),((s_5,0),(s_3,0))\rangle$	$\langle((s_3,0),(s_4,0)),((s_4,0),(s_5,0))\rangle$	$\langle((s_4,0),(s_2,0)),((s_3,0),(s_2,0))\rangle$	$\langle((s_4,0),(s_2,0)),((s_5,0),(s_3,0))\rangle$

Table 4: 2TLCq-ROF decision matrix by e_3.

	$\hbar_1$	$\hbar_2$	$\hbar_3$	$\hbar_4$
λ_1	$\langle((s_5,0),(s_3,0)),((s_3,0),(s_2,0))\rangle$	$\langle((s_2,0),(s_3,0)),((s_3,0),(s_2,0))\rangle$	$\langle((s_6,0),(s_2,0)),((s_4,0),(s_5,0))\rangle$	$\langle((s_{71},0),(s_2,0)),((s_1,0),(s_2,0))\rangle$
λ_2	$\langle((s_6,0),(s_1,0)),((s_3,0),(s_2,0))\rangle$	$\langle((s_2,0),(s_3,0)),((s_5,0),(s_3,0))\rangle$	$\langle((s_5,0),(s_2,0)),((s_2,0),(s_6,0))\rangle$	$\langle((s_3,0),(s_2,0)),((s_4,0),(s_7,0))\rangle$
λ_3	$\langle((s_3,0),(s_2,0)),((s_3,0),(s_5,0))\rangle$	$\langle((s_2,0),(s_3,0)),((s_2,0),(s_7,0))\rangle$	$\langle((s_4,0),(s_2,0)),((s_3,0),(s_5,0))\rangle$	$\langle((s_7,0),(s_3,0)),((s_1,0),(s_3,0))\rangle$
λ_4	$\langle((s_2,0),(s_4,0)),((s_3,0),(s_4,0))\rangle$	$\langle((s_4,0),(s_2,0)),((s_3,0),(s_7,0))\rangle$	$\langle((s_5,0),(s_2,0)),((s_1,0),(s_2,0))\rangle$	$\langle((s_4,0),(s_3,0)),((s_2,0),(s_3,0))\rangle$
λ_5	$\langle((s_6,0),(s_4,0)),((s_1,0),(s_5,0))\rangle$	$\langle((s_4,0),(s_6,0)),((s_5,0),(s_1,0))\rangle$	$\langle((s_2,0),(s_2,0)),((s_1,0),(s_1,0))\rangle$	$\langle((s_1,0),(s_1,0)),((s_2,0),(s_2,0))\rangle$
λ_6	$\langle((s_2,0),(s_1,0)),((s_2,0),(s_1,0))\rangle$	$\langle((s_1,0),(s_2,0)),((s_1,0),(s_2,0))\rangle$	$\langle((s_3,0),(s_2,0)),((s_6,0),(s_5,0))\rangle$	$\langle((s_2,0),(s_3,0)),((s_5,0),(s_6,0))\rangle$
λ_7	$\langle((s_2,0),(s_3,0)),((s_4,0),(s_5,0))\rangle$	$\langle((s_1,0),(s_3,0)),((s_4,0),(s_3,0))\rangle$	$\langle((s_2,0),(s_7,0)),((s_3,0),(s_3,0))\rangle$	$\langle((s_5,0),(s_1,0)),((s_4,0),(s_2,0))\rangle$

Table 5: Collective the 2TLCq-ROF assessing matrix by the 2TLCq-ROFHWA operator.

	Collective assessment matrix	
Alternatives	$\hbar_1$	$\hbar_2$
λ_1	$\langle((s_4,0.1104),(s_3,0.2121)),((s_3,0.3992),(s_3,-0.0131))\rangle$	$\langle((s_2,-0.2220),(s_4,0.1377),(s_4,0.0177),(s_4,-0.1636))\rangle$
λ_2	$\langle((s_4,0.3900),(s_3,0.2269)),((s_4,-0.0636),(s_3,-0.3423))\rangle$	$\langle((s_6,-0.3618),(s_3,0.2121)),((s_3,-0.3501),(s_4,-0.3015))\rangle$
λ_3	$\langle((s_4,-0.4988),(s_2,-0)),((s_3,-0.0131),(s_4,-0.4888))\rangle$	$\langle((s_2,0.4392),(s_3,-0.2782)),((s_4,-0.4214),(s_4,-0.4626))\rangle$
λ_4	$\langle((s_3,-0.4560),(s_4,-0.3231)),((s_2,-0.1639),(s_3,0.2730))\rangle$	$\langle((s_3,0.2607),(s_4,0.1274)),((s_4,-0.4888),(s_5,0.2652))\rangle$
λ_5	$\langle((s_4,0.4042),(s_4,0.3162)),((s_2,0.1513),(s_3,0.2636))\rangle$	$\langle((s_4,0.3162),(s_4,0.4042)),((s_3,0.2636),(s_2,0.1513))\rangle$
λ_6	$\langle((s_5,-0.2594),(s_5,-0.4421)),((s_3,0.3176),(s_2,0.4301))\rangle$	$\langle((s_5,-0.4421),(s_5,-0.2594)),((s_2,0.4301),(s_3,0.3176))\rangle$
λ_7	$\langle((s_3,-0.2008),(s_3,0.2121)),((s_5,-0.3164),(s_3,0.1141))\rangle$	$\langle((s_4,-0.1736),(s_4,-0.2260)),((s_3,0.2588),(s_4,-0.3015))\rangle$
Alternatives	$\hbar_3$	$\hbar_4$
λ_1	$\langle((s_5,-0.1136),(s_3,-0.4560),(s_3,0.4760),(s_4,0.3572))\rangle$	$\langle((s_5,0.3895),(s_4,0.0637),(s_2,-0.0876),(s_2,0.2596))\rangle$
λ_2	$\langle((s_4,-0.1528),(s_4,-0.3231)),((s_2,-0),(s_5,-0.4502))\rangle$	$\langle((s_2,0.4392),(s_4,-0.3231)),((s_4,-0.1739),(s_3,0.3992))\rangle$
λ_3	$\langle((s_3,0.2607),(s_4,-0.3231)),((s_3,-0),(s_3,-0.4655))\rangle$	$\langle((s_5,0.2476),(s_3,0)),((s_2,0.3664),(s_3,-0.0087))\rangle$
λ_4	$\langle((s_5,-0.2419),(s_2,0.4721)),((s_2,0.0056),(s_4,0.1656))\rangle$	$\langle((s_4,-0),(s_3,-0.2782)),((s_3,-0.3540),(s_3,-0.4478))\rangle$
λ_5	$\langle((s_4,0.0637)(s_2,-0)),((s_2,-0.2521),(s_3,0.4067))\rangle$	$\langle((s_2,-0.1587),(s_4,0.0459)),((s_4,0.1656),(s_2,0.1513))\rangle$
λ_6	$\langle((s_4,-0.2112),(s_4,0.4229)),((s_5,-0.4196),(s_3,0.4961))\rangle$	$\langle((s_4,0.4229),(s_4,-0.2112)),((s_3,0.4961),(s_5,-0.4196))\rangle$
λ_7	$\langle((s_3,0.3791),(s_5,0.3429)),((s_4,-0.4888),(s_2,0.2596))\rangle$	$\langle((s_5,0.0936),(s_2,0.3572)),((s_3,-0.0828),(s_3,-0.3423))\rangle$

accordance with their interaction and identify the most suitable one. Each decision expert uses the 2TLCq-ROFNs to assess each network security service provider's ability to control each attribute.

6.1. The Outcomes of a Case Study

6.1.1. Decision-Making Procedure Based on the 2TLCq-ROFHWA Operator. On the basis of 2TLCq-ROFNs matrix

Table 6: Assessing values of favorable- and nonfavorable-type attributes by the 2TLCq-ROFHWA operator.

	Assessed values of favorable attributes	Assessed values of nonfavorable attributes
Alternatives		
$\daleth_1$	$\langle((s_4,-0.0223),(s_3,0.0357)),((s_5,0.4604),(s_6,-0.4488))\rangle$	$\langle((s_4,-0.4918),(s_3,0.1659)),((s_6,-0.4243),(s_6,-0.1948))\rangle$
$\daleth_2$	$\langle((s_3,-0.1058),(s_3,-0.1778)),((s_6,0.4078),(s_6,-0.0561))\rangle$	$\langle((s_4,0.3583),(s_3,0.0065)),((s_4,0.3236),(s_6,-0.1917))\rangle$
$\daleth_3$	$\langle((s_4,-0.2054),(s_2,0.1860)),((s_6,-0.3941),(s_6,0.0175))\rangle$	$\langle((s_3,-0.4656),(s_3,-0.1525)),((s_5,0.2148),(s_5,-0.0104))\rangle$
$\daleth_4$	$\langle((s_3,-0.1086),(s_3,-0.4202)),((s_5,0.3485),(s_6,-0.2301))\rangle$	$\langle((s_4,-0.3919),(s_3,0.1491)),((s_5,-0.3007),(s_6,0.2438))\rangle$
$\daleth_5$	$\langle((s_3,-0.1620),(s_3,0.3348)),((s_6,0.0219),(s_6,-0.4349))\rangle$	$\langle((s_4,-0.3433),(s_3,0.2963)),((s_4,0.4429),(s_5,-0.3404))\rangle$
$\daleth_6$	$\langle((s_4,-0.3514),(s_3,0.3253)),((s_6,0.1586),(s_6,0.2394))\rangle$	$\langle((s_4,-0.3057),(s_4,-0.0024)),((s_5,0.2002),(s_5,0.2980))\rangle$
$\daleth_7$	$\langle((s_4,-0.3787),(s_2,0.2501)),((s_6,0.2304),(s_6,-0.2224))\rangle$	$\langle((s_3,0.1682),(s_4,0.0718)),((s_5,0.2776),(s_5,-0.0865))\rangle$

Table 7: Assessing outcomes of alternatives and ranking order by utilizing the 2TLCq-ROF-COPRAS.

Alternatives	Benefit attributes scores $\mathsf{F}(\breve{\alpha}_\kappa)$	Cost attributes scores $\mathsf{F}(\beta_\kappa)$	Relative degree Γ_κ	Utility degree $\mathscr{U}_\kappa$	Ranking
$\daleth_1$	0.4083	0.3871	0.8749	1.0000	1
$\daleth_2$	0.3291	0.4362	0.7432	0.8494	4
$\daleth_3$	0.3737	0.4236	0.8002	0.9146	3
$\daleth_4$	0.3894	0.3938	0.8481	0.9693	7
$\daleth_5$	0.3727	0.4656	0.7607	0.8695	5
$\daleth_6$	0.3380	0.4343	0.7540	0.8617	6
$\daleth_7$	0.3521	0.4400	0.7626	0.8716	2

Table 8: Collective 2TLCq-ROF assessing matrix by the 2TLCq-ROFHWG operator.

	Collective assessment matrix	
Alternatives	$\hbar_1$	$\hbar_2$
$\daleth_1$	$\langle((s_3,-0.1510),(s_3,-0.2137)),((s_5,0.2476),(s_3,0.3791))\rangle$	$\langle((s_2,-0.4840),(s_4,-0.3015)),((s_5,-0.1524),(s_5,-0.4294))\rangle$
$\daleth_2$	$\langle((s_2,-0.2581),(s_2,0.3599)),((s_4,0.1984),(s_3,-0.2008))\rangle$	$\langle((s_4,-0.1147),(s_3,-0.2137)),((s_4,-0.2766),(s_4,0.1377))\rangle$
$\daleth_3$	$\langle((s_3,0.3691),(s_2,-0)),((s_3,0.3791),(s_4,-0.0669))\rangle$	$\langle((s_2,0.2596),(s_3,-0.4478)),((s_4,0.2507),(s_5,0.2600))\rangle$
$\daleth_4$	$\langle((s_2,0.3533),(s_3,0.2588)),((s_2,0.3572),(s_3,0.3951))\rangle$	$\langle((s_3,-0.0989),(s_3,0.4961)),((s_4,-0.0669),(s_6,-0.2770))\rangle$
$\daleth_5$	$\langle((s_2,0.1438),(s_4,0.0278)),((s_3,0.2084),(s_4,0.0368))\rangle$	$\langle((s_4,0.0278),(s_2,0.1438)),((s_4,0.0368),(s_3,0.2084))\rangle$
$\daleth_6$	$\langle((s_3,-0.4227),(s_3,0.1313)),((s_5,-0.4991),(s_3,0.3488))\rangle$	$\langle((s_3,0.1313),(s_3,-0.4227)),((s_3,0.3488),(s_5,-0.4991))\rangle$
$\daleth_7$	$\langle((s_3,-0.3423),(s_3,-0.2137)),((s_5,-0.2419),(s_4,-0.1528))\rangle$	$\langle((s_3,-0.4655),(s_4,-0.3273)),((s_4,-0.3231),(s_4,0.1377))\rangle$
Alternatives	$\hbar_3$	$\hbar_4$
$\daleth_1$	$\langle((s_4,-0.2726),(s_2,0.3533)),((s_5,-0.3732),(s_5,-0.0540))\rangle$	$\langle((s_4,0.3320),(s_3,0.2820)),((s_2,0.4721),(s_2,0.4392))\rangle$
$\daleth_2$	$\langle((s_3,0.1141),(s_3,0.2588)),((s_2,-0),(s_5,-0.1351))\rangle$	$\langle((s_2,0.2596),(s_3,0.2588)),((s_4,0.1365),(s_5,0.2476))\rangle$
$\daleth_3$	$\langle((s_3,-0.0989),(s_3,0.2588)),((s_3,0),(s_4,-0.1736))\rangle$	$\langle((s_3,0.3992),(s_3,-0)),((s_4,-0.0332),(s_4,-0.1827))\rangle$
$\daleth_4$	$\langle((s_5,-0.3164),(s_2,-0.0876)),((s_3,0.0107),(s_5,0.1435))\rangle$	$\langle((s_4,0),(s_3,-0.4478)),((s_3,0.2427),(s_3,-0.2782))\rangle$
$\daleth_5$	$\langle((s_3,0.2820),(s_2,-0)),((s_3,0.1730),(s_5,0.1343))\rangle$	$\langle((s_2,-0.3752),(s_3,-0.3275)),((s_5,0.1435),(s_3,0.2084))\rangle$
$\daleth_6$	$\langle((s_2,0.2714),(s_3,-0.1754)),((s_5,0.0585),(s_4,0.1274))\rangle$	$\langle((s_3,-0.1754),(s_2,0.2714)),((s_4,0.1274),(s_5,0.0585))\rangle$
$\daleth_7$	$\langle((s_3,-0.0131),(s_4,-0.2947)),((s_4,-0.0669),(s_2,0.4392))\rangle$	$\langle((s_5,-0.1395),t(s_2,-0.1639))),((s_4,0.2350),t(s_3,-0.2008))\rangle$

(see Tables 2–4) and Table 3 by utilizing (15), the collective 2TLCq-ROF assessing matrix is computed. The aggregated outcomes are listed in Table 5.

Construct the assessing matrix (see Table 6) of favorable- and nonfavorable-type attributes by utilizing the (15) and (44), and (45).

Calculate the scoring outcomes of alternatives for favorable ($\mathsf{F}(\breve{\alpha}_\kappa)$)- and nonfavorable ($\mathsf{F}(\beta_\kappa)$)-type attributes by utilizing (12), and establish the ranking order by using the 2TLCq-ROF-COPRAS method. The evaluation outcomes are listed in Table 7.

6.1.2. Decision-Making Procedure Based on the 2TLCq-ROFHWG Operator. On the basis of 2TLCq-ROFN matrix (see Tables 2–4) and by utilizing (34), the collective 2TLCq-ROF assessing matrix is computed. The aggregated outcomes are listed in Table 8.

Construct the assessing matrix (see Table 9) of favorable- and nonfavorable-type attributes by utilizing the (34) and (44), and (45).

Calculate the scoring outcomes of alternatives for favorable ($\mathsf{F}(\breve{\alpha}_\kappa)$)- and nonfavorable ($\mathsf{F}(\beta_\kappa)$)-type attributes by utilizing (12) and establish the ranking order by using the 2TLCq-ROF-COPRAS method. The evaluation outcomes are listed in Table 10.

6.2. Parameter Analysis. Surely, the parameter ϱ has a great influence on the ranking results. The influence of parameters on score values and ranking results based on 2TLCq-

Table 9: Assessing values of favorable- and nonfavorable-type attributes by the 2TLCq-ROFHWG operator.

	Assessed values of favorable attributes	Assessed values of nonfavorable attributes
Alternatives		
$\mathfrak{Z}_1$	$\langle((s_6, 0.2971), (s_6, -0.0599)), ((s_3, 0.3893), (s_2, 0.3551))\rangle$	$\langle((s_4, 0.3090), (s_5, -0.0370)), ((s_4, 0.1242), (s_4, 0.1305))\rangle$
$\mathfrak{Z}_2$	$\langle((s_5, 0.1244), (s_6, -0.2031)), ((s_3, 0.3356), (s_4, -0.2780))\rangle$	$\langle((s_5, 0.3839), (s_5, -0.0397)), ((s_3, -0.1818), (s_4, -0.0743))\rangle$
$\mathfrak{Z}_3$	$\langle((s_6, 0.1372), (s_6, -0.4356)), ((s_3, 0.0175), (s_3, 0.1010))\rangle$	$\langle((s_5, -0.4634), (s_5, -0.1616)), ((s_3, 0.3172), (s_4, 0.1169))\rangle$
$\mathfrak{Z}_4$	$\langle((s_6, 0.0442), (s_6, -0.2335)), ((s_2, 0.3901), (s_2, 0.4500))\rangle$	$\langle((s_5, 0.4866), (s_5, -0.3619)), ((s_3, 0.1240), (s_5, -0.2501))\rangle$
$\mathfrak{Z}_5$	$\langle((s_5, -0.0879), (s_6, -0.0028)), ((s_4, -0.3074), (s_3, -0.1011))\rangle$	$\langle((s_6, -0.4945), (s_4, 0.0610)), ((s_3, 0.2265), (s_4, -0.1764))\rangle$
$\mathfrak{Z}_6$	$\langle((s_6, -0.3032), (s_6, -0.4044)), ((s_3, 0.4362), (s_4, -0.3434))\rangle$	$\langle((s_5, -0.3116), (s_5, -0.3189)), ((s_4, -0.1944), (s_4, -0.2280))\rangle$
$\mathfrak{Z}_7$	$\langle((s_6, 0.3865), (s_5, 0.2536)), ((s_4, -0.4234), (s_3, -0.3159))\rangle$	$\langle((s_5, -0.2756), (s_6, -0.4764)), ((s_3, 0.3102), (s_3, 0.1518))\rangle$

Table 10: Assessing outcomes of alternatives and ranking order by utilizing the 2TLCq-ROF-COPRAS.

Alternatives	Benefit attributes scores $\mathsf{F}(\breve{\alpha}_\kappa)$	Cost attributes scores $\mathsf{F}(\beta_\kappa)$	Relative degree Γ_κ	Utility degree $\mathscr{U}_\kappa$	Ranking
$\mathfrak{Z}_1$	0.6620	0.5227	1.2354	1.0000	1
$\mathfrak{Z}_2$	0.5917	0.5699	1.1176	0.9047	3
$\mathfrak{Z}_3$	0.6344	0.5344	1.1953	0.9675	4
$\mathfrak{Z}_4$	0.6447	0.5467	1.1930	0.9656	6
$\mathfrak{Z}_5$	0.5988	0.5530	1.1407	0.9234	7
$\mathfrak{Z}_6$	0.6047	0.5336	1.1663	0.9441	5
$\mathfrak{Z}_7$	0.6349	0.5739	1.1571	0.9366	2

Table 11: Score values and ranking outcomes according to the parameter q by the 2TLCq-ROFHWA operator.

Parameters	$\mathsf{F}(\mathfrak{Z}_1)$	$\mathsf{F}(\mathfrak{Z}_2)$	$\mathsf{F}(\mathfrak{Z}_3)$	$\mathsf{F}(\mathfrak{Z}_4)$	$\mathsf{F}(\mathfrak{Z}_5)$	$\mathsf{F}(\mathfrak{Z}_6)$	$\mathsf{F}(\mathfrak{Z}_7)$	Ranking
$q = 2$	1.0000	0.7877	0.8865	0.9286	0.8096	0.8246	0.8228	$\mathfrak{Z}_1 > \mathfrak{Z}_4 > \mathfrak{Z}_3 > \mathfrak{Z}_6 > \mathfrak{Z}_7 > \mathfrak{Z}_5 > \mathfrak{Z}_2$
$q = 3$	1.0000	0.8177	0.8975	0.9513	0.8371	0.8394	0.8457	$\mathfrak{Z}_1 > \mathfrak{Z}_4 > \mathfrak{Z}_3 > \mathfrak{Z}_7 > \mathfrak{Z}_6 > \mathfrak{Z}_5 > \mathfrak{Z}_2$
$q = 5$	1.0000	0.8783	0.9323	0.9819	0.8096	0.8855	0.8962	$\mathfrak{Z}_1 > \mathfrak{Z}_4 > \mathfrak{Z}_3 > \mathfrak{Z}_7 > \mathfrak{Z}_6 > \mathfrak{Z}_2 > \mathfrak{Z}_5$
$q = 7$	1.0000	0.9236	0.9615	0.9950	0.9445	0.9278	0.9359	$\mathfrak{Z}_1 > \mathfrak{Z}_4 > \mathfrak{Z}_3 > \mathfrak{Z}_5 > \mathfrak{Z}_7 > \mathfrak{Z}_6 > \mathfrak{Z}_2$
$q = 11$	0.9999	0.9712	0.9901	1.0000	0.9845	0.8246	0.9776	$\mathfrak{Z}_4 > \mathfrak{Z}_1 > \mathfrak{Z}_3 > \mathfrak{Z}_5 > \mathfrak{Z}_7 > \mathfrak{Z}_2 > \mathfrak{Z}_6$
$q = 13$	1.0000	0.9821	0.9953	0.9999	0.9916	0.9866	0.9865	$\mathfrak{Z}_1 > \mathfrak{Z}_4 > \mathfrak{Z}_3 > \mathfrak{Z}_5 > \mathfrak{Z}_6 > \mathfrak{Z}_7 > \mathfrak{Z}_2$
$q = 17$	1.0000	0.9924	0.9990	0.9993	0.9970	0.9955	0.9945	$\mathfrak{Z}_1 > \mathfrak{Z}_4 > \mathfrak{Z}_3 > \mathfrak{Z}_5 > \mathfrak{Z}_6 > \mathfrak{Z}_7 > \mathfrak{Z}_2$
$q = 19$	1.0000	0.9948	0.9996	0.9993	0.9981	0.9973	0.9962	$\mathfrak{Z}_1 > \mathfrak{Z}_3 > \mathfrak{Z}_4 > \mathfrak{Z}_5 > \mathfrak{Z}_6 > \mathfrak{Z}_7 > \mathfrak{Z}_2$
$q = 23$	1.0000	0.9973	0.9999	0.9994	0.9991	0.9988	0.9981	$\mathfrak{Z}_1 > \mathfrak{Z}_3 > \mathfrak{Z}_4 > \mathfrak{Z}_5 > \mathfrak{Z}_6 > \mathfrak{Z}_7 > \mathfrak{Z}_2$
$q = 29$	1.0000	0.7877	0.8865	0.9286	0.8096	0.8246	0.8228	$\mathfrak{Z}_1 > \mathfrak{Z}_4 > \mathfrak{Z}_3 > \mathfrak{Z}_6 > \mathfrak{Z}_7 > \mathfrak{Z}_5 > \mathfrak{Z}_2$

ROFHWA and 2TLCq-ROFHWG operators are evaluated in this subsection. We fix the several values of q and evaluate the scores of the overall aggregation. Furthermore, scores are used to rank the alternatives. In Tables 11 and 12 score values are evaluated by varying q and ϱ, respectively, based on the 2TLCq-ROFHWA operator. Then, these scores are used to rank the alternatives. Ranking results are used to select the best alternative, and $\mathfrak{Z}_1$ is the best alternative based on the 2TLCq-ROFHWA operator. As the values of q and ϱ vary, the scores of the seven alternatives change as well, resulting in an irregular change accordingly, based on the 2TLCq-ROFHWA operator. The change in values of q and ϱ have a significant influence on the results of the alternative ranking. Tables 11 and 12 demonstrate that when q and ϱ are changed, the ranking results are relatively stable, and the best alternative remained unchanged. The decision preference can be represented in the actual DM process by varying the values of q and ϱ to obtain the best decision result.

We fix the several values of q and ϱ and evaluate the scores of the overall aggregation. Furthermore, scores are used to rank the alternatives. In Tables 13 and 14 score values are evaluated by varying q and ϱ, respectively, based on the 2TLCq-ROFHWG operator. Then, these scores are used to rank the alternatives. The ranking results are used to select the best alternative, and $\mathfrak{Z}_1$ is the best alternative based on the 2TLCq-ROFHWG operator. As the values of q and ϱ vary, the scores of the seven alternatives change as well, resulting in an irregular change accordingly, based on the 2TLCq-ROFHWG operator. The change in values of q and ϱ has a significant influence on the results of the alternative

Table 12: Score values and ranking outcomes according to the parameter ϱ by the 2TLq-ROFHWA operator.

Parameters	$\mathsf{F}(\mathfrak{J}_1)$	$\mathsf{F}(\mathfrak{J}_2)$	$\mathsf{F}(\mathfrak{J}_3)$	$\mathsf{F}(\mathfrak{J}_4)$	$\mathsf{F}(\mathfrak{J}_5)$	$\mathsf{F}(\mathfrak{J}_6)$	$\mathsf{F}(\mathfrak{J}_7)$	Ranking
$\varrho = 2$	1.0000	0.8607	0.9254	0.9709	0.8822	0.8739	0.8820	$\mathfrak{J}_1 > \mathfrak{J}_4 > \mathfrak{J}_3 > \mathfrak{J}_5 > \mathfrak{J}_7 > \mathfrak{J}_6 > \mathfrak{J}_2$
$\varrho = 3$	1.0000	0.8494	0.9146	0.9693	0.8695	0.8618	0.8717	$\mathfrak{J}_1 > \mathfrak{J}_4 > \mathfrak{J}_3 > \mathfrak{J}_7 > \mathfrak{J}_5 > \mathfrak{J}_6 > \mathfrak{J}_2$
$\varrho = 5$	1.0000	0.8333	0.8995	0.9662	0.8511	0.8452	0.8568	$\mathfrak{J}_1 > \mathfrak{J}_4 > \mathfrak{J}_3 > \mathfrak{J}_7 > \mathfrak{J}_5 > \mathfrak{J}_6 > \mathfrak{J}_2$
$\varrho = 7$	1.0000	0.8217	0.8887	0.9633	0.8375	0.8338	0.8460	$\mathfrak{J}_1 > \mathfrak{J}_4 > \mathfrak{J}_3 > \mathfrak{J}_7 > \mathfrak{J}_5 > \mathfrak{J}_6 > \mathfrak{J}_2$
$\varrho = 11$	1.0000	0.8048	0.8733	0.9582	0.8174	0.8183	0.8303	$\mathfrak{J}_1 > \mathfrak{J}_4 > \mathfrak{J}_3 > \mathfrak{J}_7 > \mathfrak{J}_5 > \mathfrak{J}_6 > \mathfrak{J}_2$
$\varrho = 13$	1.0000	0.7984	0.8673	0.9560	0.8095	0.8125	0.8243	$\mathfrak{J}_1 > \mathfrak{J}_4 > \mathfrak{J}_3 > \mathfrak{J}_7 > \mathfrak{J}_6 > \mathfrak{J}_5 > \mathfrak{J}_2$
$\varrho = 17$	1.0000	0.7877	0.8576	0.9519	0.7962	0.8034	0.8143	$\mathfrak{J}_1 > \mathfrak{J}_4 > \mathfrak{J}_3 > \mathfrak{J}_7 > \mathfrak{J}_6 > \mathfrak{J}_5 > \mathfrak{J}_2$
$\varrho = 19$	1.0000	0.7832	0.8535	0.9501	0.7905	0.7997	0.8102	$\mathfrak{J}_1 > \mathfrak{J}_4 > \mathfrak{J}_3 > \mathfrak{J}_7 > \mathfrak{J}_6 > \mathfrak{J}_5 > \mathfrak{J}_2$
$\varrho = 23$	1.0000	0.7754	0.8464	0.9467	0.7805	0.7935	0.8030	$\mathfrak{J}_1 > \mathfrak{J}_4 > \mathfrak{J}_3 > \mathfrak{J}_7 > \mathfrak{J}_6 > \mathfrak{J}_5 > \mathfrak{J}_2$
$\varrho = 29$	1.0000	0.7659	0.8377	0.9422	0.7680	0.7861	0.7942	$\mathfrak{J}_1 > \mathfrak{J}_4 > \mathfrak{J}_3 > \mathfrak{J}_7 > \mathfrak{J}_6 > \mathfrak{J}_5 > \mathfrak{J}_2$

Table 13: Score values and ranking outcomes according to the parameter q by the 2TLq-ROFHWG operator.

Parameters	$\mathsf{F}(\mathfrak{J}_1)$	$\mathsf{F}(\mathfrak{J}_2)$	$\mathsf{F}(\mathfrak{J}_3)$	$\mathsf{F}(\mathfrak{J}_4)$	$\mathsf{F}(\mathfrak{J}_5)$	$\mathsf{F}(\mathfrak{J}_6)$	$\mathsf{F}(\mathfrak{J}_7)$	Ranking
$q = 2$	1.0000	0.9017	0.9616	0.9661	0.9231	0.9413	0.9254	$\mathfrak{J}_1 > \mathfrak{J}_4 > \mathfrak{J}_3 > \mathfrak{J}_6 > \mathfrak{J}_7 > \mathfrak{J}_5 > \mathfrak{J}_2$
$q = 3$	1.0000	0.8984	0.9632	0.9635	0.9198	0.9410	0.9274	$\mathfrak{J}_1 > \mathfrak{J}_4 > \mathfrak{J}_3 > \mathfrak{J}_6 > \mathfrak{J}_7 > \mathfrak{J}_5 > \mathfrak{J}_2$
$q = 5$	1.0000	0.9170	0.9730	0.9706	0.9324	0.9497	0.9492	$\mathfrak{J}_1 > \mathfrak{J}_3 > \mathfrak{J}_4 > \mathfrak{J}_6 > \mathfrak{J}_7 > \mathfrak{J}_5 > \mathfrak{J}_2$
$q = 7$	1.0000	0.9461	0.9843	0.9828	0.9562	0.9650	0.9731	$\mathfrak{J}_1 > \mathfrak{J}_3 > \mathfrak{J}_4 > \mathfrak{J}_7 > \mathfrak{J}_6 > \mathfrak{J}_5 > \mathfrak{J}_2$
$q = 11$	1.0000	0.9828	0.9980	0.9979	0.9877	0.9888	0.9960	$\mathfrak{J}_1 > \mathfrak{J}_3 > \mathfrak{J}_4 > \mathfrak{J}_7 > \mathfrak{J}_6 > \mathfrak{J}_5 > \mathfrak{J}_2$
$q = 13$	0.9993	0.9901	0.9999	1.0000	0.9935	0.9938	0.9986	$\mathfrak{J}_4 > \mathfrak{J}_3 > \mathfrak{J}_1 > \mathfrak{J}_7 > \mathfrak{J}_6 > \mathfrak{J}_5 > \mathfrak{J}_2$
$q = 17$	0.9979	0.9951	0.9999	1.0000	0.9971	0.9970	0.9988	$\mathfrak{J}_4 > \mathfrak{J}_3 > \mathfrak{J}_7 > \mathfrak{J}_1 > \mathfrak{J}_5 > \mathfrak{J}_6 > \mathfrak{J}_2$
$q = 19$	0.9980	0.9965	0.9999	1.0000	0.9980	0.9979	0.9989	$\mathfrak{J}_4 > \mathfrak{J}_3 > \mathfrak{J}_7 > \mathfrak{J}_1 = \mathfrak{J}_5 > \mathfrak{J}_6 > \mathfrak{J}_2$
$q = 23$	0.9986	0.9980	0.9999	1.0000	0.9990	0.9989	0.9992	$\mathfrak{J}_4 > \mathfrak{J}_3 > \mathfrak{J}_7 > \mathfrak{J}_5 > \mathfrak{J}_6 > \mathfrak{J}_1 > \mathfrak{J}_2$
$q = 29$	0.9993	0.9991	0.9999	1.0000	0.9995	0.9994	0.9996	$\mathfrak{J}_4 > \mathfrak{J}_3 > \mathfrak{J}_7 > \mathfrak{J}_5 > \mathfrak{J}_6 > \mathfrak{J}_1 > \mathfrak{J}_2$

Table 14: Score values and ranking outcomes according to the parameter ϱ by the 2TLq-ROFHWG operator.

Parameters	$\mathsf{F}(\mathfrak{J}_1)$	$\mathsf{F}(\mathfrak{J}_2)$	$\mathsf{F}(\mathfrak{J}_3)$	$\mathsf{F}(\mathfrak{J}_4)$	$\mathsf{F}(\mathfrak{J}_5)$	$\mathsf{F}(\mathfrak{J}_6)$	$\mathsf{F}(\mathfrak{J}_7)$	Ranking
$\varrho = 2$	1.0000	0.9075	0.9693	0.9698	0.9260	0.9451	0.9392	$\mathfrak{J}_1 > \mathfrak{J}_4 > \mathfrak{J}_3 > \mathfrak{J}_6 > \mathfrak{J}_7 > \mathfrak{J}_5 > \mathfrak{J}_2$
$\varrho = 3$	1.0000	0.9046	0.9674	0.9656	0.9233	0.9440	0.9366	$\mathfrak{J}_1 > \mathfrak{J}_3 > \mathfrak{J}_4 > \mathfrak{J}_6 > \mathfrak{J}_7 > \mathfrak{J}_5 > \mathfrak{J}_2$
$\varrho = 5$	1.0000	0.9023	0.9663	0.9614	0.9214	0.9440	0.9342	$\mathfrak{J}_1 > \mathfrak{J}_3 > \mathfrak{J}_4 > \mathfrak{J}_6 > \mathfrak{J}_7 > \mathfrak{J}_5 > \mathfrak{J}_2$
$\varrho = 7$	1.0000	0.9017	0.9663	0.9594	0.9210	0.9449	0.9333	$\mathfrak{J}_1 > \mathfrak{J}_3 > \mathfrak{J}_4 > \mathfrak{J}_6 > \mathfrak{J}_7 > \mathfrak{J}_5 > \mathfrak{J}_2$
$\varrho = 11$	1.0000	0.9020	0.9672	0.9577	0.9218	0.9471	0.9329	$\mathfrak{J}_1 > \mathfrak{J}_3 > \mathfrak{J}_4 > \mathfrak{J}_6 > \mathfrak{J}_7 > \mathfrak{J}_5 > \mathfrak{J}_2$
$\varrho = 13$	1.0000	0.9025	0.9677	0.9573	0.9225	0.9482	0.9330	$\mathfrak{J}_1 > \mathfrak{J}_3 > \mathfrak{J}_4 > \mathfrak{J}_6 > \mathfrak{J}_7 > \mathfrak{J}_5 > \mathfrak{J}_2$
$\varrho = 17$	1.0000	0.9037	0.9688	0.9569	0.9240	0.9502	0.9334	$\mathfrak{J}_1 > \mathfrak{J}_3 > \mathfrak{J}_4 > \mathfrak{J}_6 > \mathfrak{J}_7 > \mathfrak{J}_5 > \mathfrak{J}_2$
$\varrho = 19$	1.0000	0.9044	0.9694	0.9569	0.9248	0.9511	0.9337	$\mathfrak{J}_1 > \mathfrak{J}_3 > \mathfrak{J}_4 > \mathfrak{J}_6 > \mathfrak{J}_7 > \mathfrak{J}_5 > \mathfrak{J}_2$
$\varrho = 23$	1.0000	0.9056	0.9703	0.9569	0.9263	0.9528	0.9342	$\mathfrak{J}_1 > \mathfrak{J}_3 > \mathfrak{J}_4 > \mathfrak{J}_6 > \mathfrak{J}_7 > \mathfrak{J}_5 > \mathfrak{J}_2$
$\varrho = 29$	1.0000	0.9075	0.9716	0.9570	0.9285	0.9550	0.9351	$\mathfrak{J}_1 > \mathfrak{J}_3 > \mathfrak{J}_4 > \mathfrak{J}_6 > \mathfrak{J}_7 > \mathfrak{J}_5 > \mathfrak{J}_2$

ranking. Tables 13 and 14 demonstrate that when q and ϱ are changed, the ranking results are relatively stable, and the best alternative remained unchanged. The decision preference can be represented in the actual DM process by varying the values of q and ϱ to obtain the best decision result.

6.3. Comparative Analysis. In this subsection, we compare our proposed work with existing work to demonstrate its reliability and efficiency. Basically, we fused the concept of 2TLq-ROFS with the concept of the complex set to present HWA, HOWA, HHA, HWG, HOWG, and HHG in the context of 2TL$C q$-ROFS. In real-world problems, the 2TL$C q$-ROFS effectively deals with uncertain and linguistic information. Determining the weight of the criteria is seen as an important aspect of dealing with the MAGDM challenges. Different criteria may have different weights, and different weights of criteria may provide different results. It is challenging for experts to obtain accurate and objective weight values from real-world data. Because the method of obtaining weight values is complicated, the experts' knowledge and biases may impact their decisions. As a result, as an objective method, the COPRAS method is an excellent solution for addressing these problems. The COPRAS method has been investigated extensively in different MAGDM issues. We use various MAGDM strategies to address the network security service provider selection problem to verify the feasibility and superiority of our proposed method. To synthesize the individual assessments of the DMs, we use the 2TL$C q$-ROFHWA and 2TL$C q$-

Table 15: Evaluation outcomes by utilizing different aggregation operators based on the 2TLCq-ROFHWA operator.

Alternatives	2TLCq-ROFH	Ranking	2TLCq-ROFWA	Ranking	2TLCq-ROFEWA	Ranking
$\mathfrak{Z}_1$	1.0000	I	1.0000	I	1.0000	I
$\mathfrak{Z}_2$	0.8494	IV	0.8771	IV	0.8607	IV
$\mathfrak{Z}_3$	0.9146	III	0.9413	III	0.9254	III
$\mathfrak{Z}_4$	0.9693	VII	0.9724	V	0.9709	V
$\mathfrak{Z}_5$	0.8695	V	0.9006	VII	0.8822	VII
$\mathfrak{Z}_6$	0.8617	VI	0.8925	VI	0.8739	VI
$\mathfrak{Z}_7$	0.8716	II	0.8970	II	0.8820	II

Table 16: Evaluation outcomes by utilizing different aggregation operators based on the 2TLCq-ROFHWG operator.

Alternatives	2TLCq-ROFH	Ranking	2TLCq-ROFWG	Ranking	2TLCq-ROFEWG	Ranking
$\mathfrak{Z}_1$	1.0000	I	1.0000	I	1.0000	I
$\mathfrak{Z}_2$	0.9047	III	0.9138	IV	0.9075	IV
$\mathfrak{Z}_3$	0.9675	IV	0.9741	III	0.9693	III
$\mathfrak{Z}_4$	0.9656	IV	0.9784	VI	0.9698	VI
$\mathfrak{Z}_5$	0.9234	VII	0.9321	VII	0.9260	VII
$\mathfrak{Z}_6$	0.9441	V	0.9486	V	0.9451	V
$\mathfrak{Z}_7$	0.9366	II	0.9447	II	0.9392	II

Table 17: Evaluation outcomes by utilizing different FSs based on the 2TLCq-ROFHWA operator.

Alternatives	2TLCq-ROFH	Ranking	2TLCFFH	Ranking	2TLCPFH	Ranking	2TLCIFH	Ranking
$\mathfrak{Z}_1$	1.0000	I	1.0000	I	1.0000	I	1.0000	I
$\mathfrak{Z}_2$	0.8494	IV	0.8177	IV	0.7877	IV	0.7833	IV
$\mathfrak{Z}_3$	0.9146	III	0.8975	III	0.8865	III	0.8990	III
$\mathfrak{Z}_4$	0.9693	VII	0.9513	VII	0.9286	VI	0.9121	VI
$\mathfrak{Z}_5$	0.8695	V	0.8371	VI	0.8096	VII	0.8134	VII
$\mathfrak{Z}_6$	0.8617	VI	0.8394	V	0.8246	V	0.8387	V
$\mathfrak{Z}_7$	0.8716	II	0.8457	II	0.8228	II	0.8252	II

Table 18: Evaluation outcomes by utilizing different FSs based on the 2TLCq-ROFHWG operator.

Alternatives	2TLCq-ROFH	Ranking	2TLCFFH	Ranking	2TLCPFH	Ranking	2TLCIFH	Ranking
$\mathfrak{Z}_1$	1.0000	I	1.0000	I	1.0000	I	1.0000	I
$\mathfrak{Z}_2$	0.9047	III	0.8984	IV	0.9017	IV	0.9171	IV
$\mathfrak{Z}_3$	0.9675	IV	0.9632	III	0.9616	III	0.9639	III
$\mathfrak{Z}_4$	0.9656	VI	0.9635	VI	0.9661	VI	0.9745	VI
$\mathfrak{Z}_5$	0.9234	VII	0.9198	VII	0.9231	VII	0.9330	VII
$\mathfrak{Z}_6$	0.9441	V	0.9410	V	0.9413	V	0.9464	V
$\mathfrak{Z}_7$	0.9366	II	0.9274	II	0.9254	II	0.9341	II

ROFHWG operators. Comparative analysis with different FSs (2TLCIFH, 2TLCPFH, 2TLCFFH), aggregation operators (2TLCq-ROFWA, 2TLCq-ROFEWA, 2TLCq-ROFWG, 2TLCq-ROFEWG), and methods (CODAS, EDAS, TOPSIS) is illustrated as follows.

6.3.1. Comparative Analysis with Different Aggregation Operators. Our proposed operator is more realistic and superior because it can evaluate the interrelationship of fused arguments and scientifically consider the complexities of humans in practical MAGDM problems, whereas the 2TLCq-ROFWA (2TLCq-ROFWG) and 2TLCq-ROFEWA (2TLCq-ROFEWG) operators are unable to evaluate the interrelationships between fused arguments and cannot consider the complexity of DMs. As a result, proposed operators are more general in expressing fuzzy information.

The 2TLCq-ROFHWA and 2TLCq-ROFHWG operators can provide more effective and flexible information fusion, making it more suitable for dealing with MAGDM problems with dependent attributes, as demonstrated in Tables 15 and 16. As a result, our technique overcomes the constraints of 2TLCq-ROFWA (2TLCq-ROFWG) and 2TLCq-ROFEWA (2TLCq-ROFEWG) aggregation operators. As a result,

Table 19: Evaluation outcomes by utilizing different methodologies based on the 2TLCq-ROFHWA operator.

Alternatives	COPRAS	Ranking	CODAS	Ranking	EDAS	Ranking	TOPSIS	Ranking
$\mathfrak{Z}_1$	1.0000	I	−0.0439	IV	0.5277	VI	−1.3229	V
$\mathfrak{Z}_2$	0.8494	IV	0.0539	VII	0.5331	VII	−1.9971	III
$\mathfrak{Z}_3$	0.9146	III	−0.2050	II	0.2846	V	−1.1370	IV
$\mathfrak{Z}_4$	0.9693	VII	−0.5126	I	0.0000	II	−1.1445	I
$\mathfrak{Z}_5$	0.8695	V	−3.3930	III	0.5648	I	0.0000	II
$\mathfrak{Z}_6$	0.8617	VI	2.7821	IV	0.7304	III	−2.7610	VII
$\mathfrak{Z}_7$	0.8716	II	1.3185	V	0.5820	IV	−2.2180	VI

Table 20: Evaluation outcomes by utilizing different methodologies based on the 2TLCq-ROFHWG operator.

Alternatives	COPRAS	Ranking	CODAS	Ranking	EDAS	Ranking	TOPSIS	Ranking
$\mathfrak{Z}_1$	1.0000	I	−1.4587	VI	0.2452	VII	−0.2422	VII
$\mathfrak{Z}_2$	0.9047	III	1.4557	II	0.4219	V	−0.5476	IV
$\mathfrak{Z}_3$	0.9675	IV	0.8752	III	0.2846	IV	−0.6408	I
$\mathfrak{Z}_4$	0.9656	VI	−1.6952	VII	0.4511	II	−0.1472	II
$\mathfrak{Z}_5$	0.9234	VII	0.4201	V	0.4725	III	−0.6044	VI
$\mathfrak{Z}_6$	0.9441	V	1.6987	I	0.0913	I	−0.5873	V
$\mathfrak{Z}_7$	0.9366	II	−1.2959	IV	0.9024	VI	−0.0653	III

2TLCq-ROFHWA and 2TLCq-ROFHWG operators are highly suitable for dealing with MAGDM in a 2TLCq-ROF environment.

6.3.2. Comparative Analysis with Different Fuzzy Sets. We compared our suggested operators to the 2TLCIFH (for $q = 1$), 2TLCPFH (for $q = 2$), and 2TLCFFH (for $q = 3$) operators in this subsection. When we set the parameter $q = 1,2,3$, we can see that the 2TLCIFH, 2TLCPFH, and 2TLCFFH operators are all special cases of our approach. Clearly, our technique can represent more fuzzy information and is applicable in a wide range of real-world MAGDM situations. Furthermore, in a complicated DM environment, the DM's risk attitude is an important factor to consider; our method can accomplish this goal by changing the parameter q, whereas 2TLCIFH, 2TLCPFH, and 2TLCFFH operators cannot dynamically adjust the parameter based on the DM's risk attitude.

The characteristic of the proposed set is that the sum of q th power of MD and NMD is constrained to unit disc instead of real numbers in the range [0, 1]. As a result, our proposed work is more effective in solving MAGDM problems. The comparison of the proposed work with existing work is shown in Tables 17 and 18. Utilizing 2TLCq-ROFH, 2TLCFFH, 2TLCPFH, and 2TLCIFH operators the optimal alternative is $\mathfrak{Z}_1$ based on the 2TLCq-ROFHWA (2TLCq-ROFHWG) operator.

6.3.3. Comparative Analysis with Different MAGDM Methods. This subsection compares the proposed method to some existing methodologies in order to highlight the superiority of our method. To begin, our developed method is compared to CODAS, EDAS, and TOPSIS methods. We carefully calculate the results of these methods and compare them with our proposed method. For the CODAS, EDAS, and TOPSIS methods, the ranking order is $\mathfrak{Z}_6 > \mathfrak{Z}_7 > \mathfrak{Z}_2 > \mathfrak{Z}_1 > \mathfrak{Z}_3 > \mathfrak{Z}_4 > \mathfrak{Z}_5$, $\mathfrak{Z}_6 > \mathfrak{Z}_7 > \mathfrak{Z}_5 > \mathfrak{Z}_2 > \mathfrak{Z}_1 > \mathfrak{Z}_3 > \mathfrak{Z}_4$, and $\mathfrak{Z}_5 > \mathfrak{Z}_3 > \mathfrak{Z}_4 > \mathfrak{Z}_2 > \mathfrak{Z}_1 > \mathfrak{Z}_7 > \mathfrak{Z}_6$, respectively, based on the 2TLCq-ROFHWA operator in Table 19. Therefore, the best alternatives are $\mathfrak{Z}_6$, $\mathfrak{Z}_6$, and $\mathfrak{Z}_5$ according to CODAS, EDAS, and TOPSIS methods, respectively. However, in our purposed method (COPRAS), the ranking order is $\mathfrak{Z}_1 > \mathfrak{Z}_4 > \mathfrak{Z}_3 > \mathfrak{Z}_7 > \mathfrak{Z}_5 > \mathfrak{Z}_6 > \mathfrak{Z}_2$, and the best (worst) alternative is $\mathfrak{Z}_1$ ($\mathfrak{Z}_2$), based on the 2TLCq-ROFHWA operator as shown in Table 19.

In Table 20 the ranking order is $\mathfrak{Z}_6 > \mathfrak{Z}_2 > \mathfrak{Z}_3 > \mathfrak{Z}_5 > \mathfrak{Z}_7 > \mathfrak{Z}_1 > \mathfrak{Z}_4$, $\mathfrak{Z}_7 > \mathfrak{Z}_5 > \mathfrak{Z}_4 > \mathfrak{Z}_2 > \mathfrak{Z}_3 > \mathfrak{Z}_1 > \mathfrak{Z}_6$, and $\mathfrak{Z}_7 > \mathfrak{Z}_4 > \mathfrak{Z}_1 > \mathfrak{Z}_2 > \mathfrak{Z}_6 > \mathfrak{Z}_5 > \mathfrak{Z}_3$ for the CODAS, EDAS, and TOPSIS methods, respectively, based on the 2TLCq-ROFHWG operator. Therefore, the best alternatives are $\mathfrak{Z}_6$, $\mathfrak{Z}_7$, and $\mathfrak{Z}_7$ according to CODAS, EDAS, and TOPSIS methods, respectively. In our purposed method (COPRAS), the ranking order is $\mathfrak{Z}_1 > \mathfrak{Z}_3 > \mathfrak{Z}_4 > \mathfrak{Z}_6 > \mathfrak{Z}_7 > \mathfrak{Z}_5 > \mathfrak{Z}_2$, based on the 2TLC$q$-ROFHWG operator as shown in Table 20. However, the best and the worst alternative remains the same that are $\mathfrak{Z}_1$ and $\mathfrak{Z}_2$ that show the reliability and effectiveness of our purposed method.

6.4. Advantages of the Proposed Work. Different aggregation operators perform different functions, and the decision expert can select appropriate aggregation operators based on the real-world DM situation. In this subsection, we try to express how the presented approach is superior. The merits of our proposed method are summarized as follows:

(i) The presented method is superior to other existing methods because they effectively handle the interdependence of the multi-input arguments. Moreover, they have monotonicity for the parameter ϱ and can impact the risk perspective of the DMs. Thus, we can conclude that the proposed methods

are significantly preferable and have more comprehensive applications. The extended 2TLC_q-ROFH-COPRAS method utilizes 2TLC_q-ROFS as the information representation, and 2TLC_q-ROF can provide more comprehensive assessment details as it combines the excellent aspects of the C$_q$-ROFS and 2TL terms. Furthermore, 2TLC_q-ROFS can tackle realistic problems both quantitatively and qualitatively. Therefore, the proposed approach is clear and has less loss of data.

(ii) The 2TLC_q-ROFH-COPRAS method can provide more versatile and robust information fusion and make it more feasible to tackle risk MAGDM problems. It is based on the Hamacher operator so that the attribute's interrelationship can be interpreted and it can be widely applied in various cases by assigning preference values with different parameter t. Thus, the 2TLC_q-ROFH-COPRAS method has an excellent ability to describe the interaction among multi-input parameters and is efficiently applied in the information fusion process.

7. Conclusions

In this work, we contributed to the development of MAGDM by analyzing difficulties in a 2TLC_q-ROF context. The theoretical basis of aggregation operators must be carefully addressed in preparation for their use in decision-making. The inadequacies of existing methods, together with the advantageous properties of Hamacher aggregation operators, led us to evaluate their capacity to generate optimal combinations of 2TLC_q-ROFNs. The following conclusions can be drawn in summary:

(1) The 2TLC_q-ROFS idea has been used to describe uncertain data. The C$_q$-ROFS is an extended version of the CIFS and CPyFS. The C$_q$-ROFS is defined by two functions that express the degree of complex-valued membership and nonmembership. A flexible parameter q in C q-ROFS will influence its values to reflect information in a broader domain.

(2) The 2TL terms can better reflect the human perception and C$_q$-ROFSs are more reliable due to the q-th power of MD and NMD. So, we developed a new concept of the 2TLC_q-ROFS by incorporating the C$_q$-ROFS with 2TL terms.

(3) We expanded the arithmetic mean, geometric mean, and hybrid operators into the 2TLC_q-ROF environment and utilized Hamacher operational rules to propose six novel aggregation operators, the 2TLC_q-ROFHWA, 2TLC_q-ROFHOWA, 2TLC_q-ROFHHA, 2TLC_q-ROFHWG, 2TLC_q-ROFHOWG, and 2TLC_q-ROFHHG operators. Several novel characteristics of these proposed operators are being considered.

(4) Additionally, we developed a novel DM technique entitled the 2TLC_q-ROF-COPRAS approach for solving 2TLC_q-ROF-MAGDM problems.

(5) Finally, we solved a problem for selecting the best network security service provider by using our newly developed MAGDM approach.

In a nutshell, the fundamental contribution of this research is that it consolidates both the role of Hamacher aggregation operators and the favorable properties of 2TLC_q-ROFNs. This model of uncertain knowledge demonstrates its versatility in presenting vague and imprecise data in complex situations. So, our proposed approach is more generic and versatile than previous approaches.

Moreover, there are some limitations to this approach that should be taken into account in future studies. Firstly, this research focuses entirely on the aggregation of the 2TLC_q-ROFNs by utilizing Hamacher AOs. Future research will include a variety of assessment knowledge, such as triangular fuzzy numbers, interval-valued IF number, trapezoidal fuzzy number, and interval-valued picture fuzzy number with the integration of Hamacher operators. Therefore, this research will continue to expand. Secondly, the one parameter in our developed approach may present DMs with a quandary regarding how to choose the proper values of parameter in parameter analysis. A methodological combination with alternative techniques may therefore be justified for determining the quantities of parameters objectively. The DM approach based on the 2TLC_q-ROF-COPRAS method, which have complicated assessments due to the involvement of two-step aggregation: (1) for benefit attributes and (2) for cost attributes. Therefore, the DM approach can be expanded further with other MAGDM methods, namely, MABAC, EDAS, CODAS, and TOPSIS. In addition, no details were given of the parameter estimation of the attribute weighting values. In the future, more attention may receive on the development of innovative types of AOs, DM strategies [47–51], and distance measures for interval-valued C$_q$-ROFSs. Furthermore, Hamacher weighted average and geometric operators will be extended to (1) 2TL complex interval-valued q-ROFSs; (2) 2TL complex simplified interval-valued q-ROFSs; and (3) 2TL complex hesitant q-ROFSs.

Data Availability

No data were used to support this study.

Ethical Approval

This article does not contain any studies with human participants or animals performed by any of the authors.

Conflicts of Interest

The authors declare that they have no conflicts of interest.

Acknowledgments

The authors extend their appreciation to the Deanship of Scientific Research at King Khalid University for funding this work through General Research Project under grant number R.G.P.2/48/43.

References

[1] L. A. Zadeh, "Fuzzy sets," *Information and Control*, vol. 8, no. 3, pp. 338–353, 1965.

[2] K. T. Atanassov, "Intuitionistic fuzzy sets," *Fuzzy Sets and Systems*, vol. 20, no. 1, pp. 87–96, 1986.

[3] R. R. Yager, "Pythagorean membership grades in multicriteria decision making," *IEEE Transactions on Fuzzy Systems*, vol. 22, no. 4, pp. 958–965, 2013.

[4] T. Senapati and R. R. Yager, "Fermatean fuzzy sets," *Journal of Ambient Intelligence and Humanized Computing*, vol. 11, no. 2, pp. 663–674, 2020.

[5] R. R. Yager, "Generalized orthopair fuzzy sets," *IEEE Transactions on Fuzzy Systems*, vol. 25, no. 5, pp. 1222–1230, 2016.

[6] D. Ramot, R. Milo, M. Friedman, and A. Kandel, "Complex fuzzy sets," *IEEE Transactions on Fuzzy Systems*, vol. 10, no. 2, pp. 171–186, 2002.

[7] A. M. D. J. S. Alkouri and A. R. Salleh, "Complex intuitionistic fuzzy sets," in *Proceedings of the AIP Conference Proceedings*, vol. 1482, no. 1, pp. 464–470, American Institute of Physics, Antalya, Turkey, April 2012.

[8] A. U. M. Alkouri and A. R. Salleh, "Complex Atanassov's intuitionistic fuzzy relation," in *Abstract and Applied Analysis*vol. 2013, Hindawi, Article ID 287382, 18 pages, Hindawi, 2013.

[9] K. Ullah, T. Mahmood, Z. Ali, and N. Jan, "On some distance measures of complex Pythagorean fuzzy sets and their applications in pattern recognition," *Complex & Intelligent Systems*, vol. 6, no. 1, pp. 15–27, 2020.

[10] P. Liu, T. Mahmood, and Z. Ali, "Complex q -rung orthopair fuzzy aggregation operators and their applications in multi-attribute group decision making," *Information*, vol. 11, no. 1, p. 5, 2020.

[11] P. Liu, Z. Ali, and T. Mahmood, "Generalized complex q-rung orthopair fuzzy Einstein averaging aggregation operators and their application in multi-attribute decision making q-rung orthopair fuzzy Einstein averaging aggregation operators and their application in multi-attribute decision making," *Complex & Intelligent Systems*, vol. 7, no. 1, pp. 511–538, 2021.

[12] M. Akram, K. Zahid, and J. C. R. Alcantud, "A new outranking method for multicriteria decision making with complex Pythagorean fuzzy information," *Neural Computing & Applications*, vol. 34, no. 10, pp. 8069–8102, 2022.

[13] M. Akram, U. Amjad, J. C. R. Alcantud, and G. Santos-García, "Complex fermatean fuzzy N-soft sets: a new hybrid model with applications," *Journal of Ambient Intelligence and Humanized Computing*, pp. 1–34, 2022.

[14] L. A. Zadeh, "The concept of a linguistic variable and its application to approximate reasoning-I," *Information Sciences*, vol. 8, no. 3, pp. 199–249, 1975.

[15] P. Liu, "Some generalized dependent aggregation operators with intuitionistic linguistic numbers and their application to group decision making," *Journal of Computer and System Sciences*, vol. 79, no. 1, pp. 131–143, 2013.

[16] J.-q. Wang, Y. Yang, and L. Li, "Multi-criteria decision-making method based on single-valued neutrosophic linguistic Maclaurin symmetric mean operators," *Neural Computing & Applications*, vol. 30, no. 5, pp. 1529–1547, 2018.

[17] P. Liu and W. Liu, "Multiple-attribute group decision-making based on power Bonferroni operators of linguisticq-rung orthopair fuzzy numbers -rung orthopair fuzzy numbers," *International Journal of Intelligent Systems*, vol. 34, no. 4, pp. 652–689, 2019.

[18] F. Herrera and L. Martnez, "A 2-tuple fuzzy linguistic representation model for computing with words," *IEEE Transactions on Fuzzy Systems*, vol. 8, no. 6, pp. 746–752, 2000.

[19] M. Zhao, G. Wei, J. Wu, Y. Guo, and C. Wei, "TODIM method for multiple attribute group decision making based on cumulative prospect theory with 2-tuple linguistic neutrosophic sets," *International Journal of Intelligent Systems*, vol. 36, no. 3, pp. 1199–1222, 2021.

[20] Y. Zhang, G. Wei, Y. Guo, and C. Wei, "TODIM method based on cumulative prospect theory for multiple attribute group decision-making under 2-tuple linguistic Pythagorean fuzzy environment," *International Journal of Intelligent Systems*, vol. 36, no. 6, pp. 2548–2571, 2021.

[21] S. Naz and M. Akram, "Novel decision-making approach based on hesitant fuzzy sets and graph theory," *Computational and Applied Mathematics*, vol. 38, no. 1, p. 7, 2019.

[22] M. Akram, S. Naz, S. A. Edalatpanah, and R. Mehreen, "Group decision-making framework under linguistic q-rung orthopair fuzzy Einstein models q-rung orthopair fuzzy Einstein models," *Soft Computing*, vol. 25, no. 15, Article ID 10309, 2021.

[23] P. Liu, S. Naz, M. Akram, and M. Muzammal, "Group decision-making analysis based on linguistic q-rung orthopair fuzzy generalized point weighted aggregation operators," *International Journal of Machine Learning and Cybernetics*, vol. 13, no. 4, pp. 883–906, 2022.

[24] M. Akram, S. Naz, and F. Ziaa, "Novel decision making framework based on complex q-rung orthopair fuzzy information q -rung orthopair fuzzy information," *Scientia Iranica*, pp. 1–34, 2021.

[25] S. Naz, M. Akram, S. Alsulami, and F. Ziaa, "Decision-making analysis under interval-valued q -rung orthopair dual hesitant fuzzy environment," *International Journal of Computational Intelligence Systems*, vol. 14, no. 1, pp. 332–357, 2021.

[26] S. Naz, M. Akram, M. Akram, M. M. A. Al-Shamiri, M. M. Khalaf, and G. Yousaf, "A new MAGDM method with 2-tuple linguistic bipolar fuzzy Heronian mean operators," *Mathematical Biosciences and Engineering*, vol. 19, no. 4, pp. 3843–3878, 2022.

[27] H. Garg, S. Naz, F. Ziaa, and Z. Shoukat, "A ranking method based on Muirhead mean operator for group decision making with complex interval-valued q-rung orthopair fuzzy numbers q -rung orthopair fuzzy numbers," *Soft Computing*, vol. 25, no. 22, pp. 14001–14027, 2021.

[28] I. Beg and T. Rashid, "An intuitionistic 2-tuple linguistic information model and aggregation operators," *International Journal of Intelligent Systems*, vol. 31, no. 6, pp. 569–592, 2016.

[29] X. Deng, G. Wei, H. Gao, and J. Wang, "Models for safety assessment of construction project with some 2-tuple linguistic Pythagorean fuzzy Bonferroni mean operators," *IEEE Access*, vol. 6, Article ID 52105, 2018.

[30] Y. Rong, Y. Liu, and Z. Pei, "Complex q-rung orthopair fuzzy 2-tuple linguistic Maclaurin symmetric mean operators and its application to emergency program selection q -rung orthopair fuzzy 2-tuple linguistic Maclaurin symmetric mean operators and its application to emergency program selection," *International Journal of Intelligent Systems*, vol. 35, no. 11, pp. 1749–1790, 2020.

[31] P. Liu and P. Wang, "Some q-Rung Orthopair Fuzzy Aggregation Operators and their Applications to Multiple-Attribute Decision Making q -rung orthopair fuzzy aggregation operators and their applications to multiple-attribute decision making," *International Journal of Intelligent Systems*, vol. 33, no. 2, pp. 259–280, 2018.

[32] H. Hamacher, "Uber logische verknupfungen unscharfer aussagen und deren zugehrige bewertungsfunktionen," *Progress in Cybernetics and Systems Research*, vol. 3, pp. 276–288, 1978.

[33] M. Akram, X. Peng, and A. Sattar, "A new decision-making model using complex intuitionistic fuzzy Hamacher aggregation operators," *Soft Computing*, vol. 25, no. 10, pp. 7059–7086, 2021.

[34] S. Faizi, W. Sałabun, S. Nawaz, A. U. Rehman, and J. Wątróbski, "Best-Worst method and Hamacher aggregation operations for intuitionistic 2-tuple linguistic sets," *Expert Systems with Applications*, vol. 181, Article ID 115088, 2021.

[35] S. S. Rawat and K. Komal, "Multiple attribute decision making based on q-rung orthopair fuzzy Hamacher Muirhead mean operators -rung orthopair fuzzy Hamacher Muirhead mean operators," *Soft Computing*, vol. 26, no. 5, pp. 2465–2487, 2022.

[36] D. Pamucar, M. Deveci, I. Gokasar, and M. Popovic, "Fuzzy Hamacher WASPAS decision-making model for advantage prioritization of sustainable supply chain of electric ferry implementation in public transportation," *Environment, Development and Sustainability*, vol. 24, pp. 1–40, 2021.

[37] E. K. Zavadskas, A. Kaklauskas, and V. Sarka, "The new method of multicriteria complex proportional assessment of projects," *Technological and Economic Development of Economy*, vol. 1, no. 3, pp. 131–139, 1994.

[38] A. Arabameri, M. Yamani, B. Pradhan, A. Melesse, K. Shirani, and D. Tien Bui, "Novel ensembles of COPRAS multi-criteria decision-making with logistic regression, boosted regression tree, and random forest for spatial prediction of gully erosion susceptibility," *The Science of the Total Environment*, vol. 688, pp. 903–916, 2019.

[39] P. Chatterjee, V. M. Athawale, and S. Chakraborty, "Materials selection using complex proportional assessment and evaluation of mixed data methods," *Materials & Design*, vol. 32, no. 2, pp. 851–860, 2011.

[40] M. Alipour, R. Hafezi, P. Rani, M. Hafezi, and A. Mardani, "A new Pythagorean fuzzy-based decision-making method through entropy measure for fuel cell and hydrogen components supplier selection," *Energy*, vol. 234, Article ID 121208, 2021.

[41] A. Balali, A. Valipour, R. Edwards, and R. Moehler, "Ranking effective risks on human resources threats in natural gas supply projects using ANP-COPRAS method: case study of Shiraz," *Reliability Engineering & System Safety*, vol. 208, Article ID 107442, 2021.

[42] M. Narang, M. C. Joshi, and A. K. Pal, "A hybrid fuzzy COPRAS-base-criterion method for multi-criteria decision making," *Soft Computing*, vol. 25, no. 13, pp. 8391–8399, 2021.

[43] F. Herrera and E. Herrera-Viedma, "Linguistic decision analysis: steps for solving decision problems under linguistic information," *Fuzzy Sets and Systems*, vol. 115, no. 1, pp. 67–82, 2000.

[44] F. Herrera and L. Martinez, "An approach for combining linguistic and numerical information based on the 2-tuple fuzzy linguistic representation model in decision-making," *International Journal of Uncertainty, Fuzziness and Knowledge-Based Systems*, vol. 8, no. 5, pp. 539–562, 2000.

[45] W. Wang and X. Liu, "Intuitionistic fuzzy geometric aggregation operators based on Einstein operations," *International Journal of Intelligent Systems*, vol. 26, no. 11, pp. 1049–1075, 2011.

[46] X. Zhang, "A novel approach based on similarity measure for Pythagorean fuzzy multiple criteria group decision making," *International Journal of Intelligent Systems*, vol. 31, no. 6, pp. 593–611, 2016.

[47] S. Ashraf, S. Abdullah, and A. O. Almagrabi, "A new emergency response of spherical intelligent fuzzy decision process to diagnose of COVID19," *Soft Computing*, pp. 1–17, 2020.

[48] B. Batool, M. Ahmad, S. Abdullah, S. Ashraf, and R. Chinram, "Entropy based pythagorean probabilistic hesitant fuzzy decision making technique and its application for fog-haze factor Assessment problem," *Entropy*, vol. 22, no. 3, p. 318, 2020.

[49] B. Batool, S. S. Abosuliman, S. Abdullah, and S. Ashraf, "EDAS method for decision support modeling under the Pythagorean probabilistic hesitant fuzzy aggregation information," *Journal of Ambient Intelligence and Humanized Computing*, pp. 1–14, 2021.

[50] G. Kou, Ö Olgu Akdeniz, H. Dinçer, and S. Yüksel, "Fintech investments in European banks: a hybrid IT2 fuzzy multidimensional decision-making approach," *Financial Innovation*, vol. 7, no. 1, pp. 39–28, 2021.

[51] G. Kou, H. Xiao, M. Cao, and L. H. Lee, "Optimal computing budget allocation for the vector evaluated genetic algorithm in multi-objective simulation optimization," *Automatica*, vol. 129, Article ID 109599, 2021.

Hindawi
Complexity
Volume 2022, Article ID 3487355, 17 pages
https://doi.org/10.1155/2022/3487355

WILEY | Hindawi

Research Article

A Two-Level Metaheuristic for the Job-Shop Scheduling Problem with Multipurpose Machines

Pisut Pongchairerks

Thai-Nichi International College, Thai-Nichi Institute of Technology, Bangkok 10250, Thailand

Correspondence should be addressed to Pisut Pongchairerks; pisut@tni.ac.th

Received 21 November 2021; Revised 1 January 2022; Accepted 18 January 2022; Published 1 June 2022

Academic Editor: Yu Zhou

This paper proposes a two-level metaheuristic consisting of lower- and upper-level algorithms for the job-shop scheduling problem with multipurpose machines. The lower-level algorithm is a local search algorithm used for finding an optimal solution. The upper-level algorithm is a population-based metaheuristic used to control the lower-level algorithm's input parameters. With the upper-level algorithm, the lower-level algorithm can reach its best performance on every problem instance. Most changes of the proposed two-level metaheuristic from its original variants are in the lower-level algorithm. A main purpose of these changes is to increase diversity into solution neighborhood structures. One of the changes is that the neighbor operators of the proposed lower-level algorithm are developed to be more adjustable. Another change is that the roulette-wheel technique is applied for selecting a neighbor operator and for generating a perturbation operator. In addition, the proposed lower-level algorithm uses an adjustable delay-time limit to select an optional machine for each operation. The performance of the proposed two-level metaheuristic was evaluated on well-known benchmark instances. The evaluation's results indicated that the proposed two-level metaheuristic performs well on most benchmark instances.

1. Introduction

The job-shop scheduling problem (JSP) is a well-known NP-hard optimization problem [1–3]. JSP involves scheduling jobs onto machines in order to minimize *makespan*, i.e., the schedule's length. Each job consists of a number of operations, where each operation must be processed on a predetermined machine with a predetermined processing time. To complete each job, all of its operations must be processed in the sequence from the first to the last operations. JSP has many variants and related problems, such as [4–7]. One of the well-known variants of JSP is the job-shop scheduling problem with multipurpose machines (MPMJSP) [8–10]. MPMJSP is defined as a generalized variant of JSP. An only difference between them is that each operation in JSP has only one predetermined machine, while each operation in MPMJSP may have more than one optional machine. This difference makes MPMJSP be closer to the real-world applications in modern factories than JSP because, nowadays, most machines have been developed for multiple tasks.

In this paper, the research's objective is to develop a high-performing algorithm for MPMJSP. To do so, this paper proposes a two-level metaheuristic, based on the framework of [5, 11, 12], consisting of upper- and lower-level algorithms. The upper-level algorithm is a population-based metaheuristic that acts as a parameter controller for the lower-level algorithm. The upper-level algorithm's population consists of the parameter-value combinations of the lower-level algorithm. In a parameter-value combination, each parameter's value is iteratively changed by a sum of two changeable opposite-direction vectors. The directions of the first and the second vectors are toward and away from, respectively, the memorized best-found value. The lower-level algorithm is a local search algorithm searching for an optimal solution of the being-solved MPMJSP problem. Like other metaheuristics, the lower-level algorithm cannot perform its best on all instances with a single combination of

input-parameter values. This drawback can be overcome when its input parameters are controlled by the upper-level algorithm.

The proposed two-level metaheuristic is modified from its original variant [12], where the main differences are in their lower-level algorithms. Their lower-level algorithms both search for an optimal solution in hybrid neighborhood structures via their optional operators. Their optional neighbor operators are similarly modified from the traditional operators (i.e., swap, insert, and reverse) by limiting a distance between positions of two members selected in a solution-representing permutation. However, while the lower-level algorithm of [12] has only three levels of the distance limit, the distance limit in this paper is adjustable to any possible range. Another main difference is in their methods of generating their hybrid neighborhood structures. To generate each neighbor solution-representing permutation, the lower-level algorithm of [12] uses a given probability to select one of two neighbor operators. Instead, the proposed lower-level algorithm uses the roulette-wheel method [13] to select one from three neighbor operators. In this paper, the roulette-wheel method is also applied to select multiple optional operators for generating a perturbation operator. A purpose of using the roulette-wheel method is to diversify more on the hybridization of the neighborhood structure.

As mentioned, each operation in MPMJSP has one or more optional machines. The lower-level algorithm proposed in this paper uses the delay-time limit (δ), as its input parameter, to make a criterion of selecting a machine for each operation. This use of δ is different from the uses of δ in the other researches, e.g., [10, 11, 14–17]. While the proposed lower-level algorithm uses δ to select a machine for each operation, the other researches use δ to select an operation into a timetable. A method of generating a schedule of the proposed lower-level algorithm is briefly presented as follows: First, an appearance order of all operations in a solution-representing permutation is used as a priority order for all operations. Then, every operation is assigned one-by-one into a schedule by the given priority order. When being assigned, each operation must be processed on the machine that satisfies δ, and it must be started as early as the machine can.

The remainder of this paper is divided into five sections. Section 2 describes MPMJSP and reviews the previous researches relevant to the proposed two-level metaheuristic. Section 3 describes the proposed two-level metaheuristic in detail. Section 4 shows experiment's results of evaluating the proposed two-level metaheuristic's performance. Section 5 then analyzes and discusses the experiment's results. Finally, Section 6 concludes the research's findings.

2. Preliminaries

In this section, the description of MPMJSP is given in Section 2.1, and the review on the previous researches relevant to the proposed two-level metaheuristic is given in Section 2.2.

2.1. Description of MPMJSP. The job-shop scheduling problem with multipurpose machines (MPMJSP) is classified as a generalization of the job-shop scheduling problem (JSP). An only difference between JSP and MPMJSP is their numbers of optional machines of each operation. That is, while each operation in JSP has only one predetermined machine, each operation in MPMJSP has one or more optional machines. MPMJSP thus becomes JSP if each of its operations has only one optional machine. A similar variant of MPMJSP is the flexible job-shop scheduling problem (FJSP) [18, 19]. MPMJSP and FJSP both are the JSP's variants where each operation may have more than one optional machine. However, the processing time of an operation in FJSP may change when changing its selected optional machine, while the processing time of each operation in MPMJSP is fixed for all of its optional machines. This means MPMJSP is a specific FJSP where, for each operation, all optional machines have the same processing time.

Notation used to describe MPMJSP in this paper is defined below:

(i) Let n denote the number of all jobs in MPMJSP.

(ii) Let m denote the number of all machines in MPMJSP.

(iii) Let J_i denote the i-th job in MPMJSP, where $i = 1, 2, \ldots, n$.

(iv) Let M_j denote the j-th machine in MPMJSP, where $j = 1, 2, \ldots, m$.

(v) Let n_i denote the number of all operations of J_i.

(vi) Let O_{ik} denote the k-th operation of J_i, where $k = 1, 2, \ldots, n_i$.

(vii) Let τ_{ik} denote the processing time of O_{ik}.

(viii) Let m_{ik} denote the number of all optional machines of O_{ik}, where $i = 1, 2, \ldots, n$, and $k = 1, 2, \ldots, n_i$.

(ix) Let $E_{ikl} \in$ all optional machines of O_{ik} that appear in $\{M_1, M_2, \ldots, M_m\}$ and denote the l-th optional machine of O_{ik}, where $l = 1, 2, \ldots, m_{ik}$. In other words, E_{ikl} is equivalent to the M_j that owns the l-th lowest value of j among all optional machines of O_{ik}. For example, suppose O_{12} has three optional machines, i.e., M_2, M_4, and M_5. Thus, $E_{121} = M_2$, $E_{122} = M_4$, and $E_{123} = M_5$.

MPMJSP comes with n given jobs $(J_1, J_2, \ldots, J_n)$ and m given machines $(M_1, M_2, \ldots, M_m)$. Each job J_i consists of a sequence of n_i given operations $(O_{i1}, O_{i2}, \ldots, O_{in_i})$ as a chain of precedence constraints. To complete each job J_i, O_{i1} must be finished before O_{i2} can start; O_{i2} must be finished before O_{i3} can start, and so on. Each O_{ik} must be processed by one of $E_{ik1}, E_{ik2}, \ldots, E_{ikm_{ik}}$ with the processing time of τ_{ik}. Each machine cannot process more than one operation at a time, and it cannot be stopped during processing an operation. At the beginning (i.e., time 0), all jobs have already arrived, and all machines have not been occupied. An optimal schedule is a feasible schedule that minimizes makespan (i.e., the schedule's length).

MPMJSP was first introduced by Brucker and Schlie [8]. They also proposed a polynomial-time algorithm for MPMJSP with two jobs. MPMJSP with three jobs belongs to NP-hard problem even if the number of all machines is two [9]. Tabu-search algorithms were developed by [9] for solving three sets of MPMJSP benchmark instances, i.e., Edata, Rdata, and Vdata. Since then, these three instance sets have been commonly used for comparing results of different algorithms on MPMJSP. To date, many algorithms have been developed for solving MPMJSP and its closely related problems [10, 18–21].

2.2. Previous Relevant Researches. Iterated local search is traditionally defined as a single-solution-based metaheuristic that can search for a global optimal solution. During an exploration, it uses a neighbor operator repeatedly to find a local optimum and then uses a perturbation operator to escape the found local optimum. Note that a perturbation operator stands for an operator that generates a new initial solution by largely modifying a found local optimal solution [22]. Some untraditional iterated local search algorithms are enhanced in their performance by using multiple initial solutions [23, 24]. The iterated local search algorithms have been successful on many optimization problems, including MPMJSP and FJSP [25, 26].

In iterated local search and related algorithms, there are three operators usually used as neighbor operators and perturbation operators. These three operators are the traditional swap, insert, and reverse operators [27]. To explain the mentioned operators, let u and v be two different integers randomly generated from 1 to D, where D represents the number of all members in a solution-representing permutation. The swap operator is to swap between the two members in the u-th and the v-th positions of the permutation. The insert operator is to remove a member from the u-th position of the permutation and then insert it back at the v-th position. The reverse operator is to reverse the sequence of all members from the u-th to the v-th positions of the permutation.

A common drawback of most metaheuristics is that their performance is dependent on their parameter-value settings. To overcome such a drawback, many applications use upper-level algorithms to control parameters of their solution-searching algorithms [11, 12, 14, 15, 28–31]. Some of them, e.g., [5], require more than two levels of algorithms for very complicated problems; however, most of them require only two levels. For solving JSP, there are two two-level metaheuristics acting as adaptive iterated local search algorithms [11, 12]. In each of the two-level metaheuristics, the upper-level algorithm controls the lower-level algorithm's input parameters, while the lower-level algorithm is a local search algorithm searching for an optimal job-shop schedule.

UPLA and MUPLA are the upper-level algorithms in [11, 12], respectively; they both are population-based algorithms searching in real-number search spaces. In each of them, the population is a number of the parameter-value combinations of the lower-level algorithm. In a parameter-value combination, each parameter's value is iteratively changed by a sum of two changeable opposite-direction vectors. The first vector's and the second vector's directions are toward and away from, respectively, the memorized best-found value. In only MUPLA, each parameter-value combination includes a different start operation-based permutation; thus, the two-level metaheuristic of [12] has a multistart property.

LOLA, the lower-level algorithm in [11], is a local search algorithm exploring in a solution space of parameterized-active schedules (i.e., hybrid schedules [16]). Its input parameters (i.e., a delay-time limit, a scheduling direction, a perturbation operator, and a neighbor operator) are controlled by UPLA, its upper-level algorithm. Because the delay-time limit (δ) is one of the input parameters controlled, UPLA then can control the solution space's size of parameterized-active schedules. Such a control of δ follows in the successes of the two-level PSOs of [14, 15]. Other techniques of controlling δ can also be found in literature. For example, the value of δ in [10] is dependent on the number of jobs and the number of machines, while the value of δ in [17] is dependent on the algorithm's iteration index. In addition, the PSO in [32] controls the value of δ by using the concept of self-adaptive parameter control [28].

LOSAP, the lower-level algorithm in [12], is a local search algorithm searching in a probabilistic-based hybrid neighborhood structure. By a given probability, LOSAP randomly uses one from two predetermined operators to generate a neighbor solution-representing permutation. In other words, based on the given probability, LOSAP can switch between the two given operators anytime during its exploration. While the search performance of LOLA [11] is mainly based on its special solution space, that of LOSAP is mainly based on its hybrid neighborhood structure. LOSAP has multiple optional operators for its perturbation and neighbor operators. These optional operators are modified from the traditional operators by limiting the distance of v from u. For generating v in LOSAP, there are three optional distance-limit levels: $[u-4, u+4]$, $[u-(D/5), u+(D/5)]$, and $[1, D]$.

3. Proposed Two-Level Metaheuristic

For solving MPMJSP, this paper proposes the two-level metaheuristic consisting of the lower- and upper-level algorithms. In this section, MPM-LOLA and MPM-UPLA represent the lower-level algorithm and the upper-level algorithm, respectively. The description of MPM-LOLA is given in Section 3.1, and the description of MPM-UPLA is given in Section 3.2.

3.1. MPM-LOLA. MPM-LOLA, as a variant of LOLA [11] and LOSAP [12], is a local search algorithm exploring in a hybrid neighborhood structure. Similar to LOLA and LOSAP, MPM-LOLA generates its neighborhood structure by using multiple optional operators. However, there are many changes of MPM-LOLA from its older variants. Although MPM-LOLA uses the delay-time limit (δ) like LOLA does, it uses δ in different way and purpose. While LOLA

uses δ to select an operation, MPM-LOLA uses δ to select an optional machine for each operation. In the remaining other parts, MPM-LOLA is more similar to LOSAP than LOLA. The major changes of MPM-LOLA from LOSAP are summarized below:

(i) While the LOSAP's solution-decoding method generates JSP's solutions, the MPM-LOLA's solution-decoding method generates MPMJSP's solutions.

(ii) MPM-LOLA is similar to LOSAP in that its optional operators are modified from the traditional operators by limiting the distance of v from u. However, while LOSAP has only three levels of distance limit, the distance limit of MPM-LOLA is adjustable to any possible range.

(iii) Unlike LOSAP, MPM-LOLA applies the roulette-wheel method to select a neighbor operator. It also applies the roulette-wheel method to select optional operators for generating a perturbation operator.

For the purpose of clarification, the description of MPM-LOLA is divided into two parts: a description of its solution-decoding method and a description of its overall procedure. The solution-decoding method is described in Section 3.1.1, and the overall procedure is described in Section 3.1.2.

3.1.1. Solution-Decoding Method. MPM-LOLA decodes a solution-representing permutation into a schedule by using the delay-time limit (δ) and the tiebreak criterion (TB). Note that TB is used only if there is more than one optional machine that satisfies δ. In this paper, every solution-representing permutation is in a form of the operation-based permutation [33, 34]. An operation-based permutation is a permutation of numbers $1, 2, \ldots, n$ where the number i ($i = 1, 2, \ldots, n$) appears n_i times. Remind that n and n_i denote the number of all jobs and the number of all operations of the job J_i, respectively. In the permutation, the number i in its k-th appearance represents the operation O_{ik}. Then, a schedule is constructed by scheduling all operations one-by-one in the order given by the permutation. Each operation must be processed by its optional machine that satisfies δ and TB, and it must be started as early as this machine can. It is noticed that the use of δ in this paper is different from those in the other researches, e.g., [10, 11, 14–16]. While MPM-LOLA uses δ to select an optional machine for each operation, the other researches use δ to select an operation into the timetable.

As mentioned above, $\delta \in [0, 1)$ and $TB \in \{\text{lowest, highest}\}$ are used to select an optional machine for each operation. If $\delta = 0$, each operation must be processed on its optional machine that can start processing earliest. When the value of δ is assigned larger, the maximum delay-time allowed for each operation is then longer; consequently, it may increase the number of optional machines that satisfy δ for each operation. If there is more than one optional machine that satisfies δ, then TB is required as a tie breaker. If TB is selected to be lowest, the lowest-indexed optional machine that satisfies δ is selected; otherwise, the highest-indexed optional machine that satisfies δ is selected.

Algorithm 1 presents the solution-decoding method used by MPM-LOLA. The algorithm uses δ and TB, as its input parameters, to transform an operation-based permutation into an MPMJSP's solution. Note that Algorithm 1 may return a different schedule from the same operation-based permutation if the values of δ and TB are changed. Notation used in Algorithm 1 is defined below:

(i) Let D denote the number of all operations in the being-solved MPMJSP instance. Thus, $D = n_1 + n_2 + \ldots + n_n$, where n_i is the number of all operations of the job J_i ($i = 1, 2, \ldots, n$).

(ii) Let Π denote the sequence of operations transformed from the operation-based permutation.

(iii) Let Φ denote the schedule transformed from Π.

(iv) Let $O_{i'k'}$ denote the k'-th operation of the job $J_{i'}$, and it represents the as-yet-unscheduled operation that is currently in its turn to be scheduled.

(v) Let $m_{i'k'}$ denote the number of all optional machines of $O_{i'k'}$.

(vi) Let $E_{i'k'l}$ denote the l-th optional machine of $O_{i'k'}$, where $l = 1, 2, \ldots, m_{i'k'}$.

(vii) Let E denote the chosen machine for processing $O_{i'k'}$. This machine must be chosen from all $E_{i'k'l}$ ($l = 1, 2, \ldots, m_{i'k'}$).

(viii) Let δ be a real number within $[0, 1)$ and denote the delay-time limit.

(ix) Let $TB \in \{\text{lowest, highest}\}$ denote the tiebreak criterion for selecting an optional machine to process $O_{i'k'}$. It is used only if there is more than one optional machine that satisfies δ. If $TB = \text{lowest}$, let E be the machine with the lowest l from all $E_{i'k'l}$ (where $l = 1, 2, \ldots, m_{i'k'}$) that satisfy δ. If $TB = \text{highest}$, let E be the machine with the highest l from all $E_{i'k'l}$ (where $l = 1, 2, \ldots, m_{i'k'}$) that satisfy δ.

(x) Let $\tau_{i'k'}$ denote the processing time of $O_{i'k'}$.

(xi) Let σ_M denote the minimum of the earliest available times of all optional machines of $O_{i'k'}$.

(xii) Let σ_J denote the earliest possible start time of $O_{i'k'}$ in the job $J_{i'}$. This means σ_J is equal to the finished time of $O_{i'k'-1}$. If $O_{i'k'}$ has no immediate-preceding operation, then σ_J is equal to 0.

(xiii) Let σ denote the earliest possible start time of $O_{i'k'}$. It is equal to the maximum between σ_M and σ_J.

3.1.2. Procedure of MPM-LOLA. MPM-LOLA generates its neighborhood structure based on multiple optional operators. These optional operators consist of d-swap, d-insert, d-reverse, D-swap, D-insert, and D-reverse operators. Note that D-swap, D-insert, and D-reverse are identical to the traditional swap, insert, and reverse operators, respectively. Notation and terminologies used to define the mentioned operators are given below:

Step 1. Receive a δ's value, a *TB*'s value, and an operation-based permutation needed to be transformed from MPM-LOLA (Algorithm 2).
Step 2. Transform the operation-based permutation taken from Step 1 into Π by changing the number i in its k-th appearance into the operation O_{ik} ($i = 1, 2, \ldots, n$; $k = 1, 2, \ldots, n_i$). For example, the operation-based permutation (3, 2, 3, 1, 1, 2) is transformed into $\Pi = (O_{31}, O_{21}, O_{32}, O_{11}, O_{12}, O_{22})$.
Step 3. Transform Π into Φ by using Steps 3.1 to 3.6.
Step 3.1. Let $\Phi \longleftarrow$ an empty schedule, and let $t \longleftarrow 1$.
Step 3.2. Let $O_{i'k'} \longleftarrow$ the leftmost as-yet-unscheduled operation in Π.
Step 3.3. Find σ_M, σ_j, and σ of $O_{i'k'}$.
Step 3.4. Let $E \longleftarrow$ the machine, chosen from all $E_{i'k'l}$ ($l = 1, 2, \ldots, m_{i'k'}$), that can start processing not-later-than $\sigma + \delta\tau_{i'k'}$. If there is more than one machine that can be chosen as E, then choose one of them that has the lowest l if TB = lowest; otherwise, choose one of them that has the highest l.
Step 3.5. Modify Φ by assigning E to process $O_{i'k'}$. In the schedule, let E start processing $O_{i'k'}$ as early as possible.
Step 3.6. If $t < D$, then $t \longleftarrow t + 1$ and repeat from Step 3.2. Otherwise, go to Step 4.
Step 4. Return Φ as the complete schedule to MPM-LOLA (Algorithm 2).

Algorithm 1: Solution-decoding method.

(i) Let u and v be integers used to point at the two member positions in an operation-based permutation.

(ii) Let d denote a distance limit of v from u. It is used for specifying d-swap, d-insert, and d-reverse.

(iii) Let D denote the number of all members in the solution-representing permutation, which equals the number of all operations in the MPMJSP instance. Thus, $D = n_1 + n_2 + \ldots + n_n$, where n_i is the number of all operations of the job J_i.

(iv) d-swap is to swap two members in the u-th and the v-th positions in the permutation. Let u be randomly selected from 1 to D. Then, let v be randomly selected from $\max(1, u - d)$ to $\min(u + d, D)$ except u.

(v) d-insert is to remove a member from the u-th position in the permutation and then insert it into the v-th position. Let u be randomly selected from 1 to D. Then, let v be randomly selected from $\max(1, u - d)$ to $\min(u + d, D)$ except u.

(vi) d-reverse is to reverse the positions of all members from the u-th to the v-th positions in the permutation. Let u be randomly selected from 1 to D. Then, let v be randomly selected from $\max(1, u - d)$ to $\min(u + d, D)$ except u.

(vii) D-swap is to swap two members in the u-th and the v-th positions in the permutation. Let u and v be two different integers randomly selected from 1 to D.

(viii) D-insert is to remove a member from the u-th position in the permutation and then insert it into the v-th position. Let u and v be two different integers randomly selected from 1 to D.

(ix) D-reverse is to reverse the positions of all members from the u-th to the v-th positions in the permutation. Let u and v be two different integers randomly selected from 1 to D.

Before an execution, eight MPM-LOLA's input parameters must be assigned values. The first input parameter, denoted by P, is the start operation-based permutation. The remaining seven input parameters consist of two parameters for specifying a perturbation operator, three parameters for generating its neighbor operators, and two parameters for selecting an optional machine. In MPM-LOLA, the perturbation operator is to randomly use one from D-swap, D-insert, and D-reverse on the start operation-based permutation n times (remind that n denotes the number of all jobs). In each of these n random selections, the roulette-wheel technique is applied to select one from D-swap, D-insert, and D-reverse. The probabilities of selecting D-swap and D-insert in the roulette wheel are the second and the third input parameters of MPM-LOLA, respectively. Consequently, the probability of selecting D-reverse is unity subtracted by the sum of the probabilities of selecting D-swap and D-insert.

The fourth to the sixth input parameters are used to generate MPM-LOLA's neighbor operators (i.e., d-swap, d-insert, and d-reverse). The fourth input parameter, denoted by d, is the distance limit of v from u for specifying d-swap, d-insert, and d-reverse. Then, MPM-LOLA uses the roulette-wheel technique to randomly select one from d-swap, d-insert, and d-reverse to generate a neighbor solution-representing permutation. In the roulette wheel, the probabilities of selecting d-swap and d-insert are the fifth and the sixth input parameters, respectively. The probability of selecting d-reverse is thus unity subtracted by the sum of the probabilities of selecting d-swap and d-insert.

The delay-time limit (δ) and the tiebreak criterion (TB) are the MPM-LOLA's seventh and eighth input parameters, respectively. These two input parameters are used to select an optional machine for each operation in constructing a schedule. Thus, instead of using δ and TB by MPM-LOLA itself, MPM-LOLA transfers the values of δ and TB into its solution-decoding method (Algorithm 1).

The overall procedure of MPM-LOLA is given in Algorithm 2. Notation used in Algorithm 2 is defined below:

Step 1. Receive values of its eight input parameters (i.e., P, ρ_S, ρ_I, d, ρ_{NS}, ρ_{NI}, δ, and TB) from MPM-UPLA (Algorithm 3).
Step 2. Generate P_0 from P by using Steps 2.1 to 2.4.
  Step 2.1. Let $r \longleftarrow 1$.
  Step 2.2. Randomly generate $p \sim U[0, 1)$.
  Step 2.3. Modify P by using D-swap if $p < \rho_S$, D-insert if $\rho_S \leq p < \rho_S + \rho_I$, and D-reverse otherwise.
  Step 2.4. If $r < n$, let $r \longleftarrow r + 1$ and repeat from Step 2.2. Otherwise, let $P_0 \longleftarrow P$ and go to Step 3.
Step 3. Execute Algorithm 1, with the taken values of δ and TB, for transforming P_0 into S_0.
Step 4. Find a local optimal schedule by using Steps 4.1 to 4.5.
  Step 4.1. Let $t_L \longleftarrow 0$.
  Step 4.2. Randomly generate $p \sim U[0, 1)$.
  Step 4.3. Generate P_1 from P_0 by using d-swap if $p < \rho_{NS}$, d-insert if $\rho_{NS} \leq p < \rho_{NS} + \rho_{NI}$, and d-reverse otherwise.
  Step 4.4. Execute Algorithm 1, with the taken values of δ and TB, for transforming P_1 into S_1.
  Step 4.5. Update P_0, S_0, and t_L by using Steps 4.5.1 to 4.5.3.
    Step 4.5.1. If $Makespan(S_1) < Makespan(S_0)$, then let $P_0 \longleftarrow P_1$ and $S_0 \longleftarrow S_1$, and repeat from Step 4.1.
    Step 4.5.2. If $Makespan(S_1) = Makespan(S_0)$, then let $P_0 \longleftarrow P_1$ and $S_0 \longleftarrow S_1$, and repeat from Step 4.2.
    Step 4.5.3. If $Makespan(S_1) > Makespan(S_0)$, then let $t_L \longleftarrow t_L + 1$. If $t_L < D^2$, repeat from Step 4.2; otherwise, go to Step 5.
Step 5. Return P_0 and S_0 as the final (best-found) operation-based permutation and the final (best-found) schedule, respectively, to MPM-UPLA (Algorithm 3).

Algorithm 2: MPM-LOLA's procedure.

(i) Let D denote the number of all operations in the being-solved MPMJSP instance. Thus, $D = n_1 + n_2 + \ldots + n_n$, where n_i is the number of all operations of the job J_i.

(ii) Let d denote the distance limit of v from u in the operation-based permutation for specifying d-swap, d-insert, and d-reverse.

(iii) Let ρ_S and ρ_I, which are real numbers within [0, 1), denote the probabilities of selecting D-swap and D-insert, respectively. Thus, the probability of selecting D-reverse is $1 - \rho_S - \rho_I$.

(iv) Let ρ_{NS} and ρ_{NI}, which are real numbers within [0, 1), denote the probabilities of selecting d-swap and d-insert, respectively. Thus, the probability of selecting d-reverse is $1 - \rho_{NS} - \rho_{NI}$.

(v) Let δ, which is a real number within [0, 1), denote the delay-time limit for selecting an optional machine for each operation.

(vi) Let $TB \in \{\text{lowest, highest}\}$ denote the tiebreak criterion for selecting an optional machine for each operation.

(vii) Let P denote the start operation-based permutation.

(viii) Let P_0 denote the current best-found operation-based permutation. An initial P_0 is generated from P via the perturbation operator.

(ix) Let S_0, which is decoded from P_0, denote the current best-found schedule. In addition, $Makespan(S_0)$ stands for the makespan of S_0.

(x) Let P_1 denote the current neighbor operation-based permutation.

(xi) Let S_1, which is decoded from P_1, denote the current neighbor schedule. In addition, $Makespan(S_1)$ stands for the makespan of S_1.

3.2. MPM-UPLA. MPM-UPLA is an upper-level algorithm of the proposed two-level metaheuristic. It uses the same framework of the upper-level algorithms of [11, 12]. MPM-UPLA is thus a population-based search algorithm that acts as a parameter controller. It evolves the MPM-LOLA's input-parameter values, so that MPM-LOLA can return its best performance on every single MPMJSP instance. At the t-th iteration, the MPM-UPLA's population consists of N combinations of the MPM-LOLA's input-parameter values, i.e., $C_1(t)$, $C_2(t)$, ..., $C_N(t)$. In short, let a *parameter-value combination* stand for a combination of the MPM-LOLA's input-parameter values. Let $C_g(t) \equiv (c_{1g}(t), c_{2g}(t), \ldots, c_{9g}(t))$ denote the g-th parameter-value combination (where $g = 1, 2, \ldots, N$) in the population at the t-th iteration. It represents the value combination of the MPM-LOLA's input parameters, i.e., P, ρ_S, ρ_I, d, ρ_{NS}, ρ_{NI}, and TB.

The delay-time limit, δ, is an important MPM-LOLA's input parameter controlled by MPM-UPLA. However, the value of δ is not assigned as a member in $C_g(t)$, but it is controlled by the MPM-UPLA's iteration index, t. At the first MPM-UPLA's iteration ($t = 1$), the value of δ is set to be 0.0 for MPM-LOLA. For every next 50 MPM-UPLA's iterations, the value of δ is increased by 0.2 for MPM-LOLA. This setting of δ was based on the result of a preliminary study of this research. It found that the control of δ using the MPM-UPLA's iteration index usually performs better than the control of δ using $C_g(t)$.

The transformations from the $C_g(t)$'s members into MPM-LOLA's parameter values are described below:

(i) Let $c_{1g}(t)$ represent P. In other words, P is directly equal to $c_{1g}(t)$ in the transformation.

(ii) Let $c_{2g}(t)$, $c_{3g}(t)$, and $c_{4g}(t) \in \mathbb{R}$ be used together to determine the values of ρ_S and ρ_I. Their transformations are given in (1) and (2).

$$\rho_S = \frac{\max\left(0, c_{2g}(t)\right)}{\max\left(0, c_{2g}(t)\right) + \max\left(0, c_{3g}(t)\right) + \max\left(0, c_{4g}(t)\right)}, \quad (1)$$

$$\rho_I = \frac{\max\left(0, c_{3g}(t)\right)}{\max\left(0, c_{2g}(t)\right) + \max\left(0, c_{3g}(t)\right) + \max\left(0, c_{4g}(t)\right)}. \quad (2)$$

(iii) Let $c_{5g}(t) \in \mathbb{R}$ be used to determine the value of d. In its transformation, let d be equal to the rounded integer from $1 + Dc_{5g}(t)$, where D is the number of all operations in the MPMJSP instance. After that, reassign $d = 1$ if $d < 1$, and reassign $d = D$ if $d > D$.

(iv) Let $c_{6g}(t)$, $c_{7g}(t)$, and $c_{8g}(t) \in \mathbb{R}$ be used together to determine the values of ρ_{NS} and ρ_{NI}. Their transformations are given in (3) and (4).

$$\rho_{NS} = \frac{\max\left(0, c_{6g}(t)\right)}{\max\left(0, c_{6g}(t)\right) + \max\left(0, c_{7g}(t)\right) + \max\left(0, c_{8g}(t)\right)}, \quad (3)$$

$$\rho_{NI} = \frac{\max\left(0, c_{7g}(t)\right)}{\max\left(0, c_{6g}(t)\right) + \max\left(0, c_{7g}(t)\right) + \max\left(0, c_{8g}(t)\right)}. \quad (4)$$

(v) Let $c_{9g}(t) \in \mathbb{R}$ be used to determine the value of TB. In its transformation, let TB = lowest if $c_{9g}(t) < 0.5$, and let TB = highest if $c_{9g}(t) \geq 0.5$.

The overall procedure of MPM-UPLA is given in Algorithm 3. Notation used in Algorithm 3 is defined below:

(i) Let N denote the number of all parameter-value combinations in the MPM-UPLA's population.

(ii) Let $C_g(t) \equiv (c_{1g}(t), c_{2g}(t), \ldots, c_{9g}(t))$ denote the g-th parameter-value combination (where $g = 1, 2, \ldots, N$) in the MPM-UPLA's population at the t-th iteration.

(iii) Let $Score(C_g(t))$ denote the performance score of $C_g(t)$. Note that the lower the performance score, the better the performance.

(iv) After executing MPM-LOLA with the parameter values given by $C_g(t)$, let its final (best-found) operation-based permutation and final (best-found) schedule be denoted by $P_{fg}(t)$ and $S_{fg}(t)$, respectively.

(v) Let $Makespan(S_{fg}(t))$ denote the makespan of $S_{fg}(t)$.

(vi) Let $C_{\text{best}} \equiv (c_{1\text{best}}, c_{2\text{best}}, \ldots, c_{9\text{best}})$ denote the best parameter-value combination ever found by the population. In addition, let $Score(C_{\text{best}})$ denote the performance score of C_{best}.

(vii) Let S_{best} denote the best schedule ever found by the population.

4. Experiment's Results

In this paper, an experiment was conducted to compare MPM-UPLA's results with those of TS, PSO, and CP. Let TS, PSO, and CP represent the tabu-search algorithm [9], the particle swarm optimization algorithm [10], and the ILOG constraint programming optimizer [20], respectively. These three algorithms were chosen because they perform well on the same benchmark instance sets used in this paper's experiment. In Sections 4 and 5, let MPM-UPLA stand for the whole two-level metaheuristic, i.e., MPM-UPLA combined with MPM-LOLA. The reason is that MPM-UPLA uses MPM-LOLA as its component when solving MPMJSP.

In the comparison, this paper's experiment used three benchmark instance sets, i.e., Edata, Rdata, and Vdata, taken from [9, 20, 21]. Each instance set consists of 66 instances, modified from the well-known JSP benchmark instances [35–39]. The difference among the three instance sets is the number of optional machines of each operation in their instances. In Edata, the average number of optional machines of each operation is 1.15, and the maximum number of optional machines of each operation is 2 or 3. In Rdata, the average number and the maximum number of optional machines of each operation are 2 and 3, respectively. In Vdata, the average number and the maximum number of optional machines of each operation are $0.5m$ and $0.8m$, respectively (where m = the number of all machines in an instance).

The parameter settings of MPM-UPLA used in the experiment are shown below:

(i) The population of MPM-UPLA consisted of three parameter-value combinations (i.e., $N = 3$ in Algorithm 3).

(ii) The stopping criterion of MPM-UPLA was to stop when any of the below conditions was satisfied:

(a) The 1,000-th iteration (i.e., $t = 1{,}000$ in Algorithm 3) was reached.

(b) The 150-th minute of computational time was reached.

(c) The known optimal solution was found. If the optimal solution has been yet unknown, its lower bound [20, 21] was used instead.

(iii) MPM-UPLA was coded in C# and executed on an Intel® Core™ i7-3520M @ 2.90 GHz with RAM of 4 GB (3.87 GB useable).

(iv) For each instance, MPM-UPLA was executed five trials with different random-seed numbers.

With the above settings, the experiment's results on Edata, Rdata, and Vdata are presented in Tables 1 to 3, respectively. These tables first show the name, size, and best-known solution value of each instance. The best-known solution value, given by literature, stands for the upper bound of the optimal solution value. For each instance, each table then shows the best-found solution values of TS [9], PSO [10], CP [20], and MPM-UPLA. The best-found solution values of TS, PSO, and CP are their best solution values taken from their original articles [9, 10] and [20], respectively. For MPM-UPLA, its best-found solution value on each instance is a minimum of the best-found solution values from its five trials in this experiment. Each table also shows an average of the best-found solution values, the average number of used iterations, and the average computational time from the MPM-UPLA's five trials on each instance.

Step 1. Receive a value of N and a stopping criterion from a user. Let $t \longleftarrow 1$, $\delta \longleftarrow 0.0$, and $Score(C_{\text{best}}) \longleftarrow +\infty$.
Step 2. Generate $C_g(t) \equiv (c_{1g}(t), c_{2g}(t), \ldots, c_{9g}(t))$, where $g = 1, 2, \ldots, N$, by using Steps 2.1 to 2.4.
Step 2.1. Let $g \longleftarrow 1$.
Step 2.2. Randomly generate $c_{1g}(t)$ from any possible operation-based permutation.
Step 2.3. Randomly generate $c_{2g}(t), c_{3g}(t), \ldots, c_{9g}(t) \sim U[0, 1)$.
Step 2.4. If $g < N$, let $g \longleftarrow g + 1$ and repeat from Step 2.2. Otherwise, go to Step 3.
Step 3. Evaluate $Score(C_g(t))$, and update C_{best} and S_{best} by using Steps 3.1 to 3.6.
Step 3.1. Let $g \longleftarrow 1$.
Step 3.2. Transform $C_g(t)$ into the values of P, ρ_S, ρ_I, d, ρ_{NS}, ρ_{NI}, and TB.
Step 3.3. Execute MPM-LOLA (Algorithm 2) with the last-updated values of P, ρ_S, ρ_I, d, ρ_{NS}, ρ_{NI}, TB, and δ in order to receive $P_{fg}(t)$ and $S_{fg}(t)$.
Step 3.4. Let $Score(C_g(t)) \longleftarrow Makespan(S_{fg}(t))$.
Step 3.5. If $Score(C_g(t)) \leq Score(C_{\text{best}})$, then let $C_{\text{best}} \longleftarrow C_g(t)$, $Score(C_{\text{best}}) \longleftarrow Score(C_g(t))$, and $S_{\text{best}} \longleftarrow S_{fg}(t)$.
Step 3.6. If $g < N$, let $g \longleftarrow g + 1$ and repeat from Step 3.2. Otherwise, go to Step 4.
Step 4. Update $C_g(t+1)$, where $g = 1, 2, \ldots, N$, by using Steps 4.1 to 4.5.
Step 4.1. Let $g \longleftarrow 1$.
Step 4.2. Let $c_{1g}(t+1) \longleftarrow P_{fg}(t)$.
Step 4.3. If $(t+1) \bmod 50 = 0$, let $\delta \longleftarrow \delta + 0.2$. After that, reassign $\delta \longleftarrow 0.999$ if $\delta \geq 1.0$.
Step 4.4. If $(t+1) \bmod 50 = 0$, randomly generate $c_{2g}(t+1), c_{3g}(t+1), \ldots, c_{9g}(t+1) \sim U[0, 1)$. Otherwise, generate $c_{qg}(t+1)$, where $q = 2, 3, \ldots, 9$, by using the below equation. Let u_1 and $u_2 \sim U[0, 1)$.

$$c_{qg}(t+1) = \begin{cases} c_{qg}(t) + 0.05u_1 - 0.01u_2 & \text{if } c_{qg}(t) < c_{q\text{best}}, \\ c_{qg}(t) - 0.05u_1 + 0.01u_2 & \text{if } c_{qg}(t) > c_{q\text{best}}, \\ c_{qg}(t) + 0.01u_1 - 0.01u_2 & \text{if } c_{qg}(t) = c_{q\text{best}}. \end{cases}$$

Step 4.5. If $g < N$, then let $g \longleftarrow g + 1$ and repeat from Step 4.2. Otherwise, go to Step 5.
Step 5. If the stopping criterion is not met, then let $t \longleftarrow t + 1$ and repeat from Step 2. Otherwise, return S_{best} as the final result to the user.

Algorithm 3: MPM-UPLA's procedure.

Notation and terminologies used for each instance in Tables 1 to 3 are given as follows:

(i) Let *Instance* column present the name of each instance.

(ii) Let n and m denote the number of all jobs and the number of all machines, respectively, in the instance.

(iii) Let a *solution* denote an MPMJSP's schedule, and let a *solution value* denote a makespan of an MPMJSP's schedule.

(iv) Let *BKS* column present the best-known solution value given by literature, e.g., [20, 21]. If the best-known solution value has been proven to be an optimal solution value, it is presented without parentheses. Otherwise, it is an upper bound of the optimal solution value and is presented within parentheses.

(v) If the best-found solution value of MPM-UPLA is better than the best-known solution value given by literature, let the best-found solution value of MPM-UPLA become the new best-known solution value. When such a case occurs, an arrow symbol ($\longrightarrow$) is given in front of the value.

(vi) Let *Best* represent the best-found solution value of each algorithm. *Best* of MPM-UPLA was taken from the five trials in this experiment. *Bests* of TS, PSO, and CP were taken from [9, 10] and [20], respectively. N/A means the best-found solution value does not appear in the original article.

(vii) Let *Avg* represent the average of the best-found solution values of the five trials of MPM-UPLA.

(viii) Let *No of Iters* and *Time* stand for the average number of iterations and the average computational time (in HH:MM:SS format), respectively, until the MPM-UPLA's stopping criterion is met.

For each instance set, Table 4 shows *Avg %BD* of each algorithm on each instance category. Of each algorithm, *%BD* of each instance denotes a percent deviation of the best-found solution value from the best-known solution value. Then, *Avg %BD* denotes an average of *%BDs* of all instances in their category. In Table 4, each instance is classified into one of 13 instance categories, based on its source and size. The details of these 13 categories are given below:

(i) M6-20 consists of three instances, i.e., M6, M10, and M20.

(ii) LA1-5 consists of five 10-job/5-machine instances, i.e., LA1, LA2, ..., LA5.

(iii) LA6-10 consists of five 15-job/5-machine instances, i.e., LA06, LA07, ..., LA10.

(iv) LA11-15 consists of five 20-job/5-machine instances, i.e., LA11, LA12, ..., LA15.

(v) LA16-20 consists of five 10-job/10-machine instances, i.e., LA16, LA17, ..., LA20.

Table 1: Results on Edata.

Instance	n, m	BKS	Best of TS [9]	Best of PSO [10]	Best of CP [20]	MPM-UPLA			
						Best	Avg	No of Iters	Time
M6	6, 6	55	57	55	55	55	55.0	1	< 1 sec.
M10	10, 10	871	917	892	877	873	875.0	1000	0:26:10
M20	20, 5	1088	1109	1116	1088	1090	1090.2	1000	0:31:11
LA1	10, 5	609	611	609	609	609	609.0	1	< 1 sec.
LA2	10, 5	655	655	655	655	655	655.0	3	< 1 sec.
LA3	10, 5	550	573	567	567	550	550.0	89	0:00:19
LA4	10, 5	568	578	582	568	568	568.0	25	0:00:05
LA5	10, 5	503	503	503	503	503	503.0	1	< 1 sec.
LA6	15, 5	833	833	833	833	833	833.0	1	< 1 sec.
LA7	15, 5	762	765	765	765	762	762.0	377	0:04:02
LA8	15, 5	845	845	845	845	845	845.0	3	0:00:01
LA9	15, 5	878	878	878	878	878	878.0	1	< 1 sec.
LA10	15, 5	866	866	866	866	866	866.0	1	< 1 sec.
LA11	20, 5	1103	1106	1103	1106	1103	1103.0	246	0:05:09
LA12	20, 5	960	960	960	960	960	960.0	1	0:00:02
LA13	20, 5	1053	1053	1053	1053	1053	1053.0	1	0:00:01
LA14	20, 5	1123	1151	1123	1123	1123	1123.0	2	0:00:02
LA15	20, 5	1111	1111	1111	1111	1111	1111.0	2	0:00:03
LA16	10, 10	892	924	893	904	892	892.0	4	0:00:07
LA17	10, 10	707	757	707	707	707	707.0	3	0:00:04
LA18	10, 10	842	864	847	843	842	842.0	250	0:06:00
LA19	10, 10	796	850	820	799	796	796.0	161	0:04:20
LA20	10, 10	857	919	859	857	857	857.0	6	0:00:11
LA21	15, 10	1009	1066	1057	1044	1021	1025.0	1000	1:42:08
LA22	15, 10	880	919	912	887	882	883.2	1000	1:39:29
LA23	15, 10	950	980	994	950	950	950.0	68	0:06:38
LA24	15, 10	908	952	939	913	909	909.2	1000	1:39:33
LA25	15, 10	936	970	974	955	945	945.2	1000	1:31:55
LA26	20, 10	1106	1169	1173	1143	1115	1123.0	543	2:30:09
LA27	20, 10	1181	1230	1247	1188	1182	1188.8	552	2:30:12
LA28	20, 10	1142	1204	1195	1153	1149	1149.0	566	2:30:08
LA29	20, 10	1107	1210	1175	1128	1124	1130.2	555	2:30:08
LA30	20, 10	(1193)	1253	1262	1241	1220	1223.4	551	2:30:19
LA31	30, 10	(1532)	1596	1620	1552	1541	1541.0	195	2:30:31
LA32	30, 10	1698	1769	1743	1698	1698	1698.0	2	0:01:19
LA33	30, 10	1547	1575	1578	1560	1547	1547.0	2	0:01:22
LA34	30, 10	1599	1627	1662	1609	1608	1608.8	259	2:30:09
LA35	30, 10	1736	1736	1736	1736	1736	1736.0	1	0:01:06
LA36	15, 15	1160	1247	1202	1160	1160	1161.8	307	1:49:22
LA37	15, 15	1397	1453	1425	1397	1397	1397.0	41	0:11:14
LA38	15, 15	1141	1185	1209	1146	1143	1148.2	424	2:30:18
LA39	15, 15	1184	1226	1220	1184	1186	1187.4	423	2:30:14
LA40	15, 15	1144	1214	1197	1174	1150	1153.6	391	2:30:05
ABZ5	10, 10	1167	N/A	N/A	1176	1167	1167.0	235	0:06:08
ABZ6	10, 10	925	N/A	N/A	925	925	925.0	35	0:00:49
ABZ7	20, 15	(610)	N/A	N/A	638	619	621.0	150	2:30:44
ABZ8	20, 15	(637)	N/A	N/A	654	648	650.0	152	2:30:37
ABZ9	20, 15	644	N/A	N/A	668	655	656.6	155	2:30:26
CAR1	11, 5	6176	N/A	N/A	6176	6176	6182.0	723	0:03:37
CAR2	13, 4	6327	N/A	N/A	6455	6432	6433.6	1000	0:05:05
CAR3	12, 5	6856	N/A	N/A	6856	6856	6875.8	780	0:04:25
CAR4	14, 4	7789	N/A	N/A	7789	7789	7789.0	1	< 1 sec.
CAR5	10, 6	7229	N/A	N/A	7229	7229	7229.0	41	0:00:15
CAR6	8, 9	7990	N/A	N/A	8478	7990	7990.0	62	0:00:33
CAR7	7, 7	6123	N/A	N/A	6123	6123	6123.0	6	0:00:01
CAR8	8, 8	7689	N/A	N/A	7689	7689	7689.0	9	0:00:04
ORB1	10, 10	977	N/A	N/A	988	977	977.0	223	0:06:25
ORB2	10, 10	865	N/A	N/A	870	865	865.0	53	0:01:21
ORB3	10, 10	951	N/A	N/A	960	952	952.0	1000	0:26:46

Table 1: Continued.

Instance	n, m	BKS	Best of TS [9]	Best of PSO [10]	Best of CP [20]	MPM-UPLA			
						Best	Avg	No of Iters	Time
ORB4	10, 10	984	N/A	N/A	1016	984	984.0	255	0:06:47
ORB5	10, 10	842	N/A	N/A	865	842	842.0	215	0:05:27
ORB6	10, 10	958	N/A	N/A	1004	958	958.0	93	0:02:48
ORB7	10, 10	387	N/A	N/A	387	389	389.0	1000	0:26:27
ORB8	10, 10	894	N/A	N/A	894	894	894.0	15	0:00:23
ORB9	10, 10	933	N/A	N/A	933	933	933.0	121	0:03:14
ORB10	10, 10	933	N/A	N/A	937	933	933.0	226	0:06:02

Table 2: Results on Rdata.

Instance	n, m	BKS	Best of TS [9]	Best of PSO [10]	Best of CP [20]	MPM-UPLA			
						Best	Avg	No of Iters	Time
M6	6, 6	47	47	47	47	47	47.0	1	< 1 sec.
M10	10, 10	686	737	724	686	686	686.0	29	0:01:10
M20	20, 5	1022	1028	1025	1024	1022	1022.0	22	0:00:46
LA1	10, 5	(571)	574	574	573	571	571.0	1000	0:04:50
LA2	10, 5	529	535	534	534	530	530.8	1000	0:04:51
LA3	10, 5	477	481	480	478	478	478.0	1000	0:05:43
LA4	10, 5	502	509	506	504	502	502.8	878	0:04:31
LA5	10, 5	457	460	459	458	457	457.6	648	0:03:03
LA6	15, 5	799	801	800	799	799	799.0	15	0:00:13
LA7	15, 5	749	752	750	750	749	749.0	158	0:02:38
LA8	15, 5	765	767	767	766	765	765.0	183	0:02:54
LA9	15, 5	853	859	854	854	853	853.0	100	0:01:29
LA10	15, 5	804	806	806	805	804	804.0	274	0:03:55
LA11	20, 5	1071	1073	1072	1072	1071	1071.0	3	0:00:07
LA12	20, 5	936	937	936	936	936	936.0	2	0:00:04
LA13	20, 5	1038	1039	1039	1038	1038	1038.0	2	0:00:03
LA14	20, 5	1070	1071	1070	1071	1070	1070.0	4	0:00:07
LA15	20, 5	1089	1093	1090	1091	1089	1089.0	67	0:02:21
LA16	10, 10	717	717	732	717	717	717.0	2	0:00:05
LA17	10, 10	646	646	654	646	646	646.0	1	0:00:02
LA18	10, 10	666	674	694	666	666	666.0	72	0:02:49
LA19	10, 10	700	725	730	703	700	701.2	534	0:22:48
LA20	10, 10	756	756	756	757	756	756.0	1	0:00:03
LA21	15, 10	(829)	861	916	845	844	846.6	617	2:30:04
LA22	15, 10	(753)	790	839	775	772	774.6	754	2:30:05
LA23	15, 10	(832)	884	892	857	850	856.2	665	2:30:04
LA24	15, 10	(801)	825	870	818	821	823.0	723	2:30:06
LA25	15, 10	(782)	823	858	805	802	804.0	785	2:30:04
LA26	20, 10	(1059)	1086	1114	1074	1067	1068.2	218	2:30:31
LA27	20, 10	(1087)	1109	1141	1101	1095	1098.4	249	2:30:15
LA28	20, 10	(1077)	1097	1135	1084	1083	1086.0	227	2:30:07
LA29	20, 10	(996)	1016	1046	1006	1003	1004.6	258	2:30:08
LA30	20, 10	(1072)	1105	1148	1087	1087	1090.2	257	2:30:15
LA31	30, 10	⟶1520	1532	1549	1525	1520	1523.2	61	2:16:01
LA32	30, 10	(1658)	1668	1691	1664	1659	1660.4	65	2:30:56
LA33	30, 10	(1498)	1511	1530	1502	1498	1500.2	70	2:30:47
LA34	30, 10	(1536)	1542	1556	1542	1536	1537.2	70	2:31:01
LA35	30, 10	(1550)	1559	1577	1556	1551	1551.8	73	2:31:01
LA36	15, 15	1023	1054	1119	1034	1026	1033.0	213	2:30:17
LA37	15, 15	1062	1122	1190	1084	1084	1086.0	219	2:30:21
LA38	15, 15	954	1004	1063	973	976	976.0	249	2:30:18
LA39	15, 15	1011	1041	1131	1018	1024	1025.2	258	2:30:26
LA40	15, 15	955	1009	1057	984	977	984.0	169	2:30:33
ABZ5	10, 10	954	N/A	N/A	962	959	960.0	1000	0:48:07
ABZ6	10, 10	807	N/A	N/A	807	807	807.0	4	0:00:08
ABZ7	20, 15	(527)	N/A	N/A	544	547	548.8	57	2:32:24

Table 2: Continued.

Instance	n, m	BKS	Best of TS [9]	Best of PSO [10]	Best of CP [20]	MPM-UPLA			
						Best	Avg	No of Iters	Time
ABZ8	20, 15	(540)	N/A	N/A	555	561	565.2	67	2:31:02
ABZ9	20, 15	(539)	N/A	N/A	562	555	565.2	68	2:31:18
CAR1	11, 5	(5035)	N/A	N/A	5057	5050	5053.4	1000	0:07:21
CAR2	13, 4	(5986)	N/A	N/A	5987	5986	5986.0	1000	0:05:45
CAR3	12, 5	(5623)	N/A	N/A	5626	5625	5629.2	1000	0:10:00
CAR4	14, 4	(6515)	N/A	N/A	6518	6515	6515.2	1000	0:07:25
CAR5	10, 6	5615	N/A	N/A	5764	5680	5691.4	1000	0:09:24
CAR6	8, 9	6147	N/A	N/A	6147	6147	6147.0	17	0:00:12
CAR7	7, 7	4425	N/A	N/A	4432	4425	4430.6	803	0:04:07
CAR8	8, 8	5692	N/A	N/A	5692	5692	5692.0	99	0:00:54
ORB1	10, 10	746	N/A	N/A	763	746	746.0	20	0:00:40
ORB2	10, 10	696	N/A	N/A	703	696	698.4	807	0:32:37
ORB3	10, 10	712	N/A	N/A	720	715	716.0	1000	0:44:29
ORB4	10, 10	753	N/A	N/A	753	753	753.0	8	0:00:22
ORB5	10, 10	639	N/A	N/A	643	639	639.0	325	0:15:04
ORB6	10, 10	754	N/A	N/A	766	754	754.0	145	0:05:35
ORB7	10, 10	302	N/A	N/A	302	302	303.4	866	0:38:49
ORB8	10, 10	639	N/A	N/A	651	641	641.0	1000	0:42:24
ORB9	10, 10	694	N/A	N/A	694	694	694.0	33	0:01:27
ORB10	10, 10	742	N/A	N/A	750	742	743.4	847	0:41:27

Table 3: Results on Vdata.

Instance	n, m	BKS	Best of TS [9]	Best of PSO [10]	Best of CP [20]	MPM-UPLA			
						Best	Avg	No of Iters	Time
M6	6, 6	47	47	47	47	47	47.0	1	< 1 sec.
M10	10, 10	655	655	655	655	655	655.0	1	0:00:01
M20	20, 5	1022	1023	1024	1023	1022	1022.0	4	0:00:10
LA1	10, 5	570	573	571	570	570	570.2	431	0:02:30
LA2	10, 5	529	531	530	529	529	529.0	134	0:00:43
LA3	10, 5	477	482	479	478	477	477.8	875	0:04:58
LA4	10, 5	502	504	504	502	502	502.0	345	0:01:48
LA5	10, 5	457	464	460	458	457	457.4	527	0:02:43
LA6	15, 5	799	802	799	799	799	799.0	6	0:00:05
LA7	15, 5	749	751	750	750	749	749.0	103	0:01:47
LA8	15, 5	765	766	766	766	765	765.0	96	0:01:39
LA9	15, 5	853	854	855	854	853	853.0	28	0:00:28
LA10	15, 5	804	805	805	804	804	804.0	124	0:02:04
LA11	20, 5	1071	1073	1071	1071	1071	1071.0	1	0:00:03
LA12	20, 5	936	940	936	936	936	936.0	1	0:00:03
LA13	20, 5	1038	1040	1038	1038	1038	1038.0	4	0:00:08
LA14	20, 5	1070	1071	1070	1070	1070	1070.0	2	0:00:03
LA15	20, 5	1089	1091	1090	1090	1089	1089.0	36	0:01:21
LA16	10, 10	717	717	717	717	717	717.0	1	0:00:02
LA17	10, 10	646	646	646	646	646	646.0	1	0:00:02
LA18	10, 10	663	663	663	663	663	663.0	1	0:00:02
LA19	10, 10	617	617	619	617	617	617.0	3	0:00:10
LA20	10, 10	756	756	756	756	756	756.0	1	0:00:02
LA21	15, 10	(802)	826	819	804	817	822.2	501	2:30:08
LA22	15, 10	(735)	745	755	736	755	756.4	536	2:30:11
LA23	15, 10	(812)	826	828	815	826	831.2	533	2:30:06
LA24	15, 10	(775)	796	790	775	793	797.4	589	2:30:06
LA25	15, 10	(753)	770	775	756	768	770.2	562	2:30:08
LA26	20, 10	(1053)	1058	1058	1054	1073	1075.8	267	2:30:24
LA27	20, 10	1084	1088	1091	1084	1106	1110.2	260	2:30:20
LA28	20, 10	1069	1073	1076	1070	1091	1094.6	253	2:30:20
LA29	20, 10	(994)	995	1003	995	1010	1013.6	241	2:30:18
LA30	20, 10	(1069)	1071	1078	1072	1085	1093.8	222	2:30:17

Table 3: Continued.

Instance	n, m	BKS	Best of TS [9]	Best of PSO [10]	Best of CP [20]	MPM-UPLA			
						Best	Avg	No of Iters	Time
LA31	30, 10	1520	1521	1524	1522	1538	1540.6	82	2:31:00
LA32	30, 10	(1658)	1658	1664	1661	1681	1686.6	79	2:31:10
LA33	30, 10	(1498)	1498	1503	1500	1511	1519.2	79	2:31:12
LA34	30, 10	1535	1536	1541	1537	1557	1561.4	84	2:30:49
LA35	30, 10	1549	1553	1555	1551	1563	1570.8	74	2:31:05
LA36	15, 15	948	948	955	948	948	948.0	4	0:03:21
LA37	15, 15	986	986	993	986	986	986.0	54	0:49:27
LA38	15, 15	943	943	943	943	943	943.0	1	0:00:38
LA39	15, 15	922	922	945	922	922	922.0	27	0:24:02
LA40	15, 15	955	955	955	955	955	955.0	1	0:00:41
ABZ5	10, 10	859	N/A	N/A	860	859	859.0	12	0:00:53
ABZ6	10, 10	742	N/A	N/A	742	742	742.0	1	0:00:04
ABZ7	20, 15	(495)	N/A	N/A	495	535	536.0	86	2:30:44
ABZ8	20, 15	(509)	N/A	N/A	509	554	554.8	84	2:30:58
ABZ9	20, 15	(499)	N/A	N/A	500	540	541.8	85	2:31:11
CAR1	11, 5	5005	N/A	N/A	5013	5007	5007.0	1000	0:08:30
CAR2	13, 4	5929	N/A	N/A	5930	5929	5929.0	255	0:01:22
CAR3	12, 5	(5598)	N/A	N/A	5600	5601	5601.4	1000	0:10:41
CAR4	14, 4	6514	N/A	N/A	6517	6514	6514.0	199	0:01:22
CAR5	10, 6	(4913)	N/A	N/A	4932	4935	4941.0	1000	0:11:21
CAR6	8, 9	5486	N/A	N/A	5486	5486	5486.0	1	0:00:01
CAR7	7, 7	4281	N/A	N/A	4281	4281	4281.0	1	0:00:00
CAR8	8, 8	4613	N/A	N/A	4613	4613	4613.0	2	0:00:02
ORB1	10, 10	695	N/A	N/A	695	695	695.0	1	0:00:01
ORB2	10, 10	620	N/A	N/A	620	620	620.0	1	0:00:04
ORB3	10, 10	648	N/A	N/A	648	648	648.0	1	0:00:02
ORB4	10, 10	753	N/A	N/A	753	753	753.0	1	0:00:02
ORB5	10, 10	584	N/A	N/A	584	584	584.0	1	0:00:04
ORB6	10, 10	715	N/A	N/A	715	715	715.0	1	0:00:01
ORB7	10, 10	275	N/A	N/A	275	275	275.0	10	0:00:32
ORB8	10, 10	573	N/A	N/A	573	573	573.0	1	0:00:02
ORB9	10, 10	659	N/A	N/A	659	659	659.0	1	0:00:03
ORB10	10, 10	681	N/A	N/A	681	681	681.0	1	0:00:03

(vi) LA21-25 consists of five 15-job/10-machine instances, i.e., LA21, LA22, . . ., LA25.

(vii) LA26-30 consists of five 20-job/10-machine instances, i.e., LA26, LA27, . . ., LA30.

(viii) LA31-35 consists of five 30-job/10-machine instances, i.e., LA31, LA32, . . ., LA35.

(ix) LA36-40 consists of five 15-job/15-machine instances, i.e., LA36, LA37, . . ., LA40.

(x) ABZ5-6 consists of two 10-job/10-machine instances, i.e., ABZ5 and ABZ6.

(xi) ABZ7-9 consists of three 20-job/15-machine instances, i.e., ABZ7, ABZ8, and ABZ9.

(xii) CAR1-8 consists of eight instances, i.e., CAR1, CAR2, . . ., CAR8.

(xiii) ORB1-10 consists of ten 10-job/10-machine instances, i.e., ORB1, ORB2, . . ., ORB10.

In addition to the 13 categories, Table 4 includes four more instance categories, i.e., M6-LA40, SM-M6-LA40, M6-ORB10, and SM-M6-ORB10. These additional categories were used for comparing performance of the algorithms. SM in SM-M6-LA40 and SM-M6-ORB10 indicates that these categories contain only small-to-medium instances. Let instances be defined as small-to-medium instances if their $nm < 150$ and large instances otherwise (where $n =$ the number of jobs and $m =$ the number of machines). The details of these four additional categories are given below:

(i) M6-LA40 consists of the first 43 instances of all 66 instances, starting from M6 to LA40. These 43 instances were used by TS [9] and PSO [10] in their original articles.

(ii) SM-M6-LA40 consists of all 23 small-to-medium instances from M6-LA40.

(iii) M6-ORB10 consists of all 66 instances, starting from M6 to ORB10. These 66 instances were used by CP [20] in its original article.

(iv) SM-M6-ORB10 consists of all 43 small-to-medium instances from M6-ORB10.

5. Result Analysis and Discussion

This section analyzes and discusses the results shown in Section 4. Like Section 4, MPM-UPLA in this section stands for the whole two-level metaheuristic, i.e., MPM-UPLA

Table 4: Avg %BDs.

Category	No. of instances	n, m	Edata				Rdata				Vdata			
			TS	PSO	CP	MPM-UPLA	TS	PSO	CP	MPM-UPLA	TS	PSO	CP	MPM-UPLA
M6-20	3	Vary	3.62	1.66	0.23	0.14	2.67	1.94	0.07	0.00	0.03	0.07	0.03	0.00
LA01-05	5	10, 5	1.25	1.11	0.62	0.00	0.91	0.67	0.42	0.08	0.78	0.37	0.09	0.00
LA06-10	5	15, 5	0.08	0.08	0.08	0.00	0.37	0.18	0.10	0.00	0.20	0.12	0.08	0.00
LA11-15	5	20, 5	0.55	0.00	0.05	0.00	0.17	0.06	0.07	0.00	0.22	0.02	0.02	0.00
LA16-20	5	10, 10	5.46	0.79	0.37	0.00	0.95	2.36	0.11	0.00	0.00	0.06	0.00	0.00
LA21-25	5	15, 10	4.34	4.10	1.37	0.50	4.65	9.49	2.58	2.31	2.21	2.33	0.23	2.13
LA26-30	5	20, 10	5.92	5.64	2.16	1.06	2.30	5.53	1.15	0.83	0.30	0.70	0.11	1.82
LA31-35	5	30, 10	2.38	2.87	0.55	0.23	0.65	1.82	0.35	0.02	0.08	0.35	0.14	1.16
LA36-40	5	15, 15	5.01	3.85	0.61	0.17	4.51	11.08	1.77	1.65	0.00	0.79	0.00	0.00
ABZ5-6	2	10, 10	N/A	N/A	0.39	0.00	N/A	N/A	0.42	0.26	N/A	N/A	0.06	0.00
ABZ7-9	3	20, 15	N/A	N/A	3.66	1.64	N/A	N/A	3.42	3.55	N/A	N/A	0.07	8.38
CAR1-8	8	Vary	N/A	N/A	1.02	0.21	N/A	N/A	0.42	0.19	N/A	N/A	0.08	0.07
ORB1-10	10	10, 10	N/A	N/A	1.39	0.06	N/A	N/A	0.96	0.07	N/A	N/A	0.00	0.00
M6-LA40	43	Vary	3.16	2.26	0.69	0.24	1.87	3.76	0.77	0.57	0.44	0.56	0.08	0.59
SM-M6-LA40	23	$nm <$ 150	2.07	0.65	0.27	0.02	0.87	0.96	0.16	0.02	0.26	0.13	0.04	0.00
M6-ORB10	66	Vary	N/A	N/A	0.96	0.26	N/A	N/A	0.87	0.57	N/A	N/A	0.07	0.78
SM- M6-ORB10	43	$nm <$ 150	N/A	N/A	0.67	0.07	N/A	N/A	0.55	0.24	N/A	N/A	0.04	0.01

combined with MPM-LOLA. The performance of MPM-UPLA was compared with the performance of TS [9], PSO [10], and CP [20] via three performance indicators. These indicators are the number of instances achieved in finding the best-known solutions, the number of instances won by an algorithm against another, and the average percent deviation of the algorithm's best-found solution value from the best-known solution value (*Avg %BD*). Of each instance, the best-known solution value means the best solution value found by the published literature. An only exception is in LA31 of Rdata, where its best-known solution value was taken from the best-found solution value of MPM-UPLA. The reason is that, in LA31 of Rdata, MPM-UPLA found the better solution than the previously published best-known solution.

For each instance set, this section separates analyses on the first 43 instances from those on all 66 instances. The reason is that the results of TS and PSO were given on only the 43 instances in their original articles [9, 10], while the results of CP were given on the 66 instances in its original article [20]. In addition, this section separates analyses on small-to-medium instances from those on all given instances. Note that all instances with $nm < 150$ are defined as small-to-medium instances (where n = the number of jobs and m = the number of machines). Sections 5.1 to 5.3 show the analyses and discussions via the three given indicators. Then, Section 5.4 provides an overall summary from Sections 5.1 to 5.3.

5.1. The Number of Instances Achieved in Finding the Best-Known Solutions. Of each instance set, this section first compares the number of instances achieved in finding the best-known solutions by MPM-UPLA with those by TS, PSO, and CP on the first 43 instances. The numbers of instances achieved by each algorithm in Edata, Rdata, and Vdata were counted from Tables 1, 2, and 3, respectively. For the first 43 instances, MPM-UPLA obviously outperforms the three other algorithms on all three instance sets, especially Rdata. Of each instance set, the comparison results are given below:

(i) For the first 43 instances of Edata, the algorithms TS, PSO, CP, and MPM-UPLA reach the best-known solutions on 10, 15, 22, and 27 instances, respectively.

(ii) For the first 43 instances of Rdata, the algorithms TS, PSO, CP, and MPM-UPLA reach the best-known solutions on 4, 4, 8, and 24 instances, respectively. MPM-UPLA also found a new best-known solution value (i.e., 1520) for LA31 of Rdata. This value is defined as the optimal solution value because it equals the optimal solution value's lower bound given in [20].

(iii) For the first 43 instances of Vdata, the algorithms TS, PSO, CP, and MPM-UPLA reach the best-known solutions on 14, 13, 23, 28 instances, respectively.

Of each instance set, this section then compares the number of instances achieved by MPM-UPLA with that by CP on all 66 instances. For all 66 instances, MPM-UPLA outperforms CP on all three instance sets, especially Rdata. Of each instance set, the comparison results are given below:

(i) For all 66 instances of Edata, CP and MPM-UPLA reach the best-known solutions on 32 and 44 instances, respectively.

(ii) For all 66 instances of Rdata, CP and MPM-UPLA reach the best-known solutions on 14 and 38 instances, respectively.

(iii) For all 66 instances of Vdata, CP and MPM-UPLA reach the best-known solutions on 39 and 45, respectively.

Thus, as a conclusion, MPM-UPLA outperforms TS, PSO, and CP in finding the best-known solutions on all three instance sets, especially Rdata. On Rdata, the number of instances achieved by MPM-UPLA is more than double the number of instances achieved by each of the others. Moreover, MPM-UPLA also found the new best-known solution value on LA31 of Rdata.

5.2. The Number of Instances Won. This section first compares the number of instances won by MPM-UPLA with those by TS, PSO, and CP on the first 43 instances of each instance set. Note that in the first 43 instances, there are 23 small-to-medium instances included. The numbers of instances won in Edata, Rdata, and Vdata were counted from Tables 1, 2, and 3, respectively. For the first 43 instances, MPM-UPLA obviously outperforms the three other algorithms on Edata and Rdata; MPM-UPLA outperforms TS and PSO but underperforms CP on Vdata. However, when considering only the 23 small-to-medium instances, MPM-UPLA outperforms CP on Vdata. Of each instance set, the comparison results are detailed below:

(i) Out of the first 43 instances of Edata, MPM-UPLA has 33 wins, 10 draws, and 0 losses against TS; it has 28 wins, 15 draws, and 0 losses against PSO. In addition, it has 21 wins, 20 draws, and 2 losses against CP.

(ii) Out of the first 43 instances of Rdata, MPM-UPLA has 39 wins, 4 draws, and 0 losses against each of TS and PSO. In addition, it has 29 wins, 11 draws, and 3 losses against CP.

(iii) Out of the first 43 instances of Vdata, MPM-UPLA has 19 wins, 13 draws, and 11 losses against TS; it has 18 wins, 14 draws, and 11 losses against PSO. In addition, it has 7 wins, 21 draws, and 15 losses against CP. However, when considering only the 23 small-to-medium instances, MPM-UPLA has 7 wins, 16 draws, and 0 losses against CP.

Then, this section compares the number of instances won by MPM-UPLA with that by CP on all 66 instances of each instance set. Note that in the 66 instances, there are 43 small-to-medium instances included. For the 66 instances, MPM-UPLA outperforms CP on Edata and Rdata, but it underperforms CP on Vdata. However, when considering only the 43 small-to-medium instances, MPM-UPLA obviously outperforms CP on all three instance sets. For each instance set, the comparison results are detailed below:

(i) Out of all 66 instances of Edata, MPM-UPLA has 34 wins, 29 draws, and 3 losses against CP. Out of the 43 small-to-medium instances of Edata, MPM-UPLA has 17 wins, 24 draws, and 2 losses against CP.

(ii) Out of all 66 instances of Rdata, MPM-UPLA has 44 wins, 17 draws, and 5 losses against CP. Out of the 43 small-to-medium instances of Rdata, MPM-UPLA has 28 wins, 15 draws, and 0 losses against CP.

(iii) Out of all 66 instances of Vdata, MPM-UPLA has 11 wins, 35 draws, and 20 losses against CP. Out of the 43 small-to-medium instances of Vdata, MPM-UPLA has 11 wins, 30 draws, and 2 losses against CP.

As a conclusion, in terms of the number of instances won, MPM-UPLA outperforms the three other algorithms on Edata and Rdata. For Vdata, MPM-UPLA outperforms TS and PSO but underperforms CP. However, when considering only small-to-medium instances, MPM-UPLA outperforms CP on Vdata.

5.3. Avg %BD. This section analyzes *Avg %BDs* in Table 4. To do so, it first analyzes *Avg %BDs* of the first 43 instances of each instance set. Then, it analyzes those of the 23 small-to-medium instances of the first 43 instances. In Table 4, the rows M6-LA40 and SM-M6-LA40 provide *Avg % BDs* of the first 43 instances and those of the 23 small-to-medium instances, respectively. For *Avg %BDs* of the first 43 instances, MPM-UPLA outperforms the three other algorithms on Edata and Rdata, but it underperforms the three other algorithms on Vdata. When considering only the 23 small-to-medium instances, MPM-UPLA obviously outperforms the three other algorithms on all three instance sets. Of each instance set, the analysis results are detailed below:

(i) For the first 43 instances of Edata, MPM-UPLA's *Avg %BD* (i.e., 0.24%) is much better than those of TS, PSO, and CP (i.e., 3.16%, 2.26%, and 0.69%, respectively). Based on these 43 instances, paired t tests concluded that the mean *%BD* of MPM-UPLA is significantly better than those of TS, PSO, and CP (with p values of 3×10^{-10}, 1×10^{-8}, and 0.0002, respectively). When considering only the 23 small-to-medium instances, MPM-UPLA's *Avg %BD* (i.e., 0.02%) is also much better than those of TS, PSO, and CP (i.e., 2.07%, 0.65%, and 0.27%, respectively).

(ii) For the first 43 instances of Rdata, MPM-UPLA's *Avg %BD* (i.e., 0.57%) is much better than those of TS, PSO, and CP (i.e., 1.87%, 3.76%, and 0.77%, respectively). Based on these 43 instances, paired t tests concluded that the mean *%BD* of MPM-UPLA is significantly better than those of TS, PSO, and CP (with p values of 4×10^{-7}, 1×10^{-7}, and 0.00004, respectively). When considering only the 23 small-to-medium instances, MPM-UPLA's *Avg %BD* (i.e., 0.02%) is also much better than those of TS, PSO, and CP (i.e., 0.87%, 0.96%, and 0.16%, respectively).

(iii) For the first 43 instances of Vdata, MPM-UPLA's *Avg %BD* (i.e., 0.59%) is worse than those of TS, PSO, and CP (i.e., 0.44%, 0.56%, and 0.08%, respectively). However, when considering only the 23 small-to-medium instances, MPM-UPLA's *Avg %BD* (i.e., 0.00%) is better than those of TS, PSO,

and CP (i.e., 0.26%, 0.13%, and 0.04%, respectively). Based on the 23 small-to- medium instances, paired t tests concluded that the mean *% BD* of small-to-medium instances of MPM-UPLA is significantly better than those of TS, PSO, and CP (with p values of 0.001, 0.0007, and 0.004, respectively).

Of each instance set, this section then compares *Avg % BDs* of MPM-UPLA and CP from all 66 instances and from their 43 small-to-medium instances. In Table 4, the rows M6-ORB10 and SM-M6-ORB10 provide *Avg %BDs* of all 66 instances and those of the 43 small-to-medium instances, respectively. For all 66 instances, MPM-UPLA outperforms CP on Edata and Rdata, but it underperforms CP on Vdata. However, when considering only the 43 small-to-medium instances, MPM-UPLA obviously outperforms CP on all three instance sets. Of each instance set, the comparison results are detailed below:

(i) For all 66 instances of Edata, MPM-UPLA's *Avg % BD* (i.e., 0.26%) is better than CP's *Avg %BD* (i.e., 0.96%). A paired t-test concluded that the mean *% BD* of MPM-UPLA is significantly better than the mean *%BD* of CP (with p value of 0.00001). When considering only the 43 small-to-medium instances, MPM-UPLA's *Avg %BD* (i.e., 0.07%) is also better than CP's *Avg %BD* (i.e., 0.67%).

(ii) For all 66 instances of Rdata, MPM-UPLA's *Avg % BD* (i.e., 0.57%) is better than CP's *Avg %BD* (i.e., 0.87%). A paired t-test concluded that the mean *% BD* of MPM-UPLA is significantly better than the mean *%BD* of CP (with p value of 0.00002). When considering only the 43 small-to-medium instances, MPM-UPLA's *Avg %BD* (i.e., 0.24%) is also better than CP's *Avg %BD* (i.e., 0.55%).

(iii) For all 66 instances of Vdata, MPM-UPLA's *Avg % BD* (i.e., 0.78%) is worse than CP's *Avg %BD* (i.e., 0.07%). However, when considering only the 43 small-to-medium instances, MPM-UPLA's *Avg % BD* (i.e., 0.01%) is better than CP's *Avg %BD* (i.e., 0.04%). Based on the 43 small-to-medium instances, a paired t-test concluded that the mean *%BD* of small-to-medium instances of MPM-UPLA is significantly better than that of CP (with p value of 0.002).

As a conclusion, based on *Avg %BDs*, MPM-UPLA obviously outperforms the three other algorithms on Edata and Rdata, but it underperforms the three other algorithms on Vdata. When considering only the small-to-medium instances, MPM-UPLA outperforms the three other algorithms on all three instance sets.

5.4. Overall Summary. In the number of instances achieved in finding the best-known solutions, MPM-UPLA outperforms the three other algorithms on all three sets of instances. In the number of instances won, MPM-UPLA outperforms the three other algorithms on Edata and Rdata; MPM-UPLA outperforms TS and PSO but underperforms CP on Vdata. However, when considering only small-to-medium instances, MPM-UPLA outperforms CP on Vdata in the number of instances won. In *Avg %BD*, MPM-UPLA outperforms the three other algorithms on Edata and Rdata, but it underperforms the three other algorithms on Vdata. However, when considering only small-to-medium instances, MPM-UPLA outperforms the three other algorithms on Vdata. As a conclusion, MPM-UPLA usually performs very well on the MPMJSP instances where each operation has less than four optional machines (e.g., the instances in Edata and Rdata). When each operation has many optional machines (i.e., $\geq 0.5m$ optional machines), MPM-UPLA usually performs well on only small-to-medium instances (i.e., the instances of $nm < 150$).

6. Conclusion

In this paper, a two-level metaheuristic was proposed for solving MPMJSP. The two-level metaheuristic consists of MPM-UPLA and MPM-LOLA as its upper- and lower-level algorithms, respectively. MPM-UPLA, a population-based algorithm, acts as the MPM-LOLA's parameter controller. MPM-LOLA is a local search algorithm, searching for an MPMJSP's optimal solution. MPM-LOLA has many changes from its older variants, such as perturbation and neighbor operators. It also uses a unique method to select an optional machine for each operation. The MPM-UPLA's function is to evolve the MPM-LOLA's input-parameter values, so that MPM-LOLA can perform its best for every single instance. In this paper's experiment, the performance of the two-level metaheuristic was evaluated on the three instance sets, i.e., Edata, Rdata, and Vdata. The experiment's results indicated that the two-level metaheuristic performs very well on Edata and Rdata. For Vdata, the two-level metaheuristic usually performs well on only the category of small-to-medium instances. Thus, a future research should be focused to enhance the two-level metaheuristic's performance, especially on large instances of Vdata.

Data Availability

The data used to support the findings of this study are available from the author upon request.

Conflicts of Interest

The author declares that there are no conflicts of interest.

References

[1] A. S. Jain and S. Meeran, "Deterministic job-shop scheduling: past, present and future," *European Journal of Operational Research*, vol. 113, no. 2, pp. 390–434, 1999.

[2] B. Çaliş and S. Bulkan, "A research survey: review of AI solution strategies of job shop scheduling problem," *Journal of Intelligent Manufacturing*, vol. 26, no. 5, pp. 961–973, 2015.

[3] C. Cebi, E. Atac, and O. K. Sahingoz, "Job shop scheduling problem and solution algorithms: a review," in *Proceedings of the 11th International Conference on Computing,*

Communication and Networking Technologies, Kharagpur, India, July 2020.

[4] J. Zhang, G. Ding, Y. Zou, S. Qin, and J. Fu, "Review of job shop scheduling research and its new perspectives under Industry 4.0," *Journal of Intelligent Manufacturing*, vol. 30, pp. 1809–1830, 2019.

[5] P. Pongchairerks, "A job-shop scheduling problem with bi-directional circular precedence constraints," *Complexity*, vol. 2021, Article ID 3237342, 19 pages, 2021.

[6] F. Zhao, X. He, and L. Wang, "A two-stage cooperative evolutionary algorithm with problem-specific knowledge for energy-efficient scheduling of no-wait flow-shop problem," *IEEE Transactions on Cybernetics*, vol. 51, no. 11, pp. 5291–5303, 2021.

[7] F. Zhao, L. Zhao, L. Wang, and H. Song, "An ensemble discrete differential evolution for the distributed blocking flowshop scheduling with minimizing makespan criterion," *Expert Systems with Applications*, vol. 160, Article ID 113678, 2020.

[8] P. Brucker and R. Schlie, "Job-shop scheduling with multi-purpose machines," *Computing*, vol. 45, pp. 369–375, 1990.

[9] J. Hurink, B. Jurisch, and M. Thole, "Tabu search for the job-shop scheduling problem with multi-purpose machines," *OR Spektrum*, vol. 15, pp. 205–215, 1994.

[10] P. Pongchairerks and V. Kachitvichyanukul, "A particle swarm optimization algorithm on job-shop scheduling problems with multi-purpose machines," *Asia-Pacific Journal of Operational Research*, vol. 26, no. 2, pp. 161–184, 2009.

[11] P. Pongchairerks, "A two-level metaheuristic algorithm for the job-shop scheduling problem," *Complexity*, vol. 2019, Article ID 8683472, 11 pages, 2019.

[12] P. Pongchairerks, "An enhanced two-level metaheuristic algorithm with adaptive hybrid neighborhood structures for the job-Shop scheduling problem," *Complexity*, vol. 2020, Article ID 3489209, 15 pages, 2020.

[13] J. Grefenstette, "Proportional selection and sampling algorithms," in *In Evolutionary Computation 1: Basic Algorithms and Operators*, T. Bäck, D. B. Fogel, and Z. Michalewicz, Eds., Taylor & Francis Group, New York, NY, USA, 2000.

[14] P. Pongchairerks and V. Kachitvichyanukul, "A two-level particle swarm optimisation algorithm for open-shop scheduling problem," *International Journal of Computing Science and Mathematics*, vol. 7, no. 6, pp. 575–585, 2016.

[15] P. Pongchairerks and V. Kachitvichyanukul, "A two-level particle swarm optimisation algorithm on job-shop scheduling problems," *International Journal of Operational Research*, vol. 4, no. 4, pp. 390–411, 2009.

[16] C. Bierwirth and D. C. Mattfeld, "Production scheduling and rescheduling with genetic algorithms," *Evolutionary Computation*, vol. 7, no. 1, pp. 1–17, 1999.

[17] P. Pongchairerks, "Efficient local search algorithms for job-shop scheduling problems," *International Journal of Mathematics in Operational Research*, vol. 9, no. 2, pp. 258–277, 2016.

[18] J. Xie, L. Gao, K. Peng, X. Li, and H. Li, "Review on flexible job shop scheduling," *IET Collaborative Intelligent Manufacturing*, vol. 1, no. 3, pp. 67–107, 2019.

[19] X. Li and L. Gao, "Review for flexible job shop scheduling," in *Engineering Applications of Computational Methods*, vol. 2, Berlin, Germany, Springer, 2020.

[20] D. Behnke and M. J. Geiger, "Test instances for the flexible job shop scheduling problem with work centers," Logistics Management Department, Hamburg, Germany, RR-12-01-01, 2012.

[21] G. A. Kasapidis, D. C. Paraskevopoulos, P. P. Repoussis, and C. D. Tarantilis, "Flexible job shop scheduling problems with arbitrary precedence graphs," *Production and Operations Management*, vol. 30, no. 11, pp. 4044–4068, 2021.

[22] H. R. Lourenço, O. C. Martin, and T. Stützle, "Iterated local search," in *International Series in Operations Research and Management Science*, vol. 57, Springer, Boston, MA, USA, 2003.

[23] M. Avci and S. Topaloglu, "A multi-start iterated local search algorithm for the generalized quadratic multiple knapsack problem," *Computers & Operations Research*, vol. 83, pp. 54–65, 2017.

[24] P. Venkatesh, A. Singh, and R. Mallipeddi, "A multi-start iterated local search algorithm for the maximum scatter traveling salesman problem," in *Proceedings of the IEEE Congress on Evolutionary Computation*, pp. 1390–1397, Wellington, New Zealand, June 2019.

[25] A. Ishigaki and S. Takaki, "Iterated local search algorithm for flexible job shop scheduling," in *Proceedings of the 6th IIAI International Congress on Advanced Applied Informatics*, pp. 947–952, Hamamatsu, Japan, July 2017.

[26] D. de C. Bissoli and A. R. S. Amaral, "A hybrid iterated local search metaheuristic for the flexible job shop scheduling problem," in *Proceedings of the XLIV Latin American Computer Conference (CLEI)*, pp. 149–157, Sao Paulo, Brazil, October 2018.

[27] P. Guo, W. Cheng, and Y. Wang, "Parallel machine scheduling with step-deteriorating jobs and setup times by a hybrid discrete cuckoo search algorithm," *Engineering Optimization*, vol. 47, no. 11, pp. 1564–1585, 2015.

[28] A. E. Eiben, R. Hinterding, and Z. Michalewicz, "Parameter control in evolutionary algorithms," *IEEE Transactions on Evolutionary Computation*, vol. 3, no. 2, pp. 124–141, 1999.

[29] S.-J. Wu and P.-T. Chow, "Genetic algorithms for nonlinear mixed discrete-integer optimization problems via meta-genetic parameter optimization," *Engineering Optimization*, vol. 24, no. 2, pp. 137–159, 1995.

[30] T. Brys, M. M. Drugan, and A. Nowé, "Meta-evolutionary algorithms and recombination operators for satisfiability solving in fuzzy logics," in *Proceedings of the 2013 IEEE Congress on Evolutionary Computation*, pp. 1060–1067, IEEE, Cancun, Mexico, June 2013.

[31] P. Cortez, M. Rocha, and J. Neves, "A meta-genetic algorithm for time series forecasting," in *Proceedings of the Workshop on Artificial Intelligence Techniques for Financial Time Series Analysis, 10th Portuguese Conference on Artificial Intelligence (EPIA 2001)*, pp. 21–31, Porto, Portugal, December 2001.

[32] P. Pongchairerks, "A self-tuning PSO for job-shop scheduling problems," *International Journal of Operational Research*, vol. 19, no. 1, pp. 96–113, 2014.

[33] M. Gen and R. Cheng, *Genetic Algorithms and Engineering Design*, John Wiley & Sons, New York, NY, USA, 1997.

[34] C. Bierwirth, "A generalized permutation approach to job shop scheduling with genetic algorithms," *OR Spektrum*, vol. 17, no. 2-3, pp. 87–92, 1995.

[35] H. Fisher and G. L. Thompson, "Probabilistic learning combinations of local job-shop scheduling rules," in *In Industrial Scheduling*, J. F. Muth and G. L. Thompson, Eds., pp. 225–251, Prentice-Hall, Englewood, NJ, USA, 1963.

[36] S. Lawrence, *Resource Constrained Project Scheduling: An Experimental Investigation of Heuristic Scheduling Techniques (Supplement)*, Carnegie Mellon University, Pittsburgh, PA, USA, 1984.

[37] D. Applegate and W. Cook, "A computational study of the job-shop scheduling problem," *ORSA Journal on Computing*, vol. 3, no. 2, pp. 149–156, 1991.
[38] J. Adams, E. Balas, and D. Zawack, "The shifting bottleneck procedure for job shop scheduling," *Management Science*, vol. 34, no. 3, pp. 391–401, 1988.
[39] J. Carlier and E. Pinson, "An algorithm for solving the job-shop problem," *Management Science*, vol. 35, no. 2, pp. 164–176, 1989.

Hindawi
Complexity
Volume 2022, Article ID 8014975, 9 pages
https://doi.org/10.1155/2022/8014975

Research Article

Complex Management Countermeasures of Postgraduate Education Quality Based on Comparison of International Training Models

Youling Wan [1] **and Zhiming Guo** [1,2]

[1]*School of Food and Biological Engineering, Jiangsu University, Zhenjiang 212013, China*
[2]*International Joint Research Laboratory of Intelligent Agriculture and Agri-products Processing (Jiangsu University), Jiangsu Education Department, Zhenjiang 212013, China*

Correspondence should be addressed to Zhiming Guo; guozhiming@ujs.edu.cn

Received 14 April 2022; Revised 1 May 2022; Accepted 16 May 2022; Published 24 May 2022

Academic Editor: Yu Zhou

Graduate students are an important engine of national and regional development and the dominant force of contemporary scientific and technological innovation. It has become the historical mission of high-level research universities to provide strong talent support for the construction of innovative powerful countries with human resources. This investigation performed a systematic and comparative analysis of international postgraduate training models. The whole process of multidimensional training countermeasures and suggestions were proposed. Those specifically included updating the training concept, optimizing the curriculum structure, innovating teaching methods, strengthening practical training, strengthening the responsibility of the tutor, and expanding the international vision. After investigation and analysis, this research pointed out that the conditions of establishing and perfecting the examination system, evaluation mechanism, and incentive measures related to postgraduate education were guaranteed. Multiple measures to improve the quality of graduate students have certain reference significance for the current graduate education.

1. Introduction

Graduate students are the main force of future scientific and technological innovation. Their academic ability, style, ambition, and international vision determine the height of national or regional scientific and technological innovation and the speed of building an innovative country [1, 2]. How to improve the quality of postgraduate education in the new era has become the focus of international industry learning and research circles and has become an important topic for the sustainable and high-quality development of universities and research institutes around the world [3]. Graduate students, as high-level talents, play an important role in serving national strategy and improving national comprehensive strength and competitiveness [4]. Under the background of the new era, it has become the historical mission of high-level research universities to improve the quality of postgraduate training and provide strong talent support for the construction of an innovative country and a powerful country with human resources.

The profound changes in the international situation have driven every country to amend new requirements for national education. Graduate education has become the primary foundation of a nation's talent and technological competition, as they play an essential role in significant innovations in the world. Therefore, both developed and developing countries attach great importance to high-level graduate education [5]. Currently, all countries are vigorously developing cutting-edge science and technology to seize the commanding heights of the world's technology and industry. As the world is encountering changes unseen in a century, the new round of scientific and technological

revolution and industrial transformation has triggered a profound adjustment of the world structure. The reform of the global governance system and international order has been accelerated: the contradiction between the internationalization of higher education and the national nature of schooling continues to collide; moreover, the development and the "Belt and Road" program increased the demands on higher education. These changes in the international situation have brought unprecedented opportunities and challenges to the development of graduate education.

The strategy of scientific and technological power in the new era puts forward new requirements for postgraduate education. Graduate education plays an important role in improving national innovation ability, serving social and economic construction, and promoting the modernization of the national governance systems and governance abilities. The guiding plan of "double first-class" construction of China's higher education puts forward that it is necessary to reform the training mode and system of postgraduates, enhance the innovation ability of postgraduates, and vigorously cultivate advanced, sophisticated, and urgently needed talents [6]. The United States has closely linked the development of higher education to national competitiveness and put forward plans to ensure national security and prosperity [7, 8]. Germany proposed to build excellent universities and clusters and strongly support the innovation of education [9]. Japan proposes "two capacities, one environment, one learning network, and one set of mechanisms" to cultivate diverse capacities with high aspirations to lead and support sustainable social development [10].

2. Comparative Analysis of International Postgraduate Training Models

Quality is the lifeline of postgraduate education, and how to improve the quality of postgraduate training is the focus of global concern. Graduate education in Europe and the United States, which has a history of more than 100 years, has gradually developed from two stages of "standardized education, certificate-based quality" and "external ranking based on the pursuit of excellence" to the current stage of "focusing on students' learning effect and promoting students' development" [11, 12]. The complete training process covers enrollment, course teaching, training links, scientific research, thesis work, etc. Most international high-level universities are very strict in enrollment, selection, teaching process, and thesis work, and other links, graduate courses, and papers are quite high requirements and set extremely strict assessment standards.

2.1. Student Selection and Enrollment. In Western countries, universities have greater rights to enroll students independently, without government intervention [13]. Therefore, every university can recruit and select prospective students according to their criteria. Students usually need to provide their transcripts, diploma, and 2-3 recommendation letters from their professors during admission. In higher education, these recommendation letters are far more convincing than mere scores [14]. On the other hand, the graduate admission test, i.e., the Unified National Graduate Entrance Examination, is an admission requirement for all graduate schools in mainland China. Therefore, the selection criteria of the universities tend to be unified, and the stipulated arrangement is still relatively limited.

2.2. Curriculum and Teaching. In most international universities, conducting innovative research or professional training pieces is the principal component of graduate studies [15]. The teaching content does not advocate the so-called "designated teaching resources" yet often incorporates the latest research topics and results [16]. Graduate students are trained to focus on the knowledge and skills essential for scientific research through seminars, forum discussions, experiments, and more. On the other hand, graduate education in China adopts the segmented learning style. In the first year of the study, graduate students will take courses to gain knowledge and focus on their research later in the second year of the study. As a result, graduate students in China seem to be gradually ignoring the quality of teaching, as taking the courses is just simply counting the credits needed to be obtained in the first year of their study.

2.3. Comparison of Academic Training. Most international universities actively implement interdisciplinary learning plans and research topics, and their curriculum setting emphasizes the intersection and penetration between academic disciplines and fields [17]. Some universities frequently invite guest teachers to provide students with great high-level courses and lectures that comprise diverse novel knowledge. In addition, to meet the needs of interdisciplinary talents with innovation capability, universities add multidisciplinary approaches to broaden the knowledge and skills of graduate students. They positively influence their interdisciplinary problem-solving in science, technology, social economy, and their comprehensive ability to deal with complex problems. In contrast, the multidisciplinary learning plans and cross-integration of scientific research topics are very limited in mainland China. There are specific barriers between disciplines and colleges of the same university.

2.4. Stage Evaluation Comparison. Both the US and the UK graduate education systems have strict and systematic teaching curriculum arrangements. Students are not allowed to begin writing their thesis or dissertation before completing the courses. Although graduate students have different learning forms, i.e., scientific research is the central component of the study, course completion is still the primary requirement before the thesis work. Most high-level international universities have stringent teaching processes and training assessments [18]. The requirements for graduate courses are very high. If the students could not meet the criteria, they might be dropped out. It has been vastly reported that the graduation rate is much lower than the admission rate across the United States. However, these

requirements are essential to cultivating and screening high-quality graduate students. In contrast, higher education in mainland China adopts the "strict enrollment" model to screen high-quality students at the very beginning. Much to the professors' amazement, most graduate students can graduate very smoothly. Unless students voluntarily give up continuing their studies, they are uncommonly dropping out of school.

2.5. Focus on Capability Comparison. The core of graduate education in most international universities is scientific research. Every professor and student must have significant independent research. However, professors must not make rulings on students' research direction and content. Professors will guide the students by implying some research methods and providing corresponding references and frameworks [19]. In the process of learning and doing research, it is essential to attach great importance to the students' opinions and give them enough space to express and practice their thoughts to cultivate their critical thinking, encourage the exploration of new knowledge, and advocate a high degree of independent research and innovation [20]. After an extensive investigation in the early stage, it was found that most universities in China mainly emphasize the publishing of high-quality academic papers and writing dissertations for the graduation conditions and degree awarding standards of doctoral and master's degrees. To ensure the successful graduation of students, the supervisors had to pay more attention to the cultivation of students' writing ability. In view of the pressure of graduation, students mainly participate in the research topic of their supervisor as assistants, and they are unlikely to explore freely according to their scientific interests. In the long run, they cannot form their independent scientific thinking.

3. Countermeasures for Improving the Quality of Postgraduate Training

In recent years, with the expansion of the postgraduate education scale, China's postgraduate education is no longer elite in the traditional sense. Graduate education tends to be popular, and quite several graduates are application-oriented talents facing the demand of social production [21, 22]. At the same time, some disadvantages affect the high-quality development of graduate education. (1) The degree of learning and application of graduate students is not high, and the current training scheme cannot fully adapt to the social demand for graduate students' ability. (2) Compared with the rapid development of science and technology, the curriculum of graduate students lags, and there is a disjointed phenomenon of learning and application. (3) The teaching method of the course is single, and the students' sense of classroom acquisition is low. (4) Fewer opportunities for students go deep into the production line, lack of adequate practical training, weak vocational competence, and increasing employment pressure on graduates. (5) With the expansion of the enrollment scale and the increasing work pressure on tutors, the sense of responsibility in guiding students tends to weaken. (6) The international vision of graduate students is limited, and the international communication ability cannot meet the expectation of the country and society. By comparing and analyzing the differences between international graduate education systems [23], it is not difficult to find out that the only way to improve the quality of graduate education is to effectively deal with the shortcomings and disadvantages of the current graduate education. The framework of the overall theoretical system of postgraduate education quality improvement countermeasures proposed in this study is shown in Figure 1. The improvement and solution of the above problems need a series of multidimensional measures in the whole process of cultivation.

3.1. Optimization of Culture Program. The development of the graduate training scheme should be in line with the national strategies and needs and the frontiers of the disciplines. Sometimes, it is beneficial to take first-class universities at home and abroad as reliable examples, understand the differences, and adapt the training characteristics to promote the development of the graduate training scheme to be more advanced, forward-looking, and systematic [24]. Based on making clear the orientation of key points and self-orientation, the graduate student training program suitable for their development is made scientifically and rationally. At the same time, it is necessary to reflect differentiation and individualization according to different subject areas and degree types in every higher education institution [25]. Moreover, to support a stable model of the cultivation of top graduate talents, every higher education institution needs to grasp the specifications of degree award, properly, refine the degree award standards, integrate the subject resources, build a subject sharing research platform, and form a high-level subject platform.

The evaluation standard of talent quality should be incorporated into the training process of graduate students. Industries, enterprises, institutions, and universities are actively absorbed to jointly design training programs and discuss curriculum settings. It will be preferable if experts from industry, enterprises, institutions, and universities could design the training plan together to discuss the curriculum settings and clarify teaching goals and the practice standards while adhering to the goals to meet the needs of the society by focusing on detailed solutions on how to face the challenges of the new era.

Furthermore, quality consciousness should run through the whole process of training, and the mechanism of separation and elimination should be set up in the links of the dissertation proposal and dissertation defense, to extend the study period according to the situation and stimulate the research potential of graduate students. Simultaneously, it is also essential to ensure that the requirements of each link of the training program comply with the national regulations of graduate education. Efforts should be made to build a system conducive to improving endogenous quality, strengthening the construction of a quality assurance system, and forming a self-discipline mechanism for secondary colleges, subject

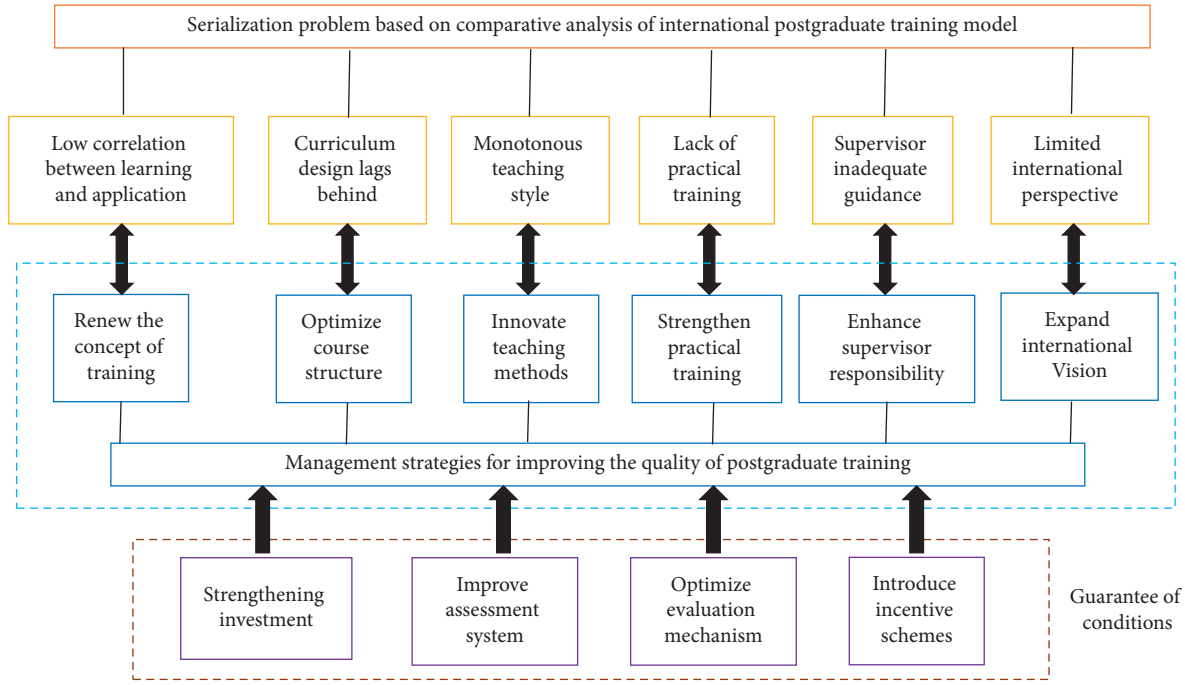

Figure 1: Frame diagram of the overall theoretical system of postgraduate education quality improvement countermeasures.

direction, graduate supervisors, lecturers, and management teams. Therefore, system construction promotes the continuous improvement of the quality assessment mechanism.

3.2. Optimization of Syllabus and Curriculum. Strengthening the core curriculum is imperative as it often reflects the significance of the study. The graduate school curriculum should cover all essential principles, techniques, and the latest research findings from a wide range of research directions [26, 27]. Notably, it must cover introductory courses and frontier innovative training and reflect the characteristics of the discipline and the overall strong point of the education team. It will be preferable to build a collaborative curriculum development team by selecting a pivotal teacher to serve as the course leader with 2–4 more teachers to participate in the curriculum construction and jointly undertake the course teaching and the formulation of the teaching plan and the preparation of the syllabus.

It is essential to develop professional courses according to the needs of different levels and types of graduate education. High-quality implementation of research-based instruction is needed throughout the graduate training process to form a high-level graduate curriculum system that is in line with international standards. In addition, every graduate school needs to develop its specialized course program to keep up with the current discipline/academic development. All schools are encouraged to welcome guest teachers to participate in graduate training activities to enhance knowledge sharing among academics, broaden students' intellectual horizons, and strengthen the link between theory and practice of the graduate study.

Humanity as the basis of graduate education cannot be neglected. In the curriculum setting, apart from quality education, it is also essential to strengthen academics, morals, and humanities, vocational ethics education, and comprehensively improve academic literacy [28]. The ideological and political construction of the curriculum should be promoted solidly, and the sense of responsibility for linking scientific research with national needs should be stimulated. The national spirit education with patriotism and spirit education with innovation and entrepreneurship are strengthened, and the double improvement of humanistic quality and scientific spirit [29]isrealized. Academic postgraduates should pay attention to cultivating their innovative thinking, while professional postgraduates should strengthen their entrepreneurial spirit and professional competence.

3.3. Promoting Innovation in Teaching Approaches. It is essential to change the teaching model by taking course quality as a critical indicator to measure graduate training. It is imperative to classify the scientific design courses, increase a couple of seminars, practical and research-based courses, provide forward-looking content for postgraduate training, and improve the innovation and entrepreneurship education curriculum system for graduate students [30]. It is necessary to continuously improve the teaching procedure and increase the quality of the course through intensive lectures and practice, for example, by actively promoting flipped classrooms, utilizing diversified teaching methods, supporting the construction of a case database for graduate courses, and expanding the amount of information and depth of knowledge delivered to graduate students by course teaching.

It is preferable to promote a digital learning and teaching environment by accelerating the integration of scientific research and the cultivation of top-notch innovative talents

in the information environment and promoting the expansion of high-quality digital education resources under the conditions of informatization [31, 32]. All graduate education institutions are encouraged to build a batch of high-quality graduate online public courses to promote cross-disciplines and cross-university massive open online courses, micro-courses, and other advanced media courses to go beyond the traditional classroom restrictions to enrich graduate students' self-study platforms, meet the needs of personalized learning, and stimulate students' innovative consciousness.

Subsequently, it is fundamental to work on promoting the mutual recognition and credit transfer to accompany the increase in student mobility between faculties and even universities at home and abroad, such as focusing on integrated master-PhD courses, strengthening the integration and linkage of the curriculum system of different training stages, encouraging academic master students to pick classes among all degree levels, and recognizing the practical training credits of professional degree graduate students from every means of access. It is also essential to foster the credit recognition of optional doctoral courses for graduate students in the same discipline, construct an open elective course system, and provide more accessible ways for students to acquire credits.

3.4. Strengthen Scientific Practical Training. Increasing the proportion and quality of practical courses by carrying out specialized training courses to train students about various types of equipment and how to operate them could help students strengthen their practical skills and cultivate their innovative thinking [33]. Through excellent and high-quality practical courses, students are stimulated to improve their ability to solve practical problems and accustomed to independent learning and research-based learning. Hence, students transform knowledge into skills, and they are more likely to feel satisfied with the course learning.

In addition, it is essential to increase scientific research training for graduate students. Doctoral students should focus on cultivating scientific research and innovation capabilities, and professional degree master's students should focus on improving their practice and application capabilities. Through typical, comprehensive, and advanced experimental projects and scientific research topics, graduate students are trained to master the fundamental processes and methods of scientific experiments so that students could experience the scientific research environment, familiarize themselves with scientific research equipment, integrate into the scientific research team, and participate in project activities [34, 35]. Accordingly, all scientific research training should be problem-oriented to nurture students' skills for innovation and research for them to be able to conduct exploratory research by themselves. Graduate students are encouraged to explore freely according to their interests and to improve original innovation in scientific research.

Furthermore, it is essential to promote more scientific research activities through academic conferences, open forums, lectures by guest teachers, and more as they can be helpful for students to improve their innovative thinking and motivate them to increase the number and quality of innovations they create. Yet, for these activities, to successfully facilitate the academic exchange and help students nurture their organizational skills and coordination capabilities, it is essential to guide them to form a "self-organized, actively contributed, and self-expressed" academic community, to let students express their thoughts more actively, mutually inspire each other with innovations, exhibit their academic achievements, and strengthen the awareness of scientific research integrity. To increase efforts to promote cross-school and cross-cultural exchanges and communication, postgraduates are actively organized to participate in various social activities and practice exercises, to improve their employment competitiveness and professional competence.

3.5. Improvement of Supervisors' Responsibilities. It is fundamental to give every supervisor the primary responsibility to lead and guide their students according to their style and ideologies. Supervisors can demonstrate and give students moral education and scientific ethics [36]. Letting them have a subjective initiative in their role as a supervisor could further strengthen their sense of responsibility for the quality of the graduate training. Hence, it will be preferable to give every supervisor the right and responsibility to participate in the enrollment selection, training link assessment, award evaluation, employment recommendation, and more.

Besides, higher education institutions are urgently called to facilitate supervisors to join the jointly group mentoring model through organizing joint combined exchange training between mentors and off-campus scientific research institutions and enterprises, regulating a certain proportion of supervisor's occupation mobility, and utilizing the unique role of off-campus trainers in cultivating students' innovation and entrepreneurship capabilities [37]. The guidance mode of the tutor's research group was advocated, which could give full play to the advantages and specialties of each group member in postgraduate training. Supervisor team building can effectively relieve the work pressure and education pressure of graduate tutors.

Likewise, it is essential to continuously strengthen the supervisor's management team by enriching the selection and management mechanism; providing appropriate and sufficient training for newly elected supervisors; implementing a rotation system for senior supervisors; expanding the domestic and foreign academic exchange and cooperation system for supervisors; facilitating them to participate in industry and enterprise practice; raising the quality of supervisor's archives management system for graduate teaching; promoting supervisors to balance the relationship between graduate training, scientific research, and social services; and inspiring all supervisors to devote themselves entirely to the graduate training and focus on the quality of graduate education.

3.6. Expansion of International Vision. The education curriculum should reflect not only national but also international components. In the new era of education, colleges and universities are encouraged to open bilingual and English

courses and actively use foreign classic original textbooks. Through the teaching team construction policy of "Excellent, Young and International," the investment in foreign experts and teachers is increased. There is an urgent need for a graduate curriculum that is aligned with international standards and faculty that can engage in a truly equal dialogue in a global dialogue. Young teachers with overseas backgrounds and visiting experience are encouraged to conduct special lectures and interactive exchanges for graduate students to expand the international elements of the curriculum [38, 39].

It is essential to set up a multinational training environment by exploring the convergence management of overseas graduate education. For instance, it would be preferable to arrange overseas and local students together in the same class and research group to equally compete on the same platform; significantly improve the overseas academic exchanges and scientific research experience of graduate students; gradually promote the general study of graduate education with high-quality courses and greatly support doctoral students to participate in international academic exchanges and research program; and pilot some fields of study and research teams throughout the entire process of international teaching and training.

Consequently, it is essential to build an international education environment. High education institutions are encouraged to carry out comprehensive cooperation with world-renowned universities and research institutions in personnel training, scientific research, cultural exchanges, and more as well as promote the establishment of stable overseas study and practice bases in various fields of study and increase the promotion of international cooperation projects; accommodate high-level international academic conferences; increase the global influence and popularity of schools, disciplines, and experts to create an excellent international scientific research and practice platform for the students; and improve the quality of the graduate education in the international level.

4. Conditional Guarantee for the Quality Improvement of Graduate Education

4.1. Expanding and Raising Funding for Education. The enhancement of the overall planning of expanding and raising funds from the national government, universities, research projects, professional institutions, enterprises, and more is essential to support the whole process of graduate education. To create a harmonious and sustainable graduate education environment, most of the funds should be invested in scientific research and discipline construction to support the structure of the graduate curriculum, including the teaching process and practical teaching, especially for the professional degree graduates [40]. Accordingly, it will be crucial to improve the award policy system, increase the optimization of scholarships and funding, significantly raise the standards of graduate student awards, increase the budget for graduate students with financial difficulties, and further promote and improve the scientific research-oriented tutor funding system.

These scholarships and research funding programs could hopefully help graduate students finish their graduate education smoothly without stressing about financial problems and difficulties. Hopefully, it will result in more fantastic achievements. With the establishment of special funding for graduate academic activities, students participate more actively in intellectual salons and forums and scientific and technological practices, therefore promoting their theoretical innovations. Accordingly, to be able to build the circumstances mentioned above, all graduate education institutions are encouraged to adapt to the current development of the national graduate education funding mechanism, to link up performance indicators such as the quality of the graduate courses and the qualification rate of dissertations with the graduate education funding, and to develop a quality-centric graduate education funding allocation mechanism.

4.2. Establishing a Better Institution System and Regulation. First, it is essential to strengthen the standardization and institutionalization of graduate education and regard the improvement of the system as a necessary part of the connotation of improving the quality of the graduates. Likewise, the importance of improving the secondary management of graduate education and strengthening the construction of the graduate management team cannot be neglected. Every faculty and research institution plays an essential role in the whole process of graduate education [41]. Therefore, the core indicators of faculty and research institution performance evaluation should include the quality of its graduate education to encourage every faculty and research institution to improve its graduate education system and management continuously.

In the new era of education, every institution is encouraged to strengthen the information construction of graduate education management and implement an intelligent monitoring system of the whole process of the training process, including course teaching and assessment, thesis proposal, annual reports, professional training, and special lectures. Following the growth of the technology, the implementation of quality control throughout the entire process of training becomes easier as institutions could build student and lecture systems that could monitor and facilitate the whole training process. Both students and lecturers can access both the course credits and the graduate thesis system and receive notifications and announcements. In addition, through the system, lecturers, supervisors, and graduate students could jointly monitor and evaluate the quality of graduate training. Hence, this evaluation system should be set as an anonymous online system divided into three different stages, i.e., the pre-lecture design stage, lecture observation stage, and after-lecture evaluation stage. Meanwhile, it is also essential to improve the dynamic adjustment mechanism of the supervisor position. Single research orientation should be changed, efforts to train new supervisors should be intensified, and provincial recruitment should be implemented. Some measures such as suspending the recruitment or even canceling supervisor qualifications will also be needed to some extent. However, as the supervisors majorly

influence the students' development, the central element of supervisor evaluation should be linked to the development of their students.

4.3. Optimizing Educational Evaluation Mechanism. As evaluation is an essential component in the education development process, it is necessary to establish and refine the self-evaluation system for degree authorization points and carry out regular evaluation and trial basis international peer evaluation for the degree programs [35, 42]. Through the periodical evaluation of the degree programs, it is expected that the quality of the whole graduate training will be increased as it necessitates graduates' research ability and practical ability, demands academic exchanges, and appraises the quality of dissertations and other vital indicators. Moreover, it highlights the significant role of the graduate education team in discipline construction and promotes the gradual return of discipline construction to the standard of talent training.

Furthermore, by establishing a dynamic adjustment mechanism for the admission, early notice, and withdrawal of the degree authorization points, the dynamic adjustment of the degree programs will be linked to the evaluation results of the national and provincial degree authorization points and the school subject assessment results at the same time. Hence, the survival of the fittest will be carried out along with the results. Accordingly, it is essential to gradually establish and refine the dynamic adjustment mechanism for degree programs that is compatible with the orientation of the school, the quality of graduate education, and economic and social development; emphasize the quality evaluation based on the employer's feedback and comprehensively highlight the importance of supervision, identification, diagnosis, regulation, and improvement; and guide employers to scientifically and reasonably determine the job descriptions and responsibilities, adhere to post-fixed salary, getting paid according to work, preferential work and preferential remuneration, establish an incentive mechanism that emphasizes actual performance and contribution, establish the ideal employment orientation, and promote the appropriateness of the job.

4.4. Establishing the Incentive Mechanism. To further strengthen the construction of graduate education teams, i.e., lecturers, supervisors, and management personnel, it is essential to establish an incentive mechanism for the quality of graduate education, thoroughly improve the evaluation system for the classification appraisal and assessment of academic and professional graduate degree supervisors, establish a feedback mechanism for the quality of graduate training [43], implement rewards and disciplines based on enrollment indicators, and link the quality of graduate training and supervisors with enrollment indicators. Besides that, all results and achievements, amount of work, and quality evaluation results of the graduate training must not be omitted in the series of teachers, supervisors, and professional technical job evaluation requirements to increase the standard and enthusiasm of the lecturers and supervisors in giving lectures and guiding the students.

In addition, it is also compulsory to actively carry out the selection of the best graduate courses, lecturers, and supervisors, improve the reward policies for curriculum construction achievements, and increase the funding for teachers to undertake postgraduate course construction and teaching reform projects [44, 45]. To build an excellent graduate education team, an achievement award is a requisite method to encourage the lecturers to devote themselves to research and teaching, supervisors to care about the development of students, and the management personnel to carry out research-based management.

5. Conclusion

Graduate education is a systematic project. Following the challenges and opportunities in the new era, the graduate training model is constantly adjusted and optimized to meet the different needs of the society for solid talents. To cultivate the ability of postgraduates to have dreams and lofty aspirations, to lead and support the sustainable development of society, and to have an international perspective and social development responsibilities, the quality of postgraduate education needs to keep pace with the times and continue to improve. As widely known, the quality of graduate training is reflected through the overall connotative development of colleges and universities, which requires long-term accumulation and perfection. Accordingly, it is necessary to expand and deepen the training objectives, training methods, training process, and quality assurance of graduate students. The development of graduate education should be planned pragmatically to serve the national economic construction.

Data Availability

No data were used to support this study.

Conflicts of Interest

The authors declare that they have no conflicts of interest.

Acknowledgments

This study was supported by the particular project commissioned by Graduate Education and Teaching Reform of Jiangsu Province, Higher Education Planning and Development of Jiangsu University (G201912), Key Project on Higher Education Teaching Reform in Jiangsu Province (2021JSJG108), Key Project on Higher Education Teaching Reform in Jiangsu University (2021JGZZ003), Evaluation Project of Jiangsu Higher Education Association Committee (2020-Y04), and the Outstanding Young Teachers of Blue Project in Jiangsu Province.

References

[1] C. Zhaohui and A. Anning, "Exploring the affiliation between teachers' professional development and students' academic performance in higher education in China," *Thermal Science*, vol. 24, no. 1, pp. 301–311, 2020.

[2] A. A. Al-Asmar, Y. Oweis, N. H. Ismail, A. H. A. Sabrah, and I. M. Abd-Raheam, "The predictive value of high school grade point average to academic achievement and career satisfaction of dental graduates," *BMC Oral Health*, vol. 21, no. 1, p. 300, 2021.

[3] L. M. Harrison-Bernard, A. C. Augustus-Wallace, F. M. Souza-Smith, F. Tsien, G. P. Casey, and T. P. Gunaldo, "Knowledge gains in a professional development workshop on diversity, equity, inclusion, and implicit bias in academia," *Advances in Physiology Education*, vol. 44, no. 3, pp. 286–294, 2020.

[4] A. S. Chmiel, M. Shaha, and D. K. Schneider, "Introduction of blended learning in a master program: developing an integrative mixed method evaluation framework," *Nurse Education Today*, vol. 48, pp. 172–179, 2017.

[5] Y. Shen and G. Hu, "Chinese graduate students' perceptions of plagiarism: a mixed-methods study," *Accountability in Research*, vol. 28, no. 4, pp. 197–225, 2021.

[6] J. Li and E. Xue, *How talent Cultivation Contributes to Creating World-Class Universities in China: A Policy Discourse Analysis*, Educational Philosophy and Theory, AUSTRALASIA, 1970.

[7] P. S. Cahn, A. Makosky, K. A. Truong et al., "Introducing the language of antiracism during graduate school orientation," *Journal of Diversity in Higher Education*, vol. 15, no. 1, pp. 1–6, 2022.

[8] D. Grote, A. Patrick, C. Lyles, D. Knight, M. Borrego, and A. Alsharif, "STEM doctoral students' skill development: does funding mechanism matter?" *International Journal of Stem Education*, vol. 8, no. 1, p. 50, 2021.

[9] M. Thom, "The rough journey into arts entrepreneurship," *Education + Training*, vol. 59, no. 7/8, pp. 720–739, 2017.

[10] R. Sakurai and T. Uehara, "Effectiveness of a marine conservation education program in Okayama, Japan," *Conservation Science and Practice*, vol. 2, no. 3, p. e167, 2020.

[11] P. H. Koehn and J. I. Uitto, "Evaluating sustainability education: lessons from international development experience," *Higher Education*, vol. 67, no. 5, pp. 621–635, 2014.

[12] A. Stanitznig, E. Leitner, P. Winter, and T. Wittek, "Survey of teaching of ruminant medicine to veterinary students in veterinary schools in Europe and the USA by questionnaire," *Berliner und Münchener Tierärztliche Wochenschrift*, vol. 132, no. 7-8, pp. 397–404, 2019.

[13] A. Sahin, H. C. Waxman, E. Demirci, and V. S. Rangel, "An investigation of harmony public school students' college enrollment and STEM major selection rates and perceptions of factors in STEM major selection," *International Journal of Science and Mathematics Education*, vol. 18, no. 7, pp. 1249–1269, 2020.

[14] C. Avery, B. L. Castleman, M. Hurwitz, B. T. Long, and L. C. Page, "Digital messaging to improve college enrollment and success," *Economics of Education Review*, vol. 84, Article ID 102170, 2021.

[15] W. D. Hendricson, S. Seitz, and D. K. English, "Case report of a program to enhance dental students' interest in academic dentistry," *Journal of Dental Education*, vol. 83, no. 9, pp. 1047–1056, 2019.

[16] B. Taebi and W. E. Kastenberg, "Teaching engineering ethics to PhD students: a berkeley-delft initiative," *Science and Engineering Ethics*, vol. 25, no. 6, pp. 1763–1770, 2019.

[17] T. Yuret, "Path to success: an analysis of US educated elite academics in the United States," *Scientometrics*, vol. 117, no. 1, pp. 105–121, 2018.

[18] A. B. d. Carvalho, H. L. Resende, R. M. D. Faria, and J. A. Toledo, "Content analysis of two Brazilian external evaluations of medical programs: ENADE and REVALIDA," *Revista Brasileira de Educação MédicaAssociação Brasileira de Educação Médi*, vol. 45, no. 1, p. e033, 2021.

[19] K. Benati and J. Fischer, "Beyond human capital: student preparation for graduate life," *Education + Training*, vol. 63, no. 1, pp. 151–163, 2020.

[20] S. Lavy and W. Ayuob, "Teachers' sense of meaning associations with teacher performance and graduates' resilience: a study of schools serving students of low socio-economic status," *Frontiers in Psychology*, vol. 10, 2019.

[21] G. Fang and S. Wan, "Peer effects among graduate students: evidence from China," *China Economic Review*, vol. 60, Article ID 101406, 2020.

[22] Y. Zhou, H. Li, and F. Shahzad, "Does college education promote entrepreneurship education in China?" *Sage Open*, vol. 11, no. 3, p. 215824402110316, 2021.

[23] J. Collins, N. Brown, and J. Leigh, "Making sense of cultural bumps: supporting international graduate teaching assistants with their teaching," *Innovations in Education & Teaching International*, vol. 1, pp. 1–11, 2021.

[24] A. Kumari, D. T. Wu, K. K. Motiani, K. Y. Wu, M. Palumbo, and S. D. Tran, "Career pathways and professional skills of postgraduate students from a dental research-intensive programme," *European Journal of Dental Education*, vol. 23, no. 2, pp. 143–150, 2019.

[25] J. L. Mateos-González and P. Wakeling, "Exploring socioeconomic inequalities and access to elite postgraduate education among English graduates," *Higher Education*, vol. 83, no. 3, pp. 673–694, 2022.

[26] K. McManus, C. Metrejean, K. Schweitzer, J. Cooley, and T. Warholak, "Quality improvement and safety in US pharmacy schools," *American Journal of Pharmaceutical Education*, vol. 83, no. 9, pp. 7042–1905, 2019.

[27] R. Roller-Wirnsberger, T. Masud, M. Vassallo et al., "European postgraduate curriculum in geriatric medicine developed using an international modified Delphi technique," *Age and Ageing*, vol. 48, no. 2, pp. 291–299, 2019.

[28] A. Tekian, O. ten Cate, E. Holmboe, T. Roberts, and J. Norcini, "Entrustment decisions: implications for curriculum development and assessment," *Medical Teacher*, vol. 42, no. 6, pp. 698–704, 2020.

[29] S. Preece, "Postgraduate students as plurilingual social actors in UK higher education," *Language Culture and Curriculum*, vol. 33, no. 2, pp. 126–141, 2020.

[30] Y. Wan and Z. Guo, "Improving the sense of gain of graduate students in food science," *Journal of Food Quality*, vol. 2021, pp. 1–7, 2021.

[31] F. D. Guillén-Gámez and M. J. Mayorga-Fernández, "Quantitative-comparative research on digital competence in students, graduates and professors of faculty education: an analysis with ANOVA," *Education and Information Technologies*, vol. 25, no. 5, pp. 4157–4174, 2020.

[32] S. Parramore, "Online active-learning: information literacy instruction for graduate students," *Reference Services Review*, vol. 47, no. 4, pp. 476–486, 2019.

[33] G. R. Fassakhova, V. G. Rosa, R. I. Lilya, G. C. Lyubov, and I. M. Rezida, "Problems of training qualified personnel for agriculture," in *Proceedings of the International Scientific-Practical Conference - Agriculture and Food Security: Technology, Innovation, Markets, HUMAN RESOURCES (FIES 2019)*, Kazan, Russia, Feb 2020.

[34] T. W. Bolsen, B. R. Fairbanks, E. E. Aviles et al., "Merging undergraduate teaching, graduate training, and producing research: lessons from three collaborative experiments," *PS: Political Science & Politics*, vol. 52, no. 1, pp. 117–122, 2019.

[35] O. Leonchuk and D. O. Gray, "Scientific and technological (human) social capital formation and Industry-University Cooperative Research Centers: a quasi-experimental evaluation of graduate student outcomes," *The Journal of Technology Transfer*, vol. 44, no. 5, pp. 1638–1664, 2019.

[36] A. V. Grigoryeva and E. A. Terentev, "Doctoral students' academic supervision: a systematic review of approaches to conceptualization and empirical analysis," *University Management: Practice and Analysis*, vol. 25, no. 1, pp. 49–61, 2021.

[37] M. Jacobsen, S. Friesen, and S. Becker, "Online supervision in a professional doctorate in education: cultivating relational trust within learning alliances," *Innovations in Education & Teaching International*, vol. 58, no. 6, pp. 635–646, 2021.

[38] A. Hines, "University of Houston. Getting ready for a post-work future," *Foresight and STI Governance*, vol. 13, no. 1, pp. 19–30, 2019.

[39] L. Li, "Education supply chain in the era of Industry 4.0," *Systems Research and Behavioral Science*, vol. 37, no. 4, pp. 579–592, 2020.

[40] A. Graddy-Reed, L. Lanahan, and J. D'Agostino, "Training across the academy: the impact of R&D funding on graduate students," *Research Policy*, vol. 50, no. 5, Article ID 104224, 2021.

[41] K. Byoung-Joo, W. Park, K. Min-Hee, and L. Jung, "The perspectives of graduate school deans on institution-level, faculty-level, and government-level graduate school improvement," *Journal of Higher Educational Research*, vol. 3, no. 2, pp. 55–82, 2020.

[42] F. Guo, Y. Luo, L. Liu, J. Shi, and H. Coates, "Analysing mechanisms for evaluating higher education outcomes in China," *Higher Education Policy*, vol. 32, no. 4, pp. 557–575, 2019.

[43] Y. Song, "Sorting, school performance and quality: evidence from China," *Journal of Comparative Economics*, vol. 47, no. 1, pp. 238–261, 2019.

[44] H. Lim and H. Y. Park, "Graduate student researchers' learning experiences and perceived Identity in University-Research Institute Cooperation program in Korea," *Asian Journal of Education*, vol. 21, no. 4, pp. 1127–1155, 2020.

[45] M. Mimirinis, "What do undergraduate students understand by excellent teaching?" *Higher Education Research and Development*, vol. 41, no. 2, pp. 466–480, 2022.

Hindawi
Complexity
Volume 2022, Article ID 7436256, 23 pages
https://doi.org/10.1155/2022/7436256

Research Article

Priority Roles of Stakeholders for Overcoming the Barriers to Implementing Education 4.0: An Integrated Fermatean Fuzzy Entropy-Based CRITIC-CODAS-SORT Approach

Roselyn Gonzales[1], **Rose Mary Almacen**[1], **Gamaliel Gonzales**[1,2], **Felix Costan**[1], **Decem Suladay**[1], **Lynne Enriquez**[1], **Emily Costan**[1], **Nadine May Atibing**[3], **Joerabell Lourdes Aro**[3], **Samantha Shane Evangelista**[3], **Fatima Maturan**[3], **Egberto Selerio Jr.**[3], and **Lanndon Ocampo**[3,4]

[1]*College of Education at Danao Campus, Cebu Technological University, Danao 6004, Philippines*
[2]*Educational Research and Resource Center, Cebu Technological University, Danao 6004, Philippines*
[3]*Center for Applied Mathematics and Operations Research, Cebu Technological University, Cebu City 6000, Philippines*
[4]*Department of Industrial Engineering, Cebu Technological University, Cebu City 6000, Philippines*

Correspondence should be addressed to Lanndon Ocampo; lanndonocampo@gmail.com

Received 29 January 2022; Revised 1 April 2022; Accepted 13 April 2022; Published 9 May 2022

Academic Editor: Yu Zhou

This work defines various stakeholder roles (or strategies) to overcome the barriers to implementing Education 4.0 (EDUC4), which were recently identified in the domain literature. The stakeholder roles are evaluated against these barriers, and such evaluation is structured as a multicriteria sorting problem. To this end, an integrated entropy-based CRITIC-CODAS-SORT under a Fermatean fuzzy (FF) environment addresses epistemic uncertainties inherent in decision-making. The FF CRITIC assigns the priority weights of the barriers, while the FF CODAS-SORT determines the high-priority stakeholder roles. A case of an HEI evaluating 57 possible roles of 5 stakeholders is demonstrated here. Findings suggest the lack of collaboration, apprehensive stakeholders, cybersecurity threats, health issues, and cost as crucial barriers to the HEI. The sorting process yields 13 high-priority roles, encompassing those within the influence of the government (i.e., cybersecurity awareness, allocation of necessary funds, designing more aligned curricula, and streamlining the basic education agenda), university management (i.e., investing in efficient technologies and forging extensive stakeholder collaboration), human resource function (i.e., implementing periodic skills training for educators), and educators (i.e., engaging in continuous learning about cybersecurity threats, integrating awareness of applicable laws against cyberbullying, devising alternative cost-efficient teaching strategies, taking part in initiatives to improve curricula, efficient preparation of learning materials, and participating in skills development initiatives). Various managerial insights are offered as inputs to the design of initiatives in EDUC4 implementation.

1. Introduction

In recent years, Education 4.0 (EDUC4) has been recognized as a framework for learning institutions so that teaching and learning will be aligned with the fourth industrial revolution (4IR). EDUC4 characterizes a learning process highly associated with technologies such as virtual learning environments [1], adaptive internet of things (IoT) [2], and artificial intelligence (AI) [3]. These technologies have a curriculum design that reflects technology-based environments [4]. Despite these advances in the teaching-learning process linked to EDUC4, developing economies encounter barriers in its implementation due to resource scarcity, educational politics, and cultural aspects. For instance, the response of Malaysia in EDUC4 faces challenges ranging from limited and inefficient educational resources, outdated

teaching styles, and inadequate infrastructure, to a lack of close linkages among educational institutions [5]. In Pakistan, they found no framework that provides the base for EDUC4 with the lack of resources, improper implementation of relevant policies, and inexperienced human resources [6]. A recent review by Costan et al. [7], with an empirical work of Gonzales et al. [8], comprehensively identified these EDUC4 implementation barriers, with a particular focus on developing economies.

Current literature (e.g., [3, 9]) highlighted some essential roles of stakeholders in overcoming the barriers of implementing EDUC4 and putting such an initiative into action. Although Costan et al. [7] established the barriers through a systematic literature review, there is no existing literature about identifying specific functions of the stakeholders that can better address the barriers to EDUC4 implementation, especially in a developing economy. Mourtzis [10] reported the relevance of the teaching factory concept for successful EDUC4 implementation, but the degree of participation of the stakeholders so that a university could dynamically execute the teaching factory direction is not clear. This implies that stakeholders' roles in taking the EDUC4 initiative are not straightforward. For instance, we expect to improve government investments in social and human capital [11] and prepare for the costly challenges of rapid technological advancements and developing ICT competencies. Thus, overcoming the barriers to EDUC4 implementation needs a thorough understanding of stakeholder roles so that educational managers, human resources, educators, ICT function, and other relevant stakeholders can function systematically in any policy direction toward EDUC4.

In this work, evaluating stakeholder roles in overcoming different barriers to implementing EDUC4 is structured as multiple-attribute decision-making (MADM) problem, where barriers are treated as "evaluation criteria" and stakeholder roles as "evaluation alternatives." In addressing this problem, we proposed the integration of the CRiteria Importance through Intercriteria Correlation (CRITIC) and multiple criteria sorting (MCS) method based on the COmbinative Distance-based ASsessment (CODAS) approach (i.e., CODAS-SORT) under Fermatean fuzzy set (FFS) environment to account for epistemic uncertainties in expert decision-making. The Fermatean fuzzy (FF) CRITIC assigns priority weights of implementation barriers, while the FF CODAS-SORT sorts the stakeholder roles by identifying those high roles for strategic implementation of EDUC4. Unlike other priority weight allocation methods (e.g., analytic hierarchy process, best-worst method, and full consistency method), the CRITIC developed by Diakoulaki et al. [12] provides an efficient technique for generating priority weights of criteria or attributes from a decision matrix. The mental workload required from decision-makers in eliciting judgments is significantly minimized, particularly in a huge number of attributes (e.g., 50 attributes). Recent applications of the CRITIC method were reported in the MADM literature (e.g., [13–15]). On the other hand, the CODAS method, proposed by Ghorabaee et al. [16], offers an efficient yet powerful MADM platform based on Euclidean distance, similarly conceptualized with the Technique for Order of Preference by Similarity to Ideal Solution (TOPSIS). Such applications of the CODAS and its extensions have been increasing in the literature (e.g., [17–19]). The CODAS-SORT, with a variant offered by Ouhibi and Frikha [20], is part of the family of MCS methods that assigns a set of elements (e.g., alternatives) to predefined classes under an evaluation based on multiple criteria. A brief discussion of the background of MCS is found elsewhere (e.g., [21]), and the performance of the CODAS-SORT is found to be comparable with TOPSIS-SORT and VIKORSORT [21, 22], but with a more efficient computational framework.

Due to the presence of vagueness and uncertainty inherent in both CRITIC and CODAS-SORT, the use of the FFS addresses these conditions by overcoming the limitations of the classical fuzzy set [23] and the intuitionistic fuzzy set [24] or the Pythagorean fuzzy set [25]. This particular argument on epistemic uncertainties has been repeatedly mentioned in several other works in the field of management [26–28]. Proposed by Senapati and Yager [29], the FFS is deemed more capable of handling higher uncertainties than the previously developed fuzzy environments. Although the FF CRITIC has been recently offered in the literature [30, 31], the integration of FFS within CODAS-SORT is not yet explored, so is the application of an integrated FF CRITIC-CODAS-SORT in an MADM problem. This forms the methodological contribution of this work. A case study in a publicly funded HEI in the central Philippines demonstrates the application of the proposed approach. Ultimately, the main contributions of this work advance both the literature on EDUC4 and MCS by developing an integrated approach based on FF CRITIC-CODAS-SORT in systematically identifying high-priority stakeholder roles in overcoming the barriers to EDUC4 implementation. Determining these important roles would inform the design of initiatives and policy directions of different stakeholders in advancing the implementation of EDUC4 in an HEI.

The remainder of this paper is arranged as follows. Section 2 reviews the relevant literature. Section 3 presents some background of FFS, the CRITIC, and CODAS methods. Section 4 details the methodology by illustrating the case study environment and demonstrates the application of the proposed FF CRITIC-CODAS-SORT in identifying the high-priority stakeholder roles. The findings and some key policy insights are discussed in Section 5. It ends with concluding remarks and a discussion of future works in Section 6.

2. Literature Review

Previous works have investigated the barriers to EDUC4 implementation in various aspects: human resources [2, 3], change management [32], technological infrastructure [33, 34], and financial [35], among others. A systematic literature review by Costan et al. [7] reported a comprehensive identification of the barriers to EDUC4 in developing economies. In their work, 12 barriers were identified. These barriers include cybersecurity threats, costly, skill gap of the human capital, apprehensive stakeholders, lack of

training resources, lack of collaboration, knowledge gap for the customization of curriculum design, insufficient available technologies, health issues, time constraint for material preparation, the complexity of learning platforms, and insufficient foundation in basic foundation. The initiatives in addressing these barriers are complex, and the policy directions are ideally dependent on economic characteristics and the willpower of the stakeholders. Notably, the implementation strategies are contextually unique, and there is a need to capture the evidence of changes among the key players, such as the policy-makers, educators (enablers), and learners (receivers) [4]. For example, a study on the design framework for Indonesian higher education using blockchain technology (i.e., an EDUC4 component) concentrates on investing in human resources and social capital [11].

As part of the clusters of barriers identified by Costan et al. [7], managing human resources requires the need for a sustainable program that enhances labor market demands, such as upskilling and reskilling of university graduates aligned with the requirements of the industries [36] to increase productivity [6] and harmonize human and artificial intellectual capital [3]. The policies and practices necessary for upgrading human resources are imperative in EDUC4 implementation. On the other hand, as a technology-based environment, EDUC4 requires ICTs to be integrated into the teaching-learning process. In Malaysian Schools, Ghavifekr and Wong [37] suggest that the utilization of ICTs and the digital revolution have been the focal points in this direction. They demonstrated that the ICT leadership of school principals impacts teachers' effective ICT utilization. Finally, as front liners in the implementation process, the role of educators in exercising the strategic initiatives of the HEI managers is equivalent to the quality of the target competencies. Hamilton [34] postulated teachers' human side efforts while working with AI and other technologies in a university experience. Customized adaptive learning, redefined assessment, and intelligent and smart approaches are some initiatives for enhanced delivery of learning outcomes under an EDUC4 environment.

Previous studies revealed that stakeholders, that is, government, university management, human resource function, ICT function, and educators, play crucial roles in implementing EDUC4 [3, 9, 34]. The macro-level role of the government goes beyond policy-making and funding sources. For instance, in the Philippines, the government and its faculties are committed to the following functions: (1) provide training to educators for lesson delivery, curriculum design, and instructional materials development, (2) align and device initiatives that will complement basic education and EDUC4, (3) craft protocols to safeguard from cybersecurity attacks and to promote healthy use of technologies, (4) strengthen collaboration efforts from internationally recognized higher education institutions (HEIs) and intragovernment agencies, (5) benchmark technologies used by successful implementers of EDUC4, and (6) ensure and evaluate that EDUC4 responds to the sustainable development goals. Moreover, the government's massive role in EDUC4 translates to the seamless coordination between delivering agencies and the HEIs. As a decision-making body, the role of HEI managers is to carry out strategic initiatives to achieve target goals, including pedagogical and evaluation assessments, relevant approaches to promote cybersecurity awareness, applicable measures in learning material preparation, and essential and cost-efficient technologies for content delivery.

Different findings emerged in the literature on EDUC4 implementation. For example, Ramírez-Montoya et al. [38] identified that decision-makers and the social and academic communities play important roles in developing reasoning for complexity. Critical thinking competency has been given importance in the EDUC4 framework in their work. Thus, HEIs must understand that training in complex reasoning is necessary for the academe. Gonzales et al. [8] identified that the financial aspect and lack of training resources are the most prominent barriers among developing economies. HEIs shall take the primary responsibility for overcoming these barriers. As supported by González-Pérez and Ramírez-Montoya [39], the need to incorporate educational practices into the core components of EDUC4 becomes imperative. They added that schools and teachers do not possess the twenty-first-century skill frameworks with the EDUC4 components to develop future skills. The school leadership towards ICT utilization impacts teachers' active ICT utilization, leading to an increase in students' academic performance [37]. The IT integration in schools towards the EDUC4 system has been a great challenge among administrators. López et al. [40] highlighted that leadership in EDUC4 can lead to students' success in attaining the skills and competencies to become IT leaders in modern industries. Due to the university's decentralized design, instructors might use whatever other technology they consider appropriate for their classes at the risk of losing official backing [41]. The ongoing training for using digital educational resources and their integration into traditional practices is important to ease the transition process, with the COVID-19 crisis emphasizing such importance.

Likewise, the need to fully align the practices of various academic disciplines into the EDUC4 framework is discussed in the literature. For example, Bilotta et al. [42] revealed that methods and technologies introduced by big data, automation, virtual and augmented reality, robotics, and ICT will fit with EDUC4, with a case in the tourism industry. Still, the students are not yet trained on techniques, issues, and methods related to the emerging framework. Goldin et al. [43] proposed an architecture to help users recognize how to digitalize education and create a better plan on how EDUC4 can be implemented into the IT landscape of the universities. Another stream emphasizes that professors must possess competencies for innovation, complex problem-solving, entrepreneurship, collaboration, international perspective, leadership, and connection with the needs of society [33]. Emerging literature also focuses on the alignment to engineering education, emphasizing that the education sector mainly benefits from the recent technological progress [9]. They proposed the four core components of EDUC4 in higher education: (1) competencies, (2) learning methods, (3) ICTs, and (4) infrastructure. The 4IR requires that the education system do everything in time

to support the transformation of the curriculum with the requirements of EDUC4 [44]. Thus, it is evident in the literature that the roles of stakeholders are always linked to the EDUC4 transition, either implicitly or explicitly. However, despite the need to systematically understand these roles, the current literature offers limited insights.

3. Preliminaries

3.1. Fermatean Fuzzy Set. The fuzzy set theory has been well-regarded for dealing with imprecise information and uncertainties. It was developed primarily by Zadeh [23] as an application for the numerous valued logic to illustrate the behavior of complex electrical systems. An extension of the fuzzy set theory was introduced by Atanassov [24], which is the intuitionistic fuzzy set (IFS). It is characterized by a membership function, a non-membership function, and a hesitancy degree that expresses support, opposition, and neutrality in eliciting information [24], extending the concept of membership functions of Zadeh's fuzzy set theory. It is defined as follows:

Definition 1 (see [24]). Let Δ be a non-empty universe of discourse. The IFS F has the general form

$$F = \{(x, \mu_F(x), \nu_F(x)) : x \in \Delta\}, \tag{1}$$

where $\mu_F(x) : \Delta \longrightarrow [0,1]$ and $\nu_F(x) : \Delta \longrightarrow [0,1]$ such that $0 \le (\mu_F(x) + \nu_F(x)) \le 1$ for all $x \in \Delta$. Furthermore, $\mu_F(x)$ and $\nu_F(x)$ refer to the degree of membership and degree of non-membership of the element $x \in \Delta$ in the set F, respectively.

However, in practical application, decision-makers may elicit their judgment fulfilling a set condition either to an assisting or opposing degree greater than 1. Thus, Yager [25] introduced the notion of Pythagorean fuzzy sets (PFS) to address this possible condition, whose illustration is given as follows:

Definition 2 (see [25]). Let Δ be a non-empty universe of discourse, and the PFS $\mathscr{P}$ can be presented as follows:

$$\mathscr{P} = \{(x, \mu_{\mathscr{P}}(x), \nu_{\mathscr{P}}(x)) : x \in \Delta\}, \tag{2}$$

where $\mu_{\mathscr{P}}(x) : \Delta \longrightarrow [0,1]$ and $\nu_{\mathscr{P}}(x) : \Delta \longrightarrow [0,1]$ such that $0 \le (\mu_{\mathscr{P}}(x))^2 + (\nu_{\mathscr{P}}(x))^2 \le 1$ for all $x \in \Delta$. Furthermore, $\mu_{\mathscr{P}}$ and $\nu_{\mathscr{P}}(x)$ refer to the degree of membership and degree of non-membership of the element $x \in \Delta$ in the set $\mathscr{P}$, respectively. For any $\mathscr{P}$ and $x \in \Delta$, the degree of indeterminacy, $\pi_{\mathscr{P}}(x)$, can be calculated by

$$\pi_{\mathscr{P}}(x) = \sqrt{1 - (\mu_{\mathscr{P}}(x))^2 - (\nu_{\mathscr{P}}(x))^2}. \tag{3}$$

However, the PFS could not handle certain conditions. For instance, $\mu_{\mathscr{P}} = 0.9$ and $\nu_{\mathscr{P}} = 0.6$ suggest that $0.9^2 + 0.6^2 \le 1$. Thus, Senapati and Yager [29] proposed the notion of the FFS to provide a tool for handling uncertain information more efficiently and is more flexible in capturing uncertain information than IFS and PFS. The features and operators of FFS are defined as follows:

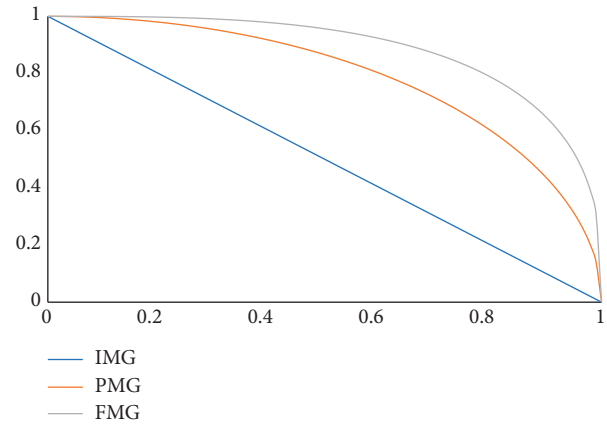

Figure 1: Comparison of space of FMGs, PMGs, and IMGs.

Definition 3 (see [29]). Let Δ be a non-empty universe of discourse. The Fermatean fuzzy set T in Δ can be presented as follows:

$$T = \{(x, \mu_T(x), \nu_T(x)) : x \in \Delta\}, \tag{4}$$

where $\mu_T(x) : \Delta \longrightarrow [0,1]$ and $\nu_T(x) : \Delta \longrightarrow [0,1]$ such that $0 \le (\mu_T(x))^3 + (\nu_T(x))^3 \le 1$ for all $x \in \Delta$. Furthermore, $\mu_T(x)$ and $\nu_T(x)$ refer to the degree of membership and degree of non-membership of the element x in the set T, respectively. Meanwhile, the degree of indeterminacy, $\pi_T(x)$, is identified through

$$\pi_T(x) = \sqrt[3]{1 - (\mu_T(x))^3 - (\nu_T(x))^3}. \tag{5}$$

Figure 1 shows the difference among the spaces related to intuitionistic membership grades (IMG), Pythagorean membership grades (PMG), and Fermatean membership grades (FMG). In general, these fuzzy sets are part of a class of q-rung orthopair fuzzy sets in which the sum of the q^{th} power of the membership function and the q^{th} power of the non-membership function is bounded by 1 [45]. For instance, $q = 1$ implies IFS; $q = 2$ implies PFS.

Definition 4 (see [29]). Suppose that $T = (\mu_T, \nu_T)$, $T_1 = (\mu_{T_1}, \nu_{T_1})$, and $T_2 = (\mu_{T_2}, \nu_{T_2})$ are three distinct FFS and $\alpha > 0$, then the following are the operators for the FFS:

$$\begin{aligned}
T_1 \cap T_2 &= \left(\min\{\mu_{T_1}, \mu_{T_2}\}, \max\{\nu_{T_1}, \nu_{T_2}\}\right),\\
T_1 \cup T_2 &= \left(\max\{\mu_{T_1}, \mu_{T_2}\}, \min\{\nu_{T_1}, \nu_{T_2}\}\right),\\
T^c &= (\nu_T, \mu_T),\\
T_1 \oplus T_2 &= \left(\sqrt[3]{\mu_{T_1}^3 + \mu_{T_2}^3 - \mu_{T_1}^3\mu_{T_2}^3}, \nu_{T_1}\nu_{T_2}\right),\\
T_1 \otimes T_2 &= \left(\mu_{T_1}\mu_{T_2}, \sqrt[3]{\nu_{T_1}^3 + \nu_{T_2}^3 - \nu_{T_1}^3\nu_{T_2}^3}\right),\\
\alpha T &= \left(\sqrt[3]{1 - \left(1 - \mu_T^3\right)^\alpha}, (\nu_T)^\alpha\right),\\
T^\alpha &= \left((\mu_T)^\alpha, \sqrt[3]{1 - \left(1 - \nu_T^3\right)^\alpha}\right).
\end{aligned} \tag{6}$$

Additional operations on subtraction and division of FFS were introduced by Senapati and Yager [46].

Definition 5 (see [46]). Assume $T_1 = (\mu_{T_1}, \nu_{T_1})$, and $T_2 = (\mu_{T_2}, \nu_{T_2})$ are two distinct FFS, then

$$T_1 \boxminus T_2 = \left(\sqrt[3]{\frac{\mu_{T_1}^3 - \mu_{T_2}^3}{1 - \mu_{T_2}^3}}, \frac{\nu_{T_1}^3}{\nu_{T_2}^3} \right) \text{if } \mu_{T_1} \geq \mu_{T_2}, \nu_{T_1} \leq \min\left\{ \nu_{T_2}, \frac{\nu_{T_2}\pi_{T_1}}{\pi_{T_2}} \right\}. \tag{7}$$

$$T_1 \boxminus T_2 = \left(\frac{\mu_{T_1}}{\mu_{T_2}}, \sqrt[3]{\frac{\nu_{T_1}^3 - \nu_{T_2}^3}{1 - \nu_{T_2}^3}} \right) \text{if } \mu_{T_1} \leq \min\left\{ \mu_{T_2}, \frac{\mu_{T_2}\pi_1}{\pi_2} \right\}, \nu_{T_1} \geq \nu_{T_2}. \tag{8}$$

Definition 6 (see [29]). Assume $T_i = (\mu_{T_i}, \nu_{T_i})$ $(i = 1, 2, \ldots, n)$ be a set of FFS and $w = (w_1, w_2, \ldots, w_n)^K$ be the corresponding weight vector for $\sum_i w_i = 1$. Then, the FF weighted average *FFW* aggregation operator is defined by

$$FFWA(T_1, T_2, \ldots T_n) = \left(\sum_{i=1}^{n} w_i \mu_{T_i}, \sum_{i=1}^{n} w_i \nu_{T_i} \right). \tag{9}$$

Senapati and Yager [29] provided the concept of a score function score: $T \longrightarrow \mathbb{R}$, where T is an FFS and is the basis for ranking FFS alongside the accuracy function. However, the score function cannot rank the FFS in some special cases precisely. Thus, Mishra and Rani [47] proposed a novel FF score function to provide the shortcomings of the existing score function. The features of this score function are defined as follows:

Definition 7 (see [47]). Suppose that $T = (\mu_T, \nu_T)$ is an FFS, the score function for T is defined as follows:

$$S(T) = \frac{1}{2}\left[\left(\mu_T^3 - \nu_T^3 - ln\left(1 + \pi_T^3\right) \right) + 1 \right], \tag{10}$$

where π_T is the corresponding indeterminacy degree. For all μ_T and ν_T, provided that $\mu_T^3 + \nu_T^3 \leq 1$, $S(T) \in [0, 1]$.

Mishra and Rani [47] show that S is increasing monotonically with respect to μ_T and decreasing monotonically with respect to ν_T. The following provides the basis for ranking FFS according to S.

Theorem 1 [47]. *For any two FFS $T_1 = (\mu_{T_1}, \nu_{T_1})$ and $T_2 = (\mu_{T_2}, \nu_{T_2})$, if $\mu_{T_1} > \mu_{T_2}$ and $\nu_{T_1} < \nu_{T_2}$, then $S(T_1) > S(T_2)$.*

The Euclidean distance is also defined in FFS.

Definition 8 (see [29]). Let $T_1 = (\mu_{T_1}, \nu_{T_1})$ and $T_2 = (\mu_{T_2}, \nu_{T_2})$ be two distinct FFS. Then, the Euclidean distance between T_1 and T_2 is

$$d(T_1, T_2) = \sqrt{\frac{1}{2}\left[\left(\mu_{T_1}^3 - \mu_{T_2}^3\right)^2 + \left(\nu_{T_1}^3 - \nu_{T_2}^3\right)^2 + \left(\pi_{T_1}^3 - \pi_{T_2}^3\right)^2 \right]}. \tag{11}$$

3.2. The CRITIC Method. Diakoulaki et al. [12] initially proposed the CRITIC method, which determines the priority weights of elements of a given set through an aggregation process. Accordingly, the underlying notion of the CRITIC method is the significant information that can be drawn from the criteria set that contains the contrast and conflict concentration between criteria [12, 48, 49]. The contrast intensity and degree of variability among scores within the criterion are captured through computing the standard deviation. Additionally, the CRITIC method obtains the pairwise linear correlation coefficients among criteria in evaluating their conflicting relationships. Thus, CRITIC collectively analyses sufficient information contained in the set of evaluation criteria and, in general, the set of homogeneous decision elements.

Definition 9 (see [12]). Let U be a finite set of m alternatives. Then, given a system of n evaluation criteria c_j $(j = 1, \ldots, n)$, the MADM problem in its general form is presented as follows:

$$\max\{c_1(u), c_2(u), \ldots, c_n(u) | a \in U\}. \tag{12}$$

In this case, for every criterion c_j, a membership function x_j is defined that maps the values of c_j to the interval $[0, 1]$. This transformation is based on the concept of the ideal point. Thus, a value close to the ideal c_j^* is the best performance in criterion j and close to the anti-ideal value c_{j^*} is the worst performance in criterion j. The steps in determining the criteria weights using the CRITIC method are as follows. Note that, in general, the criteria set can be a set of any homogeneous decision elements.

Step 1: Determine the set of n criteria and m alternatives constructed as a hierarchical MADM problem.

Step 2: Evaluate the performance score a_{ij} of the i^{th} $(i = 1, \ldots, m)$ alternative with respect to the j^{th} $(j = 1, \ldots, n)$ criterion.

Step 3: Compute the normalized matrix $X = (x_{ij})_{m \times n}$ where the normalized score x_{ij} describes a linear normalization of a_{ij} scores and represents

$$x_{ij} = \frac{a_{ij} - a_{j^*}}{a_j^* - a_{j^*}}, \tag{13}$$

where $a_j^* = \max_i a_{ij}$ and $a_{j^*} = \min_i a_{ij}$ for $j = 1, \ldots, n$.

Step 4: Generate a vector x_j denoting the normalized scores of all m alternatives. Vector x_j is calculated using the following equation:

$$x_j = \left(x_{1j}, x_{2j}, \ldots, x_{mj}\right). \tag{14}$$

Step 5: Compute the standard deviation of each x_j by the following formula:

$$\sigma_j = \sqrt{\frac{\sum_{i=1}^{m}\left(x_{ij} - \overline{x}_j\right)^2}{m}}, \tag{15}$$

where $\overline{x}_j = \sum_{i=1}^{m} x_{ij}/m$. Aside from standard deviation, Diakoulaki et al. [12] suggest that the use of entropy or variance is also possible.

Step 6: Construct a symmetric matrix $R = (r_{jk})_{n\times n}$ where r_{jk} denotes the linear correlation coefficient of two vectors x_j and x_k, $j,k \in \{1,\ldots,n\}$, using the following formula:

$$r_{jk} = \frac{\sum_{i=1}^{m}\left(x_{ij} - \overline{x}_j\right)\left(x_{ik} - \overline{x}_k\right)}{\sqrt{\sum_{i=1}^{m}\left(x_{ij} - \overline{x}_j\right)^2 \sum_{i=1}^{m}\left(x_{ik} - \overline{x}_k\right)^2}}, \tag{16}$$

where $r_{jk} \in [-1,1]$. Obviously, when $j = k$, then $r_{jk} = 1$.

Step 7: Compute the amount of information z_j as follows:

$$z_j = \sigma_j \sum_{k=1}^{n}\left(1 - r_{jk}\right), \tag{17}$$

where the higher value of z_j implies that the criterion j contains more information.

Step 8: Determine the criteria weights according to the following formula:

$$w_j = \frac{z_j}{\sum_{k=1}^{n} z_k}. \tag{18}$$

3.3. The CODAS Method. The CODAS method was initially proposed by Ghorabaee et al. [16], wherein the desirability of the alternatives is determined based on l^1-norm and l^2-norm indifference spaces for criteria. In this method, a combinative form of the Euclidean distance and the secondary measure, Taxicab distance, is used to calculate the assessment score of alternatives wherein the alternative has a greater distance from the negative ideal solution is more desirable. The steps of the CODAS method for MADM problems are presented as follows:

Step 1. Construct the decision matrix A that is represented as follows:

$$A = \left(a_{ij}\right)_{m\times n} = \begin{pmatrix} a_{11} & a_{12} & \cdots & a_{1n} \\ a_{21} & a_{22} & \cdots & a_{2n} \\ \vdots & \vdots & \vdots & \vdots \\ a_{m1} & a_{m2} & \cdots & a_{mn} \end{pmatrix}, \tag{19}$$

where $a_{ij} \geq 0$ denotes the performance value of i^{th} ($i \in \{1,2,\ldots,m\}$) alternative with respect to the j^{th} ($j \in \{1,2,\ldots,n\}$) criterion (or attribute).

Step 2. Determine normalized decision matrix $N = (n_{ij})_{m\times n}$ according to the type of each criterion using the linear normalization of performance values as follows:

$$n_{ij} = \begin{cases} \dfrac{a_{ij}}{\max\limits_i a_{ij}}, & \text{if } j \in P, \\ \dfrac{\min\limits_i a_{ij}}{a_{ij}}, & \text{if } j \in C, \end{cases} \tag{20}$$

where P and C represent the sets of benefit and cost criteria (or attributes), respectively, and n_{ij} denotes the normalized performance values.

Step 3. Calculate the weighted normalized decision matrix $B = (b_{ij})_{m\times n}$ as follows:

$$b_{ij} = w_j n_{ij}, \tag{21}$$

wherein $\sum_{j=1}^{n} w_j = 1$, w_j denotes the weight of the j^{th} criterion, and $0 < w_j < 1$. w_j can be determined through any priority weight generation method (e.g., CRITIC).

Step 4. Determine the negative ideal solution as follows:

$$b_* = \left(b_{j*}\right)_{1\times n}. \tag{22}$$

$$b_{j*} = \min_i b_{ij}. \tag{23}$$

Step 5. Calculate the Euclidean d_i and Taxicab t_i distances of alternatives from the negative ideal solution using the following equation:

$$d_i = \sqrt{\sum_{j=1}^{m}\left(b_{ij} - b_{j*}\right)^2}, \quad \forall i = 1,\ldots,n. \tag{24}$$

$$t_i = \sum_{j=1}^{m}\left|b_{ij} - b_{j*}\right|, \quad \forall i = 1,\ldots,n. \tag{25}$$

Step 6. Construct the relative assessment matrix $H = (h_{ik})_{m\times m}$ presented as follows:

$$h_{ik} = \left(d_i - d_k\right) + \left(\beta\left(d_i - d_k\right) \times \left(t_i - t_k\right)\right), \tag{26}$$

where $k \in \{1,2,\ldots,m\}$ and β is a threshold function that can be set by the decision-maker and defined as follows:

$$\beta = \begin{cases} 1, & \text{if } d_i - d_k \geq \rho, \\ 0, & \text{if } d_i - d_k < \rho. \end{cases} \tag{27}$$

If the difference between the Euclidean distances of the two alternatives is less than ρ, then these two alternatives are also compared by the Taxicab distance.

Step 7. Calculate the assessment score (S_i) of each alternative as follows:

$$S_i = \sum_{k=1}^{m} h_{ik}, \tag{28}$$

wherein the alternative with the highest S_i value is the most desirable. Given the simplicity of the CODAS for the decision-makers and its success, a sorting method was developed by Ouhibi and Frikha [20] called CODAS-SORT. In an MCS problem, the decision-maker aims to assign alternatives to predefined classes. For brevity, the steps of the CODAS-SORT are not repeated here. Despite the introduction of the CODAS-SORT, some technical issues in the sorting process proposed by Ouhibi and Frikha [20] are evident, which prompted an introduction of a modified CODAS-SORT variant, along with the integration of FFS.

4. Methodology

4.1. Case Study Background. To keep up with the consequential dynamics that continue to reshape life, economies, industries, and jobs in developing economies, HEIs should embrace the emerging trends of EDUC4, including personalized learning, remote learning opportunities, an abundance of educational tools, project-based learning, and innovation-based education. In this context, the curriculum and learning outcomes require twenty-first-century skills to address the urgency of essential modernization. Current reports predict that AI will transform the hiring behavior of tech-driven companies. Calibrating to the industry requirements propels the HEIs to remodel their curriculum to integrate life skills into the programs through immersion with real-world stakeholders such as the industry, society, and entrepreneurial networks. Government investments with industry and local society across all aspects of the education value chain, from curricula and faculty to infrastructure, research, study experience, and placements, should expand partnerships. The collaborative models with global experts from academia and industry should also advance in-site research opportunities for small and medium enterprises with limited research groundwork. The faculty may be able to develop a group of champion faculty members coming from different departments who are leading the way in developing digital skills or new innovative teaching techniques utilizing various technologies.

Cebu Technological University (CTU) Danao Campus is a component campus of the CTU, a state university in the central Philippines. Following existing guidelines in Philippine institutions, the operating expenditures among state universities and colleges for personnel services, maintenance, and other operating expenses and the capital outlays are coming from government subsidies allocated through the General Appropriations Act (GAA)—the annual national expenditure budget of the government. Aside from the GAA funds, incomes are also generated from various fees and grants provided by international and local institutions. With the recent rise of the university in various rankings and its expanded role in the national development agenda, CTU is pushing for innovation efforts in its different functions, including instruction and research. Among these efforts is directed towards attaining an environment fostering EDUC4. Since CTU Danao Campus is positioning itself as a globally competitive campus of the university and alignment to EDUC4 is inevitable, efforts are becoming grounded for its realization. Although efforts and activities are evident, an integrative framework, particularly on the design of these initiatives, is missing.

The government resources remained significantly deficient to support the massive task to consolidate the efforts to address barriers related to financial resources and to recalibrate CTU to stay relevant in the age of EDUC4, resulting in struggling levels of university-industry collaboration, insufficient industry-relevant research consortiums, and underdeveloped research infrastructure and cutting-edge laboratories and equipment. The initiatives of CTU 4.0 transformation, coined by the university through EDUC4, are underway; however, government funding priorities should be enforced not only for the operating expenditures but also for the innovation disbursements targeting the significant deficiencies in attaining the inevitable EDUC4 transformation to become a globally competitive educational institution. Although the Philippine government's spending on public higher education exhibited an upward trend, the corresponding increase in government appropriation to state universities means that these universities shall prioritize expenses to expedite solutions for the implementation barriers to enhance research funding, talent, infrastructure, and links with the industry. However, there are inadequate policies, mechanisms, and understanding of how these barriers will be directed. One possible direction is that the constrained allocation of public funding should move toward a performance-based approach for campus research and capital expenditures to concentrate on attaining EDUC4.

In this regard, following a series of strong evidence in the literature, stakeholders play a substantial role in guiding the university for the design, planning, and implementation of any initiative, which includes the direction leaning toward EDUC4. In the current setting, the following stakeholders are relevant for CTU Danao: (1) the Philippine government (i.e., represented by the trifocal agencies Commission on Higher Education (CHED), Department of Education (DepEd), and Technical Education and Skills Development Authority (TESDA)), (2) university management (i.e., from the top management down to academic departments), (3) human resource, (4) ICT function, and (5) educators. Identifying the crucial roles of these stakeholders in systematically overcoming the barriers of EDUC4 implementation is an essential agenda for CTU Danao in its efforts for EDUC4. This agenda would help establish institutional-level policies to describe the impacts, show findings, and provide recommendations for a conceptual-analytical framework for implementing EDUC4. Furthermore, although idiosyncrasies exist, the insights would yield comparative results with other developing economies' strategic priorities and policy actions addressing implementation barriers.

4.2. Proposed Procedure. Figure 2 shows the methodological framework of the Fermatean fuzzy CRITIC-CODAS-SORT approach in establishing the degree to which the stakeholder roles overcome the barriers of EDUC4 implementation.

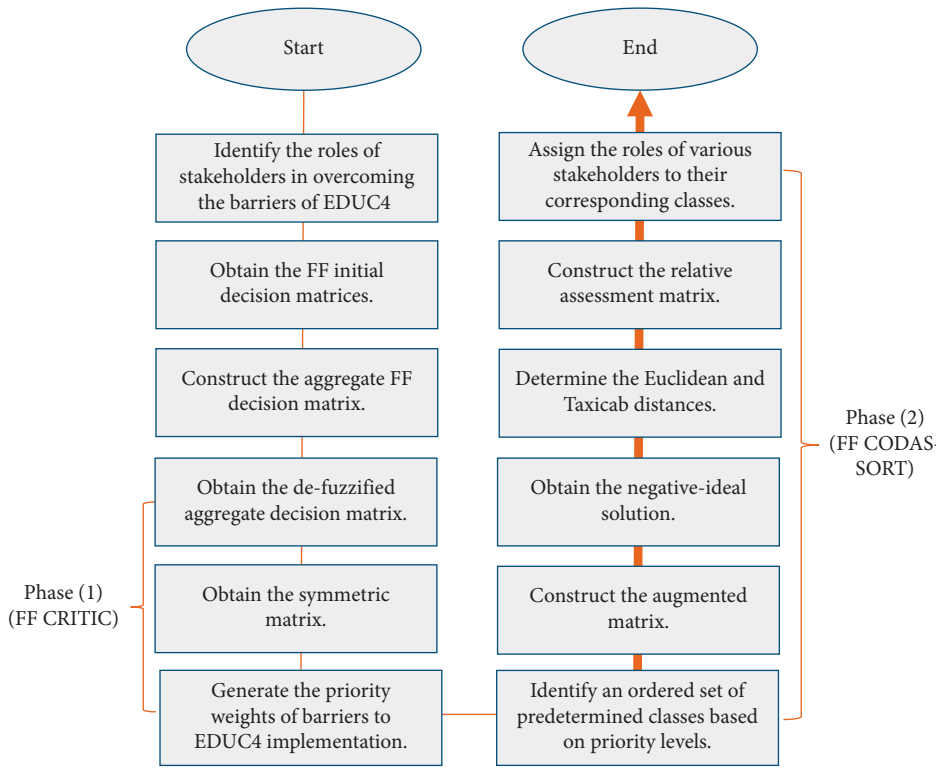

Figure 2: The methodological framework.

Note that due to idiosyncrasies, the implementation of the proposed framework is intended for a single case (e.g., an HEI).

The proposed methodological framework consists of two main phases: (1) obtaining the priority weights of the barriers to EDUC4 implementation through FF CRITIC and (2) sorting the stakeholder roles in addressing these barriers via FF CODAS-SORT. In this framework, the weights generated from phase (1) are integrated into phase (2). The application of the proposed approach is discussed as follows:

Step 1. Identify the roles of stakeholders. This study identified the roles of stakeholders in overcoming the barriers to EDUC4 implementation of a case university (i.e., CTU) through a focus group discussion of domain expert decision-makers. They were chosen in such a way that satisfies the following qualifications: (1) must be affiliated with the HEI in the case environment, (2) must have a PhD degree, (3) must have at least five years of experience in a supervisory or administrative function, and (4) must have at least five years of experience working with the HEI in the case environment. As shown in Table 1, five stakeholders, that is, government, university management, human resource function, ICT function, and educators, were identified along with their corresponding roles in overcoming the barriers identified by Costan et al. [7] (see Table 2). In the case study, the government comprises frontline institutions consisting of the CHED, DepEd, and TESDA. They are the trifocal institutions associated with the educational system in the Philippines. The university management consists of those in the organizational hierarchy ranging from the chairs of the academic departments, deans of colleges, campus directors, vice presidents, and president, to the board of regents. The human resource function oversees the functional areas of human resource management, including staffing, development, compensation, safety and health, human resource information system, and employee and labor relations. On the other hand, the ICT function manages communication, data management, cybersecurity, and technology development. Lastly, the educators represent the teaching staff of the university.

Step 2. Obtain the FF initial decision matrices. Initial decision matrices $\widetilde{A}^k = (\widetilde{a}_{ij}^k)_{m\times n}$, for $k = 1, \ldots, K$, where $\widetilde{a}_{ij}^k = (\mu_{\widetilde{a}_{ij}}^{\sim k}, \nu_{\widetilde{a}_{ij}}^{\sim k})$ represents the degree of relevance of stakeholder role i in overcoming a barrier to EDUC4 implementation j elicited by the k^{th} decision-maker in linguistic terms, were constructed. These matrices were transformed into FF decision matrices using the linguistic scale shown in Table 3.

Phase 1. Implementation of the FF CRITIC.

The processes in steps 3 to 5 discuss the integration of FF CRITIC in assigning priority weights to barriers to EDUC4 implementation.

Step 3. Construct the aggregate FF decision matrix. The aggregate FF decision matrix $\widetilde{A} = (\widetilde{a}_{ij})_{m\times n}$ is

Table 1: Stakeholder roles in overcoming the barriers of EDUC4 implementation.

Stakeholders	Codes	Roles
Government (i.e., CHED, DepEd, and TESDA)	G1	Investing in endpoint protection against cybersecurity attacks (e.g., malware, phishing, and trojans, among others)
	G2	Delivering up-to-date training of human resources (e.g., educators) about cybersecurity threats
	G3	Inclusion of cybersecurity awareness in the basic education curriculum
	G4	Allocating more funds to support the necessary inclusive activities in the implementation of EDUC4
	G5	Implementing initiatives to direct linkages among stakeholders in different areas of cooperation (e.g., industry-CHED and international organizations)
	G6	Updating of curricular offerings based on the labor market signals posed by I4.0
	G7	Forging heightened information dissemination drives about EDUC4 to all stakeholders
	G8	Designing an overall policy agenda, including road mapping, in the implementation of EDUC4
	G9	Positioning the EDUC4 implementation within the UN Sustainable Development Goals
	G10	Promoting cross-functional collaboration that involves different functional expertise in various relevant government offices
	G11	Designing the curricula in line with the implementation and sustainment of EDUC4
	G12	Designing appropriate measures for the emergence of new technologies that affect learning (e.g., addiction to gaming and social media)
	G13	Promotion and creation of initiatives that yield social and psychological benefits to foster healthy behaviors
	G14	Creation of network infrastructure to lessen the complexity of learning platforms
	G15	Fostering opportunities for the emergence of self-organization, dynamic activities with AIs
	G16	Streamlining alignment initiatives of the basic education agenda (e.g., human resources and curricula) to EDUC4
University management (from the top management down to academic departments)	U17	Engaging in initiatives in promoting cybersecurity awareness among university members (i.e., educators, learners, and staff)
	U18	Designing measures that are security-cognizant (e.g., centralized IT governance, uniform control, segregation of networks, enhanced strategic alignment, and accountability), including stringent access regulators to shield sensitive data and information
	U19	Investing in efficient technologies (e.g., virtual classrooms, enablement or process audit, analytic tools for strategic planning, and the hybrid or fully automated process of project management), which are known to reduce overall costs and improve the experience of the university stakeholders
	U20	Constant training and capability upgrading of educators in terms of technical competencies and behavioral stamina for supporting adaptability, reliability, productivity, and total well-being as they align with the demands of EDUC4
	U21	Fostering transformational support and environmental and institutional framework for university educators, learners, and staff for adapting to the EDUC4 atmosphere
	U22	Engaging stakeholders in dialogues that emphasize the alignment of EDUC4 with global inclusive agenda (e.g., UN-SDGs)
	U23	Exploring the translation of the EDUC4 framework into pedagogy, assessment, and the design of an instructional system
	U24	Forging extensive collaboration with various stakeholders (e.g., policy-makers, academic experts, university networks, educators, education leaders, learners, and industry partners) to provide space and training resources for implementing EDUC4
	U25	Benchmarking of established and favorable practices for EDUC4 implementation
	U26	Establishing measures that would allow more time for the educators in preparing learning materials, conducting research and development projects, and attending to continuous learning opportunities inclined to EDUC4

Table 1: Continued.

Stakeholders	Codes	Roles
	U27	Established intensified policies of college entry requirements, particularly in evaluating the readiness of candidate learners in an EDUC4 environment
Human resource function	H28	Incorporating data privacy and protection orientation during personnel hiring
	H29	Restricting access of any information and sites only to its trusted users or known parties
	H30	Designing non-ambiguous measures for the protection of the human resource from insider threats, which may expose potentially damaging contents
	H31	Implementing information drives for personnel and other stakeholders on how to protect themselves against phishing, social engineering (e.g., acquiring login credentials), and other cybersecurity attacks
	H32	Designing initiatives that would encourage cybersecurity culture among university educators
	H33	Participating actively in university-wide efforts for cost-efficient initiatives in building human capabilities required in EDUC4 implementation
	H34	Periodic training of the human resources on the skills (i.e., especially digital readiness and customization of curriculum design) fitting to the current demands of EDUC4
	H35	Designing policies for personnel hiring, merit, and promotions system (i.e., including collaboration as an indicator) relevant to EDUC4 to ensure that the most competent and qualified employees are hired and retained
	H36	Initiating forums among stakeholders (e.g., educators, parents, and local governments) to discuss the pressing need for EDUC4 adoption
	H37	Establishing programs to coach or support employees who seek to acquire external training grants and collaboration
	H38	Designing a recognition system that recognizes and acknowledges the collaborative endeavors of the educators and staff
	H39	Integrating health issues as an integral part of the personnel development efforts (e.g., periodic health monitoring and health benefits) of the university
ICT function	I40	Investing in collaboration efforts with IT experts capable of addressing cybersecurity threats
	I41	Designing robust infrastructure against cybersecurity threats
	I42	Initiating inclusive programs (e.g., information dissemination, training, workshops, and continuous learning) that would encourage an IT culture among university stakeholders
	I43	Directing the IT infrastructure needs of the university, including maintenance of equipment, that would support the implementation of EDUC4
	I44	Forging constant collaboration with IT experts to seek efficient and effective IT solutions for EDUC4 needs
Educators	E45	Engaging in continuous learning initiatives about relevant cybersecurity threats at the university (i.e., data breaches on student information, denial of service attacks, and phishing)
	E46	Integrating awareness of applicable laws to cyberbullying in (virtual) classroom teaching
	E47	Devising alternative cost-efficient teaching strategies in the delivery of required learning outcomes while upholding the implementation of EDUC4
	E48	Initiating collaboration efforts with other educators (i.e., inside or outside the university) in the delivery of cost-efficient methods in EDUC4 implementation
	E49	Participating in inclusive efforts (e.g., training, workshops, formal education, focus group discussions, symposiums, and industry immersion) for upgrading and aligning necessary skills (including an emphasis on handling complex learning platforms) for implementing EDUC4
	E50	Taking part in efforts to demonstrate the need and relevance of EDUC4 to stakeholders (i.e., parents, investors, local governments, and immediate community)
	E51	Involvement in the planning, selection, and maintenance efforts of technologies to support teaching-learning under an EDUC4 environment
	E52	Establishing holistic initiatives for linkage and collaboration with foreign universities, industry, non-government organizations, government offices, and international organizations, among others, in the delivery of intended

Table 1: Continued.

Stakeholders	Codes	Roles
		learning outcomes, along with their support infrastructure, within the context of EDUC4
	E53	Participation in efforts for increased visibility in online forums and platforms to possibly establish collaboration
	E54	Taking part in the design, development, and improvement of innovative curricula aligned to EDUC4
	E55	Integrating health standards, including the mental health of learners, in designing their intended learning outcomes consistent with EDUC4
	E56	Promoting ways to efficiently prepare learning materials, including the use of advanced ICTs
	E57	Participating in skills development initiatives aimed at equipping educators with the capabilities in handling different complex learning platforms

Table 2: Barriers to EDUC4 implementation [7].

Code	Barrier	Brief description
B1	Cybersecurity threat	The threat of information leakage, security attacks, and misusage of technology
B2	Costly	Implementation of EDUC4 requires high costs (e.g., acquisition of equipment and maintenance)
B3	Skills gap of the human capital	Insufficient knowledge and experience of the human capital in using digital technology for education and lack of specific skills (i.e., critical thinking and emotional intelligence)
B4	Apprehensive stakeholders	Apprehension of some stakeholders (i.e., learners, educators, and administrators) to EDUC4
B5	Lack of training resources	The lack of training resources (i.e., facility and materials) for professional development
B6	Lack of collaboration	Lack of collaboration with other sectors (i.e., community, government, other HEIs, and industry) that is essential in successfully implementing EDUC4
B7	Knowledge gap for the customization of curriculum design	Current lack of knowledge to create a customized curriculum design to enhance learner's skills (i.e., creativity and critical thinking) and promote skills-based training
B8	Insufficient available technologies	Due to the rapid advancement of technology, developing countries cannot catch up with developed countries; some technology might already be available in some countries but not in others
B9	Health issues	Prolonged exposure to the technology that may cause health issues in the physical and mental well-being of the learners and educators
B10	Time constraint for material preparation	The time needed to prepare and teach in a virtual learning platform that requires more time than the traditional one
B11	Complexity of learning platforms	The challenge that the users (i.e., learners and educators) face in utilizing the virtual learning platform
B12	Insufficient foundation in basic foundation	Students with proper primary education, an essential component in implementing EDUC4, are rare

Table 3: Linguistic evaluation scale.

Linguistic term	Non-FFS scores	FFS
Extremely low	1	(0.1, 0.9)
Low	2	(0.25, 0.6)
Moderately low	3	(0.4, 0.5)
Medium	4	(0.5, 0.4)
Moderately high	5	(0.6, 0.3)
High	6	(0.7, 0.2)
Extremely high	7	(0.9, 0.1)

constructed, where $\tilde{a}_{ij}$ is obtained using equation (9) and w_i is the corresponding weight of k^{th} decision-maker. In this study, the length of service holding a supervisory or managerial position and level of administrative function were used to assign weights to decision-makers. Following the agreement of the decision-makers, the following are used to generate their importance weights to the decision-making problem. To give more credit to their current administrative functions, the scores of 5, 4, 3, and 2 are assigned to Campus Director, Assistant Campus Director, Dean, and Program Chair, respectively. For instance, the importance weight of DM3 is computed as: $0.2022 = 14/87 * 4/3.1839$, where 14 is the number of years holding a supervisory or managerial position, 87 is the sum of column (2) of Table 4, and 3.1839 is the sum of all products of normalized column (2) and the scores associated with their current administrative functions of all decision-makers. Analogous to equation (9), $\tilde{A}$ is shown in Table 5, where

$$\tilde{a}_{ij} = FFWA\left(\tilde{a}_{ij}^1, \tilde{a}_{ij}^2, \ldots, \tilde{a}_{ij}^K\right) = \left(\sum_{k=1}^{K} w_k \mu_{\tilde{a}_{ij}}, \sum_{k=1}^{K} w_k \nu_{\tilde{a}_{ij}}\right), \quad (29)$$

Table 4: Assignment of weights of decision-makers.

Decision-maker	No. of years holding a supervisory or managerial position	Current administrative function	Importance weight
DM1	5	Program chair	0.0361
DM2	13	Program chair	0.0939
DM3	14	Assistant campus director	0.2022
DM4	10	Dean	0.1083
DM5	12	Program chair	0.0866
DM6	17	Dean	0.1841
DM7	16	Campus director	0.2888

where w_k is the importance weight of k^{th} decision-maker.

Step 4. Obtain the defuzzified aggregate decision matrix A. The defuzzified aggregate decision matrix $A = (a_{ij})_{m\times n}$ was obtained using equation (10) to transform the aggregate evaluation scores in FFS to their corresponding crisp (non-FFS) values. The resulting matrix is shown in Table 6. Instead of equation (15), the entropy e_j method was used in this work as presented in the following equation:

$$e_j = \frac{1}{\ln(m)} \sum_{i=1}^{m} a_{ij} \ln\left(a_{ij}\right) \text{ for } j = 1, \ldots, n. \tag{30}$$

Step 5. Obtain the symmetric matrix R. The symmetric matrix R was constructed using equation (16) and is shown in Table 7.

Step 6. Generate the priority weights w_j, $j = 1, \ldots, m$, of barriers to EDUC4 implementation. The information value z_j is calculated using equation (17). Furthermore, the two values, e_j and z_j, are used to obtain the priority weights w_j using equation (18). The w_j values are presented in Table 8.

Phase 2. Implementation of the FF CODAS-SORT

Here, steps 6 to 10 discuss the application of FF CODAS-SORT in sorting the roles of various stakeholders in overcoming the different barriers to EDUC4 implementation.

Step 6. Identify an ordered set of predetermined classes based on priority levels. In general, L $(e = 1, \ldots, L)$ classes can be predefined for the MCS process. These classes generate $L - 1$ limit profiles. Each e class contains lower and upper boundaries, denoted by l_e^a and l_e^b, where $l_e^b = l_{e+1}^a$. In this work, $L = 3$ classes (i.e., low relevance, moderate relevance, and high relevance) and two limit profiles are introduced.

Step 7. Construct the augmented matrix $\overline{A}$. The aggregate FF decision matrix in step 3 with the $L - 1$ limit profiles identified in step 6 is used to construct the augmented matrix $\overline{A} = (\overline{a}_{ij})_{m\times n}$. The resulting matrix is presented in Table 9.

Step 8. Obtain the negative ideal solution b_*. $\overline{A}$ was used to obtain the negative ideal solution $\widetilde{b}_* = (\widetilde{b}_{j*})_{1\times n}$ using equation (23). Considering that the elements in $\overline{A}$ are FFS, then Definition 7 and Theorem 1 discussed in Section 3.1 were used to obtain $\widetilde{b}_*$. The resulting vector is illustrated in Table 10.

Step 9. Determine the Euclidean and Taxicab distances. The Euclidean distance $D_i(\overline{a}_{ij}, \widetilde{b}_{j*})$ between each stakeholder role i (including the limit profiles) and the ideal negative solution b_{j*} obtained in step 8 is calculated using the following equation:

$$D_i\left(\overline{a}_{ij}, \widetilde{b}_{j*}\right) = \sum_{j=1}^{m} w_j d\left(\overline{a}_{ij}, b_{j*}\right), \tag{31}$$

where w_j represents the priority weights of barriers to EDUC4 implementation obtained from FF CRITIC in step 5 in Section 3.2 and $d(\overline{a}_{ij}, b_{j*})$ is calculated using equation (11).

On the other hand, the Taxicab distance $\widetilde{t}_i(\overline{a}_{ij}, \widetilde{b}_{j*})$ between each stakeholder role i (including the limit profiles) and the ideal negative solution b_{j*} obtained in step 8 in Section 3.2. is calculated analogously using equation (25). Considering that both elements are FFS, equation (7) was used to obtain their difference. Then, equation (10) was used to transform the obtained Taxicab distance $\widetilde{t}_i(\overline{a}_{ij}, \widetilde{b}_{j*})$ to their corresponding crisp value $t_i(\overline{a}_{ij}, \widetilde{b}_{j*})$. Both the Euclidean and Taxicab distances are shown in Table 11.

Step 10. Construct the relative assessment matrix. Following step 6 in Section 3.2, the relative assessment matrix $H = (h_{i\kappa})_{m\times L-1}$ is calculated, where $h_{i\kappa}$ is shown in equation (32), and the resulting matrix is featured in Table 12. The threshold parameter is set to be $\rho = 0.02$.

$$\begin{aligned} h_{i\kappa} = &\left(D_i\left(\overline{a}_{ij}, \widetilde{b}_{j*}\right) - D_\kappa\left(\overline{a}_{\kappa j}, \widetilde{b}_{j*}\right)\right) \\ &+ \left(\beta\left(D_i\left(\overline{a}_{ij}, \widetilde{b}_{j*}\right) - D_\kappa\left(\overline{a}_{\kappa j}, \widetilde{b}_{j*}\right)\right)\right. \\ &\times \left.\left(t_i\left(\overline{a}_{ij}, \widetilde{b}_{j*}\right) - t_\kappa\left(\overline{a}_{\kappa j}, \widetilde{b}_{j*}\right)\right)\right). \end{aligned} \tag{32}$$

where $\kappa = 1, \ldots, L - 1$ and β is a threshold function defined in equation (27).

Step 11. Assign the roles of various stakeholders to the predefined classes.

Suppose that $h_{i\kappa}(L2)$ is the highest limiting profile, then the stakeholder role i can be classified as follows:

class L_{high} if $h_{ik}(L2) \geq 0$.

class L_{mod} if $h_{ik}(L2) < 0$ and $h_{ik}(L1) \geq 0$.

Table 5: Aggregate FF decision matrix.

Codes	B1	B2	B3	B4	B5	B6
G1	(0.8675, 0.1217)	(0.5798, 0.3238)	(0.6184, 0.3036)	(0.5498, 0.3502)	(0.6069, 0.2913)	(0.6404, 0.2921)
G2	(0.7989, 0.1614)	(0.6960, 0.2365)	(0.7036, 0.2184)	(0.6014, 0.2986)	(0.7542, 0.1783)	(0.6773, 0.2516)
G3	(0.8495, 0.1361)	(0.5621, 0.3448)	(0.6487, 0.2549)	(0.6350, 0.2650)	(0.6708, 0.2292)	(0.7412, 0.2155)
G4	(0.6545, 0.2819)	(0.8567, 0.1325)	(0.6437, 0.2870)	(0.7253, 0.2036)	(0.7354, 0.1866)	(0.6051, 0.2949)
G5	(0.5838, 0.3238)	(0.6231, 0.2769)	(0.6271, 0.2729)	(0.8783, 0.1108)	(0.6047, 0.2953)	(0.8675, 0.1217)
G6	(0.5960, 0.3256)	(0.5534, 0.3502)	(0.8502, 0.1303)	(0.6032, 0.2968)	(0.6220, 0.2780)	(0.5823, 0.3177)
G7	(0.5119, 0.4011)	(0.6112, 0.2924)	(0.6274, 0.3014)	(0.8783, 0.1108)	(0.4946, 0.4054)	(0.8675, 0.1217)
G8	(0.5599, 0.3495)	(0.5112, 0.3870)	(0.7527, 0.2014)	(0.7942, 0.1729)	(0.6076, 0.2924)	(0.6957, 0.2130)
G9	(0.5227, 0.3773)	(0.5968, 0.3014)	(0.6783, 0.2217)	(0.5755, 0.3245)	(0.5361, 0.3621)	(0.6686, 0.2383)
G10	(0.5469, 0.3617)	(0.5274, 0.3848)	(0.6112, 0.2888)	(0.8061, 0.1523)	(0.5859, 0.3325)	(0.8567, 0.1325)
G11	(0.5412, 0.3682)	(0.5401, 0.3635)	(0.7729, 0.1787)	(0.6415, 0.2585)	(0.7116, 0.2069)	(0.4989, 0.3993)
G12	(0.7166, 0.2087)	(0.7332, 0.2087)	(0.6119, 0.3152)	(0.5635, 0.3365)	(0.6906, 0.2383)	(0.5906, 0.3130)
G13	(0.5809, 0.3227)	(0.5329, 0.3708)	(0.6166, 0.2816)	(0.6856, 0.2390)	(0.5300, 0.3682)	(0.6292, 0.2744)
G14	(0.5729, 0.3347)	(0.7801, 0.1906)	(0.6588, 0.2498)	(0.4986, 0.4014)	(0.5325, 0.3632)	(0.4585, 0.4415)
G15	(0.6574, 0.2646)	(0.7729, 0.1780)	(0.6783, 0.2401)	(0.5816, 0.3184)	(0.7245, 0.1939)	(0.5491, 0.3509)
G16	(0.5408, 0.3722)	(0.5599, 0.3437)	(0.8343, 0.1426)	(0.5560, 0.3440)	(0.7011, 0.2155)	(0.4986, 0.4014)
U17	(0.8487, 0.1274)	(0.6567, 0.2653)	(0.7318, 0.2155)	(0.5224, 0.3769)	(0.6112, 0.2924)	(0.6199, 0.2838)
U18	(0.8134, 0.1433)	(0.8126, 0.1581)	(0.6318, 0.2751)	(0.6029, 0.2971)	(0.6058, 0.2924)	(0.6235, 0.2765)
U19	(0.8144, 0.1599)	(0.8458, 0.1433)	(0.6047, 0.3224)	(0.6444, 0.2740)	(0.6209, 0.2957)	(0.7130, 0.2379)
U20	(0.6155, 0.2968)	(0.7209, 0.2202)	(0.8502, 0.1303)	(0.6040, 0.2960)	(0.8025, 0.1542)	(0.5549, 0.3451)
U21	(0.6278, 0.3000)	(0.5729, 0.3307)	(0.6740, 0.2260)	(0.6892, 0.2108)	(0.6625, 0.2560)	(0.7542, 0.1729)
U22	(0.5448, 0.3552)	(0.5310, 0.3671)	(0.5238, 0.3762)	(0.8415, 0.1292)	(0.5498, 0.3502)	(0.8235, 0.1437)
U23	(0.5249, 0.3827)	(0.6090, 0.2946)	(0.8321, 0.1448)	(0.5599, 0.3401)	(0.8235, 0.1437)	(0.6040, 0.2960)
U24	(0.5394, 0.3588)	(0.6014, 0.3022)	(0.6271, 0.2949)	(0.8675, 0.1181)	(0.8307, 0.1365)	(0.9000, 0.1000)
U25	(0.5480, 0.3606)	(0.5718, 0.3318)	(0.6148, 0.3159)	(0.6292, 0.2708)	(0.5671, 0.3329)	(0.7245, 0.1939)
U26	(0.5675, 0.3455)	(0.5036, 0.4000)	(0.5274, 0.3910)	(0.4693, 0.4307)	(0.5599, 0.3401)	(0.5307, 0.3693)
U27	(0.5664, 0.3458)	(0.4960, 0.4076)	(0.6588, 0.2596)	(0.6108, 0.2892)	(0.4715, 0.4267)	(0.4946, 0.4162)
H28	(0.8343, 0.1419)	(0.6199, 0.2838)	(0.6365, 0.2819)	(0.5329, 0.3671)	(0.6256, 0.2744)	(0.5982, 0.3000)
H29	(0.8134, 0.1433)	(0.6632, 0.2368)	(0.5527, 0.3509)	(0.5343, 0.3657)	(0.6935, 0.2336)	(0.5386, 0.3758)
H30	(0.8487, 0.1274)	(0.6199, 0.2838)	(0.6072, 0.2928)	(0.5473, 0.3527)	(0.5650, 0.3350)	(0.6036, 0.2964)
H31	(0.7722, 0.1787)	(0.5599, 0.3437)	(0.6812, 0.2458)	(0.6307, 0.2693)	(0.6271, 0.2729)	(0.6513, 0.2487)
H32	(0.8408, 0.1390)	(0.6112, 0.2924)	(0.6783, 0.2401)	(0.6617, 0.2383)	(0.6668, 0.2332)	(0.7072, 0.1964)
H33	(0.5253, 0.3747)	(0.6184, 0.2852)	(0.6740, 0.2531)	(0.6220, 0.2780)	(0.6097, 0.3123)	(0.7578, 0.1711)
H34	(0.5635, 0.3549)	(0.6957, 0.2166)	(0.8783, 0.1108)	(0.5570, 0.3430)	(0.8783, 0.1108)	(0.6325, 0.2783)
H35	(0.4982, 0.4018)	(0.5520, 0.3516)	(0.6199, 0.2986)	(0.6899, 0.2390)	(0.6458, 0.2726)	(0.7245, 0.2032)
H36	(0.4700, 0.4242)	(0.5148, 0.3888)	(0.4455, 0.4502)	(0.8675, 0.1217)	(0.4823, 0.4159)	(0.6769, 0.2451)
H37	(0.4184, 0.4845)	(0.7043, 0.2177)	(0.8502, 0.1303)	(0.5466, 0.3534)	(0.7245, 0.1975)	(0.5776, 0.3390)
H38	(0.4119, 0.4769)	(0.5819, 0.3217)	(0.6076, 0.3108)	(0.5397, 0.3585)	(0.6184, 0.3036)	(0.7473, 0.1910)
H39	(0.5458, 0.3578)	(0.6227, 0.2809)	(0.5982, 0.3000)	(0.6097, 0.2859)	(0.5928, 0.3108)	(0.6069, 0.2913)
I40	(0.8675, 0.1217)	(0.7686, 0.1910)	(0.6675, 0.2509)	(0.6307, 0.2693)	(0.6516, 0.2668)	(0.7101, 0.2083)
I41	(0.8596, 0.1202)	(0.5895, 0.3141)	(0.6177, 0.2823)	(0.5224, 0.3733)	(0.6924, 0.2347)	(0.6870, 0.2455)
I42	(0.5632, 0.3491)	(0.6935, 0.2285)	(0.6639, 0.2581)	(0.8126, 0.1545)	(0.5794, 0.3390)	(0.8502, 0.1267)
I43	(0.6307, 0.2877)	(0.8018, 0.1690)	(0.5238, 0.3848)	(0.6708, 0.2292)	(0.6841, 0.2159)	(0.6166, 0.2816)
I44	(0.6783, 0.2401)	(0.6783, 0.2253)	(0.6415, 0.2585)	(0.6617, 0.2383)	(0.5874, 0.3126)	(0.8206, 0.1397)
E45	(0.9000, 0.1000)	(0.6567, 0.2653)	(0.7469, 0.1827)	(0.6415, 0.2585)	(0.8603, 0.1253)	(0.6343, 0.2657)
E46	(0.8451, 0.1310)	(0.6004, 0.3227)	(0.5440, 0.3596)	(0.8271, 0.1401)	(0.5787, 0.3433)	(0.8126, 0.1581)
E47	(0.5231, 0.3805)	(0.6292, 0.2794)	(0.7195, 0.1989)	(0.6040, 0.2960)	(0.8892, 0.1072)	(0.7191, 0.2206)
E48	(0.5036, 0.4000)	(0.5744, 0.3256)	(0.6242, 0.2758)	(0.6448, 0.2661)	(0.6661, 0.2632)	(0.8783, 0.1108)
E49	(0.4473, 0.4379)	(0.6957, 0.2166)	(0.8206, 0.1397)	(0.6217, 0.2819)	(0.8603, 0.1253)	(0.6379, 0.2621)
E50	(0.4314, 0.4574)	(0.5946, 0.3199)	(0.4910, 0.4072)	(0.7989, 0.1686)	(0.5484, 0.3498)	(0.7650, 0.1823)
E51	(0.4217, 0.4671)	(0.6675, 0.2361)	(0.7332, 0.1852)	(0.5437, 0.3563)	(0.5903, 0.3097)	(0.5545, 0.3491)
E52	(0.4260, 0.4733)	(0.5209, 0.4011)	(0.6776, 0.2444)	(0.6087, 0.2913)	(0.6588, 0.2596)	(0.7224, 0.1996)
E53	(0.6195, 0.2841)	(0.6014, 0.3022)	(0.6162, 0.2838)	(0.6108, 0.2892)	(0.5061, 0.3939)	(0.7643, 0.1830)
E54	(0.4401, 0.4451)	(0.5347, 0.3690)	(0.8278, 0.1491)	(0.7545, 0.1838)	(0.8567, 0.1289)	(0.6108, 0.2928)
E55	(0.5646, 0.3390)	(0.7152, 0.2069)	(0.6159, 0.2841)	(0.6964, 0.2036)	(0.5235, 0.3801)	(0.5278, 0.3722)
E56	(0.7787, 0.1704)	(0.8126, 0.1581)	(0.7924, 0.1556)	(0.7458, 0.1917)	(0.8271, 0.1401)	(0.5653, 0.3347)

Table 5: Continued.

Codes	B1	B2	B3	B4	B5	B6
E57	(0.6047, 0.2953)	(0.7513, 0.1996)	(0.8415, 0.1390)	(0.6596, 0.2440)	(0.8603, 0.1253)	(0.6866, 0.2422)
Codes	B7	B8	B9	B10	B11	B12
G1	(0.5202, 0.3791)	(0.7422, 0.2144)	(0.5061, 0.3931)	(0.4545, 0.4412)	(0.5152, 0.3848)	(0.4567, 0.4462)
G2	(0.5123, 0.3733)	(0.7069, 0.2220)	(0.4480, 0.4314)	(0.4491, 0.4448)	(0.4736, 0.4220)	(0.6018, 0.3112)
G3	(0.6679, 0.2523)	(0.7542, 0.1949)	(0.6162, 0.3072)	(0.4560, 0.4397)	(0.5437, 0.3520)	(0.5708, 0.3513)
G4	(0.5606, 0.3394)	(0.8134, 0.1487)	(0.5134, 0.3776)	(0.5260, 0.3740)	(0.4939, 0.4061)	(0.6578, 0.2404)
G5	(0.4238, 0.4455)	(0.5700, 0.3282)	(0.3957, 0.4798)	(0.4116, 0.4722)	(0.3870, 0.4823)	(0.5199, 0.3787)
G6	(0.7513, 0.1996)	(0.7397, 0.1892)	(0.6162, 0.3072)	(0.3859, 0.4996)	(0.5166, 0.3773)	(0.6949, 0.2321)
G7	(0.5614, 0.3426)	(0.6426, 0.2668)	(0.4588, 0.4256)	(0.4116, 0.4722)	(0.4108, 0.4603)	(0.4736, 0.4256)
G8	(0.7087, 0.2300)	(0.6625, 0.2375)	(0.6466, 0.2780)	(0.3556, 0.5137)	(0.4736, 0.4119)	(0.7152, 0.2094)
G9	(0.6480, 0.2704)	(0.6076, 0.2906)	(0.6870, 0.2538)	(0.4116, 0.4722)	(0.4538, 0.4354)	(0.7224, 0.2224)
G10	(0.5866, 0.3173)	(0.6191, 0.2903)	(0.4899, 0.3939)	(0.4227, 0.4664)	(0.6841, 0.2404)	(0.8112, 0.1614)
G11	(0.7845, 0.1578)	(0.7946, 0.1545)	(0.6581, 0.2697)	(0.7805, 0.1755)	(0.7816, 0.1675)	(0.8523, 0.1238)
G12	(0.6675, 0.2325)	(0.6646, 0.2574)	(0.6188, 0.2812)	(0.4282, 0.4556)	(0.4076, 0.4671)	(0.7007, 0.2238)
G13	(0.6794, 0.2531)	(0.5780, 0.3296)	(0.7235, 0.2191)	(0.5722, 0.3314)	(0.5892, 0.3144)	(0.6513, 0.2487)
G14	(0.5025, 0.3931)	(0.6209, 0.2884)	(0.4722, 0.4260)	(0.7440, 0.2173)	(0.8285, 0.1513)	(0.7144, 0.2072)
G15	(0.6025, 0.2975)	(0.7448, 0.1830)	(0.5354, 0.3581)	(0.4949, 0.4087)	(0.5303, 0.3697)	(0.6632, 0.2368)
G16	(0.6697, 0.2505)	(0.7722, 0.1892)	(0.6292, 0.2986)	(0.7321, 0.2152)	(0.7509, 0.1964)	(0.8227, 0.1386)
U17	(0.5617, 0.3314)	(0.6487, 0.2549)	(0.4628, 0.4220)	(0.5029, 0.4007)	(0.5881, 0.3119)	(0.5231, 0.3805)
U18	(0.4542, 0.4314)	(0.6989, 0.2300)	(0.3773, 0.5029)	(0.3574, 0.5119)	(0.5498, 0.3495)	(0.4906, 0.3986)
U19	(0.5888, 0.3242)	(0.8097, 0.1700)	(0.5235, 0.3700)	(0.5599, 0.3621)	(0.7061, 0.2412)	(0.7498, 0.2029)
U20	(0.6249, 0.2874)	(0.6206, 0.2794)	(0.5321, 0.3715)	(0.4841, 0.4116)	(0.5917, 0.3166)	(0.5036, 0.3899)
U21	(0.6762, 0.2552)	(0.7563, 0.1928)	(0.5462, 0.3473)	(0.5101, 0.3791)	(0.4502, 0.4354)	(0.6047, 0.2910)
U22	(0.5455, 0.3671)	(0.4585, 0.4271)	(0.4195, 0.4650)	(0.4245, 0.4646)	(0.4206, 0.4632)	(0.4339, 0.4516)
U23	(0.6502, 0.2755)	(0.7823, 0.1755)	(0.5040, 0.3895)	(0.6148, 0.2852)	(0.5253, 0.3747)	(0.6314, 0.2686)
U24	(0.5852, 0.3224)	(0.5491, 0.3509)	(0.5043, 0.3791)	(0.4704, 0.4152)	(0.4444, 0.4412)	(0.5094, 0.3946)
U25	(0.6004, 0.3383)	(0.5477, 0.3523)	(0.4823, 0.4130)	(0.4556, 0.4300)	(0.4354, 0.4502)	(0.4632, 0.4224)
U26	(0.6856, 0.2469)	(0.6177, 0.2805)	(0.6635, 0.2653)	(0.8191, 0.1606)	(0.7473, 0.2105)	(0.7809, 0.1751)
U27	(0.5433, 0.3498)	(0.4653, 0.4303)	(0.4877, 0.3957)	(0.3939, 0.4953)	(0.4639, 0.4260)	(0.5181, 0.3895)
H28	(0.4072, 0.4639)	(0.3993, 0.4845)	(0.3758, 0.4935)	(0.3791, 0.4921)	(0.4664, 0.4271)	(0.4617, 0.4274)
H29	(0.5603, 0.3390)	(0.6996, 0.2329)	(0.5466, 0.3534)	(0.4152, 0.4729)	(0.7004, 0.2480)	(0.5848, 0.3188)
H30	(0.5076, 0.3863)	(0.6126, 0.2910)	(0.5137, 0.3845)	(0.3556, 0.5235)	(0.4585, 0.4372)	(0.4000, 0.4747)
H31	(0.5116, 0.3884)	(0.5058, 0.3942)	(0.7458, 0.2014)	(0.4744, 0.4249)	(0.5949, 0.3087)	(0.6715, 0.2610)
H32	(0.5336, 0.3664)	(0.5715, 0.3285)	(0.7087, 0.2238)	(0.4401, 0.4635)	(0.3379, 0.5801)	(0.4747, 0.4188)
H33	(0.7715, 0.1794)	(0.5661, 0.3321)	(0.5256, 0.3780)	(0.5094, 0.3906)	(0.4928, 0.4155)	(0.6083, 0.2910)
H34	(0.8379, 0.1419)	(0.7415, 0.2076)	(0.5513, 0.3480)	(0.5581, 0.3419)	(0.7542, 0.1931)	(0.6480, 0.2740)
H35	(0.5794, 0.3347)	(0.5148, 0.3888)	(0.5256, 0.3780)	(0.4928, 0.4054)	(0.4740, 0.4159)	(0.4747, 0.4188)
H36	(0.5159, 0.3841)	(0.4394, 0.4444)	(0.4733, 0.4260)	(0.4585, 0.4451)	(0.4560, 0.4375)	(0.4653, 0.4282)
H37	(0.5888, 0.3332)	(0.5188, 0.3794)	(0.5437, 0.3599)	(0.5307, 0.3693)	(0.4704, 0.4195)	(0.5116, 0.4004)
H38	(0.6209, 0.2827)	(0.6000, 0.3036)	(0.6386, 0.2834)	(0.4271, 0.4722)	(0.3509, 0.5715)	(0.4653, 0.4282)
H39	(0.5025, 0.3968)	(0.4513, 0.4426)	(0.7975, 0.1736)	(0.5087, 0.3852)	(0.3758, 0.5032)	(0.4379, 0.4556)
I40	(0.5188, 0.3769)	(0.6206, 0.2996)	(0.5863, 0.3119)	(0.4664, 0.4372)	(0.4032, 0.4819)	(0.4563, 0.4372)
I41	(0.4877, 0.4061)	(0.6025, 0.3213)	(0.6278, 0.2899)	(0.4845, 0.4191)	(0.3675, 0.5069)	(0.4531, 0.4404)
I42	(0.5881, 0.3339)	(0.5480, 0.3502)	(0.5235, 0.3758)	(0.5108, 0.3931)	(0.5032, 0.3960)	(0.4877, 0.4199)
I43	(0.4700, 0.4300)	(0.5700, 0.3484)	(0.4924, 0.4032)	(0.5520, 0.3480)	(0.5682, 0.3271)	(0.4928, 0.4007)
I44	(0.4881, 0.4119)	(0.5412, 0.3809)	(0.4455, 0.4538)	(0.5527, 0.3473)	(0.5278, 0.3675)	(0.4401, 0.4390)
E45	(0.4484, 0.4354)	(0.5755, 0.3285)	(0.5971, 0.2975)	(0.4300, 0.4538)	(0.5563, 0.3394)	(0.5809, 0.3184)
E46	(0.6083, 0.3137)	(0.5621, 0.3415)	(0.7119, 0.2123)	(0.6141, 0.2895)	(0.6498, 0.2827)	(0.6004, 0.3032)
E47	(0.8018, 0.1693)	(0.7137, 0.2152)	(0.5278, 0.3657)	(0.7011, 0.2278)	(0.5812, 0.3188)	(0.6202, 0.2834)
E48	(0.5722, 0.3462)	(0.5690, 0.3310)	(0.5426, 0.3563)	(0.4978, 0.4061)	(0.5090, 0.3910)	(0.6245, 0.2791)
E49	(0.7881, 0.1715)	(0.6303, 0.2697)	(0.5426, 0.3563)	(0.5534, 0.3466)	(0.5477, 0.3523)	(0.5350, 0.3686)
E50	(0.6224, 0.2942)	(0.5534, 0.3502)	(0.5235, 0.3718)	(0.3899, 0.4949)	(0.4173, 0.4726)	(0.3819, 0.4971)
E51	(0.7004, 0.2162)	(0.6433, 0.2549)	(0.5079, 0.3874)	(0.4495, 0.4444)	(0.4531, 0.4451)	(0.5462, 0.3574)
E52	(0.7729, 0.1780)	(0.6126, 0.2874)	(0.5740, 0.3195)	(0.4798, 0.4159)	(0.4029, 0.4726)	(0.4574, 0.4361)
E53	(0.5224, 0.3733)	(0.5386, 0.3596)	(0.5123, 0.3975)	(0.4570, 0.4466)	(0.4097, 0.4801)	(0.3744, 0.5047)
E54	(0.7708, 0.1801)	(0.6729, 0.2560)	(0.5379, 0.3610)	(0.7267, 0.2058)	(0.6747, 0.2339)	(0.6224, 0.2812)
E55	(0.6097, 0.3123)	(0.5715, 0.3267)	(0.8101, 0.1614)	(0.5256, 0.3780)	(0.5303, 0.3679)	(0.5043, 0.3993)
E56	(0.6097, 0.3087)	(0.7181, 0.2292)	(0.6931, 0.2531)	(0.7563, 0.1910)	(0.6426, 0.2574)	(0.7072, 0.2253)
E57	(0.7881, 0.1715)	(0.6433, 0.2549)	(0.5513, 0.3477)	(0.7751, 0.1827)	(0.8134, 0.1628)	(0.7552, 0.2061)

Table 6: Defuzzified aggregate decision matrix.

Codes	B1	B2	B3	B4	B5	B6	B7	B8	B9	B10	B11	B12
G1	0.6772	0.2947	0.3286	0.2703	0.3191	0.3499	0.2479	0.4704	0.2379	0.2045	0.2442	0.2049
G2	0.5549	0.4117	0.4212	0.3140	0.4876	0.3899	0.2436	0.4250	0.2027	0.2015	0.2165	0.3136
G3	0.6425	0.2796	0.3599	0.3460	0.3836	0.4689	0.3797	0.4872	0.3264	0.2054	0.2659	0.2856
G4	0.3645	0.6562	0.3534	0.4484	0.4619	0.3173	0.2790	0.5786	0.2438	0.2521	0.2294	0.3696
G5	0.2978	0.3343	0.3382	0.6989	0.3170	0.6772	0.1902	0.2868	0.1742	0.1814	0.1708	0.2478
G6	0.3077	0.2729	0.6439	0.3157	0.3333	0.2971	0.4831	0.4676	0.3264	0.1676	0.2459	0.4106
G7	0.2406	0.3228	0.3370	0.6989	0.2299	0.6772	0.2792	0.3533	0.2086	0.1814	0.1829	0.2161
G8	0.2776	0.2416	0.4851	0.5472	0.3196	0.4120	0.4270	0.3746	0.3567	0.1554	0.2177	0.4355
G9	0.2497	0.3099	0.3921	0.2912	0.2598	0.3810	0.3585	0.3197	0.4007	0.1814	0.2049	0.4442
G10	0.2673	0.2520	0.3230	0.5667	0.2989	0.6562	0.3006	0.3300	0.2285	0.1868	0.3979	0.5749
G11	0.2627	0.2624	0.5146	0.3526	0.4311	0.2330	0.5323	0.5481	0.3688	0.5260	0.5277	0.6480
G12	0.4373	0.4586	0.3221	0.2813	0.4054	0.3041	0.3801	0.3761	0.3302	0.1906	0.1806	0.4176
G13	0.2956	0.2569	0.3282	0.3996	0.2552	0.3401	0.3923	0.2928	0.4457	0.2882	0.3028	0.3626
G14	0.2885	0.5252	0.3703	0.2326	0.2573	0.2064	0.2358	0.3317	0.2153	0.4728	0.6046	0.4347
G15	0.3683	0.5146	0.3915	0.2964	0.4477	0.2697	0.3150	0.4745	0.2597	0.2297	0.2553	0.3753
G16	0.2621	0.2781	0.6149	0.2752	0.4183	0.2326	0.3817	0.5133	0.3389	0.4570	0.4827	0.5947
U17	0.6413	0.3675	0.4565	0.2495	0.3228	0.3310	0.2803	0.3599	0.2110	0.2352	0.3021	0.2496
U18	0.5787	0.5773	0.3425	0.3153	0.3181	0.3347	0.2056	0.4153	0.1641	0.1563	0.2703	0.2284
U19	0.5803	0.6358	0.3153	0.3547	0.3314	0.4320	0.3019	0.5724	0.2509	0.2766	0.4236	0.4810
U20	0.3264	0.4425	0.6439	0.3163	0.5608	0.2743	0.3354	0.3319	0.2564	0.2233	0.3047	0.2367
U21	0.3374	0.2888	0.3873	0.4046	0.3739	0.4876	0.3886	0.4903	0.2680	0.2417	0.2032	0.3172
U22	0.2663	0.2560	0.2505	0.6280	0.2703	0.5959	0.2658	0.2083	0.1857	0.1878	0.1864	0.1937
U23	0.2506	0.3208	0.6110	0.2784	0.5959	0.3163	0.3604	0.5287	0.2370	0.3264	0.2516	0.3424
U24	0.2623	0.3138	0.3370	0.6772	0.6085	0.7445	0.2991	0.2697	0.2382	0.2157	0.1998	0.2397
U25	0.2681	0.2879	0.3246	0.3403	0.2843	0.4477	0.3105	0.2686	0.2222	0.2065	0.1945	0.2111
U26	0.2836	0.2357	0.2514	0.2132	0.2784	0.2556	0.3993	0.3292	0.3746	0.5883	0.4774	0.5265
U27	0.2827	0.2304	0.3700	0.3227	0.2148	0.2286	0.2658	0.2112	0.2271	0.1711	0.2111	0.2456
H28	0.6149	0.3310	0.3466	0.2572	0.3368	0.3112	0.1810	0.1748	0.1652	0.1665	0.2122	0.2098
H29	0.5787	0.3753	0.2723	0.2583	0.4089	0.2603	0.2787	0.4161	0.2677	0.1827	0.4164	0.2990
H30	0.6413	0.3310	0.3193	0.2683	0.2825	0.3160	0.2395	0.3241	0.2434	0.1537	0.2070	0.1766
H31	0.5135	0.2781	0.3945	0.3417	0.3382	0.3626	0.2416	0.2376	0.4756	0.2165	0.3079	0.3833
H32	0.6266	0.3228	0.3915	0.3738	0.3793	0.4261	0.2578	0.2879	0.4272	0.1947	0.1373	0.2175
H33	0.2516	0.3296	0.3863	0.3333	0.3204	0.4927	0.5124	0.2835	0.2515	0.2401	0.2277	0.3203
H34	0.2799	0.4119	0.6989	0.2760	0.6989	0.3430	0.6213	0.4696	0.2715	0.2769	0.4873	0.3583
H35	0.2323	0.2717	0.3302	0.4045	0.3562	0.4475	0.2936	0.2436	0.2515	0.2288	0.2174	0.2175
H36	0.2144	0.2436	0.1991	0.6772	0.2218	0.3898	0.2447	0.1971	0.2158	0.2059	0.2057	0.2115
H37	0.1823	0.4221	0.6439	0.2677	0.4476	0.2919	0.3012	0.2470	0.2652	0.2556	0.2151	0.2404
H38	0.1808	0.2965	0.3186	0.2626	0.3286	0.4778	0.3320	0.3125	0.3486	0.1878	0.1428	0.2115
H39	0.2669	0.3338	0.3112	0.3219	0.3060	0.3191	0.2354	0.2028	0.5524	0.2402	0.1635	0.1949
I40	0.6772	0.5080	0.3794	0.3417	0.3623	0.4293	0.2472	0.3308	0.3006	0.2109	0.1767	0.2059
I41	0.6618	0.3031	0.3291	0.2499	0.4076	0.4010	0.2259	0.3135	0.3380	0.2226	0.1603	0.2039
I42	0.2801	0.4090	0.3753	0.5774	0.2933	0.6440	0.3006	0.2690	0.2503	0.2407	0.2359	0.2243
I43	0.3408	0.5594	0.2497	0.3836	0.3987	0.3282	0.2137	0.2853	0.2289	0.2720	0.2855	0.2293
I44	0.3915	0.3920	0.3526	0.3738	0.3015	0.5909	0.2255	0.2615	0.1986	0.2726	0.2539	0.1981
E45	0.7445	0.3675	0.4775	0.3526	0.6631	0.3453	0.2024	0.2909	0.3104	0.1917	0.2758	0.2959
E46	0.6346	0.3116	0.2655	0.6022	0.2924	0.5773	0.3190	0.2799	0.4314	0.3255	0.3597	0.3128
E47	0.2496	0.3399	0.4412	0.3163	0.7213	0.4402	0.5594	0.4336	0.2540	0.4179	0.2961	0.3314
E48	0.2357	0.2903	0.3354	0.3554	0.3774	0.6989	0.2871	0.2858	0.2647	0.2316	0.2399	0.3355
E49	0.2015	0.4119	0.5909	0.3327	0.6631	0.3489	0.5377	0.3414	0.2647	0.2731	0.2686	0.2585
E50	0.1918	0.3069	0.2276	0.5548	0.2693	0.5029	0.3328	0.2729	0.2507	0.1697	0.1837	0.1666
E51	0.1862	0.3799	0.4591	0.2655	0.3040	0.2737	0.4174	0.3545	0.2396	0.2017	0.2033	0.2672
E52	0.1871	0.2462	0.3906	0.3206	0.3700	0.4448	0.5146	0.3243	0.2904	0.2205	0.1780	0.2066
E53	0.3307	0.3138	0.3277	0.3227	0.2378	0.5018	0.2499	0.2618	0.2412	0.2050	0.1795	0.1628
E54	0.1973	0.2583	0.6033	0.4880	0.6562	0.3225	0.5113	0.3850	0.2611	0.4502	0.3878	0.3334
E55	0.2819	0.4356	0.3274	0.4131	0.2499	0.2534	0.3204	0.2880	0.5731	0.2515	0.2555	0.2362
E56	0.5233	0.5773	0.5446	0.4758	0.6022	0.2828	0.3206	0.4386	0.4078	0.4904	0.3537	0.4254
E57	0.3170	0.4831	0.6279	0.3713	0.6631	0.4007	0.5377	0.3545	0.2715	0.5177	0.5785	0.4885

Table 7: Symmetric matrix.

	B1	B2	B3	B4	B5	B6	B7	B8	B9	B10	B11	B12
B1	1.0000	0.2590	−0.1662	−0.2301	0.0126	−0.1239	−0.4585	0.1409	0.0449	−0.1913	−0.0171	−0.1273
B2	0.2590	1.0000	0.1005	−0.1488	0.2557	−0.2422	−0.1695	0.3351	−0.1374	0.1141	0.1984	0.0497
B3	−0.1662	0.1005	1.0000	−0.2748	0.6608	−0.3537	0.5629	0.3920	0.0216	0.3315	0.3429	0.3388
B4	−0.2301	−0.1488	−0.2748	1.0000	−0.1245	0.6632	−0.1297	−0.2358	−0.1066	−0.1425	−0.1851	−0.1200
B5	0.0126	0.2557	0.6608	−0.1245	1.0000	−0.1449	0.4607	0.3755	−0.0618	0.3727	0.2944	0.1982
B6	−0.1239	−0.2422	−0.3537	0.6632	−0.1449	1.0000	−0.1466	−0.2892	−0.2537	−0.3072	−0.3409	−0.2640
B7	−0.4585	−0.1695	0.5629	−0.1297	0.4607	−0.1466	1.0000	0.3878	0.1485	0.4291	0.3640	0.4303
B8	0.1409	0.3351	0.3920	−0.2358	0.3755	−0.2892	0.3878	1.0000	−0.0462	0.3072	0.3869	0.5385
B9	0.0449	−0.1374	0.0216	−0.1066	−0.0618	−0.2537	0.1485	−0.0462	1.0000	0.1987	0.0515	0.2311
B10	−0.1913	0.1141	0.3315	−0.1425	0.3727	−0.3072	0.4291	0.3072	0.1987	1.0000	0.7582	0.5991
B11	−0.0171	0.1984	0.3429	−0.1851	0.2944	−0.3409	0.3640	0.3869	0.0515	0.7582	1.0000	0.7171
B12	−0.1273	0.0497	0.3388	−0.1200	0.1982	−0.2640	0.4303	0.5385	0.2311	0.5991	0.7171	1.0000

Table 8: Priority weights of the barriers to EDUC4 implementation.

Barriers	e_j	z_j	w_j
B1	0.9769	11.5827	0.0988
B2	0.9901	10.2825	0.0877
B3	0.9894	8.9476	0.0763
B4	0.9871	11.8796	0.1013
B5	0.9862	8.5806	0.0732
B6	0.9872	12.6392	0.1078
B7	0.9882	9.0134	0.0769
B8	0.9901	8.6214	0.0735
B9	0.9893	10.7923	0.0920
B10	0.9827	8.3830	0.0715
B11	0.9822	8.2799	0.0706
B12	0.9842	8.2754	0.0706

class L_{low} if $h_{ik}(L2) < 0$ and $h_{ik}(L1) < 0$.

The final classification of the roles of various stakeholders to overcome barriers to EDUC4 implementation is illustrated in Figure 3.

5. Results and Discussion

In promoting a workable EDUC4 implementation roadmap, this work offers the application of the proposed FF entropy-based CRITIC-CODAS-SORT in evaluating the stakeholder roles for overcoming the barriers to implementing EDUC4. The applicability of the proposed framework is positioned to analyze the conditions describing an HEI. In the proposed approach, the FF CRITIC determines the priority barriers, while FF CODAS-SORT identifies the high-priority stakeholder roles that could guide the case HEI in formulating policy directions appropriate for its implementation of EDUC4. Identifying the relevant and priority barriers is essential for an HEI at different managerial levels to accomplish activities attuned to addressing these barriers. A set of expert decision-makers at the university level elicited judgments on the relevance of various stakeholder roles in overcoming the barriers to implementing EDUC4 in developing economies recently identified in the literature. Consequently, the insights generated strategic views to design appropriate approaches for the implementation agenda. Results show that the top five most relevant barriers associated with the case HEI in developing initiatives for EDUC4 implementation are the lack of collaboration (B6; i.e., external fund sourcing and industry linkages), apprehensive stakeholders (B4; i.e., low motivation, fear of the unknown and limited technical know-how), cybersecurity threats (B1; i.e., no infrastructure against cybersecurity attracts), health issues (B9; i.e., concerns on-screen time and cyber stress), and costly (B2; i.e., ICT infrastructure and fast-changing upgrades). These findings draw parallel insights with recent studies concerning the readiness of the HEIs in developing economies. For example, Jamaludin et al. [4] raised concerns about the managerial and financial readiness of HEIs in the ASEAN countries. Thus, aside from the costs associated with EDUC4 implementation, the administrative aspect is essential in ensuring effective collaboration and dealing with apprehensive stakeholders. Another emerging literature emphasized that curriculum design for EDUC4 implementation must include teaching industrial cybersecurity to accelerate the next-generation programmers and cybersecurity researchers [50]. Lastly, Hariharasudan and Kot [51] emphasized the relevance of health issues following their observation that one of IoT's most critical industrial applications in the EDUC4 era includes medical, health, and elderly care. These works in the literature justify the priority judgments of educational decision-makers at a university level from a developing economy perspective.

In addition, the decision-makers of the case HEI positioned insufficient foundation in basic education (B12; i.e., lack of learner's proper primary education), the complexity of learning platforms (B11; i.e., difficulty in utilizing virtual learning platforms), and time constraint for material preparation (B10; i.e., time constraint in preparation for virtual learning platform) among the minor priority barriers in achieving EDUC4. Unlike the other top priority barriers (i.e., B2, B9, B1, B6, and B4), the least three priorities barriers (i.e., B10, B11, and B10) are construed along with case-specific conditions of the HEI wherein limited or no control is available due to the trifocal education system [52] with each has own mandates and budgetary directions.

Table 9: Augmented FF decision matrix.

Codes	B1	B2	B3	B4	B5	B6
G1	(0.8675, 0.1217)	(0.5798, 0.3238)	(0.6184, 0.3036)	(0.5498, 0.3502)	(0.6069, 0.2913)	(0.6404, 0.2921)
G2	(0.7989, 0.1614)	(0.6960, 0.2365)	(0.7036, 0.2184)	(0.6014, 0.2986)	(0.7542, 0.1783)	(0.6773, 0.2516)
G3	(0.8495, 0.1361)	(0.5621, 0.3448)	(0.6487, 0.2549)	(0.6350, 0.2650)	(0.6708, 0.2292)	(0.7412, 0.2155)
G4	(0.6545, 0.2819)	(0.8567, 0.1325)	(0.6437, 0.2870)	(0.7253, 0.2036)	(0.7354, 0.1866)	(0.6051, 0.2949)
G5	(0.5838, 0.3238)	(0.6231, 0.2769)	(0.6271, 0.2729)	(0.8783, 0.1108)	(0.6047, 0.2953)	(0.8675, 0.1217)
G6	(0.5960, 0.3256)	(0.5534, 0.3502)	(0.8502, 0.1303)	(0.6032, 0.2968)	(0.6220, 0.2780)	(0.5823, 0.3177)
G7	(0.5119, 0.4011)	(0.6112, 0.2924)	(0.6274, 0.3014)	(0.8783, 0.1108)	(0.4946, 0.4054)	(0.8675, 0.1217)
G8	(0.5599, 0.3495)	(0.5112, 0.3870)	(0.7527, 0.2014)	(0.7942, 0.1729)	(0.6076, 0.2924)	(0.6957, 0.2130)
G9	(0.5227, 0.3773)	(0.5968, 0.3014)	(0.6783, 0.2217)	(0.5755, 0.3245)	(0.5361, 0.3621)	(0.6686, 0.2383)
G10	(0.5469, 0.3617)	(0.5274, 0.3848)	(0.6112, 0.2888)	(0.8061, 0.1523)	(0.5859, 0.3325)	(0.8567, 0.1325)
G11	(0.5412, 0.3682)	(0.5401, 0.3635)	(0.7729, 0.1787)	(0.6415, 0.2585)	(0.7116, 0.2069)	(0.4989, 0.3993)
G12	(0.7166, 0.2087)	(0.7332, 0.2087)	(0.6119, 0.3152)	(0.5635, 0.3365)	(0.6906, 0.2383)	(0.5906, 0.3130)
G13	(0.5809, 0.3227)	(0.5329, 0.3708)	(0.6166, 0.2816)	(0.6856, 0.2390)	(0.5300, 0.3682)	(0.6292, 0.2744)
G14	(0.5729, 0.3347)	(0.7801, 0.1906)	(0.6588, 0.2498)	(0.4986, 0.4014)	(0.5325, 0.3632)	(0.4585, 0.4415)
G15	(0.6574, 0.2646)	(0.7729, 0.1780)	(0.6783, 0.2401)	(0.5816, 0.3184)	(0.7245, 0.1939)	(0.5491, 0.3509)
G16	(0.5408, 0.3722)	(0.5599, 0.3437)	(0.8343, 0.1426)	(0.5560, 0.3440)	(0.7011, 0.2155)	(0.4986, 0.4014)
U17	(0.8487, 0.1274)	(0.6567, 0.2653)	(0.7318, 0.2155)	(0.5224, 0.3769)	(0.6112, 0.2924)	(0.6199, 0.2838)
U18	(0.8134, 0.1433)	(0.8126, 0.1581)	(0.6318, 0.2751)	(0.6029, 0.2971)	(0.6058, 0.2924)	(0.6235, 0.2765)
U19	(0.8144, 0.1599)	(0.8458, 0.1433)	(0.6047, 0.3224)	(0.6444, 0.2740)	(0.6209, 0.2957)	(0.7130, 0.2379)
U20	(0.6155, 0.2968)	(0.7209, 0.2202)	(0.8502, 0.1303)	(0.6040, 0.2960)	(0.8025, 0.1542)	(0.5549, 0.3451)
U21	(0.6278, 0.3000)	(0.5729, 0.3307)	(0.6740, 0.2260)	(0.6892, 0.2108)	(0.6625, 0.2560)	(0.7542, 0.1729)
U22	(0.5448, 0.3552)	(0.5310, 0.3671)	(0.5238, 0.3762)	(0.8415, 0.1292)	(0.5498, 0.3502)	(0.8235, 0.1437)
U23	(0.5249, 0.3827)	(0.6090, 0.2946)	(0.8321, 0.1448)	(0.5599, 0.3401)	(0.8235, 0.1437)	(0.6040, 0.2960)
U24	(0.5394, 0.3588)	(0.6014, 0.3022)	(0.6271, 0.2949)	(0.8675, 0.1181)	(0.8307, 0.1365)	(0.9000, 0.1000)
U25	(0.5480, 0.3606)	(0.5718, 0.3318)	(0.6148, 0.3159)	(0.6292, 0.2708)	(0.5671, 0.3329)	(0.7245, 0.1939)
U26	(0.5675, 0.3455)	(0.5036, 0.4000)	(0.5274, 0.3910)	(0.4693, 0.4307)	(0.5599, 0.3401)	(0.5307, 0.3693)
U27	(0.5664, 0.3458)	(0.4960, 0.4076)	(0.6588, 0.2596)	(0.6108, 0.2892)	(0.4715, 0.4267)	(0.4946, 0.4162)
H28	(0.8343, 0.1419)	(0.6199, 0.2838)	(0.6365, 0.2819)	(0.5329, 0.3671)	(0.6256, 0.2744)	(0.5982, 0.3000)
H29	(0.8134, 0.1433)	(0.6632, 0.2368)	(0.5527, 0.3509)	(0.5343, 0.3657)	(0.6935, 0.2336)	(0.5386, 0.3758)
H30	(0.8487, 0.1274)	(0.6199, 0.2838)	(0.6072, 0.2928)	(0.5473, 0.3527)	(0.5650, 0.3350)	(0.6036, 0.2964)
H31	(0.7722, 0.1787)	(0.5599, 0.3437)	(0.6812, 0.2458)	(0.6307, 0.2693)	(0.6271, 0.2729)	(0.6513, 0.2487)
H32	(0.8408, 0.1390)	(0.6112, 0.2924)	(0.6783, 0.2401)	(0.6617, 0.2383)	(0.6668, 0.2332)	(0.7072, 0.1964)
H33	(0.5253, 0.3747)	(0.6184, 0.2852)	(0.6740, 0.2531)	(0.6220, 0.2780)	(0.6097, 0.3123)	(0.7578, 0.1711)
H34	(0.5635, 0.3549)	(0.6957, 0.2166)	(0.8783, 0.1108)	(0.5570, 0.3430)	(0.8783, 0.1108)	(0.6325, 0.2783)
H35	(0.4982, 0.4018)	(0.5520, 0.3516)	(0.6199, 0.2986)	(0.6899, 0.2390)	(0.6458, 0.2726)	(0.7245, 0.2032)
H36	(0.4700, 0.4242)	(0.5148, 0.3888)	(0.4455, 0.4502)	(0.8675, 0.1217)	(0.4823, 0.4159)	(0.6769, 0.2451)
H37	(0.4184, 0.4845)	(0.7043, 0.2177)	(0.8502, 0.1303)	(0.5466, 0.3534)	(0.7245, 0.1975)	(0.5776, 0.3390)
H38	(0.4119, 0.4769)	(0.5819, 0.3217)	(0.6076, 0.3108)	(0.5397, 0.3585)	(0.6184, 0.3036)	(0.7473, 0.1910)
H39	(0.5458, 0.3578)	(0.6227, 0.2809)	(0.5982, 0.3000)	(0.6097, 0.2859)	(0.5928, 0.3108)	(0.6069, 0.2913)
I40	(0.8675, 0.1217)	(0.7686, 0.1910)	(0.6675, 0.2509)	(0.6307, 0.2693)	(0.6516, 0.2668)	(0.7101, 0.2083)
I41	(0.8596, 0.1202)	(0.5895, 0.3141)	(0.6177, 0.2823)	(0.5224, 0.3733)	(0.6924, 0.2347)	(0.6870, 0.2455)
I42	(0.5632, 0.3491)	(0.6935, 0.2285)	(0.6639, 0.2581)	(0.8126, 0.1545)	(0.5794, 0.3390)	(0.8502, 0.1267)
I43	(0.6307, 0.2877)	(0.8018, 0.1690)	(0.5238, 0.3848)	(0.6708, 0.2292)	(0.6841, 0.2159)	(0.6166, 0.2816)
I44	(0.6783, 0.2401)	(0.6783, 0.2253)	(0.6415, 0.2585)	(0.6617, 0.2383)	(0.5874, 0.3126)	(0.8206, 0.1397)
E45	(0.9000, 0.1000)	(0.6567, 0.2653)	(0.7469, 0.1827)	(0.6415, 0.2585)	(0.8603, 0.1253)	(0.6343, 0.2657)
E46	(0.8451, 0.1310)	(0.6004, 0.3227)	(0.5440, 0.3596)	(0.8271, 0.1401)	(0.5787, 0.3433)	(0.8126, 0.1581)
E47	(0.5231, 0.3805)	(0.6292, 0.2794)	(0.7195, 0.1989)	(0.6040, 0.2960)	(0.8892, 0.1072)	(0.7191, 0.2206)
E48	(0.5036, 0.4000)	(0.5744, 0.3256)	(0.6242, 0.2758)	(0.6448, 0.2661)	(0.6661, 0.2632)	(0.8783, 0.1108)
E49	(0.4473, 0.4379)	(0.6957, 0.2166)	(0.8206, 0.1397)	(0.6217, 0.2819)	(0.8603, 0.1253)	(0.6379, 0.2621)
E50	(0.4314, 0.4574)	(0.5946, 0.3199)	(0.4910, 0.4072)	(0.7989, 0.1686)	(0.5484, 0.3498)	(0.7650, 0.1823)
E51	(0.4217, 0.4671)	(0.6675, 0.2361)	(0.7332, 0.1852)	(0.5437, 0.3563)	(0.5903, 0.3097)	(0.5545, 0.3491)
E52	(0.4260, 0.4733)	(0.5209, 0.4011)	(0.6776, 0.2444)	(0.6087, 0.2913)	(0.6588, 0.2596)	(0.7224, 0.1996)
E53	(0.6195, 0.2841)	(0.6014, 0.3022)	(0.6162, 0.2838)	(0.6108, 0.2892)	(0.5061, 0.3939)	(0.7643, 0.1830)
E54	(0.4401, 0.4451)	(0.5347, 0.3690)	(0.8278, 0.1491)	(0.7545, 0.1838)	(0.8567, 0.1289)	(0.6108, 0.2928)
E55	(0.5646, 0.3390)	(0.7152, 0.2069)	(0.6159, 0.2841)	(0.6964, 0.2036)	(0.5235, 0.3801)	(0.5278, 0.3722)
E56	(0.7787, 0.1704)	(0.8126, 0.1581)	(0.7924, 0.1556)	(0.7458, 0.1917)	(0.8271, 0.1401)	(0.5653, 0.3347)
E57	(0.6047, 0.2953)	(0.7513, 0.1996)	(0.8415, 0.1390)	(0.6596, 0.2440)	(0.8603, 0.1253)	(0.6866, 0.2422)
L2	(0.7020, 0.2665)	(0.6682, 0.2242)	(0.6851, 0.2476)	(0.6851, 0.2369)	(0.6936, 0.2347)	(0.7020, 0.2428)

Table 9: Continued.

Codes	B1	B2	B3	B4	B5	B6
L1	(0.4950, 0.3779)	(0.4712, 0.3179)	(0.4831, 0.3511)	(0.4831, 0.3359)	(0.4890, 0.3328)	(0.4950, 0.3444)
Codes	B7	B8	B9	B10	B11	B12
G1	(0.5202, 0.3791)	(0.7422, 0.2144)	(0.5061, 0.3931)	(0.4545, 0.4412)	(0.5152, 0.3848)	(0.4567, 0.4462)
G2	(0.5123, 0.3733)	(0.7069, 0.2220)	(0.4480, 0.4314)	(0.4491, 0.4448)	(0.4736, 0.4220)	(0.6018, 0.3112)
G3	(0.6679, 0.2523)	(0.7542, 0.1949)	(0.6162, 0.3072)	(0.4560, 0.4397)	(0.5437, 0.3520)	(0.5708, 0.3513)
G4	(0.5606, 0.3394)	(0.8134, 0.1487)	(0.5134, 0.3776)	(0.5260, 0.3740)	(0.4939, 0.4061)	(0.6578, 0.2404)
G5	(0.4238, 0.4455)	(0.5700, 0.3282)	(0.3957, 0.4798)	(0.4116, 0.4722)	(0.3870, 0.4823)	(0.5199, 0.3787)
G6	(0.7513, 0.1996)	(0.7397, 0.1892)	(0.6162, 0.3072)	(0.3859, 0.4996)	(0.5166, 0.3773)	(0.6949, 0.2321)
G7	(0.5614, 0.3426)	(0.6426, 0.2668)	(0.4588, 0.4256)	(0.4116, 0.4722)	(0.4108, 0.4603)	(0.4736, 0.4256)
G8	(0.7087, 0.2300)	(0.6625, 0.2375)	(0.6466, 0.2780)	(0.3556, 0.5137)	(0.4736, 0.4119)	(0.7152, 0.2094)
G9	(0.6480, 0.2704)	(0.6076, 0.2906)	(0.6870, 0.2538)	(0.4116, 0.4722)	(0.4538, 0.4354)	(0.7224, 0.2224)
G10	(0.5866, 0.3173)	(0.6191, 0.2903)	(0.4899, 0.3939)	(0.4227, 0.4664)	(0.6841, 0.2404)	(0.8112, 0.1614)
G11	(0.7845, 0.1578)	(0.7946, 0.1545)	(0.6581, 0.2697)	(0.7805, 0.1755)	(0.7816, 0.1675)	(0.8523, 0.1238)
G12	(0.6675, 0.2325)	(0.6646, 0.2574)	(0.6188, 0.2812)	(0.4282, 0.4556)	(0.4076, 0.4671)	(0.7007, 0.2238)
G13	(0.6794, 0.2531)	(0.5780, 0.3296)	(0.7235, 0.2191)	(0.5722, 0.3314)	(0.5892, 0.3144)	(0.6513, 0.2487)
G14	(0.5025, 0.3931)	(0.6209, 0.2884)	(0.4722, 0.4260)	(0.7440, 0.2173)	(0.8285, 0.1513)	(0.7144, 0.2072)
G15	(0.6025, 0.2975)	(0.7448, 0.1830)	(0.5354, 0.3581)	(0.4949, 0.4087)	(0.5303, 0.3697)	(0.6632, 0.2368)
G16	(0.6697, 0.2505)	(0.7722, 0.1892)	(0.6292, 0.2986)	(0.7321, 0.2152)	(0.7509, 0.1964)	(0.8227, 0.1386)
U17	(0.5617, 0.3314)	(0.6487, 0.2549)	(0.4628, 0.4220)	(0.5029, 0.4007)	(0.5881, 0.3119)	(0.5231, 0.3805)
U18	(0.4542, 0.4314)	(0.6989, 0.2300)	(0.3773, 0.5029)	(0.3574, 0.5119)	(0.5498, 0.3495)	(0.4906, 0.3986)
U19	(0.5888, 0.3242)	(0.8097, 0.1700)	(0.5235, 0.3700)	(0.5599, 0.3621)	(0.7061, 0.2412)	(0.7498, 0.2029)
U20	(0.6249, 0.2874)	(0.6206, 0.2794)	(0.5321, 0.3715)	(0.4841, 0.4116)	(0.5917, 0.3166)	(0.5036, 0.3899)
U21	(0.6762, 0.2552)	(0.7563, 0.1928)	(0.5462, 0.3473)	(0.5101, 0.3791)	(0.4502, 0.4354)	(0.6047, 0.2910)
U22	(0.5455, 0.3671)	(0.4585, 0.4271)	(0.4195, 0.4650)	(0.4245, 0.4646)	(0.4206, 0.4632)	(0.4339, 0.4516)
U23	(0.6502, 0.2755)	(0.7823, 0.1755)	(0.5040, 0.3895)	(0.6148, 0.2852)	(0.5253, 0.3747)	(0.6314, 0.2686)
U24	(0.5852, 0.3224)	(0.5491, 0.3509)	(0.5043, 0.3791)	(0.4704, 0.4152)	(0.4444, 0.4412)	(0.5094, 0.3946)
U25	(0.6004, 0.3383)	(0.5477, 0.3523)	(0.4823, 0.4130)	(0.4556, 0.4300)	(0.4354, 0.4502)	(0.4632, 0.4224)
U26	(0.6856, 0.2469)	(0.6177, 0.2805)	(0.6635, 0.2653)	(0.8191, 0.1606)	(0.7473, 0.2105)	(0.7809, 0.1751)
U27	(0.5433, 0.3498)	(0.4653, 0.4303)	(0.4877, 0.3957)	(0.3939, 0.4953)	(0.4639, 0.4260)	(0.5181, 0.3895)
H28	(0.4072, 0.4639)	(0.3993, 0.4845)	(0.3758, 0.4935)	(0.3791, 0.4921)	(0.4664, 0.4271)	(0.4617, 0.4274)
H29	(0.5603, 0.3390)	(0.6996, 0.2329)	(0.5466, 0.3534)	(0.4152, 0.4729)	(0.7004, 0.2480)	(0.5848, 0.3188)
H30	(0.5076, 0.3863)	(0.6126, 0.2910)	(0.5137, 0.3845)	(0.3556, 0.5235)	(0.4585, 0.4372)	(0.4000, 0.4747)
H31	(0.5116, 0.3884)	(0.5058, 0.3942)	(0.7458, 0.2014)	(0.4744, 0.4249)	(0.5949, 0.3087)	(0.6715, 0.2610)
H32	(0.5336, 0.3664)	(0.5715, 0.3285)	(0.7087, 0.2238)	(0.4401, 0.4635)	(0.3379, 0.5801)	(0.4747, 0.4188)
H33	(0.7715, 0.1794)	(0.5661, 0.3321)	(0.5256, 0.3780)	(0.5094, 0.3906)	(0.4928, 0.4155)	(0.6083, 0.2910)
H34	(0.8379, 0.1419)	(0.7415, 0.2076)	(0.5513, 0.3480)	(0.5581, 0.3419)	(0.7542, 0.1931)	(0.6480, 0.2740)
H35	(0.5794, 0.3347)	(0.5148, 0.3888)	(0.5256, 0.3780)	(0.4928, 0.4054)	(0.4740, 0.4159)	(0.4747, 0.4188)
H36	(0.5159, 0.3841)	(0.4394, 0.4444)	(0.4733, 0.4260)	(0.4585, 0.4451)	(0.4560, 0.4375)	(0.4653, 0.4282)
H37	(0.5888, 0.3332)	(0.5188, 0.3794)	(0.5437, 0.3599)	(0.5307, 0.3693)	(0.4704, 0.4195)	(0.5116, 0.4004)
H38	(0.6209, 0.2827)	(0.6000, 0.3036)	(0.6386, 0.2834)	(0.4271, 0.4722)	(0.3509, 0.5715)	(0.4653, 0.4282)
H39	(0.5025, 0.3968)	(0.4513, 0.4426)	(0.7975, 0.1736)	(0.5087, 0.3852)	(0.3758, 0.5032)	(0.4379, 0.4556)
I40	(0.5188, 0.3769)	(0.6206, 0.2996)	(0.5863, 0.3119)	(0.4664, 0.4372)	(0.4032, 0.4819)	(0.4563, 0.4372)
I41	(0.4877, 0.4061)	(0.6025, 0.3213)	(0.6278, 0.2899)	(0.4845, 0.4191)	(0.3675, 0.5069)	(0.4531, 0.4404)
I42	(0.5881, 0.3339)	(0.5480, 0.3502)	(0.5235, 0.3758)	(0.5108, 0.3931)	(0.5032, 0.3960)	(0.4877, 0.4199)
I43	(0.4700, 0.4300)	(0.5700, 0.3484)	(0.4924, 0.4032)	(0.5520, 0.3480)	(0.5682, 0.3271)	(0.4928, 0.4007)
I44	(0.4881, 0.4119)	(0.5412, 0.3809)	(0.4455, 0.4538)	(0.5527, 0.3473)	(0.5278, 0.3675)	(0.4401, 0.4390)
E45	(0.4484, 0.4354)	(0.5755, 0.3285)	(0.5971, 0.2975)	(0.4300, 0.4538)	(0.5563, 0.3394)	(0.5809, 0.3184)
E46	(0.6083, 0.3137)	(0.5621, 0.3415)	(0.7119, 0.2123)	(0.6141, 0.2895)	(0.6498, 0.2827)	(0.6004, 0.3032)
E47	(0.8018, 0.1693)	(0.7137, 0.2152)	(0.5278, 0.3657)	(0.7011, 0.2278)	(0.5812, 0.3188)	(0.6202, 0.2834)
E48	(0.5722, 0.3462)	(0.5690, 0.3310)	(0.5426, 0.3563)	(0.4978, 0.4061)	(0.5090, 0.3910)	(0.6245, 0.2791)
E49	(0.7881, 0.1715)	(0.6303, 0.2697)	(0.5426, 0.3563)	(0.5534, 0.3466)	(0.5477, 0.3523)	(0.5350, 0.3686)
E50	(0.6224, 0.2942)	(0.5534, 0.3502)	(0.5235, 0.3718)	(0.3899, 0.4949)	(0.4173, 0.4726)	(0.3819, 0.4971)
E51	(0.7004, 0.2162)	(0.6433, 0.2549)	(0.5079, 0.3874)	(0.4495, 0.4444)	(0.4531, 0.4451)	(0.5462, 0.3574)
E52	(0.7729, 0.1780)	(0.6126, 0.2874)	(0.5740, 0.3195)	(0.4798, 0.4159)	(0.4029, 0.4726)	(0.4574, 0.4361)
E53	(0.5224, 0.3733)	(0.5386, 0.3596)	(0.5123, 0.3975)	(0.4570, 0.4466)	(0.4097, 0.4801)	(0.3744, 0.5047)
E54	(0.7708, 0.1801)	(0.6729, 0.2560)	(0.5379, 0.3610)	(0.7267, 0.2058)	(0.6747, 0.2339)	(0.6224, 0.2812)
E55	(0.6097, 0.3123)	(0.5715, 0.3267)	(0.8101, 0.1614)	(0.5256, 0.3780)	(0.5303, 0.3679)	(0.5043, 0.3993)
E56	(0.6097, 0.3087)	(0.7181, 0.2292)	(0.6931, 0.2531)	(0.7563, 0.1910)	(0.6426, 0.2574)	(0.7072, 0.2253)
E57	(0.7881, 0.1715)	(0.6433, 0.2549)	(0.5513, 0.3477)	(0.7751, 0.1827)	(0.8134, 0.1628)	(0.7552, 0.2061)
L2	(0.6536, 0.2551)	(0.6344, 0.2664)	(0.6319, 0.2766)	(0.6389, 0.2879)	(0.6463, 0.3191)	(0.6648, 0.2776)
L1	(0.4608, 0.3619)	(0.4474, 0.3779)	(0.4456, 0.3922)	(0.4505, 0.4083)	(0.4557, 0.4525)	(0.4688, 0.3937)

Table 10: The negative ideal solution.

Barriers	b_{j*}
B1	(0.4119, 0.4769)
B2	(0.4712, 0.3179)
B3	(0.4455, 0.4502)
B4	(0.4693, 0.4307)
B5	(0.4715, 0.4267)
B6	(0.4585, 0.4415)
B7	(0.4072, 0.4639)
B8	(0.3993, 0.4845)
B9	(0.3773, 0.5029)
B10	(0.3556, 0.5235)
B11	(0.3379, 0.5801)
B12	(0.3744, 0.5047)

Table 11: Euclidean d_i and Taxicab distances t_i.

	d_i	t_i		d_i	t_i		d_i	t_i
G1	0.0746	0.5108	U21	0.0875	0.5700	I41	0.0754	0.4995
G2	0.0885	0.5561	U22	0.0676	0.4410	I42	0.0912	0.5483
G3	0.1003	0.5871	U23	0.0905	0.5795	I43	0.0691	0.5177
G4	0.1031	0.5979	U24	0.1075	0.5575	I44	0.0754	0.5154
G5	0.0873	0.4811	U25	0.0531	0.4699	E45	0.1043	0.5741
G6	0.0863	0.5578	U26	0.0783	0.5136	E46	0.1176	0.6093
G7	0.0875	0.4920	U27	0.0346	0.3747	E47	0.1081	0.6203
G8	0.0916	0.5378	H28	0.0528	0.3532	E48	0.0794	0.5339
G9	0.0679	0.5162	H29	0.0763	0.5350	E49	0.0964	0.5813
G10	0.0990	0.5612	H30	0.0606	0.4408	E50	0.0611	0.4313
G11	0.1198	0.6391	H31	0.0828	0.5533	E51	0.0558	0.4770
G12	0.0815	0.5515	H32	0.0857	0.5161	E52	0.0665	0.4879
G13	0.0741	0.5449	H33	0.0762	0.5430	E53	0.0537	0.4320
G14	0.0773	0.5078	H34	0.1228	0.6449	E54	0.1097	0.6101
G15	0.0835	0.5693	H35	0.0585	0.4879	E55	0.0743	0.5265
G16	0.1040	0.6095	H36	0.0530	0.3793	E56	0.1396	0.6846
U17	0.0790	0.5363	H37	0.0669	0.4968	E57	0.1415	0.6918
U18	0.0779	0.4736	H38	0.0529	0.4341	L2	0.0997	0.6226
U19	0.1206	0.6351	H39	0.0568	0.4625	L1	0.0235	0.2935
U20	0.0861	0.5664	I40	0.0932	0.5476			

Consequently, the authorities of each of these systems are emanated from decision- and policy-makers at the national to the classroom level. Decision-makers formulate policies, structures, implementation strategies, and evaluation procedures based on various legislations, public opinion, education studies, technological advances, societal demands, industry demands, research findings, national testing, new leadership, accreditation, cross-country evaluation, and available funds. The barrier B12 (i.e., insufficient foundation in basic education) is the least among the preidentified 12 barriers. Nevertheless, B12 is associated with the top five priority barriers when addressed accordingly. For instance, B6 (i.e., lack of collaboration) components may be managed by identifying the gaps between CHED preservice teacher training and DepEd recommended curriculum's Most Important Learning Competencies. The actions to bridge the gap through collaboration should stress the importance of DepEd working closely with CHED for the curriculum of general education courses and the close supervision of TESDA for the national competency training under the senior high school curriculum of DepEd. With this coordination, the connection between these government educational agencies shall see these gaps closed. On the other hand, B10 and B11 are deemed low-bearing barriers. For example, learning platforms are as common as social network sites (e.g., Google, LinkedIn, and Facebook). Educators have already integrated these sites as educational delivery tools in the learning environment. These platforms are coined as an "alternative to the institutions' current Learning Management Systems (LMS)" in the delivery of asynchronous and synchronous learning [53]. LMS in HEIs is becoming responsive for organizing and distributing course materials. Since 2014, the case HEI has embarked on faculty development programs for the online LMS training and invested in the curriculum development and material preparation aligned with the LMS to make learning flexible and attuned to the requirements of EDUC4. Thus, the experts view these barriers with less priority.

The use of the FF CODAS-SORT reveals the high-priority stakeholder roles in overcoming EDUC4 implementation barriers. For the government, these roles include the inclusion of cybersecurity awareness in the basic education curriculum (G3), allocating more funds to support the necessary inclusive activities in the implementation of EDUC4 (G4), designing the curricula in line with the implementation and sustainment of EDUC4 (G11), and streamlining alignment initiatives of the basic education agenda (e.g., human resources and curricula) to EDUC4 (G16). As pointed out in the domain literature, governments play a vital role in designing, implementing, and monitoring EDUC4. With regard to cybersecurity threats, the Philippine government, through its arms (i.e., CHED, DepEd, and TESDA), may promote the inclusion of cybersecurity awareness in the basic education curriculum to cater to such concerns. The CHED may organize a pool of experts to roam around the universities for such an agenda. On the other hand, allocating more funds to support the necessary inclusive activities in the implementation of EDUC4 is also encouraged by the government to cater to the skills gap of human capital, to add training resources, and also for the Philippines to catch up with the developed countries in terms of technological gaps. The Philippine government may also encourage its arms to design curricula that align with the implementation and sustainment of EDUC4. CHED shall strengthen the collaboration among its agencies to address the knowledge gap for the customization of curriculum design and insufficient foundation of basic education. This initiative may include retooling human resources (e.g., educators, educational managers, and ICT personnel) to bridge the complexity of learning platforms.

For the university managers, the high-priority roles include investing in efficient technologies (e.g., virtual classrooms, enablement or process audit, analytic tools for strategic planning, and the hybrid or fully automated process of project management), which are known to reduce overall costs and improve the experience of the university stakeholders (U19) and forging extensive collaboration with various stakeholders (e.g., policy-makers, academic experts, university networks, educators, education leaders, learners, and industry partners) to provide space and training

Table 12: The relative assessment matrix.

	h_j (L2)	h_j (L1)		h_j (L2)	h_j (L1)		h_j (L2)	h_j (L1)
G1	−0.0251	0.0569	U20	−0.0137	0.0735	H39	−0.0429	0.0358
G2	−0.0113	0.0757	U21	−0.0122	0.0755	I40	−0.0066	0.0805
G3	0.0006	0.0918	U22	−0.0322	0.0465	I41	−0.0243	0.0575
G4	0.0033	0.0963	U23	−0.0093	0.0796	I42	−0.0085	0.0780
G5	−0.0124	0.0700	U24	0.0078	0.0978	I43	−0.0306	0.0514
G6	−0.0134	0.0732	U25	−0.0466	0.0319	I44	−0.0243	0.0584
G7	−0.0122	0.0705	U26	−0.0214	0.0616	E45	0.0046	0.0958
G8	−0.0081	0.0784	U27	−0.0652	0.0110	E46	0.0179	0.1147
G9	−0.0319	0.0499	H28	−0.0469	0.0298	E47	0.0084	0.1045
G10	−0.0007	0.0881	H29	−0.0235	0.0603	E48	−0.0203	0.0637
G11	0.0205	0.1210	H30	−0.0392	0.0394	E49	−0.0033	0.0870
G12	−0.0183	0.0674	H31	−0.0169	0.0688	E50	−0.0387	0.0395
G13	−0.0256	0.0582	H32	−0.0141	0.0703	E51	−0.0439	0.0353
G14	−0.0224	0.0604	H33	−0.0236	0.0606	E52	−0.0332	0.0472
G15	−0.0162	0.0709	H34	0.0237	0.1254	E53	−0.0460	0.0319
G16	0.0043	0.0983	H35	−0.0412	0.0383	E54	0.0100	0.1055
U17	−0.0207	0.0635	H36	−0.0468	0.0299	E55	−0.0254	0.0577
U18	−0.0218	0.0598	H37	−0.0328	0.0480	E56	0.0430	0.1526
U19	0.0211	0.1212	H38	−0.0468	0.0310	E57	0.0455	0.1562

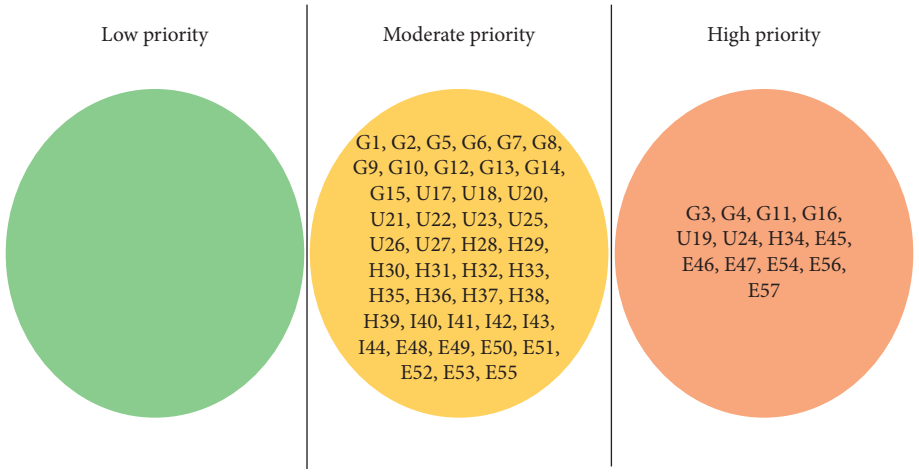

Figure 3: Sorting of the roles of various stakeholders.

resources for implementing EDUC4 (U24). Investments in efficient technologies would generally address the barriers related to cost (B2), lack of available technologies (B8), and complexity of learning platforms (B11). This role may be straightforward as EDUC4 implementation is associated with technology-intensive environments. Investing in those efficient technologies may integrate necessary activities for fully automated teaching and learning, resulting in increased productivity for educators. HEI managers may source these technologies from extensive collaborations with various stakeholders, providing inputs and learning experiences using such technologies. Forging partnerships require necessary diplomatic skills that HEI managers must possess. One efficient approach that is more applicable to the case HEI is to engage government institutions in finding collaborators as they can organize various stakeholders for an identified collaborative agenda. Nevertheless, the triple helix approach (i.e., government, industry, and academia) in initiating collaborations is rich in the literature (see [54]).

For the human resource function, periodic training of the human resources on the skills (i.e., especially digital readiness and customization of curriculum design) fitting to the current demands of EDUC4 emerges as a high-priority role (H34). The HEI managers and their governing boards may work together to examine existing policies and guidelines in hiring teaching and non-teaching personnel to include the skills relevant to EDUC4 as part of the selection criteria. On the other hand, incumbent personnel could be submitted to rigorous training and seminars to transform the workforce into becoming EDUC4 ready. In this manner, the HEIs could effectively address the skill gap of the human capital barrier, particularly those related to the lack of skills

(B3) and training resources (B5). To make the training and seminars relevant and need-based, periodic inventories on personnel training needs and the timely response of the human resource personnel to the identified needs could help the HEIs retain the best and most qualified personnel while addressing the demands of EDUC4.

Due to the danger primarily posed by online threats at the university level, educators can engage in continuous learning initiatives about relevant cybersecurity threats (i.e., data breaches on student information, denial of service attacks, and phishing; E45). This initiative will equip them with the necessary skills to help safeguard crucial information of learners and other members of the university. This may be achieved by integrating awareness of applicable laws to cyberbullying in (virtual) classroom teaching (E46). On the other hand, they can also devise alternative cost-efficient teaching strategies to deliver required learning outcomes geared to EDUC4 while upholding the implementation of EDUC4 (E47) and taking part in the design, development and improvement of innovative curricula aligned to EDUC4 (E54). Educators can also promote ways to efficiently prepare learning materials, including advanced ICTs (E56). They can also participate in skills development initiatives to equip them with the capabilities in handling different complex learning platforms (E57).

6. Conclusion and Future Work

While the recent literature has identified barriers to implementing EDUC4 in developing economies, holistic insights into overcoming these barriers remain largely unknown. This gap poses the relevance of the roles of various stakeholders in generating insights for the design of strategies and initiatives in the implementation of EDUC4. In this work, designed for HEIs, an analytic evaluation tool based on integrating Fermatean fuzzy sets into a hybrid entropy-based CRITIC-CODAS-SORT for evaluating various stakeholder roles is proposed. With the entropy-based CRITIC assigning priority weights to the recently reported 12 barriers and the CODAS-SORT identifying those roles with high priority, the incorporation of FFS into the integrated methodology addresses epistemic uncertainties inherent in decision-making. Through a focus group discussion of experts on a case HEI in a developing economy, the roles of various stakeholders, including the government, university management, human resource, ICT function, and educators, were identified. The application of FF CRITIC yields the following most relevant barriers to EDUC4 implementation in developing economies: lack of collaboration, apprehensive stakeholders, cybersecurity threats, health issues, and costs.

To overcome these barriers, the proposed methodology finds the following high-priority stakeholder roles. The government must consider the inclusion of cybersecurity awareness in the basic education curriculum, allocating more funds to support the necessary inclusive activities in the implementation, designing the curricula in line with the implementation and sustainment of EDUC4, and streamlining alignment initiatives of the basic education agenda (e.g., human resources and curricula) to EDUC4 in its priority agenda. On the other hand, HEIs must invest in efficient technologies to reduce the overall costs of implementing EDUC4 and enhance the experience of university stakeholders. Also, they need to forge extensive collaboration with various stakeholders to provide the necessary resources for EDUC4 implementation. The human resource management function of HEIs must implement periodic training of educators on the skills required of EDUC4. Finally, educators have the highest number of critical roles, including engaging in continuous learning initiatives about relevant cybersecurity threats at the university; integrating awareness of applicable laws to cyberbullying in (virtual) classroom teaching; devising alternative cost-efficient teaching strategies in the delivery of required learning outcomes while upholding the implementation of EDUC4; taking part in the design, development, and improvement of innovative curricula aligned to EDUC4; promoting ways to efficiently prepare learning materials; including the use of advanced ICTs; and participating in skills development initiatives aimed at equipping educators with the capabilities in handling different complex learning platforms.

The high-priority roles offer some insights into the design of specific initiatives in implementing EDUC4 in HEIs, not just in the case of university but in comparable HEIs, particularly in developing economies. Although idiosyncrasies exist, these insights may be relevant in other HEIs with similar conditions. Investigating how these roles or strategies may work out in practice is an interesting future endeavor and is highly suggested as a follow-up to this work. Furthermore, if available, the utilization of statistical data and analysis may be opted to cross-reference the findings of this study empirically. For instance, gathering data on the increase of utilization of digital technologies and other compositions of EDUC4 in different settings where some of these strategies are implemented may provide some idea on the actual effectiveness of the strategies, which can validate the results of this work based on expert decisions.

Data Availability

The perception data used to support the findings of this study are included within the article.

Conflicts of Interest

The authors declare that they have no conflicts of interest.

References

[1] M. Huba and Š. Kozák, "From E-learning to industry 4.0," in *Proceedings of the 2016 International Conference on Emerging eLearning Technologies and Applications*, pp. 103–108, IEEE, Stary Smokovec, Slovakia, November 2016.

[2] M. I. Ciolacu and P. Svasta, "Education 4.0: AI empowers smart blended learning process with biofeedback," in *Proceedings of the 2021 IEEE Global Engineering Education Conference*, pp. 1443–1448, IEEE, Vienna, Austria, April 2021.

[3] K. V. Vodenko and S. A. Lyausheva, "Science and education in the form 4.0: public policy and organization based on human

and artificial intellectual capital," *Journal of Intellectual Capital*, vol. 21, no. 4, pp. 549–564, 2020.

[4] R. Jamaludin, E. McKAY, and S. Ledger, "Are we ready for education 4.0 within ASEAN higher education institutions? Thriving for knowledge, industry and humanity in a dynamic higher education ecosystem?" *Journal of Applied Research in Higher Education*, vol. 12, no. 5, pp. 1161–1173, 2020.

[5] N. Abdul Razak, H. M. Alakrash, and Y. Sahboun, "English language teachers' readiness for the application of technology towards fourth industrial revolution demands," *Asia-Pacific Journal of Information Technology & Multimedia*, vol. 7, no. 2, pp. 89–98, 2018.

[6] R. Butt, H. Siddiqui, R. A. Soomro, and M. M. Asad, "Integration of industrial revolution 4.0 and IOTs in academia: a state-of-the-art review on the concept of Education 4.0 in Pakistan," *Interactive Technology and Smart Education*, vol. 17, no. 4, pp. 337–354, 2020.

[7] E. Costan, G. Gonzales, R. Gonzales et al., "Education 4.0 in developing economies: a systematic literature review of implementation barriers and future research agenda," *Sustainability*, vol. 13, no. 22, Article ID 12763, 2021.

[8] G. Gonzales, F. Costan, D. Suladay et al., "Fermatean fuzzy DEMATEL and MMDE algorithm for modelling the barriers of implementing education 4.0: insights from the Philippines," *Applied Sciences*, vol. 12, no. 2, p. 689, 2022.

[9] J. Miranda, C. Navarrete, J. Noguez et al., "The core components of education 4.0 in higher education: three case studies in engineering education," *Computers & Electrical Engineering*, vol. 93, Article ID 107278, 2021.

[10] D. Mourtzis, "Development of skills and competences in manufacturing towards education 4.0: a teaching factory approach," in *Proceedings of the 3rd International Conference on the Industry 4.0 Model for Advanced Manufacturing*, J. Ni, V. D. Majstorovic, and D. Djurdjanovic, Eds., pp. 194–210, Belgrade, Serbia, June 2018.

[11] U. Rahardja, A. N. Hidayanto, T. Hariguna, and Q. Aini, "Design framework on tertiary education system in Indonesia using blockchain technology," in *Proceedings of the 2019 7th International Conference on Cyber and IT Service Management (CITSM)*, vol. 7, pp. 1–4, Jakarta, Indonesia, November 2019.

[12] D. Diakoulaki, G. Mavrotas, and L. Papayannakis, "Determining objective weights in multiple criteria problems: the CRITIC method," *Computers & Operations Research*, vol. 22, no. 7, pp. 763–770, 1995.

[13] T. K. L. Nguyen, H. N. Le, V. H. Ngo, and B. A. Hoang, "CRITIC Method and Grey system theory in the study of global electric cars," *World Electric Vehicle Journal*, vol. 11, no. 4, p. 79, 2020.

[14] B. Pan, S. Liu, Z. Xie, Y. Shao, X. Li, and R. Ge, "Evaluating operational features of three unconventional intersections under heavy traffic based on CRITIC method," *Sustainability*, vol. 13, no. 8, p. 4098, 2021.

[15] S. Wang, G. Wei, J. Lu, J. Wu, C. Wei, and X. Chen, "GRP and CRITIC method for probabilistic uncertain linguistic MAGDM and its application to site selection of hospital constructions," *Soft Computing*, vol. 26, no. 1, pp. 237–251, 2022.

[16] M. K. Ghorabaee, E. K. Zavadskas, Z. Turskis, and J. Antucheviciene, "A new combinative distance-based assessment (CODAS) method for multi-criteria decision-making," *Economic Computation & Economic Cybernetics Studies & Research*, vol. 50, no. 3, pp. 25–44, 2016.

[17] D. Pamučar, I. Badi, K. Sanja, and R. Obradović, "A novel approach for the selection of power-generation technology using a linguistic neutrosophic CODAS method: a case study in Libya," *Energies*, vol. 11, no. 9, p. 2489, 2018.

[18] V. Simic, S. Karagoz, M. Deveci, and N. Aydin, "Picture fuzzy extension of the CODAS method for multi-criteria vehicle shredding facility location," *Expert Systems with Applications*, vol. 175, Article ID 114644, 2021.

[19] F. Lei, G. Wei, and X. Chen, "Model-based evaluation for online shopping platform with probabilistic double hierarchy linguistic CODAS method," *International Journal of Intelligent Systems*, vol. 36, no. 9, pp. 5339–5358, 2021.

[20] A. Ouhibi and H. Frikha, "CODAS-SORT: a new CODAS based method for sorting problems," in *Proceedings of the 2019 6th International Conference on Control, Decision and Information Technologies*, pp. 855–860, Paris, France, April 2019.

[21] L. Ocampo, R. A. Tanaid, A. M. Tiu, E. Selerio Jr, and K. Yamagishi, "Classifying the degree of exposure of customers to COVID-19 in the restaurant industry: a novel intuitionistic fuzzy set extension of the TOPSIS-Sort," *Applied Soft Computing*, vol. 113, p. 107906, 2021.

[22] L. Ocampo and K. Yamagishi, "Multiple criteria sorting of tourist sites for perceived COVID-19 exposure: the use of VIKORSORT," *Kybernetes*, 2021.

[23] L. A. Zadeh, "Fuzzy sets," *Information and Control*, vol. 8, no. 3, pp. 338–353, 1965.

[24] K. T. Atanassov, "Intuitionistic fuzzy sets," *Fuzzy Sets and Systems*, vol. 20, no. 1, pp. 87–96, 1986.

[25] R. R. Yager, "Pythagorean fuzzy subsets," in *Proceedings of the 2013 joint IFSA world congress and NAFIPS annual meeting (IFSA/NAFIPS)*, pp. 57–61, Edmonton, AB, Canada, June 2013.

[26] G. Kou, Ö. Olgu Akdeniz, H. Dinçer, and S. Yüksel, "Fintech investments in European banks: a hybrid IT2 fuzzy multidimensional decision-making approach," *Financial Innovation*, vol. 7, no. 1, p. 39, 2021.

[27] Y. Meng, H. Wu, W. Zhao, W. Chen, H. Dinçer, and S. Yüksel, "A hybrid heterogeneous Pythagorean fuzzy group decision modelling for crowdfunding development process pathways of fintech-based clean energy investment projects," *Financial Innovation*, vol. 7, no. 1, p. 33, 2021.

[28] M. Rahiminezhad Galankashi, F. Mokhatab Rafiei, and M. Ghezelbash, "Portfolio selection: a fuzzy-ANP approach," *Financial Innovation*, vol. 6, no. 1, p. 17, 2020.

[29] T. Senapati and R. R. Yager, "Some new operations over Fermatean fuzzy numbers and application of Fermatean fuzzy WPM in multiple criteria decision making," *Informatica*, vol. 30, no. 2, pp. 391–412, 2019.

[30] A. R. Mishra, P. Rani, and K. Pandey, "Fermatean fuzzy CRITIC-EDAS approach for the selection of sustainable third-party reverse logistics providers using improved generalized score function," *Journal of Ambient Intelligence and Humanized Computing*, vol. 13, no. 1, pp. 295–311, 2022.

[31] M. Kamali Saraji, D. Streimikiene, and G. L. Kyriakopoulos, "Fermatean fuzzy CRITIC-COPRAS method for evaluating the challenges to industry 4.0 adoption for a sustainable digital transformation," *Sustainability*, vol. 13, no. 17, p. 9577, 2021.

[32] J. P.-L. Tan, S. S. Choo, T. Kang, and G. A. D. Liem, "Educating for twenty-first century competencies and future-ready learners: research perspectives from Singapore," *Asia Pacific Journal of Education*, vol. 37, no. 4, pp. 425–436, 2017.

[33] M. S. Ramírez-Montoya, M. I. Loaiza-Aguirre, A. Zúñiga-Ojeda, and M. Portuguez-Castro, "Characterization of the

teaching profile within the framework of education 4.0," *Future Internet*, vol. 13, no. 4, p. 91, 2021.

[34] M. Hamilton, "Envisioning Education 4.0-A scenario planning approach to predicting the future," in *Future Directions in Digital Information*pp. 267–283, Chandos Publishing, 2021, https://www.sciencedirect.com/book/9780128221440/future-directions-in-digital-information.

[35] R. E. Indrajit, B. Wibawa, and A. Suparman, "University 4.0 in developing countries," *International Journal of Socio-technology and Knowledge Development*, vol. 13, no. 3, pp. 33–59, 2021.

[36] V. Agarwal, K. Mathiyazhagan, S. Malhotra, and T. Saikouk, "Analysis of challenges in sustainable human resource management due to disruptions by Industry 4.0: an emerging economy perspective," *International Journal of Manpower*, 2021.

[37] S. Ghavifekr and S. Y. Wong, "Technology leadership in Malaysian schools," *International Journal of Asian Business and Information Management*, vol. 13, no. 2, pp. 1–18, 2022.

[38] M. S. Ramírez-Montoya, I. M. Castillo-Martínez, J. Sanabria-Z, and J. Miranda, "Complex thinking in the framework of education 4.0 and open innovation-A systematic literature review," *Journal of Open Innovation: Technology, Market, and Complexity*, vol. 8, no. 1, p. 4, 2022.

[39] L. I. González-Pérez and M. S. Ramírez-Montoya, "Components of Education 4.0 in 21st century skills frameworks: systematic review," *Sustainability*, vol. 14, no. 3, p. 1493, 2022.

[40] H. A. López, P. Ponce, A. Molina, M. S. Ramírez-Montoya, and E. Lopez-Caudana, "Design framework based on TEC21 educational model and Education 4.0 implemented in a Capstone Project: a case study of an electric vehicle suspension system," *Sustainability*, vol. 13, no. 11, p. 5768, 2021.

[41] S. Iglesias-Pradas, Á. Hernández-García, J. Chaparro-Peláez, and J. L. Prieto, "Emergency remote teaching and students' academic performance in higher education during the COVID-19 pandemic: a case study," *Computers in Human Behavior*, vol. 119, Article ID 106713, 2021.

[42] E. Bilotta, F. Bertacchini, L. Gabriele, S. Giglio, P. S. Pantano, and T. Romita, "Industry 4.0 technologies in tourism education: nurturing students to think with technology," *Journal of Hospitality, Leisure, Sports and Tourism Education*, vol. 29, Article ID 100275, 2021.

[43] T. Goldin, E. Rauch, C. Pacher, and M. Woschank, "Reference architecture for an integrated and synergetic use of digital tools in education 4.0," *Procedia Computer Science*, vol. 200, pp. 407–417, 2022.

[44] B. Marković and A. Đurić, "Education 4.0 for industry 4.0," in *Proceedings of the International Conference on Machine and Industrial Design in Mechanical Engineering*, pp. 723–733, Springer, Novi Sad, Serbia, June 2021.

[45] R. R. Yager, "Generalized orthopair fuzzy sets," *IEEE Transactions on Fuzzy Systems*, vol. 25, no. 5, pp. 1222–1230, 2017.

[46] T. Senapati and R. R. Yager, "Fermatean fuzzy sets," *Journal of Ambient Intelligence and Humanized Computing*, vol. 11, no. 2, pp. 663–674, 2019.

[47] A. R. Mishra and P. Rani, "Multi-criteria healthcare waste disposal location selection based on Fermatean fuzzy WASPAS method," *Complex & Intelligent Systems*, vol. 7, no. 5, pp. 2469–2484, 2021.

[48] X. Shen, X. Zhang, L. Lan, Q. Liao, and Z. Luo, "Another robust NMF: rethinking the hyperbolic tangent function and locality constraint," *IEEE Access*, vol. 7, Article ID 31089, 2019.

[49] X. Peng, X. Zhang, and Z. Luo, "Pythagorean fuzzy MCDM method based on CoCoSo and CRITIC with score function for 5G industry evaluation," *Artificial Intelligence Review*, vol. 53, no. 5, pp. 3813–3847, 2020.

[50] T. M. Fernández-Caramés and P. Fraga-Lamas, "Use case based blended teaching of IIoT cybersecurity in the industry 4.0 era," *Applied Sciences*, vol. 10, no. 16, p. 5607, 2020.

[51] A. Hariharasudan and S. Kot, "A scoping review on digital English and education 4.0 for industry 4.0," *Social Sciences*, vol. 7, no. 11, p. 227, 2018.

[52] A. B. De Guzman, "The dynamics of educational reforms in the Philippine basic and higher education sectors," *Asia Pacific Education Review*, vol. 4, no. 1, pp. 39–50, 2003.

[53] D. C. Suladay and G. G. Gonzales, "A modified delphi study to identify course delivery modes in Cebu Technological University," *Journal of Agriculture and Technology Management*, vol. 18, no. 2, pp. 1–9, 2015.

[54] A. Galvao, C. Mascarenhas, C. Marques, J. Ferreira, and V. Ratten, "Triple helix and its evolution: a systematic literature review," *Journal of Science and Technology Policy Management*, vol. 10, no. 3, pp. 812–833, 2019.

Hindawi
Complexity
Volume 2022, Article ID 8942773, 8 pages
https://doi.org/10.1155/2022/8942773

Review Article

Credit Risk Measurement, Decision Analysis, Transformation and Upgrading for Financial Big Data

Wenshuai Wu

Guangdong Academy of Decision Sciences, Sun Yat-sen University, Guangzhou, Guangdong 510275, China

Correspondence should be addressed to Wenshuai Wu; wuwsh8@163.com

Received 9 December 2021; Revised 12 April 2022; Accepted 15 April 2022; Published 2 May 2022

Academic Editor: Yu Zhou

There is no well-built theory on credit risk measurement and decision analysis for financial big data, and an effective and scientific evaluation system for them has not been formed. A review of them can contribute to grasping the abovementioned topics, understanding current issues, analyzing research problems, mastering research challenges, and predicting future research directions. Besides, this paper points out four research directions of credit risk measurement and decision analysis for financial big data. Moreover, this paper can provide some guidance directions and insights for practitioners, researchers, financial institutions, and government departments who have an interest in complex decision-making in big data.

1. Introduction

With the rapid development of Internet finance, cloud computing, the Internet of things, and big data techniques, the data generated by society from structured data, semi-structured data, and unstructured data, such as credit card data, e-commerce data, resume data, picture data, audio data, and video data, are proliferating at an unprecedented speed, which marks the arrival of the big data era [1–4]. In 2012, the United Nations issued a white paper on big data government affairs, which listed big data as a historical opportunity globally. In 2013, the United States proposed to invest USD 200 million to promote the development of big data industries for upgrading the "big data strategy" according to the national will. The strong advantages of big data have attracted more countries and regions to join the process of exploring and applying big data. In China, the 14th five-year development plan for big data has also been issued for emphasizing the need to focus on developing key technologies of big data, innovating big data service mode, cultivating big data product system, and supporting the development of big data industry. Research on financial big data is not only a requirement for the development of society, but it is also conducive to grasping the operational status in order to better promote the transformation and upgrading of the structure of the financial industry and maintain regional financial stability [2].

The financial field is deeply involved in the calculation of big data events [5]. The financial credit system is not only an important part of the social credit system but also one of the most basic research fields [6]. Financial institutions employ credit scoring models to identify potential borrowers and to determine loan pricing and collateral requirements by measuring credit risk [7–9]. Effective measurement of credit risk is the core of credit risk management. Besides, the measurement of credit risk depends on massive data, which are difficult to improve the accuracy of analysis results [10, 11] because of complex characteristics such as multi-source heterogeneity, timeliness, sociality, and emergence. Therefore, for financial big data, such as bank customer information data, credit management data, and financial transaction information data, the problem of developing the effective technologies of credit risk measurement and decision analysis is a challenging and difficult issue [12].

Although some scholars are engaged in the research of financial big data, most of them have focused on theoretical and policy research [13–15]. For financial big data, there is still a lack of systematic and scientific theories and methods to measure credit risk, in order to explore the evaluation mechanism. Besides, there are also decision-making risks in

the choice of credit risk models in the big data environment. Moreover, big data not only bring unprecedented challenges to the traditional profit model, operation management, and customer service mode of financial institutions but also bring urgent needs to the transformation and upgrading of the financial industry. At present, the key research topics for financial institutions or even government departments are as follows: how to research and develop the effective technologies of credit risk measurement and decision analysis for financial big data to make the technological leap and promote the transformation and upgrading of the financial industry. So, this paper surveys the key technologies of credit risk measurement and decision analysis for financial big data, which are conducive to enhancing the driving force of technological innovation and promoting the upgrading of the financial industry.

The rest of this paper is organized as follows: Section 2 summarizes the related research. Section 3 introduces some research problems. In Section 4, some research challenges are proposed. In Section 5, future research directions regarding credit risk measurement and decision analysis for financial big data are presented. Finally, Section 6 concludes this paper.

2. Related Works

2.1. The Complexity of Big Data. The field of complexity science emerged at the end of the 20th century. However, the following questions persist: What is complexity? What is complexity science? There has always been some controversy surrounding this topic in academia. When the development of complexity science is discussed, big data technology has developed with vigor and vitality. Big data have the following five characteristics, known as the five Vs: (1) [16] Volume refers to a huge amount of data, more than 1000 T or even up to 1 billion T. (2) Variety refers to a wide range of data types, such as pictures, audio, video, network logs, and geographic location information. (3) Value indicates that the data purification value is low; that is, the data value density is relatively low. (4) Velocity refers to strong timeliness requirements, in that the effective information needs to be collected, processed, and fed back in time. (5) Veracity requires high accuracy, which reflects the quality of data [17, 18]. Complexity is one of the key factors restricting the efficiency and quality of big data processing, and it is an important factor for big data to become a scientific problem.

The representative achievement of complexity research is the "open complex giant system" theory, proposed by Qian [19, 20]. The core achievements of this theory are the "comprehensive integration method from qualitative to quantitative" and the "comprehensive integration seminar hall system of the man-machine combination." After decades of development, the basic technology and method system are formed. In recent years, with the development of big data techniques, the practical process of applying big data has been gradually accelerated. Many countries have launched and implemented national big data strategies. The US has taken big data as a strategic resource and accelerated the sharing, opening, development, and application of data resources to aid in industrial transformation and upgrading. Big data have brought unprecedented opportunities [13, 15, 21] for industrial transformation and upgrading. However, opportunities and challenges coexist.

At present, big data face three major theoretical problems [22–24]. The first is how to deal with big data effectively, the second is how to describe the complexity and uncertainty of big data, and the third is how to model the big data system. Based on cloud storage and cloud computing, how to use information technology to deal with unstructured and semistructured data effectively has become a cutting-edge scientific research issue of common concern. Besides, how to explore the effective methods and execute the system modeling for big data are important issues for knowledge discovery in big data. The subsequent problem is that of decision heterogeneity and data heterogeneity, the relationship between decision heterogeneity and data heterogeneity for knowledge discovery and management decision-making in big data should be studied in depth. Owing to the complexity of big data, this problem is clearly an important research issue, which presents new challenges to data mining theory and technology [7, 25–27]. At present, analysis of the complexity of big data has mostly focused on specific data sets and algorithm measurement levels. At the system level, the work of analyzing the complexity of big data, exploring its mechanism, and finding the basic methods is of great significance.

2.2. Credit Risk Measurement. Throughout the research process of credit risk measurement, from the credit risk measurement method initially relying on the subjective judgment of experts to the modern credit risk evaluation model based on statistics, operations research, and artificial intelligence, the credit risk measurement model has constantly developed and improved. The research on the credit risk measurement can be roughly divided into five models: experience judgment model, mathematical-statistical model, structural model, internal rating model, and artificial intelligence model.

In the experience judgment model, the credit scoring technology mainly relies on expert experience for scoring. Credit experts score applicants according to the applicant's materials and some elements of credit analysis. The commonly used methods include the 5C element analysis method, 5P element analysis method, and 5W element analysis method [28]. The characteristics of the experience judgment model mainly adopt the expert analysis method. The credit person in charge makes a subjective judgment on the credit status of the business object and then makes credit decisions, which have strong subjectivity.

In the late 1960s [29], the mathematical-statistical model is gradually developed to avoid the subjective influence of empirical judgment. The representative models include the zeta model [1], discriminant analysis model [30], regression analysis model [31–33], mathematical programming model [34, 35], multiobjective optimization model [36–38], and decision tree model [39].

With the rapid development of the capital market, the nonintermediation of financing and securitization, and the

emergence of many financial innovation tools, the complexity of credit risk became more significant. To solve the development of the capital market and the complexity of credit risk, the structural model based on capital market theory and information science theory is put forward in the 1990s, such as the KMV model [40], credit metrics model [41], credit portfolio view model [42], and risk measurement model based on option pricing technology [43, 44].

The Basel Committee launches the draft of the New Basel Capital Accord in 2001, pointing out that qualified banks should use the internal rating model to measure credit risk. The Office of the Comptroller of the Currency (OCC) defines the key components and characteristics of the internal rating system in 2003.

There are many assumptions in the application of the previous models, but the real data are difficult to fit with the proposed assumptions. With the development of artificial intelligence and computer technology, the artificial intelligence model has begun to enter the field of credit risk measurement. The representative models include the expert system [45], neural network [46], genetic algorithm [47, 48], and support vector machine (SVM) [49, 50].

Research on the credit risk measurement has attracted great attention in academic and application circles, and some research results have been obtained [51–55]. Altman [29], based on Beaver [56], using the Bayesian discriminant idea and linear discriminant technology, established the famous Z-score model to judge whether an enterprise defaults or goes bankrupt. In 1977, the Z-score model was extended by Altman [29] to propose the zeta model. Ohlson [57] took the financial ratio as the index and applied the logistic regression model to predict enterprise default probability. Altman et al. [58] used a neural network to predict bankruptcy and found that the neural network model was superior to the multivariate discriminant analysis method in performance. Jarrow and Turnbull [59] employed an arbitrage-free valuation technique for pricing derivatives on financial securities subject to credit risk. Vapnik [60] applied the SVM method to financial crisis early warnings, because of its strong operability and high prediction accuracy, and recently, the SVM method has been actively researched. Based on the credit conversion matrix, Morgan used the idea of value at risk to calculate the volatility of enterprise value by considering the loss rate of enterprise default loans and proposed the Risk-Metrics model [41]. Yu et al. [61] proposed a modified least-squares SVM classification, called the C-VLSSVM classification model, to evaluate credit risk. Yu et al. [62] applied a multiscale neural network model to address financial crisis events. Li et al. [63] proposed a software process model to measure and manage credit risk, in which the risk management and cost control module help to improve the risk management in the software development process. Based on the theories and methods of multicriteria decision making (MCDM) and data mining, Kou and Wu [64] proposed an analytic hierarchy model (AHM) to solve the model selection problem of credit risk assessment. Florez-Lopez and Ramon-Jeronimo [65] developed a correlated-adjusted decision forest model for ensemble strategy evaluation in credit risk assessment. Sousa et al. [66] proposed a new dynamic modeling framework to evaluate credit risk. Zhang et al. [24] proposed multiple instance learning models with transaction data for credit risk assessment. Yamanaka [67] presented a random thinning model for top-down-type credit risk assessment. Song et al. [68] indicated that ensemble learning methods perform better in default prediction than statistical techniques and individual classifiers. Huang et al. [69] proposed a GMM-based method to estimate model parameters and test model-implied restrictions for specification analysis of structural credit risk models. Lappas and Yannacopoulos [70] proposed a model combining genetic algorithm and expert knowledge for feature selection in credit risk assessment [71]. In summary, the research on the credit risk measurement model has mainly focused on the improvement and innovation of the above models.

Because most researchers focus on designing new methods and developing new models [10], they are rarely able to address and analyze the mining results in-depth, so many users cannot easily and effectively grasp and use them, resulting in wastage of knowledge and data resources [64]. Besides, although major commercial banks, such as the People's Bank of China, Bank of China, Industrial Commercial Bank of China, and China Construction Bank, have developed some credit scoring models suitable for the banks' business systems, the data information establishing these models lacks accuracy because of the difficulty of sharing data among banks. In addition, these models are customized for their own business systems, so they lack universality. Moreover, under the background of the financial big data era, many studies have not considered the big data environment and its characteristics, and big data have the characteristics of multisource heterogeneity, timeliness, sociality, and emergence, so research faces new and severe challenges, and the measurement of credit risk has become more and more complex. Furthermore, there is a risk of decision-making in the technology selection of big data. Therefore, there is no well-built theory on credit risk measurement and decision analysis for financial big data, and an effective and scientific evaluation system has not been formed.

3. Research Problems

So far, the research on credit risk measurement has attracted extensive discussion and study, and some related results have been achieved [54, 55, 72, 73]. However, most studies on credit risk measurement have mainly focused on the improvement and innovation of the models. At the same time, some researchers have focused on the introduction of model principles, and others have focused on the comparative analysis of various models. Besides, the data between financial institutions are difficult to share, and the reliable data information in the establishment of the model lacks accuracy. Moreover, these methods rarely combine the application domain background, decision-making objectives, background knowledge, and preferences of users.

Although some scholars are engaged in the research of financial big data, most of them have focused on theoretical

and policy research [13–15]. There is still a lack of unified standards for the acquisition, storage, and management of big data [74, 75]. For big data finance, there is also a lack of work to analyze big data using the basic theories and methods of system science, explore its mechanism, and find the basic evaluation system. In addition, there is a risk of decision-making in the model selection of big data. Besides, big data bring unprecedented challenges to the traditional profit model, operational management, and customer service mode of financial institutions. Therefore, this paper aims to excavate complex and heterogeneous massive data for financial institutions to develop key technologies for credit risk measurement and decision analysis to realize technological breakthroughs and improve financial risk prevention and control. Moreover, this paper can provide a decision-making basis for financial institutions and government departments to formulate relevant financial policies and realize the development strategy of the financial industry driven by technological innovation.

4. Research Challenges

In recent years, many large databases have been established in the financial industry, scientific research institutions, and government departments. Considerable multisource heterogeneous data have been accumulated. With the rapid development of computer technology, the era of big data has come. Big data can help to extract the value of data and make better decisions [76]. Big data finance has become an emerging hot research topic in recent years [22, 77]. In February 2011, Science magazine launched its first special issue on data processing: "Dealing with data," which discussed a variety of problems related to the rapid growth of data. In December of the same year, it published another special issue to discuss the replicability and reproduction of massive data. Ke and Shi [7] pointed out that big data have attracted increasing attention from academia and the industry [23]. As the core of the modern economy, finance is an important force that promotes the economic development of a region and even a country. Financial institutions have more inherent advantages in big data applications: (1) financial enterprises can accumulate a large amount of high-value density data, such as liabilities, assets, capital revenue, customer identity, and payment transactions; (2) financial institutions have a relatively sufficient capital budget, which can not only attract high-end talent in the field of big data but also easily adapt the latest big data technology.

Based on the five Vs of big data and complexity characteristics, big data are mostly stored in nonrelational databases, such as Google's BigTable, Amazon's Dynamo, and Hadoop's HBase, which have a flexible architecture design. In 2011, Ghoting et al. [78] proposed the SystemML and NIMBLE systems to design and implement a series of MapReduce primitives for data mining algorithms. Besides, algorithms, such as data clustering and classification, based on MapReduce have also been implemented and applied in many fields [32, 79]. Recently, the practical process of applying big data has gradually accelerated. From the early scientific research to applications in the fields of biology and physics, it has begun to spread to more fields, such as the Internet and finance. In the era of big data, the competition among financial institutions is intensifying on the network information platform, where "data are king."

Big data have brought unprecedented opportunities for the vigorous development of financial institutions [13]. From a marketing perspective, big data can more clearly and accurately obtain the needs and preferences of potential customers to attract customers through precision marketing or personalized intelligent recommendation. From the perspective of risk management, through deep mining of transaction data from multiple angles and channels, the financial industry can monitor financial risks in real-time and give early warnings of potential financial risks in time to reduce the cost of credit risk management. However, any financial activity has risks. For financial institutions, credit risk management is the key to the operation and management of financial institutions and has become the core issue in current social management. At present, although some scholars have engaged in research on financial big data, most of them have focused on theoretical and policy research [14], and there is still a lack of unified standards for the acquisition, storage, and management of big data [74, 75]. Besides, for financial big data, the work of using the basic theories and methods of system science to analyze big data, explore its mechanism, and find the basic evaluation system is also ambiguous. What's more, how to research and develop the key technologies of credit risk measurement and decision analysis for financial big data to make the technological leap is a key research topic for financial institutions and government departments.

5. Research Directions

McKinsey's research showed that the financial industry ranked first in the value potential index of big data. Big data have brought new opportunities and development impetus to the financial industry. The great significance of big data should be fully recognized. Future research directions are summarized as follows.

5.1. Theoretical Research on the Complexity Mechanism of Credit Risk Measurement for Financial Big Data. Big data have multisource heterogeneity, timeliness, sociality, and emergence; hence, research on financial credit risk measurement faces new and great challenges. However, most researchers have focused on designing new models or developing new algorithms [10], ignoring the big data environment and its characteristics. In view of this difficult problem, this research direction is to carry out theoretical research on the complexity mechanism of financial credit risk measurement. First, this research is to study the complexity and uncertainty of big data, the complexity of the big data process, and the complexity of the knowledge system involved in processing big data. Second, this research is to discuss and research the basic connotation of data, information, and knowledge to deeply research the characteristics of the financial big data industry and analyze the

challenges of the traditional credit risk measurement model. Finally, this research is to further discuss the essential feature of financial credit risk in the big data environment and carry out theoretical research on the complexity mechanism of credit risk measurement for financial big data.

5.2. Technology Development of Data Mining Models of Credit Risk Measurement. The complexity of big data is a key factor restricting the efficiency and quality of big data processing, and it is also an important factor for big data to become a key scientific problem. Facing the requirements of big data analysis, the traditional data processing, and analysis methods cannot meet the needs of data analysis in the big data environment. Three principles should be followed in big data analysis: all data, hybridity, and correlation. These are also the key characteristics that distinguish big data analysis from traditional data analysis. As an important technology of information processing, data mining aims to mine, extract, and identify valuable patterns, potential knowledge, and laws from massive data, in order to effectively guide business decision-making and scientific theoretical research. In this research direction, for financial big data, first, this research is to study the influencing factors of industrial upgrading based on the collection, processing, storage, and management technology of big data for determining the important factors, key areas, and key directions affecting big data innovation in the financial industry. Second, this research is to effectively screen and match data indicators in the data cloud platform from the three dimensions of personal credit, enterprise credit, and government credit to establish a credit risk measurement index system suitable for the financial industry. Finally, based on data mining models, relying on big data processing platforms (the big data offline processing platform, interactive processing platform, and stream processing platform), combined with Python and the big data ecosystem environment (Hadoop, Spark, HBase, Hive), this research is to develop new data mining models and technologies for credit risk measurement to give the system the advantages of scalability and high availability for seeking a technical breakthrough to solve the problem of credit risk measurement.

5.3. Method Development of Decision Analysis for Secondary Mining and Knowledge Discovery Based on MCDM. In the fields of data mining, machine learning, and big data analysis, many researchers have mostly focused on designing new models or developing new algorithms [10], and they have rarely been able to deeply process, analyze, and display the mined results. Therefore, it is difficult for users to understand the mined results, and the probability of mastering is lower, so the users cannot easily and effectively master and use the results, which causes the wastage of knowledge and data resources. Besides, the rough knowledge, generated by data mining, still needs to be filtered by decision-makers to obtain useful decision-making knowledge. Therefore, how to further integrate domain knowledge and rough knowledge into the decision-making knowledge to guide decision-making is a recognized and challenging scientific problem. If the process of extracting "rough knowledge" through data mining or big data analysis is called "primary mining," then the process of combining rough knowledge with quantified domain knowledge (e.g., expert experience, common sense, instinct, situational knowledge, and user preferences) to produce "decision knowledge" is called "secondary mining." For financial big data, based on the MCDM method [25, 80, 81], this research direction is to carry out secondary mining and knowledge discovery from a multicriteria, multidimensional, multistage, and multistate perspective to develop new decision analysis methods for financial big data. What's more, this research is committed to transforming the rough knowledge of data mining into the decision-making knowledge required by decision-makers to overcome the previous elite decision-making mode of "intuition and experience" which subverts the traditional research thinking mode and transforms "causal thinking" into "relevant thinking" in the big data era.

5.4. Countermeasure Research for the Transformation and Upgrading of the Financial Industry. With the transformation of economic structure to consumption structure, the original credit market cannot meet the demands of the social economy. In addition, there are obvious deficiencies in the coverage and availability of financial credit investigation data sources. The strong market demand poses a severe challenge to the financial industry. At the same time, in the era of big data, the competition among financial enterprises is more and more intense, and the traditional "intuition and experience" elite decision-making mode has gradually failed. Therefore, in this research direction, first, this research is based on industrial upgrading theory and economic growth theory, integrating cross scientific fields such as data mining, MCDM [82, 83], computer science, operations research, and artificial intelligence to carry out theoretical research on the operational mechanism of financial industry upgrading for financial big data. Second, the research is to combine the development status and characteristics of the financial industry in order to strive to explore the characteristics and operational law of big data in the development and management decision-making of the financial industry. Finally, the research is to further explore the development countermeasure suitable for the transformation and upgrading of the financial industry by providing big data management consulting and decision support services.

6. Conclusion

Financial credit risk analysis is the primary work and key link of risk management of financial institutions, which is related to the survival of financial institutions and social stability. The application of big data in the financial industry has attracted increasing attention. However, for the analysis of the financial credit risk for big data, no scientific evaluation and decision-making system has been formed. Besides, the research in this field has mostly focused on the improvement and innovation of the models and has rarely analyzed the mining results deeply. In addition, the research

has also rarely incorporated the corresponding application field background, decision-making objectives, background knowledge, and preferences of users. With the gradual deepening of economic globalization, the competition among enterprises is becoming fiercer and fiercer, and the traditional elite decision-making method of "intuition and experience" has gradually failed.

With the advent of the big data era, the cost of data acquisition is reducing. However, the amount of data is multiplying exponentially, and the data structure is becoming more and more complex. Human thinking has shifted from "causal thinking" to "relevance thinking" in the big data era. For financial big data, the work on using the basic theories and methods of system science to analyze financial credit risk, exploring its complex mechanism, and finding its evaluation system for financial big data is very meaningful. Therefore, based on the major needs of national economic and social development, this paper surveys theoretical research and technical development on credit risk measurement and decision-making analysis for financial big data. Besides, four research directions are pointed out as follows: first, considering new requirements and new challenges from the complex characteristics of multisource heterogeneity, timeliness, and the five Vs of big data, one direction is to perform theoretical research on the complex mechanism of credit risk measurement for financial big data. Second, because of the complexity of big data, another research direction is to develop new data mining models and technologies for credit risk measurement to achieve a technical breakthrough. Third, the results of mining are hard to understand, so another research direction is to carry out secondary mining and knowledge discovery for reconciling the knowledge gap, based on MCDM methods, in order to overcome the previous elite decision-making mode of "intuition and experience," which subverts the traditional research thinking mode and transforms "causal thinking" into "relevant thinking" in the big data era. Fourth, given the industrial upgrading theory and economic growth theory, the last direction is to carry out countermeasure research on the transformation and upgrading of the financial industry by providing big data management consulting and decision support services. Moreover, the review can contribute to grasping the previous topics, understanding current issues, analyzing research problems, mastering research challenges, and predicting future research directions. Furthermore, this paper can also provide a decision-making basis for financial institutions and government departments to formulate relevant financial industry policies to promote a great leap forward in the development of the financial industry [84–88].

Data Availability

The data used to support the findings of this study are included within the article.

Conflicts of Interest

The authors declare that they have no financial conflicts of interest related to the paper.

References

[1] S. Zhang, W. Xiong, W. Ni, and X. Li, "Value of big data to finance: observations on an internet credit Service Company in China," *Financial Innovation*, vol. 1, p. 17, 2015.

[2] T. K. Chen, H. H. Liao, and W. H. Chen, "CEO ability heterogeneity, board's recruiting ability and credit risk," *Review of Quantitative Finance and Accounting*, vol. 49, no. 4, pp. 1005–1039, 2017.

[3] Q. Zha, G. Kou, H. Zhang et al., "Opinion dynamics in finance and business: a literature review and research opportunities," *Financial Innovation*, vol. 6, p. 44, 2020.

[4] P. Jovanovic, S. Nadal, O. Romero, A. Abelló, and B. B. Quarry, "Quarry: a user-centered big data integration platform," *Information Systems Frontiers*, vol. 23, no. 1, pp. 9–33, 2021.

[5] M. M. Hasan, J. Popp, and J. Oláh, "Current landscape and influence of big data on finance," *Journal of Big Data*, vol. 7, no. 1, pp. 21–17, 2020.

[6] T. Kariya, Y. Yamamura, and K. Inui, "Empirical credit risk ratings of individual corporate bonds and derivation of term structures of default probabilities," *Journal of Risk and Financial Management*, vol. 12, no. 3, pp. 124–129, 2019.

[7] M. Ke and Y. Shi, "Big data, big change: in the financial management," *Open Journal of Accounting*, vol. 03, no. 04, pp. 77–82, 2014.

[8] P. K. Roy and K. Shaw, "A multi-criteria credit scoring model for SMEs using hybrid BWM and TOPSIS," *Financial Innovation*, vol. 7, no. 1, p. 77, 2021.

[9] M. Fleckenstein and F. A. Longstaff, "The market risk premium for unsecured consumer credit risk," *The Review of Financial Studies*, 2022.

[10] X. Q. Cheng, S. H. Liu, X. Q. Sun et al., "Combating emerging financial risks in the big data era: a perspective review," *Fundamental Research*, vol. 1, no. 5, pp. 595–606, 2021.

[11] W. H. Jiang, L. Xu, Z. S. Chen, K. Govindan, and K. S. Chin, "Financing equilibrium in a capital constrained supply Chain: the impact of credit rating," *Transportation Research Part E: Logistics and Transportation Review*, vol. 157, Article ID 102559, 2022.

[12] L. Yu, L. Yu, and K. Yu, "A high-dimensionality-trait-driven learning paradigm for high dimensional credit classification," *Financial Innovation*, vol. 7, no. 1, pp. 32–20, 2021.

[13] M. E. Mccue and A. M. Mccoy, "The scope of big data in one medicine: unprecedented opportunities and challenges," *Frontiers in Veterinary Science*, vol. 4, p. 194, 2017.

[14] B. Tissot, *Financial Big Data and Policy Work: Opportunities and Challenges*, Publications Office of the European Union, Luxembourg, 2019.

[15] Z. B. Zhou, M. Gao, H. L. Xiao, R. Wang, and W. B. Liu, "Big data and portfolio optimization: a novel approach integrating DEA with multiple data sources," *Omega*, vol. 104, p. 102479, 2021.

[16] A. N. Berger and W. S. Frame, "Small business credit scoring and credit availability," *Journal of Small Business Management*, vol. 45, no. 1, pp. 5–22, 2007.

[17] D. Howe, M. Costanzo, P. Fey et al., "Big data: the future of biocuration," *Nature*, vol. 455, pp. 47–50, 2008.

[18] A. Gandomi and M. Haider, "Beyond the hype: big data concepts, methods, and analytics," *International Journal of Information Management*, vol. 35, no. 2, pp. 137–144, 2015.

[19] J. Y. Yu, "Qian Xuesen's research on open complex giant systems," *Systems Engineering theory & Practice*, vol. 5, pp. 8–12, 1992.

[20] N. Wang, "The making of an intellectual hero: Chinese narratives of qian xuesen," *The China Quarterly*, vol. 206, pp. 352–371, 2011.
[21] K. Fanning and E. Drogt, "Big data: new opportunities for M&A," *Journal of Corporate Accounting & Finance*, vol. 25, no. 2, pp. 27–34, 2014.
[22] Y. Shi, "Big data and new challenges for science and technology," *Science, Technology and Development*, vol. 10, no. 1, pp. 25–30, 2014a.
[23] Y. Shi, "Big data history, current status, and challenges going forward," *The Bridge*, vol. 44, no. 4, pp. 4–11, 2014b.
[24] T. Zhang, W. Zhang, Xu. Wei, and H. Hao, "Multiple instance learning for credit risk assessment with transaction data," *Knowledge-Based Systems*, vol. 161, pp. 65–77, 2018.
[25] W. Wu, Z. Xu, G. Kou, and Y. Shi, "Decision-making support for the evaluation of clustering algorithms based on MCDM," *Complexity*, vol. 2020, no. 2, pp. 1–17, 2020b.
[26] H. Y. Qiu, C. Liu, and X. M. Zhang, "Intelligent design of tennis player training schedule based on big data of complexity," *Complexity*, vol. 2021, no. 1, pp. 1–11, 2021.
[27] M. E. Zmijewski, "Methodological issues related to the estimation of financial distress Prediction models," *Journal of Accounting Research*, vol. 22, pp. 59–86, 1984.
[28] S. M. Abbadi and S. M. A. Karsh, "Methods of evaluating credit risk used by commercial banks in Palestine," *International Research Journal of Finance and Economics*, vol. 111, pp. 146–159, 2013.
[29] E. I. Altman, "Financial ratios, discrimiant analysis and the prediction of corporate bankruptcy," *The Journal of Finance*, vol. 23, no. 4, pp. 589–609, 1968.
[30] C. Fraley and A. E. Raftery, "Model-based clustering, discriminant analysis, and density estimation," *Journal of the American Statistical Association*, vol. 97, no. 458, pp. 611–631, 2002.
[31] J. C. Wiginton, "A note on the comparison of logit and discriminant models of consumer credit behavior," *Journal of Financial and Quantitative Analysis*, vol. 15, no. 3, pp. 757–770, 1980.
[32] F. Campobasso and A. Fanizzi, "Goodness of fit measures and model selection in a fuzzy least squares regression analysis," *Studies in Computational Intelligence*, vol. 465, pp. 241–257, 2013.
[33] C. Jiang, Z. Wang, and H. Zhao, "A prediction-driven mixture cure model and its application in credit scoring," *European Journal of Operational Research*, vol. 277, no. 1, pp. 20–31, 2019.
[34] Y. Peng, G. Kou, Y. Shi, and Z. Chen, "A multi-criteria convex quadratic programming model for credit data analysis," *Decision Support Systems*, vol. 44, no. 4, pp. 1016–1030, 2008.
[35] Z. Chen, Y. Li, Y. Wu, and J. Luo, "The transition from traditional banking to mobile internet finance: an organizational innovation perspective-a comparative study of Citibank and ICBC," *Financial Innovation*, vol. 3, no. 1, p. 12, 2017.
[36] G. Kou, Y. Peng, Y. Shi, M. Wise, and W. Xu, "Discovering credit cardholders' behavior by multiple criteria linear programming," *Annals of Operations Research*, vol. 135, no. 1, pp. 261–274, 2005.
[37] Y. Shi, Y. Peng, G. Kou, and Z. Chen, "Classifying credit card accounts for business intelligence and decision making: a multiple-criteria quadratic programming approach," *International Journal of Information Technology and Decision Making*, vol. 04, no. 04, pp. 581–599, 2005.
[38] W. Wu and Y. Peng, "Extension of grey relational analysis for facilitating group consensus to oil spill emergency management," *Annals of Operations Research*, vol. 238, no. 1-2, pp. 615–635, 2016.
[39] N. O. Bakir, "A decision tree model for evaluating countermeasures to secure cargo at United States southwestern ports of entry," *Decision Analysis*, vol. 5, no. 4, pp. 230–248, 2008.
[40] K. M. V. Corporate, *Credit Monitor Overview*, San Francisco California, 1993.
[41] J. P. Morgan, "CreditMetrics-technical document," *Jp Morgan*, vol. 5, no. 3, pp. 48–51, 1997.
[42] T. Wilsom, *Credit Risk Modeling: A New Approach*, Mckinsey Inc, New York, 1997.
[43] F. A. Longstaff and E. F. Schwartz, "A simple approach to valuing risky fixed and floating rate debt," *The Journal of Finance*, vol. 50, no. 3, pp. 789–819, 1995.
[44] Z. S. Chen, X. Zhang, K. Govindan, X. J. Wang, and K. S. Chin, "Third-party reverse logistics provider selection: a computational semantic analysis-based multi-perspective multi-attribute decision-making approach," *Expert Systems with Applications*, vol. 166, p. 114051, 2021.
[45] A. Bahrammirzaee, A. R. Ghatari, P. Ahmadi, and K. Madani, "Hybrid credit ranking intelligent system using expert system and artificial neural networks," *Applied Intelligence*, vol. 34, no. 1, pp. 28–46, 2011.
[46] J. A. Marshall, "Neural networks for pattern recognition," *Neural Networks*, vol. 8, no. 3, pp. 493-494, 1995.
[47] J. Galindo and P. Tamayo, "Credit risk assessment using statistical and machine learning: basic methodology and risk modeling applications," *Computational Economics*, vol. 15, no. 1/2, pp. 107–143, 2000.
[48] P. Pawiak, M. Abdar, J. Pawiak, V. Makarenkov, and U. R. Acharya, "DGHNL: a new deep genetic hierarchical network of learners for prediction of credit scoring," *Information Sciences*, vol. 516, pp. 401–418, 2020.
[49] Z. Huang, H. Chen, C. J. Hsu, W. H. Chen, and S. Wu, "Credit rating analysis with support vector machines and neural networks: a market comparative study," *Decision Support Systems*, vol. 37, no. 4, pp. 543–558, 2004.
[50] J. H. Trustorff, P. M. Konrad, and J. Leker, "Credit risk prediction using support vector machines," *Review of Quantitative Finance and Accounting*, vol. 36, no. 4, pp. 565–581, 2011.
[51] M. Jacobs Jr, "The impact of asset price bubbles on credit risk measures," *Journal of Financial Risk Management*, vol. 04, no. 04, pp. 251–266, 2015.
[52] W. Wu and D. G. Mcmillan, "Dynamic linkages in credit risk: modeling the time-varying correlation between the money and derivatives markets over the crisis period," *Journal of Risk*, vol. 16, no. 2, pp. 51–59, 2013.
[53] A. Pichler, "A quantitative comparison of risk measures," *Annals of Operations Research*, vol. 254, no. 1-2, pp. 251–275, 2017.
[54] R. Chen, Z. Wang, L. Yang, C. T. Ng, and T. C. E. Cheng, "A study on operational risk and credit portfolio risk estimation using data analytics," *Decision Sciences*, vol. 53, no. 1, pp. 84–123, 2020, https://doi.org/10.1111/deci.12473.
[55] M. Mahbobi, S. Kimiagari, and M. Vasudevan, "Credit risk classification: an integrated predictive accuracy algorithm using artificial and deep neural networks," *Annals of Operations Research*, 2021.
[56] W. H. Beaver, "Beaver financial ratios as predictors of failures," *Journal of Accounting Research*, vol. 4, pp. 71–102, 1966.
[57] J. A. Ohlson, "Financial ratios and the probabilistic prediction of bankruptcy," *Journal of Accounting Research*, vol. 18, no. 1, pp. 109–131, 1980.

[58] E. I. Altman, G. Marco, and F. Varetto, "Corporate distress diagnosis: comparisons using linear discriminant analysis and neural networks (the Italian experience)," *Journal of Banking & Finance*, vol. 18, no. 3, pp. 505–529, 1994.

[59] R. A. Jarrow and S. M. Turnbull, "Pricing derivatives on financial securities subject to credit risk," *The Journal of Finance*, vol. 50, no. 1, pp. 53–85, 1995.

[60] V. N. Vapnik, *The Nature of Statistical Learning Theory*, Springer, New York, 1995.

[61] L. Yu, S. Wang, and J. Cao, "A modified least squares support vector machine classifier with application to credit risk analysis," *International Journal of Information Technology and Decision Making*, vol. 08, no. 04, pp. 697–710, 2009.

[62] L. Yu, S. Wang, K. K. Lai, and F. Wen, "A multi-scale neural network learning paradigm for financial crisis forecasting," *Neurocomputing*, vol. 73, no. 4–6, pp. 716–725, 2010.

[63] J. Li, M. Li, D. Wu, and H. Song, "An integrated risk measurement and optimization model for trustworthy software process management," *Information Sciences*, vol. 191, no. 1, pp. 47–60, 2012.

[64] G. Kou and W. Wu, "An analytic hierarchy model for classification algorithms selection in credit risk analysis," *Mathematical Problems in Engineering*, vol. 2014, no. 11-12, pp. 1–7, 2014.

[65] R. Florez-Lopez and J. M. Ramon-Jeronimo, "Enhancing accuracy and interpretability of ensemble strategies in credit risk assessment. A correlated-adjusted decision forest proposal," *Expert Systems with Applications*, vol. 42, no. 13, pp. 5737–5753, 2015.

[66] M. R. Sousa, J. Gama, and E. Brandão, "A new dynamic modeling framework for credit risk assessment," *Expert Systems with Applications*, vol. 45, pp. 341–351, 2016.

[67] S. Yamanaka, "Random thinning model with a truncated credit quality vulnerability factor: application to top-down-type credit risk assessment," *International Journal of Financial Engineering*, vol. 06, no. 03, Article ID 1950024, 2019.

[68] Y. Song, YY. Wang, X. Ye, D. J. Wang, Y. Q. Yin, and Y. Z. Wang, "Multi-view ensemble learning based on distance-to-model and adaptive clustering for imbalanced credit risk assessment in P2P lending," *Information Sciences*, vol. 525, no. 4, pp. 182–204, 2020.

[69] J. Z. Huang, Z. Shi, and H. Zhou, "Specification analysis of structural credit risk models," *Review of Finance*, vol. 24, no. 1, pp. 45–98, 2020.

[70] P. Z. Lappas and A. N. Yannacopoulos, "A machine learning approach combining expert knowledge with genetic algorithms in feature selection for credit risk assessment," *Applied Soft Computing*, vol. 107, Article ID 107391, 2021.

[71] R. A. Jarrow and D. Lando, "A markov model for the term structure of credit risk spreads," *Review of Financial Studies*, vol. 10, no. 2, pp. 481–523, 1997.

[72] D. E. Allen, R. J. Powell, and A. K. Singh, "Take it to the limit: innovative CVaR applications to extreme credit risk measurement," *European Journal of Operational Research*, vol. 249, no. 2, pp. 465–475, 2016.

[73] M. Gubareva and M. R. Borges, "Rethinking economic capital management through the integrated derivative-based treatment of interest rate and credit risk," *Annals of Operations Research*, vol. 266, no. 1-2, pp. 71–100, 2017.

[74] C. Liu and C. O. Sergeevna, "For intelligent debugging management of offshore oil engineering with big data," *Journal of Intelligent and Fuzzy Systems*, vol. 40, no. 4, pp. 6091–6101, 2021.

[75] S. Y. Wang, "An interview with Shouyang Wang: research Frontier of big data-driven economic and financial forecasting," *Data Science and Management*, vol. 1, no. 1, pp. 10–12, 2021.

[76] A. Pérez-Martín, A. Pérez-Torregrosa, and M. Vaca, "Big Data techniques to measure credit banking risk in home equity loans," *Journal of Business Research*, vol. 89, pp. 448–454, 2018.

[77] A. A. Bressan, "Big data as a revolutionary tool in finance," *Journal of Financial Innovation*, vol. 1, no. 2, pp. 1–7, 2015.

[78] A. Ghoting, R. Krishnamurthy, E. Pednault et al., "SystemML: declarative machine learning on MapReduce," in *Proceedings of the 2011 IEEE 27th International Conference on Data Engineering (ICDE)*, pp. 231–242, Hannover, Germany, 2011.

[79] J. J. Grefenstette, "Credit assignment in rule discovery systems based on genetic algorithms," *Machine Learning*, vol. 3, no. 2-3, pp. 225–245, 1988.

[80] W. Wu and Z. Xu, "Hybrid TODIM method with crisp number and probability linguistic term set for urban epidemic situation evaluation," *Complexity*, vol. 2020, no. 4, pp. 1–11, 2020.

[81] W. Wu, Z. Xu, and G. K. Kou, "Evaluation of group decision making based on group preferences under a multi-criteria environment," *Technological and Economic Development of Economy*, vol. 26, no. 6, pp. 1187–1212, 2020a.

[82] G. Kou, Ö. Olgu Akdeniz, H. Dinçer, and S. Yüksel, "Fintech investments in European banks: a hybrid IT2 fuzzy multidimensional decision-making approach," *Financial Innovation*, vol. 7, no. 1, pp. 39–28, 2021a.

[83] G. Kou, H. Xiao, M. Cao, and L. H. Lee, "Optimal computing budget allocation for the vector evaluated genetic algorithm in multi-objective simulation optimization," *Automatica*, vol. 129, p. 109599, 2021b.

[84] M. Cao, R. Chychyla, and T. Stewart, "Big data analytics in financial statement audits," *Accounting Horizons*, vol. 29, no. 2, pp. 423–429, 2015.

[85] W. S. Frame and L. Woosley, "Credit scoring and the availability of small business credit in low- and moderate-income areas," *Financial Review*, vol. 39, no. 1, pp. 35–54, 2004.

[86] Z. Lin, A. B. Whinston, and S. Fan, "Harnessing Internet finance with innovative cyber credit management," *Financial Innovation*, vol. 1, p. 5, 2015.

[87] X. Wu, X. Zhu, G. Q. Wu, and W. Ding, "Data mining with big data," *IEEE Transactions on Knowledge and Data Engineering*, vol. 26, no. 1, pp. 97–107, 2014.

[88] W. Wu, G. Kou, Y. Peng, and D. Ergu, "Improved AHP-group decision-making for investment strategy selection," *Technological and Economic Development of Economy*, vol. 18, no. 2, pp. 299–316, 2012.

Hindawi
Complexity
Volume 2022, Article ID 1695265, 14 pages
https://doi.org/10.1155/2022/1695265

Research Article

A BP Neural Network-Based GIS-Data-Driven Automated Valuation Framework for Benchmark Land Price

Lei Wu,[1] **Yu Zhang**,[2] **Yongchang Wei**,[2] **and Fangyu Chen**[2]

[1]*Business College, Shaoxing University, Shaoxing, China*
[2]*Institute of Operations Management and System Engineering, School of Business Administration, Zhongnan University of Economics and Law, Wuhan, China*

Correspondence should be addressed to Fangyu Chen; cfyconan@126.com

Received 25 January 2022; Accepted 6 April 2022; Published 28 April 2022

Academic Editor: Yu Zhou

The automated valuation of benchmark land price plays an essential role in regulating land demand in Chinese real-estate market as the big data are currently accumulated rapidly. However, this problem becomes highly challenging due to the multidimension, large volume, and nonlinearity of the land price-influencing factors. In this paper, an effective data-driven automated valuation framework is proposed for valuing real estate assets by combining a GIS (geographic information system) and neural network technologies. This framework can automatically obtain the values of spatial factors affecting land price from GIS and generate training set data for training the neural network to identify the complex relationship between all kinds of factors and benchmark land prices. The effectiveness and universality of the framework is verified via the data of benchmark land prices in Wuhan. The framework can be applied for automated benchmark land price valuation in other cities.

1. Introduction

In China, the benchmark land price is one of the main means for the government to control land demand at the macrolevel. The benchmark land price essentially reflects the average level of land prices in a certain area of a town, as well as its spatial distribution pattern. It can macroscopically guide land space utilization and investment behaviors and can be used as the basis for bulk land valuation. The benchmark land price is relatively stable over certain periods, generally being in line with the real estate market and urban development requirements [1, 2]. However, with the development of the social economy and the progress of urbanization, there exists a gap between the benchmark land price and the actual price of the land market. When this gap reaches a certain level, the benchmark land price needs to be reevaluated, which is a basic business in asset valuation. However, there are defects in the current commonly used benchmark land price valuation approaches. Firstly, there is a large subjectivity in the process of dealing with the benchmark land price impact factors. Secondly, when evaluating an entire city, the resulting large amount of data result in low work efficiency. Facing the huge land transaction market, the application effect of traditional benchmark land price valuation approaches has become increasingly unsatisfactory. It is therefore necessary to establish a reasonable automated benchmark land price valuation framework.

When constructing an automated benchmark land price valuation framework, we are faced with several challenges: (1) benchmark land prices often take an entire city as the valuation object, involving a large number of land parcels. Therefore, benchmark land price valuation has higher requirements for data collection and processing; (2) there are multiple dimensions of the factors affecting the benchmark land price, and many factors have no quantitative indicators. In traditional valuation, the value of these factors is often determined based on experience, which decreases the objectivity of the valuation process; (3) the mechanisms of impact factors on the benchmark land price are complicated, which cannot be reflected by simple linear relations; (4) considering the above three reasons, benchmark land price

valuation is often carried out every few years. Therefore, the guiding role of the benchmark land price in real estate transactions is reduced. The current valuation approaches cannot meet the efficiency and accuracy requirements for assessing a large number of lands. Thus, the valuation methods need to improve their applicability and timeliness.

In recent years, the development and application of the GIS technology have provided a basis for large-scale geographic data collection which is updated in real time [3]. Xu and Li [4] conducted a sustainability analysis through GIS for urban residential development which considered the impacts of benchmark land prices. On the other hand, artificial intelligence technology has also begun to play a role in the field of valuation. Neural networks can map complex nonlinear relationships between an input and output, as well as handling multidimensional complex data well. In addition, the self-training processes of neural networks avoid the need for human subjective interference. Therefore, based on data collected by GIS, this paper attempts to integrate artificial intelligence and batch valuation to design an automated valuation framework for the benchmark land price.

The critical innovation of this paper lies in the framework we proposed for benchmark price valuation. We use the GIS technology to establish a geographic information database to collect geographic data. To deal with the incommensurability of impact factors, we unify the quantitative criteria of these factors by using GIS-based spatial data quantification and weight setting. Considering the nonlinear interactions and relationships between impact factors and land prices, a pricing model based on BP neural networks is constructed, in order to reduce subjectivity and uncertainty of valuation and improve the effectiveness of valuation results. Finally, taking Wuhan as an example, the effectiveness of our framework is verified and the corresponding limitations are discussed.

The rest of this article is organized as follows: Section 2 summarizes the relevant literature from three aspects: benchmark land price valuation, automated valuation technology, and artificial intelligence technology in land price valuation. Section 3 introduces the automated valuation framework; Section 4 uses the residential benchmark land price valuation in Wuhan as a data source to verify the effectiveness of the framework. The paper is concluded in Section 5.

2. Literature Review

This part will summarize the related research from three aspects: (1) benchmark land price valuation, (2) automated valuation, and (3) application of artificial intelligence technology in valuation field.

2.1. Benchmark Land Price. Wang [5] proposed to predict the price curve of commercial and residential land through the urban population size and income level. The results showed that population size and income level had a positive impact on urban benchmark land price. Moreover, the benchmark land price for different land-use types often varies greatly; for example, the benchmark land price of general commercial land is typically higher than that of residential land. De Groot [6] developed a comprehensive valuation framework of ecological services and socioeconomic benefits. By introducing landscape ecology, this valuation framework could accurately reflect the value of the land itself. Davis and Heathcote [7] found a close relationship between the price of residential land in the United States and the current housing price. Demetriou [8], in a case study based in Cyprus, found that location characteristics, legal factors, physical attributes, and economic conditions had more impact on the value of land than other factors. Yang et al. [9] pointed out that demographic and economic factors have an influence on the residential land price in major cities of China and also found that the GDP has a great influence. Burian et al. [10] divided the impact factors of land price into three aspects: social, environmental, and economic. Compared with social and environmental factors, the impact of economic factors on land price was found to be relatively small. Glumac et al. [11] proposed a hedonic urban land price index which could quantify the spatial effect of land and the impact of macropolicies on land transaction volume. Li et al.[12] concluded that the price of urban land is not only influenced by the city itself but also by its interaction with nearby cities. They calculated the interaction intensity between cities based on a gravity model, in order to obtain the urban land price of a certain area. Yuan et al. [13] focused on the difference of land prices caused by land marketization and fiscal decentralization. Nakamura [14] proposed a land pricing model which considers six factors: entrepreneurship, nature conservation, resource recycling, social vitality, financial viability of local governments, and environmental quality. Tan et al. [15] considered that a newly opened subway station was more likely to raise land prices nearby than a central station. In addition, earthquake risk [16] and noise [17] have also been shown to affect the land price under special circumstances.

From the above analysis, it can be seen that the factors affecting land price mainly focus on the natural environment, economic society, population, infrastructure construction, and the correlations among relevant cities.

2.2. Automated Valuation. In the theoretical research of automated valuation, various models have been proposed and their adaptability has been studied. Berry and Bednarz [18] and Pace and Gilley [19] proposed automated valuation for public purposes, such as for the collection of property taxes, where the hedonic price index was considered as an appropriate method. IAAO [20] applied the three valuation processes of AVM (automated valuation model)—namely, model specification, model calibration, and model test and quality assurance—to the valuation research of benchmark land price. Aragonés-Beltrán et al. [21] proposed a method based on ANP which they applied to the valuation of industrial land value, demonstrating that it could accurately model complex environments. Metzner and Kindt [22] further developed the hedonic price index by extracting, comparing, and integrating parameters from a large number

of studies in the literature. Taking Cyprus as a case study, Demetriou [23] developed an automated valuation model (AVM) using geographic information system (GIS) data, which had a higher valuation efficiency and greatly reduced the use of time and resources. The general valuation process has also begun to shift from empirical to systematic and standard. Renigier-Biłozor [24] proposed an automated valuation model with decision theory and data mining to assess real-estate values. In response to the multidimensional factors that affect land prices, Bencure et al. [25] adopted AHP to integrate multiple factors into one model, in order to achieve the automated valuation of land. It can be seen that the most critical process in automated valuation or batch valuation models is dealing with large-scale parameters, as well as integrating multiple parameters with different characteristics into one valuation model.

2.3. Application of Artificial Intelligence Technology in Valuation. Artificial intelligence technology has been applied in assets valuation areas such as box office revenue [26], stock value [27–29], and the auction price of paintings [30]. In real estate valuation, artificial intelligence technology has been widely used, especially in developed countries [31]. The most commonly used models are artificial neural networks (ANNs). ANNs can obtain the nonlinear relationships between real-estate characteristics and real-estate prices but do not have many parameter limits, such as in traditional statistical methods [32].

Peterson and Flanagan [33] found that, compared with the linear hedonic price index model, the artificial neural network evidently had lower pricing error and higher pricing accuracy, which can lead to better predictions in a volatile pricing environment. Follow-up studies indicated that, in different situations, ANN and multiple linear regression each have their own advantages and the advantages and disadvantages of the two are not absolute. When the homogeneity of the data set is low, a valuation method based on AI is more appropriate [34]. ANN, as a "black box" data-driven method, has the major disadvantage of complexity [35], which limits its use by valuators. Multiple regression analysis is more transparent and explanatory than ANN. Geographically weighted regression can be used to achieve an optimal balance between the accuracy of the valuation and the transparency of the methodology [36].

Furthermore, Bin et al. [37] used the long short-term memory (LSTM) model to improve an automatic valuation model based on Boosting Tree to predict house prices in the next few months or a year. Poursaeed et al. [38] believed that the internal and external appearance affect the value of a house and thus proposed to evaluate the visual characteristics of houses by use of convolutional neural networks (CNNs). In addition to artificial neural networks, other methods have also been used in the field of real estate valuation, such as Random Forest [39, 40], Fuzzy Logic System [41, 42], and Genetic Algorithms [43].

The related research illustrates that the wide application of artificial intelligence provides an opportunity to conduct automated valuation. The benchmark land price is an important tool for the government to implement macrocontrol on the land market, and it is a business in asset valuation. The introduction of any new method must comply with the criteria for asset valuation. As a basic approach for land valuation, the market approach selects multiple factors that affect land value, quantifies the differences between the reference objects and the evaluated land with respect to these factors after determining the weights of these factors, and finally determines the land value. In essence, it is a multi-objective decision problem, and an optimization method can be introduced to improve the decision efficiency [44, 45]. The calculation process of the BP neural network [46] conforms to the basic idea of the traditional market approach, which considers the effect of comparable impact factors. More importantly, BP neural network can make up for the shortcoming of the simple linear assumption in the market approach to the influencing mechanism of the impact factors. Moreover, there are many factors affecting benchmark land prices and, so, the first problem to be solved is data collection and integration of multidimensional factors. Therefore, based on the GIS and BP neural network, we propose a framework of automated benchmark land price valuation with the function of spatial data collection and processing.

3. Automated Valuation Framework

In this paper, we propose an automated benchmark land price valuation framework based on the BP neural network. In this framework, the land use must be determined first, as plots with different uses yield different benchmark land price types. Then, the impact factors of land price are selected, according to the land-use type, to form a value impact system. The sample data to train the neural network are collected with the assistance of the GIS. Finally, after training and testing, the neural network-based valuation model can execute the automated valuation of benchmark land prices.

The basic procedure of the framework is shown in Figure 1.

3.1. Impact Factors Selection. According to different specific uses, different functional attribute values of the same plot yield different benchmark prices. For example, the value of commercial land is mainly related to its geographical location, local economic development, lifestyles of residents, and surrounding business services; the land area, mode of land leasing, location of the district, GDP, paid-in foreign investment, unemployment, tenure of district mayor, gross industrial production, and total industrial asset affect the industrial land price [47]; meanwhile, residential land value is closely related to the surrounding cultural environment, traffic, and public facilities. After determining the specific use of the land, it is necessary to choose the corresponding impact factors. As the most common transaction object in the land trading market, the valuation of residential land has attracted the most attention [48].

For residential land benchmark pricing, impact factors exist in many aspects. Dale and McLaughlin [49] proposed

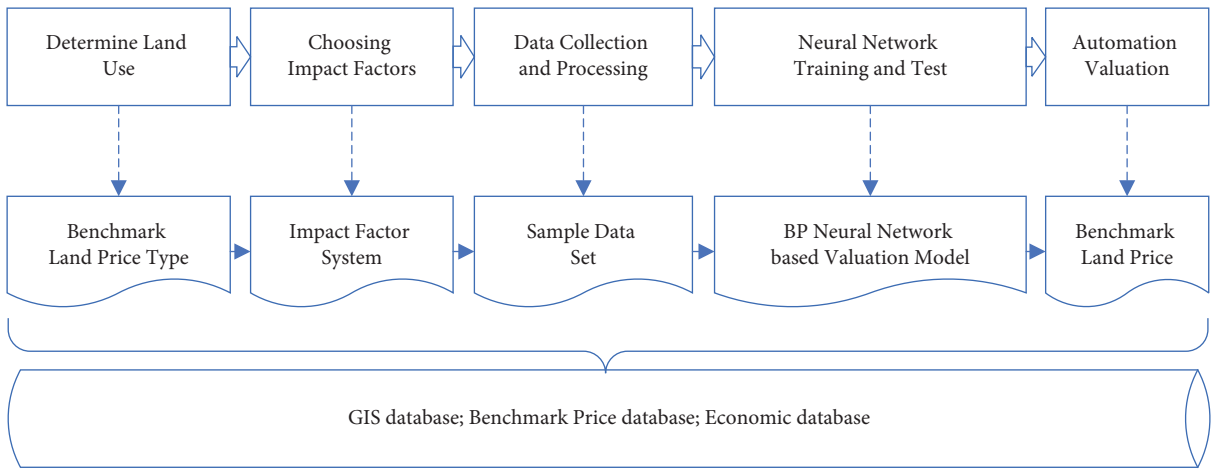

Figure 1: Basic procedure of the automated valuation framework.

that land price depends on various factors, such as economy, society, environment, and law. By using the Delphi method, China's local government found that the impact factors for the land price were business services, public facilities, population density, transportation facilities, and so on [1]. Residential land price is also influenced by the environment and ecology [50]. Xu and Coors [51] took socioeconomic level, regional pressure of environmental constraints, population pressure, and transportation pressure as the most important impact factors affecting urban residential land price. Yang et al. [9] used geographically weighted regression (GWR) to analyze the relationships between residential land prices and housing prices. They screened out three main impact factors—immigrant population, gross domestic product (GDP), and residential investment—and found that the impact of GDP on the residential land price was more significant than other factors in the prior three years. It has been observed that location, business services, and education resources have a great influence on the spatial layout of residential land prices. The benchmark land price is the basic reference for residential land prices. The government also considers the same factors when pricing. As the basic consensus of the industry, to meet the requirements of the evaluation criteria, in this paper, we chose business services, environment, traffic, public facilities, and GDP per capita as the five dimensions for impact factors of residential land price. According to the different connotations of these five dimensions, the specific impact factors of residential land price were summarized into the valuation system shown in Table 1.

3.2. Data Collection and Preprocessing. The premise of automated valuation is that there are a lot of standardized samples and data. As benchmark land price valuation is carried out for an entire administrative region, we imported the corresponding plot information into GIS, in order to establish a geographic information database for collecting and processing data in real time.

It should be noted that some impact factors can be quantified by GIS, such as distance to the nearest business service center and driving time to the nearest train station. The accessibility of the road network can be quantified by the number of arterial roads around the plot. The indices which are difficult to quantify, such as intensity of nearby scenic location and intensity of medical support, can be processed by an index scoring method. The standards for index scoring are shown in Table 2, which is offered by our project collaborator.

3.3. Backpropagation Neural Network Training. In our neural network, the input value of the input layer corresponds to the matrix of preprocessed data of impact factors. The output layer corresponds to the predicted value of the residential benchmark land price without renormalization. The quantified values of 13 benchmark land price impact factors were selected as the input, while the output is the residential benchmark land price. The proposed BP neural network, therefore, reflects the mapping relationship of 13 independent variables to 1 dependent variable.

Based on the above analysis, the specific operation process was as follows:

Step 1: establish the value impact system of residential benchmark land price valuation

Step 2: use GIS and index scoring method to collect impact factor data

Step 3: process the collected parameters and data by the *mapminmax* function

$$X = \frac{2(x - x_{\min})}{x_{\max} - x_{\min}} - 1, \tag{1}$$

where X is the value after processing, x is the value of the impact factor, $x_{\min}$ is the minimum value in this kind of impact factor, and $x_{\max}$ is the maximum value in this kind of impact factor

Step 4: establish a BP neural network model and determine the number of network layers, the number of input layer nodes, the number of hidden layer nodes, the number of output layer nodes, training functions, performance functions, and so on

Table 1: Impact factors of residential benchmark land price.

	Parameter	Unit
Business service	Distance to the nearest business service center, D_{bsc}	m
Economic	GDP per capita in the district of the current sample, G	RMB/year
Environmental	Distance to the nearest scenic location, D_{sce}	m
	Intensity of nearby scenic location, I_{sce}	n/a
Public facilities	Distance to the nearest primary school, D_p	m
	Distance to the nearest middle school, D_m	m
	Distance to the nearest hospital, D_h	m
	Intensity of medical support, I_h	n/a
Traffic	Distance to the nearest bus stop, D_{bus}	m
	Distance to the nearest subway station, D_{sub}	m
	Driving time to the nearest train station, T_t	min
	Driving time to the nearest airport, T_a	min
	Accessibility of road network, A_r	n/a

Table 2: Standards for index scoring.

Index	Excellent (9–10)	Good (6–8)	Medium (4-5)	Inferior (2-3)	Worst (0-1)
I_h	There are 6–10 tertiary level-a hospitals within 5 kilometers	There are tertiary level-a hospitals within 5 kilometers, but the number of them is less than 6, or there are 8–10 tertiary level-a hospitals within 5 kilometers	There are 4–7 tertiary level-a hospitals within 10 kilometers	There are 1–3 tertiary level-a hospitals within 10 kilometers	Others
I_{sce}	There are class 5A tourist attractions within 5 kilometers and there are more than 5 class 5A tourist attractions within 1 kilometer	There are class 5A tourist attractions within 10 kilometers or there are class 3A/4A tourist attractions within 5 kilometers. The number of tourist attractions within 1 kilometer is less than 6	There are class 3A/4A tourist attractions within 10 kilometers; there are tourist attractions within 1 kilometer	There are no famous tourist attractions, but there are tourist attractions within 1 kilometer	There are no famous tourist attractions and there are no tourist attractions within 1 kilometer

In view of the incommensurability of the original data, we use the mapminmax function to eliminate differences between impact factors.

Step 5: train the model to process residential benchmark land price samples

Step 6: test the BP neural network model. When it successfully passes the test, the model can then be used to evaluate and update the residential benchmark land price in real time.

4. Case Analysis

4.1. Data Collection. We selected the most representative data samples from the 10 central districts of Wuhan, based on the latest residential benchmark land price data for 2018. The 110 groups of residential benchmark land price valuation project information were used to train and test the model. The related data sources are shown in Table 3.

All the collected information was imported to the GIS database to draw an electronic vector map of Wuhan, as shown in Figure 2. This map can be used to obtain the geographic characteristics of the impact factors, which were used to analyze the correlations between the target plot benchmark price and each impact factor.

Table 3: Data sources.

	Data source
Land price	Wuhan Natural Resources and Planning Bureau https://zrzyhgh.wuhan.gov.cn/pc-315-180285.html
GIS	Geographical information monitoring cloud platform https://www.dsac.cn/
GDP data	Wuhan Municipal Bureau of Statistics https://tjj.wuhan.gov.cn/

Combining the data collection and preprocessing steps mentioned in Section 3.2, the values of the impact factors for each sample point were finally obtained. Table 4 shows 10 groups of sample data, and the descriptive statistics of the whole data set is provided in Table 5.

4.2. Valuation Model Construction

4.2.1. Design of BP Neural Network Structure. The effect of the BP neural network model is affected by the number of hidden layer nodes [52]. A reasonable number of hidden

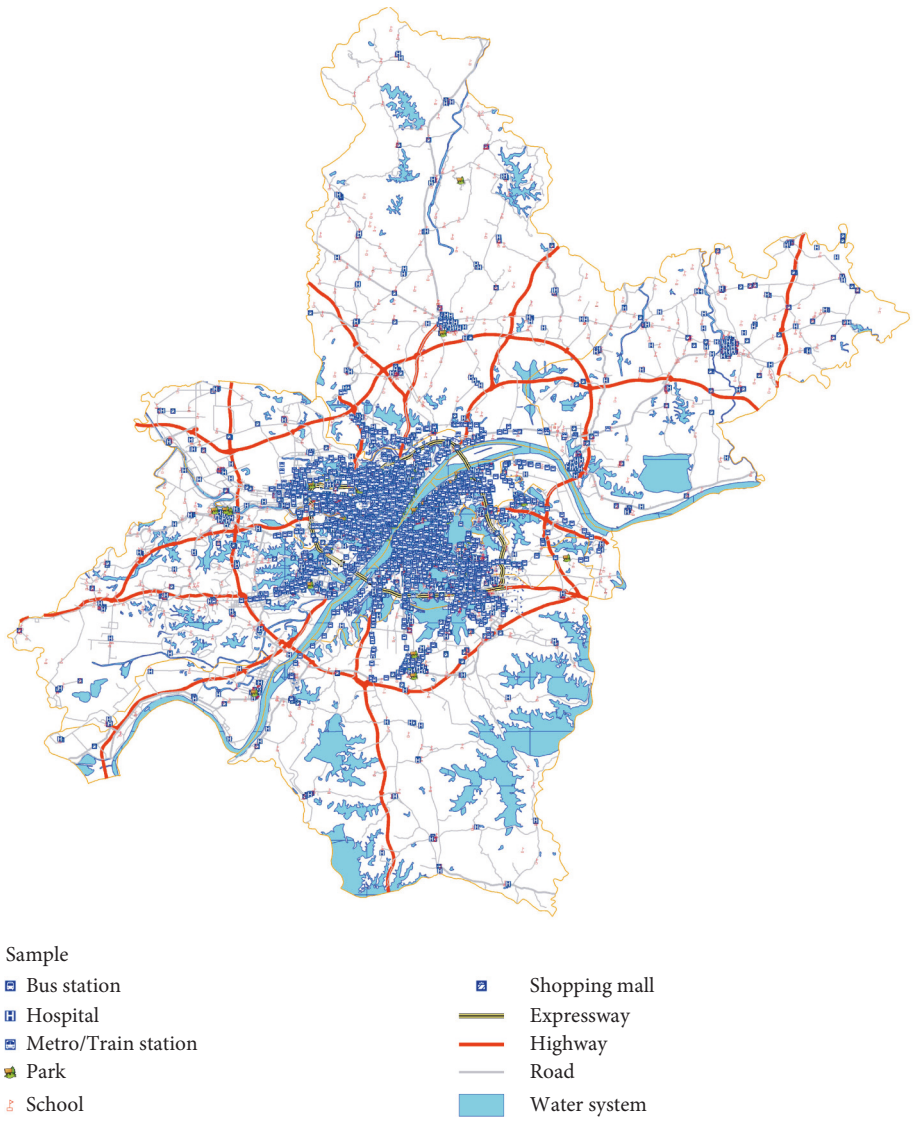

Figure 2: Electronic vector map of Wuhan.

Table 4: Factor quantification.

ID	D_{bsc}	G	D_{sce}	I_{sce}	D_p	D_m	D_h	I_h	D_{bus}	D_{sub}	T_t	T_a	A_r	Price
1	1000	81489	97	8	269	541	2200	9	31	1100	27	44	6	11270
2	1100	64355	552	9	292	650	1300	10	160	1600	20	55	5	10575
3	1700	64355	300	7	602	875	2700	10	185	348	16	48	5	9860
4	1300	132141	830	7	599	360	1600	9	132	1200	16	37	5	6894
5	3100	59765	325	6	650	730	3200	8	400	680	23	38	6	6522
6	1900	81489	635	5	778	795	3900	9	196	501	15	34	6	6487
7	771	132141	760	6	116	280	936	7	53	742	21	36	5	7037
8	1500	132141	1500	4	328	420	2800	7	128	796	20	36	5	7037
9	1700	62239	150	8	613	779	3100	8	752	1900	25	60	5	6659
10	1000	132141	100	7	631	764	2500	6	445	722	11	59	6	6306

layer nodes not only leads to better performance but can also greatly save the amount of training time required. We selected the following empirical formula to determine the number of hidden layer nodes:

$$M = \sqrt{n+m} + a, \tag{2}$$

where m is the number of input layer nodes; n is the number of output layer nodes; and a is a number in $[1, 10]$.

Table 5: Descriptive statistics.

Parameter	Max	Min	Mean	Standard deviation	Kurtosis	Skewness	Coefficient of variation
D_{bsc}	32100	382	3211.991	3915.932	34.133	5.309	1.219
G	132141	57810	84931.173	25478.534	−0.655	0.799	0.3
D_{sce}	7800	97	1269.327	1268.117	9.283	2.734	0.999
I_{sce}	9	1	3.027	2.436	−0.679	0.871	0.805
D_p	6200	32	1270.736	1053.044	6.696	2.212	0.829
D_m	10100	97	1435.636	1305.607	17.186	3.19	0.909
D_h	54000	912	8106.227	8863.934	9.307	2.647	1.093
I_h	10	2	4.855	2.559	−0.926	0.546	0.527
D_{bus}	2100	31	482.273	446.313	3.219	1.769	0.925
D_{sub}	32600	29	4506.845	6943.069	4.835	2.354	1.541
T_t	68	11	30.845	190.591	−0.366	0.758	0.448
T_a	90	19	52.1	15.998	−0.688	0.128	0.307
A_r	6	2	4.155	0.96	−0.648	0.128	0.231
Price	6059	408	2236	1403.913	−0.157	0.866	0.628

Table 6: Model parameters and equations.

Model parameters	Value
Network layer	3
Number of input layer nodes	13
Normalization function (map min max)	$2(x - x_{\min})/x_{\max} - x_{\min} - 1$
Number of hidden layer nodes	10
Error tolerance	0.01
Hidden layer activation function	$\log sig(x) = 1/1 + e^{-x}$
Output layer activation function	$\tan sig(x) = 2/1 + e^{-2x}$
Learning rate	0.01
Mean square error (MSE)	$mse = \sum_i^N e_i^2/N$

N is the vector length and e_i is the error caused by the predicted value of the i^{th} sample-the actual value.

According to this formula, the ideal number of hidden layer nodes was calculated to be between 4 and 14.

After a series of training simulations and tests, the optimal BP structure was determined to be 13-10-1. The other model parameters and equations are shown in Table 6.

4.2.2. Training of BP Neural Network Model. Considering the limited sample size, we used 10-fold cross-validation to train the BP network, obtaining the following 10 sets of test residential benchmark land price results (Figure 3).

The test error results of the ten groups are shown in Table 7.

From the previous results, it can be seen that there was a certain gap in the size of the MSE obtained by these 10 groups of experiments, but the overall error was within 2%, which is acceptable in practice. We randomly selected a group of data sets to evaluate the experimental results; the results are shown in Figure 4.

According to the above results, it can be seen that the model reached the best verification state at the 1^{st} epoch, where the mean square error was at the lowest value. Moreover, the regression analysis shows that the training data set, testing data set, and overall data set all showed a linear relationship between the values, with a correlation coefficient close to 1, as shown in Figure 5.

4.2.3. Test of BP Neural Network Model. In order to make the test results more intuitive and easier to understand, the training output obtained by the model was denormalized to the predicted value of residential benchmark land price, as shown in Table 8. We compared the actual value with the predicted value, and the absolute error and relative error were given as well. The relative error is calculated as follows:

$$\varepsilon = \frac{|y - \hat{y}|}{y}, \tag{3}$$

where y is the actual benchmark land price, $\hat{y}$ is the forecast benchmark land price, and ε is the relative error. The result of the error analysis is shown in Table 9.

According to the obtained results, it can be seen that the error of the model itself was relatively small, further reflecting the applicability of the framework. It proves that, in addition to real estate [24], the automatic evaluation can also be used in land evaluation [8, 22, 23, 53] as well. Moreover, from the results, the validity of the five dimensions of impact factors on residential land price is consistent with the previous practice results of the valuation industry.

4.3. Results Analysis. Using GIS, the error comparison data were reflected in the form of a heat map, as shown in Figure 6

Figure 6(a) illustrates that Wuhan's benchmark land prices showed a trend of gradual decreasing from the central city to its surroundings, consistent with the distribution of land prices in most Chinese cities. Among the surrounding urban areas, it is worth noting that the prices in the Huangpi and Xinzhou districts (in the northeast) were higher than

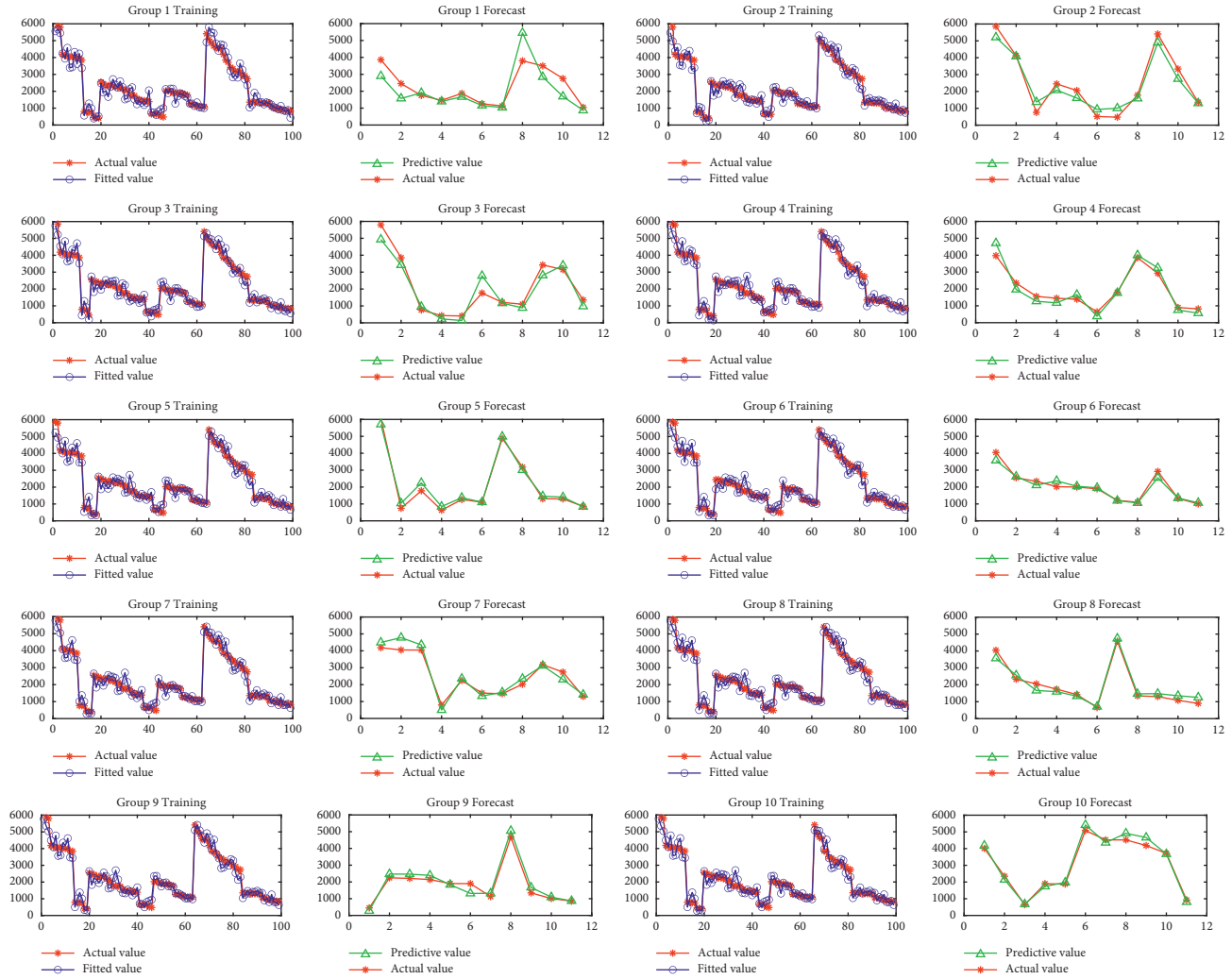

Figure 3: Ten-fold cross-validation results.

Table 7: MSE (mean square error) of ten groups.

Group	Group 1	Group 2	Group 3	Group 4	Group 5	Group 6	Group 7	Group 8	Group 9	Group 10
MSE	0.0186	0.013624	0.013539	0.0038203	0.01039	0.0055963	0.014904	0.011278	0.007668	0.01005

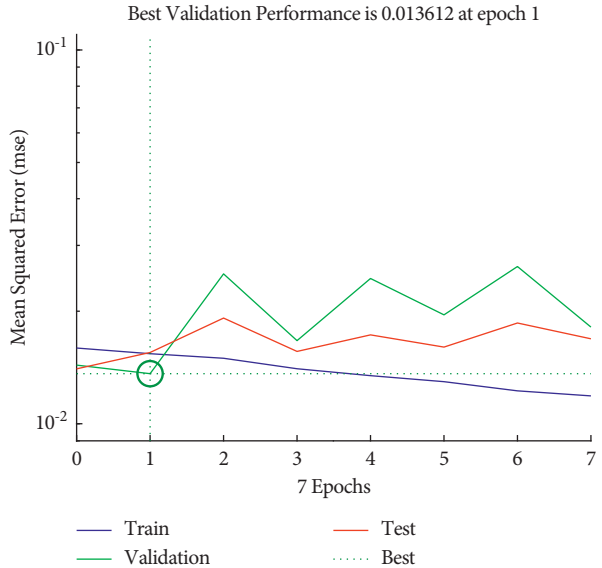

Figure 4: Model iteration curve.

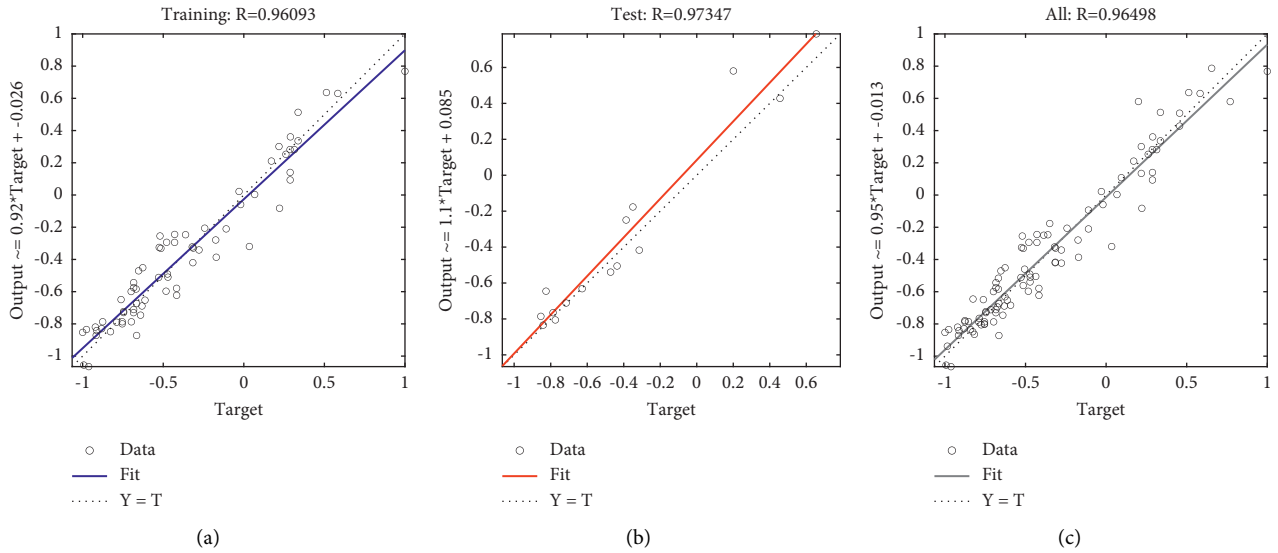

Figure 5: Dynamic changes of the metrics: (a) training set, (b) test set, and (c) all data sets.

Table 8: Training value and error analysis of benchmark land price.

ID	Actual price	Predict price	Absolute error	Relative error (%)
1	11270	10999.46462	270.5353781	2.40
2	10575	10659.02123	84.02122615	0.79
3	9860	8826.97559	1033.02441	10.48
4	6894	7187.927573	293.9275729	4.26
5	6522	7401.075705	879.075705	13.48
6	6487	7234.729173	747.729173	11.53
7	7037	6535.341643	501.658357	7.13
8	6659	7747.381349	1088.381349	16.34
9	6306	5906.933983	399.0660173	6.33
10	6732	6434.807979	297.1920212	4.41
11	6845	5251.461686	1593.538314	23.28
12	6725	5674.98795	1050.01205	15.61
13	1895	1661.540296	233.4597037	12.32
14	1895	2283.207164	388.2071638	20.49
15	1895	2670.394473	775.3944734	40.92
16	1895	1908.185993	13.1859925	0.70
17	1835	1934.873953	99.8739528	5.44
18	1835	1805.847641	29.15235895	1.59
19	1835	2855.693002	1020.693002	55.62
20	3919	4632.610073	713.610073	18.21
21	5187	3953.243253	1233.756747	23.79
22	5187	4556.753877	630.2461229	12.15
23	4069	3953.086687	115.9133129	2.85
24	4025	4598.903646	573.9036462	14.26
25	4025	3475.743022	549.2569775	13.65
26	4699	4949.017147	250.0171472	5.32
27	4515	4217.909246	297.0907538	6.58
28	4025	4361.910531	336.910531	8.37
29	3815	3931.892256	116.8922562	3.06
30	4463	3607.50109	855.4989099	19.17
31	3520	4055.871363	535.8713631	15.22
32	3415	4836.723094	1421.723094	41.63
33	3415	4104.835694	689.8356941	20.20
34	3415	3345.341087	69.65891264	2.04
36	3212	2956.042133	255.9578668	7.97
37	3160	3562.980096	402.9800956	12.75

Table 8: Continued.

ID	Actual price	Predict price	Absolute error	Relative error (%)
38	3160	2629.756478	530.2435215	16.78
39	3031	2332.130699	698.8693008	23.06
40	3031	2275.117362	755.8826377	24.94
41	3020	3297.434768	277.4347683	9.19
42	1835	2039.899685	204.8996846	11.17
43	1835	2265.600497	430.6004969	23.47
44	1835	2145.251377	310.2513772	16.91
45	1835	1750.940692	84.05930814	4.58
46	1835	1715.068536	119.9314645	6.54
47	1835	2009.052246	174.052246	9.49
48	3919	4717.376442	798.3764421	20.37
49	3919	3936.573752	17.57375157	0.45
50	3878	4018.82728	140.8272798	3.63
51	3878	4527.441176	649.4411755	16.75
52	3878	3351.890981	526.1090188	13.57
53	3878	4077.416773	199.4167731	5.14
54	3720	3876.882547	156.882547	4.22
55	3720	3440.412065	279.587935	7.52
56	3738	4000.18481	262.1848097	7.01
57	2560	2133.729179	426.2708206	16.65
58	2560	1420.83742	1139.16258	44.50
59	2432	2360.789	71.2109995	2.93
60	2432	2182.210975	249.789025	10.27
61	2314	2399.249307	85.24930743	3.68
62	2287	2195.412277	91.5877227	4.00
63	2287	2077.668831	209.3311689	9.15
64	2287	2118.524751	168.475249	7.37
65	8223	8289.125271	66.12527122	0.80
66	8196	8811.482363	615.4823632	7.51
67	8346	8875.026878	529.0268777	6.34
68	8429	6519.027601	1909.972399	22.66
69	8429	7357.134108	1071.865892	12.72
70	6894	8249.076233	1355.076233	19.66
71	6725	7561.213903	836.2139027	12.43
72	6725	7638.856438	913.8564382	13.59
73	5899	5864.577641	34.42235919	0.58
74	5730	5774.474114	44.47411434	0.78
75	5000	5044.700066	44.70006623	0.89
76	5000	4685.049398	314.9506024	6.30
77	5153	5721.648844	568.6488439	11.04
78	5187	5610.268719	423.2687185	8.16
79	5187	4225.477747	961.5222526	18.54
80	4289	3399.523071	889.4769294	20.74
81	4289	4000.231472	288.768528	6.73
82	3020	2155.479456	864.5205444	28.63
83	3020	2671.458994	348.541006	11.54
84	2945	3029.856262	84.8562621	2.88
85	2945	2858.285059	86.71494149	2.94
86	2880	2405.414772	474.585228	16.48
87	2880	2812.938556	67.06144369	2.33
88	2880	2970.800195	90.80019471	3.15
89	2880	2498.657799	381.3422013	13.24
90	2287	2946.780872	659.7808721	28.85
91	2170	1862.63273	307.3672698	14.16
92	2170	2242.295835	72.29583527	3.33
93	2170	2571.335509	401.3355094	18.49
94	1895	2366.274084	471.2740842	24.87
95	1895	2828.802786	933.8027861	49.28
96	1895	1997.013051	102.0130515	5.38

Table 8: Continued.

ID	Actual price	Predict price	Absolute error	Relative error (%)
97	1895	1751.015159	143.984841	7.60
98	1895	1975.518443	80.51844309	4.25
99	1895	1671.076755	223.9232445	11.82
100	7037	5139.590024	1897.409976	26.96
101	4654	3993.050653	660.949347	14.20
102	4463	3198.501774	1264.498226	28.33
103	3720	4700.273197	980.2731969	26.35
104	3520	3110.062106	409.9378942	11.65
105	2314	2125.805912	188.1940884	8.13
106	9052	9357.966337	305.9663367	3.38
107	7878	9116.477395	1238.477395	15.72
108	5622	5651.900916	29.900916	0.53
109	5309	4895.078181	413.9218192	7.80
110	2890	2453.368521	436.6314791	15.11

Table 9: Error analysis.

Error	Value
Relative average absolute error (RAAE)	0.13
Root means absolute error (RMAE)	22.133
Coefficient of determination (R^2)	0.913
Standard deviation ratio (RSR)	416.002
Nash–Sutcliffe coefficient (NS)	0.915
Root means squared error (RMSE)	642.659
Mean absolute percentage error (MAPE)	12.665

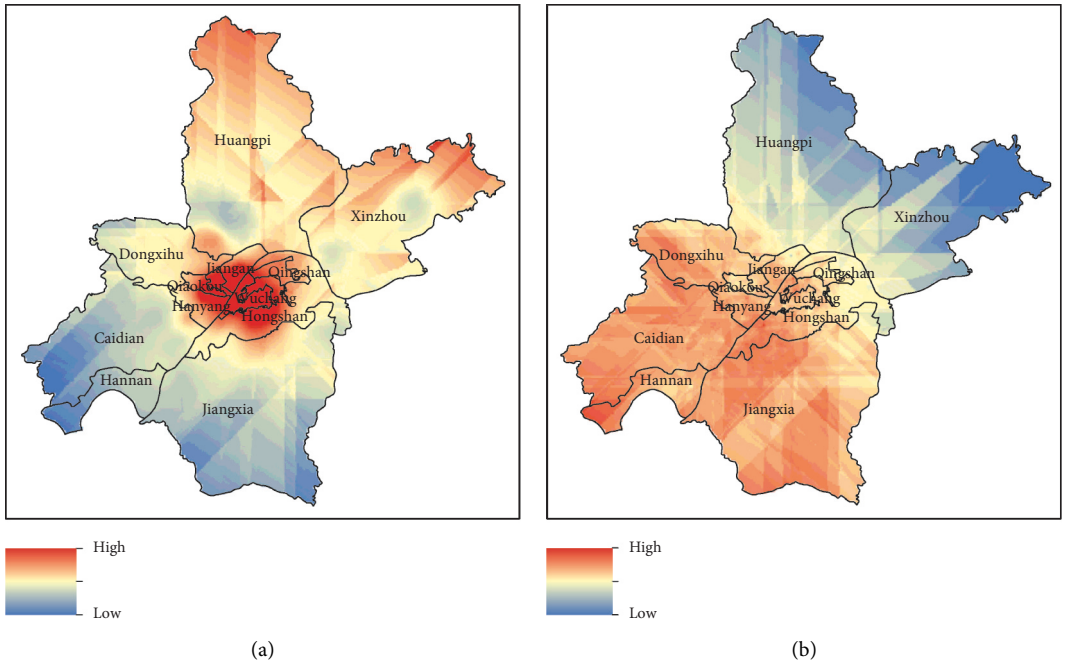

Figure 6: Actual land price and relative error heat map: (a) actual land price and (b) relative error.

those of the Caidian and Hannan districts (in the southwest). This is mainly because there are more natural scenic spots in the Huangpi district than in the southwest urban districts, and an important part of the nationally planned Wuhan Yangtze River Economic Belt, The Yangtze River New City, is located at the junction of Huangpi and Xinzhou districts. These factors have promoted an increase in land prices. In Figure 6(b), it can be seen that, although the predicted value

has a good fit with the actual benchmark land price, there were still some deviations in some regions. The deviations indicate that the price in the northeast was overestimated and the price in the southwest was underestimated. The sensitivity of the model to environmental and economic factors caused the price of the urban area in the northeast to be overestimated. The urban area in the southwest is a national automobile industry base, and the related employed population has a high demand for housing. The impact mechanism of the industrial base on local land prices was not fully reflected in the model. However, these factors have strong localization features. Under the premise of ensuring the universality of the framework, these factors can be added separately when conducting the valuation for specific cities.

Overall, the main reasons for the deviations between the predicted value and the actual value of the benchmark land price were as follows: (1) when quantifying the impact factors of residential benchmark land price, some factors used an index scoring method, which affected the accuracy of the valuation. (2) The heterogeneity of certain factors was ignored. For example, when considering the impact of the school district, only the distance to the nearest primary and middle schools was selected as the main consideration. However, school rankings have a more obvious impact on land prices, which was ignored in the model. (3) The analysis of macrofactors was not very comprehensive; for example, the impact of some government regional support policies was not considered in depth.

5. Conclusion

As one of the main means of the Chinese government's macrocontrol of land demand, the benchmark land price needs to be adjusted, in a timely manner, along with economic development. The traditional benchmark land price valuation process has the drawback of being subjective and unable to process large amounts of data. In recent years, the development and application of the GIS technology has provided a basis for the collection and real-time update of large-scale geographic data. Therefore, in this paper, we propose an automated valuation framework based on GIS data and neural networks. This framework automatically extracts spatial data which affects land prices through the GIS database, thus reducing data distortion. Using an impact factor valuation system to avoid the incommensurability of the data, we finally designed an automated valuation model based on the BP neural network model, effectively reducing the subjectivity and uncertainty of the valuation.

In the case study, in which we took Wuhan as an example, we found that although there were still some errors in the model training and testing results, they generally met the accuracy requirements. It can be seen that the BP neural network had good performance in automated valuation. The model can also be applied to the prediction of residential benchmark land prices outside Wuhan. If there are a few factors that affect the benchmark land price significantly, the model can be further adjusted. As data continue to accumulate, the fitness of the BP neural network can be further improved. This is of great practical significance for regulating the order of the Chinese land market, formulating relevant land management laws and allowing the public to more conveniently receive land transaction information.

Due to the project schedule requirements, the number of samples data provided by the collaborator is not large, and the effectiveness of the proposed framework needs to be further verified with a larger data set in the future work. In addition, except for the spatial data obtained from the GIS, more data require manual collection. The way to introduce data mining and web crawling technology to improve the automation of the proposed framework is also a focus of future work.

Data Availability

The data are available on request to the corresponding author after the paper is published.

Conflicts of Interest

The authors declare that they have no conflicts of interest.

Acknowledgments

This work was supported by the major projects of National Social Science Foundation of China Study and explains the spirit of the Fifth Plenary Session of the 19th CPC Central Committee (under grant no. 21ZDA028), the MOE (Ministry of Education in China) Project of Humanities and Social Sciences (under grant no. 21YJA630094), and Teaching and Research Project of Zhongnan University of Economics and Law in 2018 (under grant no. YB2018019).

References

[1] L. H. Li and A. Walker, "Benchmark pricing behaviour of land in China's reforms," *Journal of Property Research*, vol. 13, no. 3, pp. 183–196, 1996.

[2] C. r. Ding, "The benchmark land price system and urban land use efficiency in China," *Chinese Geographical Science*, vol. 11, no. 4, pp. 306–314, 2001.

[3] S. P. Chen, D. C. Zhuang, and H. X. Zhang, "Gis-based spatial autocorrelation analysis of housing prices oriented towards a view of spatiotemporal homogeneity and nonstationarity: a case study of Guangzhou, china," *Complexity*, vol. 2020, Article ID 1079024, 16 pages, 2020.

[4] Z. Xu and Q. Li, "Integrating the empirical models of benchmark land price and gis technology for sustainability analysis of urban residential development," *Habitat International*, vol. 44, pp. 79–92, 2014.

[5] R. Wang, "The structure of Chinese urban land prices: estimates from benchmark land price data," *The Journal of Real Estate Finance and Economics*, vol. 39, no. 1, pp. 24–38, 2009.

[6] R. De Groot, "Function-analysis and valuation as a tool to assess land use conflicts in planning for sustainable, multi-functional landscapes," *Landscape and Urban Planning*, vol. 75, no. 3-4, pp. 175–186, 2006.

[7] M. A. Davis and J. Heathcote, "The price and quantity of residential land in the United States," *SSRN Electronic Journal*, vol. 54, no. 8, pp. 2595–2620, 2007.

[8] D. Demetriou, "A spatially based artificial neural network mass valuation model for land consolidation," *Environment*

and Planning B: Urban Analytics and City Science, vol. 44, no. 5, pp. 864–883, 2017.

[9] S. Yang, S. Hu, W. Li, C. Zhang, and J. E. A. Torres, "Spatiotemporal effects of main impact factors on residential land price in major cities of China," *Sustainability*, vol. 9, no. 11, p. 2050, 2017.

[10] J. Burian, K. Macku, J. Zimmermannova, and B. Kocvarova, "Spatio-temporal changes and dependencies of land prices: a case study of the city of olomouc," *Sustainability*, vol. 10, no. 12, p. 4831, 2018.

[11] B. Glumac, M. Herrera-Gomez, and J. Licheron, "A hedonic urban land price index," *Land Use Policy*, vol. 81, pp. 802–812, 2019.

[12] C. Li, Y. Meng, Y. Li, J. Ge, and C. Zhao, "Inter-metropolitan land-price characteristics and patterns in the beijing-tianjin-hebei urban agglomeration in China," *Sustainability*, vol. 11, no. 17, p. 4726.

[13] F. Yuan, Y. D. Wei, and W. Xiao, "Land marketization, fiscal decentralization, and the dynamics of urban land prices in transitional China," *Land Use Policy*, vol. 89, Article ID 104208, 2019.

[14] H. Nakamura, "Relationship among land price, entrepreneurship, the environment, economics, and social factors in the value assessment of Japanese cities," *Journal of Cleaner Production*, vol. 217, no. 1, pp. 144–152, 2019.

[15] R. Tan, Q. He, K. Zhou, and P. Xie, "The effect of new metro stations on local land use and housing prices: the case of wuhan, China," *Journal of Transport Geography*, vol. 79, no. 1, Article ID 102488, 2019.

[16] T. Gu, M. Nakagawa, M. Saito, and H. Yamaga, "Public perceptions of earthquake risk and the impact on land pricing: the case of the uemachi fault line in Japan," *The Japanese Economic Review*, vol. 69, no. 4, pp. 374–393, 2018.

[17] J. Batog, I. Forys, R. Gaca, M. Gluszak, and J. Konowalczuk, "Investigating the impact of airport noise and land use restrictions on house prices: evidence from selected regional airports in Poland," *Sustainability*, vol. 11, no. 2, p. 412, 2019.

[18] B. J. L. Berry and R. S. Bednarz, "A hedonic model of prices and assessments for single-family homes: does the assessor follow the market or the market follow the assessor?" *Land Economics*, vol. 51, no. 1, pp. 21–40, 1975.

[19] R. K. Pace and O. W. Gilley, "Estimation employing a priori information within mass appraisal and hedonic pricing models," *The Journal of Real Estate Finance and Economics*, vol. 3, no. 1, pp. 55–72, 1990.

[20] I. A. O. A. Officers, *Standard on Automated Valuation Models (AVMs)*, International Association of Assessing Officers, Kansas City, MO, USA, 2003.

[21] P. Aragonés-Beltrán, J. Aznar, J. Ferrís-Oñate, and M. García-Melón, "Valuation of urban industrial land: an analytic network process approach," *European Journal of Operational Research*, vol. 185, no. 1, pp. 322–339, 2008.

[22] S. Metzner and A. Kindt, "Determination of the parameters of automated valuation models for the hedonic property valuation of residential properties," *International Journal of Housing Markets and Analysis*, vol. 11, no. 1, pp. 73–100, 2018.

[23] D. Demetriou, "Automating the land valuation process carried out in land consolidation schemes," *Land Use Policy*, vol. 75, pp. 21–32, 2018.

[24] M. Renigier-Biłozor, A. Janowski, and M. d'Amato, "Automated valuation model based on fuzzy and rough set theory for real estate market with insufficient source data," *Land Use Policy*, vol. 87, Article ID 104021, 2019.

[25] J. C. Bencure, N. K. Tripathi, H. Miyazaki, S. Ninsawat, and S. M. Kim, "Development of an innovative land valuation model (ilvm) for mass appraisal application in sub-urban areas using ahp: an integration of theoretical and practical approaches," *Sustainability*, vol. 11, no. 13, p. 3731, 2019.

[26] D. Barman, N. Chowdhury, and R. K. Singha, "To predict possible profit/loss of a movie to be launched using mlp with back-propagation learning," in *Proceedings of the 2012 International Conference on Communications, Devices and Intelligent Systems (CODIS), 2012 International Conference on Communications, Devices and Intelligent Systems (CODIS)*, pp. 322–325, Kolkata, India, December 2012.

[27] Q. Cao, K. B. Leggio, and M. J. Schniederjans, "A comparison between fama and French's model and artificial neural networks in predicting the Chinese stock market," *Computers & Operations Research*, vol. 32, no. 10, pp. 2499–2512, 2005.

[28] S. S. Roy, R. Chopra, K. C. Lee, C. Spampinato, and B. M. ivatlood, "Random forest, gradient boosted machines and deep neural network for stock price forecasting: a comparative analysis on south Korean companies," *International Journal of Ad Hoc and Ubiquitous Computing*, vol. 33, no. 1, pp. 62–71, 2020.

[29] A. Bose, C. H. Hsu, S. S. Roy, K. C. Lee, B. Mohammadi-ivatloo, and S. Abimannan, "Forecasting stock price by hybrid model of cascading multivariate adaptive regression splines and deep neural network," *Computers & Electrical Engineering*, vol. 95, Article ID 107405, 2021.

[30] M. Aubry, R. Kräussl, G. Manso, and C. Spaenjers, "Machine learning, human experts, and the valuation of real assets," *Tech. Rep., CFS Working Paper Series*, , 2019.

[31] R. B. Abidoye and A. P. C. Chan, "Valuers' receptiveness to the application of artificial intelligence in property valuation," *Pacific Rim Property Research Journal*, vol. 23, no. 2, pp. 175–193, 2017.

[32] C. Chun Lin and S. B. Mohan, "Effectiveness comparison of the residential property mass appraisal methodologies in the USA," *International Journal of Housing Markets and Analysis*, vol. 4, no. 3, pp. 224–243, 2011.

[33] S. Peterson and A. Flanagan, "Neural network hedonic pricing models in mass real estate appraisal," *Journal of Real Estate Research*, vol. 31, no. 2, pp. 147–164, 2009.

[34] J. Zurada, A. Levitan, and J. Guan, "A comparison of regression and artificial intelligence methods in a mass appraisal context," *Journal of Real Estate Research*, vol. 33, no. 3, pp. 349–388, 2011.

[35] G. Spellman, "An application of artificial neural networks to the prediction of surface ozone concentrations in the United Kingdom," *Applied Geography*, vol. 19, no. 2, pp. 123–136, 1999.

[36] W. J. McCluskey, M. McCord, P. T. Davis, M. Haran, and D. McIlhatton, "Prediction accuracy in mass appraisal: a comparison of modern approaches," *Journal of Property Research*, vol. 30, no. 4, pp. 239–265, 2013.

[37] J. Bin, S. Tang, Y. Liu et al., "Regression model for appraisal of real estate using recurrent neural network and boosting tree," in *Proceedings of the 2017 2nd IEEE International Conference on Computational Intelligence and Applications (ICCIA)*, pp. 209–213, Beijing, China, September 2017.

[38] O. Poursaeed, T. A. V. S. Matera, and S. Belongie, "Vision-based real estate price estimation," *Machine Vision and Applications*, vol. 29, no. 4, pp. 667–676, 2018.

[39] A. Prinzie and D. Van den Poel, "Random forests for multiclass classification: random multinomial logit," *Expert Systems with Applications*, vol. 34, no. 3, pp. 1721–1732, 2008.

[40] E. A. Antipov and E. B. Pokryshevskaya, "Mass appraisal of residential apartments: an application of random forest for valuation and a cart-based approach for model diagnostics," *Expert Systems with Applications*, vol. 39, no. 2, pp. 1772–1778, 2012.

[41] H. Kuşan, O. Aytekin, and İ. Özdemir, "The use of fuzzy logic in predicting house selling price," *Expert Systems with Applications*, vol. 37, no. 3, pp. 1808–1813, 2010.

[42] S. Amri and G. A. Tularam, "Performance of multiple linear regression and nonlinear neural networks and fuzzy logic techniques in modelling house prices," *Journal of Mathematics and Statistics*, vol. 8, no. 4, pp. 419–434, 2012.

[43] J. J. Ahn, H. W. Byun, K. J. Oh, and T. Y. Kim, "Using ridge regression with genetic algorithm to enhance real estate appraisal forecasting," *Expert Systems with Applications*, vol. 39, no. 9, pp. 8369–8379, 2012.

[44] S. Teng, L. Hay Lee, and E. Peng Chew, "Multi-objective ordinal optimization for simulation optimization problems," *Automatica*, vol. 43, no. 11, pp. 1884–1895, 2007.

[45] G. Kou, H. Xiao, M. H. Cao, and L. H. Lee, "Optimal computing budget allocation for the vector evaluated genetic algorithm in multi-objective simulation optimization," *Automatica*, vol. 129, Article ID 109599, 2021.

[46] P. Samui, S. S. Roy, and V. E. Balas, *Handbook of Neural Computation*, Academic Press, Cambridge, Massachusetts, 2017.

[47] J. Cheng, "Data analysis of the factors influencing the industrial land leasing in shanghai based on mathematical models," *Mathematical Problems in Engineering*, pp. 1–11, 2020.

[48] M. Al-Omari, "The Role of Reliable Land Valuations in Land Management and Land Administration Systems efficiency," in *Proceedings of the FIG Working Week*, Stockholm, Sweden, June 2008.

[49] P. Dale and J. McLaughlin, *Land Administration*, Oxford University Press, Oxford, UK, 2003.

[50] R. B. Hammer, S. I. Stewart, R. L. Winkler, V. C. Radeloff, and P. R. Voss, "Characterizing dynamic spatial and temporal residential density patterns from 1940–1990 across the north central United States," *Landscape and Urban Planning*, vol. 69, no. 2-3, pp. 183–199, 2004.

[51] Z. Xu and V. Coors, "Combining system dynamics model, gis and 3d visualization in sustainability assessment of urban residential development," *Building and Environment*, vol. 47, no. 1, pp. 272–287, 2012.

[52] E. Bahadır, "Prediction of prospective mathematics teachers' academic success in entering graduate education by using back-propagation neural network," *Journal of Education and Training Studies*, vol. 4, no. 5, pp. 113–122, 2016.

[53] D. Demetriou, "The assessment of land valuation in land consolidation schemes: the need for a new land valuation framework," *Land Use Policy*, vol. 54, pp. 487–498, 2016.

Hindawi
Complexity
Volume 2022, Article ID 5381208, 10 pages
https://doi.org/10.1155/2022/5381208

Research Article

Credit Index Screening Model of Family Farms and Family Ranches Based on Fuzzy Bayesian Theory of Depth Weighting

Zhanjiang Li and Qinjin Zhang

College of Economics and Management, Inner Mongolia Agricultural University, Hohhot, China

Correspondence should be addressed to Zhanjiang Li; lizhanjiang582@163.com

Received 20 January 2022; Revised 26 February 2022; Accepted 21 March 2022; Published 26 April 2022

Academic Editor: Hui Xiao

The construction of credit evaluation index system of Chinese family farm and pasture is not only a theoretical problem but also of great practical significance. In this paper, based on the depth-weighted Bayesian theory and fuzzy mathematics, the improved depth-weighted fuzzy Bayesian hybrid algorithm model is proposed to solve the unbalanced problem of default status of family farm and pasture and to build the index system with the ability of three categories of default identification. In this paper, the characteristics of the first one is based on fuzzy set theory, the definition of fuzzy linguistic assessment of different default set, family ranches characteristic is converted to the corresponding index of pasting with triangular fuzzy mathematical model, and then through the inner method converting triangular fuzzy number into accurate output data to deal with the blur and uncertainty about the state of the fuzzy default transformation is realized. Second, based on the insensitive characteristic of ROC curve to skewness samples, the depth weighting of characteristic indexes in nondefault, low default and high-default states was completed by constructing multiclassification ROC curve, which solved the practical problem of sample imbalance in different default states of family farms and ranches, and selected the index system with significant discrimination ability for default states by integrating default identification ability.

1. Introduction

China is a big agricultural country, and agriculture is the basic industry of our country. According to statistics, as of 2020, the number of family farms and family ranches registered in the national directory system exceeded 3 million, and 117,000 demonstration family farms and family ranches at or above the county level were established. As an important part of the new type of agricultural management, family farms and family ranches has become the main force to promote the development of modern agriculture and an indispensable force in the process of agricultural modernization. However, the difficulty in financing is the main problem that has always troubled the sustainable development of family farms and family ranches. The development of family farms and family ranches cannot be separated from the support of the financial system, so the construction of a scientific and reasonable credit evaluation index system plays a fundamental role in solving this problem. If the credit index system is not properly selected, no matter what evaluation method is adopted, accurate credit evaluation results cannot be obtained. Therefore, the construction of credit evaluation index system plays a fundamental role in solving this problem. Therefore, the construction of credit evaluation index system for family's farms and ranches is not only a theoretical problem but also of great practical significance. However, due to some problems existing in our family's farms and ranches and the information asymmetry between commercial banks and financial institutions, a credit index system that matches the operating characteristics of family's farms and ranches has not been established. As a result, most of the existing credit evaluation indexes of family's farms and ranches are based on the index system of companies and enterprises, and there is no system suitable for the credit evaluation standard of family's farms and ranches. Therefore, there are some problems in the evaluation process, such as the index cannot be determined and the index division is vague. How to establish an effective credit index system for family's farms and ranches is an important problem that needs to be solved urgently.

2. Research status of family farm and pasture credit index screening model

2.1. Method-Based Index Screening

2.1.1. A Credit Index Screening Model Based on Mathematical Statistics. Zhou and Su [1] selected the index combination by invading the neighborhood component analysis in the credit risk field, and extrapolated the optimal index combination based on the maximum AUC of default prediction accuracy [1]. Yan et al. [2] screened out the indicators that can significantly distinguish loss given default through the nonparametric *K*-nearest neighbor discriminant method, making up for the shortage of the traditional research that only focuses on the indicators that can significantly distinguish the default status, and they used R-clustering to sort by criteria categories, ensuring that the indicators clustered in one category have the same economic meaning and data characteristics [2]. Traczynski [3] uses the average method of Bayesian model to select default forecast indicators, and proposes that only the ratio of total liabilities to total assets and the volatility of market returns are reliable default forecast indicators in the overall sample and individual industry groups [3]. Dahiya et al. [4] used two feature selection methods, chi-square test and principal component analysis, to screen important features, and proposed a hybrid bagging algorithm (FS-HB) based on feature selection, which improved the credit risk assessment method [4].

2.1.2. A Credit Index Screening Model Based on Artificial Intelligence. Zhou et al. [5] processed the German credit samples through the XGBoost algorithm, screened the credit indicators according to the importance obtained, and then analyzed the credit indicators and classification characteristics of the samples based on the random forest classification [5]. Wang et al. [6] selected 10 features which affect the credit risk of small and medium-sized enterprises from the 53 original features by single norm kernel feature selection, and proposed that the mortgage and pledge status is the most important factor that affects credit risk [6]. Bai et al. [7] studied the characteristics affecting farmers' creditworthiness through fuzzy rough sets and fuzzy C-means clustering method. The results show that the characteristics related to education and skills can have a significant impact on farmers' creditworthiness [7]. Li AND Yang [8] used SVM model to conduct the first round of index screening, and conducted the second round of index screening based on the principle of minimum square sum of deviation of cluster variables, and finally constructed a relatively effective credit evaluation index system [8].

2.1.3. Credit Index Screening Model Based on Other Methods. Kou et al. [9] proposed a new allocation rule combined with VEGE to solve the multiobjective decision optimization problem [9]. Fallahpour et al. [10] used sequential floating forward selection algorithm as a wrapper technique to determine the optimal subset of features to ensure that the selected index combination has strong default identification capability [10]. Based on information theory, Hu et al. [11] proposed a feature selection method of dynamic association and joint mutual information maximization (DRJMIM) to screen the feature with the largest amount of information. The comparison results of five competitive feature selection methods show that the method obtains the highest classification accuracy while selecting a small number of features [11]. Hai et al. [12] deleted the indicators of information redundancy through correlation analysis, and then used significance discrimination to screen out indicators that can significantly distinguish farmers' default status [12]. Nikolic et al. [13] obtained all possible combinations of model indicators by running the logistic regression model step-by-step forward or backward through the indicators, and selected the model with the highest predictive power and containing 8 financial ratios according to the GINI performance on the validation data set [13].

2.2. The Second Is the Study of Family Farm and Pasture Credit.

Ni and Zhang [14] divided China's new agricultural operation subjects into three types, namely family operation, cooperative operation and enterprise operation, according to the different characteristics of operation subjects. Based on the principles of comprehensiveness, systematicness and comprehensiveness, the credit evaluation index system is successively constructed around the above three business entities [14]. Shen and Lu [15] based on 5 *c* criterion system and the new type of agricultural management main body, marketization, specialization and scale moderation intensive characteristics, preliminary constructs the evaluation index, through partial correlation coefficient method and the Probit regression model, delete a significant sex difference of ability to identify, to ensure that the final build 18 indexes has significant identification ability and with the new default Consistent with credit characteristics of agricultural operating subjects [15]. When Basak [16] studied the financing difficulties of agricultural operators in Howla District of West Bengal, he revealed that the number of family population, bank deposits and the relationship between banks and farmers were important factors affecting the availability of loans [16].

There are three problems in the existing credit index screening model: first, although the previous credit index screening model can distinguish the credit status of default and nondefault of the sample, due to the fuzziness of the characteristics of high default and low default, it does not explain the characteristics of high default and low default of the sample, ignoring that high-default loss and low default loss are a kind of credit characteristics with different properties. Second, the existing credit index selection models are all based on the premise of sample balance. In reality, the default samples of family's farms and ranches are not balanced. The number of default samples is much smaller than the number of nondefault samples. How to solve the problem of sample imbalance is an extremely important problem faced by the existing credit index selection research. Third, most of the existing researches only focus on the qualitative research of family's farms and

ranches, but lack the quantitative analysis of the credit status of family's farms and ranches. As a result, the credit evaluation system of family's farms and ranches has no choice but to use the index system of companies and enterprises, which leads to the problems that the index cannot be determined and the index division is fuzzy in the evaluation process. Therefore, how to construct a credit index system with default judgment ability for family's farms and ranches is an important problem that needs to be solved urgently.

Aiming at the problems that emerge in the existing credit index screening model, this paper constructs a family farms and family ranches credit index screening model based on depth-weighted fuzzy Bayesian, and carries out empirical analysis on the data from the Inner Mongolia family farms and family ranches survey data, a commercial bank credit database, and the city statistical yearbook. From this, this paper finally puts forward a new improved depth-weighted fuzzy Bayesian algorithm for nonequilibrium samples, which can define and distinguish default states in different degrees, and improves the existing multicategory credit index screening model.

The article is organized as follows. Section 2 discusses the principle of building the family farming and pasture credit index screening model, Section 3 describes the method of building the family farming and pasture credit index screening model, Section 4 explains the specific process of building the family farming and pasture credit index screening model and tests the model, and Section 5 draws the conclusion and summarizes the innovation of the research.

3. Depth Weighted Fuzzy Bayesian Model Principle

3.1. The Difficulty of the Problem

Difficulty 1. How to solve the fuzziness problem corresponding to the default state caused by the fuzziness phenomenon and realize the deterministic transformation of multiclass uncertain variables.

Difficulty 2. Which method should be adopted to solve the unbalanced problem of default state of household farm samples?

3.2. The Method to Solve the Difficulty. The solution to the first difficulty is to standardize the sample data of family's farms and ranches, convert the uncertain variables into definite triangular fuzzy numbers based on fuzzy theory, and then and then converting the fuzzy numbers into precise data defuzzification by inner method, so as to realize the definite conversion of fuzzy default status, and calculate the prior probability and conditional probability to judge the sample category. The solution to the first difficulty is shown in Figure 1.

The solution to difficulty 2: based on the fact that the importance of the index characteristics of different family's farms and ranches is discrepant and the sensitivity curve is not sensitive to unbalanced data, the weights corresponding to different indexes are obtained through the analysis of experimental samples, the selection and weighting of the important index characteristics of family's farms and ranches are realized, and the problem of sample skewness of family's farms and ranches is solved. The solution to difficulty 2 is shown in Figure 2.

3.3. Credit Index Screening Model Construction Principle. The construction principle of fuzzy Bayesian family farms and family ranches credit index screening model based on depth weighting is shown in Figure 3.

4. Depth-Weighted Fuzzy Bayesian Model

4.1. Fuzzy Bayesian Model

4.1.1. Naive Bayes. Let's say: $P(C_j|X)$ is the posterior probability of family farms and family ranches X, the family farms and family ranches data set is $X = \{x_1, x_2, \ldots, x_k\}$, $p(x_1, x_2, \ldots, x_k|C_j)$ is the conditional probability, $P(C_j)$ is the prior probability, V is the total number of indicators, and $C(x)$ is the classification decision function.

$$\begin{cases} P(C_j|X) = \dfrac{P(\mathrm{x}_1, \mathrm{x}_2, ..., \mathrm{x}_k|C_j) \cdot P(C_j)}{P(\mathrm{x}_1, \mathrm{x}_2, ..., \mathrm{x}_k)}, \\ P(x_i, C_P) = \dfrac{\text{when category } C_p\text{, the number of family farms and pastures under index } x_j + 1}{\text{total number of family farms and ranches classified } C_p + |V|}, \\ P(C_P) = \dfrac{\text{total number of family farms and ranches classified } C_p}{\text{total number of family farms and ranches}}, \\ P(x_1, x_2, \ldots, x_k|c) = \prod_{i=1}^{k} P(x_i|c), \\ C(x) = \arg\max P(c) P(\mathrm{x}_1, x_2, \ldots, x_k|c). \end{cases} \tag{1}$$

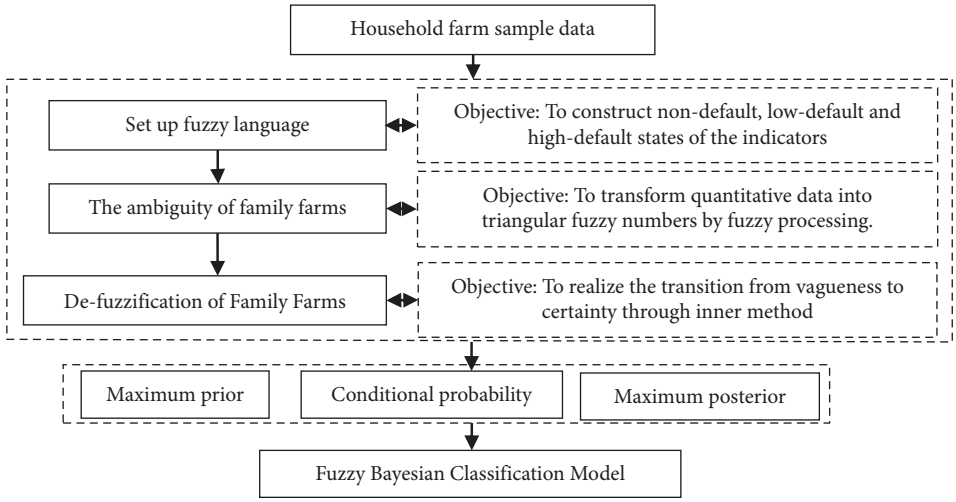

Figure 1: Principle for solving difficulty one.

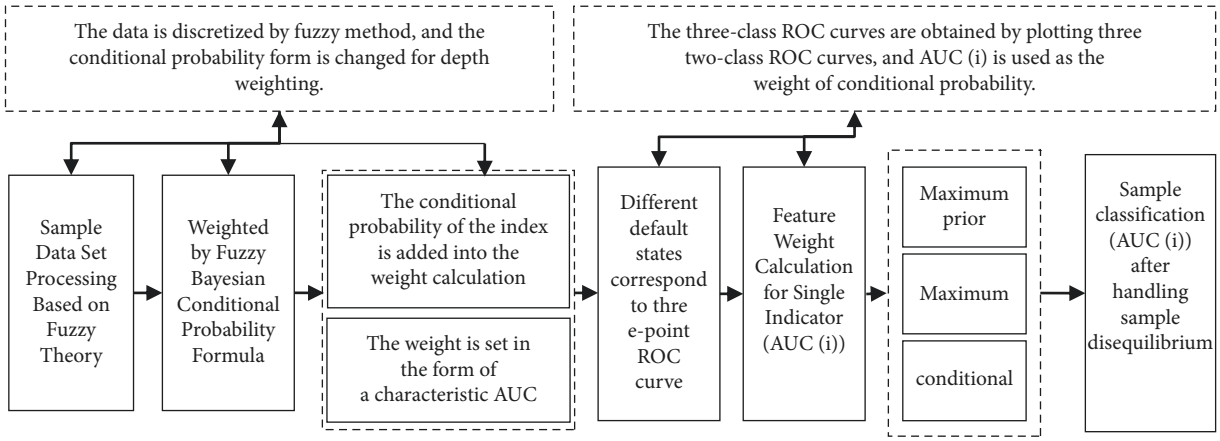

Figure 2: Principle for solving difficulty two.

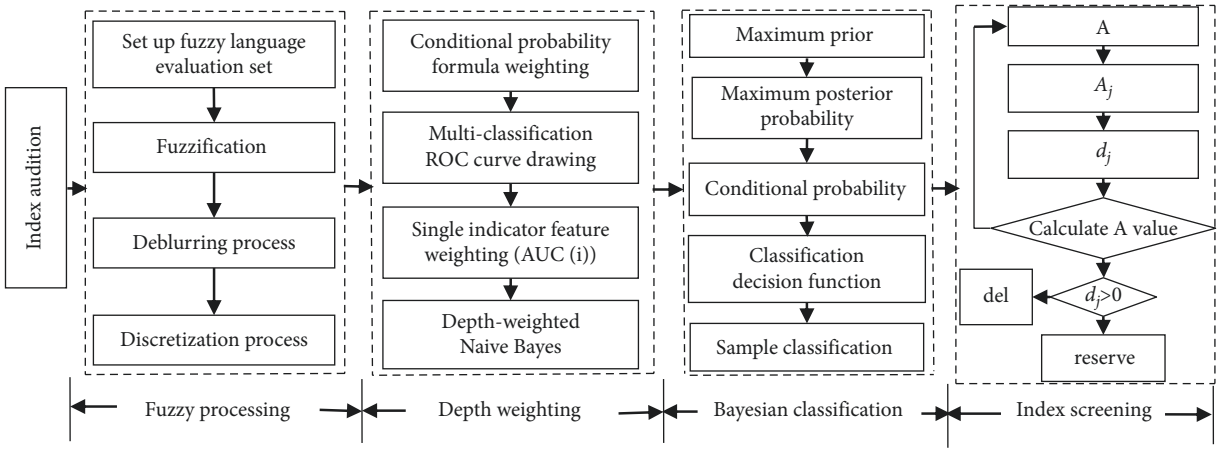

Figure 3: Technology roadmap.

The meaning of model (1): it represents the process of solving the classification of family farms and family ranches samples under classical conditions, and the classification results of family farms and family ranches based on Naive Bayes classifier without considering the fuzziness of variables and the sample disequilibrium problem.

4.1.2. The Fuzziness of Family's Farms and Ranches

Step 1. Triangular fuzzy numbers.

As a mathematical model representing the membership degree distribution of each sample attribute in the data set, triangle fuzzy number can be applied to credit

evaluation to reflect the uncertainty and fuzziness of default risk. It is a simple and efficient mathematical method that can be used to explain fuzzy phenomenon and describe fuzzy set.

Let us say $v = (v_1, v_2, v_3)$ is a triangular fuzzy number, v_1 is the lower line of the fuzzy number, v_2 is the most probable value, v_3 is the upper line of the triangular fuzzy number, and $\mu(x)$ is the corresponding membership function.

$$\mu(x) = \begin{cases} \dfrac{x - v_1}{m - v_1}, & x \in [v_1, v_2], \\ \dfrac{x - v_3}{m - v_3}, & x \in [v_2, v_3], \\ 0, & x \in (-\infty, v_1 t \cup n[v_3, +\infty). \end{cases} \tag{2}$$

The meaning of formula (2): indicates the triangular fuzzy number and membership function corresponding to the sample data of the family farms and family ranches, which is used to realize the fuzzification process of the family farms and family ranches.

Step 2. Construction of fuzzy language evaluation set for default risk.

First, a language assessment system is established for the possibility of family farms and family ranches default. Due to the fuzziness of sample data in family farms and family ranches, a fuzzy language assessment set is set through fuzzy language assessment such as nondefault, low default, high-default, etc. The fuzzy assessment set of relevant attribute indicators: $A = \{\text{nondefault, low default, high-default}\}$, and the fuzzy language assessment set is converted into triangular fuzzy numbers for classification. The construction of fuzzy language assessment set and corresponding triangular fuzzy numbers is shown in Table 1.

4.1.3. The Family's Farms and Ranches Is Defuzzified. Let $v = (v_1, v_2, v_3)$ be a triangular fuzzy number, α, β, γ, be a parameter, I_x be a definite value corresponding to the fuzzy number, I_y be a corresponding membership degree, and the process of deblurring is as follows.

$$\begin{cases} \alpha = \sqrt{(v_3 - v_2)^2 + 1}, \\ \beta = v_3 - v_1, \\ \gamma = \sqrt{(v_2 - v_1)^2 + 1}, \\ I_x = \dfrac{v_1\alpha + v_2\beta + v_3\gamma}{\alpha + \beta + \gamma}, \\ I_y = \dfrac{\beta}{\alpha + \beta + \gamma}. \end{cases} \tag{3}$$

The meaning of model (3): the triangular fuzzy number defuzzification of uncertain variables in family's farms and ranches is converted into accurate variables, and the interval is divided to discretize the continuous variables, so as to classify the samples by using the naive Bayesian classifier and realize the deterministic transformation of fuzzy default state.

4.2. Depth-Weighted Bayesian Model. This paper uses the characteristic that the ROC curve is not sensitive to unbalanced data, constructs a multiclass average ROC curve based on the sample characteristics of nondefault, low default and high-default family's farms and ranches, and realizes the sample weighting of the index characteristics of family's farms and ranches based on AUC(i) [17–20].

Step 1: drawing of multiclassification ROC curve

Under each of the existing nondefault, low default and high-default categories, the probability that the required test sample is that category can be obtained. According to different categories, the false positive rate (FPR) and true positive rate (TPR) under each threshold are calculated to draw one ROC curve, so that a total of three ROC curves can be drawn. Finally, the three ROC curves are averaged to obtain the final ROC curve.

Step 2: depth-weighted Bayesian model

Let's say: $c(x)$ is the depth-weighted Bayesian classification decision function, $P_{W_i}(x_i|c_i)$ is the conditional probability, $n(x_i|c)$ is the number of x_i in class c, $n(c)$ is the number of all samples in class c, n_i is the number of different eigenvalues in the I-th feature index, and W_i is the depth-weighted weight of the I-th feature.

$$\begin{cases} c(x) = \arg\max P(c) \prod_{i=1}^{m} P_{W_i}(x_i|c_i)^{W_i}, \\ P_{W_i}(\mathrm{x}_i|c_i) = \dfrac{n(\mathrm{x}_i|c) + 1}{n(c) + n_i}, \\ W_i = \dfrac{1}{1 - \mathrm{AUC}(i)^2}. \end{cases} \tag{4}$$

The meaning of model (4): by weighting the indicators of the three types of family's farms and ranches under different default conditions and using the characteristic that the ROC curve is not sensitive to biased data, the problem of unbalanced family farms and family ranches samples is solved, and the classification of family farms and family ranches samples under unbalanced conditions is realized.

4.3. Index Screening

4.3.1. The Credit Index Identification Ability. Suppose: A-default judgment ability of all indicators (percentage of correct judgment for high-default family's farms and ranches, low-default family's farms and ranches and nondefault family's farms and ranches), which can be expressed as credit judgment ability of all selected indicators for

Table 1: Data discretization process.

Discretized node	Subinterval division	New corresponding attribute
0.195	[0,0.195]	U
0.728	(0.195,0.728]	V
0.872	(0.728,0.872]	W
1.000	(0.872,1.000]	X

family's farms and ranches; A_0 represents the percentage of all nondefault samples judged correctly; A_1 represents the percentage of all low default samples judged correctly; A_2 represents the percentage of all high-default samples judged correctly. The formula for the credit identification ability of all indicators is:

$$A = \frac{(A_0 + A_1 + A_2)}{3}. \tag{5}$$

The meaning of formula (5): it can be used to describe the credit appraisal ability of all indicators of audition under different default conditions for all samples of family's farms and ranches.

4.3.2. The Identification Ability after Deleting Item j. Set A_j-the default judgment ability of other indicators except the J-th indicator; A_0^j- Percentage of nondefault samples of other indicators other than the J-th indicator that are judged correctly; A_1^j-Indicates the percentage of low default samples for indicators other than the J-th indicator that are judged to be correct. The formula of credit identification ability after deleting item j is

$$A = \frac{\left(A_0^j + A_1^j + A_2^j\right)}{3}. \tag{6}$$

Meaning of formula (6): credit identification ability of all remaining indicators after deleting the j-th indicator.

4.3.3. The Influence of Credit Indicators. Set: d_j-the degree of impact of the J-th indicator on the credit evaluation results; A_j-the credit appraisal ability of the remaining indicators except for the j indicator to all family's farms and ranches; A-all indicators of credit worthiness for all household farms. The formula for the influence of the indicator is

$$d_j = A - A_j. \tag{7}$$

The use of formula (7): reflects the degree of influence of the J-th indicator on the credit evaluation results. If d_j is a real number greater than 0, indicating that the remaining indicators have weaker default identification ability after deleting the J-th indicator, then the indicator should be retained; otherwise, the indicator should be deleted.

5. Empirical Study

5.1. Indicator System and Sample Data. This paper selects 1814 household farm credit data from Inner Mongolia, China, and sets four criteria levels as shown in column (2) of Table 2. A total of 44 household farm credit evaluation indicators are obtained from the audition, among which 1,586 are nondefaulting household farms, 190 are low-defaulting household farms, 38 are high-defaulting household farms. Line 45 of Table 2 indicates the real credit default status of the household farm, of which 0 indicates that the household farm credit status is nondefault, 1 indicates that the household farm credit status is low default, and 2 indicates that the household farm is high-default. The sea election indicators are derived from literature [21, 22], and the sample data of family's farms and ranches are shown in Table 2.

5.2. Sample Fuzzification and Deblurring

5.2.1. Data Obfuscation. Due to the fuzziness of the family farms and family ranches data, the definitions of nondefault, low default and high-default are uncertain. Therefore, the set fuzzy language evaluation set is converted into triangular fuzzy numbers for sample classification. The fuzzy language evaluation set and triangular fuzzy number of family's farms and ranches are shown in Table 3.

5.2.2. Data Deobfuscation. The fuzzy language evaluation set and the corresponding triangular fuzzy numbers are deblurred by the inner method so as to obtain the corresponding accurate values and realize the transformation of the sample data from fuzzy to definite. The fuzzy data and corresponding accurate values of the household farm samples are shown in Table 1.

5.3. Depth Weighted Fuzzy Bayesian Classification

5.3.1. Calculation of AUC(i) for Three Categories. Based on the three-category problem of family farms and family ranches and pasture in this paper, the weight of the depth-weighted sample index is calculated by SPSS. According to the way of drawing the ROC curve in the two categories, one ROC curve is drawn for each category. Therefore, three ROC curves are drawn, and the average of the three ROC curves is taken to obtain the three-category ROC curve corresponding to the index in this paper. The ROC curve is shown in Figure 4, and the AUC(i) corresponding to each index is obtained as the weight value and applied to the calculation of conditional probability. The calculation results of the index AUC(i) are shown in Table 4, column (4).

5.3.2. Depth Weighted Fuzzy Bayesian Classification. The new attribute values obtained after the data fuzzification, deblurring and discretization of the family farms and family ranches samples are applied to the depth-weighted Naive

Table 2: Index system of household farming and pastoral land selection at sea.

(1) serial number	(2) The standard layer	(3) The index name	(4) Indicator type	(5) sample 1	...	(1818) sample 1814
1	Basic situation	Academic degree (X_{11})	Forward direction	0.200		0.400
...		...	...	...	...	...
11		House value ($X_{1.11}$)	Forward direction	0.130		0.000
12	Repayment ability	Skills of lenders and their families (X_{21})	Forward direction	0.500		0.000
...		...	...	...	...	...
24		Annual education expenses for the lender's children ($X_{2.13}$)	Forward direction	1.000		1.000
25	Willingness to repay	Living conditions (X_{31})	Forward direction	1.000		0.500
...		...	...	...	...	
38		Joint guarantee relationship ($X_{3.14}$)	Forward direction	1.000		0.500
39	Macro environment	Per capita net income of rural households (yuan) (X_{41})	Forward direction	0.089		0.205
...		...	...	...	...	
44		Engel coefficient (X_{46})	Negative direction	0.628		0.201
45	Credit status of family's farms and ranches			0	...	2

Table 3: Fuzzy language evaluation sets and corresponding indicators.

Language evaluation set	Triangular fuzzy number	Corresponding exact value	Grade of membership
Nondefault	(0.00,0.00,0.25)	0.195	0.195
Low default	(0.00,050,0.70)	0.728	0.239
High default	(0.70,1.00,1.00)	0.872	0.426

Bayes algorithm, and the categories of the family farms and family ranches test samples are obtained according to the maximum posterior rule by calculating the conditional probability and the prior probability of the model. The calculation results are shown in line 46 of Table 4.

5.4. Index Screening

5.4.1. All Indicators Credit Indicator Identification Ability. The classification result of the family farms and family ranches is obtained through the depth-weighted fuzzy Bayes. The result is shown in the 46 lines of Table 4. The calculation result is substituted into equation (5) to calculate the credit identification ability A of all the sea selection indicators for the family farms and family ranches, and the calculation result $A = 0.85$.

5.4.2. Identification Ability after Deleting Item j of the Index. All the index data after the deletion of the j index are subjected to a depth-weighted fuzzy Bayesian hybrid classifier to obtain three classification results, and the classification results are substituted into the formula (6) to obtain the credit identification ability A_j of all the indexes except the j index for the family farms and family ranches. The results of A_j calculation are shown in column (4) of Table 4.

5.4.3. Index Influence d_j Calculation. d_j is the difference between the credit identification ability of all indicators and the identification ability of all remaining indicators after deleting the j indicator, which is expressed as the impact ability of the j indicator on credit evaluation. If d_j is a real number greater than 0, indicating that the default identification ability of the remaining indicators after deleting the j indicator is weaker, then the indicator should be retained, otherwise, the indicator should be deleted. Substituting A and A_j calculated above into equation (7), the influence of each index is calculated. The calculation results of d_j are shown in column (5) of Table 4.

5.5. Construction of Credit Index System and Effectiveness Test. After fuzzy processing and index selection of household farm credit indicators, a credit index system of household

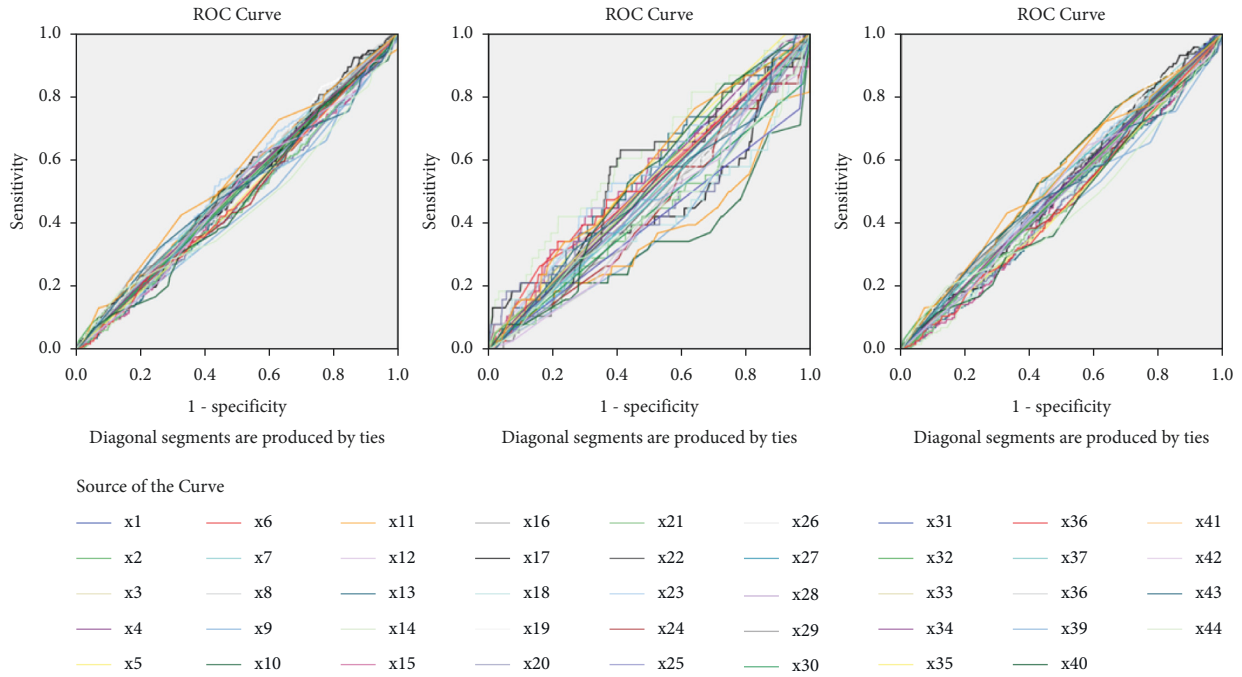

Figure 4: ROC curve of three classifications.

Table 4: Screening results of depth-weighted fuzzy Bayesian indicators.

(1) serial number	(2) The standard layer	(3) The index name	(4) AUC(i)	(5) sample 1	...	(1818) sample 1814	(1819) A_j	(1819) d_j	(1820) selection results
1	Basic situation	Academic degree (X_{11})	0.508	V		V	0.74	0.11	Reserve
...		...	...	...	...	...	...	...	...
11		House value ($X_{1.11}$)	0.477	U		U	0.73	0.12	Reserve
12	Repayment ability	Skills of lenders and their families (X_{21})	0.509	V		U	0.64	0.21	Reserve
...		...	...	...	...	...	...	...	...
24		Annual education expenses for the lender's children ($X_{2.13}$)	0.469	X		X	0.92	−0.07	Delete
25	Willingness to repay	Living conditions (X_{31})	0.466	X		V	0.87	−0.02	Delete
...		...	...	...	...	...	...	...	...
38		Joint guarantee relationship ($X_{3.14}$)	0.499	X		V	0.87	−0.02	Delete
39	Macro environment	Per capita net income of rural households (yuan) (X_{41})	0.472	U		V	0.87	−0.02	Delete
...		...	...	...	...	...	...	...	...
44		Engel coefficient (X_{46})	0.443	V		V	0.73	0.12	Reserve
45	Credit status of Family's farms and ranches			0	...	2	—	—	—
46	Fuzzy Bayesian classification of Family's farms and ranches			0	...	2	—	—	—

farm credit with 16 credit indicators was finally constructed, as shown in Table 5, column (3).

Through SPSS software, the effectiveness analysis of constructing the index system is carried out on the samples of high and low default states. The ROC curve is shown in Figure 5. The blue curve in the figure represents the identification results of high and low loss given default of 16 indexes finally screened out based on the depth-weighted fuzzy Bayesian model. The area under the blue curve AUC = 0.586, AUC > 0.5, which indicates that the depth-

Table 5: Credit evaluation indicator system.

(1) serial number	(2) The standard layer	(3) The index name	(4) Indicator type
1	Basic situation	Academic degree	Forward direction
2		Age	Interval type
3		House value	Forward direction
4	Repayment ability	Skills of lenders and their families	Forward direction
5		Annual net income is a multiple of GDP per capita	Forward direction
6		Total property	Forward direction
7		Net income of lenders	Forward direction
8		Expenditure-income ratio	Negative direction
9	Willingness to repay	Living conditions	Forward direction
10		Private lending	Forward direction
11		Is there any default	Forward direction
12		Loan records of lenders	Forward direction
13		Is there any guarantee	Forward direction
14		Ensure personnel strength	Forward direction
15	Macroenvironment	Per capita net income of rural households (yuan)	Forward direction
16		Engel coefficient	Negative direction

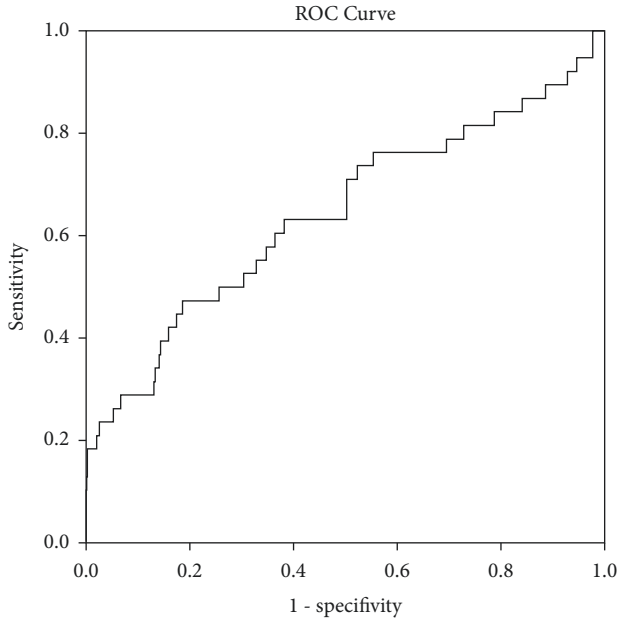

Figure 5: ROC curve.

weighted fuzzy Bayesian model has good effect in distinguishing high and low loss given default, and the constructed credit evaluation index system for family's farms and ranches has strong default identification ability and is effective.

6. Conclusion

6.1. Main Conclusions. In this paper, the fuzzy Bayesian mixed three-classification model with depth weighting is used to obtain 16 family farms and family ranches credit evaluation indexes with significant discrimination ability for nondefault, low default and high-default states, which are represented by five different levels: educational background (basic situation), skill status of lenders and their families (repayment ability), the amount of bank loans that lenders have not repaid (repayment willingness), whether there is guarantee (guarantee for guarantee), Engel coefficient (macroenvironmental factors).

6.2. Main Contributions

(1) Based on the theory of fuzzy mathematics, the uncertain variables are fuzzified by the triangular fuzzy numbers, and the triangular fuzzy numbers are fuzzified randomly by using the inner method, and different types of default situations are defined and interpreted, thus realizing the change of fuzzy default status of family's farms and ranches from fuzzy to definite.

(2) Based on the characteristic that the ROC curve is not sensitive to biased samples, the depth weighting of characteristic indicators under nondefault, low default and high-default conditions is completed by constructing a multiclassification ROC curve, which solves the practical problem of unbalanced samples in family's farms and ranches. The index system with significant discriminant ability for default status is selected based on default discriminant ability.

6.3. Policy Suggestions. In order to ensure the sustainable development of family farms and family ranches, effectively alleviate home loans difficult, the current situation of the financing difficulties, the work family farms and family ranches, identification and evaluation of credit risk monitoring, commercial Banks at all levels need to change the past mistake to use the index system of companies, to construct our country the characteristic of the family farms and family ranches loan credit rating index system. On the other hand, in order to promote the national agricultural benefit policy and strive to ensure that more family farms and family ranches get loans, the government or regulatory authorities should create conditions and guide banks at all levels to

increase the proportion of loans to family farms and family ranches. From the perspective of banks, the credit decision-making model that can guarantee the bank's target profit and maximize family farms and family ranches may be one of the effective ways to improve the financing difficulties of family farms and family ranches. And that is what we are going to focus on [23, 24].

Data Availability

The empirical sample of this paper is the credit data of 1814 family farms and ranches in Inner Mongolia, which comes from the database of a Commercial bank in China.

Conflicts of Interest

The authors declare that they have no conflicts of interest.

Acknowledgments

The research was supported by the National Natural Science Foundation of China (72161033), Natural Science Foundation of Inner Mongolia Autonomous Region of China (2020MS07009), Inner Mongolia Science and Technology Project of China (201605053), and Inner Mongolia Autonomous Region Graduate Scientific Research Innovation Project of China (S20210213Z).

References

[1] Y. Zhou and X. T. Su, "Enterprise credit risk forecast based on optimal index combination," *Journal of Systems Management*, vol. 30, no. 5, pp. 817–838, 2021.

[2] L. Yan, Z. J. Li, and X. J. Zhen, "Empirical study on indicators selection model based on nonparametric K-nearest neighbor identification and R clustering analysis," *Complexity*, vol. 2018, pp. 1–9, 2018.

[3] J. Traczynski, "Firm default prediction: A Bayesian model-averaging approach," *Journal of Financial and Quantitative Analysis*, vol. 52, no. 3, pp. 1211–1245, 2017.

[4] S. Dahiya, S. S. Handa, and N. P. Singh, "A feature selection enabled hybrid-bagging algorithm for credit risk evaluation," *Expert Systems*, vol. 34, no. 6, pp. 122–139, 2017.

[5] Y. S. Zhou, J. L. Cui, L. Y. Zhou, H. X. Sun, and S. Q. Liu, "Research on individual credit risk assessment based on improved stochastic forest model," *Credit Information*, vol. 38, no. 1, pp. 28–32, 2020.

[6] L. Wang, Y. G. Chen, H. Jiang, and J. Yao, "Imbalanced credit risk evaluation based on multiple sampling, multiple kernel fuzzy self-organizing map and local accuracy ensemble," *Applied Soft Computing*, vol. 1, pp. 1–11, 2020.

[7] C. Bai, B. Shi, F. Liu, and J. Sarkis, "Banking credit worthiness: Evaluating the complex relationships," *Omega*, vol. 83, pp. 26–38, 2019.

[8] Z. Li and C. Yang, "Establishment of the credit indicator system of micro enterprises based on support vector machine and R-type clustering," *Mathematical Problems in Engineering*, vol. 2018, Article ID 6390720, 11 pages, 2018.

[9] G. Kou, H. Xiao, M. H. Cao, and L. H. Lee, "Optimal computing budget allocation for the vector evaluated genetic algorithm in multiobjective simulation optimization," *Automatica*, vol. 129, pp. 1–14, 2021.

[10] S. Fallahpour, E. N. Lakvan, and M. H. Zadeh, "Using an ensemble classifier based on sequential floating forward selection for financial distress prediction problem," *Journal of Retailing and Consumer Services*, vol. 34, pp. 159–167, 2017.

[11] L. Hu, W. Gao, K. Zhao, P. Zhang, and F. Wang, "Feature selection considering two types of feature relevancy and feature interdependency," *Expert Systems with Applications*, vol. 93, pp. 423–434, 2017.

[12] L. P. Hai, B. F. Shi, and G. R. Peng, "A credit risk evaluation index system establishment of petty loans for farmers based on correlation analysis and significant discriminant," *Journal of Software*, vol. 8, no. 9, pp. 2344–2351, 2013.

[13] N. Nikolic, N. Zarkic-Joksimovic, D. Stojanovski, and I. Joksimovic, "The application of brute force logistic regression to corporate credit scoring models: Evidence from Serbian financial statements," *Expert Systems with Applications*, vol. 40, no. 15, pp. 5932–5944, 2013.

[14] X. Ni and Q. Zhang, "Research on credit evaluation index system of new agricultural operating subjects in China," *Agricultural Outlook*, vol. 15, no. 6, pp. 23–27, 2019.

[15] Y. T. Shen and M. Y. Lu, "Study on credit evaluation index system of new agricultural operating subject," *Xinjiang farming economy*, vol. 24, no. 9, pp. 55–62, 2017.

[16] A. Basak, "The role of urban cooperative banks and non-agricultural cooperative credit societies in financial inclusion: A study in howrah District, West Benga," *The IUP Journal of Management Research*, vol. 13, no. 3, pp. 81-82, 2015.

[17] T. Kim, B. D. Chung, and J. S. Lee, "Incorporating receiver operating characteristics into naive Bayes for unbalanced data classification," *Computing*, vol. 3, pp. 1–16, 2016.

[18] E. A. Krupinski, "Receiver operating characteristic (ROC) analysis," *Frontline learning research*, vol. 5, no. 3, pp. 31–42, 2017.

[19] L. Jiang, C. Li, S. Wang, and L. Zhang, "Deep feature weighting fornaive Bayes and its application to text classification," *Engineering Applications of Artificial Intelligence*, vol. 52, pp. 26–39, 2017.

[20] F. M. Zhang, W. J. Hua, and R. Y. Li, "Stability analysis of several comprehensive evaluation methods," *System Science and Mathematics*, vol. 39, no. 4, pp. 595–610, 2019.

[21] G. T. Chi and S. L. Yu, "Credit rating method based on maximum ability to identify default," *Journal of Management Sciences in China*, vol. 22, no. 11, pp. 106–126, 2019.

[22] H. H. Chen, "Research on the selection method of evaluation index based on reflection image correlation matrix," *China Management Science*, vol. 29, pp. 1–10, 2021.

[23] B. F. Shi, J. Wang, and G. T. Chi, "Inclusivity finance, bank credit and merchant microfinance: A perspective of risk level matching," *Chinese Management Science*, vol. 25, no. 9, pp. 28–36, 2017.

[24] B. Shi, J. Wang, J. Qi, and Y. Cheng, "A novel imbalanced data classification approach based on logistic regression and Fisher discriminant," *Mathematical Problems in Engineering*, vol. 2015, Article ID 945359, 12 pages, 2015.

Hindawi
Complexity
Volume 2022, Article ID 9483256, 18 pages
https://doi.org/10.1155/2022/9483256

WILEY | Hindawi

Research Article

Sustainable Strategic Alliance Partner Selection Using a Neutrosophic-Based Decision-Making Model: A Case Study in Passive Component Manufacturing

Huai-Wei Lo,[1] **Dong-Shang Chang**,[2] **and Lee-Te Huang**[2]

[1]*Department of Business Administration, Chaoyang University of Technology, Taichung, Taiwan*
[2]*Department of Business Administration, National Central University, Taoyuan, Taiwan*

Correspondence should be addressed to Lee-Te Huang; 108481007@cc.ncu.edu.tw

Received 21 February 2022; Revised 28 March 2022; Accepted 29 March 2022; Published 23 April 2022

Academic Editor: Hui Xiao

The electronics manufacturing industry is in an era of collaborative thinking and rapid change, as the rise of strategic alliances (SAs) plays a critical role in supply chain management. Strategic alliance (SA) collaboration is one of the most common strategies in the electronics industry, helping companies to complement each other. Most organizations or alliances operate together to produce more beneficial technologies for mutual benefit based on the sustainability thinking, such as in the areas of 5G, electric vehicles, aerospace, and smart healthcare. As the prompt evolution of information technology and electronics has a deep impact on global business activities, selecting partners based on a sustainability perspective is an urgent task. This paper proposes a complete sustainable SA partner selection framework to select the optimal partners. A neutrosophic-based decision-making model is used in the analysis. The neutrosophic ITARA technique is proposed to generate a set of criteria objective weights, and the neutrosophic TOPSIS technique is applied to determine the performance and priority of sustainable SA partners. This study introduces neutrosophic fuzzy logic to reflect the uncertainty in complex problems. Real-world data from a multinational passive component manufacturing company are used for case demonstration and analysis. The framework and methodology proposed in this study have many contributions to the electronics industry, including the establishment of assessment criteria, the identification of criteria, and the provision of partner selection practices. For academic research, the proposed model can be replicated in other areas of assessment and selection issues.

1. Introduction

Due to the lack of material, financial, technical, or managerial resources, companies form alliances with other organizations to collaborate so that they can share resources with each other and promote sustainable development [1]. However, many studies have illustrated the functions, benefits, risks, or developmental limitations of business alliances [2]. Chang et al. [3] state that the goal of strategic alliances (SAs) is to integrate the strengths or resources of multiple companies so that supply chain management systems can realize resource sharing and market diversification. Gnyawali and Ryan Charleton [4] show that the benefits that companies gain from alliances include new functions, skills, and knowledge resources. On the other hand, through the formation of alliances, it is possible to obtain access to new products and market opportunities that they cannot obtain internally. In general, the formation of SAs involves formal legal or private informal partnerships where supply chain partners can assist each other's strengths and weaknesses in order to decrease the operational risks of the companies.

In a highly competitive global market, companies are increasingly using SAs and acquisitions and mergers to acquire external knowledge (e.g., Toyota with Mazda, Panasonic, and SoftBank). As a result, SAs are also seen as a means of accumulating resources and participating in the codevelopment of technologies, products, systems, and services. Understanding the factors that contribute to successful SAs among organizations has become an important

field of inquiry among practitioners and researchers [5]. With the current boom in new technologies such as 5G, electric vehicles, aerospace, smart healthcare, and Industry 4.0, many electronics manufacturing industries are forming SAs to develop these areas together.

Different from the general manufacturing industry, the electronics manufacturing industry is classified as one of the energy-intensive industries (EIIs), and the electronic component manufacturing industry is one of its subsectors. The "electronic component manufacturing industry" is upstream of various computer and information industries, following the electronic component research and development and design industries, and is engaged in the manufacture of basic components for computer, communication, information, home electronic equipment, and other related products, and can be divided into four categories according to product characteristics: semiconductor manufacturing, passive electronic component manufacturing, printed circuit board manufacturing, and other electronic component manufacturing [6, 7]. Taiwan's electronic component manufacturing industry has developed early and has a complete upstream, midstream, and downstream all-inclusive industrial chain. The upstream side (raw materials) includes ceramic substrates, alumina substrates, conductive pastes, and electrode metals. The midstream side (manufacturing) includes resistors, capacitors, and inductors. The downstream side (product application) includes modems, gateways, routers, and hubs. In the process of business development, various strategies can be successful or unsuccessful at different stages. How to maintain a competitive advantage and continue to grow is the most important issue for business survival.

However, while the electronic component manufacturing industry has brought the development of economic and industrial clusters to the region, the negative emissions and waste from production activities can cause environmental damage [6]. As international organizations and environmental groups become more conscious of sustainability, many economic, environmental, and social criteria and regulations are being developed to require companies to operate in a manner that minimizes negative impacts on the environment and people's lives. If the notion of sustainable development is leaded into the selection of SA partners, energy consumption, harmful pollution, waste emissions, and corporate social responsibility (CSR) in the supply chain can be significantly controlled.

Therefore, the sustainable performance of SA partners plays a key role in the administration of any industry. The selection of a sustainable SA partner is based on a set of sustainability criteria to assess the performance of the alliance partner in order to select the optimal partner to become a member of the supply chain. However, the assessment and selection process involves several complex criteria or indicators, and a multiple criteria decision-making (MCDM) is the most appropriate way to approach this issue. The main aims of this study can be divided into the following three items.

(i) To construct an assessment framework for sustainable SA partner selection.

(ii) To determine the discriminatory power of the criteria in the assessment system, i.e., the criteria weights.

(iii) To consolidate the performance of the alliance partners assessed and prioritize them.

Since sustainable SA partner selection is a difficult and complex problem, it is difficult to use crisp value to reflect the actual feelings and judgments of experts. Therefore, neutrosophic fuzzy logic (here, single-valued trapezoidal neutrosophic numbers, SVTNNs is adopted) is introduced to reflect the ambiguity of the actual environment in the paper. Furthermore, the uncertainty of the experts in the assessment is measured by three parameters such as truth, falsity, and indeterminacy. The implementation process of this study can be divided into two phases: first, a framework for assessing the sustainability strategy of alliance partners in passive component manufacturing is proposed, which consists of six dimensions, which can be subdivided into 29 criteria. In the second phase, we develop a hybrid model based on neutrosophic theory, the neutrosophic ITARA technique to gain objective weights of sustainability criteria, and apply the neutrosophic TOPSIS technique to determine the performance and prioritization of sustainable SA partners. Our proposed neutrosophic ITARA improves the practicality of original ITARA. Neutrosophic ITARA not only introduces the aspiration level (AL) concept into the ITARA calculation process but also uses neutrosophic fuzzy sets to interpret uncertainty information. In addition, the neutrosophic TOPSIS extends the concept of TOPSIS in determining the variation of each alternative with respect to the normalized reference ideal, using the ideal and nonideal solutions to map the relative position of each assessed item. The improved neutrosophic TOPSIS not only overcomes the practical limitations of TOPSIS but also facilitates the examination of the attributes where the assessed items are underperforming. The proposed model is valid and reliable for assessing sustainable SA partners. This study provides insight into which criteria are discriminatory to the assessment system, and the company or organization can focus on these criteria to strengthen them. In addition, the results of the neutrosophic TOPSIS can be used to observe which criteria are underperforming in their current state, and alternative partners can develop improvement strategies based on these underperforming criteria to enhance the sustainability performance of the organization. In short, this study has the following features and contributions:

(i) This paper proposes a sustainable SA partner assessment framework to discuss the selection of the passive component manufacturing partners. However, only a few studies have measured the performance of alternative partners from a perspective of substainability. The proposed framework incorporates the concept of sustainability to make the assessment framework more comprehensive.

(ii) The proposed model developed (integrated neutrosophic, ITARA, and TOPSIS) is novel since it has not been proposed in other partner selection

studies. Neutrosophic ITARA can generate an objective set of criterion weights based on the assessed performance data of SA partners, and it does not require the release of a questionnaire for the pairwise comparison of criteria such as the analytic hierarchy process (AHP) and best-worst method (BWM). Moreover, neutrosophic TOPSIS improves on the original TOPSIS method and results in a more reliable ranking of alternative partners.

(iii) The research framework of this paper is reproducible and not limited to being used by any certain industry. Only minor adjustments to industry-appropriate assessment criteria are required.

The structure and content of the other sections of this paper are described below. Section 2 reviews the literature on SA partners and presents the proposed assessment framework system. Section 3 describes the methodology used in this study, which includes SVTNNs, neutrosophic ITARA, and neutrosophic TOPSIS. Section 4 illustrates the feasibility and effectiveness of the proposed model using a real case of a multinational passive component manufacturer. Section 5 discusses the advantages and contributions of this paper. Section 6 concludes the full discussion and provides future research directions.

2. Literature Review

SAs are an important form of cooperation among companies or organizations, and there is a lot of literature on the selection and assessment of the SA partners. By forming SAs, the partners can pool their strengths and existing resources to achieve their targets, reduce risks, share knowledge, and gain access to potential markets [8]. In the last two decades, the topics of SAs have extended from conceptual development to a more rigorous expert-based decision support system.

However, despite the popularity of SAs across all industries and sectors, there are still a large number of failed alliance operations [3]. In addition to inherent risks, one of the most frequently cited reasons for alliance failure is incompatibility among partners. Selecting the suitable partners can generate important competitive advantages and enhance the chances of success of SA operations. Therefore, selecting the right SA partners is an important task in the performance of an industry alliance. Finding the right partners requires careful screening, which can be a time-consuming and complicated procedure. It also takes time to understand the expectations and goals of the partners. The following subsections present the proposed assessment framework and research gaps.

2.1. Proposed Sustainable SA Partner Assessment Framework. This section reviews a large body of past research on SA partners and develops an assessment framework by the collaboration of several experts in the field. The sustainable SA partner assessment framework proposed in this paper is based on a perspective of sustainability, with several key dimensions added to form a comprehensive and complete assessment system. The dimensions can be composed of economy resource (E), environmental protection (G), social (S), innovation capability (I), organizational management (O), and risk factor (R). The six dimensions can be subdivided into 29 criteria that adequately reflect the key factors of SA partners, as shown in Tables 1–6. Table 1 presents the criteria of economic sustainability, including firm size (E1), financial strength (E2), material cost/selling price (E3), mergers/acquisitions (E4), and joint investment (E5), which are highly related to corporate economic activity.

Table 2 presents the dimension of environmental sustainability, which focuses on the perspective of environmental protection and is composed of environmental certification (G1), green resource integration (G2), pollution discharge treatment (G3), clean energy use (G4), and recycling/renewable capacity (G5).

Table 3 introduces the relevant indicators of social sustainability, including worker education and safety and health (S1), information sharing (S2), social contribution (S3), stakeholders' rights protection (S4), and local employment opportunities (S5).

The passive component manufacturing pays special attention to the innovation and R&D capabilities of partners, so innovation capability is a dimension in the evaluation system. In Table 4, the criteria are core technical patent (I1), product's life cycle (I2), manufacturing process capability (I3), R&D capability (I4), and supply chain integration (I5).

Organizational management is a common and important topic of strategic alliances. Table 5 shows the important organizational management key indicators, which include trust and commitment (O1), partners' complementarity (O2), corporate branded image (O3), and customer relationship management (CRM) capability (O4).

The last dimension is the risk factor. In practice, risk control is one of the keys to the success or failure of a strategic alliance. Businesses must understand whether the alliance can afford to take the potential risks. According to Table 6, this dimension can be divided into external legitimacy (R1), geographical fit (R2), collaborating stability (R3), government policy (R4), and potential competitor (R5) criteria.

2.2. Research Gap. In the keenly competitive global environment, seeking mutually beneficial partners is a key factor to maintain the competitiveness of enterprises. There have been many researchers evaluating partners for different industries. Wang et al. [44] proposed a hybrid model that combines grey theory and data envelopment analysis (DEA) to explore the partner selection issues in the global aerospace and defense industry. Their study examined the financial performance of the world's 35 largest aerospace and defense companies. Wang et al. [45] also used DEA to evaluate the operational performance of 20 IC packaging and testing enterprises. The findings suggest that what causes alliances to fail is that each partner tries to maximize personal interests rather than their cooperative interests. Chang et al. [3] developed a green SA evaluation framework to select the most suitable marketing partners for the biopharmaceutical industry. Their research focused on five dimensions of

Table 1: The economy resource dimension and its criteria.

Dimension	Criterion	Description	References
Economy resource (E)	Firm size (E1)	Corporate capital, turnover, number of employees, and market share, among other factors.	Elia et al. [19]; Padovani et al. [20]
	Financial strength (E2)	Information on corporate assets and liabilities, profit and loss, solvency, internal controls, board of directors' functions, and business status.	Cardoni et al. [21]; Padovani et al. [20]
	Material cost/selling price (E3)	All direct and indirect fixed and variable costs of materials, labor, equipment, plants, operations, marketing, and net/gross profit margins.	Gaustad et al. [22]; Lo et al. [7]
	Mergers/ acquisitions (E4)	Assessing whether the company can merge with other companies or has the value to do so.	Yu et al. [23]; Cacciolatti et al. [12]
	Joint investment (E5)	The willingness of the companies to invest their respective existing and superior resources in the joint venture in order to achieve joint capital, shared risk, and shared revenue.	Cacciolatti et al. [12]; Vendrell-Herrero et al. [24]

Table 2: The environmental protection dimension and its criteria.

Dimension	Criterion	Description	References
Environmental protection (G)	Environmental certification (G1)	The company should comply with the environmental regulations of international organizations and governments and obtain several environmental certifications and certificates.	Thorne et al. [9]; Ge et al. [10]
	Green resource integration (G2)	The company should respect the natural environment and protect the ecology in the green production system.	Huang and Li [11]
	Pollution discharge treatment (G3)	The company should actively implement environmental policies to reduce pollutant emissions and improve the efficiency of its energy use.	Chang et al. [3]
	Clean energy use (G4)	The company should strive to develop efficient and clean technologies for the production of passive components and promote the use of energy that does not pollute the environment.	Cacciolatti et al. [12]
	Recycling/renewable capacity (G5)	In the R&D and production process, enterprises should stress the importance of the recycling and reclamation of materials and consumables.	D'Amato et al. [13]

Table 3: The social dimension and its criteria.

Dimension	Criterion	Description	References
Social (S)	Worker education and safety and health (S1)	Attaching importance to the education, training, and physical health of our employees. The work environment controls the concentration of harmful substances and measures the ergonomics of workers' actions.	Mani et al. [30]; Gul [31]
	Information sharing (S2)	The company in the SA partnership can publish all production process information in a timely and accurate manner on a common information platform.	Russo and Cesarani [32]; Lee [33]
	Social contribution (S3)	The company should serve the public selflessly and assume greater CSR. The company shall comply with ethical norms and promote economic development in order to improve social well-being and improve the quality of life of society.	Muñoz and Kimmitt [34]; Chang et al. [3]
	Stakeholders' rights protection (S4)	Valuing the interests and rights of SA partners and all stakeholders in the supply chain.	Bhaumik et al. [35]; Nguyen et al. [36]
	Local employment opportunities (S5)	The company can bring more employment opportunities to local residents and promote fairness to maintain the employment rights of people.	Fernando et al. [37]; Burke and Stephens [38]

performance, including economic resource, innovation capability, organizational management, risk factors, and environmental protection. A hybrid BWM and TOPSIS model was used in their study. The study shows that innovation capability is the most important factor in SA for the biopharmaceutical industry. Tang and Hsu [46] applied a hierarchy structural fuzzy ANP (H-S FANP) approach to assess key factors of marketing SA development in the mobile telecommunication industry. Their study pointed out that H-S FANP can effectively identify the interaction of key factors. In addition to the above literature, there are many approaches to discussing SA selection and evaluation issues.

Table 4: The innovation capability dimension and its criteria.

Dimension	Criterion	Description	References
Innovation capability (I)	Core technical patent (I1)	The company currently holds patents of key core technologies. The strategy of developing patents is to develop potential markets to ensure the company's competitive advantage.	Sun et al. [25]
	Product's life cycle (I2)	The company develops products that go through an introductory phase, a growth phase, a maturity phase, and a decline phase. Usually, companies expect to produce products with a longer life cycle.	da Costa et al. [26]
	Manufacturing process capability (I3)	Under fixed production conditions and stable control, whether the company's manufacturing process matches the quality required by customers.	Gunasekaran et al. [27]
	R&D capability (I4)	Whether the company has the leading technologies and knowledge based on R&D, a clear understanding of market needs, and the ability to innovate products.	Martínez-Noya and Narula [28]
	Supply chain integration (I5)	The company's ability to integrate the supply chain, including all product processes such as incoming materials, production, inventory, and sales.	Nguyen and Tran [29]

Table 5: The organizational management dimension and its criteria.

Dimension	Criterion	Description	References
Organizational management (O)	Trust and commitment (O1)	A stable foundation for SA cohesion, trust, and termination penalties can be effective tools to motivate commitment and increase alliance effectiveness.	Alaaraj et al. [14]
	Partners' complementarity (O2)	Different resources, capabilities and technologies can be integrated and managed to enhance the complementary nature of the SA.	Mindruta et al. [15]; Hu et al. [16]
	Corporate branded image (O3)	The perception and impression of the company's brand fully reflect its values. The excellent brand image of the company increases profits and creates more channels to increase the market share of products.	Singh et al. [17]
	CRM capability (O4)	The service level of the company to meet the needs of customers. The main purpose is to use a high-performance information management system to analyze customer needs and process orders quickly.	Aldaihani and Ali [18]

Table 6: The risk factor dimension and its criteria.

Dimension	Criterion	Description	References
Risk factor (R)	External legitimacy (R1)	The company and alliance partners must obtain legalization from the local government before they can operate and trade in transnational economic organizations, and must avoid violating legal and criminal liabilities.	Zhang et al. [39]
	Geographical fit (R2)	When organizing economic activities in different regions, the company must evaluate cultural differences and business operations of the region in advance in order to avoid losses and reputational damage to the company.	Huertas-García et al. [40]
	Collaborating stability (R3)	The ambition of the company is to achieve the common goals of the SA.	Li and Nguyen [41]
	Government policy (R4)	The company operates in accordance with and supports the policies, laws, and regulations set by the local government.	Byun et al. [42]
	Potential competitor (R5)	The company should collect timely intelligence and information to assess potential competitors; otherwise, it may be threatened or even eliminated from the market.	Kim [43]

The examples include statistical probability theory [1], multiple linear regression [5, 9, 12], and combined AHP with TOPSIS [8].

In terms of SA evaluation criteria, most of the research still focuses on the marketing capabilities, financial indicators, and innovation capabilities of alternatives. However, only a few articles incorporate green awareness as an assessment perspective. In order to make up for this research gap, this study proposes a more comprehensive evaluation framework, which summarizes the economic resource, environmental protection, social, innovation capability, organizational management, and risk factor dimensions. In

addition, this study proposes a novel neutrosophic fuzzy-based MCDM model that not only effectively measures the integration performance of partners but also takes into account broader information uncertainty.

3. Methodology

The architecture of the analysis process for passive component SA partner assessment is shown in Figure 1. The methodology consists of three implementation procedures, namely, SVTNNs, neutrosophic ITARA, and neutrosophic TOPSIS. First, assessment criteria and alternative partners are identified, and assessment data for all alternative partners are generated through an actual survey. These data are used to obtain final scores using the SVTNNs conversion rule. Neutrosophic ITARA is then used to generate weights for the criteria with their importance ranking. Finally, neutrosophic TOPSIS is used to integrate the performance of the alternative partners and to determine their priority. The calculation process is described in detail below.

3.1. Basic Concepts and Definitions of the SVTNN. Zadeh [47] first proposed the concept of fuzzy sets (FSs), mainly to explore the theory of information fuzziness and the uncertainty of the assessment environment. Then, Atanassov [48] conducted an extended study on fuzzy sets by proposing intuitionistic fuzzy sets (IFSs). However, in order to reflect experts' judgment more precisely, Smarandache [49] proposed neutrosophic logic that combines the three parameters of truth ($T_{\tilde{\theta}}$), falsity ($F_{\tilde{\theta}}$), and indeterminacy ($I_{\tilde{\theta}}$) to fully interpret the uncertainty in the expert's assessment. Decision-making models based on neutrosophic set theory have been proposed by many researchers [50–54], and they believe that neutrosophic set theory is effective and practical in practice. The SVTNN is one of the methods of neutrosophic set theory, which overcomes some drawbacks of traditional intuitionistic fuzzy numbers. SVTNNs have two advantages. That is, they contain three fuzzy parameters (truth, falsity, and indeterminacy) to measure multifaceted uncertainty and use trapezoidal fuzzy numbers to encompass more latent information. SVTNNs can be explicated by the following definitions [55]:

Definition 1. $T_{\tilde{\theta}}$, $F_{\tilde{\theta}}$, and $I_{\tilde{\theta}}$ have a fixed range, which indicates that all three values are in [0, 1], and can also be expressed in percentage form. A regular SVTNN ($\tilde{\theta}$) has 7 elements, which are represented as $\tilde{\theta} = \left\{(\theta_1, \theta_2, \theta_3, \theta_4), (T_{\tilde{\theta}}, F_{\tilde{\theta}}, I_{\tilde{\theta}})\right\}$. It belongs to a special neutrosophic set in the real number set R, where $\mu_{\tilde{\theta}}$, $\lambda_{\tilde{\theta}}$, and $\nu_{\tilde{\theta}}$ are expressed as truth-membership (TM), falsity-membership (FM), and indeterminacy-membership (IM). The three membership functions can be defined by

$$\mu_{\tilde{\theta}}(x) = \begin{cases} \dfrac{(x-\theta_1)T_{\tilde{\theta}}}{(\theta_2-\theta_1)} & \theta_1 \le x \le \theta_2, \\ T_{\tilde{\theta}} & \theta_2 \le x \le \theta_3, \\ \dfrac{(\theta_4-x)T_{\tilde{\theta}}}{(\theta_4-\theta_3)} & \theta_3 \le x \le \theta_4, \\ 0 & \text{otherwise.} \end{cases} \tag{1}$$

$$\lambda_{\tilde{\theta}}(x) = \begin{cases} \dfrac{\left(\theta_2 - x + F_{\tilde{\theta}}(x-\theta_1)\right)}{(\theta_2-\theta_1)} & \theta_1 \le x \le \theta_2, \\ F_{\tilde{\theta}} & \theta_2 \le x \le \theta_3, \\ \dfrac{\left(x - \theta_3 + F_{\tilde{\theta}}(\theta_4-x)\right)}{(\theta_4-\theta_3)} & \theta_3 \le x \le \theta_4, \\ 1 & \text{otherwise.} \end{cases} \tag{2}$$

$$\nu_{\tilde{\theta}}(x) = \begin{cases} \dfrac{\left(\theta_2 - x + I_{\tilde{\theta}}(x-\theta_1)\right)}{(\theta_2-\theta_1)} & \theta_1 \le x \le \theta_2, \\ I_{\tilde{\theta}} & \theta_2 \le x \le \theta_3, \\ \dfrac{\left(x - \theta_3 + I_{\tilde{\theta}}(\theta_4-x)\right)}{(\theta_4-\theta_3)} & \theta_3 \le x \le \theta_4, \\ 1 & \text{otherwise.} \end{cases} \tag{3}$$

An SVTNN can be broken down into two parts. The first part is the general form of trapezoidal fuzzy numbers $(\theta_1, \theta_2, \theta_3, \theta_4)$, the minimum value of the fuzzy numbers is θ_1, and the maximum value is θ_4. In addition, θ_2 and θ_3 are the intermediate values, where it is not required θ_2 to be equal to θ_3. The second part is neutrosophic logic $(T_{\tilde{\theta}}, F_{\tilde{\theta}}, I_{\tilde{\theta}})$. $T_{\tilde{\theta}}$, $F_{\tilde{\theta}}$, and $I_{\tilde{\theta}}$ denote the truth, falsity, and indeterminacy of the trapezoidal fuzzy numbers, respectively. $T_{\tilde{\theta}}$, $F_{\tilde{\theta}}$, and $I_{\tilde{\theta}}$ are independent, so the sum of $T_{\tilde{\theta}}$, $F_{\tilde{\theta}}$, and $I_{\tilde{\theta}}$ is not required to be equal to 1.

Definition 2. SVTNN provides three useful indexes, which are final score ($sc(\theta)$), accuracy ($l(\theta)$), and certainty ($c(\theta)$) indexes, as in

$$sc(\theta) = \frac{(\theta_1 + 2\theta_2 + 2\theta_3 + \theta_4)\left(2 + T_{\tilde{\theta}} - F_{\tilde{\theta}} - I_{\tilde{\theta}}\right)}{18}, \tag{4}$$

$$l(\theta) = \frac{(\theta_1 + 2\theta_2 + 2\theta_3 + \theta_4)\left(T_{\tilde{\theta}} - F_{\tilde{\theta}}\right)}{6}, \tag{5}$$

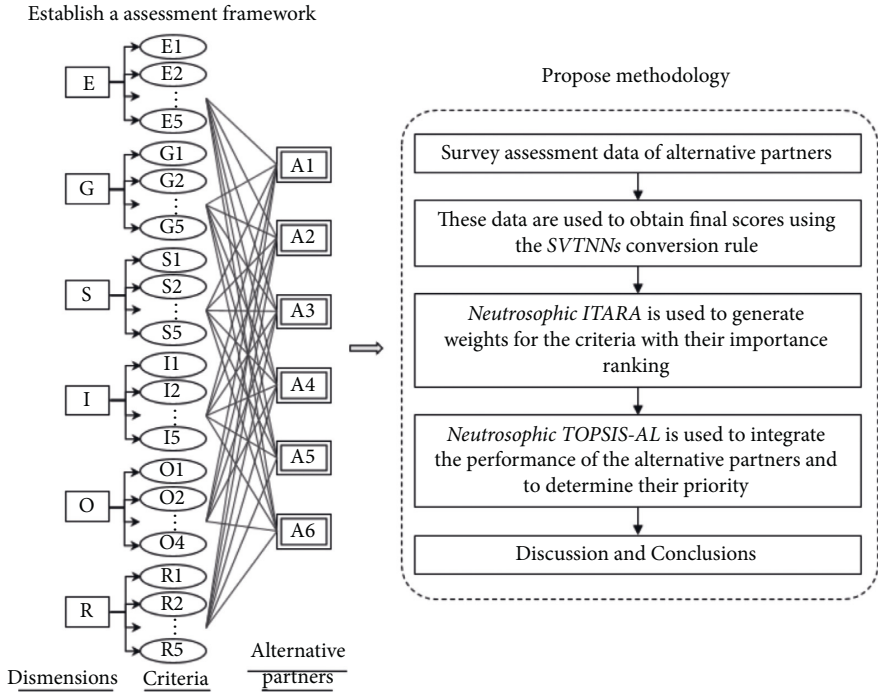

Figure 1: The analysis process chart.

$$c(\theta) = \frac{(\theta_1 + 2\theta_2 + 2\theta_3 + \theta_4)T_{\tilde{\theta}}}{6}. \quad (6)$$

Definition 3. Suppose that there are two SVTNNs here, namely $\tilde{su} = \left\{(su_1, su_2, su_3, su_4), (T_{su}\sim, F_{su}\sim, I_{su}\sim)\right\}$ and $\tilde{sv} = \left\{(sv_1, sv_2, sv_3, sv_4), (T_{sv}\sim, F_{sv}\sim, I_{sv}\sim)\right\}$; therefore, $\tilde{su}$ and $\tilde{sv}$ can be compared with each other, which is defined as follows:

(i) Suppose $sc(su) > sc(sv)$, then $\tilde{su} > \tilde{sv}$, and it indicates that $\tilde{su}$ is absolutely better than $\tilde{sv}$.

(ii) Suppose $sc(su) = sc(sv)$ and $l(su) > l(sv)$, then $\tilde{su} > \tilde{sv}$, and it indicates that $\tilde{su}$ is better than $\tilde{sv}$.

(iii) Suppose $sc(su) = sc(sv)$, then $\tilde{sv} > \tilde{su}$, and it indicates that $\tilde{su}$ is worse than $\tilde{sv}$.

Suppose $sc(su) = sc(sv)$, $l(su) = l(sv)$, and $c(su) > c(sv)$, then $\tilde{su} > \tilde{sv}$. Obviously, $\tilde{su}$ is better than $\tilde{sv}$. Suppose $c(su) < c(sv)$, then $\tilde{sv} > \tilde{su}$. When $c(su) = c(sv)$, it indicates that $\tilde{su}$ and $\tilde{sv}$ are the same.

3.2. Determining the Weights of the Criteria: Neutrosophic ITARA. There are many different methods to generate the weights of the criteria, which can be broadly classified into two types, namely, subjective and objective weighting methods. Subjective weighting methods are obtained through pairwise comparisons of criteria by experts or decision makers, such as AHP, analytic network process (ANP), decision making trial and evaluation laboratory (DEMATEL), and BWM. On the other hand, objective weighting methods are applied to train the appropriate weights of criteria from existing performance data, including CRITIC, entropy, and ITARA. The ITARA technique proposed by Hatefi [56] is a relatively new technique, which determines the weights by measuring the dispersion of the data. The greater the dispersion of data, the greater the ability of the criterion to discriminate how good the alternative partners are, and therefore the greater the weight assigned to it. Dispersion logic (DL) and indifference threshold (IT) are the two core parameters of ITARA. DL determines the dispersion of two adjacent data, while IT is the minimum allowed degree of difference.

Unfortunately, conventional ITARA only takes into account the distance between two adjacent partners but ignores the difference between the data itself and the AL. Suppose that there are 5 alternative partners with a rating of $\{3, 3, 2, 1, 1\}$ and $\{10, 10, 9, 8, 8\}$ (on a scale of 1 to 10) for 2 criteria. Although the deviations for the two sets of data are the same, the distances from the AL (10) are different. However, through the conventional ITARA, it assigns equal weights to both criteria. Therefore, this paper refers to the study of Lo et al. [57] to improve the conventional ITARA and incorporate SVTNNs to convert expert qualitative judgments into quantitative data. The steps of implementing the neutrosophic ITARA are detailed as follows.

Step 1. Collect the performance data of the alternative partners to build the initial neutrosophic assessment matrix $\tilde{\theta}$.

In this paper, m alternative partners (A_i, $i = 1, 2, \ldots, m$) are assessed under n assessment criteria (C_j, $j = 1, 2, \ldots,$

n), respectively. The initial assessment matrix obtained is shown in equation (7). Due to the inclusion of the concept of AL, the AL ($d_{\text{aspire}, j}$) is added as a benchmarking basis. The assessment team assesses the performance of the alternative partners based on the interpretation variables set in Table 7 and then measures the uncertainty of each assessment based on Table 8.

$$\widetilde{\theta} = \begin{bmatrix} \widetilde{\theta}_{11} & \widetilde{\theta}_{12} & \cdots & \widetilde{\theta}_{1n} \\ \widetilde{\theta}_{21} & \widetilde{\theta}_{22} & \cdots & \widetilde{\theta}_{2n} \\ \vdots & \vdots & \ddots & \vdots \\ \widetilde{\theta}_{m1} & \widetilde{\theta}_{m2} & \cdots & \widetilde{\theta}_{mn} \\ \widetilde{\theta}_{\text{aspire},1} & \widetilde{\theta}_{\text{aspire},2} & \cdots & \widetilde{\theta}_{\text{aspire},n} \end{bmatrix}_{(m+1)\times n}. \tag{7}$$

Step 2. Convert the linguistic variables into crisp values to form the matrix $sc(\theta)$.

The elements in the neutrosophic assessment matrix $\widetilde{\theta}$ are converted into crisp values (final scores) by (4) to form the matrix $sc(\theta)$:

$$sc(\theta) = \begin{bmatrix} sc(\theta_{11}) & sc(\theta_{12}) & \cdots & sc(\theta_{1n}) \\ sc(\theta_{21}) & sc(\theta_{22}) & \cdots & sc(\theta_{2n}) \\ \vdots & \vdots & \ddots & \vdots \\ sc(\theta_{m1}) & sc(\theta_{m2}) & \cdots & sc(\theta_{mn}) \\ sc\left(\theta_{\text{aspire},1}\right) & sc\left(\theta_{\text{aspire},2}\right) & \cdots & sc\left(\theta_{\text{aspire},n}\right) \end{bmatrix}_{(m+1)\times n}. \tag{8}$$

Step 3. Determine the IT_j for each criterion.

In this step, we develop a reasonable IT_j, $j = 1, 2, \ldots, n$. The IT_j reflects the experts' allowable range for the degree of dispersion.

Step 4. Create a normalized assessment matrix **A**

The normalization procedure is performed by (9) so that the values of the elements in the normalized assessment matrix **A** (10) fall in the range of 0 to 1.

$$a_{ij} = \frac{sc(\theta)_{ij}}{\sum_{i=1}^{m} sc(\theta)_{ij}}, \tag{9}$$

$$A = \left[a_{ij}\right]_{(m+1)\times n}. \tag{10}$$

Here, IT_j is also converted to NIT_j by normalization:

$$NIT_j = \frac{IT_{ij}}{\sum_{i=1}^{m} sc(\theta)_{ij}}, \quad j = 1, 2, \ldots, n. \tag{11}$$

Step 5. Arrange the elements of matrix **A** (in ascending order).

The elements of matrix **A** are arranged in ascending order to form a matrix β, as in equation (12). The AL $\beta_{\text{aspire},j}$ must be the maximum, so it will be arranged as the last.

$$\beta = \begin{bmatrix} \beta_{11} & \beta_{12} & \cdots & \beta_{12} \\ \beta_{21} & \beta_{22} & \cdots & \beta_{2n} \\ \vdots & \vdots & \ddots & \vdots \\ \beta_{m1} & \beta_{m2} & \cdots & \beta_{mn} \\ \beta_{\text{aspire},1} & \beta_{\text{aspire},2} & \cdots & \beta_{\text{aspire},n} \end{bmatrix}_{(m+1)\times n}. \tag{12}$$

Step 6. Calculate the degree of dispersion γ_{ij}

The dispersion of two adjacent alternative partners can be defined by equation (13). Similarly, the AL $\beta_{\text{aspire},j}$ must be subtracted from the previous data.

$$\gamma_{ij} = \beta_{i+1,j} - \beta_{ij}. \tag{13}$$

Step 7. Consider the difference between γ_{ij} and NIT_j

When $\gamma_{ij} > NIT_j$, it indicates that the dispersion of the two adjacent alternative partners is greater than the acceptable range for the decision makers. Therefore, δ_{ij} is used to represent the difference between γ_{ij} and NIT_j. Conversely, when $\gamma_{ij} \le NIT_j$, it indicates that γ_{ij} is not significant. Therefore, δ_{ij} is set to 0. The summary of the above can be shown in

$$\delta_{ij} = \begin{cases} \gamma_{ij} - NIT_j, \gamma_{ij} > NIT_j, \\ 0, \gamma_{ij} \le NIT_{j.} \end{cases} \tag{14}$$

Step 8. Generate a set of objective weights for the criteria.

The equation $v_j = (\sum_i^m \delta_{ij}^p)^{1/p}$ is a method to calculate multidimensional distances, and usually, the p values range from 1 to ∞. The Euclidean distance ($p = 2$) is used to define the distance between alternative partners, as shown in

$$v_j = \left(\sum_{i}^{m} \delta_{ij}^2\right)^{1/2}. \tag{15}$$

v_j is further normalized to conform to the concept of MCDM so that $w_j \ge 0$ and $\sum_{j=1}^{n} w_j = 1$:

$$w_j^1 = \frac{v_j}{\sum_{j=1}^{n} v_j}. \tag{16}$$

On the other hand, Lo et al. [57] proposed to incorporate ITARA by increasing the coefficient of variation (cv) as an index reflecting the overall dispersion (Equation (17)) so that the final objective criterion weight is shown in equation (18). ε is generally set to 0.5.

$$w_j^2 = \frac{cv_j}{\sum_{j=1}^{n} cv_j}, \tag{17}$$

$$w_j^* = \varepsilon\left(w_j^1\right) + (1 - \varepsilon)\left(w_j^2\right). \tag{18}$$

Table 7: Grade scale of performance assessment [3].

Linguistic variables	Code	Fuzzy numbers
Very poor	VP	(0, 1, 1, 2)
Poor	P	(2, 3, 3, 4)
Fair	F	(4, 5, 5, 6)
Good	G	(6, 7, 7, 8)
Very good	VG	(8, 9, 9, 10)

Table 8: Linguistic variables and corresponding fuzzy numbers in the neutrosophic part [58].

Linguistic variables	Code	Fuzzy numbers
No confidence	N	(0, 0, 0)
Low confidence	L	(0.6, 0.2, 0.2)
Fairly low confidence	FL	(0.7, 0.1, 0.1)
Medium confidence	M	(0.8, 0.1, 0)
Fairly high confidence	FH	(0.8, 0.2, 0.2)
High confidence	H	(0.9, 0.1, 0.1)
Absolutely high confidence	AH	(1, 0, 0)

3.3. Calculation of the Total Performance Scores of the Alternative Partners: Neutrosophic TOPSIS. This study integrates TOPSIS with neutrosophic logic theory to reflect the practical assessment of environmental uncertainty and uses the AL as the benchmark for the highest rating. The detailed TOPSIS procedure is described as follows.

Step 1. Use the matrix $sc(\theta)$ in Section 3.2 as the initial assessment matrix.

Step 2. Build the normalized assessment matrix **F** of neutrosophic TOPSIS.

The conventional normalization approach is to take the largest valuation of the alternative partners as the denominator, but this is equivalent to choosing only one relatively good apple in a basket. Therefore, this study introduces the AL concept into Step 2. Here, we add the AL and the worst level (WL) to the performance matrix. The normalized assessment matrix **F** of TOPSIS is created:

$$F = \left[f_{ij}\right]_{(m+2)\times n}, \tag{19}$$

where $f_{ij} = sc(\theta)_{ij}/sc(\theta)_{\text{aspire},j}$ and $sc(\theta)_{\text{aspire},j} = 10$ (the highest level of the assessment scale).

Step 3. Construct a weighted normalized assessment matrix **X.**

Taking into account the different degrees of the discriminative power of the criteria, the weight values generated by neutrosophic ITARA (w_j^*) are multiplied with the normalized assessment matrix **F**, which is calculated as in equation (20). The weighted normalized assessment matrix $\boldsymbol{X}$ is obtained as in equation (21).

$$x_{ij} = f_{ij} \cdot \left(w_j^*\right), \tag{20}$$

$$\mathrm{X} = \left[x_{ij}\right]_{(m+2)\times n}. \tag{21}$$

Step 4. Define positive and negative ideal solutions (PIS and NIS)

The values of PIS and NIS of the alternative partners should be 1 and 0 after normalization. The PIS and NIS of the alternative partners are shown:

$$\rho_j^+ = (1 \cdot w_1, 1 \cdot w_2, \ldots, 1 \cdot w_n) = (w_1, w_2, \ldots, w_n), \tag{22}$$

$$\rho_j^- = (0.1 \cdot w_1, 0.1 \cdot w_2, \ldots, 0.1 \cdot w_n). \tag{23}$$

Step 5. Calculate the difference between the PIS and NIS of the alternative partners.

Equations (24) and (25) are used to calculate the separation (Euclidean distance squared) between the PIS and NIS of the alternative partner *i*.

$$\mathrm{d}_i^* = \sum_{j=1}^{n} \sqrt{\left(\rho_j^+ - x_{ij}^{**}\right)^2}, \tag{24}$$

$$\mathrm{d}_i^- = \sum_{j=1}^{n} \sqrt{\left(x_{ij}^{**} - \rho_j^-\right)^2}. \tag{25}$$

Step 6. Calculate the closeness coefficient (CC_i) of the alternative partners.

The closeness coefficient CC_i is a reliable ranking index. According to Kuo [59], this ranking index takes into account the distance of all alternative partners from PIS

and NIS to overcome the shortcomings of the ranking index proposed by traditional TOPSIS, then, CC_i is shown:

$$CC_i = w^+\left(\frac{d_i^-}{\sum_{i=1}^m d_i^-}\right) - w^-\left(\frac{d_i^*}{\sum_{i=1}^m d_i^*}\right), \begin{cases} -1 \le CC_i \le 1 \\ 0 \le w^+ \le 1 \\ 0 \le w^- \le 1 \end{cases}, \quad i = 1, 2, \ldots, m, \tag{26}$$

where w^+ and w^- indicate the importance of PIS and NIS. Generally speaking, we set 0.5 to indicate equal importance to these two reference indicators. On the other hand, when CC_i is greater than 0, it indicates alternative partner i has higher performance. Conversely, when the CC_i is less than 0, it indicates that partner i has a relatively low performance.

4. A Real Case as a Data Demonstration

This study uses a multinational passive component manufacturer to illustrate the proposed neutrosophic-based DM model. Section 4 presents the problem description of the case study, followed by a description of the implementation processes of neutrosophic ITARA and TOPSIS in the case.

4.1. Background Description and Data Collection. The passive component manufacturing industry has developed early compared to other electronic industries, initially producing in the original equipment manufacturer (OEM) mode, and later shifting to the original design manufacturer (ODM) mode in order to increase added value and grasp key customers. After the rise of the semiconductor industry, passive components have almost become a traditional industry in the electronics industry, playing the role of driving the peripheral and equipment industries. The downstream application manufacturers are mainly computer equipment manufacturers, followed by the communication products market. The main products of passive components are capacitors (storing and releasing electrical energy in the form of static electricity), resistors (reducing voltage and limiting current to regulate circuit characteristics), inductors (generating electromagnetic flux to prevent electromagnetic interference), oscillators, and filters. After experiencing slow demand and oversupply in the communications and information market in 2000, the computer-related equipment, communications, and consumer electronics industries have been recovering since 2003, and the passive component boom has rebounded locally and internationally. The capacity utilization rate of various companies has gradually increased, and the companies have expanded their territories by expanding their production capacity and merging and acquiring with SAs in the industry.

In recent years, the case company has a deep understanding of the importance of technological capability and has been investing a fixed percentage of its annual revenue in technological research and development and innovation since 2000, devoting itself to various special product developments such as miniaturization, cost-efficiency optimization, green environmental protection, and independent research and development of materials to comply the trend of 3C products that are light, thin, and short with multifunctional integration. The passive components produced by the case company are widely used in various electronic products, from computer information, communication devices, consumer electronics, and even applications across electric vehicles, smart healthcare, and Industry 4.0. In the future, the case company expects to establish a SA to integrate the supply chain for electric vehicle production. Unfortunately, there is not yet a complete "sustainability concept" system for assessing SA partners, but rather a focus on the R&D and profitability of the alternative partners. Traditionally, SA decisions have been made mostly through meetings of senior executives to determine goals. Therefore, the case company needs a complete system for assessing sustainable SA partners and using scientific and computational tools to support SA strategy formulation.

The case company has a DM team consisting of senior executives, which includes the chairman, CEO, general manager, and division managers. The DM team assessed the performance of the six alternative partner companies based on the assessment framework developed in Section 2. Table 9 presents the joint assessment of the DM team. For example, based on the linguistic variables in Tables 7 and 8, A1 is rated as good (G) and absolutely high confidence (AH) on the scale of criterion E1. Next, we convert the elements in Table 9 into SVTNNs, as in Table 10. According to the above example, {G, AH} can be converted into one SVTNN, i.e., {(6, 7, 7, 8), (1, 0, 0)}, where 6 is the fuzzy lower bound, 8 is the fuzzy upper bound, and 7 is the fuzzy intermediate value (because it is a trapezoidal fuzzy number, there are two 7s). In addition, the truth is 1 and the falsity and indeterminacy are 0. According to equation (4), the SVTNNs can be converted into final scores as shown in Table 11. Subsequent neutrosophic ITARA and TOPSIS calculations are based on this table as initial input.

4.2. Using Neutrosophic ITARA to Generate the Objective Weights. Table 12 shows the initial assessment matrix for the sustainability alliance partners (which has been converted to

Table 9: Performance data of the six alternative partners (linguistic variables).

Criterion	Alternative					
	A1	A2	A3	A4	A5	A6
E1	{G, AH}	{G, FH}	{F, H}	{G, FH}	{VG, M}	{VG, H}
E2	{P, H}	{VG, M}	{VG, H}	{G, H}	{G, AH}	{F, M}
E3	{VG, H}	{F, H}	{VG, M}	{G, H}	{G, FH}	{P, H}
E4	{F, M}	{G, AH}	{G, FH}	{F, FH}	{G, H}	{F, H}
E5	{G, AH}	{VG, H}	{P, H}	{F, H}	{P, H}	{G, AH}
G1	{F, H}	{P, H}	{G, FH}	{G, FH}	{G, H}	{G, H}
G2	{G, H}	{F, FH}	{F, AH}	{F, M}	{G, H}	{G, M}
G3	{VG, H}	{F, H}	{G, M}	{F, H}	{G, H}	{P, H}
G4	{F, H}	{G, M}	{P, H}	{VG, M}	{G, H}	{G, FH}
G5	{VG, M}	{F, H}	{VG, FH}	{P, H}	{VG, M}	{G, AH}
S1	{G, M}	{VG, FH}	{G, AH}	{G, AH}	{G, AH}	{VG, FH}
S2	{P, FL}	{G, H}	{VG, H}	{F, AH}	{G, H}	{P, M}
S3	{G, M}	{G, M}	{VG, M}	{VG, M}	{G, AH}	{VG, M}
S4	{P, H}	{G, FH}	{F, H}	{P, H}	{G, AH}	{VG, M}
S5	{VG, FH}	{G, M}	{VG, M}	{G, M}	{G, AH}	{P, H}
I1	{G, H}	{VG, FH}	{F, H}	{VG, AH}	{G, M}	{F, M}
I2	{VG, FH}	{P, H}	{F, H}	{G, AH}	{VG, H}	{VG, H}
I3	{G, M}	{G, M}	{VG, H}	{G, M}	{G, AH}	{G, AH}
I4	{G, M}	{F, FL}	{P, FH}	{VG, H}	{G, FL}	{VG, L}
I5	{VG, FH}	{G, M}	{VG, H}	{G, M}	{VG, H}	{G, M}
O1	{G, H}	{F, H}	{G, AH}	{G, FH}	{G, H}	{G, FH}
O2	{F, M}	{G, M}	{F, H}	{G, AH}	{VG, FH}	{G, H}
O3	{G, H}	{G, AH}	{VG, M}	{P, H}	{VG, M}	{G, H}
O4	{G, H}	{VG, M}	{G, AH}	{VG, H}	{F, H}	{VG, H}
R1	{G, FH}	{F, H}	{G, H}	{G, AH}	{VG, H}	{G, AH}
R2	{P, H}	{VG, M}	{G, H}	{VG, H}	{G, FH}	{F, H}
R3	{VG, H}	{G, FH}	{F, H}	{P, H}	{VG, M}	{VG, H}
R4	{G, H}	{VG, H}	{VG, M}	{G, FH}	{G, AH}	{P, H}
R5	{G, FH}	{P, H}	{G, AH}	{G, AH}	{VG, M}	{G, AH}

Table 10: Performance data of the six alternative partners (SVTNNs).

Criterion	Alternative					
	A1	A2	A3	A4	A5	A6
E1	{(6, 7, 7, 8), (1, 0, 0)}	{(6, 7, 7, 8), (0.8, 0.2, 0.2)}	{(4, 5, 5, 6), (0.9, 0.1, 0.1)}	{(6, 7, 7, 8), (0.8, 0.2, 0.2)}	{(8, 9, 9, 10), (0.8, 0.1, 0)}	{(8, 9, 9, 10), (0.9, 0.1, 0.1)}
E2	{(2, 3, 3, 4), (0.9, 0.1, 0.1)}	{(8, 9, 9, 10), (0.8, 0.1, 0)}	{(8, 9, 9, 10), (0.9, 0.1, 0.1)}	{(6, 7, 7, 8), (0.9, 0.1, 0.1)}	{(6, 7, 7, 8), (1, 0, 0)}	{(4, 5, 5, 6), (0.8, 0.1, 0)}
E3	{(8, 9, 9, 10), (0.9, 0.1, 0.1)}	{(4, 5, 5, 6), (0.9, 0.1, 0.1)}	{(8, 9, 9, 10), (0.8, 0.1, 0)}	{(6, 7, 7, 8), (0.9, 0.1, 0.1)}	{(6, 7, 7, 8), (0.8, 0.2, 0.2)}	{(2, 3, 3, 4), (0.9, 0.1, 0.1)}
E4	{(4, 5, 5, 6), (0.8, 0.1, 0)}	{(6, 7, 7, 8), (1, 0, 0)}	{(6, 7, 7, 8), (0.8, 0.2, 0.2)}	{(4, 5, 5, 6), (0.8, 0.2, 0.2)}	{(6, 7, 7, 8), (0.9, 0.1, 0.1)}	{(4, 5, 5, 6), (0.9, 0.1, 0.1)}
E5	{(6, 7, 7, 8), (1, 0, 0)}	{(8, 9, 9, 10), (0.9, 0.1, 0.1)}	{(2, 3, 3, 4), (0.9, 0.1, 0.1)}	{(4, 5, 5, 6), (0.9, 0.1, 0.1)}	{(2, 3, 3, 4), (0.9, 0.1, 0.1)}	{(6, 7, 7, 8), (1, 0, 0)}
⋮	⋮	⋮	⋮	⋮	⋮	⋮
R5	{(6, 7, 7, 8), (0.8, 0.2, 0.2)}	{(2, 3, 3, 4), (0.9, 0.1, 0.1)}	{(6, 7, 7, 8), (1, 0, 0)}	{(6, 7, 7, 8), (1, 0, 0)}	{(8, 9, 9, 10), (0.8, 0.1, 0)}	{(6, 7, 7, 8), (1, 0, 0)}

Table 11), with each alternative partner having a performance score under each criterion. The data volume of the initial assessment matrix $sc(\theta)$ is 6×29 pieces of data, which are used to generate the objective weights of the criteria.

The sum of the final scores of the alternative partners for each criterion can be found in Table 12. The members of the DM team are asked to jointly develop an allowed difference, IT, for each criterion, which can be set to a different value for each criterion. Then, the objective weighting and ranking of the criteria can be calculated according to the neutrosophic ITARA process in Section 3.2, as shown in Table 13. The top five criteria are environmental certification (G1), information sharing (S2), joint investment (E5), stakeholder' rights protection (S4), and green resource integration (G2)

4.3. Using Neutrosophic TOPSIS to Integrate the Performance of Alternative Partners. The assessment and selection process of sustainable SA partners cannot be discussed using traditional cost-benefit analysis (CBA) because it involves a

Table 11: Performance data of the six alternative partners (final scores).

Criterion	Alternative					
	A1	A2	A3	A4	A5	A6
E1	7.0	5.6	4.5	5.6	8.1	8.1
E2	2.7	8.1	8.1	6.3	7.0	4.5
E3	8.1	4.5	8.1	6.3	5.6	2.7
E4	4.5	7.0	5.6	4.0	6.3	4.5
E5	7.0	8.1	2.7	4.5	2.7	7.0
⋮	⋮	⋮	⋮	⋮	⋮	⋮
R5	5.6	2.7	7.0	7.0	8.1	7.0

Table 12: The initial assessment matrix $sc(\theta)$.

	E1	E2	E3	E4	E5	⋯	R5
A1	7.0	2.7	8.1	4.5	7.0	⋯	5.6
A2	5.6	8.1	4.5	7.0	8.1	⋯	2.7
A3	4.5	8.1	8.1	5.6	2.7	⋯	7.0
A4	5.6	6.3	6.3	4.0	4.5	⋯	7.0
A5	8.1	7.0	5.6	6.3	2.7	⋯	8.1
A6	8.1	4.5	2.7	4.5	7.0	⋯	7.0
AL	10	10	10	10	10	⋯	10
Sum	48.9	46.7	45.3	41.9	42.0	⋯	47.4
IT	0.5	0.5	0.5	0.5	0.5	⋯	0.5

number of criteria other than cost or benefit in addition to many qualitative criteria that cannot be measured using instruments or equipment tools. As a result of the extensive literature review, MCDM has excellent analytical capabilities in dealing with MCDM issues, and it can meet the development needs of decision-makers/operators in order to support companies in formulating appropriate improvement strategies. Due to the ambiguity of the information and the uncertainty of the assessment environment, this study combines the neutrosophic fuzzy technique into TOPSIS, in addition to the AL and the WL as the basis for the assessment of the alternative partners, avoiding the consideration of the relative preference solution of the current solution. The procedure can be performed according to Section 3.3.

Table 14 presents the input data of neutrosophic TOPSIS, which is actually the same as the initial data of neutrosophic ITARA, with the difference that neutrosophic TOPSIS adds the AL and the WL as the two parameters of the calculation. Table 15 presents the results of the neutrosophic TOPSIS analysis, which shows the difference between the AL and the WL (d^* and d^-) for each partner, with A5 being the partner closest to the AL and furthest from the WL, with a gap of 0.069 and 0.128, respectively. It is worth mentioning that the AL and the WL are appropriate as a basis for judging the alternative partners so that it is possible to distinguish which partner is relatively good and which is relatively bad. In this case, the closeness coefficient obtained for A4 is negative, −0.002, which means that it is relatively poor among the available partners. The order of preference of the alternative partners is A5 >> A3 >> A1 >> A6 >> A2 >> A4.

5. Discussion

Due to the raging COVID-19 epidemic, the operation of global industrial chains was disrupted in one fell swoop. Now, even in the postepidemic era, business owners are thinking about how to improve operational flexibility, reallocate production resources, or significantly reduce their reliance on a single factor of production. Fortunately, due to the development of trends in 5G, electric vehicles, aerospace, smart healthcare, and Industry 4.0, many passive component makers have increased their revenue due to the surge in demand in the electronics market. The case company mainly produces passive components related products. They understand that developing SAs is an important means to enhance the competitiveness of the company, and the benefits brought by successful SAs are long-term and sustainable.

As far as we know, few previous studies in the literature have examined the assessment framework of SA partners for passive component manufacturing, especially the sustainability assessment criteria that have not been well proposed. In this study, we propose a model for assessing sustainable SA partners to bring a comprehensive assessment framework and approach to the industry. First, through an extensive literature review and expert interviews, six dimensions and 29 criteria were identified. Next, neutrosophic ITARA was used to obtain the criteria weights and neutrosophic TOPSIS was applied to prioritize the alternative partners.

According to the neutrosophic ITARA results in Table 13, environmental certification (G1) is the most discriminating criterion, with a weight value of 0.047. This result indicates that

Table 13: Calculation results of neutrosophic ITARA.

Criterion	E1	E2	E3	E4	E5	G1	G2	G3	G4	G5	S1	S2	S3	S4	S5	I1	I2	I3	I4	I5	O1	O2	O3	O4	R1	R2	R3	R4	R5
v_j	0.038	0.051	0.053	0.062	0.067	0.086	0.078	0.063	0.055	0.059	0.045	0.067	0.029	0.056	0.072	0.041	0.059	0.030	0.056	0.029	0.057	0.058	0.071	0.039	0.034	0.053	0.060	0.060	0.063
w_j^1	0.024	0.032	0.033	0.039	0.042	0.054	0.049	0.039	0.035	0.037	0.028	0.042	0.018	0.035	0.045	0.026	0.037	0.019	0.035	0.018	0.036	0.036	0.045	0.024	0.022	0.033	0.038	0.038	0.04
cv_j	0.272	0.367	0.382	0.346	0.464	0.379	0.327	0.404	0.381	0.36	0.161	0.466	0.169	0.474	0.326	0.307	0.36	0.187	0.4	0.184	0.269	0.286	0.327	0.233	0.256	0.382	0.378	0.339	0.332
w_j^2	0.029	0.039	0.04	0.036	0.049	0.04	0.034	0.042	0.04	0.038	0.017	0.049	0.018	0.05	0.034	0.032	0.038	0.02	0.042	0.019	0.028	0.03	0.034	0.024	0.027	0.04	0.04	0.036	0.035
w_j^*	0.026	0.035	0.037	0.038	0.046	0.047	0.042	0.041	0.037	0.037	0.023	0.046	0.018	0.043	0.04	0.029	0.037	0.019	0.039	0.019	0.032	0.033	0.04	0.024	0.024	0.037	0.039	0.037	0.037
Rank	23	19	17	11	3	1	5	6	14	12	26	2	29	4	7	22	13	27	10	28	21	20	8	24	25	16	9	18	15

Table 14: The initial assessment matrix of the neutrosophic TOPSIS.

	E1	E2	E3	E4	E5	⋯	R5
A1	7.0	2.7	8.1	4.5	7.0	⋯	5.6
A2	5.6	8.1	4.5	7.0	8.1	⋯	2.7
A3	4.5	8.1	8.1	5.6	2.7	⋯	7.0
A4	5.6	6.3	6.3	4.0	4.5	⋯	7.0
A5	8.1	7.0	5.6	6.3	2.7	⋯	8.1
A6	8.1	4.5	2.7	4.5	7.0	⋯	7.0
AL	10	10	10	10	10	⋯	10
WL	0	0	0	0	0	⋯	0

Table 15: The analysis results of the neutrosophic TOPSIS.

Alternative partner	d^*	d^-	CC	Rank
A1	0.088	0.115	0.002	3
A2	0.089	0.113	0.000	5
A3	0.086	0.118	0.006	2
A4	0.091	0.111	−0.002	6
A5	0.069	0.128	0.023	1
A6	0.090	0.114	0.000	4
AL	0	0.191	0.107	
WL	0.191	0	-0.135	

the performance of the G1 criterion varies considerably among the alternative partners. Since companies have different competitive strategies and environmental regimes, investment in the criteria may vary. In different countries, there are many different environmental certifications, such as JIS, NRTL, VDE, RoHS, and CE. As environmental protection issues gradually become the focus of international attention, governments and private enterprises are paying more and more attention to green materials, green processes, or green products, and therefore gradually setting up standards and regulations, and giving rise to green-related certifications or environmental labels, and enterprises obtaining green-related certifications or environmental labels are relatively gaining the recognition and trust of customers and general consumers in terms of green protection. Besides, other criteria that are among the top five in importance are communication and information sharing (S2), joint investment (E5), stakeholders' rights protection (S4), and green resource integration (G2) are all criteria of particular importance to alternative partners, as improved performance on these indicators can significantly improve overall performance.

In the ranking of the alternative partners, A5 is currently the optimal performing SA partner. A5 is a multinational manufacturer of high-frequency antennas for GPS, automotive navigation cables, NFC, and more. The partner has a wide sales channel and masters the technology of high-frequency antenna production. In recent years, the case company wants to develop new technologies and sales channels for electric vehicle components, and A5's support in this part can make a great contribution and help the case company's future business development. In addition to A5, A3 is the second-ranked alternative partner, and the case company can determine how many companies it needs to include in the SA based on its competitive strategy.

Since G1 is the most discriminating criterion in this case, a sensitivity analysis is performed to detect the influence of this criterion on the analysis results. The weight of G1 is set in the range of 0.01 to 0.09, and the interval unit of each change is 0.01. Other criteria are assigned in proportion to the neutrosophic ITARA weights. Table 16 is the ranking of alternative partners by performing nine sensitivity analyses. A5 still belongs to the top one alternative partner in the nine analysis results. According to Figure 2, the ranking status of the alternatives can be clearly seen. Except for A5 and A3, the rest of the alternative partners will change with the weight of G1, which shows the necessity of formulating the criteria weights.

This study compared six neutrosophic-based MCDM methods to illustrate their differences, including neutrosophic simple additive weighting (SAW), neutrosophic additive ratio assessment (ARAS), neutrosophic weighted aggregated sum product assessment (WASPAS), neutrosophic *vlse kriterijumska optimizacija i kompromisno resenje* in Serbian (VIKOR), neutrosophic original TOPSIS, and our proposed model. Table 17 presents the calculation results of the six methods and the ranking of alternative partners. With the exception of neutrosophic VIKOR, the ranking results for the other five methods are the same. In this paper, our model extends the concept of original TOPSIS in determining the variation of each alternative with respect to the normalized reference ideal, using the AL and WL solutions to map the relative position of each assessed partner. Compared with the other five methods, our model can obtain more potential gap information of alternative partners. In addition, the proposed model not only overcomes the practical limitations of the original TOPSIS but also facilitates the examination of the attributes with which the assessed partners are underperforming.

Table 16: The ranking of alternative partners by performing nine sensitivity analyses.

	Run 1	Run 2	Run 3	Run 4	Run 5	Run 6	Run 7	Run 8	Run 9
G1 weight	0.01	0.02	0.03	0.04	0.05	0.06	0.07	0.08	0.09
A1	4	4	3	3	3	4	4	4	5
A2	3	3	4	4	5	6	6	6	6
A3	2	2	2	2	2	2	2	2	2
A4	6	6	6	6	6	5	5	5	4
A5	1	1	1	1	1	1	1	1	1
A6	5	5	5	5	4	3	3	3	3

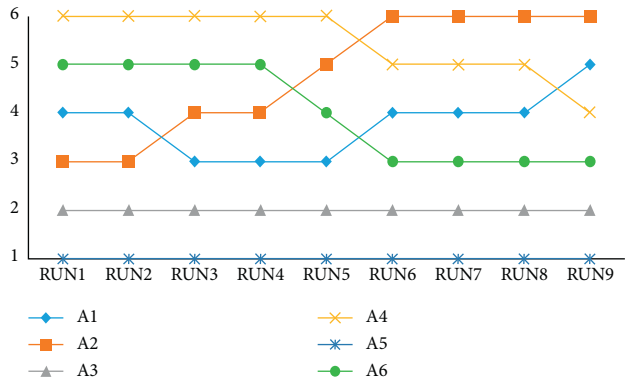

Figure 2: Line graph of sensitivity analysis results.

Table 17: Comparison of six neutrosophic-based MCDM methods.

	Neutrosophic SAW		Neutrosophic ARAS		Neutrosophic WASPAS		Neutrosophic VIKOR		Neutrosophic TOPSIS (original)		Neutrosophic TOPSIS (our model)	
	SAW	Rank	K	Rank	Q	Rank	R	Rank	CC	Rank	CC	Rank
A1	0.581	3	0.163	3	0.564	3	0.955	5	0.565	3	0.002	3
A2	0.572	5	0.160	5	0.558	5	0.995	6	0.558	5	0.000	5
A3	0.600	2	0.168	2	0.583	2	0.702	3	0.580	2	0.006	2
A4	0.572	6	0.160	6	0.555	6	0.500	2	0.549	6	-0.002	6
A5	0.667	1	0.187	1	0.659	1	0.350	1	0.649	1	0.023	1
A6	0.577	4	0.162	4	0.558	4	0.831	4	0.558	4	0.000	4

6. Conclusion and Future Work

This paper presents a systematic and sustainable SA partner assessment model that provides a tool for selecting and assessing SA partners in passive component manufacturing industries. This hybrid MCDM model not only reduces the subjectivity of management decisions but also measures the uncertainty of information. There is no academic research that comprehensively examines the recruitment of SA members in passive component manufacturing industries. This paper integrates several state-of-the-art approaches, including neutrosophic fuzzy logic, neutrosophic ITARA, and neutrosophic TOPSIS techniques to consider various realistic factors such as the consideration of information uncertainty and the introduction of the aspiration level concept. According to neutrosophic ITARA calculations, environmental certification (G1) is the most discriminative criterion. On the other hand, the order of preference of the alternative partners is A5 >> A3 >> A1 >> A6 >> A2 >> A4.

Our study illustrates the validity and reliability of the proposed model. It should bring several benefits to the case company:

(i) Identifying the most appropriate SA partners for passive component manufacturers;

(ii) Providing criteria for sustainability assessment of partners; and

(iii) Helping analysts to be more systematic in the DM process.

The model concept proposed in this study is novel, but there are still some limitations to overcome. The proposed model can be programmed in collaboration with academics from information backgrounds to jointly develop software for SA selection to facilitate its application by more academic researchers and industry managers. In addition, the interdependence among the criteria has not been discussed in this paper, and in the future, the DEMATEL technique can be

combined to determine the mutual influential relationships of criteria.

Data Availability

All data generated or analyzed during the study are included in this manuscript.

Conflicts of Interest

All authors declare that they have no conflicts of interest.

Authors' Contributions

L.-T. H. conceptualized and investigated the study and curated the data. H.-W.L. contributed to the methodology. H.-W.L. and L.-T. H. prepared the original draft. D.-S. C. performed the review and editing work.

References

[1] W. L. Ko, S. Y. Kim, J.-H. Lee, and T. H. Song, "The effects of strategic alliance emphasis and marketing efficiency on firm value under different technological environments," *Journal of Business Research*, vol. 120, pp. 453–461, 2020.

[2] N. Butigan and Đ. Benić, "The impact of membership in strategic alliances on the profitability of firms in the retail sector," *Croation Economic Survey*, vol. 19, no. 2, pp. 47–82, 2017.

[3] M. H. Chang, J. J. Liou, and H. W. Lo, "A hybrid MCDM model for evaluating strategic alliance partners in the green biopharmaceutical industry," *Sustainability*, vol. 11, no. 15, p. 4065, 2019.

[4] D. R. Gnyawali and T. Ryan Charleton, "Nuances in the interplay of competition and cooperation: towards a theory of coopetition," *Journal of Management*, vol. 44, no. 7, pp. 2511–2534, 2018.

[5] T.-H. Liu and Y.-C. Hsiao, "Fitting cooperative mode in inter-organizational strategic alliance: a perspective from innovative and financial performances," *The Journal of Technology Transfer*, vol. 44, no. 1, pp. 73–96, 2019.

[6] T.-W. Chang, C.-J. Pai, H.-W. Lo, and S.-K. Hu, "A hybrid decision-making model for sustainable supplier evaluation in electronics manufacturing," *Computers & Industrial Engineering*, vol. 156, p. 107283, 2021.

[7] H.-W. Lo, J. J. H. Liou, H.-S. Wang, and Y.-S. Tsai, "An integrated model for solving problems in green supplier selection and order allocation," *Journal of Cleaner Production*, vol. 190, pp. 339–352, 2018.

[8] G. Büyüközkan, O. Feyzioğlu, and E. Nebol, "Selection of the strategic alliance partner in logistics value chain," *International Journal of Production Economics*, vol. 113, no. 1, pp. 148–158, 2008.

[9] L. Thorne, L. S. Mahoney, K. Gregory, and S. Convery, "A comparison of Canadian and U.S. CSR strategic alliances, CSR reporting, and CSR performance: insights into implicit-explicit CSR," *Journal of Business Ethics*, vol. 143, no. 1, pp. 85–98, 2017.

[10] H. Ge, S. Chen, and Y. Chen, "International alliance of green hotels to reach sustainable competitive advantages," *Sustainability*, vol. 10, no. 2, p. 573, 2018.

[11] J.-W. Huang and Y.-H. Li, "How resource alignment moderates the relationship between environmental innovation strategy and green innovation performance," *Journal of Business & Industrial Marketing*, vol. 33, no. 3, pp. 316–324, 2018.

[12] L. Cacciolatti, A. Rosli, J. L. Ruiz-Alba, and J. Chang, "Strategic alliances and firm performance in startups with a social mission," *Journal of Business Research*, vol. 106, pp. 106–117, 2020.

[13] D. D'Amato, S. Veijonaho, and A. Toppinen, "Towards sustainability? Forest-based circular bioeconomy business models in Finnish SMEs," *Forest Policy and Economics*, vol. 110, p. 101848, 2020.

[14] S. Alaaraj, Z. A. Mohamed, and U. S. Ahmad Bustamam, "External growth strategies and organizational performance in emerging markets," *Review of International Business and Strategy*, vol. 28, no. 2, pp. 206–222, 2018.

[15] D. Mindruta, M. Moeen, and R. Agarwal, "A two-sided matching approach for partner selection and assessing complementarities in partners' attributes in inter-firm alliances," *Strategic Management Journal*, vol. 37, no. 1, pp. 206–231, 2016.

[16] T. Hu, A. Jain, and A. Delios, "Centrality asymmetry and partner complementarity as influences on alliance dissolution," *British Journal of Management*, vol. 32, no. 1, pp. 59–79, 2021.

[17] J. Singh, B. Crisafulli, and L. T. Quamina, "'Corporate image at stake': the impact of crises and response strategies on consumer perceptions of corporate brand alliances," *Journal of Business Research*, vol. 117, pp. 839–849, 2020.

[18] F. M. F. Aldaihani and N. A. B. Ali, "Impact of social customer relationship management on customer satisfaction through customer empowerment: a study of Islamic Banks in Kuwait," *International Research Journal of Finance and Economics*, vol. 170, no. 170, pp. 41–53, 2018.

[19] S. Elia, A. Messeni Petruzzelli, and L. Piscitello, "The impact of cultural diversity on innovation performance of MNC subsidiaries in strategic alliances," *Journal of Business Research*, vol. 98, pp. 204–213, 2019.

[20] E. Padovani, D. W. Young, and E. Scorsone, "The role of a municipality's financial health in a firm's siting decision," *Business Horizons*, vol. 61, no. 2, pp. 181–190, 2018.

[21] A. Cardoni, G. H. Tompson, M. Rubino, and P. Taticchi, "Measuring the impact of organizational complexity, planning and control on strategic alliances' performance," *Measuring Business Excellence*, vol. 24, no. 4, pp. 531–551, 2020.

[22] G. Gaustad, M. Krystofik, M. Bustamante, and K. Badami, "Circular economy strategies for mitigating critical material supply issues," *Resources, Conservation and Recycling*, vol. 135, pp. 24–33, 2018.

[23] B. Yu, H. Xu, and F. Dong, "Vertical vs. Horizontal: how strategic alliance type influence firm performance?" *Sustainability*, vol. 11, no. 23, p. 6594, 2019.

[24] F. Vendrell-Herrero, E. Gomes, O. F. Bustinza, and K. Mellahi, "Uncovering the role of cross-border strategic alliances and expertise decision centralization in enhancing product-service innovation in MMNEs," *International Business Review*, vol. 27, no. 4, pp. 814–825, 2018.

[25] W. Sun, Y. Zhao, and L. Sun, "Big data analytics for venture capital Application : Towards innovation performance improvement," *International Journal of Information Management*, vol. 50, pp. 557–565, 2020.

[26] L. G. da Costa, J. C. E. Ferreira, V. Kumar, and J. A. Garza-Reyes, "Benchmarking of sustainability to assess practices and performances of the management of the end of life cycle of electronic products: a study of Brazilian manufacturing

companies," *Clean Technologies and Environmental Policy*, vol. 24, pp. 1173–1189, 2022.

[27] A. Gunasekaran, Y. Y. Yusuf, E. O. Adeleye, T. Papadopoulos, D. Kovvuri, and D. A. G. Geyi, "Agile manufacturing: an evolutionary review of practices," *International Journal of Production Research*, vol. 57, no. 15-16, pp. 5154–5174, 2019.

[28] A. Martínez-Noya and R. Narula, "What more can we learn from R&D alliances? A review and research agenda," *BRQ Business Research Quarterly*, vol. 21, no. 3, pp. 195–212, 2018.

[29] N.-T. Nguyen and T.-T. Tran, "Raising opportunities in strategic alliance by evaluating efficiency of logistics companies in Vietnam: a case of Cat Lai Port," *Neural Computing & Applications*, vol. 31, no. 11, pp. 7963–7974, 2019.

[30] V. Mani, A. Gunasekaran, and C. Delgado, "Enhancing supply chain performance through supplier social sustainability: an emerging economy perspective," *International Journal of Production Economics*, vol. 195, pp. 259–272, 2018.

[31] M. Gul, "A fuzzy-based occupational health and safety risk assessment framework and a case study in an international port authority," *Journal of Marine Engineering & Technology*, vol. 19, no. 4, pp. 161–175, 2020.

[32] M. Russo and M. Cesarani, "Strategic alliance success factors: a literature review on alliance lifecycle," *International Journal of Business Administration*, vol. 8, no. 3, pp. 1–9, 2017.

[33] H. Lee, "Alliance models among value chain participants in foreign markets: a focus on Korean LSPs," *The Asian Journal of Shipping and Logistics*, vol. 37, no. 3, pp. 268–279, 2021.

[34] P. Muñoz and J. Kimmitt, "Social mission as competitive advantage: a configurational analysis of the strategic conditions of social entrepreneurship," *Journal of Business Research*, vol. 101, pp. 854–861, 2019.

[35] S. Bhaumik, N. Driffield, A. Gaur, T. Mickiewicz, and P. Vaaler, "Corporate governance and MNE strategies in emerging economies," *Journal of World Business*, vol. 54, no. 4, pp. 234–243, 2019.

[36] T. H. D. Nguyen, N. Chileshe, R. Rameezdeen, and A. Wood, "External stakeholder strategic actions in projects: a multi-case study," *International Journal of Project Management*, vol. 37, no. 1, pp. 176–191, 2019.

[37] Y. Fernando, C. J. Chiappetta Jabbour, and W.-X. Wah, "Pursuing green growth in technology firms through the connections between environmental innovation and sustainable business performance: does service capability matter?" *Resources, Conservation and Recycling*, vol. 141, pp. 8–20, 2019.

[38] M. J. Burke and J. C. Stephens, "Political power and renewable energy futures: a critical review," *Energy Research & Social Science*, vol. 35, pp. 78–93, 2018.

[39] H. Zhang, M. N. Young, J. Tan, and W. Sun, "How Chinese companies deal with a legitimacy imbalance when acquiring firms from developed economies," *Journal of World Business*, vol. 53, no. 5, pp. 752–767, 2018.

[40] R. Huertas-García, J. Lengler, and C. Consolación-Segura, "Co-branding strategy in cause-related advertising: the fit between brand and cause," *The Journal of Product and Brand Management*, vol. 26, no. 2, pp. 135–150, 2017.

[41] M. Li and B. Nguyen, "When will firms share information and collaborate to achieve innovation?" *The Bottom Line*, vol. 30, no. 1, pp. 65–86, 2017.

[42] J. Byun, T.-E. Sung, and H.-w. Park, "A network analysis of strategic alliance drivers in ICT open ecosystem: with focus on mobile, cloud computing, and multimedia," *Multimedia Tools and Applications*, vol. 77, no. 12, pp. 14725–14744, 2018.

[43] K.-H. Kim, "Cooperative or competitive in alliance formation: alliance patterns with respect to rivals," *Canadian Journal of Administrative Sciences - Revue Canadienne des Sciences de l Administration*, vol. 34, no. 3, pp. 277–290, 2017.

[44] C.-N. Wang, X.-T. Nguyen, T.-D. Le, and M.-H. Hsueh, "A partner selection approach for strategic alliance in the global aerospace and defense industry," *Journal of Air Transport Management*, vol. 69, pp. 190–204, 2018.

[45] C.-N. Wang, Y.-C. Peng, M.-H. Hsueh, and Y.-H. Wang, "The selection of strategic alliance in IC packaging and testing industry with DEA resampling comparative evaluation," *Applied Sciences*, vol. 11, no. 1, p. 204, 2020.

[46] J.-W. Tang and T.-H. Hsu, "Utilizing the hierarchy structural fuzzy analytical network process model to evaluate critical elements of marketing strategic alliance development in mobile telecommunication industry," *Group Decision and Negotiation*, vol. 27, no. 2, pp. 251–284, 2018.

[47] L. A. Zadeh, "Fuzzy sets as a basis for a theory of possibility," *Fuzzy Sets and Systems*, vol. 1, no. 1, pp. 3–28, 1978.

[48] K. T. Atanassov, "Intuitionistic fuzzy sets, Intuitionistic Fuzzy Sets," in *Intuitionistic Fuzzy Sets*, pp. 1–137, Physica, Heidelberg, 1999.

[49] F. Smarandache, "A unifying field in logics: neutrosophic logic," in *Philosophy*, pp. 1–141, American Research Press, 1999.

[50] D. Pamučar and D. Božanić, "Selection of a location for the development of multimodal logistics center: application of single-valued neutrosophic MABAC model," *Infinite Study*, vol. 2, 2019.

[51] D. Stanujkić, D. Karabašević, G. Popović et al., "A single-valued neutrosophic extension of the EDAS method," *Axioms*, vol. 10, no. 4, p. 245, 2021.

[52] M. Yazdani, A. Ebadi Torkayesh, Ž. Stević, P. Chatterjee, S. Asgharieh Ahari, and V. Doval Hernandez, "An interval valued neutrosophic decision-making structure for sustainable supplier selection," *Expert Systems with Applications*, vol. 183, p. 115354, 2021.

[53] D. Pamucar, F. Ecer, and M. Deveci, "Assessment of alternative fuel vehicles for sustainable road transportation of United States using integrated fuzzy FUCOM and neutrosophic fuzzy MARCOS methodology," *The Science of the Total Environment*, vol. 788, p. 147763, 2021.

[54] S. Das, B. K. Roy, M. B. Kar, S. Kar, and D. Pamučar, "Neutrosophic fuzzy set and its application in decision making," *Journal of Ambient Intelligence and Humanized Computing*, vol. 11, no. 11, pp. 5017–5029, 2020.

[55] R.-x. Liang, J.-q. Wang, and L. Li, "Multi-criteria group decision-making method based on interdependent inputs of single-valued trapezoidal neutrosophic information," *Neural Computing & Applications*, vol. 30, no. 1, pp. 241–260, 2018.

[56] M. A. Hatefi, "Indifference threshold-based attribute ratio analysis: a method for assigning the weights to the attributes in multiple attribute decision making," *Applied Soft Computing*, vol. 74, pp. 643–651, 2019.
[57] H.-W. Lo, C.-C. Hsu, C.-N. Huang, and J. J. H. Liou, "An ITARA-TOPSIS based integrated assessment model to identify potential product and system risks," *Mathematics*, vol. 9, no. 3, p. 239, 2021.
[58] A. Vafadarnikjoo, M. Tavana, T. Botelho, and K. Chalvatzis, "A neutrosophic enhanced best-worst method for considering decision-makers' confidence in the best and worst criteria," *Annals of Operations Research*, vol. 289, no. 2, pp. 391–418, 2020.
[59] T. Kuo, "A modified TOPSIS with a different ranking index," *European Journal of Operational Research*, vol. 260, no. 1, pp. 152–160, 2017.

Hindawi
Complexity
Volume 2022, Article ID 2501869, 12 pages
https://doi.org/10.1155/2022/2501869

Research Article

Investigation of Fire-Fighting Evacuation Indication System in Industrial Plants Based on Virtual Reality Technology

Zhi Tang[1], **Die Zhang**[1], **Jiajing Du**[2], **Wenlan Bao**[1], **Weiran Zhang**[1], **and Jiaqin Liu**[1]

[1]*College of Mechanical Engineering, Donghua University, Shanghai 201620, China*
[2]*North Automatic Control Technology Institute, Taiyuan 030000, China*

Correspondence should be addressed to Zhi Tang; tangzhi@dhu.edu.cn

Received 6 January 2022; Revised 21 March 2022; Accepted 2 April 2022; Published 15 April 2022

Academic Editor: Yu Zhou

The fire safety of industrial buildings has always been a great concern. An excellent evacuation indicator system can guide the personnel to escape quickly, thus reducing the casualties. In this study, we present a virtual simulation fire scene based on virtual reality to explore the impact of different colors, brightness values, and flashing frequencies on escape time in case of fire emergencies. The presented scene can help shorten the time required for evacuation in an industrial plant by identifying the escape path under the fire and smoke environment and improve the escape efficiency. The results show that the green color is the most suitable color for evacuations; the escape efficiency increases with an increase in brightness, and there is no significant difference between the escape times under high and medium brightness; the evacuation time decreases with an increase in the flicker frequency. Based on these experimental results, the fire evacuation indicating system is designed. A virtual reality verification experiment is used to compare the escape efficiency of the improved design with an original factory's indicating system. The verification results show that the improved scheme reduces the evacuation time and significantly improves the psychological stress on the evacuees. This work provides a theoretical basis for safe evacuation designs.

1. Introduction

Recently, the problem of fire has become increasingly prominent. According to the data provided by the Fire and Rescue Department of the Ministry of Emergency Management, 252000 fire alarms were reported in China during 2020, including commercial buildings, industrial plants, warehouses, hotels, museums, and ancient buildings. Among these buildings, the industrial factories usually have high-density products and a considerable economic value [1, 2]. It is well known that fires in industrial plants can easily spread to nearby products, resulting in a series of secondary fires [3, 4]. Furthermore, an incident analysis that focuses on the evacuation phase has indicated the presence of a clear correlation between a delayed evacuation and a high number of fire deaths [5]. In an emergency situation, every single second plays a vital role in reducing the number of claimed lives [6]. Therefore, evacuation efficiency is particularly important.

As it is not possible to completely mitigate the fire risk [7], an effective fire evacuation indication system that enables quick evaluation of people should be designed. The existing work shows that there are three critical factors for successful fire evacuation: (1) organizational evacuation efficiency, (2) information regarding safe navigation, and (3) emotion of the evacuees [8–10]. In addition, a large amount of smoke caused by fire is one of the main reasons leading to human casualties. The smoke not only causes dyspnea but also hinders the vision leading to poor visibility and panic among the affected. An effective evacuation indication system improves the evacuation speed in the presence of dense smoke. Consequently, the number of casualties can be significantly reduced and the evacuation process can be completed calmly and efficiently.

The current research regarding fire safety considers real experiments, such as fire drills and abandoned site experiments. Guillaume et al. conducted real-scale fire tests of one-bedroom

apartments [11]. Software-based fire scene simulation models and crowd evacuation simulation models [12], and fire simulation models based on numerical methods [13], have also been used in fire-related research. Furthermore, a large number of scholars have studied the evacuation behavior in fire based on microscopic or macroscopic simulation-optimization [14]. Teng et al. extended object-oriented techniques to solve multi-objective simulation optimization problems by exploiting the concept of Pareto optimality to narrow the search space [15]. Kou et al. proposed an assignment rule integrated with the vector evaluation genetic algorithm (VEGA) to solve the multi-objective simulation optimization problem to improve search efficiency in stochastic environments [16]. Abdelghany et al. proposed a simulation-optimization framework integrating a genetic algorithm (GA) and a microscopic pedestrian simulation allocation model to realize an evacuation plan [17].

It is worth noting that real experiments not only have ethical issues associated with them but also have a high cost. The software-based simulation models and numerical models cannot obtain a realistic dataset directly based on the behaviors and responses of evacuees. Recently, the development of virtual reality has brought a new perspective on the research work regarding fire safety. Kinateder et al. [18] analyzed the strengths, weaknesses, opportunities, and threats (SWOT) of virtual reality as a fire research tool. The results showed that virtual reality could effectively help the researchers in understanding the behavior of individuals who escaped fire. Zou et al. [19] used virtual reality to analyze whether the conflict between social information and emergency signs in a smoke-filled tunnel affected the evacuation process. The results showed that the negative behavior of a few individuals would hinder the process of safe evacuation.

Ronchi et al. [20] suggested the design of flashlights at the emergency entrances and exits of road tunnels based on the experiments performed using virtual reality. The results showed that the performance of green or white flash was better than that of blue; the flash frequencies of 1 Hz and 4 Hz were better than the flash frequency of 0.25 Hz. In addition, the LEDs performed better compared to single-frequency or dual-frequency flashbulbs. Cao et al. [21] performed fire simulation experiments in a virtual museum and showed that providing an escape route plan in case of fire emergency makes evacuation easier and less time consuming. Chobbok et al. [22] conducted experiments using virtual reality and proved that the exit signs with graphic assistance have an obvious guidance value. Max et al. [23] explored the colored signs that the participants were most likely to infer as exit signs in a simulated emergency evacuation using virtual reality.

In short, many researchers have proved that virtual reality can effectively simulate the real scenes with high fidelity [24]. The existing works mostly focus on the role of guiding signs and escape route planning in case of a fire, and the impact of groups on individual escape behavior. However, these works ignore the importance of the visibility of evacuation signs in the presence of fire and dense smoke. A few researchers have objectively put forward specific improvement methods for increasing the evacuation efficiency in the presence of dense smoke. The evacuation signs directly interact with people in the fire evacuation system. The visibility of signs in the presence of fire and smoke determines the evacuation efficiency. The navigation becomes very difficult when the signs cannot provide complete spatial information [25].

Therefore, in order to fill the research gap and address the problems of poor escape efficiency of traditional evacuation indication systems, first, this work simulates a factory fire smoke scene based on virtual reality to explore the effects of different colors, brightness, and flicker frequencies on evacuation time. Second, based on the experimental results, the best color, brightness, and flashing frequency are selected to improve the evacuation indication systems in industrial plants. Last, by considering an industrial plant as the prototype, comparative verification experiments between the original evacuation and improved evacuation indication systems are performed. Figure 1 shows the experimental process. The schemes are evaluated in terms of reaction and evacuation time, psychology state assessment, and the system usability scale (SUS). The experimental results show that the improved evacuation indication system significantly enhances the escape efficiency and reduces the short-term pressure on evacuees in the presence of a fire. The highlights of this study are as follows: (1) smoke, flame, and sound effects are added to the virtual fire environment to improve the authenticity of the environment; (2) based on virtual reality technology, the influence of the evacuation indication system color, brightness, and flicker frequency on evacuees is explored; (3) the evacuation indication system is improved based on the experimental data.

2. Materials and Methods

2.1. Experiment Method. In these experiments, 3 Dimensions Studio Max (3D Max) software is used to design the 3D scenes in the virtual environment and V-Ray is used to render the real scenes. We use Unity to develop a factory scene similar to the real world. The programming language C# is used to realize the interaction between the participants and the experimental scene. A virtual factory environment includes the factory equipment and materials. Additionally, it also includes static fluorescent lamps and dynamic exit sign lamps. The lighting effect of the real factory scene is fitted through parameter design. Furthermore, we use a particle system for simulating a real fire smoke scene.

2.2. Design of Experiment. The experiment is divided into two stages: a pre-experiment and formal experiment. During the former, the participants play a simple virtual reality maze game. Its purpose is to enable the participants to adapt to the virtual environment, get familiar with the operation mode, and complete the adaptive training. The formal experiment is based on an existing evacuation indication system and depicts a real scene of a factory fire. This experiment is further divided into three sub-experiments to explore the influence of different color indicators on the direction selection by the participants, the visibility of indicators with different brightness, and the visibility of different flicker frequency indicators when a fire occurs in an industrial plant. During the evacuation process, different aspects of participants' behavior are recorded to form the dataset.

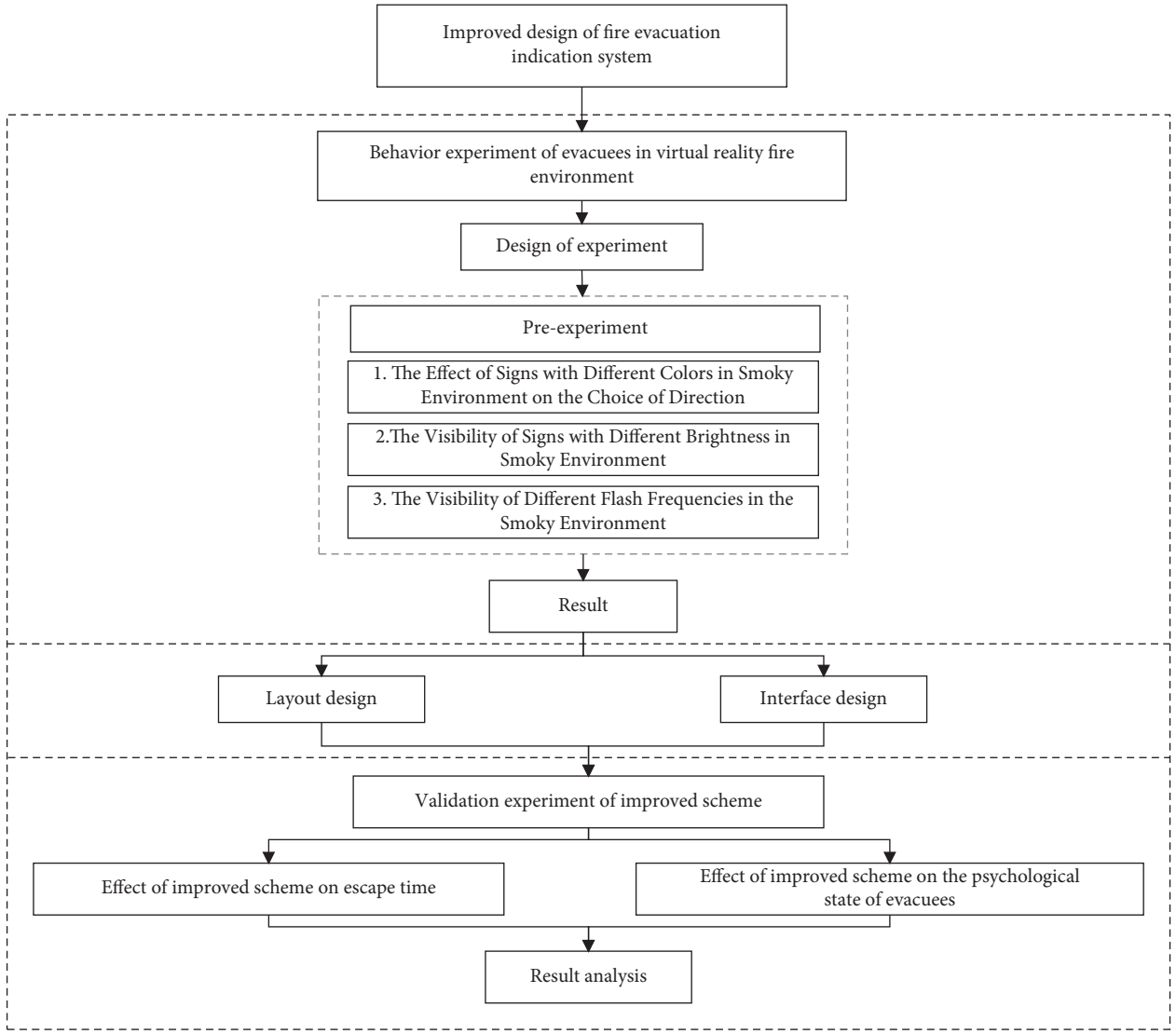

Figure 1: Experimental evacuee behavior and verification process.

2.3. Participants' Information. We recruited 24 participants to perform this experiment, including 10 males and 14 females. The ages of all the participants range from 20 to 28 years (mean age = 22.9, standard deviation = 1.44). The participants are required to be in good emotional and physical conditions. In addition, they should have a normal or corrected vision. Before the experiment, the participants are required to sign an information and consent form. The participants are also informed of the precautions required during the experiment. Each participant takes part in three experiments. If any participant feels any physical discomfort during the experiment, he/she can exit the process at any time.

2.4. Instruments Used in Experiment. The experiment is performed in the virtual simulation laboratory of Mechanical Engineering College, Donghua University. The effective space of the laboratory is three meters in both length and width. The indoor floor of the laboratory is flat and there is no interference from any other electronic devices, which ensures the normal operation of the virtual experiment.

The hardware used in the experiment includes HTC VIVE virtual reality equipment and laptops. Similarly, the software includes the game development engine Unity. The HTC VIVE VR device consists of a head-mounted display (HDM), two handheld controllers, a tracking display, and a two-controller locator (lighthouse).

2.4.1. Building of Visual Factory Fire Scene. The internal structure of a certain motor assembly plant is considered as the prototype for this experiment. We use 3D Max to model the factory, which is then imported into Unity for scene editing and development. Scripts enabling the participants to interact with the scene are written in the C programming language, as shown in Figure 2. In addition to the original production equipment in the workshop, fire-fighting equipment related to the experiment, such as indicators,

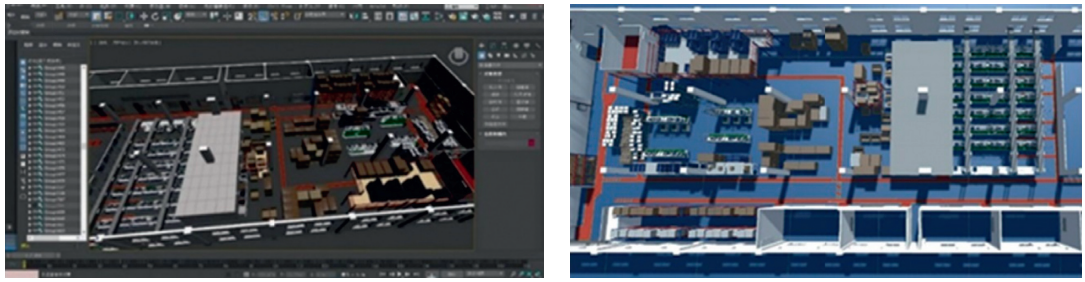

(a) (b)

Figure 2: The 3D factory model. (a) Model in 3D Max. (b) Model in Unity.

emergency lights, and fire extinguishers, are also present. The flame and smoke of incendiary objects lead to low visibility and creation of psychological panic and tension.

In the Unity framework, various parameters in the particle system provided by the software are adjusted to simulate the effect of real flame and smoke environment. In addition, the smoke alarm is triggered at the onset of the fire, and the sound module is added when the scene is restored. The direction of rotation of head-mounted display is controlled, and the speed is set equal to the speed of normal walking. The height of the human head-mounted display in the virtual scene is similar to that in the real environment. The scripts on the left- and right-hand controllers are added to achieve forward control. A camera script to control the helmet is added to realize the field of view and change the direction.

2.5. Experimental Procedure

2.5.1. Pre-Experiment. Prior to participating in the formal experiment, all the participants played a simple visual reality game of labyrinth, as shown in Figure 3. The aim of this game is to allow the participants to adapt to the visual environment and become familiar with the experimental operations. When the participants exit the door of the labyrinth, "Mission Complete" is displayed on the interface, which indicates that the participants have completed the adaptive training.

2.5.2. Formal Experiment

Experiment 1. Effect of Signs with Different Colors in Smoky Environment on the Choice of Direction

During the testing phase, the participants are present in a virtual factory scenario. Each participant is assigned a head-mounted display and a handheld controller, and a virtual factory fire scene is presented as the program starts. In order to control other variables in the experiment, the participants make choices based on the variables without being affected by the surrounding environment. Artificial changes are made to the virtual factory so that the surrounding environment is consistent. In Figure 4, the red flame icon in the factory plan denotes the location of fire. There are fire locations on the left and right sides of the start point, and the

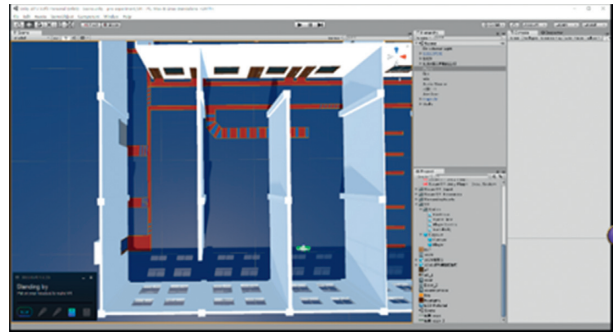

Figure 3: Adaptive environment scenario.

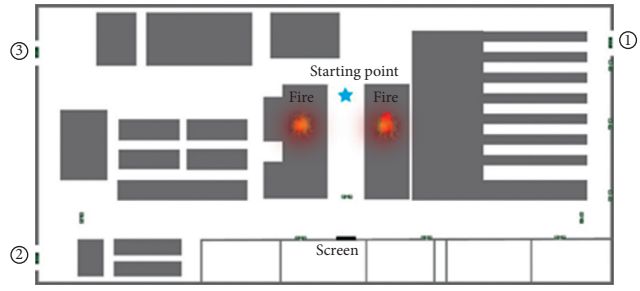

Figure 4: Floor plan of the test environment.

smoke fills the surroundings of the participants. The fire is large enough to release the smoke that spreads to the whole factory. After the onset of fire, the smoke alarms on the left and right sides go off. There is an arrow indicating the direction of evacuation on the monitor in front of the participants. The participants are required to make an escape choice according to the arrow indication and their experience, that is, they can choose to leave from either left or right. A transparent collider is set up in the Unity system when a participant traverses a certain distance after the T intersection. When the participant hits this collider, the virtual device displays "Mission Complete." The colors selected by each subject are recorded during the experiment.

The red color has the best visibility and strongest penetration ability in the presence of smoke or smog. The green color has the best semantic meaning. The blue color is particularly effective as an emergency signal [26]. Therefore, we use green, red, and blue colors in the experiment, as shown in Figure 5.

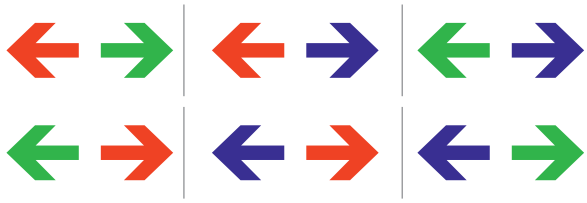

Figure 5: Arrow color map used in the experiment.

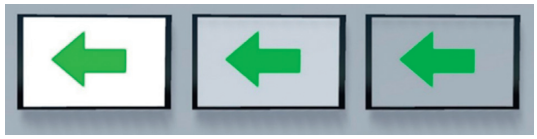

Figure 6: Schematic diagram of indicator brightness.

Experiment 2. Visibility of Signs with Different Brightness in Smoky Environment

The scene and interaction in this experiment are similar to the first experiment. In this experiment, the monitor shows a green arrow. The participants are asked to make an escape choice according to the direction indicated by the arrows. Note that the arrows appear randomly indicating either left or right direction.

Considering the human visual system, the brightness of an acceptable liquid crystal display (LCD) is up to 400 cd/m^2. The range of brightness of the human eye without fatigue is between 120 cd/m^2 to 150 cd/m^2. It is stipulated that the minimum brightness of white and green or white and red multi-color sign lamps in the factory should not be less than 5 cd/m^2, and the maximum brightness should not be more than 300 cd/m^2. Therefore, the maximum, minimum, and intermediate values, that is, 300 cd/m^2, 150 cd/m^2, and 5 cd/m^2, respectively, are selected as the experimental variables in this experiment. During the experiment, the brightness of the screen is changed each time, as shown in Figure 6. Three variables, namely high brightness, low brightness, and medium brightness are used for the convenience of subsequent statistics, and their corresponding parameter values in Unity are 1, 0.5, and 0.017, respectively. In order to eliminate the influence of other factors, the participants repeat two groups of experiments, that is, each participant completes six experiments. The random brightness sequence also appears six times. The brightness and completion time of each occurrence are recorded.

Experiment 3. Visibility of Different Flash Frequencies in the Smoky Environment

Nilsson et al. [27] observed that compared with the standard emergency exit design, the flashing lights increase the recognition of personnel. In daily life, the frequency of flashing lights working as a warning, such as the flashing light used in the car turn indicator and traffic signal light, is about 1 Hz. Therefore, 1 Hz is selected as the lower frequency. In order to ensure that normal people can observe the flickering warning light in any state, including fatigue and high tension, 30 Hz is selected as the higher flickering frequency. In order to systematically study the influence of different scintillation frequencies on the visibility in the presence of smoke, 1 Hz, 15 Hz, and 30 Hz frequencies are selected as the analysis parameters.

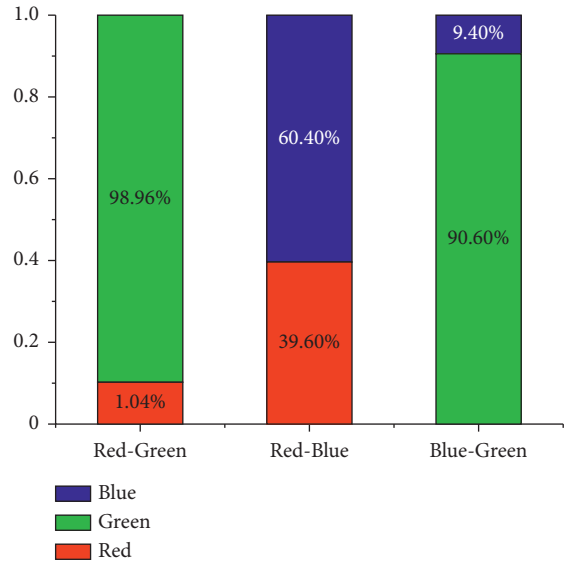

Figure 7: Statistics of experimental results.

In this experiment, the scenes and interactions are exactly similar to those of experiments one and two. There is only one green arrow on the monitor, which appears randomly towards the left or right. The participants see three different flashing frequencies, each of brightness 300 cd/m^2, which is similar to the brightness used in experiment two. The flashing frequencies are 1 Hz, 15 Hz, and 30 Hz. In order to ensure that the flickering is not affected by other factors, the random brightness sequence appears six times, and the flickering frequency is recorded each time. The participants repeat two groups of experiments, and each group participates in all six experiments. The resulting data of these experiments are included in the final statistics.

3. Results and Discussion

3.1. Analysis of the Influence of Different Color Indications on Direction Selection. Based on the statistical analysis of choices made by the participants, it can be gathered that the number of effective choices per person is 12, with a total of 24 participants. There are a total of 288 choices, among which the red is selected 39 times, green is selected 182 times, and blue is selected 67 times. According to the statistics, when the graph consists of red and green arrows, the proportion of choosing green is 98.96%; when the graph consists of blue and green arrows, the proportion of choosing green is 90.6%; and when the graph contains red and blue arrows, the proportion of selecting blue is 60.4%. As shown in Figure 7, green is the most selected color, indicating that it is considered as the safest color and can help the participants to respond quickly.

In the presence of a green arrow, 21 participants choose the green arrow, accounting for 87.5% of the total selections. The statistics show that there are only three participants who

make a random choice when the green arrow appears. After the experiment, these three participants are interviewed briefly and asked about the reasons behind their choices. The participants elaborate that they are more focused on the scene and their own experience during the experiment; therefore, they choose the direction they think is safer instead of making a choice indicated by the arrows. In fact, these participants also consider the green indicator to be safe. When red and blue arrows appear, 87.5% of the participants choose blue, and a small number of participants sometimes choose red due to the repetition of the experiment. These participants explain that the red and blue colors do not have any clear semantics regarding the safe direction. Therefore, these participants make choices according to their personal preferences. Note that 33.3% of the participants do not choose the red arrow in any case. In the postexperiment interviews, the participants explain that they consider red as the "dangerous" color; therefore, they choose the direction opposite to that shown by the red arrow.

3.2. Analysis of Visibility of Indicators with Different Brightness. The completion time and corresponding data of all the participants under different frequencies and brightness are used in the SPSS software for one-way ANOVA. In this experiment, the one-way ANOVA is used to analyze the influence of brightness on the time consumed for choosing the direction of evacuation. As listed in Table 1, the completion time in the brightness variable experiment is termed as "Time 1."

The one-way ANOVA shows that the brightness significantly affects the evacuation efficiency, with $F_{0.05}(2,141) = 17.469$, $p < 0.05$. Note that there is a significant difference between the average brightness of three cases, that is, 9.100 s (5 cd/m^2), 6.922 s (150 cd/m^2), and 6.324 s (300 cd/m^2), among all the three groups. The higher the brightness, the shorter the completion time of the experiment. The average completion times corresponding to low, medium, and high brightness are 9.100 s, 6.922 s, and 6.3240 s, respectively. There is a large difference between the average completion times for the low and medium brightness, and a small difference between the medium and high brightness. Table 2 lists the test results.

The analysis shows that the significance of low and medium brightness is $p < 0.05$. Therefore, the difference between the low and medium brightness significantly impacts the evacuation efficiency. The significance of low and high brightness is $p < 0.05$. Therefore, it can be concluded that in a scene, the difference between low and high brightness significantly affects the evacuation efficiency. However, the significance of medium and high brightness is $p > 0.05$. Therefore, it can be concluded that the difference between medium and high brightness has no significant impact on the evacuation efficiency.

The experimental results show that higher brightness leads to higher evacuation efficiency. However, there is no considerable difference between the effects of medium and high brightness values on the evacuation efficiency. The difference may lie in other errors in the experiment. Therefore, high or medium brightness can be selected when designing the evacuation indicating system.

3.3. Analysis of the Visibility of Indicators with Different Flickering Frequencies. The completion time in the flickering frequency variable experiment is termed "time 2." The one-way ANOVA of this experiment is used to analyze the effect of frequency on the time required to choose the direction of evacuation. We use SPSS to perform variance analysis of time 2 as compared to different flickering frequencies. The results are listed in Table 3.

According to the experimental results, $F_{0.05}(2,141) = 11.165$ and $p < 0.05$. The one-way ANOVA shows that brightness has a considerable impact on the evacuation efficiency. There is a significant difference between the average times of three cases, that is, 7.886 s (1 Hz), 6.716 s (15 Hz), and 5.825 s (30 Hz). The average completion times corresponding to the low, middle, and high frequencies are 7.886 s, 6.716 s, and 5.825 s, respectively. The higher the frequency, the lower the completion time. The difference between the two adjacent groups needs to be tested afterwards. The test results are provided in Table 4.

The analysis shows that the significance values of low and medium frequencies, low and high frequencies, and medium and high frequencies are $p < 0.05$. Therefore, the difference between low, medium, and high frequencies has a significant impact on the evacuation efficiency. The experimental results show that the higher the frequency, the faster and more effective the evacuation process.

4. Scenario Design

4.1. Factory Instructions Layout Design. We present a case study of the layout of an indicating system using an unmodified electrical plant as a factory prototype. The main purpose of the system is the efficient evacuation of the people. Therefore, it provides escape information to the individuals at each decision point to facilitate fast and appropriate decision making. The green squares in Figure 8 represent the location of the display, which are installed on the nearby walls by considering all the safety factors.

4.2. Indicating Interface Design. We arrange the colors selected in experiment 1 to highlight the escape direction, route, and exit. The arrows, routes, and safety exits are presented in bright green. The overall background is presented in dark blue. The base map represents a real-life view of a factory. The interface displays the location of the flame and the surrounding smoke and its concentration. Thus, it is convenient for the trapped individuals to recognize the magnitude of the fire. Additionally, the interface also displays the density of the individuals on a particular route, which is useful to the escapees for independently choosing a more efficient route. The indicated direction changes based on the amount of smoke diffusion, as shown in Figure 9. The route displayed on the system interface denotes the safest and most efficient path obtained based on the real-time analysis of data using various factors. Note that the maps in

Table 1: Analysis of completion time in brightness variable experiment.

Time1	Square sum	Degrees of freedom	Mean square	F	Significance (n_p^2)
Intergroup	204.940	2.000	102.470		
Intragroup	827.099	141.000	5.866	17.469	0.000
Total	1032.038	143.000			

Table 2: Standard error and significance of reaction time between two different brightness values.

Brightness (cd/m^2)	Mean difference (I–J)	Standard error	Significance (n_p^2)
5–150	2.178313*	0.494383	0.000
5–300	2.776042*	0.494383	0.000
150–300	0.597729	0.494383	0.229

Note. *The significance level of the mean difference is 0.05.

Table 3: Experimental data analysis results of time 2.

Time 2	Square sum	Degree of freedom	Mean square	F	Significance (n_p^2)
Intergroup	102.591	2	51.296		
Intragroup	647.795	141	4.594	11.165	0.000
Total	750.386	143			

Table 4: Standard error and significance of reaction time between two different frequencies.

Frequency (Hz)	Mean difference (I–J)	Standard error	Significance (n_p^2)
1–15	1.17063*	0.43753	0.008
1–30	2.06119*	0.43753	0.000
15–30	0.89056*	0.43753	0.044

Note. *The significance level of the mean difference is 0.05.

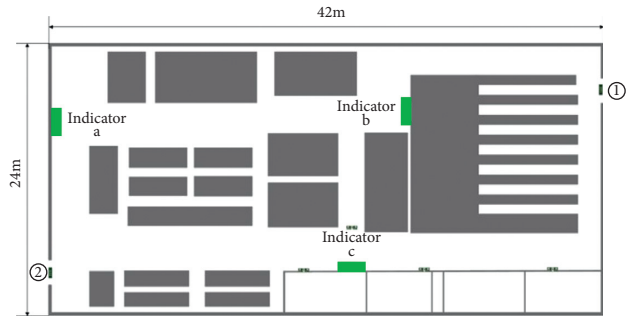

Figure 8: Layout of the factory instructions.

the display devices at different locations are different or are partially enlarged instead of a fixed and static standard map.

In experiment 2, the required evacuation time should decrease with an increase in the brightness. However, the difference between the times for high and medium brightness values is not significant ($p > 0.05$). Therefore, the energy-saving factors are also considered in the design. In case of an emergency power-off, the brightness on the display device lies in the medium range, that is, 150 cd/m^2.

In experiment 3, we observe that the escape efficiency is higher in the presence of high flickering compared to that in its low. In case of an emergency, it is necessary to transmit the most straightforward information to the individuals. Therefore, the system uses the simplest and most intuitive arrows to indicate directions, and the warning light flashes at a frequency of 30 Hz. At the same time, the warning light flickering is accompanied by a brief text, that is, "Follow the arrows and escape quickly!" to warn the individuals to evacuate quickly.

5. Design Verification and Evaluation

5.1. Instruments Used. The instruments used in the verification experiment are the same as those used in the experiments in Section 2. In addition, short stress state questionnaire (SSSQ) [28] is introduced to measure the psychological level of participants. It is a short stress state questionnaire prepared according to the Dundee Stress State Questionnaire (DSSQ) [29] and appears to be a reliable short measure of stress state, which is sensitive to task stressors. At present, the SSSQ has been widely used in the evaluation of short-term mental state changes in medicine, virtual reality, and other fields [30, 31]. It is a 24-item questionnaire that divides stress into three high-order factors: engagement, distress, and worry, which reveals the changes of emotional status throughout the experiment. Each question in the SSSQ has a score between 0 and 5, indicating totally inconsistent to totally consistent.

5.2. Participants. We recruit 36 participants to verify the proposed design. All the participants are between 18 and 28 years old, with a moderate male to female ratio.

(a) (b) (c)

Figure 9: Indication presented in the interface; (a) small smoke concentration; (b) dense smoke; (c) arrows indicating the escape routes.

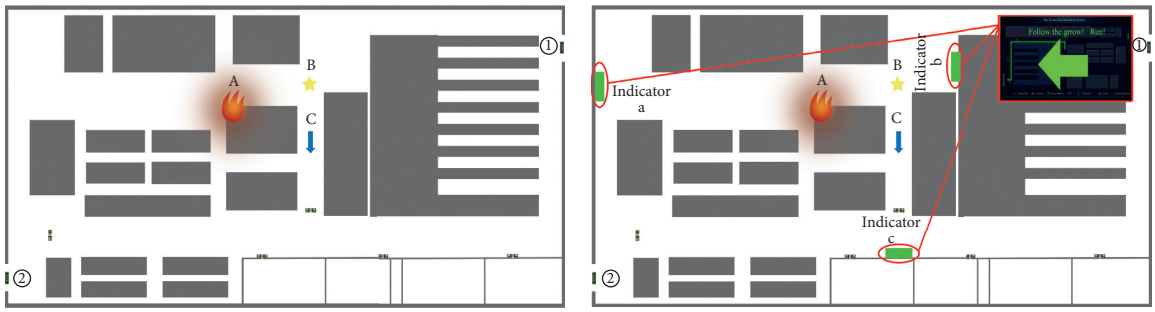

(a) (b)

Figure 10: Top view of the experimental scene. Points A, B, and C represent the fire source, starting position, and route of travel, respectively. (a) Control group; (b) experimental group.

5.3. Verification of Experimental Design. Based on virtual reality technology, we explore the changes in the escape times and psychological states to verify the effectiveness of the improved scheme. The safety exit signs, emergency lights, smoke alarms, and other necessary devices are added to the scene according to the original evacuation instruction system. The scene represents an unmodified motor packaging factory, as shown in Figure 10.

There are two exits in the factory building denoted as ① and ②. The arrows representing the safety exit signs at each location point to the safety exits. The safety signs at each T-shaped intersection are two-way arrows. The experiment is divided into two groups: 18 participants take part in the original industrial plant scene experiment, that is, the control group; the remaining 18 participants take part in the industrial plant scene experiment of the newly designed evacuation indicator system, that is, the experimental group. Compared to the control group, the experimental group has the same factory facilities except for the indicator system. In addition, the starting positions of participants in the scene at the time of accident are also the same. The moving speed in the scene is about 1.5 m/s in reality.

Prior to the experiment, all participants are required to fill the SSSQ independently as the pretest data. After the participants put on the virtual reality devices, the starting scene is represented by B in Figure 10. The arrow points represent the forward direction of the subject. The fire starts at the predefined position and will gradually increase during the experiment. There will be a large amount of smoke in front of the participants, hindering the vision, as shown in Figure 11. The inspection team adds the proposed fire-fighting evacuation system-related equipment and display

Figure 11: A participant is experimenting in the VR fire environment.

instruments. When the fire is small, there is no safety hazard on the path leading to ②, and the indicating system starts to show the escape route through ②. As the fire spreads, there is a safety hazard on the path leading to ②, and the instructing system changes the display of the escape route to ①. The remaining conditions and operations are the same as those of the control group. In addition, all participants are required to fill the SSSQ as post-test data after the completion of the experiment, and the participants in the experimental group are required to fill out the SUS questionnaire.

Three times are recorded during the two sets of experiments, that is, the time when the participant starts moving denoted as reaction time 1, the time after passing a T-shaped intersection denoted as reaction time 2, and the time required to reach the exit denoted as the escape time. The usual path is blocked due to the location of the fire. At the same time, a collider is set up in the Unity software around the fire so that the individuals cannot escape from

the usual path. Therefore, each subject passes through a T-junction in the forward direction.

5.4. Verification of Experimental Results and Analysis

5.4.1. Effect of the Improved Scheme on Escape Time. In the control group, 16 participants choose exit ① and two participants choose exit ②. After the experiment, the individuals report that the main reasons for choosing ① are as follows: first, the individuals think that the fire location is on the right-hand side. Therefore, they consider the exit as unsafe and choose the direction opposite to the fire source. Second, the individuals think that there is a door on the left, which seems to be closer to the direction of the safety exit. All the participants in the experimental group escape according to the instructions, that is, nine people choose ① and nine people choose ②. All the data are imported into SPSS. The three datasets collected from the two sets of experiments are compared separately, and the relevant sample t-test is performed. The results are shown in Figure 12.

Figure 11 compares the average time of the two groups of experiments. Based on the data of reaction time 1, reaction time 2, and the escape time, the time spent by the experimental group in each stage is less compared to the control group. This proves that after adding the improved evacuation indication system, the time required by the evacuees to select the path at each intersection is shortened. However, whether the design of fire evacuation indication system affects the escape efficiency needs to be discussed. Assumptions are present as follows:

> Null hypothesis H0: The design of the fire evacuation indication system does not affect the escape efficiency.
>
> Alternative hypothesis H1: The design of the fire evacuation indication system impacts the escape efficiency.

For each pair of data samples, the relevant sample t-test is performed, as listed in Table 5.

The significance level is $\alpha = 0.05$, which is a two-tailed test. The degree of freedom is df = 15, and the critical value is equal to tcrit = 2.131, which is obtained by checking the t critical value table. The corresponding t-values of the three data sets are 3.440, 2.747, and 3.322, respectively. The 95% confidence interval of the difference does not contain zero, and tobs > tcrit in the three sets. The actual t score is higher than the critical value. Therefore, the null hypothesis H0 is rejected, showing that the design of the fire evacuation indicating system has a significant impact on the evacuation efficiency.

The results of data processing show that the reaction time 1 (1.375 ± 0.549, average = 1.375 s, standard error of mean (SEM) = 0.549 s) of the experimental group is significantly less compared to the reaction time 1 (2.109 ± 1.066) of the control group, which is 0.734 s and $p < 0.05$ (two-tailed test). The reaction time 2 (8.130 ± 1.032) of the experimental group is significantly less compared to the reaction time 2 (9.878 ± 3.268) of the control group, where the difference between the two is 1.748 s and $p < 0.05$ (two-tailed test). The escape time of the experimental group (25.284 ± 3.061) is significantly less compared to the escape time of the control group (30.664 ± 7.531), that is, the difference between the two is 5.380 s and $p < 0.05$ (two-tailed test).

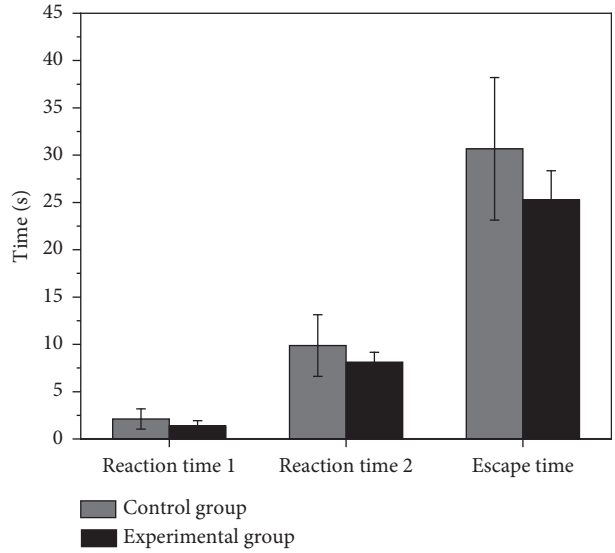

Figure 12: Average time for the control and experimental groups after the VR evacuation experiment. The error bars represent the standard error of the difference between the two groups.

Reaction time 1 is the first intuitive reaction of the participants entering the scene. The experimental group is 0.734 s faster compared to the control group. The results of reaction time 2 show that the average reaction time of the experimental group is 1.748 s less compared to the control group, and the experimental group avoids hesitation during decision making. Especially when people are in a state of tension and panic, they subconsciously follow the instructions of a clear escape direction. The final escape time of the experimental group is 5.380 s less than that of the control group, which is 17.5% higher compared to the original setting. The movement speed set in the experiment is constant; therefore, the difference in the escape times is caused by the time to make decisions. The hesitation at each T-junction leads to additional time consumption. Reducing the reaction time can quicken the response in the branch road, avoid congestion, and speed up the escape from the scene. It shows that the improved scheme significantly impacts the reaction and escape times, which greatly improves the escape efficiency: the escape efficiency increases by 17.5% compared to the original evacuation system. Grosshandler et al. found that the heat flow and temperature could be determined by a formula based on exponential growth [32]. The oxygen concentration decreases quickly, and the smoke concentration rises sharply, which can cause death in a short time [33]. Therefore, improving the evacuation efficiency can effectively reduce the physiological injuries to the evacuees and improve the survival rate.

5.4.2. SSSQ Result and Analysis. Four groups of questionnaire data prior to and after the experiment are collected. The final data are obtained by subtracting the score obtained

Table 5: Outputs of sample t-tests of three groups.

	Mean difference	95% confidence interval of difference		t	Significance (two tailed)
		Lower limit	Upper limit		
Reaction time of control group 1−reaction time of experimental group 1	0.734	0.279	1.189	3.440	0.004
Reaction time of control group 2−reaction time of experimental group 2	1.748	0.392	3.105	2.747	0.015
Escape time of control group−Escape time of experimental group	5.380	1.928	8.832	3.322	0.005

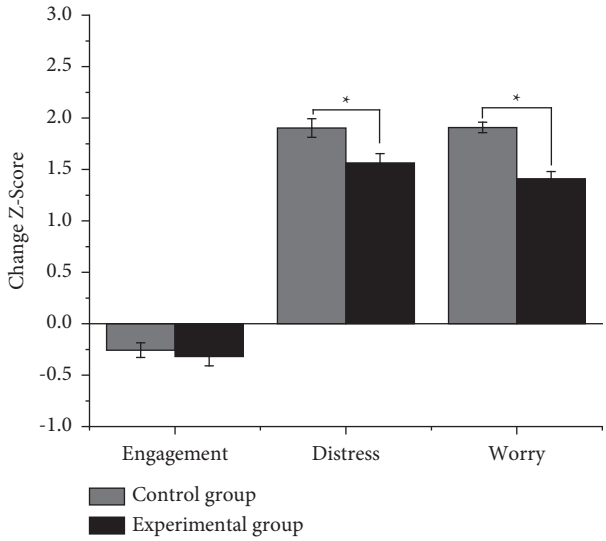

Figure 13: The average score for the control and experimental groups. The error bars represent the standard error of the difference between the two groups. Asterisks denote significant differences between the control and experimental groups. Change Z-score- = post-test score−pretest score.

after the experiment from that prior to the experiment. Six groups of data are obtained according to three high-order factors in the questionnaire. All data are imported into SPSS. Six datasets collected from the two groups of experiments are compared, and the relevant sample t-test is performed. The results are shown in Figure 13.

The statistical analysis in Figure 13 shows that the average "Engagement" scores decrease in two groups. The "Engagement" score is -0.26 ± 0.07 (average ± SEM) in the control group, while it is -0.32 ± 0.09 in the experimental group. No significant difference is found between the Engagement scores in the control and experimental groups ($t(18) = 0.529$, $p = (0.605)$, $p > 0.05$). Note that the "Distress" and "Worry" scores of both groups increase after the virtual reality fire experiment. The average "Distress" score of the control group (1.90 ± 0.09) increases more than that of the experimental group (1.56 ± 0.09). The average "Worry" score of the control group (1.91 ± 0.05) increases more than that of the experimental group (1.41 ± 0.07). In the postexperiment interviews, the participants explain that they are the most confused and afraid when facing the choice of fork roads. The evacuation indication system of the experimental group points out a clear direction, alleviating the inner pressure and fear and giving hope. The control group faces a randomly selected branch road during the escape process. It is not known whether the road ahead is safe in the smoke environment; therefore, the whole process is carried out under great pressure. We find a significant difference between the control and experimental groups in terms of SSSQ distress ($t(18) = 2.636$, $p = 0.002$, $p < 0.05$) and SSSQ worry ($t(18) = 5.757$, $p = 0.000$, $p < 0.05$). This means that the evacuation indication system of the experimental group has obvious interactions with the evacuees in the virtual reality fire environment, consequently reducing the pressure on the evacuees.

5.5. Usability Questionnaire Analysis. The SUS is a simple and quick questionnaire used to assess the usability of a specific device or product. It can produce accurate overall results in case of a small dataset. The SUS system availability scale is used to evaluate the availability of the improved fire evacuation system.

The 18 participants of the control group who participated in the verification experiment are required to fill the SUS system availability questionnaire after the completion of the experiment. The final score of the fire evacuation indication system is equal to 86.806 points. Considering the SUS score curve classification range [34], the corresponding level is $A+$, and the overall usability evaluation standard is satisfied.

6. Conclusions

Based on an existing virtual reality simulation experiment, this work investigated the influence of different colors, brightness values, and flicker frequencies on escape efficiency in case of a fire emergency. The main conclusions of this work are as follows:

(1) Green color was the most suitable escape indicator in case of a fire and smoky environment.

(2) Among the brightness levels of 300 cd/m^2, 150 cd/m^2, and 5 cd/m^2 selected in the experiment, the escape efficiency increased with an increase in the brightness. It was the highest when the brightness of the escape indicator was 300 cd/m^2.

(3) Within the identifiable range of human vision, the required escape time became shorter as the flicker frequency increased. The flicker frequency of 30 Hz resulted in the highest escape efficiency.

In addition, the fire evacuation indication system was designed according to the experimental results. The escape efficiency for the improved design and the original factory indication system was compared based on virtual reality

verification experiments to verify the effectiveness of the proposed scheme. The experimental results showed that the response and escape times in the improved scheme were reduced by 0.734 s and 5.380 s, respectively, and the overall escape efficiency increased by 17.5%. In addition, the evacuation indication system of the experimental group had obvious interaction with the evacuees in the virtual reality fire, which reduced the stress of the evacuees. The SUS score was *A*+, which met the availability standard.

The results of this work not only provided the designers with a theoretical basis and practical value for building fire evacuation system design but also highlighted the value of virtual reality for collecting human behavioral data during fire incidents. The high effectiveness of the scheme also emphasized the potential of virtual reality in future research.

Data Availability

The data used to support the findings of this study are available from the corresponding author upon request.

Conflicts of Interest

The authors declare that they have no conflicts of interest.

Acknowledgments

This work was supported by National Natural Science Foundation of China (grant no. 51775106).

References

[1] V. Stejskal, J. Hubert, R. Aulicky, and Z. Kucerova, "Overview of present and past and pest-associated risks in stored food and feed products: European perspective," *Journal of Stored Products Research*, vol. 64, pp. 122–132, 2015.

[2] L. Ding, F. Khan, and J. Ji, "Risk-based safety measure allocation to prevent and mitigate storage fire hazards," *Process Safety and Environmental Protection*, vol. 135, pp. 282–293, 2020.

[3] J.-Y. Ma, "Analysis on the fire risk existing in the storage of textile materials and textile goods," *Procedia Engineering*, vol. 71, pp. 271–275, 2014.

[4] N. Ren, J. de Vries, X. Zhou, M. Chaos, K. V. Meredith, and Y. Wang, "Large-scale fire suppression modeling of corrugated cardboard boxes on wood pallets in rack-storage configurations," *Fire Safety Journal*, vol. 91, pp. 695–704, 2017.

[5] D. Bensilum, "Quantification of behaviour for engineering design standards and escape time calculations," *Safety Science*, vol. 38, no. 2, pp. 157–182, 2001.

[6] O. Hosseini, M. Maghrebi, and M. F. Maghrebi, "Determining optimum staged-evacuation schedule considering total evacuation time, congestion severity and fire threats," *Safety Science*, vol. 139, p. 16, 2021.

[7] J.-H. Lee, W.-J. Kim, and W.-H. Hong, "Fires and fire prevention measures in Korea from 1392 to 1910," *Fire Safety Journal*, vol. 61, pp. 116–126, 2013.

[8] G. Proulx, "Evacuation time and movement in apartment buildings," *Fire Safety Journal*, vol. 24, no. 3, pp. 229–246, 1995.

[9] G. Proulx, "A stress model for people facing a fire," *Journal of Environmental Psychology*, vol. 13, no. 2, pp. 137–147, 1993.

[10] K. Fridolf, D. Nilsson, and H. Frantzich, "Fire evacuation in underground transportation systems: a review of accidents and empirical research," *Fire Technology*, vol. 49, no. 2, pp. 451–475, 2013.

[11] E. Guillaume, F. Didieux, A. Thiry, and A. Bellivier, "Real-scale fire tests of one bedroom apartments with regard to tenability assessment," *Fire Safety Journal*, vol. 70, pp. 81–97, 2014.

[12] J. Wang, J. Li, J. Li et al., "Performance optimization of the obstacle to corner bottleneck under emergency evacuation," *Journal of Building Engineering*, vol. 45, p. 45, 2022.

[13] L. M. Dorin, I. Vlad, and N. Ilinca, "Experimental and numerical study on the influence of mechanical ventilation on the survival conditions in a room set on fire," *Modelling in Civil and Environmental Engineering*, vol. 16, no. 2, 2021.

[14] X. Li, B. Huang, Z. Liu, X. Zhang, and J. Sun, "A novel method for planning a staged evacuation," *Journal of Systems Science and Complexity*, vol. 25, no. 6, pp. 1093–1107, 2012.

[15] S. Teng, L. Hay Lee, and E. Peng Chew, "Multi-objective ordinal optimization for simulation optimization problems," *Automatica*, vol. 43, no. 11, pp. 1884–1895, 2007.

[16] G. Kou, H. Xiao, M. H. Cao, and L. H. Lee, "Optimal computing budget allocation for the vector evaluated genetic algorithm in multi-objective simulation optimization," *Automatica*, vol. 129, 2021.

[17] A. Abdelghany, K. Abdelghany, H. Mahmassani, and W. Alhalabi, "Modeling framework for optimal evacuation of large-scale crowded pedestrian facilities," *European Journal of Operational Research*, vol. 237, no. 3, pp. 1105–1118, 2014.

[18] M. Kinateder, E. Ronchi, D. Nilsson et al., "Virtual reality for fire evacuation research," in *Proceedings of the 2014 Federated Conference on Computer Science and Information Systems*, Warsaw, Poland, September 2014.

[19] H. Zou, N. Li, and L. Cao, "Emotional response-based approach for assessing the sense of presence of subjects in virtual building evacuation studies," *Journal of Computing in Civil Engineering*, vol. 31, no. 5, Article ID 04017028, 2017.

[20] E. Ronchi, D. Nilsson, S. Kojić et al., "A virtual reality experiment on flashing lights at emergency exit portals for road tunnel evacuation," *Fire Technology*, vol. 52, no. 3, pp. 623–647, 2016.

[21] L. Cao, J. Lin, and N. Li, "A virtual reality based study of indoor fire evacuation after active or passive spatial exploration," *Computers in Human Behavior*, vol. 90, pp. 37–45, 2019.

[22] C. Kim, M. Hur, Y. Oh, J.-H. Choi, and J.-J. Jeong, "The effect of the running-man emergency exit sign and its installed location on human directional choice," *Applied Cognitive Psychology*, vol. 30, no. 6, pp. 1014–1019, 2016.

[23] M. Kinateder, W. H. Warren, and K. B. Schloss, "What color are emergency exit signs? Egress behavior differs from verbal report," *Applied Ergonomics*, vol. 75, pp. 155–160, 2018.

[24] K. Krosl, D. Bauer, M. SchwaRzler, H. Fuchs, G. Suter, and M. Wimmer, "A VR-based user study on the effects of vision impairments on recognition distances of escape-route signs in buildings," *The Visual Computer*, vol. 34, no. 6-8, pp. 911–923, 2018.

[25] K. L. Lovelace, M. Hegarty, and D. R. Montello, "Elements of good route directions in familiar and unfamiliar environments, Spatial Information Theory," in *Cognitive and Computational Foundations of Geographic Information Science*, C. Freksa and D. M. Mark, Eds., pp. 65–82, 1999.

[26] T. Yamada and Y. Akizuki, *Visibility and Human Behavior in Fire Smoke*, Springer, New York, NY, USA, 2016.

[27] D. Nilsson, H. Frantzich, and W. Saunders, "Coloured flashing lights to mark emergency exits - experiences from evacuation experiments," *Fire Safety Science*, vol. 8, pp. 569–579, 2005.

[28] W. S. Helton, W. College, and O. Wilmington, "Validation of a short stress state questionnaire," *Proceedings of the Human Factors and Ergonomics Society Annual Meeting*, vol. 48, no. 11, pp. 1238–1242, 2004.

[29] G. Matthews, L. Joyner, and K. Gilliland, "Validation of a comprehensive stress state questionnaire: towards a state big three?".

[30] R. M. S. Clifford, S. Jung, S. Hoermann, M. Billinghurst, and R. W. Lindeman, "Creating a stressful decision making environment for aerial firefighter training in virtual reality," in *Proceedings of the 2019 IEEE Conference on Virtual Reality and 3D User Interfaces (VR)*, pp. 181–189, Osaka, Japan, March 2019.

[31] N. H. Alsuraykh, M. L. Wilson, P. Tennent, and S. Sharples, "How stress and mental workload are connected," in *Proceedings of the 13th EAI International Conference on Pervasive Computing Technologies for Healthcare*, pp. 371–376.

[32] W. L. Grosshandler, N. Bryner, D. Madrzykowski, and K. Kuntz, "Report of the technical investigation of the station nightclub fire (NIST NCSTAR 2)," *Nist Ncstar*, vol. 1, 2005.

[33] L. Zhang, X. Wu, M. Liu, W. Liu, and B. Ashuri, "Discovering worst fire scenarios in subway stations: a simulation approach," *Automation in Construction*, vol. 99, pp. 183–196, 2019.

[34] T. Tullis, B. Albert, and T. Tallis, *User Experience Measurement*, Mechanical Engineering Press, 2009.

Hindawi
Complexity
Volume 2022, Article ID 3519989, 10 pages
https://doi.org/10.1155/2022/3519989

Research Article

Maintaining Diversity in Parallel Problem Solving: The Influence of Network Structure and Learning Strategy

Hua Zhang [1] **and Chunhui Cao** [2]

[1]*Business School of Huaqiao University, Quanzhou, Fujian, China*
[2]*School of Business and Management, Shanghai International Studies University, Shanghai, China*

Correspondence should be addressed to Chunhui Cao; chunhui.cao@shisu.edu.cn

Received 28 November 2021; Revised 1 March 2022; Accepted 3 April 2022; Published 14 April 2022

Academic Editor: Yu Zhou

Recent research on maintaining diversity in parallel problem solving takes into consideration only network structure, without considering the agents' learning strategies. In this paper, we use a simulation study to extend March's classic model by using locomotion and assessment as agents' problem-solving strategies. First, we present a simulation framework that consists of external environment, communication networks, and agents' learning strategies. Second, based on the framework, we develop March's model to depict external environment. Third, we introduce four archetypical networks: a regular network, a small-world network, a preferentially attached network, and a totally connected network as agents' communication structure. Finally, we design three experiments to explore the performance implication of locomotors and assessors under different networks. Results suggest that network structure affects performance more than learning strategy. The more efficient the network is at diffusing knowledge, the better the performance in the short run but the worse in the long run. Locomotors can help keep diversity; a high proportion of locomotors' team has a better final performance but need more equilibrium time. Furthermore, moderate composition among locomotors and assessors increases costly interaction uncertainty. We discuss the findings' implications for the regulatory mode and problem-solving literature.

1. Introduction

Much of practical problems consist of a "large number of parts that interact in a nonsimple way" [1]; such complex problem solving can be conceptualized as a parallel problem-solving process, which is the popular phenomenon in social science and engineering. A useful metaphor of a "rugged performance landscape" is introduced by Levinthal and Siggelkow to illustrate the complex problems and search process [2–4]. Problem complex arises from choices spanning over the horizontal dimensions and each possible combination of choices is represented as a performance score along the vertical dimension. The performance landscape is full of peaks meaning the higher score and valleys representing the lower score. As boundedly rational actors, agents are randomly located on the landscape [5, 6]. They interact with each other and hold different learning strategy to improve the team performance.

Facing parallel problem agents are hampered by a myopic search process. Since most of these peaks are "local" peaks, one that is easily leading the agents stuck into the local optima. Although current computational modeling research on problem solving guides us to how to assess the nature of the fitness landscape, two key factors need to be addressed in order to generate more meaningful contributions: network structure and learning strategy. The core part in understanding parallel problem solving is how team members solve problems collectively. Social network literature assumes that agents gain information from their communication network. We assume that agents will explore the problem space meanwhile watching the others [7]. Agents look at what other agents are doing. If they find a superior solution from their neighbors with who are connected, they will imitate that solution. Network structure, therefore, determines how well the knowledge about the solution is diffused in the team. In parallel problem solving,

communication network affects the collective performance. Furthermore, although several studies have examined the outcomes of agents' cognitive representation, they have paid less attention to locomotion and assessment, two popular orientations towards movement [8]. According to regulatory mode theory, we define locomotion as shifts from state to state and assessment as comparison between options [9]. Overall, consistent with extant literature, we move beyond a simple rugged performance landscape, since such traditional model cannot take network structure and behavior orientations into account. We, therefore, propose a computational model linking network structure and locomotion and assessment orientations together, which could then shed light on how to maintain diversity in parallel problem-solving research.

The main contributions of this paper are summarized as follows:

(1) To the best of our knowledge, ours is the first study to simulate locomotion and assessment orientations in a computational model to explore the nonlinear relationship between search behavior and dynamic environment, extending the traditional March's model.

(2) We extend the current research on regulatory mode theory in the context of interaction pattern. Most studies on regulatory mode are rooted in psychology. We highlight its value in predicting agents' problem-solving strategy and believe this may shed light on artificial intelligence research.

The rest of the paper is organized as follows. "Related Work" introduces the related work about NK model, March's model, and their variants. "Model" proposes the definition and characteristics of performance landscape, searching strategy, and our algorithm. The experimental results are reported and analyzed in "Result" part. "Conclusion" part concludes the performance implications of search strategies on changing performance landscapes and discusses the future work.

2. Related Work

2.1. Exploration versus Exploitation in Parallel Problem Solving. Imagine the situation of a team leader who takes in charge of the whole software development process, during which all the team members face the complex problem and share the new knowledge to solve the problem. This scenario is what we label parallel problem solving, in which all the team members face the same complex problem, and any agent who gets progress will not affect others [10]. The payoff of any agent's achievement is independent of others'. Besides, agents can observe other agents' action, absorb and learn the successful solution, and explore the next new possible alternatives based on the previous one. Facing the parallel problem solving, there are two challenges confronting the team leader: one is how to organize the interpersonal communication structure among the team members. According to the previous literature, network structure influences the learning speed, and there is a significant tradeoff between learning speed and average performance. The other one is to how to control the ratio between assessment and locomotion, which are popular cognitive behavior model among team members. Psychologists have paid considerable attention to the consequences of locomotion versus assessment, which definitely affect the learning speed and affect the final performance. In a word, the team leader should decide what kind of communication structure is applied. Is it better to let team members involve in a density network, a proven successful solution will spread fast among the team.

The balance between learning speed with final performance can be seen as the trade-off between exploration and exploitation [11, 12]. According to the seminal research of James March, exploration can be viewed as introduction of new information and development of new solutions, while exploitation involves developing existing knowledge [13]. In March's simulation model, there are fast learners and slow learners. Fast learners exploit the organization's existing knowledge, which leads to a high-performance level in the short run. Fast learners, however, are likely to reduce the diversity of organizational solutions, which leads to a low performance level in the long run. Slow learners, though less efficient, allowed the firm to keep diversity of agents' solutions, which enables the team to explore a higher-level performance of possible combinations of solutions and leads the team to an optimal equilibrium. March's work demonstrates the trade-off between exploration and exploitation, which represents a fundamental conflict between short-run and long-run development in almost all complex self-adaptive systems. In Lazer and Friedman's computational work, parallel problem solving can also be seen as a balancing of exploration and exploitation [14]. In parallel problem solving, agents can explore the possibility of combination of solutions or exploit the existing solutions by imitating the neighbor's solution through interpersonal network.

2.2. Network Structure. Agents will learn each other's solution through interpersonal network. In March's model, an organizational code was designed to represent a hub-like structure in which agents' superior solutions are put together, and agents, in turn, can learn from the organizational code. Although there seems no communication structure in March's model, March in fact implicitly assumed a hub-like interpersonal network. Miller et al. extended March's model by adding direct interpersonal learning, in which agents are randomly situated within a grid [15]. Agents can contact their direct four neighbors and learn from the best one. If the neighbors are inferior to the focal agent, agent then engages in "distant learning" by randomly drawing any other four agents from the whole organization and choose the best one to imitate. Believing that network structure will amplify the trade-off between exploration and exploitation, Lazer demonstrated the impact on the final performance level of networks: a linear network, a totally connected network, a variety of random networks, and a variety of small-world networks [14]. The results show that an efficiency network,

which is very good at disseminating information and promoting agents imitate each other, will reduce the diversity in team and lead to a higher performance level in the short run but lower level in the long run, while inefficient network maintains diversity and leads to a higher performance level in the long run. Fang et al. follow the exploration and exploitation research stream and propose a very special network structure: semi-isolated subgroups [16]. In their simulation mode, organization is divided into some subgroups and there are some hub-like actors that connect the subgroups. Then, they explore how the degree of subgroup isolation and intergroup connectivity affects the trade-off between exploration and exploitation. Their model demonstrates that moderate levels of intergroup links will maintain the diversity and perform best. Particularly, Fang's model assumes that exploration happens in each subgroup, in which agents conduct parallel problem solving and are isolated from the other subgroups, while exploitation happens in intergroup, in which agents learn superior solution across the group. In this way, a productive balance between exploration and exploitation will be achieved.

As we noted above, prior research has found that parallel problem solving involves the balance of exploration and exploitation and that communication network structure may amplify the problem by controlling the learning speed among agents [17–19]. Efficient network may reduce the diversity and destroy the possibility of future exploration. Some special network like semi-isolated subgroup may help to solve this problem.

2.3. Assessment versus Locomotion in Learning. Although many scholars admit that network structure plays an important role in balancing the trade-off of exploration and exploitation, little attention has been paid to agents' learning strategies, which fundamentally affect learning rate and maintaining diversity. Prior studies following the March's milestone work view the innovation and imitation as the basic behavior rules among agents [20, 21]. Each step agent either explores another new combination of knowledge element (innovation) or imitates other's solution directly or indirectly. Actually, in practice, there is a wide range of behaviors; also psychologists have paid considerable attention to the behavior type under knowledge diffusion situation. It is certainly useful to consider more useful behavior rules when we simulate the team process.

Recent research has focused on agents' strategies as a mechanism for problem solving. Wu's seminal research proposed dummy queries to cover up user queries and thus protect user privacy [22–24]. Shigen et al. established the malware propagation model in WSNs according to the mixed Nash equilibrium strategy [25]. Zhou et al. proposed a Heterogeneous Susceptible-Infectious-Removed-Dead (HSIRD) model based on epidemiology to represent the HSN communication connectivity [26]. In a word, agents' strategies are, indeed, conducive to performance.

According to regulatory mode theory, locomotion and assessment modes are considered to be both more general and more independent behavior rules [8, 9]. Regulatory mode theory proposes that locomotion involves movement from state to state. Traditional mode theory believes that locomotion refers to moving from the current state to a desired or valuable end, but recent studies show that the destination is unnecessary desirable or valuable, a locomotion can be any change of position. A locomotion prefers "move" to "stay"; even the current state is proven to be inherently positive. Most generally, "assessment" refers to comparing the current state and the end state. The keywords for assessment are measuring, interpreting, evaluating, and making comparisons.

In parallel problem-solving context, as the essential nature of assessment involves comparing oneself to some norms, agents with a high assessment orientation are sensitive to social standards and they want to improve their performance. High assessors are more likely to conduct long-distance learning, that is, considering the whole alternatives in team and choosing the best one to imitate. By contrast, as the essential nature of locomotion involves moving from one state to another without particular destination, agents with a high locomotion orientation intent to do "something, anything, other than the same thing." High locomotors are more likely to explore any possible combination of knowledge element by themselves or imitate the direct neighbors' solution. Although this movement may lead to an inferior solution, the movement itself satisfies the locomotors' desire.

3. Model

3.1. Simulation Framework. In this section, we describe the simulation experiment design and model draw on March's work. In Figure 1, we show the simulation framework adopted by this paper as well as examples (where the green profile represents the locomotors while the red represent the assessors). From Figure 1, we can see that simulation model consists of external environment, communication networks, and agents' learning strategies, which will be described, respectively, as follows. Besides, three experiments are set to explore the relationship between agents' search behavior and dynamic environment.

We regard an agents' team as a complex adaptive system facing complex problem, where agents interact with one another based on communication network. In particular, we view agents as carriers of ideas and knowledge and team performance as a result that emerges from interactions among agents. Based on self-regulation theory, agents are either assessors or locomotors distinguished by different learning strategy. This assumption of learning strategy makes our paper distinct from March's (1991) work. In experiment 1 and experiment 2, we will explore the performance implication of communication network with the same learning strategy, which means all the team members are locomotors or assessors. In experiment 3, team consists of both locomotors and assessors. Particularly, the proportion of locomotors and assessors is designed as 0.1, 0.2, 0.3, 0.4, 0.5, 0.6, 0.7, 0.8, 0.9, 1. We will explore the performance implication of these different proportions under different network structures.

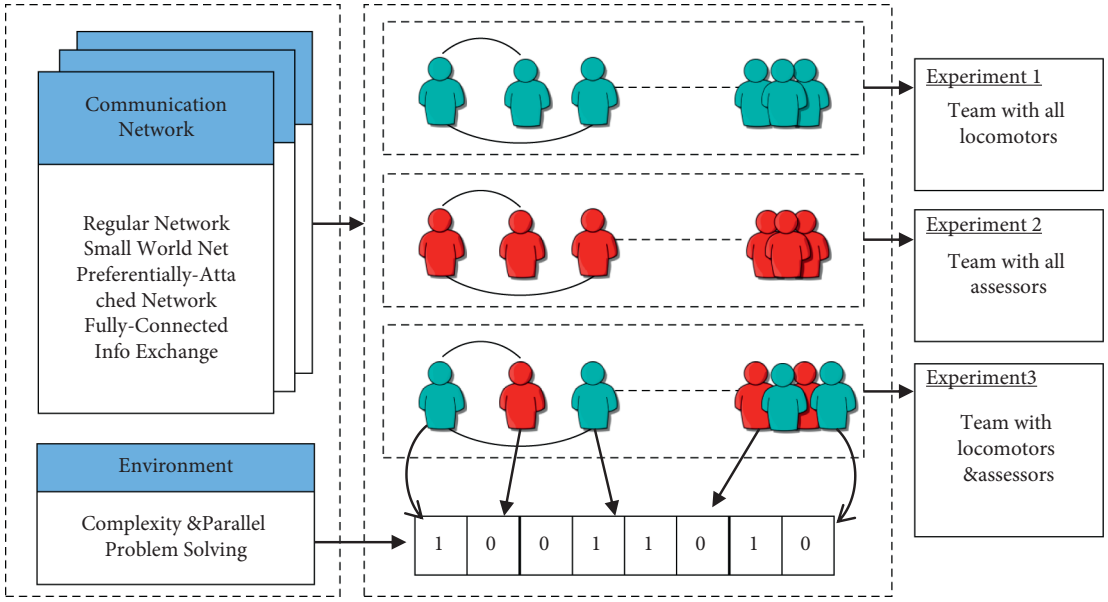

Figure 1: Simulation experiment framework.

3.2. External Environment Landscapes. To simulate the complex problem solving, prior literature uses NK landscape or March's model to model the degree to which alternative choices are correlated with one another. In NK model, N represents the number of distinct choices in an overall solution. The variable K refers to the extent to which the payoff of one choice depends on others [27, 28]. The landscape is the mapping from N choices to a payoff value. The variable N definitely determines the complexity of landscape, while the variable controls the degree of rugged landscape (see Figure 2). Similarly, March used m-dimensional vector to model the external environment, in which every dimension is randomly assigned the value of 1 or −1. The bigger m is, the more rugged the external environment landscape is.

Both models can perfectly depict the complex environment and parallel problem solving. For instance, a number of decisions constitute the solution of a team's software develop process, including the decisions about which programming language should be chosen, Java or Python, which jobs should be done in team or outsourcing. Notice that the payoff of some particular choice is correlated with others; for example, team members are more likely to use Python rather than Java, so if team leaders decide to do themselves, then Python will be preferred. Consider the situation agents will learn each other from interpersonal network, and Miller et al.'s extending work has been demonstrated successfully, we adopt March's classic model [15].

Agents have their own knowledge about the external environment; their beliefs about each of the M dimensions can be the value 1, 0, or −1, which reflect the right, absent, and wrong. All the agents can adjust their knowledge through their own learning strategies, which determine the extent to which dimensions of the beliefs match each other.

3.3. Network Structure. Implicit in March's model is the assumption that agents learn from an organizational code, which reflects the most beliefs among better performers. By contrast, Miller extended March's model by introducing the interpersonal networks. Agents can learn from each other and it is unnecessary to exchange knowledge mediated by organization codes. Following the prior literature, in our simulation model, we examined four archetypical networks: a regular network, a preferentially attached network, a variety of small-world networks, and a totally connected network.

A regular network is one in which each node connects to its four direct neighbors (see Figure 3(a)). The regular network likes grid in Miller.'s research mentioned before. To hold the density constant, we use the same number of links to construct a small-world network. A small-world network is constructed based on Watts and Strogatz's model. Both high cluster parameter and short path distances can be seen in a small-world network. To keep the same number of network ties with regular network, we then randomly cut down some local links and rewire the long-distance nodes. In this way, as Figure 3(b) demonstrates, the average path distance in regular network will be lowered. If we rewire more local links, the average path distance would drop rapidly. In the meantime, fixed number of neighbors makes sure the high cluster parameter, which makes the regular network into a small-world network.

A preferentially attached network reflects Matthew's effect, which indicates that the more friends you already have, the more new friends you will have. New links preferentially attached to the nodes whose links are the most. In our model, every agent links to another at a certain proportion; occasionally agent may become isolated vertex with very low probability (see Figure 3(c)).

A totally connected network (see Figure 3(d)) is one in which every node connects with every other node. In simulation, we keep the number of nodes constant, and then construct a totally connected network.

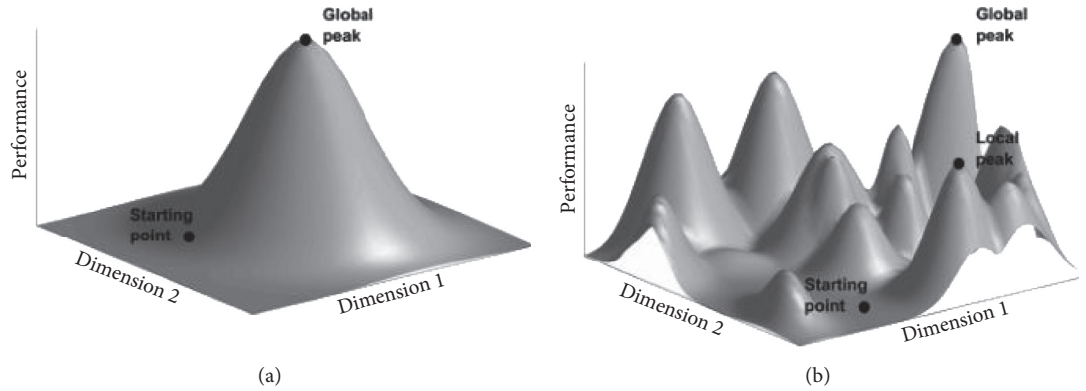

Figure 2: Stylized performance landscapes (from [29]).

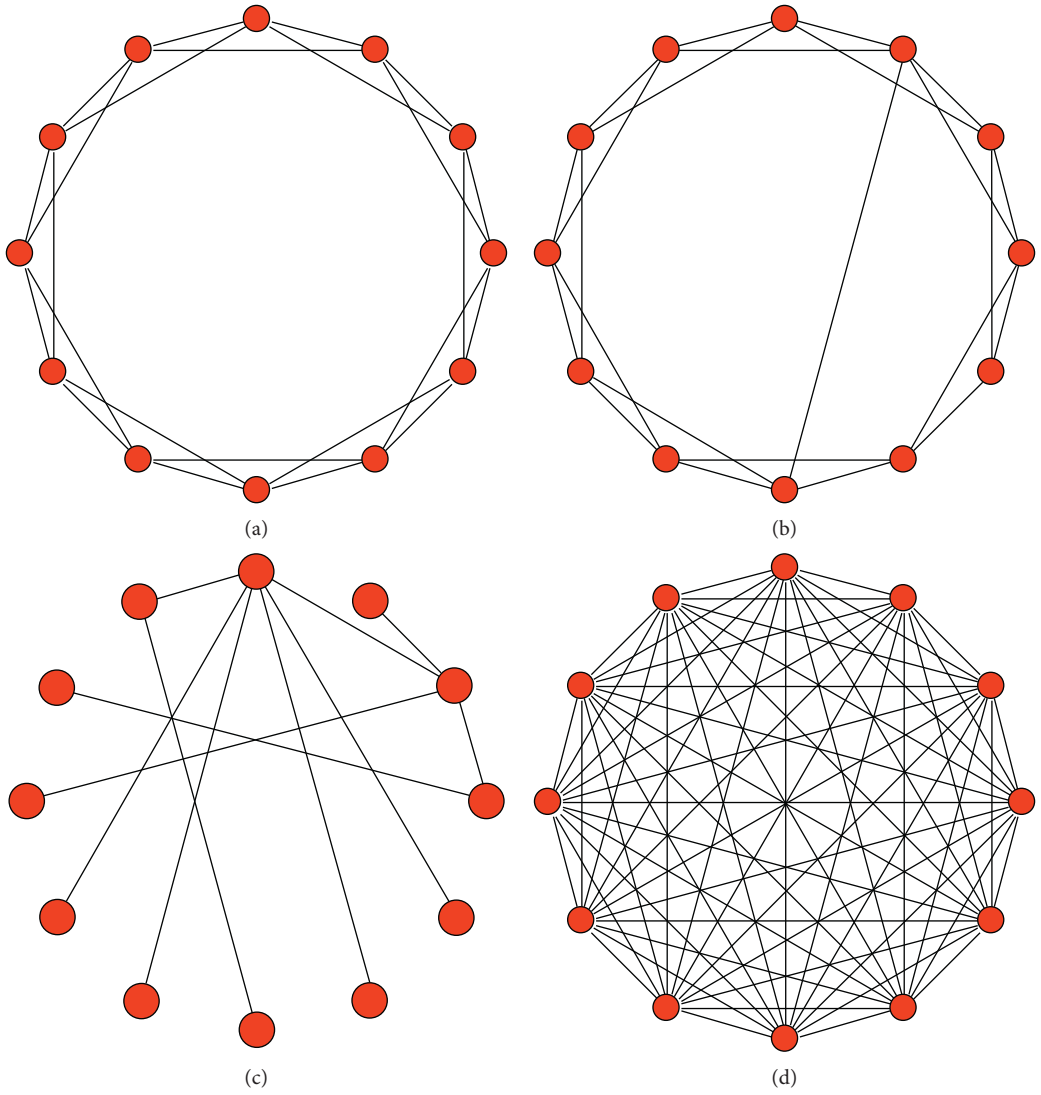

Figure 3: Graphic representation of the four network types. (a) Regular network. (b). Small-world network. (c) Preferentially attached network. (d) Totally connected network.

Because of the same number of network ties and nodes, regular network and small-world network have the same density which is defined as the potential ties divided by the real existing ties. Obviously, the density of a totally connected network is the maxim, 1. The average path distance, which is defined as the steps one node takes to reach another

one, is quite different among the three networks. In simulation, we will explore the impact of density and average path distance on final performance.

3.4. Learning Strategies. Having introduced the complex network properties of the model, we will turn our attention to agents' learning strategies, accounting for regulatory mode theory locomotion refers to moving from one state to another. Assessment refers to measurement, comparison, and evaluation. Locomotors keep moving while assessors love evaluating. A proportion q $(0 < q < 1)$ of the beliefs is constructed to reflect the difference between the two agents.

Agents learn through complex interpersonal network. In each period, agents involve finding the best performers among their neighbors who are directly connected. Once best performers are identified, agent will update q proportion of the beliefs to that superior neighbor. Consider the characteristic of locomotion and assessment we discussed above, locomotors have low value of q proportion because of their intent to move. Locomotors cannot wait for a long evaluation time to move from one state to another; they are eager to change the status quo no matter what this change will lead to their future performance. On the contrary, assessors love comparing the details between their beliefs to the superior neighbors. A high value of q proportion of assessor's beliefs will be updated according to their superior neighbors.

Another two situations should be taken into our consideration: if all the neighbors have the equal best beliefs, then locomotors or assessors will choose one randomly as the target to imitate. If all the neighbors have beliefs inferior to the agents, then the agents stop updating their beliefs. Implicit in this design of learning strategies is the assumption that agents can learn from each other in their own way. It is reasonable to assume that different learning strategies lead to different learning rate, regardless of the structure of the interpersonal network. Even though the interpersonal network's density may be the same, the aggregate team-level performance differs depending on the composition of assessors and locomotors. Implication in design of the different imitation proportion q of assessors and locomotors is the assumption the agents differ in their frequency with which they update beliefs. We incorporate this assumption into the model by having considering the agents different learning strategies. These output differences are reflected in the speed the team gets equilibrium and the final performance achieved.

4. Results

4.1. Implementation. We use MATLAB R2011b to construct our model and its picture software toolkit to report the final result figures. We consider a team of 50 agents who engage in solving a parallel problem. The problem is modeled as an m-dimensional vector whose element is assigned 1 or −1 randomly. Agents hold the same m-dimensional vector whose element is assigned 1, −1, or 0, respectively, meaning the right, the wrong, and not sure with the reality. The agents' initial beliefs are randomly generated, and those 50 agents are randomly placed on complex interpersonal network. Four networks are designed following the algorithm discussed above. Every agent's performance is calculated as the proportion of their right beliefs. In each period $t = 1, 2, 3, \ldots, T$, all agents seek the best performance of neighbors and update their beliefs with a certain probability, and we tracked the average performance of the team. Through repeated attempts and experiments, we put 200 as the equilibrium time when all the agents had the same performance levels. We adjusted the parameter values of the model and let every simulation model run for 100 times and calculated the average performance. The detailed summary of model parameters can be seen in Table 1.

4.2. Analysis

4.2.1. Experiment 1: Locomotion Learning Strategy on Different Network Structures. Figure 4 shows the performance over 100 simulations of four interpersonal networks under locomotion learning strategy over time. When all the agents are locomotors, Figure 3 demonstrates clearly the four patterns: the totally connected network is the first one to find the best solution and outperforms the other networks in the short run, but in the long run, regular network and small-world network perform better than it. Because of the isolate nodes, preferentially attached network cannot be a single component, which leads to the worst performance level.

When we focus on three single-component network structure: regular network, small-world network, and totally connected network, we can get the conclusion that having fewer communication opportunities will improve the long-run performance. Our model is close enough to the prior literature, March's model and Miller's model. The fully connected network drives out diversity with a very fast speed, which leads to a local optimum. On the contrary, regular network and small-world network can keep the diversity for quite a long time, which means that most agents' beliefs are worse than the best one in team, but a better solution will be found in the long run. The diversity will allow the regular network and small-world network to improve the solution in the long run and finally reach the global optimum. Small-world network is much more efficiency at diffusing knowledge due to the short average path even though they have the same density. When we compare the results of regular network and small-world network, we can conclude the more efficiency at diffusing information the lower performance level they reach in the long run.

4.2.2. Experiment 2: Assessment Learning Strategy in Different Network Structures. When all the team members are assessors, we can get four similar performance curves as Figure 5 shows. Figure 5 demonstrates a very clear trade-off between effective at information diffusing and final performance level. Fully connected network has the maximum density and small-world network has the shorter average path, which let all the agents quickly update their beliefs when they find the best neighbor. Furthermore, compared to

Table 1: Summary of model parameters.

Parameter type	Name	Definition	Values
Team	L	Number of team members	50
	P	Proportion of locomotors and assessors	
Communication network	RU	Regular network	None
	PA	Preferentially attached network	None
	SW	Small-world network	None
	TC	Totally connected network	None
Task characteristic	M	Number of beliefs	30
	K	Task complication	4
Learning strategy	Locomotion	Imitating the best performer with a low q to change the status quo	0.2
	Assessment	Evaluate the detailed beliefs of the best performer with a high q	0.8

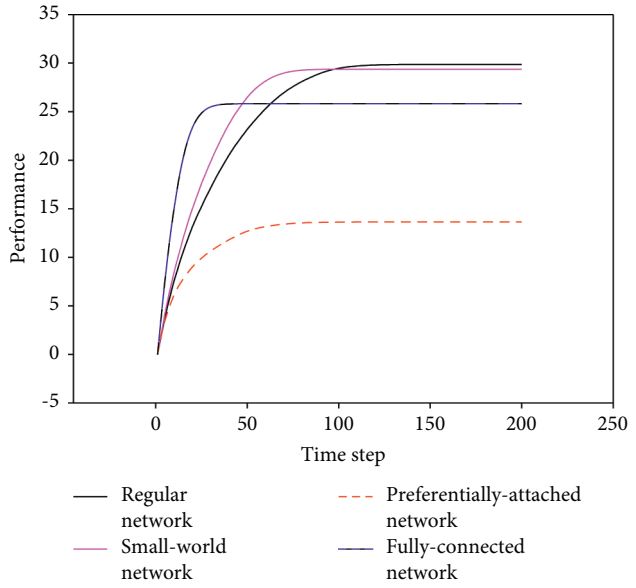

Figure 4: Locomotion learning in different network structures.

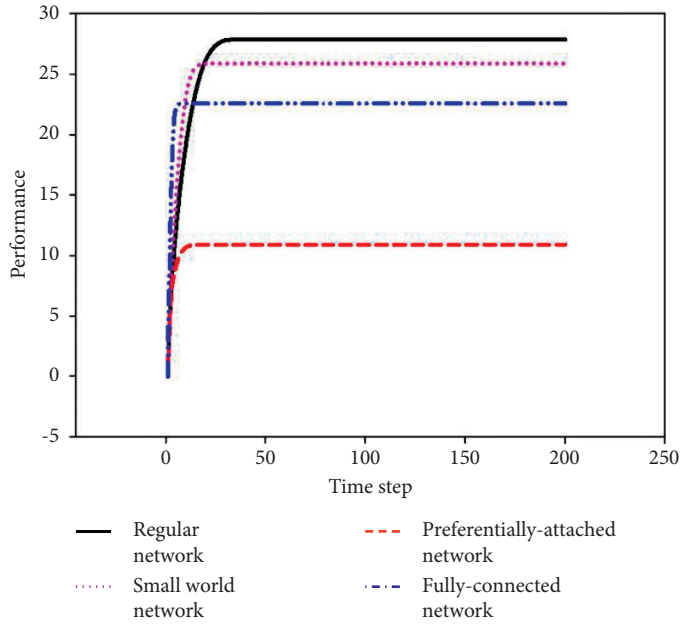

Figure 5: Assessment learning in different network structures.

locomotors, assessors are more influenced by their neighbors. Due to their strong concerns with comparing their own solution to the best neighbors', assessors are more likely than locomotors to evaluate and imitate continuously to the best neighbor's solution, which leads to a high value of proportion of m-dimensional vector changed. In a word, assessors are distinct from locomotors by higher self-evaluation concerns, which leads to more sensitivity to performance "standards." Assessors are the best learners who try their best to imitate the target.

As we discussed above, the results in Figure 5 can be explained by the agents' learning rate. Assessors learn faster than locomotors which makes the comparison of short-run performance and long-run performance on the four complex interpersonal networks much clearer. This "tack effect" makes fully connected network find the best solution in extremely quick time (less than 10 periods); all the assessors climbed uphill from the best solution that exists in team. Although regular network reaches the highest performance level in the long run, its convergence time is too short (no more than 40 periods). As we discussed above, as well as final performance level, the equilibrium time will be reported in the next section.

4.2.3. Experiment 3: Final Performance Level and Equilibrium Time in Four Complex Networks. The literature on knowledge sharing highlights the importance of effective knowledge diffusion, which is believed to lead to a high-performance level, while diversity is found to be beneficial to the final performance level. Figure 6 demonstrates these two positive and negative effects. Learning strategies and communication networks both affect knowledge diffusion and diversity. More specifically, fully connected network and assessment both positively affect knowledge diffusion, which facilitates the best solution exchanged, but negatively reduces diversity, which is also important for final performance level. Although regular network and locomotion are inefficient in diffusing the solution, they keep the diversity, which leads to a high final performance level.

Equilibrium time is a proxy for diversity. A high value of equilibrium time reflects the fact that it takes the agents a long time to climb the performance hill. Figure 6 shows that the combination of regular network with locomotors is the best way to keep diversity. Although both regular network and locomotion help keep diversity, their strength is quite different. Obviously, network has much more powerful strength to do that way. In a real team situation, controlling the frequency of communication in a team is a quite effective way to keep diversity. In fact, it is not always the case that all the team members are locomotors or assessors; we should consider the performance of different composition of the two leaning strategies.

4.2.4. Experiment 3: Equilibrium Time and Final Performance Level among Different Team Compositions. Prior literature on team composition from social, psychology, and organization is used to explain how team composition influences the team performance. According to the

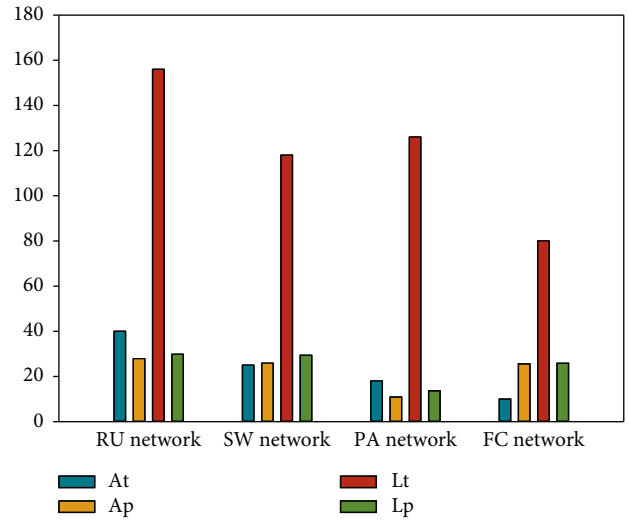

Figure 6: Final performance level and equilibrium time assessors and locomotors.

organization theory and complexity research, some common variables such as personal demographics, personality attributes, values, and other characteristics (KSAOs) are considered as the main mechanism to influence team performance. Generally speaking, deep-level composition variables, such as cognitive pattern and behavioral mode, and some psychological variables have a much stronger influence on performance than surface-level variables which can be knowledge, skill, or other personal demographics. It is not convenient or high cost to measure team member's behavioral pattern; simulation research gives us a valuable opportunity to construct a virtual experiment to explore how team composition affects the performance.

Consider a team with both locomotors and assessors, how this different composition affects the equilibrium time and final performance level. We designed 10 teams with 10 percent to 100 percent locomotors. Figure 7 tells us that the equilibrium time in general will be long very significantly as the proportion of locomotors increases. Locomotors prefer to move to change the current state. For locomotors, they could accept performance decline as long as escape from the current state. A little change can satisfy locomotors' motivation to move. A team composed of many locomotors will face a large innovative space because much more diversity will be maintained among team members, which leads to higher final performance level and longer equilibrium time (as Figure 8 shows).

What surprised us is that when the proportion of locomotors is 0.4, the team performance declines. When the proportion of locomotors is moderate, as 0.5 or 0.6 for example, the performance growth slows down. This result reflects the complexity of a self-adaptive system: when the proportion of locomotors or assessors is moderate, the interaction is quite complex and nonlinear, which leads to performance growth slow down or even decline. On the contrary, a majority or minority of locomotors or assessors shows a clear relationship between equilibrium time, final performance level, and team composition. Furthermore,

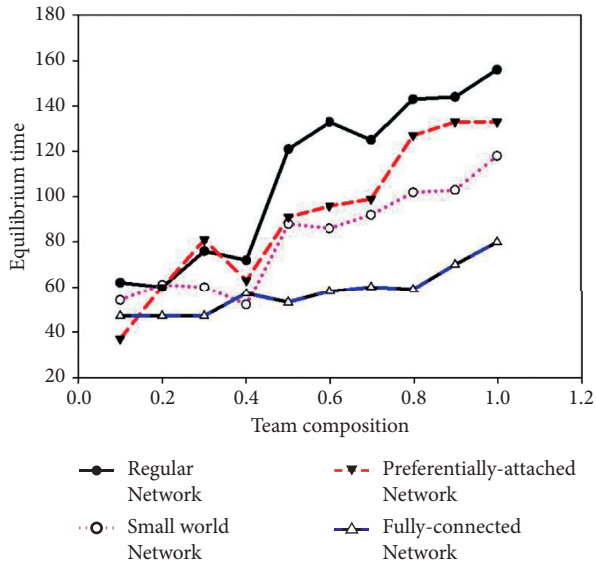

Figure 7: Equilibrium time among different team compositions.

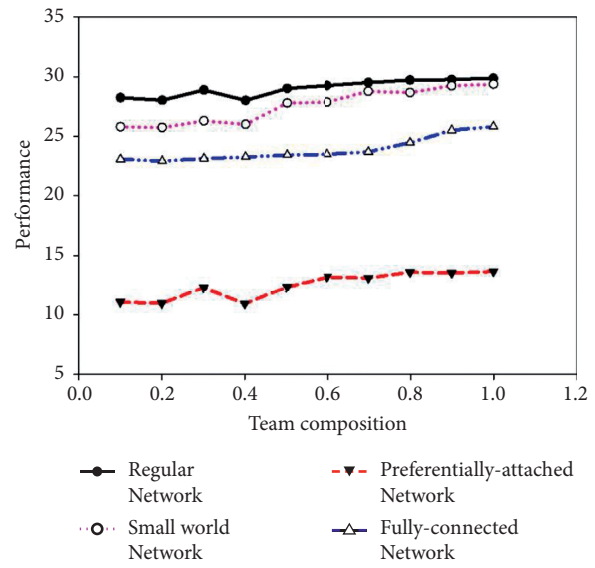

Figure 8: Final performance level of different team compositions.

Figure 7 again shows us that network configuration is the main power influencing the team performance notwithstanding the proportion of locomotors or assessors is large or small. Regular network, which can keep diversity best, will achieve a high-performance level all the time. No matter what composition the team is, the more efficient the team configuration at diffusing knowledge, the better the final performance in the long run and the worse in the short run.

5. Contribution and Discussion

In this paper, we extend Miller's model by considering the locomotion and assessment and explore the performance implication of network structure and agents learning strategies. Given the current limited understanding of performance implication of agents' learning strategies, we consider regulatory mode theory and introduce locomotion and assessment modes into our model to simulate the real team on parallel problem solving. Simulation results indicate that both network structure and agents' learning strategies can affect team performance.

Our simulation results conclude both positive and negative effect of network structure on team performance. Efficient network is good at diffusing knowledge, which reduces diversity, which positively affects the short-run performance but negatively related to the long-run performance. Fully connected network is very efficient at disseminating knowledge; that is, once a solution is proven to be better, it will spread to the whole team simultaneously because all the agents are connected with each other, which leads to a high-performance level in the short run but a low-performance level in the long run, because only one solution exists among agents, cohesive network reduces the diversity, which can improve the performance in the long run. According to regular mode theory, in our model assessors are more likely than locomotors to imitate the best performed neighbors, which leads to a similar effect like network structure. The more assessors (or less locomotors) a team has, the shorter (or the longer) equilibrium time it will be, and the higher (or the lower) short-term performance and the lower (or the higher) long-term performance.

To balance the exploration and exploitation in team, managers should compose the team ahead of time to maintain team competitiveness. Members who hold different learning strategies should be selected to optimally fit each other. From the simulation results, we can conclude that assessors are good at exploiting current knowledge, which helps team survive in the short run, while for the team who has a majority of locomotors, they should realize their long run potential. Locomotors are slow learners who are preferred to maintain diversity. Team can facilitate future learning where a majority of locomotors exists. Furthermore, moderate composition among locomotors and assessors increases costly interaction uncertainty. The complexity of this moderate composition leads to performance growth slow down or even decline. This simulation results seem to argue for composing team under less complexity. Prior literature overlooks the role of complexity in maintaining the competitive strength. It is a great challenge to managers to configure the moderate locomotors or assessors.

There is huge potential for extending our simulation model. Some dimensions should be taken into the future consideration, such as exploring the implication of changing environment. While we construct model in a stable external environment, one may imagine some exogenous shocks which are episodic or smoothly continuously would alter the problem landscape. Does that reduce the value of locomotors learning in the long run, or does it help assessors to maintain diversity which yields competitiveness in the long run? Any of these dynamic factors would be reasonable to add to our model, such as turnover. Prior studies have demonstrated that turnover can be advantageous if the environment changing is turbulent. Likewise, if turnover is permitted, the dynamic proportion between locomotors and

assessors would facilitate team adaptive ability to a changing environment. Furthermore, we hope our simulation results be supported in empirical research. In a real experiment or actual team, empirical investigation should be done to test our propositions and extend our validity.

Data Availability

We use simulation to build and test our model. All the codes are written by the authors. If you are interested in their coding, contact the corresponding author.

Conflicts of Interest

The authors declare that they have no conflicts of interest regarding the publication of this paper.

Acknowledgments

This study was supported by grants from the Ministry of Education in China "Project of Humanities and Social Sciences" (Project no. 17YJA630132), National Social Science Foundation (Project no. 21BGL054), and National Natural Science Foundation of China (Project no. 71802137).

References

[1] H. Simon, "The architecture of complexity," *Proceedings of the American Philosophical Society*, vol. 106, pp. 467–482, 1962.

[2] D. A. Levinthal, "Adaptation on rugged landscapes," *Management Science*, vol. 43, no. 7, pp. 934–950, 1997.

[3] N. Siggelkow, "Evolution toward fit," *Administrative Science Quarterly*, vol. 47, no. 1, 159 pages, 2002.

[4] D. A. Levinthal and M. Warglien, "Landscape design: designing for local action in complex worlds," *Organization Science*, vol. 10, no. 3, pp. 342–357, 1999.

[5] G. Gavetti and D. Levinthal, "Looking forward and looking backward: cognitive and experiential search," *Administrative Science Quarterly*, vol. 45, no. 1, pp. 113–137, 2000.

[6] G. Gavetti, D. A. Levinthal, and J. W. Rivkin, "Strategy making in novel and complex worlds: the power of analogy," *Strategic Management Journal*, vol. 26, no. 8, pp. 691–712, 2005.

[7] G. Gavetti and A. Menon, "Evolution cum agency: toward a model of strategic foresight," *Strategy Science*, vol. 1, no. 3, pp. 207–233, 2016.

[8] E. T. Higgins, A. W. Kruglanski, and A. Pierro, "Regulatory mode: locomotion and assessment as distinct orientations," *Advances in Experimental Social Psychology*, vol. 35, pp. 293–344, 2003.

[9] A. W. Kruglanski, E. P. Thompson, E. T. Higgins et al., "To "do the right thing" or to "just do it": locomotion and assessment as distinct self-regulatory imperatives," *Journal of Personality and Social Psychology*, vol. 79, no. 5, pp. 793–815, 2000.

[10] D. A. Levinthal, "A behavioral approach to strategy-what's the alternative?" *Strategic Management Journal*, vol. 32, no. 13, pp. 1517–1523, 2011.

[11] D. A. Levinthal, "Mendel in the C-suite: design and the evolution of strategies," *Strategy Science*, vol. 2, no. 4, pp. 282–287, 2017.

[12] J. P. Davis, K. M. Eisenhardt, and C. B. Bingham, "Developing theory through simulation methods," *Academy of Management Review*, vol. 32, no. 2, pp. 480–499, 2007.

[13] G. James, "Exploration and exploitation in organizational learning," *Organization Science*, vol. 2, no. 1, pp. 71–87, 1991.

[14] D. Lazer and A. Friedman, "The network structure of exploration and exploitation," *Administrative Science Quarterly*, vol. 52, no. 4, pp. 667–694, 2007.

[15] K. D. Miller, M. Zhao, and R. J. Calantone, "Adding interpersonal learning and tacit knowledge to march's exploration-exploitation model," *Academy of Management Journal*, vol. 49, no. 4, pp. 709–722, 2006.

[16] C. Fang, J. Lee, M. A. Schilling, and Schilling, "Balancing exploration and exploitation through structural design: the isolation of subgroups and organizational learning," *Organization Science*, vol. 21, no. 3, pp. 625–642, 2010.

[17] R. Durrett and V. Limic, "Rigorous results for the NK model," *Annals of Probability*, vol. 31, pp. 1713–1753, 2003.

[18] M. Ganco, "NK model as a representation of innovative search," *Research Policy*, vol. 46, no. 10, pp. 1783–1800, 2017.

[19] M. Ganco and G. Hoetker, "NK modeling methodology in the strategy literature: bounded search on a rugged landscape," *Research Methodology in Strategy and Management*, vol. 5, pp. 237–268, 2009.

[20] H. E. Posen and D. Martignoni, "Revisiting the imitation assumption: w," *Strategic Management Journal*, vol. 39, no. 5, pp. 1350–1369, 2018.

[21] D. A. Levinthal and A. Marino, "Three facets of organizational adaptation: selection, variety, and plasticity," *Organization Science*, vol. 26, no. 3, pp. 743–755, 2015.

[22] Z. Wu, S. Shen, X. Lian, X. Su, and E. Chen, "A dummy-based user privacy protection approach for text information retrieval," *Knowledge-Based Systems*, vol. 195, pp. 1–14, 2020.

[23] Z. Wu, G. Li, S. Shen, X. Lian, E. Chen, and G. Xu, "Constructing dummy query sequences to protect location privacy and query privacy in location-based services," *World Wide Web*, vol. 24, no. 1, pp. 25–49, 2020.

[24] Z. Wu, S. Shen, H. Zhou, H. Li, C. Lu, and D. Zou, "An effective approach for the protection of user commodity viewing privacy in e-commerce website," *Knowledge-Based Systems*, vol. 220, pp. 1–12, 2021.

[25] S. Shigen, Z. Haiping, F. Sheng et al., "HSIRD: a model for characterizing dynamics of malware diffusion in heterogeneous WSNs," *Journal of Network and Computer Applications*, vol. 146, pp. 1–14, 2019.

[26] H. Zhou, S. Shen, and J. Liu, "Malware propagation model in wireless sensor networks under attack-defense confrontation," *Computer Communications*, vol. 162, pp. 51–58, 2020.

[27] O. Baumann, "Models of complex adaptive systems in strategy and organization research," *Mind & Society*, vol. 14, no. 2, pp. 169–183, 2015.

[28] O. Baumann and N. Siggelkow, "Dealing with complexity: integrated vs. chunky search processes," *Organization Science*, vol. 24, no. 1, pp. 116–132, 2013.

[29] O. Baumann and N. Stieglitz, ""Effective search in rugged performance landscapes: a Review and Outlook," *Journal of Management*, vol. 45, no. 1, pp. 285–318, 2019.

Hindawi
Complexity
Volume 2022, Article ID 8705997, 11 pages
https://doi.org/10.1155/2022/8705997

Research Article

Theoretical Model Development for Energy Motion of Dusty Turbulent Flow of Fibre Suspensions in a Rotational Frame

Shams Forruque Ahmed

Science and Math Program, Asian University for Women, Chattogram 4000, Bangladesh

Correspondence should be addressed to Shams Forruque Ahmed; shams.f.ahmed@gmail.com

Received 19 January 2022; Revised 9 March 2022; Accepted 15 March 2022; Published 12 April 2022

Academic Editor: Yu Zhou

Fibre suspension has garnered considerable attention in turbulent flows that are used in many industries. Solid particles, such as dust particles, notably affect the turbulent flow field in a rotational frame. In assessing their impacts, the dusty turbulent flow for fibre suspensions needs to be studied in a frame of rotation that can be substantially applied in many industries. This study, therefore, aims to build a theoretical model for the energy motion of dusty turbulent flow of fibre suspensions in a rotational frame. The turbulence momentum equation was considered to formulate the model in presence of dusty fluid rotating flow of fibre suspensions. The newly derived equation was derived in second-order correlation tensors $F_{i,j}$, $W_{i,j}$, $G_{i,j}$, $S_{i,j}$, $X_{i,j}$, $Y_{i,j}$, $Q_{i,j}$, and $R_{i,j}$ at any two points in the flow domain, where the tensors were expressed as space, time, and distance functions. The developed model is a considerable improvement because it takes into account all of the potential influential parameters that could affect the motion of turbulent energy, such as dust particles, suspending particles (fibres), and rotating frame. However, the impact of these parameters on turbulence energy motion must be evaluated in order to assess the performance of turbulence systems utilized in a variety of industries, such as paper manufacturing. The present theoretical development will contribute to open up experimental and numerical research opportunities for the advancement of the industry, science, and technology.

1. Introduction

The flows of turbulent are often found in moving objects, for example, various moving vehicles, which affect flow resistance to the bodies of the objects. Turbulent flow motions define the fluid flow behaviours based on mass conservation, energy, and momentum laws [1]. In the second-order pressure-velocity correlation, Hinze and Uberoi [2] derived the turbulent motion at any two points in the flow domain. The correlations between velocity and pressure fluctuations were taken into account in his study. However, the effect of any potential turbulent motion parameters was not considered. The turbulent flows are greatly affected by the introduction of fibres into the flow. In several parts of the industry, fibre injections into the turbulent flow are used, for example, in environmental engineering, paper manufacturing, chemical engineering, the manufacture of composite materials, and the textile industry. The property of the fibre suspension has a notable effect on product quality. The complexity in turbulent fibre motion arises mainly from the translational and revolutionary dynamics of the particles, which are driven by forces and torques, depending on the form and the orientation of the particles [3]. Over the last thirty years, numerous studies have been undertaken on turbulent flows of fibre suspensions. A preliminary study on turbulent motion of fibre (ice crystals) suspension was conducted by Cho et al. [4]. Atmospheric turbulence associated with their effect on fibre orientation was investigated in their study. The mean fibre orientation was not significantly affected by the atmospheric turbulence. Fluid motion equations were solved with a spectral approach by Lin et al. [5], and the trajectories of fibre were determined on slim body theory. Although a key parameter to define the fibre orientations on a broad scale was found to be the Stokes number, its orientation effect on the fibre is not significant and the ratio of fibre direction has a minimum influence on the orientation distribution of fibre.

Particle motions in the flows of turbulent are a fundamental issue for applications [6], for example, atmospheric clouds, and spray combustion engines. In an accurate understanding between dust particle collisions and growth [7–9], humid terrestrial clouds, cool stars [10], brown dwarves, and cloud production of planets, the interactions between turbulent and the particles have been considered. The evolution of the particles' size is dependent on the particle collision rate which can be significantly increased by turbulent motions [11]. In the presence of small-sized particles, Bhatti et al. [12] studied the electro-osmotic flow of non-Newtonian fluid moving in a sinusoidal fashion in a Darcy–Brinkman–Forchheimer medium. The Jeffrey fluid model was used to investigate non-Newtonian effects. The Debye length approximation, Poisson–Boltzmann equation, and ionic Nernst–Planck equation were employed to construct the mathematical model. The effect of parameters on both fluid and particle phases was also discussed. The present effects have been proven to be advantageous in the design and manufacture of microfluidic devices for determining the transport mechanism.

A precise and exact calculation of the collision rate includes an accurate understanding of the collision rate impacts caused by turbulence and preferential or clustering particle concentrations. Several studies [13–21] have been carried out on the motion of the dusty turbulent flow. The characteristics of the dust particles [22–25] mainly rely on the particle size of the turbulence scale. The particles compete over fluid impacts and collisions on turbulent flow into the neighbourhoods of the particle. In a study conducted by [26], entropy generation and irreversibility processes that occur as a result of partial slip on magnetic dusty fluid caused by a peristaltic wave via a porous conduit were studied. The results demonstrated that the presence of dust particles in the fluid causes the flow to decelerate. In the presence of a strong magnetic field, Mahanthesh [27] investigated the effect of Hall current on the two-phase boundary layer flow of an electrically conducting dusty fluid over a permeable stretched sheet. Using appropriate similarity transformations, the governing equations were reduced from a set of partial differential to ordinary differential equations. The author reported that, in controlling the friction factor on the sheet, the dust particles' mass concentration can be employed as a control parameter. It was also revealed that suction and injection have opposing effects on the formation of the momentum boundary layer. In the presence of dust particles, the effect of Hall current on the time-dependent flow of a nanofluid was also investigated by Gireesha et al. [28]. The boundary layer approximation notion was used for modeling the governing equations for nanofluid as well as dust phases. Increases in heat transfer rate were found to be proportional to Hall current and unsteadiness.

The motions between a particle of the fluid and the suspended fibre rely on fluid dynamics fundamental of turbulence characteristics with the velocity pressure correlations of fluctuating components. A good number of [15, 29–35] studies have been undertaken in rotating systems to analyze the motion of turbulent flows. The mean rotation induces dynamical influences on turbulent flows through the pressure-stream-rate correlation in the transport equations. The rotation produces the auxiliary body force-like Coriolis and centrifugal force in rotating turbulent flows, accompanied by the turbulent structures. Consequently, the momentum transfer mechanism suffers from complexity. However, most research studies did not take into account or address the rotational impacts of the system at different angles, owing to rotational frame complications. Coriolis force plays a critical role in a turbulent flow rotating system [36, 37]. To measure the impact of the Coriolis force, You et al. [30, 35] directed an experimental-based study on the rotating turbulent flow. The velocity for particle images was considered in this study to calculate the flow profile. Because of the Coriolis effect, the flow domains between the leading and trailing sides were found to be different [30]. Coriolis force widened the vortex nearby the front side and intimidated the vortex nearby the trailing end. The force of Coriolis showed major effects in the flow field on the vortices. It was also revealed that not only the secondary flow but also the Coriolis force influences the flow domain which must not be overlooked.

Due to the simplification of laminar flow, it is shown through comprehensive literature surveys that several research studies were undertaken on assessing the behaviour of laminar fibre motion. However, the turbulent fibre motion studies are still inadequate because of the complexities of fibre motion and turbulence. Flow phenomena generated in the flow domain are complex if it includes any type of solid particle such as dust particles into the turbulent fibre flow. The dust particles can range from 1 to 400 μm diameters, with particles more than 100 μm settling down towards the formation source [38]. The overall range of the particle sizes can be classified into three categories: lower than 1 μm, 1–20 μm, and more than 20 μm, which are referred to as ultrafine, fines, and large particles, respectively. However, the smaller particles are comparatively difficult to remove or separate from the airstream because they have a stronger inclination to stay in suspension.

In a frame of rotation, the dusty turbulent flow becomes more complex. However, some mathematical models were developed on the energy motion of turbulent flow in second-order correlation tensors by considering dust particles [13], fibre suspension [39], dust particles with fibre suspensions [40], a rotating frame [32], and dust particles in a frame of rotation [15]. Nevertheless, any of these articles did not consider all of the parameters that can influence turbulence energy motion, such as dust particles, fibre suspension, and rotational frame. The main fact behind this is because of its complexity level in mathematical modeling. As a result, the previous models cannot be considered fully complete and feasible, and they must be improved by taking into account all of these influential parameters in order to make the model feasible. By considering all of these parameters, the present study thus constructs a model for the energy motion of dusty rotating turbulent flow of fibre suspensions. To address the research gaps and improve the previous models, the present study introduced correlation tensors $W_{i,j}$, $X_{i,j}$, $Y_{i,j}$, and $R_{i,j}$, which represent the correlations between fluid velocities,

angular velocities, and fluid velocities, angular velocities produced due to the rotation, and the suspending fluid velocities in the fluid flow domain. The resulting partial differential equation model can be generalized to time-space fractional order, making it valuable to the broader scientific community. Based on a numerical investigation, the DNS (direct numerical simulation) method can be applied to the rotation of dusty rigid fibres with different lengths relative to the neighbouring fluid in the channel flow. Due to its high precision, the spectral element method (SEM) may be used to solve the newly developed equation, and SEM applications are also suggested for future research.

2. Methodology

A turbulent flow domain was considered in a rotational frame to formulate and develop the present model. The fluid flow domain comprised fibre suspensions in the existence of dust particles. The mathematical formulation of the model was directed with the equation of momentum for viscid turbulent incompressible flow. The mathematical consequences were sequentially added to the momentum equation. To find the relationships among the velocities of fluid, fibres, and dust particles in the rotational frame, any two points, C and D, were chosen at a distance r in the turbulent flow field. Point C was regarded as the origin of the system coordinate since no difference exists in representing the relationships of turbulence momentum between the points if any of the two points is assumed as the source (origin). The independent variables ψ_k were chosen to differentiate the influences between distance and position. The method of averaging was used to express first-, second-, and third-order pressure-velocity correlations between the two points, C and D. These correlations were demonstrated in a second-order partial differential equation by introducing second-order correlation tensors and following averaging method and tensor properties.

3. Model Formulation and Development

The equation of momentum and the continuity for viscid turbulent incompressible flow are represented by [32, 41]

$$\begin{aligned}\frac{\partial u_i}{\partial t}+u_j\frac{\partial u_i}{\partial x_j}&=-\frac{1}{\rho}\frac{\partial p}{\partial x_i}+\upsilon\frac{\partial^2 u_i}{\partial x_j\partial x_j}-2\varepsilon_{ijl}\Omega_j u_l,\\ \frac{\partial u_i}{\partial x_i}&=0,\end{aligned}\tag{1}$$

with the fluid velocity components of $u_i(x,t)$, fluid density ρ, pressure $p(x,t)$, suspending fluids' kinematical viscosity υ, three-dimensional permutation symbol ε_{ijl}, rotation vector Ω_j, dissipation of turbulence ε, position x, and time t.

For the turbulent flow with dust (solid) particles, the following equations are obtained:

$$\begin{aligned}\frac{\partial u_i}{\partial t}+u_j\frac{\partial u_i}{\partial x_j}&=-\frac{1}{\rho}\frac{\partial p}{\partial x_i}+\upsilon\frac{\partial^2 u_i}{\partial x_j\partial x_j}-2\varepsilon_{ijl}\Omega_j u_l\\ &\quad+\frac{KN}{\rho}(v_i-u_i),\end{aligned}\tag{2}$$

$$\frac{\partial u_i}{\partial x_i}=0,\tag{3}$$

$$\frac{\partial v_i}{\partial t}+v_j\frac{\partial u_i}{\partial x_j}=-\frac{K}{m_s}(u_i-v_i),\tag{4}$$

with dust (solid) particle velocity components $v_i(x,t)$, dust particle mass for single-spherical $m_s=4/3\pi R_s^3\rho_s$ with radius R_s, Stoke's formula for the drag $K=6\pi R_s\rho\nu$, $KN/\rho=f$ frequency dimension, and dust particle density number N. It is noted that the term $KN/\rho(v_i-u_i)$ appears in equation (2) due to the solid dust particles existent in the field of turbulent flow [14]. The fluid is presumed to be air and treated as multiphase since this present study comprises fibre suspensions and dust particle interactions into the dusty turbulent flow in the frame of rotation.

In presence of fibre, the equation of turbulent motion (3) gives

$$\begin{aligned}\frac{\partial u_i}{\partial t}+u_j\frac{\partial u_i}{\partial x_j}&=-\frac{1}{\rho}\frac{\partial p}{\partial x_i}+\upsilon\frac{\partial^2 u_i}{\partial x_j\partial x_j}-2\varepsilon_{\mathrm{ijl}}\Omega_j u_l\\ &\quad+\frac{KN}{\rho}(v_i-u_i)\\ &\quad+\frac{\mu_f}{\rho}\frac{\partial}{\partial x_j}\left[a_{\mathrm{ijlm}}\varepsilon_{\mathrm{lm}}-\frac{1}{3}\left(I_{ij}a_{lm}\right)\varepsilon_{lm}\right],\end{aligned}\tag{5}$$

with the apparent viscosity of fibre suspension μ_f, the turbulent intensity of fibre suspension I_{ij}, tensor strain rate $\varepsilon_{lm}=1/2(\partial u_l/\partial x_m+\partial u_m/\partial x_l)$, and fourth- and second-order tensors for fibre orientation a_{ijlm} and a_{lm}, respectively. The term $\mu_f/\rho\partial/\partial x_j[a_{ijlm}\varepsilon_{lm}-1/3(I_{ij}a_{lm})\varepsilon_{lm}]$ occurs in equation (5) because of the fibres poured into the turbulent flow domain [42].

For a rotating frame, the turbulence momentum equation is given by [32]

$$\begin{aligned}\frac{\partial u_i}{\partial t}+u_j\frac{\partial u_i}{\partial x_j}&=-\frac{1}{\rho}\frac{\partial p}{\partial x_i}+\upsilon\frac{\partial^2 u_i}{\partial x_j\partial x_j}\\ &\quad-2\varepsilon_{ijl}\Omega_j u_l-2\left(\Omega_i u_i\eta_i\right)\sin\theta,\end{aligned}\tag{6}$$

where $-2(\Omega_i u_i\eta_i)\sin\theta=-2(\overline{\Omega}\times\overline{u})$ denotes the Coriolis force, where η, Ω_i, and θ specify unit vector normal to $\overline{u}$ and $\overline{\Omega}$, angular velocity, and the angle makes between $\overline{u}$ and $\overline{\Omega}$, respectively.

Therefore, combining equations (5) and (6), a new equation is obtained as follows:

$$\frac{\partial u_i}{\partial t} + u_j \frac{\partial u_i}{\partial x_j} = -\frac{1}{\rho}\frac{\partial p}{\partial x_i} + v\frac{\partial^2 u_i}{\partial x_j \partial x_j} - 2\varepsilon_{ijl}\Omega_j u_l + \frac{KN}{\rho}(v_i - u_i) + \frac{\mu_f}{\rho}\frac{\partial}{\partial x_j}\left[a_{\text{ijlm}}\varepsilon_{lm} - \frac{1}{3}\left(I_{ij}a_{lm}\right)\varepsilon_{lm}\right] - 2(\Omega_i u_i \eta_i)\sin\theta. \tag{7}$$

Equation (7) represents the new energy equation of motion for fibre suspended dusty rotating turbulent flow.

Suppose C and D are any two points in the turbulent flow field and assume c and d be the directions along with the points C and D, respectively. Therefore, u_c and u_d can be used as the components of the velocity along with C and D directions. Suppose that $\overline{U_i}$ is the mean velocity, time independent, and constant throughout the considered domain.

Thus, $(U_i = \overline{U}_i + u_i)_C$ and $(U_j = \overline{U}_j + u_j)_D$.

All the terms have a value, which can be calculated from the equations of u_i at C point and of u_j at D point.

At point C, the turbulence momentum can be written from equation (7) for u_i:

$$\frac{\partial u_i}{\partial t} + (\overline{U}_k + u_k)\frac{\partial u_i}{\partial x_k} = -\frac{1}{\rho}\frac{\partial p}{\partial x_i} + v\frac{\partial^2 u_i}{\partial x_k \partial x_k} - 2\varepsilon_{ikl}\Omega_k u_l + f(v_i - u_i) + \frac{\mu_f}{\rho}\frac{\partial}{\partial x_k}\left[a_{\text{iklm}}\varepsilon_{lm} - \frac{1}{3}(I_{ik}a_{lm})\varepsilon_{lm}\right] - 2(\Omega_i u_i \eta_i)\sin\theta. \tag{8}$$

Since, for incompressible fluids, $(u_i \partial u_k/\partial x_k)_C = 0$, equation (8) yields

$$\frac{\partial}{\partial t}(u_i)_B + [\overline{U}_k + (u_k)_C]\left(\frac{\partial}{\partial x_k}\right)_C (u_i)_C + \left(u_i\frac{\partial u_k}{\partial x_k}\right)_C = -\frac{1}{\rho}\left(\frac{\partial}{\partial x_i}\right)_C p_C + v\left(\frac{\partial^2}{\partial x_k \partial x_k}\right)_C (u_i)_C - 2[(\varepsilon_{ikl}\Omega_k u_l)_C + (\Omega_i u_i \eta_i)_C \sin\theta] + f(v_i - u_i)_C + \frac{\mu_f}{\rho}\left(\frac{\partial}{\partial x_k}\right)_C\left[a_{\text{iklm}}\varepsilon_{lm} - \frac{1}{3}(I_{ik}a_{lm})\varepsilon_{lm}\right]_C. \tag{9}$$

Multiplying equation (9) by $(u_j)_D$,

$$\begin{aligned}(u_j)_D\frac{\partial}{\partial t}(u_i)_C + [\overline{U}_k + (u_k)_C]\left(\frac{\partial}{\partial x_k}\right)_C (u_i)_C(u_j)_D + (u_i)_C\left(\frac{\partial}{\partial x_k}\right)_C (u_k)_C(u_j)_D \\ = -\frac{1}{\rho}\left(\frac{\partial}{\partial x_i}\right)_C p_B(u_j)_D + v\left(\frac{\partial^2}{\partial x_k \partial x_k}\right)_C (u_i)_C(u_j)_D - 2[(\varepsilon_{ikl}\Omega_k u_l)_C + (\Omega_i u_i \eta_i)_C \sin\theta](u_j)_D \\ + f(v_i - u_i)_C(u_j)_D + \frac{\mu_f}{\rho}\left(\frac{\partial}{\partial x_k}\right)_C\left[a_{\text{iklm}}\varepsilon_{lm} - \frac{1}{3}(I_{ik}a_{lm})\varepsilon_{lm}\right]_C(u_j)_D,\end{aligned} \tag{10}$$

where $(u_j)_D$ is taken as constants for the differential system at C point.

Likewise, the turbulence momentum equations for u_j are obtained at D point:

$$\frac{\partial u_j}{\partial t} + (\overline{U}_k + u_k)\frac{\partial u_j}{\partial x_k} = -\frac{1}{\rho}\frac{\partial p}{\partial x_j} + v\frac{\partial^2 u_j}{\partial x_k \partial x_k} - 2\varepsilon_{jkl}\Omega_k u_l + f\left(v_j - u_j\right) + \frac{\mu_f}{\rho}\frac{\partial}{\partial x_k}\left[a_{\mathrm{jklm}}\varepsilon_{lm} - \frac{1}{3}\left(I_{jk}a_{lm}\right)\varepsilon_{lm}\right] - 2\left(\Omega_j u_j \eta_j\right)\sin\theta. \tag{11}$$

By using the condition of incompressible fluids, $(u_j \partial u_k/\partial x_k)_D = 0$, equation (11) gives

$$\frac{\partial}{\partial t}\left(u_j\right)_D + [\overline{U}_k + (u_k)_D]\left(\frac{\partial}{\partial x_k}\right)_D\left(u_j\right)_D + \left(u_j\frac{\partial u_k}{\partial x_k}\right)_D = -\frac{1}{\rho}\left(\frac{\partial}{\partial x_j}\right)_D p_D + v\left(\frac{\partial^2}{\partial x_k \partial x_k}\right)_D\left(u_j\right)_D - 2\left[\left(\varepsilon_{jkl}\Omega_k u_l\right)_D + \left(\Omega_j u_j \eta_j\right)_D \sin\theta\right] + f\left(v_j - u_j\right)_D + \frac{\mu_f}{\rho}\left(\frac{\partial}{\partial x_k}\right)_D\left[a_{\mathrm{jklm}}\varepsilon_{lm} - \frac{1}{3}\left(I_{jk}a_{lm}\right)\varepsilon_{lm}\right]_D. \tag{12}$$

Multiplying equation (12) by $(u_i)_C$, the following is obtained:

$$\begin{aligned}(u_i)_C\frac{\partial}{\partial t}\left(u_j\right)_D &+ [\overline{U}_k + (u_k)_D]\left(\frac{\partial}{\partial x_k}\right)_D\left(u_j\right)_D(u_i)_C + \left(u_j\right)_D\left(\frac{\partial}{\partial x_k}\right)_D(u_k)_D(u_i)_C \\ &= -\frac{1}{\rho}\left(\frac{\partial}{\partial x_j}\right)_D p_D(u_i)_C + v\left(\frac{\partial^2}{\partial x_k \partial x_k}\right)_D\left(u_j\right)_D(u_i)_C - 2\left[\left(\varepsilon_{jkl}\Omega_k u_l\right)_D + \left(\Omega_j u_j \eta_j\right)_D \sin\theta\right](u_i)_C \\ &+ f\left(v_j - u_j\right)_D(u_i)_C + \frac{\mu_f}{\rho}\left(\frac{\partial}{\partial x_k}\right)_D\left[a_{\mathrm{jklm}}\varepsilon_{lm} - \frac{1}{3}\left(I_{jk}a_{lm}\right)\varepsilon_{lm}\right]_D(u_i)_C,\end{aligned} \tag{13}$$

where $(u_i)_C$ are taken as constants for differential systems at D point.

Summing equations (10) and (13),

$$\begin{aligned}\frac{\partial}{\partial t}(u_i)_C\left(u_j\right)_D &+ \left[\left(\frac{\partial}{\partial x_k}\right)_C(u_i)_C(u_k)_C\left(u_j\right)_D + \left(\frac{\partial}{\partial x_k}\right)_D(u_i)_C(u_k)_D\left(u_j\right)_D\right] + \overline{U}_k\left[\left(\frac{\partial}{\partial x_k}\right)_C(u_i)_C\left(u_j\right)_D + \left(\frac{\partial}{\partial x_k}\right)_D(u_i)_C\left(u_j\right)_D\right] \\ &= -\frac{1}{\rho}\left[\left(\frac{\partial}{\partial x_i}\right)_C p_C\left(u_j\right)_D + \left(\frac{\partial}{\partial x_j}\right)_D p_C(u_i)_C\right] + v\left[\left(\frac{\partial^2}{\partial x_k \partial x_k}\right)_C + \left(\frac{\partial^2}{\partial x_k \partial x_k}\right)_D\right](u_i)_C\left(u_j\right)_D \\ &- 2\left[(\varepsilon_{ikl}\Omega_k u_l)_C\left(u_j\right)_D + \left(\varepsilon_{jkl}\Omega_k u_l\right)_D(u_i)_C\right] - 2\left[(\Omega_i u_i \eta_i)_C\left(u_j\right)_D + \left(\Omega_j u_j \eta_j\right)_D(u_i)_C\right]\sin\theta \\ &+ f\left[(v_i - u_i)_C\left(u_j\right)_D + \left(v_j - u_j\right)_D(u_i)_C\right] \\ &+ \frac{\mu_f}{\rho}\left[\left(\frac{\partial}{\partial x_k}\right)_C\left(a_{\mathrm{iklm}}\varepsilon_{lm} - \frac{1}{3}I_{ik}a_{lm}\varepsilon_{lm}\right)_C\left(u_j\right)_D + \left(\frac{\partial}{\partial x_k}\right)_D\left(a_{\mathrm{jklm}}\varepsilon_{lm} - \frac{1}{3}I_{jk}a_{lm}\varepsilon_{lm}\right)_D(u_i)_C\right].\end{aligned} \tag{14}$$

In order to represent the relationships of turbulence momentum between D and C point, no difference exists if C or D is assumed as the source (origin) of the system coordinate. Point C was regarded as origin here. Suppose the

variables ψ_k are independent and used to differentiate the influences between distance and position, where $\psi_k = (x_k)_D - (x_k)_C$.

Therefore, the following relations are obtained:

$$\left(\frac{\partial}{\partial x_k}\right)_C = -\frac{\partial}{\partial \psi_k},$$
$$\left(\frac{\partial}{\partial x_k}\right)_D = \frac{\partial}{\partial \psi_k}, \tag{15}$$
$$\left(\frac{\partial^2}{\partial x_k \partial x_k}\right)_C = \left(\frac{\partial^2}{\partial x_k \partial x_k}\right)_D = \frac{\partial^2}{\partial \psi_k \partial \psi_k}.$$

Using these relations and averaging all the terms, equation (15) yields

$$\begin{aligned}
&\frac{\partial}{\partial t}\overline{(u_i)_C(u_j)_D} - \frac{\partial}{\partial \psi_k}\overline{(u_i)_C(u_k)_C(u_j)_D} + \frac{\partial}{\partial \psi_k}\overline{(u_i)_C(u_k)_D(u_j)_D} = -\frac{1}{\rho}\left[-\frac{\partial}{\partial \psi_i}\overline{p_C(u_j)_D} + \frac{\partial}{\partial \psi_j}\overline{p_D(u_i)_C}\right] \\
&+ 2\upsilon\frac{\partial^2}{\partial \psi_k \partial \psi_k}\overline{(u_i)_C(u_j)_D} + f\left[\overline{(v_i)_C(u_j)_D} - 2\overline{(u_i)_C(u_j)_D} + \overline{(u_i)_D(v_j)_C}\right] \\
&- 2\left[\overline{(\varepsilon_{ikl}\Omega_k u_l)_C(u_j)_D} + \overline{(\varepsilon_{jkl}\Omega_k u_l)_D(u_i)_C}\right] - 2\left[\overline{(\Omega_i u_i \eta_i)_C(u_j)_D} + \overline{(\Omega_j u_j \eta_j)_D(u_i)_C}\right]\sin\theta \\
&- \frac{\mu_f}{\rho}\frac{\partial}{\partial \psi_k}\left[\overline{(a_{\mathrm{iklm}}\varepsilon_{lm})_C(u_j)_D} - \frac{1}{3}\overline{(I_{ik}a_{lm}\varepsilon_{lm})_C(u_j)_D} - \overline{(a_{\mathrm{jklm}}\varepsilon_{lm})_D(u_i)_C} + \frac{1}{3}\overline{(I_{jk}a_{lm}\varepsilon_{lm})_D(u_i)_C}\right].
\end{aligned} \tag{16}$$

Equation (16) yields the mean energy motion of dusty turbulent flow for fibre suspensions in a rotational frame, where the motion of fibres of turbulent flow is at average speed $\overline{U}_k$ with respect to the system coordinate. Due to the constant derivative, the coefficient term $\overline{U}_k$ was omitted in this equation. The equation consists of the double correlations of velocity $\overline{(u_i)_C(u_j)_D}$, pressure-velocity $\overline{p_C(u_j)_D}$, and triple-velocity such as $\overline{(u_i)_C(u_k)_C(u_j)_D}$, where the terms are located at a certain distance from each other. The correlations of pressure-velocity $\overline{p_D(u_i)_C}$ and $\overline{p_D(u_j)_C}$ form first-order tensor as the pressure is taken as a scalar. Likewise, triple correlations of velocity, $\overline{(u_i)_C(u_k)_D(u_j)_D}$ and $\overline{(u_i)_C(u_k)_C(u_j)_D}$, make third-order tensors. The double correlations are displayed in Figure 1, while the triple correlations are illustrated in Figure 2, respectively, at points C and D, where r is the distance from C to D.

The correlations of the order first, second, and third can be labelled by $(K_{p,j})_{C,D}$, $(W_{i,j})_{C,D}$, and $(S_{ik,j})_{C,D}$, respectively. Thus, the correlations of pressure-velocity and velocity give

$$\begin{aligned}
\left(K_{i,p}\right)_{C,D} &= \overline{(u_i)_C p_D}, \\
\left(k_{p,j}\right)_{C,D} &= \overline{p_C(u_j)_D}, \\
\left(W_{i,j}\right)_{C,D} &= \overline{(u_i)_C(u_j)_D}, \\
\left(S_{ik,j}\right)_{C,D} &= \overline{(u_i)_C(u_k)_C(u_j)_D}, \\
\left(S_{i,kj}\right)_{C,D} &= \overline{(u_i)_C(u_k)_D(u_j)_D}, \\
\left(F_{i,j}\right)_{C,D} &= \overline{(v_i)_C(u_j)_D}, \\
\left(G_{i,j}\right)_{C,D} &= \overline{(u_i)_C(v_j)_D},
\end{aligned} \tag{17}$$

where p denotes the pressure which is not an index such as dummy j or i, and therefore, the summation should not be used to p.

The terms of $\overline{(\varepsilon_{\mathrm{jkl}}\Omega_k u_l)_D(u_i)_C}$, $\overline{(\varepsilon_{\mathrm{ikl}}\Omega_k u_l)_C(u_j)_D}$, $\overline{(\Omega_i u_i \eta_i)_C(u_j)_D}$, and $\overline{(\Omega_j u_j \eta_j)_D(u_i)_C}$ form the correlation tensors of second order those can be represented by $M_{i,j}$, $N_{i,j}$, $H_{i,j}$, and $L_{i,j}$, accordingly, while $\overline{(a_{\mathrm{jklm}}\varepsilon_{lm})_D(u_i)_C}$ and $\overline{(I_{jk}a_{lm}\varepsilon_{lm})_D(u_i)_C}$ form the correlation tensor of third order

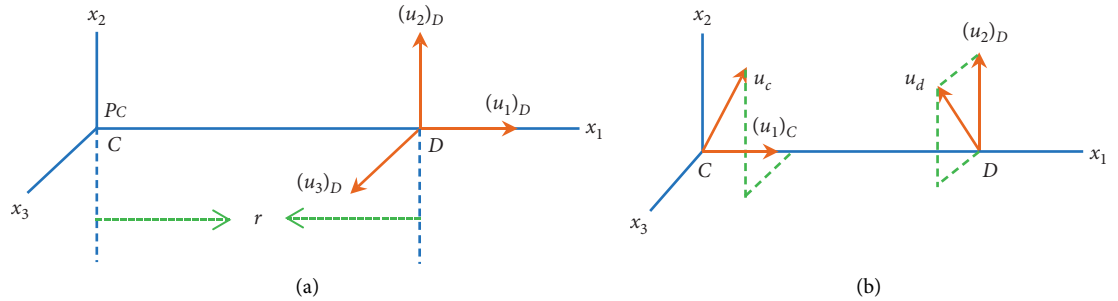

Figure 1: Correlations between C and D points. (a) The pressure at C and the velocity at D. (b) Velocities u_c at C and u_d at D.

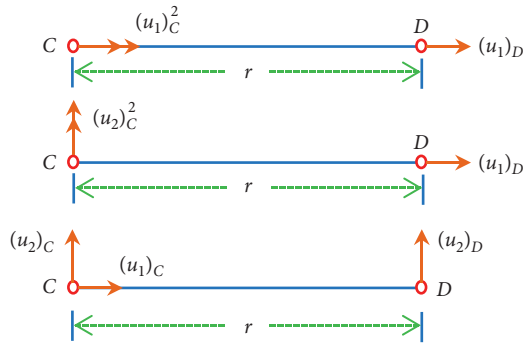

Figure 2: Triple correlations for the velocity at C and D.

and expressed as $Q_{i,jk}$ and $R_{i,jk}$, respectively. Consequently, the followings are obtained:

$$\begin{aligned}
\left(M_{i,j}\right)_{C,D} &= \overline{\left(\varepsilon_{ikl}\Omega_k u_l\right)_C\left(u_j\right)_D},\\
\left(N_{i,j}\right)_{C,D} &= \overline{\left(\varepsilon_{jkl}\Omega_k u_l\right)_D\left(u_i\right)_C},\\
\left(D_{i,jk}\right)_{C,D} &= \overline{\left(u_i\right)_C\left(a_{\mathrm{jklm}}\varepsilon_{lm}\right)_D},\\
\left(H_{i,j}\right)_{C,D} &= \overline{\left(\Omega_i u_i \eta_i\right)_C\left(u_j\right)_D},\\
\left(L_{i,j}\right)_{C,D} &= \overline{\left(\Omega_j u_j \eta_j\right)_D\left(u_i\right)_C},\\
\left(Q_{ik,j}\right)_{C,D} &= \overline{\left(a_{\mathrm{iklm}}\varepsilon_{lm}\right)_C\left(u_j\right)_D},\\
\left(R_{i,jk}\right)_{C,D} &= \overline{\left(u_i\right)_C\left(I_{jk}a_{lm}\varepsilon_{lm}\right)_D},\\
\left(R_{ik,j}\right)_{C,D} &= \overline{\left(I_{ik}a_{lm}\varepsilon_{lm}\right)_C\left(u_j\right)_D}.
\end{aligned} \tag{18}$$

Using the above correlation terms, equation (16) yields

$$\begin{aligned}
\frac{\partial}{\partial t}W_{i,j} - \frac{\partial}{\partial \psi_k}S_{ik,j} + \frac{\partial}{\partial \psi_k}S_{i,kj} &= -\frac{1}{\rho}\left(-\frac{\partial}{\partial \psi_i}K_{p,j} + \frac{\partial}{\partial \psi_j}K_{i,p}\right) + 2\upsilon\frac{\partial^2}{\partial \psi_k \partial \psi_k}W_{i,j} + f\left(F_{i,j} - 2W_{i,j} + G_{i,j}\right)\\
&- 2\left[\left(M_{i,j} + N_{i,j}\right) + \left(H_{i,j} + L_{i,j}\right)\sin\theta\right] + \frac{\mu_f}{\rho}\frac{\partial}{\partial \psi_k}\left[\left(Q_{i,jk} - Q_{ik,j}\right) + \frac{1}{3}\left(R_{ik,j} - R_{i,jk}\right)\right],
\end{aligned} \tag{19}$$

where the terms of correlations used in equation (19) are to the considering points, C and D.

The double pressure-velocity correlations are zero for incompressible and isotropic turbulence, which means

$$\begin{aligned}
\left(k_{p,j}\right)_{C,D} &= 0,\\
\left(k_{i,p}\right)_{C,D} &= 0.
\end{aligned} \tag{20}$$

In the field of isotropic turbulence, the invariance condition under the reflection to C is followed by

$$\begin{aligned}
\overline{\left(u_i\right)_C\left(u_k\right)_D\left(u_j\right)_D} &= -\overline{\left(u_k\right)_C\left(u_j\right)_C\left(u_i\right)_D},\\
\text{or}&\\
\left(s_{i,kj}\right)_{C,D} &= -\left(s_{kj,i}\right)_{C,D}.
\end{aligned} \tag{21}$$

Thus, the simplification of equation (19) gives

$$\begin{aligned}
\frac{\partial}{\partial t}W_{i,j} - \frac{\partial}{\partial \psi_k}\left(S_{ik,j} + S_{kj,i}\right) &= 2\upsilon\frac{\partial^2}{\partial \psi_k \partial \psi_k}W_{i,j} - 2\left[\left(M_{i,j} + N_{i,j}\right) + \left(H_{i,j} + L_{i,j}\right)\sin\theta\right]\\
&+ f\left(F_{i,j} - 2W_{i,j} + G_{i,j}\right) + \frac{\mu_f}{\rho}\left[-\frac{\partial}{\partial \psi_k}\left(Q_{jk,i} + Q_{ik,j}\right) + \frac{1}{3}\frac{\partial}{\partial \psi_k}\left(R_{ik,j} + R_{jk,i}\right)\right].
\end{aligned} \tag{22}$$

Table 1: Equation of motions for turbulent flow in second-order tensors of pressure-velocity correlation.

Turbulent motion	Considered parameters	References
$\frac{\partial}{\partial t}W_{i,j} - S_{i,j} = 2[\upsilon\partial^2/\partial\psi_k\partial\psi_k W_{i,j} - X_{i,j} - Y_{i,j}\sin\theta] + f(F_{i,j} - 2W_{i,j} + G_{i,j}) - \mu_f/\rho(Q_{i,j} - 1/3R_{i,j})$	(i) Momentum for turbulent flow (ii) Fibre suspensions (iii) Dust particles (iv) Rotating frame	This study
$\partial/\partial t W_{i,j} - S_{i,j} = 2[\upsilon\partial^2/\partial\psi_k\partial\psi_k W_{i,j} - X_{i,j}] + f(F_{i,j} - 2W_{i,j} + G_{i,j}) - \frac{\mu_f}{\rho}(Q_{i,j} - 1/3R_{i,j})$	(i) Momentum for turbulent flow (ii) Fibre suspensions (iii) Dust particles	Ahmed et al. [40]
$\partial/\partial t W_{i,j} - S_{i,j} = 2[\upsilon\partial^2/\partial\psi_k\partial\psi_k W_{i,j} - X_{i,j} - Y_{i,j}\sin\theta] + f(F_{i,j} - 2W_{i,j} + G_{i,j})$	(i) Momentum for turbulent flow (ii) Dust particles (iii) Rotating frame	Ahmed [15]
$\partial/\partial t W_{i,j} - S_{i,j} = 2[\upsilon\partial^2/\partial\psi_k\partial\psi_k W_{i,j} - X_{i,j} - Y_{i,j}\sin\theta]$	(i) Momentum for turbulent flow (ii) Rotating frame	Ahmed [32]
$\partial/\partial t W_{i,j} - S_{i,j} = 2\upsilon\partial^2/\partial\psi_k\partial\psi_k W_{i,j}$	(iii) Motion for turbulent flow	Hinze and Uberoi [2]

The terms $\partial/\partial\psi_k(Q_{jk,i} + Q_{ik,j})$, $\partial/\partial\psi_k(S_{ik,j} + S_{kj,i})$, $\partial/\partial\psi_k(R_{ik,j} + R_{jk,i})$, $(M_{i,j} + N_{i,j})$, and $(H_{i,j} + L_{i,j})$ form tensors of second order that can be represented by $Q_{i,j}$, $S_{i,j}$, $R_{i,j}$, $X_{i,j}$, and $Y_{i,j}$, respectively, and expressed as

$$\begin{aligned} Q_{i,j} &= \frac{\partial}{\partial\psi_k}\left(Q_{jk,i} + Q_{ik,j}\right), \\ S_{i,j} &= \frac{\partial}{\partial\psi_k}\left(S_{ik,j} + S_{kj,i}\right), \\ R_{i,j} &= \frac{\partial}{\partial\psi_k}\left(R_{ik,j} + R_{jk,i}\right), \\ X_{i,j} &= \left(M_{i,j} + N_{i,j}\right), \\ Y_{i,j} &= \left(H_{i,j} + L_{i,j}\right). \end{aligned} \tag{23}$$

Therefore, equation (23) yields

$$\begin{aligned} \frac{\partial}{\partial t}W_{i,j} - S_{i,j} = 2\left[\upsilon\frac{\partial^2}{\partial\psi_k\partial\psi_k}W_{i,j} - X_{i,j} - Y_{i,j}\sin\theta\right] \\ + f\left(F_{i,j} - 2W_{i,j} + G_{i,j}\right) - \frac{\mu_f}{\rho}\left(Q_{i,j} - \frac{1}{3}R_{i,j}\right). \end{aligned} \tag{24}$$

This newly derived equation expresses the energy motion of dusty rotating turbulent flow of fibre suspensions in 2nd order tensors.

4. Results and Discussion

The energy motion equation of the dusty turbulent flow of fibre suspension (19) was derived in a rotational frame. This new equation was developed in the 2nd order tensors of pressure-velocity and velocity-velocity correlation at any two points C and D of the fluid flow field. All of these tensors were expressed as coordinates of time, space, and distance. The present model was compared to the relevant existing models to assess its feasibility which is summarized in Table 1.

Dynamic behaviours of the particles in turbulent flow fields are a major concern related to the applications. Fibre suspensions in a fluid flow or gas have been known for some time to reduce the shear stress generated by the motion of the fluid through a solid surface under the conditions of turbulent flow. In absence of dust particles into the flow domain, $f = 0$, and consequently, the newly developed equation (24) becomes

$$\begin{aligned} \frac{\partial}{\partial t}W_{i,j} - S_{i,j} = 2\left[\upsilon\frac{\partial^2}{\partial\psi_k\partial\psi_k}W_{i,j} - X_{i,j} - Y_{i,j}\sin\theta\right] \\ - \frac{\mu_f}{\rho}\left(Q_{i,j} - \frac{1}{3}R_{i,j}\right). \end{aligned} \tag{25}$$

Equation (25) signifies the energy motion for turbulent flow of fibre suspensions in a rotational frame in the tensors of 2nd order. Here, the correlation tensors, $S_{i,j}, W_{i,j}, X_{i,j}, Y_{i,j}, Q_{i,j}, F_{i,j}, G_{i,j}$, and $R_{i,j}$ express the velocity relationships at any two points C and D (Figure 2) in the flow domain. The tensors, $S_{i,j}$ and $W_{i,j}$, represent the fluid velocity correlations, $Q_{i,j}$ and $R_{i,j}$, indicate the correlations between the suspending fibres and fluid velocities, $F_{i,j}$ and $G_{i,j}$, describe the velocity correlations between fluid and dust particles while $X_{i,j}$ and $Y_{i,j}$ defines the correlations between fluid velocities, and angular velocities between fluid and fibre formed due to the rotation.

Fibre suspensions in the fluid have been known sometimes to reduce the shear stress generated by the motion of the fluid through a solid surface under the conditions of turbulent flow. If fibres are not available in the fluid flow domain, the apparent viscosity $\mu_f = 0$ for suspending fluid; equation (25) thus yields the form

$$\frac{\partial}{\partial t}W_{i,j} - S_{i,j} = 2\left[\upsilon\frac{\partial^2}{\partial\psi_k\partial\psi_k}W_{i,j} - X_{i,j} - Y_{i,j}\sin\theta\right]. \quad (26)$$

Equation (26) expresses the energy motion of turbulent flow in the correlation tensors in a rotating frame.

Owing to the broad applications to both geophysical and engineering fluid mechanics, turbulent flow is commonly researched in the rotational frame, for example, in combustion systems, rotary shafts, rotational heat exchangers, turbine blade passages, centres of the nuclear reactor, rotated heat exchangers, combustion systems, and rotor shafts. In almost all of these complicated systems, a coordinate with nonrotation is usually used to investigate the problems. For these types of rotating systems, the Coriolis effect performs a critical role in the fluid flow field as mentioned earlier. In the nonrotational frame, the Coriolis effects do not produce in the fluid flow field, which means the term due to the Coriolis effect $Y_{i,j}$ vanishes, and therefore, equation (26) gives

$$\frac{\partial}{\partial t}W_{i,j} - S_{i,j} = 2\left[\upsilon\frac{\partial^2}{\partial\psi_k\partial\psi_k}W_{i,j} - X_{i,j}\right]. \quad (27)$$

Equation (27) signifies the energy motion for turbulent flow of 2nd-order correlation tensors.

If no energy dissipation generated by turbulence, $X_{i,j} = 0$, therefore, equation (27) yields

$$\frac{\partial}{\partial t}W_{i,j} - S_{i,j} = 2\upsilon\frac{\partial^2}{\partial\eta_k\partial\eta_k}W_{i,j}. \quad (28)$$

Equation (28) describes the turbulence motion in the 2nd-order tensors which was obtained by Hinze and Uberoi [2].

5. Conclusion and Future Directions

A new energy motion equation was derived for dusty rotating turbulent flows of fibre suspensions using the method of averaging. Fibre suspension in rotating turbulent flow was taken into account in presence of solid (dust) particles to develop the present theoretical model in second-order correlation tensors. The turbulent fibre suspension flow was subjected to both average fluid motion and random motion caused by fluctuating fluid velocity components. Comparing the present theoretical model to previous relevant models revealed a good agreement, as seen in Table 1, in comparison to previous models, the present model represents a significant improvement as it considers all of the potential influential parameters that could affect the motion of turbulent energy, for instance, dust particles, suspending particles (fibres), and rotating frame. However, the impact of these parameters on turbulence energy motion needs to be assessed to measure the performance of the turbulence system used in several industries.

The present model should be optimized in future studies to identify the most influential parameters affecting the turbulence systems. However, taking into account the nonlinearity, discrete nature, constrained parameters, and boundary conditions of turbulence systems, it is extremely difficult to design the most suitable model that accurately represents reality. Considering all of these difficulties, the future study can develop a physical model for a turbulent channel flow that depicts the modeled system in its physical form through both experimental and numerical studies. The difference between angular velocities of fluid and fibre at the fibre centre of mass should be calculated by estimating the slip spin, which enables a direct comparison of fibre rotation as well as fibre orientation with the carrier flow's local parameters. The findings of the future study could provide physical mechanisms underlying fibre rotation in the closed region of the channel walls, emphasizing how particularly fibres spin in relation to the fluid when swept or ejected. Future research in this field can significantly contribute to natural sciences, technologies, and industries.

Nomenclature

$u_i(x,t)$:	Fluid velocity components (m s^{-1})
ρ:	Fluid density (kg m^3)
$p(x,t)$:	Pressure (Pa)
υ:	Kinematical viscosity of suspending fluids (m^2 s^{-1})
ε_{ijl}:	Three-dimensional permutation symbol
Ω_j:	Rotation vector
ε:	Dissipation of turbulence
x:	Position (m)
$v_i(x,t)$:	Dust (solid) particle velocity components (m s^{-1})
$m_s = 4/3\pi R_s^3\rho_s$:	Dust particle mass (kg)
R_s:	Dust particle radius
$K = 6\pi R_s\rho\nu$:	Stoke's formula for the drag
$KN/\rho = f$:	Frequency dimension
N:	Dust particle density number
μ_f:	Apparent viscosity of fibre suspension (kg $m^{-1}s^{-1}$)
I_{ij}:	Turbulent intensity of fibre suspension
$\varepsilon_{lm} = 1/2\,(\partial u_l/\partial x_m + \partial u_m/\partial x_l)$:	Tensor strain rate
a_{lm}:	Second-order tensors for fibre orientation
a_{ijlm}:	Fourth-order tensors for fibre orientation
$-2\,(\Omega_i u_i\eta_i)\sin\theta = -2\,(\overline{\Omega}\times\overline{u})$:	Coriolis force
η:	Unit vector normal to $\overline{u}$ and $\overline{\Omega}$
Ω_i:	Angular velocity
θ:	Angle makes between $\overline{u}$ and $\overline{\Omega}$
C, D:	Any two points in the turbulent flow field
c, d:	Directions along with the points C and D, respectively
u_c, u_d:	Components of the velocity along with C and D directions

$\psi_k = (x_k)_D - (x_k)_C$:	Considered independent variables
r:	Distance between any two points C and D in the flow filed
t:	Time (s)
$S_{i,j}$, $W_{i,j}$:	Fluid velocity correlations
$Q_{i,j}$, $R_{i,j}$:	Correlations between the suspending fibres and fluid velocities
$F_{i,j}$, $G_{i,j}$:	Velocity correlations between fluid and dust particles
$X_{i,j}$:	Correlations between the velocities of fluid and fibre
$Y_{i,j}$:	Angular velocities between fluid and fibre formed due to the rotation.

Data Availability

No data were used to support this study.

Conflicts of Interest

The authors declare that they have no conflicts of interest.

Acknowledgments

The author highly expresses his gratitude to Asian University for Women, Chattogram, Bangladesh, for their support to carry out this study.

References

[1] L. Zhang, N. Qin, and B. Ahmad, "Explicit iterative solution of a Caputo-Hadamard–type fractional turbulent flow model," *Mathematical Methods in the Applied Sciences*, pp. 1–11, 2020.

[2] J. O. Hinze and M. S. Uberoi, "Turbulence," *Journal of Applied Mechanics*, vol. 27, no. 3, p. 601, 1960.

[3] D. Dotto and C. Marchioli, "Orientation, distribution, and deformation of inertial flexible fibers in turbulent channel flow," *Acta Mechanica*, vol. 230, no. 2, pp. 597–621, 2019.

[4] H.-R. Cho, J. V. Iribarne, and W. G. Richards, "On the orientation of ice crystals in a cumulonimbus cloud," *Journal of the Atmospheric Sciences*, vol. 38, no. 5, pp. 1111–1114, 1981.

[5] J. Lin, X. Shi, and Z. Yu, "The motion of fibers in an evolving mixing layer," *International Journal of Multiphase Flow*, vol. 29, no. 8, pp. 1355–1372, 2003.

[6] J. R. Singler, "Global attractor for a low order ODE model problem for transition to turbulence," *Mathematical Methods in the Applied Sciences*, vol. 40, no. 8, pp. 2896–2906, 2017.

[7] J. R. Picardo, L. Agasthya, R. Govindarajan, and S. S. Ray, "Flow structures govern particle collisions in turbulence," *Physical Review Fluids*, vol. 4, Article ID 032601, 2019.

[8] A. Pumir and M. Wilkinson, "Collisional aggregation due to turbulence," *Annual Review of Condensed Matter Physics*, vol. 7, no. 1, pp. 141–170, 2016.

[9] X.-Y. Li, A. Brandenburg, G. Svensson, N. E. L. Haugen, B. Mehlig, and I. Rogachevskii, "Condensational and collisional growth of cloud droplets in a turbulent environment," *Journal of the Atmospheric Sciences*, vol. 77, no. 1, pp. 337–353, 2020.

[10] C. Helling, M. Jardine, and F. Mokler, "Ionization in atmospheres of brown dwarfs and extrasolar planets. II. Dust-induced collisional ionization," *The Astrophysical Journal*, vol. 737, no. 1, p. 38, 2011.

[11] K. Gustavsson, E. Meneguz, M. Reeks, and B. Mehlig, "Inertial-particle dynamics in turbulent flows: caustics, concentration fluctuations and random uncorrelated motion," *New Journal of Physics*, vol. 14, Article ID 115017, 2012.

[12] M. M. Bhatti, A. Zeeshan, F. Bashir, S. M. Sait, and R. Ellahi, "Sinusoidal motion of small particles through a Darcy-Brinkman-Forchheimer microchannel filled with non-Newtonian fluid under electro-osmotic forces," *Journal of Taibah University for Science*, vol. 15, no. 1, pp. 514–529, 2021.

[13] S. F. Ahmed, "Derivation of turbulent energy in presence of dust particles," *American Journal of Applied Mathematics*, vol. 1, no. 4, pp. 71–77, 2013.

[14] N. Kishore and M. S. A. Sarker, "Rate of change of vorticity covariance in MHD turbulent flow of dusty incompressible fluid," *International Journal of Energy Research*, vol. 14, no. 5, pp. 573–577, 1990.

[15] S. F. Ahmed, "Turbulent energy for dusty fluid in a rotating system," *International Journal of Applied Mathematics and Mechanics*, vol. 9, pp. 50–61, 2013.

[16] V. Di Sarli, E. Danzi, L. Marmo, R. Sanchirico, and A. Di Benedetto, "CFD simulation of turbulent flow field, feeding and dispersion of non-spherical dust particles in the standard 20 L sphere," *Journal of Loss Prevention in the Process Industries*, vol. 62, Article ID 103983, 2019.

[17] M. Liberman, N. Kleeorin, I. Rogachevskii, and N. E. L. Haugen, "Mechanism of unconfined dust explosions: turbulent clustering and radiation-induced ignition," *Physical Review*, vol. 95, Article ID 051101, 2017.

[18] H. Homann, T. Guillot, J. Bec, C. W. Ormel, S. Ida, and P. Tanga, "Effect of turbulence on collisions of dust particles with planetesimals in protoplanetary disks," *Astronomy & Astrophysics*, vol. 589, p. A129, 2016.

[19] M. A. Liberman, N. Kleeorin, I. Rogachevskii, and N. E. L. Haugen, "Multipoint radiation induced ignition of dust explosions: turbulent clustering of particles and increased transparency," *Combustion Theory and Modelling*, vol. 22, no. 6, pp. 1084–1102, 2018.

[20] B. Mahanthesh, O. D. Makinde, B. J. Gireesha, K. L. Krupalakshmi, and I. L. Animasaun, "Two-phase flow of dusty Casson fluid with Cattaneo-Christov heat flux and heat source past a cone, wedge and plate," *Defect and Diffusion Forum*, vol. 387, pp. 625–639, 2018.

[21] B. J. Gireesha, B. Mahanthesh, R. S. R. Gorla, and P. T. Manjunatha, "Thermal radiation and Hall effects on boundary layer flow past a non-isothermal stretching surface embedded in porous medium with non-uniform heat source/sink and fluid-particle suspension," *Heat and Mass Transfer*, vol. 52, no. 4, pp. 897–911, 2016.

[22] S. Shah and R. Singh, "Lie symmetries for analyzing interaction of a characteristic shock with a singular surface in a non-ideal reacting gas with dust particles," *Mathematical Methods in the Applied Sciences*, vol. 44, no. 5, pp. 3804–3818, 2021.

[23] J. Jena, "Lie group transformations for self-similar shocks in a gas with dust particles," *Mathematical Methods in the Applied Sciences*, vol. 32, no. 16, pp. 2035–2049, 2009.

[24] M. Radhika, B. Mahanthesh, K Siddabasappa, and K. Thriveni, "Solar radiative heat-driven Sakiadis flow of a dusty

nanoliquid with Brownian motion and an exponential space-based heat source: k," *Heat Transfer*, vol. 50, no. 2, pp. 1232–1251, 2021.

[25] R. SR Gorla, "Two-phase boundary layer flow, heat and mass transfer of a dusty liquid past a stretching sheet with Thermal radiation," *International Journal of Industrial Mathematics*, vol. 8, pp. 279–292, 2016.

[26] M. M. Bhatti and S. I. Abdelsalam, *Thermodynamic Entropy of a Magnetized Ree-Eyring Particle-fluid Motion with Irreversibility Process: A Mathematical Paradigm*, Wiley Online Library, Hoboken, NJ, USA, 2021.

[27] B. Mahanthesh, "Hall effect on two-phase laminar boundary layer flow of dusty liquid due to stretching of an elastic flat sheet," *Mapana - Journal of Sciences*, vol. 16, no. 3, pp. 13–26, 2017.

[28] B. J. Gireesha, B. Mahanthesh, G. T. Thammanna, and P. B. Sampathkumar, "Hall effects on dusty nanofluid two-phase transient flow past a stretching sheet using KVL model," *Journal of Molecular Liquids*, vol. 256, pp. 139–147, 2018.

[29] S. Akar, S. Rashidi, and J. A. Esfahani, "Second law of thermodynamic analysis for nanofluid turbulent flow around a rotating cylinder," *Journal of Thermal Analysis and Calorimetry*, vol. 132, no. 2, pp. 1189–1200, 2018.

[30] H. You, H. Li, R. You, Z. Tao, and J. Shi, "Experimental investigations of turbulent flow in a rotating ribbed channel in terms of the effect of coriolis force," *Turbo Expo: Power for Land, Sea, and Air: American Society of Mechanical Engineers*, Article ID V05AT16A004, 2019.

[31] Q.-Q Xun and B.-C Wang, "Hybrid RANS/LES of turbulent flow in a rotating rib-roughened channel," *Physics of Fluids*, vol. 28, Article ID 075101, 2016.

[32] S. F. Ahmed, "Derivation of turbulent energy in a rotating system," *Journal of Computational and Applied Research in Mechanical Engineering*, vol. 3, pp. 75–83, 2013.

[33] M. Rosales, T. Pérez, and J. L. Nava, "Computational fluid dynamic simulations of turbulent flow in a rotating cylinder electrode reactor in continuous mode of operation," *Electrochimica Acta*, vol. 194, pp. 338–345, 2016.

[34] A. A. Avramenko, I. V. Shevchuk, and A. V. Kravchuk, "Turbulent incompressible microflow between rotating parallel plates," *European Journal of Mechanics - B: Fluids*, vol. 71, pp. 35–46, 2018.

[35] R. You, H. Li, Z. Tao, K. Wei, and G. Xu, "PIV measurements of turbulent flows in a smooth channel with the heated boundary under rotation conditions," *Applied Thermal Engineering*, vol. 123, pp. 1021–1033, 2017.

[36] S. F. Ahmed and M. A. Sarker, "Fiber motion in dusty fluid turbulent flow in a rotating system," *International Journal of Applied Mathematics and Mechanics*, vol. 10, pp. 92–109, 2014.

[37] G. Shalini and B. Mahanthesh, "Rayleigh-Benard convection in a dusty Newtonian nanofluid with and without coriolis force," *Journal of Nanofluids*, vol. 7, no. 6, pp. 1240–1246, 2018.

[38] D. Kumar and D. Kumar, *Sustainable Management of Coal Preparation*, Woodhead Publishing, Sawston, Cambridge, 2018.

[39] S. Ahmed and M. Sarker, "Derivation of turbulent energy of fiber suspensions," *Journal of Computational and Applied Research in Mechanical Engineering*, vol. 4, pp. 155–163, 2015.

[40] S. F. Ahmed, M. Hafez, and Y.-M. Chu, "Conversion of energy equation for fiber suspensions in dusty fluid turbulent flow," *Results in Physics*, vol. 19, Article ID 103341, 2020.

[41] T. R. Osborn, "Estimates of the local rate of vertical diffusion from dissipation measurements," *Journal of Physical Oceanography*, vol. 10, no. 1, pp. 83–89, 1980.

[42] L. Jian-Zhong, L. Jun, Z. Li, and J. A. Olson, "New equation of turbulent fibre suspensions and its solution and application to the pipe flow," *Chinese Physics*, vol. 14, no. 6, pp. 1185–1192, 2005.

Hindawi
Complexity
Volume 2022, Article ID 6460838, 16 pages
https://doi.org/10.1155/2022/6460838

Research Article

Ranking of Search Requests in the Digital Information Retrieval System Based on Dynamic Neural Networks

Viera Bartosova,[1] **Svetlana Drobyazko**,[2] **Sergii Bogachov**,[3] **Olga Afanasieva**,[4] **and Maria Mikhailova**[5]

[1]*University of Zilina, Univerzitna 8215, 010 26, Zilina, Slovakia*
[2]*The European Academy of Sciences Ltd., 71-75 Shelton Street, London WC2H 9JQ, UK*
[3]*Financial University Under the Government of the Russian Federation, 49 Leningradsky Prospekt, Moscow 125993, Russia*
[4]*Moscow Aviation Institute (National Research University), Volokolamskoe Shosse 4, Moscow 125993, Russia*
[5]*Medical Sciences, Sechenov First Moscow State Medical University, 8-2 Trubetskaya Str., Moscow 119991, Russia*

Correspondence should be addressed to Svetlana Drobyazko; svetlana.drobyazko@yahoo.com

Received 20 November 2021; Revised 1 March 2022; Accepted 15 March 2022; Published 11 April 2022

Academic Editor: Yu Zhou

The article is devoted to the problem of optimization of search request ranking algorithms in the digital information retrieval system. The algorithm of functioning of the neural network ranking unit based on Hopfield neural network is built. The ability to generate a ranked list of pages found as a result of the request in the digital information retrieval system can be provided by solving two problems of integer optimization: the problem of assignment of combinatorial sets of criteria for assessing the relevance of web page search and the problem of sorting of numbers—relevance values. The architecture of the neural network model based on the dynamic Hopfield neural network with binary output function designed for combinatorial optimization of the final list of documents found in the digital information retrieval system was synthesized. Promising variants of neural network models with binary output function of neurons for synthesis of the optimal evaluation plan with a combinatorial set of criteria by solving the problem of assignment were built. It has been proven that the built models differ in the rules for determining the coefficients of synaptic connections and external shifts; each of the created rules can be used independently or in different combinations with one another. In the course of analytical research, it was found that the optimization formulation of the problem of sorting of relevance values of search pages is identical to the problem of assignment of combinatorial groups of evaluation criteria provided that the elements of the performance matrix of the latter are defined as linear combinations of relevance values.

1. Introduction

In the process of development of the Internet and the growth of data from local area networks, the probability of the existence of the required information increases, and the possibility of finding it decreases. Proper search for the necessary information becomes a common problem. New methods and tools are needed that solve the problems of relevant search in extremely large amounts of information. The goal of digital information retrieval systems (DIRS) developers is to provide the user with a search engine results page (SERP) that is as relevant as possible to the content of the personal request (to ensure relevance and accuracy of the search), while generating as much SERP as possible containing the requested information (to ensure completeness of the search).

The development of search engines is impossible without their intellectualization, which includes the use of semantic-syntactic analysis of texts, natural language tools, intelligent algorithms for determining the significance and information resources for the user, obtaining additional information about documents by analyzing hypertext structure and user preferences, and many other tools. In the DIRS, a request is generated as a keyword or a combination of keywords related to logical operations. To search for the same textual information, different keywords are used, the choice of

which is subjective [1]. But even if the keywords are defined and the request consists of only one word, the search result may differ when using different search engines. This is due to different procedures for indexing the text of documents in different search engines, as well as due to the fact that the search result can be represented as a very large list of found documents. The number of documents found in the list when searching by a keyword can be reduced by continuing the search, but already among these found documents (a number of search engines provide this option), using another keyword as a request. Increasing the number of keywords and continuing the search procedure in the found documents allows to reduce the number of found documents to a reasonable value, at which viewing the text of documents on the topic of interest is already real. That is why the right choice of a sufficient number of keywords, and even better word combinations, is a challenge, especially when working with unfamiliar material. Neural networks are becoming a software and system necessity that can effectively solve these problems. All of this determines the high level of relevance and necessity of this research.

2. Related Work

Among all variety of types of problems of mathematical programming, there are problems in which the set of acceptable alternatives is known or infinite, and it is based on certain rules of combinatorics. Such problems constitute a class of combinatorial optimization problems. Since the problems of combinatorial programming are reduced to the choice of a finite set of alternatives, in principle, each such problem may be solved by a complete search. It is natural to state the question of the complexity of the algorithms that implement this method. In this case, when the authors say about a dynamic binary Hopfield neural network, they can get a higher effect. As is known, in static neural networks, the absence of feedback guarantees their unconditional stability. They cannot enter in some mode when an output continuously switches between states and is not suitable for use. But this very desirable property is not achieved for free; networks without feedback have more limited capabilities compared to those with feedback. Since networks with feedback have pathways for transmission of signals from outputs to inputs, the response of such networks is dynamic; that is, after using a new input, the output is calculated and, transmitted via feedback, modifies the input [2]. Then, the output is calculated again; the process is repeated again and again. For a stable network, successive iterations lead to smaller output changes until the output becomes constant. The problem of stability is solved by the Hopfield neural network, which is a subset of networks with feedback, which outputs eventually reach a steady state. This is the main advantage.

A number of fundamental works on the theory of intelligent search processes in DIRS [2–4] state that without effective ranking search results lose importance because they may include references to tens and hundreds of thousands of documents. In such conditions, ranking is a general problem imperative, and the main problems of development of scientific bases of architectural principles of DIRS are insufficient theoretical elaboration of approaches used in practice, relatively low level of use of developed mathematical mechanisms, and lag of theoretical developments from rapidly changing search needs of computer users.

A number of scientists and experts [5–8] point out that the ranking of requests in search engines is a rather complex process. Developers are constantly trying to improve ranking algorithms, usually pursuing two major goals—to improve search quality and reduce the possibility of artificial influences on the ranking of results. One or another DIRS can take into account many factors, which one way or another affect the state of a particular document in the issuance of a particular request. At the present stage of technical development, most DIRSs are based on various complex modifications of the same ranking method [9, 10]. The method is reduced to calculation of the relevance of SERP to the search phrase based on two factors—internal and external ones [11]: document relevance = (internal factor (search phrase) + external factor (search phrase) confidence coefficient). An internal factor in the ranking method is roughly the density of the search phrase in the body of the page multiplied by the coefficient of thematic relevance of the page to the search phrase. An external factor in the ranking method is the number of links to the page with the text of the link corresponding to the search phrase multiplied by the coefficient of thematic relevance of links to the search phrase and the confidence coefficient of the link to the website. Specific changes to this formula apply to all documents in the search engine database. Then, the issuance is sorted in descending order of relevance. Documents, whose relevance is less than a certain threshold, do not appear in the issuance [12].

According to [13, 14], the above global difficulties of search in DIRS cause low adequacy of the information found on request of the user, i.e., return of a large volume of uninformative pages by the system. The problem may be exacerbated by the low speed of receiving answers from the Internet, the need for the user to view all found documents and evaluate their information content in a nonautomated mode. An alternative to secondary search procedures can be the development of fast algorithms for selecting and sorting returned SERPs according to the functions of significance of information resources and relevance of requests. The problem of optimal representation of a limited set of SERPs from some set found in order to maximize the total relevance of the request is presented by the problem of combinatorial optimization in this scientific work. The formation of the final list of found documents is provided by a recurrent procedure of application of the developed combinatorial algorithms.

3. The Method of Ranking of DIRS Requests Based on Neural Network Solving of Combinatorial Problems

3.1. The General Sequence of the Method. The importance of research and development of working algorithms is determined by the need to maintain and develop high

performance of DIRS with a large amount of indexed information and compliance with the vector criterion of significance. In practice, this often leads to the impossibility of applying those algorithms that have proven themselves well in experimental studies in DIRS. In our case, high-performance requirements for DIRS are provided by a neural network computing basis, which allows to parallelize tasks; that is, the algorithm allows to perform resource-intensive precision ranking operations for requests that have a chance to be in high enough places in the issuance by the results of a rougher assessment of their relevance. The SERP ranking method developed by the author is based on two facts:

(1) The increase in the number of search objects contradicts the need to implement in a limited time interval complex assessments of the relevance of content of the information found to the requirements of the search request. Therefore, existing information technologies do not provide effective implementation of search engines without parallelization of their methods and algorithms or exponential increase in the productivity of computing resources.

(2) The complexity of the mathematical support of the algorithms for presenting the found documents and the complexity of the tasks solved using DIRS themselves do not exclude the set of criteria of relevance. In accordance with this set, the selection criteria for the found documents are already presented as Pareto-optimal. This feature is poorly reflected in the algorithmic support of the final stage of search and presentation of SERPs in DIRS [15, 16].

The general sequence of the method of ranking before delivery of search result to the user that was developed by the authors can be presented by four stages:

(1) The set *"A1"* of content correspondences (significance criteria) between the information request and SERP (search result) is dynamically determined, and also the initial set "*P*" of the found pages which is exposed to ranking is designated.

(2) The table of correspondence of the set *"P"* of the found pages with the set of significance criteria is built. The table defines the initial data for solving the ranking problem within the combinatorial assignment problem.

(3) A neural network model for solving the ranking problem based on a dynamic binary Hopfield neural network is formed.

(4) Having initialized the neural network with random input vectors, one obtains the required sequence of SERP indices in accordance with a given set of relevance criteria in DIRS.

The algorithm of search for information relevant to the information needs of the user is the main advantage of DIRS. By relevance, the authors mean the correspondence between the required and the retrieved information. Construction of the optimal sequence of application of certain tools at each step of the search determines its effectiveness. The proposed method allows to solve the problem of choice and can give a clear idea of the types, purposes, and properties of DIRS. Within the two main classes of information retrieval systems: (1) search engines and (2) search directories, the authors identify the search categories: (a) by keywords; (b) with Boolean logic of word combinations; (c) by word combinations; (d) taking into account the distance between words; (e) case sensitive; (f) semantic (conceptual); (g) according to a pattern (similarity); and (h) by document margins. The method of search engine operation proposed by the authors provides automatic indexing of a large number of documents, but it has no advanced tools of artificial intelligence for expert evaluation of information. This explains the low relevance of the results of search engines (relevance means the degree of correspondence of the search results to the user query). Search directories provide more relevant results at the expense of manual preprocessing of queries by editors.

3.2. Representation of the Method of Ranking by the Neural Network Solution of Combinatorial Sorting of SERPs. The first stage consists in determining the set of content correspondences *"A1"* and the formation of the initial set of ranked search pages—a trivial method that mainly depends on the characteristics of a certain DIRS. The formed set of content correspondences is denoted as a set of significance criteria "*V*" (importance of search request) of DIRS at generation of SERPs, $V = \{v_u\}$, $u = 1, \ldots, U$; U is the total number of DIRS request significance criteria. Suppose that as a result of a request a set of search pages D is found $\{d_j\}$, $j = 1, \ldots,$ M, where M is the total number of pages found by DIRS per search request. Each document d_j, $j = 1, \ldots,$ M, according to each criterion v_u, $u = 1, \ldots, U$, has a certain relevance r_{ui}, $u = 1, \ldots, U$, $j = 1, \ldots,$ M. From a given set of search pages M, it is necessary to form a set of pages S, in which the total S is relevant: $\sum_{u=1}^{U} \sum_{j=1}^{S} r_{uj}$ by all criteria of significance will be maximum [17]. To ensure the completeness of the selection from the set of alternatives, we will consider the total relevance of r_{ij} of any SERP d_j in relation to a group of various combinations of criteria v_u (Figure 1).

We assume that the ith group of DIRS request criteria consists of k criteria with U, where U is the total number of DIRS request significance criteria. The number of variants of alternate selection of k criteria with U is $U!/(U-k)!$. In the formed subsets of k criteria, each group has its own position. However, from the permutations of the criteria in the space covered by the subset, the number of the corresponding document does not change.

The number of subsets with different potencies is U. Therefore, the maximum number of groups of criteria for the significance of the request (or works in terms of the assignment problem) will be

$$N = \frac{\sum_{k=1}^{U} U!}{k!\,(U-k)!}, \tag{1}$$

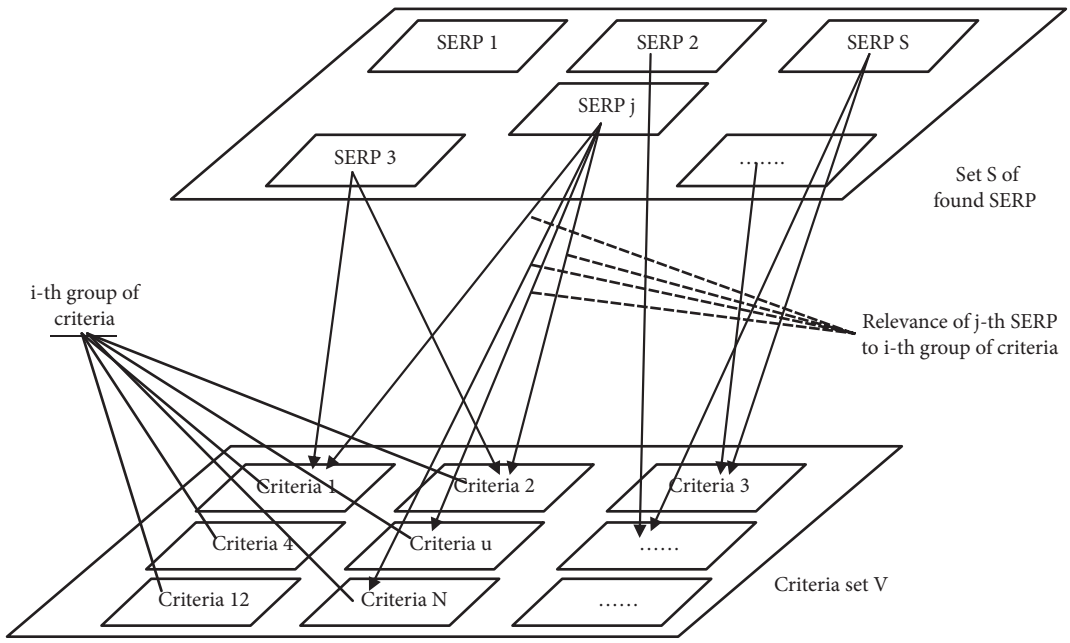

Figure 1: A group of search algorithm criteria in DIRS.

where U is the total number of criteria for the significance of the request in DIRS.

In this regard, there arises a need to develop an efficient and fast neural network algorithm to solve the problem of assignment of one SERP from set S to each group of request criteria that the problem of ranked representation of found DIRS documents is reduced to.

At the second stage of the ranking method implementation, it is necessary to distribute SERPs by groups of criteria in such a way that each page is preferably evaluated by one group of criteria, each group of criteria is preferably used for evaluation of one page, and the total relevance of the SERP by all combinatorial groups of DIRS significance criteria is maximum [18].

We designate through $R = \|r_{ji}\| - N \times M$ the performance matrix (Table 1), whose elements r_{ji} form the relevance of the document with the number j relative to the group of criteria with the number i, M is the total number of SERPs found by DIRS, and N is the total number of combinatorial groups of criteria of request significance.

We designate through $X = \|x_{ji}\| - N \times M$ the matrix of the unknown, whose element x_{ji} takes the value "1," if an SERP with the number j will be evaluated as having maximum relevance by the group of criteria with the number i, and the value "0" otherwise. We present the constraints of the mathematical model as a system of equations:

$$\begin{cases} \sum_{j=1}^{M} x_{ji} \le 1, i = \overline{1, N}, \\ \sum_{i=1}^{N} x_{ji} \le 1, j = \overline{1, M}, \\ x_{ji} \in \{0, 1\}, j = \overline{1, M}, i = \overline{1, N}. \end{cases} \tag{2}$$

Table 1: Input parameters of the assignment problem in DIRS.

	Criteria group 1	...	Criteria group i	...	Criteria group N
SERP *1*	r_{11}	...	r_{1i}	...	r_{1N}
SERP ...	...	...	...	...	...
SERP j	r_{j1}	...	r_{ji}	...	...
SERP ...	...	...	...	...	...
SERP M	r_{M1}	...	r_{Mj}	...	r_{MN}

In the given system, the first equation means that each SERP is evaluated by one group of criteria. According to the second equation, each group of criteria is used to evaluate one search page. The conditions of the third equation are natural constraints on the introduced variables. Given this, we determine the destination matrix X, which forms the criterion of optimality:

$$F(X) = \sum_{j=1}^{M} \sum_{i=1}^{N} r_{ji} x_{ji} \longrightarrow \max. \tag{3}$$

Problems (2)-(3) are called assignment problems with an additive criterion of optimality. When considering the assignment problem in its standard form, it is assumed that the number of different combinatorial groups of criteria is equal to the number of SERPs: $M = N$. It is not difficult to demonstrate that by introducing fictitious groups of criteria or fictitious SERPs found, the open mathematical model (2) is made equivalent to the following model [19]:

$$\begin{cases} \sum_{j=1}^{M} x_{ji} \le 1, i = \overline{1,N}, \\ \sum_{i=1}^{N} x_{ji} \le 1, j = \overline{1,M}, \\ 0 \le x_{ji} \le 1, j = \overline{1,M}, i = \overline{1,N}, \\ N = M. \end{cases} \quad (4)$$

Based on the fact that the matrix of condition constraints (4) is absolutely unimodular (an integer matrix is called absolute or completely unimodular, if any of its minors is equal to ("1," "–1," or "0"), then any pivot of the mathematical model (4) is an integer, hence the equivalence of the mathematical models (2) and (4) [20]. In addition, since conditions (4) and conditions of invariance of variables automatically imply that variables cannot be more than "0," the initial mathematical model (2) is equivalent (in terms of finding the optimal solution to the assignment problem) to the mathematical model with constraints (4), conditions $M = N$ and constraints $x \ge 0$, $j = 1,2,...,M$. Suppose, for example, that the number of SERP documents found exceeds the number of criteria (groups of criteria) N. We introduce additional fictitious criteria (groups of criteria) with indices: $j = N+1, ..., M$. Suppose that the coefficients of the assignment table are equal to zero. In this case, we obtain the problem formulated in the standard form. If in the optimal plan of this problem $x_{ji} = 1$, then the search page j is evaluated by a fictitious criterion (group of criteria), that is, remains without work [21]. The method using a neural network model allows to rank SERPs both in the case of many V (significance criteria) and in the extreme case of $V = 1$.

We reformulate the ranking problem as follows. Suppose there is a set of numbers—the values of the relevance of SERPs found as a result of a DIRS request: $\{r_i\}$, $i \in N = 1, ..., n$. It is necessary to arrange the numbers in ascending order, that is, to find this permutation of indices $j = \pi(i)$, then $\forall j \in 1 \ldots (n-1) \_ r_j \le r_j + 1$. We build the solution of this problem on the basis of using a neural-like model synthesized above to solve combinatorial optimization problems. For the purpose, we reduce the formulated problem of sorting of numbers to some optimization problem. To do this, we prove this statement. Suppose that there is an arbitrary set of numbers $\{r_i\}$, $i \in N = 1, ..., n$ and a monotonically increasing series of positive numbers $\{a_j\}$, $j \in N = 1, ..., n$, such that $\forall j \in 1 \ldots (n-1) \_ a_j \le a_j + 1$. On the set of various substitutions $\{\pi(i)\} = \text{Π}$, $j = \pi(i)$ and set the linear functional as follows:

$$J[\pi(i)] = \sum_{j=1}^{n} a_j r_j. \quad (5)$$

We designate permutation $j^* = \pi^*(i)$, which sorts in ascending order a given arbitrary set of numbers $\{r_i\}$, that is, satisfies the condition:

$$\pi*(i) = \arg\max_{\pi(i) \in \text{Π}} \{J[\pi(i)]\} = \arg\max_{\pi(i) \in \text{Π}} \left\{ \sum_{j=1}^{n} a_j r_j \right\}. \quad (6)$$

To prove this statement, we take an arbitrary substitution $\pi(i)$, which generates the next permutation of the initial set of numbers $(r_1, r_2, \ldots, r_k, \ldots, r_j, \ldots, r_i, \ldots r_n)$ (Figure 2(a)). For certainty, we assume that $k < l$ і $r_k \ge r_i$; that is, this pair of numbers in this permutation is not sorted in the sense of the problem formulated above. We take the second substitution $\pi*(i)$ obtained from the first transposition of the kth and ith elements. This substitution will correspond to the permutation of the initial set of numbers: $(r_1, r_2, \ldots, r_l, \ldots, r_j, \ldots, r_k, \ldots r_n)$, which differs from the first one in that the number r_i is in the kth place and the number r_k is accordingly in the lth place (Figure 2(b)) [22]. In such a permutation, this pair of numbers will be sorted in the format of the problem.

We determine the values of the functional (5) on the substitutions $\pi(i)$, і $\pi*(i)$:

$$\begin{aligned} J[\pi(i)] &= \sum_{\substack{j \in N \\ \overline{\{k,l\}}}}^{n} a_j r_j + a_k r_k + a_l r_l \\ J[\pi*(i)] &= \sum_{\substack{j \in N \\ \overline{\{k,l\}}}}^{n} a_j r_j + a_k r_l + a_l r_k, \end{aligned} \quad (7)$$

and find their difference: $\Delta kl = J[\pi*(i)] - J[\pi(i)] = a_k r_l - a_l r_k - (a_k r_k + a_l r_l) = (a_k - a_l) \times (r_l + r_k)$. On the strength of the accepted assumption $k < l$ and $r_k \ge r_i$, so, firstly, r_l-$r_k \le 0$; secondly, a_k–$a_l < 0$, as the series of numbers $\{a_j\}$ is monotonically increasing by definition. From which, it follows

$$\Delta kl = J[\pi*(i)] - J[\pi(i)] \ge 0, \quad (8)$$

that is, the value of the input linear functional (5) in the permutation, in which some pair of numbers is sorted, is greater than or equal to the value of this functional in the permutation, which differs only in that the selected pair of numbers is not sorted.

At the third and fourth stages of the method implementation, a neural network model for solving the ranking problem based on a dynamic binary Hopfield neural network is formed and used.

4. Binary Hopfield Neural Network-Based SERP Ranking Model

4.1. Synthesis of Architecture and Parameters of the Hopfield Neural Network. We consider the neural network interpretation of the problem of ranking by many criteria as a problem of assignment provided that the problem of assignment is reduced to the standard form (the number of groups of criteria is equal to the number of ranked documents) [23, 24]. We define the architecture of the neural

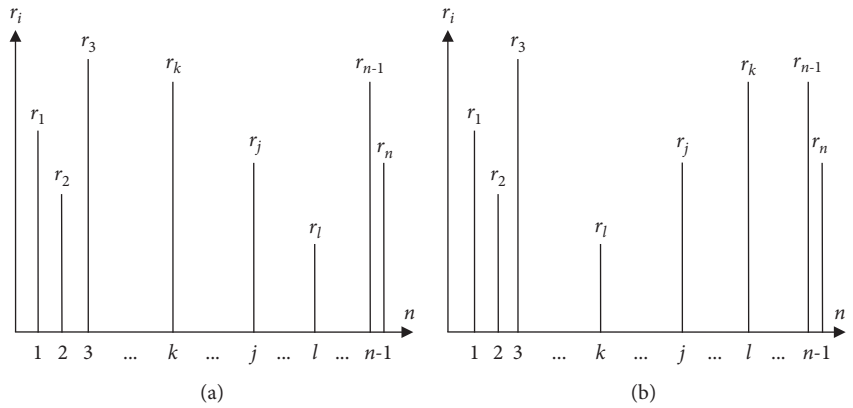

Figure 2: (a, b) Permutations of the initial set of numbers.

network by solving problem (2) under constraints (3). We include in consideration a network of binary neurons, which is a matrix with dimension of $n \times n$, where $n = N - M$ is the number of SERP or groups of criteria. A ranking model can be based on a neural network (Figure 3) containing arbitrary feedbacks by which the transmitted firing returns to the neuron and it performs its function again [25].

In dynamic neural networks, instability is manifested in wandering changes in the states of neurons, which does not lead to steady states. In the general case, the answer to the question of the stability of the dynamics of an arbitrary system with feedbacks is extremely difficult and is still open [26] (Figure 3).

It is assumed that the discrete Hopfield neural network used have the following characteristics: (1) one layer of elements (input elements representing the input sample are not taken into account); (2) each element is connected to all other elements, but not to itself; (3) only one element is refreshed in one stage; (4) elements are refreshed randomly, but on average each element must be refreshed to the same extent (with the same frequency); and (5) element output is limited to "0" or "1"; that is, the output function is binary [27].

The Hopfield network is recurrent in the sense that, for each input sample, the network output is reused as input until a steady state is reached. After "start," the appropriately organized (programmed) neural network changes its state, gradually moving to steady state. This mode identifies the result—a SERP evaluation plan with many groups of criteria, which may not match the exact solution. Random search procedures are usually used to clarify the result [28].

It is convenient to assume that the Hopfield network has no input elements, as the input vector simply determines the initial values of the activity of the elements. The elements are refreshed when all elements transmit their activity values according to the available weighted value of connections, after which the sum of terms is calculated (i.e., a scalar term is taken). The activity value of the element is based on the use of some activation rule. Each integer variable x_{ij} is matched to the output signal of the ijth neuron u_{ij}, which is in the ith row and in the jth column of the network matrix.

$$\left(x_{ij} = 1\right) \Leftrightarrow \left(u_{ij} = 1\right), \forall i, j \in \overline{1, N.} \tag{9}$$

The matrix of the network in the state of rest, where neurons with single-output signals are presented in the form of shaded squares, is given in Figure 4. A set of firing neurons is interpreted as a plan of assignments. According to (10), we interpret constraint (2) and objective function (3); as a result, we obtain (11)–(14).

$$\sum_{j=1}^{n} u_{ji} = 1, \forall i \in \overline{1, n,} \tag{10}$$

$$\sum_{i=1}^{n} u_{ji} = 1, \forall j \in \overline{1, n,} \tag{11}$$

$$\sum_{j=1}^{n} \sum_{i=1}^{n} u_{ji} = n, \tag{12}$$

$$\Phi(u) = \sum_{j=1}^{n} \sum_{i=1}^{n} u_{ji} r_{ji} \longrightarrow \max, \tag{13}$$

where u_{ji} is Hopfield neural network output value (Figure 3) and R_{ji} is performance matrix value (Table 1) whose elements r_{ji} represent the relevance of the search page with the number j in relation to the criterion (group of criteria) with the number i.

We build the energy function $E^0(u)$, whose minimization ensures the fulfillment of constraints (11)–(13) and the solution of problem (14). We build it in the following form:

$$E^0(u) = E^0_{\psi}(u) + E^0_{\Phi}(u), \tag{14}$$

where the last term provides the optimization of the cost function and up to constant $F > 0$ is unambiguously determined as follows:

$$E^0(u) = -F \sum_{j=1}^{n} \sum_{i=1}^{n} u_{ji} r_{ji}, \tag{15}$$

and the first term ensures the fulfillment of constraints and can be built in several ways. According to the first of them,

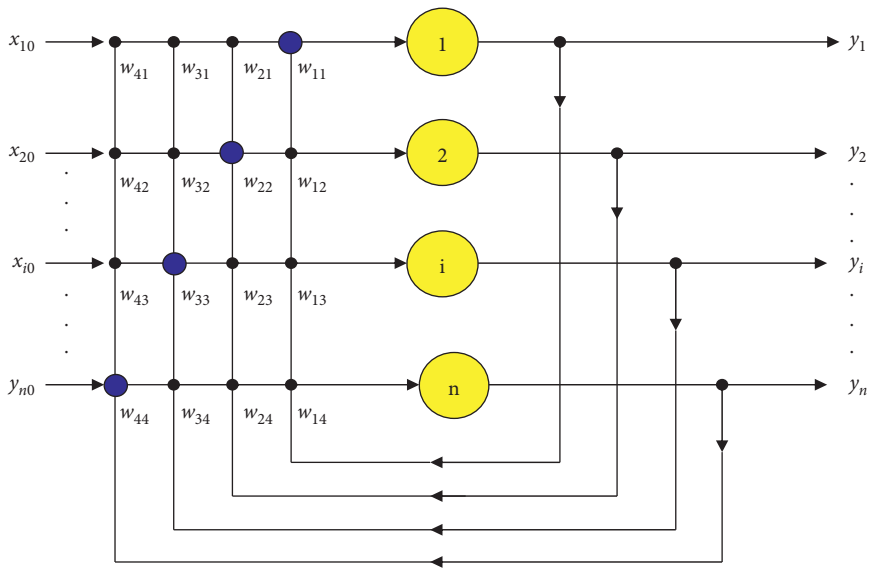

Figure 3: Hopfield neural network in the problem of SERP ranking (x: input search requests within a separate DIRS, y: neuron outputs, and w: values of offsets and synaptic connections).

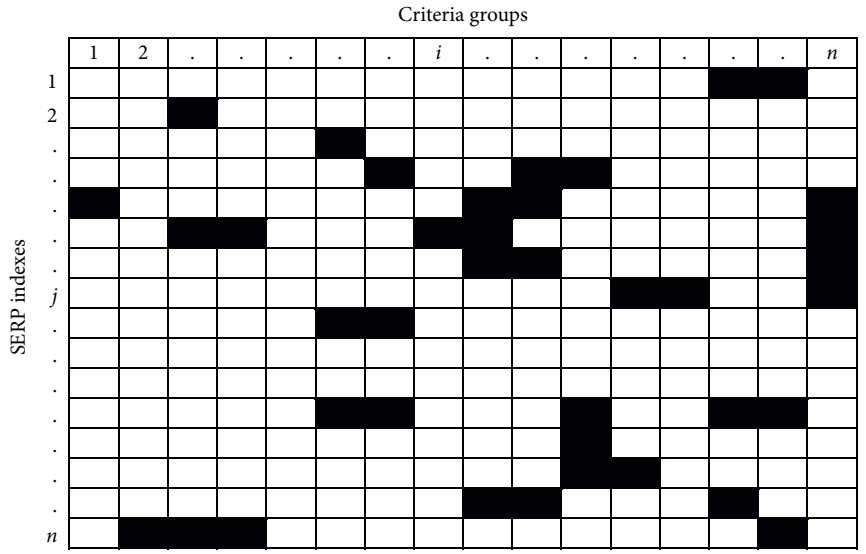

Figure 4: Assignment plan: Hopfield neural network matrix in the state of rest.

this component of the energy function being built has the following form:

$$E_{\psi}^{0}(u) = \frac{A}{2}\sum_{j=1}^{n}\sum_{i=1}^{n}\sum_{v\neq i}^{n} u_{ji}u_{jv} + \frac{B}{2}\sum_{j=1}^{n}\sum_{i=1}^{n}\sum_{\mu\neq j}^{n} u_{ji}u_{\mu i} + \frac{C}{2}\left(\sum_{j=1}^{n}\sum_{i=1}^{n} u_{ji} - n^{2}\right), \tag{16}$$

where A, B, and C are positive constants. The first term takes the minimum and zero value only if each row of the matrix $\{u_{ij}\}$ contains no more than one element, the second term takes the minimum zero value if each column of the matrix contains no more than one element, and finally the third term takes the minimum zero value if the whole matrix $\{u_{ij}\}$ contains exactly n elements.

The built function $E_{\psi}^{0}(u)$ reaches its minimum in all states that correspond to the set of constraints (11)–(13) and represent a plan of assignments. According to the second method to build this component of the energy function being built, we have

$$E_{\psi}^{0}(u) = \frac{A}{2}\sum_{j=1}^{n}\sum_{i=1}^{n} u_{ji} - 1^{2} + \frac{B}{2}\sum_{i=1}^{n}\sum_{j=1}^{n} u_{ji} - 1^{2}, \tag{17}$$

where the first term takes the minimum zero value only if any row of the matrix $\{u_{ij}\}$ contains only one firing neuron, and the second term takes the minimum zero

value if any column of the matrix contains exactly one firing neuron.

In general, the above function takes the minimum zero value only in states that meet constraints (11)-(12) and represent a plan of assignments. Combining the function (16) with the function (17) or the function (18), we build the energy function in its finished form:

$$E^0(u) = \frac{A}{2}\sum_{j=1}^{n}\sum_{i=1}^{n}\sum_{v\neq i}^{n} u_{ji}u_{jv} + \frac{B}{2}\sum_{j=1}^{n}\sum_{i=1}^{n}\sum_{\mu\neq j}^{n} u_{ji}u_{\mu i} + \frac{C}{2}\left(\sum_{j=1}^{n}\sum_{i=1}^{n} u_{ji} - n^2\right) - F\sum_{j=1}^{n}\sum_{i=1}^{n} u_{ji}r_{ji}, \tag{18}$$

or

$$E^0(u) = \frac{A}{2}\sum_{j=1}^{n}\left(\sum_{i=1}^{n} u_{ji} - 1^2\right) + \frac{B}{2}\left(\sum_{i=1}^{n}\sum_{j=1}^{n} u_{ji} - 1^2\right) - F\sum_{j=1}^{n}\sum_{i=1}^{n} u_{ji}r_{ji}. \tag{19}$$

We define network parameters having compared one of the obtained functions with the energy function put down in the general form:

$$E(u,T,I) = -\frac{1}{2}\sum_{j=1}^{n}\sum_{i=1}^{n}\sum_{\mu=1}^{n}\sum_{v=1}^{n} T_{ji\mu v}u_{ji}u_{\mu v} + \sum_{j=1}^{n}\sum_{i=1}^{n} u_{ji}I_{ji}, \tag{20}$$

where $T_{ji\mu v}$ is the coefficient of connection between the input of the ijth neuron and the output of the μvth neuron and I_{ji} is shift of the ijth neuron.

In this formula, for the energy function of the network, the time parameter is intentionally omitted due to the fact that in determining the synapses and external shifts, it does not play a significant role for both discrete-time networks and continuous-time networks. Moreover, this formula should be used when determining the parameters of synthesized networks, both with discrete and continuous states. The reason for this is the fact that the energy functions of networks with discrete and continuous states differ only in the presence of the integral term in the latter, which does not explicitly depend on the values of synapses and external shifts [29, 30].

In order to determine the parameters of the network in accordance with the built energy function (19), we give the formula for this function in the form

$$E^0(u) = \frac{A}{2}\sum_{j=1}^{n}\sum_{i=1}^{n}\sum_{v\neq i}^{n} u_{ji}u_{jv} + \frac{B}{2}\sum_{j=1}^{n}\sum_{i=1}^{n}\sum_{\mu\neq j}^{n} u_{ji}u_{\mu i} + \frac{C}{2}\sum_{j=1}^{n}\sum_{i=1}^{n}\sum_{\mu=1}^{n}\sum_{v=1}^{n} u_{ji}u_{\mu v} - \mathrm{C}n\sum_{j=1}^{n}\sum_{i=1}^{n} u_{ji} - F\sum_{j=1}^{n}\sum_{i=1}^{n} u_{ji}r_{ji} + \frac{C}{2}n^2, \tag{21}$$

and equate the coefficients for the linear and quadratic terms of the last formula and energy (21). The last term can be excluded from consideration, as it does not depend on the state of the network. Matching of linear terms allows to determine the value of external shifts, and matching of quadratic terms allows to determine the synaptic connections between neurons. Analysis of the first term of the built energy function indicates that any neuron in the network must have synaptic connections with the coefficient—A with all neurons of the row of the same name (condition $\mu = i$) except the considered neuron itself (condition $v \neq j$).

The second term dictates the presence of connections with the coefficient—B between the neurons of the column of the same name (condition $v = j$) in addition to its own feedback (condition $\mu \neq i$). The third term indicates that all neurons in the network are connected to each other by synapses with the coefficients—C. With the help of the Kronecker symbol—δ_{ji}, we form the resulting formula for synaptic connections of the network in the form

$$T_{ji\mu v} = -A\delta_{i\mu}(1-\delta_{iv}) - B\delta_{iv}(1-\delta_{i\mu}) - C = = -A\delta_{i\mu} - B\delta_{iv} + (A+B)\delta_{i\mu}\delta_{iv} - C, \_i, j, \mu, v \in \overline{1,n}. \tag{22}$$

Analysis of the fourth and fifth terms of the built energy function shows that all neurons in the network must be fed external offsets in the form

$$I_{ji} = -Cn - Fc_{ji}, i, j \in \overline{1,n}. \tag{23}$$

As a rule, in practical problems, it is assumed that $F = 1$ and A = B; then all nonzero connections have the same weight, which is equal to A. Moreover, when analyzing formulas (23) and (24), one can see that the presence of global connections with the coefficient C of each neuron with each one in the end state of the network corresponds to the plan of assignments ensures the application of a combined signal, which is equal to Cn and compensated by the constant offset Cn to any neuron from all other neurons. Therefore, to simplify the structure of network synapses, global connections with weight C and part of offset Cn can be ignored in the first approximation [31]. In this case, a simplified network structure for the synthesis of the optimal SERP assessment plan, by solving the assignment problem, can be represented as shown in Figure 5.

The required model of a neural network with binary output function of neurons contains a matrix of nxn neurons, each of which is fed an external offset equal to the corresponding performance $I_{ji} = -r_{ji}$, and the output signal of any neuron u_{ji}, with the coefficient A, is fed to the inputs of all neurons of the same rows and columns. In order not to complicate the graphical model (Figure 5.), the connections and shifts of only one neuron N_{ji} are shown in it. An example of a plan of assignments is represented by a set of excited (put in bold) neurons. Another variant of network parameters for the optimal SERP assessment plan can be obtained using the built energy function in the form of (20). Similar to the above procedure, we give this expression in a new form (21):

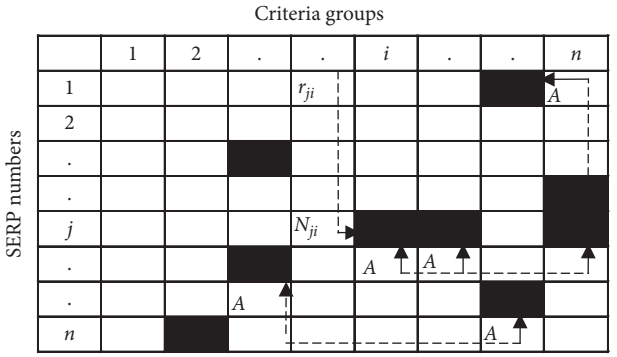

Figure 5: Dynamic neural network relaxing to its energy minimum interpreted as the maximum total value of relevance in the combinatorial group of criteria.

$$E^0(u) = \frac{A}{2}\sum_{j=1}^{n}\sum_{i=1}^{n}\sum_{\nu=1}^{n} u_{ji}u_{j\nu} + \frac{B}{2}\sum_{j=1}^{n}\sum_{i=1}^{n}\sum_{\mu=1}^{n} u_{ji}u_{\mu i} - A\sum_{j=1}^{n}\sum_{i=1}^{n} u_{ji} - B\sum_{j=1}^{n}\sum_{i=1}^{n} u_{ji} - F\sum_{j=1}^{n}\sum_{i=1}^{n} u_{ji}r_{ji} + \frac{n}{2}(A+B), \tag{24}$$

and compare the coefficients for linear and quadratic terms, discarding the last term. As a result, we obtain

$$T_{ji\mu\nu} = -A\delta_{i\mu} - \delta_{i\nu}, \quad I_{ji} = -(A+B) - Fr_{ji}, i, j, \mu, \nu \in \overline{1, n.} \tag{25}$$

In addition to the above functions, one can use various combinations of functions (17) and (18) to build the energy function $E^0(u)$. As a result, one will obtain different variants of neural network parameters. When building a neural network with continuous states, it is necessary to provide conditions for finding rest points in the corners of the n-dimensional cube of its state space. Another way to ensure strict binarity of the output signals of neurons in steady states is to add to the energy function being built an additional component that reaches a minimum value in the states of the network in which the output signals of neurons take the value "0" or "1." An example of such a function is as follows:

$$E^0_\beta(u) = \frac{G}{2}\sum_{j=1}^{n}\sum_{i=1}^{n} u_{ji}\left(1 - u_{ji}\right) = \frac{G}{2}\sum_{j=1}^{n}\sum_{i=1}^{n} u_{ji} - \frac{G}{2}\sum_{j=1}^{n}\sum_{i=1}^{n} u_{ji}^2, \tag{26}$$

where $G > 0$ is constant. Adding this term to the earlier built energy function, for example, in the form of (19), we obtain

$$E^0(u) = \frac{A}{2}\sum_{j=1}^{n}\sum_{i=1}^{n}\sum_{\nu\neq i}^{n} u_{ji}u_{j\nu} + \frac{B}{2}\sum_{j=1}^{n}\sum_{i=1}^{n}\sum_{\mu\neq i}^{n} u_{ji}u_{\mu i} + \frac{C}{2}\sum_{j=1}^{n}\sum_{i=1}^{n}\sum_{\mu=1}^{n}\sum_{\nu=1}^{n} u_{ji}u_{\mu\nu} - \frac{G}{2}\sum_{j=1}^{n}\sum_{i=1}^{n} u_{ji}^2 - Cn\left(\sum_{j=1}^{n}\sum_{i=1}^{n} u_{ji} - tFn\sum_{j=1}^{n}\sum_{i=1}^{n} u_{ji}r_{ji} + h\frac{C}{2}n_i^2\right), \tag{27}$$

from where we define the following parameters of the search neural network:

$$T_{ji\mu\nu} = -A\delta_{i\mu}\left(1 - \delta_{i\nu}\right) - B\delta_{i\nu}\left(1 - \delta_{i\mu}\right) - C + G\delta_{i\mu}\delta_{i\nu} = -A\delta_{i\mu} - B\delta_{i\nu} + (A + B + G)\delta_{i\mu}\delta_{i\nu} - C, \quad I_{ji} = -Cn - Fr_{ji}, j, \mu, \nu \in \overline{1, n.} \tag{28}$$

Combining formulas (27) and (21), we can build the energy function as follows:

$$E^0(u) = \frac{A}{2}\sum_{j=1}^{n}\sum_{i=1}^{n}\sum_{\nu=1}^{n} u_{ji}u_{j\nu} + \frac{B}{2}\sum_{j=1}^{n}\sum_{i=1}^{n}\sum_{\mu=1}^{n} u_{ji}u_{\mu i} - \frac{G}{2}\sum_{j=1}^{n}\sum_{i=1}^{n} u_{ji}^2 + \frac{G}{2}\sum_{j=1}^{n}\sum_{i=1}^{n} u_{ji} - A\sum_{j=1}^{n}\sum_{i=1}^{n} u_{ji} - B\sum_{j=1}^{n}\sum_{i=1}^{n} u_{ji} - F\sum_{j=1}^{n}\sum_{i=1}^{n} u_{ji}r_{ji} + \frac{n}{2}(A+B), \tag{29}$$

where the required network parameters are determined as follows:

$$T_{ji\mu\nu} = -A\delta_{i\mu} - B\delta_{i\nu} + G\delta_{i\mu}\delta_{i\nu}, \quad I_{ji} = \left(A + B - \frac{G}{2}\right) - Fr_{ji}, j, \mu, \nu \in \overline{1, n.} \tag{30}$$

The ranking of documents in the case of a single criterion of significance, i.e., in the extreme case of $V = 1$, is implemented under the following assumption: there are many values of relevance of the SERP list found as a result of the DIRS request: $\{r_i\}$, $i \in N = 1, \ldots, n$. As a result of ranking, the numbers are arranged in ascending order of indices $j = \pi(i)$ so that $\forall j \in 1 \ldots (n-1), r_j \leq r_{j+1}$.

The pair of numbers $\{r_k, r_l\}$ was chosen arbitrarily. Similar proofs can be provided for any other pair of numbers. Specifically, condition (9) will be valid for different pairs of adjacent elements. Due to the fact that any permutation can be represented by the superposition of transposition of adjacent elements, the maximum value of the linear function (5) will be achieved at the permutation in

which all pairs of adjacent elements are sorted, which corresponds to the above solution of SERP sorting problem [32, 33].

Thus, the initial problem of finding a sorting permutation is reduced to the optimization of the linear function with a set of various permutations, whose solution is defined in the form of (6). To solve this problem using a neural network, we present its neural network interpretation. We assume an arbitrary substitution $j = \pi(i)$ in the form of a matrix of neurons $[V_{ij}]$ with *nxn* dimension as follows:

$$(j = \pi(i)) \Leftrightarrow \left(V_{ij} = 1\right), \forall i, j \in \overline{1, n}. \tag{31}$$

At the content level, the excited state of the neuron $V_{ij} = 1$ corresponds to the fact that the ith element of the initial set of values of relevance r occupies the jth position in the substitution $\pi(i)$. There must be exactly one excited neuron in any row and in each column of such a matrix, so the limitations of the form are valid:

$$\sum_{i=1}^{n} V_{ij} = 1, \forall j \in \overline{1, n}. \tag{32}$$

The neural network interpretation of the optimizing function (5) will be presented as follows:

$$\phi(V) = \sum_{j=1}^{n} a_j \sum_{i=1}^{n} r_j V_{ij} \longrightarrow \max_{M}. \tag{33}$$

Comparing the last formula with the results of the neural network interpretation of the assignment problem in the forms (11)–(14), we conclude that the optimization formulation of the SERP sorting problem is identical to the formulation of the assignment problem provided that the elements of the performance matrix are defined as follows:

$$c_{ij} = a_j r_i \_ i, j \in 1, \ldots, n. \tag{34}$$

Therefore, the further building of the neural network for solving the problem (6) will completely coincide with the building of the network for solving the SERP assignment problem. The parameters of networks for solving both the first and second problems will be determined by the same formula [34, 35]. Specifically, using the parameters of the network to solve the assignment problem taking into account the condition (35), we obtain the network parameters to solve the sorting problem in the following form:

$$\begin{aligned} T_{ji\mu\nu} &= -A\delta_{i\mu} - \delta_{i\nu}, \\ I_{ji} &= -(A + B) - Fr_{ji}, j, \mu, \nu \in \overline{1, n}. \end{aligned} \tag{35}$$

Using another formula to determine the parameters of the network for solving the assignment problem, one can obtain a family of neural networks to solve the problem of sorting data in DIRS.

4.2. Use of the Model through Relaxation of the Hopfield Network Energy Function. At the fourth stage of the method implementation, the Hopfield neural network is initiated by an input random vector that "relaxes" to its energy minimum, and the output results of each of the neurons are interpreted as an index according to which DIRS requests should be ranked. The input vector specifies the initial states of all elements—neurons. The element to be updated is selected randomly. The selected element receives weighted signals from all other neurons and changes its state. Another element is selected and the process is repeated. The neural network reaches the point when none of its elements, being already selected for updating, does not change its state. In the general case, the end rest point U^*, to which the network will pass in the process of energy minimization, will be determined by its initial state U° and the relief of the energy function $E\ (U, T, I)$ set in the space of states M [36, 37]. We turn to the simplified version of the network to solve the problem of assignment presented in Figure 3.

In this case, the relief of the energy function will be determined by the module of synaptic connections $T = A$ and the performance matrix $\{r_{ji}\}$. With a rather wide range of values of the elements of this matrix and an arbitrary value of the module of connections T, the network not only does not guarantee the transition to the end state, which corresponds to the global maximum of the optimizing function but may have end steady states that do not correspond to any plan of assignments. This situation can be addressed by introducing additional matching of the values of the module of connections and external shifts of the network, which are the input data of the problem, by scaling the latter [38]. The selection of the scaling factor of the input data of the problem is based on the results of the study of the influence of the module of connections T on the relief of the energy function E for some specific variant of the performance matrix.

We consider a practical version of the problem with the size of 2×2 with the performance matrix as follows: $r_{ji} = \begin{pmatrix} 1 & 2 \\ 4 & 3 \end{pmatrix}$. Each initial state U of the network is matched by a four-bit binary code, which is a rolled matrix $\{u_{ji}\}$, and the change in the energy function and its components depending on the state of the network is examined. A graph of change in the own component of the energy function is presented in Figure 6:

$$E_0 = -\frac{1}{2} \sum_{j=1}^{n} \sum_{i=1}^{n} \sum_{\mu=1}^{n} \sum_{\nu=1}^{n} T_{ji\mu\nu} u_{ji} u_{\mu\nu}, \tag{36}$$

determined by the value of the module of connections and obtained at $T = 1$.

Regardless of the value of the module of connections, this component takes the minimum (zero) value in the states corresponding to the plans ("1001" and "0110") or characterized by the presence of no more than one excited neuron. The full line shows the graph of the change of the forced component of the energy function $E_c = -\sum_{j=1}^{n} \sum_{i=1}^{n} I_{ji} u_{ji}$, which is determined by external shifts in accordance with the performance matrix and does not depend on the value of the module of connections. Graphs of changes in the full energy function $E = E_0 + E_c$ at different values of the module of connections T are shown by solid lines. As can be seen from the analysis of the presented

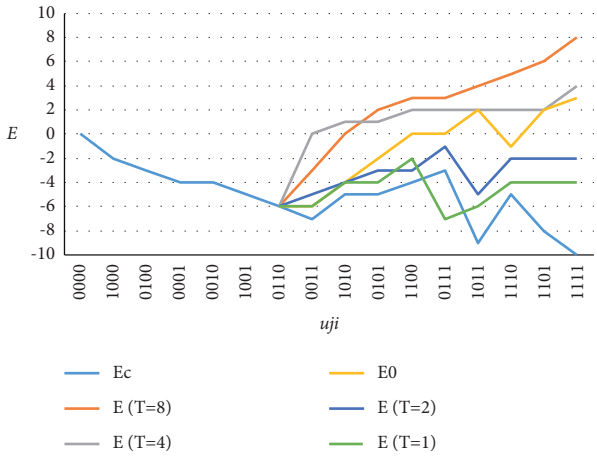

Figure 6: Change in the own component of the energy function.

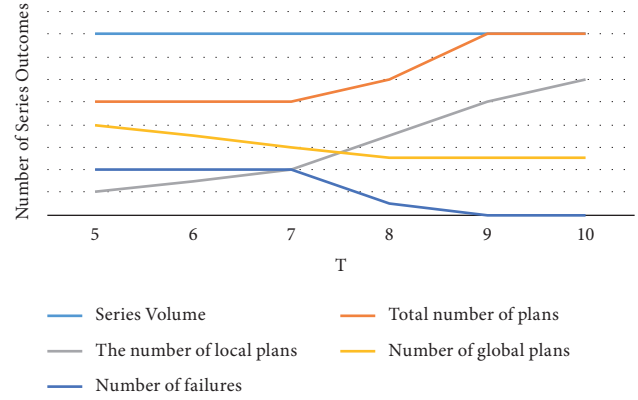

Figure 7: Implementations of evolutionary network processes depending on the module of connections (T).

results, at rather small values of the module of connections the relief of the energy function is complex and multiextreme. Despite the fact that in this case the four-dimension space of the network states is reflected on the integer axis, even such a simplified representation allows to conclude that with increasing value of T the relief of the energy function becomes more regular, the number of local minima decreases, and global extremum is identified, which corresponds to the optimal plan of assignments "0110" [39]. More constructive conclusions can be drawn from the results of the study of the quality of solving the problem of assignment at different values of the module of connections. For the purpose, we consider the problem of assignment with the matrix: $\begin{pmatrix} 10 & 5 & 4 & 6 \\ 6 & 4 & 9 & 7 \\ 1 & 8 & 3 & 6 \\ 5 & 3 & 7 & 2 \end{pmatrix}$. Totally, in this case, there are 24 possible plans of assignments of criteria of evaluation of the found SERPs where the values of cost function are within the range from 11 to 32. The last value corresponds to the optimal solution, which is the only one. A family of initial states of the network $U^{(0)}$ is set, each of which consists of one excited neuron and all other excited neurons. Thus, by sequentially sorting all the neurons, a series of sixteen implementations of the evolutionary processes of the network from different initial states with the above selected performance matrix and the specific value of the module of connections T is carried out. The results of solving the problem in six series, which correspond to the values of the module of connections from 5 to 10 that are presented in Figure 7.

At large values of T, close to the maximum element of the performance matrix $r_{\max}$, out of sixteen solutions in a series six results give the optimal plan of assignments. With that, ten other solutions of the series correspond to local maxima, whose cost function value is not less than 28. This condition is maintained with a further increase in the module of connections. The module of connections is reduced to a value close to the average for all elements of the performance matrix, which leads to an increase in the number of strictly optimal solutions, a decrease in the number of locally optimal solutions, and the emergence of stable conditions not meeting the plans of assignments, whose number is growing.

Based on the above results, the following practical recommendations can be made. When solving the problem of assignment, using a neural network, the value of the module of synaptic connections should be within the range from the average to the maximum element of the performance matrix [40]. In practice, when changing the values of the module of synaptic connections is a difficult technical problem, this recommendation should be implemented through scaling the input performance values before their input into the network, in the form of neuron shifts at the given value of T. The scaling factor k_m is selected from the range of $k_m \in [r_{\text{mid}}/T; r_{\max}/T]$, and the shift signals are defined in the form of $I_{ji} = r_{ji}/k_m$, $j, i = 1, \ldots n$. The final selection is made in each specific case depending on the required quality of the solution and the available time [41]. If it is necessary to promptly obtain a solution of the problem that is not necessarily fundamental, but close enough to it by a single call to the network, the scaling factor is selected, which is close to $k_m = r_{\max}/T$. If it is necessary to obtain strictly optimum solution and there is a possibility to call to the network several times, the factor is selected, which is close to $k_m = r_{\text{mid}}/T$, a series of solutions for various initial states of the network is found, and among the found plans of assignments of groups of criteria for SERPs, the best plan is assigned.

5. Neural Network Request Ranking Algorithm for DIRS

We define the basic neural network request ranking algorithm for DIRS. A general block diagram of the developed neural network ranking algorithm with a vector relevance criterion is given in Figure 8. In the first three stages, the input data of the algorithm are formed [42, 43]. At the first stage, the number of Z starts of neural network relaxation is set to its energy minimum.

At the second stage, based on statistical, dynamic internal, and dynamic external factors, the vector of relevance criteria of the found SERPs is formed: v_i, i = l,...,N. Since the

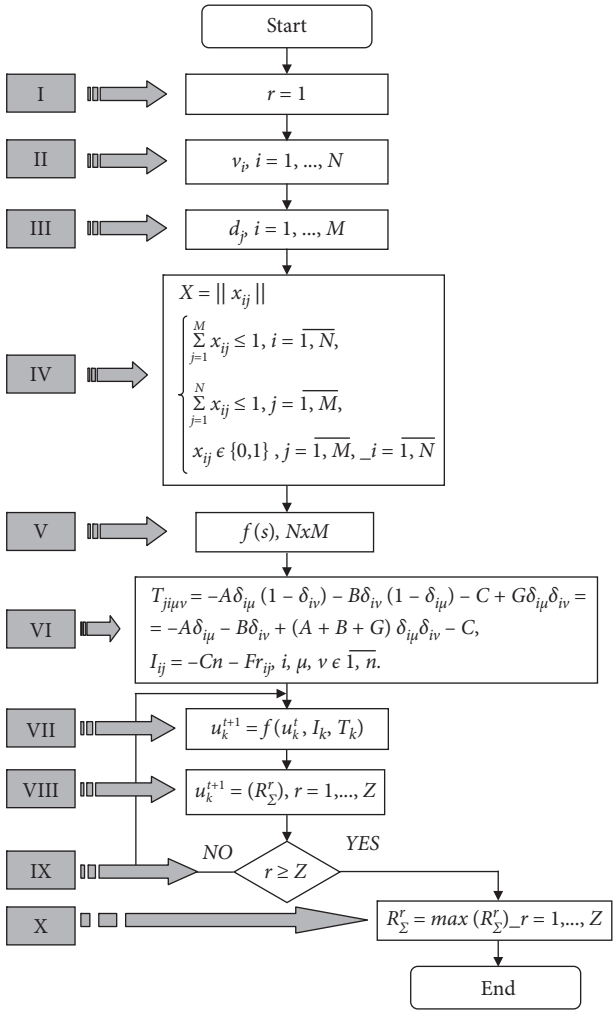

Figure 8: Block diagram of the neural network ranking algorithm with the vector relevance criterion.

criteria v_i are one order more than SERP d_j, the criteria are combinatorially grouped by all possible combinations without repetition and each group is taken as a destination unit. At the third stage, the unordered part of the set of found SERPs to be ranked. d is selected: d_j, $j = 1, ..., M$. At the fourth stage, the table $X = \|x_{ji}\|$ of correspondence of D set of the found SERP to the V set of significance criteria is built.

The input data for solving the ranking problem within the combinatorial assignment problem are defined in the table. At the fifth stage, the structure of the neural network model is defined—the type of activation function $f(s)$, the number of $N \times N$ neurons—which depends on the dimensionality of the vectors of the input data and the mode of operation (asynchronous mode). At the sixth stage, using formulas (23), (24), and (31), the coefficients of connectivity $T_{ji\mu v}$ and shift I_{ji} of the model of binary Hopfield neural network are calculated: $u = f(u,I,T)$, where u–neuron outputs, I–shift values, and T–coefficients of synaptic connections. At the seventh stage, the initialization of the neural network is implemented by a random input vector u^0; as a result of subsequent iterations of which, the neural network is set to equilibrium $u_k^{t+1} = f(u_k^t, I_k, T_k)$.

At the eighth stage, an unambiguous interpretation of the output signals of neurons binary Hopfield neural network is carried out. Interpretation of neural network outputs allows to obtain the desired sequence of SERP indices according to a given set of DIRS relevance criteria, and the total relevance value of $R_\sum^r$ on the rth start of the neural network. Stages 7–9 are performed after achievement of the set quantity of 2 starts of relaxation of a neural network to its energy minimum (check of the condition $r \ge Z$ at stage 9). At the final stage 10, the SERP presentation sequence is selected, whose total relevance value, $R_\Sigma^r = \max(R_\Sigma^r)\_r = 1, \ldots, Z$, is maximum.

6. Practical Implementation of the Neural Network Search Request Ranking Algorithm in DIRS

The developed and implemented algorithms and methods for synthesizing the parameters of the neural network ranking unit allow determining the parameters of the network up to constant coefficients and can be used alone or in various combinations with each other. In this regard, the experimental results of comparing the quality of solving problems of assignment on neural-like networks, the parameters of which were determined at different values of constants in equations, are of practical interest. The authors consider the example of equations that define the parameters of the neural network model in the ranking unit for solving the problem of assignment with dimension of 20 to 200 links found on Internet. To evaluate the quality of the solution, the authors use the parameter:

$$\Phi_{ig}(c) = \frac{\phi_{cp}(c) - \phi(c, x*)}{\phi_{cp}(c) - \phi\left(c, x^{\min}\right)}, \tag{37}$$

where $\phi_{cp}(c)$ is the average value of the cost function for the whole set of valid solutions x for a specific set of search request parameters.

In this equation, c denotes a set of input data of the problem, which, depending on the type of problem, will be a performance matrix $[c_{ij}]$. The values of $\phi_{cp}(c)$ and $\phi(c, x^{\min})$ are determined by a complete search. To evaluate the statistically average value of quality $\Phi_w\ (c)$, different variants of the input data randomly selected from the range [0,1] are considered, for each of which 10 solutions of different initial conditions of evolution of the network V^0 are obtained. Table 1 presents the results of the evaluation of the statistically average value of quality $\Phi_w(c)$ for solving the problem of assignment for different dimensions and the above rules for determining network parameters (Table 2).

The above results testify to quite acceptable quality of problem solving by means of the synthesized models of the neural network ranking unit.

To determine the efficiency of neural network ranking compared to traditional ranking methods, experiments were conducted with various search requests and samples of web links from 20 to 200. Table 3 summarizes the data on the time of problem solving.

Table 2: Results of the experimental evaluation of the quality of the solution of the vector ranking problem with the number of ranked links from 20 to 200.

Network parameters (equations)	Number of ranked documents in a request				
	20	40	80	100	200
(4.6)	+0.980	0.960	0.975	0.988	0.887
(4.7)	1.000	0.999	0.999	0.958	0.898
(4.8)	1.000	0.999	1.000	1.000	0.899

Table 3: Results of experimental comparison of the efficiency of problem solving with the number of ranked links from 20 to 200.

Ranking algorithm	CPU run time (s)		
	20 links	80 links	200 links
Vector neural network ranking	5,1667e – 004	2,1667e – 002 (10 model runs)	0,1211 (5 model runs)
Scalar neural network ranking	6,379e – 004	9,8623ee – 002 (10 model runs)	0,5274 (5 model runs)
Sorting the relevance of found links by the "bubble" method	1,1437e – 003	0.5274	8.4578
Sorting the relevance by selection of the largest element	1,3496e – 003	0.8305	9.6424
Ranking by sorting the array of values by insert	2,0054e – 003	0.9846	11.2836
Exhaustive search	10.2159	—	—

Table 4: Examples of 20 search requests of the prototype of DIRS search engine.

No.	Search request	No.	Search request
1	Syllabus	11	Bright
2	Wear	12	Kalman filter
3	Periodic	13	Hill
4	Analyzing the response	14	Probably an increase
5	Revive	15	Tragic
6	Test period	16	Ophthalmology
7	Speak	17	Link
8	Waiting for the storm	18	Verse
9	Exemplary subject	19	Connect
10	Album	20	Early

Table 4 shows examples of search requests of the prototype of DIRS search engine.

Investigation of the sequential dynamics of the neural network block during the ranking of web links. Although within this variant of the organization of the Internet ranking block, in turn, a number of subvariants can be identified, the latter will differ slightly from each other in their efficiency, so without loss of generality, the authors settled on one of them. It is implemented in two main steps. At the first step, the calculation of binary functions from the current variables of the model state is carried out. It is implemented in the form of a sequential process of variable sampling: the sum of Hopfield neural network inputs from the transfer buffer to the calculation unit of the binary output function, the implementation of the output function, and the transfer of the final output of one neuron to the buffer. The second step is to sequentially determine for each neuron the right part of the numerical scheme for obtaining the final difference. Adding the execution time of two consecutive steps, the authors obtain the desired estimate of the implementation time of one ranking step for a sequential version of the organization of the block. Table 5 presents the results of measuring the ranking time of different requests depending on the size of the sample being ranked.

Table 5: Time of ranking operation *(c)* depending on the sample size in the sequential implementation of the block.

Search request	$N = 20$	$N = 80$	$N = 200$
Syllabus	0.37×10^{-3}	0.133×10^{-2}	0.854
Wear	0.13×10^{-3}	0.932×10^{-2}	0.86
Periodic	0.273×10^{-3}	0.563×10^{-2}	0.34
Analyzing the response	0.57×10^{-3}	0.3×10^{-2}	0.618
Revive	0.34×10^{-3}	0.758×10^{-2}	0.62
Test period	0.8545 ч 10^{-3}	0.34×10^{-2}	0.32
Speak	0.62×10^{-3}	0.348×10^{-2}	0.68
Waiting for the storm	0.45×10^{-3}	0.598×10^{-2}	0.63
Exemplary subject	0.864 ч 10^{-3}	0.555×10^{-2}	0.51
Album	0.12×10^{-3}	0.995×10^{-2}	0.436
Bright	0.386×10^{-3}	0.774×10^{-2}	0.68
Kalman filter	0.56×10^{-3}	0.578×10^{-2}	0.657
Hill	0.78 ч 10^{-3}	0.42×10^{-2}	0.942
Probably an increase	0.655 ч 10^{-3}	0.233×10^{-2}	0.85
Tragic	0.30 ч 10^{-3}	0.177×10^{-2}	0.773
Ophthalmology	0.471×10^{-3}	0.893×10^{-2}	0.6
Link	0.89×10^{-3}	0.64×10^{-2}	0.835
Verse	0.535×10^{-3}	0.88×10^{-2}	0.579
Connect	0.644×10^{-3}	0.45×10^{-2}	0.848
Early	0.55×10^{-3}	0.518×10^{-2}	0.87

In the structure of the implementation of this variant of the ranking block, there is an element of parallel summation of *N+1* number of neurons. This summation is carried out using the tree of two-input software adders. The most significant contribution to the duration τ, which depends on dimension of the model, is the time of calculating the sum $\sum_{i=1}^{n} u_{ji} I_{ji}$, where *uji* and I_{ij} are neuron output and the size of its bias. The contribution of sum calculation to the total time can be reduced by using adders with a large number of inputs.

The family of intermediate variants of parallelization is naturally generated by the assumption of the presence of not one, as was the case in an absolutely sequential version, but several traditional serial processors, each of which simulates a group of neurons in an absolutely sequential scheme. The more processors, the less time τ. The limit case when the number of

Table 6: Time of ranking operation (c) depending on the sample size in the parallel implementation of the block.

Search request	$N = 20$	$N = 80$	$N = 200$
Syllabus	0.62×10^{-4}	0.156×10^{-3}	0.976×10^{-2}
Wear	0.826×10^{-4}	0.386×10^{-3}	0.68×10^{-2}
Periodic	0.64×10^{-4}	0.185×10^{-3}	0.8×10^{-2}
Analyzing the response	0.428×10^{-4}	0.567×10^{-3}	0.462×10^{-2}
Revive	0.596×10^{-4}	0.28×10^{-3}	0.486×10^{-2}
Test period	0.95×10^{-4}	0.653×10^{-3}	0.593×10^{-2}
Speak	0.396×10^{-4}	0.56×10^{-3}	0.542×10^{-2}
Waiting for the storm	0.605×10^{-4}	0.97×10^{-3}	0.457×10^{-2}
Exemplary subject	0.864×10^{-4}	0.74×10^{-3}	0.51×10^{-2}
Album	0.76×10^{-4}	0.869×10^{-3}	0.436×10^{-2}
Bright	0.725×10^{-4}	0.774×10^{-3}	0.678×10^{-2}
Kalman filter	0.461×10^{-4}	0.578×10^{-3}	0.542×10^{-2}
Hill	0.146×10^{-4}	0.42×10^{-3}	0.47×10^{-2}
Probably an increase	0.475×10^{-4}	0.233×10^{-3}	0.825×10^{-2}
Tragic	0.486×10^{-4}	0.177×10^{-3}	0.589×10^{-2}
Ophthalmology	0.565×10^{-4}	0.893×10^{-3}	-0.46×10^{-2}
Link	0.982×10^{-4}	0.475×10^{-3}	0.728×10^{-2}
Verse	0.214×10^{-4}	0.79×10^{-3}	0.5×10^{-2}
Connect	0.47×10^{-4}	0.35×10^{-3}	0.48×10^{-2}
Early	$0{,}445 \times 10^{-4}$	$0{,}764 \times 10^{-3}$	$0{,}974 \times 10^{-2}$

neurons is equal to the number of processors τ will be determined by the time of absolutely sequential implementation of the model of one neuron. Approximately for this family of parallelization variants, one can consider $\tau \sim N^2/\pi$.

An additional number of families of different variants give hypotheses about the parallelization of the implementation of certain operations in the model of one neuron.

Table 6 presents the results of measuring the ranking time of different requests depending on the size of the sample being ranked.

A comparison of Tables 5 and 6 shows a significant gain in ranking time with an increase in the number of ranked web links and the degree of parallelization of the neural network ISS (intellectual subsystem) block. Knowing the methods of parallelization of the neural network and substituting the corresponding values of the parallelization parameters, we can evaluate the efficiency of this specific example of the ranking block based on the ISS server. In conclusion, it should be noted that the methods considered in the study do not exhaust all possible variants for parallelization, and hence all possible variants for hardware implementation of the Hopfield neural network in the web search ranking block. For example, a broad family of parallelization variants allows using pipelined methods of arithmetic operations in the ranking block, which may be one of the areas of further studies on creation of a class of digital neuro accelerators for web search. The results of experimental tests of neural network ranking procedures showed high efficiency of the latter in the adapted multicore architecture of hardware and software.

7. Conclusion

An analysis of the existing capabilities of modern information retrieval systems and problems of intelligent search for textual information related to the need to solve discrete optimization problems was carried out. The analysis showed that as of today the neural network is not fully used in information retrieval systems to solve problems of optimal representation of the found SERPs. The analysis of neural network models of optimization of information retrieval procedures applicable in algorithms of information retrieval systems was carried out. So, the choice of method to solve the optimization problem in the operation of DIRS is determined by the original set of alternatives. With a small number of ranked SERPs, the use of accurate methods becomes effective; otherwise, heuristic methods are used for solving a specific optimization problem where neural networks have advantages. The solution of optimization problems with the help of neural networks is based on the properties of the latter to minimize the energy function of the stability of states corresponding to some local minima of the network energy.

A method of ranking documents in DIRS based on a neural network solution of combinatorial problems of assignment and sorting was developed. The solution of these problems with the help of neural network is due to the need to solve an integer problem of optimizing the large dimension of the found SERPs. The architecture of the neural network model of ranking of SERPs based on the dynamic binary Hopfield neural network was created. Several variants of neural network models with binary output function of neurons were created for the synthesis of the optimal evaluation plan based on a combinatorial set of criteria by solving the problem of assignment. The models differ in the rules for determining the coefficients of synaptic connections and external shifts, and practical recommendations for their selection are provided.

The algorithm of operation of the neural network ranking unit at various values of significance criterion was developed. During analytical studies, it was established that the optimization formulation of the problem of sorting of the values of relevance of documents is identical to the formulation of the problem of assignment of combinatorial groups of evaluation criteria, provided that the elements of the performance matrix of the latter are defined as linear combinations of relevance values.

Data Availability

No data were used to support this study.

Consent

Consent is not applicable.

Conflicts of Interest

The authors declare that they have no conflicts of interest regarding the publication of this paper.

Authors' Contributions

Conceptualization was prepared by V. B. and S. D.; methodology and investigation were conducted by S. D.; software and resources were obtained by S. B.; validation was

performed by M. M. and O. A.; formal analysis was done by V. B.; data curation and project administration were carried out by O. A.; the original draft was prepared by M. M.; review and editing were performed by V .B.; visualization was carried out by S. B.; supervision was done by S.D.; and funding acquisition was done by M. M. All authors have read and agreed to the published version of the manuscript.

References

[1] V. Maurya, P. Pandey, and L. S. Maurya, "Effective information retrieval system," *International Journal of Emerging Technology and Advanced Engineering*, vol. 3, no. 4, p. 787, 2013.

[2] W. Arms, *Manuscript of Digital Libraries*, MIT Press, Cambridge, MA, USA, 2002.

[3] T. M. Cover and T. A. Joy, *Elements of Information Theory*, John Wiley & Sons Interscience Publication, Hoboken, USA, 1991.

[4] G. Kowalski and M. T. Maybury, *Information Storage and Retrieval Systems*, Springer, New York, NY, USA, 2005.

[5] F. Crestani, "Spoken query processing for interactive information retrieval," *Data & Knowledge Engineering*, vol. 41, no. 1, pp. 105–124, 2002.

[6] P. A. Mohan, *Residue Number Systems: Algorithms and Architectures*, Kluwer Academic Pub, Boston, Flordia, USA, 2002.

[7] E. Greengrass, "Information retrieval: a survey by ed greengrass," *Information Retrieval*, vol. 141-163, 2002.

[8] E. Brynjolfsson and A. McAfee, *Race against the Machine: How the Digital Revolution Is Accelerating Innovation, Driving Productivity, and Irreversibly Transforming Employment and the Economy*, Digital Frontier Press, Lexington, Massachusetts, USA, 2012.

[9] G. Forman, "A pitfall and solution in multi-class feature selection for text classification," in *Proceedings of the 21st International Conference on Machine Learning*, Banff, Canada, January, 2004.

[10] W. Xue and H. Deng, "Unstructured queries based on mobile user context," *International Journal of Pervasive Computing and Communications*, vol. 8, no. 4, pp. 368–394, 2012.

[11] J. Bruna, W. Zaremba, A. Szlam, and Y. LeCun, "Spectral Networks and Locally Connected Networks on Graphs," pp. 1312–6203, 2013, https://arxiv.org/abs/1312.6203.

[12] K. Jarvelin and J. Kekalainen, "IR evaluation methods for retrieving highly relevant documents," in *In: Proceedings of the 23rd Annual International ACM SIGIR Conference on Research and Development in Information Retrieval*, N. J. Belkin, P. Ingwersen, and M. K. Leong, Eds., pp. 41–48, ACM, New York, NY, USA, 2010.

[13] Y. Chang, I. Ounis, and M. Kim, "Query reformulation using automatically generated query concepts from a document space," *Information Processing & Management*, vol. 42, no. 2, pp. 453–468, 2006.

[14] G. Chowdhury, *Introduction to Modern Information Retrieval*, Facet Publishing, UK, . edition, 2010.

[15] A. F. Ward, "Supernormal: how the Internet is changing our minds and our memories," *Psychological Inquiry*, vol. 24, 2013.

[16] K. Agbele, E. Ayetiran, and O. Babalola, "A context-adaptive ranking model for effective information retrieval system," *International Journal of Information Science*, vol. 8, no. 1, pp. 1–12, 2018.

[17] R. T. Rolls, "The representation and storage of information in neural networks in the primate cerebral cortex and hippocampus," in *The Computing Neuron*, R. Durbin, C. Miall, and G. Mitchison, Eds., Addison-Weley, Reading, MA, 1989.

[18] C. Hillar, N. Tran, and K. Koepsell, "Robust Exponential Binary Pattern Storage in Little-Hop-Eld Networks," pp. 1206–2081, 2012, https://arxiv.org/abs/1206.2081.

[19] L. Gibson, B. Finnie, and J. Stuart, "A mathematical model for exploring the evolution of organizational structure," *International Journal of Organizational Analysis*, vol. 23, no. 1, pp. 21–40, 2015.

[20] Yi-An Lai, C.-C. Hsu, W. H. Chen, Mi-Y. Yeh, and S.-De Lin, "Prune: preserving proximity and global ranking for network embedding," *Advances in Neural Information Processing Systems*, pp. 5263–5272, 2017.

[21] Z. Bar-Yossef and Li-T. Mashiach, "Local approximation of pagerank and reverse pagerank," in *Proceedings of the 17th ACM Conference on Information and Knowledge Management*, pp. 279–288, Singapore, July, 2008.

[22] M. E Newman, "Finding community structure in networks using the eigenvectors of matrices," *Physical review. E, Statistical, nonlinear, and soft matter physics*, vol. 74, no. 3, pp. 036104–104, 2006.

[23] B. Krose and V. D P. Smagt, *An Introduction to Neural Networks*, University of Amsterdam, Amsterdam, Switzerland, 1996.

[24] W. Wang and X.-G. Xia, "A closed-form robust Chinese remainder theorem and its performance analysis," *IEEE Transactions on Signal Processing*, vol. 58, no. 11, pp. 5655–5666, 2010.

[25] D. Anderson and G. McNeill, "Artificial Neural Network Technology," Report, 1992.

[26] J. J. Hopfield, "Neural networks and physical systems with emergent collective computational abilities," *Proceedings of the National Academy of Sciences*, vol. 79, no. 8, pp. 2554–2558, 1982.

[27] J. Schmidhuber, "Deep learning in neural networks: an overview," *Neural Networks*, vol. 61, no. 1, pp. 85–117, 2015.

[28] G. A. Kohring, "A high-precision study of the Hopfield model in the phase of broken replica symmetry," *Journal of Statistical Physics*, vol. 59, no. 3-4, pp. 1077–1086, 1990.

[29] V. Gripon and C. Berrou, "Sparse neural networks with large learning diversity," *IEEE Transactions on Neural Networks*, vol. 22, no. 7, pp. 1087–1096, 2011.

[30] R. B. González, *Index Compression for Information Retrieval Systems*, University of A Coruña, A. Coruña, PhD Thesis, 2008.

[31] M. Zhang and Y. Chen, "Link prediction based on graph neural networks," in *Proceedings of the 32nd Conference on Neural Information Processing Systems (NeurIPS 2018)*, Montréal, Canada, February, 2018.

[32] C. Aicher, A. Z. Jacobs, A. Clauset, and A. Clauset, "Learning latent block structure in weighted networks," *Journal of Complex Networks*, vol. 3, no. 2, pp. 221–248, 2015.

[33] S. Sreenivasan and I. Fiete, "Grid cells generate an analog error-correcting code for singularly precise neural computation," *Nature Neuroscience*, vol. 14, no. 10, pp. 1330–1337, 2011.

[34] K. Siau and W. Wang, "Building trust in artificial intelligence, machine learning, and robotics," *Cutter Business Technology Journal*, vol. 31, no. 2, pp. 47–53, 2018.

[35] R. Baeza-Yates and B. Ribeiro-Neto, *Modern Information Retrieval*, Addison&Wesley, Boston, USA, 2011.

[36] S. J. Russell and P. Norvig, *Artificial Intelligence: A Modern Approach*, Prentice-Hall, Hoboken, New Jersey, USA, 2010.
[37] M. Neumann, R. Garnett, C. Bauckhage, and K. Kersting, "Propagation kernels: efficient graph kernels from propagated information," *Machine Learning*, vol. 102, no. 2, pp. 209–245, 2016.
[38] C. T. Meadow, B. R. Boyce, D. H. Kraft, and C. L. Barry, *Text Information Retrieval Systems*, Academic Press, Cambridge, Massachusetts, USA, 2007.
[39] B. Croft, D. Metzler, and T. Strohman, *Search Engines: Information Retrieval in Practice*, Pearson, New York, NY. USA, 2010.
[40] C. J. Van Risjbergen, *The Geometry of Information Retrieval*, Cambridge University Press, Cambridge, MA, USA, 2004.
[41] V. Sutton, *Innovations in Information Retrieval: Perspectives for Theory and Practice*, Library Management, 2012.
[42] M. Levene, "Search engines: information retrieval in practice," Pearson Education, New York, NY. USA, 2011.
[43] S. Buettcher, C. Clarke, and G. Cormack, *Information Retrieval: Implementing and Evaluating Search Engines*, MIT Press, Cambridge, MA, USA, 2010.

Hindawi
Complexity
Volume 2022, Article ID 7993599, 14 pages
https://doi.org/10.1155/2022/7993599

Research Article

Cooperative Production Behavior of Fresh Agricultural Product Suppliers under Regional Product Standardization Construction

Yang Yang[1], **Guanxin Yao**[1,2] **and Xueru Fan**[1]

[1]*School of Management, Jiangsu University, Zhenjiang 212013, China*
[2]*Jiangsu Modern Logistics Research Base, Yangzhou University, Yangzhou 225009, China*

Correspondence should be addressed to Guanxin Yao; 2111810009@stmail.ujs.edu.cn

Received 13 December 2021; Revised 10 February 2022; Accepted 1 March 2022; Published 11 April 2022

Academic Editor: Yu Zhou

From the perspective of regional product standardization construction, the evolutionary game models of standardized collaborative production of fresh agricultural product suppliers with or without government participation were built respectively, and the stability of the main strategy choice was discussed. The results show that when the standardization of regional fresh agricultural product is low and the participants' willingness to cooperate is high, the government can choose not to participate in the guidance, but if the government participates in the guidance but does not participate properly, it will have a reverse inhibition effect. When the standardization degree of regional fresh agricultural product is high, the government must effectively guide and regulate, regardless of the initial will of the participants. When government participation is effective, standardized production subsidies can promote the choice of collaborative strategies, while revenue-sharing mechanism and cost-sharing mechanism have little effect.

1. Introduction

Under the background of consumption upgrading and market competition, the development of agricultural industrialization has become an important way to accelerate the development of China's rural economy and realize the strategy of rural revitalization, and standardization is an important symbol of industrialization. In recent years, more and more landmark associations have cooperated with retailers such as "Jingdong Fresh" and "Hema Fresh" to realize the development of agricultural industrialization, and the high-standard fresh agricultural products created are also favored by consumers. More and more regions have begun to formulate production standards for fresh agricultural products and take the road of industrialization, such as "Dongtai Watermelon" and "Yangcheng Lake Hairy Crab", which are quite effective.

However, the standardization of most fresh agricultural products in China is still relatively low at present, which is mainly affected by the "small farmers" production mode. From the perspective of standardized production, the small-scale agricultural production economic model is difficult to bear the cost of standardized production (technology introduction, equipment purchase, professional staffing, etc.) and thus cannot realize the development of agricultural industrialization, resulting in the fresh agricultural product industry still staying in the small-scale agricultural economic model, which is a vicious circle. From the perspective of product standardization, fresh agricultural products with different quality, specification, and packaging have different requirements for cold chain logistics, which cannot carry out unified standardized logistics operation, reduce the efficiency of cold chain logistics, increase the cost of cold chain logistics, and cannot obtain the scale effect of industrial agglomeration. Under the background that logistics has already become the "third-party profit source" of industrial industry, cold chain logistics cannot fully meet the basic preservation and transportation needs, which undoubtedly restricts the further industrialization of fresh agricultural products.

In the process of China's modernization, small-scale peasant economy has always been regarded as the object of

transformation, so as to continuously promote agricultural development [1]. Agricultural organization is regarded as the only way for "small-scale peasant economy" to connect the development of modern agriculture [2]. Under the dual influence of market and policy, many agricultural industrialization organization modes have emerged, such as "company + farmer," "company + farmer cooperative + farmer," "company + family farm," and many scholars have conducted in-depth research on the problems under different development modes [3–7]. However, under the influence of changes in world conditions, national conditions, and agricultural conditions, such as the increase in the risk of international trade in agricultural products, the accelerated transformation of the domestic food consumption structure, and the continuous increase in the requirements for high-quality agricultural development, the above-mentioned agricultural industry development model shows problems such as insufficient cooperation with agriculture, insufficient effect of leading agriculture, and insufficient comprehensive competitiveness [8]. The root cause is that in the above-mentioned agricultural industrialization development model, the main body of fresh agricultural product supply has a low degree of organization, resulting in low autonomy, weak voice, and high dependence on the company.

So how should we break the "small peasant economy" situation, improve the standardization of fresh agricultural products, and promote the development of industrialization? Referring to the definition of synergy and the elaboration of synergistic effect in literature [9], the horizontal collaborative production behavior of fresh agricultural product suppliers can break individual boundaries, integrate resources and allocate them rationally, expand the scale of fresh agricultural product production, jointly introduce standardized production equipment, promote the formation of regional product standardization, and finally realize the industrialization of fresh agricultural product.

Based on this, the main research questions of this study are as follows: (1) what impact does the degree of regional standardization have on the collaborative production behavior of fresh agricultural product suppliers? (2) How should the government guide the suppliers of fresh agricultural product to carry out highly standardized collaborative production behaviors?

In order to answer the above questions, from the perspective of regional standardization construction, we will first build an evolutionary game model of fresh agricultural product supply entities without government participation and explore the decision-making law of collaborative behavior of fresh agricultural product supply entities. Then, an evolutionary game is constructed with government participation and the role of the government is explored in the collaborative process.

The rest of the study is organized as follows: in Section 2, we present the literature review. In Section 3, we make basic assumptions and notation. Section 4 and Section 5 construct the evolutionary game model without government participation and government participation, respectively. Section 6 presents the numerical examples. We conclude this study in Section 7.

2. Literature Review

In this section, we will briefly review the relevant literature based on two streams of research: high-quality development of fresh agricultural product industry and cooperative behavior analysis based on the evolutionary game.

There are many studies on the high-quality development of the fresh agricultural product industry. Generally speaking, scholars have studied and explored it from three perspectives. The first angle is to improve the quality of fresh agricultural products. He et al. [10] conducted a literature review on quality and operational management issues in food supply chains from four aspects: storage issues, distribution issues, marketing issues, and food traceability and safety issues, providing researchers with a starting point for research. Lin et al. [11] have designed supply chain contracts together with food safety mechanisms that can greatly improve food safety, consumer confidence, and food supply chain profits. Yu et al. [12] studied the impact of government subsidies on food safety. Wang et al. [13] found that the consumption form of online shopping of agricultural products can promote the development of agriculture from high-speed growth to high-quality development. The second angle is the standardization of fresh agricultural products. As the carrier of scientific and technological achievements, standardization can promote the specialization of agricultural production, promote the rational utilization of natural resources, improve competitiveness and sustainable development, and ensure the quality and safety of agricultural products [14]. Yu [15] believed that agricultural standardization can not only ensure quality, reduce production and transaction costs, and form economies of scale but also correct the negative externalities of production and realize the sustainable utilization of resources and the sustainable development of agriculture. Geng and Li [16] believed that standardization can achieve economies of scale, and based on the microdata of mutton sheep scale farms (households), it is confirmed that the economies of scale effect under the standardized breeding mode in the park are significantly better than the family breeding mode, which can improve agricultural productivity. The research of Wang et al. [17] has proved that agricultural technical standards have significantly promoted the promotion of international competitiveness of agriculture. Ma et al. [18] took apple planting as an example, and the study showed that improving apple growers' awareness of standardized production and the degree of organization of fruit farmers can solve the dilemma of quality and safety. Based on the empirical test of 771 fruit farmers in Hebei, Jiangsu, and Jiangxi provinces, Chen et al. [19] confirmed that standardized production can inhibit the occurrence of "lemon market" in the process of regional public brand of agricultural products and effectively improve farmers' income and promote the process of agricultural modernization. Yu et al. [20] studied the impact of standardized label certification on retailer behavior and found that when two suppliers adopted an asymmetric

certification strategy, retailers tended to purchase products with organic labels. The third angle is how to promote the industrialization of fresh agricultural products. Zhang et al. [21] believed that the leading enterprises of agricultural industrialization are the most important driving bodies for the development of agricultural industrialization. From the perspective of network organization, Deng and Li [22] suggested that the high-quality development of grain industrialization should be guided by improving the main body of the network. Zhou [1] believed that the economic effect in the development of rural industrialization needs to be closely combined with the ability of self-development. In order to promote the development of fishery industrialization, Sheng et al. [23] proposed a development mechanism of "internal and external linkage and trinity" of policies, driving forces, and paths.

Next, we review literature related to collaborative behavior analysis based on the evolutionary game. There is a lot of research in this area, and it is widely used, especially in the application of collaborative innovation problems. Xu et al. [24], Su et al. [25], Zhou and Ren [26], Hou and Li [27] used evolutionary game models to study collaborative innovation in military-civilian integration, collaborative innovation between enterprises and universities, collaborative innovation in low-carbon technologies, and collaborative innovation in the Internet of Things industry. In addition, some scholars have used evolutionary game models to study issues such as project and organization collaboration (Liu et al. [28], Chen et al. [29], Sun et al. [30]), supply chain collaboration (Qu et al. [31], Long et al. [32]), information collaboration (Yang et al. [33], Zhang et al. [34]), and collaborative supervision and governance (Lei et al. [35], Zhang et al. [36]).

It can be seen from the above literature that, on the one hand, synergistic factors have not been considered in the current research on the high-quality development of the fresh agricultural product industry. On the other hand, although the application of evolutionary games is very extensive, few people have used it to study the collaborative behavior of fresh agricultural product suppliers, and there is no literature focusing on the impact of regional standardization on collaborative decision-making. This study noticed the above deficiencies and carried out research, hoping to provide some guidance for the development of the fresh agricultural product industry.

3. Basic Assumptions and Symbol Description

It is assumed that there are only two fresh agricultural product suppliers A and B of the same type in a certain region (such as two fresh agricultural product growers and two fresh agricultural product manufacturers), and they have two strategy choices: standardized collaborative production and nonstandardized collaborative production. The probabilities of coordinated and uncoordinated strategy set are $(x, 1-x)$ and $(y, 1-y)$, respectively.

(1) When both of them choose uncoordinated strategy, they produce independently, the output is Q_1 and Q_2, the unit production cost is C_1 and C_2, and the price of fresh agricultural product is p. At this time, the regional product standardization degree is 0.

(2) Consumers are more interested in high-standardized and high-quality fresh agricultural products, so it is assumed that consumers have a certain consumption preference μ for standardized fresh agricultural products.

(3) When both of them choose the cooperative strategy, the scale effect of cooperative production can be obtained. Producing the same quantity of fresh agricultural products (Q_1 and Q_2) can reduce the production cost with a ratio of $\varnothing$. The standardized collaborative production behavior of fresh agricultural product suppliers can bring about the homogenization of the quality and the unification of the specifications of fresh agricultural products in the region. At this time, the standardization degree of fresh agricultural products in the region is θ. The unit cost paid by the supplier of fresh agricultural product for product standardization is $1/2C\theta^2$ (including the cost of mechanical equipment, production technology, precooling and fresh-keeping equipment, packaging technology, etc.).

(4) When the two parties cooperate, the cost paid for the standardization of fresh agricultural products is shared between them in proportion β, and the benefits from standardization are shared in proportion α.

(5) When one party chooses the collaborative strategy and the other party chooses the uncollaborative strategy, although one party carries out standardized production, it cannot reach a unified standard. At this time, the standardization degree of fresh agricultural products in the region is 0.

4. Strategy Stability Analysis without Government Participation

According to the assumptions, we can get the payment matrix of fresh agricultural product suppliers without government participation, as listed in Table 1. It is assumed that the benefits of participating in cooperation are greater than the benefits obtained when choosing a noncooperative strategy.

According to the relevant theory of evolutionary game and the algorithm of expected return, we can get the expected return and average return of fresh agricultural product supplier A as follows:

Table 1: Payment matrix of fresh agricultural product suppliers without government participation.

A	B	
	Coordinated (y)	Uncoordinated $(1-y)$
Coordinated (x)	$pQ_1 + \alpha\mu\theta\,(Q_1+Q_2) - (1-\varnothing)C_1Q_1 - \beta 1/2C\theta^2\,(Q_1+Q_2)$, $pQ_2 + (1-\alpha)\mu\theta\,(Q_1+Q_2) - (1-\varnothing)C_2Q_2 - (1-\beta)1/2C\theta^2\,(Q_1+Q_2)$	$pQ_1 - C_1Q_1 - 1/2C\theta^2Q_1$, $pQ_2 - C_2Q_2$
Uncoordinated $(1-x)$	$pQ_1 - C_1Q_1$, $pQ_2 - C_2Q_2 - 1/2C\theta^2Q_2$	$pQ_1 - C_1Q_1$, $pQ_2 - C_2Q_2$

$$\begin{cases} E\pi_{A1}^{x} = y\alpha\mu\theta(Q_1+Q_2) - (1-\varnothing y)C_1Q_1 + pQ_1 - \beta y\dfrac{1}{2}C\theta^2(Q_1+Q_2) - (1-y)\dfrac{1}{2}C\theta^2Q_1, \\ E\pi_{A1}^{1-x} = pQ_1 - C_1Q_1, \\ E\overline{\pi_{A1}} = xE\pi_{A1}^{x} + (1-x)E\pi_{A1}^{1-x}. \end{cases} \tag{1}$$

Then, the replication dynamic equation of fresh agricultural product supplier A's collaborative strategy is as follows:

$$F_1(x) = \frac{\mathrm{d}x}{\mathrm{d}t} = x(1-x)\left[y\alpha\mu\theta(Q_1+Q_2) + \varnothing yC_1Q_1 - \beta y\frac{1}{2}C\theta^2(Q_1+Q_2) - (1-y)\frac{1}{2}C\theta^2Q_1\right]. \tag{2}$$

Similarly, the expected income and average income of fresh agricultural product supplier B can be obtained as follows:

$$\begin{cases} E\pi_{B1}^{y} = x(1-\alpha)\mu\theta(Q_1+Q_2) - (1-\varnothing x)C_2Q_2 + pQ_2 - (1-\beta)x\dfrac{1}{2}C\theta^2(Q_1+Q_2) - (1-x)\dfrac{1}{2}C\theta^2Q_2, \\ E\pi_{B1}^{1-y} = pQ_2 - C_2Q_2, \\ E\overline{\pi_{B1}} = yE\pi_{B1}^{y} + (1-y)E\pi_{B1}^{1-y}. \end{cases} \tag{3}$$

Then, the replication dynamic equation of fresh agricultural product supplier B's collaborative strategy is as follows:

$$F_1(y) = \frac{\mathrm{d}y}{\mathrm{d}t} = y(1-y)\left[x(1-\alpha)\mu\theta(Q_1+Q_2) + \varnothing xC_2Q_2 - (1-\beta)x\frac{1}{2}C\theta^2(Q_1+Q_2) - (1-x)\frac{1}{2}C\theta^2Q_2\right]. \tag{4}$$

Proposition 1. *When $y > y_1^*$, the stable strategy of fresh agricultural product supplier A is to participate in collaboration; when $y < y_1^*$, the stable strategy of fresh agricultural product supplier A is uncoordinated; when $y = y_1^*$, the stable strategy of fresh agricultural product supplier A cannot be determined, where $y_1^* = 1/2C\theta^2Q_1/\alpha\mu\theta\ (Q_1+Q_2) + \varnothing C_1Q_1 - \beta 1/2C\theta^2\,(Q_1+Q_2) + 1/2C\theta^2Q_1$.*

Proof. $N(y) = y\alpha\mu\theta(Q_1+Q_2) + \varnothing yC_1Q_1 - \beta y1/2C\theta^2(Q_1+Q_2) - (1-y)1/2C\theta^2Q_1$

$$\frac{\partial N(y)}{\partial y} = \alpha\mu\theta(Q_1 + Q_2) + \varnothing C_{1Q_1} - \beta\frac{1}{2}C\theta^2(Q_1 + Q_2) + \frac{1}{2}C\theta^2 Q_1 > 0. \tag{5}$$

Therefore, $N(y)$ is the increasing function of y. When $y > y_1^*$, $N(y) > 0$, $F_1(x)|_{x=1} = 0$, $F_1'(x)|_{x=1} < 0$, $x = 1$ is stable, that is, the stable strategy of fresh agricultural product supplier A is coordination; when $y < y_1^*$, $N(y) < 0$, $F_1(x)|_{x=0} = 0$, $F_1'(x)|_{x=0} < 0$, $x = 0$ is stable, the stable strategy of fresh agricultural product A is uncoordinated; when $y = y_1^*$, $N(y) = 0$, $F_1(x) = 0$, $F_1'(x) = 0$, the stability strategy cannot be determined. □

Proposition 2. *When $x > x_1^*$, the stable strategy of fresh agricultural product supplier B is synergy; when $x < x_1^*$, the stable strategy of fresh agricultural product supplier B is uncoordinated; when $x = x_1^*$, the stability strategy of fresh agricultural product supplier B cannot be determined, where $x_1^* = 1/2C\theta^2 Q_2/(1-\alpha)\mu\theta(Q_1 + Q_2) + \varnothing C_2 Q_2 - (1-\beta)1/2C\theta^2(Q_1 + Q_2) + 1/2C\theta^2 Q_2$.*

Proof. $N(x) = x(1-\alpha)\mu\theta(Q_1 + Q_2) + \varnothing x C_2 \quad Q_2 - (1-\beta)x1/2C\theta^2(Q_1 + Q_2) - (1-x)1/2C\theta^2 Q_2$

$$\frac{\partial N(x)}{\partial x} = (1-\alpha)\mu\theta(Q_1 + Q_2) + \varnothing C_2 Q_2 - (1-\beta)\frac{1}{2}C\theta^2(Q_1 + Q_2) + \frac{1}{2}C\theta^2 Q_2 > 0. \tag{6}$$

Therefore, $N(x)$ is the increasing function of x. When $x > x_1^*$, $N(x) > 0$, $F_1(y)|_{y=1} = 0$, $F_1'(y)|_{y=1} < 0$, $y = 1$ is stable, that is, the stable strategy of fresh agricultural product supplier A is coordination; when $x < x_1^*$, $N(x) < 0$, $F_1(y)|_{y=0} = 0$, $F_1'(y)|_{y=0} < 0$, $y = 0$ is stable, that is, the stable strategy of fresh agricultural product A is uncoordinated; when $x = x_1^*$, $N(x) = 0$, $F_1(y) = 0$, $F_1'(y) = 0$, the stability strategy cannot be determined. □

Inference 1. The choice of cooperative strategy among the suppliers of fresh agricultural product is mutually reinforcing. When the cooperative probability of one side is higher, the possibility of the other side is also higher.

Proposition 3. *There are two stable points in the game system of standardized collaborative production of fresh agricultural product suppliers without government participation, which are $(0,0)$ and $(1,1)$, respectively. The final game result depends on the initial state of the participants.*

Proof. Let $F_1(x) = 0$ and $F_1(y) = 0$, then we can get five local equilibrium points: $O(0,0)$, $A(0,1)$, $B(1,0)$, $C(1,1)$, $D(x_1^*, y_1^*)$, where $x_1^* = 1/2C\theta^2 Q_2/(1-\alpha)\mu\theta \quad (Q_1 + Q_2) + \varnothing C_2 Q_2 - (1-\beta)1/2C\theta^2(Q_1 + Q_2) + 1/2C\theta^2 Q_2$ and $y_1^* = 1/2C\theta^2 Q_1/\alpha\mu\theta(Q_1 + Q_2) + \varnothing C_1 Q_1 - \beta 1/2C\theta^2 \quad (Q_1 + Q_2) + 1/2C\theta^2 Q_1$.

And, according to formulas (2) and (4), the Jacobian matrix J_1 of the two-dimensional dynamic system I is as follows: $J_1 = \begin{bmatrix} \partial F_1(x)/\partial x & \partial F_1(x)/\partial y \\ \partial F_1(y)/\partial x & \partial F_1(y)/\partial y \end{bmatrix} = \begin{bmatrix} a_{11} & a_{12} \\ a_{21} & a_{22} \end{bmatrix}$, where $a_{11} = (1-2x)[y\alpha\mu\theta(Q_1 + Q_2) + \varnothing y C_1 Q_1 - \beta y 1/2C\theta^2(Q_1 + Q_2) - (1-y)1/2C\theta^2 Q_1]$, $a_{12} = x(1-x) \quad [\alpha\mu\theta(Q_1 + Q_2) + \varnothing C_1 Q_1 - \beta 1/2C\theta^2 \quad (Q_1 + Q_2) + 1/2C\theta^2 Q_1]$, $a_{21} = y(1-y)[(1-\alpha)\mu\theta(Q_1 + Q_2) + \varnothing C_2 Q_2 - (1-\beta)1/2C\theta^2(Q_1 + Q_2) + 1/2C\theta^2 Q_2]$, and $a_{22} = (1-2y)[x(1-\alpha)\mu \quad \theta(Q_1 + Q_2) + \varnothing x C_2 Q_2 - (1-\beta) \quad x1/2C\theta^2(Q_1 + Q_2) - (1-x)1/2C\theta^2 Q_2]$.

According to Jacobian matrix local stability analysis method, the stability of five points is analyzed and the results are listed in Table 2.

It can be seen that there are two stable points in the game system of standardized collaborative production of fresh agricultural product suppliers, namely, $O(0,0)$ and $C(1,1)$. The phase diagram of system evolution is shown in Figure 1. □

5. Stability Analysis of System Strategy with Government Participation

Government synergy factors are introduced into the model, assuming that the government participates in synergy mainly through three means. First, the standard θ of fresh agricultural products is formulated in the region. When the suppliers of fresh agricultural product choose standardized collaborative production, they must meet the standards formulated by the government, so as to complete the standardization construction of regional fresh agricultural products. When one supplier of fresh agricultural product participates in collaboration, while the other party does not, the noncooperative party will get free-riding income U from the cooperative party. The second is to give standardized production cost subsidy a. The third is to impose a penalty of F on those who enjoy "free-rider" benefits in nonstandard production.

According to the assumed conditions, the payment matrix of fresh agricultural product suppliers can be obtained, as listed in Table 3.

The expected income and average income of fresh agricultural product supplier A are as follows:

Table 2: Stability analysis of local equilibrium point of system without government participation.

Local equilibrium points	trJ_1	$\det J_1$	Stability
$O\ (0,0)$	−	+	ESS
$A\ (0,1)$	+	+	Unstable
$B\ (1,0)$	+	+	Unstable
$C\ (1,1)$	−	+	ESS
$D\ (x_1^*, y_1^*)$	0	−	Saddle point

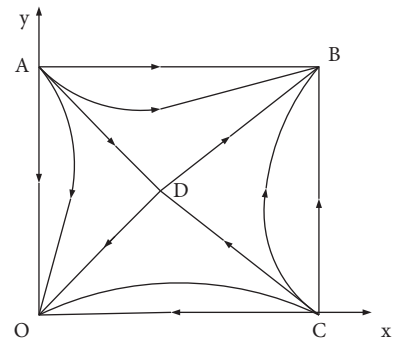

Figure 1: Phase diagram of system evolution without government participation.

Table 3: Payment matrix of fresh agricultural product suppliers A and B with government participation.

A	B	
	Coordinated (y)	Uncoordinated $(1-y)$
Coordinated (x)	$pQ_1 + \alpha\mu\overline{\theta}\,(Q_1+Q_2) - (1-\varnothing)C_1Q_1 - \beta 1/2\,(C-a)\overline{\theta}^2\,(Q_1+Q_2)$, $pQ_2 + (1-\alpha)\mu\overline{\theta}\,(Q_1+Q_2) - (1-\varnothing)C_2Q_2 - (1-\beta)1/2\,(C-a)\overline{\theta}^2\,(Q_1+Q_2)$	$pQ_1 + \mu\overline{\theta}Q_1 - C_1Q_1 - 1/2C\overline{\theta}^2Q_1 - U$, $pQ_2 - C_2Q_2 + U - F$
Uncoordinated $(1-x)$	$pQ_1 - C_1Q_1 + U - F$, $pQ_2 + \mu\overline{\theta}Q_2 - C_2Q_2 - 1/2C\overline{\theta}^2Q_2 - U$	$pQ_1 - C_1Q_1 - F$, $pQ_2 - C_2Q_2 - F$

$$\begin{cases} E\pi_{A2}^{x} = y\alpha\mu\overline{\theta}(Q_1+Q_2) - (1-\varnothing y)C_1Q_1 + pQ_1 - y\beta\dfrac{1}{2}(C-a)\overline{\theta}^2(Q_1+Q_2) + (1-y)\mu\overline{\theta}Q_1, \\ -(1-y)\dfrac{1}{2}C\overline{\theta}^2Q_1 - U, \\ E\pi_{A2}^{1-x} = pQ_1 - C_1Q_1 + yU - F, \\ \overline{E\pi_{A2}} = xE\pi_{A2}^{x} + (1-x)E\pi_{A2}^{1-x}. \end{cases} \tag{7}$$

Then, the replication dynamic equation of fresh agricultural product supplier A's collaborative strategy is as follows:

$$F_2(x) = \frac{\mathrm{d}x}{\mathrm{d}t} = x(1-x)\left[y\alpha\mu\overline{\theta}(Q_1+Q_2) + \varnothing yC_1Q_1 - y\beta\frac{1}{2}(C-a)\overline{\theta}^2(Q_1+Q_2) + (1-y)\mu\overline{\theta}Q_1 - (1-y)\frac{1}{2}C\overline{\theta}^2Q_1 - U + F\right]. \tag{8}$$

Similarly, the expected income and average income of fresh agricultural product supplier B can be obtained as follows:

$$\begin{cases} E\pi_{B2}^{y} = x(1-\alpha)\mu\overline{\theta}(Q_1+Q_2) - (1-\varnothing x)C_2Q_2 + pQ_2 - x(1-\beta)\dfrac{1}{2}(C-a)\overline{\theta}^2(Q_1+Q_2) + (1-x)\mu\overline{\theta}Q_1 - (1-x)\dfrac{1}{2}C\overline{\theta}^2Q_2 - U, \\ E\pi_{B2}^{1-y} = pQ_2 - C_2Q_2 + xU - F, \\ E\overline{\pi_{B2}} = yE\pi_{B2}^{y} + (1-y)E\pi_{B2}^{1-y}. \end{cases} \tag{9}$$

Then, the replication dynamic equation of fresh agricultural product supplier B's collaborative strategy is as follows:

$$F_2(y) = \frac{\mathrm{d}y}{\mathrm{d}t} = y(1-y)\left[x(1-\alpha)\mu\overline{\theta}(Q_1+Q_2) + \varnothing xC_2Q_2 - x(1-\beta)\frac{1}{2}(C-a)\overline{\theta}^2(Q_1+Q_2) + (1-x)\mu\overline{\theta}Q_2 - (1-x)\frac{1}{2}C\overline{\theta}^2Q_2 - U + F\right]. \tag{10}$$

According to formulas (8) and (10), the two-dimensional dynamic system II can be obtained, and the Jacobian matrix J_2 is as follows: $J_2 = \begin{bmatrix} \partial F_2(x)/\partial x & \partial F_2(x)/\partial y \\ \partial F_2(y)/\partial x & \partial F_2(y)/\partial y \end{bmatrix} = \begin{bmatrix} b_{11} & b_{12} \\ b_{21} & b_{22} \end{bmatrix}$.

$$\begin{aligned} b_{11} &= (1-2x)\left[y\alpha\mu\overline{\theta}(Q_1+Q_2) + \varnothing yC_1Q_1 - y\beta\frac{1}{2}(C-a)\overline{\theta}^2(Q_1+Q_2) + (1-y)\mu\overline{\theta}Q_1 - (1-y)\frac{1}{2}C\overline{\theta}^2Q_1 - U + F\right], \\ b_{12} &= x(1-x)\left[\alpha\mu\overline{\theta}(Q_1+Q_2) + \varnothing C_1Q_1 - \beta\frac{1}{2}(C-a)\overline{\theta}^2(Q_1+Q_2) - \mu\overline{\theta}Q_1 + \frac{1}{2}C\overline{\theta}^2Q_1\right], \\ b_{21} &= y(1-y)\left[(1-\alpha)\mu\overline{\theta}(Q_1+Q_2) + \varnothing C_2Q_2 - (1-\beta)\frac{1}{2}(C-a)\overline{\theta}^2(Q_1+Q_2) - \mu\overline{\theta}Q_2 + \frac{1}{2}C\overline{\theta}^2Q_2\right], \\ b_{22} &= (1-2y)\left(x(1-\alpha)\mu\overline{\theta}(Q_1+Q_2) + \varnothing xC_2Q_2 - x(1-\beta)\frac{1}{2}(C-a)\overline{\theta}^2(Q_1+Q_2) + (1-x)\mu\overline{\theta}Q_2 - (1-x)\frac{1}{2}C\overline{\theta}^2Q_2 - U + F\right). \end{aligned} \tag{11}$$

Let $F_2(x) = 0$ and $F_2(y) = 0$, then we can get five local equilibrium points: $O_2(0,0)$, $A_2(0,1)$, $B_2(1,0)$, $C_2(1,1)$, and $D_2(x_2^*, y_2^*)$:

$$\begin{aligned} y_2^* &= \frac{U - F - \mu\overline{\theta}Q_1 + 1/2C\overline{\theta}^2Q_1}{\alpha\mu\overline{\theta}(Q_1+Q_2) + \varnothing C_1Q_1 - \beta 1/2(C-a)\overline{\theta}^2(Q_1+Q_2) - \mu\overline{\theta}Q_1 + 1/2C\overline{\theta}^2Q_1}, \\ x_2^* &= \frac{U - F - \mu\overline{\theta}Q_2 + 1/2C\overline{\theta}^2Q_2}{(1-\alpha)\mu\overline{\theta}(Q_1+Q_2) + \varnothing C_2Q_2 - (1-\beta)1/2(C-a)\overline{\theta}^2(Q_1+Q_2) - \mu\overline{\theta}Q_2 + 1/2C\overline{\theta}^2Q_2}. \end{aligned} \tag{12}$$

The stability of five points is analyzed, and the results are listed in Table 4.

$O_2(0,0)$ is the stable point of the dynamic system when the conditions $\mu\overline{\theta}Q_1 - 1/2C\overline{\theta}^2Q_1 - U + F < 0$ and $\mu\overline{\theta}Q_2 - 1/2C\overline{\theta}^2Q_2 - U + F < 0$ are satisfied; when the conditions $\alpha\mu\overline{\theta}(Q_1+Q_2) + \varnothing C_1Q_1 - \beta 1/2(C-a)\overline{\theta}^2(Q_1+Q_2) - U + F > 0$ and $(1-\alpha)\mu\overline{\theta}(Q_1+Q_2) + \varnothing C_2Q_2 - (1-\beta)1/2(C-a)\overline{\theta}^2(Q_1+Q_2) - U + F > 0$ are satisfied, $C_2(1,1)$ is the stable point of the system.

Inference 2. Condition one: when $U - F > \alpha\mu\overline{\theta}(Q_1+Q_2) + \varnothing C_1Q_1 - \beta 1/2(C-a)\overline{\theta}^2(Q_1+Q_2)$ and $U - F > (1-\alpha)\mu\overline{\theta}(Q_1+Q_2) + \varnothing C_2Q_2 - (1-\beta)1/2(C-a)\overline{\theta}^2(Q_1+Q_2)$, the stable point of the system is $O_2(0,0)$. Condition two:

Table 4: Stability analysis of local equilibrium point of system with government participation.

Local equilibrium point	trJ_2	$\det J_2$	Stability
$O_2\ (0,0)$	U	+	ESS when conditions are met
$A_2\ (0,1)$	+	U	Unstable/saddle point
$B_2\ (1,0)$	+	U	Unstable/saddle point
$C_2\ (1,1)$	U	+	ESS when conditions are met
$D_2\ (x_2^*, y_2^*)$	0	−	Saddle point

when $\mu\overline{\theta}Q_1 - 1/2C\overline{\theta}^2Q_1 < U - F < \alpha\mu\overline{\theta}(Q_1 + Q_2) + \varnothing C_1Q_1 - \beta 1/2\,(C-a)\overline{\theta}^2\,(Q_1 + Q_2)$ and $\mu\overline{\theta}Q_2 - 1/2C\overline{\theta}^2Q_2 < U - F < (1-\alpha)\mu\overline{\theta}(Q_1 + Q_2) + \varnothing C_2\quad Q_2 - (1-\beta)1/2\,(C-a)\overline{\theta}^2\,(Q_1 + Q_2)$, the stable points of the system are $O_2\,(0,0)$ and $C_2\,(1,1)$. Condition three: when $U - F < \mu\overline{\theta}Q_1 - 1/2C\overline{\theta}^2Q_1$ and $U - F < \mu\overline{\theta}Q_2 - 1/2C\overline{\theta}^2Q_2$, the stable point of the system is $C_2\,(1,1)$.

The evolution phase diagram of game system with government participation in different situations is shown in Figure 2. Figure 2(a) shows the evolution process of the system when condition one is met. At this time, the suppliers of fresh agricultural product tend to choose uncoordinated strategies. Figure 2(b) shows the evolution process of the system when condition two is met. At this time, the suppliers of fresh agricultural product may all choose uncoordinated strategies or collaborative strategies, depending on the initial state. Figure 2(c) shows the evolution process of the system when condition three is met. At this time, the suppliers of fresh agricultural product tend to choose collaborative strategy.

Inference 3. Free-rider income is not conducive to the choice of standardized collaborative production strategy of fresh agricultural product suppliers, and the government's penalty for not implementing standardized production is conducive to the choice of standardized collaborative production strategy of fresh agricultural product suppliers.

6. Simulation Analysis

In order to show more intuitively and clearly the influence of key parameters on the stability strategy of evolutionary game players, the evolution trajectory of dynamic game system is numerically simulated by using Matlab software. According to the basic assumptions and realistic basis, the relevant parameters are initially assigned as follows: $\varnothing = 0.3$, $Q_1 = 200$, $Q_2 = 250$, $C_1 = 5$, $C_1 = 4.5$, $\alpha = \beta = 0.5$, $\mu = 1$, $\theta = 1$, and $C = 2$.

Firstly, the stability of the equilibrium point of the system is verified without government participation. Assuming that the initial states of fresh agricultural product suppliers are $(0.5, 0.5)$ and $(0.4, 0.4)$, respectively, the evolution process of the system is shown in Figure 3(a). It can be found that the stable point of the system is $(1,1)$ when the initial state of fresh agricultural product supplier is 0.5, and $(0,0)$ when the initial cooperative probability is reduced to 0.4. Figure 3(b) shows that the stable point of the system is $(1,1)$ when the initial cooperative probability of fresh agricultural product supplier A is 0.4 and that of fresh agricultural product supplier B is 0.5. Figure 3(c) shows the stable point $(1,1)$ of the system when the initial cooperative probability of fresh agricultural product supplier A is 0.5 and that of fresh agricultural product supplier B is 0.4. It can be seen that the evolution direction of the system is (coordinated,coordinated) when the initial collaboration probability of participants is high and is (uncoordinated, uncoordinated) when the initial collaboration probability of participants is low. However, when the cooperative probability of one participant is low, the promotion of the cooperative probability of the other participant will promote its choice of cooperative strategy, that is, the cooperative strategy choice of fresh agricultural product suppliers is mutually reinforcing.

Secondly, the stability of the equilibrium point of the system is verified with government participation. Let $a = 1$, $\overline{\theta} = 1$, $U = 450$, and $F = 30$, then condition 1 in Inference 2 is satisfied. Assuming that the initial state of fresh agricultural product supplier is $(0.5, 0.5)$, the evolution process of the system is shown in Figure 4(a). It can be found that the stable points of the system are $(0,0)$ when the initial cooperative probabilities are 0.5, respectively. Let $a = 1$, $\overline{\theta} = 1$, $U = 450$, and $F = 150$, then the second condition in Inference 2 is met and it is assumed that the initial states of fresh agricultural product suppliers are $(0.5, 0.5)$ and $(0.8, 0.8)$, respectively, and the evolution process of the system is shown in Figure 4(b). It can be found that the stable point of the system is $(0,0)$ when the initial cooperative probability of participants is 0.5 and is $(1,1)$ when the initial cooperative probability of participants rises to 0.8. Let $a = 1$, $\overline{\theta} = 1$, $U = 450$, and $F = 400$, then the third condition in Inference 2 is met and it is assumed that the initial state of fresh agricultural product supplier is $(0.5, 0.5)$, and the evolution process of the system is shown in Figure 4(c). It can be found that the stable points of the system are $(1,1)$ when the initial cooperative probability is 0.5, respectively. It can be seen that with the participation of the government, the supplier of fresh agricultural product will tend to choose uncoordinated strategy when the free-riding income obtained from the other party's standardized production is still large after deducting the government penalty. On the contrary, they will tend to choose the cooperative strategy.

Thirdly, the influence of government participation is explored on the system evolution results. When $\theta = \overline{\theta} = 1$, it is assumed that the initial cooperative probability of participants is 0.5, and the evolution process and results of the system under the conditions of no government participation and government participation are compared. As shown in Figure 5, x and y represent the evolution path of agent strategy without government participation and $x1$ and $y2$ represent the evolution path of agent strategy with

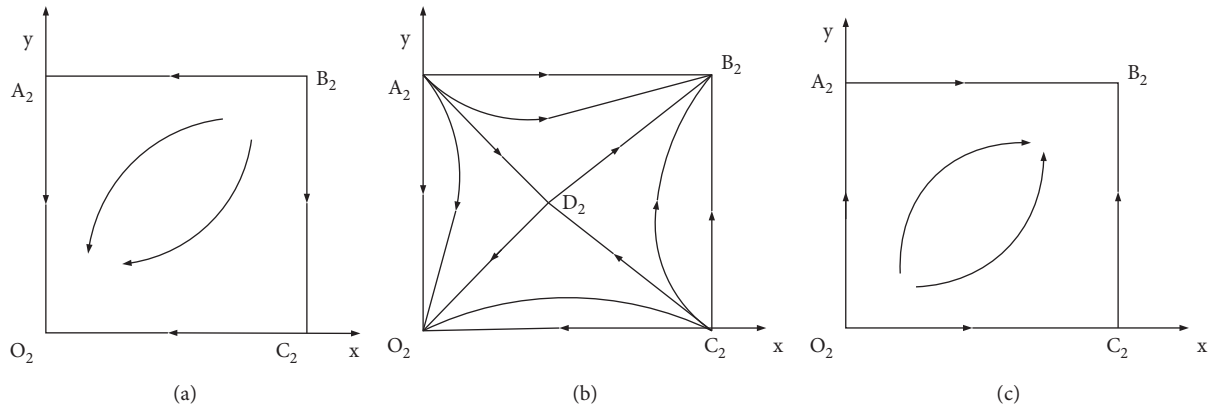

Figure 2: Phase diagram of system evolution with government participation.

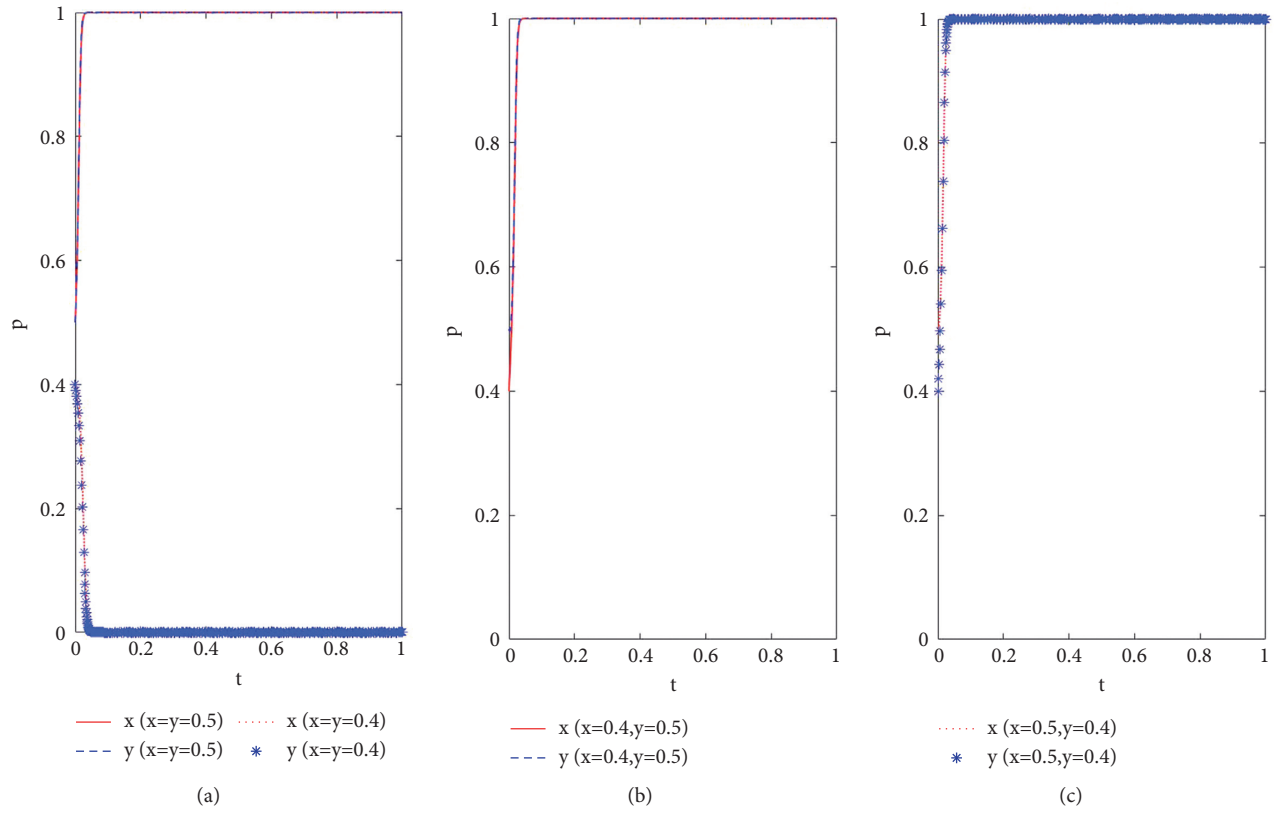

Figure 3: Evolution process of game system without government participation.

government participation. And, Figure 5(a) shows the evolution process of the system without government participation and with government participation meeting condition one; Figure 5(b) shows the evolution process of the system without government participation and with government participation meeting condition two; Figure 5(c) shows the evolution process of the system without government participation and with government participation meeting condition three. By comparison, it can be found that under the same initial cooperative probability, only when the third condition is met, the government participation can positively promote the evolution of the system to the $(1, 1)$ direction. That is to say, when the government participates, it is necessary to effectively control the free-rider behavior and increase the punishment; otherwise, the government participation will inhibit the standardized collaborative production behavior of fresh agricultural product suppliers.

Let $\theta = \overline{\theta} = 2$, then it is assumed that the initial cooperative probability of the subjects in the system without government participation and the system with government participation is both (0.5, 0.5). Comparing the evolution process of the system with or without government participation and satisfying condition three, it is represented by

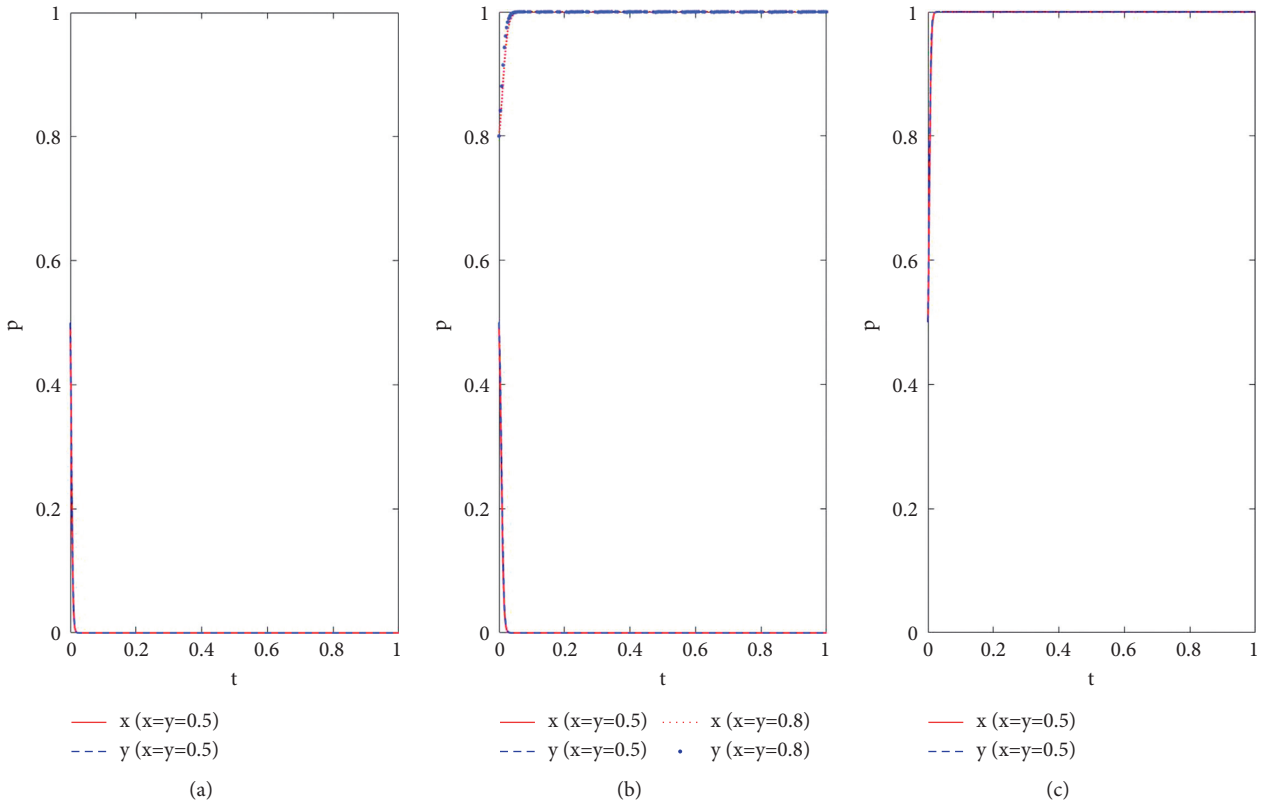

Figure 4: Evolution process of game system with government participation.

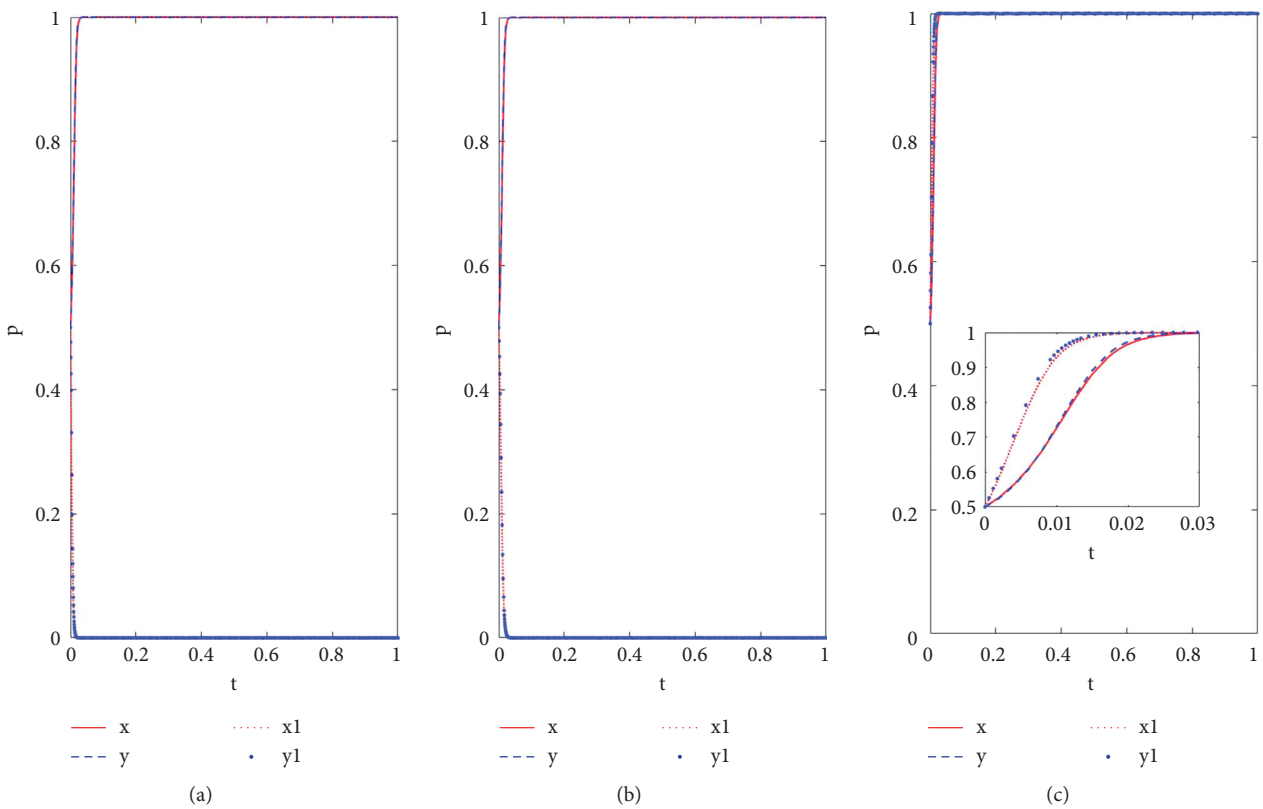

Figure 5: Influence of government participation on the evolution results of game system.

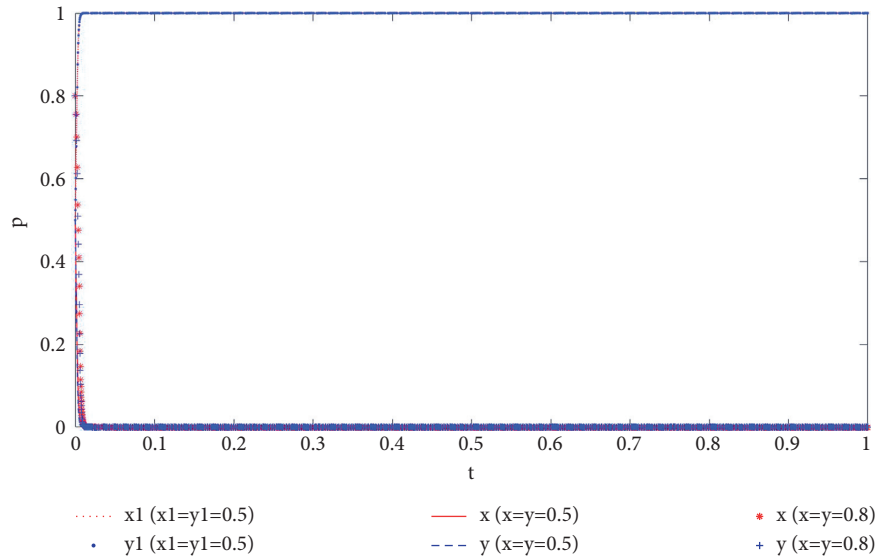

Figure 6: Influence of standardization degree on evolution results of two game systems.

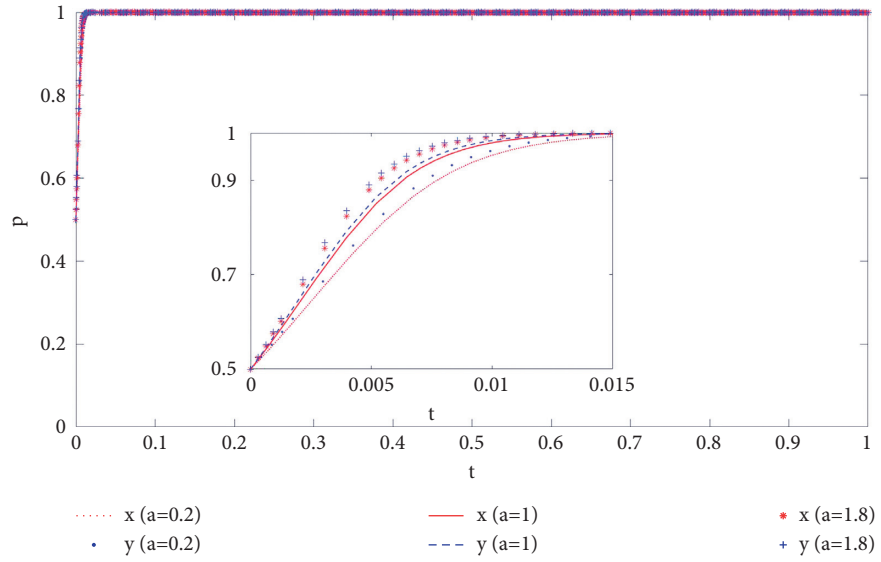

Figure 7: Influence of standardized cost subsidy on system evolution results.

lines x and y and lines $x1$ and $y1$, respectively, as shown in Figure 6. It can be seen from the figure that when the standardization of fresh agricultural products is improved, the evolution direction of the system without government participation is $(0, 0)$, and that of the system with government participation is $(1, 1)$. From this, it can be concluded that when the degree of standardization is higher, it is more necessary for the government to participate in coordination, guidance, and encouragement.

Finally, the influence of other parameters on the system evolution results is explored with the effective participation of the government.

(1) *Standardized Cost Subsidy*. Take $\overline{\theta} = 2$ and $a = (0.2, 1, 1.8)$, respectively, with the effective participation of the government, assuming that the initial cooperative probability of subjects is $(0.5, 0.5)$, and the process of system evolution is shown in Figure 7. With the increase of the government standardized cost subsidy, fresh agricultural product suppliers are evolving in the $(1, 1)$ direction faster, that is, the government standardized cost subsidy is conducive to promoting fresh agricultural product suppliers to choose standardized collaborative production strategies.

(2) *Benefit Sharing Coefficient and Cost-Sharing Coefficient*. Keeping other parameters unchanged, take $\alpha = 0.5$, $\beta = (0.2, 0.5, 0.8)$, and $\alpha = (0.2, 0.5, 0.8)$, $\beta = 0.5$, respectively. The evolution process of the system is shown in Figure 8. It can be seen from the figure that when the profit-sharing coefficient is constant, with the increase of the cost-sharing coefficient, the evolution rate of the subject in the

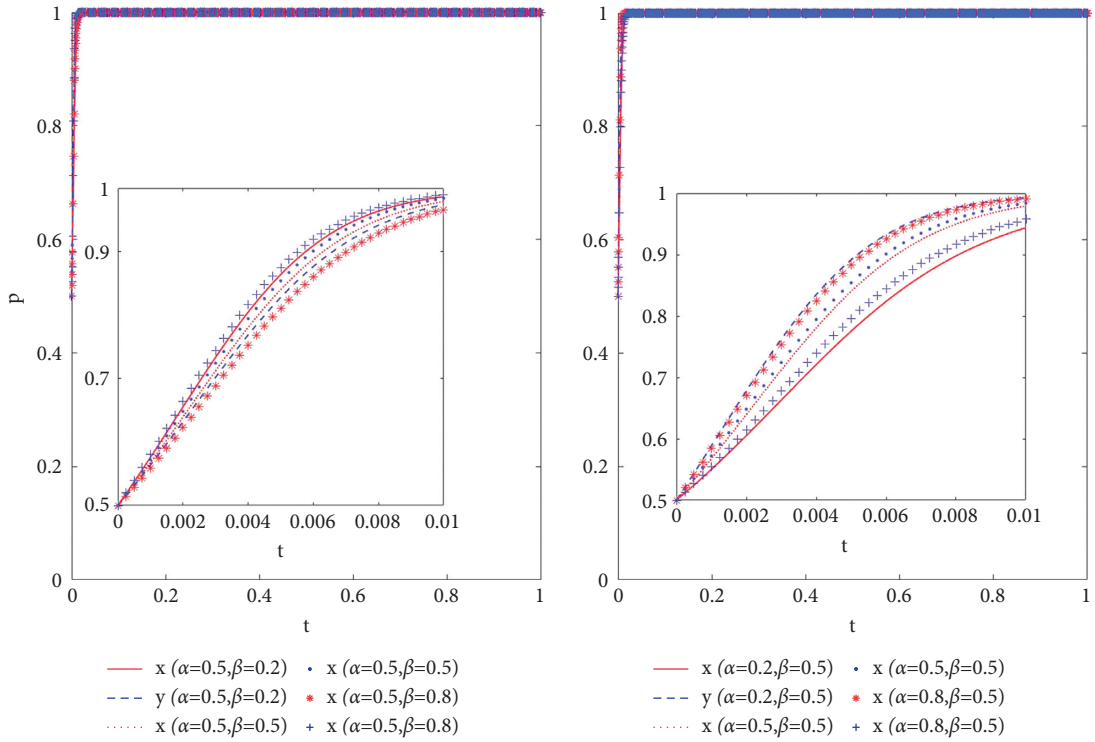

Figure 8: Influence of revenue sharing coefficient and cost sharing coefficient on system evolution results.

direction of 1 becomes slower; when the cost-sharing coefficient is constant, with the increase of the profit-sharing coefficient, the evolution rate of the subject in the direction of 1 becomes faster, but the overall evolution direction remains unchanged. That is, with the effective participation of the government, the revenue-sharing mechanism and cost-sharing mechanism have little influence on the strategy selection results of the fresh agricultural product suppliers.

7. Conclusion

Taking the regional product standardization construction as the goal, this study constructs the evolutionary game model of collaborative production of fresh agricultural product suppliers, explores the decision-making rules of standardized collaborative production behavior of fresh agricultural product suppliers, and finally finds the following conclusions:

(1) When the standardization degree of regional fresh agricultural products is low, the cost for standardization of fresh agricultural products suppliers is low, and the choice of cooperative strategy of fresh agricultural product suppliers without government participation is only related to the initial intention. However, when the government participates, it is necessary to strictly supervise the free-riding behavior; otherwise, government participation will inhibit the choice of standardized collaborative production strategy of fresh agricultural products.

(2) When the standardization degree of regional fresh agricultural products is high, the cost for standardization is high, and the suppliers of fresh agricultural product are unwilling to actively participate in standardized collaborative production without government participation. Only when the government enforces high standards and does a good job in supervising and punishing free-riding behaviors, the suppliers of fresh agricultural product will be willing to participate in standardized collaborative production.

(3) With the government's effective participation, it can effectively supervise and punish the free-rider behavior, and the standardized cost subsidy is conducive to promoting the supplier of fresh agricultural product to choose the standardized collaborative production strategy. At this time, the profit-sharing coefficient and cost-sharing coefficient have little influence on the selection of standardized collaborative production strategy of fresh agricultural product suppliers.

There are several limitations in the study, which may be worth further exploration. First of all, this study does not consider the scale and individual attributes of fresh agricultural product suppliers. In fact, fresh agricultural product suppliers of different scales and attributes have different risk tolerance and willingness to cooperate. Secondly, the formulation and measurement of the standardization degree of fresh agricultural products are also an issue worthy of further discussion.

Data Availability

The [DATA TYPE] data used to support the findings of this study are available from the corresponding author upon request

Conflicts of Interest

The authors declare that they have no conflicts of interest.

Acknowledgments

This research was supported by the National Natural Science Foundation of China (no. 72103178), Jiangsu Social Science Key Fund Project (no. 20GLA002), and Jiangsu Postgraduate Innovation Plan (no. SJKY19_2519).

References

[1] D. M. Zhou, "The development dilemma and social influences of rural industrialization: a sociology investigation based on industrial poverty alleviation project of T county in southeast Guizhou," *Journal of Ethnic Culture*, vol. 13, no. 2, pp. 25–36, 2021, Chinese.

[2] Z. M. Qin and H. W. Lu, "Subdivision organization: the concrete path of organic connection between small and weak farmers and modern agricultural development-taking the agricultural development of two poverty-stricken villages in Guangxi as an example," *Jianghan Forum*, vol. 11, pp. 125–131, 2021, Chinese.

[3] Q. Lin, W. H. Fu, and Y. J. Wang, "The internal financing decisions of "company + farmer" contract farming supply chain," *System Engineering - Theory & Practice*, vol. 41, no. 5, pp. 1162–1178, 2021, Chinese.

[4] M. Wu, B. H. Zhao, and Y. X. Zong, "Research on the behavioral mechanism of contract form selection between agricultural companies and farmers: multi-case analysis based on aquatic vegetable industry," *Agricultural Economic Issues*, vol. 12, pp. 74–86, 2020, Chinese.

[5] M. Mao, L. L. Jia, and Z. T. Bao, "Research on the competition and structure of "company & cooperative & farmer" supply chain," *Chinese journal of systems science*, vol. 30, no. 2, pp. 59–64, 2022, Chinese.

[6] Y. Q. Cui, B. J. Liu, and B. J. Liu, "Optimization model analysis of new order agricultural cooperation model," *Chinese Journal of Management Science*, vol. 28, no. 12, pp. 140–150, 2020, https://doi.org/10.16381/j.cnki.issn1003-207x.2020.12.014 Chinese.

[7] J. G. Li, "Farmers + family farm agricultural management mode innovation - management of farm household, the construction of agricultural system," *Journal of Tianjin Normal University*, vol. 3, pp. 75–80, 2017.

[8] Z. Zhong, W. Y. Jiang, and Z. J. Zhao, "Main forms and operating mechanisms of agro-industrial alliance-based on research on three typical cases," *Study & Exploration (Chinese)*, vol. 307, no. 2, pp. 91–101, 2021.

[9] H. Haken, *Advanced Synergetics: Instability Hierarchies of Self-Organizing Systems and Devices*, Springer-Verlag Press, New York, USA, 1983.

[10] Y. He, H. F. Huang, H. D. Li, C. M. Shi, and S. J. Wu, "Quality and operations management in food supply chains: a literature review," *Journal of Food Quality*, vol. 2018, Article ID 7279491, 14 pages, 2018.

[11] D.-Y. Lin, C.-J. Juan, and C.-C. Chang, "Managing food safety with pricing, contracts and coordination in supply chains," *IEEE ACCESS*, vol. 7, Article ID 150892, 2019.

[12] Y. N. Yu, Y. He, and M. Salling, "Pricing and safety investment decisions in food supply chains with government subsidy," *Journal of Food Quality*, vol. 202118 pages, 2021, https://doi.org/10.1155/2021/6616096, Article ID 6616096.

[13] K. S. Wang, Y. Hao, and R. Qin, "High quality development of agriculture, transaction system change and promotion of consumption of online agricultural products-influence of novel coronavirus pneumonia on fresh e-commerce development," *Research on Economics and Management (Chinese)*, vol. 41, no. 4, pp. 21–31, 2020.

[14] Y. Y. Nie, S. X. Yang, Z. J. Qu, and H. Chen, "Construction of eco-agriculture standard system under the sixth-order industrialization theory: taking Anhui as an example," *China Science and Technology Forum*, vol. 3, pp. 58–65, 2018, Chinese.

[15] L. Yu, "Analysis of the government's promotion of agricultural standardization," *Agricultural Economic Issues*, vol. 9, pp. 26–35, 2007, Chinese.

[16] N. Geng and B. L. Li, "Analysis on the scale effect of standardized farmers-empirical evidence from meat sheep farmers in Huairen County, Shanxi Province," *Agricultural Technology and Economy*, vol. 3, pp. 36–44, 2016, Chinese.

[17] H. Wang, L. Z. Gan, and J. Qiao, "Dynamic impact of technical standards on agricultural international competitiveness: direct and mediating effects," *International Business-Journal of University of International Business and Economics*, vol. 5, pp. 1–12, 2019, Chinese.

[18] X. D. Ma and X. X. Huo, "Apple standardized production and improving recommendations: based on Shandong、Shaanxi and Gansu 960 apple growers' field investigation in China," *Agricultural Economic Issues*, vol. 3, pp. 37–48, 2019, Chinese.

[19] C. Chen, Y. Kong, and L. Xu, "Impact of regional public brands and standardized production on operating income of fruit growers: based on empirical test of 771 fruit farmers in Hebei, Jiangsu and Jiangxi Province," *Journal of Agro-Forestry Economics and Management*, vol. 20, no. 5, pp. 569–577, 2021, Chinese.

[20] Y. Yu, Y. He, X. Zhao, and L. Zhou, "Certify or not? an analysis of organic food supply chain with competing suppliers," *Annals of Operations Research*, 2019.

[21] Y. L. Zhang, M. Z. Wang, J. F. Qian, and Y. S. Liao, "Development characteristics, problems of leading enterprises in agricultural industrialization in China and its development thoughts," *Agricultural Economic Problems*, vol. 8, pp. 135–144, 2021, Chinese.

[22] Q.-Q. Deng and E.-L. Li, "Models and optimal path of grain industrialization based on the perspective of network organization," *Journal of Natural Resources*, vol. 36, no. 6, pp. 1602–1615, 2021.

[23] C. W. Sheng, J. Zhu, B. T. Yu, and Q. F. Feng, "The industrialization of China's fisheries: development pattern, synergistic mechanism and internationalization transformation experience inspirations," *Economic Issues*, vol. 6, pp. 47–54, 2021, Chinese.

[24] X. D. Xu, Z. L. Wang, Y. F. Zhu, and X. C. Luo, "Subject behavior of collaborative innovation in civil-military integration: an evolutionary game analysis," *Mathematical Problems in Engineering*, vol. 2021, Article ID 6698895, 7 pages, 2021.

[25] N. Su, Z. Shi, X. Zhu, and Y. Xin, "An evolutionary game model of collaborative innovation between enterprises and

colleges under government participation of China," *Sage Open*, vol. 11, no. 1, Article ID 215824402199485, 2021.

[26] K. Zhou and T. Ren, "Low-carbon technology collaborative innovation in industrial cluster with social exclusion: an evolutionary game theory perspective," *Chaos: An Interdisciplinary Journal of Nonlinear Science*, vol. 31, no. 3, Article ID 033124, 2021.

[27] J. Hou and B. Li, "The evolutionary game for collaborative innovation of the IoT industry under government leadership in China: an IoT infrastructure perspective," *Sustainability*, vol. 12, no. 9, pp. 3648–9, 2020.

[28] K. Liu, Y. Liu, H. Zhou, Y. Kou, Q. Ji, and D. Li, "Evolutionary game and numerical simulation of participants' collaborative behavior in integrated project delivery project," *Alexandria Engineering Journal*, vol. 60, no. 1, pp. 373–385, 2021.

[29] F. Chen, S. Liu, and A. Appolloni, "Horizontal coordination of I-LNGOs in the humanitarian supply chain: an evolutionary game approach," *Sustainability*, vol. 12, no. 15, pp. 5953–15, 2020.

[30] C. S. Sun, M. Wang, and F. Y. Zhai, "Research on the collaborative application of BIM in EPC projects: the perspective of cooperation between owners and general contractors," *Advances in Civil Engineering*, vol. 2021, Article ID 4720900, 14 pages, 2021.

[31] G. Qu, Y. Wang, L. Xu, W. Qu, Q. Zhang, and Z. Xu, "Low-carbon supply chain emission reduction strategy considering the supervision of downstream enterprises based on evolutionary game theory," *Sustainability*, vol. 13, no. 5, pp. 2827–5, 2021.

[32] Q. Long, X. Tao, Y. Shi, and S. Zhang, "Evolutionary game analysis among three green-sensitive parties in green supply chains," *IEEE Transactions on Evolutionary Computation*, vol. 25, no. 3, pp. 508–523, 2021.

[33] F. Yang, L. Yang, and P. Li, "The dynamic game of knowledge hiding behavior from organizational members: to hide or not to hide?" *Complexity*, vol. 202115 pages, 2021, https://doi.org/10.1155/2021/1713890, Article ID 1713890.

[34] Z. W. Zhang, Y. J. Xue, J. X. Li, L. M. Gong, and L. Wang, "Supply chain logistics information collaboration strategy based on evolutionary game theory," *IEEE ACCESS*, vol. 8, 2020 https://doi.org/10.1109/ACCESS.2020.2978943, Article ID 46102.

[35] L. C. Lei, S. Gao, and R. X. Chen, "How to solve the problem of big data killing: evolutionary game in e-commerce market based on collaborative supervision of government and consumers," *Journal of Systems Management*, vol. 30, no. 4, pp. 664–675, 2021, https://doi.org/10.3969/j.issn.1005-2542.2021.04.006.

[36] N. Zhang, X. X. Zhang, M. Lei, and Y. J. Yang, "Multiagent collaborative governance for targeted poverty alleviation from the perspective of stakeholders," *Complexity*, vol. 2020, Article ID 8276392, 21 pages, 2020.

Hindawi
Complexity
Volume 2022, Article ID 4547212, 14 pages
https://doi.org/10.1155/2022/4547212

WILEY | Hindawi

Research Article

A Comparison of Metaheuristic Techniques for Solving Optimal Sitting and Sizing Problems of Capacitor Banks to Reduce the Power Loss in Radial Distribution System

Tongfei Lei,[1] Saleem Riaz,[2] Hira Raziq,[3] Munira Batool ,[3] Feng Pan,[1] and Jianfeng Wang[1]

[1]*College of Mechanical Engineering, Xijing University, Xi'an 710123, China*
[2]*School of Automation, Northwestern Polytechnical University, Xi'an, Shaanxi, China*
[3]*Department of Electrical Engineering, University of Engineering and Technology, Taxila, Pakistan*

Correspondence should be addressed to Munira Batool; munira.batool@uettaxila.edu.pk

Received 31 December 2021; Revised 9 March 2022; Accepted 10 March 2022; Published 25 March 2022

Academic Editor: Yu Zhou

The losses in the radial distribution system are inevitable which needs to be minimized for the proper transmission of power to the end customers. This problem can be solved by the allocation of capacitor banks at proper locations with appropriate sizing. These allocations need an efficient approach for the performance enhancement of RDS. In this paper, several metaheuristic techniques such as particle swarm optimization (PSO), Harmony search, Bat, Cuckoo, and Grey-wolf (GW) algorithms are employed to find the size of capacitor banks. Loss sensitivity analysis is considered for the indication of candidate buses where a capacitor has to be installed to reduce the total system losses and ultimately increase efficiency. Cost-effectiveness, power loss minimization, and voltage enhancement can be determined and compared for these 5 techniques and are implemented on the IEEE-34 bus system to illustrate the efficacy of each of them. The results show the advantages and drawbacks of the techniques separately. The simulations are carried out in MATLAB.

1. Introduction

The voltage in a radial distribution system goes on decreasing from the substation to the end customer due to the losses generated in lines. The percentage of losses in the form of I^2R in a radial distribution system is 10–13% of generated power. Power loss minimization and voltage profile improvement are one of the most important technical issues to deal with. These issues can be reduced by employing distributed generation units at different locations of the system. Similarly, losses can also be reduced by allocating capacitor banks at suitable locations in the system. Two important scenarios are incorporating capacitor which is the basic step for the minimization of the losses and the allocation of these capacitors at the specific locations in a system which is the main objective. Locating capacitor banks in a radial distribution system is done through some heuristic techniques. Based on the approach of these techniques size and position of a capacitor can be found [1–4]. Allocation at a certain position is critical for the system so it is really important to place the CB at a certain specified location if not placed properly that will not only lead to increased losses but also results in the failure of a system. Hence classical methods have been used by researchers to solve the optimal sizing and location of a capacitor. One of the approaches is teaching strategy-based algorithm. In this, the size and position are determined by student and instructor relation-based schemes [5, 6].

To allocate the position and size of capacitors for the control of active and reactive power flow in the power system some genetic algorithms have been used. These genetic algorithms with some modifications shows better performance when compared with their standard counterparts [7–9]. To reduce the power loss and to find the exact location and size of the capacitor different genetic algorithms with some improvements are found to be more promising. One of the bio-inspired algorithms is the monkey search algorithm which uses the strategy of the monkeys for the sizing and allocating the capacitor banks

[10]. The PSO optimization technique improves the result by repetitively improving a solution concerning the task given to it. The adopted PSO algorithm shows some improvements in the conventional PSO [11].

A direct search algorithm was implemented on standard bus system and exhibit better power loss reduction, voltage characterization with less cost when compared with PSO. The algorithm searches for all possible locations in the system by a specific capacitor size and places the capacitor on the bus providing a significant reduction in operating power loss. The correct sizes are chosen to be the standard sizes available on the market i.e., different capacitor sizes are considered. The integration of renewable energy resources i.e. wind with the distributed system leads to higher power losses and voltage reduction due to varying wind speed. The intermittent nature of the wind creates the unbalance power which has to be improved with the PSO algorithm. Modifications are carried out in the objective function of the algorithm to obtain adequate results. Hybrid searching algorithms combine two or more algorithms and use the advantages of one algorithm on the other and results in improved results than if both of them are used individually [12–14]. The recursive techniques are used for the estimation of unknown matrix for linear system. The repetitiveness leads to exact location and dimension of the unknown variable by estimating different values in a continuous loop until correct standard is achieved and putting them in the matrix. For the reliability and high efficiency of the system specific equipment and size of the material is necessary. The supercapacitor nowadays is getting popular due to its robust nature of fast charging and discharging. For integration of supercapacitor in the energy storage system require the specific size and the parameter of the supercapacitor. The capacitor allocation in the power system requires the suitable optimization technique. Some of the researchers had used plant growth optimization to minimize the power losses. Loss sensitivity can be employed for the determination of the specific location for the employment of capacitor and the optimization technique is used for the size of the capacitor. In recent times a new algorithm i.e. Bacterial Foraging Optimization algorithm was incorporated for finding the solution of the problem by minimizing the power loss [15–18]. For several years the researchers try to minimize the power losses but that results in large compensating locations that will make the system complex and costly so minimizing the number of locations at which capacitors are to be installed is challenging. So, in the following research, the compensating locations are minimized to two or three and better results are to be achieved, with less complexity and cost-effectiveness compared to other techniques available in the literature. Budget allocation for genetic algorithm improves the search efficiency for selecting the highest solution for the optimization problem. The allocation can be extended to multi-objective optimization problem for correct selection of a candidate solution [19].

Iterative control method is used to locate the specific position and time of the fault by its repetitive property. Designing the iterative control strategy is a difficult task for both linear and nonlinear systems. Some error convergence techniques i.e Norm optimal, P-type, PD^{α}-type iterative control are implemented. The data produced in each iteration is used for the next iteration for improvement in control system. The optimal control scheme based on optimization shows improves performance of the iterative control algorithm. For system optimization Convergence speed of iterative control algorithm is important and is improved by applying optimal control scheme [20–25]. The efficiency of a system is based on the optimization approach. Different strategies based on the failure management is proposed for the maintenance management of a system. The maintenance and failure cost increase with time that urges for the optimization based on the complexity of the system [26, 27].

A harmonic search algorithm has been used to solve optimal placement and sizing of the capacitor bank. Fuzzy-based GA has been used to determine the optimal size with the multi-objective functions to minimize the energy cost and enhance the voltage profile [28]. BAT algorithm is implied to calculate the optimal size of the capacitor. The loss sensitivity factor determines the best and fewer number of locations for capacitor placement. This technique is slightly different than the other existing techniques based on LSF approach for sizing of capacitor [7]. Furthermore, the Cuckoo algorithm has been used more frequently than the BAT algorithm by researchers due to better power loss minimization but one of the drawbacks of the algorithm is the number of locations cannot be minimized [29]. Similarly, the Grey wolf algorithm is introduced to compensate for all the issues associated with power loss minimization effectively and efficiently. The convergence rate is higher than the other optimization techniques available. Similarly, the cost is lower than the direct and teaching-based algorithms [30, 31].

The foremost and primary aim of this work has to reduce the total power loss of the system. The proposed algorithms are verified on the IEEE 34-bus radial distribution system. The acquired outcomes are matched with the other present methods and the results are comparably shown in the table. MATLAB software is used for the Load flow analysis of IEEE standard bus system.

The main contributions of the paper are as follows:

(i) Proposal of various optimization algorithms to find the accurate size of capacitor banks for power loss reduction in distribution network

(ii) Step-by step implementation of proposed algorithms on the standard IEEE bus system for finiding the most suitable technique

(iii) Selection of most suitable technique for power loss reduction and voltage improvement of distribution

network by comparitive analysis of implemented optimization algorithm

(iv) Validating the effective operation of the proposed techniques using numerical analysis

2. Materials and Methods

The algorithms presented in the paper are applied to the IEEE 34-bus radial distribution system shown in Figure 1. The line and bus data are given in [33]. The total real and reactive powers are 4636.5 KW and 2873.5 KW respectively. The real and the reactive power losses of the system without the incorporation of capacitors are 223.85 kW and 66.47 kVAR.

The exact and precise approach for Distribution load flow is used for the determination of P, Q losses, and voltages. The model of distribution system is given in Figure 2.

Where m, m+1 = buses.

V_m, V_{m+1} = voltages at bus m and $m+1$, respectively.

J_m = branch current.

From Figure 2 above the expression of V_{m+1} can be written as

$$V_{m+1} = V_m - J_m(R_m + \mathrm{jX}_m), \tag{1}$$

where $V = \mathrm{IR}$ and $J = (\mathrm{BIBC}) \times (I)$, which is the Matrix representation of branch current in each line, BIBC is the Bus current Injection to branch current matrix.

As the formula of complex power is given as

$$S = \mathrm{VI}^*, \qquad I = \left(\frac{S}{|V|}\right)^*, \tag{2}$$

where S=P + jQ.

Putting the value of S in I,

$$I = \left(\frac{P_m + \mathrm{jQ}_m}{|V_m|}\right)^*. \tag{3}$$

2.1. Expression for Active Power Loss.

$$\begin{aligned} P_{\mathrm{Loss}(m,m+1)} &= I^2 * R_m \\ &= \left(\frac{S_m}{|V_m|}\right)^2 R_m, \quad \text{where } S = \sqrt{P^2 + Q^2} \\ &= \frac{\left(P_m^2 + Q_m^2\right)}{|V_m|^2} * R_m. \end{aligned} \tag{4}$$

The $P_{\mathrm{Loss}(m,m+1)}$ is the active power loss in the line section between buses m and $m+1$.

2.2. Expression for Reactive Power Loss.

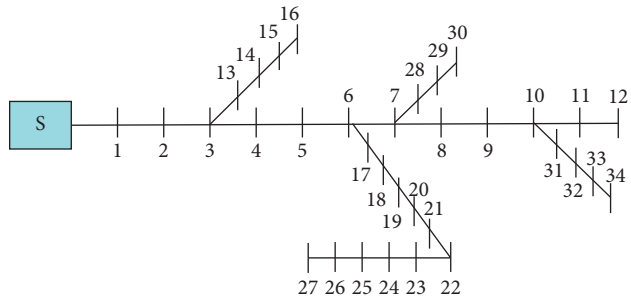

Figure 1: IEEE-34 bus radial distribution system [32].

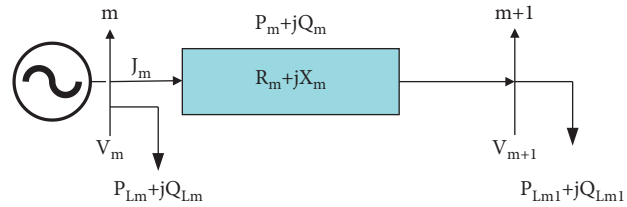

Figure 2: Distribution system [7].

$$\begin{aligned} Q_{\mathrm{Loss}(m,m+1)} &= \left(\frac{S_m}{|V_m|}\right)^2 * X_m, \\ &= \frac{\left(P_m^2 + Q_m^2\right)}{|V_m|^2} * X_m, \end{aligned} \tag{5}$$

where $Q_{\mathrm{Loss}(m,m+1)}$ = Reactive power loss in the line section between buses m and $m+1$.

P_m and Q_m = Active and Reactive power flowing out of bus m,

X_m = Reactance of the line section between buses m and $m+1$,

V_m = Magnitude of voltage at bus m.

2.3. Sum of Active Power Loss. The total power loss can be computed by adding up all the branch losses. The expression for total power loss is mentioned as follows:

$$P_{t,\mathrm{loss}} = \sum_{m=1}^{\mathrm{nb}} P_{\mathrm{Loss}(m,m+1)}. \tag{6}$$

2.4. Sum of Reactive Power Loss. The equation for total reactive power loss is

$$Q_{t,\mathrm{loss}} = \sum_{m=1}^{\mathrm{nb}} Q_{\mathrm{Loss}(m,m+1)}. \tag{7}$$

2.5. Objective Function for the Problem. The objective function is used for the minimization of power loss in the system. The mathematical formulation of the objective function is given by

$$\text{Minimize}\,(F) = \min\left(P_{t,\text{loss}}\right). \tag{8}$$

subject to the following operating constraints.

2.5.1. Power Balance.

$$P_{\text{ss}} = \sum_{m=2}^{n} P_{\text{Lm}} + \sum_{m=1}^{\text{nb}} P_{\text{Loss}^{(m,m+1)}} - \sum_{m=1}^{\text{nb}} P_{\text{cap},m}, \tag{9}$$

where P_{Lm} = real power load at bus m.
$P_{\text{cap},m}$ = reactive power supplied by capacitor.
m = bus number
n = total number of buses
nb = total number of the branches.

2.5.2. Voltage Deviation Limit.

$$V_{m,\min} \le \left|V_m\right| \le V_{m,\max}, \tag{10}$$

where $V_{m,min}$ and $V_{m,\max}$ = minimum and maximum voltage limits at bus m.

2.5.3. Reactive Power Compensation.

$$Q_{\text{cm},\min} \le Q_{\text{cm}} \le Q_{\text{cm},\max}, \quad m = 1, \ldots, N_B, \tag{11}$$

where $Q_{\text{cm},\min}$ and $Q_{\text{cm},\max}$ = minimum and maximum reactive power limits of compensated bus m.

2.6. Loss Sensitivity Factor for Node Selection. LSF approach is employed to assess the sensitivity of the buses and is useful for the selection of candidate buses for locating capacitor. The LSF values for all lines and buses are calculated by sorting these values in descending order. Those nodes which have the largest value of LSF are considered to be the candidate buses and capacitors will be only installed on those nodes. Following are the advantages of LSF:

(i) It helps to figure out the buses on which capacitors are to be installed
(ii) It reduces the search space for optimization
(iii) It is easy and simple to implement

Assume there are two nodes m and n connected through a branch k. LSF can be calculated by partial derivative of the system losses with respect to reactive power consumption at the destination node n as follows:

$$\frac{\partial P_{\text{lineloss}}}{\partial Q_m} = \frac{2Q_m R_k}{\left|V_m\right|^2}, \tag{12}$$

where $P_{\text{loss}\,(m,n)}$ Power loss in nodes m and n, Q_{mn} is reactive power in nodes m and n

$$\frac{\partial Q_{\text{lineloss}}}{\partial Q_m} = \frac{2Q_m X_k}{\left|V_m\right|^2}, \tag{13}$$

where $Q_{[m]}$ is reactive power beyond node m, R_k = resistance of a branch k, $X_{[k]}$ is the reactance of the branch k.

2.6.1. Unit of LSF. As the formula of LSF is given as

$$\begin{aligned}
\frac{\partial P_{\text{loss}}}{\partial Q_m} &= \frac{2Q_m R_k}{\left|V_m\right|^2} \\
&= \frac{V_{\text{ar}}.\Omega}{V.V}, \\
\frac{V_{\text{ar}}.A^{-1}}{V} \text{ as } \frac{V}{\Omega} &= \text{Amp\&}\frac{\Omega}{V} = A^{-1} \\
&= \frac{V_{\text{ar}}}{\text{AV}} \\
&= \frac{\text{AV}}{\text{AV}} \\
&= \text{no unit.}
\end{aligned} \tag{14}$$

Hence, it is concluded from this derivation that LSF has no unit.

2.6.2. Net Savings. Parameters utilized for the net savings are energy rate Ce = \$0.06/kWh, the cost of capacitor that has to be incorporated Ccl = \$1000/each location, cost of buying capacitor Cc = \$3.0/kVAR, T = 8760. The total savings can be given by

$$\text{Netsavings} = \left[\left(C_e * P_{\text{Loss}}^{\text{Cap}} * T\right) - \left(C_{\text{cl}} * N_{\text{BC}}\right) - \left(C_c * T_c\right)\right], \tag{15}$$

where N_{BC} = number of buses that are compensated.

(1) T_c = total rating of a capacitor
(2) $P_{\text{Loss}}^{\text{Cap}}$ = total power loss of the system with capacitor [7]

2.7. Algorithms. Five algorithms namely PSO, Harmony search, BAT, Cuckoo, and Grey-wolf are defined and discussed. The properties of each of them make them unique in solving complex problems. Flowcharts show the working hierarchy of the techniques in tackling difficult tasks.

2.7.1. Particle Swarm Optimization Technique. PSO technique is originated from basic two concepts:

(i) The Examination of swarming modes of animals like bird or fish
(ii) The area of mutative computation is like a genetic algorithm [11]

As the name suggests it works on having a swarm of particles. The particles are considered as the set of possible solutions in the population of a swarm. The particles will roam around the space based on mathematical formulas. The particle's motion is governed by their own best positions and that of the swarms. Once the best position is located it will lead the other swarm to achieve the best location. The process is repetitive and expects to find suitable results. The flowchart shown below in Figure 3 demonstrates the hierarchy of the technique.

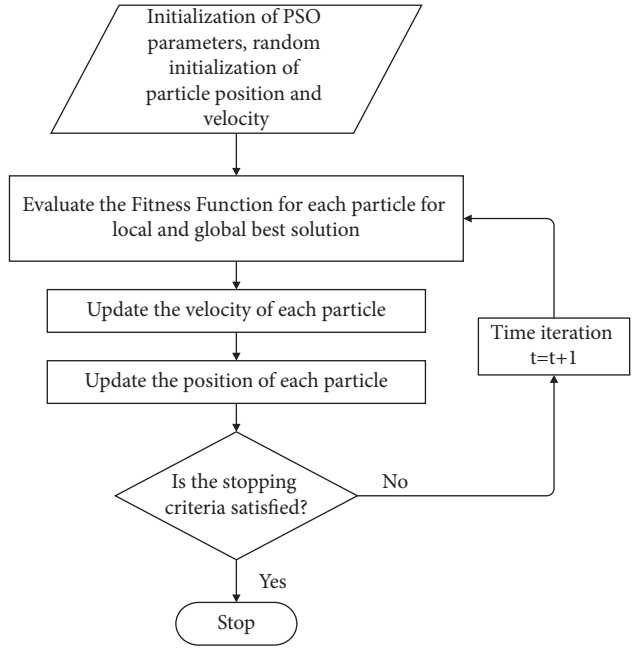

Figure 3: PSO algorithm flow chart.

2.7.2. Harmony Search Algorithm. The harmony search algorithm is based on the creation of pleasant harmony by using different musical instruments and their pitches by the musician. The musician searching for new harmonies for the uniqueness of their sound made the basis for this algorithm. In this searching strategy, the algorithm finds the best solution to the problem with less computational time and rapid convergence. Figure 4 shows the flowchart of the scheme.

2.7.3. BAT Algorithm. From the nature of environmental systems, intelligent-based algorithms have been derived. Bat Algorithm (BA) was first introduced by Xin-She-Xang to optimize the engineering problem [35], is built on the microbat's property of echolocation concerning varying pulse rates of diffusion and noise shown in Figure 5.

BAT algorithm is based on the following:

(i) Echolocation behavior of microbats

(ii) Variation in frequency

(iii) Variation in loudness

2.7.4. Cuckoo Algorithm. The cuckoo algorithm is built based on the cuckoo bird's behavior of laying eggs in the nests of other birds. It is used for the optimization of complex problems i.e. Global optimization problems and NP-hard problems that can be efficiently resolved. The important property of the algorithm is its operation of flight for updating the search space for the new solution generation. One of its properties is the modification of the solution during the iterations by adding small changes [36–38]. The flowchart of the algorithm is shown below in Figure 6.

2.7.5. Grey-Wolf Algorithm. The grey-Wolf algorithm is based on the leadership hierarchy and the behavior of grey wolves as they hunt their prey in a group form. Hierarchy has four levels alpha, beta, delta, and omega with each of the levels designated with different responsibilities. The topmost alphas are the organizers and decision-makers for the entire group, which each of them has to follow. Beta advises the alpha in the decision-making process and manages the group according to the orders given by the alpha. The bot-tom-most omega is the one to solve the problems among the different levels of the group. Delta is assigned to warn the wolves in case of danger, provide food to the group, caring for them if any one of them gets sick.

Another stimulating feature of the grey wolves is the hunting of their prey in the form of groups i.e. they search for their prey, encircle them and attack them collectively. This hierarchy scheme with the hunting mechanism made the basis for the optimization problem. The hierarchy scheme and hunting behavior are shown via pyramid and flowchart below in Figures 7 and 8 respectively.

3. Results and Discussion

Loss sensitivity analysis is carried out on IEEE-34 bus system Voltage profile improvement and power loss minimization graphs [7] can be seen for the base case and the proposed schemes as discussed below.

3.1. IEEE Radial 34 Bus System LSF. Loss sensitivity analysis at each node of the IEEE-34 bus system is calculated for the indication of candidate buses where capacitor has to be installed to reduce the total system losses which in turn increases the efficiency of the RDS. The loss sensitivity factor is calculated using Microsoft excel and the results are shown in Figure 9.

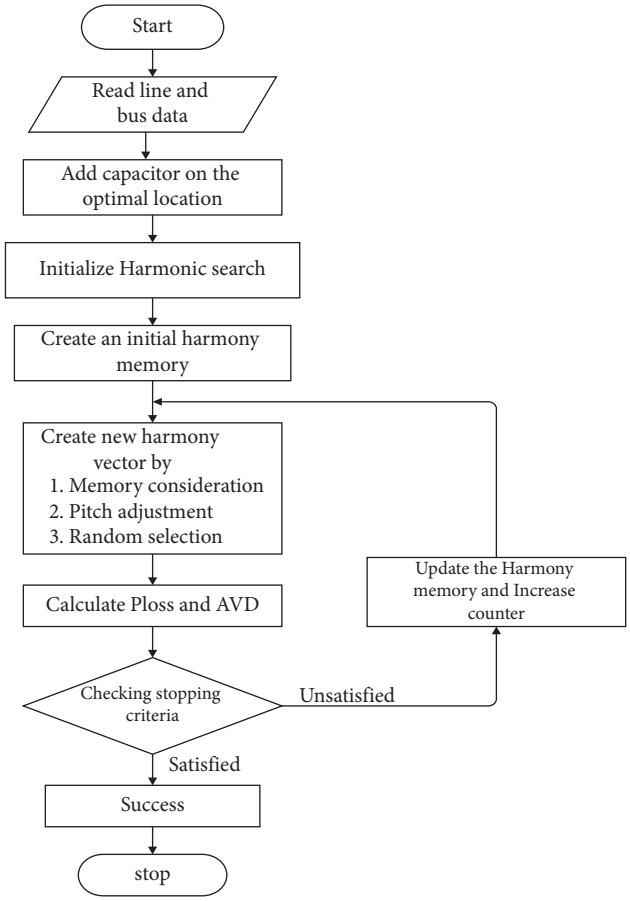

Figure 4: Harmony search algorithm flowchart [34].

3.2. Voltage Profile and Power Loss in an IEEE-34 Bus System. Voltage and power loss in the 34-bus system have been determined with and without capacitors. The voltage is enhanced and power loss minimization occurs.

3.2.1. Base Case. Voltage and power loss without capacitor incorporation are shown in Figure 10. The maximum voltage is 1 pu and the minimum voltage is 0.9423 pu. These values are taken as the base values for the other results in which the capacitor is allocated in the system. Real Power loss is 223.85 kW while reactive power loss in the base case is 66.4783 kVAR.

3.2.2. Proposed Method. Allocation of capacitor in power system leads to improved voltages and power loss minimization. Different techniques are used for locating and sizing of capacitor for voltage improvement and power loss minimization as shown in Table 1. Outputs of BAT and grey wolf are shown in Figures 11 and 12.

For the Bat algorithm, the maximum voltage is 1 pu but the minimum voltage is 0.95 pu which is a considerable improvement from the base case. Similarly, real power loss is 165.34 kW, and reactive power loss is 49.95 kVAr which is minimized then the base case.

Grey-wolf gives the most satisfactory result among the 5 optimization problems. Voltages and power losses show the best results among the proposed techniques. The minimum voltage is 0.9507 pu which is the highest among the proposed algorithms similarly active and reactive powers are 159.29 kW and 47.812 kVAR, respectively.

Table 1 compare the metaheuristic techniques and the base case. Capacitor sizes and their location at nodes in the 34-bus system are mentioned. Different parameters such as minimum and maximum voltages, kVAR injected, active and reactive power losses, percentage power loss reduction and cost analysis have been compared based on different algorithms. The results show satisfactory outputs after the incorporation of CBs.

The comparison of the real power losses for different algorithms is shown in Figure 13 Without capacitors the losses are the highest among them. The grey-wolf have the lowest losses hence the highest optimization.

The net savings for the PSO algorithm is the lowest i.e. $18398 and are highest for Bat and GWO algorithms $21711 and $20115 respectively shown in Figure 14. This is one of the advantages of the Bat and GWO in terms of cost.

Power loss reduction is one of the most important features of the power system. For the proper functioning of the system, the losses should be the least otherwise it will lead to other system problems. The power loss reduction is the lowest in PSO and highest in the Grey-wolf optimization technique as shown below in Figure 15.

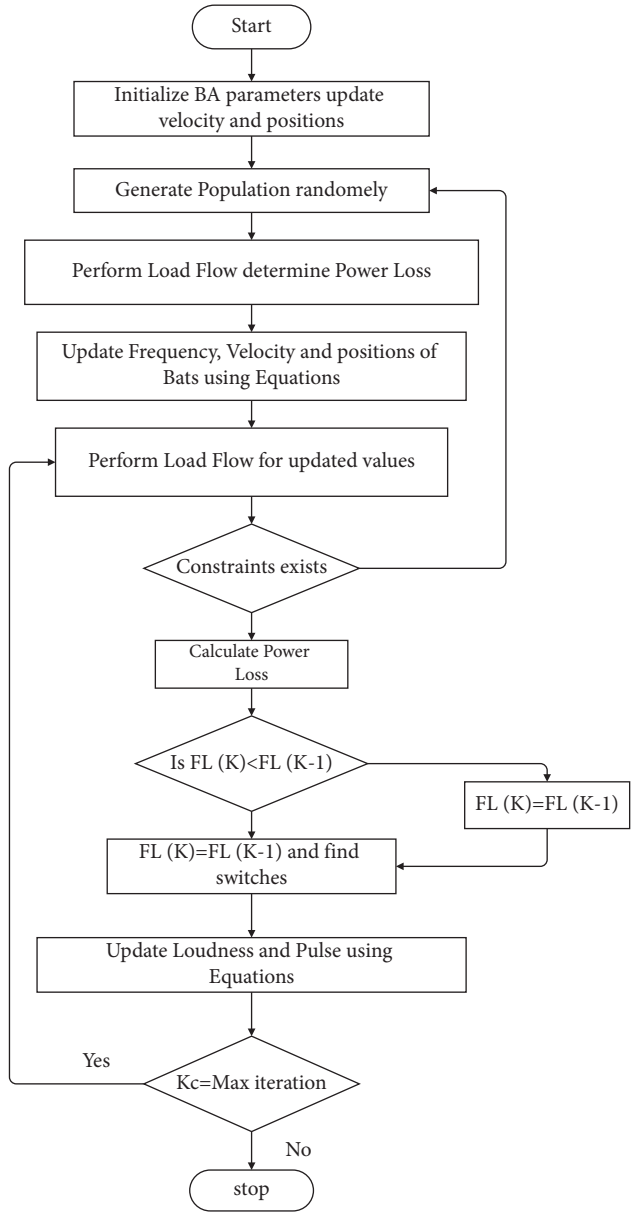

Figure 5: Bat algorithm flowchart.

Table 2 compares the metaheuristic techniques based on their different approach towards optimization of a problem. It can be seen from Figure 10(a) that the minimum voltage that appeared without compensation kVAR is 0.9423 p.u but as soon as kVAR is injected the voltage profile gets improved and the minimum voltage hence appears is 0.9507 p.u shown in Figure 10(b). If one looks at the power loss graph in Figure 11(a) it can be seen that the power loss has also been reduced power loss at node 1 is about 30.1754 kW Figure 10(a)) but after the capacitor placement, it reduces to about 25.4049 kW shown in Figure 11(b). Using GWO nearly 28.84% real power loss and 28.0777% reactive power loss have been reduced. Moreover, comparison Tables 1 and 2 predicts the pros and cons of each of the techniques. PSO technique converges very slowly and does not have appreciable power loss minimization as far as other techniques are concerned GWO can better minimize the power losses as compared to other techniques and also converges quickly but BAT algorithm can minimize the locations where capacitors have to be installed. The cuckoo algorithm gives better power loss reduction whereas the harmony search algorithm can have minimum kVAR injected and ultimately the number of candidate buses. So a hybrid algorithm could be developed using this research that could achieve superiority over all the mentioned techniques.

A. Future work.

(1) Using system reconfiguration techniques and then applying the algorithm.

(2) System power loss minimization could be accomplished by optimal location of DG (distributed generation).

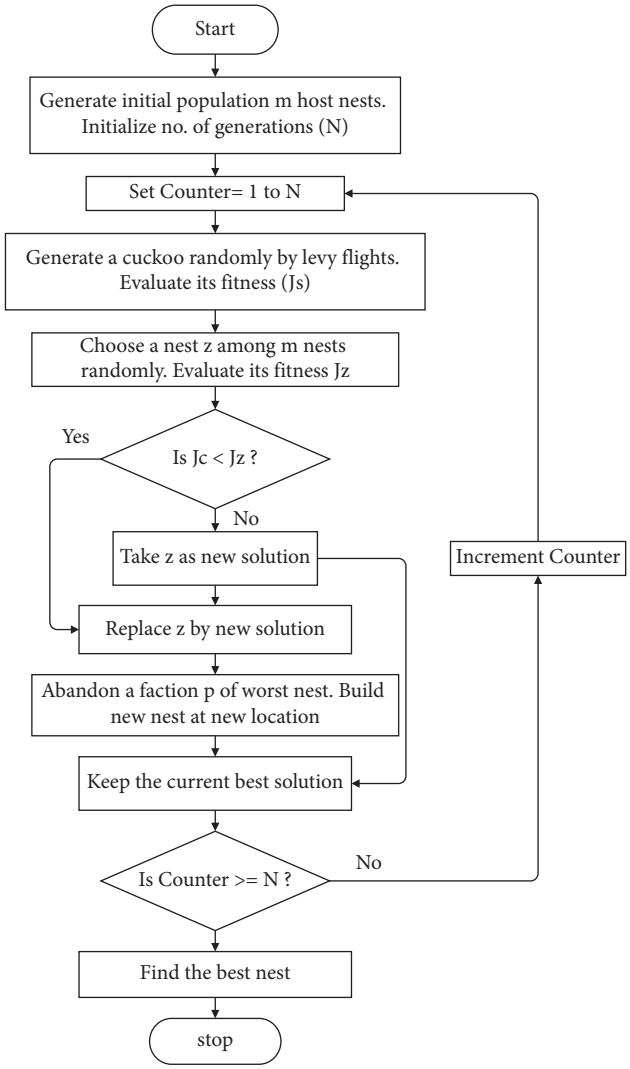

Figure 6: Cuckoo algorithm flow chart [39].

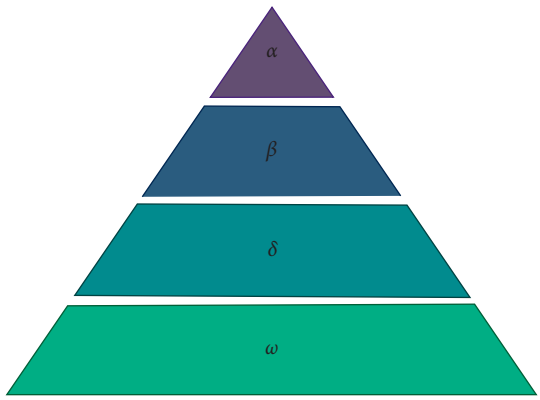

Figure 7: GWO pyramid [40].

(3) An improved Bat algorithm based on the novel initialization technique for global optimization problem could be developed.

(4) Another technique is used that is the hybrid between different techniques, for example, Bat algorithm (BA) and Artificial Bee Colony (ABC) which enables a communication strategy. In this technique, the drawbacks or the bad individuals or bats are covered by good agents of the artificial bee colony and vice versa. At every iteration, the advantages got

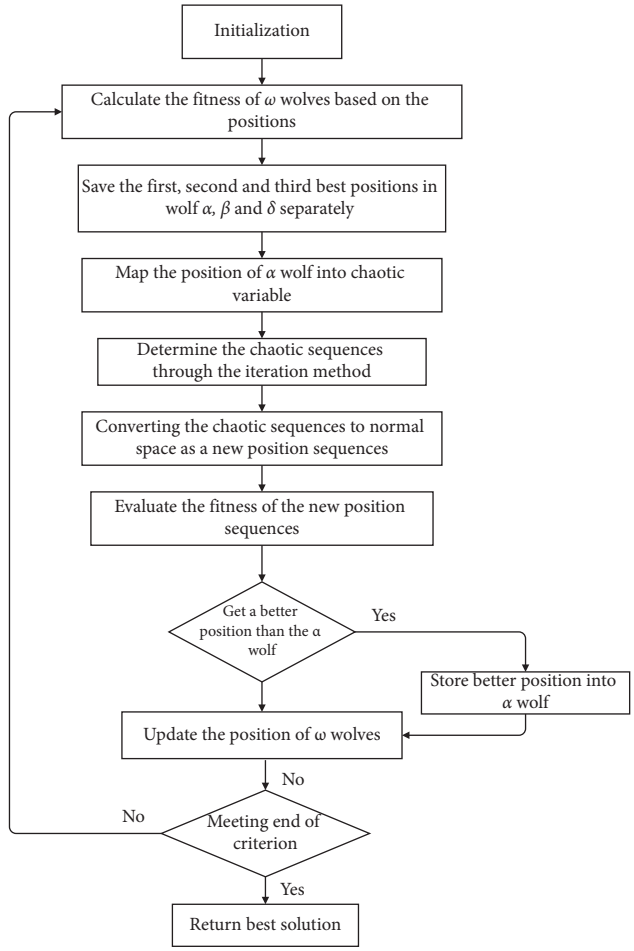

Figure 8: Grey wolf algorithm flow chart [41].

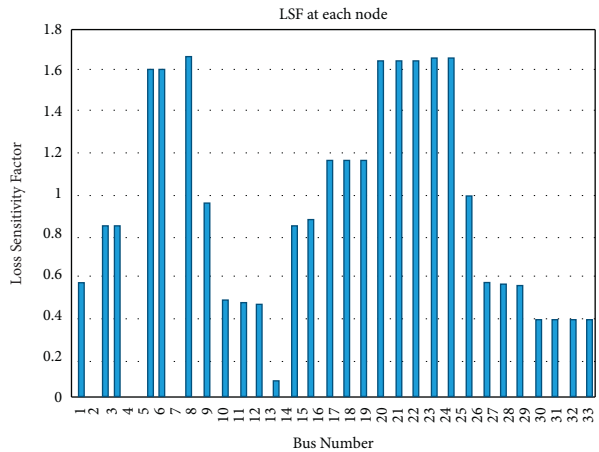

Figure 9: LSF at each node IEEE-34 bus system.

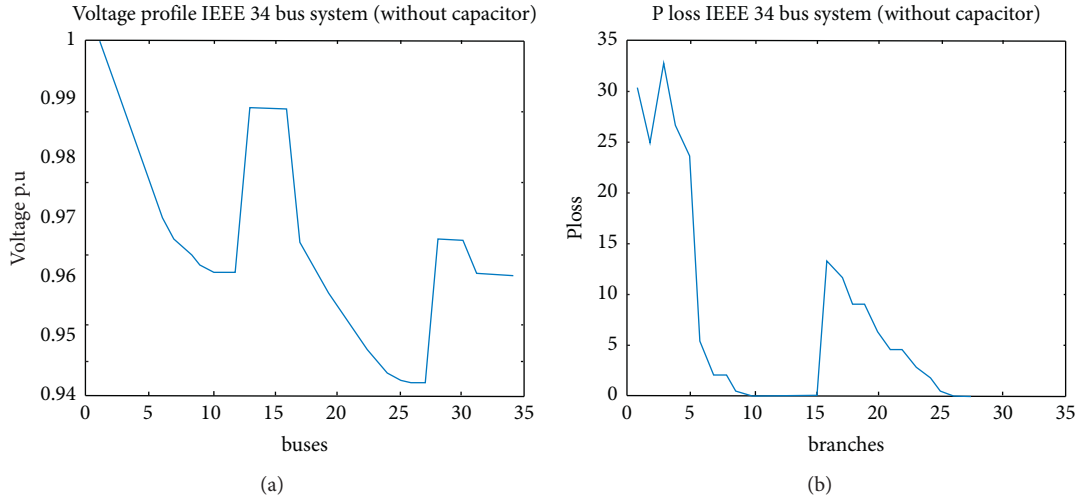

Figure 10: (a) Voltage profile IEEE-34 bus system. (b) Power loss (kW) at each node IEEE-34 bus system.

Table 1: Results comparison of metaheuristic techniques on an IEEE-34 bus system.

Parameter	Base case	PSO [34]	Harmonic search	BAT	Cuckoo	Grey wolf
Capacitor size and sitting (node)	—	781 (19) 803 (22) 479 (20)	1000 (19) 800 (26)	650 (10) 1150 (25)	10 (650) 19 (850) 25 (700)	500(10) 500(25) 660 (19) 290 (22)
Minimum voltage (node)	0.9423 (bus 27)	—	0.9501 (27)	0.9500 (27)	0.9503 (27)	0.9507 (27)
Maximum voltage (node)	1.00 (bus 1)	—	1.00 (1)	1.00 (1)	1.00 (1)	1.00 (1)
Real power loss (kW)	223.85	168.6	167.9468	165.3482	160.3	159.29
Reactive power loss (kVAR)	66.4783	49.9924	49.0422	49.9579	48.8243	47.8127
% P loss reduction	—	24.6817	24.9735	26.1343	28.3895	28.84%
% Q loss reduction	—	24.7989	26.2282	24.8508	26.556	28.0777
kVAR injected	—	2063	1800	1800	2200	1950
Computation time (s)	0.903117	17.809493	9.892012	2.005097	0.14682	0.43199
Net savings ($)	—	18398	20635	21711	19194	20115

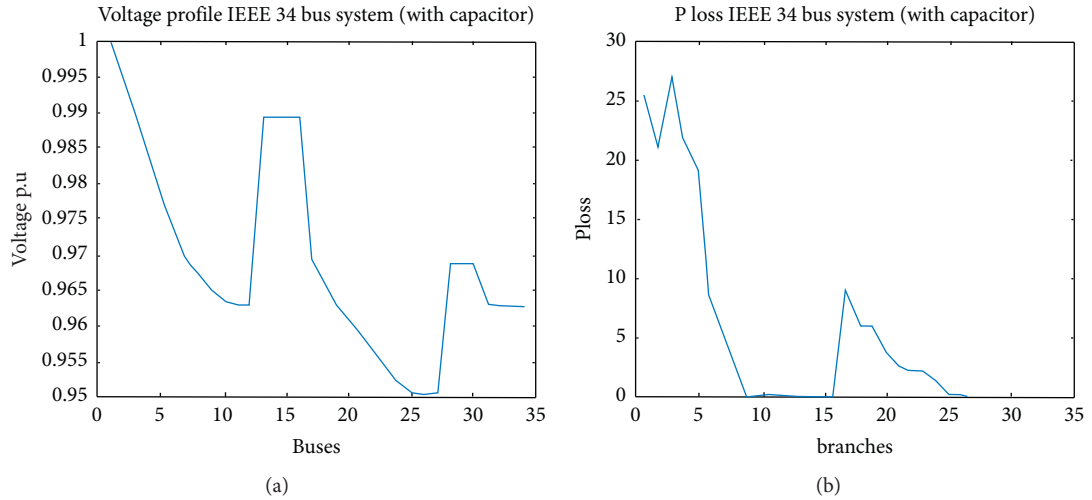

Figure 11: BAT (a) Voltage profile after kVAR compensation IEEE-34 bus system. (b) Power loss after kVAR compensation IEEE- 34 bus system.

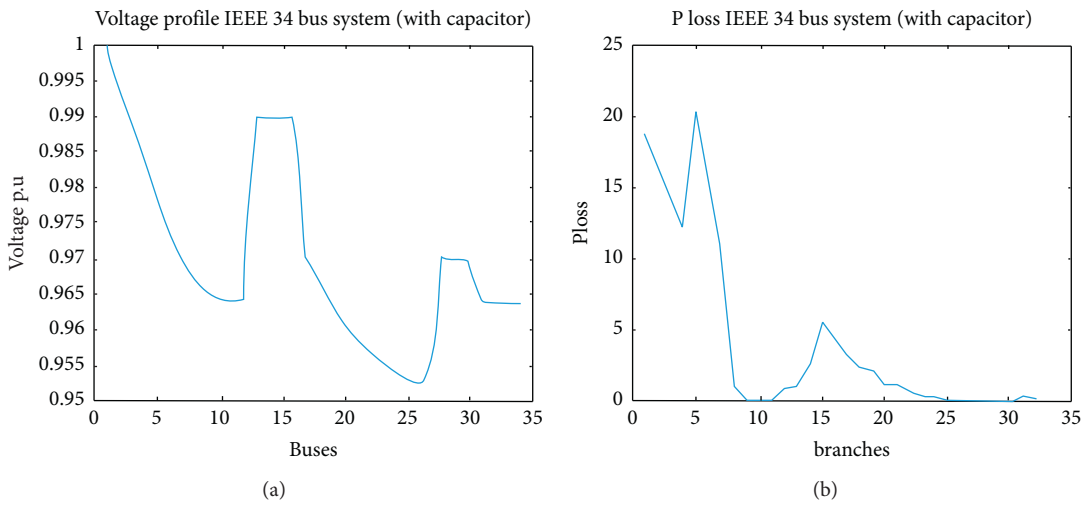

Figure 12: GWO (a) Voltage profile after kVAR compensation IEEE-34 bus system. (b) Power loss after kVAR compensation IEEE- 34 bus system.

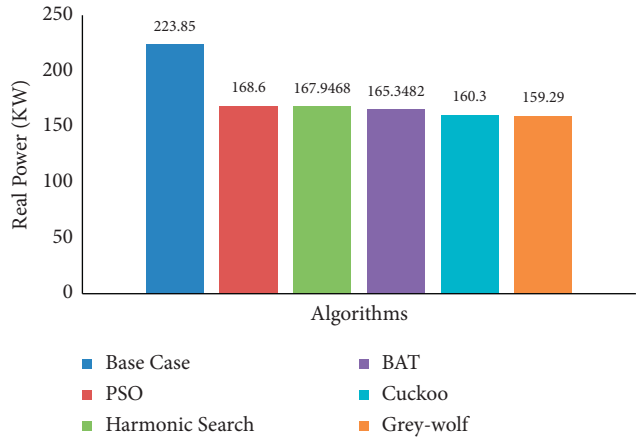

Figure 13: comparison of Real power losses for different techniques.

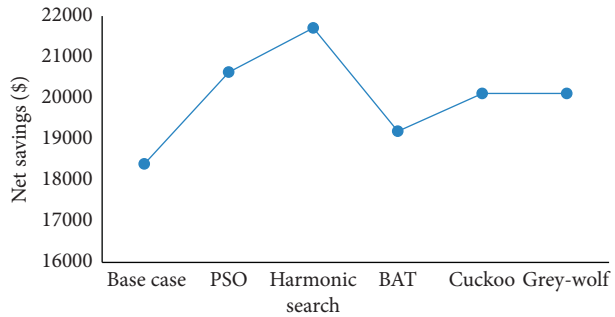

Figure 14: Net savings in different techniques.

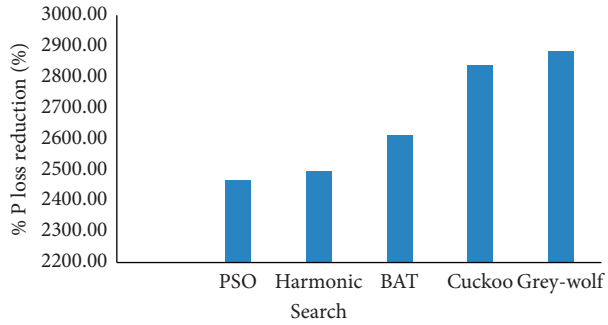

Figure 15: Power loss reduction for different techniques.

Table 2: Comparison of metaheuristic techniques.

PSO	Harmonic search	Bat	Cuckoo	Grey-wolf
Based on the concept of swarm intelligence for solving complex problems	Inspired by the musical process of searching for a perfect state of harmony. Inspired by the musical process of searching for a perfect state of harmony. Inspired by the musical process of searching for a perfect state of harmony.	Inspired by the echolocation behavior of bats. It is a bio-inspired algorithm. Inspired by the echolocation behavior of bats. It is a bio-inspired algorithm. Inspired by the echolocation behavior of bats. It is a bio-inspired algorithm.	Inspired by the behavior of cuckoo species e.g. off-spring parasites. Inspired by the behavior of cuckoo species e.g. off-spring parasites. Inspired by the behavior of cuckoo species, e.g., off-spring parasites.	The hierarchy scheme and hunting mechanism of grey wolves made the basis of this optimization problem

increased and accuracy and convergence is achieved in a better way. BA is up to 78% and original ABC is at 11% on finding the near best solution improvement.

4. Conclusion

In this paper, five techniques have been applied to the IEEE-34 bus test system for optimally locating the capacitor banks. The size of the CBs is another issue that has been optimized. The importance of these algorithms in RDS has been pointed out by comparing the results with the base case. Sizing and sitting of the capacitors can also be done without the algorithmic approach but that will increase the chances of risk and in turn reliability of a system becomes less which makes the use of these techniques necessary. Comparison between different algorithms can be carried out to find the best technique for the given problem. PSO is applied for the allocation of CBs but the results do not assure a reliable solution to the problem. Bat algorithm shows satisfactory results by determining the best and minimum optimal locations at which capacitor should be placed. Harmonic search and cuckoo algorithm has been used in the search for better results than the previous ones. The cuckoo algorithm shows better power loss minimization than Bat but the locations of the CBs cannot be minimized which is one of its drawbacks. Similarly, the Grey wolf algorithm is introduced to compensate for the issue of power loss minimization and shows better performance, converges rapidly in an effective and efficient manner.

Abbreviations and Acronyms

PSO: Particle swarm optimization
GWO: Grey wolf optimization
CSA: Cuckoo search algorithm
HSA: Harmony search algorithm
LSF: Loss sensitivity factor.

Data Availability

The data are available, and simulation data can be provided on demand.

Conflicts of Interest

The authors declare that they have no conflicts of interest to report regarding the present study.

Authors' Contributions

Saleem Riaz and Tongfei Lei conceptualized and designed the study; Tongfei Lei took part in methodology, acquired funding, prepared the original draft, and reviewed and edited the manuscript; Hira Raziq provided software and provided resources and took part in data curation; Tongfei Lei and Jianfeng wang validated the study; Munira Batool took part in formal analysis; Feng Pan investigated and visualized the study; Saleem Riaz supervised the study and took part in project administration. All authors have read and agreed to the published version of the manuscript.

Acknowledgments

This research work was financially supported by the Foundation for Advanced Talents of Xijing University (grant number XJ17B03).

References

[1] A. R. Abul'Wafa, "Optimal capacitor allocation in radial distribution systems for loss reduction: a two stage method," *Electric Power Systems Research*, vol. 95, pp. 168–174, Feb. 2013.

[2] I. A. Kowsalya M and M. Kowsalya, "Optimal size and siting of multiple distributed generators in distribution system using bacterial foraging optimization," *Swarm and Evolutionary Computation*, vol. 15, pp. 58–65, 2014.

[3] A. Mohamed Imran, M. Kowsalya, and D. P. Kothari, "A novel integration technique for optimal network reconfiguration and distributed generation placement in power distribution networks," *International Journal of Electrical Power & Energy Systems*, vol. 63, pp. 461–472, 2014.

[4] X. Feng, Q. Li, and K. Wang, "Waste plastic triboelectric nanogenerators using recycled plastic bags for power generation," *ACS Appl. Mater. Interfaces*, vol. 13, no. 1, pp. 400–410, 2021.

[5] C. Liu, Q. Li, and K. Wang, "State-of-charge estimation and remaining useful life prediction of supercapacitors," *Renewable and Sustainable Energy Reviews*, vol. 150, Article ID 111408, Oct. 2021.

[6] S. Sultana and P. K. Roy, "Optimal capacitor placement in radial distribution systems using teaching learning based optimization," *International Journal of Electrical Power & Energy Systems*, vol. 54, pp. 387–398, 2014.

[7] K. R. Devabalaji, A. M. Imran, T. Yuvaraj, and K. Ravi, "Power loss minimization in radial distribution system," *Energy Procedia*, vol. 79, pp. 917–923, 2015.

[8] N. Kanwar, N. Gupta, K. R. Niazi, and A. Swarnkar, "Improved meta-heuristic techniques for simultaneous capacitor and DG allocation in radial distribution networks," *International Journal of Electrical Power & Energy Systems*, vol. 73, pp. 653–664, Dec. 2015.

[9] K. Wang, C. Liu, J. Sun et al., "State of charge estimation of composite energy storage systems with supercapacitors and lithium batteries," *Complexity*, vol. 2021, pp. 1–15, 2021.

[10] F. G. Duque, L. W. De Oliveira, E. J. De Oliveira, A. L. M. Marcato, and I. C. Silva, "Allocation of capacitor banks in distribution systems through a modified monkey search optimization technique," *International Journal of Electrical Power & Energy Systems*, vol. 73, pp. 420–432, May 2015.

[11] K. Balu and V. Mukherjee, "Siting and sizing of distributed generation and shunt capacitor banks in radial distribution system using constriction factor particle swarm optimization," *Electric Power Components and Systems*, vol. 48, no. 6-7, Article ID 2020935, pp. 697–710, 2020.

[12] M. Ramalinga Raju, K. V. S. Ramachandra Murthy, and K. Ravindra, "Direct search algorithm for capacitive compensation in radial distribution systems," *International Journal of Electrical Power & Energy Systems*, vol. 42, no. 1, pp. 24–30, 2012.

[13] H. S. Ramadan, A. F. Bendary, and S. Nagy, "Particle swarm optimization algorithm for capacitor allocation problem in distribution systems with wind turbine generators," *International Journal of Electrical Power & Energy Systems*, vol. 84, pp. 143–152, Jan. 2017.

[14] H. Lotfi, R. Ghazi, and M. b. Naghibi-Sistani, "Multi-objective dynamic distribution feeder reconfiguration along with capacitor allocation using a new hybrid evolutionary algorithm," *Energy Systems*, vol. 11, no. 3, pp. 779–809, Aug. 2020.

[15] Y. Hua, N. Wang, and K. Zhao, "Simultaneous unknown input and state estimation for the linear system with a rank-deficient distribution matrix," *Mathematical Problems in Engineering*, vol. 2021, pp. 1–11, 2021.

[16] X. Feng, Y. Zhang, L. Kang et al., "Integrated energy storage system based on triboelectric nanogenerator in electronic devices," *Frontiers of Chemical Science and Engineering*, vol. 15, no. 2, pp. 238–250, 2021.

[17] R. S. Rao, S. V. L. Narasimham, and M. Ramalingaraju, "Optimal capacitor placement in a radial distribution system using Plant Growth Simulation Algorithm," *International Journal of Electrical Power & Energy Systems*, vol. 33, no. 5, pp. 1133–1139, Jun. 2011.

[18] K. R. Devabalaji, K. Ravi, and D. P. Kothari, "Optimal location and sizing of capacitor placement in radial distribution system using Bacterial Foraging Optimization Algorithm," *International Journal of Electrical Power & Energy Systems*, vol. 71, pp. 383–390, Oct. 2015.

[19] G. Kou, H. Xiao, M. Cao, and L. H. Lee, "Optimal computing budget allocation for the vector evaluated genetic algorithm in multi-objective simulation optimization," *Automatica*, vol. 129, Article ID 109599, 202199.

[20] S. Riaz, H. Lin, F. Afzal, and A. Maqbool, "Design and implementation of novel LMI-based iterative learning robust nonlinear controller," *Complexity*, vol. 2021, pp. 1–13, 2021.

[21] S. Riaz, H. Lin, and M. P. Akhter, "Design and implementation of an accelerated error convergence criterion for norm optimal iterative learning controller," *Electronics*, vol. 9, no. 11, pp. 1766–1815, 2020.

[22] S. Riaz, H. Lin, M. Waqas, F. Afzal, K. Wang, and N. Saeed, "An accelerated error convergence design criterion and implementation of lebesgue-p norm ILC control topology for linear position control systems," *Mathematical Problems in Engineering*, vol. 2021, pp. 1–12, 2021.

[23] S. Riaz, H. Lin, M. Mahsud, D. Afzal, A. Alsinai, and M. Cancan, "An improved fast error convergence topology for PDα-type fractional-order ILC," *Journal of Interdisciplinary Mathematics*, vol. 24, no. 7, p. 2021, 2021.

[24] S. Riaz, H. Lin, M. Bilal Anwar, and H. Ali, "Design of PD-type second-order ILC law for PMSM servo position control," *Journal of Physics: Conference Series*, vol. 1707, no. 1, Article ID 012002, 2020.

[25] S. Riaz, H. Lin, and H. Elahi, "A novel fast error convergence approach for an optimal iterative learning controller," *Integrated Ferroelectrics*, vol. 213, no. 1, pp. 103–115, 2021.

[26] Y. Zhou, G. Kou, H. Xiao, Y. Peng, and F. E. Alsaadi, "Sequential imperfect preventive maintenance model with failure intensity reduction with an application to urban buses," *Reliability Engineering & System Safety*, vol. 198, Article ID 106871, 2020.

[27] Y. Zhou, M. Zhang, G. Kou, and Y. Li, "Travel preference of bicycle-sharing users: a multi-granularity sequential pattern mining approach," *International Journal of Computers, Communications & Control*, vol. 17, no. 1, pp. p1-14, 2022.

[28] Y. Wang, S. Riaz, Z. Bao, and W. Zhang, "Accelerated iterative learning control for linear discrete time invariant switched systems," *Mathematical Problems in Engineering*, vol. 2002, Article ID 5738826, 10 pages, 2022.

[29] K. R. Devabalaji, T. Yuvaraj, and K. Ravi, "An efficient method for solving the optimal sitting and sizing problem of capacitor banks based on cuckoo search algorithm," *Ain Shams Engineering Journal*, vol. 9, no. 4, pp. 589–597, Dec. 2018.

[30] S. Kola Sampangi and J. Thangavelu, "Optimal capacitor allocation in distribution networks for minimization of power loss and overall cost using water cycle algorithm and grey wolf optimizer," *International Transactions on Electrical Energy Systems*, vol. 30, no. 5, May 2020.

[31] U. Sultana, A. B. Khairuddin, A. S. Mokhtar, N. Zareen, and B. Sultana, "Grey wolf optimizer based placement and sizing of multiple distributed generation in the distribution system," *Energy*, vol. 111, pp. 525–536, Sep. 2016.

[32] A. Kavousi-Fard, A. Abasi, H. Rezazade, and J. Ansari, "An intelligent approach for optimal capacitor placement problem as a reliability reinforcement strategy," *Journal of Intelligent and Fuzzy Systems*, vol. 29, no. 5, pp. 1857–1867, 2015, Jan. 2015.

[33] M. Chis, M. M. A. Salama, and S. Jayaram, "Capacitor placement in distribution systems using heuristic search strategies," *IEE Proceedings - Generation, Transmission and Distribution*, vol. 144, no. 3, pp. 225–230, 1997.

[34] K. R Devabalaji and K Ravi, "Optimal placement and sizing of capacitor in radial distribution system using harmony search algorithm," *Proceeding Electr. Eng. Comput. Sci. Informatics*, vol. 1, no. 1, 2014.

[35] M. Seyedmahmoudian, T. Kok Soon, E. Jamei et al., "Maximum power point tracking for photovoltaic systems under partial shading conditions using bat algorithm," *Sustainability*, vol. 10, no. 5, p. 1347, 2018.

[36] "Nabic 2009 - world congress on nature and biologically inspired computing," 2021, http://www.mirlabs.org/nabic09/.

[37] X.-S. Yang and S. Deb, "Cuckoo search: recent advances and applications," *Neural Computing & Applications*, vol. 24, no. 1, pp. 169–174, 2013.

[38] "Combining cuckoo and tabu algorithms for solving quadratic assignment problems | Request PDF," 2021, https://www.researchgate.net/publication/284295446_Combining_cuckoo_and_tabu_algorithms_for_solving_quadratic_assignment_problems.

[39] K. Premkumar and B. V. Manikandan, "Bat algorithm optimized fuzzy PD based speed controller for brushless direct current motor," *Engineering Science and Technology, an International Journal*, vol. 19, no. 2, pp. 818–840, Jun. 2016.

[40] Y. Xing, D. Wang, and L. Wang, "A novel dynamic generalized opposition-based grey wolf optimization algorithm," *Algorithms*, vol. 11, no. 4, p. 47, 2018.

[41] H. Moazami Goodarzi and M. H. Kazemi, "An optimal autonomous microgrid cluster based on distributed generation droop parameter optimization and renewable energy sources using an improved grey wolf optimizer," *Engineering Optimization*, vol. 50, no. 5, Article ID 1355970, pp. 819–839, 2017.

Hindawi
Complexity
Volume 2022, Article ID 4605455, 9 pages
https://doi.org/10.1155/2022/4605455

Research Article

Optimal Pricing Decisions for Dual-Channel Supply Chain: Blockchain Adoption and Consumer Sensitivity

Rong Zhang,[1] Zhiwei Xia,[1] and Bin Liu[2]

[1]*Research Center of Logistics, Shanghai Maritime University, Shanghai 201306, China*
[2]*Business School, University of Shanghai for Science and Technology, Shanghai 200093, China*

Correspondence should be addressed to Bin Liu; liubhnau@163.com

Received 20 January 2022; Revised 3 March 2022; Accepted 4 March 2022; Published 19 March 2022

Academic Editor: Yu Zhou

Counterfeiting is common in many industries. For the authenticity of online channel products and to combat counterfeiting, many companies have begun to use blockchain technology to trace product information. This paper investigates a dual-channel supply chain consisting of one manufacturer and one retailer, in which the manufacturer sells its standard products through the retailer and adopts blockchain technology to launch the online channel to sell the traceable products. A Stackelberg game is developed to depict the pricing decision and channel strategy choice for the manufacturer. It shows that both the manufacturer and the retailer can benefit from blockchain adoption. And the longer it takes for product traceability, the lower the price of online traceable products. It is beneficial for the manufacturer when consumers in the market are less concerned about information transparency. For consumer sensitivity, as consumers' acceptance of direct sales channels increases, the selling prices of online traceable products have risen. Furthermore, as the traceability time-sensitivity coefficient increases, the sales price of the traceable products decreases, and the retail price of offline standard products rises. The conclusion of this paper has a certain guiding role for the dominant manufacturers in choosing whether to apply blockchain technology to improve the demand for traceable products.

1. Introduction

According to data from the National Bureau of Statistics, the national online retail sales in 2020 were 11.76 trillion RMB, while the online retail sales of physical goods were 9.76 trillion RMB Yuan, accounting for 24.9% of the total retail sales of consumer goods [1]. Although the online consumer market has continued to grow and develop in recent years, online consumers cannot access products and cannot effectively distinguish between the authenticity and reliability of product-related information. Products in the categories of fresh agriculture, mother and baby, alcohol, beauty and makeup, second-hand goods, luxury goods, cross-border goods, and medicine are often replaced by imposters on the Internet. For the manufacturer, to meet consumers' personalized preferences and pursue consumers' demand for product traceability, the manufacturer needs to deal with the problem of enhancing their profits while relieving channel conflicts, as well as the issue of consumers' demand for product traceability by considering product information transparency. At present, there are shortcomings in the product sales chain, such as opaque product information, difficulty tracing the origin of products, and difficulty proving the authenticity of products, etc. By adopting blockchain technology, we can make use of its decentralized, nontemperable, traceable, collective maintenance, and open and transparent features [2]. Therefore, after setting a unique label for the product, the logistics information of each product can be tracked and recorded, and consumers who purchase products supported by blockchain technology can trace the source of the product. For example, Wyeth products, by adopting the anticounterfeiting traceability service of JD blockchain, enable consumers to purchase with confidence [3]. In 2016, Walmart tested the traceability of mangoes in a store, and it took 6 days, 18 : 26, to trace the mangoes back to their farm of origin. But after adopting blockchain technology, the traceability is completed, and all relevant information is obtained in only 2.2 seconds [4]. The

above are the results of the application of blockchain technology in enterprise practice, and the following is the theoretical research on the application of blockchain technology in practice by scholars.

In terms of research on the impact of blockchain technology on supply chain decision-making, scholars at home and abroad mainly focus on the impact of blockchain technology on traditional supply chain goals, customer viscosity, traceability, transaction costs, and social welfare. Kshetr [5] and Tian [6] propose that the application of blockchain to the supply chain will improve transparency and responsibility and increase customers' trust in product features. Kamblea et al. [7] believe that traceability is the most important reason for the realization of blockchain technology in the agricultural supply chain. Zhang et al. [8] combine blockchain technology with the Internet of Things and big data to solve the difficult problem of collecting reliable data in life cycle assessment. Tönnissen and Frank [9] use a case analysis method to explain how to use blockchain technology in supply chain operations and management. Christoph and Stephan [10] propose that blockchain can limit the impact of opportunism, environmental and behavioral uncertainty in the supply chain, thereby reducing transaction costs. Yan and Zhang [11] discuss the influence of risk aversion coefficient and blockchain technology application degree on supply chain decision-making. Liang and Xiao [12] analyze the impact of the introduction of specific parameters such as blockchain technology on the channel selection of a dual-channel supply chain. Furthermore, many scholars have focused on investigating the dual-channel supply chain when the manufacturer provides homogeneous products. Chen et al. [13], Tang et al. [14], and Zhou and Ye [15] examine the influence of nonprice factors such as product quality on the sales of a single product in different channels. Wan et al. [16], Li et al. [17] reflect the negative impact of retailer services on the online channel and find that implementing product differentiation is beneficial to both online and offline channels. Dan et al. [18] investigate the impact of retail services in retail channels and customer loyalty on pricing decisions in dual-channel supply chains. In terms of supply chain pricing, Huang et al. [19] investigated the impact of supply chain members' altruistic preference behavior on the pricing decisions of supply chain members when consumers' green preferences were considered. Xu et al. [20] consider optimal pricing decisions and profit issues in centralized and decentralized systems of dual-channel supply chains under mandatory carbon emission regulation. Hosseini-Motlagh et al. [21]conduct a study on energy-saving efforts in remanufacturing and forward logistics in closed-loop supply chains and analyze how remanufacturing and energy-saving efforts affect competitive selling prices and recycling rates. Motlagha et al. [22] point out the impact of demand interruption on RSC in a reverse supply chain (RSC) system and obtain the optimal pricing under demand interruption and a harmonized scheme using a combined two-part tariff contract.

Our paper contributes to the literature on whether direct sales channels adopt blockchain technology and channel pricing strategies. In the existing dual-channel supply chain research, considering the few factors of blockchain technology, the research on the traceability time of online traceable product information transparency is also rarely involved. Christoph and Stephan [10] also focus on considering whether different dual-channel structures under homogeneous products need to introduce blockchain technology. This paper starts from the perspective of manufacturers opening online direct sales channels and introducing traceable products through channel invasion based on a single channel. Focus on consumer channel preferences, the level of transparency of blockchain product information, the differentiation of online and offline products and services in direct dual-channel pricing, and the decision on whether to bring traceable products online.

To sum up, this paper introduces blockchain technology into the dual-channel and provides some guidance for whether the online channel adopts blockchain technology. Furthermore, the impact on manufacturers and consumers is explained from the perspective of manufacturer information transparency. We will study how to help manufacturers adopt blockchain technology in direct sales channels to solve the problem of product inauthenticity and traceability. How manufacturers' costs change and how consumer sensitivities affect manufacturers when adopting blockchain technology. Specifically, we will solve the following research issues:

(1) Under what conditions will the manufacturer adopt blockchain technology to offer traceable products?

(2) How should the manufacturer introduce traceable products to alleviate channel conflicts? What are the effects of adopting blockchain technology on the prices and profits of both the manufacturer and retailer?

2. Problem Description

The manufacturer sells standard products through offline traditional retail channels and sells traceable products through online direct sales channels, as shown in Figure 1. In this study, the manufacturer, as the leader of the Stackelberg game, decides the selling price in the direct channel and the wholesale price for the retailer. Then, the retailer, as the follower, determines the retail price of standard products. Third, both the manufacturer and the retailer are completely rational decision-makers, which means that both make optimal decisions based on the principle of maximizing their profits.

The retailer wholesales the standard product from the manufacturer at the wholesale price w and sells it to consumers at the retail price p_r. The manufacturer sells the traceable products directly to consumers at the price p_d. We denote consumers' acceptance level of the online channel as θ, where $(0 \le \theta \le 1)$, and the consumers' valuation of the products as v , which is uniformly distributed on. Then, the consumers' valuation of the online products is θv.

Consumer utility of the online direct sales channel is related to the level of transparency of traceable products'

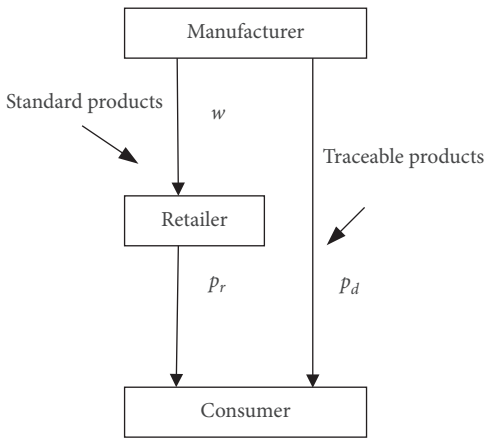

Figure 1: Dual-channel supply chain model for online traceable products.

information (product information includes transaction information, origin information, product information, and logistics information) and the time of traceable products' traceability. Therefore, the consumer utility of the online retail channel can be expressed as $U_d = \theta v - p_d + e - \beta t$. We denote the level of traceable products' information transparency as e $(0 \le e \le 1)$, which the larger the value, the more realistic the product. The consumers' sensitivity to the traceable products' traceability sensitivity to time is β and the time spent waiting for product traceability from the consumer is t. Then, the consumer utility of the offline retail channel can be expressed as $U_r = v - p_r$.

When the manufacturer and the retailer sell these two products at the same time, which product consumers choose depends on the size of the consumer's surplus value. So, when $U_d > U_r$ and $U_d > 0$, we have $p_d - e + \beta t/\theta < v < p_r - p_d + e - \beta t/1 - \theta$, and consumers choose to buy online traceable products. When $U_r > U_d$ and $U_r > 0$, we have $v > \max(p_r - p_d + e - \beta/1 - \theta, p_d - e + \beta t/\theta)$, and consumers choose to buy standard products offline. When $U_d = U_r$, we have $v = p_r - p_d + e - \beta t/1 - \theta$, under which there is no difference in the utility of consumers buying two products.

Through the residual value function, we get the online direct sales channel demand Q_d and the offline retail channel demand Q_r respectively as

$$Q_d = \begin{cases} \dfrac{p_r - p_d + e - \beta t}{1-\theta} - \dfrac{p_d - e + \beta t}{\theta}, & p_r > \dfrac{p_d - e + \beta t}{\theta}, \\ 0, & \text{others}, \end{cases}$$

$$Q_r = \begin{cases} 1 - \dfrac{p_r - p_d + e - \beta t}{1-\theta}, & p_r > \dfrac{p_d - e + \beta t}{\theta}, \\ 1 - \dfrac{p_r - e + \beta t}{\theta}, & \text{others}. \end{cases} \tag{1}$$

3. Dual-Channel Supply Chain Decision Model

3.1. Dual-Channel Supply Chain Model for Online Traceable Products. The manufacturer and the retailer each make decisions for their profit maximization, and their profit functions are, respectively,

$$\pi_m = wQ_r + \left(\frac{p_d}{-l/t}\right)Q_d - \frac{e^2}{2}, \tag{2}$$

$$\pi_r = (p_r - w)Q_r. \tag{3}$$

We denote the cost of each traceability of the manufacturer as l/t, and the cost of single traceability is related to time t. Furthermore, the shorter the traceability time, the higher the cost. We refer to Aspremont [23]and other documents for the explanation and the form of innovation input cost. We denote one-time fixed cost to be paid by the manufacturer for introducing blockchain technology as $e^2/2$, which implies that the higher the level of transparency of traceable products information, the higher the cost, where $p_d > l/t$.

When $p_r \le (p_d - e + \beta t)/\theta$, the online direct sales channel has zero sales, that is, consumers will only buy standard offline products, so this situation is outside the scope of the study. When $p_r > (p_d - e + \beta t)/\theta$, both sales channels have their own demand. Therefore, using the inverse solution method, the retailer's optimal response is obtained as

$$p_r = \frac{(p_d + w - \theta - e + \beta t + 1)}{2}. \tag{4}$$

From the first stage of the game, the manufacturer determines the sales price of online traceable products p_d and the wholesale price of offline standard products w, and the optimal solution is

$$p_d = \frac{\theta + e - \beta t + l/t}{2}, \tag{5}$$

$$p_r = \frac{3 + \beta t - e - \theta + l/t}{2}, \tag{6}$$

$$w^* = \frac{1}{2}, \tag{7}$$

$$p_d^* = \frac{2\beta t\theta(1-\theta) + \left(2\theta^2 - 3\theta + 2\right)l/t + \theta^3 - \theta^2 + \theta/2}{\left(4\theta^2 - 5\theta + 2\right)}. \tag{8}$$

Substituting equations (7) and (8) into (4), the optimal selling price of offline retail channels can be derived as

$$p_r^* = \frac{\theta(\beta t + l/t)(\theta - 1) - \theta^3 + 4\theta^2 - 4\theta + 2/3}{4\theta^2 - 5\theta + 2}. \tag{9}$$

Therefore, the maximum profits of the manufacturer and the retailer are, respectively,

$$e^* = \frac{(\beta t + l/t)(2-\theta) + \theta^2 - \theta}{4\theta^2 - 5\theta + 2},$$
$$\pi_r^* = \frac{(1-\theta)\left[(\beta t + l/t)\theta - \theta^2 + \theta - 1/2\right)]^2}{\left(4\theta^2 - 5\theta + 2\right)^2}, \tag{10}$$
$$\pi_m^* = \frac{(\theta-2)\left(\beta^2 t^2 + 2\beta l + l^2/t^2\right) + 2(1-\theta)(\beta t + \theta l/t) + \theta^3 - \theta + 1/2}{2\left(4\theta^2 - 5\theta + 2\right)}.$$

Proposition 1. *As the level of information transparency of online traceable products increases, the selling price of online traceable products also increases, while the retail price of standard offline products and the profitability of the retailer decrease.*

Proof. Solving for the first-order condition of the optimal selling price p_d of the online traceable products, the optimal selling price p_r of the offline standard product, and the maximum profit π_r of the retailer for the level of information transparency of the traceable products e, respectively, we can gain

$$\frac{\partial p_r}{\partial e} = -\frac{1}{4} < 0,$$
$$\frac{\partial p_d}{\partial e} = \frac{1}{2} > 0. \tag{11}$$

□

Proposition 2. *shows that the manufacturer improves the level of information transparency of online direct marketing channels. Thus, consumers' pursuit of information transparency makes them more inclined to purchase traceability products online. Thus, the manufacturer raises the sales price of online traceability products. The retailer is at a competitive disadvantage due to the impact of online direct marketing channels. Therefore, the only choice is to lower the sales price to maintain sales volume.*

Proposition 3. *As the time-sensitivity factor β for the traceability of the traceable products increases, the selling price of the traceable products decreases, while the retail price of standard offline products increases.*

Proof. Solving for the first-order necessary condition of the optimal selling price p_d of the traceable products and the optimal selling price p_r of the offline standard product for the time-sensitivity coefficient β of the traceability of the traceable products, respectively, we can get

$$\frac{\partial p_r}{\partial \beta} = \frac{t\theta(1-\theta)}{4\theta^2 - 5\theta + 2} > 0,$$
$$\frac{\partial p_d}{\partial \beta} = -\frac{2t\theta(1-\theta)}{4\theta^2 - 5\theta + 2} < 0. \tag{12}$$

□

Proposition 4. *shows that as the time-sensitive factor of traceability of traceable products increases, the price of traceable products decreases. As a result, the manufacturer lowers the price of traceable products to offset the long wait time for consumers. In contrast, consumers' increased trust in standard offline products have led retailers to raise prices.*

3.2. Comparison of the Dual-Channel Supply Chains of Online Traceable Products and Standard Product. When direct sales channels do not adopt blockchain technology to sell traceability products, the supply chain becomes a dual-channel supply chain of standard products (indicated by the superscript "S"). Therefore, the consumer utility of online direct sales channels and offline retail channels are, respectively,

$$U_d^S = \theta v - p_d^S,$$
$$U_r^S = v - p_r^S. \tag{13}$$

The profits of the manufacturer and the retailer are, respectively,

$$\pi_m^S = w^S Q_r^S + p_d^S Q_d^S,$$
$$\pi_r^S = \left(p_r^S - w_s\right) Q_r^S. \tag{14}$$

Using the same method, the optimal decision of the standard product dual-channel supply chain can be obtained as

$$w^{S*} = \frac{1}{2},$$
$$p_d^{S*} = \frac{\theta}{2},$$
$$p_r^{S*} = \frac{3-\theta}{4},$$
$$\pi_r^{S*} = \frac{1-\theta}{16}, \tag{15}$$
$$\pi_m^{S*} = -\frac{1+\theta}{8}.$$

Proposition 5. *When $\beta t + l/t < 1/4$, compared with the dual-channel supply chain of standard products, the retail price, the sales price of traceable products, and the profit of retailers in*

the dual-channel supply chain using blockchain will all increase.

Proof.

$$p_r - p_r^S = \frac{\theta(\theta-1)(4\beta t-1)+l/t\left(4\theta^2-6\theta+4\right)}{2\left(4\theta^2-5\theta+2\right)} > 0,$$

$$p_d - p_d^S = \frac{\theta(\theta-1)(4\beta t+4l/t-1)}{4\left(4\theta^2-5\theta+2\right)} > 0, \tag{16}$$

$$\pi_r - \pi_r^S = \frac{\theta(1-\theta)(4\beta t+4l/t-1)\left[4\theta(\beta t+l/t)-\left(8\theta^2-9\theta+4\right)\right]}{16\left(4\theta^2-5\theta+2\right)^2} > 0.$$

□

Proposition 6. *shows that after adding an online traceability service based on a standard product dual channel, the cost of the online direct sales channel increases. As a result, the manufacturer takes advantage of consumers' preference for online traceable products to increase prices in online direct sales channels. For the retailer, the emergence of traceable products has eased the channel competition brought about by selling homogeneous products online and offline. The retailer no longer needs to cut prices to retain consumers, and profits have also improved to a certain extent compared to standard product dual-channel supply chains.*

4. Numerical Analysis

4.1. Effect of Consumer Online Channel Acceptance on Price. Numerical tests are conducted by taking $\beta = 0.02, t = 2, l = 0.3$ and θ variations in the range [0, 1], respectively, to obtain the effect of changes in consumer online channel acceptance level θ on price. Figure 2 shows that as θ gradually increases from 0 to 1, the sales price of online traceable products tends to increase, while the sales price of offline standard products tends to decrease. As consumer acceptance of online direct sales channels increases, consumers will be more likely to buy products online. Therefore, the manufacturer increases the selling price of online traceable products. For the retailer, due to the impact of direct sales channels, the retailer is at a disadvantage and can only choose to lower sales prices to maintain sales.

4.2. Comparison of the Manufacturer' Profits in the Dual-Channel Supply Chain of the Traceable Products and Standard Products. Numerical experiments are conducted by taking $\beta = 0.02$, $t = 2$, $l = 0.3$, and θ within the range of [0, 1] respectively. It can obtain a comparison of the profits of the two types of dual-channel supply chains used by the manufacturer. Figure 3 shows that when consumers' acceptance of the direct sales channel is not big. Therefore, the blockchain input cost of the direct sales channel cannot be offset, which makes the manufacturer's profit decline. In addition, when the acceptance of direct selling channels is higher than a certain value, the profit of the dual-channel supply chain adopting blockchain is always higher than that of the standard product dual-channel supply chain. When θ is constant, and as β increases, the manufacturer's profit in the dual-channel traceability product decreases. Only when θ is too large and β is small enough, the profit of the manufacturer adopting the blockchain be greater than the profit of the manufacturer not adopting the blockchain.

4.3. Effect of Traceability Time on Price. Numerical experiments are conducted by taking $\theta = 0.8$, $\beta = 0.02$, $l = 0.3$, and t within the range of [0, 10] respectively. It can be used to obtain the effect of traceability time on price. Figure 4 shows that when the traceability time of the traceable products continues to increase for direct sales channels, the sales price of traceable products continues to drop. For the retailer, the retail prices of offline standard products show a trend of rising first and then falling. When t increases to a critical value, it is always higher than the direct selling price.

5. Extension

This section extends our basic model by introducing consumers' sensitivity parameters to the level of information transparency of traceable products to check the robustness of the conclusions. Specifically, after introducing parameters, a new dual-channel model is constructed. Then, we solve the corresponding optimal solution. Finally, we graphically explore the impact of the changes in the sum on manufacturers and retailers.

5.1. The Model by Introducing Consumers' Sensitivity Parameters. The new model introduces consumers' sensitivity to the transparency level of blockchain product information γ, and other parameters are the same as the basic model. Therefore, the consumer utility of the online direct sales channel can be expressed as $U_d = \theta v - p_d + \gamma e - \beta t$. And the consumer utility of the offline retail channel can be expressed as $U_r = v - p_r$.

Through the residual value function, we get the online direct sales channel demand Q_d and the offline retail channel demand Q_r, respectively, as

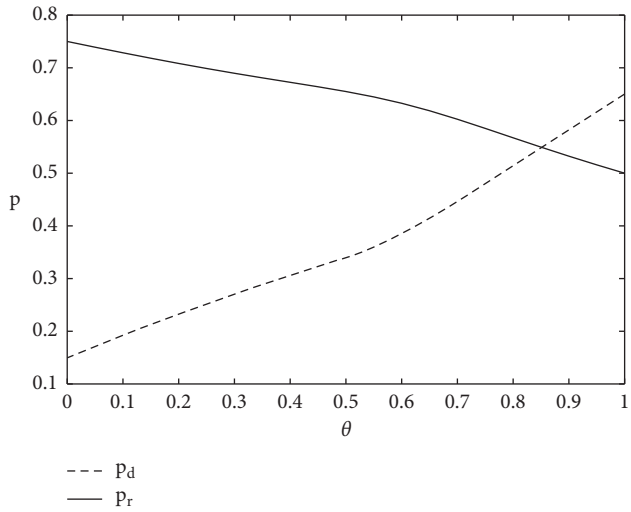

Figure 2: Effect of θ on price.

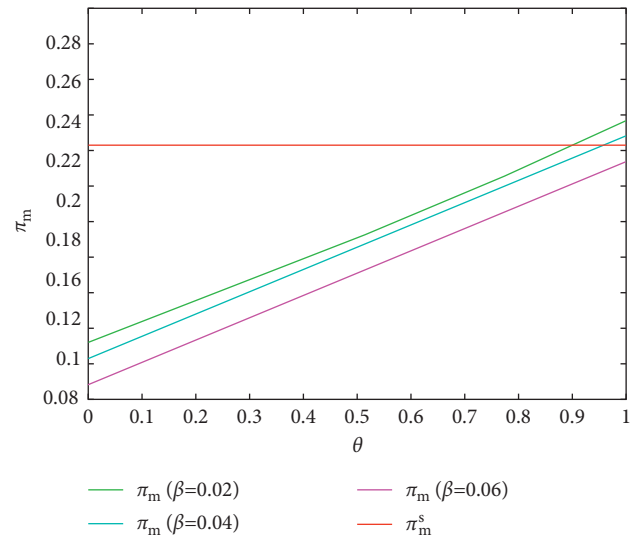

Figure 3: Effect of θ on the manufacturer's profit in the dual-channel supply chain adopting blockchain.

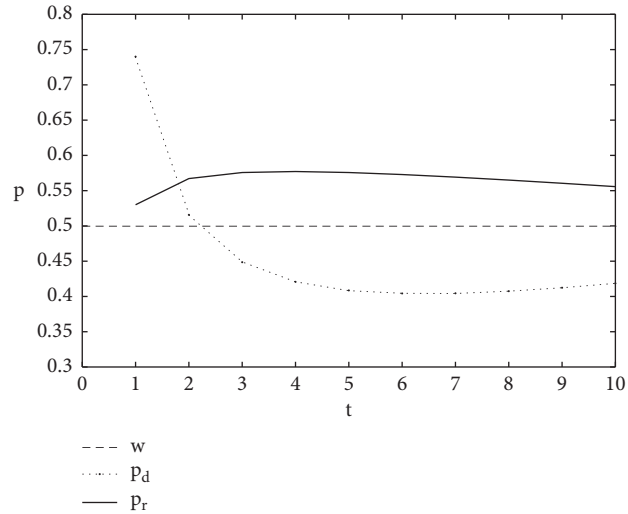

Figure 4: Effect of t on price.

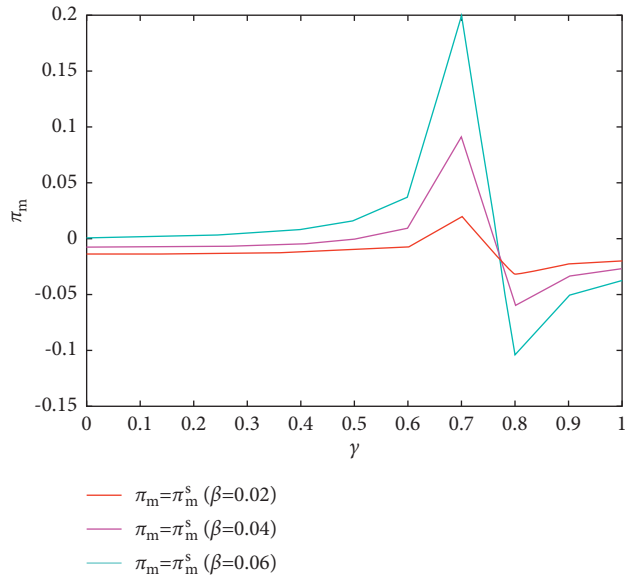

Figure 5: Effect of γ on the profit of the manufacturer.

$$Q_d = \begin{cases} \dfrac{p_r - p_d + \gamma e - \beta t}{1-\theta} - \dfrac{p_d - \gamma e + \beta t}{\theta}, & p_r > \dfrac{p_d - \gamma e + \beta t}{\theta}, \\ 0, & \text{others}, \end{cases}$$

$$Q_r = \begin{cases} 1 - \dfrac{p_r - p_d + \gamma e - \beta t}{1-\theta}, & p_r > \dfrac{p_d - \gamma e + \beta t}{\theta}, \\ 1 - \dfrac{p_r - \gamma e + \beta t}{\theta}, & \text{others}. \end{cases} \tag{17}$$

The manufacturer and the retailer each make decisions for their profit maximization, and their profit functions are, respectively,

$$\pi_m = wQ_r + \left(p_d - \frac{l}{t}\right)Q_d - \frac{\eta e^2}{2}, \qquad \pi_r = (p_r - w)Q_r. \tag{18}$$

According to the basic model solving method, the optimal solution is

$$\pi_r^* = \frac{(1-\theta)\left[2\eta\theta\left(\beta t + l/t + 1 - \theta - \gamma^2\right)\right]^2}{4\left[\gamma^2(\theta-2) + 4\eta\theta(1-\theta)\right]^2},$$

$$\pi_m^* = \frac{(2-\theta)\left(\eta\beta^2 t^2 + 2\eta\beta l + \eta l^2/t^2\right) + 2\eta\theta(\beta t + l/t)(\theta - 1) + \eta\theta\left(1-\theta^2\right) - 1/2\gamma^2}{2\left[\gamma^2(\theta-2) + 4\eta\theta(1-\theta)\right]}. \tag{19}$$

5.2. Consumers' Sensitivity to the Level of Information Transparency of Traceable Products. Numerical tests are conducted by taking $\theta = 0.8$, $t = 2$, $l = 0.3, \eta = 1$ and γ variations in the range [0, 1), respectively. Therefore, we can get the impact of changes in consumers' sensitivity to the transparency level of traceable product information on manufacturers and retailers.

Figure 5 shows that when consumers' sensitivity to information transparency is lower than a certain value, the increase in consumers' sensitivity to traceability time will increase the manufacturer's profit. However, when it is higher than a certain value, consumers' increased sensitivity to time will reduce the manufacturer's profit. Therefore, the sensitivity of consumers to information transparency should not be too high, which will be more conducive to the increase of the manufacturers' profits.

Figure 6 shows that the profit of retailers with dual channels of traceability products is always higher than that of retailers with dual channels of common products. In addition, when consumers' sensitivity to information transparency is lower than a certain value, the increase in consumers' sensitivity to traceability time will increase the retailer's profit. However, when it is higher than a certain value, consumers' increased sensitivity to time will reduce the retailer's profit. Therefore, the sensitivity of consumers to information transparency should not be too high, which will be more conducive to the increase of retailer's profits.

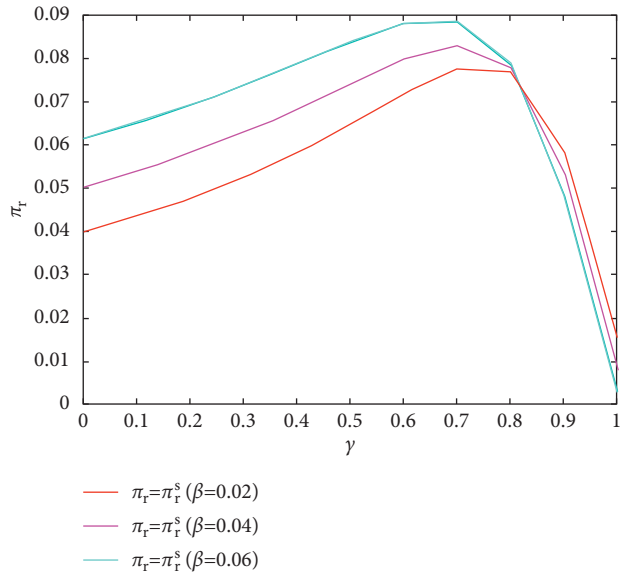

Figure 6: Effect of γ on the profit of the retailer.

6. Conclusion

This paper investigates the dual-channel supply chain for online traceable products and uses the Stackelberg game to find the optimal decisions for the manufacturer and the retailer and compares the results with the product prices and profits of the dual-channel supply chain for standard products. In addition, we also extend the model by considering consumers' sensitivity to the transparency of traceable product information. We can draw the following conclusions:

(1) The inclusion of traceable products in the dual-channel supply chain of standard products can increase the profits of both the manufacturer and the retailer and can mitigate channel competition.

(2) When consumers' acceptance of online channels exceeds a certain threshold, the manufacturer's profits will increase. But when consumers' acceptance of online channels is below a certain threshold, the manufacturer's profits will decrease. The manufacturer can obtain higher profits by controlling the transparency level of blockchain product information while also improving brand awareness.

(3) When the manufacturer adds online traceable products to their standard product dual-channel supply chains, they can mitigate the impact of online direct sales channels on offline retail channels, thus allowing the retailer to realize a degree of increased product sales prices and profits.

The conclusions of this article have a certain guiding effect on whether the dominant manufacturer chooses to apply the dual-channel supply chain model that considers the adoption of blockchain online.

This paper analyzes the impact of blockchain technology on dual-channel supply chain pricing from a manufacturer-dominated perspective. If we consider the complete information setting in this paper, However, in the presence of customer loyalty, the coordination problem of the supply chain with asymmetric information is an interesting and challenging issue. It can be further expanded in future research, such as further analyzing the role of blockchain in combination with social welfare and considering the impact of blockchain technology on sustainable development.

Data Availability

The data used to support the findings of this study are included within the article.

Conflicts of Interest

All authors declare that there are no possible conflicts of interest.

Acknowledgments

The authors acknowledge the support of the National Natural and Science Foundation of China with Grant no. 71971134.

References

[1] National Bureau of Statistics of the People's Republic of China, *China Statistical Yearbook*, China Statistics Press, Beijing, China, 2020.

[2] S. Saberi, M. Kouhizadeh, J. Sarkis, and L. Shen, "Blockchain technology and its relationships to sustainable supply chain management," *International Journal of Production Research*, vol. 57, no. 7, pp. 2117–2135, 2019.

[3] Y. Wang and J. Jia, "Scanning "code" on JD.com APP food blockchain traceability information improves food safety transparency," *Barcode and Information System*, vol. 148, no. 6, pp. 19–21, 2018.

[4] D. Bai, "Walmart: blockchain traces food source information in just 2.2 seconds," *Sales and Marketing*, vol. 21, p. 1, 2018.

[5] N. Kshetri, "1 Blockchain's roles in meeting key supply chain management objectives," *International Journal of Information Management*, vol. 39, no. 4, pp. 80–89, 2018.

[6] F. Tian, "An Agri-Food Supply Chain Traceability System for China Based on RFID & Blockchain Technology," in *Proceedings of the 13th International Conference on Service Systems and Service Management (ICSSSM)*, Kunming, China, June 2016.

[7] S. S. Kamble, A. Gunasekaran, and R. Sharma, "Modeling the blockchain enabled traceability in agriculture supply chain," *International Journal of Information Management*, vol. 52, no. 6, pp. 67–96, 2020.

[8] A. Zhang, R. Y. Zhong, M. Farooque, K. Kang, and V. G. Venkatesh, "Blockchain-based life cycle assessment: an implementation framework and system architecture," *Resources, Conservation and Recycling*, vol. 152, no. 5, pp. 104–135, 2020.

[9] S. Tönnissen and T. Frank, "Analysing the impact of blockchain-technology for operations and supply chain management: an explanatory model drawn from multiple case studies," *International Journal of Information Management*, vol. 52, no. 6, pp. 146–170, 2020.

[10] G. S. Christoph and M. W. Stephan, "Blockchain and supply chain relations: a transaction cost theory perspective," *Journal of Purchasing and Supply Management*, vol. 25, no. 4, pp. 100–124, 2019.

[11] A. Yan and J. Zhang, "A study on supply chain subject with a risk-aversion retailer based on block chain techonlogy," *Industrial Engineering & Management*, vol. 23, no. 6, pp. 33–42, 2018.

[12] X. Liang and J. Xiao, "Blockchain-based dual-channel supply chain pricing decision and online channel selection strategy," *Chinese Journal of Management Science*, vol. 1-12, 2021, https://kns.cnki.net/kcms/detail/detail.aspx?FileName=ZGGK2021060900A&DbName=DKFX2021.

[13] J. Chen, L. Liang, D. Q. Yao, and S. Sun, "Price and quality decisions in dual-channel supply chains," *European Journal of Operational Research*, vol. 259, pp. 935–948, 2016.

[14] C. Tang, Y. Honglin, E. Cao, and K. K. Lai, "Channel competition and coordination of a dual-channel supply chain with demand and cost disruptions," *Applied Economics*, vol. 50, no. 46, pp. 4999–5016, 2018.

[15] Y. Zhou and X. Ye, "Differential game model of joint emission reduction strategies and contract design in a dual-channel supply chain," *Journal of Cleaner Production*, vol. 190, Article ID 592607, 2018.

[16] W. Yao, B. Dan, and C. Liu, "Improvement strategy of dual-channel supply chain based on differentiated product and service negative spillover effect," *Chinese Journal of Management*, vol. 11, no. 5, pp. 758–763, 2014.

[17] w. Li, K. Li, and G. An, "Decisions of dual channel supply chain when considering channel power and service negative spillover effect," *Chinese Journal of Management*, vol. 14, no. 5, pp. 767–774, 2017.

[18] B. Dan, G. Xu, and C. Liu, "Pricing policies in a dual-channel supply chain with retail services," *International Journal of Production Economics*, vol. 139, no. 1, pp. 312–320, 2012.

[19] H. Huang, J. Zhang, X. Ren, and X. Zhou, "Greenness and pricing decision of cooperative supply chanins considering altruistic preferences," *International Journal of Environmental Research and Public Health*, vol. 16, no. 1, p. 51, 2019.

[20] J. Xu, Q. Qi, and Q. Bai, "Coordinating a dual-channel supply chain with price discount contracts under carbon emission capacity regulation," *Applied Mathematical Modelling*, vol. 56, pp. 449–468, 2018.

[21] S.-M. Hosseini-Motlagh, M. Johari, S. Ebrahimi, and P. Rogetzer, "Competitive channels coordination in a closed-loop supply chain based on energy-saving effort and cost-tariff contract," *Computers & Industrial Engineering*, vol. 149, Article ID 106763, 2020.

[22] S. M. H Motlagha, M. N. Harzvilia, T. M. Choi, and S. Ebrahimi, "Reverse supply chain systems optimization with dual channel and demand disruptions: sustainability, CSR investment and pricing coordination," *Information Sciences*, vol. 503, pp. 606–634, 2019.

[23] C. D. Aspremont and A. Jacquenmin, "Cooperative and non-cooperative R & D in duopoly with spillovers," *The American Economic Review*, vol. 78, no. 5, pp. 1133–1137, 1988.

Hindawi
Complexity
Volume 2022, Article ID 4572145, 14 pages
https://doi.org/10.1155/2022/4572145

Research Article

Performance Analysis of Grid-Connected Distributed Generation System Integrating a Hybrid Wind-PV Farm Using UPQC

Tongfei Lei,[1] Saleem Riaz,[2] Noor Zanib,[3] Munira Batool,[3] Feng Pan,[1] and Shaoguo Zhang[1]

[1]*College of Mechanical Engineering, Xijing University, Xi'an 710123, China*
[2]*School of Automation, Northwestern Polytechnical University, Shaanxi, Xi'an, China*
[3]*Department of Electrical Engineering, University of Engineering and Technology, Taxila, Pakistan*

Correspondence should be addressed to Saleem Riaz; saleemriaznwpu@mail.nwpu.edu.cn

Received 14 January 2022; Accepted 4 March 2022; Published 18 March 2022

Academic Editor: Yu Zhou

This work presents a distributed generation system (DG) that combines system of a wind turbine (WT) and photovoltaic (PV) using a unified power quality conditioner (UPQC). Along with providing active power (AP) to the utility grid, Wind-PV-UPQC improves PQ indicators, for example, voltage drops/surges, harmonics of grid voltages, and PF. Since Wind-PV-UPQC depends on dual compensation scheme, the parallel converter works as a sinusoidal voltage source, while the series converter works as a sinusoidal current source. In this way, a smooth transition from grid operation to island operation and vice versa can be achieved without load voltage transitions. In addition, in order to overcome the problems through abrupt solar radiation or wind speed variations, a faster power balance is achieved between the wind turbines, the PV array, and the grid, as FFCL pursue the production of the current references of series converter. Consequently, the dynamic reactions of the converter currents and the voltage of dc bus are enhanced. A comprehensive analysis of flow of the AP through the converters is done to ensure a proper understanding of how Wind-PV-UPQC works. Finally, the simulation results are shown to estimate the dynamic and static performance of Wind-PV-UPQC in conjunction with the power distribution system.

1. Introduction

Today, electricity generation via renewable energy sources (RESs) has increased significantly, especially due to the increasing needs for electrical energy as well as intense worldwide struggles to reduce the dangerous environmental impact of contaminant energy sources, for example, coal, oil, gas, and others [1–6]. As a result, greenhouse effect and the global warming have enforced several states to sign a contract in Paris at the 2015 Climate change conference this century to toughen international measures to keep global temperature growth well below 2 degrees Celsius. Countries around the world tend to use renewable energy as a clean, useable, and cheaper energy source to achieve a high degree of integration of twenty percent by 2020 [7–10].

In this context, RES-based distributed generation systems (DG) have helped to discover new modern way out for developing traditional energy structures. The use of DGs is more attractive as it improves the quality of the system, reduces CO_2 emissions, and reduces losses in transmission and distribution systems [1, 11–15]. Though the core purpose of DGs is to provide real power to the grid, its multifunctionality may be extended to include the active power line conditioning targets [16–22]. In this situation, in addition to generating energy, an integrated DGs can also perform, instantaneously, active power line compensation, thus contributing to the improvement of the power quality indicators (PQ) [23]. Photovoltaic and wind energy included in this scenario are potential sources of DGs, as they simply require sunshine and wind to produce energy wherever assets are plentiful, comparatively clean, and free [24, 25]. The weakness of wind turbines and photovoltaics, in addition to being able to generate electricity, creates a series of current and voltage harmonics caused through the existence of different sorts of photovoltaic devices and wind turbines and power inverters. In addition to the rise in the amount of

nonlinear loads associated with the network, it ultimately leads to a deterioration in the quality of the network.

UPQC has been proposed to improve and overcome power quality because of the presence of nonlinear loads and the incorporation of photovoltaic and wind turbines in the utility grid. UPQC is used to recompense for quality problems of supply voltage, e.g., harmonics, flicker, sag, swell, and quality issues of load current such as harmonics, unbalances, reactive currents, and neutral current. As a general rule, steady-state (voltage imbalances and voltage harmonics) or nonpersistent (voltage sag and swell) PQ events related to line voltages may be resolved or alleviated by series active power filters, so-called dynamics voltage restorers [26, 27]. In contrast, PQ issues produced thru load configuration or even nonlinear properties of load currents may often be overwhelmed via using parallel active power filters. On the other hand, single-phase or three-phase arrangements of the UPQC are further suitable to simultaneously reduce PQ events from mains and load. In other words, systems of UPQC may perform series active power filters and parallel active power filter functionality at once. Two compensation schemes, "traditional" and "dual/inverted," were chosen to control UPQC. These schemes are described according to the control methods of UPQC's serial and parallel converters. With traditional UPQC, the controlled variables (current and voltage) are nonsinusoidal, so the series converter works as a nonsinusoidal voltage source, whereas the parallel converter works as a nonsinusoidal current source. Variables controlled by dual UPQC are always sinusoidal. Hence, the series converter works as a sinusoidal current source, whereas the parallel converter works as a sinusoidal voltage source. It should be noted that the dual UPQC controls the relevant variables (output voltages and input currents) because the series converter directly controls the input currents to remain in phase, symmetrical, and sinusoidal with the mains voltages while the parallel converter controls the balanced output voltages to remain sinusoidal and regulated [28–37]. Iterative control method is used to locate the specific position and time of the fault by its repetitive property. The data produced in each iteration is used for the next iteration for improvement in control system. The modeling of iterative control method for linear and nonlinear system is difficult work. The optimal control scheme based on optimization improves performance of the iterative control algorithm. For system optimization, convergence speed of iterative control algorithm is important and is improved by applying optimal control scheme [38–43].

Typically, grid-connected photovoltaic systems can be used with either a single stage (S-S) or two-stage energy conversion [44, 45]. In a single stage system of photovoltaic, maximum power point tracking (MPPT) monitoring must be done by a DC/AC converter [46, 47], while in a two-stage system of photovoltaic, this job is typically taken over via a DC/DC boost converter [48]. Whatever the topology of the photovoltaic structure, the power balance between the system of photovoltaic and the electrical grid is achieved thru regulating the dc bus voltage of the inverter.

In [49], a 3-Φ three-wire (3P3W) single stage system of photovoltaic layout is presented by utilizing two 3-wire voltage source inverters working using UPQC. However, experimental results are presented only considering its work like a dynamic voltage restorer. The elimination of harmonics from the mains voltage and the parallel active power filters process are not considered. In [50], the double stage PV system was implemented on a system of three-phase three-wire using simple computer simulations. However, harmonic suppression is not considered for line voltage or load current. A combined study of UPQC using distributed generation is described in [26]. UPQC power quality degradation in microgrids powered by wind turbines and photovoltaic energy system was implemented in [51]. As a result, PI and FLC were able to improve the power supply quality and reduce degradation in output power.

In this article, the features of Wind-PV-UPQC can be highlighted as follows:

(1) Improvement of PQ indicators through series-parallel conditioning capabilities of power lines. Therefore, poor voltage harmonics and voltage regulation can be overcome because of the capability of the series active power filtering.

(2) Furthermore, effectual power factor (PF) correction may be made by capability of the active power filtering in parallel. It should be noted that parallel-series active filtering may continue in operation even if photovoltaic wind system is out of service due to maintenance work or during the night.

(3) Injecting the energy generating from a wind and photovoltaic energy system to the grid. Single-phase and three-phase consumers may or may not be connected to the system in this scenario. When there is no load, the system works similarly to traditional DGs in that universal active filtering can be disabled.

The control loop of dc bus regulates the sinusoidal currents amplitudes supplied to network via the series inverter, for which the voltage reference of dc bus is determined through the MPPT procedure. Usually, the reaction of dynamics of the dc bus regulation loop should be slower as compared to the current regulation loops of the grid-connected inverter. It is therefore absolutely necessary to adequately adjust the gains of the two controllers mentioned, as the control circuit of dc bus should not degrade the current control loops performance, in order to ensure that undeformed currents are supplied to the network. On the other hand, sudden fluctuations in solar radiation or in wind speed can cause significant fluctuations in the circuit voltage of dc bus [46], which may change the correct balance of Wind-PV-UPQC power and thus affect the current references calculation of inverter.

To solve this issue, this article too recommends using a feedforward control loop (FFCL) working in combination with the control loop of dc bus to speed up the control of current references of series converter. As a result, even with rapid changes in solar irradiation or wind speed, the dc bus voltage fluctuations are sufficiently damped, accelerating the

system's power equalization. The response time of the voltage of dc bus and overvoltage/undervoltage are significantly reduced as the dynamics are also improved.

This paper is structured as follows: second part presents the explanation of the system of Wind-PV-UPQC along with the control structures including two NPC inverters connected back to back. Also, the strategies are used to create the input references of the serial and parallel converters as well as the FFCL and its core purpose. Third part analyzes the flow of energy via the Wind-PV-UPQC, whereas fourth part shows the results of advanced simulation to feature the double compensation scheme and FFCL achievement. Lastly, fifth part describes conclusions.

2. Wind-PV-UPQC System Configuration

Figure 1 illustrates the power circuit's block diagram of 3-phase 4-wire Wind-PV-UPQC used during the simulation tests. It is consisting of two three-level neutral point clamped (NPC) inverters that are connected back to back. According to the assumed double compensation strategies, the LC and L filters are coupled to the output of the respective parallel and series PWM converters. The NPC series converter is connected to the utility grid via three single-phase coupling transformers. A neutral point clamped module is frequently known as a three-level module. Every branch of the neutral point clamped inverter has four transistors that could be controlled, providing an entire of $2^4 = 16$ possible conditions. However, only 3 of these conditions could be realized, because others produce short circuits on the dc link. The three possible conditions result in three various output voltages: 0 V, $V_{\mathrm{DC}}/2$, $-V_{\mathrm{DC}}/2$. The center point of the DC link capacitor is connected to the neutral point of the 3P4W power supply and the load, so that charge imbalances can be compensated.

2.1. Operation of UPQC with Dual Compensation Strategy. With the double compensation scheme, the series inverter must be regulated as a sinusoidal current source. In this study, the symmetrical and sinusoidal currents of the series inverter are regulated to be directly in phase with the fundamental positive sequence constituents of the mains voltages. This compensates for load asymmetries and reactive power and provides efficient power factor correction by eliminating harmonic currents. Also, the high impedance path generated via the sinusoidal current controlled series inverter enforces load current harmonics to stream via parallel inverter.

In contrast, the parallel inverter must be regulated as a sinusoidal voltage source to deliver regulated, symmetrical, and sinusoidal voltages to the load. In this article, the output voltages are regulated so that they are always in phase with the positive sequence fundamental constituents of the mains voltages. In this situation, when the input and output voltage amplitudes are different from each other, only real power may be taken through the utility grid or injected into the utility grid with the series inverter in order to sustain the power stability of the system. Furthermore, the low impedance path formed through the voltage controlled sine wave parallel inverter permits current harmonics of load to flow thru the parallel inverter.

It may be noted that the static (voltage asymmetries and harmonics) and unstable (voltage spikes and dips) power quality actions occur through the series transformers, leading to indirect voltage suppression/compensations.

Because input references are sinusoidal, it is not necessary to calculate nonsinusoidal input references using specific techniques typically used in conventional compensation strategy. Also, the dq input references in the synchronous rotating reference frame are continuous because the regulated voltage and current values in the SRF abc are sinusoidal. This permits the utilization of a conventional proportional-integral (PI) controller through zero static error.

2.2. Series Converter References Current and Parallel Converter Output References Voltage. The signal flowchart presented in Figure 2(a) shows the control loop of series current. First, load currents $(i_{L\_a}, i_{L\_b}, i_{L\_c})$ are dignified and converted to the dq axis of the SRF from the stationary reference frame of the *abc* axis, so as to the current i_{L_d} may be attained directly as

$$i_{L\_d} = \sqrt{\frac{2}{3}}\left[\cos\theta - \frac{1}{2}\cos\theta + \frac{\sqrt{3}}{2}\sin\theta - \frac{1}{2}\cos\theta + \frac{\sqrt{3}}{2}\sin\theta\right] \begin{bmatrix} i_{L\_a} \\ i_{L\_b} \\ i_{L\_c} \end{bmatrix}. \tag{1}$$

The current i_{L_d} consists of the harmonic and active constituents of the load currents, where $\cos\theta$ and $\sin\theta$ are the coordinates of the rotating unit vector. A PLL [52] is utilized to evaluate the phase angle of the line voltage $\theta = \theta_{pll}$.

The average value of i_{L_d} $(i_{L\_d_{dc}})$ is obtained with a low pass filter (LPF), so that $i_{L\_d_{dc}}$ in SRF are active constituents of abc load currents. Lastly, the input current reference of the series converter on the *d*-axis is specified as

$$i^*_{se\_d} = i_{L\_d_{dc}} + i_{dc} - i_{ff}, \tag{2}$$

where i_{dc} is the PI controller DC link voltage output signal and i_{ff} is the expected current. The variable i_{dc} characterizes the quantity of active power processed by the series NPC inverter to ensure the power stability of the UPQC and thereby control the voltage of dc bus. In other words, i_{dc} adjusts the amplitude of $i^*_{se\_d}$ to regulate the energy flow thru the system of Wind-PV-UPQC to perform energy balancing. Together with i_{dc}, the quantity i_{ff} will accelerate the balance of power as described in the next section. Since symmetrical and sinusoidal currents are anticipated in the utility grid, both the quadrature current $i^*_{se\_q}$ and the zero component $i^*_{se\_0}$ are set to zero.

The signal flow diagram presented in Figure 2(b) shows control loop of parallel voltage. As mentioned earlier,

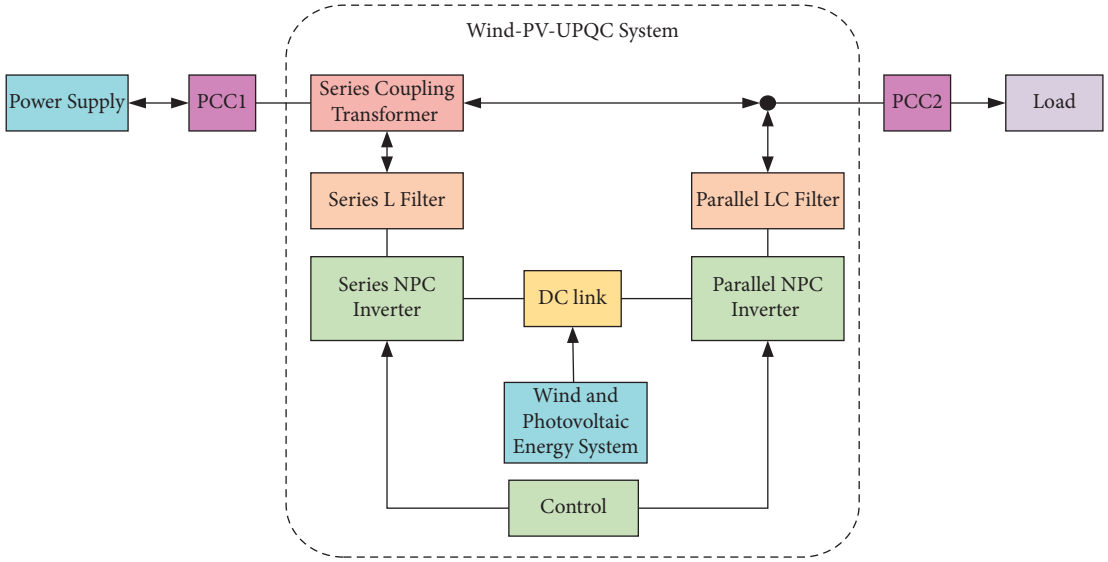

Figure 1: Block diagram of the Wind-PV-UPQC System.

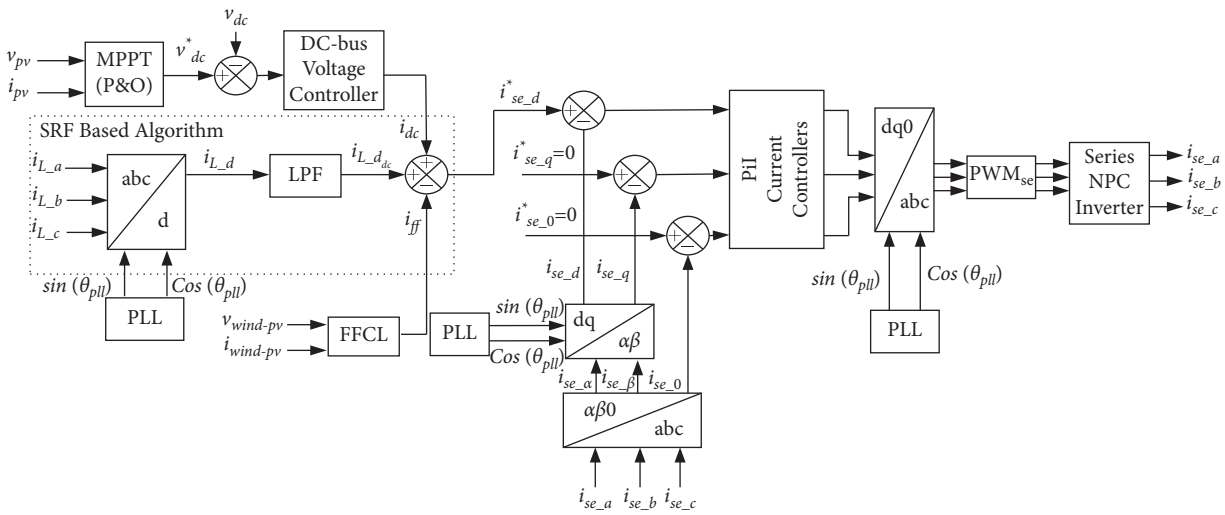

(a)

Figure 2: Continued.

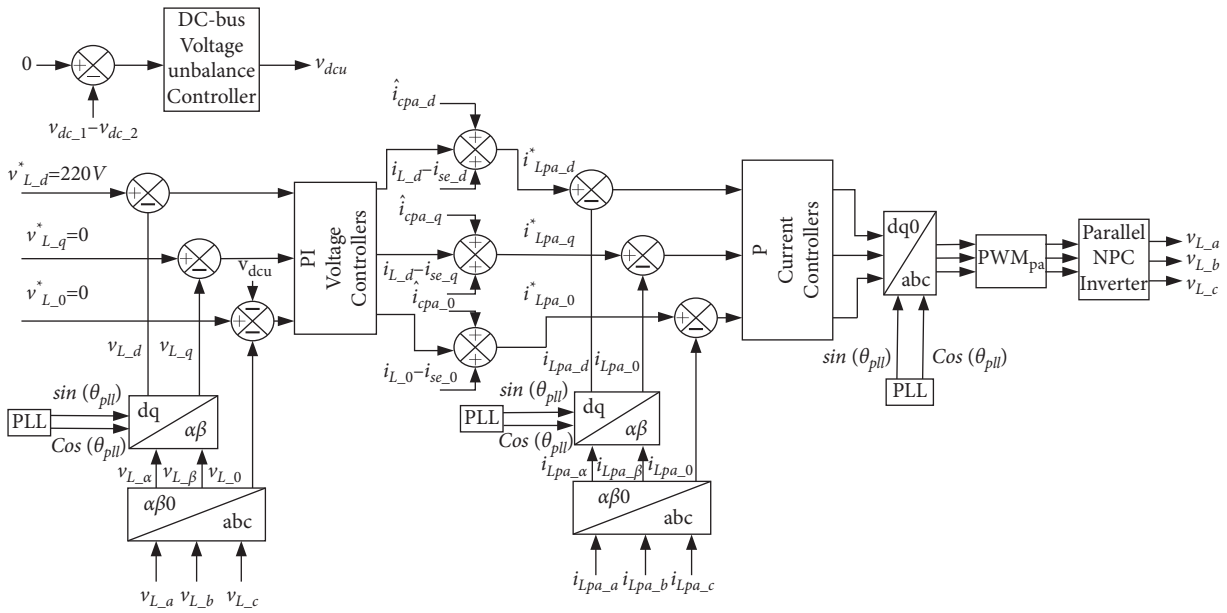

(b)

Figure 2: Signal flow diagrams of control loops of the series and parallel converters. (a) Series currents reference generation and control loops; (b) parallel reference voltages generation and control loops.

parallel converter's input voltage references are set to $V^*_{L\_abc}$ in the SRF (abc axes) and $V^*_{L\_d}$ directly on the SRF axis (d-axis) as presented in Figure 2(a). Since symmetrical and sinusoidal voltages are supplied to load, the quadrature voltage $V^*_{L\_q}$ and the zero sequence component $V^*_{L\_0}$ are set to zero [19].

2.3. Calculation of i_{ff}. In the case of particularly sudden changes in wind speed or solar radiation, voltage fluctuations occur in the dc bus of the inverter, which interfere with the calculation of inverter current references and the correct operation of the inverter. Therefore, FFCL is necessary to reduce the amplitude of these oscillations because FFCL allows to speed up the calculation of input current references during the occurrence of rapid changes in wind speed or solar irradiance [18, 19, 48]. The action is represented by FFCL (i_{ff}) shown in Figure 2(a).

Suppose that the supply voltage grid and the grid-connected series inverters currents are symmetrical. The wind photovoltaic system is also assumed to operate under ideal conditions, so system losses are negligible. In this scenario, all the active power drawn from the photovoltaic wind turbine is fed into the grid with $P_{ac} = P_{\text{wind-pv}}$, that is,

$$P_{\text{wind-pv}} = v_{\text{wind-pv}} i_{\text{wind-pv}} = (v_{dc1} + v_{dc2}) i_{\text{wind-pv}} = \frac{3V_{s\_pk} I_{s\_pk}}{2}, \tag{3}$$

where $v_{dc\,1}$ and $v_{dc\,2}$ represent the dc bus voltage of NPC inverter, while $i_{\text{wind-pv}}$ represents the current of the wind photovoltaic system; and V_{s_pk} and I_{s_pk} are peak magnitude of mains voltage and current, correspondingly, so that V_{s_pk} is assessed using the PLL scheme [52].

$$I_{s\_pk} = \frac{2(v_{dc\,1} + v_{dc\,2}) i_{\text{wind-pv}}}{3V_{s\_pk}}. \tag{4}$$

Lastly, the current i_{ff} characterized in the dq rotating frame is specified by

$$i_{ff} = \sqrt{\frac{3}{2}}.I_{s\_pk}. \tag{5}$$

So, i_{ff} in (5) is used to calculate the input current reference series inverter ($i^*_{se\_d}$) in the dq axis.

As can be noted, the current i_{ff} therefore makes it possible to improve the dynamic response of both the voltage of DC link and the currents of the utility grid-connected series inverters.

3. Flow of Active Power through the Parallel and Series NPC Inverter

The flow of active power via the system of Wind-PV-UPQC is shown in Figure 3. It is determined by considering the following: (1) the difference among the RMS network and the voltage of load; (2) the amount of energy produced by the wind and photovoltaic power system; and (3) the volume of energy consumed through the load. To create analysis, the following active powers are used in Figures 3(a) to 3(c): grid power P_s, load power P_L, wind turbine and photovoltaic generator power $P_{\text{wind-pv}}$, power of series converter P_{se}, and power of parallel converter P_{pa}.

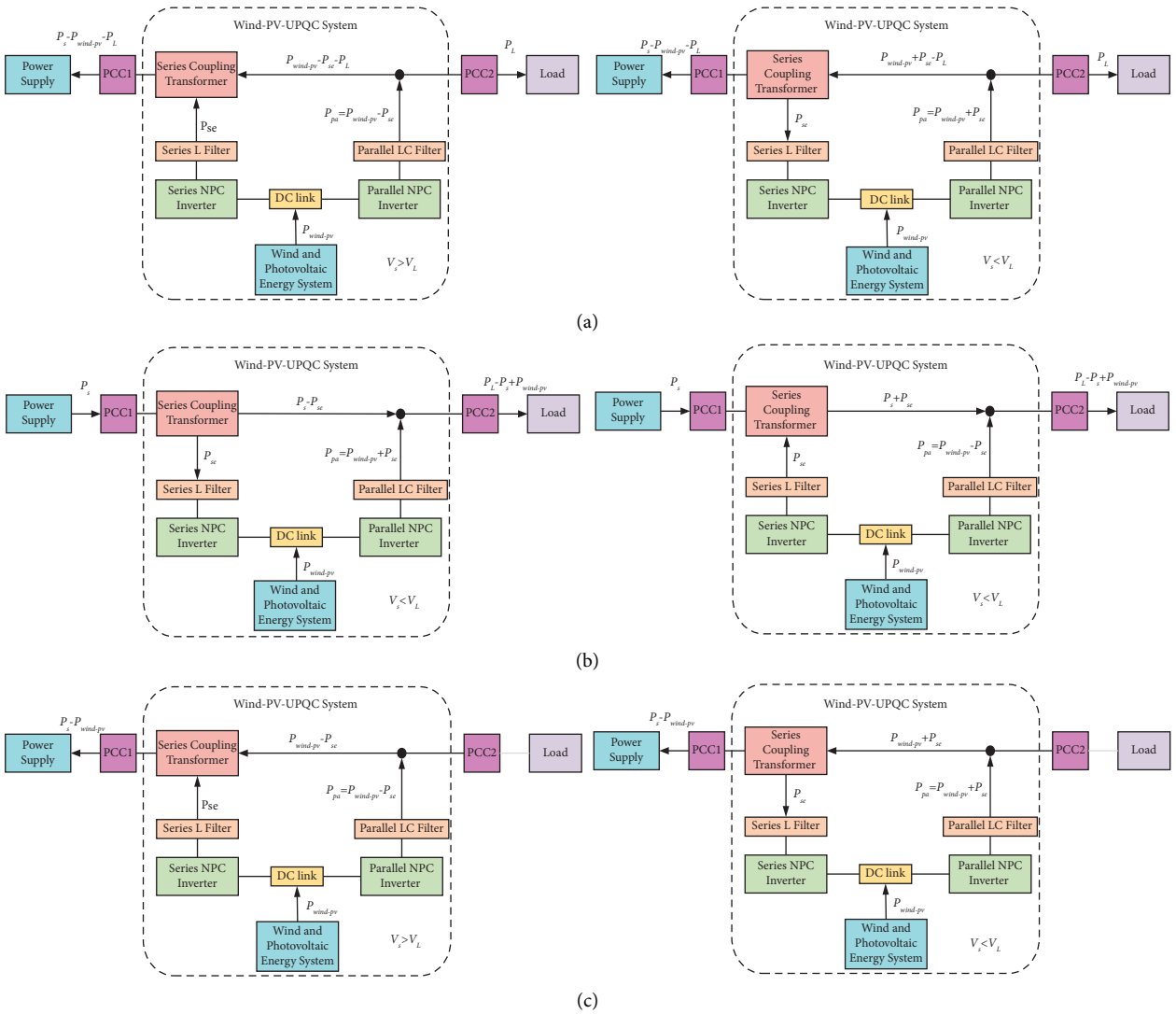

Figure 3: Flow of active power by the system of Wind-PV-UPQC. (a) $P_{\text{wind-pv}} > P_L$; (b) $P_{\text{wind-pv}} > P_L$; (c) $P_L = 0$.

In an ideal case, when $V_s = V_L$, all the energy is controlled via parallel converter and there is no flow of real power via the series converter.

In Figure 3(a), as $P_L \neq 0$ W, $P_{\text{wind-pv}} > P_L$, and $V_s > V_L$, in this scenario, the amount of the energy generated by the wind and photovoltaic energy system is sent to the utility grid via the parallel and series converter and the rest is delivered to load via parallel converter. If $V_s > V_L$, in this scenario, the amount of the energy generated by the wind and photovoltaic energy system is supplied to the grid through parallel converter and the rest is directed to load.

In Figure 3(b), as $P_L \neq 0$ W, $P_{\text{wind-pv}} < P_L$, and $V_s > V_L$, in this scenario, all energy generated through the wind and photovoltaic energy system is supplied to load via parallel converter and the rest is exhausted from the utility grid. As can be noted, amount of the energy provided thru the utility grid to the load proceeds through parallel and series converters. If $V_s > V_L$, in this scenario, the energy generated through the wind and photovoltaic energy system is supplied to load via the parallel and series converters and the rest is exhausted from the utility grid.

In Figure 3(c), as $P_L = 0$ W and $V_s > V_L$, in this scenario, all energy generated through the wind and photovoltaic energy system is supplied to the grid via the parallel and series converters. The bulk of energy is constantly controlled via the parallel converter. If $V_s < V_L$, in this scenario, all energy generated through the wind and photovoltaic energy system is supplied to the utility grid via the parallel NPC inverter. The real power consumed through the series converter proceeds by the parallel converter.

Table 1 presents the conditions that are used to regulate the power flow through the NPC inverter.

4. Simulation Results

The steady-state and dynamic performance of the Wind-PV-UPQC system are analyzed by simulating the system in MATLAB/Simulink software. The simulation of the system is

Table 1: Conditions assumed to regulate the flow of active power by the Wind-PV-UPQC.

Modes		RMS voltages	Load power	Wind-PV power
1	a	$V_s > V_L$	$P_L > 0$	$P_{\text{wind-pv}} > P_L$
	b	$V_s < V_L$		
2	a	$V_s > V_L$	$P_L > 0$	$P_{\text{wind-pv}} < P_L$
	b	$V_s < V_L$		
3	a	$V_s > V_L$	$P_L = 0$	$P_{\text{wind-pv}} > 0$
	b	$V_s > V_L$		

performed based on the block diagram of circuit shown in Figure 1. Sinusoidal Pulse Width Modulation (SPWM) technique is utilized in series and parallel NPC inverters [53]. For the simulation $5.0505e-6$ s solver step size is used. Detailed system parameters and three-phase nonlinear load are given in Appendix.

4.1. Performance of Wind-PV-UPQC in Steady-State Condition. This subsection describes the steady-state results where the Wind-PV-UPQC works in three operating modes (OPM). These OPMs are illustrated in Figure 4 taking into account the various operating conditions to which the Wind-PV-UPQC is exposed. In OPM 1, the system of Wind-PV-UPQC works without load and injects only active power into the utility grid. OPM 2 happens while there is instantaneous power of wind turbine and solar irradiation is needed by native loads linked to the system of Wind-PV-UPQC, so that $P_{\text{wind-pv}} < P_L$. In OPM 3 that arises at night (without solar radiation), with Wind-PV-UPQC coupled to asymmetrical and distorted utility grid with $P_{\text{wind-pv}} = 0$ W, the system only works as a UPQC.

Figures 5 and 6 show steady-state results for a system of Wind-PV-UPQC supplying real power to the utility grid, taking into consideration a 3-Φ full-bridge rectifier followed via an R load. In Figure 5, the load is detached and only active power is interjected into the utility grid (OPM 1). Therefore, all the power generated through the system of wind and photovoltaic is interjected into the utility grid and the system losses are updated, where $P_{\text{wind-pv}}$ is approximately 3500 W. As can be noticed, the currents of source are sinusoidal and reverse to the phase according to the particular mains voltages, although three-phase output voltages keep regulated, symmetrical, and sinusoidal. It has also been noted that almost all of the real power is interjected into the utility grid via parallel inverter.

OPM 2 happens while $P_{\text{wind-pv}} < P_L$, as presented in Figure 6. Note that the Wind-PV-UPQC system feeds the load in conjunction with the grid. Since wind and photovoltaic power is less than the actual power required by the load, the system draws power from the utility grid. As can be seen, the system of Wind-PV-UPQC in OPM 2 performs active power line conditioning. By eliminating current harmonics and compensating for load asymmetries, sinusoidal and symmetrical mains currents are obtained. Moreover, regulated and practically sinusoidal and symmetrical load voltages are attained.

In OPM 3, Figure 7 shows the operation of Wind-PV-UPQC. In this situation, it is connected to a programmable AC power supply that delivers biased input voltages, for example, voltage imbalances, harmonics, and faults. As you can see, parallel and series inverters both are performing active line filtering. The output voltages (v_{L_abc}) are consistently balanced, free of harmonics, and regulated even under the distorted voltage conditions. Since the voltages of output are controlled sinusoidally and symmetrically, the difference among the voltages of input and output occurs in series coupling transformers (v_{Tse_abc}).

Table 2 shows the total harmonic distortion (THD) and RMS values of currents and voltages connected to the utility grid and the load. As can be noticed, THDs of output voltages and mains currents are reduced in all operating modes. It is also noticed that the THD values of current and voltages are within limits described in IEEE 519 Standard. In addition, Table 2 presents the PF for the network and the load. It should be noted that effectual PF corrections are attained. From the steady results shown in Figures 5–7 and Table 2, it may be proved that the system can work in various operating mode and provides regulated, balanced, and sinusoidal voltages to the loads. Also, the system can efficiently feed/drain power to/from the grid with high PF.

4.2. Performance of Wind-PV-UPQC in Dynamic Condition. The dynamic performance of the system of Wind-PV-UPQC has been tested taking into account sudden changes in wind speed and solar radiation such as 100% to 0% and 0% to 100%. The dynamic consequences of wind speed changes and sudden changes in solar radiation are shown in Figures 8 where the total dc bus voltage (V_{dc}), grid voltage (v_{sa}), and current (i_{sa}) across PCC 1, the voltage of load (v_{La}) across PCC 2, dc bus controller output signal (i_{dc}), feedforward current (i_{ff}), and power of wind and photovoltaic system ($P_{\text{wind-pv}}$) are shown. The tests were carried out by disconnecting and reconnecting the wind and photovoltaic systems from the dc bus. Figure 8 illustrates the outcomes when i_{ff} is accustomed to speed up the production of series converter current references. According to the results, if i_{ff} is used during transitions in wind and photovoltaic systems, the dc bus voltage fluctuations are reduced.

As you can see, Wind-PV-UPQC performs active filtering while the wind and photovoltaic system is off. By eliminating current harmonics and compensating for load asymmetries, sinusoidal and symmetrical mains currents are

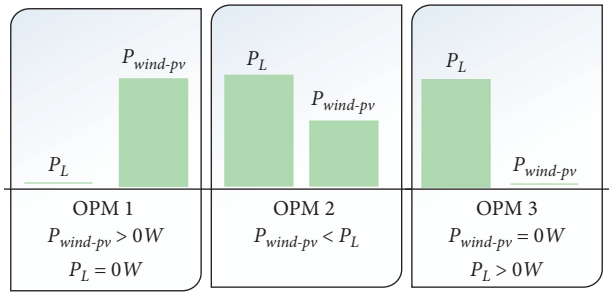

Figure 4: Operating modes described in the steady-state simulation results.

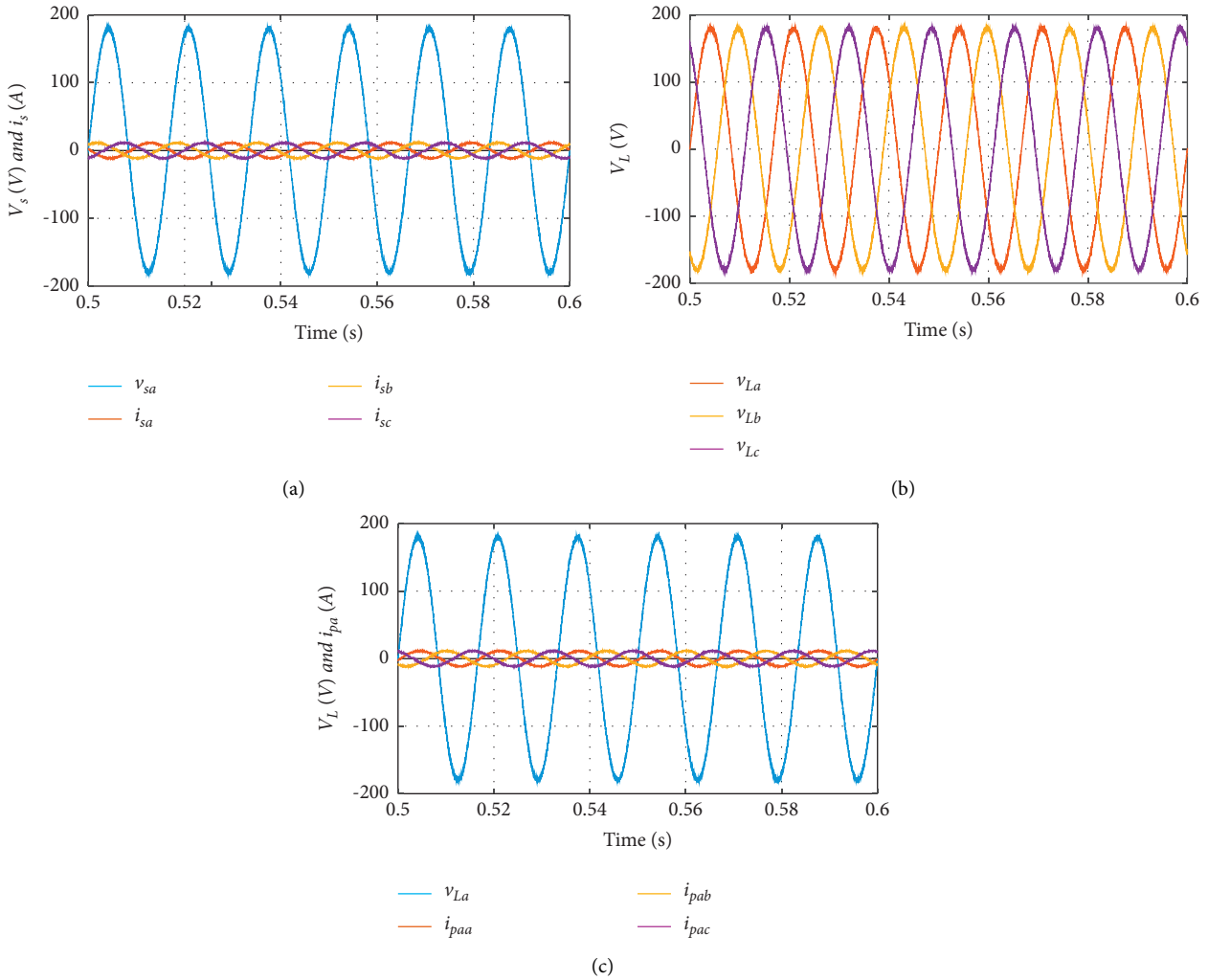

Figure 5: Only active power interjection is performing by Wind-PV-UPQC into the grid with $P_L = 0$ W and $P_{\text{wind–pv}} = 3500$ W. (a) Grid voltage currents, (b) load voltages, (c) load voltage and parallel converter currents.

obtained. Moreover, regulated and practically sinusoidal and symmetrical load voltages are attained. The Wind-PV-UPQC system then provides approximately 3500 W of real power to the load and the grid when the wind and photovoltaic system are connected. It also illustrates that the grid current dynamic response is quick when the wind and photovoltaic system is exposed to sudden power changes, because of using FFCL.

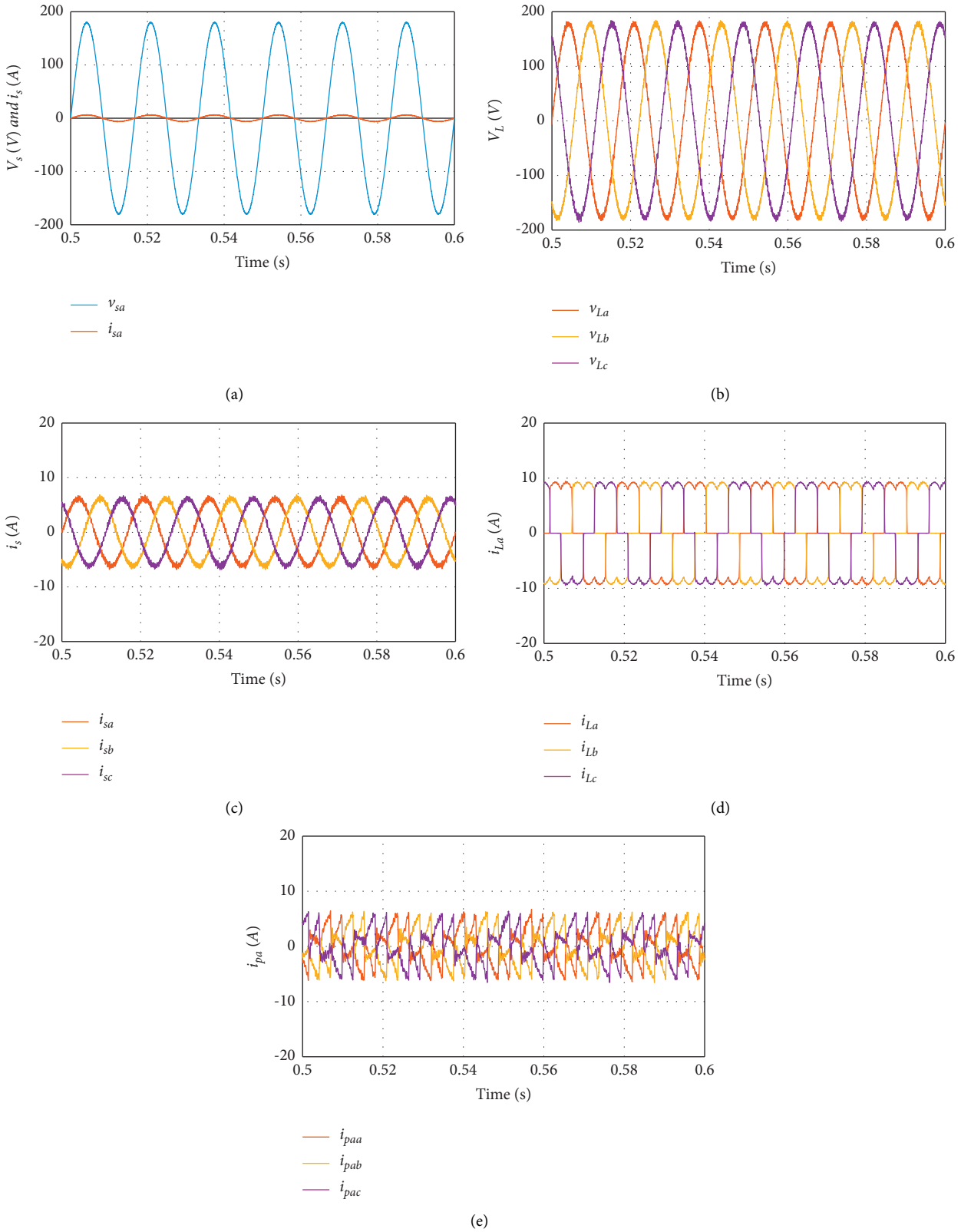

FIGURE 6: Active filtering along with active power interjection is performed by Wind-PV-UPQC with $P_{\text{wind-pv}} < P_L$. (a) Grid voltage and current, (b) load voltage, (c) grid currents, (d) load current, (e) parallel converter current.

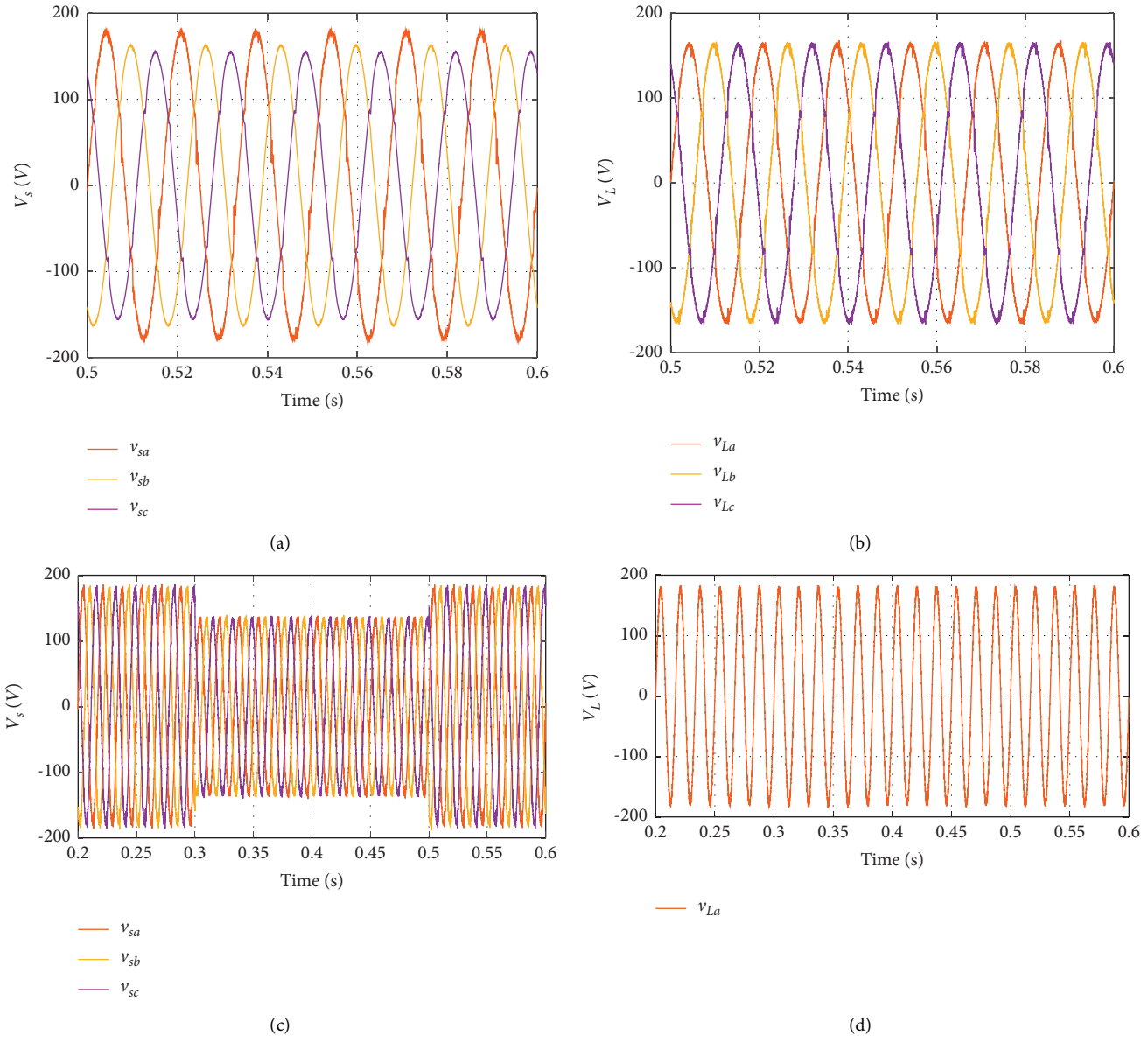

Figure 7: Wind-PV-UPQC coupled to asymmetrical and distorted utility grid $P_{\text{wind-pv}} = 0$ W; (a) voltages of grid; (b) load voltages; (c) grid voltages of Phase "a" intended for voltage sags (25%), (d) output voltage of Phase "a" intended for voltage sags (25%).

Table 2: Conditions assumed to regulate the flow of real power via the Wind-PV-UPQC.

Operating conditions	RMS values of the currents (A) and voltages (V)											
	v_{sa}	v_{sb}	v_{sc}	i_{sa}	i_{sb}	i_{sc}	v_{La}	v_{Lb}	v_{Lc}	i_{La}	i_{Lb}	i_{Lc}
OPM1	127	127	127	8.02	8.01	8.04	128	128	128	—	—	—
OPM 2	127	127	127	4.34	4.35	4.36	126	126	126	7.18	7.19	7.18
OPM 3	126	116	106	7.18	7.16	7.14	115	116	116	6.39	6.40	6.40
	Total harmonic distortion (%)											
OPM1	1.8	1.9	1.9	2.5	2.6	2.4	2.4	1.9	1.6	—	—	—
OPM 2	1.7	1.8	1.7	5.5	5.5	4.8	2.5	2.2	1.7	29	29	28
OPM 3	10.6	9.9	9.9	4.5	3.9	3.9	2.2	2.0	1.5	29	28	29

Table 2: Continued.

Operating conditions	RMS values of the currents (A) and voltages (V)											
	v_{sa}	v_{sb}	v_{sc}	i_{sa}	i_{sb}	i_{sc}	v_{La}	v_{Lb}	v_{Lc}	i_{La}	i_{Lb}	i_{Lc}
	Power factor (PF)											
	Utility grid						Load					
	Phase "a"	Phase "b"	Phase "c"				Phase "a"	Phase "b"	Phase "c"			
OPM1	−0.99	−0.99	−0.99				—	—	—			
OPM 2	0.99	0.98	0.98				0.96	0.96	0.96			
OPM 3	1.0	0.98	0.99				0.96	0.96	0.96			

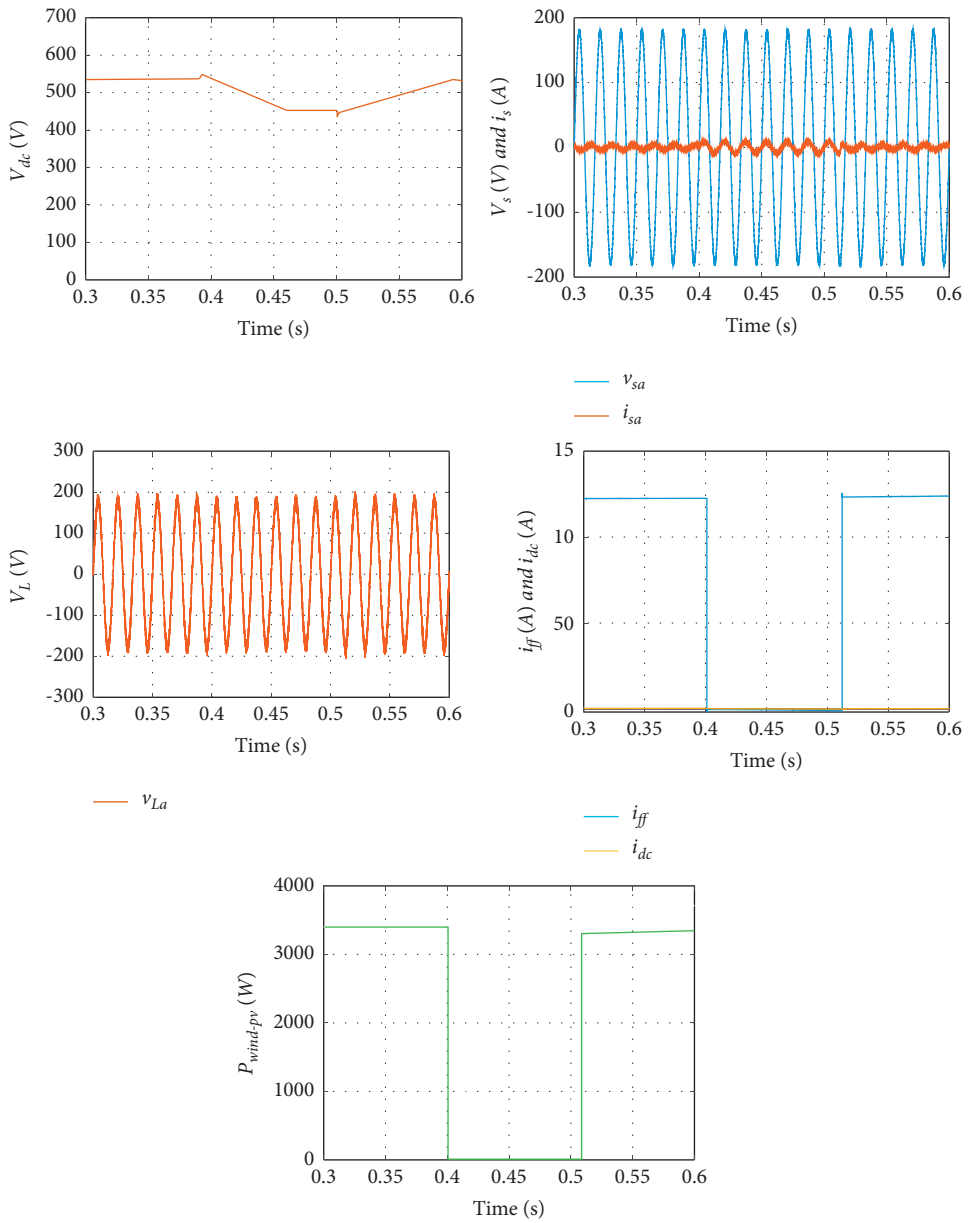

Figure 8: Active filtering along with active power interjection is performed by Wind-PV-UPQC with $P_{\text{wind-pv}} > P_L$. Voltage of dc bus V_{dc}, Phase "a" grid current and grid voltage, load voltage, i_{ff} current, i_{dc} current, and Wind and Photovoltaic power $P_{\text{wind-pv}}$ for sudden wind and solar irradiance variations using FFCL.

5. Conclusion

In this paper, a DG system named Wind-PV-UPQC is proposed, which combines a 3P4W grid-connected wind and photovoltaic energy conversion system using a unified power quality conditioner and also performs the duties of an UPQC dual compensation scheme, along with FFCL. The arrangement, called Wind-PV-UPQC, consists of two 3-level NPC inverters connected back to back. In addition to supplying active energy from the arrangement of wind photovoltaic, the wind photovoltaic-UPQC arrangement was capable of realizing series and parallel conditioning of power lines. The dynamic and steady-state performance of the system was assessed in distorted/disturbed line voltage situations, containing dips, asymmetries, and harmonics. In addition to the series compensation, an effective compensation of the reactive power is obtained through compensating the reactive power of the load by eliminating the harmonic currents of the load. The efficiency of the FFCL acting on the current references of the series converter was correctly evaluated for sudden changes in wind speed and solar irradiance. Wind-PV-UPQC can be seen to be a good solution for modern distribution systems via integrating distributed generation with improved power quality.

Appendix

Simulation parameters: Utility grid voltage: 127.27 V (L-N), 60 Hz; voltage of Dc link: 616 V; capacitance of Dc link: 2200 μF; parallel converter interfacing inductor: 1.73 mH; parallel converter interfacing capacitor: 60 μF; series converter interfacing inductor: 3.5 mH; NPC inverters switching frequency = 20 kHz; $P_{\text{wind-pv}} = 3.5$ kW; three-phase full-bridge rectifier followed by resistive load ($R = 33.3\ \Omega$ and $40\ \Omega$).

PV array parameters: $I_{\text{sc}} = 8.49$ A; $I_{\text{mp}} = 7.96$ A; $V_{\text{oc}} = 37.5$ V; $V_{\text{mp}} = 30.8$ V; $P_{\text{pv}} = 2.0$ kW.

Wind turbine parameters: Wind speed: 12 m/s; blade pitch angle: 0°; $P_{\text{wind}} = 1.5$ kW.

Data Availability

The data used to support the findings of this study are available from the corresponding author upon request.

Conflicts of Interest

The authors declare that they have no conflicts of interest.

Authors' Contributions

Conceptualization was done by Saleem Riaz and Tongfei Lei; methodology was done by Tongfei Lei; software was done by Noor Zanib; validation was done by Tongfei Lei and Jianfeng wang; formal analysis was done by Munira Batool; investigation was done by Feng Pan; resources were done by Noor Zanib; data curation was done by Noor Zanib; writing—original draft preparation was done by Tongfei Lei; writing—review and editing was done by Tongfei Lei; visualization was done by Feng Pan; supervision was done by Saleem Riaz; project administration was done by Saleem Riaz; funding acquisition was done by Tongfei Lei. All authors have read and agreed to the published version of the manuscript.

Acknowledgments

This research work was financially supported by Shaanxi Provincial Science and Technology Department: Grant no. 2020JM-644.

References

[1] J. Rocabert, A. Luna, F. Blaabjerg, and P. Rodríguez, "Control of power converters in AC microgrids," *IEEE Transactions on Power Electronics*, vol. 27, no. 11, pp. 4734–4749, 2012.

[2] A. Al-Quraan and M. Al-Qaisi, "Modelling, design and control of a standalone hybrid PV-wind micro-grid system," *Energies*, vol. 14, no. 16, pp. 4849–16, 2021.

[3] O. Lodin, N. Khajuria, S. Vishwakarma, and G. Manzoor, "Modeling and simulation of wind solar hybrid system using matlab/simulink," *International Journal of Innovative Technology and Exploring Engineering*, vol. 8, no. 9S, pp. 218–224, 2019.

[4] A. F. Bendary and M. M. Ismail, "Battery charge management for hybrid PV/Wind/Fuel cell with storage battery," *Energy Procedia*, vol. 162, pp. 107–116, 2019.

[5] K. Wang, C. Liu, J. Sun et al., "State of charge estimation of composite energy storage systems with supercapacitors and lithium batteries," *Complexity*, vol. 2021, Article ID 8816250, 15 pages, 2021.

[6] C. Liu, Q. Li, and K. Wang, "State-of-charge estimation and remaining useful life prediction of supercapacitors," *Renewable and Sustainable Energy Reviews*, vol. 150, Article ID 111408, 2021.

[7] A. Benali, M. Khiat, T. Allaoui, and M. Denai, "Power quality improvement and low voltage ride through capability in hybrid wind-PV farms grid-connected using dynamic voltage restorer," *IEEE Access*, vol. 6, pp. 68634–68648, 2018.

[8] J. Hossain and H. R. Pota, *Robust Control for Grid Voltage Stability: High Penetration of Renewable Energy: Power Systems*, Springer, Singapore, 2014.

[9] M. Malinowski, J. I. Leon, and H. Abu-Rub, "Solar photovoltaic and thermal energy systems: Current Technology and future trends," *Proceedings of the IEEE*, vol. 105, no. 11, pp. 2132–2146, 2017.

[10] Y. Zhou, M. Zhang, G. Kou, and Y. Li, "Travel preference of bicycle-sharing users: A multi-granularity sequential pattern mining approach," *International Journal of Computers, Communications & Control*, vol. 17, no. 1, 2022.

[11] S. Samal, P. K. Hota, and P. K. Barik, "Performance improvement of a distributed generation system using unified power quality conditioner," *Technology and Economics of Smart Grids and Sustainable Energy*, vol. 5, no. 1, 2020.

[12] M. Badoni, B. Singh, and A. Singh, "Implementation of echo-state network-based control for power quality improvement," *IEEE Transactions on Industrial Electronics*, vol. 64, no. 7, pp. 5576–5584, 2017.

[13] S. Bahrami and M. H. Amini, "A decentralized trading algorithm for an electricity market with generation uncertainty," *Applied Energy*, vol. 218, pp. 520–532, 2018.

[14] Y. Hua, N. Wang, and K. Zhao, "Simultaneous unknown input and state estimation for the linear system with a rank-deficient

distribution matrix," *Mathematical Problems in Engineering*, vol. 2021, Article ID 6693690, 11 pages, 2021.

[15] C. Liu, Y. Zhang, J. Sun, Z. Cui, and K. Wang, "Stacked bidirectional LSTM RNN to evaluate the remaining useful life of supercapacitor," *International Journal of Energy Research*, vol. 46, no. 3, pp. 3034–3043, 2021.

[16] S. Kumar and B. Singh, "A multipurpose PV system integrated to a three-phase distribution system using an LWDF-based approach," *IEEE Transactions on Power Electronics*, vol. 33, no. 1, pp. 739–748, 2018.

[17] F. M. de Oliveira, S. A. O. da Silva, F. R. Durand, L. P. Sampaio, V. D. Bacon, and L. B. G. Campanhol, "Grid-tied photovoltaic system based on PSO MPPT technique with active power line conditioning," *IET Power Electronics*, vol. 9, no. 6, pp. 1180–1191, 2016.

[18] L. B. G. Campanhol, S. A. O. Da Silva, A. A. De Oliveira, and V. D. Bacon, "Dynamic performance improvement of a grid-tied PV system using a feed-forward control loop acting on the NPC inverter currents," *IEEE Transactions on Industrial Electronics*, vol. 64, no. 3, pp. 2092–2101, 2017.

[19] L. B. G. Campanhol, S. A. O. Da Silva, A. A. De Oliveira, and V. D. Bacon, "Single-stage three-phase grid-tied pv system with universal filtering capability applied to DG systems and AC microgrids," *IEEE Transactions on Power Electronics*, vol. 32, no. 12, pp. 9131–9142, 2017.

[20] S. Devassy and B. Singh, "Design and performance analysis of three-phase solar PV integrated UPQC," in *Proceedings of the 2016 IEEE 6th International Conference on Power Systems (ICPS)*, New Delhi, India, March 2016.

[21] K. Palanisamy, D. P. Kothari, M. K. Mishra, S. Meikandashivam, and I. Jacob Raglend, "Effective utilization of unified power quality conditioner for interconnecting PV modules with grid using power angle control method," *International Journal of Electrical Power & Energy Systems*, vol. 48, no. 1, pp. 131–138, 2013.

[22] G. Kou, H. Xiao, M. Cao, and L. H. Lee, "Optimal computing budget allocation for the vector evaluated genetic algorithm in multi-objective simulation optimization," *Automatica*, vol. 129, Article ID 109599, 2021.

[23] X. Zhang, Y. Zhao, H. Lin, S. Riaz, and H. Elahi, "Real-time fault diagnosis and fault-tolerant control strategy for Hall sensors in permanent magnet brushless DC motor drives," *Electronics*, vol. 10, no. 11, p. 1268, 2021.

[24] J. Zhao, F. Li, Z. Wang, P. Dong, G. Xia, and K. Wang, "Flexible PVDF nanogenerator-driven motion sensors for human body motion energy tracking and monitoring," *Journal of Materials Science: Materials in Electronics*, vol. 32, no. 11, pp. 14715–14727, 2021.

[25] Y. Zhou, G. Kou, H. Xiao, Y. Peng, and F. E. Alsaadi, "Sequential imperfect preventive maintenance model with failure intensity reduction with an application to urban buses," *Reliability Engineering & System Safety*, vol. 198, Article ID 106871, 2020.

[26] B. Han, B. Bae, H. Kim, and S. Baek, "Combined operation of unified power-quality conditioner with distributed generation," *IEEE Transactions on Power Delivery*, vol. 21, no. 1, pp. 330–338, 2006.

[27] J. G. Nielsen, M. Newman, H. Nielsen, and F. Blaabjerg, "Control and testing of a dynamic voltage restorer (DVR) at medium voltage level," *IEEE Transactions on Power Electronics*, vol. 19, no. 3, pp. 806–813, 2004.

[28] S. A. O. Da Silva, L. B. G. Campanhol, G. M. Pelz, and V. De Souza, "Comparative performance analysis involving a three-phase UPQC operating with conventional and dual/inverted power-line conditioning strategies," *IEEE Transactions on Power Electronics*, vol. 35, no. 11, pp. 11652–11665, 2020.

[29] J. He, Y. W. Li, F. Blaabjerg, and X. Wang, "Active harmonic filtering using current-controlled, grid-connected DG units with closed-loop power control," *IEEE Transactions on Power Electronics*, vol. 29, no. 2, pp. 642–653, 2014.

[30] F. Briz, P. Garcia, M. W. Degner, D. Diaz-Reigosa, and J. M. Guerrero, "Dynamic behavior of current controllers for selective harmonic compensation in three-phase active power filters," *IEEE Transactions on Industry Applications*, vol. 49, no. 3, pp. 1411–1420, 2013.

[31] B. A. Angélico, L. B. G. Campanhol, and S. A. Oliveira da Silva, "Proportional-integral/proportional-integral-derivative tuning procedure of a single-phase shunt active power filter using Bode diagram," *IET Power Electronics*, vol. 7, no. 10, pp. 2647–2659, 2014.

[32] B. L. G. Costa, V. D. Bacon, S. A. O. Da Silva, and B. A. Angelico, "Tuning of a PI-mr controller based on differential evolution metaheuristic applied to the current control loop of a shunt-APF," *IEEE Transactions on Industrial Electronics*, vol. 64, no. 6, pp. 4751–4761, 2017.

[33] W. R. N. Santos, E. R. C. da Silva, C. B. Jacobina et al., "The transformerless single-phase universal active power filter for harmonic and reactive power compensation," *IEEE Transactions on Power Electronics*, vol. 29, no. 7, pp. 3563–3572, 2014.

[34] A. Teke, M. E. Meral, M. U. Cuma, M. Tümay, and K. Ç. Bayindir, "OPEN unified power quality conditioner with control based on enhanced phase locked loop," *IET Generation, Transmission & Distribution*, vol. 7, no. 3, pp. 254–264, 2013.

[35] B. W. Franca, L. F. Da Silva, M. A. Aredes, and M. Aredes, "An improved iUPQC controller to provide additional grid-voltage regulation as a STATCOM," *IEEE Transactions on Industrial Electronics*, vol. 62, no. 3, pp. 1345–1352, 2015.

[36] V. Khadkikar and A. Chandra, "A novel structure for three-phase four-wire distribution system utilizing Unified Power Quality Conditioner (UPQC)," *IEEE Transactions on Industry Applications*, vol. 45, no. 5, pp. 1897–1902, 2009.

[37] R. A. Modesto, S. A. O. Da Silva, A. A. De Oliveira, and V. D. Bacon, "A versatile unified power quality conditioner applied to three-phase four-wire distribution systems using a dual control strategy," *IEEE Transactions on Power Electronics*, vol. 31, no. 8, pp. 5503–5514, 2016.

[38] S. Riaz, H. Lin, M. Waqas, F. Afzal, K. Wang, and N. Saeed, "An accelerated error convergence design criterion and implementation of lebesgue-p norm ILC control topology for linear position control systems," *Mathematical Problems in Engineering*, vol. 2021, Article ID 5975158, 12 pages, 2021.

[39] S. Riaz, H. Lin, and M. P. Akhter, "Design and implementation of an accelerated error convergence criterion for norm optimal iterative learning controller," *Electronics*, vol. 9, no. 11, p. 1766, 2020.

[40] S. Riaz, H. Lin, M. Bilal Anwar, and H. Ali, "Design of PD-type second-order ILC law for PMSM servo position control," *Journal of Physics: Conference Series*, vol. 1707, no. 1, Article ID 012002, 2020.

[41] S. Riaz, H. Lin, F. Afzal, and A. Maqbool, "Design and implementation of novel LMI-based iterative learning robust nonlinear controller," *Complexity*, vol. 2021, Article ID 5577241, 13 pages, 2021.

[42] S. Riaz, H. Lin, and H. Elahi, "A novel fast error convergence approach for an optimal iterative learning controller," *Integrated Ferroelectrics*, vol. 213, no. 1, pp. 103–115, 2021.

[43] S. Riaz, H. Lin, M. Mahsud, D. Afzal, A. Alsinai, and M. Cancan, "An improved fast error convergence topology for PDα-type fractional-order ILC," *Journal of Interdisciplinary Mathematics*, vol. 24, no. 7, pp. 2005–2019, Article ID 1984567, 2021.

[44] S. B. Kjaer, J. K. Pedersen, and F. Blaabjerg, "A review of single-phase grid-connected inverters for photovoltaic modules," *IEEE Transactions on Industry Applications*, vol. 41, no. 5, pp. 1292–1306, 2005.

[45] W. Li, Y. Gu, H. Luo, W. Cui, X. He, and C. Xia, "Topology review and derivation methodology of single-phase transformerless photovoltaic inverters for leakage current suppression," *IEEE Transactions on Industrial Electronics*, vol. 62, no. 7, pp. 4537–4551, 2015.

[46] L. Wu, Z. Zhao, and J. Liu, "A single-stage three-phase grid-connected photovoltaic system with modified MPPT method and reactive power compensation," *IEEE Transactions on Energy Conversion*, vol. 22, no. 4, pp. 881–886, 2007.

[47] M. C. Cavalcanti, A. M. Farias, K. C. Oliveira, F. A. S. Neves, and J. L. Afonso, "Eliminating leakage currents in neutral point clamped inverters for photovoltaic systems," *IEEE Transactions on Industrial Electronics*, vol. 59, no. 1, pp. 435–443, 2012.

[48] S. A. O. Da Silva, L. P. Sampaio, F. M. De Oliveira, and F. R. Durand, "Feed-forward DC-bus control loop applied to a single-phase grid-connected PV system operating with PSO-based MPPT technique and active power-line conditioning," *IET Renewable Power Generation*, vol. 11, no. 1, pp. 183–193, 2017.

[49] M. Cabral Cavalcanti, G. Medeiros de Souza Azevedo, B. de Aguiar Amaral, F. de Assis dos Santos Neves, D. Carvalho Moreira, and K. Carneiro de Oliveira, "A grid connected photovoltaic generation system with compensation of current harmonics and voltage sags," *Eletrônica de Potência*, vol. 11, no. 2, pp. 93–101, 2006.

[50] S. Devassy and B. Singh, "Dynamic performance of solar PV integrated UPQC-P for critical loads," in *Proceedings of the 2015 Annual IEEE India Conference (INDICON)*, New Delhi, India, December 2015.

[51] K. S. Srikanth, T. K. Mohan, and P. Vishnuvardhan, "Notice of Removal: Improvement of power quality for microgrid using fuzzy based UPQC controller," in *Proceedings of the 2015 International Conference on Electrical, Electronics, Signals, Communication and Optimization (EESCO)*, Visakhapatnam, India, January 2015.

[52] V. D. Bacon and S. A. O. da Silva, "Performance improvement of a three-phase phase-locked-loop algorithm under utility voltage disturbances using non-autonomous adaptive filters," *IET Power Electronics*, vol. 8, no. 11, pp. 2237–2250, 2015.

[53] I. Colak, E. Kabalci, and R. Bayindir, "Review of multilevel voltage source inverter topologies and control schemes," *Energy Conversion and Management*, vol. 52, no. 2, pp. 1114–1128, 2011.